# CHANGES IN FOREST ECOSYSTEM NUTRITION

EDITED BY: Friederike Lang, Roland Bol, Jaane Krüger, Sebastian Loeppmann, Klaus Kaiser and Stephan Hättenschwiler

PUBLISHED IN: Frontiers in Forests and Global Change and Frontiers in Environmental Science

frontiers Research Topics

ISSN 1664-8714
ISBN 978-2-88971-499-5
DOI 10.3389/978-2-88971-499-5

## About Frontiers

Frontiers is more than just an open-access publisher of scholarly articles: it is a pioneering approach to the world of academia, radically improving the way scholarly research is managed. The grand vision of Frontiers is a world where all people have an equal opportunity to seek, share and generate knowledge. Frontiers provides immediate and permanent online open access to all its publications, but this alone is not enough to realize our grand goals.

## Frontiers Journal Series

The Frontiers Journal Series is a multi-tier and interdisciplinary set of open-access, online journals, promising a paradigm shift from the current review, selection and dissemination processes in academic publishing. All Frontiers journals are driven by researchers for researchers; therefore, they constitute a service to the scholarly community. At the same time, the Frontiers Journal Series operates on a revolutionary invention, the tiered publishing system, initially addressing specific communities of scholars, and gradually climbing up to broader public understanding, thus serving the interests of the lay society, too.

## Dedication to Quality

Each Frontiers article is a landmark of the highest quality, thanks to genuinely collaborative interactions between authors and review editors, who include some of the world's best academicians. Research must be certified by peers before entering a stream of knowledge that may eventually reach the public - and shape society; therefore, Frontiers only applies the most rigorous and unbiased reviews.
Frontiers revolutionizes research publishing by freely delivering the most outstanding research, evaluated with no bias from both the academic and social point of view. By applying the most advanced information technologies, Frontiers is catapulting scholarly publishing into a new generation.

## What are Frontiers Research Topics?

Frontiers Research Topics are very popular trademarks of the Frontiers Journals Series: they are collections of at least ten articles, all centered on a particular subject. With their unique mix of varied contributions from Original Research to Review Articles, Frontiers Research Topics unify the most influential researchers, the latest key findings and historical advances in a hot research area! Find out more on how to host your own Frontiers Research Topic or contribute to one as an author by contacting the Frontiers Editorial Office: frontiersin.org/about/contact

# CHANGES IN FOREST ECOSYSTEM NUTRITION

Topic Editors:
**Friederike Lang,** University of Freiburg, Germany
**Roland Bol,** Helmholtz-Verband Deutscher Forschungszentren (HZ), Germany
**Jaane Krüger,** University of Education Freiburg, Germany
**Sebastian Loeppmann,** Christian-Albrechts-Universität zu Kiel, Germany
**Klaus Kaiser,** Martin Luther University Halle-Wittenberg, Germany
**Stephan Hättenschwiler,** UMR5175 Centre d'Ecologie Fonctionnelle et Evolutive (CEFE), France

**Citation:** Lang, F., Bol, R., Krüger, J., Loeppmann, S., Kaiser, K., Hättenschwiler, S., eds. (2021). Changes in Forest Ecosystem Nutrition. Lausanne: Frontiers Media SA. doi: 10.3389/978-2-88971-499-5

# Table of Contents

frontiers in Forests and Global Change

EDITORIAL
published: 30 August 2021
doi: 10.3389/ffgc.2021.752063

# Editorial: Changes in Forest Ecosystem Nutrition

*Friederike Lang[1]*, Jaane Krüger[1], Klaus Kaiser[2], Roland Bol[3,4] and Sebastian Loeppmann[5,6]*

*[1] Chair of Soil Ecology, Faculty of Environment and Natural Resources, University of Freiburg, Freiburg, Germany, [2] Soil Science and Soil Protection, Martin Luther University Halle-Wittenberg, Halle, Germany, [3] Research Centre Jülich, Institute of Bio- and Geosciences, Agrosphere (IBG-3), Jülich, Germany, [4] School of Natural Sciences, Bangor University, Bangor, United Kingdom, [5] Biogeochemistry of Agroecosystems, Georg-August-University, Göttingen, Germany, [6] Department of Soil Science, Institute of Plant Nutrition and Soil Science, Christian-Albrechts-University, Kiel, Germany*

**Keywords: phosphorus, nitrogen, cross-scale nutritional interactions, nutrient use efficiency, disturbance, scales of ecosystem nutrition**

## Editorial on the Research Topic

## Changes in Forest Ecosystem Nutrition

Forests strongly depend on natural nutrient resources since fertilization is not a common forest management practice in most parts of the world. Soils and above- and belowground interactions play a crucial role in regulating the retention, distribution, and uptake of nutrients. The high relevance of nutrition for health and productivity of forests has been demonstrated by recent research data obtained by extensive forest monitoring around the world. For example, nutrient availability was the most decisive factor explaining net forest ecosystem productivity (NEP) for a global population of 92 forest sites (Fernández-Martínez et al., 2014). Also, changes in phosphorus (P) and nitrogen (N) nutrition have been emphasized in recent studies on European forests (Jonard et al., 2015; Etzold et al., 2020). These findings stress the necessity of addressing forest nutrition via holistic ecosystem approaches (**Figure 1**), as was recently outlined for P (Lang et al., 2016).

Linking trees' nutrient supply with the abundance and activity of other organisms present in different ecosystem compartments has a long tradition in forest-related research. Thus, vast information on relationships between soils and site conditions, nutrient cycling and composition, and productivity of vegetation has been collected systematically over long periods of time, and then used to develop empirical models of forest growth (e.g., Barnes et al., 1982). However, forest ecosystem interactions are exposed to quickly changing environmental conditions. Recent drivers of forest nutrition include (a) higher global atmospheric N deposition leading to increased productivity (Etzold et al., 2020) and causing nutrient imbalances (Peñuelas et al., 2012); (b) climate change affecting the recycling of nutrients (Medlyn et al., 2011) and increasing forest disturbance (Gleason et al., 2010); or (c) changes in management intensity leading to increased removal of nutrients with biomass (Vadeboncoeur et al., 2014). Such changes in nutritional conditions are expected to translate into detrimental effects on forest ecosystems. Therefore, proper management of forests for preserving their functioning requires timely updating of empirical knowledge about ecosystem interactions and their feedbacks to nutrition.

OPEN ACCESS

***Edited and reviewed by:***
*Frank Hagedorn, Swiss Federal Institute for Forest, Switzerland*

****Correspondence:***
*Friederike Lang*
*fritzi.lang@bodenkunde.uni-freiburg.de*

***Specialty section:***
*This article was submitted to Forest Soils, a section of the journal Frontiers in Forests and Global Change*

***Received:*** *02 August 2021*
***Accepted:*** *05 August 2021*
***Published:*** *30 August 2021*

***Citation:***
*Lang F, Krüger J, Kaiser K, Bol R and Loeppmann S (2021) Editorial: Changes in Forest Ecosystem Nutrition. Front. For. Glob. Change 4:752063. doi: 10.3389/ffgc.2021.752063*

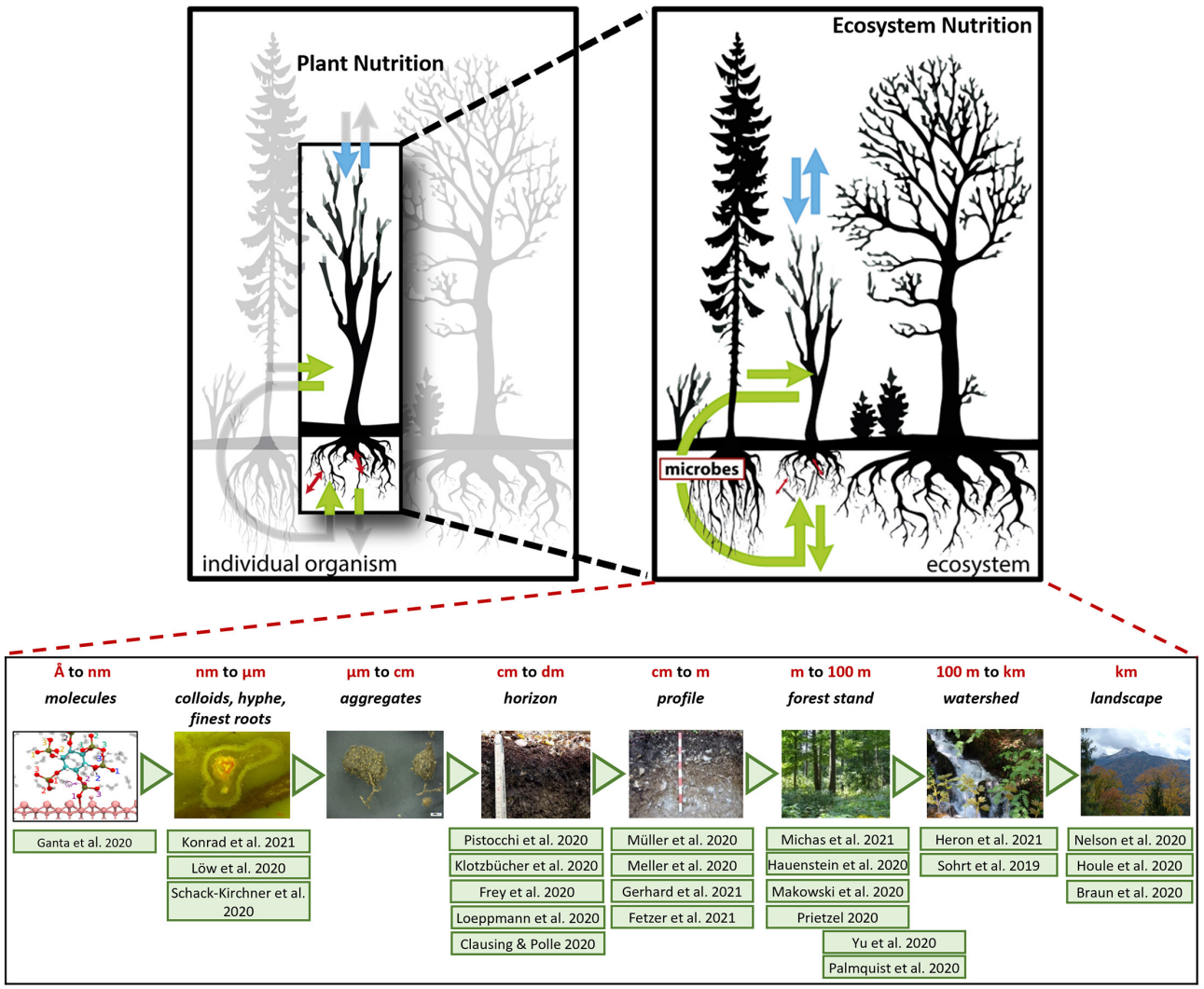


**FIGURE 1 |** In contrast to plant nutrition, which focuses on individual target plants, ecosystem nutrition covers all ecosystem compartments and their interactions **(Top)**. The different articles within the Research Topic Changes in Forest Ecosystem Nutrition address manifold compartments and interactions on a wide range of spatial scales **(Bottom)**.

Many new approaches of ecosystem nutrition have been compiled in the Research Topic "Changes in Forest Ecosystem Nutrition," covering spatial scales (**Figure 1**) from the molecular level (Ganta et al.) up to landscapes (Houle et al.). Those approaches are complementary to the traditional concepts of plant nutrition, which focus on one-way relationships between soil and plants. Key factors in P ecosystem nutrition at discrete scale levels were P speciation in soils (Klotzbücher et al.; Konrad et al.), nutrient mobilization by root exudates (Schack-Kirchner et al.), microbial (Michas et al.), and fungal communities (Müller et al.), identification of P sources and uptake processes (Pistocchi et al.; Hauenstein et al.), P-efficiency of mycorrhizal fungi (Clausing and Polle), the impact of beech provenances (Meller et al.) and root surface distribution (Loew et al.). The topic also addresses factors effective along different scale levels, such as P leaching within soils (Makowski et al.; Gerhard et al.; Fetzer et al.) or at catchment scale (Sohrt et al.), element coupling during microbial non-steady state conditions at profile scale (Loeppmann et al.) or stand scale (Palmqvist et al.), and P heterogeneity at stand scale (Prietzel) and at the scale of landscapes (Yu et al.). In addition, the topic extents to the impact of certain drivers of ecosystem nutrition, including land-use (Heron et al.), pedogenetic and ecosystem succession (Nelson et al.), climate change (Houle et al.) and of N deposition (Braun et al.; Frey et al.).

Overall, the range of publications in the Research Topic impressively illustrates that plant nutrition approaches considering only processes immediately relevant to vitality and yield of individual plants are not sufficient to address recent challenges linked to human impact on forest ecosystems. The importance of saprophytic symbiotic microorganisms – including their community composition, abundance, and activity

– for nutrient turnover in forest ecosystems, and the linkages between above- and below-ground biota, as well as relations to ecosystem services need to be carefully considered. At the scale of ecosystems, heterogeneity and its structuring effects, seasonality, and links to nutrient transport by soil water or within organisms, become crucial factors. Based on the compiled studies, we postulate that for understanding their resilience against and vulnerability to global change, ecosystem nutrition processes need to be characterized based on their emergent interacting, hierarchy, spatial and temporal structure, and robustness. Sound evaluation of the human impact on forest ecosystem nutrition needs assessment beyond nutrient budgets and contents, by considering all relevant key factors that link mobilization and immobilization processes, and therefore shape the nutrient use efficiency of forests at the ecosystem level.

## AUTHOR CONTRIBUTIONS

FL prepared the draft. JK compiled the figures. RB, SL, and KK revised the draft. All authors approved the final submission.

## ACKNOWLEDGMENTS

The idea for this Research Topic resulted from the discussion within the Priority Programme 1685 *Ecosystem Nutrition–Forest strategies for limited phosphorus resources* funded by the German Research Foundation (DFG). We greatly thank all authors and reviewers for their contributions to this special issue as well as the support of the editorial office.

## REFERENCES

Barnes, B. V., Pregitzer, K. S., Spies, T. A., and Spooner, V. H. (1982). Ecological forest site classification. *J. Forestry* 80, 493–498.

Etzold, S., Ferretti, M., Reinds, G. J., Solberg, S., Gessler, A., Waldner, P., et al. (2020). Nitrogen deposition is the most important environmental driver of growth of pure, even-aged and managed European forests. *Forest Ecol. Manage.* 458:117762. doi: 10.1016/j.foreco.2019.117762

Fernández-Martínez, M., Vicca, S., Janssens, I. A., Sardans, J., Luyssaert, S., Campioli, M., et al. (2014). Nutrient availability as the key regulator of global forest carbon balance. *Nature Climate Change* 4:471–476. doi: 10.1038/nclimate2177

Gleason, S. M., Read, J., Ares, A., and Metcalfe, D. J. (2010). Species-soil associations, disturbance, and nutrient cycling in an Australian tropical rainforest. *Oecologia* 162, 1047–1058. doi: 10.1007/s00442-009-1527-2

Jonard, M., Fürst, A., Verstraeten, A., Thimonier, A., Timmermann, V., Potočić, N., et al. (2015). Tree mineral nutrition is deteriorating in Europe. *Global Change Biol.* 21, 418–430. doi: 10.1111/gcb.12657

Lang, F., Bauhus, J., Frossard, E., George, E., Kaiser, K., Kaupenjohann, M., et al. (2016). Phosphorus in forest ecosystems: New insights from an ecosystem nutrition perspective. *J. Plant Nutr. Soil Sci.* 179, 129–135. doi: 10.1002/jpln.201500541

Medlyn, B. E., Duursma, R. A., and Zeppel, M. J. B. (2011). Forest productivity under climate change: a checklist for evaluating model studies. *WIREs Clim. Change* 2, 332–355. doi: 10.1002/wcc.108

Peñuelas, J., Sardans, J., Rivas-ubach, A., and Janssens, I. A. (2012). The human-induced imbalance between C, N and P in Earth's life system. *Global Change Biol.* 18, 3–6. doi: 10.1111/j.1365-2486.2011.02568.x

Vadeboncoeur, M. A., Hamburg, S. P., Yanai, R. D., and Blum, J. D. (2014). Rates of sustainable forest harvest depend on rotation length and weathering of soil minerals. *Forest Ecol. Manage.* 318, 194–205. doi: 10.1016/j.foreco.2014.01.012

**Conflict of Interest:** The authors declare that the research was conducted in the absence of any commercial or financial relationships that could be construed as a potential conflict of interest.

**Publisher's Note:** All claims expressed in this article are solely those of the authors and do not necessarily represent those of their affiliated organizations, or those of the publisher, the editors and the reviewers. Any product that may be evaluated in this article, or claim that may be made by its manufacturer, is not guaranteed or endorsed by the publisher.

frontiers in Forests and Global Change

ORIGINAL RESEARCH
published: 17 December 2019
doi: 10.3389/ffgc.2019.00085

# Phosphorus Fluxes in a Temperate Forested Watershed: Canopy Leaching, Runoff Sources, and In-Stream Transformation

*Jakob Sohrt[1]*, David Uhlig[2†], Klaus Kaiser[3], Friedhelm von Blanckenburg[2], Jan Siemens[4], Stefan Seeger[1], Daniel A. Frick[2], Jaane Krüger[5], Friederike Lang[5] and Markus Weiler[1]*

[1] Chair of Hydrology, University of Freiburg, Freiburg im Breisgau, Germany, [2] GFZ German Research Centre for Geosciences, Section Earth Surface Geochemistry, Potsdam, Germany, [3] Soil Science and Soil Protection, Martin Luther University Halle-Wittenberg, Halle (Saale), Germany, [4] iFZ Research Centre for Biosystems, Land Use and Nutrition, Institute of Soil Science and Soil Conservation, Justus Liebig University Giessen, Giessen, Germany, [5] Chair of Soil Ecology, University of Freiburg, Freiburg im Breisgau, Germany

OPEN ACCESS

**Edited by:**
Edith Bai,
Institute of Applied Ecology (CAS), China

**Reviewed by:**
John T. Van Stan,
Georgia Southern University, United States
Ingeborg Callesen,
University of Copenhagen, Denmark

***Correspondence:**
Jakob Sohrt
jakob.sohrt@posteo.de

**†Present address:**
David Uhlig,
Institute of Bio- and Geosciences (IBG-3) Agrosphere, Forschungszentrum Jülich, Jülich, Germany

**Specialty section:**
This article was submitted to Forest Soils, a section of the journal Frontiers in Forests and Global Change

**Received:** 25 September 2019
**Accepted:** 02 December 2019
**Published:** 17 December 2019

**Citation:**
Sohrt J, Uhlig D, Kaiser K, von Blanckenburg F, Siemens J, Seeger S, Frick DA, Krüger J, Lang F and Weiler M (2019) Phosphorus Fluxes in a Temperate Forested Watershed: Canopy Leaching, Runoff Sources, and In-Stream Transformation. Front. For. Glob. Change 2:85. doi: 10.3389/ffgc.2019.00085

Declining foliar phosphorus (P) levels call increasing attention to the cycling of this element in temperate forests. We explored the fluxes of P in a temperate mixed deciduous forest ecosystem in six distinct hydrological compartments: Bulk precipitation and throughfall, soil water draining laterally from three different soil depths (0–15, 15–150, 150–320 cm below soil surface), groundwater, creek and spring discharge, which were sampled at daily to bi-weekly resolution from March 2015 to February 2016. Atmospheric P fluxes into the ecosystem were equally partitioned between wet and dry deposition. Approximately 10% of the foliar P stock was lost annually by foliar leaching during late summer. The concentrations of dissolved P in soil water from the forest floor and upper mineral topsoil followed a pronounced seasonal cycle with higher concentrations during the vegetation period. The concentrations of P dissolved in soil water decreased with increasing soil depth. Using an end member mixing analysis (EMMA) we found that P sources feeding the spring water were both soil water from greater depths or groundwater with season specific contributions. Atmospheric P fluxes into the ecosystem determined in this study and P-release from weathering reported for the research site were large enough to compensate P losses with runoff. This suggests that declining foliar P levels of forests are unlikely the result of a dwindling total P supply, but rather caused by tree nutrition imbalances or alternative stressors.

**Keywords: hydrological P cycle, canopy P balance, atmospheric P deposition, groundwater, discharge, soil water, EMMA, periphyton**

## INTRODUCTION

The primary productivity of forest ecosystems is often limited or co-limited by P availability (Elser et al., 2000, 2007; Vitousek et al., 2010; Achat et al., 2016). Over the past decades, foliar P concentrations were observed to decline in temperate forests but it is not yet clear whether this decline indicates P limitation (Duquesnay et al., 2000; Jonard et al., 2014; Talkner et al., 2015). Thus, better constraints on P cycling in forest ecosystems are required to identify the mechanisms of the respective forest ecosystem functioning (Lang et al., 2016, 2017).

The P cycle in temperate forests depends mainly on the general boundary conditions of the past and present, which are the drivers of the local ecosystem development (Walker and Syers, 1976). Important boundary conditions include lithology as the original source of most ecosystem P as well as climate and topography as controls of the water cycle, erosion-sedimentation, weathering processes and soil development, through which the bio-availability of P is determined (Laliberté et al., 2013). Fluxes of P across the ecosystem boundaries occur through runoff and atmospheric transport, which may result in either net gains or losses (Newman, 1995; Mahowald et al., 2008; Buendia et al., 2010; Tipping et al., 2014). The P deposition in bulk precipitation and throughfall mostly exceeds the P export by discharge (Cole and Rapp, 1981; Sohrt et al., 2017), but this does not necessarily imply that the overall P balance is positive. The P exports from an ecosystem via atmospheric pathways, e.g., pollen dispersion, are hard to quantify, which likely causes overestimation of net atmospheric deposition (Doskey and Ugoagwu, 1989; Newman, 1995; Tipping et al., 2014). Average estimates for above canopy atmospheric deposition mostly range from 10 to 100 mg P $m^{-2}$ $a^{-1}$; discharge losses are typically in the range of 1–10 mg P $m^{-2}$ $a^{-1}$ (Cole and Rapp, 1981; Sohrt et al., 2017).

In comparison to abiotic fluxes *across* ecosystem boundaries, *internal* P fluxes within ecosystems associated with biotic processes are much larger (Rodin et al., 1967; Cole and Rapp, 1981; Turner, 1981; Compton and Cole, 1998; Ilg et al., 2009; Bol et al., 2016). Litterfall represents a flux of 100 to 500 mg P $m^{-2}$ $a^{-1}$, about 60–80% of which is contained in foliar litter (Sohrt et al., 2017). Plant nutrient uptake from soil necessarily exceeds nutrient fluxes from litter fall, since P in growing tissue and losses via dead roots or herbivory have to be additionally compensated for. Another biotic flux within temperate forests highly relevant to the internal P cycling is related to bacteria and fungi. The microbial biomass comprises on average 20–40% of the total biomass P, which cycles at the scale of weeks to months (Raubuch and Joergensen, 2002; Spohn and Widdig, 2017), whereas P contained in woody biomass may persist for years to decades. While its measurement is still challenging, microbial uptake and subsequent leaching from dead microbial biomass must be considered as major internal fluxes in the P cycle of temperate forests (Horwath, 2017).

Quantifying P fluxes within the hydrological cycle has been identified as a priority to close gaps in a full quantification of P cycling in forest ecosystems (Bol et al., 2016). Fundamental observations made so far include the following: When passing through the canopy, rainwater is on average enriched 2-fold in P and the P content is doubled again during percolation through the forest floor (Sohrt et al., 2017). Beneath the forest floor, dissolved P concentrations and fluxes decline with increasing depth since P is effectively retained during percolation through the upper mineral soil (Cole and Rapp, 1981; Persson and Broberg, 1985; Jansson et al., 1986; Killingbeck, 1986; Stevens et al., 1989; Brown and Iles, 1991; Qualls and Haines, 1991; Saa et al., 1993; Sparling et al., 1994; Compton and Cole, 1998; Kaiser et al., 2001a,b; Sohrt et al., 2017). In contrast to throughfall and water in the forest floor, soil water, and groundwater in the weathered and fractured bedrock features the lowest dissolved P contents of all hydrological compartments (Dillon and Kirchner, 1975; Timmons et al., 1977; Reckhow et al., 1980; Mulholland et al., 1990; Qualls et al., 2002; Schwärzel et al., 2012; Verheyen et al., 2015). Thus, due to the large variation of P concentrations, discharge generation from either groundwater or soil water sources may control the P concentrations of stream water. Supporting evidence for this assumption stems from time series of dissolved P contents in groundwater and discharge in forested headwaters showing that P concentrations in discharge are consistently higher and more variable than in groundwater (Verheyen et al., 2015).

However, the dissolved P concentrations in forest headwater catchments are not only controlled by the contribution from different runoff sources, but also by abiotic adsorption/desorption processes or biotic in-stream processes. For example, biota in the stream channel can seasonally act both as a source and sink of P, effectively shaping the P concentration in lower order forest streams (Gregory, 1978; Munn and Meyer, 1990; Hill et al., 2001; Mulholland, 2004; Winkelmann et al., 2014). A short period of higher P concentrations in streamflow has been observed when freshly fallen litter enters the stream, which is attributed to P leached from litter (Triska et al., 1975). A simultaneous pulse of P leaching from the forest floor directly after litter fall has also been reported (Gosz et al., 1973; Baldwin, 1999). After initial leaching of rapidly mobilizable P, net retention of P in microbial biomass in the stream takes place, which may extend into the early summer of the following year, causing a depression of P concentrations (Sedell et al., 1975; Mulholland, 1992, 2004; Mulholland and Hill, 1997). By applying a radioactive phosphate tracer ($^{32}PO_4^{3-}$), Elwood et al. (1983), and Mulholland et al. (1985) showed that the average uptake length of phosphate between desorption and resorption in low-order forest streams is in the range of 5–160 m, and that the uptake length increases from the time of litter fall to summer. Similar mean uptake lengths have been recorded for ammonium, while mean uptake lengths for nitrate appear to be substantially larger (Peterson et al., 2001; Webster et al., 2001; Bernhardt and Likens, 2002). Apart from the in-stream heterotrophic decomposer community, periphyton can also shape P concentrations. Since the primary productivity of periphyton is limited by sunlight, its P consumption and hence decreasing P concentrations are restricted to the time before spring budbreak (Friberg et al., 1997; Mulholland and Hill, 1997; Hill et al., 2001; Winkelmann et al., 2014). As a consequence, P concentrations in low order forest streams appear to be either chemostatic, with little or no changes in response to discharge and seasonality (Meyer and Likens, 1979; Benning et al., 2012), or biotically controlled, with minima in spring and fall (Mulholland, 1992, 2004; Rosemond, 1994; Mulholland and Hill, 1997; Roberts et al., 2007; Zelazny and Siwek, 2012; Bernal et al., 2015; Verheyen et al., 2015).

In summary, a number of studies addressed single fluxes of P in great details, but studies exploring relationships between multiple input and output fluxes are scarce, especially for forested catchments. We therefore aimed to quantify hydrological output fluxes of P and relate them to P gains from atmospheric deposition. By sampling water at daily to bi-weekly resolution from six distinct hydrological compartments—bulk precipitation, throughfall, subsurface flow

in three depth increments, groundwater, spring discharge, and creek discharge—we determined mobilization and transport of P as well as their temporal variation. We focus on the P canopy balance, the relative contribution of P from soil water and groundwater to discharge in a spring and a first order headwater, and the respective P fluxes. In this way, we intend to spotlight P fluxes in different hydrological compartments and their relation to each other as well as to investigate, whether the observed changes in forests P cycles are explained by unbalanced P budgets.

## Study Site

The study was conducted at the "Conventwald" research site located in the Black Forest, Germany (48°02'0 N, 07°96'0 E). Our study area consists of two neighboring watersheds: the "creek" catchment with long-term discharge monitoring of a headwater creek, and the "spring" catchment. The average elevation of the two headwater catchments was 840 m a.s.l., mean annual temperature was 6.6°C, and mean annual precipitation was 1,749 mm $a^{-1}$. Being part of the European "Level II" (ICP Forest) environmental monitoring network, the Conventwald was equipped some decades ago with instruments to monitor bulk precipitation and throughfall, soil moisture, soil water, and stream discharge in the creek catchment. New instrumentation in the spring catchment included 10 m long collectors for lateral subsurface flow, collecting water at three depth intervals (0–15, 15–150, 150–320 cm below soil surface), a groundwater well with a depth of 15 m drilled through the saprolite into the fractured bedrock and a weir at the spring catchment. The subsurface flow collectors including their installation are described in detail in Bachmair and Weiler (2012).Time series of soil moisture, bulk precipitation, throughfall, and plant-phenological data were kindly provided by the Forest Research Institute of Baden-Wuerttemberg (FVA). With a surface area of 0.086 $km^2$, the creek catchment was slightly larger than the spring catchment with an area of 0.077 $km^2$. Exposition was south-east for the creek catchment and south-south-west for the spring catchment. The average slope was about 20° at both catchments. In the creek catchment, an open channel bed was present, reaching up to 40% of the way from the catchment outlet to the ridge, the upper part of which was ephemeral. By contrast, the spring catchment had no permanent surface water flow at all and was instead drained by a spring at the catchment outlet. It was evident, however, that this spring did not represent the complete discharge from the catchment area, as additional below ground discharge was visible some meters down-slope in the form of water leaking from a road cut. The existence of below ground discharge was also evident since the specific discharge from the spring catchment is only ∼60% of that from the creek catchment, which, given their topographic and hydrological similarity, was not plausible. Therefore, below ground discharge from the spring catchment was estimated in such a way that its average specific discharge (discharge rates normalized to catchment area) matches that of the creek catchment.

At the creek catchment the vegetation consisted of European beech [*Fagus sylvatica (L.),* ∼69%] and White fir (*Abies alba (Mill.),* ∼31%) (Lang et al., 2017). At the spring catchment, the tree species distribution was slightly different with 45% Norway spruce [*Picea abies (L.)*], 40% European beech [*Fagus sylvatica (L.)*], 15% Douglas fir [*Pseudotsuga menziesii (Mirb.)*] and small amounts of White fir [*Abies alba (Mill.)*] [personal communications, Forest Research Institute Baden-Wuerttemberg (FVA), 2018]. The soil type in both catchments was a Hyperdystric Skeletic Folic Cambisol with a loamy or sandy loamy texture and a mor-type moder forest floor atop (Lang et al., 2017). The soils have formed on periglacial slope deposits and the uppermost meter of soil had a rock fragment content of about 70% (Lang et al., 2017). The dominant fraction of P in the forest floor is organically bound. In the mineral soil, the portion of organically-bound P decreased with depth and, in turn, that of P bound to secondary Fe- and Al oxides increased (Lang et al., 2017; Uhlig and von Blanckenburg, 2019b).Weathered bedrock was found at a depth of 7 m and parent bedrock (paragneiss) at 15 m (Uhlig and von Blanckenburg, 2019a). The dominant P-containing mineral in unweathered paragneiss bedrock was apatite, as inferred from scanning electron microscopic imaging in combination with elemental analyses with energy-dispersive X-ray spectroscopy (unpublished data).

As the Conventwald study site is part of the ICP Forest sites, extensive scientific background information is available on the topics of hydrology (Uhlenbrook et al., 1998; Hangen et al., 2001), soils (Kohler et al., 2000), and plant water use (Rennenberg and Schraml, 2000; Magh et al., 2017). The Conventwald site is also part of the DFG-funded priority *project (SPP 1685): Ecosystem Nutrition—Forest Strategies for limited Phosphorus Resources*, providing background information on soil P speciation (Prietzel et al., 2016; Lang et al., 2017; Stahr et al., 2017; Werner et al., 2017), colloidal P transport in soil water and streamflow (Missong et al., 2016, 2017; Gottselig et al., 2017), and on P cycling in plant and microbial biomass (Heuck et al., 2015; Bergkemper et al., 2016; Zavišić et al., 2016).

# METHODS

## Sampling

Sample collection was carried out from 01.03.2015 to 25.02.2016. Daily samples of groundwater, creek, and spring discharge were taken at midnight with automatic samplers. Bulk precipitation, throughfall, and lateral subsurface water were sampled in bulk containers and collected twice a week. To avoid contamination, the precipitation samplers were covered with a netting of 0.5 mm mesh size. Stemflow was only assessed with respect to water flow (no P concentrations). For the purpose of this study, water flow associated with stemflow was included into the throughfall fraction and assumed to feature comparable P concentrations. For some tree species stemflow has been found to be highly enriched in P compared to throughfall (Schroth et al., 2001; Neal et al., 2003). However, the few available studies on Fagus species' stemflow P concentrations found them to be roughly equivalent to throughfall (Voigt, 1960; Nihlgård, 1970). The reson for this may be, that Fagus sylvatica produces relatively large quantities of stemflow, causing a dilution effect. All precipitation samples with visible particular contamination were excluded from further analysis. All samples were stored

in polypropylene bottles that were cleaned prior to sampling with P-free detergent and deionized water (Milli-Q, 18 MΩ·cm). After collection, all samples were filtered through membranes of 0.8 μm pore size (Supor-800, Pall Laboratories) and aliquots for analyses were taken. Sample acidification to pH 3 with ultrapure concentrated nitric acid was restricted to samples used for P analysis. All aliquots were stored at 8°C.

To assess the mobilization and retention of P in water passing through canopy, forest floor and mineral soil, changes in concentrations and fluxes of P in bulk precipitation, throughfall, runoff from the forest floor (ca. 0–15 cm), and the upper mineral soil (15–150 cm) over time were compared. Only 17 samples could be collected from the deepest soil layer (150–320 cm), and thus, the temporal variability of P concentrations in this hydrological compartment was not assessed. Continuous time series of water levels were recorded at weirs at the outlet of the two catchments and at the groundwater well. Water levels in the weirs were transformed into discharge using discharge rating curves. From March to June 2015, three peaks in deep groundwater levels were not fully recorded, since the sensor (Ott Orpheus Water Level Logger) was placed too low and the maximum measureable head was exceeded.

## Analytical Methods

Total P concentrations were measured in the "HELGES" Laboratory at GFZ Potsdam (von Blanckenburg et al., 2016) using a high resolution Inductively-Coupled-Plasma Mass Spectrometer (ICP-MS; Element 2, Thermo Fisher Scientific, Bremen, Germany). Tests prior to the measurements showed that matrix-matched calibration was not needed, since no significant matrix effects were observed in the concentration range of the major elements. Accuracy and precision of the P determination was assessed using two international reference standards (National Research Council of Canada, SLRS-5, and U.S. Geological Survey, M-212) as well as four laboratory standards resembling a typical river-water matrix containing major constituents (Ca, Mg, K, Si, Na, S, P) and trace constituents (Cu, Ni, Zn, Ti, and Fe) prepared from single element standards. The overall uncertainty of the P measurement was below 10% for the encountered range of concentrations. Concentrations of Ca, Na, K, Mg, and S were analyzed at GFZ Potsdam using Inductively Coupled Plasma Optical Emission Spectrometer (ICP-OES; 720ES, Varian, Mulgrave, Australia) following the procedure described by Schuessler et al. (2016) with relative uncertainties better than 10%. Concentrations of total dissolved carbon (C) and nitrogen (N), and dissolved inorganic carbon (DIC) were analyzed using a Shimadzu (Kyoto, Japan) Vcpn analyzer. DIC concentrations were all below the detection limit of 50 $\mu g\ l^{-1}$. Thus, dissolved carbon concentrations are considered as organic carbon. Chloride was measured with an ion chromatograph (790 Personal IC, Metrohm, Filderstadt, Germany) at the Chair of Soil Ecology, University of Freiburg.

## Data Evaluation

Due to its high aerodynamic roughness, the canopy was expected to act as an efficient aerosol trap. As a result, P derived from dry deposition should have increased the P concentration in throughfall compared to bulk precipitation. In addition, P may have been leached from leaves, pollen, insects, and microorganisms within the canopy. To estimate fluxes of wet and dry P deposition as well as canopy leaching, the canopy balance model of Ulrich (1983) was used. The model is based on three assumptions. First, dissolved sodium (Na) in throughfall is only from wet deposition and leaching from atmospheric dust because Na is neither taken up nor released by the plant canopy in relevant amounts. Second, the relation between wet and dry deposition observed for Na is transferable to other elements, including P. Third, the fraction of dissolved P in throughfall that is neither accounted for by dry or wet deposition must originate from foliar leaching. There was no general exclusion of outlier values. Only samples with visible particular contamination were excluded, which was mostly due to insects getting into the sampler.

To assess the contributions of different hydrological compartments to discharge, we performed an end member mixing analysis (EMMA) using the software package EMMAgeo in the R Environment (Dietze and Dietze, 2013). Three end members were identified by applying the annual average concentrations of eight elements/parameters (Ca, Na, K, Mg, S, DOC, Si, Cl) from water from the forest floor (0–15 cm), the mineral soil (15–320 cm), and groundwater. The model was calibrated to daily time series of those elements in the discharge of the spring catchment. The application of the EMMA was restricted to the spring catchment for two reasons: First, given that the element concentrations of the end members were exclusively inferred from the spring catchment we refrained from transferring the data to the adjacent catchment for reasons of small-scale heterogeneity. Second, the simulation of in-stream transformation processes that likely occur in headwater catchments is beyond the scope of EMMA.

We then tested whether the calculated discharge contributions from soil- and groundwater (when considering the dissolved P concentrations in those compartments) would lead to a simulated P concentration in discharge that is similar to the one actually observed in spring discharge using simple linear regression analysis. In doing so, we could infer whether the sources of discharge imposed a control on discharge P contractions.

Similarity of temporal variation between data series was assessed with linear models using the lm() function, and 2-sample *t*-tests for comparing group averages were assessed using the *t*-test function in R Environment (Dietze and Dietze, 2013). The raw data used in this study is partially available as a supplement to this study (**Supplementary Table 1**).

# RESULTS

## Hydrological Conditions

The hydrological conditions in the catchments during the study period were characterized by three distinct periods: Spring and summer until June 2015 were relatively wet, followed by a relatively dry period with a marked water deficit which ended in November 2015 and then by a period of rewetting, which extended into January 2016. With a precipitation sum of 1,118 mm $a^{-1}$ the study period was unusually dry compared

to the long-term average annual precipitation of 1,749 mm $a^{-1}$ (average 1961–1996).

From March to June 2015, soil moisture, groundwater level and discharge fluxes responded rapidly to precipitation events (**Figure 1**), which suggested that in this period the hydrological compartments were well connected. In the groundwater well, a fill-and-spill behavior could be observed: At ground water levels between 8 and 6.3 m below the surface, relatively strong variability occurred corresponding to the occurrence of precipitation, but peaks of groundwater level consistently stopped at around 6.3 m below ground (**Figure 1C**). The groundwater table did not react immediately to precipitation events but with a lag time of 1–2 days. Still, until the beginning of June, all main discharge events in the creek and spring catchment were associated with corresponding changes of the groundwater table depth.

At the beginning of June 2015, soil moisture was only 5% below that of the wetter spring period but strong hydrological changes were observed, indicating the start of the drier summer period: The rainfall-runoff event occurring mid of June produced smaller increases in discharge and soil moisture compared to events with similar amounts of precipitation in the previous months (**Figures 1A,B,D**). The groundwater seemed to be disconnected from precipitation events from the beginning of June until December. The slowly declining groundwater level indicated continuous drainage of the groundwater during this period. Small fluctuations in discharge occurred after precipitation events in both catchments, which were more pronounced in the creek catchment.

At the end of November and early December 2015, two large precipitation events occurred. The first event elevated soil moisture to pre-summer level and caused substantial discharge in both catchments. No groundwater recharge occurred after the first precipitation event, and the observable increase in the groundwater level was small even after the second precipitation event. Pre-summer groundwater levels were only reached as late as in January 2016. Thus, the rewetting took 1.5 months.

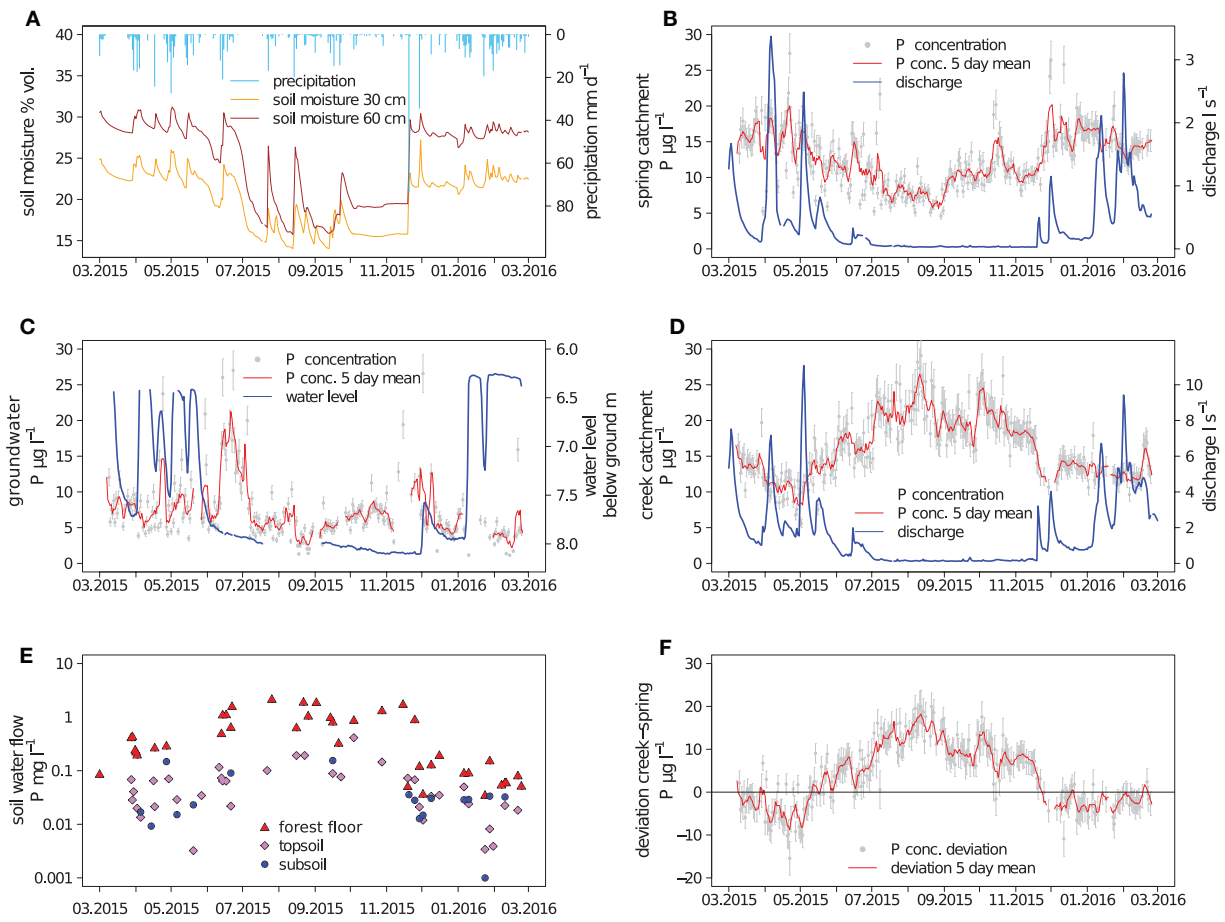


**FIGURE 1 |** Hydrological variables and phosphorus (P) concentrations; bulk precipitation and soil moisture **(A)**. Discharge and dissolved P concentrations in the spring and creek catchment **(B,D)**; water level and P concentrations in the groundwater **(C)**. P concentrations of lateral subsurface flow **(E)**; deviation of P concentration in discharge between the creek and spring catchment **(F)**; depth intervals of subsurface flow were 0–15 cm (forest floor), 15–150 cm (upper mineral soil), and 150–320 cm (deeper mineral soil); uncertainty bars represent the standard deviation of the arithmetic mean.

## Phosphorus Concentrations

Phosphorus concentrations in bulk precipitation were on average 5.8 $\mu g\ l^{-1}$ (**Table 1**). Relatively high P concentrations in bulk precipitation (>10 $\mu g\ l^{-1}$) were found during the vegetation period, lower P concentrations (<5 $\mu g\ l^{-1}$) in the dormant season. Phosphorus concentrations in throughfall were on average 140 $\mu g\ l^{-1}$ and peaked from late summer to leaf abscission in autumn. Peak P concentrations in throughfall were >1,000 $\mu g\ l^{-1}$. Phosphorus concentrations in bulk precipitation and throughfall were not significantly correlated ($p$ >0.05, not shown). Interestingly, the high throughfall fluxes of P from July to October appear to have been driven by increases in throughfall P concentrations rather than by high amounts of precipitation. Only 24% of the annual precipitation were recorded in this period but 71% of the total P flux with throughfall.

Disentangling the canopy P fluxes into wet and dry atmospheric deposition and canopy leaching by applying the canopy balance model (Ulrich, 1983) suggested that the vast majority of P fluxes with throughfall originated from foliar P leaching (**Figures 2C,D**). Within the first 3 months of the vegetation period after budbreak in April, no notable canopy leaching was detected. From July to November, canopy leaching steadily increased, with P fluxes higher than 10 mg $m^{-2}$ $month^{-1}$ (**Figures 2B,C**). The highest wet and dry P depositions were found from April to August, with one outlier in February 2016 (**Figure 2A**).

For groundwater and discharge of the two catchments, nearly continuous series of daily samples could be collected. In groundwater, the average P concentration was 7 $\mu g\ l^{-1}$, showing no clear indication of systematic seasonal variation (**Figure 1C**). One period of higher P concentrations occurred in June 2015, with concentrations up to 25 $\mu g\ l^{-1}$. Phosphorus concentrations in groundwater were not significantly correlated to concentrations and fluxes of P in lateral soil water flow at any depth increment or discharge ($p$ >0.05, not shown). Day-to-day variations of P concentrations in groundwater were in a similar range to those in discharge water.

Phosphorus concentrations in discharge in the spring were on average 12 $\mu g\ l^{-1}$ and were significantly ($p$ <0.05, not shown) smaller than the average P concentration in the creek water of 16 $\mu g\ l^{-1}$. Phosphorus concentrations in discharge water from the two catchments displayed a nearly inverse seasonal pattern: Creek P concentrations were elevated during the vegetation period (**Figure 1F**), when spring P concentrations show a seasonal minimum. Day-to-day variations of P concentrations in discharge water were comparable between the two catchments.

While almost every recorded precipitation event was associated with the generation of lateral flow in the forest floor, not all events could be sampled. Over the measurement period, 39 lateral flow events were sampled in the forest floor (0–15 cm), 36 events from the upper mineral soil (15–150 cm), and 17 samples from the deeper mineral soil (150–320 cm). With average concentrations of 700 $\mu g\ P\ l^{-1}$ and maximum concentrations as high as 1,500 $\mu g\ P\ l^{-1}$, near-surface lateral flow in the forest floor was significantly enriched in P compared to throughfall; the highest concentrations usually occurred during the vegetation period (**Figure 1D**). In the upper mineral soil (15–150 cm), P concentrations in lateral subsurface flow were significantly reduced by about one order of magnitude in comparison to lateral flow from the forest floor. Phosphorus concentrations in the deeper mineral soil at 150–320 cm were not significantly smaller than the concentrations in the upper mineral soil ($p$ <0.05, not shown).

**TABLE 1** | Concentrations and fluxes of P and water in the study area.

| | Mean P concentration | P flux | Water flux |
|---|---|---|---|
| | $\mu g\ l^{-1}$ (SD) | mg $m^{-2}$ $a^{-1}$ (uncertainty) | mm $m^{-2}$ $a^{-1}$ |
| Bulk open precipitation | 5.9 (±10) | 7.4 (± 1) | 944 |
| Bulk throughfall precipitation | 150 (±24) | 60 (± 6) | 769 |
| Dry deposition | | 9.7 (+2.4/−2.0)[a] | |
| Canopy leaching | | 43 (+8.8/−9.2)[a] | |
| Organic layer water flow | 570(±600) | 0.001[d] | 0.002[d] |
| Mineral soil | 43 (±38) | 20[d] | 446[d] |
| Groundwater | 7.1 (±4.2) | 2.5[d] | 166[d] |
| Discharge spring | 13 (±4.0) | 9.2 (± 1.0)[c] | 613[c] |
| Discharge creek | 16 (±4.5) | 7.9 (± 1.0) | 613 |
| P Balance spring catchment | | 7.8 (+4.1/−3.7)[b] | |
| P Balance creek catchment | | 9.1 (+3.9/−3.5)[b] | |

[a] *Calculated according to Ulrich (1983).*
[b] *Bulk open prec.*
*+Dry deposition−discharge P flux.*
[c] *Including ungagged below-ground discharge with total specific discharge assumed to be equal to creek catchment.*
[d] *Calculated with EMMA.*

## End Member Mixing Analysis

During the high-flow period from March to June 2015, spring discharge was dominated by water with a solute composition (Ca, Na, K, Mg, S, Cl, DOC) matching best that of water from the mineral soil (top- and subsoil grouped together, 15–320 cm) (**Figures 3A,B**), with a relative contribution to discharge of up to 90%. During the summer low-flow period, groundwater became the dominant source of discharge with over 95% discharge contribution, which was reversed again at the end of November after two large precipitation-runoff events, raising the fraction of water from the mineral soil in discharge to around 50% initially. According to the EMMA, water from the forest floor hardly contributed to the mixture with contributions of about 0.2%. The model uncertainty, i.e., the ability of the model to simulate a mixture from the end members with an element composition matching the measured composition at a given day, was lowest in the high-flow period and highest in the low-flow period (**Figure 3C**).

Since the actual P concentrations of the end members are known but not included in the fitting process of the EMMA, it can be tested how well the actual P concentrations in

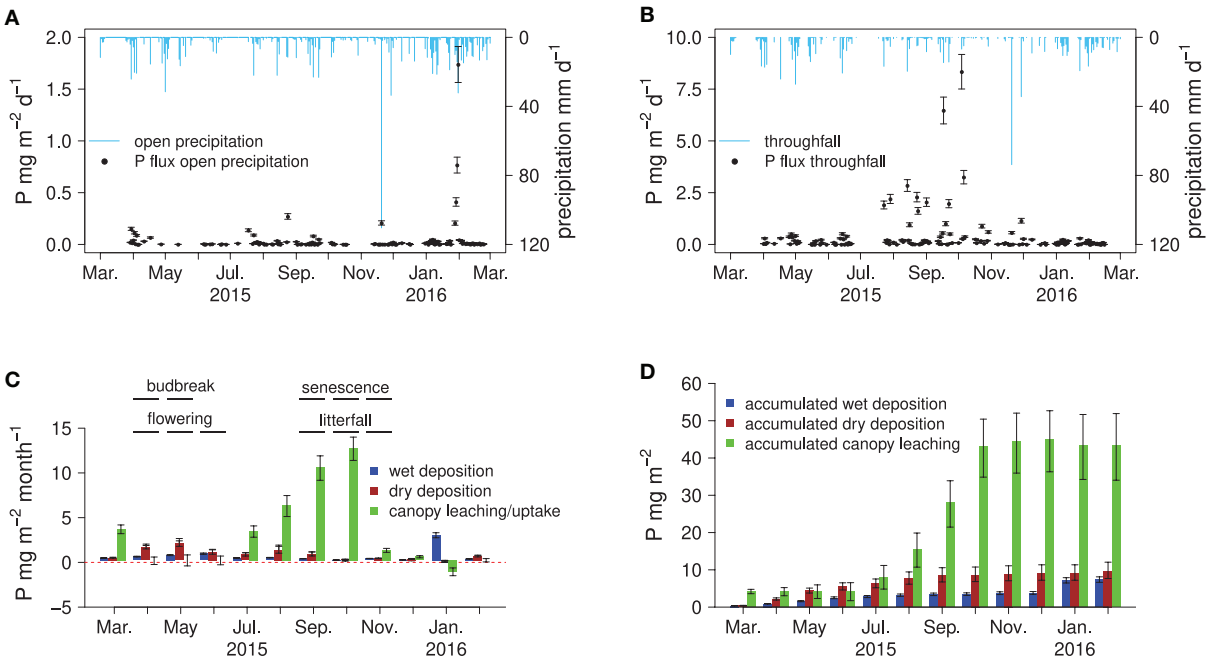


**FIGURE 2 |** Fluxes of P in bulk precipitation and throughfall, monthly, and accumulated atmospheric P deposition to the forest floor: daily fluxes of P in open precipitation **(A)** and throughfall **(B)**, the canopy P balance with monthly fluxes of wet deposition, dry deposition, canopy leaching, and some phenological indicators measured on site **(C)**, and accumulated fluxes of P in wet deposition, dry deposition, and canopy leaching **(D)**.

spring discharge can be simulated using the simulated end member composition. In doing so, it becomes apparent that the P concentration in spring discharge is systematically overestimated by the calculated end member composition (**Figure 4**). If the EMMA model uncertainty is used to weigh the data points for a linear regression between measured and simulated P concentrations in spring discharge, only a moderately good fit ($R^2 = 0.38$) is achieved with a slope significantly larger than one (**Figure 4D**). Given that the model uncertainty is small in the low-flow period, the EMMA provides reliable results for this period. Also, weekly and seasonal variations in P concentrations in spring discharge are well-predicted by the EMMA. In summary, EMMA predicts that water from the mineral soil (15–320 cm) is the largest contributor to discharge (66% over the whole observation period), followed by groundwater with 34% and water from the forest floor with only 0.02%. For the P fluxes leaving the spring catchment, the differences are even more pronounced, with the mineral soil being the dominant source with 93%, followed by groundwater with 6 and 0.5% from the forest floor (**Figure 4E**). The variability of discharge is much higher than the variability of P concentrations therein. Because of this, the bulk of the accumulated discharge P flux is confined to the high-flow periods (**Figure 4F**). This also means, that discharge itself is a more accurate predictor for the discharge P flux than the associated P concentration, so that the temporal pattern of P fluxes can be somewhat accurately represented by our approach (**Figures 4E,F**).

## The P Balance of the Catchments

Based on the results from the canopy balance and the EMMA, we calculated not only the mean annual P concentrations in the hydrological compartments, but also estimated the annual P fluxes that enter or leave the ecosystem as well as some that result from cycling within the ecosystem (**Table 1**). Disregarding mineral weathering for which we do not have direct measurements in this study, the P balance would be negative if only wet deposition is regarded as a true input to the ecosystem but clearly positive if dry deposition is regarded as input (**Table 1**). The uncertainties presented for the P fluxes (**Table 1**) represent the effect of the standard deviation of P measurements of individual samples on the calculated P fluxes. In the case of wet- and dry deposition the additional inclusion of the model uncertainty results in an asymmetric uncertainty range. The uncertainty for the catchment balances is the maximum range of uncertainty resulting from the individual balance components. Uncertainties for the measured water fluxes were not determined.

# DISCUSSION

## P Inputs via Atmospheric Deposition

The question whether the atmospheric dry deposition of P can be regarded as a true input to the site is of high relevance for the overall P balance. The answer depends on whether dry deposition in forests stems from external or internal sources. One possible internal source is pollen dispersion, which can contribute substantially to atmospheric dry P deposition (Doskey

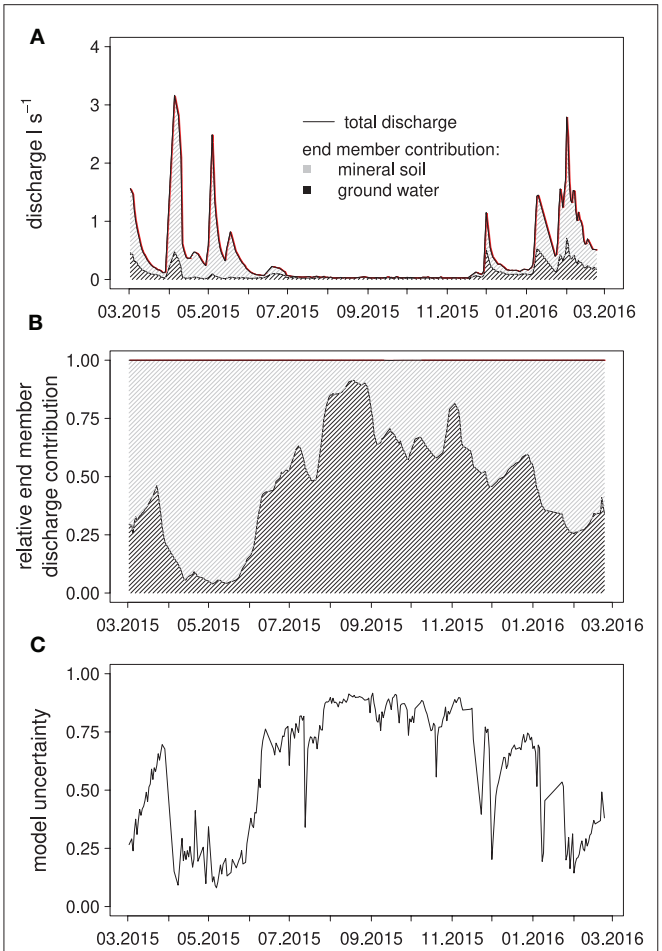


**FIGURE 3 |** Results of the EMMA: Calculated absolute contributions of the end members to spring discharge **(A)**; water from the forest floor was used as an end member but ended up not contributing significant amounts to the simulated discharge composition, simulated, end member contributions to discharge **(B)** and relative model uncertainty **(C)**.

and Ugoagwu, 1989; Tipping et al., 2014). The calculated high P dry deposition fluxes (May to June) at our study site intersect with the period of pollen dispersion (**Figure 2C**). Although their size of 10–100 μm exceeds the pore size (0.8 μm) of the used filters by 2–3 orders of magnitude, P might have been leached out of pollen increasing the P concentration in throughfall. However, we have to consider that pollen are not only entering the forest canopy, but are also exported from the forest. Therefore, without detailed investigation it is not clear whether a net P input or export occurs by pollen dispersion.

Further, the assumption of Na behaving conservatively during canopy passage underlying the canopy balance model of Ulrich (1983) has been challenged. In particular, it has been shown, that especially young (broad-) leaves do loose Na via foliar leaching (Tukey Jr, 1970; Staelens et al., 2007; Thimonier et al., 2008). Disregarding foliar leaching of Na could cause overestimation of dry deposition and underestimation of foliar leaching of P in the canopy balance model used in this study. The underestimation of foliar leaching could be small relative to the total foliar leaching of P. The estimate for dry deposition, however, could be more severely affected, since as much as 45 % of throughfall Na enrichment may be due to foliar leaching (Thimonier et al., 2008).

Foliar P leaching dominates the overall canopy P balances of our catchments. Direct evidence of foliar P leaching is still lacking in the literature and indirect estimates of foliar P leaching are much lower than the amount derived from this study, ranging from a maximum of 20 mg m$^{-2}$ a$^{-1}$ to net uptake of P into the foliage during canopy passage (Long et al., 1956; Tukey Jr, 1966; Miller et al., 1976; Duquesnay et al., 2000; Kopavcek et al., 2009; Runyan et al., 2013). At 50 mg m$^{-2}$ a$^{-1}$, the calculated foliar leaching flux of P in this study translates into about 10% of the average total P content in mature leaves of a deciduous forest (Sohrt et al., 2017). This implies, that foliar resorption of P, which is generally assumed to be solely responsible for the deviation of the P content in mature foliage and foliar litterfall (Killingbeck, 1986, 1996; Duchesne et al., 2001; Côté et al., 2002), may generally be overestimated if foliar leaching is assumed to be negligible.

Leaching of P from the canopy was virtually absent in the first 3 months of the vegetation period. This implies that young leaves are able to avoid significant losses of P via leaching. Two months before the first indications of leaf senescence occurred, leaching of P from the canopy was already significantly increased, which means the leaves lose P in their later life cycle. Almost half of the total throughfall deposition is due to leaching from the canopy during the first 2 months of leaf senescence. The increase in leaching from the canopy may be due to the stepwise reduction in leaf functionality during senescence, causing the leaves to become more "leaky." In addition, progressing microbial degradation of the senescent foliage may come into effect: The relevant decomposer organisms are already present on the foliar surfaces before senescence and generally become active before leaf abscission (Snajdr et al., 2011). This could cause damage to the leaves and subsequent leaching of soluble substances with throughfall, although the initial binding form of leached P was not addressed in this study. Interestingly, during the last month of leaf senescence (November), the P foliar leaching decreased again to very small fluxes, although precipitation amounts stayed constant and leaf abscission was only completed by the end of November after a rainstorm event. Hence, the bulk of foliar P leaching occurs before the final stages of senescence Besides below-average amounts of bulk open precipitation there was no apparent occurrence of vegetation stressors such as pests or strong storm events. Potential sources of P inputs are arable fields in the Rhine valley or the City of Freiburg just 7 km west of the study site. Considering also the predominant westerly winds in the area, deposition of P-rich dust from agricultural and urban settings is, hence, the most likely cause for the P enrichment in throughfall water.

## End Member Mixing Analysis

It is apparent that the EMMA performed best during the low-flow period, when calculated groundwater contribution to discharge was high, and worse during high-flow periods, when water from the mineral soil was the dominant source of discharge water. This indicated that the sampled groundwater body directly

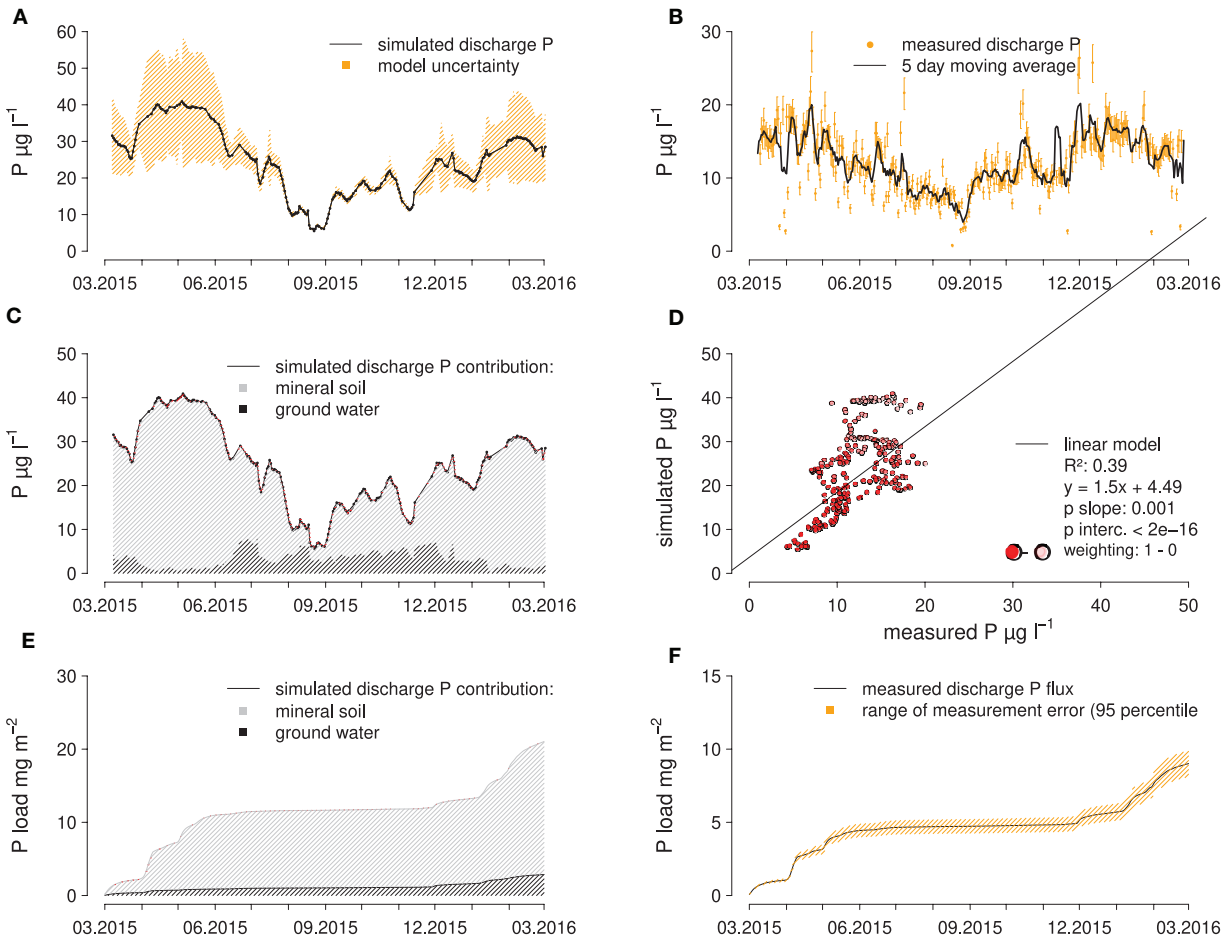


**FIGURE 4 |** Results of EMMA compared to measured data: simulated **(A)** and measured **(B)** discharge P concentrations, contribution of end members to simulated discharge P concentrations **(C)**, scatter plot of measured vs. simulated discharge P concentrations **(D)**, as well as simulated **(E)**, and measured **(F)** cumulative P fluxes in the creek catchment.

contributes to discharge without large changes in chemical composition, and thus, was a suitable end member. Water from the forest floor, on the other hand, was almost absent from the mixtures calculated with the EMMA, meaning that it likely did not contribute to spring discharge at all. The reason was likely that the spring lacked a sufficiently long interception interface with the thin forest floor, in contrast to more linear creeks for example.

Overall, water from the mineral soil was responsible for 65% of total discharge according to the EMMA. Periods with higher fractions of soil water in discharge were consistently associated with higher model uncertainties. From these results it can be deduced that our model was missing an important end member that presumably contributed large parts of discharge during high-flow events. A possible candidate would be water from soil layers below our maximum sampling depth.

When simulating discharge P concentrations in the spring catchment from the end member contributions suggested by the EMMA, P concentrations were strongly overestimated during the high-flow period in spring when the model inaccuracy was also highest. During the rest of the study period, discharge P concentrations are still overestimated but less pronounced. The reason for the systematic overestimation could be the fact that P is known to easily attach to or react with a variety of soil components, while the elements that were used to calibrate the EMMA may behave more conservatively. The fact that P concentrations in subsurface flow declined sharply with increasing depth across the sampled soil layers implies that, at least in those layers, P immobilization by sorption took place. Still, simulated discharge P concentrations are significantly correlated to measured concentrations, which suggests that changes in discharge contribution of different water sources are an important control of P concentrations in spring discharge.

## Deviations of Discharge P Concentrations Between the Two Catchments

We identified contrary seasonal variations in discharge P concentrations in the creek and the spring catchment, although

the adjacent catchments are similar in topography, soil type, lithology, and vegetation cover. The only difference is that the creek catchment has an open channel bed, which is absent in the spring catchment. Here we provide two potential reasons explaining the difference.

The first is that an open channel bed has the potential to receive discharge contributions directly from precipitation and surface runoff, which would be absent for spring discharge. Since throughfall, surface runoff, and shallow subsurface flow are highly enriched in P compared to groundwater, significant inputs of water via these flow paths should control the P concentrations in spring discharge. Given that these flow paths should contribute relatively more water to discharge in the creek than in the spring, larger average P concentrations and larger temporal variations of P concentrations would be expected for the creek compared to spring, especially during rainfall-runoff events. However, P concentrations in the creek water were highest in the dry period (with lacking near surface runoff) and there were no increases in discharge P with rainfall-runoff events. Consequently, there were no indications of near-surface runoff being the controlling pathway of P export at the study site for either of the two sites.

The second possible explanation of the difference in seasonal variations in discharge P between the creek and the spring catchment were in-stream transformation processes. It has been demonstrated that retention of P by in-stream biomass can strongly affect variations in discharge P: Periphyton growth is associated with uptake of discharge P in spring until leaf flushing (Friberg et al., 1997; Mulholland and Hill, 1997; Hill et al., 2001; Winkelmann et al., 2014). Heterotrophic microbial growth on leaf litter entering the stream can cause a similar effect in autumn and winter since these microbes are initially N- and P- rather than C-limited (Gregory, 1978; Munn and Meyer, 1990; Bernhardt and Likens, 2002; Rier and Stevenson, 2002; Stelzer et al., 2003; Mulholland, 2004; Hill et al., 2010). During summer, periphyton activity is decreased due to shading by trees, and P limitation of in-stream heterotrophic decomposers may be reduced, as the litter from the previous autumn is increasingly depleted of accessible C sources. In this time, the in-stream biomass may become a source of discharge P rather than being a sink. Since the seasonal pattern of P concentrations in the creek is in line with this concept, it seems probable that the deviation in P concentrations in discharge between the two studied catchments is due to biotic P turnover in the creek, which would be mostly absent in the spring discharge, leading to the observed differences in the seasonal pattern of P concentrations in discharge between the two catchments.

## P Balance of the Study Area

In line with earlier studies on the subject (e.g., Cole and Rapp, 1981; Sohrt et al., 2017), the analysis of P fluxes in bulk precipitation and throughfall in combination with the application of the Ulrich (1983) canopy balance model suggested that atmospheric P inputs alone might compensate P losses with drainage and runoff in temperate forests. However, especially the estimated dry deposition flux is connected with uncertainties. The P discharge flux quantified in this study allows for a comparison with the study site's P weathering flux determined by Uhlig and von Blanckenburg (2019a) amounting to 76 ± 17 mg $m^{-2}$ $a^{-1}$. This flux exceeds the P discharge flux presented in this study by an order of magnitude. As the integration timescales for cosmogenic nuclide-derived weathering fluxes ($10^3$-$10^5$ year) and gauging-derived discharge fluxes ($10^0$-$10^1$ year) differ by orders of magnitudes, timescale effects could account for this discrepancy. Since bulk precipitation during the study period was only 60% of the 30-year average, the mean annual discharge, and thus, P export was likely less than usual. However, accounting for timescale effects by normalizing the respective P fluxes to fluxes of sodium does not eliminate the discrepancy between the P discharge flux and the P weathering flux (unpublished data). Sodium was chosen because Na is an "inert" element with respect to nutrient uptake and neoformation of secondary minerals during chemical weathering. Such discrepancy, quantifiable through a metric called sodium normalized "dissolved export efficiency" ($DEE^{X}_{Na}$, Uhlig et al., 2017; Schuessler et al., 2018) can be observed across the globe (Uhlig et al., 2017; Schuessler et al., 2018). Potential fluxes of P that could (in combination) explain this systematic discrepancy include underestimated P exports with litter and wood (de Oliveira Garcia et al., 2018), transiently increasing P stocks in biomass in growing forests, and net P export via pollen dispersion.

It appears that the sum of P release from weathering (Uhlig and von Blanckenburg, 2019a) together with atmospheric P inputs determined in this study likely compensate P losses with runoff. Therefore, declining foliar P levels are unlikely the result of a P depletion of the forest ecosystem.

# CONCLUSIONS

The common observation, that percolating water becomes strongly enriched in dissolved P during the passage through the canopy and the forest floor, where the highest P concentrations are recorded, was confirmed by this study. This trend was found to be reversed when the water came into contact with the mineral soil, where dissolved P was effectively retained, causing the P concentration in soil water at about 3 m depth to be en par with that in the creek water. P export from the catchment via spring water was found to be driven by runoff from mineral soils and by groundwater discharge. Also in the investigated creek, a potential contribution of near-surface runoff to P exports appeared to be negligible or superimposed by in-stream P cycling.

Wet and dry deposition were found to be in a similar range. Even if only wet deposition was assumed to be a true input into the ecosystem, it outweighed the losses by discharge at our study site, so that the overall P balance of both catchments was positive during the study period. Together with the potential inflow of P through mineral weathering this supports the idea that declining foliar P levels of forest ecosystems are unlikely to be related to a declining total P supply, but rather to imbalances of tree nutrition, e.g., due to nitrogen fertilization, or alternative stressors, such as drought. Detailed investigations of atmospheric N and P deposition and the inclusion of fluxes resulting from mineral weathering are necessary to reduce major uncertainties of forest P budgets.

## DATA AVAILABILITY STATEMENT

All datasets for this study are included in the article/**Supplementary Material**.

## AUTHOR CONTRIBUTIONS

JSo and MW conceived and designed the experiment. JSo was responsible for installation of field equipment, sampling, the integrative data analyses and visualization. DF, DU, FB, FL, JK, KK, and SS contributed analyses and data. JSo conceptualized and wrote the paper as lead author. All authors contributed to the interpretation of the findings and the final manuscript.

## FUNDING

This study was carried out under a grant from the DFG-funded project SPP 1685 Ecosystem Nutrition-Forest Strategies for Limited Phosphorus Resources (DFG WE 4598/7-1).

## ACKNOWLEDGMENTS

We are thankful for the data contributions from the Federal Forest Research Institute of Baden-Württemberg (Heike Puhlmann, FVA Freiburg). We acknowledge Jutta Schlegel, Ruth Magh, Franziska Zieger, and Lisa Dankwerth for sample management. Measurements for DOC were carried out by Christine Krenekwitz (Soil Science and Soil Protection, Martin Luther University Halle-Wittenberg), CL was measured by Petra Wiedemer and Nicole Specht (Soil Ecology, University of Freiburg).

## SUPPLEMENTARY MATERIAL

The Supplementary Material for this article can be found online at: https://www.frontiersin.org/articles/10.3389/ffgc.2019.00085/full#supplementary-material

**Supplementary Table 1 |** Water fluxes and elemental concentrations at the Conventwald research site 2014–2016.

## REFERENCES

Achat, D. L., Pousse, N., Nicolas, M., Brédoire, F., and Augusto, L. (2016). Soil properties controlling inorganic phosphorus availability: general results from a national forest network and a global compilation of the literature. *Biogeochemistry* 127, 255–272. doi: 10.1007/s10533-015-0178-0

Bachmair, S., and Weiler, M. (2012). *Technical Report on Experimental Hillslope Hydrology, Hydronotes*. University of Freiburg, Freiburg, Germany

Baldwin, D. S. (1999). Dissolved organic matter and phosphorus leached from fresh and 'terrestrially'aged river red gum leaves: implications for assessing river–floodplain interactions. *Freshw. Biol.* 41, 675–685. doi: 10.1046/j.1365-2427.1999.00404.x

Benning, R., Schua, K., Schwärzel, K., and Feger, K. (2012). Fluxes of nitrogen, phosphorus, and dissolved organic carbon in the inflow of the lehnmühle reservoir (Saxony) as compared to streams draining three main land-use types in the catchment. *Adv. Geosci.* 32, 1–7. doi: 10.5194/adgeo-32-1-2012

Bergkemper, F., Schöler, A., Engel, M., Lang, F., Krüger, J., Schloter, M., et al. (2016). Phosphorus depletion in forest soils shapes bacterial communities towards phosphorus recycling systems. *Environ. Microbiol.* 18, 1988–2000. doi: 10.1111/1462-2920.13188

Bernal, S., Lupon, A., Ribot, M., Sabater, F., and Martí, E. (2015). Riparian and in-stream controls on nutrient concentrations and fluxes in a headwater forested stream. *Biogeosciences* 12, 1941–1954.

Bernhardt, E. S., and Likens, G. E. (2002). Dissolved organic carbon enrichment alters nitrogen dynamics in a forest stream. *Ecology* 83, 1689–1700. doi: 10.1890/0012-9658(2002)083[1689:DOCEAN]2.0.CO;2

Bol, R., Julich, D., Brödlin, D., Siemens, J., Kaiser, K., Dippold, M. A., et al. (2016). Dissolved and colloidal phosphorus fluxes in forest ecosystems-an almost blind spot in ecosystem research. *J. Plant Nutr. Soil Sci.* 179, 425–438. doi: 10.1002/jpln.201600079

Brown, A. H. F., and Iles, M. A. (1991). Water chemistry profiles under four tree species at Gisburn, NW England. *Forestry* 64, 169–187. doi: 10.1093/forestry/64.2.169

Buendia, C., Kleidon, A., and Porporato, A. (2010). The role of tectonic uplift, climate, and vegetation in the long-term terrestrial phosphorous cycle. *Biogeosciences* 7, 2025–2038. doi: 10.5194/bg-7-2025-2010

Côté, B., Fyles, J. W., and Djalilvand, H. (2002). Increasing N and P resorption efficiency and proficiency in northern deciduous hardwoods with decreasing foliar N and P concentrations. *Ann. For. Sci.* 59, 275–281. doi: 10.1051/forest:2002023

Cole, D. W., and Rapp, M. O. (1981). "Elemental cycling in forest ecosystems," in *Dynamic Properties of Forest Ecosystems,* ed D. E. Reichele (Cambridge: Cambridge University Press), 341–409.

Compton, J. E., and Cole, D. W. (1998). Phosphorus cycling and soil P fractions in douglas-fir and red alder stands. *For. Ecol. Manag.* 110, 101–112. doi: 10.1016/S0378-1127(98)00278-3

de Oliveira Garcia, W., Amann, T., and Hartmann, J. (2018). Increasing biomass demand enlarges negative forest nutrient budget areas in wood export regions. *Sci. Rep.* 8:5280. doi: 10.1038/s41598-018-22728-5

Dietze, M., and Dietze, E. (2013). *EMMAgeo: End-Member Modelling Algorithm and Supporting Functions for Grain-Size Analysis*. R package version 0.9. 0.

Dillon, P. J., and Kirchner, W. (1975). The effects of geology and land use on the export of phosphorus from watersheds. *Water Res.* 9, 135–148. doi: 10.1016/0043-1354(75)90002-0

Doskey, P. V., and Ugoagwu, B. J. (1989). Atmospheric deposition of macronutrients by pollen at a semi-remote site in northern Wisconsin. *Atmos. Environ.* 23, 2761–2766. doi: 10.1016/0004-6981(89)90556-8

Duchesne, L., Ouimet, R., Camiré, C., and Houle, D. (2001). Seasonal nutrient transfers by foliar resorption, leaching, and litter fall in a northern hardwood forest at lake clair watershed, quebec, Canada. *Can. J. For. Res.* 31, 333–344. doi: 10.1139/x00-183

Duquesnay, A., Dupouey, J., Clement, A., Ulrich, E., and Le Tacon, F. (2000). Spatial and temporal variability of foliar mineral concentration in beech (*Fagus sylvatica*) stands in northeastern France. *Tree Physiol.* 20, 13–22. doi: 10.1093/treephys/20.1.13

Elser, J. J., Bracken, M. E. S., Cleland, E. E., Gruner, D. S., Harpole, W. S., Hillebrand, H., et al. (2007). Global analysis of nitrogen and phosphorus limitation of primary producers in freshwater, marine and terrestrial ecosystems. *Ecol. Lett.*10, 1135–1142. doi: 10.1111/j.1461-0248.2007.01113.x

Elser, J. J., Fagan, W. F., Denno, R. F., Dobberfuhl, D. R., Folarin, A., Huberty, A., et al. (2000). Nutritional constraints in terrestrial and freshwater food webs. *Nature* 408, 578–580. doi: 10.1038/35046058

Elwood, J. W., Newbold, J. D., O'Neill, R. V., and Van Winkle, W. (1983). "Resource spiralling: an operational paradigm for analyzing lotic ecosystems," in *Dynamics of Lotic Ecosystems,* eds T. D. Fontaine III and S. M. Bartell (Ann Arbor, MI: Ann Arbor Science), 3–27.

Friberg, N., Winterbourn, M., Shearer, K., and Larsen, S. (1997). Benthic communities of forest streams in the South Island, New Zealand: effects of forest type and location. *Arch. Hydrobiol.* 138, 289–306.

Gosz, J. R., Likens, G. E., and Bormann, F. H. (1973). Nutrient release from decomposing leaf and branch litter in the hubbard brook forest, New Hampshire. *Ecol. Monogr.* 43, 173–191. doi: 10.2307/1942193

Gottselig, N., Nischwitz, V., Meyn, T., Amelung, W., Bol, R., Halle, C., et al. (2017). Phosphorus binding to nanoparticles and colloids in forest stream waters. *Vadose Zone J.* 16, 1–12. doi: 10.2136/vzj2016.07.0064

Gregory, S. V. (1978). Phosphorus dynamics on organic and inorganic substrates in streams. *Int. Ver. Theor. Angew. Limnol. Verh* 20, 1340–1346. doi: 10.1080/03680770.1977.11896696

Hangen, E., Lindenlaub, M., Leibundgut, C., and Von Wilpert, K. (2001). Investigating mechanisms of stormflow generation by natural tracers and hydrometric data: a small catchment study in the black forest, Germany. *Hydrol. Process*. 15, 183–199. doi: 10.1002/hyp.142

Heuck, C., Weig, A., and Spohn, M. (2015). Soil microbial biomass C: N: P stoichiometry and microbial use of organic phosphorus. *Soil Biol. Biochem*. 85, 119–129. doi: 10.1016/j.soilbio.2015.02.029

Hill, B. H., McCormick, F. H., Harvey, B. C., Johnson, S. L., Warren, M. L., and Elonen, C. M. (2010). Microbial enzyme activity, nutrient uptake and nutrient limitation in forested streams. *Freshwater Biol.* 55, 1005–1019. doi: 10.1111/j.1365-2427.2009.02337.x

Hill, W. R., Mulholland, P. J., and Marzolf, E. R. (2001). Stream ecosystem responses to forest leaf emergence in spring. *Ecology* 82, 2306–2319. doi: 10.1890/0012-9658(2001)082[2306:SERTFL]2.0.CO;2

Horwath, W. R. (2017). "The role of the soil microbial biomass in cycling nutrients," in *Microbial Biomass: A Paradigm Shift in Terrestrial Biogeochemistry*, ed K. R. Tate (London: World Scientific), 41–66.

Ilg, K., Wellbrock, N., and Lux, W. (2009). Phosphorus supply and cycling at long-term forest monitoring sites in Germany. *Eur. J. For. Res*. 128, 483–492. doi: 10.1007/s10342-009-0297-z

Jansson, M., Persson, G., and Broberg, O. (1986). Phosphorus in acidified lakes: the example of lake gårdsjön, Sweden. *Hydrobiologia* 139, 81–96. doi: 10.1007/BF00770243

Jonard, M., Fürst, A., Verstraeten, A., Thimonier, A., Timmermann, V., Potočić, N., et al. (2014). Tree mineral nutrition is deteriorating in Europe. *Glob. Chang. Biol*. 21, 418–430 doi: 10.1111/gcb.12657

Kaiser, K., Guggenberger, G., Haumaier, L., and Zech, W. (2001a). Seasonal variations in the chemical composition of dissolved organic matter in organic forest floor layer leachates of old-growth Scots pine (*Pinus sylvestris* L.) and European beech (*Fagus sylvatica* L.) stands in northeastern Bavaria, Germany. *Biogeochemistry* 55, 103–143. doi: 10.1023/A:1010694032121

Kaiser, K., Guggenberger, G., and Zech, W. (2001b). Organically bound nutrients in dissolved organic matter fractions in seepage and soil water of weakly developed forest soils. *Acta. Hydrochim. Hydrobiol.* 28, 411–419. doi: 10.1002/1521-401X(20017)28:7<411::AID-AHEH411>3.0.CO;2-D

Killingbeck, K. T. (1986). Litterfall dynamics and element use efficiency in a Kansas gallery forest. *Am. Midl. Nat*. 116, 180–189. doi: 10.2307/2425950

Killingbeck, K. T. (1996). Nutrients in senesced leaves: keys to the search for potential resorption and resorption proficiency. *Ecology* 77, 1716–1727. doi: 10.2307/2265777

Kohler, M., Wilpert, K., and Hildebrand, E. (2000). The soil skeleton as a source for the short-term supply of base cations in forest soils of the black forest (Germany). *Water Air Soil Pollut*. 122, 37–48. doi: 10.1023/A:1005277909113

Kopavcek, J., Turek, J., Hejzlar, J., and Santruckova, H. (2009). Canopy leaching of nutrients and metals in a mountain spruce forest. *Atmos. Environ*. 43, 5443–5453. doi: 10.1016/j.atmosenv.2009.07.031

Laliberté, E., Grace, J. B., Huston, M. A., Lambers, H., Teste, F. P., Turner, B. L., et al. (2013). How does pedogenesis drive plant diversity? *Trends Ecol. Evol*. 28, 331–340. doi: 10.1016/j.tree.2013.02.008

Lang, F., Bauhus, J., Frossard, E., George, E., Kaiser, K., Kaupenjohann, M., et al. (2016). Phosphorus in forest ecosystems: new insights from an ecosystem nutrition perspective. *J. Plant Nutr. Soil Sci*. 179, 129–135. doi: 10.1002/jpln.201500541

Lang, F., Krüger, J., Amelung, W., Willbold, S., Frossard, E., Bünemann, E. K., et al. (2017). Soil phosphorus supply controls P nutrition strategies of beech forest ecosystems in Central Europe. *Biogeochemistry* 136, 5–29. doi: 10.1007/s10533-017-0375-0

Long, W., Sweet, D., and Tukey, H. (1956). Loss of nutrients from plant foliage by leaching as indicated by radioisotopes. *Science* 123, 1039–1040. doi: 10.1126/science.123.3206.1039-a

Magh, R.-K., Grün, M., Knothe, V. E., Stubenazy, T., Tejedor, J., Dannenmann, M., et al. (2017). Silver-fir (Abies alba MILL.) neighbors improve water relations of European beech (*Fagus sylvatica* L.), but do not affect N nutrition. *Trees* 32, 337–348. doi: 10.1007/s00468-017-1557-z

Mahowald, N., Jickells, T. D., Baker, A. R., Artaxo, P., Benitez-Nelson, C. R., Bergametti, G., et al. (2008). Global distribution of atmospheric phosphorus sources, concentrations and deposition rates, and anthropogenic impacts. *Glob. Biogeochem. Cycles* 22:4026. doi: 10.1029/2008GB003240

Meyer, J. L., and Likens, G. (1979). Transport and transformation of phosphorus in a forest stream ecosystem. *Ecology* 60, 1255–1269.

Miller, H., Cooper, J. M., and Miller, J. (1976). Effect of nitrogen supply on nutrients in litter fall and crown leaching in a stand of Corsican pine. *J. Appl. Ecol*. 13, 233–248. doi: 10.2307/2401943

Missong, A., Bol, R., Nischwitz, V., Krüger, J., Lang, F., Siemens, J., et al. (2017). Phosphorus in water dispersible-colloids of forest soil profiles. *Plant Soil* 427, 71–86. doi: 10.1007/s11104-017-3430-7

Missong, A., Bol, R., Willbold, S., Siemens, J., and Klumpp, E. (2016). Phosphorus forms in forest soil colloids as revealed by liquid-state 31P-NMR. *J. Plant Nutr. Soil Sci*. 179, 159–167. doi: 10.1002/jpln.201500119

Mulholland, P. J. (1992). Regulation of nutrient concentrations in a temperate forest stream: roles of upland, riparian, and instream processes, Limnol. *Oceanogr*. 37:1512–1526. doi: 10.4319/lo.1992.37.7.1512

Mulholland, P. J. (2004). The importance of in-stream uptake for regulating stream concentrations and outputs of N and P from a forested watershed: evidence from long-term chemistry records for walker branch watershed. *Biogeochemistry* 70, 403–426. doi: 10.1007/s10533-004-0364-y

Mulholland, P. J., and Hill, W. R. (1997). Seasonal patterns in streamwater nutrient and dissolved organic carbon concentrations: separating catchment flow path and in-stream effects. *Water Resour. Res*. 33, 1297–1306. doi: 10.1029/97WR00490

Mulholland, P. J., Newbold, J. D., Elwood, J. W., and Webster, J. R. (1985). Phosphorus spiralling in a woodland stream: seasonal variations. *Ecology* 66, 1012–1023. doi: 10.2307/1940562

Mulholland, P. J., Wilson, G. V., and Jardine, P. M. (1990). Hydrogeochemical response of a forested watershed to storms: effects of preferential flow along shallow and deep pathways. *Water Resour. Res*. 26, 3021–3036. doi: 10.1029/WR026i012p03021

Munn, N. L., and Meyer, J. L. (1990). Habitat-specific solute retention in two small streams: an intersite comparison. *Ecology* 71, 2069–2082. doi: 10.2307/1938621

Neal, C., Reynolds, B., Neal, M., Hughes, S., Wickham, H., Hill, L., et al. (2003). Soluble reactive phosphorus levels in rainfall, cloud water, throughfall, stemflow, soil waters, stream waters and groundwaters for the upper river severn area, plynlimon, mid wales. *Sci. Total Environ.* 314, 99–120. doi: 10.1016/S0048-9697(03)00099-8

Newman, E. I. (1995). Phosphorus inputs to terrestrial ecosystems. *J. Ecol*. 83, 713–726. doi: 10.2307/2261638

Nihlgård, B. (1970). Precipitation, its chemical composition and effect on soil water in a beech and a spruce forest in south Sweden. *Oikos* 21, 208–217. doi: 10.2307/3543676

Persson, G., and Broberg, O. (1985). Nutrient concentrations in the acidified lake gårdsjön: the role of transport and retention of phosphorus, nitrogen and DOC in watershed and lake. *Ecol. Bull*. 37, 158–175.

Peterson, B. J., Wollheim, W. M., Mulholland, P. J., Webster, J. R., Meyer, J. L., Tank, J. L., et al. (2001). Control of nitrogen export from watersheds by headwater streams. *Science* 292, 86–90. doi: 10.1126/science.1056874

Prietzel, J., Klysubun, W., and Werner, F. (2016). Speciation of phosphorus in temperate zone forest soils as assessed by combined wet-chemical fractionation and XANES spectroscopy. *J. Plant Nutr. Soil Sci*. 179, 168–185. doi: 10.1002/jpln.201500472

Qualls, R. G., and Haines, B. L. (1991). Geochemistry of dissolved organic nutrients in water percolating through a forest ecosystem. *Soil Sci. Soc. Am. J.* 55, 1112–1123. doi: 10.2136/sssaj1991.03615995005500040036x

Qualls, R. G., Haines, B. L., Swank, W. T., and Tyler, S. W. (2002). Retention of soluble organic nutrients by a forested ecosystem. *Biogeochemistry* 61, 135–171. doi: 10.1023/A:1020239112586

Raubuch, M., and Joergensen, R. G. (2002). C and net N mineralisation in a coniferous forest soil: the contribution of the temporal variability of microbial biomass C and N. *Soil Biol. Biochem*. 34, 841–849. doi: 10.1016/S0038-0717(02)00016-0

Reckhow, K. H., Beaulac, M. N., and Simpson, J. T. (1980). *Modeling Phosphorus Loading and Lake Response Under Uncertainty: A Manual and Compilation of Export Coefficients*. Washington, DC: EPA publication

Rennenberg, H., and Schraml, C. (2000). Sensitivität von ökotypen der buche (*Fagus sylvatica* L.) gegenüber trockenstressforstwiss. *Cent.bl.* 119, 51–61. doi: 10.1007/BF02769126

Rier, S. T., and Stevenson, R. J. (2002). Effects of light, dissolved organic carbon, and inorganic nutrients [2pt] on the relationship between algae and heterotrophic bacteria in stream periphyton. *Hydrobiologia* 489, 179–184. doi: 10.1023/A:1023284821485

Roberts, B. J., Mulholland, P. J., and Hill, W. R. (2007). Multiple scales of temporal variability in ecosystem metabolism rates: results from 2 years of continuous monitoring in a forested headwater stream. *Ecosystems* 10, 588–606.

Rodin, L. E., Bazilevich, N. I., Fogg, G. E., Technica, S., and Rodin, L. B. (ed) (1967). *Production and Mineral Cycling in Terrestrial Vegetation*. Edinburgh: Oliver & Boyd Edinburgh.

Rosemond, A. D. (1994). Multiple factors limit seasonal variation in periphyton in a forest stream. *J. N. Am. Benthol. Soc.* 13, 333–334. doi: 10.2307/1467363

Runyan, C. W., Lawrence, D., Vandecar, K. L., and D'odorico, P. (2013). Experimental evidence for limited leaching of phosphorus from canopy leaves in a tropical dry forest. *Ecohydrology* 6, 806–817. doi: 10.1002/eco.1303

Saa, A., Trasar-Cepeda, M. C., Gil-Sotres, F., and Carballas, T. (1993). Changes in soil phosphorus and acid phosphatase activity immediately following forest fires. *Soil Biol. Biochem.* 25, 1223–1230. doi: 10.1016/0038-0717(93)90218-Z

Schroth, G., Elias, M. E. A., Uguen, K., Seixas, R., and Zech, W. (2001). Nutrient fluxes in rainfall, throughfall and stemflow in tree-based land use systems and spontaneous tree vegetation of central Amazonia. *Agric. Ecosyst. Environ.* 87, 37–49. doi: 10.1016/S0167-8809(00)00294-2

Schuessler, J. A., Kämpf, H., Koch, U., and Alawi, M. (2016). Earthquake impact on iron isotope signatures recorded in mineral spring water. *J. Geophys. Res. Solid Earth* 121, 8548–8568. doi: 10.1002/2016JB013408

Schuessler, J. A., Von Blanckenburg, F., Bouchez, J., Uhlig, D., and Hewawasam, T. (2018). Nutrient cycling in a tropical montane rainforest under a supply-limited weathering regime traced by elemental mass balances and Mg stable isotopes. *Chem. Geol.* 497, 74–87. doi: 10.1016/j.chemgeo.2018.08.024

Schwärzel, K., Ebermann, S., and Schalling, N. (2012). Evidence of double-funneling effect of beech trees by visualization of flow pathways using dye tracer. *J. Hydrol.* 470, 184–192. doi: 10.1016/j.jhydrol.2012.08.048

Sedell, J. R., Triska, F. J., and Triska, N. S. (1975). The processing of conifer and hardwood leaves in two coniferous forest streams: I. weight loss and associated invertebrates. *Verh. Internat. Verein. Limnol.* 19, 1617–1627. doi: 10.1080/03680770.1974.11896227

Snajdr, J., Cajthaml, T., Valášková, V., Merhautová, V., Petránková, M., Spetz, P., et al. (2011). Transformation of quercus petraea litter: successive changes in litter chemistry are reflected in differential enzyme activity and changes in the microbial community composition. *FEMS Microbiol. Ecol.* 75:291–303. doi: 10.1111/j.1574-6941.2010.00999.x

Sohrt, J., Lang, F., and Weiler, M. (2017). Quantifying components of the phosphorus cycle in temperate forests. *Wiley Interdiscip. Rev. Water* 4:e1243. doi: 10.1002/wat2.1243

Sparling, G. P., Hart, P. B. S., August, J. A., and Leslie, D. M. (1994). A comparison of soil and microbial carbon, nitrogen, and phosphorus contents, and macro-aggregate stability of a soil under native forest and after clearance for pastures and plantation forest. *Biol. Fertil. Soils* 17, 91–100. doi: 10.1007/BF00337739

Spohn, M., and Widdig, M. (2017). Turnover of carbon and phosphorus in the microbial biomass depending on phosphorus availability. *Soil Biol. Biochem.* 113, 53–59. doi: 10.1016/j.soilbio.2017.05.017

Staelens, J., De Schrijver, A., and Verheyen, K. (2007). Seasonal variation in throughfall and stemflow chemistry beneath a European beech (*Fagus sylvatica*) tree in relation to canopy phenology. *Can. J. For. Res.* 37, 1359–1372. doi: 10.1139/X07-003

Stahr, S., Graf-Rosenfellner, M., Klysubun, W., Mikutta, R., Prietzel, J., and Lang, F. (2017). Phosphorus speciation and C: N: P stoichiometry of functional organic matter fractions in temperate forest soils. *Plant Soil* 427, 53–69. doi: 10.1007/s11104-017-3394-7

Stelzer, R. S., Heffernan, J., and Likens, G. E. (2003). The influence of dissolved nutrients and particulate organic matter quality on microbial respiration and biomass in a forest stream. *Freshwater Biol.* 48, 1925–1937. doi: 10.1046/j.1365-2427.2003.01141.x

Stevens, P., Hornung, M., and Hughes, S. (1989). Solute concentrations, fluxes and major nutrient cycles in a mature Sitka-spruce plantation in Beddgelert Forest, North Wales, For. *Ecol. Manag.* 27:1–20. doi: 10.1016/0378-1127(89)90078-9

Talkner, U., Meiwes, K. J., Potočić, N., Seletković, I., Cools, N., De Vos, B., et al. (2015). Phosphorus nutrition of beech (*Fagus sylvatica* L.) is decreasing in Europe. *Ann. For. Sci.* 72, 919–928. doi: 10.1007/s13595-015-0459-8

Thimonier, A., Schmitt, M., Waldner, P., and Schleppi, P. (2008). Seasonality of the Na/Cl ratio in precipitation and implications of canopy leaching in validating chemical analyses of throughfall samples. *Atmos. Environ.* 40, 9106–9117. doi: 10.1016/j.atmosenv.2008.09.007

Timmons, D., Verry, E., Burwell, R., and Holt, R. (1977). Nutrient transport in surface runoff and interflow from an aspen-birch forest. *J. Environ. Qual.* 6, 188–192. doi: 10.2134/jeq1977.00472425000600020018x

Tipping, E., Benham, S., Boyle, J., Crow, P., Davies, J., Fischer, U., et al. (2014). Atmospheric deposition of phosphorus to land and freshwater. *Environ. Sci. Process Impacts* 16, 1608–1617. doi: 10.1039/C3EM00641G

Triska, F. J., Sedell, J. R., and Buckley, B. (1975). The processing of conifer and hardwood leaves in two coniferous forest streams: II. biochemical and nutrient changes. *Verh. Internat. Verein. Limnol.* 16, 1628–1639. doi: 10.1080/03680770.1974.11896228

Tukey Jr, H. (1966). Leaching of metabolites from above-ground plant parts and its implications. *Bull. Torrey Bot. Club* 93, 385–401. doi: 10.2307/2483411

Tukey Jr, H.B. (1970). The leaching of substances from plants. *Annu. Rev. Plant Physiol. Plant Mol. Biol.* 21, 305–324. doi: 10.1146/annurev.pp.21.060170.001513

Turner, J. (1981). Nutrient cycling in an age sequence of western Washington Douglas-fir stands. *Ann. Bot.* 48, 159–170. doi: 10.1093/oxfordjournals.aob.a086109

Uhlenbrook, S., Holocher, J., Leibundgut, C., and Seibert, J. (1998). "Hydrology, water resources and ecology in headwaters," in *Using a Conceptual Rainfall-Runoff Model on Different Scales by Comparing a Headwater With Larger Basins,* eds U. Tappeiner, N. E. Peters, R. G. Craig, and K. Kovar (Wallingford: IAHS), 297–305.

Uhlig, D., Schuessler, J. A., Bouchez, J., Dixon, J. L., and von Blackenburg, F. (2017). Quantifying nutrient uptake as driver of rock weathering in forest ecosystems by magnesium stable isotopes. *Biogeosciences* 14, 3111–3128. doi: 10.5194/bg-14-3111-2017

Uhlig, D., and von Blanckenburg, F. (2019b). Geochemical and isotope data on rock weathering, and nutrient balances during fast forest floor turnover in montane, temperate forest ecosystems. *GFZ Data Services*. doi: 10.5880/GFZ.3.3.2019.004

Uhlig, D., and von Blanckenburg, F. V. (2019a). How slow rock weathering balances nutrient loss during fast forest floor turnover in montane, temperate forest ecosystems. *Front. Earth Sci.* 7, 1–28. doi: 10.3389/feart.2019.00159

Ulrich, B. (1983). "Interaction of forest canopies with atmospheric constituents: $SO_2$, alkali and earth alkali cations and chloride," in *Effects of Accumulation of Air Pollutants in Forest Ecosystems,* eds B. Ulrich and J. Pankrath (Berlin: Umweltbundesamt), 33–45.

Verheyen, D., Van Gaelen, N., Ronchi, B., Batelaan, O., Struyf, E., Govers, G., et al. (2015). Dissolved phosphorus transport from soil to surface water in catchments with different land use, *Ambio* 44, 228–240. doi: 10.1007/s13280-014-0617-5

Vitousek, P. M., Porder, S., Houlton, B. Z., and Chadwick, O. A. (2010). Terrestrial phosphorus 968 limitation: mechanisms, implications, and nitrogen-phosphorus interactions. *Ecol. Appl.* 20, 5–15.

Voigt, G. K. (1960). Alteration of the composition of rainwater by trees. *Am. Midl. Nat.* 63, 321–326. doi: 10.2307/2422795

von Blanckenburg, F., Wittmann, H., and Schuessler, J. A. (2016). HELGES: Helmholtz Laboratory for the geochemistry of the earth surface. *J. Large Scale Res. Facil.* 2, 1–5. doi: 10.17815/jlsrf-2-141

Walker, T. W., and Syers, J. K. (1976). The fate of phosphorus during pedogenesis. *Geoderma* 15, 1–19. doi: 10.1016/0016-7061(76)90066-5

Webster, J., Tank, J., Wallace, J., Meyer, J., Eggert, S., Ehrman, T., et al. (2001). Effects of litter exclusion and wood removal on phosphorus and nitrogen retention in a forest stream, Internationale Vereinigung fur

Theoretische und Angewandte Limnologie. *Verhandlungen* 27, 1337–1340. doi: 10.1080/03680770.1998.11901453

Werner, F., de la Haye, T. R., Spielvogel, S., and Prietzel, J. (2017). Small-scale spatial distribution of phosphorus fractions in soils from silicate parent material with different degree of podzolization. *Geoderma* 302, 52–65. doi: 10.1016/j.geoderma.2017.04.026

Winkelmann, C., Schneider, J., Mewes, D., Schmidt, S. I., Worischka, S., Hellmann, C., et al. (2014). Top-down and bottom-up control of periphyton by benthivorous fish and light supply in two streams. *Freshw Biol*. 59, 803–818. doi: 10.1111/fwb.12305

Zavišić, A., Nassal, P., Yang, N., Heuck, C., Spohn, M., Marhan, S., et al. (2016). Phosphorus availabilities in beech (*Fagus sylvatica* L.) forests impose habitat filtering on ectomycorrhizal communities and impact tree nutrition. *Soil Biol. Biochem*. 98, 127–137. doi: 10.1016/j.soilbio.2016.04.006

Zelazny, M., and Siwek, J. P. (2012). Determinants of seasonal changes in streamwater chemistry in small catchments with different land use: case study from Poland's Carpathian foothills. *Pol. J. Environ. Stud*. 21, 791–804.

**Conflict of Interest:** The authors declare that the research was conducted in the absence of any commercial or financial relationships that could be construed as a potential conflict of interest.

frontiers in Forests and Global Change

ORIGINAL RESEARCH
published: 31 March 2020
doi: 10.3389/ffgc.2020.00033

# Foliar Nutrient Concentrations of European Beech in Switzerland: Relations With Nitrogen Deposition, Ozone, Climate and Soil Chemistry

*Sabine Braun*[1]*, *Christian Schindler*[2] and *Beat Rihm*[3]

[1] Institute for Applied Plant Biology, Witterswil, Switzerland, [2] Swiss TPH, University of Basel, Basel, Switzerland, [3] Meteotest, Berne, Switzerland

Excess deposition of the mineral nutrient nitrogen (N) is a serious threat for European forests. Its effect on foliar nutrient concentrations of *Fagus sylvatica*, along with other predictors, was analyzed in the present study which bases on 30 year's observation data in 74 forest monitoring plots in Switzerland. The data include gradients in soil chemistry, climate, nitrogen (N) deposition, and ozone concentration. This long-term forest monitoring study shows that foliar concentrations of phosphorus (P), magnesium (Mg), and potassium (K) decreased over time. Current foliar P concentrations indicate acute P deficiency, assessed both from the concentration and the N:P ratio thresholds. In addition, also the relation between N deposition and foliar concentrations of N and P changed over time. Initially, the N concentrations were positively and the P concentrations not correlated with N deposition. Today, N concentrations are negatively and P strongly negatively related, suggesting a progressive N saturation. Interactions between N deposition and soil chemistry suggest an impaired uptake of K and P at higher N loads. The decline of foliar Mg concentrations seems to be a result of soil acidification mediated by N deposition. Additionally, ozone impaired foliar P uptake. We could observe an increase in leaf weight over time while there was no time trend in P and K mass per leaf. This could be interpreted as a dilution effect but detailed regression analysis argues against the dilution hypothesis. Overall, the changing relation between N deposition and foliar N and P support the nitrogen saturation hypothesis.

**Keywords: nitrogen deposition, phosphorus, potassium, magnesium, fructification, soil acidification**

OPEN ACCESS

***Edited by:***
*Friederike Lang,*
*University of Freiburg, Germany*

***Reviewed by:***
*Gregory Alexander Van Der Heijden,*
*INRA Centre Nancy-Lorraine, France*
*Junwei Luan,*
*International Center for Bamboo and Rattan, China*

***Correspondence:**
*Sabine Braun*
*sabine.braun@iap.ch*

***Specialty section:***
*This article was submitted to Forest Soils, a section of the journal Frontiers in Forests and Global Change*

***Received:*** *30 September 2019*
***Accepted:*** *05 March 2020*
***Published:*** *31 March 2020*

***Citation:***
*Braun S, Schindler C and Rihm B (2020) Foliar Nutrient Concentrations of European Beech in Switzerland: Relations With Nitrogen Deposition, Ozone, Climate and Soil Chemistry. Front. For. Glob. Change 3:33. doi: 10.3389/ffgc.2020.00033*

## INTRODUCTION

The assessment of tree mineral nutrition is part of the UNECE forest monitoring program ICP Forests (International Co-operative Programme on Assessment and Monitoring of Air Pollution Effects on Forests; ICP Forests, 2016). On the plots of this program, a deterioration of nutrition has been observed in the last two decades (Jonard et al., 2015; Talkner et al., 2015), and phosphorus (P) is the element most often declining in these studies. Unbalanced tree nutrition will affect growth and thus limit the uptake of increased atmospheric $CO_2$ (Blanes et al., 2013). It will also have consequences for tree health and mortality (see e.g., St. Chaboussou, 1973; St. Clair et al., 2005; Vitousek et al., 2010; Sardans et al., 2012; Christina et al., 2015).

In permanent forest monitoring plots in Switzerland, decreases in foliar N and P concentrations have been observed for the last 30 years in European beech (*Fagus sylvatica*) (Braun et al., 2018). P concentrations have reached very low levels, far below the thresholds for normal nutrition. K and Mg concentrations have decreased, too, and leaves are showing an increasing incidence of Mg deficiency symptoms. Possible drivers for these changes may be progressive nitrogen saturation, soil acidification, changes of growth or climate or increasing tree age.

Increased tree productivity as a consequence of high nitrogen deposition, increased $CO_2$ concentration or increased temperature has been proposed to be responsible for the changes in foliar nutrient concentrations (Pretzsch et al., 2014; Jonard et al., 2015). Dilution effects, when nutrients are dispersed over a larger biomass, may occur during the first stage of excess nitrogen addition, as long as N is still limiting (Menge and Field, 2007). When N deposition continues, this stage is, however, followed by a stage of nitrogen saturation (Aber et al., 1989; Emmett, 2007) characterized by an increase of nitrate concentration in soil solution (Aber et al., 1989). This may affect roots (Boxman et al., 1998b) or mycorrhiza (Nilsson and Wallander, 2003; Suz et al., 2014) and therefore nutrient uptake. Saturation may develop slowly, leading to changes in the responses to excessive N (Emmett, 2007; McNulty et al., 2017). Thus, a decadal perspective in monitoring is needed given the inherently slow processes involved.

Climate change and increased fructification of beech have been proposed as reasons for the decrease in foliar P concentrations (Talkner et al., 2015). While increasing temperatures will rather increase nutrient uptake (BassiriRad, 2000), increasing drought occurrence and intensity is expected to act in the opposite way (Kreuzwieser and Gessler, 2010). Since increasing temperature and pronounced drought events are often linked it is difficult to judge which process will be predominant.

In the case of Ca and Mg, a decrease of foliar concentrations is usually explained by soil acidification and the corresponding depletion of the exchangeable pools in the soils by leaching. Visible Mg deficiency in Norway spruce has been a forest decline symptom in parts of Germany affected by high acid loads in the 1980's (Cape et al., 1990; Elling et al., 2007). For anthropogenic soil acidification, both sulfur or nitrogen inputs are relevant. After the reduction of sulfur emissions achieved in the 1990's, the relative importance of nitrogen for soil acidification has become more important although sulfur is still leaching from the soils. Today's soil acidifying inputs are mainly mediated by nitrogen as sulfur deposition became very low (Augustin and Achermann, 2012).

The objective of the present paper was to disentangle the contribution of these possible factors, along with the role of edaphic predictors. Growth data for the study have been presented by Braun et al. (2017b). They show a marked decrease in stem increment, both on the basis of individual tree measurements and on plot surface.

# MATERIALS AND METHODS

## Permanent Monitoring Plots

The study was conducted based on data from a network of long-term forest monitoring plots in Switzerland which was initiated in 1984. The plots cover a variety of soil types (including vertisols, cambisols, and rendzic leptosols) and environmental conditions (**Table_Supplementary 1**). Seventy-four beech plots were included in this study (**Figure_Supplementary 1**), each consisting of 60 mature *Fagus* trees on a surface area of 0.1–2 ha. The observation period of this study covers the time from 1984 to 2015, with harvests every 3–4 years (total of 9 harvests). The number of plots was 52 in 1984 and increased to 93 in 2015.

## Soil Analysis

The solid phase of the soil was sampled in all plots once between 2005 and 2010. An Edelman auger (Eijkelkamp) was used for taking the samples at 6–8 points per plot in different horizons. The samples were pooled by horizon. Soil samples were air dried and passed through a 2 mm sieve. Exchangeable base cations and pH($CaCl_2$) were determined as described in Braun et al. (2003). Plant available P was extracted using 2% citric acid at a ratio of 1:10 (Hort et al., 1998; Manghabati et al., 2018). Total N and acid extractable P were determined after a Kjeldahl digestion. For P this digestion procedure yields lower values than real totals (Hornburg and Lüer, 1999). Lime ($CaCO_3$) was determined by measuring the volume of $CO_2$ evolved by addition of HCl. For data analysis, the element stocks in kg $ha^{-1}$ were cumulated over the uppermost 40 or 60 cm, considering layer thickness, bulk density and stone content in the calculation. Bulk density was estimated in the field according to Sponagel et al. (2005) and adjusted for the content of organic carbon. pH and base saturation were averaged over the uppermost 40 cm. C:N ratios as well as total N and P concentrations were calculated for the forest floor or the uppermost mineral soil horizon, if no humic horizon was present (e.g., mull humus forms). This fraction is called "uppermost horizon" in the following.

## Soil Solution

Soil solution was sampled in a subset of 19 plots covering a large range of chemical properties, starting between 1997 and 2002. Ceramic cups (Soilmoisture Inc., USA) were installed in 2–3 depths per plot and 5–8 replicates per depth. Depths varied per plot according to soil profile but a frequent sampling pattern was 20, 50, and 80 cm. Samples were collected monthly. The samples were combined per depth to one mixed sample per plot. Anions were analyzed in filtered samples using ion chromatography (Dionex GP50) with suppressed electrochemical detection (Dionex ED50). For the analysis of cations, samples were acidified after sampling. Ca, Mg, and Al were measured using atomic absorption spectrophotometry, K using flame emission spectrophotometry (Varian 240 AA).

## Shoot Harvest and Plant Analysis

Shoots used for nutrient analysis were harvested every 4 years in July by helicopter from the top crown of the same eight trees per plot, starting in 1984. The shoots were visually assessed

for discoloration symptoms (quantified as percentage of leaves affected) and for fructification by counting fruits or fruit scars on short shoots of different age. Leaves were dried, ground, and analyzed for N, P, K, Ca, Mg, and Mn according to Walinga et al. (1995). A subset of samples from previous harvests was reanalyzed each time to avoid systematic shifts in the analytical results. Quality control was achieved by analysis of certified samples (NIST apple leaves, National Institute of Standards and Technology, Gaithersburg, USA) and by taking part in a sample exchange program (WEPAL, University of Wageningen).

Ten leaves per tree were dried at 80°C and weighed. Nutrient contents in the leaves were obtained by multiplication of the dry weight per leaf with the concentration. The dry weight determination was not available for the years 1984 and 1995.

## Climate

Meteorological data were interpolated for each plot from the nearest eight monitoring stations of the Federal Office of Meteorology and Climatology (MeteoSwiss) as described in Braun et al. (2017b). The resulting daily averages were used in the regression analysis or as input to the hydrological model Wasim-ETH (Schulla, 2013). With this model the following drought indicators were calculated:

i. Ratio between actual and potential evapotranspiration (ETa/ETp).
ii. Site water balance (SWB): cumulated difference between precipitation and potential evapotranspiration at a daily basis, with added water storage capacity of the soil (available water capacity). The cumulation started on January 1st. The lowest value reached during summer was used in the data analysis.
iii. Temperature, precipitation and drought indicators for the harvest year were averaged over the time between start of the season and the harvest date. Start and end of the season were taken from phenological data of beech budbreak and discoloration observed by MeteoSwiss and adjusted for altitude as described in Braun et al. (2017b). The season length thus differs between plots.

## Nitrogen Deposition

We used for this study modeled nitrogen deposition covering all relevant dry and wet N components at a high spatial resolution, which gives an estimate of total deposition into forests. In Switzerland, ammonia ($NH_3$) contribution to nitrogen deposition is quite high (Rihm and Achermann, 2016). The model based on emission inventories and dispersion models for the years 1990, 2000, 2007, and 2010 and was validated against measurements of $NO_2$, $NH_3$ and of ion concentrations in the precipitation (Rihm and Achermann, 2016) and against total deposition estimates by measurements of the single components with micrometeorological methods (Thimonier et al., 2018). Spatial resolution of the model was 1 ha for gaseous $NO_2$ and $NH_3$ and 1 $km^2$ for wet deposition. The years between the model years were interpolated linearly. Such an interpolation is feasible as nitrogen emissions do not change very rapidly.

## Ozone Flux

In earlier studies, annual ozone ($O_3$) flux, expressed as the phytotoxic ozone dose over the threshold of 1 nmol $m^{-2}$ $s^{-1}$ ($POD_1$), proved to be the best measure for ozone exposure of forest trees (Braun et al., 2014). It was calculated using the Central European parameterization for beech (UNECE, 2017) for the years 1991–2015. The model $DO_3SE$ (Emberson et al., 2000) was applied to monitoring data from 30 ozone monitoring stations, and the resulting annual flux values were mapped as described in Braun et al. (2014). Raster cell size was 250 m. The model was run including soil water (Büker et al., 2012) assuming medium soil water storage. Only annual ozone fluxes were available for analysis. It was therefore not possible to calculate ozone flux between budbreak and harvest date for an analysis of harvest year's ozone.

## Statistics

Aim of the data analysis was the simultaneous evaluation of a broad range of possible covariates for foliar nutrient concentrations and ratios and to identify the most significant ones. A multivariable regression model was used with a backwards selection of predictors. The covariates included initially in the model are listed below. They were selected based on theoretical considerations.

i. Soil analysis
   a. exchangeable stocks of K, Mg, Ca, or Mn (sum 0–40 cm) in kg $ha^{-1}$, log transformed
   b. citrate extractable stocks of P (sum 0–40 cm) in kg $ha^{-1}$, log transformed.
   c. stocks of N (Kjeldahl) and P (acid extractable) in t/ha (sum 0–60 cm)
   d. base saturation in % (average 0–40 cm)
   e. pH($CaCl_2$) (average 0–40 cm)
   f. $CaCO_3$ (lime, sum 0–40 cm) in t $ha^{-1}$, log transformed.

ii. Meteorological parameters of the current or the previous year: In the year of the harvest they were averaged over the time between beech budbreak observed by the phonological network of MeteoSwiss and harvest date ("harvest year spring"), in the previous year over the time between beech budbreak and the following 85 days ("previous year spring") or the whole season extending from budbreak to observed discoloration ("previous year season").
   a. air temperature
   b. precipitation
   c. ratio between actual and potential evapotranspiration (ETa/ETp)
   d. site water balance: minimum value within each growing season.

iii. Time (continuous)
   iv. Age: tree age at the beginning of the study for each plot as recommended for cohort studies (Glenn, 2007). In a dataset including a range of age classes, this procedure allows to disentangle the effects of age and of time.
   v. Species composition: proportion of deciduous trees in the forest stand.

The number of plots allowed to include about 7 predictors with variations within plots and about 100 with variations within plot and time (Braun et al., 2017a). The covariates were subjected to a backwards removal procedure, based on the Akaike Information Criterion (AIC) which should be minimized. Linearity was tested using linear, quadratic or cubic functions of covariates using the function poly. Stocks of soil nutrients were tested for different depths (0–40, 0–60, 0–80 cm). The stocks accumulated over 40 cm proved to be the best predictors. As the arrangement of data in clusters of sites and years required a mixed linear regression model with site and year as random factors, the lmer function in R (version 1.1–15, package lme4, Bates et al., 2015) was used. Concentration predictors usually have a lognormal distribution. They were log-transformed if this led to an improvement of the AIC. After identification of the main effects, all possible interactions were tested one by one. Interactions which were significant in this screening procedure were added to the main model and subjected to another backward selection procedure. Residuals were checked for normal distribution using probability plots (qqplots) and for homoscedasticity and outliers using plots of residuals vs. fitted values. In case of non-conformance the dependent variable was transformed, and outliers which could clearly be visually identified in the Tukey-Anscombe plot were removed. In no case the removal of outliers changed the results. All variables were centered by subtracting the mean. Predictions and confidence intervals were extracted from the regression models using the R function ggpredict (R package ggeffects, version 0.14.0; Lüdecke, 2018). This function averages all covariates except the one(s) of interest. Plots with confidence bands were then produced using ggplot2 (Wickham, 2009). For the presentation of the results in the table, the significance of predictors with quadratic and cubic terms was tested using analysis of variance (R package car, function Anova, Fox and Weisberg, 2011). Collinearity of the predictors in the final models was tested using the variance inflation factor R function vif, package "car" (Fox and Weisberg, 2011). In most cases the factors were <2.5, in one case (manganese in soil, base saturation and lime) 4.3 and 5.2, respectively.

The number of plots has not been constant during the observation time. The monitoring program started with 52 plots in 1984. It increased to 93 in 2015. As the unequal number may introduce artifacts in time trends, predictions from a mixed regression with years as factor are shown in **Figure 1** in addition to the raw concentrations. The covariates ozone, fructification, the chemistry of soil solution and leaf weight were not available for all years and/or plots. They were thus included with a reduced dataset (**Table_Supplementary 2**). As a starting point for these regressions, the same covariates as for the regression with all plots were used, but they were subjected to a further removal of predictors increasing the AIC.

For the regression analysis of soil solution data, the average concentrations of the corresponding element in the soil solution of the year preceding the leaf harvest and in depths of <70 cm were used. The effect of soil solution chemistry on foliar concentrations was tested by comparing the AIC of a model with and without soil solution.

Fructification was not included as predictor in the general analysis as it is not an independent predictor: foliar nutrient concentrations may affect fructification and vice versa. It has, however, increased strongly during the observation period so its significance for the development of foliar concentrations of beech was assessed by comparing the time trend in regression models with and without fructification. Fructification, measured as number of fruits per short shoot in the respective season, was included for the current and the previous year in the same model. Attention was paid to the fruit coefficient on the one hand and on the time coefficient on the other hand. A change of the time coefficient would be an indication that fructification plays a role in explaining the observed time trend in the foliar nutrient concentrations.

The status of the nutrient supply was evaluated using the concentration thresholds published by Göttlein (2015) which base on a very large and well-documented data set compiled by van den Burg (1985, 1990). Recommendations for harmonized nutrient ratios in the compilations of van den Burg were summarized by Flückiger and Braun (1998).

# RESULTS

## Time Trend of Element Foliar Concentrations and Contents

Over time, foliar concentrations of N, P, K, and Mg have decreased significantly (**Figure 1**). This is shown by the significance of the regression with time in **Table 1**. The observed time trend was not affected by the increasing number of plots as the values corrected for this do not differ from the uncorrected values (black squares in **Figure 1**). The increasing trend of Ca concentration in beech leaves is not significant as the variations between years are large. Inclusion of fructification reduced the variation for this element between years but the time trend remained insignificant (see **Table 4**). Changes of N and P concentrations were largely parallel resulting in rather constant N:P ratios. The N:K ratio have slightly decreased but this decrease is not significant as the variations from year to year are mostly explained by meteorological covariates (see also **Figure 7**). The time trend in Mn is not significant either.

Mg deficiency symptoms have increased since 1984 in parallel to the decreasing concentrations (**Figure_Supplementary 2**). Leaves with intercostal chloroses were clearly related to foliar Mg concentrations, less to Mg content (**Figure_Supplementary 3**).

The only element which was significantly associated with tree age was N. With increasing age foliar concentrations of N decreased. Age may thus have contributed to the decrease in foliar N concentrations but its inclusion in the regression model did not replace time as significant predictor. When looking at contents instead of concentrations there is no significant time trend (**Figure 2**, **Table 1**).

## Relations of Foliar Nutrients With Soil Chemistry of the Solid Phase

Foliar N concentrations were not related to soil chemistry. Foliar P was higher, when the stock of acid extractable soil P cumulated over the uppermost 40 cm was high

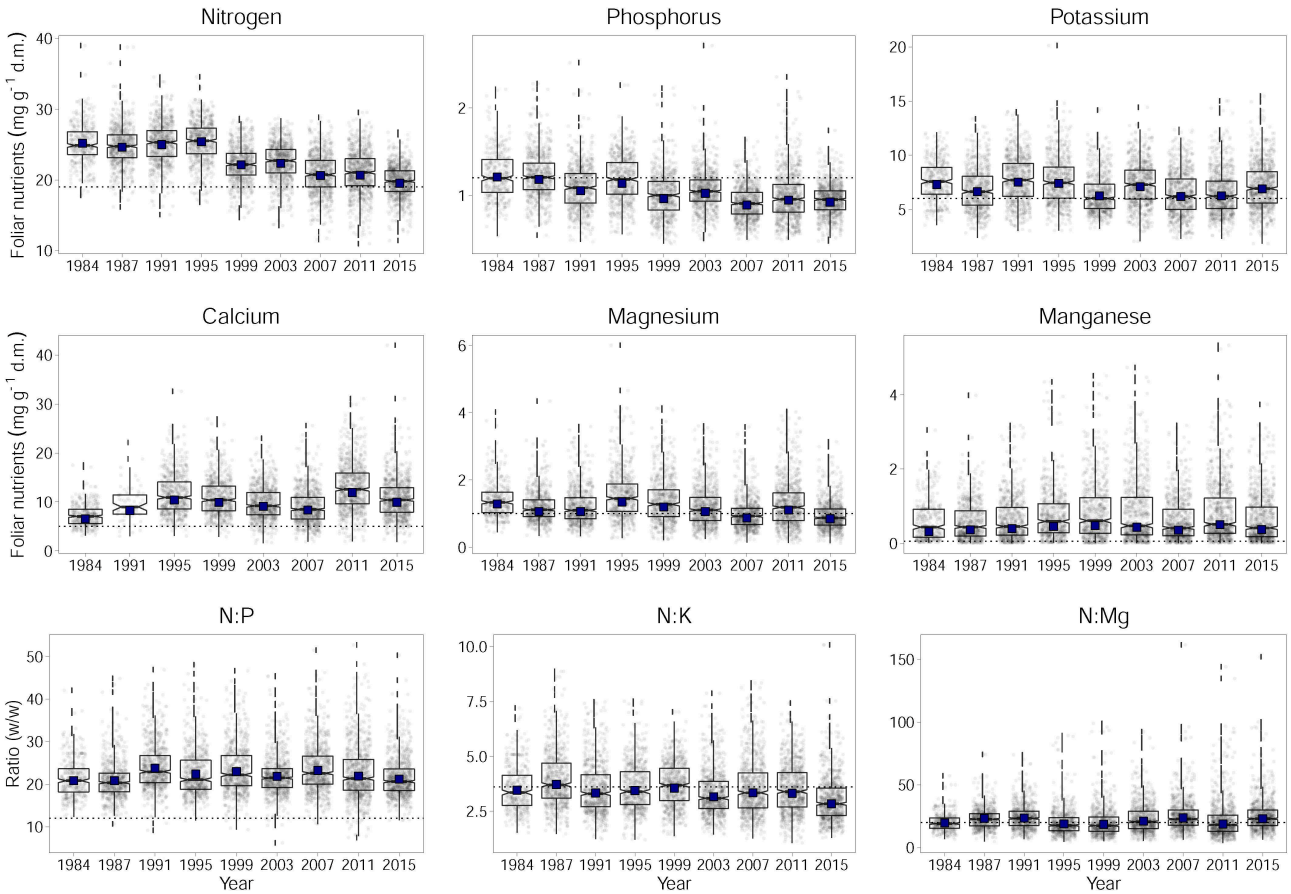


**FIGURE 1 |** Development of foliar nutrient concentrations of N, P, K, Ca, Mg, and Mn for *Fagus sylvatica per* dry matter (d.m.) and the ratios of N to P, K, and Mg. Horizontal dashed lines indicates lower limits of normal ranges according to Göttlein (2015) and the upper limits of normal ranges for the ratios according to Flückiger and Braun (2003). Adjusted annual levels for the annually changing set of plots (by considering plot as a random effect) with year as fixed effect are given as black squares.

(**Figure 3** left). For foliar Ca, the best predictor was base saturation. Foliar K, Mg, and Mn were related with the exchangeable pools of the corresponding element in the soil (K: **Figure_Supplementary 5**, Mg: **Figure_Supplementary 6** left, Mn: **Figure_Supplementary 7** left). Mn was also related with base saturation (**Figure_Supplementary 7** center). If Mn is analyzed in an univariate spline regression with pH($CaCl_2$) as predictor, the foliar concentrations reflect the pH window of high Mn availability between pH 4 and 5 (**Figure_Supplementary 7** right). The soil chemistry predictors for the foliar ratios to nitrogen were similar as for the corresponding single elements. Foliar N:P was related with acid extractable P in soil (**Figure_Supplementary 8**).

## Development of Soil Solution Chemistry Over Time and Relations With Foliar Chemistry

Mg was the only element showing significant relations between foliar concentration and concentration in soil solution (20–40 cm depths), as indicated by the negative AIC difference (**Table 2, Figure_Supplementary 6** right). Mg in soil solution was almost as good as predictor for foliar Mg as exchangeable Mg in soil, and the inclusion of soil solution chemistry along with exchangeable Mg into the regression model for foliar Mg decreased the magnitude of the time coefficient considerably (**Table 3**). By introducing soil solution Mg, the explained variance for fixed variables increased from 16.9 to 19.2%.

During the observation period, all base cations as well as $NO_3^-$ concentrations in the soil solution have decreased significantly (**Table_Supplementary 3**). The decrease in Mg concentrations is illustrated in **Figure_Supplementary 9**. The Al concentrations have increased but in beech plots the increase was small and not significant. The BC/Al ratio has, however decreased significantly in the plots with European beech which indicates a progressing acidification.

## Relations of Tree Nutrition With Nitrogen Deposition

The relations of element concentrations with N deposition partially depended on other covariates as suggested by significant interaction terms. For foliar P concentration there were significant interactions with time and pH($CaCl_2$). On average

**TABLE 1 |** Associations between element concentrations, ratios, and contents in foliage of *Fagus sylvatica* and different predictor variables.

| | Concentrations (mg $g^{-1}$ d.m.) | | | | | | Ratios (w/w) | | | Contents (mg $leaf^{-1}$) | | | | | |
|---|---|---|---|---|---|---|---|---|---|---|---|---|---|---|---|
| | **N** | **P** | **K** | **Ca** | **Mg** | **Mn** | **N:P** | **N:K** | **N:Mg** | **N** | **P** | **K** | **Ca** | **Mg** | **Mn** |
| Explained variance incl. random variables | 0.511 | 0.609 | 0.437 | 0.587 | 0.434 | 0.778 | 0.607 | 0.462 | 0.415 | 0.327 | 0.409 | 0.433 | 0.449 | 0.391 | 0.772 |
| Explained variance fixed only | 0.310 | 0.333 | 0.135 | 0.424 | 0.155 | 0.666 | 0.251 | 0.136 | 0.163 | 0.024 | 0.091 | 0.084 | 0.271 | 0.125 | 0.561 |
| N Deposition | ns | −− | −−− | + | sss2 | | sss3 | +++ | | | | −− | | | |
| Time | −−− | −−− | −− | | − | | | | | | | | | | |
| Age | −−− | | | | | | | | | −−− | | | | | |
| Extractable fraction in soil 0–40 cm | | +++ | +++ | | +++ | sss3 | −−− | −−− | sss3 | | +++ | ++ | | sss3 | sss3 |
| pH($CaCl_2$) | | −−− | | | | | | | | ++ | | | | | |
| Soil base saturation 0–40 cm | | | | +++ | | sss3 | | | | | | | +++ | | sss3 |
| Air temperature CS | | | | | | | | | sss2 | | | | | ++ | |
| Air temperature PVEG | | | | +++ | | | | | | | | | ++ | | |
| ETa/ETp CS | | | | ns | | | | +++ | | | | −− | | | |
| ETa/ETp PVEG | | | | | | | | | +++ | ++ | +++ | sss2 | | | |
| SWB PVEG | | | | | −−− | | | | | | | | | | |
| N deposition * time | − | −−− | | | | | +++ | +++ | | | | | | | |
| N deposition * pH($CaCl_2$) | | +++ | | | | | | | | | | | | | |
| N deposition * extractable fraction | | | −−− | | | | +++ | +++ | | | | | | | |
| Base saturation * ETa/ETp CS | | | | +++ | | | | | | | | | | | |
| Extractable fraction 0–40 cm*Eta/ETP CS | | | | | | | | | | | | −−− | | | |

*–, negative association; +, positive association; s, spline regression with degree given as number after the letters, significant with $p < 0.001$ (3 symbols), $p < 0.01$ (2 symbols), $p < 0.05$ (1 symbol), $p > 0.05$ (ns; shown only when there are significant interactions with this predictor). Empty fields: not included in the regression model (delta AIC between the model including or excluding the corresponding predictor >-2). CS, current spring, PS, previous spring; PVEG, previous season; SWB, Site water balance. Extractable fraction: exchangeable cations according to the dependent variable or citrate extractable P.*

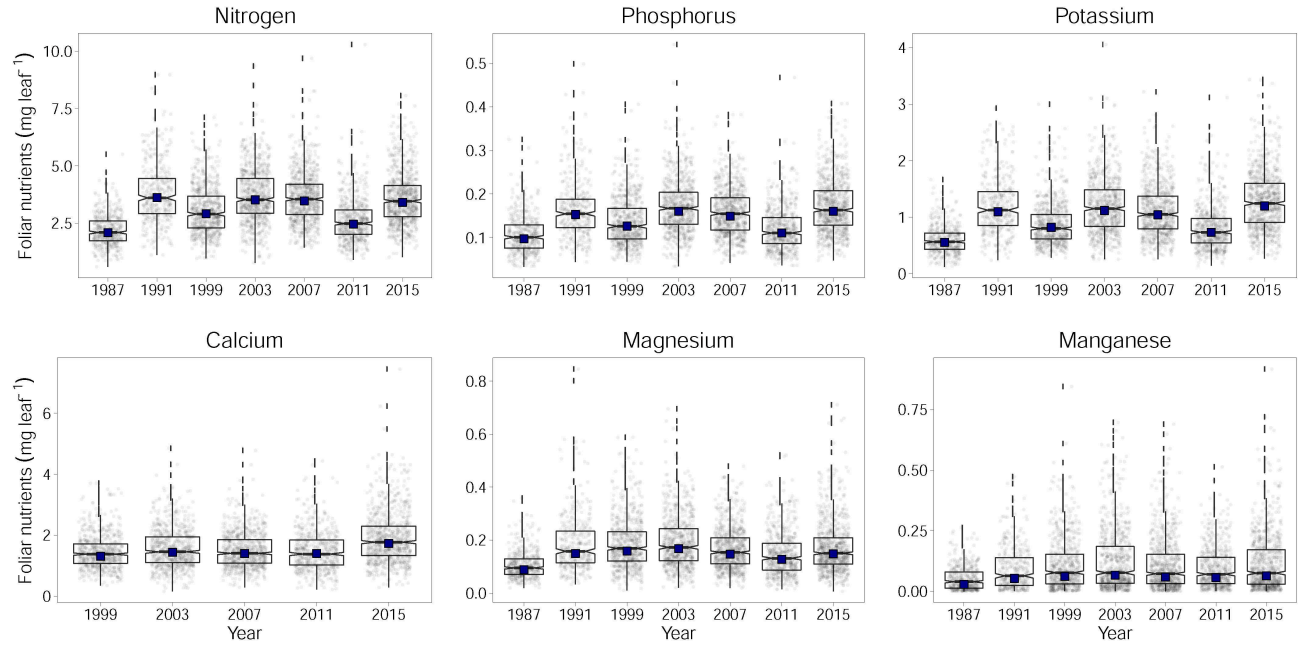


**FIGURE 2 |** Development of foliar contents for N, P, K, Ca, Mg, and Mn for *Fagus sylvatica* calculated per leaf. Adjusted annual levels for the annually changing set of plots (by considering plot as a random effect) with year as fixed effect are given as black squares. The development is different when foliar contents are looked at instead of foliar concentrations (**Figure 2**). This contrasting development of concentrations and contents is mainly due to increasing leaf dry weight (**Figure_Supplementary 4**): while the specific leaf area slightly decreased throughout the observation period, leaf area increased (data not shown).

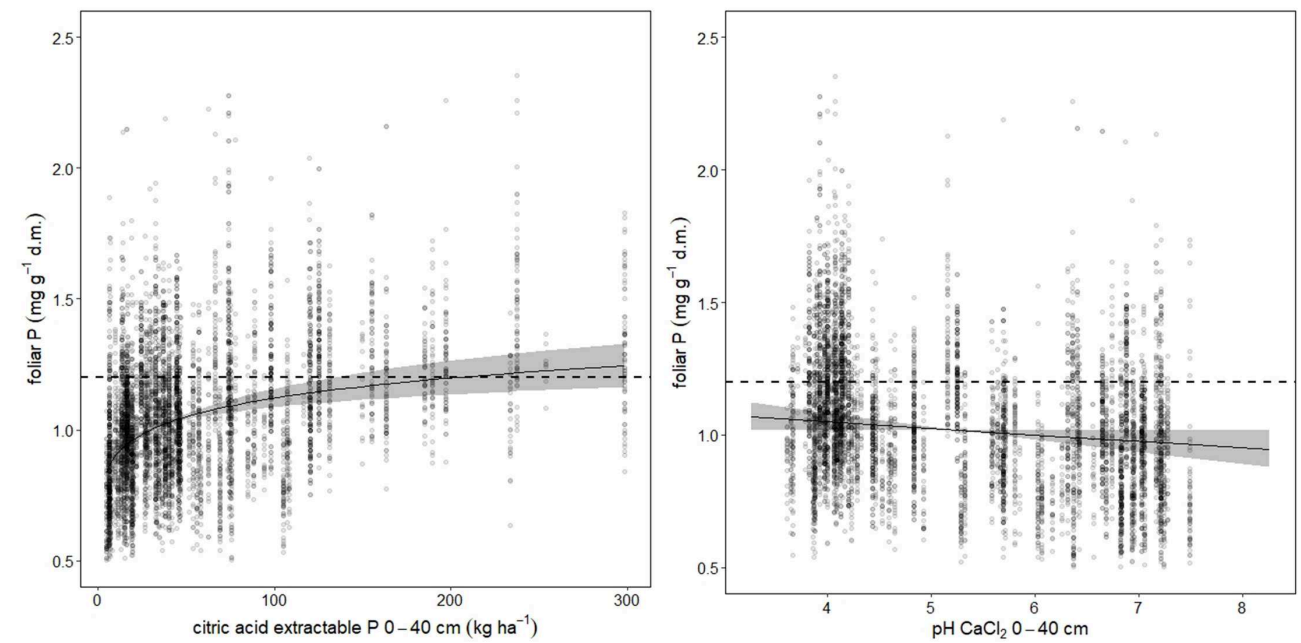


**FIGURE 3 |** Soil chemistry predictors for foliar P. The dotted lines indicate the lower threshold of normal nutrition according to Göttlein (2015), the gray bands the 95% confidence intervals. Total variance explained is 60.9%, while citric acid extractable P (left graph) accounted for 41.5%, and pH (right graph) for 31.6%.

over the whole observation period there was no significant correlation between foliar N concentration and N deposition but N deposition was positively correlated with foliar N in the beginning of the observation period (1984) and negatively in 2015 (**Figure 4** left). Foliar P was negatively related to N deposition in beech. This relation was inexistent in the

beginning and got stronger over time as suggested by the significant interaction between N deposition and time (**Figure 4** center). The negative relation between foliar P and N deposition was stronger at low pH($CaCl_2$) (**Figure_Supplementary 10**). Similarly, the ratio of N:P in beech leaves responded much more to acid extractable P in soil at low N deposition (**Figure_Supplementary 11**). The uptake of K on soils with a high concentration of exchangeable K was only higher when N deposition was low (**Figure 4** right). There was also a significant positive correlation of N deposition with the N:K ratio (**Figure 5** right). The relation between foliar K and N deposition remains significant also when contents instead of concentrations are looked at (**Figure_Supplementary 12**).

## Relations of Foliar Nutrients With Ozone Flux

The ozone flux in the year preceding the harvest was correlated significantly and negatively with foliar P (**Figure 6**) while for N there was only a non-significant trend. The concentrations of the other foliar nutrients were not related to the ozone flux.

## Relations of Foliar Nutrients With Fructification

Regression models with foliar concentrations as dependent variable and the significant predictors according to in **Table 1** were compared to models with the number of fruits in the current and the previous year added as predictors. **Table 4** shows the coefficients for current and previous year fruits and the AIC difference to the model without fruits, **Table_Supplementary 4** the resulting time trends. The inclusion of fructification improved the model fit (as judged by the AIC) except for K. The coefficients with harvest year fruits were positive in all cases, i.e., foliar nutrient concentrations increased when fructification was high (**Table_Supplementary 5**). With previous year fruits, coefficients were positive for Ca and K concentrations and negative for N concentration. Inclusion of fruits did not affect the size of the time coefficient for any of the elements. The time trends for Ca and Mg were not significant and are shown in **Table_Supplementary 4** for information only.

It was also tested if there was a relationship with long-term average of fructification. **Table 5** shows the regression coefficients obtained when the model in **Table 1** is recalculated in presence of a long-term average per tree. In the case of P, the relation is significant: trees with more fruits have larger foliar P concentrations than trees with less fruits. For the other nutrients the AIC difference is positive, i.e., there is no significant relationship with long-term fructification average.

## Relations of Foliar Concentrations With Climate

Air temperature, precipitation, evapotranspiration ratio and site water balance were significant predictors for foliar nutrient concentrations (**Table 1**). Drought was an important predictor, quantified either as ETa/ETp ratio, precipitation or soil water balance, for the cations K (as ratio to N); (**Figure_Supplementary 16**), Mg, and Ca (**Figure_Supplementary 15**). On soils with low base saturation, foliar Ca concentrations were higher under dry than under moist conditions (**Figure_Supplementary 13**).

The only clear temperature response was found for Ca which increased with increasing temperature of the previous season (**Figure_Supplementary 14**) while a non-linear relationship was observed for the N:Mg ratio.

When all predictors except the one(s) of interest are averaged, multivariate regression models allow to extract the response functions. This can be done for either single predictors or a group of predictors and was used to estimate the time trend of foliar nutrients explained by climate. The only modification to the models necessary was to run them without year as random effect. Then all non-climatic predictors were averaged and the predicted values from the regression model were extracted and averaged by year. The results are shown in **Figure 7** for two examples with clear climatic relations: foliar concentrations of Ca and N:K

**TABLE 2 |** Regression coefficients for the relation between foliar nutrient concentrations and the concentration of the corresponding element in soil solution for beech (19 plots).

| | Coefficient for the soil solution concentration | SE | *p*-value | deltaAIC |
|---|---|---|---|---|
| N | 0.0068 | 0.0047 | 0.1477 | 8.8 |
| K | −0.0233 | 0.0233 | 0.3174 | 6.7 |
| Ca | 0.0086 | 0.0263 | 0.7430 | 7.3 |
| Mg | 0.1513 | 0.0445 | 0.0007 | −2.0 |

*DeltaAIC indicates the difference in the AIC between the model including and the model excluding the soil solution chemistry of the respective element.*

**TABLE 3 |** Regression coefficients for the relation between foliar nutrient concentrations with Mg concentration in soil solution (line 3), exchangeable Mg concentration in the soil (line 4), and time (line 5), for regression models including (left) and excluding Mg in soil solution.

| | Model with soil solution | | | Model without soil solution | | |
|---|---|---|---|---|---|---|
| Explained variance incl. random variables | 0.364 | | | 0.366 | | |
| Explained variance fixed only | 0.192 | | | 0.169 | | |
| | **Coefficient** | **SE** | ***p*-value** | **Coefficient** | **SE** | ***p*-value** |
| Mg soil solution | 0.1138 | 0.0481 | 0.0003 | | | |
| Exchangeable Mg | 0.1744 | 0.0482 | 0.0003 | 0.2058 | 0.0584 | 0.0006 |
| Time | −0.0544 | 0.0365 | 0.1316 | −0.0763 | 0.0375 | 0.0417 |

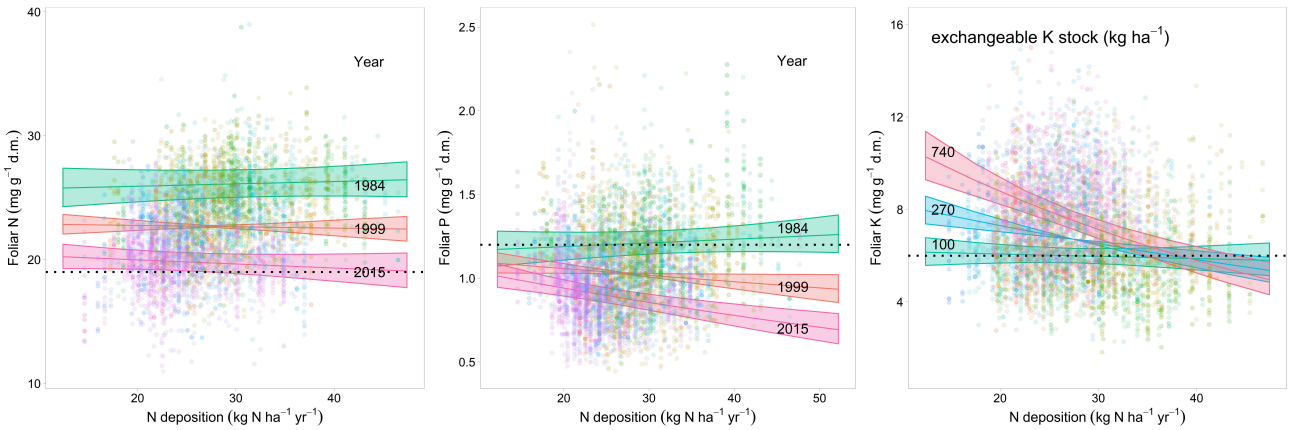


**FIGURE 4 |** Relationship between modeled N deposition and N (left), P (center), and foliar K concentrations (right) in *Fagus sylvatica*. Predicted values extracted from the regression models for 3 years (N, P) and for three levels of soil K stock (K). The lower thresholds to normal nutrition according to Göttlein (2015) are given as dashed lines. The colored bands indicate the 95% confidence intervals.

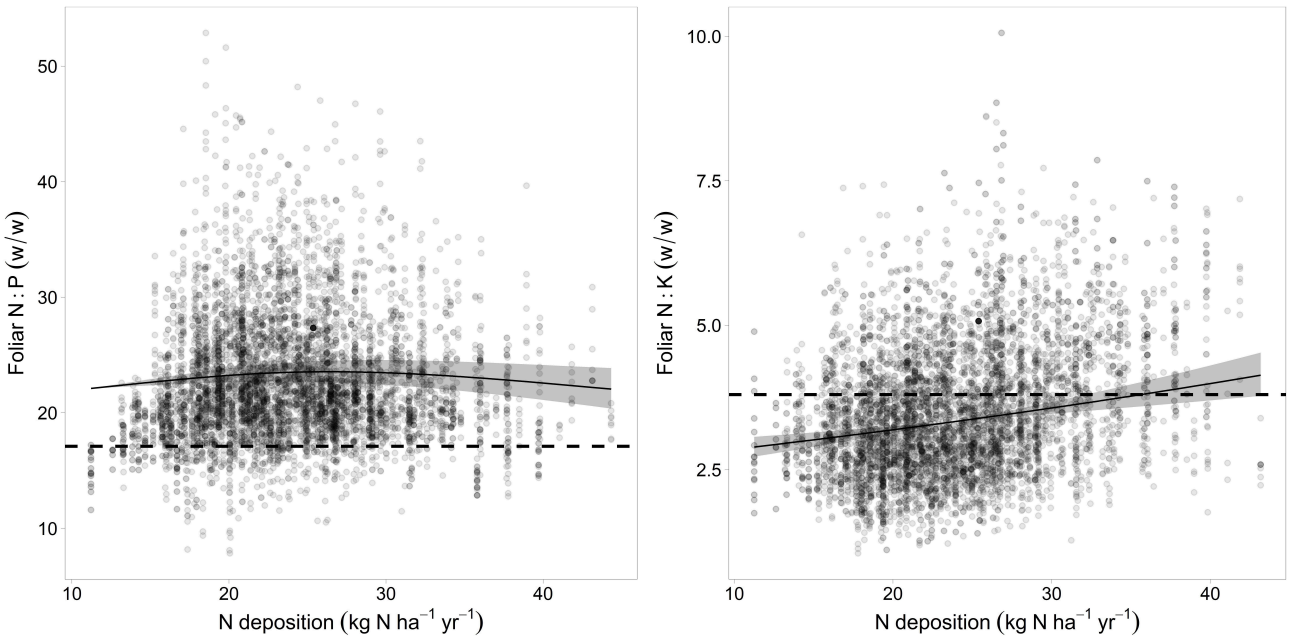


**FIGURE 5 |** Relation between N deposition and the N:P ratio (left) and N:K (right). The upper limit for harmonic ratios according to Flückiger and Braun (2003) are given as dotted lines. The gray bands indicate the 95% confidence interval.

ratios. While climate explains neither a trend nor a significant part of the variation of Ca concentrations (left part), it explains 57% of the observed negative time trend of N:K (right part).

## Leaf Weight

As increasing leaf weight is an important reason for the contrasting trends of nutrient concentrations and contents, explanatory variables for this variable were also assessed. Only fructification was a significant predictor for leaf weight (**Figure_Supplementary 17**). This relation was strongly negative. A decreasing leaf weight with increasing fructification would thus have led to smaller, not larger, leaves and does not give an explanation for the increasing leaf weight.

If leaf weight explained decreasing concentrations by dilution, its inclusion in the regression model should affect the coefficient for time. The regression models in **Table 1** were therefore recalculated adding leaf weight as additional covariate. The result is shown in **Table 6**. Only for foliar Mg the time trend got weaker after adjustment for leaf weight. This means that the time trend of Mg concentration may be partly explained by the increasing leaf weight while the others are not.

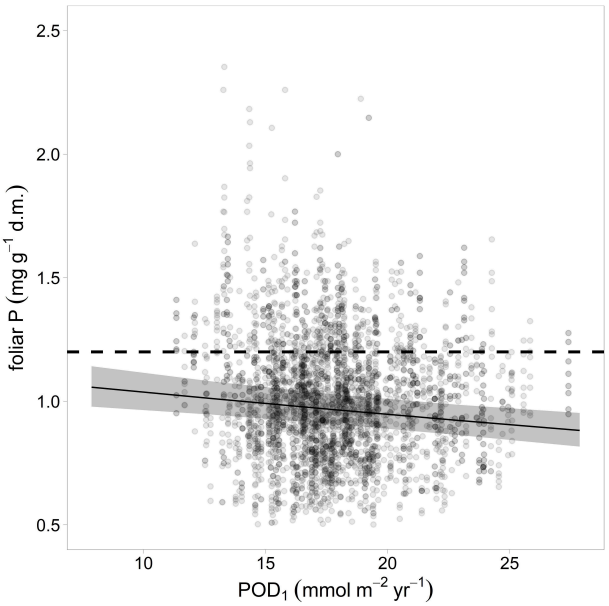


**FIGURE 6 |** Relation between ozone flux in the preceding year and foliar P. The gray bands indicate the 95% confidence interval. Ozone unit is Phytotoxic Ozone Dose at Threshold 1 (POD1).

**TABLE 4 |** Regression coefficients for the correlation of nutrient concentrations (left part) and nutrient contents (right) with the fructification of the current year (line c.y.) and of the previous year (line prev.y.).

| | | Concentrations (mg g$^{-1}$ d.m.) | | | Contents (mg leaf$^{-1}$) | | |
|---|---|---|---|---|---|---|---|
| | Fruit variable | Delta AIC | Coeff | SE | Delta AIC | Coeff | SE |
| N | c.y. | −22.5 | 0.0218 | 0.0072 | −213.8 | −0.3229 | 0.0215 |
| | prev.y. | | −0.0310 | 0.0060 | | −0.0914 | 0.0160 |
| P | c.y. | −11.8 | 0.0504 | 0.0099 | −185.3 | −0.3089 | 0.0216 |
| | prev.y. | | −0.0103 | 0.0082 | | −0.0638 | 0.0161 |
| K | c.y. | 8.2 | 0.0352 | 0.0144 | −137.6 | −0.3178 | 0.0255 |
| | prev.y. | | 0.0275 | 0.0119 | | −0.0266 | 0.0189 |
| Ca | c.y. | −106.8 | 0.2047 | 0.0189 | −10.7 | −0.1317 | 0.0262 |
| | prev.y. | | 0.0703 | 0.0151 | | 0.0073 | 0.0186 |
| Mg | c.y. | −81.0 | 0.2173 | 0.0234 | −8.9 | −0.1194 | 0.0301 |
| | prev.y. | | −0.0294 | 0.0194 | | −0.0787 | 0.0225 |

*DeltaAIC, AIC difference of the model with and without fruits. A negative difference signifies a significant fruit effect.*

**TABLE 5 |** Regression coefficients of the relation between foliar nutrient concentration and long-term average of fructification per tree (average year 2000–2015).

| Element | Coefficient for fructification | SE | deltaAIC |
|---|---|---|---|
| N | −0.0546 | 0.0228 | 2.00 |
| P | 0.1028 | 0.0315 | −3.40 |
| K | 0.0789 | 0.0461 | 3.43 |
| Mg | −0.0581 | 0.0741 | 4.74 |
| Ca | 0.0701 | 0.0578 | 4.39 |

# DISCUSSION

## Time Trend and Nutrient Levels

The negative time trend of foliar nutrient concentrations found in this study is in accordance with several other recent studies in Europe. Prietzel and Stetter (2010) observed decreasing P concentration in two Scots pine (*Pinus sylvestris*) plots between 1991 and 2007, especially at the plot with high N deposition. Talkner et al. (2015) report on a strong P decrease in leaves of *F. sylvatica* in the ICP Forests plots. Jonard et al. (2015) analyzed the development of all macronutrients in nine tree species and found P concentrations deteriorating especially in *F. sylvatica*, *Q. petraea*, and *P. sylvestris*, partially down to critical levels. In *F. sylvatica* also the N, Ca, and Mg concentrations decreased, in *Q. petraea* the N, Ca, and K concentrations decreased while the changes of element concentrations in leaves of *Q. robur* were not significant. The authors attribute this development to an increased demand due to increased tree productivity (dilution hypothesis) although no growth data are presented along with the nutrient data. For the data presented here, a dilution due to an increased growth cannot have caused the concentration decrease as in *F. sylvatica* the stem increment was decreasing during the observation time (Braun et al., 2017b). Leaf weight has increased but the regression analysis including leaf weight as a covariate argues against its significance as it did not change the time trend. The increase of nutrient concentration in years with high fructification as suggested by the positive correlation between number of fruits and foliar nutrient concentrations can be interpreted as enrichment in smaller leaves.

P concentrations have to be considered as strongly deficient in *F. sylvatica* which is also supported by the high N:P ratios. The ratios between N and P were clearly above the normal range and did not change regardless of decreasing N or P concentrations. This may be interpreted as a decrease of N uptake to keep the N:P ratios rather constant when P concentrations are low as it has been observed e.g., for *Abies pinsapo* by Blanes et al. (2012). Ratios of nutrient concentrations are independent from changes in leaf weight. While P concentrations were clearly deficient for European beech, K concentrations were still in the normal range on an average (Göttlein, 2015). N:K ratios can be considered normal, too. The Mg supply was decreasing and reached clearly deficient levels after 2003 which was also expressed in increasing visual Mg deficiency symptoms. On an average, the Mn concentrations are well within the normal range. Toxic levels, causing visible dark spots, have been detected in two plots using X-ray analysis at concentrations of 1,163 and 1,328 mg kg$^{-1}$ d.m., respectively (Flückiger and Braun, 2009) while Mn deficiency have been observed on two calcareous plots. No explanation can be given for the increasing leaf mass in the last 30 years. The increasing fructification can be excluded as reason as the relation of leaf mass with fructification was negative. There were no significant climate predictors for leaf mass but relations were found with leaf area: an increased leaf area was observed with increasing temperature and drought of the current season, and with decreasing drought of the previous season (not

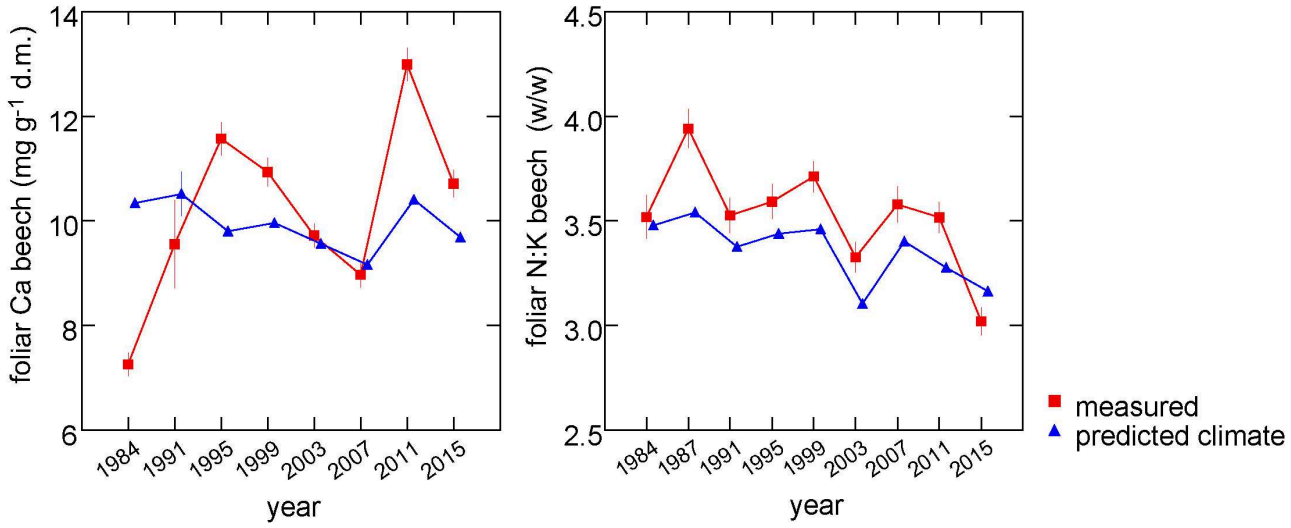


**FIGURE 7 |** Predictions from the regression model for Ca concentrations (left) and N:K ratio (right) with non-climatic variables set at their means (blue triangles). These predictions thus reflect the annual variations explained by climatic variables. The measured values are shown for comparison (red squares).

**TABLE 6 |** Comparison of the time coefficient of the regression model with the covariates listed in **Table 1** (left two columns) and including leaf weight as additional covariate (right columns).

| | Without leaf weight | | Including leaf weight | |
|---|---|---|---|---|
| **Element** | **Coeff time** | **SE** | **Coeff time** | **SE** |
| N | −0.0374 | 0.0045 | −0.0360 | 0.0047 |
| P | −0.0348 | 0.0078 | −0.0320 | 0.0074 |
| K | −0.0234 | 0.0130 | −0.0230 | 0.0130 |
| Mg | −0.0274 | 0.0200 | −0.0161 | 0.0188 |
| Ca | 0.0245 | 0.0452 | 0.0324 | 0.0034 |

shown). A possible explanation could be increased $CO_2$ in the atmosphere. In a FACE experiment with poplars, increased $CO_2$ led to a larger area per leaf and heavier leaves while the specific leaf area decreased or remained constant (Gielen et al., 2001). The latter finding was confirmed in a meta-analysis by Ainsworth and Long (2005).

## Nitrogen Deposition

Our results suggest that elevated nitrogen deposition is an important predictor for nutrition of European beech. This is in accordance with experimental evidence and gradient studies. In an N addition experiment, Balsberg-Påhlsson (1992) found a decrease of the concentrations of P and Cu in beech leaves in response to N fertilization with 40 kg N $ha^{-1}$ $yr^{-1}$ over 5 years. The fertilizer contained also small amounts of Ca and Mg. Although foliar K concentrations were unaffected, the increased N:K ratio suggests a changed K nutrition. Flückiger and Braun (1999) observed decreases in the concentrations of P, K, Mg, and Ca due to N addition in European beech and Norway spruce. In areas with high N input in the Netherlands, Houdijk and Roelofs (1993) observed low P, but also decreased Mg concentrations in Douglas fir needles.

Aber et al. (1989) suggested that P deficiency or a shortage of water limit the biotic functions when N saturation of forest ecosystems is reached. In the beginning of the saturation process, the biomass may be increasing. In our 74 European beech forests, the observed growth stimulation by nitrogen was small and detectable only at N inputs of <20 kg N $ha^{-1}$ $yr^{-1}$. In general, the stem increment has been decreasing during the last decades (Braun et al., 2017b). In the nitrogen saturation stage, an impairment of the root system (Aber et al., 1989; Boxman et al., 1998a) or of mycorrhiza (Rühling and Tyler, 1991; Wallander and Nylund, 1992) may reduce nutrient uptake and lead to reduced growth (Boxman et al., 1998a; Jönsson et al., 2004; Magill et al., 2004). Increased soil solution nitrate concentrations are also an indicator of the saturation stage. In the plots presented in this study, nitrate concentrations in 20–40 cm depth in the year 2015 were on an average 1.1 mg N $l^{-1}$ which is much higher than the limit of 0.2 mg N $l^{-1}$ for ecosystems unaffected by nitrogen set in the Mapping Manual of the UNECE Air Convention (CLRTAP, 2017). On an average, $NH^+$-N was observed in soil solution was only 0.011 mg N $l^{-1}$ (median) which suggests a rapid nitrification. In 15 of the beech stands examined in the present study, de Witte et al. (2017) observed that mycorrhizal species which are important for P uptake are reduced at higher N load. Such an impairment of mycorrhiza may lead to reductions not only in P nutrition but also in supply of other mineral nutrients—including N—and water.

Excess N deposition has certainly contributed to the low levels of P and K nutrition and the wide N:P ratios in leaves. The changing relations between foliar N and P with N deposition suggest progressive N saturation as proposed by Emmett (2007). Although N deposition has decreased by 25% during the observed period it is still considerably higher than the critical

loads for nitrogen. The average N deposition in beech plots in 2010 was 24.6 kg N $ha^{-1}$ $yr^{-1}$ (Braun et al., 2017b). While effects of this decrease on soil solution chemistry are already visible (Braun, 2018), biological processes respond much more slowly (Stevens, 2016; Verstraeten et al., 2017).

## Soil Chemistry

Favorable conditions for high K uptake were high exchangeable K concentrations in soil. High foliar P concentrations or low N:P ratios were observed at high acid extractable P concentration in the soil or at low pH. These positive relationships were, however, only valid when the nitrogen deposition was low. The observed interactions between N deposition and soil chemical parameters may beinterpreted as a reduced K and P uptake at higher N deposition. In our data there was no indication of K limitation in calcareous soils by the K-Ca-antagonism as discussed by Mellert and Ewald (2014).Lime stock of the soil was not a significant predictor for foliar K.

The significant decrease in BC/Al ratio in soil solution between 1998 and 2017 indicates an increase of acidification (Sverdrup and Warfvinge, 1993). The concentration of all base cations decreased significantly, but only foliar Mg was directly related to soil solution chemistry. This change in soil solution chemistry may therefore have contributed to the decrease in foliar Mg. Relations of foliar Mg with soil concentrations have been shown both for exchangeable Mg in soil (Ende and Evers, 1997) and for Mg in soil solution (Matzner et al., 1989). The significance of soil acidification for visible symptoms of Mg deficiency has been reported for Norway spruce in Germany e.g., by Cape et al. (1990) and Elling et al. (2007). For the chemistry of the solid soil phase no replicate in time is available for all plots. In a subset of plots, however, also a decrease in base saturation and in pH($CaCl_2$) was observed between 1996 and 2005 (Flückiger and Braun, 2009) while concentrations of citric-acid extractable P were stable (unpublished results).

The relation between foliar P concentration and pH($CaCl_2$) was linear which is not in accordance to the expectations from soil mineralogy. In acid soils P is immobilized as Al- and Fe-phosphates (Variscit, Strengit), in alkaline soils as Ca-phosphates (Apatite; Schachtschabel et al., 1998; Mellert and Ewald, 2014), with the highest availability at medium pH values. Other studies observed also a lower P availability in calcareous soils. Lower foliar P concentrations have been reported for European beech stands on limestone by Calvaruso et al. (2017), and a low P nutrition has been suggested to be responsible for a lower vitality of beech in the Bavarian alps (Ewald, 2000).

We found a clear correlation between foliar P concentrations and citric acid-soluble P stock in the soil This is in accordance to the results by Fäth et al. (2019) who also found that citrate extractable P is the best soil chemical predictor for foliar P. However, the level needed for sufficient foliar P nutrition in the present study (200 kg $P_{citr}$ $ha^{-1}$ for 0–40 cm stocks) is much higher than in the study of Fäth et al. (2019) who observed sufficient foliar P concentrations in beech at 43 kg $P_{citr}$ $ha^{-1}$ for 0–10 cm stocks and 50 kg $P_{citr}$ $ha^{-1}$, respectively, for 0–80 cm stocks. This comparison suggests that the P nutrition of beech in Switzerland is much lower even when corrected for soil P stocks.

## Climate

No temperature effects were found for N, P, and K concentrations in beech leaves which would have been expected for the actively absorbed elements (BassiriRad, 2000; Marschner, 2012). The climate effects observed in the present dataset can be summarized as increase either at high temperatures or under drought. This holds true for Mg which was higher when the minimum water balance of the previous season was low. Ca was either increased at warmer temperatures of the previous season or when the current spring was dry except on soils with high base saturation. These results may be explained by either an increased uptake when the transpiration stream is high due to high evaporative demand or by a concentration effect when drought leads to smaller leaves. The latter process has been proposed by e.g., Sardans and Peñuelas (2007) and Sardans et al. (2008) who suggested enrichment effects in Mediterranean ecosystems through reduced biomass. The decreasing N:K ratio with increasing drought is, however, not compatible with the concentration hypothesis as ratios are independent from the magnitude of the reference. In the case of N:K, drought is explaining a significant part of the observed increase. A decreased availability of nutrients in the soil as a result of reduced moisture as proposed by Kreuzwieser and Gessler (2010) would have led to decreased nutrient concentrations under dry conditions which was not observed.

## Ozone

Ozone flux was negatively related with foliar P, as a trend also with N. These changes in foliar nutrients may be a result of a decreased carbon allocation to the roots (Samuelson and Kelly, 1996; review by Cooley and Manning, 1987) affecting the symbiosis with the mycorrhizal fungi which depend on these photosynthates. Ozone was a significant predictor for the composition of ectomycorrhiza community in a gradient study in the same beech plots used for the current study (de Witte et al., 2017). Effects of ozone on nutrient uptake may therefore be expected and are in accordance to the results of Wang et al. (2015) who found decreased needle P concentrations after chamber fumigation with 60 ppb ozone and changes in the ectomycorrhizal community in hybrid larch (*L. gmelinii var. japonica _ L. kaempferi*). In the Kranzberg ozone fumigation experiment labeled N was also more allocated to the roots of fumigated trees and showed up less in the leaves of mature beech and Norway spruce (Weigt et al., 2015). However, the number of vital ectomycorrhizal root tips and mycorrhizal species richness increased in the fumigated beeches (Grebenc and Kraigher, 2007).

# CONCLUSIONS

The presented results of a 30 years time series of tree nutrition of *Fagus sylvatica* show effects of excess nitrogen deposition, of soil chemistry and of climate on tree nutrition, with interactions between the various predictors. Soil acidification is likely to have contributed to the decrease of the Mg concentration in beech leaves. Leaf weight increased in parallel to the reduction of foliar concentrations of N, P, and K. This increase in leaf

weight explained parts of the time trend in Mg, not in the other nutrients. An increase of foliar concentrations by drought was observed for Mg and for Ca on base poor soils. Climate predictors explained the negative time trend in the case of the N:K ratio, but the data show no significant effect on the actively absorbed elements N and P. The drastic increase of fructification in beech has probably contributed to the annual variation in Ca concentrations but cannot be responsible for the changes in time as fructification decreased leaf size and most elements were positively, not negatively, related with the number of fruits. The observed interactions between N deposition and soil chemical parameters indicate a reduced nutrient uptake at higher N deposition. A decreased stem increment in parallel to the decreased nutrient concentrations contradicts the "dilution by increased growth" hypothesis. The high soil nitrate concentrations and the changing relations between foliar N and P with N deposition favor also the saturation hypothesis. Saturation develops slowly over time (Aber et al., 1998; Emmett, 2007). Nutrient imbalances are important indicators for this process. It has been shown that negative effects of increased nitrogen deposition on tree development often starts with nutrient imbalances, with consequences for e.g., parasite infestations (Flückiger and Braun, 1998; Eatough Jones et al., 2004) or drought induced mortality (Magill et al., 2004). With weakened resistances against abiotic or biotic incidents, external events may trigger visible decline processes. The present study supports the hypothesis that the changes in plant nutrition are a continuous process in which the nitrogen deposition plays a prominent role.

## DATA AVAILABILITY STATEMENT

The datasets generated for this study are available on request to the corresponding author.

## AUTHOR CONTRIBUTIONS

SB: forest observation, data analysis, and writing of manuscript. CS: data analysis. BR: model of nitrogen deposition and climate data.

## FUNDING

This work was supported by Cantonal forestry departments of the cantons AG, BE, BL, BS, GR, TG, and ZH, environmental agencies of Central Switzerland Federal Office for the Environment, Berne, Switzerland.

## ACKNOWLEDGMENTS

The authors thank the Swiss Cantons of Zurich, Bern, Zug, Solothurn, Basel-Stadt and Basel-Landschaft, Aargau and Thurgau for financing the long-term forest observations and the forest authorities for their interest in our work. We thank also the Federal Office for the Environment for financial support of the data analysis and helpful comments during the preparation of this manuscript, Jan Remund from Meteotest, for the interpolation of meteorological data, Simon Tresch for his help in R graphics, Daniel Lüdecke for extensive advice in the use of the R package ggeffects, the team of the Institute for Applied Plant Biology for field and lab work as well as all the foresters and forest owners enabling the long-term forest observation. I also thank a reviewer for very careful and helpful comments.

## SUPPLEMENTARY MATERIAL

The Supplementary Material for this article can be found online at: https://www.frontiersin.org/articles/10.3389/ffgc.2020.00033/full#supplementary-material

## REFERENCES

Aber, J., McDowell, W., Nadelhoffer, K., Magill, A., Berntson, G., Kamakea, M., et al. (1998). Nitrogen saturation in temperate forest ecosystems. *BioScience* 48, 921–934. doi: 10.2307/1313296

Aber, J. D., Nadelhoffer, K. J., Steudler, P., and Melillo, J. M. (1989). Nitrogen saturation in northern forest ecosystems. *BioScience* 39, 378–386. doi: 10.2307/1311067

Ainsworth, E. A., and Long, S. P. (2005). What have we learned from 15 years of free-air CO2 enrichment (FACE)? A meta-analytic review of the responses of photosynthesis, canopy. *New Phytol.* 165, 351–371. doi: 10.1111/j.1469-8137.2004.01224.x

Augustin, S., and Achermann, B. (2012). Deposition von Luftschadstoffen in der Schweiz: Entwicklung, aktueller Stand und Bewertung. *Schweizerische Zeitschrift Forstwesen* 163, 323–330. doi: 10.3188/szf.2012.0323

Balsberg-Påhlsson, A. (1992). Influence of nitrogen fertilization on minerals, carbohydrates, amino acids and phenolic compounds in beech (*Fagus sylvatica*) leaves. *Tree Physiol.* 10, 93–100. doi: 10.1093/treephys/10.1.93

BassiriRad, H. (2000). Research review: kinetics of nutrient uptake by roots: responses to global change. *New Phytol.* 147, 155–169. doi: 10.1046/j.1469-8137.2000.00682.x

Bates, D., Maechler, M., Bolker, B., and Walker, S. (2015). Fitting linear mixed-effects models using lme4. *J. Stat. Softw.* 67, 1–48. doi: 10.18637/jss.v067.i01

Blanes, C., Viñegla, B., Merino, J., and Carreira, J. A. (2013). Nutritional status of Abies pinsapo forests along a nitrogen deposition gradient: do C/N/P stoichiometric shifts modify photosynthetic nutrient use efficiency? *Oecologia* 171, 797–808. doi: 10.1007/s00442-012-2454-1

Blanes, M. C., Emmett, B. A., Viñegla, B., and Carreira, J. A. (2012). Alleviation of P limitation makes tree roots competitive for N against microbes in a N-saturated conifer forest: a test through P fertilization and N-15 labelling. *Soil Biol. Biochem.* 48, 51–59. doi: 10.1016/j.soilbio.2012.01.012

Boxman, A. W., Blanck, K., Brandrud, T. E., Emmet, B. A., Gundersen, P., Hogervorst, R. F., et al. (1998b). Vegetation and soil biota response to experimentally-changed nitrogen inputs in coniferous forest ecosystems of the NITREX project. *For. Ecol. Manage.* 101, 65–79. doi: 10.1016/S0378-1127(97)00126-6

Boxman, A. W., van der Ven, P. J. M., and Roelofs, J. G. M. (1998a). Ecosystem recovery after a decrease in nitrogen input to a Scots pine stand at Ysselsteyn, The Netherlands. *For. Ecol. Manage.* 101, 155–163. doi: 10.1016/S0378-1127(97)00132-1

Braun, S. (2018). *Untersuchungen über die Zusammensetzung der Bodenlösung*. Bericht: Institut für Angewandte Pflanzenbiologie. Avaialble online at: http://www.bafu.admin.ch/wald.

Braun, S., Achermann, B., De Marco, A., Pleijel, H., Karlsson, P. E., Rihm, B., et al. (2017a). Epdemiological analysis of air pollution effects on vegetation: critical evaluation and recommendations. *Sci. Total Environ.* 603, 785–792. doi: 10.1016/j.scitotenv.2017.02.225

Braun, S., Hopf, S., and De Witte, L. (2018). *Wie Geht es Unserem Wald? 34 Jahre Jahre Walddauerbeobachtung*. Schönenbuch: Institut für Angewandte Pflanzenbiologie.

Braun, S., Schindler, C., and Rihm, B. (2014). Growth losses in Swiss forests caused by ozone: epidemiological data analysis of stem increment data of *Fagus sylvatica* L. and *Picea abies* Karst. *Environ. Pollut.* 192, 129–138. doi: 10.1016/j.envpol.2014.05.016

Braun, S., Schindler, C., and Rihm, B. (2017b). Growth trends of beech and Norway spruce in Switzerland: the role of nitrogen deposition, ozone, mineral nutrition and climate. *Sci. Total Environ.* 599–600, 637–646. doi: 10.1016/j.scitotenv.2017.04.230

Braun, S., Schindler, C., Volz, R., and Flückiger, W. (2003). Forest damage by the storm "Lothar" in permanent observation plots in Switzerland: the significance of soil acidification and nitrogen deposition. *Water Air Soil Pollut.* 142, 327–340. doi: 10.1023/A:1022088806060

Büker, P., Morissey, T., Briolat, A., Falk, R., Simpson, D., Tuovinen, J.-P., et al. (2012). DO3SE modelling of soil moisture to determine ozone flux to European forest trees. *Atmospheric Chem. Phys.* 12, 5537–5562. doi: 10.5194/acp-12-5537-2012

Calvaruso, C., Kirchen, G., Saint-André, L., Redon, P. O., and Turpault, M. P. (2017). Relationship between soil nutritive resources and the growth and mineral nutrition of a beech (*Fagus sylvatica*) stand along a soil sequence. *CATENA* 155, 156–169. doi: 10.1016/j.catena.2017.03.013

Cape, J. N., Freersmith, P. H., Paterson, I. S., Parkinson, J. A., and Wolfenden, J. (1990). TheNutritional-Status of Picea-Abies (L) Karst Across Europe, and implications for forest decline. *Trees Struct. Funct.* 4, 211–224. doi: 10.1007/BF00225318

Chaboussou, F. (1973). *Le Rôle du Potassium et de L'équilibre Cationique Dans la Résistance de la Plante Aux Parasites et Aux Maladies*. Au Service de l'Agriculture (SCPA) No 2, Document technique 16, Pont-de-la-Maye, 1–26.

Christina, M., Le Maire, G., Battie-Laclau, P., Nouvellon, Y., Bouillet, J. P., Jourdan, C., et al. (2015). Measured and modeled interactive effects of potassium deficiency and water deficit on gross primary productivity and light-use efficiency in Eucalyptus grandis plantations. *Glob. Change Biol.* 21, 2022–2039. doi: 10.1111/gcb.12817

CLRTAP (2017). *Mapping Critical Loads for Ecosytems. Chapter V of Manual on Methodologies and Criteria for Modelling and Mapping Critical Loads and Levels and Air Pollution Effects, Risks and Trends*. UNECE Convention on Long-range Transboundary Air Pollution.

Cooley, D. R., and Manning, W. J. (1987). The impact of ozone on assimilate partitioning in plants: a review. *Environ. Pollut.* 47, 95–113. doi: 10.1016/0269-7491(87)90040-6

de Witte, L. C., Rosenstock, N. P., van der Linde, S., and Braun, S. (2017). Nitrogen deposition changes ectomycorrhizal communities in Swiss beech forests and thereby hampers nutrient uptake. *Sci. Total Environ.* 605–606, 1083–1096. doi: 10.1016/j.scitotenv.2017.06.142

Eatough Jones, M., Paine, T. D., Fenn, M. E., and Poth, M. A. (2004). Influence of ozone and nitrogen deposition on bark beetle activity under drought conditions. *For. Ecol. Manage.* 200, 67–76. doi: 10.1016/j.foreco.2004.06.003

Elling, W., Heber, U., Polle, A., and Beese, F. (2007). *Schädigung von Waldökosystemen. Auswirkungen athropogener Umweltveränderungen und Schutzmassnahmen*. München: Elsevier, Spektrum Akademischer Verlag.

Emberson, L. D., Ashmore, M. R., Cambridge, H. M., Simpson, D., and Tuovinen, J.-P. (2000). Modelling stomatal ozone flux across Europe. *Environ. Pollut.* 109, 403–414. doi: 10.1016/S0269-7491(00)00043-9

Emmett, B. (2007). Nitrogen saturation of terrestrial ecosystems: some recent findings and their implications for our conceptual framework. *Water Air Soil Pollut. Focus* 7, 99–109. doi: 10.1007/s11267-006-9103-9

Ende, H. P., and Evers, F. H. (1997). "Visual magnesium deficiency symptoms (coniferous, deciduous trees) and threshold values (foliar, soil)," in *Magnesium Deficiency in Forest Ecosystems*, eds R. F. Hüttl and W. Schaaf (Dordrecht: Kluwer Academic Publishers), 2–22.

Ewald, J. (2000). Ist Phosphormangel für die geringe Vitalität von Buchen (*Fagus sylvatica* L.) in den Bayerischen Alpen verantwortlich? *Forstwissenschaftliches Centralblatt* 119, 276–296. doi: 10.1007/BF02769143

Fäth, J., Kohlpaintner, M., Blum, U., Göttlein, A., and Mellert, K. H. (2019). Assessing phosphorus nutrition of the main European tree species by simple soil extraction methods. *For. Ecol. Manage.* 432, 895–901. doi: 10.1016/j.foreco.2018.10.007

Flückiger, W., and Braun, S. (1998). Nitrogen deposition in Swiss forests and its possible relevance for leaf nutrient status, parasite attacks and soil acidification. *Environ. Pollut.* 102, 69–76. doi: 10.1016/S0269-7491(98)80017-1

Flückiger, W., and Braun, S. (1999). Nitrogen and its effects on growth, nutrient status and parasite attacks in beech and Norway spruce. *Water Air Soil Pollut.* 116, 99–110. doi: 10.1023/A:1005298609109

Flückiger, W., and Braun, S. (2003). "Critical limits for nutrient concentrations and ratios for forest trees - a comment. Critical Loads for Nitrogen," in *Expert Workshop on Critical Loads of Nitrogen, Proceedings*, eds B. Achermann and R. Bobbink (Berne: Swiss Agency for the Environment, Forests and Landscape SAEFL), 273–280.

Flückiger, W., and Braun, S. (2009). *Wie Geht es Unserem Wald? Bericht 3*. Schönenbuch: Institut für Angewandte Pflanzenbiologie.

Fox, J., and Weisberg, S. (2011). *An {R} Companion to Applied Edition*. Thousand Oaks, CA: Sage.

Gielen, B., Calfapietra, C., Sabatti, M., and Ceulemans, R. (2001). Leaf area dynamics in a closed poplar plantation under free-air carbon dioxide enrichment. *Tree Physiol.* 21, 1245–1255. doi: 10.1093/treephys/21.17.1245

Glenn, N. D. (2007). *Age, Period and Cohort Effects*. In: ed G. Ritzer. Wiley.

Göttlein, A. (2015). Grenzwertbereiche für die ernährungsdiagostische Einwertung der Hauptbaumarten Fichte, Kiefer, Eiche und Buche. *Allg. Forst Jagdz.* 186, 110–116.

Grebenc, T., and Kraigher, H. (2007). Changes in the community of ectomycorrhizal fungi and increased fine root number under adult beech trees chronically fumigated with double ambient ozone concentration. *Plant Biol.* 9, 279–287. doi: 10.1055/s-2006-924489

Hornburg, V., and Lüer, B. (1999). Vergleich zwischen Total- und königswasserextrahierbaren Elementgehalten in natürlichen Böden und Sedimenten. *J. Plant Nutr. Soil Sci.* 162, 131–137. doi: 10.1002/(SICI)1522-2624(199903)162:2<131::AID-JPLN131>3.0.CO;2-1

Hort, R., Gupta, S., and Häni, H. (1998). "Methodenbuch für Boden-, Pflanzen- und Lysimeterwasseruntersuchungen," in *Schriftenreihe der FAL* (Zürich-Reckenholz; Eidgenössische Forschungsanstalt für Agrarökologie und Landbau; Liebefeld-Bern: Institut für Umweltschutz und Landwirtschaft), 27, 1–228.

Houdijk, A., and Roelofs, J. G. M. (1993). The effects of atmospheric nitrogen deposition and soil chemistry on the nutritional status of *Pseudotsuga menziesii*, *Pinus nigra* and *Pinus sylvestris*. *Environ. Pollut.* 80, 79–84. doi: 10.1016/0269-7491(93)90013-E

ICP Forests (2016). Manual on Methods and Criteria for Hamonized Sampling, Assessment, Monitoring and Analysis of the Effects of Air Pollution on Forests. Revision 2016. Eberswalde: Johann Heinrich von Thünen Institute.

Jonard, M., Fürst, A., Verstraeten, A., Thimonier, A., Timmermann, V., Potocic, N., et al. (2015). Tree mineral nutrition is deteriorating in Europe. *Glob. Change Biol.* 418–430. doi: 10.1111/gcb.12657,

Jönsson, A. M., Rosengren, U., and Nihlgård, B. (2004). Excess nitrogen affects the frost sensitivity of the inner bark of Norway spruce. *Ann. Forest Sci.* 61, 293–298. doi: 10.1051/forest:2004022

Kreuzwieser, J., and Gessler, A. (2010). Global climate change and tree nutrition: influence of water availability. *Tree Physiol.* 30, 1221–1234. doi: 10.1093/treephys/tpq055

Lüdecke, D. (2018). *ggeffects: Create Tidy Data Frames of Marginal Effects for 'ggplot' From Model Outputs*. R package version 0.3.3.

Magill, A., Aber, J. D., Currie, W. S., Nadelhoffer, K. J., Martin, M. E., McDowell, W. H., et al. (2004). Ecosystem response to 15 years of chronic nitrogen additions at the Harvard Forest LTER, Massachusetts, USA. *For. Ecol. Manage.* 196, 7–28. doi: 10.1016/j.foreco.2004.03.033

Manghabati, H., Kohlpaintner, M., Ettl, R., Mellert, K.-H., Blum, U., and Göttlein, A. (2018). Correlating phosphorus extracted by simple soil extraction methods with foliar phosphorus concentrations of *Picea abies (L.) H. Karst* and *Fagus sylvatica* (L.). *J. Plant Nutr. Soil Sci.* 181, 547–556. doi: 10.1002/jpln.201700536

Marschner, P. (2012). *Marschner's Mineral Nutrition of Higher Plants*. Amsterdam; Boston; Heidelberg: Elsevier.

Matzner, E., Blanck, K., Hartmann, G., and Stock, R. (1989). "Needle chlorosis pattern in relation to soil chemical properties in two Norway spruce (*Picea abies*, Karst) forests of the German Harz mountains," in *IUFRO Conference:*

*Air Pollution and Forest Decline*, eds J. B. Bucher and I. Bucher-Wallin (Birmensdorf: Interlaken), 195–199.

McNulty, S., Boggs, J. L., Aber, J. D., and Rustad, L. E. (2017). Spruce-fir forest changes during a 30- year nitrogen saturation experiment. *Sci. Total Environ.* 605–606, 376–390. doi: 10.1016/j.scitotenv.2017.06.147

Mellert, K. H., and Ewald, J. (2014). Nutrient limitation and site-related growth potential of Norway spruce (*Picea abies* [L.] Karst) in the Bavarian Alps. *Eur. J. For. Res.* 133, 433–451. doi: 10.1007/s10342-013-0775-1

Menge, D. N. L., and Field, C. B. (2007). Simulated global changes alter phosphorus demand in annual grassland. *Glob. Change Biol.* 13, 2582–2591. doi: 10.1111/j.1365-2486.2007.01456.x

Nilsson, L. O., and Wallander, H. (2003). Production of external mycelium by ectomycorrhizal fungi 811 in a Norway spruce forest was reduced in response to nitrogen fertilization. *New Phytol.* 158, 409–418. doi: 10.1046/j.1469-8137.2003.00728.x

Pretzsch, H., Biber, P., Schütze, G., Uhl, E., and Rötzer, T. (2014). Forest stand growth dynamics in Central Europe have accelerated since 1870. *Nat. Commun.* 5:4947. doi: 10.1038/ncomms5967

Prietzel, J., and Stetter, U. (2010). Long-term trends of phosphorus nutrition and topsoil phosphorus stocks in unfertilized and fertilized Scots pine (*Pinus sylvestris*) stands at two sites in Southern Germany. *For. Ecol. Manage.* 259, 1141–1150. doi: 10.1016/j.foreco.2009.12.030

Rihm, B., and Achermann, B. (2016). *Critical Loads of Nitrogen and Their Exceedances, Swiss Contribution to the Effects-Oriented Work Programme Under the Convention on Long Range Transboundary Air Pollution (UNECE)*. Berne: Federal Office for the Environment (FOEN), 1–78.

Rühling, A., and Tyler, G. (1991). Effects of simulated nitrogen deposition to the forest floor on the macrofungal flora of a beech forest. *Ambio* 20, 261–263.

Samuelson, L. J., and Kelly, J. M. (1996). Carbon partitioning and allocation in northern red oak seedlings and mature trees in response to ozone. *Tree Physiol.* 16, 853–858. doi: 10.1093/treephys/16.10.853

Sardans, J., and Peñuelas, J. (2007). Drought changes phosphorus and potassium accumulation patterns in an evergreen Mediterranean forest. *Funct. Ecol.* 21, 191–201. doi: 10.1111/j.1365-2435.2007.01247.x

Sardans, J., Peñuelas, J., Coll, M., Vayreda, J., and Rivas-Ubach, A. (2012). Stoichiometry of potassium is largely determined by water availability and growth in Catalonian forests. *Funct. Ecol.* 26, 1077–1089. doi: 10.1111/j.1365-2435.2012.02023.x

Sardans, J., Peñuelas, J., and Ogaya, R. (2008). Drought's impact on Ca, Fe, Mg, Mo and S concentration and accumulation patterns in the plants and soil of a Mediterranean evergreen Quercus ilex forest. *Biogeochemistry* 87, 49–69. doi: 10.1007/s10533-007-9167-2

Schachtschabel, P., Blume, H. P., Brümmer, G., Hartge, K. H., and Schwertmann, U. (1998). *Lehrbuch der Bodenkunde*. Stuttgart: Enke.

Schulla, J. (2013). *Model Description WaSIM (Water balance Simulation Model)*. Zurich. Available online at: http://www.wasim.ch/de/products/wasim_description.htm

Sponagel, H., Grottenthaler, W., and Hartmann, K.-J. (2005). *Bodenkundliche Kartieranleitung*. Hannover: E.Schweizerbart'sche Verlagsbuchhandlung.

St. Clair, S. B. S., Carlson, J. E., and Lynch, J. P. (2005). Evidence for oxidative stress in sugar maple stands growing on acidic, nutrient imbalanced forest soils. *Oecologia* 145, 258–269. doi: 10.1007/s00442-005-0121-5

Stevens, C. J. (2016). How long do ecosystems take to recover from atmospheric nitrogen deposition? *Biol. Conserv.* 200, 160–167. doi: 10.1016/j.biocon.2016.06.005

Suz, L. M., Barsoum, N., Benham, S., Dietrich, H. P., Fetzer, K. D., Fischer, R., et al. (2014). Environmental drivers of ectomycorrhizal communities in Europe's temperate oak forests. *Mol. Ecol.* 23, 5628–5644. doi: 10.1111/mec.12947

Sverdrup, H., and Warfvinge, P. (1993). *The Effect of Soil Acidification on the Growth of Trees, Grass and Herbs as Expressed by the (Ca+Mg+K)/Al Ratio. Reports in Ecology and Environmental Engineering*. Lund University, Department of Chemical Engineering II, Lund, 1–108.

Talkner, U., Meiwes, K. J., Potoèiæ, N., Seletkoviæ, I., Cools, N., De Vos, B., et al. (2015). Phosphorus nutrition of Beech (*Fagus sylvatica*) is decreasing in Europe. *Ann. For. Sci* 72, 919–928. doi: 10.1007/s13595-015-0459-8

Thimonier, A., Kosonen, Z., Braun, S., Rihm, B., Schleppi, P., Schmitt, M., et al. (2018). Total depositition of nitrogen in Swiss forests: comparison of assessment methods and evaluation of changes over two decades. *Atmos. Environ.* 198, 335–350. doi: 10.1016/j.atmosenv.2018.10.051

UNECE (2017). *Mapping Critical Levels for Vegetation. Revised Chapter 3 of the UNECE Manual on Methodologies and Criteria for Modelling and Mapping Critical Loads and Levels and Air Pollution Effects, Risks and Trends*. Prepared under the Convention on Long-range Transboundary Air Pollution (UNECE) by the International Cooperative Programme on Effects of Air Pollution on Natural Vegetation and Crops (Bangor: Center for Ecology & Hydrology (CEH); ICP Vegetation), 1–66.

van den Burg, J. (1985). *Foliar Analysis for Determination of Tree Nutrient Status - A Compilation of Literature Data*. Wageningen: Rijksinstituut voor Onderzoek in de Bos- en Landschapsbouw "De Dorschkamp"; Rapport.

van den Burg, J. (1990). *Foliar Analysis for Determination of Tree Nutrient Status - A Compilation of Literature Data*. Wageningen: Rijksinstituut voor Onderzoek in de Bos- en Landschapsbouw "De Dorschkamp"; Rapport.

Verstraeten, A., Neirynck, J., Cools, N., Roskams, P., Louette, G., de Neve, S., et al. (2017). Multiple nitrogen saturation indicators yield contradicting conclusions on improving nitrogen status of temperate forests. *Ecol. Indicators* 82, 451–462. doi: 10.1016/j.ecolind.2017.07.034

Vitousek, P. M., Porder, S., Houlton, B. Z., and Chadwick, O. A. (2010). Terrestrial phosphorus limitation: mechanisms, implications, and nitrogen-phosphorus interactions. *Ecol. Appl.* 20, 5–15. doi: 10.1890/08-0127.1

Walinga, I., van der Lee, J. J., Houba, V. J., van Vark, W., and Novozamsky, I. (1995). *Plant Analysis Manual*. Dordrecht: Kluwer Academic Publishers.

Wallander, H., and Nylund, J. E. (1992). Effects of excess nitrogen and phosphorus starvation on the extramatrical mycelium of ectomycorrhizas of *Pinus sylvestris* L. *New Phytol.* 120, 495–503. doi: 10.1111/j.1469-8137.1992.tb01798.x

Wang, X., Qu, L., Mao, Q., Watanabe, M., Hoshika, Y., Koyama, A., et al. (2015). Ectomycorrhizal colonization and growth of the hybrid larch F1 under elevated $CO_2$ and $O_3$. *Environ. Pollut.* 197, 116–126. doi: 10.1016/j.envpol.2014.11.031

Weigt, R. B., Häberle, K. H., Rötzer, T., and Matyssek, R. (2015). Whole-tree seasonal nitrogen uptake and partitioning in adult *Fagus sylvatica* L. and *Picea abies* L. [Karst.] trees exposed to elevated ground-level ozone. *Environ. Pollut.* 196, 511–517. doi: 10.1016/j.envpol.2014.06.032

Wickham, H. (2009). *ggplot2: Elegant Graphics for Data Analysis*. New York, NY: Springer-Verlag.

**Conflict of Interest:** SB was employed by the company Institute for Applied Plant Biology AG, BR by the company Meteotest AG.

The remaining author declares that the research was conducted in the absence of any commercial or financial relationships that could be construed as a potential conflict of interest.

frontiers in Forests and Global Change

ORIGINAL RESEARCH
published: 05 May 2020
doi: 10.3389/ffgc.2020.00048

# Soil Phosphorus Translocation via Preferential Flow Pathways: A Comparison of Two Sites With Different Phosphorus Stocks

*Vera Makowski*, Stefan Julich, Karl-Heinz Feger and Dorit Julich*

*Institute of Soil Science and Site Ecology, Technische Universität Dresden, Tharandt, Germany*

Weather events where a dry period is followed by a heavy rainfall event appear to affect phosphorus (P) exports through preferential flow pathways from forest soils. Export rates also depend on the P stocks. To explore this, we installed zero-tension lysimeters in three trenches at two sites with contrasting soil P stocks. Lysimeters were installed in three different depths (topsoil, subsoil and deep subsoil) to explore P depth transport. We covered the forest floor above the lysimeters with tarpaulins to simulate a dry period and afterward artificially irrigated the area. This experiment was repeated three times at each site. Lysimeter samples were analyzed for concentrations of total P, organic and inorganic dissolved P and particle bound P (>0.45 μm). Loads of P and flow rates were calculated. Results reveal clear differences between sites, individual events and soil depths. At both sites, concentrations and loads of P in the topsoil lysimeters were higher than those in the subsoil. This difference was most evident at the low P site and underlines its efficiency of recycling nutrients. Dissolved inorganic P showed marked peaks in the topsoil lysimeters, whereby in the subsoil, particle-bound P peaks were partly noticeable at both sites. Depth transport of P into the subsoil depended on initial soil moisture, texture and the spatial distribution of flow pathways. Further, we observed large heterogeneity within a single site, dependent on profile-specific characteristics of the distribution of P, flow pathways and microbial biomass. We conclude that under certain conditions, there is a depth transport of P into the subsoil and therefore a potential of P exports, especially for particle-bound P. Small-scale heterogeneity hampers the clear identification of influences and illustrates the need for further research regarding soil heterogeneity.

**Keywords: heavy rainfall event, dry period, zero-tension lysimeter, P loads, forest soil**

OPEN ACCESS

***Edited by:***
*Sebastian Loeppmann, Christian-Albrechts-Universität zu Kiel, Germany*

***Reviewed by:***
*Jörg Prietzel, Technical University of Munich, Germany*
*Aamir Manzoor, University of Göttingen, Germany*

****Correspondence:***
*Vera Makowski*
*vera.makowski@tu-dresden.de*

***Specialty section:***
*This article was submitted to Forest Soils, a section of the journal Frontiers in Forests and Global Change*

***Received:*** *11 February 2020*
***Accepted:*** *06 April 2020*
***Published:*** *05 May 2020*

***Citation:***
*Makowski V, Julich S, Feger K-H and Julich D (2020) Soil Phosphorus Translocation via Preferential Flow Pathways: A Comparison of Two Sites With Different Phosphorus Stocks. Front. For. Glob. Change 3:48. doi: 10.3389/ffgc.2020.00048*

## INTRODUCTION

Phosphorus (P) is an essential nutrient for all organisms. In terrestrial ecosystems, research on P mainly focused on cultivated soils (Heckrath et al., 1995; Withers et al., 2001; Damon et al., 2014). Here, fertilizing and manure application are the main factors for P import (Linderholm et al., 2012). Exports are driven by soil erosion on the surface, subsurface leaching and tile drains (Sims et al., 1998; Turner and Haygarth, 2000). Meanwhile, P budgets in forest soils were assumed to be

balanced under natural conditions (e.g., Wood et al., 1984). Exports were attributed to soil erosion after clear cutting (e.g., Likens et al., 1970) and therefore preventable by management. Imports of P are driven by atmospheric deposition (of P-rich dust) and mineral weathering (Newman, 1995). Therefore, imports depend on the abundance of P-containing minerals in deposits and parent material. Based on that, it was hypothesized that P exports under natural conditions in forest ecosystems depend on their soil P status, i.e., total amount and availability/mobility (Lang et al., 2016). The smaller the soil P stock, the tighter the P cycling in a forest ecosystem and therefore the smaller the leaching loss ("recycling system"). Consequently, Lang et al. (2017) connected soil P stocks along a geometric sequence with different nutrition strategies of beech (*Fagus sylvatica* L.) ecosystems and confirmed their previous hypothesis. Furthermore, connections between soil P status and various influencing factors on the forest P cycle were investigated. For example, Spohn et al. (2018) found differences in P uptake by plants or microbes, depending on season and P stock of the soil at a given site. Hauenstein et al. (2018) illustrated the increasing importance of organic layers and their ability to prevent P leaching with decreasing site P status. Moreover, an increased P mobilization of microbial associated P after drying-rewetting cycles, resulting in the subsequent increased risk of P depletion, especially of sites with already low P stocks, was observed (Brödlin et al., 2019). The above-mentioned studies mainly focused on organic layers and the mineral topsoil. Research on the mineral subsoil of forests often focused on the dissolved organic P fractions (Qualls et al., 2000; Kaiser et al., 2003). A site-specific depth transport of dissolved organic P in the soil solution of forest soils could be observed by Kaiser et al. (2003). Additionally, they found peaks of dissolved organic P during rainfall events after dry periods. Recent studies found elevated amounts of P in forest streams during heavy rainfall events, compared to base flow conditions (Benning et al., 2012; Julich S. et al., 2017). Julich S. et al. (2017) quantified these amounts with up to 12 g $ha^{-1}$ per event, which accounts for up to 19% of the annual flux. These peaks seem to be more pronounced during rainfall events following a dry period and thereby are in line with the findings of Kaiser et al. (2003) and Brödlin et al. (2019). The drying of the soil and its subsequent rewetting can result in the formation of preferential flow (Jarvis, 2007; Guo and Lin, 2018). Through such preferential flow pathways (PFP), nutrients including P can quickly be transported into the subsoil without passing the sorbing soil matrix (Makowski et al., 2020). Consequently, a dry period followed by a heavy rainfall event seem to be important for soil P exports. Most research on P balances in forest soils has focused on moisture conditions mainly influenced by slow matrix flow (e.g., Ilg et al., 2009). For the collection of preferential flow, which is supposed to predominantly translocate P through forest soils, zero-tension lysimeters can be used (Allaire et al., 2009; Peters and Durner, 2009). Advantages and limitations of this approach were discussed elsewhere (e.g., Zhu et al., 2002; Barzegar et al., 2004); their applicability with regard to quantifying P transport via preferential flow in forest soils was tested in a pre-testing study by Makowski et al. (2020). The filling with coarse material prevents matrix flow from entering the lysimeter and therefore they only sample preferential flow. Further, the filling ensures tight contact to the soil above, prevents it from collapsing and increases the collection efficiency (Radulovich and Sollins, 1987). Additionally, zero-tension lysimeters are able to collect particle-associated P, which is often (partly) excluded by other sampling methods (e.g., suction cups) by their fine pores (Grossmann and Udluft, 1991). However, these colloids are important carriers for soil P, including subsoil P (Missong et al., 2017). Therefore, the aim of our study was to investigate the translocation of dissolved and particle-bound P through preferential flow pathways into the subsoil. We tested to what extent at sites with differing soil P stock significant differences in P subsoil transport occur. Thus, we hypothesize that (i) relevant loads of P are translocated into the subsoil via preferential flow pathways, and (ii) at the P-poor site, a lower amount of P is translocated into the subsoil as compared to the P-rich site.

# MATERIALS AND METHODS

## Site Description

The experiments were conducted at two sites in Germany, Mitterfels with a high soil P status (678 g $m^{-2}$ soil P) and Lüss with a low soil P status (164 g $m^{-2}$ soil P). Mitterfels (hereafter called "high P site") is a mountainous region located in the Bavarian Forest in SE Germany. The soil is a Dystric Cambisol (WRB, 2015) developed on a paragneiss. Gravel, stones and boulders mainly appeared from 20 to 30 cm soil depth and below. Their size and distribution varied strongly between replicates. Lüss (hereafter called "low P site") is located in the North German lowlands. The soil is also a Dystric Cambisol, which was formed from a glacial sandy till. The till layers cause marked differences in soil physical conditions, i.e., texture ranging from silt to gravel and stones, with a high variety within a single profile. Both sites are covered with 130-year-old beeches (*Fagus sylvatica* L.). Further site information is listed in **Table 1**, profile information in **Table 2**.

## Experimental Setup

At each site, three trenches with a minimum length of 2.5 m and a depth of 1 m were dug. The trenches served as replicates to cope with small-scale site variability. All plots possessed the same site-specific properties of tree age and parent material and are located near each other according to the experimental design of the whole research program (DFG priority programme SPP 1685 "Ecosystem Nutrition: Forest strategies for limited Phosphorus Resources").

In each trench, three zero-tension pan lysimeters were installed next to each other. The lysimeters made from polyethylene (Singh et al., 2017) had a size of 50−40 cm. A 4–5 cm rim ensured a slope within the lysimeter and promoted water flow toward the outlet in the corner with the 5-cm rim (Jemison and Fox, 1992). Additionally, the rim prevented outflow of sampled water. For a good connection to the overlying soil and to create a capillary barrier preventing matrix flow sampling, the lysimeters were filled with coarse, pre-cleaned quartz sand

**TABLE 1 |** Site characteristics of the study sites Mitterfels (high P site) and Lüss (low P site), according to Lang et al. (2017).

| | High P site | Low P site |
|---|---|---|
| Elevation (m a.s.l.) | 1023 | 115 |
| Mean annual precipitation (mm) | 1299 | 779 |
| Soil type WRB (2015) | Hyperdystric chromic folic Cambisol | Hyperdystric folic Cambisol |
| Parent material | Paragneiss | Sandy till |
| Mean soil pH (1M KCl) (L/O/A/B horizons) | 5.6 / 2.9 / 3.3 / 4.0 | 5.3 / 3.0 / 2.7 / 4.0 |
| Soil phosphorus* (g $m^{-2}$) | 678 | 164 |
| Soil nitrogen* (kg $m^{-2}$) | 1.4 | 0.7 |
| Soil carbon* (kg $m^{-2}$) | 26 | 16 |

**Stocks from forest floor to 1 m soil depth.*

**TABLE 2 |** Soil properties of the two study sites Mitterfels (high P site) and Lüss (low P site).

| | Thickness | Texture | Stone content |
|---|---|---|---|
| | cm | | Vol-% |
| **High P site** | | | |
| Organic layer | +5 / 6 / 11 | – | – |
| A(E)h | 0–3 / 5 / 2 | Loam | 0 / 0 / 0 |
| 1B | –50 / 32 / 17 | (Sandy) Loam | 75 / 0 / 0 |
| 2B | 50 / 32 / 17+ | Sandy Loam | 75 / 75 / 60 |
| **Low P site** | | | |
| Organic layer | 8 / 9 / 10 | – | – |
| A(E)h | 0–6 / 6 / 8 | Loamy Sand | 1 / 5–10 / 1 |
| 1B | –37 / 42 / 52 | Loamy Sand | 1–2 / 5–10 / 1 |
| 2B | 37 / 42 / 52+ | Loamy Sand | 1 / 5–10 / 1 |

*Shown data from profile description refer to the single replicates. First number always refers to profile 1, second number to profile 2, third number to profile 3. Texture was determined from mixed samples.*

(>200 μm). A schematic setup and a picture of a built-in sampler are given in Makowski et al. (2020). The upper lysimeters were located at 12–16 cm depth. Middle lysimeters were installed in 35–40 cm depth. The lower lysimeters were installed in the lower subsoil, in depths between 70 and 100 cm depending on profile depth and stone content (**Table 3**). Due to the high stone content at one of the replicates at the high P site, only the upper lysimeter (beneath the A-horizon) and a second lysimeter at a depth of 20 cm were installed in this trench.

After lysimeter installation, each sampler was connected to an outlet to collect preferential flow water. Soil above the lysimeters was covered with a tarpaulin to simulate a dry period. The lysimeter plots were left to settle and dry. After 4 weeks, soil moisture was determined with a TDR probe (Trime-Pico 32, IMKO, Ettlingen, Germany) (**Table 4**). Measurements were taken at the topsoil, around 10 cm below forest floor and additionally from left and right of every lysimeter. Subsequently, we simulated a large rainfall event with a rainfall intensity of 20 L $m^{-2}$ $h^{-1}$. Event duration was 4 h, thus in total, 80 L $m^{-2}$ were irrigated with watering cans. The water was evenly applied over the irrigation course and the above-sampler area. The sampled water was collected in polypropylene bottles which were pre-rinsed with distilled water. The bottles were changed every 500 mL and the elapsed time since beginning of the irrigation recorded. To prevent microbial growth, the samples were stored in cooling boxes. At the end of the day, samples were brought to a refrigeration cell and stored at 5°C. In total, three cycles of drying and rewetting were simulated at each site. Irrigation 1 was conducted in May 2018, irrigations 2 and 3 in September and October 2018, respectively. Due to the seasonal differences, irrigations were not treated as replicates.

## Laboratory Work

The volume of all water samples was determined gravimetrically and their pH value and electric conductivity were measured (S20 SevenEasy pH, Mettler Toledo, Gießen, Germany). Total phosphorus (TP) was determined by adding 200 μL of 9 M $H_2SO_4$ and 4 mL $K_2(SO_4)_2$ to 40 mL of the unfiltered sample. The solution was heated in an autoclave for 45 min at 121°C and after cooling, the samples were measured in a spectrophotometer (UV-Mini 1240, Shimadzu Deutschland GmbH, Duisburg, Germany) using the molybdenum-blue method as described in ISO 6878:2004-05 (International Organization for Standardization, 2002, 2004). For determination of the dissolved fractions, the samples were filtered through a 0.45 μm cellulose acetate filter. Total dissolved phosphorus (TDP) was measured as described for TP. Dissolved inorganic phosphorus (DIP) was defined as dissolved molybdate-reactive P and analyzed photometrically within filtrates (UV-Mini 1240, Shimadzu Deutschland GmbH, Duisburg, Germany). Dissolved organic phosphorus (DOP) was calculated by subtracting DIP from TDP. By method, DOP is defined as organic P smaller than 0.45 μm. Particle-bound P (PP) was defined as the difference between TP and TDP. Values below the detection limit (DL) were further proceeded with half of the DL.

## Calculations and Statistics

Water flow rates were calculated by dividing the collected sample volume by the lysimeter area (0.2 $m^2$) and collection time. The fraction of sampled water for each lysimeter was calculated with the amount of sampled water as a percentage share of irrigated water amounts. Multiplying measured P concentrations with the amount of collected water of each sample results in the P loads. Summing all loads of one lysimeter for one respective irrigation results in the total (cumulative) P load. Sampling times and number of samples were different for every profile, therefore results on concentrations were split into five time steps, one for each hour of irrigation and one for samples taken after the irrigation process was finished (240 to maximal 420 min after irrigation start). The concentrations and flow rates of the three replicates per site were averaged for every time step, resulting in the mean concentrations and time steps per site. For each site, standard deviations and coefficients of variation were calculated from the mean cumulative loads of every irrigation event (see **Table 5** and respective figures). Differences between sites were tested with an unpaired Wilcoxon test on the respective TP loads per lysimeter. Unpaired Wilcoxon tests were performed with RStudio Version 1.2.1335, based on R Version 3.6.1. The ratios of TP load to the TP stock in the

**TABLE 3 |** Installation depths and the fraction of sampled water of the lysimeters at the high P and low P site.

| Site | Replicate | Lysimeter | Installation depth | Fraction of sampled water (%) | | |
|---|---|---|---|---|---|---|
| | | | cm under forest floor | Irrigation 1 | Irrigation 2 | Irrigation 3 |
| High P | 1 | Upper | 12 | 65 | 68 | 41 |
| | | Middle | 34 | 66 | 45 | 58 |
| | | Lower | 68 | 3 | 0 | 0 |
| | 2 | Upper | 18 | 23 | 20 | 14 |
| | | Middle | 47 | 7 | 5 | 3 |
| | | Lower | 65 | 0 | 0 | 0 |
| | 3 | Upper | 16 | 24 | 26 | 17 |
| | | Middle | 25 | 13 | 3 | 2 |
| Low P | 1 | Upper | 13 | 28 | 24 | 16 |
| | | Middle | 45 | 3 | 6 | 7 |
| | | Lower | 82 | 0 | 0 | 0 |
| | 2 | Upper | 14 | 21 | 8 | 16 |
| | | Middle | 48 | 10 | 3 | 3 |
| | | Lower | 85 | 6 | 0 | 0 |
| | 3 | Upper | 15 | 9 | 15 | 12 |
| | | Middle | 45 | 1 | 0 | 0 |
| | | Lower | 81 | 0 | 0 | 0 |

soil were calculated. For this, the soil stock up to the respective lysimeter installation depth was taken into account. Soil stock data was taken from Lang et al. (2017).

# RESULTS

## Flow Rates and Fraction of Sampled Water

Flow rates at the high P site ranged between 0 and 9 mL $m^{-2}$ $h^{-1}$. In all three irrigations, the maximum value was measured in the middle lysimeter of one replicate. At the low P site, flow rates were lower and ranged between 0 and 2.3 mL $m^{-2}$ $h^{-1}$. Here, the maximum values were reached by the upper lysimeters. At both sites, the lysimeters started reacting from top to bottom. First samples of each replicate were drawn from the upper lysimeter, followed by the middle lysimeter. In the deep subsoil lysimeters, flow only occurred during the first irrigation experiment (**Figure 1**). The first samples at the high P site consistently were taken during the first time step, while at the low P site, sampling began during the second time step. Over the course of the individual irrigations, the mean flow rates of the upper lysimeters remained constant. The mean flow rate of the middle lysimeters at the high P site increased clearly during the experiments. Concurrently at the low P site, in the middle lysimeters flow only occurred in the last time step of the experiment. After the end of the irrigation, mean flow rates strongly decreased (see time step 5). At both sites, the range of flow rates and their means decreased with every irrigation. The flow rates and their means were highest at the high P site.

The sampled water volume as a proportion of the irrigated water volume ranged from 0 to 68% (corresponding to 0–54 L $m^{-2}$) at the high P site and from 0 to 28% (0 to 22 L $m^{-2}$) at the low P site (**Table 3**). Values of 0% state that no sample was collected from the respective lysimeter. Coefficients of variation (CV) for each lysimeter were high and varied between 0.15 and 0.78. In the upper lysimeters, more flow occurred than in the middle and lower ones.

**TABLE 4 |** Volumetric soil moisture in %, measured with TDR probe directly before irrigations.

| | High P site | | | Low P site | | |
|---|---|---|---|---|---|---|
| Irrigation | 1 | 2 | 3 | 1 | 2 | 3 |
| 10 cm depth | 17.8 | 7.8 | 16.3 | 12.8 | 4.6 | 5.8 |
| 15 cm depth | 20.5 | 10.7 | 20.6 | 14.1 | 2.2 | 3.0 |
| 45 cm depth | 24.4 | 14.0 | 24.1 | 11.9 | 2.4 | 2.9 |
| 80 cm depth | 28.7 | 9.0 | 22.8 | 16.1 | 1.9 | 3.9 |

*Values represent the arithmetic means of all replicates, with n ≥ 6. Depths refer to levels under the forest floor.*

## Concentrations of P Fractions in Preferential Flow Water

All mentioned concentrations refer to the arithmetic mean values of the three plot repetitions and the defined time steps. Standard deviations (SD) at both sites were high and indicate the variability of the replicates (**Figures 2**, **3**). At the high P site, concentrations range from below the limit of quantification (LOQ) of 5 μg $L^{-1}$ up to 115 μg $L^{-1}$ DIP in the upper lysimeter. At the low P site, they range from LOQ up to 417 μg $L^{-1}$ PP found in the lower lysimeter. Highest mean concentrations occurred with the highest standard deviations.

**TABLE 5 |** Mean cumulative TP loads (in $\mu g\ m^{-2}$) per irrigation, in brackets their coefficient of variation (CV) (–).

| | High P site | | | Low P site | | |
|---|---|---|---|---|---|---|
| **Lysimeter** | **Irrigation 1** | **Irrigation 2** | **Irrigation 3** | **Irrigation 1** | **Irrigation 2** | **Irrigation 3** |
| Upper | 4062 (0.53) | 1654 (0.52) | 770 (0.17) | 1500 (0.28) | 3354 (0.49) | 2830 (0.40) |
| Middle | 686 (0.95) | 540 (0.54) | 483 (1.0) | 631 (1.19) | 205 (0.04) | 208 (0.12) |
| Lower | 87 (-) | – | – | 1752 (-) | – | – |

*Arithmetic means and CV were calculated from the cumulative TP loads of three replicates per site.*

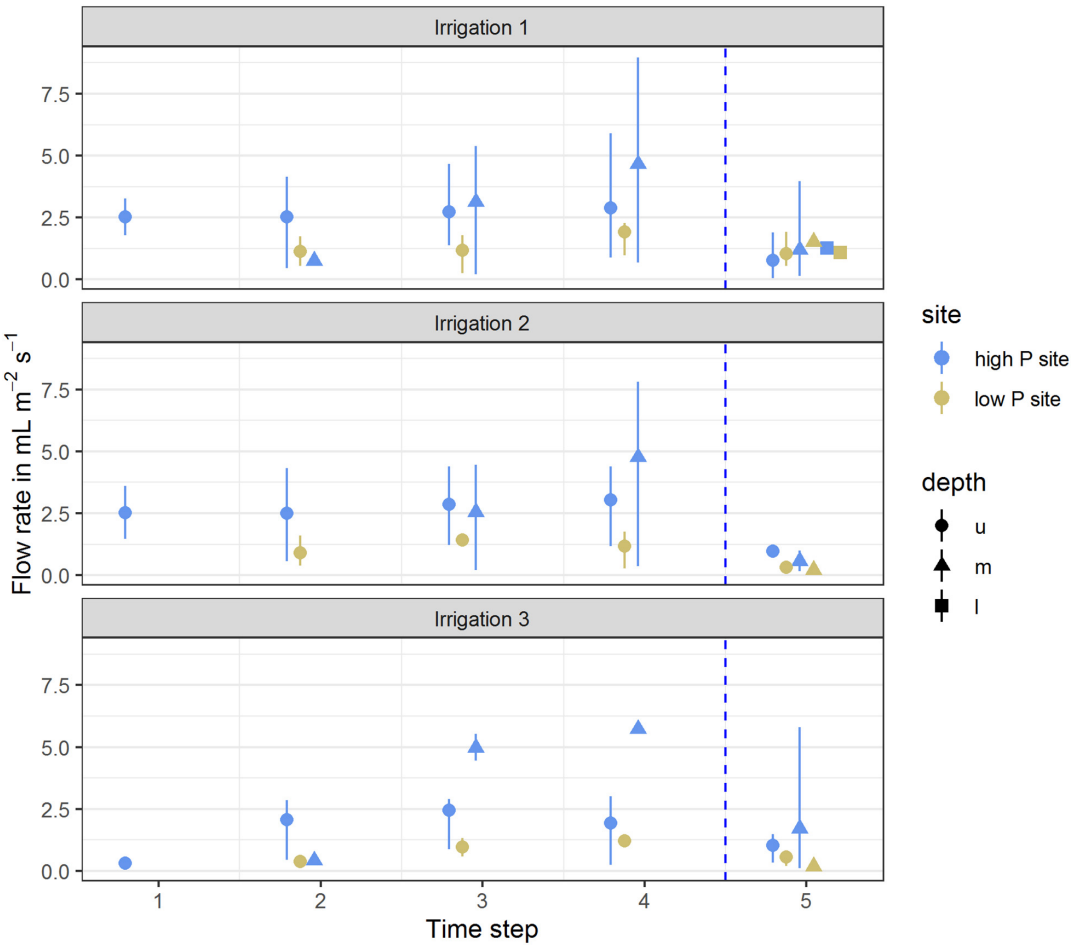


**FIGURE 1 |** Mean flow rates per time step of high (blue) and low (yellow) P sites. Arithmetic means were calculated from flow rates of all replicates per site for the respective time step. Ranges indicate the span from minimum and maximum values. Time steps 1–4 each represent 60 min of irrigation, time step 5 represents 180 min after the end of the irrigation. Depth represents the lysimeter installation depths (u – upper, m – middle, l – lower). Vertical dotted line represents the end of the irrigation impulse.

In the upper lysimeters of the high P site (**Figure 2**), high amounts (up to 115 $\mu g\ L^{-1}$) of DIP toward the end of the first irrigation were found. In the following irrigations, DIP concentrations were below 22 $\mu g\ L^{-1}$. During irrigations 2 and 3, no P fraction was clearly prevailing in the upper lysimeters. In the middle lysimeters, DOP and DIP concentrations were around the LOQ during all irrigations with a maximum of 21 $\mu g\ L^{-1}$ (DOP, irrigation 3). PP concentrations were slightly higher and reached a maximum of 89 $\mu g\ L^{-1}$ during the third irrigation. Lower lysimeters sampled only during the fifth time step of the first irrigation. Here, DIP and DOP concentrations were below the LOQ, while PP concentration reached 21 $\mu g\ L^{-1}$.

In the upper lysimeters at the low P site (**Figure 3**), DIP concentrations were up to 62 $\mu g\ L^{-1}$. During the two following irrigations, DIP concentrations in the upper lysimeters ranged between 109 and 251 $\mu g\ L^{-1}$ and therefore were clearly higher than in the first irrigation. DOP concentrations ranged between 15 and 55 $\mu g\ L^{-1}$, while PP was the smallest fraction with

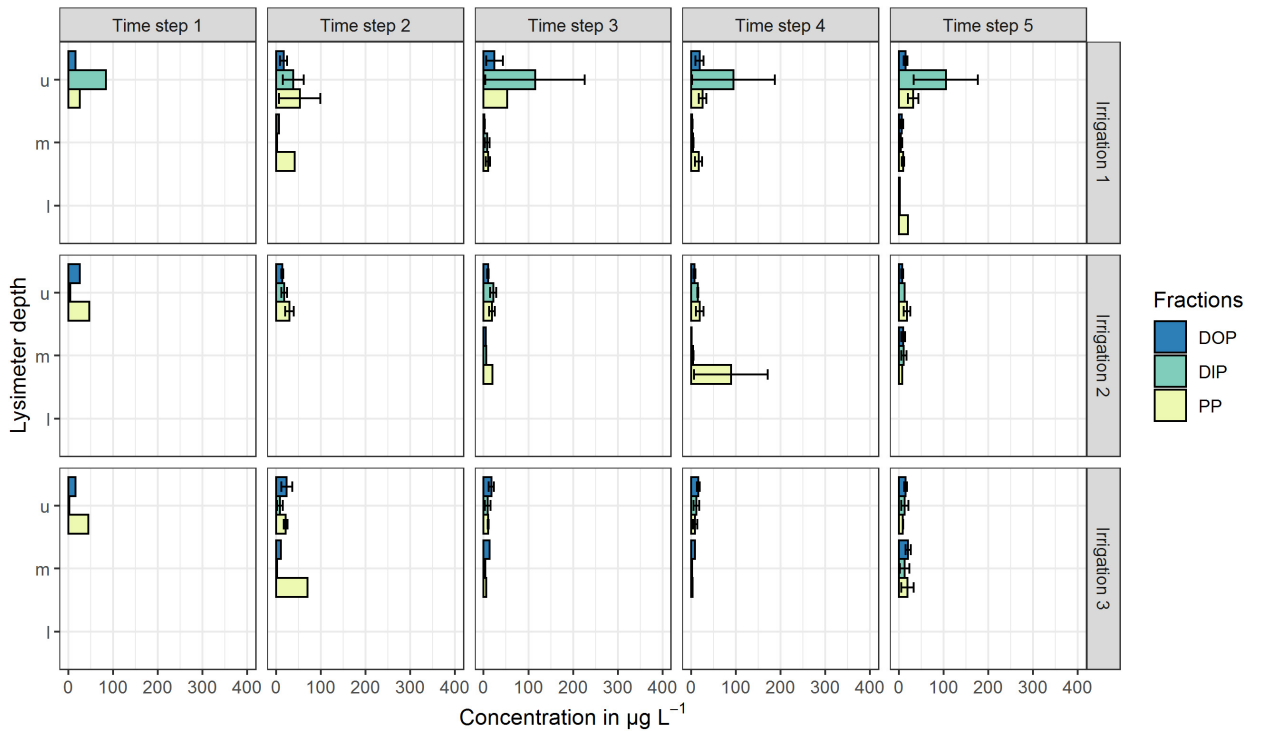


**FIGURE 2 |** Mean P concentrations in preferential-flow water collected with zero-tension lysimeters during three irrigations at the high P site. Arithmetic means were calculated from all samples drawn in the respective time step. Shown P fractions are DOP (dissolved organic P), DIP (dissolved inorganic P) and PP (particle bound P). Lysimeter depths were indicated by u (upper), m (middle) and l (lower). Time steps 1–4 each represent 60 min of irrigation, time step 5 represents 180 min after the end of the irrigation. No bar indicates that in the respective time step and/or depth, no sample was drawn. Error bars indicate the standard deviation.

values between 8 and 47 µg $L^{-1}$. By contrast, in the middle lysimeter samples, DIP concentrations were <10 µg $L^{-1}$ and DOP concentrations were constant around 30 µg $L^{-1}$ during all irrigations. The PP fraction was the main fraction during the first irrigation in the middle (136 µg $L^{-1}$) and lower (417 µg $L^{-1}$) lysimeters. The PP/TP ratios of 0.93 (middle lysimeter) and 0.99 (lower lysimeter) underline their prominent role.

## Cumulative P Loads

The P loads were calculated as means of the replicates per site and time step. Especially in the upper lysimeter, TP loads differ between sites (see **Figure 4** and **Table 5**). The lower lysimeters did not collect any samples in irrigations 2 and 3. Comparing the loads of both sites, they differ significantly ($p < 0.001$) in the upper lysimeters for the second and third irrigation. The difference between sites was not statistically significant for the results from the first irrigation ($p = 0.29$). Furthermore, loads between sites in the middle and lower lysimeters did not differ significantly. This is probably due to the high variability of the replicates. The mean TP loads, cumulated per irrigation, range from 87 to 4062 µg $m^{-2}$ (**Table 5**). The maximum TP loads were measured in the upper lysimeters at both sites. Still, the high coefficients of variation show the high variability of the replicates at each site. At the high P site, maximum mean cumulative P load (2444 µg $m^{-2}$ for DIP) occurred in the upper lysimeter during the first irrigation. The low P site also showed maximal values for DIP loads with 2525 µg $m^{-2}$ during the second irrigation and 2089 µg $m^{-2}$ during the third irrigation in the upper lysimeter. Cumulative DOP loads followed a similar pattern. The maximum at the high P site was measured in the upper lysimeter during the first irrigation (553 µg $m^{-2}$), at the low P site during the second and third irrigation (631 µg $m^{-2}$ and 449 µg $m^{-2}$). The clear maximum of the PP loads was measured in the upper lysimeter at the high P site and during the first irrigation (1058 µg $m^{-2}$). The low P sites maximum was 591 µg $m^{-2}$ (irrigation 1, middle lysimeter) and therefore clearly lower than at the high P site.

The ratios of TP loads to the respective soil P stock of the sites are given in **Figure 5**. Here, the low P site reveals higher amounts (63–144 µg $P_{water}$ $g^{-1}$ $P_{soil}$) of P mobilized in the upper lysimeters, compared to the high P site (7–37 µg $P_{water}$ $g^{-1}$ $P_{soil}$). This emphasizes the high loads of mobilized P in the topsoil of the low P site. In the middle lysimeters, load-to-stock P ratios of both sites were similar to each other and clearly lower than in the upper lysimeters. Lower lysimeter ratios could only be calculated for the first irrigation. Here, the low P sites ratio was higher (14 µg $P_{water}$ $g^{-1}$ $P_{soil}$) compared to the high P site (0.2 µg $P_{water}$ $g^{-1}$ $P_{soil}$).

# DISCUSSION

Our results demonstrate differences in terms of mobilization and transport of P between sites, depths and events. The dominating P

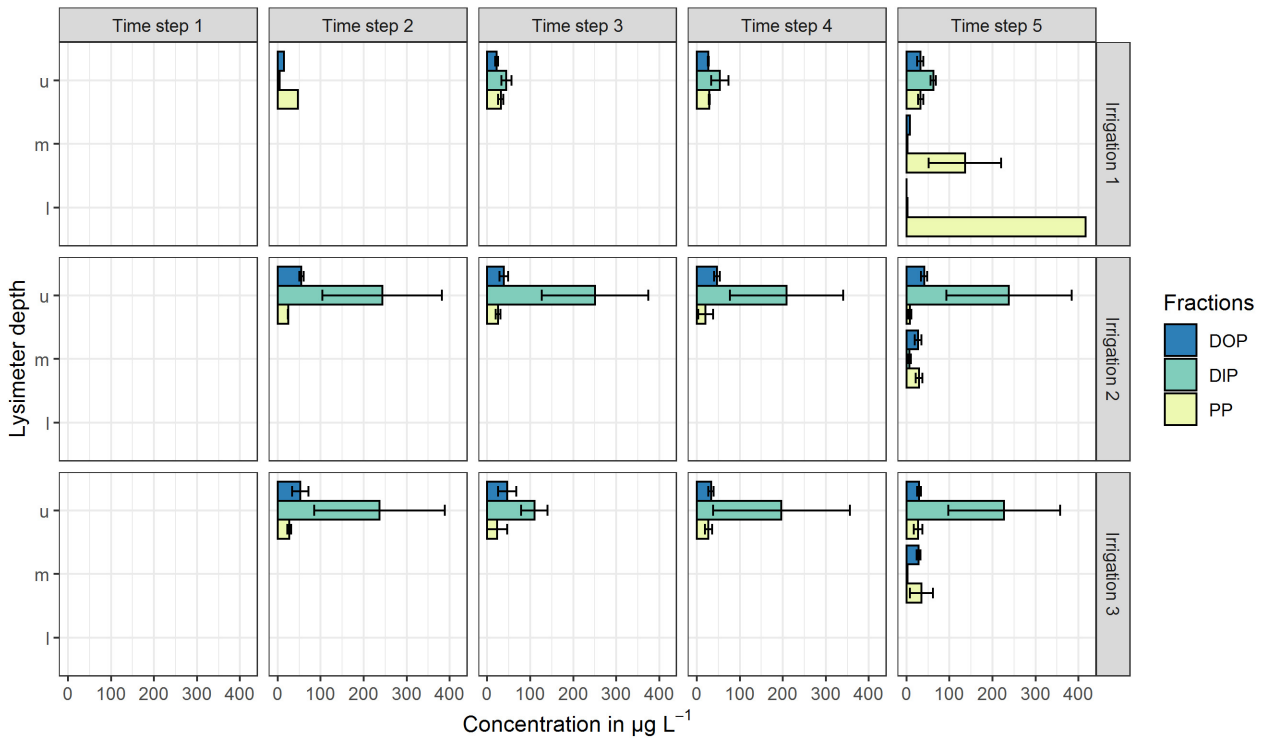


**FIGURE 3 |** Mean P concentrations in preferential-flow water collected with zero-tension lysimeters during three irrigations at the low P site. Arithmetic means were calculated from all samples drawn in the respective time step. Shown P fractions are DOP (dissolved organic P), DIP (dissolved inorganic P) and PP (particle bound P). Lysimeter depths are indicated by u (upper), m (middle) and l (lower). Time steps 1–4 each represent 60 min of irrigation, time step 5 represents 180 min after the end of the irrigation. No bar indicates that in the respective time step and/or depth, no sample was drawn. Error bars indicate the standard deviation.

fraction in our results was DIP, which is in line to the findings of similar studies (Dinh et al., 2016; Hömberg and Matzner, 2018; Brödlin et al., 2019), who investigated leachates from organic layers during drying-rewetting cycles in beech forest soils. Dinh et al. (2016) and Brödlin et al. (2019) also sampled A-Horizons, but reported higher DOP and smaller DIP shares than our results from the upper lysimeters. Therefore, preferential flow pathways seem to translocate P, often as DIP, from the organic layers into the mineral topsoil below the A-horizon. Additionally, our results contrast findings from a 27 months experiment, where DOP predominates leachates from the forest floor and mineral soil solution (Kaiser et al., 2003). However, our experiments did not always result in high DIP concentrations in the topsoil. The release of DIP into the soil solution is controlled by biotic and abiotic processes (Frossard et al., 2000). The biotic release of DIP is associated with microbial turnover and mineralization. This is especially important for sites with low P availability, where low abiotic DIP release is assumed (Frossard et al., 2000; Pistocchi et al., 2018). Therefore, high concentrations of DIP in soil water represent high microbial activity in combination with no or little plant uptake. Furthermore, soil moisture controls biotic processes with more inactive microbes and less turnover in dryer soils (Skopp et al., 1990). The microbial release of DIP following drying-rewetting cycles is assumed to be highly relevant at the P poor site (Lang et al., 2017). This is supported by our data showing that DIP was predominating in the second and third drying-rewetting cycle at the low P site. By contrast, the plant-available P fraction (corresponding to DIP) was clearly reduced at the high P site during late summer and autumn in our data. However, our methodical approach does not allow conclusions on elevated DIP uptake by plants or less microbial release as compared to the low P site. For future experimental approaches, corresponding methods should be included to answer questions on DIP release and uptake.

The observed depth transport of PP in our study confirms assumptions on the importance of the particle-bound P fraction in seepage water, also including colloids below the operationally defined size of 0.45 µm (Missong et al., 2017; Makowski et al., 2020). These observations fit to our results, where highest PP loads were found at the low P site. Colloid-associated P fluxes in soil leachates in 20 cm soil depths were detected in a range of 8–51 mg P $m^{-2}$ $a^{-1}$ (Bol et al., 2016) and may account for 12–91% of total P leached in forest soils (Missong et al., 2018). Investigations of forest streamwater revealed that colloidal DOP may account for 40–100% of the P losses, which were suggested to be mediated by preferential flow transport during storm events (Bol et al., 2016). The DOP loads in seepage water in our experiments ranged between 0 and 0.63 mg $m^{-2}$ within a period of 7 h. Literature values on annual DOP fluxes in deciduous forest soil were indicated in a range of 30–62 mg $m^{-2}$ in organic layers and 2–38 mg $m^{-2}$ in subsoil [summarized in Bol et al. (2016)]. Against this background, the observed

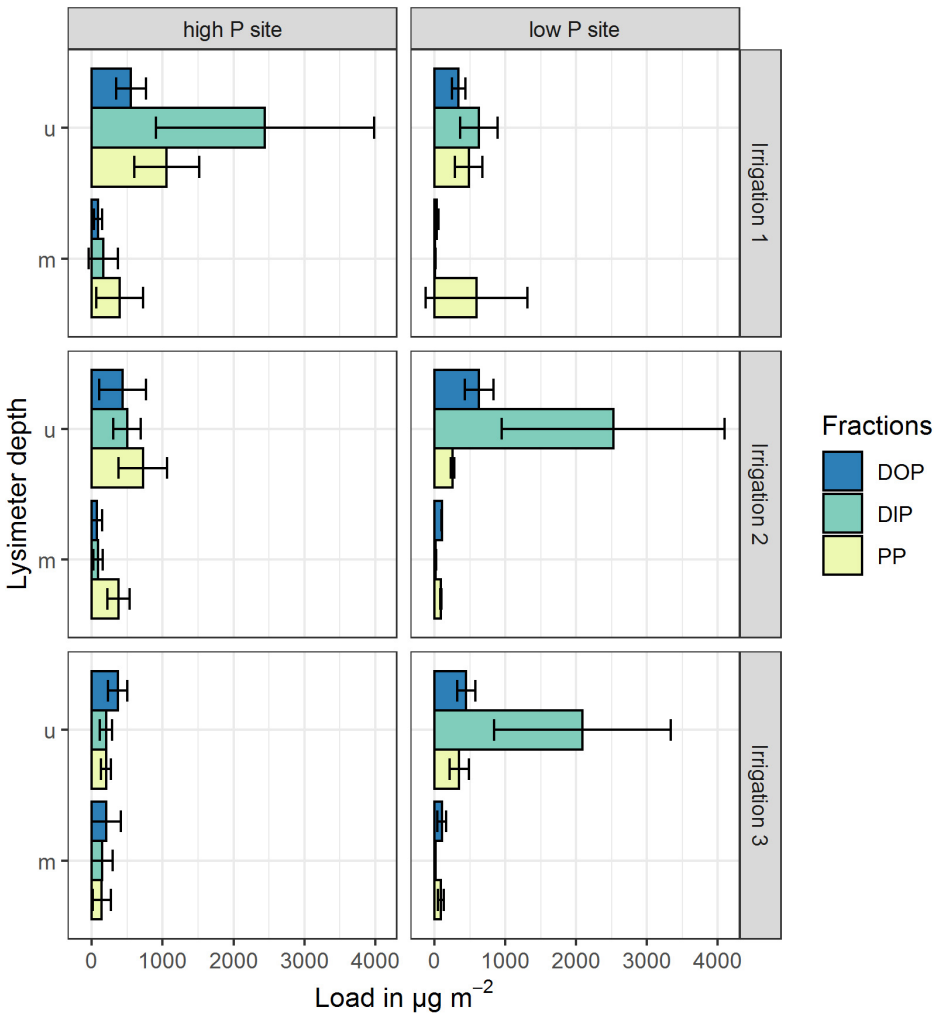


**FIGURE 4 |** Mean cumulative P loads in preferential flow water collected with zero-tension lysimeters during three irrigations at a high P and a low P site. Shown P fractions are DOP (dissolved organic P), DIP (dissolved inorganic P) and PP (particle bound P). Upper (u) and middle (m) lysimeter data are pictured, lower lysimeter data is not pictured. Values represent arithmetic means of three replicates, cumulated over the experimental period (4 h irrigation + 3 h after irrigation sampling). Error bars represent the standard deviation of the replicates.

DOP fluxes in our experiments seem to be very low, even if the occurrence of several rain events in the applied extent is considered. However, the methodical approach by using zero-tension lysimeters may explain why other studies, using suction-based approaches, detected a predominance of DOP rather than PP in soil water fluxes.

We were able to collect only few samples from middle and especially lower lysimeters resulting in the assumption that the subsoil is not well connected to water flow from upper soil layers in our experiments. Similar flow patterns were detected in a study by Bogner et al. (2008), who also found low soil moisture to be the reason for missing subsoil preferential flow in forest soils. Research on cultivated soils, which is more frequent, is contradictory concerning soil moisture and depth transport via preferential flow pathways (e.g., Granovsky et al., 1994; Kung et al., 2000), because not all PFP in the soil were activated under drier conditions. Others suggested that site-dependent differences are more dominant than soil moisture with regard to occurrence of depth flow (Weiler and Flühler, 2004). The differences in the occurrence of PFP can in our cases mainly be explained by the differences in texture and stone content. At the high P site, higher stone contents in the B-horizons lead to flow mainly along the stone surface matrix interface (Julich D. et al., 2017). At the low P site with low stone content and a coarser texture, slower and fingering-like flow is pronounced. In sum, factors such as soil moisture, texture, and stone content affect distribution and connection of PFPs to deep water flow, and consequently P fluxes through the soil profile. With regard to our first hypothesis, we can conclude that under certain conditions, preferential flow along specific pathways is able to translocate relevant loads of P into the subsoil. These loads mainly consist of PP and DOP rather than DIP.

Focusing on differences in export dynamics between sites, main aspects are the P contents of the parent material and the

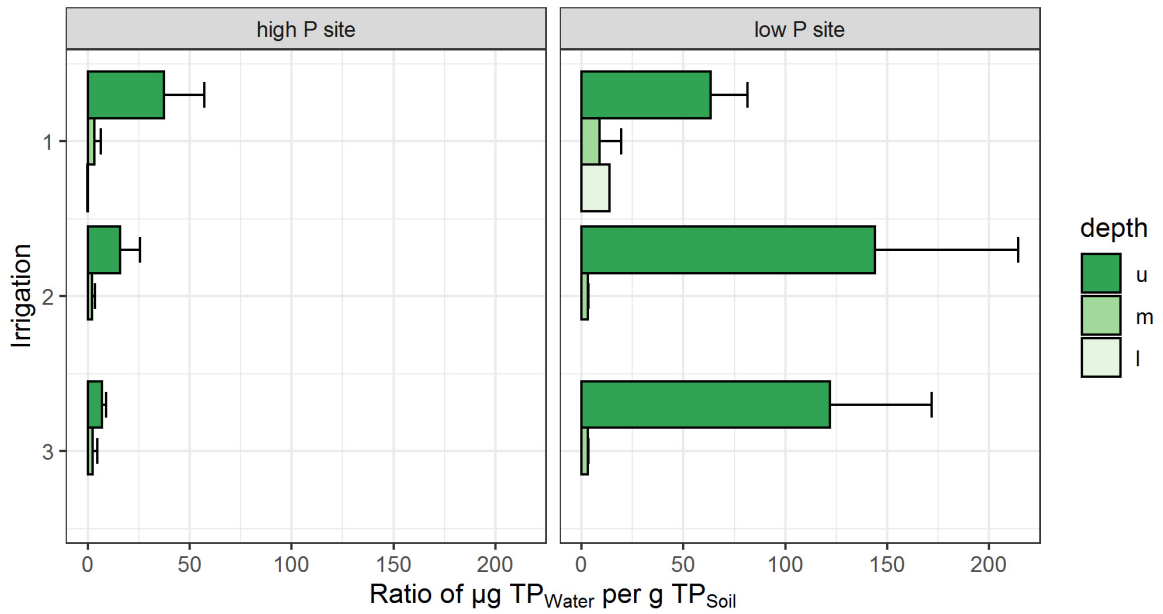


**FIGURE 5 |** Cumulative total P loads in relation to soil P stock of each site. Depth refers to the respective lysimeter installation depths (u – upper, m – middle, l – lower). Ratios represent the arithmetic means of three replicates per site. No bar indicates no samples from the respective depth and irrigation. Error bars represent the standard deviation of the replicates.

resulting soil P stock. Taking the soils P stock and the respective P loads into account, a ratio of load per stock can be specified. In the upper and middle lysimeters, this ratio differs from the P loads of the sites (**Table 5** and **Figure 5**). At the low P site, the ratio of TP in seepage to TP stocks in the overlying soil was clearly higher than at the high P site during all irrigations. This supports the results of Brödlin et al. (2019), who found higher mobilization of P at the low P site than at the high P sites. Further, we were able to detect a strong decrease of the ratios from the upper lysimeter to the middle lysimeter. For irrigations 2 and 3, our data is in line with the assumption by Lang et al. (2017) that low P sites prevent mobilized P from leaching out of the rooting zone, which is a strong indicator for tight recycling of P within the ecosystem. In relation to the soil P stock, both sites had similar amounts of P translocated in the subsoil. The results from irrigation 1 differ from that assumption. Here, high cumulative P loads were found in the lower lysimeters of the low P site and the P load to P stock ratio is higher than at the high P site (**Table 5** and **Figure 5**). However, the sample amount in the lower lysimeters was generally very low with high variability in the replicates, which represents a very small data base but high data uncertainty for the deep subsoil. Nevertheless, as the decrease of the P ratio from topsoil to subsoil is much stronger at the low P site than at the high P site, less P translocation into the subsoil can be expected here. Therefore, we found strong indications which would confirm our second hypothesis.

Furthermore, we found considerable differences between the replicates within the respective sites, indicating a high variability of preferential flow. Ranges and coefficients of variation of our data indicate a high variability of flow rates as well as P concentrations and loads within each site. Recent research on forest soils focused on the differences in nutrient/element distribution between PFP and soil matrix (Bundt et al., 2001; Backnäs et al., 2012; Bogner et al., 2012; Julich D. et al., 2017). Meanwhile, research on the heterogeneity of preferential flow mainly focused on its occurrence (Wiekenkamp et al., 2016) or spatial distribution (Jarvis et al., 2012) rather than nutrient distributions. In addition to the heterogeneous occurrence of preferential flow, distribution of soil P concentrations has shown to be highly variable within a soil profile in dependences of soil depth and contents of soil organic matter as well as pedogenic Al and Fe minerals (Werner et al., 2017). Backnäs et al. (2012) and Julich D. et al. (2017) connected high stone contents with heterogeneous flow and low P sorption conditions. Furthermore, Bundt et al. (2001) emphasized the size and role of microbial biomass in PFP. As a consequence, factors like heterogeneity of soil P, pathway type, pathway distribution and microbial biomass can explain the variability of the presented results. Further research on the spatial and temporal heterogeneity of nutrients in preferential flow appears to be important for a deeper understanding of the role of preferential flow (pathways) for nutrient translocation in natural ecosystems.

## CONCLUSION

In this study, we compared two beech-stocked sites with contrasting soil P status concerning the amount of P in preferential flow at several soil depths. We were able to show that under certain conditions, relevant amounts of P were translocated into the subsoil via preferential flow. Here, low P sites were better adapted by recycling processes and retained

higher shares of mobilized P in the main rooting zone than high P sites. Additionally, DIP was the main mobilized P fraction, while PP seemed to be important for depth transport, regardless of the soils P status. Nevertheless, driving factors for P losses from forest ecosystems were hard to identify due to the high variability within the sites. Future research must determine the conditions which lead to P export from forest ecosystems with an emphasis on soil heterogeneity. In summary, our study was able to demonstrate that P is translocated from topsoil to deeper soil regions and to give first numbers on the magnitude of this transport processes.

## DATA AVAILABILITY STATEMENT

The raw data supporting the conclusions of this article will be made available by the authors, without undue reservation, to any qualified researcher.

## AUTHOR CONTRIBUTIONS

SJ, K-HF, and DJ conceived the experimental approach. VM was responsible for the installation of equipment in the field, sampling, data analyzes and visual processing, supported by DJ. VM wrote the manuscript as lead author. All authors contributed equally to the discussion of the results, commented on the manuscript, read and approved the submitted manuscript.

## FUNDING

This work was funded by the Deutsche Forschungsgemeinschaft (DFG) as part of the SPP 1685 "Ecosystem Nutrition: Forest Strategies for limited Phosphorus Resources" by grant JU 2940/1-2. The Publication Fund of the TU Dresden funded the Open Access publication.

## ACKNOWLEDGMENTS

We are very grateful to Robert Endrikat for his laboratory work and support during fieldwork. We also thank Gisela Ciesielski for her support in the lab and during fieldwork, Manuela Unger and Thomas Klinger for their lab assistance and Tobias Krause and several student helpers for their help in the field. Additionally, we would like to thank our colleagues at the institute for their helpful input.

## REFERENCES

Allaire, S. E., Roulier, S., and Cessna, A. J. (2009). Quantifying preferential flow in soils: a review of different techniques. *J. Hydrol.* 378, 179–204. doi: 10.1016/j.jhydrol.2009.08.013

Backnäs, S., Laine-Kaulio, H., and Kløve, B. (2012). Phosphorus forms and related soil chemistry in preferential flowpaths and the soil matrix of a forested podzolic till soil profile. *Geoderma* 189, 50–64. doi: 10.1016/j.geoderma.2012.04.016

Barzegar, A. R., Herbert, S. J., Hashemi, A. M., and Hu, C. S. (2004). Passive pan sampler for vadose zone leachate collection. *Soil Sci. Soc. Am. J.* 68, 744–749. doi: 10.2136/sssaj2004.0744

Benning, R., Schua, K., Schwärzel, K., and Feger, K. H. (2012). Fluxes of nitrogen, phosphorus, and dissolved organic carbon in the inflow of the Lehnmühle reservoir (Saxony) as compared to streams draining three main land-use types in the catchment. *Adv. Geosci.* 32, 1–7. doi: 10.5194/adgeo-32-1-2012

Bogner, C., Borken, W., and Huwe, B. (2012). Impact of preferential flow on soil chemistry of a podzol. *Geoderma* 175, 37–46. doi: 10.1016/j.geoderma.2012.01.019

Bogner, C., Wolf, B., Schlather, M., and Huwe, B. (2008). Analysing flow patterns from dye tracer experiments in a forest soil using extreme value statistics. *Eur. J. Soil Sci.* 59, 103–113. doi: 10.1111/j.1365-2389.2007.00974.x

Bol, R., Julich, D., Brödlin, D., Siemens, J., Kaiser, K., Dippold, M. A., et al. (2016). Dissolved and colloidal phosphorus fluxes in forest ecosystems—an almost blind spot in ecosystem research. *J. Plant Nutr. Soil Sci.* 179, 425–438. doi: 10.1002/jpln.201600079

Brödlin, D., Kaiser, K., Kessler, A., and Hagedorn, F. (2019). Drying and rewetting foster phosphorus depletion of forest soils. *Soil Biol. Biochem.* 128, 22–34. doi: 10.1016/j.soilbio.2018.10.001

Bundt, M., Widmer, F., Pesaro, M., Zeyer, J., and Blaser, P. (2001). Preferential flow paths: biological "hot spots" in soils. *Soil Biol. Biochem.* 33, 729–738. doi: 10.1016/S0038-0717(00)00218-212

Damon, P. M., Bowden, B., Rose, T., and Rengel, Z. (2014). Crop residue contributions to phosphorus pools in agricultural soils: a review. *Soil Biol. Biochem.* 74, 127–137. doi: 10.1016/J.SOILBIO.2014.03.003

Dinh, M., Van, Schramm, T., Spohn, M., and Matzner, E. (2016). Drying-rewetting cycles release phosphorus from forest soils. *J. Plant Nutr. Soil Sci.* 179, 670–678. doi: 10.1002/jpln.201500577

Frossard, E., Condron, L. M., Oberson, A., Sinaj, S., and Fardeau, J. C. (2000). Processes governing phosphorus availability in temperate soils. *J. Environ. Qual.* 29, 15–23. doi: 10.2134/jeq2000.00472425002900010003x

Granovsky, A. V., McCoy, E. L., Dick, W. A., Shipitalo, M. J., and Edwards, W. M. (1994). Impacts of antecedant moisture and soil surface mulch coverage on water and chemical transport through a no-till soil. *Soil Tillage Res.* 32, 223–236. doi: 10.1016/0167-1987(94)90022-90021

Grossmann, J., and Udluft, P. (1991). The extraction of soil water by the suction-cup method: a review. *J. Soil Sci.* 42, 83–93. doi: 10.1111/j.1365-2389.1991.tb00093.x

Guo, L., and Lin, H. (2018). Addressing two bottlenecks to advance the understanding of preferential flow in soils. *Adv. Agron.* 147, 61–117. doi: 10.1016/bs.agron.2017.10.002

Hauenstein, S., Neidhardt, H., Lang, F., Krüger, J., Hofmann, D., Pütz, T., et al. (2018). Organic layers favor phosphorus storage and uptake by young beech trees (*Fagus sylvatica* L.) at nutrient poor ecosystems. *Plant Soil* 432, 289–301. doi: 10.1007/s11104-018-3804-3805

Heckrath, G., Brookes, P. C., Poulton, P. R., and Goulding, K. W. T. (1995). Phosphorus leaching from soils containing different phosphorus concentrations in the Broadbalk experiment. *J. Environ. Qual.* 24:904. doi: 10.2134/jeq1995.00472425002400050018x

Hömberg, A., and Matzner, E. (2018). Effects of drying and rewetting on soluble phosphorus and nitrogen in forest floors: an experiment with undisturbed columns. *J. Plant Nutr. Soil Sci.* 181, 177–184. doi: 10.1002/jpln.201700380

Ilg, K., Wellbrock, N., and Lux, W. (2009). Phosphorus supply and cycling at long-term forest monitoring sites in Germany. *Eur. J. For. Res.* 128, 483–492. doi: 10.1007/s10342-009-0297-z

International Organization for Standardization, (2002). *Soil quality - Determination of Particle Size Distribution in Mineral Soil Material - Method by Sieving and Sedimentation*. Geneva: ISO.

International Organization for Standardization, (2004). *Water Quality—Determination of Phosphorus: Ammonium Molybdate Spectrometric Method (DIN EN ISO 6878)*. Geneva: ISO.

Jarvis, N. J. (2007). A review of non-equilibrium water flow and solute transport in soil macropores: principles, controlling factors and consequences for water quality. *Eur. J. Soil Sci.* 58, 523–546. doi: 10.1111/j.1365-2389.2007.00915.x

Jarvis, N. J., Moeys, J., Koestel, J., and Hollis, J. M. (2012). "Preferential flow in a pedological perspective," in *Hydropedology*, ed. H. Lin (Oxford: Academic), 75–120.

Jemison, J. M., and Fox, R. H. (1992). Estimation of zero-tension pan lysimeter collection efficiency. *Soil Sci.* 154, 85–94. doi: 10.1097/00010694-199208000-199208001

Julich, D., Julich, S., and Feger, K. H. (2017). Phosphorus in preferential flow pathways of forest soils in Germany. *Forests* 8:19. doi: 10.3390/f8010019

Julich, S., Benning, R., Julich, D., and Feger, K. H. (2017). Quantification of phosphorus exports from a small forested headwater-catchment in the Eastern Ore Mountains, Germany. *Forests* 8:206. doi: 10.3390/f8060206

Kaiser, K., Guggenberger, G., and Haumaier, L. (2003). Organic phosphorus in soil water under a European beech (*Fagus sylvatica* L.) stand in northeastern Bavaria. Germany: seasonal variability and changes with soil depth. *Biogeochemistry* 66, 287–310. doi: 10.1023/B:BIOG.0000005325.86131.5f

Kung, K.-J. S., Steenhuis, T. S., Kladivko, E. J., Gish, T. J., Bubenzer, G., and Helling, C. S. (2000). Impact of preferential flow on the transport of adsorbing and non-adsorbing tracers. *Soil Sci. Soc. Am. J.* 64, 1290. doi: 10.2136/sssaj2000.6441290x

Lang, F., Bauhus, J., Frossard, E., George, E., Kaiser, K., Kaupenjohann, M., et al. (2016). Phosphorus in forest ecosystems: new insights from an ecosystem nutrition perspective. *J. Plant Nutr. Soil Sci.* 179, 129–135. doi: 10.1002/jpln.201500541

Lang, F., Krüger, J., Amelung, W., Willbold, S., Frossard, E., Bünemann, E. K., et al. (2017). Soil phosphorus supply controls P nutrition strategies of beech forest ecosystems in Central Europe. *Biogeochemistry* 136, 5–29. doi: 10.1007/s10533-017-0375-370

Likens, G. E., Bormann, F. H., Johnson, N. M., Fisher, D. W., and Pierce, R. S. (1970). Effects of forest cutting and herbicide treatment on nutrient budgets in the Hubbard Brook watershed-ecosystem. *Ecol. Monogr.* 40, 23–47.

Linderholm, K., Mattsson, J. E., and Tillman, A.-M. (2012). Phosphorus flows to and from Swedish agriculture and food chain. *Ambio* 41, 883–893. doi: 10.1007/s13280-012-0294-291

Makowski, V., Julich, S., Feger, K. H., and Julich, D. (2020). Leaching of dissolved and particulate phosphorus via preferential flow pathways in a forest soil: an approach using zero-tension lysimeters. *J. Plant Nutr. Soil Sci.* 183, 238–247. doi: 10.1002/jpln.201900216

Missong, A., Bol, R., Nischwitz, V., Krüger, J., Lang, F., Siemens, J., et al. (2017). Phosphorus in water dispersible-colloids of forest soil profiles. *Plant Soil* 427, 71–86. doi: 10.1007/s11104-017-3430-3437

Missong, A., Holzmann, S., Bol, R., Nischwitz, V., Puhlmann, H. V., Wilpert, K., et al. (2018). Leaching of natural colloids from forest topsoils and their relevance for phosphorus mobility. *Sci. Total Environ.* 634, 305–315. doi: 10.1016/j.scitotenv.2018.03.265

Newman, E. I. (1995). Phosphorus inputs to terrestrial ecosystems. *J. Ecol.* 83, 713–726. doi: 10.2307/2261638

Peters, A., and Durner, W. (2009). Large zero-tension plate lysimeters for soil water and solute collection in undisturbed soils. *Hydrol. Earth Syst. Sci.* 13, 1671–1683. doi: 10.5194/hess-13-1671-2009

Pistocchi, C., Mészáros, É, Tamburini, F., Frossard, E., and Bünemann, E. K. (2018). Biological processes dominate phosphorus dynamics under low phosphorus availability in organic horizons of temperate forest soils. *Soil Biol. Biochem.* 126, 64–75. doi: 10.1016/j.soilbio.2018.08.013

Qualls, R. G., Haines, B. L., Swank, W. T., and Tyler, S. W. (2000). Soluble organic and inorganic nutrient fluxes in clearcut and mature deciduous forests. *Soil Sci. Soc. Am. J.* 64:1068. doi: 10.2136/sssaj2000.6431068x

Radulovich, R., and Sollins, P. (1987). Improved performance of zero-tension lysimeters. *Soil Sci. Soc.Am. J.* 51, 1386–1388. doi: 10.2136/sssaj1987.03615995005100050054x

Sims, J. T., Simard, R. R., and Joern, B. C. (1998). Phosphorus loss in agricultural drainage: historical perspective and current research. *J. Environ. Qual.* 27:277. doi: 10.2134/jeq1998.00472425002700020006x

Singh, G., Kaur, G., Williard, K., Schoonover, J., and Kang, J. (2017). Monitoring of water and solute transport in the vadose zone: a review. *Vadose Zone J.* 17:160058. doi: 10.2136/vzj2016.07.0058

Skopp, J., Jawson, M. D., and Doran, J. W. (1990). Steady-state aerobic microbial activity as a function of soil water content. *Soil Sci. Soc. Am. J.* 54:1619. doi: 10.2136/sssaj1990.03615995005400060018x

Spohn, M., Zavišić, A., Nassal, P., Bergkemper, F., Schulz, S., Marhan, S., et al. (2018). Temporal variations of phosphorus uptake by soil microbial biomass and young beech trees in two forest soils with contrasting phosphorus stocks. *Soil Biol. Biochem.* 117, 191–202. doi: 10.1016/j.soilbio.2017.10.019

Turner, B. L., and Haygarth, P. M. (2000). Phosphorus forms and concentrations in leachate under four grassland soil types. *Soil Sci. Soc. Am. J.* 64:1090. doi: 10.2136/sssaj2000.6431090x

Weiler, M., and Flühler, H. (2004). Inferring flow types from dye patterns in macroporous soils. *Geoderma* 120, 137–153. doi: 10.1016/j.geoderma.2003.08.014

Werner, F., de la Haye, T. R., Spielvogel, S., and Prietzel, J. (2017). Small-scale spatial distribution of phosphorus fractions in soils from silicate parent material with different degree of podzolization. *Geoderma* 302, 52–65. doi: 10.1016/j.geoderma.2017.04.026

Wiekenkamp, I., Huisman, J. A., Bogena, H. R., Lin, H. S., and Vereecken, H. (2016). Spatial and temporal occurrence of preferential flow in a forested headwater catchment. *J. Hydrol.* 534, 139–149. doi: 10.1016/j.jhydrol.2015.12.050

Withers, P. J. A., Edwards, A. C., and Foy, R. H. (2001). Phosphorus cycling in UK agriculture and implications for phosphorus loss from soil. *Soil Use Manag.* 17, 139–149. doi: 10.1111/j.1475-2743.2001.tb00020.x

Wood, T., Bormann, F. H., and Voigt, G. K. (1984). Phosphorus cycling in a northern hardwood forest: biological and chemical control. *Science* 223, 391–393. doi: 10.1126/science.223.4634.391

WRB, (2015). *World Reference Base for Soil Resources 2014, Update 2015. International Soil Classification System for Naming Soils and Creating Legends for Soil Maps*. World Soil Resources Reports 106. Rome: FAO.

Zhu, Y., Fox, R. H., and Toth, J. D. (2002). Leachate collection efficiency of zero-tension pan and passive capillary fiberglass wick lysimeters. *Soil Sci. Soc. Am. J.* 66, 37–43. doi: 10.2136/sssaj2002.0037

**Conflict of Interest:** The authors declare that the research was conducted in the absence of any commercial or financial relationships that could be construed as a potential conflict of interest.

frontiers in Forests and Global Change

ORIGINAL RESEARCH
published: 14 May 2020
doi: 10.3389/ffgc.2020.00047

# Saprotrophic and Ectomycorrhizal Fungi Contribute Differentially to Organic P Mobilization in Beech-Dominated Forest Ecosystems

*Karolin Müller[1]*, Nadine Kubsch[1], Sven Marhan[1], Paula Mayer-Gruner[1], Pascal Nassal[1], Dominik Schneider[2], Rolf Daniel[2], Hans-Peter Piepho[3], Andrea Polle[4] and Ellen Kandeler[1]*

[1] Institute of Soil Science and Land Evaluation, University of Hohenheim, Stuttgart, Germany, [2] Genomic and Applied Microbiology & Göttingen Genomics Laboratory, Georg-August University of Göttingen, Göttingen, Germany, [3] Institute of Crop Science, University of Hohenheim, Stuttgart, Germany, [4] Forest Botany and Tree Physiology, Georg-August University of Göttingen, Göttingen, Germany

OPEN ACCESS

**Edited by:**
Sebastian Loeppmann, Christian-Albrechts-Universität zu Kiel, Germany

**Reviewed by:**
Martin Maier, Forstliche Versuchs-und Forschungsanstalt Baden-Württemberg (FVA), Germany
Matthias Gube, Georg August University Göttingen, Germany

***Correspondence:**
Karolin Müller
karolin.mueller@uni-hohenheim.de

**Specialty section:**
This article was submitted to Forest Soils, a section of the journal Frontiers in Forests and Global Change

**Received:** 19 December 2019
**Accepted:** 03 April 2020
**Published:** 14 May 2020

**Citation:**
Müller K, Kubsch N, Marhan S, Mayer-Gruner P, Nassal P, Schneider D, Daniel R, Piepho H-P, Polle A and Kandeler E (2020) Saprotrophic and Ectomycorrhizal Fungi Contribute Differentially to Organic P Mobilization in Beech-Dominated Forest Ecosystems. Front. For. Glob. Change 3:47. doi: 10.3389/ffgc.2020.00047

Phosphorus (P) is an essential nutrient, but European forest ecosystems are experiencing widespread declines in soil P concentrations. To clarify the roles of ectomycorrhizal (EM) and saprotrophic (SAP) fungi in P cycling in forest soils that differ in inorganic and organic P availability, we conducted an ingrowth tube (IGT) experiment over 18 months of exposure in five beech (*Fagus sylvatica* L.) forests in Germany. To separate the contributions of both fungal guilds *in situ*, two different types of IGTs were used: (i) open IGTs with micromesh windows to allow EM fungi to regrow into the tubes, and (ii) closed IGTs (without mesh windows) in which recolonization by EM hyphae was restricted. We then measured phosphomonoesterase, phosphodiesterase, peroxidase, and phenoloxidase activities in EM (open IGTs) and SAP (closed IGTs) dominated fungal assemblages. Shifts in fungal assemblages occurred over time, but the speed and extent of those shifts differed between the five forest sites. In three forest sites fungal community composition shifted toward greater dominance of EM fungi in open IGTs than in closed IGTs after a period of 18 months, but these changes were not apparent in two other sites. Although shifts in fungal community composition were noticeable between treatments, we found no effect on phosphomonoesterase activity. Since phosphomonoesterase is present in both fungal guilds, this indicates functional redundancy of fungi. Phosphodiesterase activity was slightly reduced in SAP dominated IGTs, indicating that SAP fungi contribute to phosphodiesterase activity to a lesser extent than do EM fungi. P cycling enzymes did not appear to have been influenced by the total P stocks of the forest sites but may have been affected by additional abiotic factors. Contrary to our expectation, phenoloxidase activity was unaffected by fungal community composition, and only peroxidase activity was higher in SAP dominated IGTs, indicating that the contribution of EM fungi to degradation of complex organic material is driven by the need to obtain nutrients in addition to C. Overall, the results of this study contribute to a better understanding of the roles of EM and SAP fungi in P cycling in forest soils.

**Keywords: organic P, inorganic P, acid phosphomonoesterase, phosphodiesterase, peroxidase, phenoloxidase**

## INTRODUCTION

Foliar P content in European beech (*Fagus sylvatica* L.) forest ecosystems is declining, suggesting that these forests may encounter future P deficiency (Jonard et al., 2015; Talkner et al., 2015). Plants take up P in the form of phosphate anions $HPO_4^{2-}$ and $H_2PO_4^-$ (Jones and Oburger, 2011). However, inorganic P ($P_{inorg}$) is frequently adsorbed to minerals and the equilibrium concentration of orthophosphates in soil solution is low; therefore, only a minor fraction of total soil P ($P_{tot}$), which is often <1%, is plant available (Condron et al., 2005; Quiquampoix and Mousain, 2005). In forest soils, a large fraction of $P_{tot}$ is bound in the organic P ($P_{org}$) pool, and this can account for 35–83% of $P_{tot}$ in beech forests (Talkner et al., 2015; Lang et al., 2017; Zederer et al., 2017). $P_{org}$ comprises orthophosphate monoesters (e.g., inositol phosphates), orthophosphate diesters (e.g., nucleic acids, phospholipids), phosphonates, and phosphate anhydrides (Condron et al., 2005). In contrast to the geochemical P cycle, for which exchange processes of soil P pools due to abiotic factors are well understood (Frossard et al., 2000), little is known about the importance of biological regulation mechanisms of the P cycle and the contributions of microbial groups to these processes (Tamburini et al., 2012).

Microorganisms are significantly involved in the P cycle through solubilization, immobilization, and mineralization of $P_{org}$ and $P_{inorg}$ (Richardson and Simpson, 2011), thus mediating the transfer of P between different pools (Plante, 2007). Ectomycorrhizal (EM) and saprotrophic (SAP) fungi are major microbial groups in forest soils and pursue functionally different lifestyles with respect to their carbon (C) acquisition strategies. EM fungi form symbioses with host trees, which supply the fungi with C through photo-assimilates such as sucrose and in return benefit from nutrients and water supplied by EM fungi (Smith and Read, 1997). Especially in nutrient poor ecosystems, mycorrhizal plants accumulate more P than non-mycorrhizal plants because the mutualistic fungi can access a larger soil volume through their branched hyphal network (Smith and Read, 1997; Lambers et al., 2008; Jansa et al., 2011). This beneficial interaction results in an increase in foliar P concentration (Wallander et al., 1997; Alvarez et al., 2009; Danielsen and Polle, 2014).

In contrast to mycorrhizal fungi associated with roots, SAP fungi degrade organic material to obtain C, thereby contributing significantly to the decomposition of organic substances in forest soils (Grinhut et al., 2007; Baldrian, 2008). Mineralization of organic compounds by SAP fungi is directly linked with the turnover of nutrients (Attiwill and Adams, 1993). The release of $P_{inorg}$ is a process catalyzed by extracellular phosphatase enzymes, which are secreted into the soil by microorganisms and plants in response to P demand (Quiquampoix and Mousain, 2005). The extent of enzyme production and excretion is highly regulated by the availability of $P_{inorg}$. Low $P_{inorg}$ availability stimulates phosphatase activity and high $P_{inorg}$ availability inhibits it (Kandeler, 1990; Burns and Dick, 2002; Kavka and Polle, 2017). In addition to their production of specific P cycle enzymes, fungi can decompose complex organic matter due to their ability to produce extracellular per- and phenoloxidases (Baldrian, 2009; Burke et al., 2014; Bödeker et al., 2014). The cleavage of high molecular weight organic carbon compounds is necessary for fungi in order to access N and P containing compounds stored in complex biotic structures such as above- and belowground plant residues. The potential to decompose complex organic matter was previously ascribed to SAP fungi, but recent studies have demonstrated that enzymes required for organic matter degradation are present also in the genomes of EM fungi (Burke and Cairney, 2002; Talbot et al., 2013). Compared to other fungal guilds (i.e., white rot and brown rot saprotrophs), however, the abundance of genes involved in soil organic matter (SOM) decomposition is lower in EM fungi (Martino et al., 2018), indicating that EM fungi may not be able to modify SOM to the same extent as free-living SAP fungi (Zak et al., 2019). Additionally, fungi and bacteria are capable of solubilizing P from recalcitrant inorganic sources (e.g., rock material) by secretion of low molecular weight organic "acid" anions such as oxalates and gluconate (Kucey et al., 1989; Gyaneshwar et al., 2002).

Here, our goal was to disentangle the contributions of EM and SAP fungal assemblages to P mobilization in forest soils. To address this goal we used open and closed ingrowth tubes (IGTs) (Wallander et al., 2001; Wallander, 2006; Wallander and Thelin, 2008). The tubes were filled with forest soil, and by a sand barrier at the top and bottom of each tube fine root accession was avoided, while nutrient and water supply from the surrounding soil into the tubes was enabled. A lateral micromesh window in the open IGTs permitted EM fungal hyphae to recolonize the IGTs, while in closed IGTs (without micromesh windows) recolonization by EM fungi was restricted. We expected that the contribution of fungal guilds to P mobilization depended on P availability in the soil. Therefore, we selected five forests along a geosequence characterized by a gradient in soil P content (Lang et al., 2017) to study fungal abundance and community composition as well as enzyme activity.

We hypothesized: (I) In closed IGTs the fungal communities are shifted toward SAP dominated assemblage because of an EM fungal dieback resulting from a lack of available photo-assimilates. In contrast, the symbiotic EM fungi are able to recolonize the soil in the open IGTs. (II) The phosphomono- and phosphodiesterase activities depend on the proportion of SAP to EM fungi, with higher phosphatase activities in EM dominated soil, since the ability to produce high levels of phosphatases are attributed to symbiotic fungi. (III) The activities of P-cycle enzymes depend on soil P stocks and therefore acid phosphomono- and phosphodiesterase activities are site specific, having lower values in forests with high P stocks and higher values in forests with limited P stocks. (IV) If EM fungi do contribute substantially to the oxidation of organic substrates, the activities of peroxidases and phenoloxidases decrease with decreasing EM abundance in the closed IGTs.

## MATERIALS AND METHODS

### Study Sites

The experiment was conducted in five even-aged beech (*Fagus sylvatica* L.) forests located across Germany (**Table 1**). The soils

**TABLE 1 |** Summary of soil characteristics at the five study sites in Bad Brückenau (BBR), Mitterfels (MIT), Vessertal (VES), Conventwald (CON), and Lüss (LUE), modified from Lang et al. (2017).

| Study sites | BBR | MIT | VES | CON | LUE |
|---|---|---|---|---|---|
| Location[a] | Bavarian Rhön | Bavarian Forest | Thuringian Forest | Black Forest | Lower Saxon Plain |
| Gauss-Krüger coordinates[a] | 3566195, 5579975 | 4564502, 5426906 | 4413076, 5608602 | 3422803, 5321010 | 3585473, 5857057 |
| Altitude (m a.s.l.)[b] | 809 | 1023 | 810 | 840 | 115 |
| Mean annual precipitation[b] | 1031 | 1299 | 1200 | 1749 | 779 |
| Soil type[b] (WRB 2015) | Dystric Skeletic Cambisol | Hyperdystric Chromic Folic Cambisol | Hyperdystric Skeletic Chromic Cambisol | Hyperdystric Skeletic Folic Cambisol | Hyperdystric Folic Cambisol |
| Parent material[b] | Basalt | Paragneis | Trachyandesite | Paragneis | Sandy till |
| Texture[b] (topsoil) (WRB 2015) | Silty clay loam | Loam | Loam | Loam | Loamy sand |
| Tree species composition[b] (%) | *Fagus sylvatica* (99), *Acer pseudoplatanus* (1) | *Fagus sylvatica* (96), *Picea abies* (2), *Abies alba* (2) | *Fagus sylvatica* (100) | *Fagus sylvatica* (69), *Abies alba* (31) | *Fagus sylvatica* (91), *Quercus petraea* (9) |
| Age beeches[b] (a) | 137 | 131 | 123 | 132 | 132 |
| pH ($H_2O$) | 3.8 | 3.6 | 3.4 | 4 | 3.5 |
| $P_{tot}$ (g $m^{-2}$) in up to 1 m soil depth[b] | 904 | 678 | 464 | 231 | 164 |
| $P_{org}$ (% of $P_{tot}$) in Ah1 horizon[b] | 54 | 69 | 66 | 71 | 50 |
| $P_{org}$ (% of $P_{tot}$) in Ah2 horizon[b] | 49 | 75 | 66 | – | 35 |
| $C_{mic}$ in 0–20 cm (μg $g^{-1}$)[b] | 1223 | 795 | 810 | 1392 | 192 |
| $N_{mic}$ in 0–20 cm (μg $g^{-1}$)[b] | 87 | 82 | 64 | 130 | 12 |

[a] *http://www.ecosystem-nutrition.uni-freiburg.de/standorte (2017).* [b] *Lang et al. (2017).*

were formed from different parent materials and differed in P stocks in decreasing order as follows: Bad Brückenau (BBR), over Mitterfels (MIT), Vessertal (VES), Conventwald (CON) to Lüss (LUE) decreasing from 904 to 164 g $P_{tot}$ $m^{-2}$ in depth to 1 m, with ∼50–70% belonging to the $P_{org}$ pool in the Ah1 horizon (**Table 1**). According to the IUSS Working Group WRB (2014), all investigated soils are cambisols with pH values from 3.4 to 4. For more soil properties of each site we refer to Lang et al. (2017) and http://www.ecosystem-nutrition.uni-freiburg.de/standorte.

## Preparation, Installation, and Sampling of Ingrowth-Tubes (IGTs)

To separate EM and SAP fungal communities, we installed *in situ* "open" and "closed" ingrowth tubes (IGTs, size: height of 10 cm, diameter of 5 cm) after descriptions of Johnson et al. (2001), Wallander et al. (2001), and Hendricks et al. (2006). The open IGTs were constructed with 340° micromesh windows (50 μm mesh size, SEFAR NITEX 03-50/37, SEFAR GmbH, Edling, Germany), surrounding the tubes, allowing EM derived hyphae, but not plant roots, to grow into the tubes from ambient soil (see **Supplementary Figure S1**). In contrast, the closed IGTs (without surrounding micromesh) did not allow any ingrowth of hyphae. All IGTs were filled with topsoil (0–20 cm) from the respective forest sites; these had been collected 1 week before tube filling and kept at 4°C. The soil was sieved (<2 mm) to minimize possible carryover of roots. The IGTs were filled to a bulk density of ∼1 g $cm^{-3}$, reflecting average bulk densities of the different forest topsoils (Lang et al., 2017). Tops and bottoms of the tubes had 2 cm mesh borders (50 μm mesh size) filled with sand to avoid fine root accession and hyphal migration of saprotrophic fungi which may have been promoted by starvation of their hyphae while nutrient foraging (Lori Phillips' and Melanie Jones' pers. comm. in Wallander et al., 2013). The sand barriers were made of a 1:1 mixture of carbonate free mineral sand of two differing grain sizes (aquarium sand 0.4–0.8 mm, aquarium sand 1.0–2.0 mm; SCHICKER Mineral GmbH, Bad Berneck, Germany) according to Wallander et al. (2001). This sand barrier was successful as at none of the harvests were plant roots found inside of our IGTs.

In spring 2014, five 30–40 year old beech trees were selected in each of the forests and four IGT treatment sets (each consisting of one open IGT and one closed IGT) were randomly installed around each selected tree at a distance of 2.5 m from the tree. The open and closed IGT of a given set were installed at a distance of 20–30 cm from each other to expose them to comparable microhabitat conditions. The IGTs were vertically buried in the top 20 cm of the soil, in close contact to the surrounding soil. The tops of the upper sand barriers were subsequently covered with a ∼3 cm thick topsoil layer and re-mulched with litter from the surrounding forest floor. For sampling, one IGT set from each tree was removed after 3 months in summer 2014, after 6 months in autumn 2014, after 14 months in summer 2015, and after 18 months in autumn 2015. At the time of removal of each IGT set, additional soil was collected from undisturbed soil in close proximity to the IGT set. Thus, 300 samples were obtained in total (5 forest sites × 3 treatments × 5 replicates × 4 time points). The control samples were also sieved at 2 mm and all samples were frozen at −20°C until further analyses. Soil water content was determined gravimetrically by drying samples at 105°C for 24 h.

## Determination of Phospholipid Fatty Acid (PLFA) Contents

For determination of microbial biomass, phospholipid fatty acid (PLFA) analysis was carried out according to Frostegård et al. (1991) and Frostegård et al. (1993). Initially, 4 g fresh soil was

mixed with 18.4 ml Bligh & Dyer reagent [chloroform, methanol, and citrate buffer (pH 4), 1:2:0.8]. For lipid fractionation, the extract was pipetted onto an extraction column and subsequently diluted with chloroform, acetone, and methanol (Frostegård et al., 1991). Fractionation occurred after alkaline methylation according to Dowling et al. (1986) via methanolic potassium hydroxide, hexane chloroform solution, and acetic acid as described by Ruess et al. (2007). The resulting PLFA methyl esters were dissolved in iso-octane and measured on a gas chromatograph (GC, AutoSystem XL, PerkinElmer Inc., Norwalk, CT, United States). The GC was equipped with a flame ionization detector, an HP-5 capillary column (cross-linked 5% phenyl methyl silicone; 50 m × 0.2 mm, film thickness: 0.33 μm) and helium as carrier gas. The initial column temperature of 70°C was held for 2 min. Temperature was then increased by 30°C $min^{-1}$ to 160°C, then by 3°C $min^{-1}$ to 280°C and held for 15 min. Injection temperature was set at 260°C. The concentration of the fatty acid methyl ester (FAME) was calculated via an internal C24:1 FAME standard, which was added to the samples before methylation. Fungal PLFAs were represented by 18:2ω6,9, gram-positive bacterial PLFAs by *i*15:0, *a*15:0, *i*16:0, *i*17:0 and gram-negative bacterial PLFAs by *cy*17:0 and *cy*19:0. The sum of gram-positive and-negative bacterial PLFAs as well as 16:1ω7 represented the sum of bacterial PLFAs. Total microbial PFLAs were calculated as the sum of all previously mentioned PLFAs plus PLFAs 15:0 and 16:1ω5 (Frostegård and Bååth, 1996; Kandeler et al., 2006).

## Molecular Analysis of Relative Fungal Abundance and Fungal Diversity (Illumina Sequencing)

Soil samples were homogenized in a ball mill Type MM400 (Retsch GmbH, Haan, Germany) in 25 ml containers fitted with a stainless steel ball (20 mm) under liquid nitrogen at 30 Hz $s^{-1}$ for 2 min. DNA isolations were initiated by transferring 250 mg sample material into a bead beating tube containing glass beads (2 ml, MO BIO Laboratories Inc., Carlsbad, CA, United States). Homogenization was conducted under liquid nitrogen for 10 min in the ball mill (30 Hz $s^{-1}$). DNA was extracted with the PowerSoil DNA isolation kit (MO BIO Laboratories Inc., Carlsbad, CA, United States). For DNA elution, a total of 100 μl nuclease-free water (AppliChem, Darmstadt, Germany) instead of buffer supplied by the kit was used for each sample. DNA yields were estimated with a NanoDrop ND-1000 spectrophotometer (Peqlab Biotechnologie GmbH, Erlangen, Germany).

To characterize fungal community composition, the internal transcribed spacer region ITS1 was amplified by PCR using the specific forward primer ITS1-F_KYO1 according to Toju et al. (2012) and the reverse primer ITS2 according to White et al. (1990). Both primers were labeled with Illumina MiSeq specific overhang adapters (Microsynth, Balgach, Switzerland), i.e., ITS1-F_KYO1 5′-TCG TCG GCA GCG TCA GAT GTG TAT AAG AGA CAG CTH GGT CAT TTA GAG GAA STA A-3′ and ITS2 5′ GTC TCG TGG GCT CGG AGA TGT GTA TAA GAG ACA GGC TGC GTT CTT CAT CGA TGC-3′. The polymerase chain reaction (PCR) mix was composed of 5 μl template DNA, 10 μl 5x Phusion GC buffer (New England Biolabs, Frankfurt a. M., Germany), 0.15 μl $MgCl_2$ (50 mM, New England Biolabs, Frankfurt a. M., Germany), 2.5 μl DMSO (5%, New England Biolabs, Frankfurt a. M., Germany), 2.5 μl BSA (8 mg/ml, Sigma Aldrich, St. Louis, MO, United States), 1 μl of each primer (10 mmol/l, Microsynth, Wolfurt, Austria), 1 μl dNTP mix (10 mM each, Thermo Fisher Scientific, Osterode am Harz, Germany), 0.5 μl Phusion high-fidelity DNA polymerase (2 U/μl, New England Biolabs, Frankfurt a. M., Germany) and adjusted to a total volume of 50 μl with nuclease-free distilled water. PCR reactions were performed in a SensoQuest Labcycler (Göttingen, Germany). The PCR program was initiated at 98°C (hold), followed by 98°C for 30 s, 25 cycles of 10 s at 98°C (denaturation), 20 s at 47°C (annealing), 20 s at 72°C (extension) and terminated at 72°C for 5 min.

PCR products were subjected to electrophoresis in 1.2% agarose gels (Biozym LE Agarose, Biozym Scientific GmbH Hessisch Oldendorf, Germany) using 1x running buffer (recipe 5x running buffer: 89 mM tris ultra, 89 mM boric acid, 2 mM EDTA, pH 8.0–8.3) and 10 × loading buffer (600 μl glycerin (99.5%), 50 μl SDS (20%), 200 μl TBE buffer (5x), 100 μl EDTA (0.5 M, pH 8.0), 10 μl bromophenol blue, 40 μl $H_2O$). Gel Red (10,000x) was used for staining (VWR International, Darmstadt, Germany). PCR products were observed using a Raytest Fluorescence Laser Scanner FLA-5100 and evaluated with the Aida Image Analyzer v. 4.27 (both: Raytest GmbH, Straubenhardt, Germany). All PCR reactions were performed in triplicate and pooled and purified using the innuPREP PCRpure kit (Analytik Jena, Jena, Germany). PCR products were run on an agarose gel again and cut in the range of 300–400 bp using the QIAquick Gel extraction kit (Qiagen GmbH, Hilden, Germany) as recommended by the manufacturer. Each sample was eluted in 20 μl nuclease-free water (AppliChem, Darmstadt, Germany) and a UV table (INTAS UV System Type N80M, Göttingen, Germany). Quantification of purified PCR products was done using the Quant-iT dsDNA HS assay Kit (Life Technologies GmbH, Darmstadt, Germany) and a Qubit fluorometer (Life Technologies GmbH, Darmstadt, Germany).

Amplicon libraries were normalized, pooled and sequenced on the Illumina MiSeq platform with MiSeq reagent kit v.3 as recommended by the manufacturer (Illumina, San Diego, CA, United States). Resulting paired-end ITS sequence datasets were merged with PEAR (version 0.9.10; Zhang et al., 2014), quality-filtered and primer clipped with *split_libraries_fastq.py* from the QIIME 1.9.0 software package (Caporaso et al., 2010). Additional primer clipping was performed with cutadapt (version 1.12) (Martin, 2011). High-quality reads were further processed with USEARCH (version 9.2.64_i86linux64; Edgar, 2010), which included, in the following order: size filter (sequences shorter 140 bp were discarded), dereplication, denoising (UNOISE), reference-based (UNITE version 7.2) chimera removal, sequence sorting by length, and OTU determination at 97% sequence identity. Finally, the high quality reads were mapped against the OTUs with USEARCH and an OTU table was generated (Edgar, 2010). Taxonomic classification of OTU sequences was inferred with *parallel_assign_taxonomy_blast.py* against the

UNITE database (version 7.2) (Kõljalg et al., 2013). Taxonomic information was added to the OTU table with biom tools (McDonald et al., 2012). Unidentified fungal OTUs were searched with BLASTn (Altschul et al., 1990) against the nt database (version March 2017) to remove non-fungal OTUs, and only reads classified as fungi were kept. Finally, unclassified OTUs and extrinsic domain OTUs (Protista, Plantae) were removed from the table by employing *filter_otu_table.py* (Caporaso et al., 2010). Sample comparisons were performed at the same surveying effort, utilizing the lowest number of sequences by random selection (3,650). Fungal sequences were assigned to functional guilds using FunGuild (Nguyen et al., 2016).

The ITS1 region sequences were deposited in the National Centre for Biotechnology Information (NCBI) Sequence Read Archive (SRA) under bioproject accession number PRJNA592056.

## Easily Soluble ($P_{sol}$) and Microbially Bound P ($P_{mic}$)

Easily soluble inorganically bound P ($P_{sol}$) and microbially bound P fractions ($P_{mic}$) were extracted according to Hedley et al. (1982). $P_{sol}$ was extracted from fresh soil equivalents to 2 g air-dried soil with 30 ml ultrapure water in presence of a 2 × 3 cm anion exchange membrane (551642S, VWR-International, Darmstadt, Germany) in bicarbonate form. To extract P bound in microbial cells, a second subsample was prepared with 1 ml hexanol in addition to the soil, ultrapure water, and anion exchange membrane ($P_{Hexanol}$). A third subsample ($P_{Control}$) included a defined P concentration of 25 μg P $g^{-1}$ soil DM (spike) for later calculation correction. All subsamples were shaken on a horizontal shaker at room temperature for 18 h. Subsequently, the membranes were washed with deionized water ($H_2O_{deion}$), dried and transferred to a fresh vessel. To remove the P bound onto the membranes, they were shaken in 20 ml 0.5 M HCl for 1 h. After dyeing 1 ml of each sample with 2 ml M&R reagent (Murphy and Riley, 1962), the subsamples were measured photometrically at 712 nm with a microplate reader (ELx808, Absorbance Microplate Reader, BioTek Instruments Inc., Winooski, VT, United States). Percent recovery of spiked P was expressed as:

$$R = \left( \frac{P_{Control} - P_{sol}}{Spike} \right) \times 100$$

Using R and the extraction factor $k_{EP}$ of 0.4 (Brookes et al., 1982) as the relative proportion of hexanol-extractable inorganic P ($P_{Hexanol}$) in total microbial P, $P_{mic}$ was calculated as following:

$$P_{mic} \left[ \mu g\ P\ g\ soil^{-1} DM \right] = \frac{P_{Hexanol} - P_{\mathrm{sol}}}{k_{EP} \times \frac{100}{R}}$$

## Potential Enzyme Activities

The activity of acid phosphomonoesterase (EC 3.1.3.2) was determined in duplicate using the phenyl phosphate method according to Hoffmann (1968), modified by Öhlinger et al. (1996). For this, a 10 ml mixed buffer (pH 5) consisting of 1 M glacial acetic acid and 1 M sodium acetate trihydrate (1:2), as well as 5 ml 0.1 M disodium phenyl phosphate dihydrate (EC 3279-54-7) as substrate solution, were added to 5 g fresh soil. In one control sub-sample, the substrate solution was replaced by $H_2O_{deion}$. All samples were incubated with constant shaking (100 rpm) in a water bath at 37°C for 3 h. Afterward, 35 ml $H_2O_{deion}$ was added, and samples were shaken and filtered. Next, 0.1 ml filtrate was added to 1 ml borate buffer (12.4 g boric acid, solubilized in 100 ml 1 M sodium hydroxide and $H_2O_{deion}$, pH adjusted to 10 and brought to 1 L volume with $H_2O_{deion}$). For measurement, 0.2 ml of 2.6-dibromchinone-4-chlorimide (EC 202-937-2) color reagent (2 mg $ml^{-1}$ ethanol, 60%) was added with 5 ml $H_2O_{deion}$. After 30 min and dilution with 13.9 ml $H_2O_{deion}$, absorbance was measured on a microplate reader (ELx808, Absorbance Microplate Reader, BioTek Instruments Inc., Winooski, VT, United States) at 630 nm.

The activity of phosphodiesterase (EC 3.1.4.2) was measured according to Browman and Tabatabai (1978), modified by Schinner et al. (2012). In duplicate, 4 ml of 0.05 M Tris(hydroxymethyl)aminomethane [Tris(THAM)] buffer (pH 8.0) and 1 ml 5 mM bis(4-nitrophenyl) phosphate sodium salt (EC 223-739-2) as substrate solution were added to 1 g fresh soil. One of these sub-samples was prepared without substrate solution to serve as control. All samples were incubated under constant shaking (100 rpm) in a water bath at 37°C for 1 h. Subsequently, 1 ml 0.5 M calcium chloride solution and 4 ml 0.1 M Tris (THAM) buffer (pH 12.0) were pipetted into the samples. Additionally, 1 ml of the substrate solution was mixed into the control sub-samples. After filtering, all samples were measured at 405 nm using a microplate reader (ELx808, Absorbance Microplate Reader, BioTek Instruments Inc., Winooski, VT, United States).

Measurements of peroxidase and phenoloxidase activities were carried out photometrically using ABTS (2,2′-azino-bis(3-ethylbenzothiazoline-6-sulphonic acid)) as substrate as described by Floch et al. (2007). A mixture of 50 ml $H_2O_{deion}$ and 0.4 g fresh soil was ultrasonically suspended (50 J $s^{-1}$). Peroxidase activity was calculated by subtracting phenoloxidase activity from total enzyme activity. To this end, microplates were prepared for total enzyme activity and phenoloxidase activity analyses separately (Bach et al., 2013). For analysis of total enzymatic activity, 50 μl soil solution was pipetted into each microplate well with 140 μl modified universal buffer [MUB; 2.42 g Tris(THAM) buffer, 2.32 g maleic acid, 2.80 g citric acid monohydrate, 1.26 g boric acid≥ 99.8% solubilized in $H_2O_{deion}$, adjusted to pH 3, brought to 1 L volume], 50 μl 2 mM ABTS substrate solution, and 10 μl $H_2O_2$. Total volume in each well was 250 μ l.

For phenoloxidase activity, 100 μl soil solution and 100 μl MUB were mixed in each microplate well and 50 μl 2 mM ABTS substrate solution was added. A reference sample without substrate was prepared for each sample. Additionally, negative controls without soil were prepared for total enzyme and phenoloxidase activity, respectively. Microplates with sample solutions and substrate were pre-incubated at 30°C for at least 5 min (Floch et al., 2007). Measurement of the resulting stable radical cation $ABTS^{*+}$ was carried out with a microplate

reader (SYNERGY HTX, BioTek Instruments Inc., Winooski, VT, United States) at 30°C at wavelength 650 nm for 30 min every 3 min.

## Statistical Analyses

Statistical analyses were performed with R version 3.5.2 (R Core Team, 2019). A linear mixed-effects model (*nlme* package version 3.1-140; Pinheiro et al., 2019) was used with treatments, harvest dates, sites, and their interaction as fixed effects; and trees (representing the replicates), position of IGT sets around the trees as cardinal direction, and sample IDs as random effects. The fit of the model was assessed based on normal distribution and heteroscedasticity of model residuals and the data were square-root or log-transformed to achieve normality of distribution when necessary. Results of the fitted models are given for the full dataset in **Supplementary Table S1** and for the exposure time of 18 months in **Supplementary Table S2**. Tukey's tests for comparison of means between open and closed IGTs at specific sampling dates, as well as control soils between forests, were run with the package *emmeans* (version 1.3.5; Lenth et al., 2019) at a significance level of 5% (see bold values in **Supplementary Tables S3**, **S4**, respectively).

Principal component analysis (PCA) was carried out on enzyme activities, PLFAs, and abundant EM and SAP genera (absolute numbers of OTUs per genus) in order to determine how enzyme activities varied as a function of fungal community differences. This was done using the "*prcomp*" function of the R stats package (R Core Team, 2019).

# RESULTS

## Shifts in the Relative Abundances and Community Structure of Ectomycorrhizal (EM) and Saprotrophic (SAP) Fungi

At 3 and 6 months after exposure of the IGTs, no shifts in the EM:SAP ratios of the fungal communities were detected (**Figures 1A,B**). In the second year, 14 and 18 months after exposure, the ratio of EM:SAP fungi in the open IGTs increased in three of five forests (MIT, CON, and LUE) (**Figure 1A**). These shifts resulted from dynamic changes in both EM and SAP fungi (**Table 2** and **Supplementary Table S3**). Highest recolonization of open IGTs was found in CON, with an increase in the relative abundance of EM fungi from 10 ± 7% to 54 ± 14% (**Table 2** and **Supplementary Table S3**) and a decrease in SAP fungi from 65 ± 5% to 21 ± 10%. Similar changes occurred in the MIT and LUE soils ($p$ = 0.002). In contrast to the strong changes in the EM and SAP fungal communities in the open IGTs, the EM:SAP fungal ratios in the closed IGTs varied only slightly over the 18 month exposure period in all the studied forests (**Figure 1B**).

Community composition of EM and SAP fungi varied among the IGTs in the investigated beech forests (**Figures 2A,B**). Unexpectedly, we detected an increase in the abundance of EM fungal genera and a decrease in SAP fungi in the BBR forest, but in the other four forests SAP fungi increased (**Figure 2B**) and EM fungi decreased (**Figure 2A**). The decrease in relative abundance of EM fungi in the closed IGTs at MIT, VES, CON and LUE was mainly due to decreases in the genera *Russula* and *Craterellus* spp. (**Figure 2A**). In the closed IGTs at BBR forest, the genera *Amanita*, *Imleria* and *Cenococcum* spp. increased in abundance (**Figure 2A**). Among SAP, *Solicoccozyma* and *Mortierella* spp. were most affected by the treatments in all forests, increasing dramatically during the exposure period (**Figure 2B**). These results show that our experimental approach with open and closed IGTs successfully established distinct EM and SAP fungal assemblages, but other fungal groups with unclear EM status (such as *Entoloma, Meliniomyces*, and *Sistotrema* spp.) were unaffected by the treatment after 18 months of exposure (**Supplementary Table S3**).

## Phospholipid Fatty Acid (PLFA) Content

Total microbial PLFA content in the closed IGTs was on average 8% lower than in the open IGTs after 18 months (**Supplementary Figure S2A**). Similar results were found for 18:2ω6,9 ($p < 0.001$), which is considered to be a fungal biomarker (**Figure 3**). The difference between open and closed IGTs was also mirrored in bacterial biomass, with the strongest decrease in VES (13%) (**Supplementary Figure S2B**). The five forests differed significantly in their fungal and bacterial PLFA contents (**Figure 3** and **Supplementary Figure S2**): BBR and CON had the highest and LUE the lowest fungal PLFA content ($p$ = 0.026). The fungal-to-bacterial ratios of PLFAs were unaffected by treatment after 18 months of IGT exposure.

## Easily Soluble P Fraction ($P_{sol}$) and Microbial Bound P ($P_{mic}$)

The content of water-extractable P ($P_{sol}$) was not influenced by the type of IGT (**Figure 4A**). However, $P_{sol}$ content was forest-specific ($p < 0.001$) with much higher values in VES than in the other forests. The microbial P ($P_{mic}$) content did not differ between treatments (**Figure 4B**), although a trend was seen, with an increase in the $P_{mic}$ content between 14 and 18 months in all forests ($p$ = 0.083, **Supplementary Table S3**). The installation of the IGTs had no effect on microbially bound P values, as the $P_{mic}$ values inside the cores did not change in comparison to the ambient soil (**Figure 4B** and **Supplementary Table S4**).

## Enzyme Activities

Acid phosphomonoesterase activities (**Figure 5A**) were ∼40-fold higher than the activities of phosphodiesterases (**Figure 5B**). The acid phosphomonoesterase activity was not significantly different between open and closed IGTs after 18 months of exposure. In contrast, phosphodiesterase activity was reduced in the closed compared to the open IGTs ($p < 0.001$), with significant differences in all forests except BBR. Both esterase activities were forest-specific (acid phosphomonoesterase: $p$ = 0.038, phosphodiesterase: $p < 0.001$).

Phenol- and peroxidase activities (**Figures 5C,D**) varied between the forest sites ($p < 0.001$) after 18 months of exposure. The treatment was only significant in CON with 44% lower phenoloxidase activity in closed than in open IGTs but no

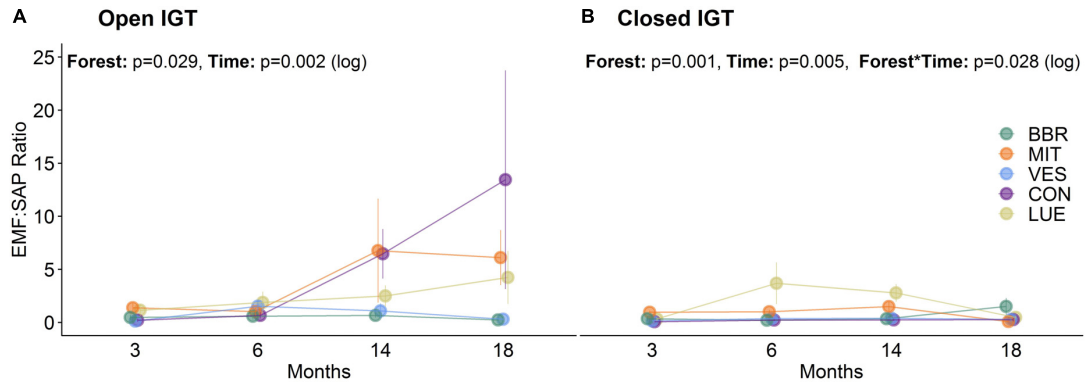


**FIGURE 1 |** Ratio of ectomycorrhizal to saprotrophic fungi (EM:SAP) in **(A)** open ingrowth tubes (IGTs) and **(B)** closed IGTs based on absolute number of OTUs in Bad Brückenau (BBR), Mitterfels (MIT), Vessertal (VES), Conventwald (CON), and Lüss (LUE) over 18 months of exposure ($n$ = 5).

**TABLE 2 |** Relative proportion of ectomycorrhizal (EM) and saprotrophic (SAP) fungi OTUs in open and closed ingrowth tubes (IGTs) based on Illumina sequencing in Bad Brückenau (BBR), Mitterfels (MIT), Vessertal (VES), Conventwald (CON), and Lüss (LUE) over 18 months of exposure ($n$ = 5).

| Parameter | Exposure Time (months) | EM fungi (% OTU) | | SAP fungi (% OTU) | |
|---|---|---|---|---|---|
| | | Open IGT | Closed IGT | Open IGT | Closed IGT |
| BBR | 3 | 17.51 ± 6.94 | 13.51 ± 6.96 | 52.29 ± 7.51 | 57.17 ± 7.83 |
| | 6 | 23.05 ± 10.23 | 12.02 ± 2.68 | 46.47 ± 4.16 | 60.79 ± 2.77 |
| | 14 | 28.93 ± 7.49 | 16.22 ± 3.6 | 47.39 ± 3.12 | 54.13 ± 6.18 |
| | 18 | 13.32 ± 2.93 | 39.69 ± 13.89 | 61 ± 3.83 | 43.34 ± 9.24 |
| MIT | 3 | 35.93 ± 9.08 | 31.46 ± 2.26 | 37.84 ± 10.82 | 33.84 ± 2.06 |
| | 6 | 33.87 ± 9.35 | 34.33 ± 3.61 | 42.93 ± 7.06 | 35.87 ± 3.03 |
| | 14 | 43.69 ± 13.41 | 32.42 ± 5.21 | 15.47 ± 4.22 | 27.53 ± 5.64 |
| | 18 | **53.85 ± 15.72** | **4.56 ± 0.95** | **11.84 ± 4.22** | **71.02 ± 5.57** |
| VES | 3 | 6.17 ± 1.75 | 7.56 ± 1.77 | 51.37 ± 3.8 | 56.32 ± 4.34 |
| | 6 | 43.2 ± 7.75 | 16.33 ± 3.58 | 34.25 ± 4.79 | 47.29 ± 1.73 |
| | 14 | 26.92 ± 12.22 | 18.52 ± 5.15 | 46.35 ± 9.21 | 52.89 ± 3.57 |
| | 18 | 14.74 ± 4.13 | 6.73 ± 3.92 | 51.99 ± 2.56 | 45.18 ± 8.67 |
| CON | 3 | 10.08 ± 7.11 | 4.28 ± 0.66 | 64.62 ± 5.11 | 65.75 ± 2.25 |
| | 6 | 24.67 ± 8.69 | 10.52 ± 4.49 | 48.18 ± 6.81 | 52.17 ± 2.18 |
| | 14 | **62.86 ± 12.74** | **11.25 ± 4.62** | **18.02 ± 7.11** | **50.47 ± 2.06** |
| | 18 | **53.61 ± 14.29** | **10.04 ± 3.67** | **21.41 ± 9.82** | **67.36 ± 11.28** |
| LUE | 3 | 30.73 ± 11.9 | 13.56 ± 6.86 | **55.39 ± 14.16** | **70.32 ± 12.03** |
| | 6 | 37.01 ± 7.96 | 53.67 ± 14.73 | 34.38 ± 8.16 | 32.36 ± 10.65 |
| | 14 | 51.02 ± 13.69 | 62.14 ± 7.03 | 37.52 ± 11.66 | 29.38 ± 6.47 |
| | 18 | **51.71 ± 13.25** | **19.3 ± 6.05** | 29.35 ± 9.37 | 45.06 ± 5.81 |

*Significant differences of EM and SAP fungi between open and closed IGTs are highlighted in bold.*

treatment effects in the other forests (**Figure 5C**). In contrast to phenoloxidase activity, the closed IGTs were higher in peroxidase activities than the open IGTs in all forests ($p$ = 0.002) (**Figure 5D**). The effect of treatment was higher in CON and LUE with increases in peroxidase activity of 21 and 34%, respectively.

Principal component analysis disclosed that the first two principal components (PCs) together accounted for 50% of the variance in enzyme activity, fungal and bacterial PLFA content, as well as abundant EM and SAP genera after 18 months of exposure (**Figure 6**). The fungal genera appeared to separate on axis PC2, while total fungal and bacterial PLFAs separated together with enzyme activities on axis PC1. LUE was clearly separate from the other forests. Additionally, in BBR and CON, closed and open IGTs separated from each other.

# DISCUSSION

## Trenching Resulted in a Shift in the Fungal Community

An experiment with two different types of ingrowth cores was used to study the importance of fungal-fungal interactions in forest sites differing in their inorganic and organic P availability. We expected a shift in fungal communities in the closed IGTs

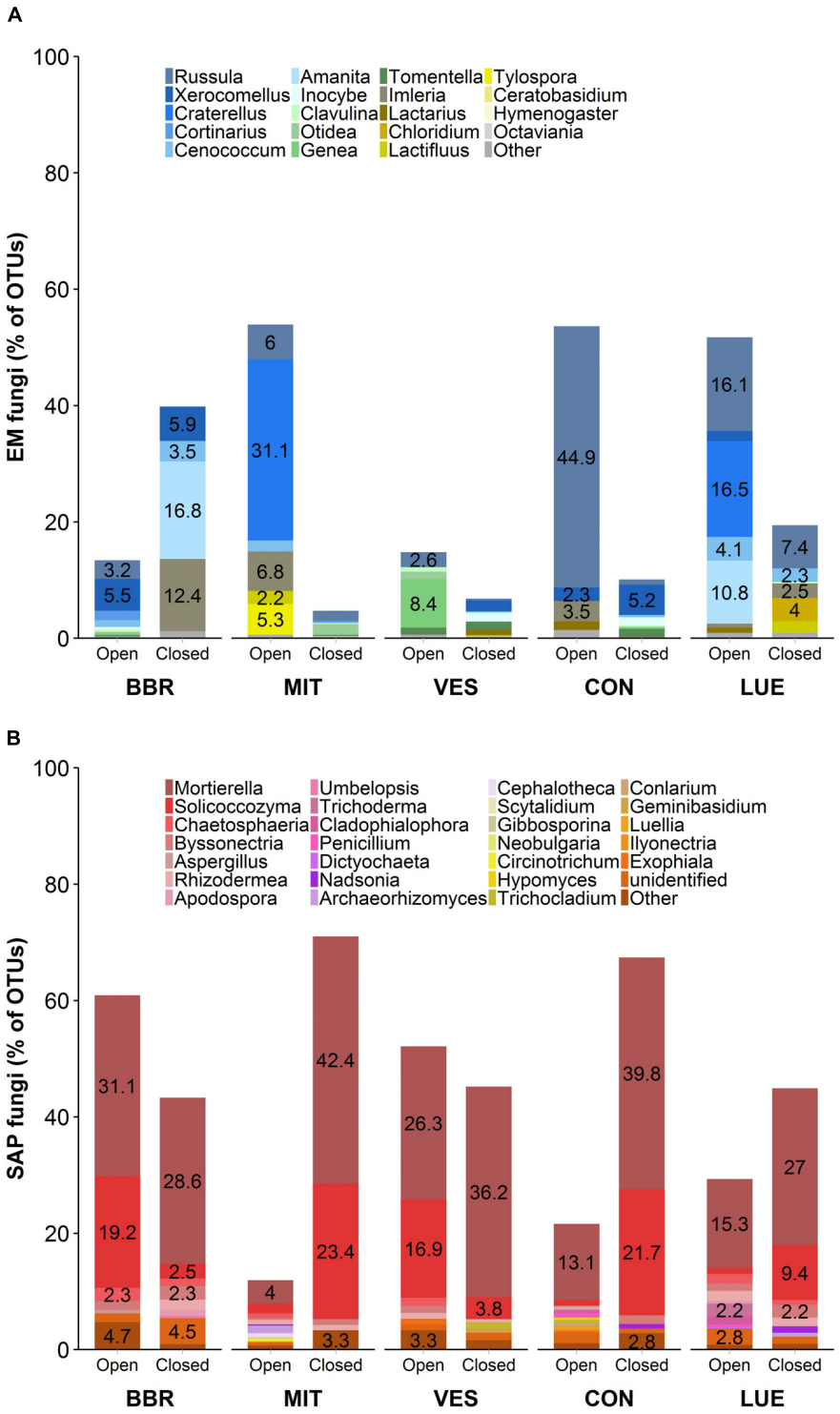


**FIGURE 2 |** Fungal community composition of **(A)** ectomycorrhizal (EM) fungi and **(B)** saprotrophic (SAP) fungi in open and closed IGTs based on Illumina Sequencing data in Bad Brückenau (BBR), Mitterfels (MIT), Vessertal (VES), Conventwald (CON), and Lüss (LUE) after 18 months of exposure ($n$ = 5).

toward SAP dominated assemblages due to the disruption in photo-assimilate availability for EM fungi. In contrast, open IGTs should have permitted the recolonization of EM fungi into the cores from the surrounding soil. Our results clearly show that shifts in fungal assemblages occurred over time, but that the speed and extent of changes differed in the five forest sites.

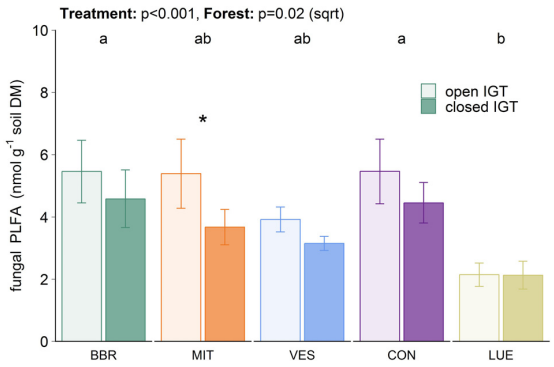


**FIGURE 3 |** Fungal biomass in open and closed ingrowth tubes (IGTs) based on phospholipid fatty acid analysis in Bad Brückenau (BBR), Mitterfels (MIT), Vessertal (VES), Conventwald (CON), and Lüss (LUE) after 18 months of exposure ($n$ = 5). Forests sharing no letter are significantly different and asterisks highlight significant differences between open and closed IGTs at the respective forest site.

In three forest sites (MIT, CON, and LUE), fungal community composition shifted toward a higher dominance of EM fungi in open IGTs after a period of 18 months, whereas these changes were not apparent in two other forests (BBR and VES). It could be that recolonization of the open IGTs occurred more slowly in BBR and VES than in the other forest sites, but it is unclear whether unidentified abiotic environmental factors may have precluded rapid fungal growth. Another possibility is that SAP fungal communities competed with EM fungi and thereby delayed the recolonization process. Therefore, our hypothesis was only supported by the results of three of the five studied sites, suggesting that additional factors not included in our study may have impacted fungal community composition and influenced the speed and extent of the colonization process of the IGTs.

The temporal dynamics of the fungal assemblages in the IGTs were influenced by the initial disruption of the fungal hyphal network of both EM and SAP fungi between the soil inside the IGTs and the surrounding soil. The exclusion of animal guilds, which graze specifically on EM or disturb the hyphal net such as Protura and earthworms (Yang et al., 2015; Bluhm et al., 2019) might have facilitated strong proliferation of EM compared to other fungi, which we found in some IGTS (MIT, CON, LUE). However, this suggestion is currently speculative since we do not know how soil animals vary among our forest sites. Based on low EM/SAP ratio in closed IGTs and higher EM/SAP ratio in open IGTs we were able to discuss the differences in fungal physiology in P-cycling. Our results are in accordance with data from Wallander et al. (2013). They found twice as much fungal biomass (measured as 18:2ω6,9 PLFA content) in a mesh bag in young Norway spruce (*Picea abies* L.) forests after 12 months of incubation than in those buried for only 2–5 months. After 18 months of exposure, we found a higher content of the fungal PLFA biomarker (18:2ω6,9) in the open IGTs than in the closed IGTs. Since EM fungi are the dominant contributors to the total 18:2ω6,9 PLFA in acidic forest soils (Wallander et al., 2001; Hagerberg and Wallander, 2002), we tentatively attribute the differences in the fungal PLFA content to recolonization by EM fungi in the open IGTs. This suggestion is supported by our amplicon data, which showed an increase in the number of EM OTUs in the open IGTs in MIT, VES, and LUE, and a stable number of EM OTUs in BBR and CON over time. In addition, SAP abundance decreased in the forest sites MIT, VES and LUE over time, whereas their abundance remained stable in BBR and CON. Overall, these changes in fungal assemblages were largely restricted to the EM and SAP fungal communities, while other fungal groups (e.g., fungi with unknown EM status or arbuscular mycorrhizal fungi) were low in OTU abundance and did not change throughout the experiment. Therefore, these groups were considered negligible in terms of P dynamics.

The EM fungal assemblages found in the open IGTs are typical for temperate beech forest sites (Lang et al., 2013). In our open IGTs, *Russula*, *Cenococcum*, and *Xerocomellus* spp. were the abundant groups after 18 months of exposure. These results agree with those of Pena et al. (2013), who found great interspecific variation in the temporal patterns of beech litter recolonization by EM fungi. In a litter bag experiment, Pena et al. (2013) observed an initial recolonization by EM fungi classified as contact or short-distance exploration types such as *Russula cuprea*, *Cenococcum geophilum, Humaria* spp., or *Sebacina* spp. (Agerer, 2001). EM fungi from the long-distance exploration types (Agerer, 2001) such as *Xerocomellus pruinatus* gained access to the litter inside the bags over the course of time. Additionally, we found *Cortinarius* spp., which have extensive SOM decomposition capacity, also in boreal forest soils (Bödeker et al., 2014). This result suggests ongoing decomposition of SOM inside the IGTs due not only to SAP fungi, but also to some EM fungi.

Fungi with the capacity to decompose complex organic material may profit from the dieback of other microorganisms by using the C and nutrients from microbial necromass in addition to plant-derived C sources. The installation of the IGTs affected the abundance and diversity of the EM fungi to a greater degree than that of the SAP fungi, as EM fungi rely on the connection with roots of their host plant. Disconnection from their host plants led to a dieback of these organisms (Högberg and Högberg, 2002; Remén et al., 2008), as seen, e.g., for *Russula* spp. in the closed IGTs in CON. Furthermore, disturbance of the soil by IGT installation may have brought litter and dead root material into closer contact than before to fungi and other microorganisms with saprotrophic properties. This could have provided SAP with a spatial advantage because new EM fungi had to grow into the open IGTs, whereas SAP could immediately establish their hyphal networks with the readily available resources, occupying free niches in the IGTs. Our results thus concur with those of Lindahl et al. (2010) in a *Pinus sylvestris* L. forest in Sweden. The authors concluded that disturbance induces rapid growth of opportunistic SAP fungi using the dying mycorrhizal mycelia. In accordance, Brabcová et al. (2016) found a specific microbial community in the vicinity of the dead mycelia of mostly non-basidiomycetous r-strategists such as *Mortierella*, *Aspergillus*, and *Penicillium* spp. In our study, *Mortierella* was the most abundant genus of SAP fungi

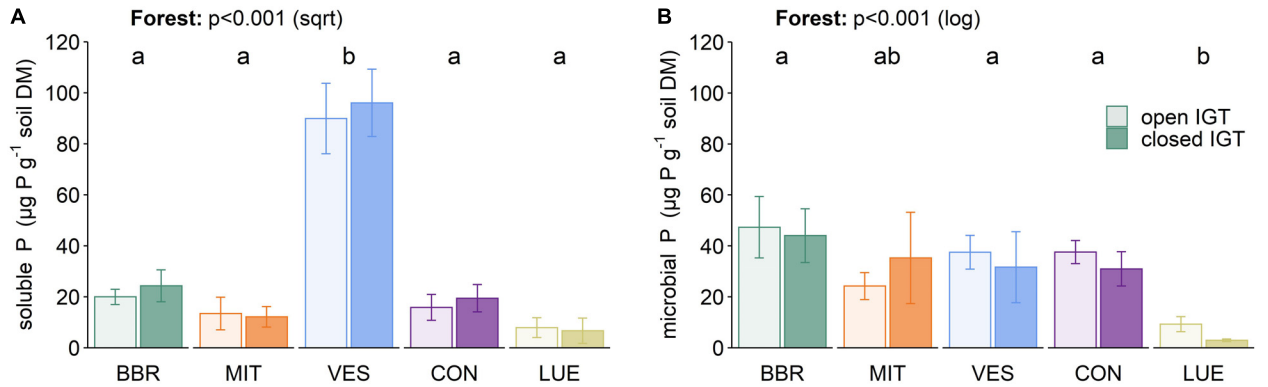


**FIGURE 4 | (A)** Soluble P and microbially bound P **(B)** in open and closed IGTs in Bad Brückenau (BBR), Mitterfels (MIT), Vessertal (VES), Conventwald (CON), and Lüss (LUE) after 18 months exposure ($n$ = 5). Forests sharing no letter are significantly different.

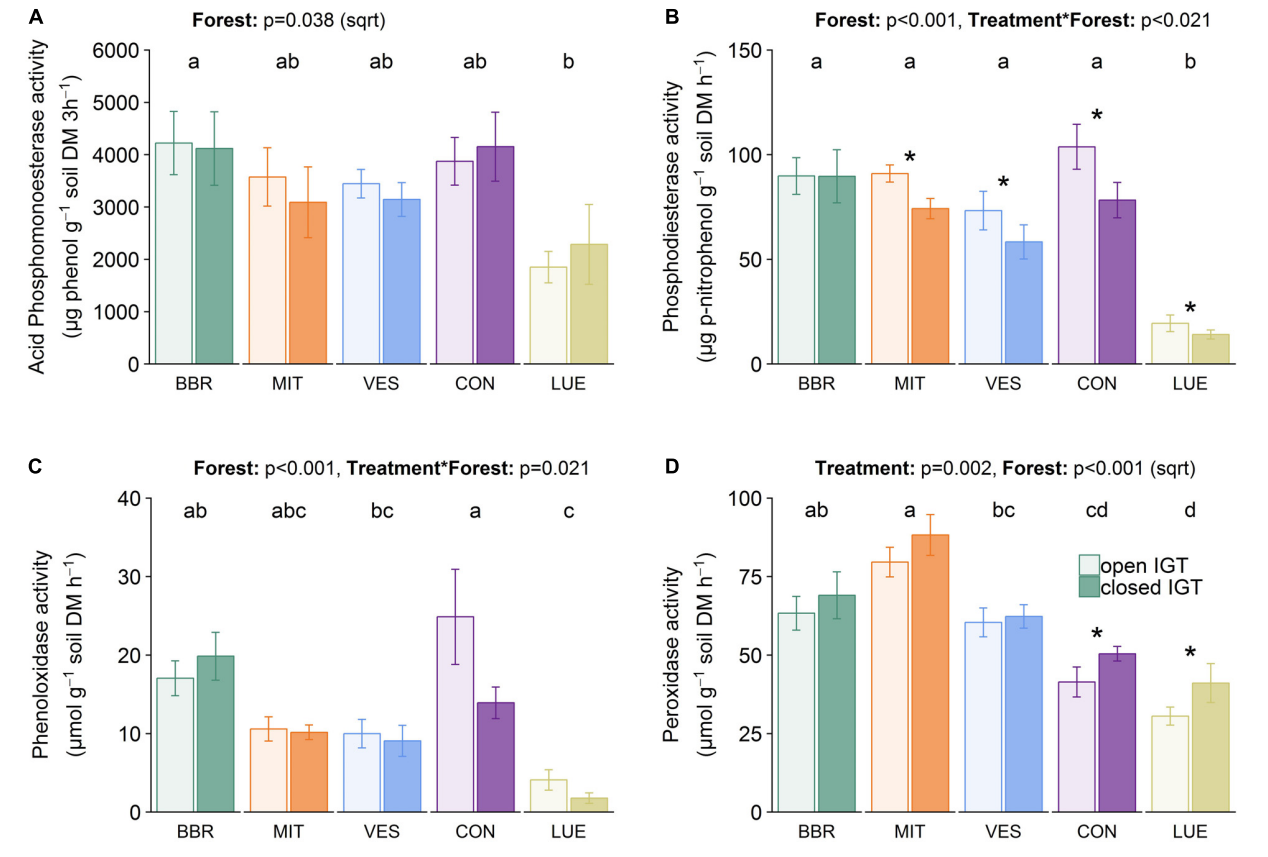


**FIGURE 5 |** Enzyme activities of **(A)** acid phosphomonoesterase, **(B)** phosphodiesterase, **(C)** phenoloxidase, and **(D)** peroxidase activity in open and closed IGTs in Bad Brückenau (BBR), Mitterfels (MIT), Vessertal (VES), Conventwald (CON), and Lüss (LUE) after 18 months of exposure ($n$ = 5). Forests sharing no letter are significantly different and asterisks highlight significant differences between open and closed IGTs at the respective forest site.

and more abundant in the closed than in the open IGTs. In particular, in MIT 42% of the SAP OTUs belonged to this genus, in comparison to only 4% in the corresponding open IGTs. Similar to the data of Buée et al. (2009), who identified *Solicoccozyma* as a highly abundant genus in different forest soils in France, this genus was also abundant in our forest soils. *Solicoccozyma* specializes in using C from cellulose in spruce forests and thus is known to be heavily involved in the decomposition of dead plant litter (Štursová et al., 2012). We assume that the dead organic material of dying EM hyphae served as a C source in addition to the available plant litter material. This source may explain the observed increase in abundance of

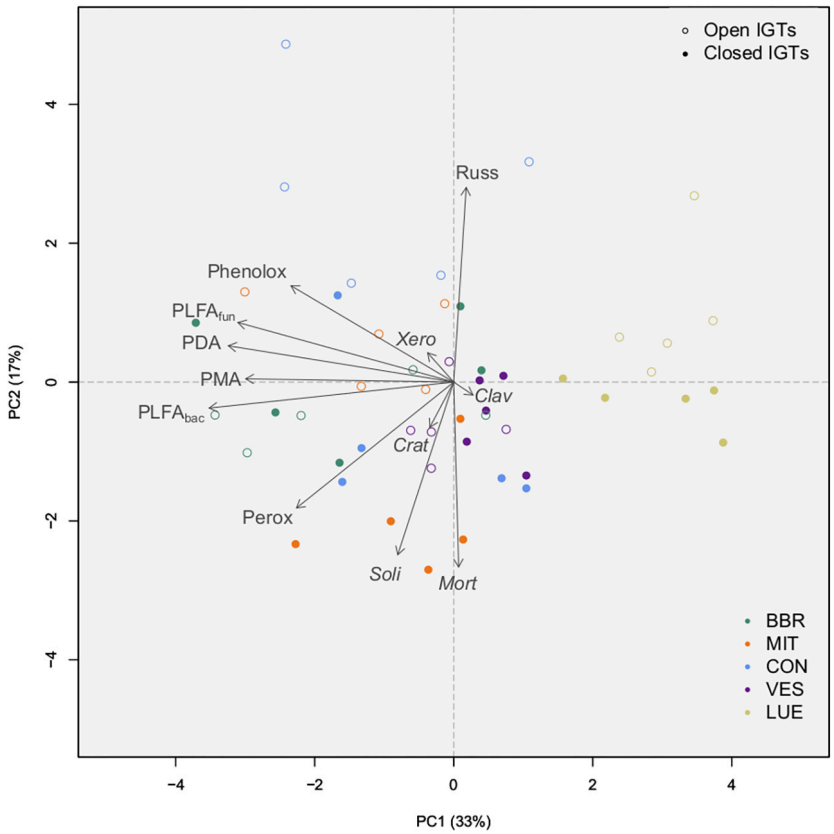


**FIGURE 6 |** Results of principal component analysis of absolute amounts of PLFAs (sum of 15:0, i15:0, a15:0, i16:0, i17:0, cy17:0, cy19:0, 16:1ω5 = bacterial PLFA, 18:2ω6,9 = fungal PLFA), absolute number of OTUs from the most abundant EM and SAP fungal genera, and absolute amount of enzyme activity groups by treatment (open IGTs, closed IGTs) and forest [Bad Brückenau (BBR), Mitterfels (MIT), Vessertal (VES), Conventwald (CON) and Lüss (LUE)]. *Clav*, *Clavulina*; *Crat*, *Craterellus*; *Mort*, *Mortierella*; PDA, Phosphodieserase activity; Perox, Peroxidase activity; Phenolox, Phenoloxidase activity; PLFA$_{bac}$, bacterial PLFA; PLFA$_{fun}$, fungal PLFA; PMA, Phosphomonoesterase activity; *Russ*, *Russula*; *Soli*, *Solicoccozyma*; Xero, *Xeromellus*.

*Solicoccozyma* in the closed IGTs in three (MIT, CON, and LUE) out of five forests.

## SAP and EM Fungal Assemblages Affected Enzyme Activities

We hypothesized that phosphomono-and phosphodiesterase activities depend on the proportion of SAP to EM fungi, with higher P cycling enzyme activities in soils dominated by EM fungi. All of our forest sites are characterized by low pH values (3.4–4) where fungi are the dominant microbial group and compete successfully with bacteria. As we cannot completely exclude the bacterial and animal contribution to the production of phosphatases, we focused on fungi community composition and related differences in P-cycling enzyme activity mainly to changes in fungal production of these enzymes and not to plants, bacteria and archaea (Nannipieri et al., 2011). Our results demonstrated that fungal community composition had no effect on phosphomonoesterase activity, while the exclusion of EM led to a decrease in phosphodiesterase activity of up to 38%. Although the shifts in fungal community composition were noteworthy between treatments, phosphomonoesterase activity was steady, suggesting some functional redundancy in fungal-derived P cycling enzymes (**Figure 6**). Therefore, the capacity to produce acid phosphomonoesterases is present in both fungal guilds to a similar extent. Our results are supported by findings of Colpaert and Laere (1996) who found, in a pot experiment with mycorrhizal and non-mycorrhizal seedlings of *Pinus sylvestris* L., considerable evidence that EM fungi produce extracellular phosphatases. Also, Dighton (1983, 1991) measured equal or even higher phosphatase activity production by EM fungi than by SAP basidiomycetes. Cell wall-bound and extracellular acid phosphomonoesterase activities have, indeed, been demonstrated for a wide taxonomic range of EM fungi (Pritsch and Garbaye, 2011), including genera which are abundant in our study, e.g., *Clavulina*, *Russula, Cenococcum, Tomentella, Lactarius*, and *Amanita* (Ho and Zak, 1979; Alvarez et al., 2005, 2006; Nygren and Rosling, 2009; Walker et al., 2014; Ning et al., 2018; Ruess et al., 2019).

In our experiment, phosphodiesterase activity was generally lower than phosphomonoesterase activity, which is in line with findings from Turner and Haygarth (2005). We found lower phosphodiesterase activities in four of our sites (exception

BBR) in SAP-dominated IGTs, indicating that SAP fungi were not as involved as EM fungi in the production and secretion of phosphodiesterases. Phosphodiesterase activity has scarcely been investigated *in situ* (Ruess et al., 2019), and to our knowledge measurements are lacking for individual EM fungal genera. The formerly held opinion that SAP fungi are the only degraders of complex organic substances that release directly plant-available P is now being revised (Lindahl and Tunlid, 2015). EM fungi have a greater capacity to produce enzymes involved in the degradation of complex organic material than was previously thought. Genomic and field studies have demonstrated that fungi have retained many degrading enzymes and that SAP and EM fungi are more functionally similar than previously considered (Baldrian, 2009; Burke et al., 2014; Bödeker et al., 2016).

Whereas phosphomono- and phosphodiesterase directly release plant-available P, phenoloxidase and peroxidase activities may indirectly contribute to P mineralization by liberating organic P-compounds from complex organic substrates, preparing them for further cleavage. Contrary to our initial hypothesis, the phenoloxidase activity remained unchanged, whereas the peroxidase activity was higher only in SAP-dominated IGTs. This indicates that EM fungi produce phenoloxidases much as SAP fungi do under similar environmental conditions. The capacity to produce substrate-specific laccases, probably the largest class of phenoloxidases in soils, is known only for some ectomycorrhizal species, e.g., *Russula delica* (Matsubara and Iwasaki, 1972). *Russula* was one of the most abundant genera in our experiment. Luis et al. (2004, 2005) investigated the diversity of basidiomycete laccase genes in beech-oak forests in Germany and they linked 108 gene sequences to specific fungal taxa. Two-thirds belonged to EM fungi and the remaining to SAP fungi. In a follow-up experiment, Kellner et al. (2009) showed that the temporal variation in EM laccase diversity peaked with autumn litterfall, while overall phenoloxidase activity in the litter layer was similar over the seasons. This indicates the importance of EM fungi as decomposers of more complex material to gain access to organic forms of P (Talbot et al., 2013), although the presence of a gene sequence in the DNA that likely codes for phenoloxidase enzymes is not adequate proof of a particular species' capacity to produce these enzymes *in situ*.

We assume from our results that peroxidase activity, at least to some extent, was derived from EM fungi. For example, *Cortinarius* spp. encode lignolytic class-II peroxidases in their genome, and their gene transcription correlates highly with peroxidase activity in a boreal pine forest soil (Bödeker et al., 2014). In agreement with these results, we found high peroxidase activities in BBR and MIT where *Cortinarius* spp. were abundant (**Figure 2**), but this genus was not found in VES, CON, and LUE, where peroxidase activity was lower. Additionally, Bödeker et al. (2014) found that Mn-peroxidase production is not a general feature of all *Cortinarius* spp. in soils. High peroxidase activity was also detected when these fungi were not abundant, indicating that the Mn-peroxidase production is not restricted to *Cortinarius*. Distinct peroxidase activity is also known for *Lactarius* spp. (Nicolás et al., 2019) and *Russula* spp. (Bödeker et al., 2009). All mentioned genera were present in our investigated forests. Although these genera are ecologically important, little is known about their specific functions as they comprise many members which have not been well studied. Therefore, the question remains as to what extent the EM fungal community is involved in the decomposition process to obtain nutrients other than C. Collectively, our results suggest that EM fungi are not only involved in the production of P cycle enzymes but also in per- and phenoloxidase production to decompose complex SOM to meet their own P needs. Therefore, we reject our third hypothesis that the exclusion of EM fungi in the closed IGTs led to a pronounced reduction in oxidase activity.

## Forest Conditions Affected P Cycle Enzyme Activities With Implications for $P_{mic}$ and $P_{sol}$

P availability is acknowledged as a key driver of the production of P cycle enzymes (Quiquampoix and Mousain, 2005), so we expected that the activity of these enzymes is dependent on soil P stock, with lower values in forests with high P stocks and higher values in forests with limited P stocks. The investigated forests were selected based on a geosequence derived from total P stock values (BBR > MIT > VES > CON > LUE, see **Table 1**) according to Lang et al. (2017). Specific phosphomonoesterase activities (enzyme activity per microbial biomass measured as PLFAs) showed an opposite gradient from the total P stock gradient, with highest enzyme activity per biomass in LUE and lowest in BBR. For specific phosphodiesterase activity, we recorded highest values in CON, intermediate values in BBR, MIT, VES, and lowest in LUE. Therefore, we can partly confirm our hypothesis.

Some evidence indicated that in addition to P availability, soil texture may influence biotic soil components and their functions. The adsorption of enzymes to clay particles can reduce enzyme activities *in situ* (Leprince and Quiquampoix, 1996) and this likely depends on the soil type (Louche et al., 2010). The specific phosphodiesterase activity was lowest in LUE, although Lang et al. (2017) identified different $P_{org}$ fractions by NMR spectroscopy, and found a high proportion of phosphodiesters of ∼20% of total $P_{org}$ in the upper 20 cm depth. They assumed that this contrast in high P substrate availability and low phosphodiesterase activity was due to either low enzyme stability at low pH values of 3.5 and/or low microbial enzyme production, resulting in a higher proportion of phosphodiesters in comparison to phosphomonoesters in LUE.

The BBR soil was not P limited for plants, as P-fertilization did not enhance photosynthesis in contrast to LUE soil (Zavišić et al., 2018). Similarly, Heuck and Spohn (2016) concluded that the soils in BBR and MIT may not be P depleted and/or that P is not the only limiting nutrient in the soil. Apart

from microbial P, N, and C supplies (Kieliszewska-Rokicka, 1992; Taniguchi et al., 2008), other abiotic factors such as moisture (Courty et al., 2007), temperature, and pH (Tibbett et al., 1998), may influence microbial activities and functions to some extent. In VES, we found much higher $P_{sol}$ values than in the other four forests (see **Figure 4A**). Surprisingly, the higher $P_{sol}$ values did not influence the specific enzyme activities of phosphomono- and phosphodiesterases, underscoring the possibility that microbially mediated P mobilization is also influenced by site-specific conditions.

## CONCLUSION

Understanding the importance of fungal-fungal interactions in forest ecosystems is necessary to better disentangle the relative contributions of EM and SAP fungi in P cycling. This study investigated phosphatase and oxidase activities in EM and SAP dominated fungal assemblages in beech forest ecosystems with differing P availabilities. Taken together, our results indicate that phosphatase and oxidase activity in EM and SAP dominated assemblages was more similar than expected, with only minor differences in phosphodiesterase and peroxidase activities. They also provide new insights into biological regulation mechanisms of the P cycle and highlight the role of EM fungi in meeting P demand for the fungi themselves and for their host plant, especially in nutrient poor ecosystems.

## DATA AVAILABILITY STATEMENT

The datasets generated for this study can be found in the National Centre for Biotechnology Information (NCBI) Sequence Read Archive (SRA), accession number: PRJNA592056.

## AUTHOR CONTRIBUTIONS

EK and SM developed the project. KM, NK, and PN wrote the manuscript, which was read and revised by all co-authors. Fieldwork was performed by PN. Soil analyses were mainly performed by PN and PM-G. DS, RD, and AP performed the molecular biological analyses and bioinformatic analysis of the sequence data. KM performed statistics and data evaluation with support by H-PP. All authors listed have made substantial, direct, and intellectual contributions to the work, and have approved it for publication.

## FUNDING

We are grateful to the Deutsche Forschungsgemeinschaft for supporting the Priority Program 1685 "Ecosystem Nutrition" by funding the projects Ka 1590/12-1 and Po 362/22-1.

## ACKNOWLEDGMENTS

We would like to thank H. Haslwimmer and S. Rudolph for help during soil analysis, T. Klein (University of Göttingen, Laboratory for Radio-Isotopes) for DNA extraction and preparation for the ILLUMINA analyses and K. Regan for English corrections. Furthermore, we thank the student helpers for supporting the extensive installation of soil cores and subsequent harvest campaigns in the field.

## SUPPLEMENTARY MATERIAL

The Supplementary Material for this article can be found online at: https://www.frontiersin.org/articles/10.3389/ffgc.2020.00047/full#supplementary-material

**FIGURE S1 | (A)** Prototype of the open IGTs and **(B)** soil filled open and closed IGTs directly before installation.

**FIGURE S2 | (A)** Microbial and **(B)** bacterial biomass based on PLFA-analysis in the open and closed IGTs in Bad Brückenau (BBR), Mitterfels (MIT), Vessertal (VES), Conventwald (CON), and Lüss (LUE) after 18 months of exposure ($n = 5$). Forests sharing no letter are significantly different and asterisks highlight significant differences between open and closed IGTs at the respective forest site.

**TABLE S1 |** Results of the nlme-Model for the IGTs in Bad Brückenau (BBR), Mitterfels (MIT), Vessertal (VES), Conventwald (CON), and Lüss (LUE), including all sampling dates ($n = 5$). Level of significance: $^{***}p < 0.001$, $^{**}p < 0.01$, $^{*}p < 0.05$, and $^{+}p < 0.1$.

**TABLE S2 |** Results of the nlme-Model for the IGTs in Bad Brückenau (BBR), Mitterfels (MIT), Vessertal (VES), Conventwald (CON), and Lüss (LUE), including only the last sampling date after 18 months of exposure ($n = 5$). Level of significance: $^{***}p < 0.001$, $^{**}p < 0.01$, $^{*}p < 0.05$, and $^{+}p < 0.1$.

**TABLE S3 |** Results of open and closed IGTs in Bad Brückenau (BBR), Mitterfels (MIT), Vessertal (VES), Conventwald (CON), and Lüss (LUE) during the experiment ($n = 5$). Bold values represent statistically significant differences (Tukey test) between open and closed IGTs at the respective forest and sampling date.

**TABLE S4 |** Results of control soil in Bad Brückenau (BBR), Mitterfels (MIT), Vessertal (VES), Conventwald (CON), and Lüss (LUE) after 18 months of exposure ($n = 5$). Superscript letters indicate results of the Tukey test, highlighting differences between forest sites.

## REFERENCES

Agerer, R. (2001). Exploration types of ectomycorrhizae. *Mycorrhiza* 11, 107–114. doi: 10.1007/s005720100108

Altschul, S. F., Gish, W., Miller, W., Myers, E. W., and Lipman, D. J. (1990). Basic local alignment search tool. *J. Mol. Biol.* 215, 403–410.

Alvarez, M., Gieseke, A., Godoy, R., and Härtel, S. (2006). Surface-bound phosphatase activity in ectomycorrhizal fungi. A comparative study between a colorimetric and a microscope-based method. *Biol. Fertil. Soils* 42:561. doi: 10.1007/s00374-005-0053-6

Alvarez, M., Godoy, R., Heyser, W., and Härtel, S. (2005). Anatomical–physiological determination of surface bound phosphatase activity in ectomycorrhizae of *Nothofagus obliqua*. *Soil Biol. Biochem.* 37, 125–132. doi: 10.1016/j.soilbio.2004.07.028

Alvarez, M., Huygens, D., Olivares, E., Saavedra, I., Alberdi, M., and Valenzuela, E. (2009). Ectomycorrhizal fungi enhance nitrogen and phosphorus nutrition of *Nothofagus dombeyi* under drought conditions by regulating assimilative enzyme activities. *Physiol. Plant.* 136, 426–436. doi: 10.1111/j.1399-3054.2009.01237.x

Attiwill, P. M., and Adams, M. A. (1993). Nutrient cycling in forests. *New Phytol.* 124, 561–582.

Bach, C. E., Warnock, D. D., van Horn, D. J., Weintraub, M. N., Sinsabaugh, R. L., Allison, S. D., et al. (2013). Measuring phenol oxidase and peroxidase activities with pyrogallol, l-DOPA, and ABTS. Effect of assay conditions

and soil type. *Soil Biol. Biochem.* 67, 183–191. doi: 10.1016/j.soilbio.2013.08.022

Baldrian, P. (2008). "Enzymes of saprotrophic basidiomycetes," in *British Mycological Society Symposia Series: Ecology of Saprotrophic Basidiomycetes*, eds L. Boddy, J. C. Frankland, and P. van West (New York, NY: Academic Press), 19–41. doi: 10.1016/s0275-0287(08)80004-5

Baldrian, P. (2009). Ectomycorrhizal fungi and their enzymes in soils. Is there enough evidence for their role as facultative soil saprotrophs? *Oecologia* 161, 657–660. doi: 10.1007/s00442-009-1433-7

Bluhm, S. L., Potapov, A. M., Shrubovych, J., Ammerschubert, S., Polle, A., and Scheu, S. (2019). Protura are unique. First evidence of specialized feeding on ectomycorrhizal fungi in soil invertebrates. *BMC Ecol.* 19:10. doi: 10.1186/s12898-019-0227-y

Bödeker, I. T. M., Clemmensen, K. E., de Boer, W., Martin, F., Olson, Å., and Lindahl, B. D. (2014). Ectomycorrhizal *Cortinarius* species participate in enzymatic oxidation of humus in northern forest ecosystems. *New Phytol.* 203, 245–256. doi: 10.1111/nph.12791

Bödeker, I. T. M., Lindahl, B. D., Olson, Å., Clemmensen, K. E., and Treseder, K. (2016). Mycorrhizal and saprotrophic fungal guilds compete for the same organic substrates but affect decomposition differently. *Funct. Ecol.* 30, 1967–1978. doi: 10.1111/1365-2435.12677

Bödeker, I. T. M., Nygren, C. M. R., Taylor, A. F. S., Olson, Å., and Lindahl, B. D. (2009). ClassII peroxidase-encoding genes are present in a phylogenetically wide range of ectomycorrhizal fungi. *ISME J.* 3:1387. doi: 10.1038/ismej.2009.77

Brabcová, V., Nováková, M., Davidová, A., and Baldrian, P. (2016). Dead fungal mycelium in forest soil represents a decomposition hotspot and a habitat for a specific microbial community. *New Phytol.* 210, 1369–1381. doi: 10.1111/nph.13849

Brookes, P. C., Powlson, D. S., and Jenkinson, D. S. (1982). Measurement of microbial biomass phosphorus in soil. *Soil Biol. Biochem.* 14, 319–329. doi: 10.1016/0038-0717(82)90001-3

Browman, M. G., and Tabatabai, M. A. (1978). Phosphodiesterase activity of soils. *Soil Sci. Soc. Am. J.* 42, 284–290. doi: 10.2136/sssaj1978.03615995004200020016x

Buée, M., Reich, M., Murat, C., Morin, E., Nilsson, R. H., Uroz, S., et al. (2009). 454 Pyrosequencing analyses of forest soils reveal an unexpectedly high fungal diversity. *New Phytol.* 184, 449–456. doi: 10.1111/j.1469-8137.2009.03003.x

Burke, D. J., Smemo, K. A., and Hewins, C. R. (2014). Ectomycorrhizal fungi isolated from old-growth northern hardwood forest display variability in extracellular enzyme activity in the presence of plant litter. *Soil Biol. Biochem.* 68, 219–222. doi: 10.1016/j.soilbio.2013.10.013

Burke, R., and Cairney, J. (2002). Laccases and other polyphenol oxidases in ecto- and ericoid mycorrhizal fungi. *Mycorrhiza* 12, 105–116. doi: 10.1007/s00572-002-0162-0

Burns, R. G., and Dick, R. P. (2002). *Enzymes in the Environment. Activity, Ecology, and Applications*. New York, NY: CRC Press.

Caporaso, J. G., Kuczynski, J., Stombaugh, J., Bittinger, K., Bushman, F. D., Costello, E. K., et al. (2010). QIIME allows analysis of high-throughput community sequencing data. *Nat. Methods* 7, 335–336.

Colpaert, J. V., and Laere, A. (1996). A comparison of the extracellular enzyme activities of two ectomycorrhizal and a leaf-saprotrophic basidiomycete colonizing beech leaf litter. *New Phytol.* 134, 133–141. doi: 10.1111/j.1469-8137.1996.tb01153.x

Condron, L. M., Turner, B. L., and Cade-Menun, B. J. (2005). "Chemistry and dynamics of soil organic phosphorus," in *Phosphorus: Agriculture and the Environment*, eds J. T. Sims and A. N. Sharpley (Madison, WI: ASA-CSSA-SSSA), 87–121. doi: 10.2134/agronmonogr46.c4

Courty, P.-E., Bréda, N., and Garbaye, J. (2007). Relation between oak tree phenology and the secretion of organic matter degrading enzymes by *Lactarius quietus* ectomycorrhizas before and during bud break. *Soil Biol. Biochem.* 39, 1655–1663. doi: 10.1016/j.soilbio.2007.01.017

Danielsen, L., and Polle, A. (2014). Poplar nutrition under drought as affected by ectomycorrhizal colonization. *Environ. Exp. Bot.* 108, 89–98. doi: 10.1016/j.envexpbot.2014.01.006

Dighton, J. (1983). Phosphatase production by mycorrhizal fungi. *Plant Soil* 71, 455–462. doi: 10.1007/978-94-009-6833-2_51

Dighton, J. (1991). Acquisition of nutrients from organic resources by mycorrhizal autotrophic plants. *Experientia* 47, 362–369. doi: 10.1007/bf01972078

Dowling, N. J. E., Widdel, F., and White, D. C. (1986). Phospholipid ester-linked fatty acid biomarkers of acetate-oxidizing sulphate-reducers and other sulphide-forming bacteria. *Microbiology* 132, 1815–1825. doi: 10.1099/00221287-132-7-1815

Edgar, R. C. (2010). Search and clustering orders of magnitude faster than BLAST. *Bioinformatics* 26, 2460–2461. doi: 10.1093/bioinformatics/btq461

Floch, C., Alarcon-Gutiérrez, E., and Criquet, S. (2007). ABTS assay of phenol oxidase activity in soil. *J. Microbiol. Methods* 71, 319–324. doi: 10.1016/j.mimet.2007.09.020

Frossard, E., Condron, L. M., Oberson, A., Sinaj, S., and Fardeau, J. C. (2000). Processes governing phosphorus availability in temperate soils. *J. Environ. Qual.* 29, 15–23. doi: 10.2134/jeq2000.00472425002900010003x

Frostegård, A., and Bååth, E. (1996). The use of phospholipid fatty acid analysis to estimate bacterial and fungal biomass in soil. *Biol. Fertil. Soils* 22, 59–65. doi: 10.1007/bf00384433

Frostegård, A., Bååth, E., and Tunlio, A. (1993). Shifts in the structure of soil microbial communities in limed forests as revealed by phospholipid fatty acid analysis. *Soil Biol. Biochem.* 25, 723–730. doi: 10.1016/0038-0717(93)90113-p

Frostegård, A., Tunlid, A., and Bååth, E. (1991). Microbial biomass measured as total lipid phosphate in soils of different organic content. *J. Microbiol. Methods* 14, 151–163. doi: 10.1016/0167-7012(91)90018-l

Grinhut, T., Hadar, Y., and Chen, Y. (2007). Degradation and transformation of humic substances by Saprotrophic fungi. Processes and mechanisms. *Fungal Biol. Rev.* 21, 179–189. doi: 10.1016/j.fbr.2007.09.003

Gyaneshwar, P., Naresh Kumar, G., Parekh, L. J., and Poole, P. S. (2002). Role of soil microorganisms in improving P nutrition of plants. *Plant Soil* 245, 83–93.

Hagerberg, D., and Wallander, H. (2002). The impact of forest residue removal and wood ash amendment on the growth of the ectomycorrhizal external mycelium. *FEMS Microbiol. Ecol.* 39, 139–146. doi: 10.1111/j.1574-6941.2002.tb00915.x

Hedley, M. J., Stewart, J. W. B., and Chauhan, B. S. (1982). Changes in inorganic and organic soil phosphorus fractions induced by cultivation practices and by laboratory incubations. *Soil Sci. Soc. Am. J.* 46, 970–976. doi: 10.2136/sssaj1982.03615995004600050017x

Hendricks, J. J., Mitchell, R. J., Kuehn, K. A., Pecot, S. D., and Sims, S. E. (2006). Measuring external mycelia production of ectomycorrhizal fungi in the field. The soil matrix matters. *New Phytol.* 171, 179–186. doi: 10.1111/j.1469-8137.2006.01742.x

Heuck, C., and Spohn, M. (2016). Carbon, nitrogen and phosphorus net mineralization in organic horizons of temperate forests. Stoichiometry and relations to organic matter quality. *Biogeochemistry* 131, 229–242. doi: 10.1007/s10533-016-0276-7

Ho, I., and Zak, B. (1979). Acid phosphatase activity of six ectomycorrhizal fungi. *Can. J. Bot.* 57, 1203–1205. doi: 10.1139/b79-144

Hoffmann, G. (1968). Eine photometrische Methode zur Bestimmung der Phosphatase-Aktivität in Böden. *Z. Pflanzenernähr. Bodenk.* 118, 161–172. doi: 10.1002/jpln.19681180303

Högberg, M. N., and Högberg, P. (2002). Extramatrical ectomycorrhizal mycelium contributes one-third of microbial biomass and produces, together with associated roots, half the dissolved organic carbon in a forest soil. *New Phytol.* 154, 791–795. doi: 10.1046/j.1469-8137.2002.00417.x

IUSS Working Group WRB (2014). "World reference base for soil resouces 2014," in *Proceedings of the International Soil Classification SYSTEM for Naming Soils and Creating Legends for Soil Maps, Word Soil Resources Reports No. 106* (Rome: FAO).

Jansa, J., Finlay, R., Wallander, H., Smith, F. A., and Smith, S. E. (2011). "Role of mycorrhizal symbioses in phosphorus cycling," in *Phosphorus in Action*, eds E. Bünemann, A. Oberson, and E. Frossard (Berlin: Springer), 137–168. doi: 10.1007/978-3-642-15271-9_6

Johnson, D., Leake, J. R., and Read, D. J. (2001). Novel in-growth core system enables functional studies of grassland mycorrhizal mycelial networks. *New Phytol.* 152, 555–562. doi: 10.1046/j.0028-646x.2001.00273.x

Jonard, M., Fürst, A., Verstraeten, A., Thimonier, A., Timmermann, V., Potočić, N., et al. (2015). Tree mineral nutrition is deteriorating in Europe. *Glob. Chang. Biol.* 21, 418–430. doi: 10.1111/gcb.12657

Jones, D. L., and Oburger, E. (2011). "Solubilization of phosphorus by soil microorganisms," in *Phosphorus in Action*, eds E. Bünemann, A. Oberson, and E. Frossard (Berlin: Springer), 169–198. doi: 10.1007/978-3-642-15271-9_7

Kandeler, E. (1990). Characterization of free and adsorbed phosphatases in soils. *Biol. Fertil. Soils* 9, 199–202. doi: 10.1007/bf00335808

Kandeler, E., Mosier, A. R., Morgan, J. A., Milchunas, D. G., King, J. Y., Rudolph, S., et al. (2006). Response of soil microbial biomass and enzyme activities to the transient elevation of carbon dioxide in a semi-arid grassland. *Soil Biol. Biochem.* 38, 2448–2460. doi: 10.1016/j.soilbio.2006.02.021

Kavka, M., and Polle, A. (2017). Dissecting nutrient-related co-expression networks in phosphate starved poplars. *PLoS One* 12:e0171958. doi: 10.1371/journal.pone.0171958

Kellner, H., Luis, P., Schlitt, B., and Buscot, F. (2009). Temporal changes in diversity and expression patterns of fungal laccase genes within the organic horizon of a brown forest soil. *Soil Biol. Biochem.* 41, 1380–1389. doi: 10.1016/j.soilbio.2009.03.012

Kieliszewska-Rokicka, B. (1992). Effect of nitrogen level on acid phosphatase activity of eight isolates of ectomycorrhizal fungus *Paxillus involutus* cultured *in vitro*. *Plant Soil* 139, 229–238. doi: 10.1007/bf00009314

Kõljalg, U., Nilsson, R. H., Abarenkov, K., Tedersoo, L., Taylor, A. F. S., Bahram, M., et al. (2013). Towards a unified paradigm for sequence-based identification of fungi. *Mol. Ecol.* 22, 5271–5277. doi: 10.1111/mec.12481

Kucey, R. M. N., Janzen, H. H., and Leggett, M. E. (1989). Microbially mediated increases in plant-available phosphorus. *Adv. Agron.* 42, 199–228. doi: 10.1016/s0065-2113(08)60525-8

Lambers, H., Raven, J., Shaver, G., and Smith, S. (2008). Plant nutrient-acquisition strategies change with soil age. *Trends Ecol. Evol.* 23, 95–103. doi: 10.1016/j.tree.2007.10.008

Lang, C., Finkeldey, R., and Polle, A. (2013). Spatial patterns of ectomycorrhizal assemblages in a monospecific forest in relation to host tree genotype. *Front. Plant Sci.* 4:103. doi: 10.3389/fpls.2013.00103

Lang, F., Krüger, J., Amelung, W., Willbold, S., Frossard, E., Bünemann, E. K., et al. (2017). Soil phosphorus supply controls P nutrition strategies of beech forest ecosystems in Central Europe. *Biogeochemistry* 136, 5–29. doi: 10.1007/s10533-017-0375-0

Lenth, R., Singmann, H., Love, J., Buerkner, P., and Herve, M. (2019). *emmeans Estimated Marginal Means, aka Least-Squares Means*. Available at: https://github.com/rvlenth/emmeans (accessed August 5, 2019).

Leprince, F., and Quiquampoix, H. (1996). Extracellular enzyme activity in soil. Effect of pH and ionic strength on the interaction with montmorillonite of two acid phosphatases secreted by the ectomycorrhizal fungus *Hebeloma cylindrosporum*. *Eur. J. Soil Sci.* 47, 511–522.

Lindahl, B. D., de Boer, W., and Finlay, R. D. (2010). Disruption of root carbon transport into forest humus stimulates fungal opportunists at the expense of mycorrhizal fungi. *ISME J.* 4, 872–881. doi: 10.1038/ismej.2010.19

Lindahl, B. D., and Tunlid, A. (2015). Ectomycorrhizal fungi-potential organic matter decomposers, yet not saprotrophs. *New Phytol.* 205, 1443–1447. doi: 10.1111/nph.13201

Louche, J., Ali, M. A., Cloutier-Hurteau, B., Sauvage, F.-X., Quiquampoix, H., and Plassard, C. (2010). Efficiency of acid phosphatases secreted from the ectomycorrhizal fungus *Hebeloma cylindrosporum* to hydrolyse organic phosphorus in podzols. *FEMS Microbiol. Ecol.* 73, 323–335. doi: 10.1111/j.1574-6941.2010.00899.x

Luis, P., Kellner, H., Zimdars, B., Langer, U., Martin, F., and Buscot, F. (2005). Patchiness and spatial distribution of laccase genes of ectomycorrhizal, saprotrophic, and unknown basidiomycetes in the upper horizons of a mixed forest cambisol. *Microb. Ecol.* 50, 570–579. doi: 10.1007/s00248-005-5047-2

Luis, P., Walther, G., Kellner, H., Martin, F., and Buscot, F. (2004). Diversity of laccase genes from basidiomycetes in a forest soil. *Soil Biol. Biochem.* 36, 1025–1036. doi: 10.1016/j.soilbio.2004.02.017

Martin, M. (2011). Cutadapt removes adapter sequences from high-throughput sequencing reads. *EMBnet J.* 17, 10–12.

Martino, E., Morin, E., Grelet, G.-A., Kuo, A., Kohler, A., Daghino, S., et al. (2018). Comparative genomics and transcriptomics depict ericoid mycorrhizal fungi as versatile saprotrophs and plant mutualists. *New Phytol.* 217, 1213–1229. doi: 10.1111/nph.14974

Matsubara, T., and Iwasaki, H. (1972). Occurrence of laccase and tyrosinase in fungi of agaricales and comparative study of laccase from *Russula delica* and *Russula pseudodelica*. *Bot. Mag.* 85, 71–83. doi: 10.1007/bf02489202

McDonald, D., Clemente, J. C., Kuczynski, J., Rideout, J. R., Stombaugh, J., Wendel, D., et al. (2012). The Biological Observation Matrix (BIOM) format or How I learned to stop worrying and love the ome-ome. *GigaScience* 1:7.

Murphy, J., and Riley, J. P. (1962). A modified single solution method for the determination of phosphate in natural waters. *Anal. Chim. Acta* 27, 31–36. doi: 10.1016/s0003-2670(00)88444-5

Nannipieri, P., Giagnoni, L., Landi, L., and Renella, G. (2011). "Role of phosphatase enzymes in soil," in *Phosphorus in Action: Biological Processes in Soil Phosphorus Cycling*, eds E. Bünemann A. Oberson and E. Frossard (Berlin: Springer).

Nguyen, N. H., Song, Z., Bates, S. T., Branco, S., Tedersoo, L., Menke, J., et al. (2016). FUNGuild. An open annotation tool for parsing fungal community datasets by ecological guild. *Fungal Ecol.* 20, 241–248. doi: 10.1016/j.funeco.2015.06.006

Nicolás, C., Martin-Bertelsen, T., Floudas, D., Bentzer, J., Smits, M., Johansson, T., et al. (2019). The soil organic matter decomposition mechanisms in ectomycorrhizal fungi are tuned for liberating soil organic nitrogen. *ISME J.* 13, 977–988. doi: 10.1038/s41396-018-0331-6

Ning, C., Mueller, M. G., Egerton-Warburton, M. L., Wilson, W. A., Yan, W., and Xiang, W. (2018). Diversity and enzyme activity of ectomycorrhizal fungal communities following nitrogen fertilization in an Urban-adjacent pine plantation. *Forests* 9:99. doi: 10.3390/f9030099

Nygren, C. M. R., and Rosling, A. (2009). Localisation of phosphomonoesterase activity in ectomycorrhizal fungi grown on different phosphorus sources. *Mycorrhiza* 19, 197–204. doi: 10.1007/s00572-008-0223-0

Öhlinger, R., Margesin, R., and Kandeler, E. (1996). "Enzymes involved in phosphorus metabolism," in *Methods in Soil Biology*, eds F. Schinner, R. Öhlinger, E. Kandeler, and R. Margesin (Berlin: Springer), 208–227. doi: 10.1007/978-3-642-60966-4_13

Pena, R., Tejedor, J., Zeller, B., Dannenmann, M., and Polle, A. (2013). Interspecific temporal and spatial differences in the acquisition of litter-derived nitrogen by ectomycorrhizal fungal assemblages. *New Phytol.* 199, 520–528. doi: 10.1111/nph.12272

Pinheiro, J., Bates, D., DebRoy, S., Sarkar, D., and R Core Team. (2019). *nlme: Linear and Nonlinear Mixed Effects Models*. Available at: https://svn.r-project.org/R-packages/trunk/nlme (accessed July 23, 2019).

Plante, A. F. (2007). "Soil biogeochemical cycling of inorgacnic nutrients and metals," in *Soil Microbiology, Ecology and Biochemistry*, Third Edn, ed. E. A. Paul (San Diego, CA: Academic Press), 389–432. doi: 10.1016/b978-0-08-047514-1.50019-6

Pritsch, K., and Garbaye, J. (2011). Enzyme secretion by ECM fungi and exploitation of mineral nutrients from soil organic matter. *Ann. For. Sci.* 68, 25–32. doi: 10.1007/s13595-010-0004-8

Quiquampoix, H., and Mousain, D. (2005). "Enzymatic hydrolysis of organic phosphorus," in *Organic Phosphorus in the Environment*, eds B. L. Turner, E. Frossard, and D. S. Baldwin (Wallingford: CAB International), 89–112. doi: 10.1079/9780851998220.0089

R Core Team (2019). *R: A Language and Environment for Statistical Computing*. Vienna: R Foundation for Statistical Computing.

Remén, C., Persson, T., Finlay, R., and Ahlström, K. (2008). Responses of oribatid mites to tree girdling and nutrient addition in boreal coniferous forests. *Soil Biol. Biochem.* 40, 2881–2890. doi: 10.1016/j.soilbio.2008.08.006

Richardson, A. E., and Simpson, R. J. (2011). Soil microorganisms mediating phosphorus availability-update on microbial phosphorus. *Plant Physiol.* 156, 989–996. doi: 10.1104/pp.111.175448

Ruess, L., Schütz, K., Migge-Kleian, S., Häggblom, M. M., Kandeler, E., and Scheu, S. (2007). Lipid composition of Collembola and their food resources in deciduous forest stands-Implications for feeding strategies. *Soil Biol. Biochem.* 39, 1990–2000. doi: 10.1016/j.soilbio.2007.03.002

Ruess, W. R., Swanson, M. M., Kielland, K., McFarland, W. J., Olson, D. K., and Taylor, L. D. (2019). Phosphorus mobilizing enzymes of alnus-associated Ectomycorrhizal Fungi in an Alaskan Boreal Floodplain. 10:554. doi: 10.3390/f10070554

Schinner, F., Öhlinger, R., Kandeler, E., and Margesin, R. (eds) (2012). *Methods in Soil Biology*. Berlin: Springer.

Smith, S. E., and Read, D. J. (1997). *Mycorrhizal Symbiosis*. San Diego, CA: Academic Press.

Štursová, M., Žifčáková, L., Leigh, M. B., Burgess, R., and Baldrian, P. (2012). Cellulose utilization in forest litter and soil. Identification of bacterial and fungal decomposers. *FEMS Microbiol. Ecol.* 80, 735–746. doi: 10.1111/j.1574-6941.2012.01343.x

Talbot, J. M., Bruns, T. D., Smith, D. P., Branco, S., Glassman, S. I., Erlandson, S., et al. (2013). Independent roles of ectomycorrhizal and saprotrophic communities in soil organic matter decomposition. *Soil Biol. Biochem.* 57, 282–291. doi: 10.1016/j.soilbio.2012.10.004

Talkner, U., Meiwes, K. J., Potočić, N., Seletković, I., Cools, N., de Vos, B., et al. (2015). Phosphorus nutrition of beech (*Fagus sylvatica* L.) is decreasing in Europe. *Ann. For. Sci.* 72, 919–928. doi: 10.3389/fpls.2019.00744

Tamburini, F., Pfahler, V., Bünemann, E. K., Guelland, K., Bernasconi, S. M., and Frossard, E. (2012). Oxygen isotopes unravel the role of microorganisms in phosphate cycling in soils. *Environ. Sci. Technol.* 46, 5956–5962. doi: 10.1021/es300311h

Taniguchi, T., Kataoka, R., and Futai, K. (2008). Plant growth and nutrition in pine (*Pinus thunbergii*) seedlings and dehydrogenase and phosphatase activity of ectomycorrhizal root tips inoculated with seven individual ectomycorrhizal fungal species at high and low nitrogen conditions. *Soil Biol. Biochem.* 40, 1235–1243. doi: 10.1016/j.soilbio.2007.12.017

Tibbett, M., Sanders, F. E., and Cairney, J. W. G. (1998). The effect of temperature and inorganic phosphorus supply on growth and acid phosphatase production in arctic and temperate strains of ectomycorrhizal *Hebeloma* spp. in axenic culture. *Mycol. Res.* 102, 129–135. doi: 10.1017/s0953756297004681

Toju, H., Tanabe, A. S., Yamamoto, S., and Sato, H. (2012). High-Coverage ITS Primers for the DNA-based identification of ascomycetes and basidiomycetes in environmental samples. *PLoS One* 7:e40863. doi: 10.1371/journal.pone.0040863

Turner, B. L., and Haygarth, P. M. (2005). Phosphatase activity in temperate pasture soils. Potential regulation of labile organic phosphorus turnover by phosphodiesterase activity. *Sci. Total Environ.* 344, 27–36. doi: 10.1016/j.scitotenv.2005.02.003

Walker, J. K. M., Cohen, H., Higgins, L. M., and Kennedy, P. G. (2014). Testing the link between community structure and function for ectomycorrhizal fungi involved in a global tripartite symbiosis. *New Phytol.* 202, 287–296. doi: 10.1111/nph.12638

Wallander, H. (2006). External mycorrhizal mycelia – the importance of quantification in natural ecosystems. *New Phytol.* 171, 240–242. doi: 10.1111/j.1469-8137.2006.01803.x

Wallander, H., Ekblad, A., Godbold, D. L., Johnson, D., Bahr, A., Baldrian, P., et al. (2013). Evaluation of methods to estimate production, biomass and turnover of ectomycorrhizal mycelium in forests soils – A review. *Soil Biol. Biochem.* 57, 1034–1047. doi: 10.1016/j.soilbio.2012.08.027

Wallander, H., Nilsson, L. O., Hagerberg, D., and Baath, E. (2001). Estimation of the biomass and seasonal growth of external mycelium of ectomycorrhizal fungi in the field. *New Phytol.* 151, 753–760. doi: 10.1046/j.0028-646x.2001.00199.x

Wallander, H., and Thelin, G. (2008). The stimulating effect of apatite on ectomycorrhizal growth diminishes after PK fertilization. *Soil Biol. Biochem.* 40, 2517–2522. doi: 10.1016/j.soilbio.2008.06.011

Wallander, H., Wickman, T., and Jacks, G. (1997). Apatite as a P source in mycorrhizal and non-mycorrhizal Pinus sylvestris seedlings. *Plant Soil* 196, 123–131.

White, T. J., Bruns, T., Lee, S., and Taylor, J. L. (1990). Amplification and direct sequencing of fungal ribosomal RNA genes for phylogenetics. *PCR Protoc.* 18, 315–322. doi: 10.1016/b978-0-12-372180-8.50042-1

Yang, N., Schützenmeister, K., Grubert, D., Jungkunst, H. F., Gansert, D., Scheu, S., et al. (2015). Impacts of earthworms on nitrogen acquisition from leaf litter by arbuscular mycorrhizal ash and ectomycorrhizal beech trees. *Environ. Exp. Bot.* 120, 1–7. doi: 10.1016/j.envexpbot.2015.06.013

Zak, D. R., Pellitier, P. T., Argiroff, W., Castillo, B., James, T. Y., Nave, L. E., et al. (2019). Exploring the role of ectomycorrhizal fungi in soil carbon dynamics. *New Phytol.* 223, 33–39. doi: 10.1111/nph.15679

Zavišić, A., Yang, N., Marhan, S., Kandeler, E., and Polle, A. (2018). Forest soil phosphorus resources and fertilization affect ectomycorrhizal community composition, beech P uptake efficiency, and photosynthesis. *Front. Plant Sci.* 9:463. doi: 10.3389/fpls.2018.00463

Zederer, D. P., Talkner, U., Spohn, M., and Joergensen, R. G. (2017). Microbial biomass phosphorus and C/N/P stoichiometry in forest floor and A horizons as affected by tree species. *Soil Biol. Biochem.* 111, 166–175. doi: 10.1016/j.soilbio.2017.04.009

Zhang, J., Kobert, K., Flouri, T., and Stamatakis, A. (2014). PEAR. A fast and accurate Illumina Paired-End reAd mergeR. *Bioinformatics* 30, 614–620. doi: 10.1093/bioinformatics/btt593

**Conflict of Interest:** The authors declare that the research was conducted in the absence of any commercial or financial relationships that could be construed as a potential conflict of interest.

The reviewer MG declared a shared affiliation, though no other collaboration, with several of the authors DS, RD, AP to the handling Editor.

frontiers in Forests and Global Change

ORIGINAL RESEARCH
published: 19 May 2020
doi: 10.3389/ffgc.2020.00054

# Mycorrhizal Phosphorus Efficiencies and Microbial Competition Drive Root P Uptake

*Simon Clausing and Andrea Polle**

*Forest Botany and Tree Physiology, University of Göttingen, Göttingen, Germany*

Phosphorus (P) availability shows large differences among different soil types, affecting P nutrition of forest trees. Chemical binding of P to soil moieties affects partitioning of P between soil particles and solution, influencing soluble P concentrations upon which plants, their associated mycorrhizal symbionts, and microbes feed. The goal of this study was to characterize root P uptake by mycorrhizal and non-mycorrhizal root tips in competition with microbes *in situ* in the organic and mineral layer of a P-rich and a P-poor forest. We used intact soil cores (0.2 m depth) from beech (*Fagus sylvatica*) forests to tracing the fate of $^{33}$P in soil, plant and microbial fractions. We used the dilution of $^{33}$P in the rhizosphere of each soil layer to estimate the enrichment with new P in mycorrhizal and non-mycorrhizal root tips and root P uptake. In soil cores from P-rich conditions, 25 and 75% of root P uptake occurred in the organic and mineral layer, respectively, whereas in the P-poor forest, 60% occurred in the organic and 40% in the mineral layer. Mycorrhizal P efficiency, determined as enrichment of new P in mycorrhizal root tips, differed between soil layers. Root P uptake was correlated with mycorrhizal P efficiency and root tip abundance but not with root tip abundance as a single factor. This finding underpins the importance of the regulation of mycorrhizal P acquisition for root P supply. The composition of mycorrhizal assemblages differed between forests but not between soil layers. Therefore, differences in P efficiencies resulted from physiological adjustments of the symbionts. Non-mycorrhizal root tips were rare and exhibited lower enrichment with new P than mycorrhizal root tips. Their contribution to root P supply was negligible. Microbes were strong competitors for P in P-poor but not in P-rich soil. Understory roots were present in the P-rich soil but did not compete for P. Our results uncover regulation of mycorrhizal P efficiencies and highlight the complexity of biotic and abiotic factors that govern P supply to trees in forest ecosystems.

**Keywords: ectomycorrhiza, rhizosphere, organic soil, mineral soil, phosphorus, radioactive labeling**

OPEN ACCESS

***Edited by:***
*Friederike Lang,*
*University of Freiburg, Germany*

***Reviewed by:***
*Tessa Camenzind,*
*Freie Universität Berlin, Germany*
*Lukas Kohl,*
*University of Helsinki, Finland*

***Correspondence:**
*Andrea Polle*
*apolle@gwdg.de*

***Specialty section:***
*This article was submitted to Forest Soils, a section of the journal Frontiers in Forests and Global Change*

***Received:*** *29 January 2020*
***Accepted:*** *14 April 2020*
***Published:*** *19 May 2020*

***Citation:***
*Clausing S and Polle A (2020) Mycorrhizal Phosphorus Efficiencies and Microbial Competition Drive Root P Uptake. Front. For. Glob. Change 3:54. doi: 10.3389/ffgc.2020.00054*

## INTRODUCTION

Plants take up phosphorus (P) as inorganic phosphate ($P_i$, $HPO_4^{2-}$, or $PO_4^{3-}$) from the soil solution (Plassard and Dell, 2010). However, this P source is scarce because $P_i$ has low diffusion rates in soil (Shen et al., 2011), is sequestered by soil minerals such as Fe and Al hydroxides (Lambers et al., 2015b; Prietzel et al., 2016) or is bound to organic matter (Ilg et al., 2008; Lambers et al., 2008).

Besides, P input into soil by P deposition is extremely low (Peñuelas et al., 2013). Consequently, weathering and P utilization lead to a shift in P availability for plants (Walker and Syers, 1976; Callaway and Nadkarni, 1991; Vitousek et al., 2010; Vincent et al., 2013) and drive P reductions during soil geological aging (Turner and Condron, 2013). As a result, different soils vary drastically in P availability (Chadwick et al., 1999; Lang et al., 2016).

Since P is an essential element for plant nutrition, plants have to adjust their acquisition strategies to cope with different P availabilities (Vance et al., 2003; Lambers et al., 2008, 2015a,b). This requirement is especially important for tree species such as beech (*Fagus sylvatica* L.), which occur on a broad range of different soil types (Leuschner et al., 2006). It has been shown that beech ecosystems along a geosequence of different P availabilities adjust their nutritional strategies from P acquisition under high P availability to P recycling when P is scarce (Lang et al., 2017). Due to differences in soil structure and nutrient availability, beech trees in P-poor soil modify their root systems to explore the organic soil layer more intensely than trees in P-rich soil (Lang et al., 2017). They further exhibit extended seasonal P acquisition (Spohn et al., 2018), stronger recycling of P resources from internal storage tissues (Netzer et al., 2017; Zavišić and Polle, 2018), and reductions in growth and photosynthesis (Yang et al., 2016), which are released upon P-fertilization (Zavišić et al., 2018). In acidic, P-poor soils, forests build up a thick organic layer from which P can be re-mobilized by decomposition (Heuck and Spohn, 2016; George et al., 2018; Zederer and Talkner, 2018). In mesocosms with reconstructed soil layers composed of homogenized organic and mineral soil, the organic layer was important for the P supply to young beech saplings (Hauenstein et al., 2018). Under field conditions, understory vegetation is present and more abundant in P-rich than P-poor beech forests (Rieger et al., 2019). To assess beech P nutrition, the potential competition of understory for nutritional resources needs to be taken into account (Nambiar and Sands, 1993). Furthermore, soil microbes are important competitors for mineral nutrients (Kuzyakov and Xu, 2013; Zhu et al., 2017).

It is well-known that ectomycorrhizal fungi play a critical role for nutrition of forest trees in temperate ecosystems (Cairney, 2011; Becquer et al., 2014; Johri et al., 2015; Nehls and Plassard, 2018). Ectomycorrhizas produce hyphal networks that overcome zones of P depletion by hyphal tunneling (Jongmans et al., 1997; Hoffland et al., 2003; Jansa et al., 2011). Mycorrhizal fungi further contribute to bioweathering by secretion of organic acids (Wallander, 2000; Balogh-Brunstad et al., 2008; Jansa et al., 2011) and to the recycling of organic-bound P by production of acidic phosphatases (Hinsinger et al., 2015; Smith et al., 2015). Already early tracer studies with radioactive $P_i$ showed that mycorrhizal roots of pine and beech accumulate more P than non-mycorrhizal roots (Kramer and Wilbur, 1949; Harley et al., 1954). In beech forests, the fraction of non-mycorrhizal root tips is generally small (Pena et al., 2010; Lang et al., 2017) but whether they play a role for P acquisition in natural forest soils, for example, in deeper soil layers, has not yet been studied. P acquisition strategies of distinct mycorrhizal communities in natural soils have mainly been studied empirically and not directly by tracing P uptake. It is therefore unknown if mycorrhizal fungal assemblages at different soil depth show physiological differences that adjust P acquisition to P availability in soil. It is further unclear whether differences in fungal assemblages and soil structures affect competition for P of beech with roots of understory plants and soil microbes. The present study was undertaken to investigate these open points.

The aims of this study were to quantify the contributions of mycorrhizal and non-mycorrhizal root tips to $P_i$ acquisition in the organic layer and mineral top soil of a P-poor and a P-rich beech forest and to elucidate the competition between beech roots, microbes and other plants roots for P uptake. To address these goals, we excised intact soil cores from two well-characterized beech forests, which constitute the high-P (HP) and low-P (LP) ends of a geosequence in Central Europe (Germany), previously characterized by Lang et al. (2017). We irrigated the soil cores with $^{33}P$, traced the distribution of the label and measured the P contents in the soluble and insoluble fractions of bulk soil, rhizosphere, beech roots, mycorrhizal and non-mycorrhizal root tips, other roots, and microbes in the organic layer and mineral topsoil. As a methodological innovation, we determined the bioavailability of $P_i$ not only in bulk but also in rhizosphere soil. We tested the following hypotheses: (i) the main P source for beech P supply is the mineral topsoil under P-rich and the organic layer under P-poor conditions. (ii) Mycorrhizal root tips exhibit different P efficiencies, thereby counteracting low P availability by relatively higher P uptake than under high P availability; the contribution of non-mycorrhizal root tips to P uptake is low. (iii) Under high P availability, beech roots do not compete with understory or microbes for $P_i$, whereas the competition is strong under low P availability.

# MATERIALS AND METHODS

## Site Characteristics

Two beech (*F. sylvatica* L.) forests, which differ strongly in soil properties and P stocks (**Supplementary Table S1**) were selected for this study: Lüss, a low-P (LP) and Bad Brückenau, a high-P (HP) site (Zavišić et al., 2016; Lang et al., 2017). Briefly, the LP forest is located in the district Celle in Lower Saxony (R: 3585473 E, H: 5857057 N; 115 m above sea level) and stocked with about 132-year-old beech trees (Haußmann and Lux, 1997). The soil type is sandy-loam from silicate substrate, containing 164 g P $m^{-2}$ to a depth of 1 m (Lang et al., 2017). The mean annual temperature was 8.0°C and the mean annual sum of precipitation 730 mm. The HP forest is situated in the biosphere reservation 'Bayerische Rhön' (R: 3566195 E, H: 5579975 N; 801 to 850 m above sea level). The mean long-term sum of annual precipitation was 1000 mm and the mean annual temperature 5.8°C. The soil type is basalt of volcanic origin, containing 904 g P $m^{-2}$ to a depth of 1 m (Lang et al., 2017). The average age of the beech stand is 137 years (Haußmann and Lux, 1997). Additional information on the research sites has been compiled in **Supplementary Table S1**.

## Collection of Soil Cores

We collected intact soil cores in the HP (27.6.2017) and the LP (19.6.2017) forest, respectively, using PVC pipes of 120 mm

diameter and a length of 200 mm. Each pipe was hammered completely into the soil at a distance of about 0.2 m to a beech tree and was pulled up containing the soil and forest floor. The soil cores remained in the PVC pipes. They were immediately transported to laboratory, kept at room temperature, weighed, watered with 100 ml of tap water, and used the next day for labeling ($n$ = 5 per forest). Soil cores of the same dimensions ($n$ = 5 per forest) for mycorrhizal inspection were harvested on the same plots about 2–3 weeks later in the same manner.

## Radioactive Labeling and Harvest

We used the soil cores for uptake studies of $^{33}P$ into roots. Pretests with soil cores collected in the same manner in 2015 showed that the roots were still active exhibiting similar uptake of the label as roots of intact plants (Spohn et al., 2018). We labeled five soil cores per forest by addition of 1850 kBq of $H_3{}^{33}PO_4$ (Hartmann Analytic GmbH, Brunswick, Germany) in 40 ml of tap water to each soil core. The added $^{33}P$ corresponded to 1.66 ng P per soil core. Each soil core was subsequently watered with 40 ml tap water to distribute the radioactive marker throughout the soil core. To avoid loss of label by through-flow a plastic saucer was placed underneath each soil core. Any through-flow was returned to the soil core. After 24 h incubation in the laboratory at 20°C, the soil cores were pushed out of the pipe and were immediately separated in organic and mineral topsoil. Each sample was further fractionated in bulk soil, rhizosphere soil, beech roots (fine roots: < 2 mm, coarse roots: > 2 mm), other roots (distinguished by color and surface structure, Hölscher et al., 2002), and residual materials (litter, fruits, twigs, and stones).

We defined rhizosphere soil as the soil adhering to roots. Our rhizosphere effectively represents the mycorrhizosphere since fungal hyphae also contribute to soil adherence (York et al., 2016) but for consistency, the term rhizosphere was used throughout this study. The rhizosphere soil was collected by streaking the adhering soil from the roots with a paintbrush. Afterward, fresh fine roots were cut into pieces of similar lengths and yielded one mixed sample per soil layer and soil core, which was immediately weighed. All other fractions were also immediately weighed. Well-mixed aliquots of soil and plant fractions were dried at 40°C for 1 week, weighed, and used for analyses of the dry mass per soil layer and plant fraction.

## Analyses of Root Tips and Mycorrhizal Species

Approximately half of the fresh beech fine roots, extracted from each soil core, were used to determine the number of root tips and mycorrhizal colonization. The sample was weighed and the number of root tips in this sample was counted under a stereomicroscope (Leica M205 FA, Wetzlar, Germany). The total number of root tips per soil layer was calculated as:

**Equation 1**

$$\text{Total number}_{\text{root tips}} = \frac{\text{Aliquot}_{\text{root tips}}}{\text{Aliquot}_{\text{fine root biomass (g)}}} \times \text{total biomass of FR (g)} \quad (1)$$

Root tips were categorized according to their visual appearance as vital ectomycorrhizal, vital non-mycorrhizal or dry (Winkler et al., 2010). Mycorrhizal root tips and non-mycorrhizal root tips were collected separately from each sample. The mean weight of mycorrhizal and non-mycorrhizal root tips was determined by collecting 100 and 200 root tips, respectively, and weighing the sample after drying (40°C for 1 week, followed by freeze-drying for 4 days and equilibration at room temperature in a desiccator with silica gel). For the analyses of P and $^{33}P$, mycorrhizal root tips were collected for each soil layer and forest type separately. The mycorrhizal samples represented a mixture of morphotypes. Mycorrhizal colonization and root vitality were calculated as:

$$\text{Mycorrhizal colonization (\%)} = \frac{\text{number of mycorrhizal root tips}}{\text{number of vital root tips}} \times 100 \quad (2)$$

$$\text{Nonmycorrhizal root tips (\%)} = \frac{\text{number of nonmycorrhizal root tips}}{\text{number of vital root tips}} \times 100 \quad (3)$$

$$\text{Root vitality (\%)} = \frac{\text{number of vital root tips}}{\text{number of all counted root tips}} \times 100 \quad (4)$$

The abundance of different morphotypes was determined under the stereomicroscope (Leica MF205) using a simplified identification key (after Agerer, 1987–2012) as described by Pena et al. (2010). For mycorrhizal species identification, morphotypes of all species were collected, which comprised at least three root tips per sample. Mycorrhizal species identities were determined after DNA extraction and ITS sequencing using the protocol of Pena et al. (2017).

## Determination of Total and Soluble Phosphorus in Roots and Soil

Dry soil and coarse and fine root samples were milled in a ball mill (Retsch MN 400, Haan, Germany) to a fine powder. For determination of total P ($P_{tot}$), about 50 mg of the powder was weighed and extracted in 25 ml of 65% $HNO_3$ at 160°C for 12 h according to Heinrichs et al. (1986). For $P_{tot}$ determination of root tips, dry root tips, either mycorrhizal or non-mycorrhizal, with weights ranging from 0.2 to 30 mg were weighed and extracted in 2 ml of 65% $HNO_3$ at 160°C for 12 h according to Heinrichs et al. (1986). For determination of soluble P ($P_{sol}$) about 100 mg of plant or soil powder was extracted in 150 ml of Bray-1 solution (0.03 N $NH_4F$, 0.025 N HCl) for 60 min on a shaker at 180 rpm (Bray and Kurtz, 1945). Microbial P was determined using the chloroform fumigation extraction method according to Brookes et al. (1985). About 5 g organic layer or 10 g mineral topsoil were fumigated for 24 h with chloroform ($CHCl_3$). The fumigated samples were extracted for 60 min on a shaker at 180 rpm in 150 ml Bray-1 solution. After P

measurement (described below), $P_{mic}$ was calculated according to Brookes et al. (1982):

$$P_{mic}\ \left(mg\ g^{-1}\right) = 2.5\ \times (P_{Chloroform\ ectract} - P_{sol}) \quad (5)$$

All extracts were filtered through phosphate free filter paper (MN 280 1/4, Macherey-Nagel, Düren, Germany). The $P_{tot}$ and Bray-1 extracts were used for elemental analysis by inductively coupled plasma–optical emission spectroscopy (ICP-OES) (iCAP 7000 Series ICP–OES, Thermo Fisher Scientific, Dreieich, Germany). P was measured at the wavelength of 185.942 nm (axial) and calibrated with a series of dilutions (0.1 to 20 mg $l^{-1}$) using the element standard for P (Einzelstandards, Bernd Kraft, Duisburg, Germany).

## Determination of $^{33}P$ by Scintillation Counting

The $P_{tot}$ and Bray-1 extracts of all soil, plant and root tip samples were used to measure $^{33}P$. For this purpose, 3 ml of plant or soil extract or 1.5 ml of root tip extracts were mixed with 10 ml of scintillation cocktail (Rotiszint eco plus, Roth, Karlsruhe, Germany). The mixture was used for detection of $^{33}P$ signals (DPM, disintegrations per minute) in a PerkinElmer scintillation counter (Tri-Carb TR/SL 3180, Waltham, MA, United States). The signal was corrected for the $^{33}P$ half-life of 25.34 days using QuantSmart (version 4.00, PerkinElmer) to take the decay time between harvest and measurements into account. A background correction value was subtracted from all samples, which was obtained by measuring only scintillation cocktail and extraction solution. $^{33}P$ concentrations in different fractions were expressed as $^{33}P$ (Bq $g^{-1}$ dry mass):

$$^{33}P\ \left(Bq\ g^{-1}\right) = \frac{DPM}{60\ \times dilution\ \times dry\ mass\ of\ the\ sample\ \left(g\right)} \quad (6)$$

To determine the whole amount of $^{33}P$ in a distinct soil or plant compartment (whole amount = WA), we multiplied the $^{33}P$ concentration (Eq. 6) with the total mass of that compartment, for example for fine roots (FR):

$$WA_{FR}\ \ ^{33}P\ \left(Bq\right) = \ ^{33}P\ \ \left(Bq\ g^{-1}\ FR\right) \times total\ biomass\ of\ FR\ \left(g\right) \quad (7)$$

The WA of $^{33}P$ in coarse roots (CR), other roots, rhizosphere soil (Rhizo) in the organic layer (OL), rhizosphere soil in the mineral layer (ML), in bulk soil (Bulk) in the organic layer and in bulk soil in the mineral layer were determined correspondingly.

## Calculation of P Uptake

Irrigation with $^{33}P$ solution ($^{33}P_{tot}$ = total $^{33}P$) leads to distribution of $^{33}P$ between soil solution (soluble $^{33}P = {}^{33}P_{sol}$) and absorption to soil particles (bound $^{33}P = {}^{33}P_{bound}$). Furthermore, only a fraction of $^{33}P$ will percolate through the organic layer into the mineral top soil, where it can be expected to result in another distribution factor between soil solution and soil particles than in the organic layer. As the consequence, $^{33}P_{sol}$ will vary depending on soil layer and forest type. Similarly, we expect that soluble P ($P_{sol}$) present in our soil cores will also vary between soil layers and forest type. Therefore, the dilution of $^{33}P$ in the P concentration of the soil will vary among different soil layer and forest types, resulting in different specific activities. We determined the specific activity of $^{33}P_{sol}$ (spec $^{33}P_{sol}$) for each soil compartment separately using the P and $^{33}P$ concentrations of the Bray-1 solution (**Supplementary Table S2**):

$$spec\ ^{33}P_{sol}\ (Bq\ mg^{-1}P_{sol}) = \frac{^{33}P_{sol}\ (Bq\ g^{-1}\ soil)}{P_{sol}\ (mg\ g^{-1}\ soil)} \quad (8)$$

We used the specific activities to determine P uptake and enrichment in plant roots, microbes and mycorrhizal and non-mycorrhizal tips after 1 day using the whole amounts of these fractions in different soil layers (cv. Eq. 7) and the corresponding specific activities (cv. Eq. 8). The specific activity of $^{33}P_{sol}$ in the bulk soil was used to calculate P uptake of microbes separately for the organic and the mineral layer:

$$P\ uptake_{microbes}(mg) = \frac{WA_{microbes}\ ^{33}P}{spec\ ^{33}P_{sol}(bulk)} \quad (9)$$

We used the specific activity of the rhizosphere to calculate P uptake of beech roots because roots absorb nutrients mainly from the rhizosphere (York et al., 2016):

$$P\ uptake_{beech}(mg) = \frac{(WA_{FR}\ ^{33}P + WA_{CR}\ ^{33}P}{spec\ ^{33}P_{sol}(rhizo)} \quad (10)$$

We calculated P $uptake_{beech}$ separately for the mineral (ML) and organic layer (OL). With P $uptake_{beech}$ in OL and in ML, we calculated the relative contribution of each soil layer to P uptake of beech roots:

$$\text{Relative P uptake in OL} = \frac{P\ uptake_{beech}\ in\ OL}{(P\ uptake_{beech}\ in\ OL + \ P\ uptake_{beech}\ in\ ML)} \quad (11)$$

The relative P uptake in the mineral layer was determined correspondingly.

Mycorrhizal (EM) and non-mycorrhizal (NM) root tips take up nutrients for their own metabolism and translocation to the host. The $^{33}P$ label in the tips should therefore not be termed "uptake" but represents enrichment of new P (ENP) as the result of P metabolism in the mycorrhiza and host allocation at a distinct time point, as exemplified previously for nitrogen (Pena and Polle, 2014; Leberecht et al., 2016). To calculate ENP in EM root tips, we used the $^{33}P$ concentration in root tips (Eq. 6), the specific activity of $^{33}P_{sol}$ in the rhizosphere (Eq. 8) and the mass of an individual EM root tip:

$$ENP_{EM}\ (mg\ root\ tip^{-1}) = \frac{^{33}P_{tot}\ of\ EM\ \times\ mass\ of\ 1\ root\ tip}{spec\ \ ^{33}P_{sol}\ (rhizo)} \quad (12)$$

ENP of non-mycorrhizal root tips was calculated accordingly. We determined and used the following masses for roots tips: 1 EM root tip in HP = 18.35 μg, in LP = 15.68 μg, and 1 NM root tip = 8.84 μg in both HP and LP.

To determine the whole amount of new P (WA ENP) in all mycorrhizal root tips of a distinct layer, we used EMP (Eq. 12) and the total number of root tips in that layer (Eq. 1):

$$\text{WA ENP}_{\text{EM}} \text{ in OL } (\text{mg}) = \text{ENP}_{\text{EM}} \times \text{ number of all EM root tips in OL} \quad (13)$$

WA ENP for EM in the mineral layer and for the non-mycorrhizal root tips in those layers were calculated correspondingly. With these values we calculated WA ENP in all root tips of the whole soil core:

$$\text{WA ENP}_{\text{soil core}} \ (\text{mg}) = \text{WA ENP}_{\text{EM}} \text{ in OL} + \text{WA ENP}_{\text{EM}} \text{ in ML} + \text{WA ENP}_{\text{NM}} \text{ in OL} + \text{WA ENP}_{\text{NM}} \text{ in ML} \quad (14)$$

Using the enrichment of new P of a distinct fraction of root tips (according to Eq. 12) and the total enrichment of new P in all root tips of the soil core (Eq. 13), we determined the relative enrichment of new P in distinct soil layer and types of root tips:

$$\text{Relative ENP}_{\text{EM}} \text{ in OL} = \frac{\text{WA ENP}_{\text{EM}} \text{ in OL}}{\text{WA ENP}_{\text{soil core}}} \quad (15)$$

The relative enrichments of new P in EM of the ML and in NM root tips per soil layer were determined correspondingly.

## Calculations of Relative Competition Intensities (RCI)

According to Grace (1995) the dynamics of mixtures can be accurately determined by the relative competition intensity. We adapted the concept originally used to compare the performance of plants in different ecological settings (Grace, 1995) to calculate the competition intensities for P between beech roots and microbes, or beech roots and other roots in our soil cores or beech roots and all competitors (= microbes + other roots). In line with Grace (1995), we reasoned that new P could end in any of these fractions and the relative amount of new P in beech roots compared to other fractions indicates their competitive strengths:

$$\text{RCI}_{\text{beech vs microbes}} = \frac{\text{P uptake}_{\text{beech}} - \text{P uptake}_{\text{microbes}}}{\text{P uptake}_{\text{beech}}} \quad (16)$$

$\text{RCI}_{\textit{beech versus other roots}}$ and $\text{RCI}_{\textit{beech versus all competitors}}$ were calculated accordingly. Negative values of RCI indicate competition; positive values or values that do not deviate from zero indicate no competition. To test whether the values deviated from zero, we used a non-parametric signed rank test. We considered $p$-values $< 0.05$ to indicate significant effects.

## Statistical Analyses

Data are shown as means ($n$ = 5 to 8 per soil layer and forest type ± SE), if not indicated otherwise. Statistical analyses were conducted with R version 3.6.0 (R Core Development Team, 2012). Normal distribution and homogeneity of variances were tested by analyzing residuals of the models and performing a Shapiro–Wilk test. Data were logarithmically transformed to meet the criteria of normal distribution and homogeneity of variances, where necessary. General linear models were used to test the factor "Forest type" with the two layers (OL and ML) as random factors; otherwise analysis of variance (ANOVA) was used. Differences between means were tested by a *post hoc* test Tukey HSD (package: 'multcomp'). Means between the two forest types were compared with Student's $t$-test. Means were considered to be significantly different from each other when $p \leq 0.05$. For relative values, a generalized linear model using Poisson distribution was used and data were considered to be significantly different from each other when $p \leq 0.05$. To detect linear relationships between variables, Pearson's correlation coefficient was determined.

For the analyses of diversity data (count data for mycorrhizal species), we used PAST version 3.22 (Hammer et al., 2001) to determine mean species abundance and to test differences in the fungal assemblages by a two-way PERMANOVA for the factors: forest type and soil layer. Bray–Curtis was used as the similarity measure.

# RESULTS

## Biomass, Total P and $^{33}$P Distribution in Soil, Roots, and Microbes Differ Between Soil Layers of P-Rich and P-Poor Soils

One day after irrigation of intact soil cores from a HP and an LP forest with $^{33}$P, we determined the masses of soil and root fractions (**Figures 1A,B**), the amounts of bound and soluble P (**Figures 1C,D**), and the amounts of $^{33}$P present in the different fractions (**Figures 1E,F**, complete statistical information: **Supplementary Tables S2, S3**). Bulk soil was always the largest mass fraction, followed by residual materials (leaf litter and twigs in the organic layer and a large stone fraction in the HP mineral soil), and rhizosphere soil (**Figures 1A,B**). LP contained more rhizosphere soil in the organic layer than HP ($p$ = 0.028), probably because the biomass of beech fine roots, from which the adhering soil was collected, was higher in the organic layer at LP than at HP ($p < 0.001$) (**Figures 1A,B** and **Supplementary Table S2**). Beside beech roots, the soil cores also contained roots from other plant species in both layers (**Figures 1A,B**). Other roots were more abundant than beech roots in the organic layer at HP ($p$ = 0.014), while they constituted a smaller fraction to that of beech roots in the organic layer at LP ($p < 0.001$) (**Figures 1A,B**). In the mineral layer, beech roots strongly dominated over other roots at HP ($p$ = 0.002) and were mostly absent at LP ($p < 0.001$) (**Figures 1A,B**).

As expected (Lang et al., 2017), the vast majority of total P was sequestered in bulk soil and the amounts of P present in

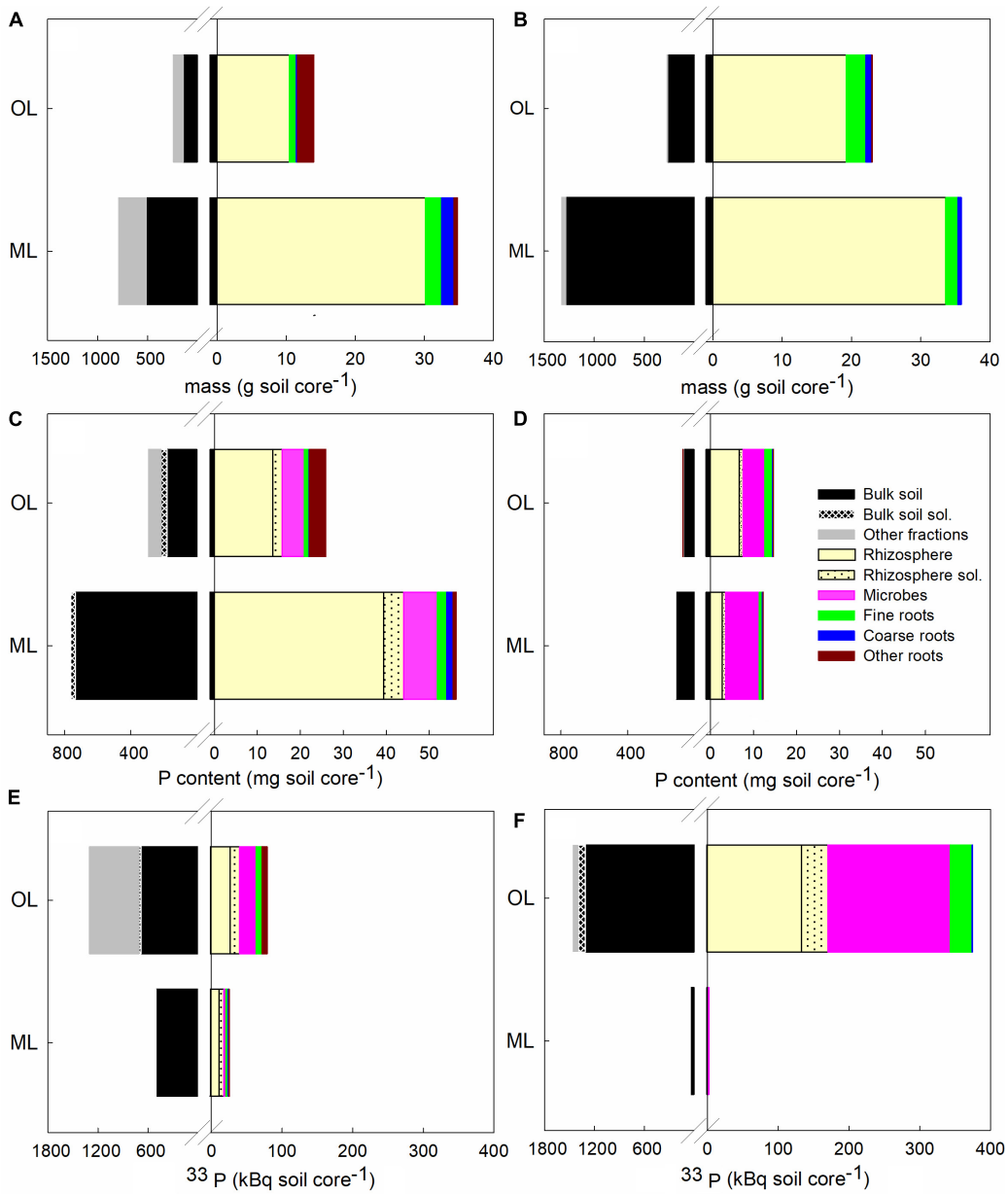


**FIGURE 1 |** Distribution of biomass, P content and $^{33}$P activity in intact soil cores 24 h after label application. Soil cores were obtained from P-rich **(A,C,E)** and P-poor **(B,D,F)** forests. Soils from the organic layer (OL) and the mineral topsoil (ML) were analyzed separately. Data indicate means ($n$ = 5). Standard errors and statistical information is shown in **Supplementary Tables S2, S3**. Colors of bars refer to bulk soil (black) with potential plant available $P_{sol}$ (white hatched), residual materials (gray), rhizosphere soil (light yellow) with potential plant available $P_{sol}$ (dotted), microbes (purple), fine roots (green), coarse roots (blue), and other roots (dark red).

most of the analyzed fractions were higher at HP than at LP (**Figures 1C,D** and **Supplementary Table S3**). Still, we noted some exceptions: the total amounts of P bound by beech fine roots ($p$ = 0.231), beech coarse roots ($p$ = 0.522), and microbes ($p$ = 0.114) in the organic layer of LP were similar to those at HP. In the mineral layer of LP, the amount of P in microbes was even higher than that of HP ($p$ = 0.003). The $P_{sol}$ content of the rhizosphere, which we considered as the potentially plant-available P pool, was higher at HP than at LP in both soil layers (organic layer: $p < 0.001$, mineral layer: $p < 0.001$) (**Figures 1C,D**).

To investigate the fate of newly added $P_i$, we studied the distribution of $^{33}$P 1 day after labeling. The majority of the label was sequestered in bulk soil and was not soluble in mild acid at HP ($p < 0.001$) and LP ($p < 0.012$), suggesting that it was immediately removed from the easily available bioactive pool (**Figures 1E,F**). Furthermore, the distribution of the added $^{33}$P showed interesting differences between the organic layer and

**TABLE 1 |** Specific activity $^{33}P$ in rhizosphere and bulk soil of beech forests.

| Site | HP | | LP | | Forest | | OL | | ML | |
|---|---|---|---|---|---|---|---|---|---|---|
| Layer | OL | ML | OL | ML | F | *p* | t | *p* | t | *p* |
| Bulk soil | 0.86 ± 0.15 | 0.27 ± 0.04 | 26.69 ± 3.60 | 0.30 ± 0.17 | 13.012 | **0.002** | 7.160 | **<0.001** | 0.638 | 0.541 |
| Rhizosphere | 6.39 ± 0.97 | 1.44 ± 0.37 | 46.17 ± 8.70 | 0.08 ± 0.04 | 8.593 | **0.009** | 4.542 | **0.002** | 3.638 | **0.007** |

*Soils were collected in a P-rich (HP) and P-poor (LP) forest and separated into organic layer (OL) and the mineral topsoil (ML) for analyses. Data indicate means (n = 5 ± SE). To compare means we used general linear models for the overall comparisons between HP and LP (OL and ML as random factor), otherwise Student's t-test. Bold letters indicate significant differences at p ≤ 0.05.*

the mineral top soil at HP and LP (**Figures 1E,F**). At LP, only a relatively small fraction of the added $^{33}P$ percolated into the mineral soil (**Figure 1F**, $p < 0.001$), while at HP, the organic layer including microbes and rhizosphere retained less $^{33}P$, resulting in a higher through flux of $^{33}P$ into the mineral layer (**Figure 1E**). These distribution patterns also influenced the specific activities of $^{33}P_{sol}$ in the rhizosphere (**Table 1**), resulting in the highest specific activity in the organic layer and the lowest in mineral soil at LP, while HP assumed intermediate specific $^{33}P$ activities (**Table 1**). Overall, the recovery of applied $^{33}P$ was at 84.7% ± 5.1 at HP and 99.2% ± 0.4 at LP (calculated with the data in **Supplementary Table S3**). It is likely that the lower recovery at HP was caused by the stone fraction in the mineral layer, which could not be measured, but probably also absorbed a portion of the added $^{33}P$.

## P Uptake and P Distribution in Beech Roots Differ Between Soil Layers in P-Rich and P-Poor Forests

The specific activities of $^{33}P_{sol}$ in rhizosphere per forest type and soil layer (**Table 1**) were used to estimate P uptake of beech roots in each layer separately. To compare the importance of soil layers for P supply at HP and LP, we normalized the data relative to P uptake of beech roots (Eq. 11 under materials and methods). We found that beech roots in our soil cores acquired about 75% of P from the mineral soil and 25% from the organic layer at HP, whereas beech roots at LP took up about 60% P from the organic and 40% from the mineral soil (**Figure 2**). These figures corresponded well to the distribution of total P in beech roots between the organic layer and mineral soil at HP (25% and 75%, respectively) and at LP (69% and 30%, respectively, calculated with the data in **Supplementary Table S3**).

## Mycorrhizal P Efficiencies Differ Between Soil Layers in P-Rich and P-Poor Soil

Regardless of forest type and soil layer, 96% of the vital root tips were colonized by ectomycorrhizal fungi (**Table 2**). In soil cores from HP about 50% of the root tips were present in the organic layer and the other 50% in the mineral soil, whereas at LP 75% of the root tips were present in the organic layer and 25% in the mineral soil (**Table 2**). In HP soil, the P concentrations of mycorrhizal root tips were similar to those of non-mycorrhizal root tips in HP soil and did not differ between soil layers (**Figure 3A**). In LP soil, the P concentrations of mycorrhizal root tips were higher than those in HP soil ($p = 0.002$), whereas those of non-mycorrhizal root tips were by far lower than those of non-mycorrhizal root tips in HP soil ($p = 0.015$, **Figure 3A**).

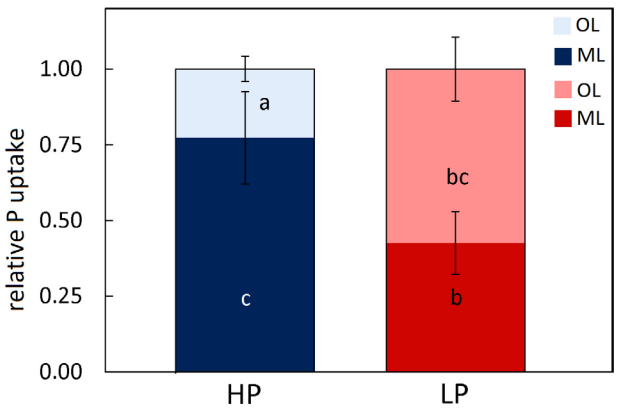


**FIGURE 2 |** Relative P enrichment in beech roots in the organic layer and mineral layer topsoil of beech (*Fagus sylvatica* L.) forests. Intact soil cores were collected in a P-rich (HP: blue) and a P-poor (LP: red) forest, irrigated with $^{33}P$ artificial soil solution and roots from the organic layer (light blue, light red) and the mineral topsoil (dark blue, dark red) were analyzed separately after 24 h of labeling. To determine P root uptake, the rhizospheric $^{33}P$ dilutions per forest and layer were used as described under materials and methods. Data indicate means ($n = 5 \pm SE$). Differences among means per forest and layer were tested by GLM using Poisson distribution. Different letters indicate significant differences at $p \leq 0.05$.

To test whether these differences were caused by differences in the abilities for P acquisition in different soil layers, we determined the $^{33}P$ enrichment of mycorrhizal and non-mycorrhizal root tips. We calculated the relative enrichment of new $P_{roottip}$ with the specific activities of $^{33}P$ in the rhizosphere of each soil layer and forest type (**Table 1**) as described under materials and methods (Eq. 12). The relative enrichment of new P per root tip indicates a mean value for the ability of the mycorrhizal root tips in that soil layer to acquire P (Eq. 15). We define this ability as mycorrhizal P efficiency. P accumulation in non-mycorrhizal root tips was treated correspondingly. The relative accumulation of new P per non-mycorrhizal root tip was low and did not differ between HP and LP (**Figure 3B**). In the mineral soil of LP, where only very little of the total added $^{33}P$ was present (**Figure 1F**), non-mycorrhizal root tips showed no measurable $^{33}P$ enrichment (**Figure 3B**). In contrast to non-mycorrhizal root tips, the relative enrichment per mycorrhizal root tip showed significant differences between soil layers and

**TABLE 2 |** Vitality, ectomycorrhizal (EM) colonization and number of beech root tips (soil core$^{-1}$) in the organic layer (OL) and mineral topsoil (ML) from a P-rich (HP) and P-poor beech (*Fagus sylvatica*) forest.

| Site | HP | | LP | | Forest | | OL | | ML | |
|---|---|---|---|---|---|---|---|---|---|---|
| Layer | OL | ML | OL | ML | F | *p* | t | *p* | t | *p* |
| Vital root tips (%) | 91.08 ± 1.44 | 84.72 ± 1.76 | 89.95 ± 1.37 | 84.76 ± 1.81 | 0.106 | 0.748 | 0.899 | 0.395 | 0.032 | 0.98 |
| EM root tips (%) | 96.39 ± 1.31 | 95.19 ± 1.77 | 97.89 ± 1.25 | 96.43 ± 1.32 | 2.271 | 0.149 | 1.308 | 0.227 | 0.887 | 0.401 |
| EM (number) | 2701.1 ± 1095.2 | 3287.1 ± 562.5 | 5324.9 ± 1150.0 | 1783.0 ± 393.1 | 0.33 | 0.575 | 1.651 | 0.137 | 2.388 | **0.044** |
| Dry (number) | 301.8 ± 136.8 | 615.2 ± 102.5 | 635.3 ± 164.5 | 317.1 ± 52.1 | 0.16 | 0.899 | 1.559 | 0.158 | 2.593 | **0.032** |
| Non-EM (number) | 11.3 ± 68.0 | 160.7 ± 39.7 | 119.2 ± 55.2 | 56.6 ± 12.3 | 1.28 | 0.272 | 0.533 | 0.609 | 2.501 | **0.037** |

*Data indicate means (n = 5 ± SE). To compare means we used general linear models (GLM) for the overall comparisons between HP and LP (OL and ML as random factor), otherwise Student's t-test. Relative data were tested by a GLM using the Poisson distribution. Bold letters indicate significant differences at p ≤ 0.05. Number = number of root tips per layer and soil core with the following dimensions, height: 0.2 m and diameter: 0.12 m.*

forest types (**Figure 3B**). In the organic layer, mycorrhizal P efficiency (per root tip) was higher at LP than at HP (**Figure 3B**). In the mineral layer, mycorrhizal P efficiency (per root tip) was lower at LP than at HP (**Figure 3B**). These differences were even more pronounced when the P enrichment in root tips was up-scaled to the whole soil core (**Figure 3C**). At HP, mycorrhizal root tips of the whole root system in the mineral layer exhibited 70% of P enrichment, followed by mycorrhizal root tips of the organic layer (26%), whereas non-mycorrhizal root tips of the mineral layer accumulated only about 4% and of the organic layer less than 0.1% ($p < 0.001$) of the total new P in root tips. At LP, mycorrhizal root tips of the whole root system in the organic layer contributed most to relative P accumulation in root tips (78%), followed by mycorrhizal root tips in the mineral layer (22%), whereas non-mycorrhizal root tips contributed less than 0.1% to P accumulation in root tips in the organic layer and nothing in the mineral layer ($p = 0.003$, **Figure 3C**).

If the enrichment of mycorrhizal root tips with new P was an indicator for root P supply, we expected that beech root P uptake is correlated with the abundance of mycorrhizal root tips and their specific enrichment with new P. In accordance with this suggestion, we found a strong relationship between the total amount of new P accumulated in all root tips of a soil layer and the estimated amount of new P taken up by beech roots in that layer (**Figure 4**). We did not find a correlation between the number of root tips and P uptake ($R = 0.332$, $p = 0.164$) indicating that the P efficiencies of mycorrhizal root tips are decisive for beech P acquisition.

## Mycorrhizal Community Structures Differ Between the HP and LP Forests but Not Between the Soil Layers

We investigated whether the observed differences in P acquisition were accompanied by differences in the mycorrhizal communities. Roots in HP and LP forests were colonized by different fungal assemblages (PERMANOVA, $p_{(forest)} = 0.012$). Ascomycota (Hyaloscyphacae, *Cenococcum geophilum*) were more abundant in LP soil, whereas Basidiomycota of the orders of Russulales and Boletales (several *Lactarius* sp., *Xerocomellus* sp.) were more abundant in the HP soils (**Figure 5**). However, there were some exceptions, *Lactarius blennius* and *Lactarius tabidus* occurred only in the LP forests, whereas *Genea hispidula* was only found the HP forest (**Figure 5**).

We further analyzed mycorrhizal community strutures in different soil layers. *Clavulina cristata* and *Rhizodermea veluwensis* occurred only in LP mineral (**Figure 5**) but these species were rare. Overall, no significant differences between the fungal assemblages in the organic layer and mineral top soil were detected (PERMANOVA, $p_{(soillayer)} = 0.747$).

## Competition of Beech Roots, Understory Roots, and Microbes for P Resources in Different Layers in P-Rich and P-Poor Forests

We expected that low P availability would result in strong competition of microbes and other roots with beech roots (i.e., negative values for RCI) and that high P availability would prevent competition. In line with this assumption, we found that the RCI for the competition of beech with microbes together with other roots at HP were not smaller than zero and higher than those at LP (**Figure 6**). Other roots, despite their relatively high abundance in the organic layer at HP (**Figure 1A**), did not significantly affect the competition of beech roots for $P_i$ (vertical lines in the bars for HP in **Figure 6**). At LP, other roots were too rare to affect the competition between beech roots and microbes. At LP, microbes outcompeted beech roots in both soil layers (**Figure 6**).

# DISCUSSION

## Soil Structure and $P_i$ Availability Impact Beech Root P Uptake

In recent years, the concept of ecosystem nutrition has gained support, which proposes a gradual shift in nutritional strategies from P acquisition to P recycling when P soil stocks are decreasing from P-rich to P-poor forest sites (Lang et al., 2016). According to this model, we expected that bio-available P varied among soil layers of P-rich and P-poor forests, resulting in differences for root P supply. Using undisturbed soil horizons for P tracing, our results support our first hypothesis and comply with previous experiments in mesocosms with young beech

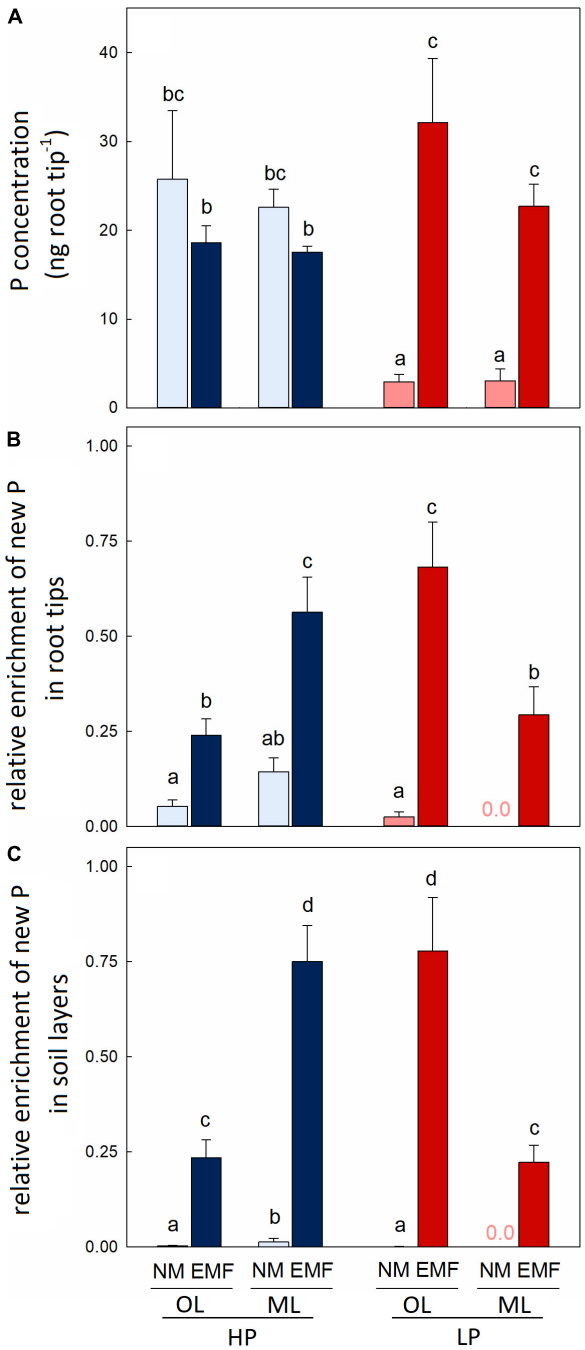


**FIGURE 3 |** P concentration **(A)**, relative net enrichment of new P in single root tips of beech trees (*Fagus sylvatica* L.) **(B)** and the relative net enrichment of new P in the sum of mycorrhizal and non-mycorrhizal root tips per forest type and soil layer **(C)**. Intact soil cores were collected in a P-rich (HP: blue) and a P-poor (LP: red) forest, irrigated with $^{33}$P artificial soil solution and mycorrhizal (EMF) and non-mycorrhizal (NM) root tips from the organic layer (light blue, light red) and the mineral topsoil (dark blue, dark red) were analyzed separately after 24 h of labeling. To determine P enrichment, the rhizospheric $^{33}$P dilutions per forest and layer were used as described under materials and methods. Data indicate means ($n$ = 5 ± SE). Differences among means per forest and layer were tested by three-way-ANOVA and Tukey HSD *post hoc* test **(A)** or by GLM using Poisson distribution **(B,C)**. Different letters indicate significant differences at $p \leq 0.05$.

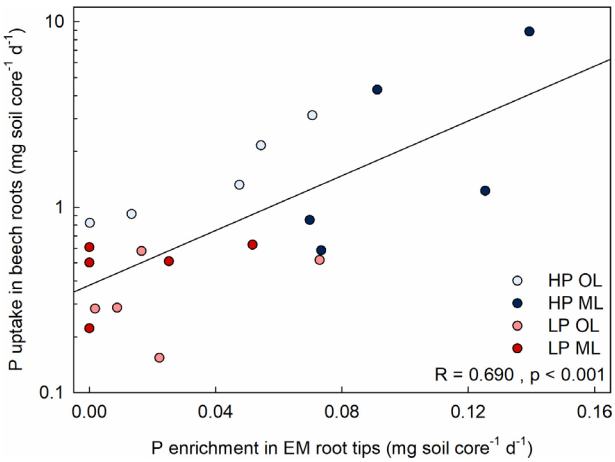


**FIGURE 4 |** Relationship between the P enrichment in mycorrhizal (EM) root tips and P uptake of beech roots. Symbols indicate individual measurements in soil cores (diameter 0.12 m, height: 0.2 m) from a P-rich (HP) and a P-poor forest (LP) in the organic layer (OL) and in mineral top soil (ML). P uptake was determined 1 day (d) after application of $^{33}$P in artificial soil solution using the specific activities for $^{33}P_{sol}/P_{sol}$ in the rhizosphere (**Table 1**) as described under materials and methods. Regression analysis was done determining Pearson correlation coefficient.

plants (Brandtberg et al., 2004; Jonard et al., 2009; Hauenstein et al., 2018; Spohn et al., 2018; Zavišić and Polle, 2018). It should be noted that our approach might have some limitations because (i) the roots were severed at the edge of the soil cylinders and (ii) only the upper portion of the whole-rooted soil profile was included. Firstly, excised fresh roots are still highly active in P uptake and translocation (Noggle and Fried, 1960; Franklin, 1969; Mejstrik and Benecke, 1969; Rubio et al., 1997). Furthermore, P root uptake in the present study corresponded well to aboveground P translocation in young intact beech trees (Yang et al., 2016; Hauenstein et al., 2018; Zavišić and Polle, 2018). Therefore, we have no evidence for confounding effects of root damage in our experimental set-up. Secondly, based on our experimental unit "soil core," we estimated a contribution of 25-to-75% of the organic layer-to-mineral layer to P root supply in the P-rich forest. Since a larger root fraction is present below the forest floor and the A horizon in HP (about 80%) than in LP soil (30%, Lang et al., 2017), the ratios for the contribution of soil layers to beech P supply may further diverge in favor of the mineral layer at HP. Our results, thus, underpin an at least twice higher contribution of the organic layer to root P acquisition (60-to-40%) under P-poor conditions. This result strongly supports that the organic layer is critical for P nutrition under P-poor conditions (Lang et al., 2017; Hauenstein et al., 2018) and underpins that our comparison of two sites concurs with field studies along a larger P gradient (Lang et al., 2017).

We demonstrated that the function of the organic layer for root P supply occurred already at a short time scale of 1 day. One reason for this finding is probably that the sorption capacity for different P species is lower in the organic layer in P-poor than in P-rich soil (Lang et al., 2017), thus, resulting in relatively higher $P_i$

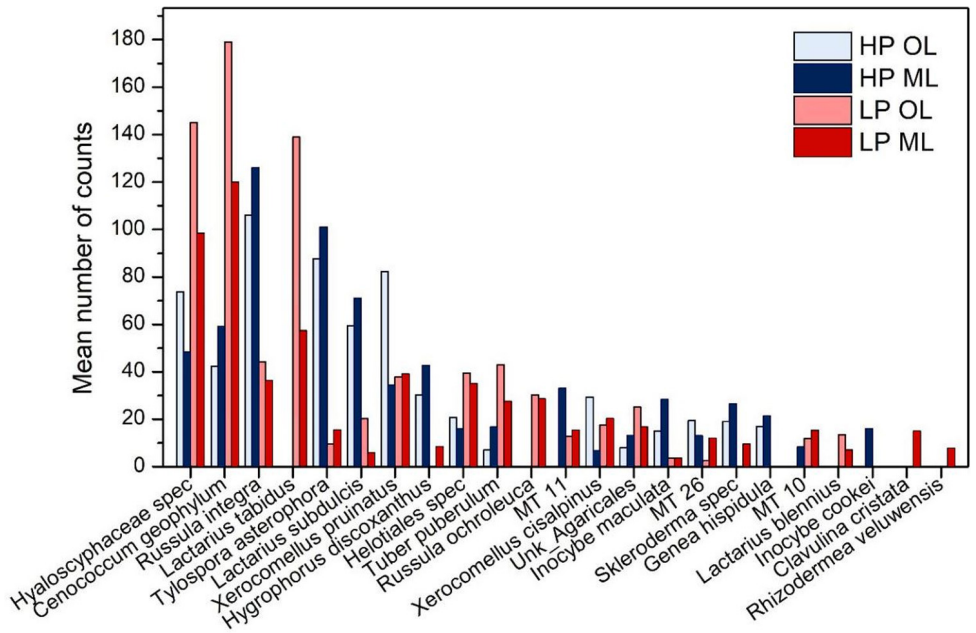


**FIGURE 5 |** Ectomycorhizal species colonizing beech (*Fagus sylvatica*) roots in P-rich (HP: blue) and P-poor (LP: red) forest soil. Species were analyzed by morphotyping and ITS sequencing of the fungal morphotypes. **Supplementary Table S4** shows additional information on species identification. Roots from the organic layer (OL, light blue, light red) and the mineral topsoil (ML: dark blue, dark red) were analyzed separately.

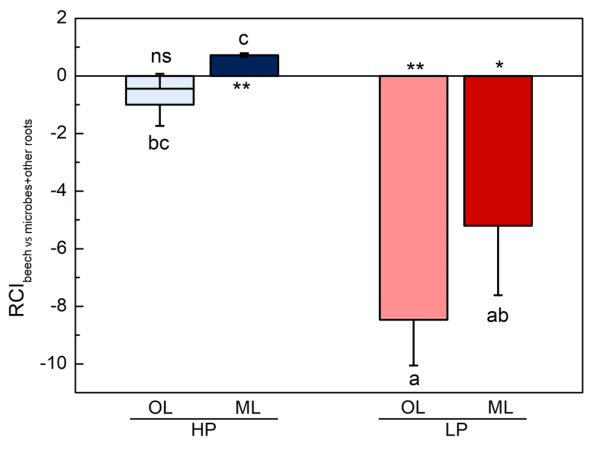


**FIGURE 6 |** Relative competition indices (RCIs) for P uptake of beech (*Fagus sylvatica*) roots and their competitors (microbes + other roots) in P-rich (HP: blue) and P-poor (LP: red) forest soil. Analyses were conducted separately for the organic layer (OL, light blue, light red) and the mineral topsoil (ML: dark blue, dark red). Data show means ($n$ = 5 ± SE per soil layer and forest type). Vertical line in bars show RCI for beech and other roots without microbes. Before ANOVA, data were normalized as follows: [log10((x−1)*−1)]. Significant deviation from zero are shown by different letters. To test for each variable, the non-parametric signed rank test was used and significant differences at $p < 0.05$ and $p < 0.01$ are indicated by * and **, respectively. ns = not significant.

bioavailability. Our results show that microbes benefited strongly but roots also obtained a higher share of P than one would expected on the basis of the low P stock in the P-poor forest. As the consequence of high plant and microbial activities (this study; Bergkemper et al., 2016; Hofmann et al., 2016) the P retention of the organic layer was high, despite its lower sorption capacity (Lang et al., 2017).

Our estimation of the relative P partitioning in roots in different layers and soil types was based on the premise that P uptake into roots occurs from the rhizosphere and therefore, we used the rhizospheric dilution of the P tracer for the estimation of root P uptake. This is a novel approach since previous studies considered either the dilution of added P in pooled soil samples (Jonard et al., 2015) or used more specifically tracer dilution in the organic layer and the mineral soil, respectively (Di et al., 2000; Hauenstein et al., 2018; Spohn et al., 2018; Zavišić and Polle, 2018). Our results indicate strong differences for soluble P and consequently for the specific dilution of the tracer ($^{33}$P/mg $P_{sol}$) between rhizosphere and bulk soil from the organic and mineral layers, respectively. The differences between bulk soil and rhizosphere might have been expected because plant roots and their associated mycorrhizal fungal symbionts exude organic acids, metal-chelating compounds and acid phosphatases that enhance solubilization of P (Leyval and Berthelin, 1993; Wallander, 2000; Casarin et al., 2004; Liu et al., 2007). These biotic activities result in an altered rhizosphere chemistry, in turn leading to higher P availability for mycorrhizal and root uptake (Wallander, 2000; Casarin et al., 2004; Liu et al., 2007). Consequently, we recommend that future studies should consider rhizospheric P availability when estimating root P uptake. Overall, our short-term tracer experiment with forest-grown roots in naturally stratified soil horizons highlight the

prominent role of the organic layer for beech P nutrition under P poor conditions und uncovered heterogeneity for bioavailable P between rhizosphere and bulk soil in different soil layers and forest types.

## Mycorrhizal P Efficiencies Regulate Beech P Uptake in Different Soil Layers but Do Not Prevent Competition With Microbes in P-Poor Soil

Roots of beech trees in temperate forests are usually almost completely colonized by a diverse spectrum of different mycorrhizal fungi (Courty et al., 2010; Pena et al., 2010, 2017). The taxonomic composition of ectomycorrhizal fungi differs between P-rich and P-poor beech forests (this study; Zavišić et al., 2016). Notably, the dominant ectomycorrhizal species present in both forest types were characterized by short hyphae of a few micrometers (short-distance exploration types) or by the absence of hyphae (contact types) (Weigt et al., 2012). Among the fungi in our study, only the Boletales, which were not very abundant (approximately 8% of the mycorrhizal root tips), produce long distance hyphae (Agerer, 1987) and may explore regions beyond the rhizosphere. Therefore, mycorrhizal P mobilization in P-rich and P-poor forests was mainly confined to the vicinity of roots. These considerations further underpin that for the assessment of P uptake by mycorrhizal root tips and plant roots, the specific activities of rhizospheric rather than those of bulk soil should be taken into account.

In our study forests, non-mycorrhizal root tips were rarely found and therefore were unimportant for gross host P provision. However, they provided insights into the benefits of P handling by mycorrhizal root tips in naturally composed fungal community. Drastically lower P concentrations in non-mycorrhizal root tips under low than under high P in soil highlight the superiority of mycorrhizas for P acquisition under P limitation. Although the beneficial influence of mycorrhiza for P provision is well-established (Nehls and Plassard, 2018), studies demonstrating mycorrhizal P facilitation in natural soils are scarce. An enhanced P enrichment of mycorrhizal root tips can be regarded as a measure for P efficiency. A relatively stronger enrichment with new P in mycorrhizal compared to non-mycorrhizal root tips, regardless of P availability in the soil, also indicated the predominance for P acquisition of mycorrhizal root tips. Despite lower P efficiency of non-mycorrhizal root tips in P-rich soil, their P concentrations, which are the result of more long-term processes, were similar to mycorrhizal root tips. This suggest that in contrast to P-limited conditions, mycorrhizal and non-mycorrhizal root tips do not compete for P under P-rich conditions.

An obvious question is whether differences in fungal community structures or differences in the regulation of P-uptake in the P-rich and P-poor forest were responsible for differences in plant supply. An ultimate answer to that question is not possible but our finding that similar fungal community structures in organic and mineral soil layers exhibited different P efficiencies suggests a strong impact of regulatory processes on P uptake. P-limitation leads to an increase in high-affinity P transporters to ensure P uptake, whereas under high P, low affinity transporters maintain P uptake (Wu et al., 2003; Desai et al., 2014; Kavka and Polle, 2016, 2017). Therefore, our initial hypothesis was that low P availability is counteracted by relatively higher P uptake efficiencies than under high P availability. However, in contrast to that assumption relatively higher P efficiencies of mycorrhizal root tips occurred in those soil layers that contributed most to P provision to roots and not in those with lower P availability. The most likely explanation for these findings is that both adaptedness of fungal assemblages to certain habitat conditions together with regulation of P supply in response to plant demand (Zavišić and Polle, 2018) were responsible for the observed root P supply. Since the abundance of root tips alone cannot predict root P uptake, it is obvious that the properties of the symbionts are essential for P acquisition. Here, any contribution of distinct taxa to P provision to the roots remained enigmatic because we used pooled samples. Previous studies have shown large differences among different fungal species for P translocation (Cumming, 1996; Brandes et al., 1998; Colpaert et al., 1999; Jentschke et al., 2001). Field studies in beech forests demonstrated high phosphatase activities in *Lactarius* sp., *Russula* sp., and *Cenococcum* sp. (Courty et al., 2005). These genera were also abundant in our investigation, suggesting a high potential to release $P_i$ from organic material. In conclusion, the significant relationship between root P uptake and mycorrhizal P enrichment corroborates that mycorrhizal P efficiency governs P provision to the host.

Plant P supply is not only affected by the complex interactions of mycorrhizal properties and geochemical soil properties but usually also by competition with other biota (Curt et al., 2005; Zhu et al., 2016). When nutrients such as P are inadequately available in the soil of natural ecosystems to suffice plant and microorganism requirements, plants are thought to be inferior in the competition (Woodmansee et al., 1981) but some studies have found that plants compete successfully with soil microorganisms (Schimel and Bennett, 2004) or are even superior under specific circumstances (Wang and Lars, 1997). Our study did neither reveal competition between beech roots and microbes nor with other understory roots in P-rich soil, even though the biomass of other roots was considerable and the biomass of microbes about 10-fold higher in the P-rich than in the P-poor forest (Bergkemper et al., 2016; Lang et al., 2017). The absence of P competition in P rich soil underpins P sufficiency for biological processes. By contrast, the competition between beech roots and microbes was strong in P-poor soil and might have precluded the establishment of further understory species. An unexpected result was that the competition strength did not differ between organic and mineral soil layers. This observation was surprising since we anticipated lower competition in the organic layer with higher P availability than in the mineral soil where P availability was lower. Possibly, the regulation of P uptake into roots by different

mycorrhizal efficiencies balances nutrient competition across different soil layers. This idea should be followed up in future studies.

## CONCLUSION

This study reveals that P uptake by plant roots is not only based on soil P stocks but differs between different layers, underlies regulation by mycorrhizal efficiencies, and faces competition with soil microbes under P-limiting conditions. Revisiting our hypotheses, we confirmed that (i) the main P source for beech P supply is the mineral topsoil under P-rich and the organic layer under P-poor conditions. Our results pinpoint different mycorrhizal efficiencies as drivers for root P uptake. As expected non-mycorrhizal root tips did not contribute markedly to root P supply in natural forest soils. However, the simplistic idea (hypothesis ii) that the mycorrhizal P enrichment is relatively higher to compensate for lower P bioavailability can be refuted because the relative mycorrhizal P enrichments were highest in those layers that contributed most to root P uptake. In agreement with our hypothesis (iii) no competition for P was detected in soil of the P-rich forest, whereas microbes were strong competitors under P-poor conditions.

In accordance with previous studies (Lang et al., 2017; Hauenstein et al., 2018), we conclude that an intact forest floor is of tremendous importance under nutrient-poor conditions for uptake and recycling of P. Our study provides insights into the mechanisms that contribute to the adaptation of ecosystems to low P availability. Obviously, forests that rely on P recycling with the majority of roots in the upper layer are at risk under climate change. When the duration and intensity of summer droughts increase, the top layer roots and microbes will be the first to be negatively affected by water shortage. Further depletion of P is expected due to lower P mineralization rates (Schimel et al., 2007) and lower P mobility in drier soil (Schachtman et al., 1998; Kreuzwieser and Gessler, 2010). This study envisages decreasing P retention as the result of declining microbial biomass and declining mycorrhizal activities in future climate scenarios.

## DATA AVAILABILITY STATEMENT

The datasets generated for this study can be found in the Dryad digital repository (https://doi.org/10.5061/dryad.4j0zpc87g). The sequences for identified mycorrhizal fungi are available in GenBank (accession numbers in **Supplementary Table S4**).

## AUTHOR CONTRIBUTIONS

SC and AP contributed to the conception and design of the study and contributed to manuscript revision and approved the final version. SC conducted the measurements, analyzed the data, and wrote the first draft of the manuscript. AP revised the draft.

## FUNDING

The project was funded by Deutsche Forschungsgemeinschaft (DFG) and was part of SPP 1685 "Ecosystem Nutrition," funding project Po362/22-2.

## ACKNOWLEDGMENTS

We are grateful to M. Franke-Klein for ICP analyses, to T. Klein (Laboratory for Radio-Isotopes, University of Goettingen) for help with mycorrhizal sequencing and to G. Lehmann (Laboratory for Radio-Isotopes, University of Goettingen) for support with radioactive labeling experiment.

## SUPPLEMENTARY MATERIAL

The Supplementary Material for this article can be found online at: https://www.frontiersin.org/articles/10.3389/ffgc.2020.00054/full#supplementary-material

## REFERENCES

Agerer, R. (ed.) (1987). *Colour Atlas of Ectomycorrhizae: With Glossary. Delivery 2*, 1th-5th del Edn. Schwäbisch Gmünd: Einhorn-Verlag.

Balogh-Brunstad, Z., Keller, C. K., Dickinson, J. T., Stevens, F., Li, C. Y., and Bormann, B. T. (2008). Biotite weathering and nutrient uptake by ectomycorrhizal fungus, *Suillus tomentosus*, in liquid-culture experiments. *Geochim. Cosmochim. Acta* 72, 2601–2618. doi: 10.1016/j.gca.2008.04.003

Becquer, A., Trap, J., Irshad, U., Ali, M. A., and Plassard, C. (2014). From soil to plant, the journey of P through trophic relationships and ectomycorrhizal association. *Front. Plant Sci.* 5:548. doi: 10.3389/fpls.2014.00548

Bergkemper, F., Schöler, A., Engel, M., Lang, F., Krüger, J., Schloter, M., et al. (2016). Phosphorus depletion in forest soils shapes bacterial communities towards phosphorus recycling systems: microbial phosphorus turnover in soil. *Environ. Microbiol.* 18, 1988–2000. doi: 10.1111/1462-2920.13188

Brandes, B., Godbold, D. L., Kuhn, A. J., and Jentschke, G. (1998). Nitrogen and phosphorus acquisition by the mycelium of the ectomycorrhizal fungus *Paxillus involutus* and its effect on host nutrition. *New Phytol.* 140, 735–743. doi: 10.1046/j.1469-8137.1998.00313.x

Brandtberg, P.-O., Bengtsson, J., and Lundkvist, H. (2004). Distributions of the capacity to take up nutrients by *Betula* spp. and *Picea abies* in mixed stands. *Forest Ecol. Manage.* 198, 193–208. doi: 10.1016/j.foreco.2004.04.012

Bray, R. H., and Kurtz, L. T. (1945). Determination of total, organic, and available forms of phosphorus in soils. *Soil Sci.* 59, 39–46. doi: 10.1097/00010694-194501000-00006

Brookes, P. C., Landman, A., Pruden, G., and Jenkinson, D. S. (1985). Chloroform fumigation and the release of soil nitrogen: a rapid direct extraction method to measure microbial biomass nitrogen in soil. *Soil Biol. Biochem.* 17, 837–842. doi: 10.1016/0038-0717(85)90144-0

Brookes, P. C., Powlson, D. S., and Jenkinson, D. S. (1982). Measurement of microbial biomass phosphorus in soil. *Soil Biol. Biochem.* 14, 319–329. doi: 10.1016/0038-0717(82)90001-3

Cairney, J. W. G. (2011). Ectomycorrhizal fungi: the symbiotic route to the root for phosphorus in forest soils. *Plant Soil* 344, 51–71. doi: 10.1007/s11104-011-0731-0

Callaway, R. M., and Nadkarni, N. M. (1991). Seasonal patterns of nutrient deposition in a *Quercus douglasii* woodland in central California. *Plant Soil* 137, 209–222. doi: 10.1007/BF00011199

Casarin, V., Plassard, C., Hinsinger, P., and Arvieu, J.-C. (2004). Quantification of ectomycorrhizal fungal effects on the bioavailability and mobilization of soil P in the rhizosphere of *Pinus pinaster*. *New Phytol.* 163, 177–185. doi: 10.1111/j.1469-8137.2004.01093.x

Chadwick, O. A., Derry, L. A., Vitousek, P. M., Huebert, B. J., and Hedin, L. O. (1999). Changing sources of nutrients during four million years of ecosystem development. *Nature* 397, 491–497. doi: 10.1038/17276

Colpaert, J. V., Van Tichelen, K. K., Van Assche, J. A., and Van Laere, A. (1999). Short-term phosphorus uptake rates in mycorrhizal and non-mycorrhizal roots of intact *Pinus sylvestris* seedlings. *New Phytol.* 143, 589–597. doi: 10.1046/j.1469-8137.1999.00471.x

Courty, P.-E., Buée, M., Diedhiou, A. G., Frey-Klett, P., Le Tacon, F., Rineau, F., et al. (2010). The role of ectomycorrhizal communities in forest ecosystem processes: NEw perspectives and emerging concepts. *Soil Biol. Biochem.* 42, 679–698. doi: 10.1016/j.soilbio.2009.12.006

Courty, P.-E., Pritsch, K., Schloter, M., Hartmann, A., and Garbaye, J. (2005). Activity profiling of ectomycorrhiza communities in two forest soils using multiple enzymatic tests: Methods. *New Phytol.* 167, 309–319. doi: 10.1111/j.1469-8137.2005.01401.x

Cumming, J. R. (1996). Phosphate-limitation physiology in ectomycorrhizal pitch pine (*Pinus rigida*) seedlings. *Tree Physiol.* 16, 977–983. doi: 10.1093/treephys/16.11-12.977

Curt, T., Coll, L., Prévosto, B., Balandier, P., and Kunstler, G. (2005). Plasticity in growth, biomass allocation and root morphology in beech seedlings as induced by irradiance and herbaceous competition. *Ann. For. Sci.* 62, 51–60. doi: 10.1051/forest:2004092

Desai, S., Naik, D., and Cumming, J. R. (2014). The influence of phosphorus availability and Laccaria bicolor symbiosis on phosphate acquisition, antioxidant enzyme activity, and rhizospheric carbon flux in Populus tremuloides. *Mycorrhiza* 24, 369–382. doi: 10.1007/s00572-013-0548-1

Di, H. J., Cameron, K. C., and McLaren, R. G. (2000). Isotopic dilution methods to determine the gross transformation rates of nitrogen, phosphorus, and sulfur in soil: a review of the theory, methodologies, and limitations. *Aust. J. Soil Res.* 38, 213–230. doi: 10.1071/SR99005

Franklin, R. E. (1969). Effect of adsorbed cations on phosphorus uptake by excised roots. *Plant Physiol.* 44, 697–700. doi: 10.1104/pp.44.5.697

George, T. S., Giles, C. D., Menezes-Blackburn, D., Condron, L. M., Gama-Rodrigues, A. C., Jaisi, D., et al. (2018). Organic phosphorus in the terrestrial environment: a perspective on the state of the art and future priorities. *Plant Soil* 427, 191–208. doi: 10.1007/s11104-017-3391-x

Grace, J. B. (1995). On the Measurement of Plant Competition Intensity. *Ecology* 76, 305–308. doi: 10.2307/1940651

Hammer, Ø., Harper, D. A. T., and Ryan, P. D. (2001). PAST: paleontological statistics software package for education and data analysis. *Palaeontol. Electron.* 4, 9–17.

Harley, J. L., Brierley, J. K., and Mccready, C. C. (1954). The uptake of phosphate by excised mycorrhizal roots of the beech. *New Phytol.* 53, 92–98. doi: 10.1111/j.1469-8137.1954.tb05225.x

Hauenstein, S., Neidhardt, H., Lang, F., Krüger, J., Hofmann, D., Pütz, T., et al. (2018). Organic layers favor phosphorus storage and uptake by young beech trees (*Fagus sylvatica* L.) at nutrient poor ecosystems. *Plant Soil* 432, 289–301. doi: 10.1007/s11104-018-3804-5

Haußmann, T., and Lux, W. (1997). *Dauerbeobachtungsflächen zur Umweltkontrolle im Wald: Level II; Erste Ergebnisse*. Bonn: BMELF (Bundesministerium für Ernährung, Landwirtschaft und Forsten).

Heinrichs, H., Brumsack, H.-J., Loftfield, N., and König, N. (1986). Verbessertes Druckaufschlußsystem für biologische und anorganische Materialien. *Z. Pflanzenernaehr. Bodenk.* 149, 350–353. doi: 10.1002/jpln.19861490313

Heuck, C., and Spohn, M. (2016). Carbon, nitrogen and phosphorus net mineralization in organic horizons of temperate forests: stoichiometry and relations to organic matter quality. *Biogeochemistry* 131, 229–242. doi: 10.1007/s10533-016-0276-7

Hinsinger, P., Herrmann, L., Lesueur, D., Robin, A., Trap, J., Waithaisong, K., et al. (2015). "Impact of roots, microorganisms and microfauna on the fate of soil phosphorus in the rhizosphere," in *Annual Plant Reviews*, Vol. 48, eds W. C. Plaxton and H. Lambers (Hoboken, NJ: John Wiley & Sons, Inc), 375–407. doi: 10.1002/9781118958841.ch13

Hoffland, E., Giesler, R., Breemen, N., van, and Jongmans, A. G. (2003). Feldspar tunneling by fungi along natural productivity gradients. *Ecosystems* 6, 739–746. doi: 10.1007/s10021-003-0191-3

Hofmann, K., Heuck, C., and Spohn, M. (2016). Phosphorus resorption by young beech trees and soil phosphatase activity as dependent on phosphorus availability. *Oecologia* 181, 369–379. doi: 10.1007/s00442-016-3581-x

Hölscher, D., Hertel, D., Leuschner, C., and Hottkowitz, M. (2002). Tree species diversity and soil patchiness in a temperate broad-leaved forest with limited rooting space. *Flora Morphol. Distrib. Funct. Ecol. Plants* 197, 118–125. doi: 10.1078/0367-2530-00021

Ilg, K., Dominik, P., Kaupenjohann, M., and Siemens, J. (2008). Phosphorus-induced mobilization of colloids: model systems and soils. *Eur. J. Soil Sci.* 59, 233–246. doi: 10.1111/j.1365-2389.2007.00982.x

Jansa, J., Finlay, R., Wallander, H., Smith, F. A., and Smith, S. E. (2011). "Role of mycorrhizal symbioses in phosphorus cycling," in *Phosphorus in Action*, eds E. Bünemann, A. Oberson, and E. Frossard (Berlin: Springer), 137–168. doi: 10.1007/978-3-642-15271-9_6

Jentschke, G., Brandes, B., Kuhn, A. J., Schröder, W. H., and Godbold, D. L. (2001). Interdependence of phosphorus, nitrogen, potassium and magnesium translocation by the ectomycorrhizal fungus *Paxillus involutus*. *New Phytol.* 149, 327–337. doi: 10.1046/j.1469-8137.2001.00014.x

Johri, A. K., Oelmüller, R., Dua, M., Yadav, V., Kumar, M., Tuteja, N., et al. (2015). Fungal association and utilization of phosphate by plants: success, limitations, and future prospects. *Front. Microbiol.* 6:984. doi: 10.3389/fmicb.2015.00984

Jonard, M., Augusto, L., Morel, C., Achat, D. L., and Saur, E. (2009). Forest floor contribution to phosphorus nutrition: experimental data. *Ann. For. Sci.* 66, 510–510. doi: 10.1051/forest/2009039

Jonard, M., Fürst, A., Verstraeten, A., Thimonier, A., Timmermann, V., Potoèiæ, N., et al. (2015). Tree mineral nutrition is deteriorating in Europe. *Glob. Change Biol.* 21, 418–430. doi: 10.1111/gcb.12657

Jongmans, A. G., van Breemen, N., Lundström, U., van Hees, P. A. W., Finlay, R. D., Srinivasan, M., et al. (1997). Rock-eating fungi. *Nature* 389, 682–683. doi: 10.1038/39493

Kavka, M., and Polle, A. (2016). Phosphate uptake kinetics and tissue-specific transporter expression profiles in poplar (*Populus× canescens*) at different phosphorus availabilities. *BMC Plant Biol.* 16:206. doi: 10.1186/s12870-016-0892-3

Kavka, M., and Polle, A. (2017). Dissecting nutrient-related co-expression networks in phosphate starved poplars. *PLoS One* 12:e0171958. doi: 10.1371/journal.pone.0171958

Kramer, P. J., and Wilbur, K. M. (1949). Absorption of radioactive phosphorus by mycorrhizal roots of pine. *Science* 110, 8–9. doi: 10.1126/science.110.2844.8

Kreuzwieser, J., and Gessler, A. (2010). Global climate change and tree nutrition: influence of water availability. *Tree Physiol.* 30, 1221–1234. doi: 10.1093/treephys/tpq055

Kuzyakov, Y., and Xu, X. (2013). Competition between roots and microorganisms for nitrogen: mechanisms and ecological relevance. *New Phytol.* 198, 656–669. doi: 10.1111/nph.12235

Lambers, H., Clode, P. L., Hawkins, H.-J., Laliberté, E., Oliveira, R. S., Reddell, P., et al. (2015a). "Metabolic adaptations of the non-mycotrophic proteaceae to soils with low phosphorus availability," in *Annual Plant Reviews*, Vol. 48, eds W. C. Plaxton and H. Lambers (Hoboken, NJ: John Wiley & Sons, Inc), 289–335. doi: 10.1002/9781118958841.ch11

Lambers, H., Martinoia, E., and Renton, M. (2015b). Plant adaptations to severely phosphorus-impoverished soils. *Curr. Opin. Plant Biol.* 25, 23–31. doi: 10.1016/j.pbi.2015.04.002

Lambers, H., Raven, J., Shaver, G., and Smith, S. (2008). Plant nutrient-acquisition strategies change with soil age. *Trends Ecol. Evol.* 23, 95–103. doi: 10.1016/j.tree.2007.10.008

Lang, F., Bauhus, J., Frossard, E., George, E., Kaiser, K., Kaupenjohann, M., et al. (2016). Phosphorus in forest ecosystems: new insights from an ecosystem nutrition perspective. *J. Plant Nutr. Soil Sci.* 179, 129–135. doi: 10.1002/jpln.201500541

Lang, F., Krüger, J., Amelung, W., Willbold, S., Frossard, E., Bünemann, E. K., et al. (2017). Soil phosphorus supply controls P nutrition strategies of beech forest ecosystems in Central Europe. *Biogeochemistry* 136, 5–29. doi: 10.1007/s10533-017-0375-0

Leberecht, M., Dannenmann, M., Tejedor, J., Simon, J., Rennenberg, H., and Polle, A. (2016). Segregation of nitrogen use between ammonium and nitrate of ectomycorrhizas and beech trees. *Plant Cell Environ.* 39, 2691–2700. doi: 10.1111/pce.12820

Leuschner, C., Meier, I. C., and Hertel, D. (2006). On the niche breadth of *Fagus sylvatica*: soil nutrient status in 50 Central European beech stands on a broad range of bedrock types. *Ann. For. Sci.* 63, 355–368. doi: 10.1051/forest:2006016

Leyval, C., and Berthelin, J. (1993). Rhizodeposition and net release of soluble organic compounds by pine and beech seedlings inoculated with rhizobacteria and ectomycorrhizal fungi. *Biol. Fertil. Soils* 15, 259–267. doi: 10.1007/BF00337210

Liu, Q., Loganathan, P., Hedley, M. J., and Grace, L. J. (2007). Effect of mycorrhizal inoculation on rhizosphere properties, phosphorus uptake and growth of pine seedlings treated with and without a phosphate rock fertilizer. *J. Plant Nutr.* 31, 137–156. doi: 10.1080/01904160701742063

Mejstrik, V., and Benecke, U. (1969). The ectotrophic mycorrhizas of *Alnus ciridis* (Chaix) D.C. and their significance in respect to phosphorus uptake. *New Phytol.* 68, 141–149. doi: 10.1111/j.1469-8137.1969.tb06427.x

Nambiar, E. K. S., and Sands, R. (1993). Competition for water and nutrients in forests. *Can. J. For. Res.* 23, 1955–1968. doi: 10.1139/x93-247

Nehls, U., and Plassard, C. (2018). Nitrogen and phosphate metabolism in ectomycorrhizas. *New Phytol.* 220, 1047–1058. doi: 10.1111/nph.15257

Netzer, F., Schmid, C., Herschbach, C., and Rennenberg, H. (2017). Phosphorus-nutrition of European beech (*Fagus sylvatica* L.) during annual growth depends on tree age and P-availability in the soil. *Environ. Exp. Bot.* 137, 194–207. doi: 10.1016/j.envexpbot.2017.02.009

Noggle, J. C., and Fried, M. (1960). A kinetic analysis of phosphate absorption by excised roots of millet, barley, and alfalfa. *Soil Sci. Soc. Am. J.* 24, 33–35. doi: 10.2136/sssaj1960.03615995002400010017x

Pena, R., Lang, C., Lohaus, G., Boch, S., Schall, P., Schöning, I., et al. (2017). Phylogenetic and functional traits of ectomycorrhizal assemblages in top soil from different biogeographic regions and forest types. *Mycorrhiza* 27, 233–245. doi: 10.1007/s00572-016-0742-z

Pena, R., Offermann, C., Simon, J., Naumann, P. S., Gessler, A., Holst, J., et al. (2010). Girdling affects ectomycorrhizal fungal (EMF) diversity and reveals functional differences in EMF community composition in a beech forest. *Appl. Environ. Microbiol.* 76, 1831–1841. doi: 10.1128/AEM.01703-09

Pena, R., and Polle, A. (2014). Attributing functions to ectomycorrhizal fungal identities in assemblages for nitrogen acquisition under stress. *ISME J.* 8, 321–330. doi: 10.1038/ismej.2013.158

Peñuelas, J., Poulter, B., Sardans, J., Ciais, P., van der Velde, M., Bopp, L., et al. (2013). Human-induced nitrogen–phosphorus imbalances alter natural and managed ecosystems across the globe. *Nat. Commun.* 4:2934. doi: 10.1038/ncomms3934

Plassard, C., and Dell, B. (2010). Phosphorus nutrition of mycorrhizal trees. *Tree Physiol.* 30, 1129–1139. doi: 10.1093/treephys/tpq063

Prietzel, J., Klysubun, W., and Werner, F. (2016). Speciation of phosphorus in temperate zone forest soils as assessed by combined wet-chemical fractionation and XANES spectroscopy. *J. Plant Nutr. Soil Sci.* 179, 168–185. doi: 10.1002/jpln.201500472

R Core Development Team (2012). *R: A Language and Environment for Statistical Computing*. Vienna: R Foundation for Statistical Computing. Available online at: https://www.r-project.org/

Rieger, I., Kowarik, I., Ziche, D., Wellbrock, N., and Cierjacks, A. (2019). Linkages between phosphorus and plant diversity in Central European forest ecosystems—complementarity or competition? *Forests* 10:1156. doi: 10.3390/f10121156

Rubio, G., Oesterheld, M., Alvarez, C. R., and Lavado, R. S. (1997). Mechanisms for the increase in phosphorus uptake of waterlogged plants: soil phosphorus availability, root morphology and uptake kinetics. *Oecologia* 112, 150–155. doi: 10.1007/s004420050294

Schachtman, D. P., Reid, R. J., and Ayling, S. M. (1998). Phosphorus uptake by plants: from soil to cell. *Plant Physiol.* 116, 447–453. doi: 10.1104/pp.116.2.447

Schimel, J., Balser, T. C., and Wallenstein, M. (2007). Microbial stress-response physiology and its implications for ecosystem function. *Ecology* 88, 1386–1394. doi: 10.1890/06-0219

Schimel, J. P., and Bennett, J. (2004). Nitrogen mineralization: challenges of a changing paradigm. *Ecology* 85, 591–602. doi: 10.1890/03-8002

Shen, J., Yuan, L., Zhang, J., Li, H., Bai, Z., Chen, X., et al. (2011). Phosphorus dynamics: from soil to plant. *Plant Physiol.* 156, 997–1005. doi: 10.1104/pp.111.175232

Smith, S. E., Anderson, I. C., and Smith, F. A. (2015). "Mycorrhizal associations and phosphorus acquisition: from cells to ecosystems," in *Annual Plant Reviews*, Vol. 48, eds W. C. Plaxton and H. Lambers (Hoboken, NJ: John Wiley & Sons, Inc), 409–439. doi: 10.1002/9781118958841.ch14

Spohn, M., Zavišić, A., Nassal, P., Bergkemper, F., Schulz, S., Marhan, S., et al. (2018). Temporal variations of phosphorus uptake by soil microbial biomass and young beech trees in two forest soils with contrasting phosphorus stocks. *Soil Biol. Biochem.* 117, 191–202. doi: 10.1016/j.soilbio.2017.10.019

Turner, B. L., and Condron, L. M. (2013). Pedogenesis, nutrient dynamics, and ecosystem development: the legacy of T.W. Walker and J.K. Syers. *Plant Soil* 367, 1–10. doi: 10.1007/s11104-013-1750-9

Vance, C. P., Uhde-Stone, C., and Allan, D. L. (2003). Phosphorus acquisition and use: critical adaptations by plants for securing a nonrenewable resource. *New Phytol.* 157, 423–447. doi: 10.1046/j.1469-8137.2003.00695.x

Vincent, A. G., Vestergren, J., Gröbner, G., Persson, P., Schleucher, J., and Giesler, R. (2013). Soil organic phosphorus transformations in a boreal forest chronosequence. *Plant Soil* 367, 149–162. doi: 10.1007/s11104-013-1731-z

Vitousek, P. M., Porder, S., Houlton, B. Z., and Chadwick, O. A. (2010). Terrestrial phosphorus limitation: mechanisms, implications, and nitrogen–phosphorus interactions. *Ecol. Appl.* 20, 5–15. doi: 10.1890/08-0127.1

Walker, T. W., and Syers, J. K. (1976). The fate of phosphorus during pedogenesis. *Geoderma* 15, 1–19. doi: 10.3390/ijerph14121475

Wallander, H. (2000). Uptake of P from apatite by *Pinus sylvestris* seedlings colonised by different ectomycorrhizal fungi. *Plant Soil* 218, 249–256. doi: 10.1023/A:1014936217105

Wang, J., and Lars, B. R. (1997). Competition for nitrogen during mineralization of plant residues in soil: microbial response to C and N availability. *Soil Biol. Biochem.* 29, 163–170.

Weigt, R. B., Raidl, S., Verma, R., and Agerer, R. (2012). Exploration type-specific standard values of extramatrical mycelium–a step towards quantifying ectomycorrhizal space occupation and biomass in natural soil. *Mycol. Prog.* 11, 287–297. doi: 10.1007/s11557-011-0750-5

Winkler, J. B., Dannenmann, M., Simon, J., Pena, R., Offermann, C., Sternad, W., et al. (2010). Carbon and nitrogen balance in beech roots under competitive pressure of soil-borne microorganisms induced by girdling, drought and glucose application. *Funct. Plant Biol.* 37, 879–889. doi: 10.1071/FP09309

Woodmansee, R., Vallis, I., and Mott, J. J. (1981). Grassland nitrogen, terrestrial nitrogen cycles. *Ecol. Bull.* 33, 443–462.

Wu, P., Ma, L., Hou, X., Wang, M., Wu, Y., Liu, F., et al. (2003). Phosphate starvation triggers distinct alterations of genome expression in Arabidopsis roots and leaves. *Plant Physiol.* 132, 1260–1271. doi: 10.1104/pp.103.021022

Yang, N., Zavisic, A., Pena, R., and Polle, A. (2016). Phenology, photosynthesis, and phosphorus in European beech (*Fagus sylvatica* L.) in two forest soils with contrasting P contents. *J. Plant Nutr. Soil Sci.* 179, 151–158. doi: 10.1002/jpln.201500539

York, L. M., Carminati, A., Mooney, S. J., Ritz, K., and Bennett, M. J. (2016). The holistic rhizosphere: integrating zones, processes, and semantics in the soil influenced by roots. *J. Exp. Bot.* 67, 3629–3643. doi: 10.1093/jxb/erw108

Zavišić, A., Nassal, P., Yang, N., Heuck, C., Spohn, M., Marhan, et al. (2016). Phosphorus availabilities in beech (*Fagus sylvatica* L.) forests impose habitat filtering on ectomycorrhizal communities and impact tree nutrition. *Soil Biol. Biochem.* 98, 127–137. doi: 10.1016/j.soilbio.2016.04.006

Zavišić, A., and Polle, A. (2018). Dynamics of phosphorus nutrition, allocation and growth of young beech (*Fagus sylvatica* L.) trees in P-rich and P-poor forest soil. *Tree Physiol.* 38, 37–51. doi: 10.1093/treephys/tpx146

Zavišić, A., Yang, N., Marhan, S., Kandeler, E., and Polle, A. (2018). Forest soil phosphorus resources and fertilization affect ectomycorrhizal community composition, beech P uptake efficiency, and photosynthesis. *Front. Plant Sci.* 9:463. doi: 10.3389/fpls.2018.00463

Zederer, D. P., and Talkner, U. (2018). Organic P in temperate forest mineral soils as affected by humus form and mineralogical characteristics and its relationship

to the foliar P content of European beech. *Geoderma* 325, 162–171. doi: 10.1016/j.geoderma.2018.03.033

Zhu, Q., Riley, W. J., and Tang, J. (2017). A new theory of plant-microbe nutrient competition resolves inconsistencies between observations and model predictions. *Ecol. Appl.* 27, 875–886. doi: 10.1002/eap.1490

Zhu, Q., Riley, W. J., Tang, J., and Koven, C. D. (2016). Multiple soil nutrient competition between plants, microbes, and mineral surfaces: model development, parameterization, and example applications in several tropical forests. *Biogeosciences* 13, 341–363. doi: 10.5194/bg-13-341-2016

**Conflict of Interest:** The authors declare that the research was conducted in the absence of any commercial or financial relationships that could be construed as a potential conflict of interest.

frontiers in Forests and Global Change

ORIGINAL RESEARCH
published: 21 May 2020
doi: 10.3389/ffgc.2020.00059

# Soil Phosphorus Heterogeneity Improves Growth and P Nutrition of Norway Spruce Seedlings

*Jörg Prietzel**

*Chair of Soil Science, Center of Life and Food Sciences Weihenstephan, Technical University München, Freising, Germany*

Phosphorus (P) nutrition of forest trees depends on soil P supply, which is poor on sites with sandy, quartz-rich soils and shallow calcareous soils. Soil P is distributed heterogeneously at different spatial scales. I tested the hypothesis that in P-limited forest ecosystems soil P enrichment in hotspots results in improved tree P nutrition and growth compared to soils where the same P amount is distributed evenly. In two field P fertilization experiments, Norway spruce (*Picea abies*) and European beech (*Fagus sylvatica*) seedlings were grown in soils with experimental homogeneous or heterogeneous P enrichment. The soils were amended with P to equal amounts of total P, but different patterns of P enrichment and/or as different P forms (orthophosphate [oPO4]; inositol hexaphosphate [IHP]). One experiment (*Achenpass*) was conducted with P-poor calcareous soil material of a Rendzic Leptosol (low-P soil), the other (*Mitterfels*) with Bw horizon material of a Cambisol that had formed on silicate bedrock and was characterized by moderate P concentrations (moderate-P soil). Half of the spruce seedlings additionally received experimentally elevated N deposition. At the low-P calcareous site, shoot and foliage biomass as well as foliar P, N, and S amounts of Norway spruce seedlings were considerably (+70–80%) and significantly larger on soils with spatially heterogeneous compared to homogeneous P distribution. Elevated N deposition reduced soil P heterogeneity effects on spruce by improving seedling growth on soils with homogeneous P distribution. No soil P form diversity effects were observed for spruce seedlings on calcareous soil. At the silicate site with moderate P supply, all seedlings showed excellent P nutrition. Here, only marginal, insignificant positive effects of heterogeneous soil P distribution were observed for the growth of spruce and beech seedlings without elevated N deposition, but foliar P concentrations of spruce seedlings increased significantly. Elevated N deposition resulted in a positive effect of heterogeneous vs. homogeneous soil P distribution on spruce growth (+39%; eta squared: 0.163; $p = 0.135$) and P nutrition. Our results showed that soil P concentration heterogeneity is beneficial for spruce growth and P nutrition at sites with P-poor calcareous soils, and at silicate sites with ongoing N eutrophication.

**Keywords: soil P heterogeneity, soil P forms, field experiment, elevated N deposition, orthophosphate, apatite, inositol hexaphosphate**

OPEN ACCESS

***Edited by:***
*Sebastian Loeppmann, Christian-Albrechts-Universität zu Kiel, Germany*

***Reviewed by:***
*Rodica Pena, University of Göttingen, Germany*
*Inger Kappel Schmidt, University of Copenhagen, Denmark*

***Correspondence:**
*Jörg Prietzel*
*prietzel@wzw.tum.de*

***Specialty section:***
*This article was submitted to Forest Soils, a section of the journal Frontiers in Forests and Global Change*

***Received:*** *10 February 2020*
***Accepted:*** *23 April 2020*
***Published:*** *21 May 2020*

***Citation:***
*Prietzel J (2020) Soil Phosphorus Heterogeneity Improves Growth and P Nutrition of Norway Spruce Seedlings. Front. For. Glob. Change 3:59. doi: 10.3389/ffgc.2020.00059*

## INTRODUCTION

For most forest ecosystems, the majority of its total phosphorus (P) stock is bound in the soil. Soil P is present as different inorganic (phosphate bound to Al, Fe, or Ca minerals; Prietzel et al., 2016) and organic P species (mostly mono- and diesters; Condron et al., 2005). Soils are the central P cycling hub of forest ecosystems, sustaining plant P supply (Walker and Syers, 1976; Wardle et al., 2004), and P acquisition traits of plants and soil microorganisms in forest ecosystems are largely determined by ecosystem P availability (Lang et al., 2016, 2017). Phosphorus nutrition of all major tree species in forests of Central Europe such as Norway spruce (*Picea abies*) and European beech (*Fagus sylvatica*) strongly depends on soil P supply which is particularly poor on sites with sandy, quartz-rich soils (Ilg et al., 2009; Achat et al., 2016; Lang et al., 2016, 2017; Augusto et al., 2017) or shallow initial calcareous soils (Prietzel et al., 2015, 2016). Insufficient P nutrition is a critical factor for growth and vitality of the key tree species in these forests. During recent decades, tree P nutrition in many European forest ecosystems has deteriorated markedly, which often has been attributed to effects of elevated atmospheric N deposition (Mohren et al., 1986; Prietzel and Stetter, 2010; Jonard et al., 2015).

Due to its low diffusivity, P in forest soils often is distributed in a heterogeneous pattern at different spatial scales (Werner et al., 2017a,b). In soil micro-regions with increased P loading mean P binding strength to soil minerals is decreased, and soil solution P concentration is increased. It can be assumed that P in hotspots can be acquired more easily by tree roots and associated mycorrhizal fungal communities than P in soil regions with lower P concentration, because plant roots and mycorrhizal fungi can acquire more soil P with little carbon investment due to localized root proliferation and increased P uptake kinetics (Caldwell et al., 1992). Enrichment of P in distinct soil hotspots thus should result in improved tree P nutrition and growth compared to soils where the same total P stock is distributed evenly. This has been shown for other plants than forest trees before. Facelli and Facelli (2002) in a mesocosm experiment showed increased growth and biomass of clover (*Trifolium subterraneum*), when P was distributed heterogeneously rather than homogeneously in the soil. However, experimental evidence for beneficial effects of heterogeneous soil P distribution on plant P nutrition still are scarce, and soil P heterogeneity effects on plant growth differ among soils and plant species with different P acquisition traits (Casper and Cahill, 1996, 1998). At present, no information is available concerning effects of soil P heterogeneity on forest tree growth and vitality.

To decrease this knowledge deficit, I conducted two field experiments using model soil ecosystems with defined spatial heterogeneity patterns of chemical soil properties, particularly P concentration and/or P speciation. I wanted to investigate whether two key European forest tree species (Norway spruce—*Picea abies* L. [Karst.]; European beech—*Fagus sylvatica*) seedlings grow faster and show better P nutrition on soils with heterogeneous compared to homogeneous P distribution. The experiment was conducted at two forest sites. One site has P-poor dolostone bedrock, the other site has silicate bedrock with moderate P content. In different experimental variants, the investigated P heterogeneity effects included P concentration heterogeneity as well as P species diversity.

The basic hypothesis was that in P-limited forest ecosystems soil P enrichment in hotspots results in improved tree P nutrition and growth compared to soils where the same P amount is distributed evenly.

Specifically, I tested the following hypotheses:

(1) Soil P heterogeneity is beneficial for P nutrition and growth of *P. abies* and *F. sylvatica*.

(2) Inorganic soil P (orthophosphate) supports P nutrition and growth of *P. abies* and *F. sylvatica* better than organic soil P (in our experiment added as inositol hexaphosphate [IHP], which is a predominant organic P form in forest soils; Turner et al., 2002, 2007).

(3) Combination of increased spatial P heterogeneity with increased P species diversity supports P nutrition and growth of *P. abies* and *F. sylvatica* better than mere presence of spatial heterogeneity.

(4) Elevated nitrogen deposition changes growth and nutrition responses of *P. abies* to different soil P heterogeneity patterns.

## MATERIALS AND METHODS

### Study Sites

The field experiments were conducted at the sites *Achenpass* (low-P calcareous site) and *Mitterfels* (moderate-P silicate site). The *Achenpass* experiment was established on a small (20 m × 20 m) plateau 47°35′43″N; 11°37′54″E) at 1,130 m elevation on the southern flank of the Guggenauer Köpfl (Mangfall Mts., Germany). The site has been described in detail earlier (Biermayer and Rehfuess, 1985; Prietzel and Ammer, 2008). The climate is cool and humid (MAT 5.5°C; MAP 2110 mm), with a precipitation maximum in July and August. The natural forest community is mixed mountain forest, consisting of Norway spruce, European beech, and silver fir (*Abies alba*), with some admixed Sycamore maple (*Acer pseudoplatanus*) and whitebeam (*Sorbus aria*). Parent material is P-poor (0.15 mg P $g^{-1}$) Triassic dolostone of the *Hauptdolomit* formation. Dominating soils are shallow Rendzic Leptosols with low P contents (Prietzel et al., 2016), in the following termed "low-P soil."

The *Mitterfels* experiment (location 48°58′35″N; 12°52′49″E) was established in 1,020 m elevation in a mature European beech stand in close vicinity to the Forest Climate Station Mitterfels of the Bavarian State Institute of Forestry (Bayerische Landesanstalt für Wald und Forstwirtschaft; LWF). The site and the soil both have been described repeatedly (Lang et al., 2016, 2017; Werner et al., 2017b). Similar to *Achenpass,* the climate at *Mitterfels* is cool and humid (MAT 4.9°C; MAP 1229 mm), with a precipitation maximum in July and August. Natural forest type is a mixed mountain forest, consisting of Norway spruce, European beech, and silver fir. The current forest is a mature pure European beech forest. Parent material is Paleozoic gneiss with moderate P content (1.38 mg P $g^{-1}$). Dominating soils are Dystric Cambisols with silt-loam texture, in the following text termed "moderate-P soil." The P speciation and important properties of a soil profile

close to the experimental plot were presented in detail in Prietzel et al. (2016) and in Werner et al. (2017b).

## Experiment Construction and Execution

### Low-P Calcareous Site Achenpass

The *Achenpass* experiment was constructed in autumn 2015. At the plateau described above, we removed the entire soil down to the solid bedrock on a 25 m² square plot. The removed soil material was separated by horizon (Ah horizon: $pH_{CaCl2}$ 6.6 / 83 mg OC $g^{-1}$/ 9 mg carbonate-C $g^{-1}$/ 0.57 mg P $g^{-1}$; BwC horizon: $pH_{CaCl2}$ 7.9 / 18 mg OC $g^{-1}$/103 mg $g^{-1}$ carbonate-C $g^{-1}$/<0.1 mg P $g^{-1}$). We leveled out the ground surface by application of dolomite grit (mean grain diameter 0.5–0.8 cm; 0.1 mg P $g^{-1}$). On the grit cover (thickness 5–15 cm, depending on original bedrock surface topography), we set up a square timber framework construction (height 40 cm), forming four 2 m × 2 m squares separated by walking stages. The four squares formed the four replicated blocks of our experiment (blocks 1–4; **Figure 1A**). Adding additional timber boards, we divided each square into four 1 m × 1 m square sections, forming the four different experimental variants A–D described below. The experimental variants A–D were arranged randomly in the different blocks (**Figure 1A**). In each 1 m × 1 m square, a PVC framework (height of PVC plates 20 cm; length 1 m) was inserted, resulting in division of each square into 36 square or rectangular compartments (**Figures 1B,C**). Then we filled each compartment with a homogenized 1:1 mixture of dolomite grit with Bw material ("BwC mixture"), which for the experimental variants A–D had been enriched with IHP and/or apatite in different ratios (**Table 1**; **Figures 2A–D**). Details concerning this procedure and other experimental design details are presented in the Supporting Information.

After all compartments had been filled with the respective BwC mixtures to the top (**Figure 1C**), we divided each 1 m × 1 m square section representing an experimental variant in each block into 4 squares (size 0.5 m × 0.5 m; area 0.25 m²) by inserting a cross made of two wooden boards in each 1 m² square. Then each square was covered with 5 cm original BwC mixture without P addition. On top we homogeneously applied a 5 cm topsoil cover of original Ah horizon material to improve water and nutrient (N, S, K) supply to the seedlings and to warrant seedling infection and colonization with appropriate, site-typical mycorrhizal fungi and soil fauna which is important for soil P cycling (Irshad et al., 2012). The construction was completed in October 2015. In May 2016, 128 seedlings of Norway spruce (*Picea abies;* height 10–15 cm) were excavated in the surrounding forest. Four seedlings each were planted in the upper left and lower right 0.25 m² squares of all 16 1m² squares representing the variants A–D in each experimental block. The squares are indicated by lower case "s" (spruce) and "s+N" (spruce with experimental N deposition) letters in **Figure 1A**. During planting, we paid utmost attention (i) to use only the uppermost Ah horizon cover as rooting medium, and (ii) to place the plants exactly on the position designated by the green circles in **Figure 1B**. This assured an equal probability of the developing tree roots to penetrate any of the four different BwC horizon compartments below each plant. In the same way, we planted four *Fagus sylvatica* seedlings (age: 1 yr) in the upper right 0.5 m × 0.5 m squares of the 16 1m² squares representing the variants A–D in each block, indicated by lower case "b" (beech) letters in **Figure 1A**. Planting positions are marked by yellow circles in **Figure 1B**. The lower left 0.25 m² square of each 1 m² square, indicated by a lower case "c" letter in **Figure 1A**, remained unplanted and served as control variant.

Growth and vitality of all trees were monitored by visual inspection and measurement of shoot heights and shoot basal diameters at the beginning and the end of each growing season, starting in May 2016. Whereas, beech seedlings showed few mortalities, initial losses were considerable (25% of planted seedlings) for spruce. Losses were replaced once in September 2016. At each growth inventory date, the spruce seedlings of subvariants "s+N" received a treatment with dilute $NH_4NO_3$ to simulate elevated atmospheric N deposition. At each date, 1.43 g $NH_4NO_3$ were dissolved in 100 mL $H_2O$, and the solution was distributed homogenously by spraying on the soil surface (0.25 m²) of each "s+N" plot, resulting in an extra input of 40 kg N $ha^{-1}yr^{-1}$ in addition to the ambient atmospheric deposition of about 10 kg N $ha^{-1}yr^{-1}$. Five $NH_4NO_3$ applications resulted in a total additional N input of 100 kg $ha^{-1}$ until termination of the *Achenpass* experiment in July 2018.

### Moderate-P Silicate Site Mitterfels

The *Mitterfels* experiment (**Table 1**; **Figures 2B**, **3C,D**) had a similar design as *Achenpass* (**Figures 3A,B**) and was constructed in summer 2014. Here, we removed the uppermost 50 cm soil—without reaching the massive bedrock—on a 25 m² square plot. The removed soil material was separated by horizon (moder-type O layer: $pH_{CaCl2}$ 3.7/400 g OC $g^{-1}$; Ah horizon: $pH_{CaCl2}$ 3.8/50 g OC $g^{-1}$/2.0 g P $kg^{-1}$; Bw horizon: $pH_{CaCl2}$ 4.4/25 mg OC $g^{-1}$/1.4 mg P $g^{-1}$). After leveling the bottom, we set up a timber framework construction identical to that at *Achenpass*. As in the *Achenpass* experiment, the square sections were assigned randomly to four different experimental variants A–D, which are described below. Each compartment in the 1 m² squares was filled with Bw material, which for the experimental variants A–D had been enriched with triple superphosphate (TSP; monocalcium phosphate $[Ca(H_2PO_4)_2^*H_2O]$) and/or inositol hexaphosphate (IHP) in different ratios (**Table 1**; **Figure 2B**). Due to its high solubility in water, amended TSP dissolves rapidly, liberating orthophosphate anions, which—similar to dissolved IHP—are instantaneously adsorbed to the abundant Al and Fe oxyhydroxides and clay minerals in the Cambisol *Mitterfels* (Werner et al., 2017b). Orthophosphate and/or IHP have been selected as P amendments because dominating P forms in the original Cambisol at *Mitterfels* are orthophosphate and IHP bound to Al/Fe oxyhydroxides and clay minerals (Prietzel et al., 2016).

The mean P concentration of 3 mg $g^{-1}$ after experimental P amendment at *Mitterfels* is at the upper level of forest soil P concentrations in Europe (Prietzel and Stetter, 2010; Lang et al., 2016, 2017; Prietzel et al., 2016), reaching or even exceeding P concentrations in P-rich, basalt-derived soils.

After all compartments had been filled with the respective enriched Bw materials to the top (**Figure 1C**), each 1 m × 1 m square section representing an experimental variant in each block

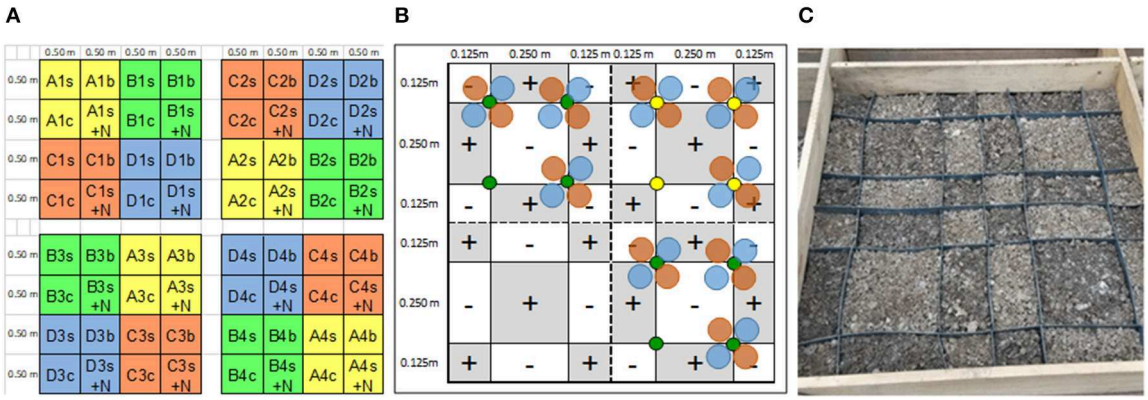


**FIGURE 1 |** Schematic view showing the layout of the P heterogeneity experiments at sites *Achenpass* and *Mitterfels*. **(A)** Distribution of the four treatment variants (A–D; capital letters; each covering four replicated 1 m² squares); the four replicated blocks of each treatment variant (1–4), and the four 1 m² subvariants (tree species: s, spruce; b, beech; +N: experimentally elevated N deposition; C: control) in each treatment variant. **(B)** Spatial arrangement of artificial soil heterogeneity in each 1 m² treatment variant. Circles indicate planting positions of spruce (green) and beech (yellow) seedling. "+" and "–" compartments are filled with identical artificial soil material for the "homogeneous" experimental variants, and with different soil materials for the "heterogeneous" variants, separated by PVC walls. **(C)** Photograph of one 1 m² tree species variant plot of the *Achenpass* experiment before being homogeneously covered with Ah horizon material.

**TABLE 1 |** Soil P enrichment patterns of "+" and "–" Compartments in different variants of the P heterogeneity experiments *Achenpass* and *Mitterfels*.

| | | | **Soil P enrichment (P form, concentration)** ***[Natural background P concentration (mg g$^{-1}$)]*** **Final P concentration [mg g$^{-1}$]** | |
|---|---|---|---|---|
| | **Pattern of added P** | **Form of added P** | **"+" Compartment** | **"–" Compartment** |
| **Low-P calcareous site Achenpass** | | | | |
| Variant A | Homogeneous<br>P concentration<br>One P form | Organic | IHP: 1<br>*(<0.1)*<br>**1** | IHP: 1<br>*(<0.1)*<br>**1** |
| Variant B | Heterogeneous<br>P concentration<br>One P form | Organic | IHP: 2<br>*(<0.1)*<br>**2** | IHP: 0<br>*(<0.1)*<br>**(<0.1)** |
| Variant C | Homogeneous<br>P concentration<br>Two P forms<br>*thoroughly mixed* | Organic + Inorganic | IHP: 0.5/Apatite: 0.5<br>*(<0.1)*<br>**1** | IHP: 0.5/Apatite: 0.5<br>*(<0.1)*<br>**1** |
| Variant D | Homogeneous<br>P concentration<br>Two P forms<br>*spatially separated* | Organic + Inorganic | IHP: 1<br>*(<0.1)*<br>**1** | Apatite: 1<br>*(<0.1)*<br>**1** |
| **Moderate-P silicate site Mitterfels** | | | | |
| Variant A | Homogeneous<br>P concentration<br>One P form | Inorganic | TSP: 2<br>*(1)*<br>**3** | TSP: 2<br>*(1)*<br>**3** |
| Variant B | Heterogeneous<br>P concentration<br>One P form | Inorganic | TSP: 4<br>*(1)*<br>**5** | TSP: 0<br>*(1)*<br>**1** |
| Variant C | Homogeneous<br>P concentration<br>Two P forms<br>*thoroughly mixed* | Organic + Inorganic | TSP: 1/IHP: 1<br>*(1)*<br>**3** | TSP: 1/IHP: 1<br>*(1)*<br>**3** |
| Variant D | Heterogeneous<br>P concentration<br>Two P forms<br>*thoroughly mixed* | Organic + Inorganic | TSP: 2/IHP 2<br>*(1)*<br>**5** | TSP: 0/IHP: 0<br>*(1)*<br>**1** |

*IHP, Inositol hexaphosphate; TSP, Triple super phosphate.*

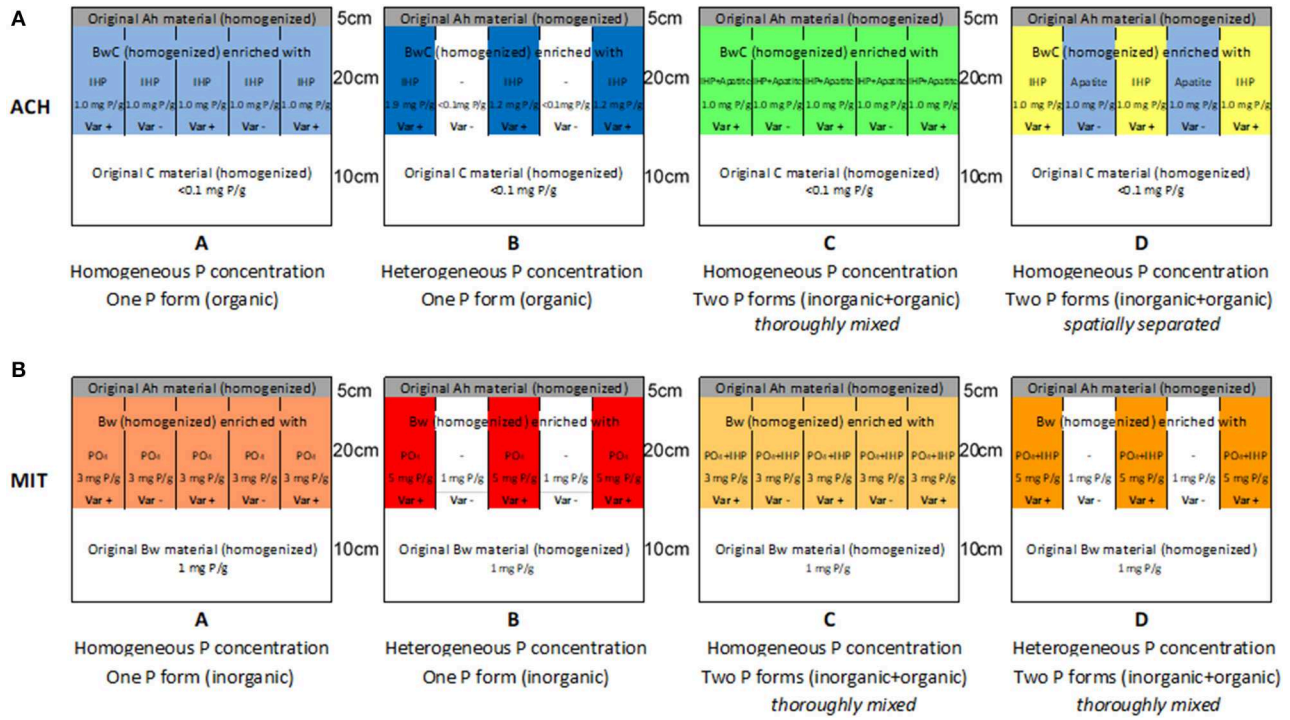


**FIGURE 2 |** Spatial P concentration heterogeneity patterns and added P forms (vertical profile of 1 m² soil squares) in different experimental variants of the experiments *Achenpass* **(A)** and *Mitterfels* **(B)**.


**FIGURE 3 |** Experiments *Achenpass* **(A,B)** and *Mitterfels* **(C,D)**. **(A,C)** Construction stage. **(B,D)** Experiment conduction stage.

was divided into 4 squares as described before for *Achenpass*. Then each square was covered with 5 cm original Bw material without P addition. On top, we homogeneously applied a 5 cm topsoil of original Ah horizon material and a 2 cm cover of original O layer material for the same reasons as mentioned for *Achenpass*. The construction was completed in August 2014.

In June 2015, 128 Norway spruce seedlings (height 5–10 cm), which had been excavated in the Dragonerfilz forest close to Peiting, Germany, and 64 European beech seedlings (age: 1 year; collected in the nearby forest) were planted in the different square compartments in the same arrangement as described above for the low-P site *Achenpass*.

As for *Achenpass*, seedling growth and vitality was recorded at the beginning and at the end of each growing season, starting in June 2015. Whereas, spruce seedlings showed few mortalities, initial losses were tremendous (75% of planted seedlings) for beech seedlings. Losses were replaced twice in June and September 2016. As described for the low-P site *Achenpass* above, at each growth inventory date, the spruce seedlings of subvariants "s+N" were treated with dilute $NH_4NO_3$, resulting in an extra input of 40 kg N $ha^{-1}yr^{-1}$ in addition to atmospheric deposition of about 20 kg N $ha^{-1}yr^{-1}$. Seven $NH_4NO_3$ applications resulted in an additional N input of 140 kg $ha^{-1}$ until termination of the *Mitterfels* experiment in August 2019.

## Post-experiment Seedling Processing

### Seedling Sampling

After termination of the experiments, we harvested the three largest of the four seedlings in each of the 48 0.25 $m^2$ squares characterized by a given combination of tree species (spruce, beech, spruce with elevated N deposition), fertilizer type (inorganic P, organic P, inorganic + organic P), and spatial pattern of fertilizer application (homogeneous, heterogeneous). This was performed by cutting the seedling shoots at the soil surface and separating foliage from non-foliage parts of each shoot. After 14-d drying at 30°C, we determined foliage and shoot dry masses of each seedling. Then we pooled the respective shoot and root material of the three trees on each 0.25 $m^2$ square, forming a three-seedling-composite sample for each 0.25 $m^2$ square. From each three-seedling-composite sample, we finely ground a subsample for foliar nutrient concentration analysis.

### Root Sampling

At *Achenpass*, we additionally sampled root material from each seedling. This was done by removing the cover topsoil above the compartment hatching and then sampling soil cores at the four positions close to the PVC hatch cross underneath each seedling indicated by large circles in the **Figure 1B**. The cores were sampled with a small auger (chamber length: 20 cm, diameter: 5 cm). The P-enriched BwC material of the two cores taken from the "+"compartments close to each seedling was pooled; the same was done for the BwC material in the two cores taken from the "–" compartments. After drying the soil samples for 14 d at 30°C, they were sieved. All visible roots were collected with a tweezer and weighed. As for shoot biomass, we pooled the root biomass of the three seedlings in a given 0.25 $m^2$ square to a three-seedling-collective.

### Foliar Nutrient Analysis

Concentrations of important elements (N, P, K, Ca, Mg) in fine-ground foliage were analyzed using a CN analyzer (N; HekaTech EA, HekaTech Comp., Wegberg, Germany) or by ICP-OES (other elements; SpectroGenesis) after pressure-digestion with hot concentrated $HNO_3$. Foliar nutrient amounts for each three-seedling-composite sample were calculated by multiplying the foliage mass of each three-seedling-composite sample with the nutrient concentration of its respective foliage sample. The values were divided by 3 to obtain the mean foliar nutrient element amounts of one seedling in each 0.25 $m^2$ square.

## Data Processing and Statistics

Based on the 48 foliar nutrient concentration as well as foliage, shoot, and root mass data obtained in each experiment, four replicate samples for each tree species/fertilizer type/spatial fertilizer pattern combination (one for each block 1–4) were available for statistical analysis. All variables were tested for normal distribution, applying a Kolmogorov-Smirnov test. Then we performed ANOVA on shoot mass, foliage mass, foliar nutrient concentrations, and foliar nutrient amounts of each separate tree species variant (spruce, spruce with N deposition, beech). Data were tested separately for each site and tree species, because not only site properties but also ages, provenience, and initial biomasses of the planted seedling varied between sites. Therefore, two one-way ANOVA tests were performed. We tested effects of fertilization regime (homogeneous *vs.* heterogeneous soil P enrichment) and fertilizer type (single P form vs. mixed P forms) on treatment mean values for statistical significance ($p < 0.05$). Because the exclusive use of statistical significance for testing experimental treatment effects recently has been criticized (Amrhein et al., 2019), we identified and rated treatment effects by combining $p$ and size effect (eta squared) values. Treatment effects were termed ***strong and significant***, if they met the following criteria: Eta squared > 0.14 and $p < 0.05$, and ***moderate*** for eta squared > 0.06.

# RESULTS

## Low-P Calcareous Site *Achenpass*

At the experimental plots of the low-P calcareous site, European beech generally developed better and showed fewer mortalities than Norway spruce. At the end of the experiment, 63 of 64 initial beech seedlings were alive (98% survival); the height of seedlings without browsing damage on average has increased by 50% between September 2016 and August 2018. For Norway spruce, survival rates were 88%, and Norway spruce with elevated N deposition showed a survival rate of 86%. Relative height increases during the experiment on average were +39% for Norway spruce, and +45% for spruce with experimental N amendment.

### Norway Spruce

Both shoot and foliage biomass of Norway spruce seedlings grown on soil with heterogeneous P amendment was considerably (shoot biomass: +72%; foliage biomass: +84%; **Figure 4**) and significantly (**Table 2**; **Supplementary Table 1**) larger than for spruces grown on soil with homogeneous P application. In contrast, root biomass was markedly smaller, and shoot/root ratios of spruce seedlings were increased by 50% on plots with heterogeneous compared to homogeneous soil P distribution. However, due to large root mass variance within experimental variants, the effects were statistically weak and insignificant. The form of applied P (IHP vs. IHP + apatite) had no effect on shoot or foliage biomass. However, due to markedly smaller root masses of spruce seedlings grown on soil with combined IHP + apatite amendment compared to exclusive IHP application, shoot/root ratios of spruce seedlings at plots

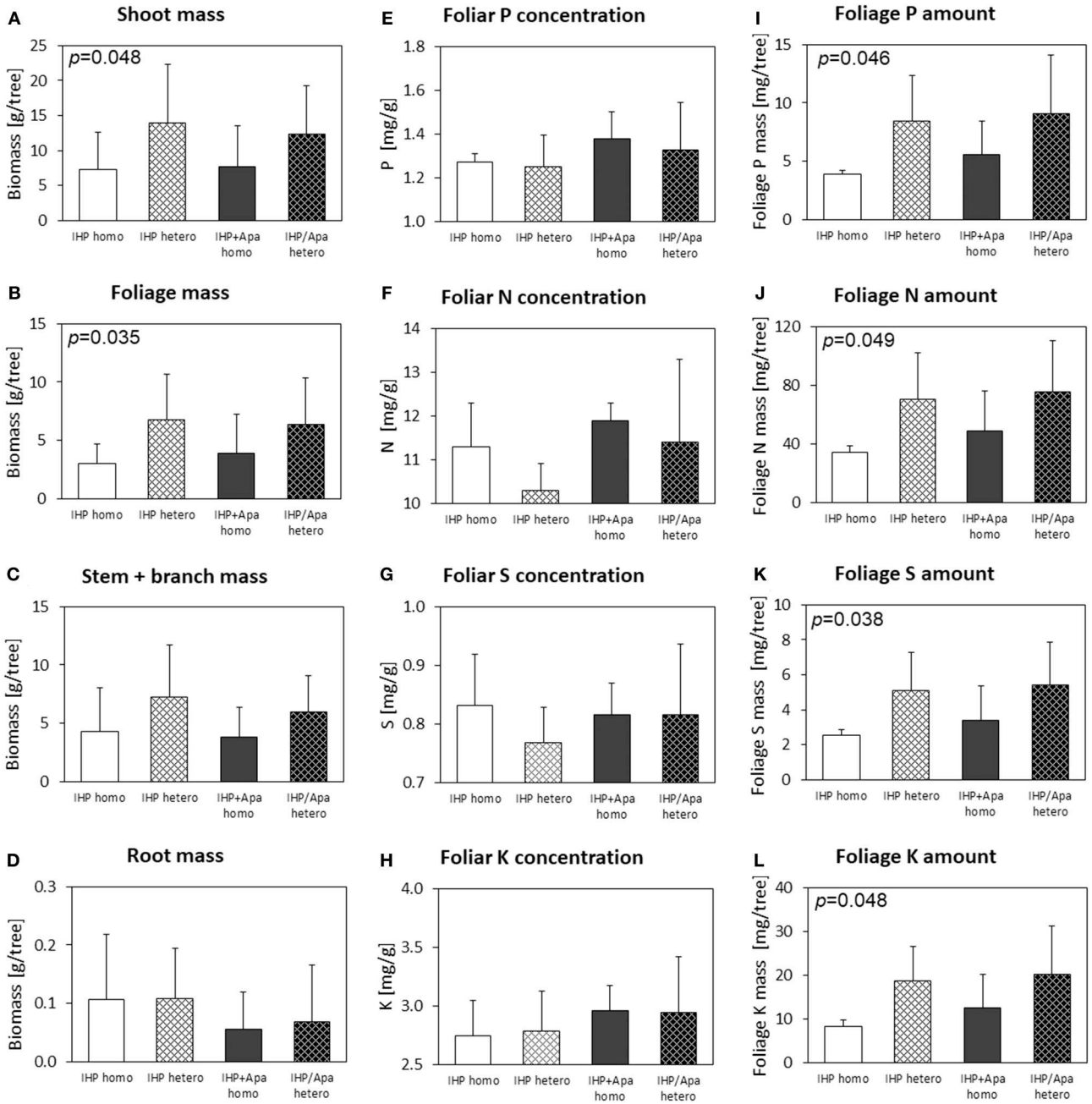


**FIGURE 4 |** Shoot **(A)**, foliage **(B)**, stem+branch **(C)**, and root **(D)** biomass, foliar concentrations of N **(E)**, P **(F)**, S **(G)**, and K **(H)**, and nutrient (P, N, S, K) amounts in foliage **(I–L)** of *Picea abies* at the low-P calcareous site. Numbers in the upper left panel corner show $p < 0.1$ for differences between mean values of homogeneous *vs.* heterogeneous P application calculated by one-way ANOVA.

fertilized with IHP + apatite were three times as large as those on plots fertilized with IHP only (**Table 2**).

Generally, Norway spruce seedlings at calcareous low-P site were characterized by insufficient N, S, and K nutrition according to the threshold values of Göttlein (2015), whereas tree seedling supply with Ca and Mg nutrition was good. The P nutritional status was latently insufficient (foliar $P < 1.3$ mg $g^{-1}$; Göttlein, 2015) for spruces on soils with IHP amendment, and sufficient for those with combined amendment of IHP and apatite. Foliar concentrations of P, N, S, and K were smaller for spruces on soils with heterogeneous compared to homogeneous P amendment, and (except K) for spruces grown on soils with IHP amendment compared to combined IHP + apatite application (**Figure 4**; **Table 2**; **Supplementary Table 1**). P nutrition was sufficient according to Göttlein (2015) for spruces with IHP + apatite treatment, but insufficient for those with exclusive IHP treatment. However, due to larger foliage masses of spruces on soil with heterogeneous compared to

homogeneous P amendment, total foliar P amounts (as well as N, S and K amounts) were markedly and significantly larger for spruces with heterogeneous soil P distribution (**Table 2**; **Supplementary Table 1**; **Figure 4**). Additionally, foliar P, N, and K amounts by trend were larger for spruces grown with combined IHP + apatite compared to pure IHP amendment. However, P fertilizer type effects generally were small. For all experimental variants, foliar N/P ratios of 8.4–8.7 indicated balanced N/P nutrition.

### Norway Spruce Subject to Experimentally Elevated N Deposition

For the spruce seedlings at the calcareous low-P site subject to artificially elevated N deposition, similar to the spruces grown under ambient N deposition shoot and foliage biomasses of seedlings with heterogeneous soil P amendment were larger than for seedlings grown on soil with homogeneous P application (**Figure 5**; **Table 2**; **Supplementary Table 2**). However, effects generally were smaller than those observed for spruces without experimental N amendment. No effects of P fertilization regime on root biomass were observed for spruce seedlings subject to experimental N deposition, most likely due to the large variation among seedlings representing a fertilization regime.

Experimentally elevated N deposition did not increase foliar N concentrations of Norway spruce seedlings at the low-P calcareous site (**Table 2**; **Supplementary Table 2**), which as the spruces without experimental N deposition were characterized by insufficient N, S, and K nutrition, but good Ca and Mg nutrition according to Göttlein (2015). The P nutrition status was also insufficient for all spruce seedlings, irrespective of the experimental variant. However, under conditions of elevated N deposition, seedlings on soils with heterogeneous P amendment showed markedly larger foliar P concentrations than seedlings on soils with homogeneous P distribution, whereas N concentrations remained unaffected (**Figure 5**; **Table 2**; **Supplementary Table 2**). Foliar N/P ratios of 8.7–9.3 in the different variants were slightly larger than for the spruce seedlings without experimental N addition, but N/P nutrition was also balanced.

Larger foliage masses of spruce seedlings on soils with heterogeneous compared to homogeneous P amendment together with increased foliar P concentrations resulted in considerably (+35%) and consistently (*p:* 0.151; eta squared: 0.141; **Supplementary Table 2**) increased amounts of P, N, S, and K in foliage of spruces with heterogeneous compared to homogeneous soil P amendment (**Table 2**; **Figure 5**). The form of applied P (IHP vs. IHP + apatite) had no consistent effect on foliar P, N, and K concentrations. In contrast to the spruce seedlings without experimental N deposition, no consistent effect of the applied P form on foliar P, N, and K amounts as well as on spruce root mass was detected.

### European Beech

Beech seedlings by trend showed larger shoot, foliage, and root biomasses for variants where P had been applied homogeneously rather than heterogeneously to the soil (**Figure 6**). However, these effects were modest and inconsistent (**Table 2**; **Supplementary Table 3**). Fertilizer P form also had no consistent effect on shoot or foliage biomass, but root biomass was consistently larger for the pure IHP compared to IHP + apatite variants. Moreover, beech root mass was larger for variants with homogeneous compared to heterogeneous soil P distribution.

The beech seedlings at the low-P calcareous site in contrast to spruce seedlings showed good, well-balanced (foliar N/P ratio: 11.1–12.0) P and N nutrition, but latent S and K deficiency. In accordance with the good P nutritional status of the beech seedlings, neither consistent spatial soil distribution nor P form effects on foliar P and N concentrations or foliar P amounts were observed (**Table 2**; **Supplementary Table 3**; **Figure 6**). Foliar K concentrations in beech seedlings were larger for heterogeneous compared to homogeneous soil P application, and larger when the same P amount was added to the soil as IHP + apatite compared to pure IHP.

## Moderate-P Silicate Site *Mitterfels*

At the moderate-P silicate site *Mitterfels,* Norway spruce seedlings showed lower mortality rates than beech seedlings during the experiment (13% vs. 22% for beech). This was mainly caused by the fact that the beech seedlings have been strongly browsed by snails and other animals. Additionally, spruce seedlings also developed markedly better than beech seedlings: Relative height increases of seedlings without browsing damage between September 2016 and August 2019 were +206, +200, and +115% for spruce, spruce with elevated N deposition, and beech, respectively. All seedlings at the moderate-P silicate site, irrespective of tree species and absence or presence of experimental N amendment showed acute N and S deficiency, as well as latent Mg deficiency (spruce only), whereas the P nutritional status was sufficient for all experimental variants. Foliar N/P ratios in all variants were consistently <7.5 for beech and <5.2 for spruce, and thus indicated imbalanced N/P nutrition with marked N limitation.

### Norway Spruce

Differences of shoot or foliage biomasses of Norway spruce seedlings with heterogeneous compared to homogeneous soil P amendment as well as TSP compared to TSP+IHP amendment were marginal and negligible compared to the biomass variation within a P amendment type (**Figure 7**; **Table 2**; **Supplementary Table 4**). However, P concentrations and amounts in Norway spruce seedling foliage were consistently larger for variants with heterogeneous compared to homogeneous P amendment. Foliar N, S, and Mg concentrations behaved the opposite way; i.e., they were decreased in variants with heterogeneous compared to homogeneous soil P amendment. Foliar N and S amounts were not consistently affected by the applied P form.

### Norway Spruce Subject to Experimentally Elevated N Deposition

Artificially elevated N deposition on average resulted in modest foliar N concentration increase of Norway spruce seedlings (**Table 3**; **Supplementary Table 5**), but the N deficiency was

**TABLE 2 |** Effects of spatial P enrichment pattern and P fertilizer type on growth and nutrition of *Picea abies* and *Fagus sylvatica* seedlings in the field experiment at the low-P calcareous site *Achenpass* (Calcaric Leptosol).

| ACHENPASS Calcareous, low-P | | | Aboveground biomass [g] | | Foliage mass [g] | | Foliar P concentration [mg/g] | | Foliar N concentration [mg/g] | | Foliar S concentration [mg/g] | | Foliar P amount [mg] | | Foliar N amount [mg] | | Foliar S amount [mg] | | Shoot/root ratio [g/g] | |
|---|---|---|---|---|---|---|---|---|---|---|---|---|---|---|---|---|---|---|---|---|
| | | *n* | MV | SD | MV | SD | MV | SD | MV | SD | MV | SD | MV | SD | MV | SD | MV | SD | MV | SD |
| **Picea abies** | | | | | | | | | | | | | | | | | | | | |
| | | | *p = 0.048* | | *p = 0.035* | | | | | | | | *p = 0.046* | | *p = 0.049* | | *p = 0.038* | | | |
| Enrichment | homogeneous | 7 | **7.9** | 3.7 | **3.7** | 1.9 | 1.33 | 0.11 | **11.6** | 0.7 | 0.82 | 0.06 | **4.8** | 2.2 | **42.7** | 21.1 | **3.0** | 1.5 | 318 | 515 |
| pattern | heterogeneous | 8 | **13.6** | 5.9 | **6.8** | 3.1 | 1.29 | 0.18 | **10.9** | 1.4 | 0.79 | 0.09 | **8.7** | 4.2 | **72.9** | 31.1 | **5.3** | 2.2 | 209 | 121 |
| P fertilizer | IHP | 7 | 11.2 | 5.9 | 5.2 | 3.0 | **1.26** | 0.11 | **10.7** | 0.9 | 0.79 | 0.07 | 6.5 | 3.7 | 54.9 | 29.9 | 4.0 | 2.1 | **128** | 85 |
| | IHP + Apatite | 8 | 10.7 | 5.8 | 5.5 | 3.1 | **1.35** | 0.17 | **11.7** | 1.3 | 0.82 | 0.09 | 7.3 | 4.2 | 62.2 | 32.3 | 4.4 | 2.3 | **376** | 458 |
| **Picea abies + N** | | | | | | | | | | | | | | | | | | | | |
| Enrichment | homogeneous | 8 | 12.5 | 6.6 | **6.2** | 3.4 | **1.17** | 0.19 | 10.9 | 1.1 | 0.80 | 0.07 | **7.1** | 3.8 | **67.2** | 36.3 | **4.9** | 2.9 | **166** | 89 |
| pattern | heterogeneous | 8 | 13.9 | 3.9 | **7.6** | 2.0 | **1.28** | 0.24 | 11.1 | 0.8 | 0.79 | 0.12 | **9.6** | 2.6 | **84.4** | 21.2 | **6.1** | 1.5 | **275** | 239 |
| P fertilizer | IHP | 8 | 13.4 | 7.0 | 6.9 | 3.6 | 1.24 | 0.20 | 11.0 | 1.2 | 0.81 | 0.09 | 8.3 | 4.0 | 75.4 | 3.9 | 5.5 | 2.9 | 236 | 129 |
| | IHP + Apatite | 8 | 13.0 | 5.3 | 7.0 | 2.0 | 1.21 | 0.25 | 11.0 | 0.8 | 0.78 | 0.10 | 8.5 | 3.0 | 76.3 | 20.6 | 5.5 | 1.6 | 195 | 231 |
| **Fagus sylvatica** | | | | | | | | | | | | | | | | | | | | |
| Enrichment | homogeneous | 8 | 24.9 | 8.1 | 7.5 | 2 | 1.76 | 0.18 | 20.2 | 2.4 | 1.44 | 0.16 | 13.3 | 4.1 | 154 | 53 | 11.0 | 3.6 | **17.0** | 10 |
| pattern | heterogeneous | 8 | 21.8 | 5.6 | 6.7 | 2.1 | 1.78 | 0.18 | 20.8 | 1.4 | 1.48 | 0.18 | 11.8 | 3.5 | 139 | 41 | 9.8 | 3.0 | **32.8** | 27.6 |
| P fertilizer | IHP | 8 | 22.6 | 6.1 | 6.9 | 1.8 | 1.80 | 0.21 | **20.0** | 2.3 | 1.42 | 0.20 | 12.4 | 4.0 | 138 | 41 | 9.8 | 2.9 | **18.0** | 16.2 |
| | IHP + Apatite | 8 | 24.0 | 8.0 | 7.4 | 2.3 | 1.75 | 0.14 | **21.0** | 1.5 | 1.49 | 0.11 | 12.8 | 3.8 | 155 | 52 | 11.0 | 3.7 | **31.9** | 25.1 |

x *Strong, significant effect (eta squared > 0.14; p < 0.05).*

x *Moderate effect (eta squared > 0.06; p > 0.05).*

*MV, Arithmetic mean value; SD, standard deviation. p-values above lines characterize the significance of differences between mean values of homogeneous vs. heterogeneous P enrichment.*

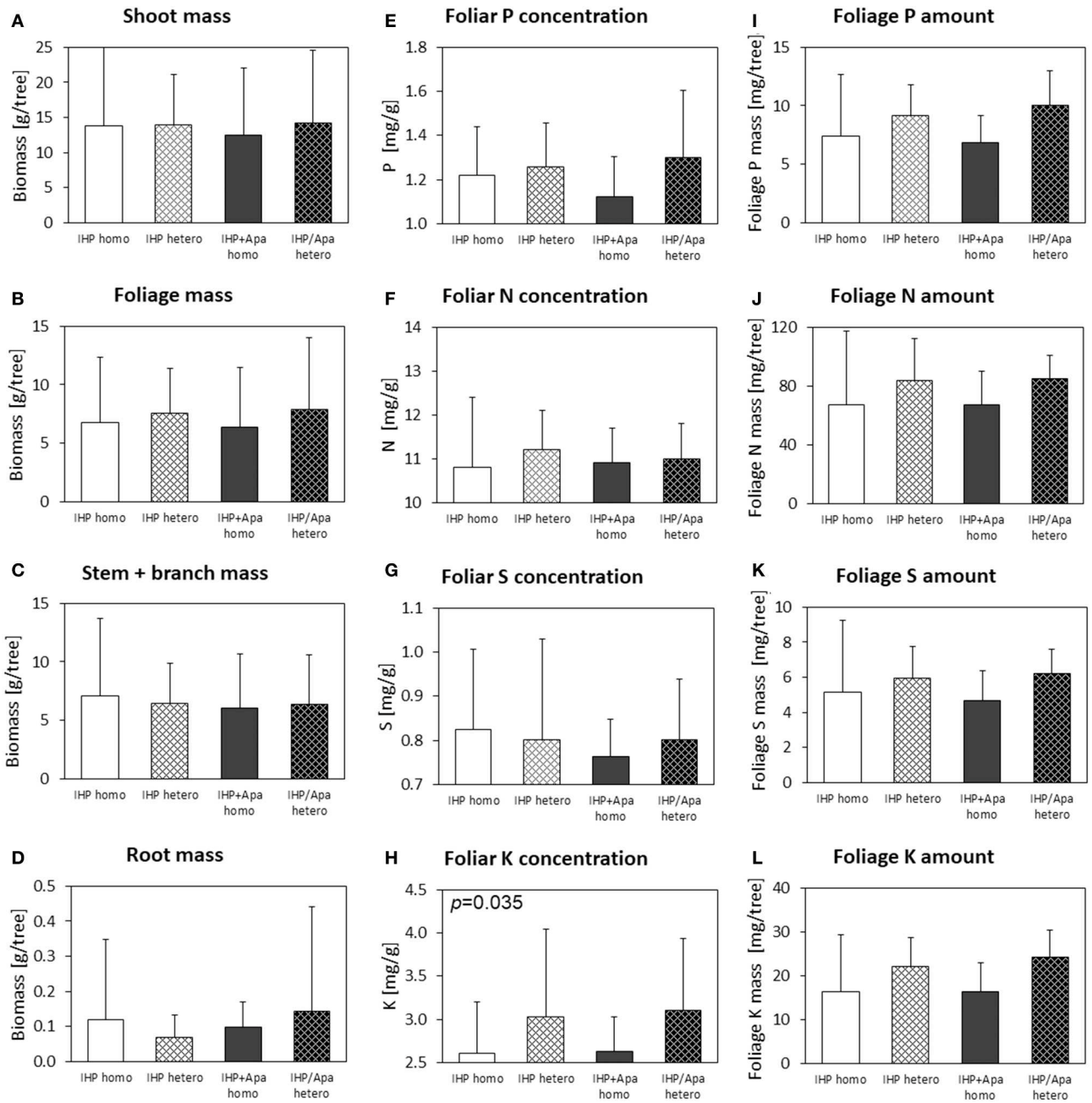


**FIGURE 5 |** Shoot **(A)**, foliage **(B)**, stem+branch **(C)**, and root **(D)** biomass, foliar concentrations of N **(E)**, P **(F)**, S **(G)**, and K **(H)**, and nutrient (P, N, S, K) amounts in foliage **(I–L)** of *Picea abies* with elevated N deposition at the low-P calcareous site. Numbers in the upper left panel corner show $p < 0.1$ for differences between mean values of homogeneous *vs.* heterogeneous P application calculated by one-way ANOVA.

far from being removed. In contrast to spruce seedlings without experimental N deposition, spruce seedlings subject to experimental N deposition showed a marked effect of the spatial soil P enrichment pattern on shoot, foliage, and stem + branch biomasses (**Table 3**; **Supplementary Table 5**), which were increased by 37, 41, and 14%, respectively, for heterogeneous compared to homogeneous soil P enrichment (**Figure 8**). Additionally, foliage biomass and by trend shoot biomass were consistently larger if the P was applied as mixture of TSP and IHP instead of pure TSP.

Foliar P concentrations of Norway spruce seedlings subject to experimentally elevated N deposition were not affected consistently by the spatial soil P enrichment pattern. However, foliar P concentrations were consistently larger and foliar S and Mg concentrations were consistently smaller when P was applied as mixture of TSP and IHP instead of pure IHP. Total P, N, S,

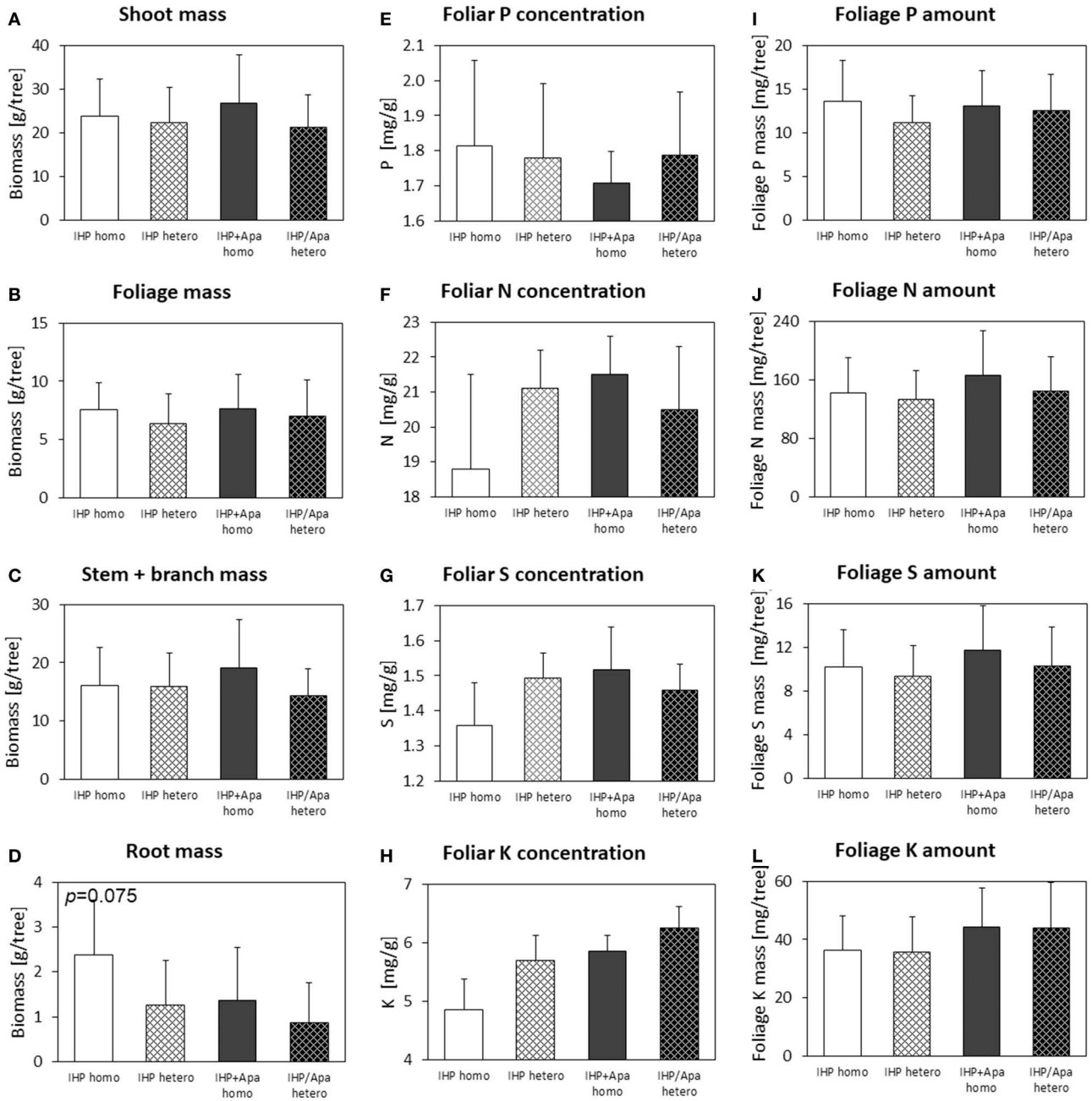


**FIGURE 6 |** Shoot **(A)**, foliage **(B)**, stem+branch **(C)**, and root **(D)** biomass, foliar concentrations of N **(E)**, P **(F)**, S **(G)** and K **(H)**, and nutrient (P, N, S, K) amounts in foliage **(I–L)** of *Fagus sylvatica* at the low-P calcareous site. Numbers in the upper left panel corner show $p < 0.1$ for differences between mean values of homogeneous vs. heterogeneous P application calculated by one-way ANOVA.

and Mg amounts in foliage biomass were largest when the P had been applied to the soil in spatial heterogeneous pattern and in two different forms, and smallest when the P had been applied homogeneously as one single P form (TSP).

## European Beech

Beech seedlings at the moderate-P silicate site by trend showed larger shoot, foliage, and stem + branch biomasses for variants with heterogeneous compared to homogeneous soil P amendment (**Figure 9**). However, the effects were modest and inconsistent (**Table 3**; **Supplementary Table 6**). Fertilizer P form also had no consistent effect on shoot or foliage biomass. Foliar P concentrations of beech seedlings were smaller for heterogeneous compared to homogenous soil P amendment, whereas the opposite was the case for foliar N, S, and Mg concentrations. Spatial or species P heterogeneity

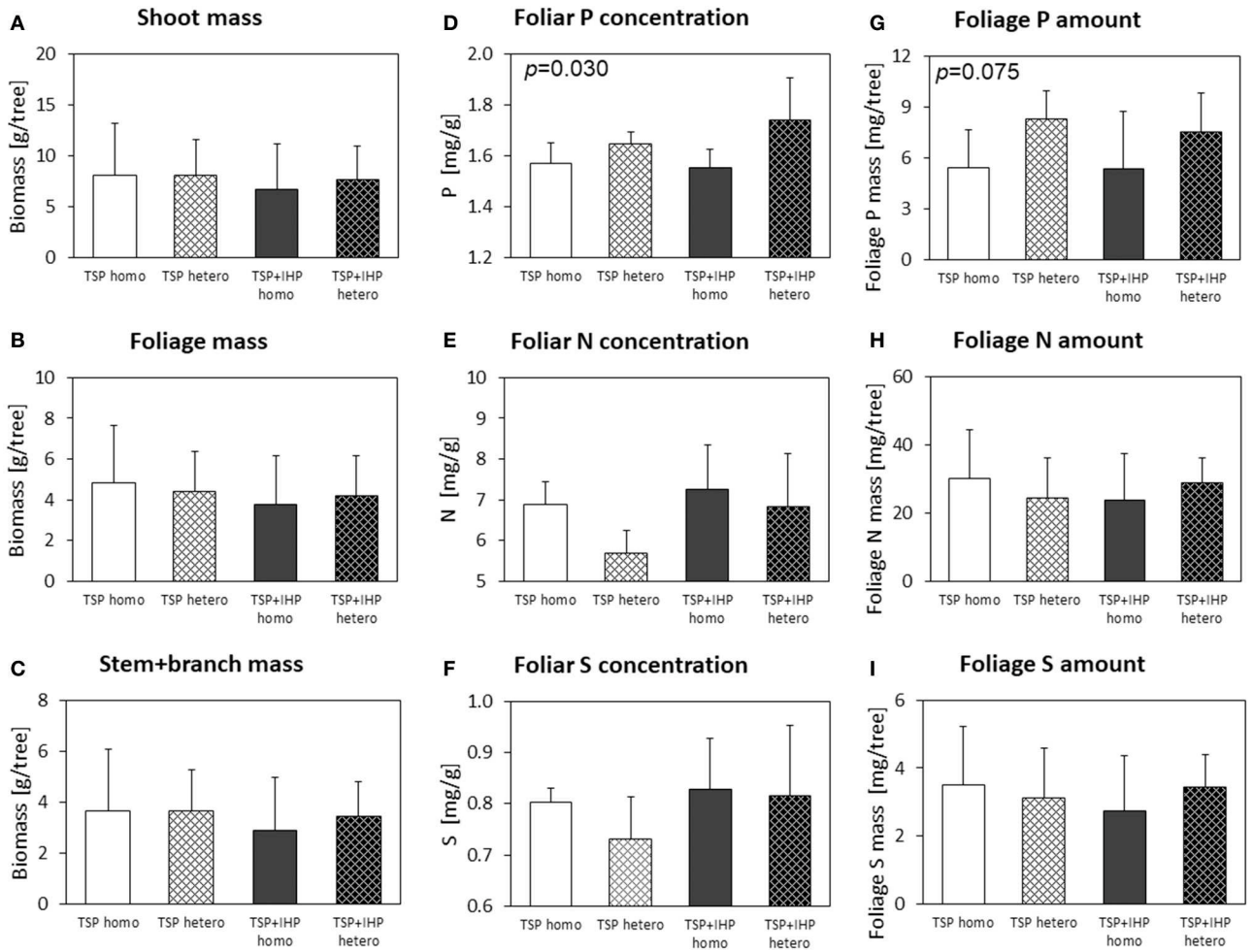


**FIGURE 7 |** Shoot **(A)**, foliage **(B)**, and stem+branch **(C)** biomass, foliar concentrations of N **(D)**, P **(E)**, and K **(F)**, and nutrient (P, N, K) amounts in foliage **(G–I)** of *Picea abies* at the moderate-P silicate site. Numbers in the upper left panel corner show $p < 0.1$ for differences between mean values of homogeneous vs. heterogeneous P application calculated by one-way ANOVA.

patterns did neither consistently affect the amounts of P nor those of N, S, or Mg in beech foliage at the silicate moderate-P site.

## DISCUSSION

### Spatial Soil P Concentration Heterogeneity Improves P Nutrition and Growth of Norway Spruce in Shallow Initial Calcareous Soils

Our study showed no consistent effects of soil P concentration heterogeneity or P species diversity on beech seedling growth. In contrast, study results clearly indicated that accumulation of a given P amount in distinct spatial soil domains (heterogeneous P soil distribution; presence of P hotspots) improves P nutrition and accelerates shoot growth of Norway spruce seedlings in initial calcareous soils with poor P supply. At the same time, smaller spruce root biomass in variants with heterogeneous compared to homogeneous soil P concentrations suggest that less photosynthesis carbon was invested for root development. Facelli and Facelli (2002) reported positive soil P concentration heterogeneity effects on the growth of the legume species *Trifolium subterraneum* in a mesocosm experiment, but the effect so far has not been shown for forest trees. Soil P concentration patchiness exists at different scales, ranging from the microscale (Hinsinger et al., 2005; Werner et al., 2017a) over the profile scale (Werner et al., 2017b) up to the stand or landscape scale (Litaor et al., 2005; Liptzin et al., 2013). It can be assumed that similar to grasses and herbs (e.g., Facelli and Facelli, 2002), also trees of different age as well as different tree species may respond differently regarding their P nutrition status and growth to soil P concentration patchiness at different scales, depending on their respective rooted soil volume. Small-scale topsoil patchiness likely is most important for seedlings with small root systems, whereas with

**TABLE 3 |** Effects of spatial P enrichment pattern and P fertilizer type on growth and nutrition of *Picea abies* and *Fagus sylvatica* seedlings in the field experiment at the moderate-P silicate site *Mitterfels* (Dystric Cambisol).

| **MITTERFELS** *Silicate, moderate-P* | | | **Aboveground biomass [g]** | | **Foliage mass** | | **Foliar P concentration** | | **Foliar N concentration [mg/g]** | | **Foliar S concentration** | | **Foliar P amount** | | **Foliar N amount [mg]** | | **Foliar S amount** | |
|---|---|---|---|---|---|---|---|---|---|---|---|---|---|---|---|---|---|---|
| | | ***n*** | **MV** | **SD** | **MV** | **SD** | **MV** | **SD** | **MV** | **SD** | **MV** | **SD** | **MV** | **SD** | **MV** | **SD** | **MV** | **SD** |
| **Picea abies** | | | | | | | | ***p = 0.030*** | | | | | | *p = 0.075* | | | | |
| Enrichment | homogeneous | 8 | 21.1 | 12.1 | 11.7 | 6.3 | **1.56** | 0.07 | **7.0** | 0.8 | 0.81 | 0.07 | **5.4** | 2.7 | 27 | 14 | 3.1 | 1.6 |
| pattern | heterogeneous | 8 | 23.7 | 8.5 | 12.9 | 5.0 | **1.70** | 0.13 | **6.3** | 1.1 | 0.77 | 0.12 | **7.9** | 1.9 | 26 | 9 | 3.3 | 1.2 |
| P fertilizer | TSP | 8 | 23.6 | 10.9 | 12.9 | 5.8 | 1.61 | 0.07 | 6.3 | 0.8 | 0.77 | 0.07 | 6.8 | 2.3 | 27 | 13 | 3.3 | 1.5 |
| | TSP+IHP | 8 | 21.2 | 10.1 | 11.8 | 5.7 | 1.65 | 0.16 | 7.0 | 1.1 | 0.82 | 0.11 | 6.4 | 2.9 | 26 | 11 | 3.1 | 1.3 |
| **Picea abies + N** | | | | | *p = 0.099* | | | | | | | | | | | | | |
| Enrichment | homogeneous | 8 | **19.4** | 7.0 | **10.4** | 3.4 | 1.44 | 0.15 | 7.1 | 0.7 | 0.69 | 0.06 | **5.4** | 1.9 | **26** | 10 | **2.4** | 0.8 |
| pattern | heterogeneous | 7 | **26.9** | 10.9 | **14.7** | 5.8 | 1.41 | 0.09 | 7.1 | 1.0 | 0.68 | 0.05 | **7.0** | 3.4 | **34** | 13 | **3.3** | 1.3 |
| P fertilizer | TSP | 8 | 21.2 | 9.4 | **11.1** | 4.8 | **1.35** | 0.07 | **6.9** | 0.9 | **0.70** | 0.06 | **4.2** | 1.5 | **25** | 10 | 2.6 | 1.1 |
| | TSP+IHP | 7 | 24.9 | 9.9 | **13.8** | 5.2 | **1.50** | 0.13 | **7.3** | 0.5 | **0.66** | 0.05 | **7.9** | 2 | **36** | 12 | 3.1 | 1.3 |
| | | | | | | | | *p = 0.057* | | | | | | ***p = 0.011*** | | *p = 0.097* | | |
| **Fagus sylvatica** | | | | | | | | | | | | *p = 0.056* | | | | | | |
| Enrichment | homogeneous | 8 | 4.8 | 2.6 | 1.5 | 0.8 | **1.56** | 0.10 | **10.0** | 1.1 | **1.05** | 0.08 | 0.78 | 0.41 | 5.4 | 2.9 | 0.53 | 0.26 |
| pattern | heterogeneous | 7 | 5.4 | 2.1 | 1.7 | 0.6 | **1.47** | 0.18 | **11.0** | 1.1 | **1.13** | 0.07 | 0.82 | 0.31 | 6.2 | 2.3 | 0.64 | 0.24 |
| P fertilizer | TSP | 8 | 5.2 | 2.1 | 1.5 | 0.5 | 1.50 | 0.19 | **10.1** | 1.4 | 1.10 | 0.08 | 0.79 | 0.22 | 5.5 | 1.9 | 0.59 | 0.18 |
| | TSP+IHP | 7 | 4.9 | 2.7 | 1.6 | 0.9 | 1.52 | 0.12 | **11.0** | 0.7 | 1.09 | 0.10 | 0.82 | 0.4 | 6.2 | 3.2 | 0.59 | 0.32 |

x *Strong, significant effect (eta squared > 0.14; p < 0.05).*

× *Moderate effect (eta squared > 0.06; p > 0.05).*

*MV, Arithmetic mean value; SD, standard deviation. p-values above lines characterize the significance of differences between mean values of homogeneous vs. heterogeneous P enrichment; p-values below lines characterize the significance of differences between mean values of different fertilizer P forms.*

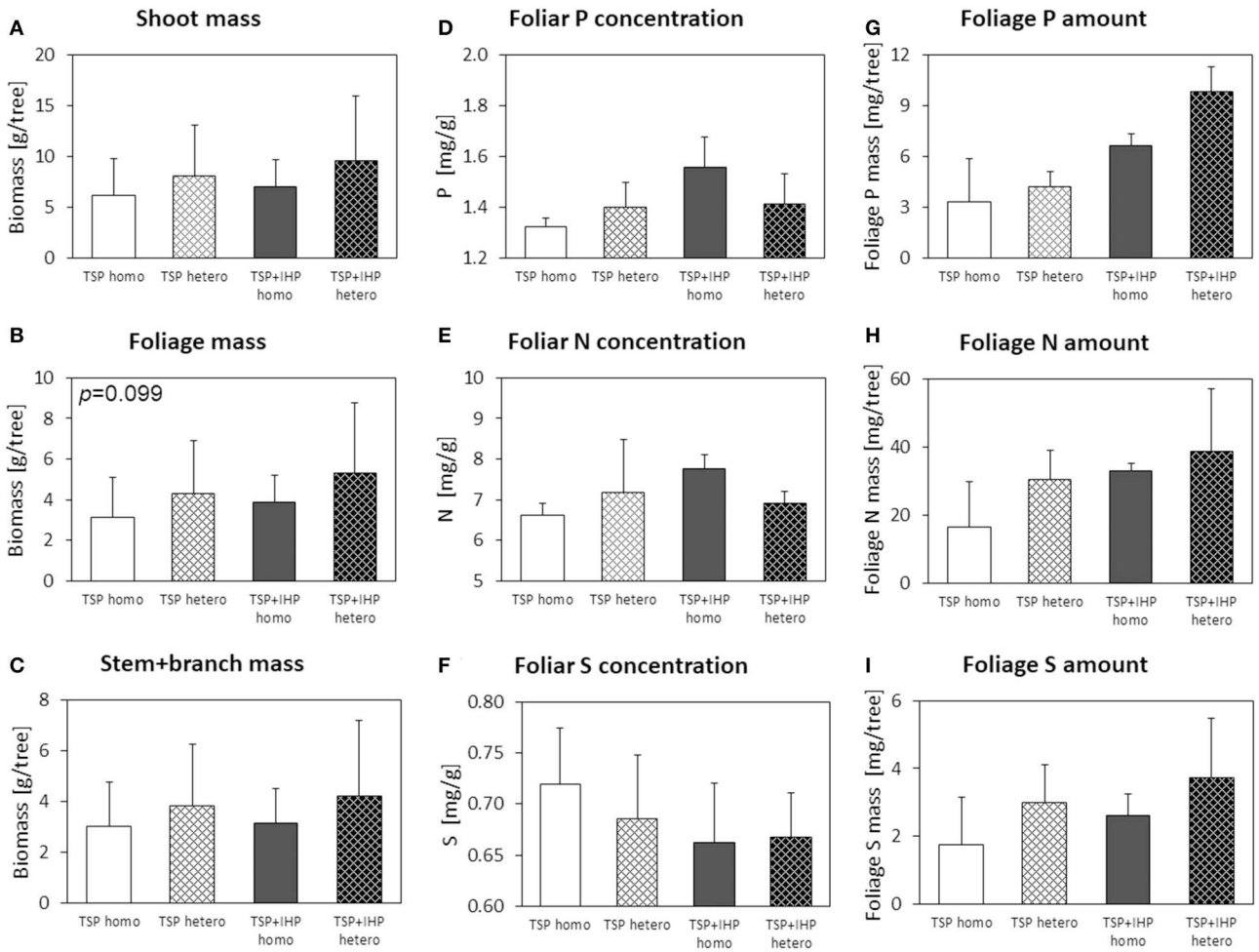


**FIGURE 8 |** Shoot **(A)**, foliage **(B)**, and stem+branch **(C)** biomass, foliar concentrations of N **(D)**, P **(E)**, and K **(F)**, and nutrient (P, N, K) amounts in foliage **(G–I)** of *Picea abies* with elevated N deposition at the moderate-P silicate site. Numbers in the upper left panel corner show $p < 0.1$ for differences between mean values of homogeneous *vs.* heterogeneous P application calculated by one-way ANOVA.

increasing tree age and rooted soil volume, larger-scaled soil P heterogeneity patterns (1–10 m) might become more relevant. Possible processes involved in the positive P hotspot effect on tree P nutrition and growth may include (i) easier mobilization of hotspot P by desorption, complexation, dissolution, (ii) enhanced enzymatic P mobilization from a larger substrate pool of organic P (Hinsinger, 2001; Hinsinger et al., 2005), (iii) increased root P uptake kinetics (Caldwell et al., 1992), and (iv) improved competitiveness of plants compared to soil microorganisms for P (Ehlers et al., 2010; Richardson and Simpson, 2011). In the artificial shallow calcareous soil in our study as well as in real-world initial calcareous soils (Celi et al., 2000; Prietzel et al., 2016), P is mostly present as Ca-bound IHP in addition to apatite-P, because IHP rapidly forms sparingly-soluble Ca-IHP precipitates at pH values >6 (Crea et al., 2006). P mobilization from Ca-IHP and apatite is achieved through cleavage of the Ca-$PO_4$ bond; in the case of IHP additionally by enzymatic cleavage of the inositol-$PO_4$ bond. In calcareous soils, Ca-$PO_4$ bond cleavage is predominantly performed through combined attack of protons and chelators from/of (poly)carboxylic acids (Hinsinger, 2001; Hinsinger et al., 2005) which are produced by plant roots, mycorrhizal fungi, and free soil microorganisms. In the case of apatite dissolution, mobilized orthophosphate can directly be taken up by plant roots. In contrast, according to current knowledge plant uptake of P derived from IHP requires prior IHP cycling through bacteria and nematodes, associated with its conversion into orthophosphate, because plants have a poor capacity to use IHP as P source (Irshad et al., 2012). In P-rich soil hotspots all processes mentioned above liberate more P from a given soil volume at a given organism expense of P-mobilizing organic acids. Moreover, soil microorganisms are particularly competitive in acquisition of nutrients as N or P at low soil concentrations (Ehlers et al., 2010; Richardson and Simpson, 2011), resulting in relatively increased microbial P immobilization ("microbial nutrient trapping"; Kuzyakov and Xu, 2013) and decreased P availability to trees. Tree root

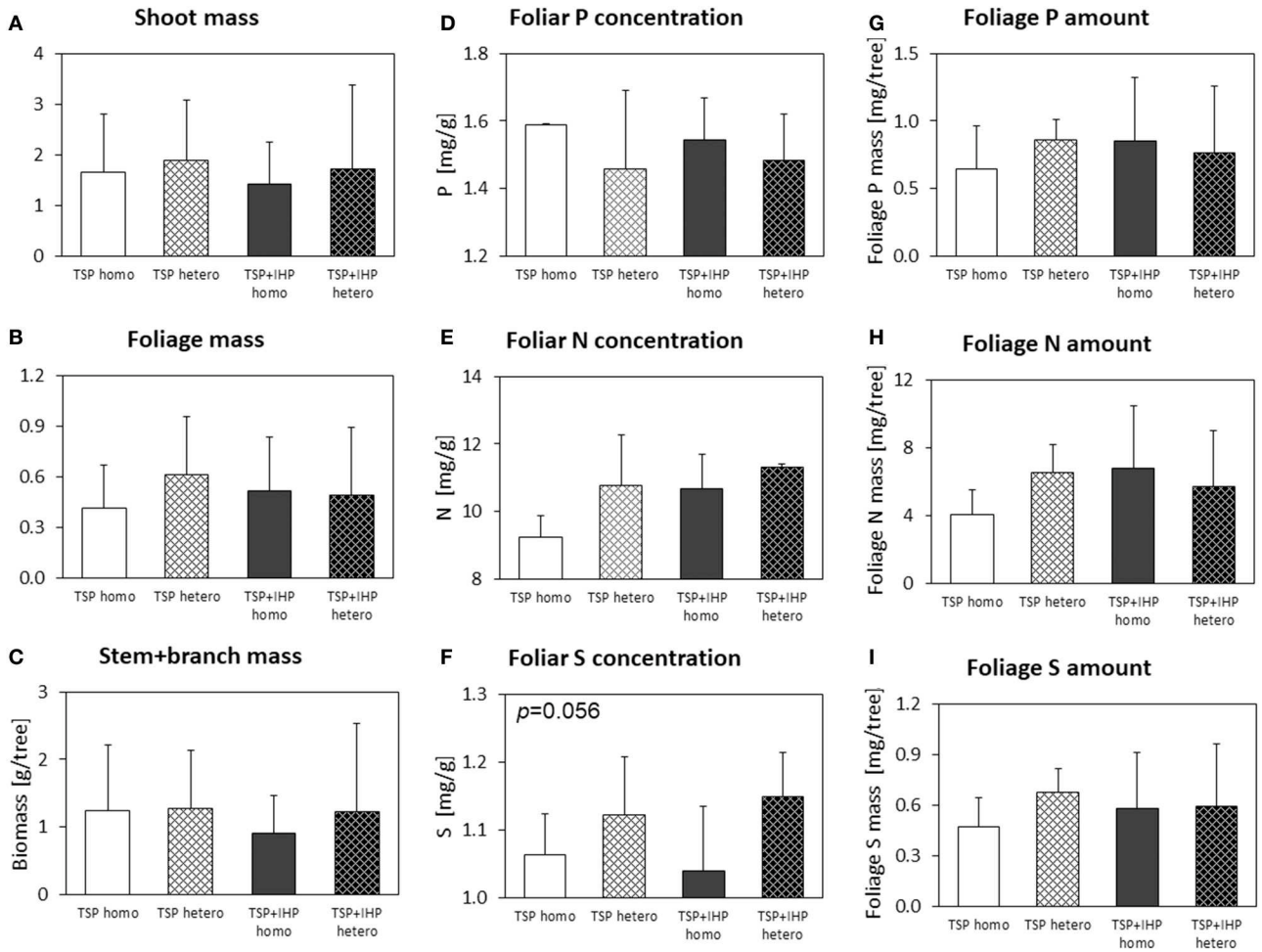


**FIGURE 9 |** Shoot **(A)**, foliage **(B)**, and stem+branch **(C)** biomass, foliar concentrations of N **(D)**, P **(E)**, and K **(F)**, and nutrient (P, N, K) amounts in foliage **(G–I)** of *Fagus sylvatica* at the moderate-P silicate site. Numbers in the upper left panel corner show $p < 0.1$ for differences between mean values of homogeneous *vs.* heterogeneous P application calculated by one-way ANOVA.

accumulation in P-rich soil compartments, as proven for roots of herbs, grasses, and crops in earlier studies (cf. references in Felderer et al., 2013) could not be proven in our study due to the large variation of soil volume-related root biomass.

In contrast to spruce, heterogeneous soil P distribution in our study showed only small and inconsistent effects on beech seedling growth and P nutrition. This is likely due to the fact that in contrast to spruce, the P nutritional status of our beech seedlings without exception was good at the moderate-P silicate site *Mitterfels* and excellent at the low-P site *Achenpass* according to the threshold values of Göttlein (2015), making a selective exploitation of P hotspots unnecessary (Noy-Meir, 1981; Facelli and Facelli, 2002). The excellent P supply of beech strongly contrasts with the poor P supply (also according to Göttlein, 2015) of spruce seedlings growing under identical soil and site conditions. Large-scale tree inventories revealed P deficiency not only for Norway spruce (Prietzel et al., 2015), but also for European beech growing on shallow calcareous soils in the Alps (Ewald, 2000). The excellent P nutrition status of our beech seedlings in contrast to the spruce seedlings at the low-P site can be explained by the fact that the spruce seedlings had been taken from the nearby forest and showed poor P nutrition at the beginning of the experiment, whereas the beech seedlings were purchased as one-year-old plants from a nursery. In contrast to the spruce seedlings, the beech seedlings at the low-P site *Achenpass* thus had a good initial P nutritional status and had probably accumulated a substantial P amount during their nursery time, which was sufficient to maintain an excellent P seedling nutrition status during the entire experiment.

No consistent soil P form diversity effects on seedling growth were present, and site- or tree species-specific effects of soil P form diversity also were absent. Yet, combined soil amendment with two different P forms in five of six experimental variants by trend resulted in larger foliage P amounts compared to variants where the same total P amount had been applied as one single

P form. This indicates that in addition to spatial P heterogeneity also P form diversity in soils may be beneficial for the P nutrition of forest trees.

### Phosphorus Concentration Heterogeneity and P Form Diversity in Acidic Soils Subject to Elevated N Deposition Improves P Nutrition and Growth of Norway Spruce

The Norway spruce variant without additional N input in our experiment at the moderate-P silicate site *Mitterfels* represents temperate conifer forest ecosystems with acidic soils formed from silicate parent material with good P supply, but N limitation. Such ecosystems are widespread in Scandinavia (Tamm, 1991), and also had been widespread in Central Europe before the onset of large-scale forest ecosystem N eutrophication by long-term elevated atmospheric N deposition (Mohren et al., 1986; Prietzel et al., 2006; Prietzel and Stetter, 2010). At such sites, according to the results of our study, soil P heterogeneity is not relevant for forest tree growth and P nutrition. According to several studies, removal of the initial N limitation in these forest ecosystems by elevated N deposition often has resulted in deterioration of the P nutritional status of conifer and broadleaf forests (Mohren et al., 1986; Ilg et al., 2009; Prietzel and Stetter, 2010; Jonard et al., 2012, 2015). Our experimental variant "Norway spruce subject to elevated atmospheric N deposition" at the moderate-P silicate site *Mitterfels* represents these forest ecosystems. In that variant we showed that spatial soil P concentration heterogeneity and P form diversity improved P nutrition and growth of Norway spruce seedlings even at sites with large mean soil P concentrations (in our study 3 mg P $g^{-1}$). It can be assumed that this is also the case for older, larger spruce trees, and also for other tree species in Central European forests subject to elevated N deposition—yet, as explained in section *Spatial Soil P Concentration Heterogeneity Improves P Nutrition and growth of Norway Spruce in Shallow Initial Calcareous Soils*, at larger spatial scales of soil P heterogeneity, which are related to the age- and species-dependent rooted soil volume. Obviously, soil P concentration heterogeneity and P form diversity plays an important, at the moment underestimated role for tree P acquisition and P cycling in forest ecosystems, and particularly in P-limited forest ecosystems with high structural and/or tree species diversity. Future experiments with defined soil P heterogeneity, including those investigating larger scales of P heterogeneity and/or different P enrichment patch sizes in three dimensions (Liu et al., 2017) will increase our understanding of soil P heterogeneity effects on forest ecosystems.

## CONCLUSION

Soil P concentration heterogeneity obviously is beneficial for growth and P nutrition of Norway spruce on P-poor shallow, calcareous soils. Moreover, it obviously is also beneficial for Norway spruce growth at sites with silicate soils characterized by moderate soil P supply and elevated atmospheric N deposition. In contrast to spatial soil P heterogeneity, soil P form diversity has minor effects on spruce seedling growth or P nutrition.

## DATA AVAILABILITY STATEMENT

The raw data supporting the conclusions of this article will be made available by the author, without undue reservation, on request to any qualified researcher.

## AUTHOR CONTRIBUTIONS

JP did all the work needed for production of this manuscript, assisted by the people listed in the Acknowledgments section.

## FUNDING

The study was funded by the German Research Foundation (grant Pr 534/6-2) as part of the Priority program SPP 1685 Ecosystem Nutrition: Forest Strategies for limited Phosphorus Resources.

## ACKNOWLEDGMENTS

I gratefully acknowledge the invaluable help of Katharina and Maximilian Prietzel during construction of the experiments. Jakob Prietzel, Agnes Eckstein, and Jasmin Seven helped in soil and tree sampling in the *Achenpass* experiment. Sigrid Hiesch, Monika Weber, and Christine Pfab assisted during soil and plant sample preparation and analysis.

## SUPPLEMENTARY MATERIAL

The Supplementary Material for this article can be found online at: https://www.frontiersin.org/articles/10.3389/ffgc.2020.00059/full#supplementary-material

## REFERENCES

Achat, D. L., Pousse, N., Nicolas, M., Brédoire, F., and Augusto, L. (2016). Soil properties controlling inorganic phosphorus availability. General results from a national forest network and a global compilation of the literature. *Biogeochemistry* 127, 255–272. doi: 10.1007/s10533-015-0178-0

Amrhein, V., Greenland, S., and McShane, B. (2019). Retire statistical significance. *Nature* 567, 305–307. doi: 10.1038/d41586-019-00857-9

Augusto, L., Achat, D. L., Jonard, M., Vidal, D., and Ringeval, B. (2017). Soil parent material - a major driver of plant nutrient limitations in terrestrial ecosystems. *Glob. Change Biol.* 23, 3808–3824. doi: 10.1111/gcb.13691

Biermayer, G., and Rehfuess, K. E. (1985). Holozäne terrae fuscae aus carbonatgesteinen in den nördlichen kalkalpen. *J. Plant Nutr. Soil Sci.* 148, 405–416. doi: 10.1002/jpln.19851480405

Caldwell, M. M., Dudley, L. M., and Lilieholm, B. (1992). Soil solution phosphate, root uptake kinetics and nutrient acquisition: implications for a patchy soil environment. *Oecologia* 89, 305–309. doi: 10.1007/BF00317406

Casper, B. B., and Cahill, J. F. Jr. (1996). Limited effects of soil nutrient heterogeneity on populations of *Abutilon theophrasti* (*Malvaceae*). *Am. J. Bot.* 83, 333–341. doi: 10.1002/j.1537-2197.1996.tb12714.x

Casper, B. B., and Cahill, J. F. Jr. (1998). Population-level responses to nutrient heterogeneity and density by *Abutilon theophrasti* (*Malvaceae*): an experimental neighborhood approach. *Am. J. Bot.* 85, 1680–1687. doi: 10.2307/2446501

Celi, L., Lamacchia, S., and Barberis, S. (2000). Interaction of inositol phosphate with calcite. *Nutr. Cycling Agroecosyst.* 57, 271–277. doi: 10.1023/A:1009805501082

Condron, L. M., Turner, B. L., and Cade-Menun, B. J. (2005). "Chemistry and dynamics of soil organic phosphorus," in *Phosphorus: Agriculture and the Environment* eds J. Thomas Sims and A. N. Sharpley (Madison, WI: American Society of Agronomy), 87–121.

Crea, P., de Robertis, A., de Stefano, C., and Sammartano, S. (2006). Speciation of phytate ion in aqueous solution. Sequestration of magnesium and calcium by phytate at different temperatures and ionic strengths, in $NaCl_{aq}$. *Biophys. Chem.* 124, 18–26. doi: 10.1016/j.bpc.2006.05.027

Ehlers, K., Bakken, L. R., Frostegard, A., Frossard, E., and Bünemann, E. K. (2010). Phosphorus limitation in a ferralsol: impact on microbial activity and cell internal P pools. *Soil Biol. Biochem.* 42, 558–566. doi: 10.1016/j.soilbio.2009.11.025

Ewald, J. (2000). Ist phosphormangel für die geringe vitalität von Buchen (*Fagus sylvatica* L.) in den Bayerischen Alpen verantwortlich? *Forstwiss. Cbl.* 119, 276–296. doi: 10.1007/BF02769143

Facelli, E., and Facelli, J. M. (2002). Soil phosphorus heterogeneity and mycorrhizal symbiosis regulate plant intra-specific competition and size distribution. *Oecologia* 133, 54–61. doi: 10.1007/s00442-002-1022-5

Felderer, B., Boldt-Burisch, K. M., Schneider, B. U., Hüttl, R. F. J., and Schulin, R. (2013). Root growth of *Lotus corniculatus* interacts with P distribution in young sandy soil. *Biogeosci* 10, 1737–1749. doi: 10.5194/bg-10-1737-2013

Göttlein, A. (2015). Grenzwertbereiche für die ernährungskundliche Einwertung der Hauptbaumarten Fichte, Kiefer, Eiche, Buche. *Allg. Forst Jagdztg.* 186, 110–116.

Hinsinger, P. (2001). Bioavailability of soil inorganic P in the rhizosphere as affected by root-induced chemical changes: a review. *Plant Soil* 237, 173–195. doi: 10.1023/A:1013351617532

Hinsinger, P., Gobran, G., Gregory, P., and Wenzel, W. (2005). Rhizosphere geometry and heterogeneity arising from root mediated physical and chemical processes. *New Phytol.* 168, 293–303. doi: 10.1111/j.1469-8137.2005.01512.x

Ilg, K., Wellbrock, N., and Lux, W. (2009). Phosphorus supply and cycling at long-term monitoring sites in Germany. *Eur. J. For. Res.* 128, 483–492. doi: 10.1007/s10342-009-0297-z

Irshad, U., Brauman, A., Villenave, C., and Plassard, C. (2012). Phosphorus acquisition from phytate depends on efficient bacterial grazing, irrespective of the mycorrhizal status of *Pinus pinaster*. *Plant Soil* 358, 148–161. doi: 10.1007/s11104-012-1161-3

Jonard, M., Fürst, A., Verstraeten, A., Thimonier, A., Timmermann, V., Potocic, N., et al. (2015). Tree mineral nutrition is deteriorating in Europe. *Glob. Change Biol.* 21, 418–430. doi: 10.1111/gcb.12657

Jonard, M., Legout, A., Nicolas, M., Dambrine, E., Nys, C., Ulrich, E., et al. (2012). Deterioration of Norway spruce vitality despite a sharp decline in acid deposition: a long-term integrated perspective. *Glob. Change Biol.* 18, 711–725. doi: 10.1111/j.1365-2486.2011.02550.x

Kuzyakov, Y., and Xu, X. (2013). Competition between roots and microorganisms for nitrogen: mechanisms and ecological relevance. *New Phytol.* 198, 656–669. doi: 10.1111/nph.12235

Lang, F., Bauhus, J., Frossard, E., George, E., Kaiser, K., Kaupenjohann, M., et al. (2016). Phosphorus in forest ecosystems: new insights from an ecosystem nutrition perspective. *J. Plant Nutr. Soil Sci.* 179, 129–135. doi: 10.1002/jpln.201500541

Lang, F., Krüger, J., Amelung, W., Willbold, S., Frossard, E., Bünemann, E. K., et al. (2017). Soil phosphorus supply controls P nutrition strategies of beech forest ecosystems in Central Europe. *Biogeochem* 136, 5–29. doi: 10.1007/s10533-017-0375-0

Liptzin, D., Sanford, R. L. Jr., and Seastedt, T. R. (2013). Spatial patterns of total and available N and P at alpine treeline. *Plant Soil* 365, 127–140. doi: 10.1007/s11104-012-1379-0

Litaor, M. I., Seastedt, T. R., Walker, M. D., Carbone, M., and Townsend, A. (2005). The biogeochemistry of phosphorus across an alpine topographic/snow gradient. *Geoderma* 124, 49–61. doi: 10.1016/j.geoderma.2004.04.001

Liu, Y., de Boeck, H., Wellens, M., and Nijs, I. (2017). A simple method to vary soil heterogeneity in three dimensions in experimental mesocosms. *Ecol. Res.* 32, 287–295. doi: 10.1007/s11284-017-1435-6

Mohren, G. M. J., van den Burg, J., and Burger, F. W. (1986). Phosphorus deficiency induced by nitrogen input in Douglas fir in the Netherlands. *Plant Soil* 95, 191–200. doi: 10.1007/BF02375071

Noy-Meir, I. (1981). "Spatial effects in modelling of arid ecosystems," in *Arid-land Ecosystems: Structure, Functioning and Management,* eds D. W. Goodall, R. A. Perry, and K. M. W. Howes (Cambridge: Cambridge University Press), 411–432.

Prietzel, J., and Ammer, C. (2008). Montane Bergmischwälder der Bayerischen Kalkalpen: Reduktion der Schalenwilddichte steigert nicht nur den Verjüngungserfolg, sondern auch die Bodenfruchtbarkeit. *Allg. Forst Jagdztg.* 179, 104–112.

Prietzel, J., Christophel, D., Traub, C., Kolb, E., and Schubert, A. (2015). Regional and site-related patterns of soil nitrogen, phosphorus, and potassium stocks and Norway spruce nutrition in mountain forests of the bavarian alps. *Plant Soil* 386, 151–169. doi: 10.1007/s11104-014-2248-9

Prietzel, J., Klysubun, W., and Werner, F. (2016). Speciation of phosphorus in temperate zone forest soils as assessed by combined wet-chemical fractionation and XANES spectroscopy. *J. Plant Nutr. Soil Sci.* 179, 168–185. doi: 10.1002/jpln.201500472

Prietzel, J., and Stetter, U. (2010). Long-term effects of atmospheric nitrogen deposition and fertilization on phosphorus nutrition in two German Scots pine (*Pinus sylvestris*) ecosystems. *For. Ecol. Manage.* 259, 1141–1150. doi: 10.1016/j.foreco.2009.12.030

Prietzel, J., Stetter, U., Klemmt, H. J., and Rehfuess, K. E. (2006). Recent carbon and nitrogen accumulation and acidification in soils of two Scots pine ecosystems in Southern Germany. *Plant Soil* 289, 153–170. doi: 10.1007/s11104-006-9120-5

Richardson, A. E., and Simpson, R. J. (2011). Soil microorganisms mediating phosphorus availability. *Plant Physiol.* 156, 989–996. doi: 10.1104/pp.111.175448

Tamm, C. O. (1991). *Nitrogen in Terrestrial Ecosystems, Questions of Productivity, Vegetational Changes, and Ecosystem Stability. Ecological Studies*. Berlin: Springer-Verlag.

Turner, B. L., Condron, L. M., Richardson, S. J., Peltzer, D. A., and Allison, V. J. (2007). Soil organic phosphorus transformations during pedogenesis. *Ecosystems* 10, 1166–1181. doi: 10.1007/s10021-007-9086-z

Turner, B. L., Paphazy, M. J., Haygarth, P. M., and Mckelvie, I. D. (2002). Inositol phosphates in the environment. *Philos. Trans. R. Soc. B.* 357, 449–469. doi: 10.1098/rstb.2001.0837

Walker, T. W., and Syers, J. K. (1976). The fate of phosphorus during pedogenesis. *Geoderma* 15, 1–19. doi: 10.1016/0016-7061(76)90066-5

Wardle, D. A., Walker, L. R., and Bardgett, R. D. (2004). Ecosystem properties and forest decline in contrasting long-term chronosequences. *Science* 305, 509–513. doi: 10.1126/science.1098778

Werner, F., de la Haye, T. R., Spielvogel,S., and Prietzel, J. (2017b). Small-scale spatial distribution of phosphorus fractions in soils from silicate parent material with different degree of podzolization. *Geoderma* 302, 52–65. doi: 10.1016/j.geoderma.2017.04.026

Werner, F., Mueller, C. W., Thieme, J., Gianoncelli, A., Rivard, C., Höschen, C., et al. (2017a). Micro-scale heterogeneity of soil phosphorus depends on soil substrate and depth. *Nat. Sci. Rep.* 7:3203. doi: 10.1038/s41598-017-03537-8

**Conflict of Interest:** The author declares that the research was conducted in the absence of any commercial or financial relationships that could be construed as a potential conflict of interest.

frontiers in Forests and Global Change

ORIGINAL RESEARCH
published: 17 June 2020
doi: 10.3389/ffgc.2020.00071

# QM/MM Molecular Dynamics Investigation of the Binding of Organic Phosphates to the 100 Diaspore Surface

*Prasanth B. Ganta*[1], *Oliver Kühn*[1,2] *and Ashour A. Ahmed*[1,2]*

[1] *Institute of Physics, University of Rostock, Rostock, Germany,* [2] *Department of Life, Light, and Matter (LLM), University of Rostock, Rostock, Germany*

The fate of phosphorus (P) in the eco-system is strongly affected by the interaction of phosphates with soil components and especially reactive soil mineral surfaces. As a consequence, P immobilization occurs which eventually leads to P inefficiency and thus unavailability to plants with strong implications on the global food system. A molecular level understanding of the mechanisms of the P binding to soil mineral surfaces could be a key for the development of novel strategies for more efficient P application. Much experimental work has been done to understand P binding to several reactive and abundant minerals especially goethite ($\alpha$-FeOOH). Complementary, atomistic modeling of the P-mineral molecular systems using molecular dynamics (MD) simulations is emerging as a new tool in environmental science, which provides more detailed information regarding the mechanisms, nature, and strength of these binding processes. The present study characterizes the binding of the most abundant organic phosphates in forest soils, inositol hexaphosphate (IHP), and glycerolphosphate (GP), to the 100 diaspore ($\alpha$-AlOOH) surface plane. Here, different molecular models have been introduced to simulate typical situations for the P-binding at the diaspore/water interface. For all models, quantum mechanics/molecular mechanics (QM/MM) based MD simulations have been performed to explore the diaspore–IHP/GP–water interactions. The results provide evidence for the formation of monodentate (**M**) and bidentate (**B**) motifs for GP and **M** and as well as two monodentate (**2M**) motifs for IHP with the surface. The calculated interaction energies suggest that GP and IHP prefer to form the **B** and **2M** motif, respectively. Moreover, IHP exhibited stronger binding than GP with diaspore and water. Further, the role of water in controlling binding strengths via promoting of specific binding motifs, formation of H-bonds, adsorption and dissociation at the surface, as well as proton transfer processes is demonstrated. Finally, the P-binding at the 100 diaspore surface plane is weaker than that at the 010 plane, studied previously (Ganta et al., 2019), highlighting the influential role of the coordination number of Al atoms at the top surface of diaspore.

**Keywords: P-efficiency, P-adsorption, inositolhexaphosphate (IHP), glycerolphosphate (GP), diaspore (AlOOH), QM/MM simulations**

OPEN ACCESS

***Edited by:***
*Friederike Lang,*
*University of Freiburg, Germany*

***Reviewed by:***
*Zachary E. Kayler,*
*University of Idaho, United States*
*Daniel Tunega,*
*University of Natural Resources and Life Sciences Vienna, Austria*

***Correspondence:**
*Ashour A. Ahmed*
*ashour.ahmed@uni-rostock.de*

***Specialty section:***
*This article was submitted to Forest Soils, a section of the journal Frontiers in Forests and Global Change*

***Received:*** *12 December 2019*
***Accepted:*** *20 May 2020*
***Published:*** *17 June 2020*

***Citation:***
*Ganta PB, Kühn O and Ahmed AA (2020) QM/MM Molecular Dynamics Investigation of the Binding of Organic Phosphates to the 100 Diaspore Surface. Front. For. Glob. Change 3:71. doi: 10.3389/ffgc.2020.00071*

## 1. INTRODUCTION

Phosphorus (P) is essential for plant growth and plays an important role in photosynthesis, energy storage, cell growth, and many other plant processes. It has been pointed out that P scarcity could arise in near future (Cordell and Neset, 2014) and to cope with this situation there is a need to understand the P cycle in forest and agro-ecosystems (Bol et al., 2016, 2018; Missong et al., 2018). In general, phosphates bind to soil components like soil organic matter (Gros et al., 2017, 2019; Ahmed et al., 2018a) and to soil minerals like Fe/Al(oxyhydr)oxides (Hens and Merckx, 2001; Jiang et al., 2015; Kruse et al., 2015; Ahmed et al., 2019) and amorphous Fe/Al hydroxide mixtures (Gypser et al., 2018). The P bound to soil minerals forms colloidal P complexes and consequently becomes unavailable to plants causing P inefficiency (Holzmann et al., 2015; Bol et al., 2016). These colloidal P complexes disperse during heavy rains and accumulate in specific regions resulting in P leaching which further reduces P availability to plants (Boy et al., 2008). Molecular level understanding of P adsorption onto these soil minerals could support efforts to improve P availability to plants (Bol et al., 2016).

Goethite ($\alpha$-FeOOH) is one of the most common and abundant soil minerals that interacts strongly with phosphates (Parfitt and Atkinson, 1976; Torrent et al., 1992; Chitrakar et al., 2006; Kubicki et al., 2012; Ahmed et al., 2019). It is a highly reactive soil mineral containing ferric ions ($Fe^{+3}$) with common surface planes as 010, 100, 110, 021 (according to *Pnma* space group) (Cornell and Schwertmann, 2003). The surface iron atoms are coordinated by 3, 4, 5, or more atoms depending on the surface plane as well as the pH of the environment. Consequently, goethite exhibits different levels of saturation according to the interaction with its environment. The same holds true for most minerals, i.e., minerals exhibit a net positive or negative surface charge based on surface (un)saturation and pH (Cornell and Schwertmann, 2003). Hence, the type of surface plane, its termination and saturation are important factors that influence the adsorption of phosphates onto soil minerals. For instance, Ahmed et al. (2018b) studied glyphosate adsorption at goethite surface with three different degrees of (un)saturation (Fe surface atoms coordinated by 3, 4, and 5 $O^{-2}/OH^{-}$ groups) and showed the effect of the surface's (un)saturation on phosphate binding stability.

In addition to surface saturation and pH, the Fe and Al ratio in amorphous Fe/Al hydroxides is also vital for understanding the phosphates' interaction with soil minerals. Gypser et al. (2018) showed the influence of the Fe:Al ratio in amorphous Fe/Al hydroxide mixtures on phosphate adsorption/desorption rates. The omnipresent Al in weathering environment results in most of Fe oxides in soils being substituted by Al and goethite is no exception (Cornell and Schwertmann, 2003). Diaspore ($\alpha$-AlOOH) is isomorphous with goethite with $Al^{+3}$ oxidation state exhibiting a higher surface energy compared to goethite (Guo and Barnard, 2011). Since amorphous Fe/Al hydroxide mixtures exist in soils, analyzing phosphate binding to diaspore provides additional insight into the P interaction with these amorphous mixtures.

Orthophosphates (Newman and Tate, 1980), inositolhexaphosphate (IHP) (Turner et al., 2002; Doolette et al., 2009; Gerke, 2015), and glycerolphosphate (GP) (Pant et al., 1999; Vincent et al., 2013; Missong et al., 2016) are the most abundant phosphates in soils. Orthophosphate interaction with goethite has been studied extensively (Parfitt and Atkinson, 1976; Torrent et al., 1992; Chitrakar et al., 2006; Ahmed et al., 2019). Yan et al. (2014) studied sorption of different phosphates involving GP and IHP on aluminum (oxyhydr)oxides. They found that the maximum adsorbed phosphate normalized to the mass of adsorbent increases with decreasing crystallinity of the minerals: $\alpha$–$Al_2O_3$ < boehmite < amorphous $Al(OH)_3$. Moreover, they concluded that the phosphate adsorption, interfacial reactions, and phosphate fate in the environment are strongly affected by molecular structure and size of phosphates, and degree of crystallinity and crystal structure of mineral surfaces. Li et al. (2017) suggested that GP adsorbs onto the goethite surface through its phosphate group forming inner-sphere complexes. IHP has six phosphate groups, and in general it exhibits strong binding with P-fixing minerals compared to other phosphates with fewer phosphate groups. Anderson and Arlidge (1962) suggested that the total number of phosphate groups in a compound determines the stability of its interaction with minerals. Ognalaga et al. (1994) showed that IHP forms inner-sphere complexes with goethite through its phosphate groups and suggested that up to four phosphate groups could be involved in binding with the mineral surface; the remaining non-interacting phosphate groups could alter the electrochemical properties of the surroundings. However, Guan et al. (2006) revealed that only three phosphate groups were bound to aluminum hydroxide while the other three groups remained free. This was based on adsorption experiments of IHP on amorphous aluminum hydroxide, FTIR characterization, and quantum chemical calculations.

Quantum chemical calculations become increasingly important when it comes to develop a mechanistic understanding of chemical processes in general. Although not yet widely used, computational chemistry approaches to environmentally relevant questions are recognized as tools to complement experimental investigations. Interestingly, as early as 1973 Tossell et al. (1973) studied electronic structure and bonding in iron oxide minerals with molecular simulations and validated this approach with experimental studies. Kwon and Kubicki (2004) used molecular simulations to resolve controversies in experimental studies related to phosphate surface complexes on iron hydroxides. In another study, Kubicki et al. (2012) demonstrated that phosphate interaction with goethite involves a variety of surface complexes in multiple configurations, which explained the difficulties one faces when interpreting, e.g., IR spectra. Moreover, Ahmed et al. (2018b) explored the possible binding mechanisms for glyphosate (GLP) with three goethite surface planes (010, 001, and 100) in the presence of water via ab initio molecular dynamics simulations. The results showed the prominence of water in controlling the GLP–goethite–water interactions. Further (Ahmed et al., 2019) investigated the molecular level mechanism of phosphate binding at the goethite–water interface referring to the possible phosphate

binding motifs formed at the modeled goethite surface planes. Moreover, the theoretical assignment of IR spectra in the latter study introduced a benchmark for characterizing experimental IR data for a distribution of adsorbed phosphate species. This incomplete list already indicates the huge potential of computational chemistry as an emerging powerful tool for detailed investigations of complex geochemical reactions and especially reaction mechanisms of P-species in soil (for a more complete overview, see also Kubicki, 2016).

Which computational methods are available today? Thinking of it in terms of a hierarchy (Kubicki, 2016; Ozboyaci et al., 2016), quantum mechanics (QM) methods are at the top because they provide, at least in principle, an unbiased ab initio description in terms of the molecular Schrödinger equation. In practice, such a treatment is not feasible except for the simplest cases. Density Functional Theory (DFT) has emerged as a low-cost alternative, which despite of the involved approximations often provides reliable results even for systems with hundreds of atoms (Kubicki, 2016). At the bottom of the hierarchy there are molecular mechanics (MM) methods, which are based on parameterized empirical functions (force fields) describing bonded and non-bonded interactions. This allows to treat millions of atoms, but unless special purpose force fields are used chemical reactions, i.e., bond making and breaking, cannot be simulated (González, M.A., 2011). Here, the hybrid QM/MM approach comes into play, combining the accuracy of QM methods with the efficiency of MM methods. In this approach, the reactive region of the molecular system is treated at the QM level while the remaining part of the system enters at the MM level (Senn and Thiel, 2009). By this, the bond changes, proton transfer events and hydrogen bonds (HBs), e.g., at water-mineral interfaces can be properly described. Besides providing energies in dependence on nuclear positions, forces on the nuclei can be calculated as well. This is prerequisite for molecular dynamics simulations which gives statistical information including thermally accessible configurations (Marx and Hutter, 2009).

In an earlier hybrid QM/MM study of IHP and GP binding to the 010 diaspore surface plane we have demonstrated a strong interaction of IHP/GP with the diaspore surface (Ganta et al., 2019). Here, IHP forms multiple intramolecular HBs with three of its phosphate groups bound to the surface, while GP is bound through its single phosphate group only. Overall, it has been found that proton transfers from phosphate to water or surface have a stabilizing effect, most likely due to the interaction of the HBs dipole with surface charges. Moreover, in case of IHP intramolecular HBs can be formed, which lead to a steric constraint that could weaken the binding to the surface. Since the interaction of IHP and GP with diaspore is not yet fully explored, in the present work we extend our previous study in two directions, i.e., we consider a chemically different surface plane and incorporate the effect of saturation of the diaspore surface on phosphates adsorption. In our previous work (Ganta et al., 2019), IHP/GP and water showed strong and spontaneous interactions with an unsaturated diaspore surface (010 in *pnma*) where the surface Al atoms are coordinated by four oxygens ($O^{-2}/OH^{-}$ groups). Here, a more saturated diaspore surface (100 in *pnma*) is selected where the surface Al atoms are coordinated by five oxygens i.e., $O^{-2}/OH^{-}$ groups. The main objective of current work is to characterize the binding mechanism of IHP and GP at this diaspore–water interface and also to understand the effect of (un)saturation of the diaspore surface on this binding mechanism.

## 2. MOLECULAR MODELING APPROACH

In general, the surface charge of a certain mineral can be determined as a function of pH via its point of zero charge (PZC) (Tan, 2011). For pH > PZC, the mineral surface is saturated with negative surface charges which attract cations. In contrast, for pH < PZC, the mineral surface is unsaturated with positive surface charges which attract anions. The phosphates in general exhibit overall negative charge and hence can be adsorbed at the partially unsaturated 100 diaspore surface (according to the *Pnma* space group) (Tan, 2011). The diaspore unit cell has four AlO(OH) units i.e., total of 16 atoms with lattice constants $a = 9.4253$, $b = 2.8452$, $c = 4.4007$ Å (see **Figure 1C**). The 100 surface plane model is generated by repetition of the diaspore unit cell as $1a \times 8b \times 5c$ along $x$, $y$, $z$ axes, respectively (see **Figure 1D**). In total, the used diaspore slab consists of 640 atoms (160 Al, 160 H, and 320 O atoms). Observe that the surface Al atoms are coordinated by five oxygen atoms (see **Figure S3B**). The phosphates IHP and GP (see **Figures 1A,B**) are modeled to have their phosphate group(s) interacting via inner-sphere complexes with surface Al atoms of diaspore (see **Figures 1F–H**, **Figures S2A–C**). The diaspore-IHP/GP complexes are then solvated using the *solvate* plugin from the VMD package (Humphrey et al., 1996) with a water layer of about 18 Å perpendicular to the surface along the $x$ axis and with a density of $\approx 1\,\mathrm{g\,cm^{-3}}$ ( see **Figure 1E**). Since we are interested in IHP/GP interaction at diaspore–water interface, the QM part of the system (see dashed box in **Figure 1E**) includes the top layer of diaspore (160 atoms), IHP (54 atoms)/GP (19 atoms), and a few water molecules ($\approx$ 53 molecules depending on the setup) surrounding IHP/GP within layer of $\approx$ 10 Å perpendicular to the diaspore surface. The enclosing QM box has a size of $22 \times 8b \times 5c$ Å i.e., $22 \times 22.7616 \times 22.0035$ Å, where $b$, $c$ are diaspore lattice constants (see **Figure 1E**). The remaining part of the system is treated at the MM level.

The initial motifs of diaspore–GP complexes include the monodentate motif **M** (1Al + 1O) (see **Figure 1F**) and bidentate motif **B** (2Al + 2O, here both oxygens are from same phosphate group) (see **Figure 1G**). Note that in contrast to this setup, in the 010 case the two oxygens bind to the same Al atom. In addition to these two, the diaspore–IHP complexes include the four monodentate motif **4M** (4Al + 4O) as experimental studies suggest that IHP forms multiple bonds with the goethite surface (Ognalaga et al., 1994; Guan et al., 2006) (see **Figure 1H**, **Figure S2C**). Note that in principle even more initial conditions/motifs could be sampled. But considering the size of the modeled systems here and the used computationally expensive QM/MM level of theory the initial configurations for the MD simulations are limited to the most common and experimentally observed binding motifs. More technical details

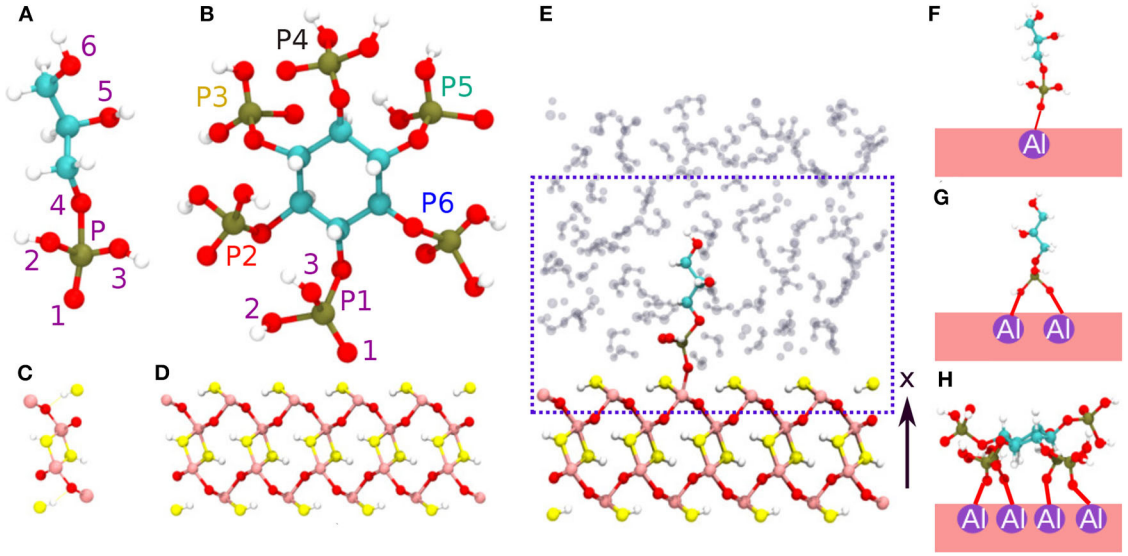


**FIGURE 1 |** Phosphates GP **(A)** and IHP **(B)**. The oxygen and phosphorus atoms are labeled here to ease the discussion of diaspore–IHP/GP–water interactions. Diaspore unit cell **(C)**, side view of the modeled diaspore surface **(D)**, diaspore–GP–water complex and the blue box including atoms described at quantum mechanical level of theory (QM part) and remaining atoms at molecular mechanics level (MM part) **(E)**, **M** motif **(F)**, **B** motif **(G)**, **4M** motif **(H)**. Pink, red, yellow, white, lime, and cyan colors correspond to Al, bridging oxygen, hydroxyl oxygen, hydrogen, phosphorus, and carbon, respectively.

about QM and MM methods and their mutual interaction adopted here is given in **Supplementary Material**. The QM/MM based MD simulations are performed for 25 ps with 0.5 fs time step and with an average temperature of 300 K maintained using canonical sampling through the velocity rescaling thermostat (CSVR) (Bussi et al., 2007). Here, for each molecular model the first 10 ps of the MD trajectory is assigned for equilibration. The last 15 ps of the trajectory is considered as the production trajectory which is used for analysis of interactions at diaspore–water interface with IHP/GP.

To analyze the interaction energies of the complexes, snapshots are taken at every 100 fs of the production trajectory and interaction energies between diaspore and IHP/GP ($E_{diaspore-IHP/GP}$), IHP/GP and water ($E_{IHP/GP-water}$), and diaspore and water ($E_{diaspore-water}$) are calculated. For example, the interaction energy $E_{int}$ between diaspore and GP for a certain diaspore–GP–water snapshot is calculated as follows:

$$E_{int} = E_{diaspore-GP} - (E_{diaspore} + E_{GP}) \quad (1)$$

where $E_{diaspore-GP}$, $E_{GP}$, and $E_{diaspore}$ denote electronic energies of the diaspore–GP complex, GP and diaspore surface, respectively. Likewise, the interaction energies for each pair of diaspore, IHP/GP and water are calculated at every 100 fs during the corresponding production trajectory. The interaction energies with water are divided by the total number of water molecules involved in the simulation box for better comparison. More details regarding the calculation of interaction energies are given in Ganta et al. (2019).

The HBs strength between IHP/GP and water as well as for the intramolecular HBs of one IHP motif are analyzed using geometrical correlations of distances between atoms in HB as discussed in Strassner (2006), Limbach et al. (2009), Yan and Kühn (2010), and Zentel and Kühn (2017). The quantities $q_1$ and $q_2$ in **Figures 4**, **6** below are defined as the deviation of the hydrogen from HB center assuming a linear HB ($q_1$) and the total HB length ($q_2$) (see **Figure 2A**). Geometrically $q_1$ and $q_2$ are defined as $q_1 = \frac{1}{2}(r_1 - r_2)$ Å and $q_2 = (r_1 + r_2)$ Å where $r_1$, $r_2$ denote the distance between donor oxygen and hydrogen ($O_D$—H) and distance between hydrogen and acceptor oxygen ($H\cdots O_A$), respectively (see **Figure 2A**). The same holds true for intramolecular HBs between phosphate groups for the IHP case (see **Figure 2B**).

A HB will be called strong if $q_1 \approx 0$ and $q_2$ is in the range 2.2-2.5 Å. Similarly, moderate and weak HBs have $q_2$ distances ranging from 2.5 to 3.2 and 3.2 to 4 Å, respectively. Also if $q_1 < 0$ the hydrogen atom stays with the donor oxygen and if $q_1 > 0$

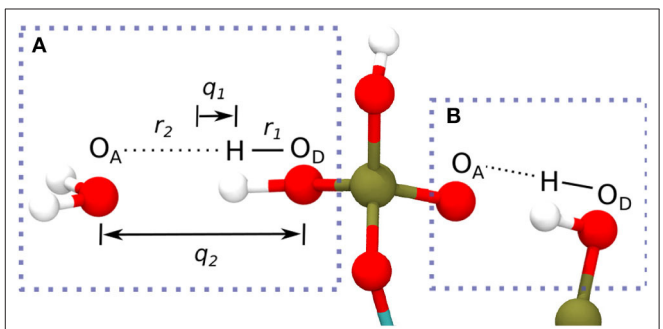


**FIGURE 2 |** Definition of coordinates $q_1$ and $q_2$ in a HB between water's oxygen ($O_A$) and IHP's oxygen ($O_D$) from a phosphate group **(A)** (Limbach et al., 2009), intramolecular HB in IHP **(B)**.

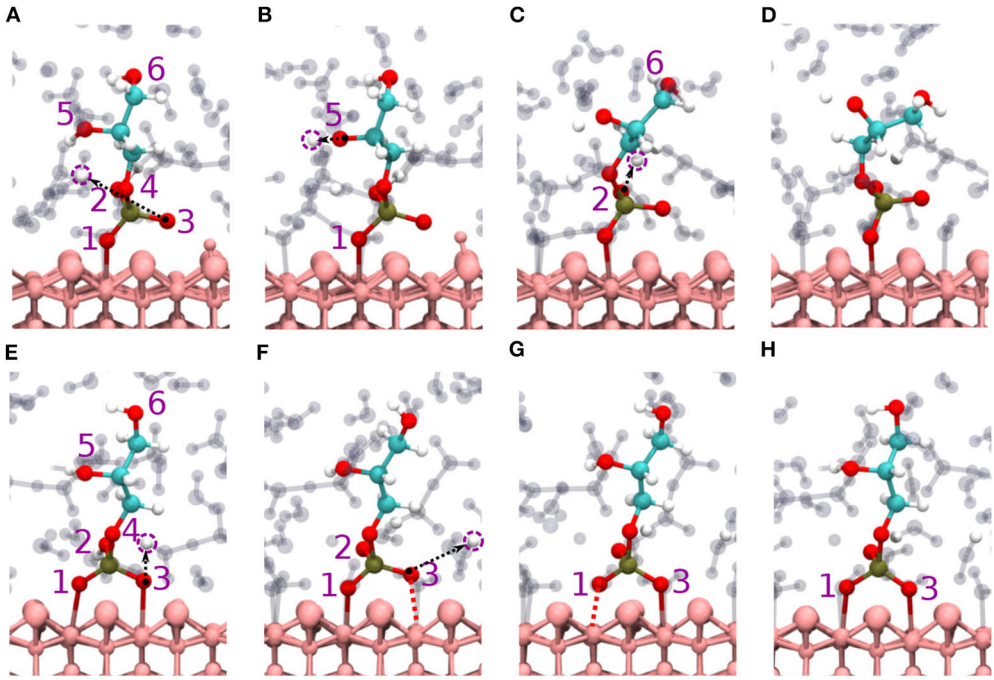


**FIGURE 3 |** Diaspore–GP–water snapshots displaying proton transfer events and GP dynamics along trajectories. Proton transfers observed during production trajectory of **M** motif from O3 to water **(A)** from O5 to water **(B)**, and from O2 to water **(C)**, GP **M** motif at 25 ps **(D)**. Proton transfer events in **B** (2Al+2O) motif from O3 to water **(E)**, from O2 to water and momentary dissociation of Al1-O1 bond **(F)**, momentary dissociation of Al2-O3 bond **(G)**, GP **B** motif at 25 ps **(H)**.

the hydrogen atom (proton) transferred to the acceptor oxygen. In the following a HB analysis is performed for the QM part of the system only as the emphasis of this study is on the interface region where the binding/adsorption process takes place.

## 3. RESULTS AND DISCUSSION

### 3.1. Diaspore–GP–Water Interactions

#### 3.1.1. GP M Motif

For the GP-**M** initial condition a stable monodentate (1Al+1O) motif is observed between GP and the diaspore surface over the course of the production trajectory with the Al-O1 average bond length of 2.3 Å (see **Figures 3A–D**). The average geometry of the $PO_4$ moiety here has root mean square deviation (RMSD) value of 0.17 Å with respect to free tetrahedral $PO_4^{3-}$ (see **Figure S2D**).

Proton transfer events from GP to the diaspore surface are not observed, instead three proton transfer events are found from O3, O5, and O2 oxygens of GP to water (see **Figures 3A–C**), respectively. On average, eight HBs are observed between GP and water in the production trajectory. Here, the GPs oxygen atoms act as HB donors ($Ox_D$) as well as acceptors ($Ox_A$). Exemplary analysis of six of the above eight HBs shows that four ($O2_A$, $O3_A$, $O5_A$, $O5_D$) are strong to moderately strong HBs and two ($O1_A$, $O6_A$) moderately strong to weak HBs (see **Figures 4A–C**).

Regarding the diaspore–water interaction, an average of 17 water molecules (out of 40 surface Al atoms) formed **M** binding motifs (Al-$O_{H_2O}$) with the diaspore surface and have average bond length of 1.9-2.3 Å. Also moderately strong HBs are observed between water and diaspore (see **Figure S1A**). This scheme of diaspore–water interactions is also observed for the other diaspore–IHP/GP–water models studied below. For the average diaspore–water interaction energy per water molecule one obtains about −3 kcal/mol for all considered models.

The time averaged interaction energy per surface bond between diaspore and GP is around −23 kcal/mol (see **Table 1**). The average GP–water interaction energy per water molecule is −2.6 k cal/mol.

#### 3.1.2. GP B Motif

The **B** motif (2Al+2O i.e., Al1-O1 and Al2-O3) is observed over the course of the production trajectory with Al1-O1 and Al2-O3 covalent bond length ranging from 2-2.7 and 1.9-2.7 Å with an average value of 2.4 and 2.3 Å, respectively (see **Figures 3E–H**). Most notably the Al2-O3 and Al1-O1 bonds are elongated and compressed in an alternating see-saw fashion as seen in **Figures 3F,G**. The **B** motif's average geometry of the $PO_4$ moiety has a RMSD value of 0.17 Å with respect to the free tetrahedral $PO_4^{3-}$.

Proton transfer events are observed from O3 and O2 oxygens to water (see **Figures 3E,F**), respectively. The **B** motif features on average a total of seven HBs between GP and water. According to **Figures 4D–F**, four ($O1_A$, $O2_A$, $O2_D$, $O5_D$) strong to moderately strong HBs and two ($O1_A$, $O6_D$) moderately strong to weak HBs are formed between GP and water.

The average interaction energy per surface bond between diaspore and GP for the **B** motif is around −15 kcal/mol. The

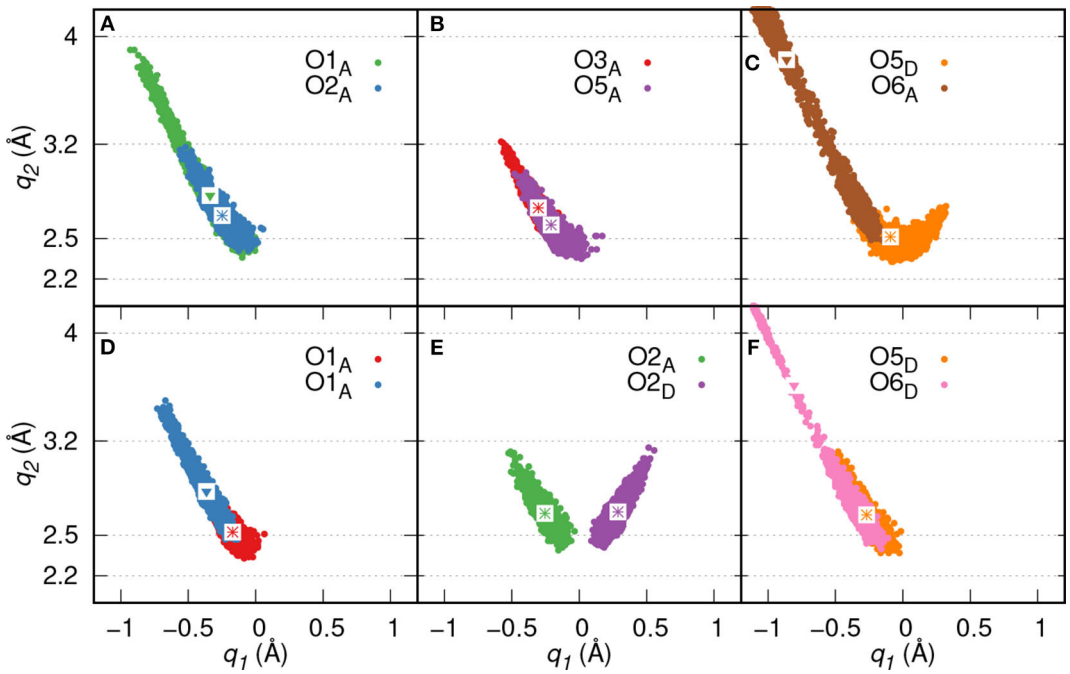


**FIGURE 4 |** HB correlation $q_2$ *vs.* $q_1$ of HBs formed between GP and water in GP's **M** motif **(A–C)** and **B** motif **(D–F)**, respectively. The average $q_1$ and $q_2$ coordinate pairs are shown as points in white square boxes. A strong to moderately strong HB is denoted as * while a moderately strong HB and a moderately strong to weak HB are denoted as • and ▼, respectively.

**TABLE 1 |** The per bond time averaged interaction energies (calculated with Equation 1) of diaspore–IHP/GP complexes and some selected bond lengths and distances.

| | | | | | |
|---|---|---|---|---|---|
| **100 diaspore surface** | | | | | |
| ***P*$_o$** | **Motif** | **E$_{int}$/bond (kcal/mol)** | **Al-*O*$_P$ (Å)** | **Al-P (Å)** | **RMSD($PO_4^{3-}$) (Å)** |
| GP | **M** | −23 | 2.3 | 3.4 | 0.17 |
| | **B** | −15 | 2.3 and 2.4 | 3.3 | 0.17 |
| IHP | **M(1)** | −33 | 2.4 | 3.5 | 0.16 |
| | **M(2)** | −18 | 2.7 | 3.6 | 0.19 |
| | **2M** | −109 | 2.1 and 2.2 | 3.3 and 3.4 | 0.18 and 0.17 |
| **010 diaspore surface (Ganta et al., 2019)** | | | | | |
| GP | **B** | −148 | 2.03 and 2.05 | 2.65 | 0.1 |
| IHP | **3M** | −145 | 1.90 and 1.88 and 1.86 | 3.25 and 3.17 and 3.18 | 0.07 and 0.08 and 0.1 |

*The RMSD difference between average phosphate geometry and isolated tetrahedral $PO_4^{3-}$ (see **Figure S2D**) is also provided. Here, $P_o$ denotes phosphate and motif denotes average motif observed during production trajectory. Further, Al-$O_P$ denotes bond distance between covalent bonded Al and $O_P$ oxygen of IHP/GP.*

per surface bond interaction energy here is smaller than for the **M** motif due to GP's see-saw type of motion over the surface. Nevertheless, the total interaction energy observed here is larger than for the **M** motif and hence the **B** motif is more likely to form.

Note that due to the formation of a strong to moderately strong HB with water, the O3 oxygen in **M** cannot easily transform into the **B** motif, i.e., the barrier is too high to be sampled in the present trajectory (see **Figure 4B**). The average GP–water interaction energy per water molecule is around −2.3 kcal/mol. The smaller value as compared with **M** could be due to the additional proton transfer event observed in that case.

## 3.2. Diaspore–IHP–Water Interactions

### 3.2.1. IHP M Motifs

Here, two initial configurations (**M**, **B** motifs) of the diaspore–IHP–water model resulted in two different **M** final motifs. In the first case, **M(1)**, the initial configuration was an **M** motif, wherein O11 oxygen is aligned to form a **M** motif with a surface Al atom (see **Figure S2A**). A stable **M** motif is observed throughout the production trajectory with average Al-O11 bond length of 2.4 Å (see **Figures 5A–D**). The series of events that are observed during the formation of the **M(1)** motif are: a proton transfer from O12 to water (see **Figure 5A**), followed by intramolecular proton transfer from O62 to O12 and formation of O13-H-O61 intramolecular HB (see **Figure 5B**). After a few femtoseconds, the O12-H-O62 HB is formed and a proton transfer is observed from O32 to water (see **Figure 5C**) to reach the final **M** motif in **Figure 5D**. The events in **Figures 5A–C** occurred within 2 ps of the simulation trajectory. Overall, a total of three protons transfer events are observed from IHP to water from O12, O53, and O32 (see **Figures 5A–C**), respectively. On average IHP has formed 19 HBs with water over the course of the production trajectory. Analyzing for illustration 12 out of these 19 HBs, IHP has formed nine ($O12_A$, $O21_A$, $O22_A$, $O23_A$, $O31_A$, $O43_A$, $O51_A$, $O53_A$,

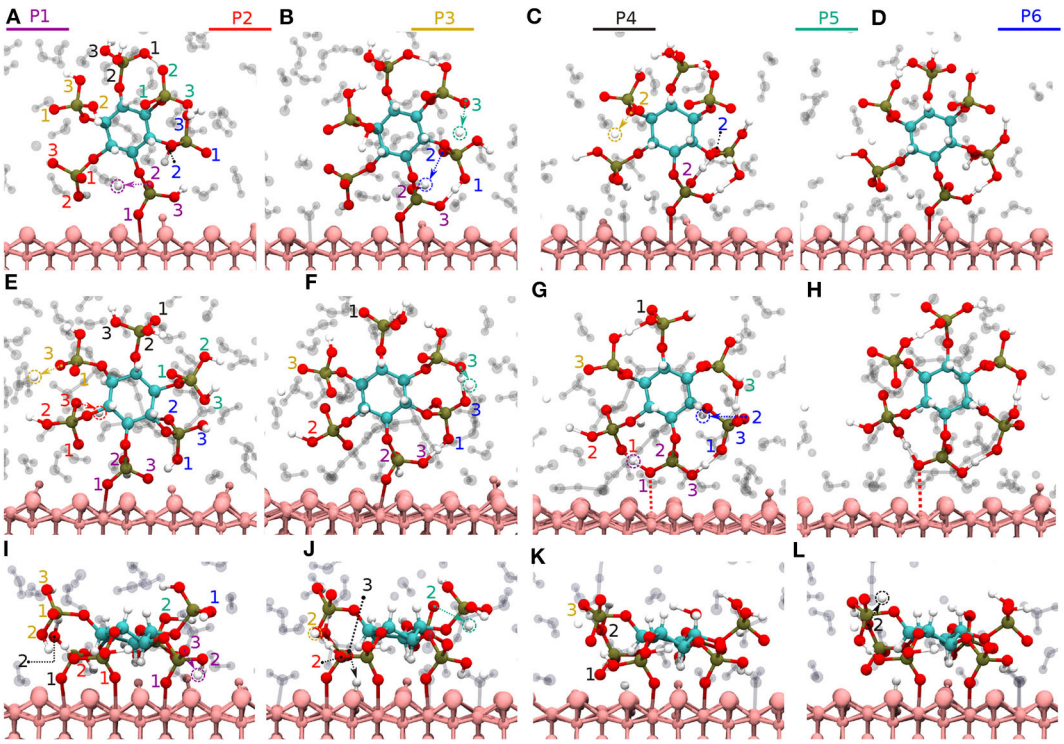


**FIGURE 5 |** Diaspore–IHP–water snapshots displaying proton transfer events and IHP dynamics along trajectories. The phosphate groups are color-coded and the oxygen atom label color denotes to the phosphate group it belongs. In **M(1)** motif, proton transfer from O12 to water **(A)**, proton transfer from O53 to water and intramolecular proton transfer from O62 to O12 **(B)**, moderately strong O12-H-O62 HB and proton sharing between O12 to O62 oxygens and proton transfer from O32 to water **(C)**, **M(1)** motif at 25 ps **(D)**. In **M(2)** motif, dissociation of Al2-O13 covalent bond due to O13-H-O61 HB and proton transfers from O23 and O33 to water **(E)**, proton transfer from O53 to water and formation of O53-H-O63 HB **(F)**, dissociation of Al1-O11 bond due to formation of O11-H-O21 HB **(G)**, **M(2)** motif at 25ps **(H)**. In **2M** motif, dissociation of Al4-O51 bond and proton transfer from O13 to water **(I)**, proton transfer from O43 to diaspore and from O32 to water, also proton sharing and HB between O22 and O32 **(J)**, and between O33 and O42 followed by dissociation of Al3-O41 bond **(K)**, proton transfer from O42 to water and **2M** motif at 25 ps **(L)**.

$O63_D$) strong to moderately strong HBs, two ($O33_D$, $O41_A$) moderately strong HBs and one ($O31_A$) moderately strong to weak HB with water (see **Figures 6A–E**). Interestingly, IHP also forms multiple intramolecular HBs, for instance, O13-H-O61, O41-H-O52, and O12-H-O62 (see **Figures 5A–C**). Analyzing the strength of the intramolecular HBs between P1 and P6 phosphate groups, one finds two (O13-H-O61, O12-H-O62) moderately strong HBs (see **Figure 6F**). The average geometry of $PO_4$ moiety has a RMSD value of 0.16 Å with respect to the free tetrahedral $PO_4^{3-}$.

The time averaged interaction energy per surface bond between diaspore and IHP is around −33 kcal/mol (see **Table 1**) and between IHP and water is around −5.5 kcal/mol per water molecule. Notice that IHP exhibits a larger interaction energy with water as well with the diaspore surface compared to GP.

For the **M(2)** motif, the initial configuration had the O11 and O13 oxygens aligned such as to form a **B** motif with adjacent surface Al atoms (see **Figure S2B**). The Al2-O13 covalent bond is dissociated during the trajectory and the **B** motif is transformed into the **M(2)** motif (see **Figures 5E,F**). Over the course of the production trajectory the Al1-O11 bond length ranges from 2.4 to 3.2 Å with an average of 2.7 Å. In more detail, the series of events that unfold in this case are as follows: From the O23 and O33 oxygens, two protons are transferred to water and the Al2-O13 covalent bond is dissociated (see **Figure 5E**). After a few femtoseconds, a proton transfer is observed from O53 to water followed by formation of an intramolecular HB between O53 and O63 oxygens (see **Figure 5F**). Also formation of the intramolecular O13-H-O61 HB is observed. With progressing simulation time an intramolecular proton transfer event is observed from O12 to O21, followed by formation of O11-H-O21 HB. Afterwards, the Al1-O11 covalent bond weakens at around 6 ps and its bond length ranges from 2.4 to 3.2 Å further on (see **Figure 5G**, **Figure S1B**). In addition, a proton transfer is observed from O62 to water (see **Figure 5G**). The snapshot at 25 ps shows that multiple inter- and intramolecular HBs are observed for IHP (see **Figure 5H**). Their characterization in terms of HB geometries leads to a similar distribution of HB strengths as for **M(1)**. Overall the average geometry of $PO_4$ moiety has RMSD value of 0.19 Å with respect to the free tetrahedral $PO_4^{3-}$.

The average interaction energy per surface bond between the diaspore surface and IHP in this case is around −18 kcal/mol. The interaction energy observed here is smaller than for the **M(1)**

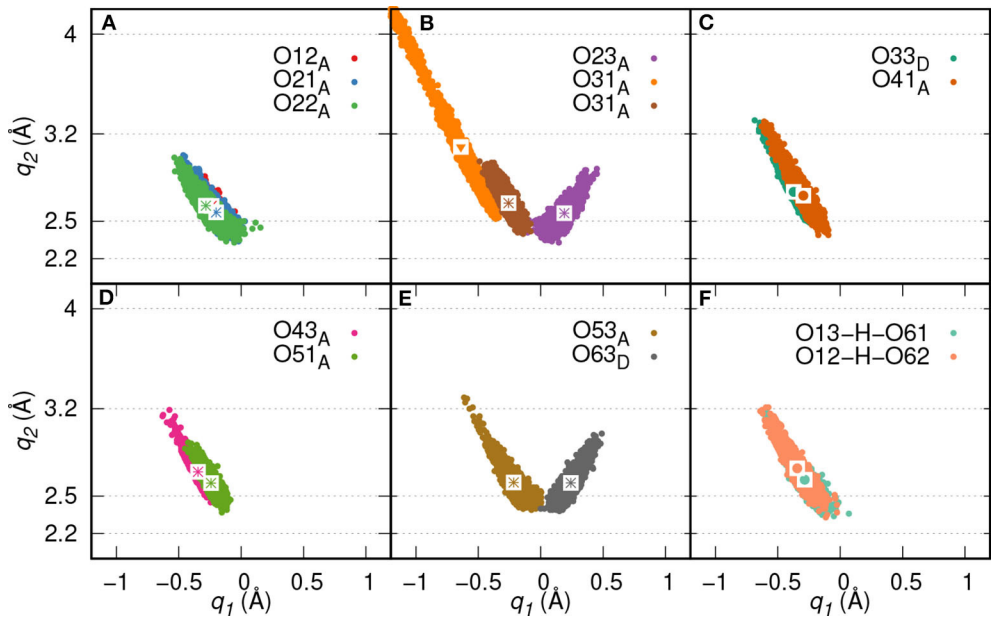


**FIGURE 6 |** HB correlation $q_2$ vs. $q_1$ of HBs formed between IHP and water **(A–E)** and between P1 and P6 phosphate groups **(F)** along trajectory of IHP's **M(1)** motif. The average $q_1$ and $q_2$ coordinate pairs are shown as points in white square boxes. A strong to moderately strong HB is denoted as * while a moderately strong HB and a moderately strong to weak HB are denoted as ● and ▼, respectively.

case as the Al1-O11 bond length is longer due to formation of O13-H-O61 and O12-H-O21 intramolecular HBs. The observed interaction energy between IHP and water here is −5.7 kcal/mol per water molecule which is slightly higher than for the **M(1)** case, probably due to additional proton transfer from IHP to water.

### 3.2.2. IHP 2M Motif

Here, IHP is initially aligned parallel to surface with the non-protonated oxygens of the four phosphate groups forming a **4M** motif, i.e., Al1-O11, Al2-O21, Al3-O41, Al4-O51 covalent bonds with the surface (see **Figure S2C**). However, only a stable **2M** motif is observed along the production trajectory with average bond lengths of Al1-O11, Al2-O21 as 2.13 and 2.22 Å, respectively. The events observed during simulation that led to the formation of **2M** motif are as follows: within a few picoseconds, the Al-O51 bond is dissociated transforming **4M** into a **3M** motif. A proton transfer is observed from O13 oxygen to water and from O43 oxygen to diaspore (see **Figures 5I,J**). Further, an intramolecular HB is observed between O22 and O32 oxygens and two proton transfer events from O32 and O52 to water (see **Figure 5J**). The Al3-O41 covalent bond is disassociated due to intramolecular HB formed between O33 and O42 oxygens (see **Figure 5K**), followed by a proton transfer event from O42 to water (see **Figure 5L**). Totally four proton transfer events are observed from IHP to water and an average of 19 HBs are formed between IHP and water. The inter- and intra-molecular HBs have a similar distribution of strengths as for **M(1)** and **M(2)**. The average geometry of the $PO_4$ moieties deviate from that of free tetrahedral $PO_4^{3-}$ with RMSD values of 0.18 and 0.17 Å.

The interaction energy between IHP and diaspore in the **2M** motif is −109 kcal/mol per bond (see **Table 1**). The interaction energy is larger here compared to **M(1)** and **M(2)** motifs due to the additional covalent bond and a proton transfer from IHP to the diaspore surface. Hence, the **2M** motif is more likely to form compared to both the **M(1)** and **M(2)** motifs. The average interaction energy per water molecule with IHP is −5.9 kcal/mol which is slightly larger than the IHP–water interaction energy observed in **M(1)** motif case due to additional proton transfer from IHP to water here.

## 3.3. Effect of Surface Saturation

In the following we will compare the present results with those of our previous work for the 010 surface plane (Ganta et al., 2019). The 010 diaspore surface plane is relatively unsaturated, i.e. the surface Al atoms are coordinated by only four oxygen atoms (see **Figure S3A**). In contrast, for the present more saturated 100 plane, surface Al atoms are coordinated by five oxygens (see **Figure S3B**). Also the 010 diaspore surface plane exhibits higher electrostatic potential compared to the 100 surface plane as shown in **Figure S6**.

For the 010 plane the largest total interaction energy was observed for the **B** and **3M** motif in case of GP and IHP, respectively (see **Table 1**). In case of 100 plane, the **B** and **2M** motifs dominate the total interaction energies. Comparing the two **B** motifs for GP one finds that the binding to 010 being 10 times stronger than to 100 surface plane. The reason for the weaker interaction energy in case of 100 is due to see-saw type

of motion of GP yielding a weakening/strengthening of Al1-O1 and Al2-O3 bonds which is not observed for the 010 plane. This can be attributed to the fact that in case of 010 plane the two oxygens are coordinated to the same Al, whereas for 100 plane the coordination is with two neighboring Al atoms, whose distances is such as to require unfavorably large $O_P$-P-$O_P$ angles for strong binding. Further stabilization of the GPs **B** motif in the 010 plane case comes from two additional proton transfers observed from GP to the diaspore surface.

Regarding the total interaction energies, the dominant binding motifs for the diaspore–IHP complexes are also different for 010 (**3M**) and 100 (**2M**). In case of 100 the total interaction energy is about two times smaller than for 010. Comparing the two motifs we note in particular that the interaction with the two surfaces is different. This is nicely illustrated by the fact that no stable **4M** motif could be observed for the 100 case. One reason for the transformation of the **4M** motif to **2M** motif is that the Al-$O_P$ bonds (regions R1 and R2, see **Figures S5A–C**) at the 100 diaspore surface are inclined due to $O_P$ and surface hydroxyl oxygen repulsion. Hence the movement of oxygens in the Al-$O_P$ bonds (regions R1 and R2) is restricted to the space between consecutive surface hydroxyl oxygens or to move away from surface (see **Figures S5A–C**). Consequently, upon equilibration the oxygens in the Al-$O_P$ bonds could dissociate from diaspore as they are confined between consecutive surface hydroxyl oxygens (see **Figures S5A–C**). In contrast for the 010 diaspore–IHP case, the oxygens in the Al-$O_P$ bonds (regions R3 and R4, **Figures S5E–G**) are not restricted and they are free to move. Hence a stable **3M** motif is observed over the course of production trajectory (see **Figures S5E–G**). Looking at it from a geometric point of view, Al-Al distances on the 010 surface are about 4.4–5.4 Å which is much larger than the 2.4 Å for the 100 surface where the **2M** motif forms (see **Figures S5D,H**). Given the typical distances between the phosphate groups in IHP, bonding to the 100 surface plane yields a higher strain and thus it becomes weaker as compared with the 010 surface plane.

In case of the 100 surface the diaspore–water interaction energy is 3.4 times smaller compared to the 010 case. In fact less than half of surface Al atoms formed **M** motifs with water compared to the 010 diaspore surface. Also the radial distribution function of diaspore surface oxygens with water hydrogens in **Figure S4** shows higher water accumulation near the 010 diaspore surface compared to the 100 diaspore surface which suggests stronger interaction for the 010 diaspore surface with water.

## 4. SUMMARY AND CONCLUSIONS

In our previous study (Ganta et al., 2019), a strong and spontaneous binding of IHP and GP with the 010 diaspore surface has been described, which provided the motivation for studying the effect of surface saturation on these interactions. Therefore, the more saturated 100 diaspore surface has been investigated here using periodic boundary QM/MM based MD simulations. The analysis of the MD trajectories showed the importance of inter- and intramolecular HBs in the formation of final motifs and also shed light on effects that lead to disassociation and association of P-O-Al bonds in the diaspore–IHP/GP–water complexes.

In case of the diaspore–GP–water complexes, the **B** motif's interaction energy per bond is 1.5 times smaller than the **M** motif. But considering the total average interaction energy, GP is more likely to form a **B** motif with the 100 diaspore surface.

Regarding the diaspore–IHP–water complexes, the interaction energy per bond follows the order **2M** > **M(1)** > **M(2)**. Here, the **M(2)** motif's interaction energy is 1.8 times smaller than the **M(1)** motif due to longer Al-$O_p$ bond length, i.e., due to movement of IHP away from the diaspore surface. Thus the **2M** motif will be also dominating considering the total interaction energy. This is due to the additional covalent bond and a proton transfer to the diaspore surface. Hence IHP is likely to form a **2M** motif with the 100 diaspore surface.

Regarding the water interaction with 100 diaspore and IHP/GP, it can be concluded that the average IHP-water interaction energy is about 2.3 times larger than the GP-water one due to IHP's higher water accessible surface area. Both IHP and GP show proton transfer events to water and formation of strong to moderately strong HBs with water. The diaspore–water interaction energy is only 1.1 times that of the GP-water case, but 2.8 times smaller than IHP-water one. Thus, water has a stronger interaction with IHP than with the 100 diaspore surface.

Of course, studying a particular perfect surface plane can at best give qualitative trends if compared to real surfaces of mineral particles in soil. Studying two abundant surface planes, however, it is possible to pinpoint important factors which influence the behavior of P-compounds at the mineral/water interface. The present investigation focused on the effects of surface saturation and thus electrostatic potential on IHP/GP adsorption. The soil minerals exhibit a positive charge with an unsaturated surface and active sites for pH < PZC. For a pH far below PZC a higher positive charge, i.e, more unsaturated surface is observed (Cornell and Schwertmann, 2003; Tan, 2011). The IHP and GP adsorption onto goethite (with PZC around 9–10) is decreased with increasing pH and reached near zero values for pH around 10 (Celi et al., 1999; Li et al., 2017). This shows that the mineral surface saturation varies with pH and thus the ability of a mineral to adsorb phosphates. Higher surface saturation leads to more negative charges on the 100 surface as compared to the 010 case. Phosphates in water are partially deprotonated and thus have an effective negative charge. Thus the phosphate groups will be attracted stronger to the 010 diaspore surface plane. The denser distribution of water around the 010 surface compared to the 100 surface and transformation of IHP's **M** and **B** motifs to **2M** motif highlight the stronger electrostatic potential of 010 surface than 100.

Comparing our previous study (Ganta et al., 2019) with the present one, it can be concluded that the diaspore surfaces with different degrees of saturation exhibit different interaction energies with phosphates. Moreover, both surface planes form multiple bonds with IHP while the **B** binding motif dominates for GP. The overall interaction energies show that IHP is bound to diaspore stronger than GP and this confirms the prevailing view that the number of phosphate groups is a decisive parameter

determining the adsorption strength (Anderson and Arlidge, 1962). This could also explain why higher percentages of IHP is found in the forest soil colloid samples than GP as revealed by liquid-state NMR measurements (Missong et al., 2016). However, not all available phosphate groups will contribute to the binding, with details depending on the surface saturation. The present study also stresses the importance of inter- and intra-molecular HBs and the observation that IHP is less protonated than solution counterparts when pH < PZC as shown by Johnson et al. (2012). For both modeled diaspore surfaces, there is no observed dissociation for the bonds involved in C-O, C-H, and C-O-P as suggested by Celi et al. (1999) and Li et al. (2017). In the present case of IHP we cannot confirm the suggestion of a **4M** motif made by Ognalaga et al. (1994).

## DATA AVAILABILITY STATEMENT

All datasets generated for this study are included in the article/**Supplementary Material**.

## AUTHOR CONTRIBUTIONS

PG has performed the present work and analyzed the results. AA and OK have suggested, designed, and supervised the scientific approach for the present study. All authors have discussed and interpreted the present results and contributed to writing the submitted manuscript.

## ACKNOWLEDGMENTS

All authors gratefully acknowledge the financial support by the German Research Foundation (DFG) as a part of the SPP 1685 Priority program Ecosystem Nutrition: Forest strategies for limited phosphorus resources. AA would like to thank the financial support by the InnoSoilPhos-project, funded by the German Federal Ministry of Education and Research (BMBF) in the frame of the BonaRes-program (No. 031A558). This research was performed within the scope of the Leibniz Science Campus Phosphorus Research Rostock. The authors thank the North German Supercomputing Alliance for providing HPC resources (project mvp00016).

## SUPPLEMENTARY MATERIAL

The Supplementary Material for this article can be found online at: https://www.frontiersin.org/articles/10.3389/ffgc.2020.00071/full#supplementary-material

## REFERENCES

Ahmed, A. A., Gros, P., Kühn, O., and Leinweber, P. (2018a). Molecular level investigation of the role of peptide interactions in the glyphosate analytics. *Chemosphere* 196, 129–134. doi: 10.1016/j.chemosphere.2017.12.162

Ahmed, A. A., Gypser, S., Leinweber, P., Freese, D., and Kühn, O. (2019). Infrared spectroscopic characterization of phosphate binding at the goethite-water interface. *Phys. Chem. Chem. Phys.* 21, 4421–4434. doi: 10.1039/C8CP07168C

Ahmed, A. A., Leinweber, P., and Kühn, O. (2018b). Unravelling the nature of glyphosate binding to goethite surfaces by ab initio molecular dynamics simulations. *Phys. Chem. Chem. Phys.* 20, 1531–1539. doi: 10.1039/C7CP06245A

Anderson, G., and Arlidge, E. Z. (1962). The adsorption of inositol phosphates and glycerophosphate by soil clays, clay minerals, and hydrated sesquioxides in acid media. *J. Soil Sci.* 13, 216–224. doi: 10.1111/j.1365-2389.1962.tb00699.x

Bol, R., Gruau, G., Mellander, P.-E., Dupas, R., Bechmann, M., Skarbøvik, E., et al. (2018). Challenges of reducing phosphorus based water eutrophication in the agricultural landscapes of Northwest Europe. *Front. Mar. Sci.* 5:276. doi: 10.3389/fmars.2018.00276

Bol, R., Julich, D., Brödlin, D., Siemens, J., Kaiser, K., Dippold, M. A., et al. (2016). Dissolved and colloidal phosphorus fluxes in forest ecosystems–an almost blind spot in ecosystem research. *J. Soil Sci. Plant Nutr.* 179, 425–438. doi: 10.1002/jpln.201600079

Boy, J., Valarezo, C., and Wilcke, W. (2008). Water flow paths in soil control element exports in an andean tropical montane forest. *Eur. J. Soil Sci.* 59, 1209–1227. doi: 10.1111/j.1365-2389.2008.01063.x

Bussi, G., Donadio, D., and Parrinello, M. (2007). Canonical sampling through velocity rescaling. *J. Chem. Phys.* 126, 014101:1–014101:6. doi: 10.1063/1.2408420

Celi, L., Lamacchia, S., Marsan, F. A., and Barberis, E. (1999). Interaction of inositol hexaphosphate on clays: adsorption and charging phenomena. *Soil Sci.* 164, 574–585. doi: 10.1097/00010694-199908000-00005

Chitrakar, R., Tezuka, S., Sonoda, A., Sakane, K., Ooi, K., and Hirotsu, T. (2006). Phosphate adsorption on synthetic goethite and akaganeite. *J. Colloid Interface Sci.* 298, 602–608. doi: 10.1016/j.jcis.2005.12.054

Cordell, D., and Neset, T.-S. (2014). Phosphorus vulnerability: a qualitative framework for assessing the vulnerability of national and regional food systems to the multi-dimensional stressors of phosphorus scarcity. *Glob. Environ. Chang.* 24, 108–122. doi: 10.1016/j.gloenvcha.2013.11.005

Cornell, R. M., and Schwertmann, U. (2003). *The Iron Oxides: Structure, Properties Reactions Occurrence and Uses*. Weinheim: Wiley-VCH Verlag GmbH and Co. KGaA.

Doolette, A., Smernik, R., and Dougherty, W. (2009). Spiking improved solution phosphorus31 nuclear magnetic resonance identification of soil phosphorus compounds. *Soil Sci. Soc. Am. J.* 73, 919–927. doi: 10.2136/sssaj2008.0192

Ganta, P. B., Kühn, O., and Ahmed, A. A. (2019). QM/MM simulations of organic phosphorus adsorption at the diaspore–water interface. *Phys. Chem. Chem. Phys.* 21, 24316–24325. doi: 10.1039/C9CP04032C

Gerke, J. (2015). Phytate (inositol hexakisphosphate) in soil and phosphate acquisition from inositol phosphates by higher plants: a review. *Plants* 4, 253–266. doi: 10.3390/plants4020253

González, M.A. (2011). Force fields and molecular dynamics simulations. *Collect. SFN 2011* 12, 169–200. doi: 10.1051/sfn/201112009

Gros, P., Ahmed, A., Kühn, O., and Leinweber, P. (2017). Glyphosate binding in soil as revealed by sorption experiments and quantum-chemical modeling. *Sci. Tot. Environ.* 586, 527–535. doi: 10.1016/j.scitotenv.2017.02.007

Gros, P., Ahmed, A. A., Kühn, O., and Leinweber, P. (2019). Influence of metal ions on glyphosate detection by FMOC-Cl. *Environ. Model. Assess.* 191:244. doi: 10.1007/s10661-019-7387-2

Guan, X.-H., Shang, C., Zhu, J., and Chen, G.-H. (2006). ATR-FTIR investigation on the complexation of myo-inositol hexaphosphate with aluminum hydroxide. *J. Colloid Interface Sci.* 293, 296–302. doi: 10.1016/j.jcis.2005.06.070

Guo, H., and Barnard, A. S. (2011). Thermodynamic modelling of nanomorphologies of hematite and goethite. *J. Mater. Chem.* 21, 11566–11577. doi: 10.1039/c1jm10381d

Gypser, S., Hirsch, F., Schleicher, A. M., and Freese, D. (2018). Impact of crystalline and amorphous iron- and aluminum hydroxides on mechanisms of phosphate adsorption and desorption. *J. Environ. Sci.* 70, 175–189. doi: 10.1016/j.jes.2017.12.001

Hens, M., and Merckx, R. (2001). Functional characterization of colloidal phosphorus species in the soil solution of sandy soils. *Environ. Sci. Technol.* 35, 493–500. doi: 10.1021/es0013576

Holzmann, S., Missong, A., Puhlmann, H., Siemens, J., Bol, R., Klumpp, E., et al. (2015). Impact of anthropogenic induced nitrogen input and liming on phosphorus leaching in forest soils. *J. Soil Sci. Plant Nutr.* 179, 443–453. doi: 10.1002/jpln.201500552

Humphrey, W., Dalke, A., and Schulten, K. (1996). VMD – visual molecular dynamics. *J. Mol. Graph.* 14, 33–38. doi: 10.1016/0263-7855(96)00018-5

Jiang, X., Bol, R., Nischwitz, V., Siebers, N., Willbold, S., Vereecken, H., et al. (2015). Phosphorus containing water dispersible nanoparticles in arable soil. *J. Environ. Qual.* 44, 1772–1781. doi: 10.2134/jeq2015.02.0085

Johnson, B. B., Quill, E., and Angove, M. J. (2012). An investigation of the mode of sorption of inositol hexaphosphate to goethite. *J. Colloid Interface Sci.* 367, 436–442. doi: 10.1016/j.jcis.2011.09.066

Kruse, J., Abraham, M., Amelung, W., Baum, C., Bol, R., Kühn, O., et al. (2015). Innovative methods in soil phosphorus research: a review. *J. Soil Sci. Plant Nutr.* 178, 43–88. doi: 10.1002/jpln.201400327

Kubicki, J. D. (ed.). (2016). *Molecular Modeling of Geochemical Reactions*. Chichester: Wiley and Sons.

Kubicki, J. D., Paul, K. W., Kabalan, L., Zhu, Q., Mrozik, M. K., Aryanpour, M., et al. (2012). ATR–FTIR and Density Functional Theory study of the structures, energetics, and vibrational spectra of phosphate adsorbed onto goethite. *Langmuir* 28, 14573–14587. doi: 10.1021/la303111a

Kwon, K. D., and Kubicki, J. D. (2004). Molecular orbital theory study on surface complex structures of phosphates to iron hydroxides-calculation of vibrational frequencies and adsorption energies. *Langmuir* 20, 9249–9254. doi: 10.1021/la0487444

Li, H., Wan, B., Yan, Y., Zhang, Y., Cheng, W., and Feng, X. (2017). Adsorption of glycerophosphate on goethite: a macroscopic and infrared spectroscopic study. *J. Soil Sci. Plant Nutr.* 181, 557–565. doi: 10.1002/jpln.201700517

Limbach, H.-H., Tolstoy, P. M., Pérez-Hernández, N., Guo, J., Shenderovich, I. G., and Denisov, G. S. (2009). Oho hydrogen bond geometries and NMR chemical shifts: from equilibrium structures to geometric H/D isotope effects, with applications for water, protonated water, and compressed ice. *Isr. J. Chem.* 49, 199–216. doi: 10.1560/IJC.49.2.199

Marx, D., and Hutter, J. (2009). *Ab Initio Molecular Dynamics: Basic Theory and Advanced Methods*. Cambridge, UK: Cambridge University Press.

Missong, A., Bol, R., Willbold, S., Siemens, J., and Klumpp, E. (2016). Phosphorous forms in forest soil colloids as revealed by liquid-state P-NMR. *J. Soil Sci. Plant Nutr.* 179, 159–167. doi: 10.1002/jpln.201500119

Missong, A., Holzmann, S., Bol, R., Nischwitz, V., Puhlmann, H., Wilpert, K., et al. (2018). Leaching of natural colloids from forest topsoils and their relevance for phosphorus mobility. *Sci. Tot. Environ.* 634, 305–315. doi: 10.1016/j.scitotenv.2018.03.265

Newman, R. H., and Tate, K. R. (1980). Soil phosphorus characterisation by 31 P Nuclear Magnetic Resonance. *Commun. Soil Sci. Plant Anal.* 11, 835–842. doi: 10.1080/00103628009367083

Ognalaga, M., Frossard, E., and Thomas, F. (1994). Glucose-1-phosphate and myo-inositol hexaphosphate adsorption mechanisms on goethite. *Soil Sci. Soc. Am. J.* 332–337. doi: 10.2136/sssaj1994.03615995005800020011x

Ozboyaci, M., Kokh, D. B., Corni, S., and Wade, R. C. (2016). Modeling and simulation of protein-surface interactions: achievements and challenges. *Q. Rev. Biophys.* 49:e4. doi: 10.1017/S0033583515000256

Pant, H. K., Warman, P. R., and Nowak, J. (1999). Identification of soil organic phosphorus by 31 P Nuclear Magnetic Resonance spectroscopy. *Commun. Soil. Sci. Plant Anal.* 30, 757–772. doi: 10.1080/00103629909370244

Parfitt, R. L., and Atkinson, R. J. (1976). Phosphate adsorption on goethite ($\alpha$-FeOOOH). *Nature* 264, 740–742. doi: 10.1038/264740a0

Senn, H. M., and Thiel, W. (2009). QM/MM methods for biomolecular systems. *Angew. Chem.* 48, 1198–1229. doi: 10.1002/anie.200802019

Strassner, T. (2006). Isotope effects in chemistry and biology. Edited by amnon kohen and hans-heinrich limbach. *Angew. Chem.* 45, 6420–6421. doi: 10.1002/anie.200585384

Tan, K. (2011). *Principles of Soil Chemistry, Fourth Edition*. Books in Soils, Plants, and the Environment. New York, NY: Taylor & Francis.

Torrent, J., Schwertmann, U., and Barron, V. (1992). Fast and slow phosphate sorption by goethite-rich natural materials. *Clays Clay Miner.* 40, 14–21. doi: 10.1346/CCMN.1992.0400103

Tossell, J. A., Vaughan, D. J., and Johnson, K. H. (1973). Electronic structure of ferric iron octahedrally coordinated to oxygen. *Nat. Phys. Sci.* 244, 42–45. doi: 10.1038/physci244042a0

Turner, B. L., Papházy, M. J., Haygarth, P. M., and Mckelvie, I. D. (2002). Inositol phosphates in the environment. *Philos. Trans. R. Soc. B* 357, 449–469. doi: 10.1098/rstb.2001.0837

Vincent, A. G., Vestergren, J., Gröbner, G., Persson, P., Schleucher, J., and Giesler, R. (2013). Soil organic phosphorus transformations in a boreal forest chronosequence. *Plant Soil* 367, 149–162. doi: 10.1007/s11104-013-1731-z

Yan, Y., and Kühn, O. (2010). Geometric correlations and infrared spectrum of adenine-uracil hydrogen bonds in $CDCl_3$ solution. *Phys. Chem. Chem. Phys.* 12, 15695–15703. doi: 10.1039/c0cp00009d

Yan, Y. P., Liu, F., Li, W., Liu, F., Feng, X. H., and Sparks, D. L. (2014). Sorption and desorption characteristics of organic phosphates of different structures on aluminium (oxyhydr)oxides. *Eur. J. Soil Sci.* 65, 308–317. doi: 10.1111/ejss.12119

Zentel, T., and Kühn, O. (2017). Properties of hydrogen bonds in the protic ionic liquid ethylammonium nitrate. *Theor Chem Acc.* 136:87. doi: 10.1007/s00214-017-2119-6

**Conflict of Interest:** The authors declare that the research was conducted in the absence of any commercial or financial relationships that could be construed as a potential conflict of interest.

frontiers in Forests and Global Change

ORIGINAL RESEARCH
published: 19 June 2020
doi: 10.3389/ffgc.2020.00065

# Contrasting Effects of Long-Term Nitrogen Deposition on Plant Phosphorus in a Northern Boreal Forest

*Kristin Palmqvist*[1]*, *Annika Nordin*[2] *and Reiner Giesler*[1,3]

[1] Department of Ecology & Environmental Science, Umeå University, Umeå, Sweden, [2] Department of Forest Genetics and Plant Physiology, Umeå Plant Science Center, Swedish University of Agricultural Sciences, Umeå, Sweden, [3] Department of Ecology & Environmental Science, Climate Impacts Research Centre, Umeå University, Umeå, Sweden

Ecosystem responses of carbon and nitrogen (N) biogeochemistry to N deposition have a high variation across sites. Phosphorus (P), which can interact strongly with N, can be the cause of some of this variation. We quantified plant N and P concentrations and estimated P stocks in aboveground foliage, and soil O-horizon P concentrations and stocks after 18 years in a long-term stand-scale (0.1 ha) N addition experiment [12.5 kg (N1) and 50 kg (N2) N $ha^{-1}$ $year^{-1}$] in a c. 100-years-old boreal spruce [*Picea abies* (L.) Karst] forest. Basal area growth had increased by 65% in the N2 treatment compared to control, along with a higher leaf area index, and lower litter decomposition rates. The higher tree growth occurred during the initial c. 10-years period thereafter resuming to control rates. We hypothesized that increased plant demand for P together with decreased recycling of organic matter in this initially N limited system may have decreased plant-available P, with possible consequences for longer-term biogeochemistry and ecosystem production. However, resin-extractable P did not differ between the three treatments (0.32 kg P $ha^{-1}$), and plant NP ratios and P concentrations and O-horizon P characteristics were similar in the N1 and control treatments. The N2 treatment doubled total P in the O-horizon (100 vs. 54 kg P $ha^{-1}$), explained by an increase in organic P. The N concentration, NP ratio, and spruce needle biomass were higher in N2, while the P stock in current year needles was similar as in the control due to a lower P concentration. In addition to P dilution, increased light competition and/or premature aging may have caused the reduction of N-stimulated growth of the trees. For the dominant understory shrub [*Vaccinium myrtillus* (L.)] no changes in growth was apparent in N2 despite a significantly higher NP ratio compared to control (15 vs. 9, respectively). We therefore conclude that increased NP ratio of vegetation cannot be used as a sole indicator of P limitation. The vegetation and O-horizon changes in N2 were still large enough to merit further studies addressing whether such high N loads may alter ecosystem biogeochemistry toward P limitation. For the lower N addition rate, relevant from an anthropogenic N deposition perspective, we suggest it had no such effect.

**Keywords: boreal forest, nitrogen deposition, phosphorus, soil, spruce (*Picea abies*), understory plants**

OPEN ACCESS

***Edited by:***
*Klaus Kaiser,*
*Martin Luther University Halle-Wittenberg, Germany*

***Reviewed by:***
*Jörg Prietzel,*
*Technical University of Munich, Germany*
*Lukas Kohl,*
*University of Helsinki, Finland*

***Correspondence:**
*Kristin Palmqvist*
*kristin.palmqvist@umu.se*

***Specialty section:***
*This article was submitted to Forest Soils, a section of the journal Frontiers in Forests and Global Change*

***Received:*** *20 February 2020*
***Accepted:*** *05 May 2020*
***Published:*** *19 June 2020*

***Citation:***
*Palmqvist K, Nordin A and Giesler R (2020) Contrasting Effects of Long-Term Nitrogen Deposition on Plant Phosphorus in a Northern Boreal Forest. Front. For. Glob. Change 3:65. doi: 10.3389/ffgc.2020.00065*

## INTRODUCTION

Nitrogen (N) is generally the most limiting nutrient for net primary productivity in boreal forest ecosystems (Binkley and Högberg, 2016; Högberg et al., 2017). If forest growth increases as a result of increasing atmospheric carbon dioxide ($CO_2$) and N deposition, the biogeochemistry of other nutrients may shift, with consequences for further responses to changing environments (Akselsson et al., 2008; From et al., 2016). For instance, the supply of phosphorus (P) could be reduced if growth increases are not matched by increased rates of P turnover (Reich et al., 2006; Peñuelas et al., 2012). Forest monitoring data in Europe documented decreasing P concentrations and increased NP ratios in tree foliage in forest trees, such as beech (*Fagus sylvatica*) and Norway spruce (*Picea abies*) (Braun et al., 2010), and according to Jonard et al. (2015), these changes are most likely caused by anthropogenic environmental changes coupled to $CO_2$ enrichment and N deposition. However, the mechanisms and controls of P nutrition of forest ecosystems remain largely unidentified (Jonard et al., 2015; Lang et al., 2016), and we know little about more long-term ecosystem effects of altered relative supplies of carbon (C), N, and P (Wang et al., 2010). In Scandinavian boreal forests, for instance, fertilization with N generally has little if any effect on the foliar concentrations of other nutrients, even when N is added in doses far above anthropogenic inputs (Jacobson and Pettersson, 2001; Nohrstedt, 2001; Nilsen and Abrahamsen, 2003; Binkley and Högberg, 2016). Therefore, we do not know if, when, and how fast a shift from N to P limitation of an ecosystem may occur (Li et al., 2016), and under which conditions a plant has an imbalanced tissue NP ratio; i.e., causing negative effects on productivity (Binkley and Högberg, 2016).

In a fertilizer experiment of a ∼100-years-old boreal spruce forest in northern Sweden, the relative basal area growth response to annual additions of 50 kg N $ha^{-1}$ $year^{-1}$ peaked after 7 years and gradually leveled off to control rates after 10 years (**Figure S1**; From et al., 2016). This also corresponded to an increased leaf area index (LAI) (**Figure S2**; Palmroth et al., 2019), emphasizing that within tree or needle competition for light (i.e., Tarvainen et al., 2016) and/or stand competition for other minerals, such as P has increased in the N treatment during the experiment, perhaps explaining why the N no longer stimulated tree growth (i.e., From et al., 2016). In the same experiment, aboveground litter input and soil C content in the O-horizon were higher, while soil respiration and litter decomposition were significantly lower in this high-N treatment as compared to the control (Maaroufi et al., 2015, 2016, 2017). To what extent these changes may be linked to a decreased P availability remains, however, unclear. Mobilization, cycling, and retention of P in an ecosystem are dependent on its species and food-web interactions. For instance, plant species differ in their NP ratio optima (Güsewell, 2004) and their abilities to use specific P forms (Turner, 2008), so the strength of a P limitation is thus species dependent. For instance, while boreal forests are mainly N limited (Binkley and Högberg, 2016), their understory plants have been suggested to be co-limited by N and P (Hedwall et al., 2017). There are studies indicating that phosphatase activity may increase in response to elevated N loads (Clarholm and Rosengren-Brink, 1995; Marklein and Houlton, 2012), but it remains uncertain to what extent different species can or even need to match an increased N availability with increased assimilation of P to maintain an unaltered NP stoichiometry. If trees dominate in the system and if they both can and need to maintain a certain NP ratio, these imply a stronger sink for P which may have negative effects for other species, i.e., understory vegetation, in the system. On the other hand, different species in the system are likely to use different P resources through niche separation and be able to store P between seasons and recycle already assimilated P between organs (Tessier and Raynal, 2003; Ahmad-Ramli et al., 2013). In addition, we do not know at what N deposition rate or dosage any P shortage effects will occur or how fast they will appear at the species or ecosystem level (Binkley and Högberg, 2016).

The objective of this study was to explore to what extent long-term N addition had affected plant P availability in a northern boreal forest. We used the above-cited spruce forest experiment in northern Sweden (Nordin et al., 2009; From et al., 2016) exposed to two N addition levels (12.5 and 50 kg N $ha^{-1}$ $year^{-1}$) for almost two decades (1996–2013), where effects on the P biogeochemistry have not been investigated before. We quantified N and P in aboveground foliage (trees, shrubs, grasses, and bryophytes) and P in the O-horizon to approach this question. We focus on the O-horizon in this study since previous studies have shown that major treatment effects on C and N were found there and with no effects in the mineral soil (Maaroufi et al., 2015). More specifically, we hypothesize (i) a buildup of organic P in the O-horizon following earlier observations of increased LAI and litter production and decreased decomposition in the highest N-treatment, and (ii) an increased NP ratio of the vegetation due to increased tissue N concentrations and possibly decreased tissue P concentrations if the plants have not been able to match the increased N availability with increased access to P. We further hypothesize (iii) that an increased plant demand for P should be manifested in a decrease in readily available soil P in the O-horizon where the main part of fine roots are found (Rosling et al., 2003; Maaroufi et al., 2015), e.g., if this demand is met by increased assimilation from the O-horizon.

## METHODS

### Study Site and Experiment

The study was done in a forest stand at Svartberget Experimental Forest (64°14′N, 19°46′E; 220 m a.s.l.) in Vindeln northern Sweden where an artificial N deposition experiment was established in 1996. Short summers and long winters characterize the climate of the region, and snow covers the ground from about the end of October until the beginning of May. Annual mean temperature (1981–2010) is 1.8°C, precipitation 614 mm $year^{-1}$ (Laudon et al., 2013), and background N deposition 1–2 kg N $ha^{-1}$ $year^{-1}$ (Pihl-Karlsson et al., 2009). Background P deposition in the area is 0.09 ± 0.01 kg $ha^{-1}$ $year^{-1}$ [average ± SE between 1995 and 2019 (2008–2013 missing)]; data provided from the Krycklan database (Laudon et al., 2013). The forest

stand where the N addition experiment is conducted grows on a gently sloping moraine and is dominated by 120-years-old Norway spruce [*Picea abies* (L.) H. Karst] (82% of all trees in the stand) with pine [*Pinus sylvestris* (L.)] being second most frequent (15%). From et al. (2016) present a detailed inventory of the trees in the stand. In brief, the forest has been naturally regenerated and has not been intensively managed during the twentieth century, mainly used by nearby farms for fuel and construction wood. During the early decades of the twentieth century, it was also used for summer-grazing cattle. The experiment covers c. 100 ha. The blocks (see below) are distributed over this area to cover the heterogeneity of the terrain with respect to slopes, drier and wetter areas. In 2014, tree heights varied from <10 m and up to 28–29 m, with mean spruce heights being 18–20 m. Tree volume but not tree height has responded to the below described N addition treatments.

The ericaceous dwarf shrub bilberry (*Vaccinium myrtillus* L.) dominates the understory covering 80% of the field layer canopy with lingonberry (*Vaccinium vitis-idaea* L.) amounting to 10% of this layer (Nordin et al., 2009). The grass, *Deschampisa flexuosa* (L.) Trin., is the only frequently occurring graminoid. Herbs are less abundant, and we selected *Maianthemum bifolium* (L.) F. W. Schmidt for this study. This broad-leaved herb is commonly found in this type of forests and is known to respond to differences in N and P availability (Giesler et al., 2002). Two feather mosses, *Hylocomium splendens* (Hedw.) Br. Eur. and *Pleurozium schreberi* (Brid.) Mit., dominate the bottom layer. Soils are podzols and classified as a Typic Haplocryods (Soil Survey Staff, 1992) developed on glacial till. The post-glacial age of the site is between 9,000 and 9,500 years BP, and the highest former shoreline in the Svartberget area is at 255–260 m above present sea level. The mineral soils are rather coarse textured with an average of coarser material exciding >2 mm accounting for 32% of the soil volume (Maaroufi et al., 2015). The fine material (<2 mm) is mainly sandy loam. The organic O-horizon is on average about 0.08 m thick, the average depth in all larger sized plots (see below) ranging from 0.04 to 0.12 m. The mineral soil consists of an about 5 cm thick eluvial E-horizon and an about 20–25-cm-thick illuvial B-horizon overlaying the parent material (C-horizon). The fine root distribution (i.e., mostly <2 mm) in the O-horizon and the upper 20 cm of the mineral soil is distributed as follows: 75% in the O-horizon, 17% in the 0–10 cm mineral soil, and 7% in the 10–20 cm mineral soil (Maaroufi et al., 2015). Selected soil properties for the O-horizon are presented in **Table 1**.

The experiment consists of three levels of N additions: 12.5 kg N $ha^{-1}$ $year^{-1}$ (N1), 50 kg N $ha^{-1}$ $year^{-1}$ (N2), and the control treatment (Control). Two plot sizes (0.1 and 0.25 ha) were randomly laid out in the stand when the experiment started (Strengbom et al., 2002; Nordin et al., 2005). The smaller plots were distributed across six blocks with Control, N1, and N2 treatments, whereas blocks with the larger plot size only have N1 and N2 treatments laid out. The sampling areas for the Control were instead placed at ∼50–100 m distance from the border of these N1 and N2 treatments within each block. The larger plots are used for destructive sampling while the smaller plots are kept intact. The N1 level was chosen to simulate upper level N deposition in the boreal region, while the N2 level is more similar to many other long-term forest fertilizer experiments. The N has been applied spreading solid ammonium nitrate ($NH_4NO_3$) granules directly after snow melt in May (before the start of the vegetation period) each year since the start in 1996. Total N doses when the data of this study were collected in 2013 and 2014 amounted to 225 or 238 for N1 treatments and 900 or 950 kg N $ha^{-1}$ for N2.

## Sampling of Plant Material

Sampling of *V. myrtillus*, *V. vitis-idaea*, *D. flexuosa*, *M. bifolium*, *H. splendens*, and *P. schreberi* was made between June 24 and July 1, 2013. The material was collected from five subplots with an area of 0.12 $m^2$ in each block and treatment plot including control areas. Biomass from the five subplots were pooled, resulting in a single measurement per plot, and dried at 50°C in paper bags for 24 h. *V. myrtillus* was separated in three fractions: current year (C) leaves, C-shoot, and older shoots. For *V. vitis-idaea*, we separated C leaves from the previous year leaves (C + 1) which were pooled with even older leaves if present (C + 2). For the other species, we used all aboveground biomass without separation. *D. flexuosa* was absent in one plot in the N2 treatment, and *M. bifolium* was absent in one plot in the N1 treatment. Spruce needles (C and C + 1) were sampled 8–10 m aboveground from three healthy-looking and representative trees on October 7–10, 2013. Needles from three to five branches around the crown were collected with a top clipper (Skogma, Hammerdal, Sweden). All C and C + 1 needles, respectively, from the three trees were pooled prior to drying at 85°C for 24 h. Please note that needle samples are commonly collected from top branches, so our sample collection may be impaired compared to other studies.

## Soil Sampling and Ion-Exchange Resin Capsules

To measure resin-extractable $NH_4$, $NO_3$, and $PO_4$-P in the field, we installed mixed bed ion-exchange resin capsules (PST1 capsule, Unibest, Bozeman, USA). The ion-exchange resin capsules were placed in the vicinity of the plant collection areas (see above), i.e., in the middle and toward the four corners in the larger treatment plots, and similarly in control areas, on June 19–20, 2013, and collected on August 29, 2013. The capsules were placed a few centimeters down in the O-horizon, but above the mineral soil, without removing the vegetation. After collection, the capsules were placed in a freezer (−18°C) until analyses.

The O-horizon was sampled on September 24, 2013, for soil chemical analyses, and a complementary sampling was done on August 27, 2019, for bulk densities. Three to six humus layer cores were taken randomly with a soil auger (0.10 m diameter) and bulked together in one composite sample in a polyethylene bag. The samples were kept in a cooler during transport to the laboratory and thereafter kept in a refrigerator at 4°C. Within 24 h of collection, the samples were sieved (4-mm mesh) in the laboratory, and a subset of the sieved soil sample was used for determination of the water content in a drying oven (105°C, 24 h) and thereafter organic matter content by loss on ignition (LOI)

**TABLE 1 |** O-horizon soil properties in the three treatments (average ± 1 SE for $n = 6$).

| Variable | Control | 12.5 kg N $ha^{-1}$ $year^{-1}$ | 50 kg N $ha^{-1}$ $year^{-1}$ | *F*-value | *p*-value |
|---|---|---|---|---|---|
| Humus thickness (cm) | 6.7 ± 0.5 | 8.0 ± 1.1 | 8.1 ± 1.1 | 0.688 | 0.518 |
| Bulk density (g $cm^{-3}$) | 0.010 ± 0.005 | 0.089 ± 0.016 | 0.110 ± 0.013 | 0.919 | 0.420 |
| Loss on Ignition (%) | 74.2 ± 3.3 | 72.1 ± 5.7 | 71.6 ± 4.2 | 0.098 | 0.907 |
| pHwater | 4.2 ± 0.05 | 4.3 ± 0.16 | 4.6 ± 0.11 | 3.236 | 0.068 |
| Al (mmol $kg^{-1}$) | 121 ± 81 | 132 ± 28 | 189 ± 34 | 1.298 | 0.302 |
| Fe (mmol $kg^{-1}$) | 209 ± 156 | 349 ± 233 | 134 ± 22 | 0.451 | 0.645 |

in a muffle furnace (550°C, 5 h). Soil pH was determined in a soil suspension (25 ml deionized water and fresh soil equivalent to 1 g of dry soil) after shaking overnight and sedimentation for 1 h before measurement. Within 3 days, P extractions were started using modifications of the Hedley sequential extraction procedure (Hedley et al., 1982; Binkley et al., 2000; Lagerström et al., 2009). Sequential extractions have been widely used to characterize soil P availability in a continuum of increasingly strong extractants under the assumption that the different fractions also reflect differences in P availability (Cross and Schlesinger, 1995). We used the following sequential extraction steps in the Hedley fractionations. In step 1, resin-extractable P was determined using an anion exchange membrane (Saggar et al., 1990; 55164 2S, BDH Laboratory Supplies, Poole, England). In steps 2–4, the following extractants were used sequentially; 0.5 M $NaHCO_3$, 0.2 M NaOH, and 1.0 M HCl. Briefly, we used fresh soil equivalent to 2.0 g dry mass that was added to a 250-ml centrifuge bottle. In step 1, 180 ml deionized water and one 9 × 62 mm anion exchange membrane (hereafter called "resin") were added. The sample was shaken overnight (16 h, 150 rpm), and the following day, the resin strips were removed. The sample was thereafter centrifuged (14,000 g, 15 min, 14,000 rpm, 5°C) after which the supernatant was discarded, and the remaining soil was used in the following steps. The resin was transferred to a bottle and eluted on a shaker (1 h, 150 rpm) with 40 ml NaCl. The eluate was immediately frozen and stored at −20°C until further analysis. This resin-extractable P fraction is hereafter referred to as "Resin P." In the following extraction steps 2–4, the soil remaining from each sequential extraction step was combined with 180 ml of extractant, shaken and centrifuged as above, and the extractant from each step was removed and stored at −20°C before the next step was started. After the final extraction (step 4), the soil remaining was washed with 180 ml of deionized water and shaken for 1 h, centrifuged, and thereafter discarding the supernatant. The soil was oven-dried (60°C, 3 days) and thereafter ground in a ball mill. A 100-mg subsample was combined with 4 ml of concentrated nitric acid ($HNO_3$) and 1 ml of hydrogen peroxide ($H_2O_2$) and digested in a microwave (180°C, 30 min) (MarsXPress, CEM, Germany). This constitutes the "Residual-P" fraction. The first two extraction steps, which involved the resin and extraction with $NaHCO_3$ solution, were designed to extract labile inorganic and organic P fractions. The third step, with NaOH extraction, is assumed to presumably extract Al and Fe surface-bound P, as well as partially stabilized organic P in soil OM. In the fourth step (1.0 M HCl), inorganic P in calcium phosphates, as well as inorganic P occluded within Al and Fe oxides, was assumed to be extracted (Cross and Schlesinger, 1995). The remaining residue fraction extracted mainly recalcitrant P. Additionally, acid-digestible Al and Fe were determined on a subset of the soil using microwave digestion as above. We acknowledge that the Hedley fractionation forms are "operationally defined" and are limited in specifically defining different P forms (see, for instance, Klotzbücher et al., 2019) but still a useful approach in comparative studies like ours to investigate the fate of native P in managed systems as suggested in a review by Negassa and Leinweber (2009).

## Chemical Analyses

The plant material was ball-milled to a fine powder in a steel cylinder, and total C and N was thereafter measured with an Elemental analyzer (Flash EA 2000, Thermo Fisher Scientific, Bremen, Germany) at a certified laboratory (Department of Forest Ecology and Management, Swedish University of Agricultural Sciences, Umeå, Sweden). This laboratory also determined total thallus P concentration after extraction in 8% $H_2SO_4$ using Kjeldahl digestion (G-189-97 Rev. 3 multitest MT7) and thereafter analyzed on a spectrophotometer at 880 nm (Auto Analyzer 3, Omniprocess, Thermo Fisher Scientific). The solutions from the sequential soil extractions were analyzed for molybdate-reactive P using a flow injection analyzer (FIAstarTM 5000 Analyzer, FOSS Analytical AB, Höganäs, Sweden). Total P in the $NaHCO_3$ and NaOH soil solutions and P, Al, and Fe in the digests were determined by inductively-coupled plasma optical-emission spectroscopy (ICP-OES; Varian Vista Ax Pro). Molybdate-reactive P is henceforth abbreviated as "Pi" assuming that the major fraction is $PO_4$-P. Molybdate non-reactive P for the $NaHCO_3$ and NaOH fractions was calculated as the difference between total P determined by ICP-OES and Pi. This fraction is henceforth abbreviated "Po" assuming that the major fraction is organically bound P. The ion-exchange resin capsules were extracted after thawing using three aliquots of 10 ml 1.0 M KCl per capsule (Gundale et al., 2008) and analyzed for $NH_4$ (method G-102-93 Rev. 5 multitest MT7), $NO_3$ (method G-189-97 Rev. 3 multitest MT7), and $PO_4$-P (method G-189-97 Rev. 3 multitest MT7) and quantified on a spectrophotometer at 520 ($NO_3$), 660 ($NH_4$), and 880 ($PO_4$) nm (Auto Analyzer 3, Omniprocess, Thermo Fisher Scientific).

## Estimation of Summed Phosphorus Pools

The trees in the six plus six blocks, including the control plots in the smaller sized blocks, but not in the larger, were examined in more detail in autumn 2014 by measuring tree diameter at breast height (DBH) of all trees and growth rates of sample trees in all plots on the whole 0.1 ha area of the smaller plots and a subsection of 0.1 ha of the larger (From et al., 2016). The DBH data were used to estimate spruce needle biomass (x) for each tree using Equation (1) (Marklund, 1988).

$$x = e\hat{}(-1.9602 + 7.8171 * (\mathrm{DBH}/(\mathrm{DBH} + 12))) \quad (1)$$

The needle biomass was summed for all trees on each 0.1-ha plot area, calculating an average for each treatment with $n = 12$ for N1 and N2 and $n = 6$ for control. Note that Equation (1) was developed for unfertilized spruce in northern Scandinavia and may have required adjustment for N-fertilized trees, as found for Scots pine (Prietzel et al., 2008). However, we did not have access to an adjusted equation for N-fertilized Norway spruce in northern Sweden. Instead, we compared our biomass estimate with data on the relative LAI on three of the blocks with smaller plots from July 2014, presented in **Figure S2**. This comparison did not reveal any significant differences between the treatments.

For estimation of the proportion of needle biomass in C and C + 1 needles, we used the models developed by Flower-Ellis and Mao-Sheng (1987) for northern Sweden and Muukkonen and Lehtonen (2004) for southern Finland, with cohort longevities being 14 and 10 years, respectively. Assuming a constant biomass production of new needles during the last 10–15 years, the proportions of C and C + 1 needles were estimated to be 11.3 and 11.0% in the former model and 17.4 and 17.0% in the latter, respectively. For estimation of the total amount of P invested in the needles, we assumed that all needle cohorts, except for the current year, had the same P concentration as the C + 1 needles. The output from both models is presented in the *Results*; a detailed inventory of cohort longevity has not been made in the stand, but a random collection of branches had up to 10–14 years of living needles (not shown).

Palmroth et al. (2019) developed equations to estimate *V. myrtillus* biomass from pinpoint inventories (Strengbom et al., 2002). A pinpoint inventory of C-leaves, C-shoots, and older shoots was made in early July 2013 in all blocks of the larger size, adding control areas as mentioned before, and biomasses were calculated using these equations. The total amount of P in leaves and shoots was then calculated by multiplying these compartments' P concentration with their respective contribution to the biomass. The aboveground biomass of *D. flexuosa* was taken from Gundale et al. (2014) and for the feathermosses from Gundale et al. (2013). The amount of P in the grass was calculated from its P concentration multiplied by its biomass and similarly for the feathermosses. For the litter, we used both biomass and P concentrations from Maaroufi et al. (2017).

The amount of <4 mm fraction in the humus soil, e.g., in kg soil $ha^{-1}$, was calculated from the dry weight of the <4 mm fraction and the total area sampled. The bulk density was determined from the dry weight and the total soil volume collected (**Table 1**). O-horizon soil P pools were then calculated from soil P concentrations and the amount of dry soil per ha.

## Statistics

The block effect was insignificant so statistical comparisons between the three different treatments (Control, N1, and N2) were analyzed with one-way ANOVA followed by Tukey *post-hoc* test. The analyses were performed using the statistical packages STATISTIX 7 (Analytical Software, Tallahasee, FL, USA). Uncertainties are reported as standard errors of the mean. Significant differences refer to the $P < 0.05$ level unless otherwise stated.

# RESULTS

## Plant Responses

Overall, the tissue N concentration was significantly higher in the N2 treatment compared to control independent of plant species (**Figure 1**, **Table 2**). This was most pronounced in the two mosses, *H. splendens* and *P. schreberi*; the concentrations were about doubled in the N2 treatment. The grass *D. flexuosa* and the herb *M. bifolium* also had a significantly higher N concentration in N2 compared to control; 72 and 38%, respectively. The differences in N concentrations were somewhat less in the spruce needles, and the leaves and shoots of the two *Vaccinium* shrubs (bilberry and lingonberry) between control and N2 ranged between 10 and 26%, in average being 21% higher in N2. In contrast, in the N1 treatment, there was no overall change in tissue N concentrations. The only exception was the moss *P. schreberi* with a significantly higher concentration in N1 compared to control (**Figure 1**, **Table 2**).

The tissue P concentrations ranged from 0.56 to 1.87 mg P $g^{-1}$ in the control, and from 0.45 to 1.23 in N2, and tended to be lower in all species and plant parts in the latter treatment (**Figure 1**). For current-year shoots of bilberry, grass and herb leaves, and the moss *P. schreberi*, this result was significant (one-way ANOVA followed by Tukey multiple comparison). For the remaining plant tissues, except for current-year bilberry leaves, the decreases of P were at a $p < 0.12$ level (**Table 2**). Concentrations for old shoots in bilberry are not shown in **Figure 1** but showed similar responses as for current-year shoots, but with lower P concentrations (0.61, 0.53, and 0.41 mg P $g^{-1}$ for the control, N1, and N2 treatments, respectively). The tissue P concentrations were on average 25% lower in N2 compared to control; the decrease ranged from 18 to 37% across the different species. The grass and the herb were the only cases where P was significantly lower also in the N1 treatment (**Figure 1**). For most of the investigated species, the concentrations were close to or below 1 mg P $g^{-1}$ in the N2 treatment. For the grass and herbs, the concentrations were, however, above 1 mg P $g^{-1}$ in the N2 treatment.

There was a clear and significantly higher NP ratio in all species in the N2 treatment compared to control; from an average NP ratio of about 10 in the control to about 20 in N2 (**Figure 1**). The NP ratio in the N2 treatment ranged from 15 to 27, with the highest value in the grass (**Figure 1**). The higher NP ratio in N2 was overall a combined effect of the higher N concentration and

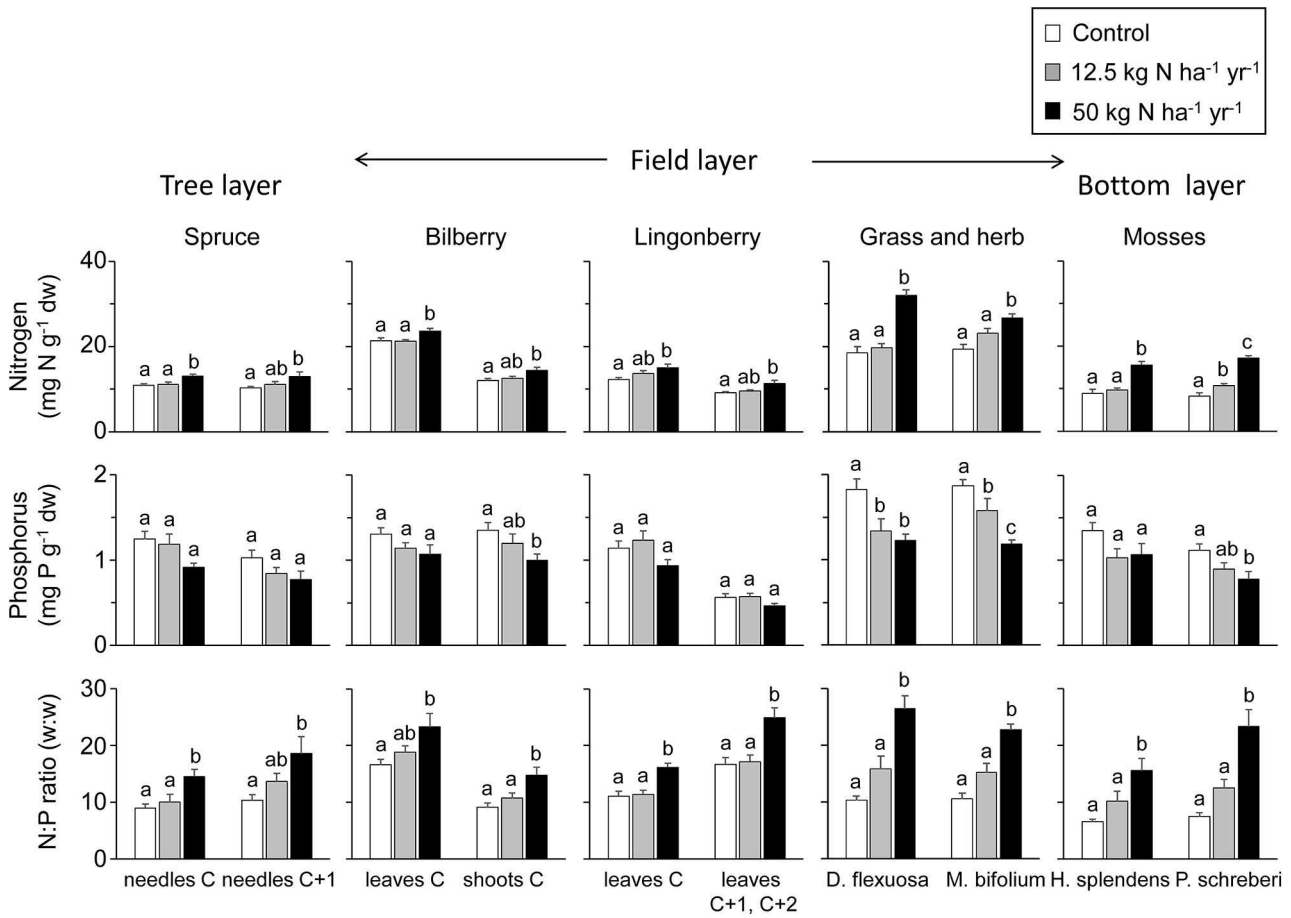


**FIGURE 1 |** Plant and moss nitrogen (N), phosphorus (P), and NP in response to N addition. Mean (+1 SE) N and P concentrations (mg $g^{-1}$), and N:P ratios (w:w) for spruce needles, leaves, shoots, and aboveground plant and moss tissues in the three treatments; control, 12.5 kg N $ha^{-1}$ $year^{-1}$ (N1), and 50 (N2) kg N $ha^{-1}$ $year^{-1}$. Different letters denote significant differences at the $p < 0.05$ level (one-way ANOVA followed by Tukey's multiple comparison of means), $n = 6$ except for the grass which was absent from one of the six N2 treatments, and the herb which was absent from one of the six N1 treatments. C denotes current year leaves or needles, C + 1 or C + 2 is leaves or needles from the preceding one or two vegetation periods.

the lower P concentration in the investigated species (**Figure 1**). In contrast, the N1 treatment did not result in any significant change in plant NP ratio in any of the species (**Figure 1**).

All plants displayed a clear response to the accumulated N dose, also expressed on the community (ecosystem) level (**Figure S3**, **Table S1**). For P, the mean decrease in tissue P concentration was 0.03 mg P $g^{-1}$ per 100 kg N $ha^{-1}$ added, while for N, the mean tissue concentration increased with 0.51 mg N $g^{-1}$ per 100 kg N $ha^{-1}$ added. The mean increase in NP ratio was 1.01 per 100 kg N $ha^{-1}$ added.

## Soil O-Horizon Concentrations

O-horizon N concentrations were far higher in the N2 treatment (**Figure 2**), with a 10-fold increase in resin capsule $NH_4$-N and a 100-fold increase in resin capsule $NO_3$-N compared to control, while no effect was found for the N1 treatment. In contrast to N, the resin capsules detected no effect of N level on $PO_4$-P (**Figure 2**). No treatment effects were found for molybdate-reactive P, independent of extractant, e.g., resin Pi, $NaHCO_3$ Pi, NaOH Pi, and HCl Pi (**Figure 3**, **Table S1**). This was also the case for $NaHCO_3$-extractable Po (**Figure 3A**). The molybdate non-reactive P concentration (NaOH Po) was 2-fold higher in the N2 treatment compared to control (**Figure 3A**). This was also reflected in a significantly higher total P in N2, from about 900 mg P $kg^{-1}$ in the control to about 1,300 mg P mg P $kg^{-1}$ in the N2 treatment, while no effects were found for the N1 treatment (**Table S2**). The average Al and Fe concentrations were 140 and 230 mmol $kg^{-1}$ and did not differ between treatments (**Table 1**). We found a linear relationship between Al and NaOH Po ($r^2 = 0.70$, $p < 0.001$; **Figure S4**) for the control and N1 treatments while three of the six N2 treatments deviated from this relationship (**Figure S4**). No significant relationship was found between NaOH Po and Fe or Al + Fe.

## Aboveground Biomass and Phosphorus Amounts in Plants and in the O-Horizon

Spruce needles comprised the largest aboveground pool of photosynthetic tissue in the forest stand and was estimated to

**TABLE 2 |** The *F*-values, degrees of freedom (df), and *p*-values from analysis of variance (ANOVA) comparing the N concentrations, P concentrations, and NP ratio across the three treatments (0, 12.5, and 50 kg N $ha^{-1}$ $year^{-1}$) in the plant species and plant parts presented in **Figure 1**; $n = 6$ except for the absence of grass in one N2 plot and the herb in one N1 plot.

| | | Nitrogen | | Phosphorus | | NP ratio | |
|---|---|---|---|---|---|---|---|
| **Species** | ***df*** | ***F*** | ***p*-value** | ***F*** | ***p*-value** | ***F*** | ***p*-value** |
| ***P. abies*** | | | | | | | |
| Needles C | 2 | 6.64 | **0.009** | 3.59 | 0.053 | 7.93 | **0.006** |
| Needles C + 1 | 2 | 3.67 | 0.051 | 2.44 | 0.121 | 5.08 | **0.021** |
| ***V. myrtillus*** | | | | | | | |
| Leaves C | 2 | 5.20 | **0.019** | 1.97 | 0.174 | 5.44 | **0.017** |
| Shoot C | 2 | 4.60 | **0.028** | 3.59 | 0.053 | 9.36 | **0.002** |
| Shoot older | 2 | 7.38 | **0.006** | 2.99 | 0.081 | 7.19 | **0.007** |
| ***V. vitis-idaea*** | | | | | | | |
| Leaves C | 2 | 3.62 | 0.052 | 2.84 | 0.090 | 16.58 | **<0.001** |
| Leaves C + 1, C + 2 | 2 | 5.55 | **0.016** | 2.87 | 0.088 | 12.6 | **0.001** |
| *D. flexuosa* | 2 | 36.31 | **<0.001** | 6.94 | **0.008** | 23.42 | **<0.001** |
| *M. bifolium* | 2 | 14.2 | **<0.001** | 18.29 | **<0.001** | 34.62 | **<0.001** |
| *H. splendens* | 2 | 21.73 | **<0.001** | 2.56 | 0.111 | 9.58 | **0.002** |
| *P. schreberi* | 2 | 61.92 | **<0.001** | 4.74 | **0.025** | 20.15 | **<0.001** |

*Bold values denote significant difference at the $p < 0.05$ level. C, current year.*

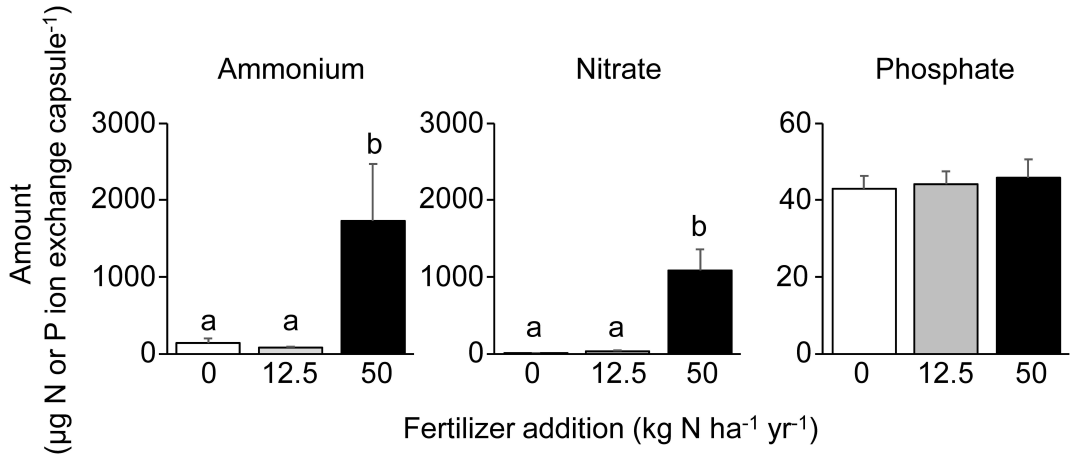


**FIGURE 2 |** Humus layer nitrogen (N) and phosphorus (P) ion concentrations. Relative humus layer (mean + 1 SE) ion concentrations of ammonium, nitrate, and phosphate in ion exchange capsules from the three treatments (0, 12.5 kg N $ha^{-1}$ $year^{-1}$, and 50 kg N $ha^{-1}$ $year^{-1}$; $n = 6$). Values presented on a per-capsule basis after extraction in 30 ml KCl. Different letters denote significant differences at the $p < 0.05$ level (one-way ANOVA followed by Tukey's multiple comparison of means).

be 12.7 and 12.2 Mg $ha^{-1}$ in the control and N1 treatments, respectively, being significantly higher in N2, 16.3 Mg $ha^{-1}$ (**Table 3**). The bilberry biomass was about 1 Mg $ha^{-1}$ in all treatments (**Table 3**). Previous studies have shown a significantly lower moss biomass in both N1 and N2 compared to control (Gundale et al., 2013); based on those observations, the summed biomass of *H. splendens* and *P. schreberi* together amounted to 4.2, 3.3, and 2.0 Mg $ha^{-1}$ in control, N1, and N2, respectively (**Table 3**). The grass had a higher biomass in N2 compared to both N1 and N2 (Gundale et al., 2014), amounting to 44, 110, and 152 kg $ha^{-1}$ in control, N1, and N2, respectively (**Table 3**). The P pool in the spruce needles was similar across treatments ranging from 10.7 to 13.5 kg $ha^{-1}$ with a minor difference between the two estimation methods. The P uptake of current year needles was also similar in the three treatments (**Table 3**), albeit with absolute values being dependent on the adopted model (see *Methods* for details). For bilberry, the estimate was 0.9 for control and 0.6 kg P $ha^{-1}$ for N2, and for the feathermosses 5.1 and 1.7 kg P $ha^{-1}$ in control and N2, respectively (**Table 3**). In the O-horizon, the total P pool was about 40% higher in the N2 treatment as compared to the control (**Table S2**). The higher total humus P content was partly caused by an almost 2-fold higher NaOH Po content in the N2 as compared to the control (**Figure 3B**).

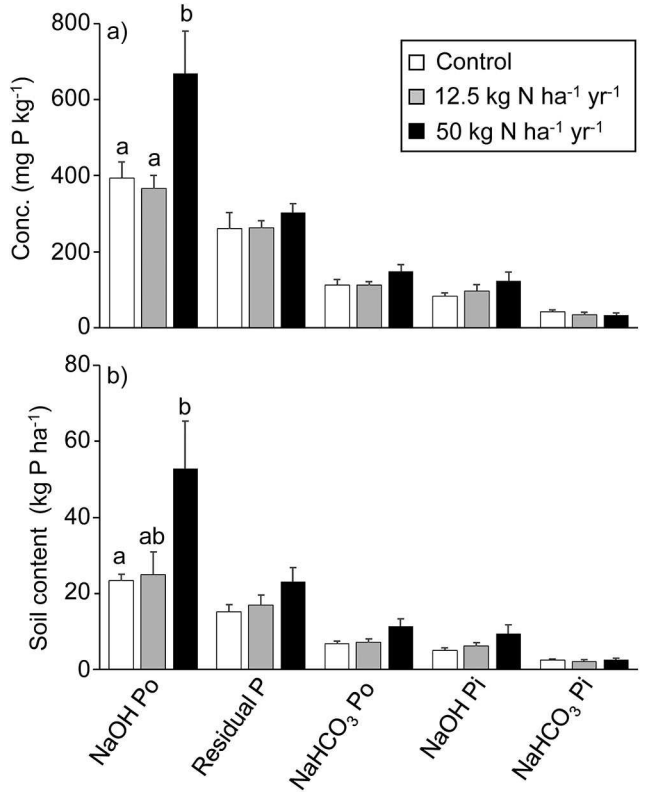


**FIGURE 3 |** Humus layer organic and inorganic phosphorus (P) concentrations. **(A)** Mean humus soil (+1 SE) inorganic ($P_i$) and organic ($P_o$) P concentration (mg P $kg^{-1}$) in different P fractions determined by Hedley P fractionation in the three treatments (0, 12.5 kg N $ha^{-1}$ $year^{-1}$, and 50 kg N $ha^{-1}$ $year^{-1}$; $n = 6$) and **(B)** the contents of the P fractions expressed in kg P $ha^{-1}$. Within each group of three histogram bars, different letters denote significant differences at the $p < 0.05$ level (one-way ANOVA followed by Tukey's multiple comparison of means).

## DISCUSSION

Overall, we found that the long-term addition of 12.5 kg N $ha^{-1}$ $year^{-1}$, which simulates upper-level N deposition across the boreal region, did not cause any detectable changes in NP ratio or P concentration of the vegetation and neither in the N or P concentrations of the O-horizon (**Figures 1–3**; **Tables 2**, **3**). Thus, an accumulated N deposition of 225 kg N $ha^{-1}$ over c. 20 years had not lowered plant P concentrations or increased the NP ratio, giving no support for our three hypotheses or any signs of emerging P limitation. In contrast, and in agreement with our first hypothesis, the higher accumulated N dose of 900 kg $ha^{-1}$ in the 50 kg N $ha^{-1}$ $year^{-1}$ treatment had doubled the total P stock in the O-horizon (100 vs. 54 kg P $ha^{-1}$), mainly explained by an increase in organic P (**Figure 3**, **Table S2**). Further, and in support of our second hypothesis, both the N concentration and the NP ratio was consistently higher in the vegetation, and the P concentration was lower in some species or plant parts, in the N2 treatment compared to control (**Figure 1**, **Table 2**). However, for the O-horizon, we did not find any decrease in P forms assumed easily plant available (**Figure 3**, **Table S2**) in this treatment, thus not supporting our third hypothesis.

### Effects of Nitrogen Additions on O-Horizon Phosphorus

We hypothesized a higher O-horizon P pool in the N2 treatment based on previous findings of higher needle litter P deposition (Maaroufi et al., 2016) and lower litter and O-horizon decomposition rates (Maaroufi et al., 2015, 2017), compared to control. Most of the P present in spruce needles are presumably organically bound as phosphate monoesters and—diesters (Koukola et al., 2006) and would thus contribute to an accumulation of organic P. More recent research also suggests that P mineralization can be driven by the decomposers' need for C (Spohn and Kuzyakov, 2013), so the overall lower rate of decomposition in N2 may thus potentially contribute to an accumulation of organic P, not only in the litter, but also in the O-horizon. While the Hedley fractionation, that we used, does not provide any detailed information on P species, a recent study by Acksel et al. (2019) found a relatively good agreement between $NaHCO_3$ and NaOH extractable Po and organic O determined with $^{31}P$ Nuclear Magnetic Resonance (NMR) spectroscopy. The here obtained proportions between inorganic and organic P also agrees well with O-horizon soils in similar boreal forests in this region of Sweden when $^{31}P$ NMR has been used: The proportion of organic P relative to total NaOH extractable P using $^{31}P$ NMR was 76% (Vincent et al., 2012) and ranged from 53 to 85% in the region (Vincent et al., 2012, 2013). A similar relationship was found here (80 ± 0.5%; mean ± SE) between Po ($NaHCO_3$ + NaOH extractable Po) and total extractable Pi and Po (resin + $NaHCO_3$ + NaOH extractable P). Other mechanisms, such as accumulation of Al and/or Fe could potentially increase organic P in the O-horizon (Giesler et al., 2002), but Al + Fe did not differ between the treatments and does not seem as a likely cause to our observations. Previous findings of increased total C in the O-horizon, decreased respiration, and decreased litter decomposition in the N2 treatment (Maaroufi et al., 2015, 2017) further support our assumption that the increase in NaOH-extractable Po reflects an increase in organic P, despite the uncertainty in the absolute amounts with the method we used.

While the buildup of organic P supports our first hypothesis, there was no reduction in P forms assumed to be more easily available in the O-horizon, such as resin and $HCO_3$-extractable P (**Figure 3**, **Table S2**) (Cross and Schlesinger, 1995), or in the resin capsules (**Figure 1**). These results are only indicative since the fractions are "operationally defined" and plants are likely to access different P forms. Still, the two independent methods we used showed no change in P despite an assumed increased demand in the N2 treatment. Notably, the resin capsules captured the increase in inorganic N in the N2 treatment, suggesting a surplus of N above plant and microbial demand while we see no change in the resin capsule P between the treatments. A previous attempt to understand ecosystem P responses to chronic N addition predicted decreased pools of available P after increased N-driven plant growth (Perring et al., 2008), but this was apparently not reflected in the O-horizon here.

**TABLE 3 |** Biomasses, P pools, and P fluxes of the major aboveground components in the three treatments.

| Component | Unit | Treatment | | |
|---|---|---|---|---|
| | | Control | N1 | N2 |
| ***P. abies*** | | | | |
| Needle biomass | (Mg ha$^{-1}$) | 12.7 | 12.2 | 16.3 |
| P uptake current year needles | (kg ha$^{-1}$ year$^{-1}$) | 1.8 (2.7) | 1.6 (2.5) | 1.7 (2.6) |
| P pool, all needles | (kg ha$^{-1}$) | 13.4 (13.5) | 10.7 (11.0) | 12.8 (12.9) |
| Needle litter P flux | (kg ha$^{-1}$ year$^{-1}$) | 1.0 | 2.6 | 1.8 |
| ***V. myrtillus*** | | | | |
| Aboveground biomass | (Mg ha$^{-1}$) | 1.1 | 1.0 | 1.0 |
| P pool, aboveground biomass | (kg ha$^{-1}$) | 0.9 | 0.7 | 0.6 |
| P, new tissues | (kg ha$^{-1}$ year$^{-1}$) | 0.5 | 0.3 | 0.3 |
| Leaf litter P flux | (kg ha$^{-1}$ year$^{-1}$) | 0.1 | 0.3 | 0.2 |
| ***Grass (D. flexuosa)*** | | | | |
| Aboveground biomass | (kg ha$^{-1}$) | 44 | 110 | 152 |
| P pool, aboveground biomass | (kg ha$^{-1}$) | 0.1 | 0.1 | 0.2 |
| ***P. schreberi and H. splendens*** | | | | |
| Aboveground biomass | (Mg ha$^{-1}$) | 4.2 | 3.3 | 2.0 |
| P pool, mosses | (kg ha$^{-1}$) | 5.1 | 3.1 | 1.7 |
| Moss litter P flux | (kg ha$^{-1}$ year$^{-1}$) | 1.1 | 0.7 | 0.2 |

*P. abies data were calculated using the needle longevity and turnover model from Flower-Ellis and Mao-Sheng (1987) with values in parentheses using the model from Muukkonen and Lehtonen (2004). See Methods for references to original data when not sampled for this study.*

However, several other studies suggest that phosphatase activity can be increased when N availability is increased (Marklein and Houlton, 2012, and references therein), increasing mineralization of organic P to more easily available forms. However, a recent study by Forsmark (2020) at the same experimental site did not find any difference in phosphatase activity between the different treatments in the O-horizon.

Another source of P is the mineral soil; these soils are young in a global perspective (Walker and Syers, 1976) and are thus relatively unweathered. A rough estimate of the total P content in the upper 0.5 m of the mineral soil using total P estimates from a nearby location (Nyänget; Melkerud et al., 2000) and the bulk density estimates for the mineral soil in Maaroufi et al. (2015) gives a total P pool of about 2,300 kg ha$^{-1}$ (bulk density 1.19 g cm$^{-3}$, soil thickness 0.5 m, and total P concentration 0.049 mg P g$^{-1}$ dry soil). Weathering is estimated to release about 0.06 kg P ha$^{-1}$ year$^{-1}$ (regional data from the Swedish Forest Soil Inventory; https://www.slu.se/en/markinventeringen). Trees in association with mycorrhizal fungi may also directly affect the release of P by biologically mediated weathering (Finlay et al., 2020), and this is not accounted for in the above estimate. For instance, the highest root tip density in a nearby podsol profile was found in the O-horizon, and there was a marked increase of root tips in the B-horizon (Rosling et al., 2003). These root tips are largely colonized with ectomycorrhizal fungi, and many of the fungal taxa found are restricted to the mineral soil (Rosling et al., 2003). It remains unclear what their function is, but we know that soil fungi can promote weathering release of P (Rosling et al., 2007) and may thus benefit tree P uptake. Also, enzymatic degradation of sorbed organic P is not necessarily restricted by P sorption (Olsson et al., 2012), an important P form in the mineral B-horizon (Wood et al., 1984). Altogether, at least trees with their deeper rooting depths have access to a large source of P in addition to the more biologically active O-horizon.

## Spruce Tree Responses

Despite the similar access to easily available P in the O-horizon in all the three treatments, the lower P concentration and higher NP ratio of the last 2 years of spruce needle cohorts in the N2 treatment emphasize that the trees had not matched the higher N concentration of the needles with more P to maintain a similar NP ratio as the untreated trees (**Figure 1**). The spruce needle biomass was calculated to be 30% higher in N2 compared to control, while the estimated total P amount in the needle biomass was similar in N2 and control due to the lower P concentration in the former (**Table 3**). Since we do not have any P data for the older needles and no detailed inventory of needle cohorts, this estimate must, however, be regarded with some caution. Nevertheless, if our estimate is correct, P assimilation on the whole tree/stand level seems to be similar in the N2 and control treatments. The additional P required to maintain a similar NP ratio in N2 as in the control amounts to ∼4 kg P ha$^{-1}$ (i.e., a ratio of c. 10, a higher P concentration to match the higher N, and 30% more needle biomass). This is a relatively small amount if we assume that plant-available P not only includes resin and $HCO_3$-extractable P which was about 14 kg P ha$^{-1}$ in the O-horizon (**Table S2**), but also the additional P in the mineral soil as discussed above, although we lack information regarding the ectomycorrhizal responses to the additional N.

The N concentration of the last two cohorts of spruce needles in N2 was c. 13 mg g$^{-1}$ (**Figure 1**), which is similar to previous data from the experiment after fewer years of treatments (Gundale et al., 2014). Maaroufi et al. (2016) found that spruce needle litter had lower N concentration than living needles in

the N2 treatment and concluded that the trees had resorbed N prior to shedding. Litter was then collected every month except during the snow-covered period to as far as possible avoid leaching of N between felling and retrieval (Maaroufi et al., 2016). However, litterfall in Norway spruce is distributed uniformly over the year (Muukkonen and Lehtonen, 2004), so some leaching of N may still have occurred during the winter. While it might be expected that P would also be resorbed with an increased demand, this is not indicated by available data. Maaroufi et al. (2016) found that needle litter P concentrations were not significantly different between the three treatments and even higher in the N2 treatment (1.2 mg $g^{-1}$) compared to the living needles in our study (0.9 mg $g^{-1}$). However, given that there was a large between-plot variation in the needle litter P concentrations (Maaroufi et al., 2016), and that needle litter mainly reflects cohorts older than 2–3 years (Muukkonen and Lehtonen, 2004), more definite conclusions are difficult to make. There are, however, no indications of any large differences in P resorption from the needles prior to their shedding in the different treatments.

Still, while the soil N data are consistent with the observed differences in plant N concentration between the three treatments, the available soil P cannot satisfactorily explain why the plants showed signs of decreased P concentration in N2. An alternative explanation may instead be that in these very N limited forest ecosystems, plants are functionally better adapted to conserve N, while mechanisms to match an extreme increase in N availability are not met by increased P assimilation and/or storage/resorption. While we cannot rule out that the forest subjected to the N2 treatment in our experiment is moving toward P-limited conditions, other limiting factors, such as increased within needle, twig, or tree self-shading (Tarvainen et al., 2016) and/or faster aging of the fertilized trees (From et al., 2016) may be equally important to explain why the trees have gradually resumed control rates of growth over the last 10 years. Hence, even if we add P in the N2 treatment, it is not clear if this can override such limitations, albeit, this is yet to be tested.

## Understory Responses

Bilberry is the dominating perennial shrub of the understory in this forest stand, both in terms of biomass and gross C assimilation (**Table 3**) (Gundale et al., 2014; Palmroth et al., 2019). The higher NP ratio of all three compartments of bilberry in the N2 treatment compared to control may indicate an emerging P shortage or P limitation of this species. However, the previously reported negative effects of the chronic N addition for bilberry during the first 10–12 years, summarized in Nordin et al. (2009), are no longer present, and yearly fluctuations in bilberry leaf biomass between 2007 and 2013 follow the same trends in all three treatments (Palmroth et al., 2019), suggesting no between-treatment difference in growth limitations. In addition, bilberry leaf litter had the same P concentration in all three treatments (Maaroufi et al., 2016) and was similar to the P concentration of the living leaves reported here, suggesting that P resorption to overwintering organs was low or not present in any of the three treatments.

The highest NP ratio of the understory plants was found in *D. flexuosa*, also having a 30% lower P concentration in N2 compared to control (**Figure 1**, **Table 2**). The grass expanded both in the N1 and the N2 treatments during the initial years of the experiment being a combined effect of parasitic attacks to bilberry, increasing light availability for the grass, and the increased availability of N *per se* (Nordin et al., 2009). During recent years, the difference in grass biomass between the treatments is still present, and there are no obvious signs of decreased growth since, and as for bilberry, yearly fluctuations in leaf biomass follow the same pattern in all three treatments (Palmroth et al., 2019). In general, there can be a large variation in NP ratio both within and between plants (Güsewell, 2004). For instance, in northern boreal forests, the same species of understory plants can differ 4-fold in NP ratio in forest types that we would still classify as typically N limited based on field layer vegetation (Giesler et al., 2002). The variation in NP ratios between different treatments for both the grass and the herb in this study (**Figure 1**) may therefore fall within a range not necessarily affecting their growth. So even if the increased NP ratios indicate a shift toward P limitation, this was not expressed as decreased growth. Moreover, photosynthetic capacities of the grass and the two *Vaccinium* shrubs have not been negatively affected by the N2 treatment (Palmroth et al., 2019), further supporting the apparent absence of emerging P limitation of the understory.

We sampled the two feathermosses, *H. splendens* and *P. schreberi*, that dominated the bottom layer of the forest when the experiment started and still do so in the control. While the former decreased significantly both in the N1 and the N2 treatments during the first 5–6 years of the experiment, the latter has similar cover and growth rate in all three treatments (Nordin et al., 2005, 2009; Gundale et al., 2013). Similar to the understory plants, the lower P concentration of *P. schreberi* in the N2 treatment (**Figure 1**) thus does not seem to be growth limiting.

# CONCLUSION

Following nearly two decades of N additions in the range of atmospheric N deposition for Europe, we found no responses indicating P limitation of tree or understory growth. However, the more extreme N addition with a total load of nearly a ton at the time of our study had increased plant NP ratios while the trees' P assimilation rate remained similar as in the control. Despite the increased NP ratio of both understory and overstory, signs of reduced growth were absent in the former and difficult to interpret in the latter. The relaxation of the trees' initial increased growth in response to the additional N may equally well be explained by increased competition for light and/or faster aging, as discussed by From et al. (2016) and not by a shortage of P. We therefore conclude that increases in NP ratio following increased N availability may not be used as a sole indicator of emerging P limitation of neither understory nor overstory vegetation. We cannot explain why P assimilation rates were not increased in the N2 treatment to match the increased assimilation of N, since access to available P in the O-horizon appeared to be higher than

demand. Additional P may further be provided from the mineral soil, and trees may have access to more P than operationally defined as labile (Richardson and Simpson, 2009). This result is intriguing, raising the question to what extent these boreal plants need or even can assimilate more P to match an increased N uptake, and whether P limitation of growth may eventually emerge. To elucidate this, further research would be needed and should include P additions to part of the plots.

## DATA AVAILABILITY STATEMENT

The datasets generated for this study are available on request to the corresponding author.

## AUTHOR CONTRIBUTIONS

KP, AN, and RG contributed to conceive the study, performed the research, analyzed the data, and wrote the paper.

## FUNDING

This project was part of a joint research program founded by FORMAS (grant 2010-00067) between the Swedish University of Agricultural Sciences and Umeå University on Sustainable Management of Carbon and Nitrogen in Future Forests and also funded by the Swedish Research Council (VR; 2019-03510) to RG.

## ACKNOWLEDGMENTS

The authors thank Ann Sehlstedt and Anneli Lundmark for help in the field and the lab, Sari Palmroth and Nadia Maaroufi for providing original data, and Dan Binkley for valuable comments on a previous version of the manuscript. The authors were grateful to the Unit for Field-based Forest Research, the Swedish University of Agricultural Sciences, in Vindeln for support in the field and for providing the tree database. We also thank one of the reviewers for helpful comments and suggestions for improvements of the previous version of the manuscript.

## SUPPLEMENTARY MATERIAL

The Supplementary Material for this article can be found online at: https://www.frontiersin.org/articles/10.3389/ffgc.2020.00065/full#supplementary-material

## REFERENCES

Acksel, A., Baumann, K., Hu, Y., and Leinweber, P. (2019). A look into the past: tracing ancient sustainable manuring practices by thorough P speciation of Northern European. *Soil Syst.* 3:72. doi: 10.3390/soilsystems3040072

Ahmad-Ramli, M. F., Cornulier, T., and Johnson, D. (2013). Partitioning of soil phosphorus regulates competition between Vaccinium vitis-idaea and *Deschampsia cespitosa*. *Ecol. Evol.* 3, 4243–4252. doi: 10.1002/ece3.771

Akselsson, C., Westling, O., Alveteg, M., Thelin, G., Fransson, A.-M., and Hellsten, S. (2008). The influence of N load and harvest intensity on the risk of P limitation in Swedish forest soils. *Sci. Total Environ.* 404, 284–289. doi: 10.1016/j.scitotenv.2007.11.017

Binkley, D., Giardina, C., and Bashkin, M.A. (2000). Soil phosphorus pools and supply under the influence of Eucaluptus saligna and nitrogen-fixing Albizia facaltaria. *For. Ecol. Manage.* 128, 241–247. doi: 10.1016/S0378-1127(99)00138-3

Binkley, D., and Högberg, P. (2016). Tamm review: Revisiting the influence of nitrogen deposition on Swedish forests. *For. Ecol. Manage.* 368, 222–239. doi: 10.1016/j.foreco.2016.02.035

Braun, S., Thomas, V. F. D., Quiring, R., and Flückiger, W. (2010). Does nitrogen deposition increase forest production? The role of phosphorus. *Environ. Pollut.* 158, 2043–2052. doi: 10.1016/j.envpol.2009.11.030

Clarholm, M., and Rosengren-Brink, U. (1995). Phosphorus and nitrogen fertilization of a Norway spruce forest-effects on needle concentrations and acid phosphatase activity in the humus layer. *Plant Soil* 175, 239–249.

Cross, A. F., and Schlesinger, W. H. (1995). A literature-review and evaluation of the Hedley fractionation-applications to the biogeochemical cycle of soil-phosphorus in natural ecosystems. *Geoderma* 64, 197–214. doi: 10.1016/0016-7061(94)00023-4

Finlay, R. D., Mahmood, S., Rosenstock, N., Bolou-Bi, W. B., Köhler, S. J., Fahad, Z., et al. (2020). Reviews and syntheses: Biological weathering and its consequences at different spatial levels–from nanoscale to global scale. *Biogeosciences* 17, 1507–1533. doi: 10.5194/bg-17-1507-2020

Flower-Ellis, J.G.K., and Mao-Sheng, Y. (1987). Vertical and cohort life-tables for needles of Norway spruce from northern Sweden. Sver. Lantbruksuniv. Inst. Skogsekol. *Skoglig Marklara Rapp*. 57, 1–24.

Forsmark, B. (2020). *Impact of nitrogen deposition on carbon stocks in coniferous forest soils* (Doctoral thesis), Sveriges lantbruksuniv., Acta Universitatis Agriculturae Sueciae.

From, F., Lundmark, T., Morling, T., Pommerening, A., and Nordin, A. (2016). Effects of simulated long-term N deposition on *Picea abies* and *Pinus sylvestris* growth in boreal forest. *Can. J. For. Res.* 46, 1396–1403. doi: 10.1139/cjfr-2016-0201

Giesler, R., Petersson, T., and Högberg, P. (2002). Phosphorus limitation in boreal forests: effects of aluminum and iron accumulation in the humus layer. *Ecosystems* 5, 300–314. doi: 10.1007/s10021-001-0073-5

Gundale, M., Sutherland, S., and DeLuca, T. H. (2008). Fire, native species, and soil resource interactions influence the spatio-temporal invasion pattern of *Bromus tectorum*. *Ecography* 31, 201–210. doi: 10.1111/j.0906-7590.2008.5303.x

Gundale, M.J., Bach, L.H., and Nordin, A. (2013). The impact of simulated chronic nitrogen deposition on the biomass and $N_2$-fixation activity of two boreal feather moss-cyanobacteria associations. *Biol Lett.* 9:20130797. doi: 10.1098/rsbl.2013.0797

Gundale, M.J., From, F., Bach, L., and Nordin, A. (2014). Anthropogenic nitrogen deposition in boreal forests has a minor impact on the global carbon cycle. *Glob. Change Biol.* 20, 276–286. doi: 10.1111/gcb.12422

Güsewell, S. (2004). N:P ratios in terrestrial plants: variation and functional significance. Tansley review. *New Phytol.* 164, 243–266. doi: 10.1111/j.1469-8137.2004.01192.x

Hedley, M. J., Stewart, J. W. B., and Chauhan, B. S. (1982). Changes in inorganic and organic phosphorus fractions induced by cultivation practices and by laboratory incubation. *Soil Sci. Soc. Am. J.* 46, 970–976. doi: 10.2136/sssaj1982.03615995004600050017x

Hedwall, P. O., Bergh, J., and Brunet, J. (2017). Phosphorus and nitrogen co-limitation of forest ground vegetation under elevated anthropogenic nitrogen deposition. *Oecologia* 185, 317–326. doi: 10.1007/s00442-017-3945-x

Högberg, P., Näsholm, T., Franklin, O., and Högberg, M. (2017). Tamm review: on the nature of the nitrogen limitation to plant growth in Fennoscandian boreal forests. *For. Ecol. Manage.* 403, 161–185. doi: 10.1016/j.foreco.2017.04.045

Jacobson, S., and Pettersson, F. (2001). Growth responses following nitrogen and N-P-K-Mg additions to previously N fertilized Scots pine and Norway spruce stands on mineral soils in Sweden. *Can. J. Forest. Res.* 31, 899–909. doi: 10.1139/x01-020

Jonard, M., Fürst, A., Verstraeten, A., Thimonier, A., Timmermann, V., Potocic, N., et al. (2015). Tree mineral nutrition is deteriorating in Europé. *Glob. Change Biol.* 21, 418–430. doi: 10.1111/gcb.12657

Klotzbücher, A., Kaiser, K., Klotzbucher, T., Wolff, M., and Mikutta, R. (2019). Testing mechanisms underlying the Hedley sequential phosphorus extraction of soils. *J. Plant Nutr. Soil Sci.* 82, 570–577. doi: 10.1002/jpln.201800652

Koukola, O., Novák, F., Hrabal, R., and Vosátka, M. (2006). Saprotrophic fungi transform organic phosphorus from spruce needle litter. *Soil Biol. Biochem.* 38, 12, 3372–3379. doi: 10.1016/j.soilbio.2006.05.007

Lagerström, A., Esberg, C., Wardle, D. A., and Giesler, R. (2009). Soil phosphorus and microbial response to a long-term wildfire chronosequence in northern Sweden. *Biogeochemistry* 95, 199–213. doi: 10.1007/s10533-009-9331-y

Lang, F., Bauhus, J., Frossard, E., George, E., Kaiser, K., Kaupenjohann, M., et al. (2016). Phosphorus in forest ecosystems: new insights from an ecosystem nutrition perspective. *J. Plant Nutr. Soil Sci.* 179, 129–135. doi: 10.1002/jpln.201500541

Laudon, H., Taberman, I., Agren, A., Futter, M., Ottosson-Lofvenius, M., and Bishop, K. (2013). The Krycklan Catchment Study–a flagship infrastructure for hydrology, biogeochemistry, and climate research in the boreal landscape. *Water Resour. Res.* 49, 7154–7158. doi: 10.1002/wrcr.20520

Li, Y., Niu, S., and Yu, G. (2016). Aggravated phosphorus limitation on biomass production under increasing nitrogen loading: a meta-analysis. *Glob. Change Biol.* 22, 934–943. doi: 10.1111/gcb.13125

Maaroufi, N. I., Nordin, A., Hasselquist, N. J., Bach, L. H., Palmqvist, K., and Gundale, M. J. (2015). Anthropogenic nitrogen deposition enhances carbon sequestration in boreal soils. *Glob. Change Biol.* 21, 3169–3180. doi: 10.1111/gcb.12904

Maaroufi, N. I., Nordin, A., Palmqvist, K., and Gundale, M. J. (2016). Chronic nitrogen deposition has a minor effect on the quantity and quality of aboveground litter in a boreal forest. *PLoS ONE* 11:e0162086. doi: 10.1371/journal.pone.0162086

Maaroufi, N. I., Nordin, A., Palmqvist, K., and Gundale, M. J. (2017). Nitrogen enrichment impacts on boreal litter decomposition are driven by changes in soil microbiota rather than litter quality. *Sci. Rep.* 7:4083. doi: 10.1038/s41598-017-04523-w

Marklein, A. R., and Houlton, B. Z. (2012). Nitrogen inputs accelerate phosphorus cycling rates across a wide variety of terrestrial ecosystems. *New Phytol.* 193, 696–704. doi: 10.1111/j.1469-8137.2011.03967.x

Marklund, L. G. (1988). Biomass functions for Scots pine, Norway spruce and birch (*Betula verrucosa B. pendula* and *B. pubescens*) in Sweden. *Rapport Inst. Skogstaxer. Sveriges Lantbruksuniv.* 73, 1–70.

Melkerud, P-A., Bain, D., Jongmans, A. G., and Kareinen, T. (2000). Chemical and mineralogical properties of three podzol profiles developed on till, fine-grained watersorted material and badly sorted outwash sand. *Geoderma* 94, 123–146.

Muukkonen, P., and Lehtonen, A. (2004). Needle and branch biomass turnover rates of Norway spruce (*Picea abies*). *Can. J. Forest Res.* 34, 2517–2527. doi: 10.1139/X04-133

Negassa, W., and Leinweber, P. (2009). How does the Hedley sequential phosphorus fractionation reflect impacts of land use and management on soil phosphorus: a review. *J. Plant Nutr. Soil Sci.* 172, 305–325. doi: 10.1002/jpln.200800223

Nilsen, P., and Abrahamsen, G. (2003). Scots pine and Norway spruce stands responses to annual N, P and Mg fertilization. *For. Ecol. Manage.* 174, 221–232. doi: 10.1016/S0378-1127(02)00024-5

Nohrstedt, H. Ö. (2001). Response of coniferous forest ecosystems on mineral soils to nutrient additions: a review of Swedish experiences. *Scand. J. For. Res.* 16, 555–573. doi: 10.1080/02827580152699385

Nordin, A., Strengbom, J., Forsum, A., and Ericson, L. (2009). Complex biotic interactions drive long-term vegetation change in a nitrogen enriched boreal forest. *Ecosystems* 12, 1204–1211. doi: 10.1007/s10021-009-9287-8

Nordin, A., Strengbom, J., Witzell, J., Näsholm, T., and Ericson, L. (2005). Nitrogen deposition and the biodiversity of boreal forests: implications for the nitrogen critical load. *Ambio* 34, 20–24. doi: 10.1639/0044-7447(2005)034[0020:NDATBO]2.0.CO;2

Olsson, R., Giesler, R., Loring, J. S., and Persson, P. (2012). Enzymatic hydrolysis of organic phosphates adsorbed on mineral surfaces. *Environ. Sci. Technol.* 46, 285–291. doi: 10.1021/es2028422

Palmroth, S., Bach, L. H., Lindh, M., Kolari, P., Nordin, A., and Palmqvist, K. (2019). Nitrogen supply and other controls of carbon uptake of understory vegetation in a boreal *Picea abies* forest. *Agric. For. Meterol.* 276:107620. doi: 10.1016/j.agrformet.2019.107620

Peñuelas, J., Sardans, J., Rivas-Ubach, A., and Janssens, A. I. (2012). The human-induced imbalance between C, N and P in Earth's life system. *Glob. Change Biol.* 18, 3–6. doi: 10.1111/j.1365-2486.2011.02568.x

Perring, M P., Hedin, L. O., Levin, S. A., and McGroddy, M., de Mazancourt, C. (2008). Increased plant growth from nitrogen addition should conserve phosphorus in terrestrial ecosystems. *Proc. Natl. Acad. Sci. U.S.A.* 105, 1971–1976. doi: 10.1073/pnas.0711618105

Pihl-Karlsson, G., Akselsson, C., Hellsten, S., Karlsson, P., and Malm, G. (2009). *Övervakning av luftföroreningar i norra Sverige—mätningar och modellering.* Report B1851. Stockholm: IVL Swedish Environmental Research Institute.

Prietzel, J., Rehfuess, K. E., Stetter, U., and Pretzsch, H. (2008). Changes of soil chemistry, stand nutrition, and stand growth at two Scots pine (*Pinus sylvestris* L.) sites in Central Europe during 40 years after fertilization, liming, and lupine introduction. *Eur. J. For. Res.* 127, 43–61. doi: 10.1007/s10342-007-0181-7

Reich, P. B., Hungate, B. A., and Luo, Y. (2006). Carbon-nitrogen interactions in terrestrial ecosystems in response to rising atmospheric carbon dioxide. *Ann. Rev. Ecol. Evol. Syst.* 17, 611–626. doi: 10.1146/annurev.ecolsys.37.091305.110039

Richardson, A. E., and Simpson, R. J. (2009). Soil microorganisms mediating phosphorus availability. *Plant Phys.* 156, 989–996. doi: 10.1104/pp.111.175448

Rosling, A., Landeweert, R., Lindahl, B. D., Larsson, K.-H., Kuyper, T. W., Taylor, A. F. S., et al. (2003). Vertical distribution of ectomycorrhizal fungal taxa in a podzol soil profile. *New Phytol.* 159, 775–783. doi: 10.1046/j.1469-8137.2003.00829.x

Rosling, A., Suttle, K. B., Johansson, E., Van Hees, P. A. W., and Banfield, J. F. (2007). Phosphorous availability influences the dissolution of apatite by soil fungi. *Geobiology* 5, 265–280. doi: 10.1111/j.1472-4669.2007.00107.x

Saggar, S., Hedley, M. J., and White, R. E. (1990). A simplified resin membrane technique for extracting phosphorus from soils. *Fertil. Res.* 24, 173–180. doi: 10.1007/BF01073586

Soil Survey Staff (1992). *Keys to Soil Taxonomy. 5th Edn.* SMSS Technical Monograph No. 19. Blacksburg, VA: Pocahontas Press.

Spohn, M., and Kuzyakov, Y. (2013). Phosphorus mineralization can be driven by microbial need for carbon. *Soil Biol. Biochem.* 61, 69–75. doi: 10.1016/j.soilbio.2013.02.013

Strengbom, J., Nordin, A., Näsholm, T., and Ericson, L. (2002). Parasitic fungus mediates change in nitrogen-exposed boreal forest vegetation. *J. Ecol.* 90, 61–67. doi: 10.1046/j.0022-0477.2001.00629.x

Tarvainen, L., Lutz, M., Räntfors, M., Näsholm, T., and Wallin, G. (2016). Increased needle nitrogen contents did not improve shoot photosynthetic performance of mature nitrogen-poor scots pine trees. *Front. Plant Sci.* 7:1041. doi: 10.3389/fpls.2016.01051

Tessier, J. T., and Raynal, D. J. (2003). Vernal nitrogen and phosphorus retention by forest understory vegetation and soil microbes. *Plant Soil* 256, 443–453, doi: 10.1023/A:1026163313038

Turner, B.L. (2008). Resource partitioning for soil phosphorus: a hypothesis. *J. Ecol.* 96, 698–702. doi: 10.1111/j.1365-2745.2008.01384.x

Vincent, A. G., Schleucher, J., Gröbner, G., Vestergren, J., Persson, P., Jansson, M., et al. (2012). Changes in organic phosphorus composition in boreal forest humus soils: the role of iron and aluminium. *Biogeochemistry* 108, 485–499. doi: 10.1007/s10533-011-9612-0

Vincent, A. G., Vestergren, J., Gröbner, G., Persson, P., Schleucher, J., and Giesler, R. (2013). Soil organic phosphorus transformations in a boreal forest chronosequence. *Plant Soil* 367, 149–162. doi: 10.1007/s11104-013-1731-z

Walker, T. W., and Syers, J. K. (1976). The fate of phosphorus during pedogenesis. *Geoderma* 15, 1–19. doi: 10.1016/0016-7061(76)90066-5

Wang, Y. P., Law, R. M., and Pak, B. (2010). A global model of carbon, nitrogen and phosphorus cycles for the terrestrial biosphere. *Biogeosciences* 7, 2261–2282. doi: 10.5194/bg-7-2261-2010

Wood, T., Bormann, F. H., and Voigt, G. K. (1984). Phosphorus cycling in a northern hardwood forest: biological and chemical control. *Science* 223, 341–393. doi: 10.1126/science.223.4634.391

**Conflict of Interest:** The authors declare that the research was conducted in the absence of any commercial or financial relationships that could be construed as a potential conflict of interest.

frontiers in Forests and Global Change

ORIGINAL RESEARCH
published: 24 June 2020
doi: 10.3389/ffgc.2020.00077

# Only Minor Changes in the Soil Microbiome of a Sub-alpine Forest After 20 Years of Moderately Increased Nitrogen Loads

*Beat Frey*[1]*, *Monique Carnol*[2], *Alexander Dharmarajah*[1], *Ivano Brunner*[1] and *Patrick Schleppi*[1]

[1] Forest Soils and Biogeochemistry, Swiss Federal Research Institute WSL, Birmensdorf, Switzerland, [2] Laboratory of Plant and Microbial Ecology, InBioS, University of Liège, Liège, Belgium

OPEN ACCESS

**Edited by:**
Klaus Kaiser,
Martin Luther University
Halle-Wittenberg, Germany

**Reviewed by:**
Chao Wang,
Institute of Applied Ecology
(CAS), China
Nadia Maaroufi,
University of Bern, Switzerland

***Correspondence:**
Beat Frey
beat.frey@wsl.ch

**Specialty section:**
This article was submitted to
Forest Soils,
a section of the journal
Frontiers in Forests and Global
Change

**Received:** 09 March 2020
**Accepted:** 22 May 2020
**Published:** 24 June 2020

**Citation:**
Frey B, Carnol M, Dharmarajah A,
Brunner I and Schleppi P (2020) Only
Minor Changes in the Soil Microbiome
of a Sub-alpine Forest After 20 Years
of Moderately Increased Nitrogen
Loads. Front. For. Glob. Change 3:77.
doi: 10.3389/ffgc.2020.00077

Soil appears to play a key role in the response of the forest ecosystems to N deposition. Twenty years of experimental moderate N addition in a sub-alpine forest increased nitrate leaching, but the soil immobilized most of the N input, gradually decreasing the C:N ratio. Exchangeable and microbial N were only slightly affected, but denitrification and $N_2O$ production were increased and soil respiration tended to be reduced while soil microbial communities were remarkably resistant. It is assumed that these changes at the process level are related to the soil microbiome, but soil microbial communities have not been assessed so far at lower taxonomical resolution in this long-term experiment. The aim of this study is to understand the underlying causes of the results obtained so far by assessing how N treatment affects the soil microbiome at different soil depths. We analyzed bacterial and fungal diversity and community structures using Illumina MiSeq sequencing and quantified the responses of the N cycling communities to elevated N loads by quantitative PCR. The microbial functions were assessed by respiration, N mineralization, and potential nitrification. Bacterial and fungal α-diversity, observed richness and Shannon diversity index, remained unchanged upon N addition. Multivariate statistics showed shifts in the structures of fungal but not bacterial communities with N load, while the changes were minor. Differences in the community compositions associated with the N treatment were mainly observed at a lower taxonomical level. We found several fungal OTUs in particular genera such as the ectomycorrhizal fungi *Hydnum*, *Piloderma*, *Amanita*, and *Tricholoma* that decreased significantly with increased N-loads. We conclude that long-term moderate N addition at this forest site did not strongly affect the soil microbiome (which remained remarkably resistant) and its functioning.

**Keywords: forest ecosystems, nitrogen, ecosystem functioning, soil microbiome, Illumina MiSeq sequencing, fungal communities, FUNGuild**

## INTRODUCTION

As a result of human activities, forests are exposed to unprecedented levels of N inputs (Bobbink et al., 2010; Schmitz et al., 2019). Biologically reactive N is mainly emitted by fossil fuel combustion or intensification of agriculture, leading to atmospheric deposition over all types of ecosystems even at long distance from sources (Galloway et al., 2008; Simpson et al., 2014). Because N is a key element in ecosystem processes (Nadelhoffer et al., 1999; Galloway et al., 2004), the effects of increased N loads on temperate forests have been intensively studied over the last three decades (e.g., Dise and Wright, 1995; Bredemeier et al., 1998; Emmett et al., 1998; Aber, 2002).

In temperate and boreal forests, reactive N inputs have been shown to alter tree growth and understory biomass, sometimes positively, sometimes negatively, depending on the N status, and other site factors (Solberg et al., 2009; Thomas et al., 2010; Gundale et al., 2014; Forstner et al., 2019a). N deposition can further accelerate soil acidification and base cation loss (Carnol et al., 1997; Högberg et al., 2006; Forstner et al., 2019a), increase N leaching (Carnol et al., 1997; Moldan and Wright, 2011; Schleppi et al., 2017), favor forest nutritional imbalances (Mooshammer et al., 2014; Zechmeister-Boltenstern et al., 2015; Forstner et al., 2019b) and affect the cycling and storage of soil organic C (Treseder, 2008; Janssens et al., 2010; Maaroufi et al., 2015). N deposition can also accelerate microbial soil processes that are part of the N cycle, such as nitrification and denitrification (Gundersen et al., 2012). However, N deposition often reduces the overall soil biological activity as measured by respiration (Janssens et al., 2010; Zhang et al., 2019) or extracellular enzyme activities (Saiya-Cork et al., 2002; Sinsabaugh et al., 2002; DeForest et al., 2004). Frey et al. (2014) reported that organic horizon SOC pools increased by 33 and 52% in hardwood and pine stands, respectively, whereas in mineral horizons SOC pools did not respond to 20 years of N addition treatment (50 kg $ha^{-1}$ $y^{-1}$). In two Norway spruce stands, Forstner et al. (2019a) also found an SOC increase in the organic layer, but compensated by a decrease in the mineral soil. The main mechanisms behind the observed increases in topsoil SOC appear to be higher litter inputs to soil via stimulated tree productivity and a slower decomposition of soil organic matter (SOM). There are, however, contradictory reports on the effect of N deposition specifically on the decomposition of less decomposable, recalcitrant SOM (Janssens et al., 2010; Forstner et al., 2019a).

Earlier reports on soils from various forests revealed that N addition reduces microbial biomass and activity (Bowden et al., 2004; Frey et al., 2004; Wallenstein et al., 2006; Demoling et al., 2008; Treseder, 2008). Shifts in fungal:bacterial (F:B) biomass ratios (decrease in fungal biomass with little change in bacterial biomass) indicate alterations in the composition of the microbial community (Wallenstein et al., 2006). The decline in fungal biomass was largely attributed to a decrease in ectomycorrhiza, which form associations with trees, suggesting that fungi are more sensitive to long-term N fertilization than bacteria. Most previous research focused on soil bacterial communities in forests (Shen et al., 2010; Turlapati et al., 2013), and we are aware of only a few studies that examined changes in soil fungal community composition following increased N loads (Boxman et al., 1998; Allison et al., 2007; Edwards et al., 2011; Maaroufi et al., 2019).

Soil microorganisms, regulated by soil N availability, are able to change the terrestrial C cycling by decomposition and formation of soil organic matter (SOM) (Uroz et al., 2016; Baldrian, 2017; Llado et al., 2017). For example, organic substrate with a high N content can be rapidly decomposed by microorganisms at the initial stage, resulting in large accumulation of microbial products and concomitant formation of stable SOM. In contrast, for substrate with a low N content, more C tends to be respired rather than stored as stable SOM (Cotrufo et al., 2013). However, it remains unclear how moderate N addition regulates soil microbial biomass and community composition in forest ecosystems, which constrains our understanding of soil C cycling in response to N deposition. Fungi dominate in the decomposition of the SOM with a low nutrient content, because their nutrient demand and metabolic activity are low compared to bacteria (Mooshammer et al., 2014; Zechmeister-Boltenstern et al., 2015; Zhou et al., 2017). Consequently, N addition may decrease the F:B ratio. Meanwhile, soil acidification induced by N addition is likely to increase the F:B, because fungi are better adapted to environments with high $H^+$ concentration than bacteria (Högberg et al., 2006; Rousk et al., 2010). However, the effect of N addition on soil microbial biomass and community composition remains unclear and the current fragmentary knowledge needs to be improved across temperate forest ecosystems (Forstner et al., 2019b).

The effects of N deposition on forests largely depend upon soil processes such as immobilization, mineralization, nitrification, and denitrification. At the time scale of decades, soils tend to accumulate most of the N inputs (Nadelhoffer et al., 1999), which is reflected in a gradually decreasing soil C:N ratio (Gundersen et al., 1998; Morier et al., 2010; Moldan and Wright, 2011). While these overall processes are well-understood and somehow quantified, the effects on the forest soil microbiome in the context of increased atmospheric N deposition remain very poorly studied, even if microorganisms are the main actors in nutrient cycling and are likely affected by N deposition. Shifts in microbial community diversity and composition through anthropogenic stressors (e.g., atmospheric N deposition) may lead to unpredictable alterations in critical ecosystem processes.

The present study builds on an existing long-term (>20 years) N addition field experiment where atmospheric N deposition is artificially increased by adding small but recurrent amounts of ammonium nitrate ($NH_4NO_3$) dissolved in water. This experiment is carried out in the Alptal valley, central Switzerland, and it simulates a moderately increased N deposition (Schleppi et al., 2017). The site is stocked by old Norway spruce trees and the soil type is a relatively nutrient-rich Gleysol. From the previous results of this field study, the soil appears to play a key role in the reaction of the ecosystem to N deposition. The experimental N addition increased nitrate leaching, but, as in the comparable studies mentioned above, the soil immobilized most of the N input, progressively decreasing its C:N ratio (Schleppi et al., 2004). Denitrification and production of $N_2O$ were increased and soil respiration tended to be reduced (Mohn et al., 2000; Krause et al., 2013). The abundance and biodiversity

of Collembola (feeding mainly on microbes) decreased due to the N treatment (Xu et al., 2009). All these effects are likely linked to modifications of the forest soil microbiome. As one of the few of this kind and duration worldwide, the experiment offers a unique chance to study how N deposition affects microbial communities in natural forest soils in the long term.

Here, we analyzed the soil microbiome in different soil horizons. More specifically, we studied the effects of the long-term N addition on (i) the soil microbial biomass (by fumigation/extraction and as the abundance of bacterial and fungal marker genes), (ii) the microbial diversity, and community structure, and (iii) various aspects of ecosystem functions such as respiration potential, N mineralization and nitrification potential, fine root traits, together with quantifying key functions of the microbiome to increased N loads by quantitative polymerase chain reactions (qPCR). Genes encoding for enzymes catalyzing major processes during N fixation (*nifH*), nitrification (bacterial *amoA*, archaeal *amoA, nxrB*), and denitrification (*nirS, nosZ*) were targeted. We specificially asked: (1) Do long-term N addition change the microbial communities?; (2) Are these changes evident in different soil layers?; (3) Are community structure shifts represented in altered microbial functions in terms of C and N cycling processes. We hypothesized that chronic N inputs to forest soils alter the soil microbiota compared to soils subjected to ambient deposition only, whereas fungal communities react more strongly than bacterial ones, with symbiotrophs more sensitive than saprotrophs. We further hypothesized that chronic but low N loads induce significant changes in N cycling gene abundances, which might therefore alter nutrient availability of the forest systems.

# MATERIALS AND METHODS

## Study Site

The present study was conducted in a subalpine Norway spruce forest (*Picea abies* (L.) Karst.) of the Alptal valley, in Central Switzerland (47°03 N, 8°43 E), at an elevation of 1,200 m a.s.l. Beside Norway spruce, the tree layer features about 15% silver fir (*Abies alba* Mill). In the herb layer, *Vaccinium* spp. (L.), *Carex* spp. (L.), *Petasites albus* [(L.) Gaertn.], *Caltha palustris* (L.), *Knautia dipsacifolia* [(Host) Kreutzer], *Chaerophyllum hirsutum* (L.), and *Lycopodium annotitum* (L.) make up most of the biomass. The climate is cool and wet, with a mean air temperature of 6°C and a mean annual precipitation of 2,300 mm. Bulk N deposition measured at the site is 12 kg $ha^{-1}$ $y^{-1}$, equally partitioned between $NH_4^+$ and $NO_3^-$. Throughfall N deposition amounts to 17 kg $ha^{-1}$ $y^{-1}$ (Schleppi et al., 1998). According to the scale of Mellert and Göttlein (2012) for foliar concentrations, the nutrition of the Norway spruce can be considered as latent deficient for N and *P*. For K, Ca, and Mg, concentrations are in the normal range. The parent rock material of the site is Flysch, composed of sedimentary conglomerates with clay-rich schists. The slope is about 20% with a west aspect. Soils are very heavy Gleysols. Because of the high clay content (on average 48%), they have a high cation-exchange capacity but a low permeability. A water table is present throughout the year, on average at a depth of 23 cm (Krause et al., 2013). The pH of the mineral soil increases with depth, from 4.6 to 5.9 on the mounds and from 5.4 to 6.9 in the depressions. Net nitrification rates (measured for of the upper 15 cm) are either positive at some locations, negative at others (N immobilization). The net overall rate is overall not significantly different from zero (Hagedorn et al., 2001b). More details about the experimental site were given previously (Schleppi et al., 2017).

## Nitrogen Treatment

The N addition experiment at Alptal started in 1995. It combines a paired-catchment design (Schleppi et al., 2017) with a replicated plot design (Mohn et al., 2000; Hagedorn et al., 2001a; Xu et al., 2009; Krause et al., 2013). The ten 20-$m^2$ plots of this latter design were sampled for this study. Each of five N-treated plots was paired with a nearby control plot of similar micro-topography and vegetation. Nitrogen was added to treated plots by sprinkling of $NH_4NO_3$ dissolved in rainwater (Schleppi et al., 2017) during precipitation events. Hence, N addition varied annually with local precipitation regime, amounting to an average of 22 kg N $ha^{-1}$ $y^{-1}$ (Schleppi et al., 2017). Control plots received the same amount of unaltered rainwater. In winter, automatic irrigation was replaced by the occasional application of concentrated $NH_4NO_3$ solution on top of the snowpack using a backpack-sprayer.

## Soil Sampling and Processing

We sampled soils in 2014 (September) and 2015 (June, September). Three intact soil cores, 5 cm in diameter and 25 cm deep, were taken from each plot, placed on ice and transported to the laboratory. Within 24 h, each core was sectioned into three soil horizons and these horizons were pooled over the three cores from a single plot. From the top to the bottom of the cores, these layers were on average 4.5 (A horizon), eight (oxic B horizon), and nine (reduced B horizon) cm in thickness. The litter layer (*L*) was separated. At the time of sampling (September), before the main needle fall of the spuce trees and before the decay of the annual plant species, there was few litter (0.06 g $cm^{-2}$ on average) on the ground. In this season, most of the litter is almost decomposed and integrated in the *A* horizon. For this reason, the *L* layer was not further considered in the present study. This sampling scheme thus yielded a total of 30 samples (2 treatments × 3 horizons × 5 replicates). Samples were homogenized by passing through a 2-mm sieve. Fine roots (<2 mm) were removed from sieved soils using forceps. Aliquots of field-moist soil were stored at 4°C up to 2 weeks for analysis of microbial activities. Subsamples were stored at −18°C until analysis of DNA. Gravimetric water content was determined from subsamples dried to constant mass at 65°C. Soil C and N concentrations were measured from milled soil material using an elemental analyzer (Euro-EA, Hekatech GmbH, Germany) coupled to a continuous flow isotope ratio mass spectrometer (Delta-V Advanced IRMS, Thermo GmbH, Germany).

## Fine-Roots Traits

After removing fine roots from soils, they were washed under rinsing demineralized water and stored in plastic bags at 4°C up to 2 weeks for analysis of fine-root traits. Firstly, the fine roots were scanned using a scanner, and the scanned pictures were

analyzed using the WinRHIZO software package (version 4.1c, Regent Instruments Inc., Québec, Canada) for morphological and architectural traits such as length, average diameter, and number of tips. Then the fine roots were dried at 60°C for 3 days, weighed, and milled. Fine-root biomass was calculated per soil volume to obtain comparable data. Specific root length (SRL; m $g^{-1}$) was calculated by combining scanned data with biomass data, and tip frequency ($cm^{-1}$) was calculated from scanned data (Brunner et al., 2019). Fine-root C and N concentrations were measured from milled root material using an elemental analyzer-continuous flow isotope ratio mass spectrometer (Euro-EA, Hekatech GmbH, Germany, interfaced with a Delta-V Advanced IRMS, Thermo GmbH, Germany).

## Potential C Mineralization Rates and N Processes and Microbial Biomass

Potential nitrification was determined using the shaken slurry method (Hart et al., 1994). 10 g of field-moist, sieved soil were shaken in 100 ml of a solution (pH 7.2) containing 1 mM $PO_4^{3-}$ and 15 mM $NH_4^+$ at 22°C in the dark. These conditions ensured a maximum $NO_3^-$ production rate with minimal N immobilization and denitrification. Homogenized sub-samples (15 ml of the slurry) were taken at 2, 6, 23.5, 26, and 29 h after the start of the incubation. These sub-samples were filtered and stored at −20°C until analysis. $NO_3^-$-N was determined colorimetrically with a continuous flow analyzer (Auto-Analyzer 3, BranLuebbe, Germany). Nitrification rates were calculated by linear regression of $NO_3^-$-N concentrations over time.

Net nitrogen mineralization was measured through a 28-days aerobic laboratory incubation of 15 g soil at constant temperature (22°C) in the dark (Hart et al., 1994). At the beginning and at the end of the incubation, inorganic N was extracted with a 1 M KCl solution (1:5 w:v) (Allen, 1989) and analyzed as described above. The mineralization rate was calculated from the net increase in inorganic N ($NH_4^+$-N and $NO_3^-$-N) during the incubation period.

The respiration potential was measured according to Robertson et al. (1999) as the $CO_2$ accumulation in the headspace (250 ml) of an amber bottle containing 20 g fresh soil, at 22°C in the dark after an overnight pre-incubation. Gas samples (4 ml) were taken at 0, 120, 150, and 180 min with an airtight syringe and analyzed with an infrared gas analyzer (EGM-4, PP Systems, UK). The respiration rate was estimated by linear regression of these measurements against time.

Soil microbial biomass C and N (MBC, MBN) were determined by the chloroform fumigation extraction method (Vance et al., 1987). Fumigations were carried out for 3 days in a vacuum desiccator with alcohol-free chloroform, followed by 0.5 M $K_2SO_4$ extraction. Dissolved organic C was measured with a Total Organic Carbon Analyzer (Labtoc, Pollution and Process Monitoring Ltd, UK) and total N was measured colorimetrically as described above. Soil MBC and MBN were calculated from the difference of total extract between fumigated and unfumigated samples, with a conversion factor of 0.45 for MBC (Jenkinson et al., 2004) and 0.54 for MBN (Joergensen and Mueller, 1996).

Water-soluble C and N were extracted from 10 g fresh sieved (4 mm) soil, following Ghani et al. (2003). First, readily soluble C and N (water soluble C and N) were extracted at room temperature with 30 ml distilled water. After 30 min agitation at 2 Hz, the suspension was centrifuged for 10 min (3,000 $min^{-1}$) and the supernatant filtered at 0.45 µm (GN-6 Metricel, Pall Corporation, US). Total organic C was measured with a Total Organic Carbon analyzer (Labtoc, Pollution and Process Monitoring Ltd, UK). Total N, $NO_3^-$N, and $NH_4^+$-N were measured colorimetrically as described above. Organic N was calculated by subtracting $NO_3^-$-N and $NH_4^+$-N from total N. After this first extraction step, labile components of soil C were extracted at 80°C (hot water extractable C and N). The centrifuge tube with the remaining wet soil was weighted to calculate the remaining water volume, and a further 60 ml distilled water was added. Samples were shaken for 30 min to re-suspend the soil, closed and placed in a pre-heated oven at 80°C for 16 h. The samples were then shaken again for 30 min, centrifuged, filtered, and analyzed as explained above. As water soluble fractions contains mineral N initially present in soils, water soluble C:N ratios were calculated as water-soluble C divided by water-soluble organic N. As initially present mineral N is mostly removed in the first extraction step, and as $NH_4^+$ in hot water extracts may result from the hydrolysis of organic N (Gregorich et al., 2003), hot water C:N ratios were calculated as hot-water-soluble C divided by hot-water-soluble total N.

## Soil DNA Extraction, MiSeq Sequencing, and Bioinformatic Analyses

Total DNA was extracted from ∼0.5 g soil using the PowerSoil DNA Isolation Kit (Qiagen). DNA was quantified using the high sensitivity Qubit assay (Thermo Fisher Scientific). The V3–V4 region of the bacterial small-subunit (16S) rRNA gene and the internal transcribed spacer region 2 (ITS2) of the eukaryotic (fungal groups, some groups of protists, and green algae) ribosomal operon were PCR amplified using primers previously described by Frey et al. (2016). PCR amplification was performed with 20 ng soil DNA and the HotStar Taq amplification kit (Qiagen, Hilden, Germany) in a final volume of 50 µL per samples (16S: 15 min at 95°C/30 cycles: 40 s at 94°C, 40 s at 58°C, 1 min at 72°C/10 min at 72°C; ITS-2: 15 min at 95°C/36 cycles: 40 s at 94°C, 40 s at 58°C, 1 min at 72°C/10 min at 72°C). PCRs were run in triplicates, pooled, and purified using Agencourt Ampure XP beads (Beckman Coulter). Bacterial and fungal amplicon pools were sent to the Génome Québec Innovation Center at McGill University (Montreal, Canada) for barcoding using the Fluidigm Access Array technology and paired-end sequencing on the Illumina MiSeq v3 platform (Illumina Inc.). Raw sequences have been deposited in the NCBI Sequence Read Archive under the BioProject accession number PRJNA595488.

Quality filtering, clustering into operational taxonomic units (OTUs) and taxonomic assignments were performed as previously described in Frey et al. (2016). In brief, a customized pipeline largely based on UPARSE (Edgar, 2013; Edgar and Flyvbjerg, 2015) implemented in USEARCH (v9.2; Edgar, 2010) was used. Filtered reads were de-replicated and singleton reads removed prior to clustering. Sequences were clustered into OTUs at 97% sequence identity (Edgar, 2013). For taxonomic

classification of the OTUs, corresponding centroid sequences were queried against selected reference databases using the naïve Bayesian classifier (Wang et al., 2007) and a minimum bootstrap support of 80%. Prokaryotic sequences were queried against the SILVA database (v132; Quast et al., 2013). Eukaryotic ITS2 sequences were first queried against a custom-made ITS2 reference database retrieved from NCBI GenBank, and sequences assigned to fungi were subsequently queried against the fungal ITS database UNITE (v8.0; Abarenkov et al., 2010). Prokaryotic centroid sequences identified as originating from organelles (chloroplast, mitochondria), as well as eukaryotic centroid sequences identified as originating from soil animals (*Metazoa*), plants (*Viridiplantae*, except green algae), or of unknown eukaryotic origin, were removed prior to data analysis.

## Quantitative PCR of Bacterial and Fungal Ribosomal Markers and Functional Genes

Relative abundances of the bacterial 16S rRNA genes, fungal ITS, and various C- and N-cycling genes were determined as previously by quantitative PCR as previously described (Frey et al., 2011; Rime et al., 2016) using an ABI7500 Fast Real-Time PCR system (Applied Biosystems). The same primers (without barcodes) and cycling conditions as for the sequencing approach were used for the 16S and ITS (Frossard et al., 2018). For qPCR analyses 2.5 ng DNA in a total volume of 25 µl containing 0.5 µM of each primer, 0.2 mg of BSA $ml^{-1}$, and 12.5 µl of QuantiTect SYBR Green PCR master mix (Qiagen, Hirlen, Germany) were used. Abundances of C- and N-cycling genes were quantified using primers and thermocycling conditions as reported in **Table S1**. Functional marker genes encoding for enzymes catalyzing major processes during methanogenesis (*mcrA*) nitrogen fixation (*nifH*), nitrification (bacterial *amoA*, archaeal *amoA, nxrB*), and denitrification (*nirS, nosZ*) are targeted. The specificity of the amplification products was confirmed by melting-curve analysis, and the expected sizes of the amplified fragments were checked in a 1.5% agarose gel stained with ethidium bromide. Three standard curves per target region (correlations $\geq$ 0.997) were obtained using tenfold serial dilutions ($10^{-1}$-$10^{-9}$ copies) of plasmids generated from cloned targets (Frey et al., 2011). Data was converted to represent average copy number of targets per µg DNA.

## Data Analysis

All statistical analyses were performed using R (v.3.6.0; R Core Team, 2017). Variables were tested for normality and homogeneity of variances using Shapiro-Wilk and Levene's tests, respectively. In case of non-normality and/or heteroscedasticity, the data were transformed by either by taking the natural logarithm or by using the Box-Cox family of power transformations. We used analysis of variance (ANOVA) to test for effects of N addition treatment, soil horizon, and their interaction on univariate response variables. *Post-hoc* differences between soil horizons were assessed with Tukey's HSD tests, and Dunnett's tests were used to check for treatment effects within horizons.

For analysis of bacterial and fungal α-diversities, observed richness (number of OTUs) and Shannon diversity index were estimated based on OTU abundance matrices rarefied to the lowest number of sequences using the R package *phyloseq* (v1.28.0; McMurdie and Holmes, 2013). To assess the main and interactive effects of N treatment and soil horizon on α-diversities a two-way ANOVA was performed. Pairwise comparisons of significant effects were conducted using Tukey's HSD *post-hoc* tests.

Bray-Curtis dissimilarities were calculated based on square root transformed relative abundances of OTUs (Hartmann et al., 2017). The effects of N treatment, soil horizon, and interactive effects on microbial community structures (ß-diversities) were assessed by conducting a permutational ANOVA (PERMANOVA, number of permutations = 9,999) with the function *adonis* implemented in the *vegan* package (v2.5.5; Oksanen et al., 2017). Canonical analysis of principal coordinates (CAP) ordinations of microbial community structures were calculated using the *ordinate* function implemented in the R package *phyloseq*.

Changes in the relative abundances of the most abundant phyla (classes, orders) were assessed by conducting a two-way analysis of variance (ANOVA). Differences were considered significant at $p < 0.05$ unless mentioned otherwise. To identify microbial genera that were significantly different between N amended and control samples we first agglomerated OTUs to the genus level, and generated subsets for each soil horizon. Differential abundance analysis by applying a negative binomial generalized linear model to the OTU count data using the *DESeq2* package (v.1.24.0; Love et al., 2014) was performed. Genera were considered significantly different (Wald test) between N-treated and control samples if the false discovery rate (adjusted *p*-value) was $< 0.05$. Fungal functional guilds were assigned within the six most abundant guilds, namely ectomycorrhizal fungi, arbuscular mycorrhizal, endophyte, undefined saprotrophs, animal pathogens, and plant pathogens, using an open annotation tool (FUNGuild) according to Nguyen et al. (2016). Only the guild assignment with "highly probable" confidence rankings was accepted.

# RESULTS

## Soil and Biological Characteristics

Overall, soil properties and processes showed only a small impact of two decades of N addition. The total C and N concentrations clearly declined with depth but were not significantly affected by the treatment (**Table 1**). The N addition, however, significantly decreased the soil C:N ratio by about two in all three layers. Hot water extractable C and N (**Figure 1**) were also very similar in the N-addition plots compared to the control plots, and concentrations of both elements clearly decreased with depth. C:N ratios in the extractable organic matter showed no effects at all, except that the ratio was lower in the hot-water than in the cold-water extract. Water soluble and hot water extractable $NH_4^+$ was not significantly affected either, even if the cumulated addition of $NH_4^+$-N amounted to 220 g $m^{-2}$, which would represent 250 mg $g^{-1}$ if it would be homogenously mixed into the 25 cm depth of the soil cores. There was a significant interaction of N addition treatment and horizon on water soluble and hot

**TABLE 1 |** Biotic and abiotic site characteristics of soil horizons (A, Bo, Br) in the control and N-added plots of the Alptal N addition experiment.

| | Control plots (mean ± *SE*, *n* = 5) | | | N-added plots (mean ± *SE*, *n* = 5) | | | ANOVA[+] *p*-values | | |
|---|---|---|---|---|---|---|---|---|---|
| | A[#] | Bo | Br | A | Bo | Br | Nitrogen | Horizon | Interaction |
| **Microbial biomass** | | | | | | | | | |
| Microbial C [mg C $g^{-1}$ soil dw] | 3.79 ± 0.56 | 1.56 ± 0.30 | 0.51 ± 0.13 | 2.98 ± 0.41 | 1.04 ± 0.19 | 0.26 ± 0.07 | 0.060 | **<0.001** | 0.68 |
| Microbial N [μg N $g^{-1}$ soil dw] | 647 ± 83 | 274 ± 55 | 75 ± 25 | 588 ± 77 | 161 ± 34 | 20 ± 11 | 0.13 | **<0.001** | 0.84 |
| Total biomass [μg DNA $g^{-1}$ soil dw] | 92 ± 10 | 69 ± 5 | 39 ± 8 | 76 ± 3 | 56 ± 7 | 15 ± 4 | **0.003** | **<0.001** | 0.65 |
| Bacterial abundance* [$10^7$ $\mu g^{-1}$ DNA] | 2.3 ± 1.2 | 2.0 ± 0.9 | 8.4 ± 0.4 | 2.8 ± 0.6 | 2.4 ± 0.9 | 1.9 ± 1.0 | 0.38 | 0.41 | 0.93 |
| Fungal abundance‡ [$10^4$ $\mu g^{-1}$ DNA] | 3.8 ± 3.0 | 1.8 ± 1.6 | 0.26 ± 0.2 | 2.1 ± 0.7 | 2.9 ± 2.2 | 0.4 ± 0.3 | 0.86 | 0.31 | 0.72 |
| **Microbial activity** | | | | | | | | | |
| Respiration [μg C $g^{-1}$ dw soil $h^{-1}$] | 199 ± 39 | 63 ± 16 | 19 ± 4 | 175 ± 32 | 56 ± 11 | 19 ± 5 | 0.56 | **<0.001** | 0.85 |
| N-mineralization [μg N $g^{-1}$ soil dw $d^{-1}$] | 2.8 ± 0.8 | 0.97 ± 0.28 | 0.17 ± 0.03 | 3.02 ± 0.91 | 0.53 ± 0.1 | 0.05 ± 0.02 | 0.78 | **<0.001** | 0.82 |
| Nitrification [ng N $g^{-1}$ soil dw $h^{-1}$] | 2.3 ± 1.4 | 4.2 ± 1.6 | 1.8 ± 1.6 | 5.6 ± 3.4 | 2.2 ± 0.8 | 0.2 ± 0.2 | 0.94 | 0.25 | 0.27 |
| **Functional genes** | | | | | | | | | |
| mcrA [$10^4$ $\mu g^{-1}$ DNA] | 3.9 ± 1.6 | 7.6 ± 1.6 | 7.5 ± 1.4 | 5.9 ± 1.0 | 10.0 ± 2.4 | 19.0 ± 9.3 | 0.13 | 0.15 | 0.45 |
| bamoA [$10^1$ $\mu g^{-1}$ DNA] | 47.0 ± 42.2 | 18 ± 11.7 | 1.7 ± 1.3 | 35.0 ± 16.8 | 8.1 ± 6.4 | 1.0 ± 0.4 | 0.62 | 0.12 | 0.95 |
| aamoA [$10^3$ $\mu g^{-1}$ DNA] | 0.2 ± 0.1 | 2.9 ± 1.5 | 1.5 ± 0.6 | 1.1 ± 0.6 | 2.1 ± 1.1 | 3.0 ± 1.8 | 0.51 | 0.24 | 0.65 |
| nrxB [$10^6$ $\mu g^{-1}$ DNA] | 1.1 ± 0.5 | 7.8 ± 1.7 | 7.7 ± 2.0 | 4.9 ± 1.4 | 10.0 ± 2.1 | 9.1 ± 0.9 | 0.06 | **0.001** | 0.73 |
| nirS [$10^7$ $\mu g^{-1}$ DNA] | 0.7 ± 0.2 | 1.9 ± 0.5 | 2.9 ± 0.7 | 1.4 ± 0.5 | 2.3 ± 0.6 | 5.7 ± 2.4 | 0.16 | **0.02** | 0.52 |
| nosZ [$10^7$ $\mu g^{-1}$ DNA] | 2.2 ± 0.5 | 3.1 ± 0.6 | 2.8 ± 0.8 | 2.6 ± 0.8 | 2.9 ± 0.5 | 3.3 ± 0.2 | 0.63 | 0.52 | 0.79 |
| nifH [$10^3$ $\mu g^{-1}$ DNA] | 0.4 ± 0.1 | 1.5 ± 0.6 | 1.8 ± 0.5 | 1.1 ± 0.5 | 1.5 ± 0.5 | 3.4 ± 0.9 | 0.08 | **0.01** | 0.46 |
| **Fine root traits** | | | | | | | | | |
| Fine root biomass [g $dm^{-3}$] | 8.1 ± 2.5 | 1.7 ± 0.9 | 0.7 ± 0.5 | 5.4 ± 1.7 | 0.7 ± 0.4 | 0.4 ± 0.3 | 0.23 | **<0.001** | 0.67 |
| Specific root length [m $g^{-1}$] | 0.7 ± 0.1 | 0.6 ± 0.1 | 0.5 ± 0.1 | 0.8 ± 0.1 | 0.5 ± 0.0 | 0.8 ± 0.2 | 0.56 | 0.38 | 0.36 |
| Mean diameter [mm] | 0.7 ± 0.0 | 0.7 ± 0.1 | 0.8 ± 0.1 | 0.7 ± 0.1 | 0.8 ± 0.1 | 0.7 ± 0.1 | 0.63 | 0.39 | 0.31 |
| Tip frequency [$cm^{-1}$] | 3.4 ± 0.4 | 2.9 ± 0.9 | 2.2 ± 0.9 | 4.0 ± 0.3 | 3.1 ± 0.1 | 2.9 ± 0.1 | 0.29 | 0.13 | 0.88 |
| Fine root C [%] | 45.4 ± 0.5 | 43.9 ± 0.5 | 42.8 ± 0.5 | 44.4 ± 0.9 | 44.4 ± 0.3 | 44.3 ± 0.3 | 0.51 | 0.14 | 0.19 |
| Fine root N [%] | 1.0 ± 0.0 | 1.0 ± 0.1 | 0.9 ± 0.1 | 1.2 ± 0.1 | 0.9 ± 0.1 | 0.9 ± 0.1 | 0.38 | 0.07 | 0.43 |
| Fine root C:N ratio | 45.5 ± 2.3 | 46.7 ± 3.8 | 48.2 ± 4.3 | 39.1 ± 3.3 | 47.9 ± 3.0 | 47.8 ± 3.0 | 0.51 | 0.18 | 0.47 |
| **Soil properties** | | | | | | | | | |
| pH ($CaCl_2$) | 4.9 ± 0.3 | 5.5 ± 0.2 | 6.0 ± 0.3 | 4.9 ± 0.3 | 5.2 ± 0.4 | 5.5 ± 0.6 | 0.45 | 0.11 | 0.81 |
| Total soil C [mg C $g^{-1}$ soil dw] | 27.3 ± 4.5 | 15.4 ± 4.0 | 6.4 ± 1.7 | 22.0 ± 2.6 | 9.4 ± 1.6 | 4.1 ± 1.0 | 0.054 | **<0.001** | 0.71 |
| Total soil N [mg N $g^{-1}$ soil dw] | 1.5 ± 0.2 | 0.9 ± 0.2 | 0.4 ± 0.1 | 1.4 ± 0.1 | 0.6 ± 0.1 | 0.3 ± 0.1 | 0.25 | **<0.001** | 0.48 |
| Soil C:N ratio | 18.3 ± 1.1 | 16.1 ± 1.5 | 16.1 ± 1.2 | 16.1 ± 0.5 | 14.9 ± 0.2 | 14.6 ± 1.4 | **0.023** | **<0.001** | 0.91 |

[+]*Effects of N treatment, horizon and their interaction were assessed by analysis of variance (ANOVA); significant values are in bold letters.*
[#]*Soil horizons: A, A horizon, 4.5 cm thick; Bo, oxic B horizon, 8 cm thick; Br, reduced B horizon, 9 cm thick.*
**Bacterial abundance, 16S rRNA gene copies.*
‡*Fungal abundance, ITS2 gene copies.*

water extractable $NO_3^-$, with higher values under N inputs in the A-horizon ($p < 0.001$). In lower layers, the tendency was even opposite pointing to reducing conditions in lower layers.

Microbial biomass C and N (**Table 1**) decreased with depth ($p < 0.001$) with a tendency of less ($p = 0.062$) microbial biomass C in N-treated plots, resulting in a lower microbial C:N ratio in the top soil layer (0–4.5 cm) with N addition (interaction N × horizon: $p = 0.007$). Respiration and N mineralisation (**Table 1**) strongly decreased with soil depth ($p < 0.001$). No effect of the N treatment could be detected, neither if process rates were expressed per soil dry mass nor per total or extractable C or N. We also found no significant interactions between horizons and N addition. Potential nitrification did not change with N addition nor with soil depth (**Table 1**).

In contrast to microbial biomass C, DNA content was significantly lower under N treatment ($p = 0.003$) and decreased with soil depth ($p < 0.001$; **Table 1**). Bacterial and fungal abundance (16S and ITS copy numbers) as well as the seven

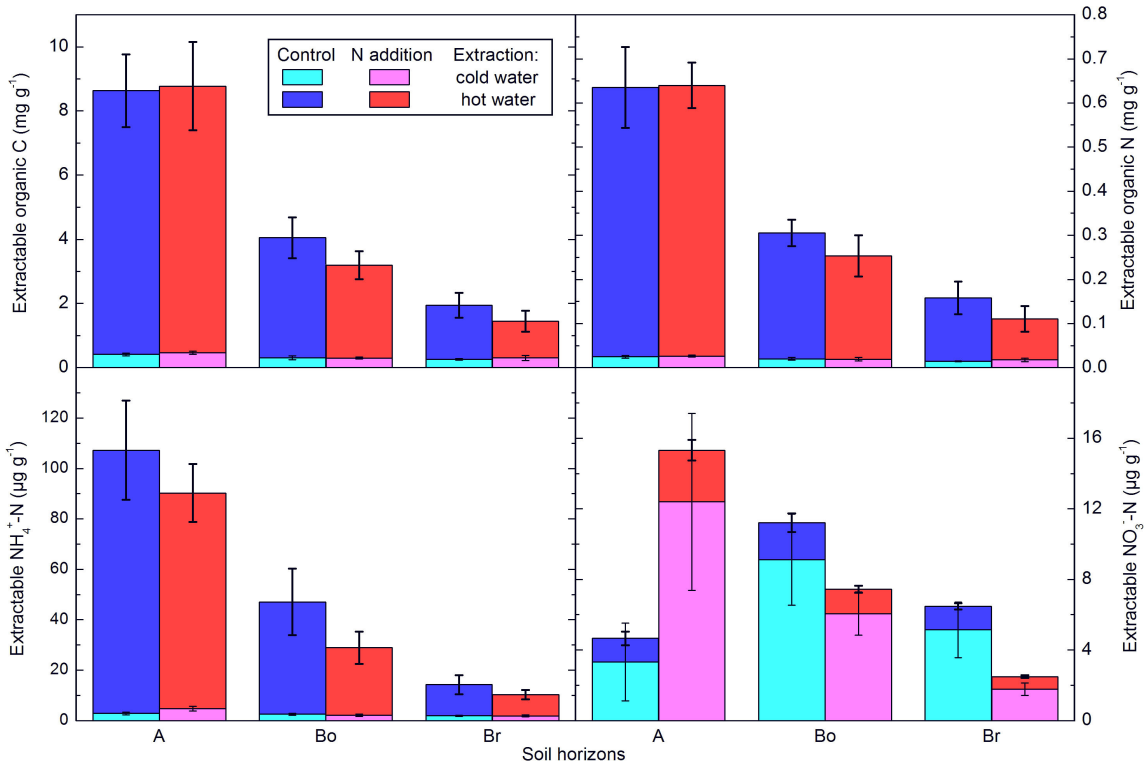


**FIGURE 1 |** Extractable C and N concentrations in the horizons of the mineral soil in the control and N-addition plots. A first extraction was done with cold water and a subsequent one with hot water. All results are from three cores per plot and given per dry soil mass as averages ± standard error ($n = 5$; A, A horizon; Bo, oxic B horizon; Br, reduced B horizon).

C- and N-cycling genes were not affected by the N addition (**Table 1**, **Figure 2**). Similarly, we found that the abundance of fungal biomass relative to bacterial (F:B ratio) did not change with the addition of N. There was a tendency of higher *nrxB* ($p = 0.06$) and *nifH* ($p = 0.08$) genes in plots with N inputs. Three functional genes (*nrxB*, *nirS*, and *nifH*) significantly increased with soil depth (**Table 1**, **Figure 2**).

N addition had no effect on fine root traits of Norway spruce. Fine root biomass, morphology (specific root length, tips, and diameter) and root chemistry (C, N) did not respond significantly to N addition (**Table 1**).

## MICROBIAL DIVERSITY AND COMMUNITY STRUCTURE

Since the results of the community analyses were similar for the three sampling times (with no or only minor changes in the soil microbiome), we decided to present only the analyses from the last sampling (September 2015). The overall microbial community analysis has been documented in the **Supplementary Results**. Bacterial α-diversity indices in control and N-added soils were unchanged ($p = 0.9$; **Table 2**, **Figure 3**). Bacterial α-diversity was also similar between different horizons under control and experimental N deposition (**Table 2**, **Table S2**). In contrast, we found a significant decline ($p = 0.05$) of fungal α-diversity indices (Richness and Shannon Index) with soil depth (**Table 2**, **Figure 3**), while neither effects of treatment (N addition) nor interactions (N × depth) on fungal α-diversity indices were recorded (**Table 2**). Among the fungal populations we found that animal pathogen (35%), ectomycorrhizal (30%), saprotroph (12%), arbuscular mycorrhizal (10%), endophyte (8%), and plant pathogen (2%) were the dominant functional guilds with a "highly probable" classification (Nguyen et al., 2016). Overall, there was a decrease of richness with N addition with strongest ($p < 0.001$; data not shown) impact on ectomycorrhizal, arbuscular mycorrhizal fungi, and endophytes (**Figure 4**). PERMANOVA analysis revealed a weak ($p = 0.06$) but not significant difference in fungal ß-diversities with N addition (**Table 2**) as also shown by canonical analysis of principal coordinates (CAP) based on the Bray-Curtis dissimilarities (**Figure 5**). In contrast, bacterial community structures were not influenced by N addition and soil depth.

### Changes in Relative Abundance of the Most Dominant Phyla (Classes, Orders) in Response to N

The relative abundance of bacterial phyla did not change between the ambient and experimental N deposition. No bacterial phyla and classes exhibited a significant change in relative abundance with the N treatment. However, we found significant ($p < 0.05$)

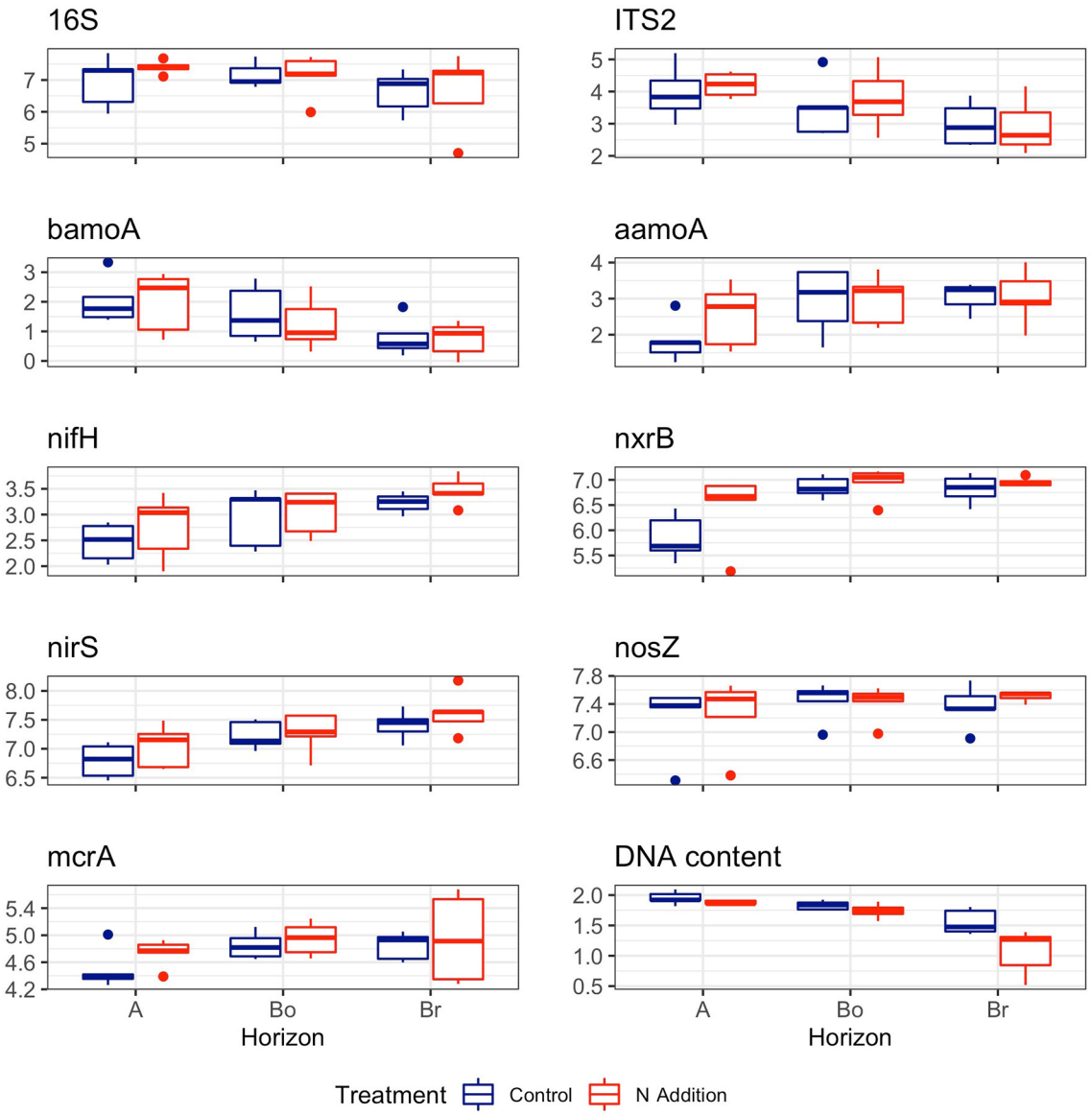


**FIGURE 2 |** DNA content and abundances of bacterial (16S), fungal (ITS2), and C- and N-cycling genes in the horizons of the mineral soil in the control and N-addition plots ($n = 5$; A, A horizon; Bo, oxic B horizon; Br, reduced B horizon). Gene copies (as log10) were given per µg DNA.

**TABLE 2 |** Treatment (N addition) and spatial (horizon) effects on α-diversity (Richness and Shannon Index) and ß-diversity (Bray-Curtis dissimilarities) in the Alptal N addition experiment.

| | **Bacteria** | | | **Fungi** | | |
|---|---|---|---|---|---|---|
| | **α-diversity*** | | **ß-diversity** | **α-diversity** | | **ß-diversity** |
| | **Richness** | **Shannon** | | **Richness** | **Shannon** | |
| Treatment | 0.90 (0.13)$^{+}$ | 0.90 (0.02) | 0.41 (1.00) | 0.28 (1.24) | 0.27 (1.29) | *0.06* (1.44) |
| Horizon | 0.85 (0.16) | 0.84 (0.18) | 0.12 (1.42) | **0.05** (3.36) | **0.05** (3.52) | 0.23 (1.13) |
| Treatment x Horizon | 0.32 (1.21) | 0.33 (1.15) | 0.97 (0.56) | 0.42 (0.90) | 0.41 (0.93) | 0.77 (0.87) |

**Effects of main factors and their interactions assessed by analysis of variance (ANOVA).*

*$^{+}$Values represent the p-values (F-ratio for each factor are given in brackets); significant values ($p < 0.05$) are in bold letters and values in italics represent $p < 0.1$.*

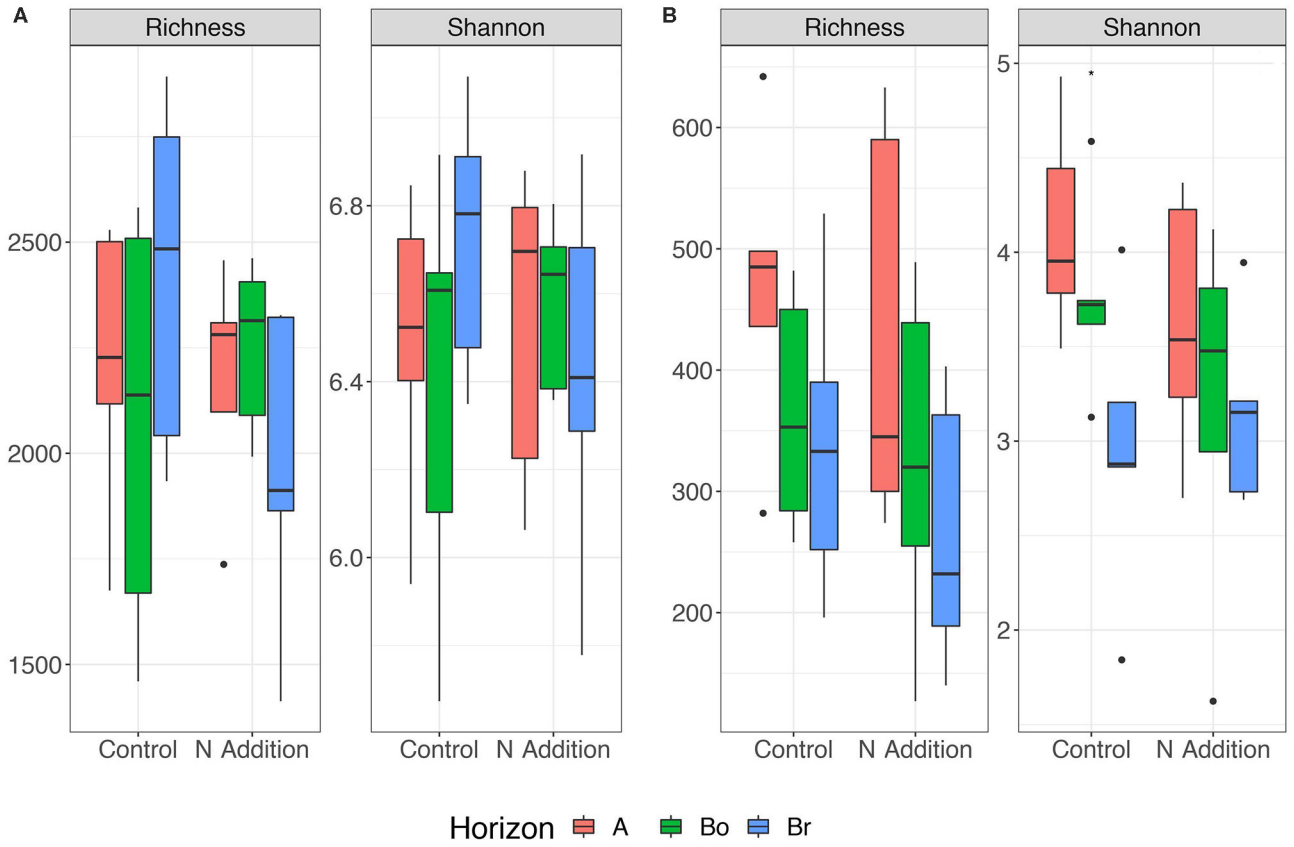


**FIGURE 3 |** Variation in Richness and Shannon index of bacterial **(A)** and fungal **(B)** communities in the horizons of the mineral soil in the control and N-addition plots ($n = 5$; A, A horizon; Bo, oxic B horizon; Br, reduced B horizon).

depth effects in the relative abundance of OTUs attributable to *Anaerolineae* (**Table 3**). Within fungi, the phylum *Basidiomycota* significantly decreased in relative abundance with N (**Table 3**). The other fungal phyla did not exhibit significant changes with the experimental N deposition treatment. A few fungal classes and orders were affected by the experimental N deposition treatment. Relative abundance of *Agaricomycetes*, *Agaricales*, and *Cantharellales* decreased ($p < 0.05$) whereas the relative abundance of *Heliotales* increased ($p < 0.1$) under experimental N addition.

## Differential Abundance of the Most Dominant Genera in Response to N Deposition

As bacterial and fungal phyla consist of various heterogeneous groups, we also investigated the changes in the differential abundance of the most common bacterial and fungal genera in response to N treatment among the three soil horizons. Since we did not find any taxa with significant ($p < 0.05$) $\log_2$ fold change in bacteria, we report on those that responded weakly ($p < 0.1$) to N addition (**Figure S1**). The majority of genera that had positive $\log_2$ fold changes upon N treatment belonged to the phylum *Proteobacteria*. Within this phylum, *Rhodoblastus* and the sulfur-oxidizing genus *Sulfurifustis* exhibited the strongest positive response to N (increase with N addition). In addition, the methane-producing *Methanocella* and *Methanolinea* showed higher positive $\log_2$ fold changes, indicating anaerobic soil conditions (**Figure S1**). The greatest negative $\log_2$ fold change in response to N addition was exhibited by genera of the phylum *Acidobacteria* such as the acidophilic *Granulicella* and *Acidipila*. Genera of the phylum *Proteobacteria* also decreased with N deposition, with *Rickettsiella* and *Inquilinus* having overall the greatest negative $\log_2$ fold change (**Figure S1**).

Within the fungal kingdom, the majority of genera that exhibited either positive or negative $\log_2$ fold changes were members of the phyla *Ascomycota* and *Basidiomycota* (**Figure 6**, **Figure S2**). The genera *Clavulina* and *Physisporinus* had the strongest positive responses to the N addition (**Figure 6**). *Clavulina* is an ectomycorrhizal fungus (*Basidiomycota*) with some saprophytic lifestyle and *Physisporinus* is a wood saprotroph (*Ascomycota*). Interestingly, fungal entomopathogens such as *Metarhizium* and *Trichoderma* (both *Ascomycota*) showed negative $\log_2$ fold changes upon treatment with N. Genera belonging to *Basidiomycota*, such as the ectomycorrhizal fungi *Membranomyces, Thelephora, Hydnum, Piloderma*, and *Amanita* were found to decrease in N-treated samples (**Figure 6**, **Figure S2**). *Membranomyces* had the largest negative $\log_2$ fold

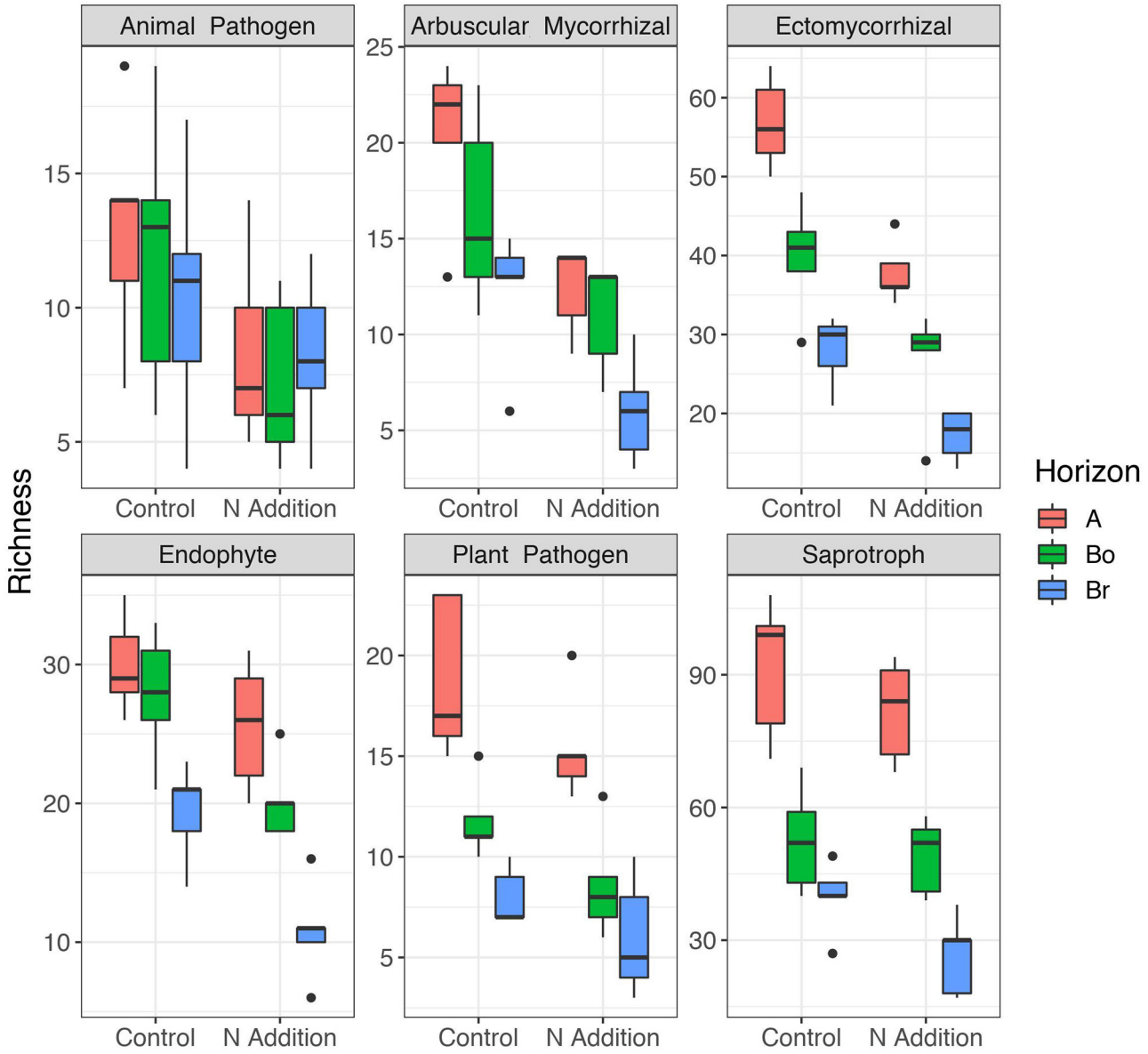


**FIGURE 4 |** Patterns of α-diversity (Richness) of the different fungal guilds in the horizons of the mineral soil in the control and N-addition plots ($n = 5$; A, A horizon; Bo, oxic B horizon; Br, reduced B horizon). Fungal functional guilds were analyzed by FUNGuild showing the six most abundant guilds. Only the guild assignment with "highly probable" confidence rankings was accepted.

change followed by *Thelephora*. Ectomycorrhizal fungi showed a mixed response with *Thelephora* declined significantly with N fertilization, while *Clavulina* increased.

## DISCUSSION

There are only a few long-term (20 years and more) N addition experiments in forest ecosystems worldwide. They all have one result in common: from an annual up to a decadal scale, added N is mainly sequestered into the soil (Cheng et al., 2019). Higher deposition rates therefore lead to an accumulation of N in the soil, with potentially effects on soil organisms and the biochemical processes that they drive. Such effects are not limited to the N cycle, but also affect C and other elements.

### Long-Term N Addition Effects on Soil Processes

In the present study we did not find any significant effect of the treatment or interaction thereof with the mineral soil layers. Similarly, for soils from the same site, Forstner et al. (2019a) also reported no significant differences in C mineralization rates with N treatment. Some studies showed an increase in forest soil

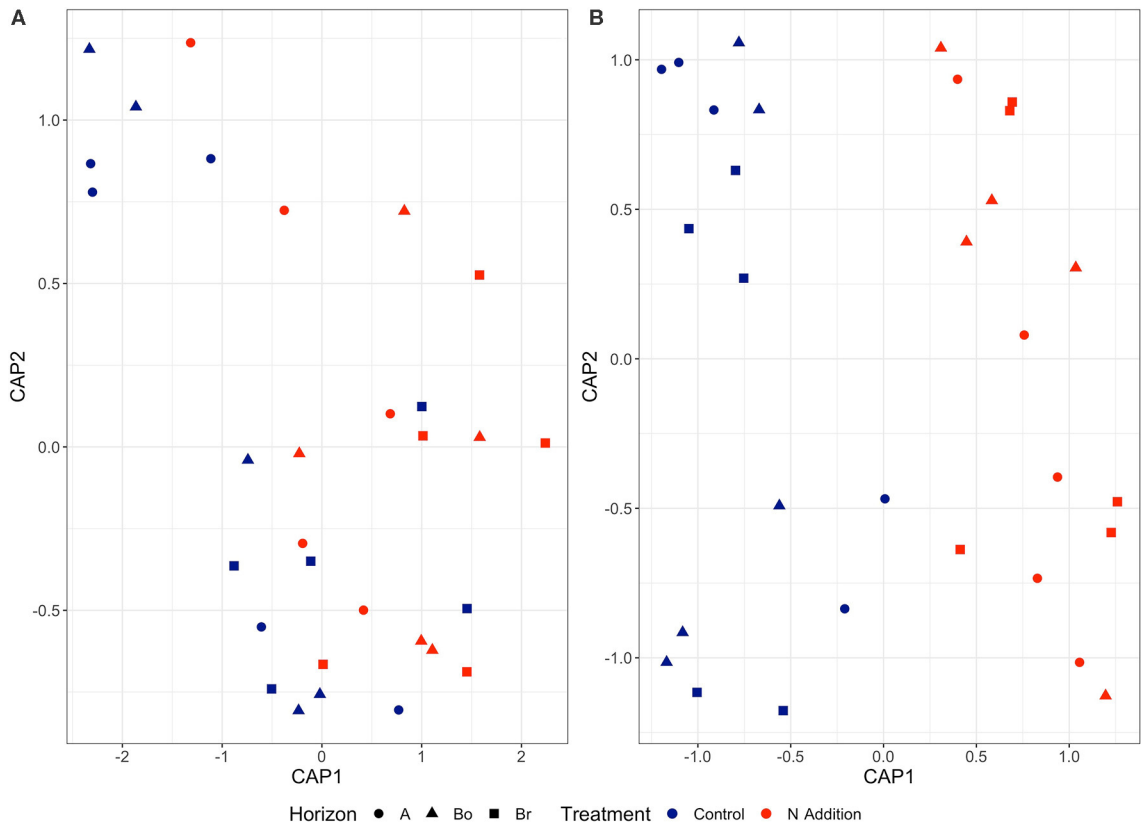


**FIGURE 5 |** Canonical analysis of principal coordinates (CAP) based on the Bray-Curtis dissimilarities for bacterial **(A)** and fungal **(B)** communities in the horizons of the mineral soil in the control and N-addition plots ($n = 5$; A, A horizon; Bo, oxic B horizon; Br, reduced B horizon). The variation in microbial community structures was explained by each CAP axis (for bacteria: CAP 1, 5.2%; CAP 2, 3.9%; for fungi: CAP 1, 15.5%; CAP 2, 9.6%).

respiration as a result of N addition (Hasselquist et al., 2012; Zhang et al., 2019), but in other reports there was no effect (e.g., Haynes and Gower, 1995; Bowden et al., 2000; Liu et al., 2017). Based on 5 years measurements with static chambers, Krause et al. (2013) found only a weak tendency of soil respiration rates to be reduced by N addition. At our site, more C tended to accumulate in the organic layer of N-addition plots, but C was decreased in the mineral soil (Forstner et al., 2019a). At the same time, the input of litter remained in the same range as for control (Krause et al., 2013). This means that neither the soil C pool nor its main fluxes in and out of the soil were significantly affected by the N treatment. Therefore, despite theoretically large potential effects, our results can only confirm that N deposition effects in relation to the C balance of forest soils are minor (Erisman et al., 2011).

At our site, in our results as well as in the previous study of Schleppi et al. (2004), the C:N ratio of the mineral soil significantly decreased as a result of the N addition. As shown by Providoli et al. (2006) using $^{15}NO_3^-$ or $^{15}NH_4^+$, most of the N from deposition entering the soil is rapidly immobilized and bound to its organic matter. This explains why the extractable inorganic N was not increased in the present study. Compared to the control plots, we observed a clear increase of extractable $NO_3^-$ in the A-horizon of the N addition plots. However, in relation to the annual $NO_3^-$ added, this represents only about one-tenth of the total. Due to the high mobility of this ion, this measurement can anyway only be considered as a snapshot. Together with the extractable $NH_4^+$, it indicates that only very little N as inorganic N is present in the soils (i.e., very little in a form that is directly available to plants and microbes).

## Long-Term N Addition Effects on Root Growth

Interestingly, no significant effects by long-term moderate N addition on any of the fine root traits of Norway spruce investigated have been observed, which is in accordance with Carnol et al. (1999). This is in contrast to what could be expected when N is added to an ecosystem (Ostonen et al., 2007; Li et al., 2015). Li et al. (2015) observed in a meta-analysis on simulated N deposition an overall significant increase of the total root biomass, with the coarse roots increasing and the fine roots decreasing significantly. In addition, they observed a significant increase of the root N concentration. However, a few fine-roots traits seemed not to be affected by N addition, in particular fine root length and diameter (Li et al., 2015). Ostonen et al. (2007) observed in their meta-analysis a significant decrease of the specific root length, whereas Li et al. (2015) did not observe any significant change of this

**TABLE 3 |** Treatment (N addition) and spatial (horizon) effects on the relative abundance of bacteria and fungi in the Alptal N addition experiment.

| Variables | Taxa | Treatment ($F_{1/29}$)* | Horizon ($F_{2/29}$) | Treatment x Horizon ($F_{2/29}$) |
|---|---|---|---|---|
| **Bacteria** | **Phylum** | | | |
| | Acidobacteria | 1.25† | 0.10 | 0.48 |
| | Actinobacteria | 0.63 | 1.05 | 0.39 |
| | Bacteroidetes | 0.81 | 1.42 | 0.64 |
| | Chloroflexi | 0.90 | **1.61*** (↑)‡ | 0.58 |
| | Nitrospirae | 1.72 | 1.32 | 0.60 |
| | Patescibacteria | 1.05 | 1.04 | 0.71 |
| | Planctomycetes | 1.00 | 1.29 | 0.52 |
| | Proteobacteria | 0.85 | 1.75 | 0.65 |
| | Rokubacteria | 0.65 | **2.46*** (↑) | 1.14 |
| | Verrucomicrobia | 1.26 | 1.32 | 0.48 |
| | **Class** | | | |
| | Alphaproteobacteria | 0.80 | 1.64 | 0.37 |
| | Anaerolineae | 0.96 | **1.74*** (↑) | 0.61 |
| | **Order** | | | |
| | Anaerolineales | 0.78 | **2.06*** (↑) | 0.65 |
| | Rhizobiales | 0.44 | 2.39 | 0.23 |
| **Fungi** | **Phylum** | | | |
| | Ascomycota | 1.04 | 0.97 | 0.78 |
| | Basidiomycota | **1.85**** (↓) | 1.19 | 0.98 |
| | Mortierellomycota | 0.63 | **1.74*** (↓) | 1.00 |
| | Rozellomycota | 1.10 | 0.63 | 1.50 |
| | **Class** | | | |
| | Agaricomycetes | **1.83**** (↓) | 1.19 | 0.98 |
| | **Order** | | | |
| | Agaricales | **1.76*** (↓) | 1.23 | 0.89 |
| | Heliotales | 1.43 | 1.04 | 0.93 |
| | Cantharellales | **2.12**** (↓) | 1.00 | 1.07 |

*Reported only the 10 most abundant bacterial and four most abundant fungal phyla and lower taxonomic levels (classes and orders) when $p < 0.1$.*
*Significance levels: *$p < 0.05$, **$p < 0.01$.*
*† F-ratio tests (F) were conducted as main tests by analysis of variance (ANOVA) to assess the significant effects of N addition, depth or their interaction. Values in bold highlight significant effects.*
**Degrees of freedom for each factor are given in brackets.*
*‡ Direction of changes in relative abundance with N or depth (from surface to lower depths); increase (↑) or decrease (↓).*

parameter. In our study, despite the fact that we did not observe any change of biomass or N concentrations in the fine roots, needle dry weight as well as needle N concentration increased significantly from the 4th year of the N addition (Krause et al., 2012). This indicates that some additional N is indeed available to tree roots but that it was transported to aboveground tree compartments. The fact that none of the fine-root traits significantly responded to the N addition is likely related to other factors limiting root growth, especially the anoxic conditions that prevail most of the time in the lower gleyic layers of the soil. Combined with waterlogging, this can indeed strongly limit root growth and, subsequently, the uptake of N (Fan et al., 2017).

## Long-Term N Addition Effects on Soil Microbial Communities

Soil microbial communities were remarkably resistant to long-term N addition. Although there have been several studies examining the effects of N deposition on microbial communities across ecosystems (Treseder, 2008; Zhou et al., 2017), ours is one of the few that comprehensively describes the long-term (>20 years) effects of moderate N addition on bacterial and fungal diversity and community structures in forest soils. Overall, the soil microbiome was relatively resistant and responded only weakly to long-term moderate N addition at our forest site. In the long-term soil microbial communities seem to be very resilient to environmental change or disturbance and adapt to new environmental conditions (Hartmann et al., 2014; Frossard et al., 2018). Another reason for the weak response of the soil microbiome might be that the added N is easily available and soluble, so it can either be washed out, or readily taken up by ectomycorrhizal fungi and roots and transported to the aboveground parts or readily immobilized in the soil (Schleppi et al., 2004; Providoli et al., 2006). Since N is not a limiting factor for the belowground communities here, more N cannot be truly used for more growth (microbial biomass). Another factor limiting the responses of N to the microbial communities is certainly the low oxygen available at lower soil depths. Because of their high clay content, Alptal soils feature anaerobic microenvironments. At this forest site a water-impermeable soil layer in the underground (gleyic soils) hinders to alleviate the oxygen limitation. All these mentioned reasons explain why we found no or only minor changes of the soil microbial communities to the moderate long-term N addition at this forest site.

The bacterial and fungal abundance remained unchanged, which is in agreement with others (Peng et al., 2017; Forstner et al., 2019b). Similarly, Hesse et al. (2015) found no change in fungal biomass in a natural maple forest in USA treated with N for 16 years. We assume that the lack of a significant effect on microbial biomass is linked to the fact that the root biomass was not affected and that the effects on C-exudate production did not alter the size of the root-associated microbes. Similarly, the abundance of C and N cycling genes were not affected by N addition.

Fungal α-diversity (Richness and Shannon Index) also remained unchanged, which is consistent with other studies with long-term N addition experiments in forests (Freedman et al., 2015; Hesse et al., 2015; Morrison et al., 2016). Morrison et al. (2016) reported no effect on fungal diversity with the addition of 50 kg N $ha^{-1}$ $yr^{-1}$ but an increase of fungal richness with higher N addition rates (150 kg N $ha^{-1}$ $yr^{-1}$). A change of fungal richness in response to N-fertilization was reported in 0–2 cm soil depth but not at lower soil depths (5 and 10 cm). Similarly, Haas et al. (2018) showed an increase in fungal diversity with nutrient addition (100 kg N $ha^{-1}$ $y^{-1}$), indicating that the effects on fungal diversity dependent on the amount of N added and soil horizon. N addition may affect microbial communities mainly as a nutrient rather than via soil acidification as suggested by Zhou et al. (2017).

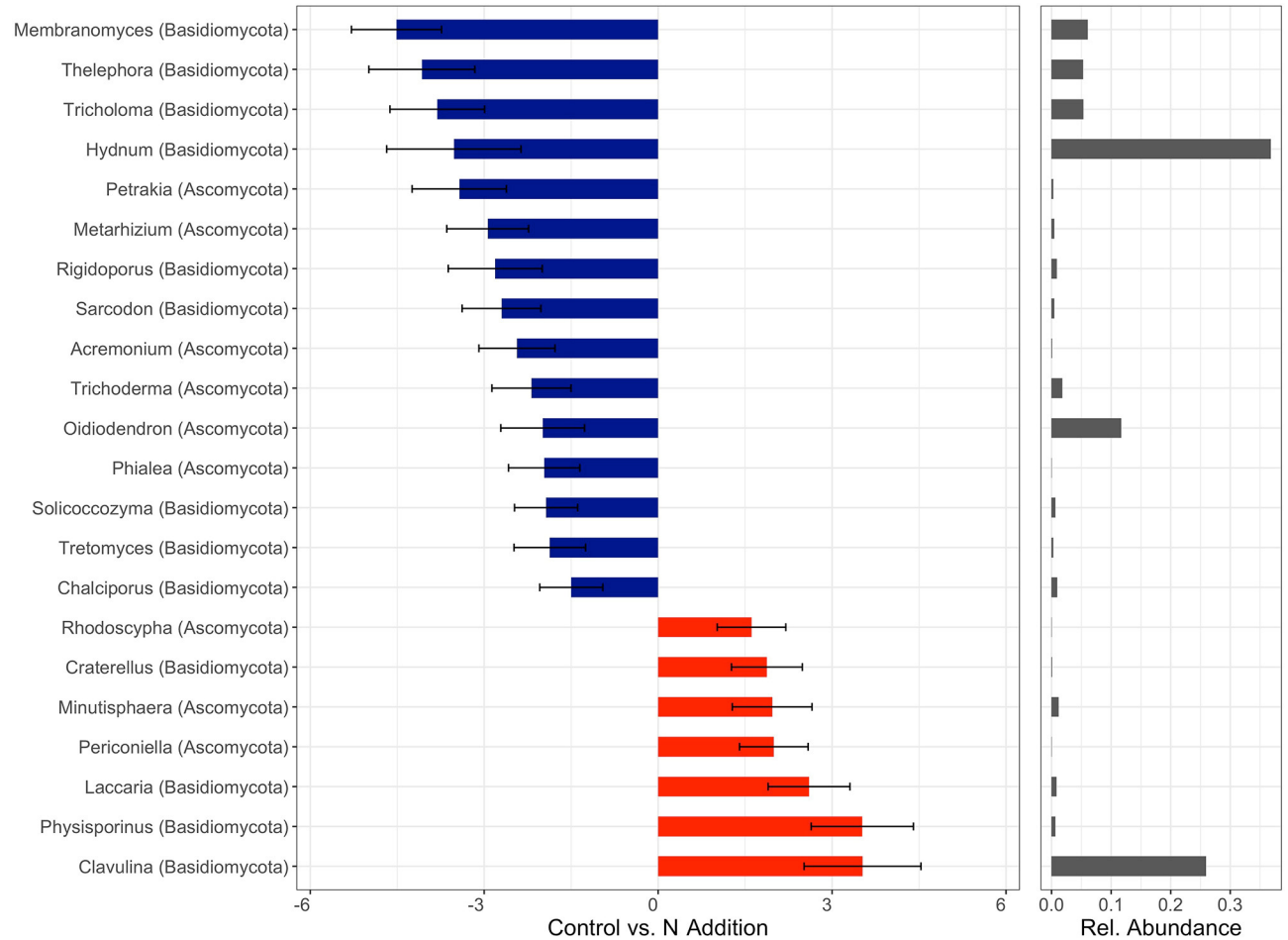


**FIGURE 6 |** Differently abundant fungal genera (statistically different $p < 0.05$) which respond to N treatments across all soil horizons with a $\log_2$-fold change > 1.0. Negative values (blue) refer to Control-upregulated genera, positive values (red) to N-Addition-upregulated genera. Bar diagrams on the right shows the relative abundance.

Long-term N additions showed weak ($p = 0.06$) changes in the structure of the fungal communities. This response was similar across depths (treatment × depth, $p = 0.77$). It was observed that elevated N deposition has either a significant influence (Eisenlord et al., 2013; Entwistle et al., 2013; Weber et al., 2013; Hesse et al., 2015; Morrison et al., 2016; van der Linde et al., 2018) or no effect (Freedman et al., 2015) on the fungal community composition. N treatments effects were dependent on soil depth in another study (Weber et al., 2013) and were most evident in very shallow surface horizons. We also expected the strongest effects of N deposition in the first (0–5 cm) soil layer according to the partitioning of N deposition (Hagedorn et al., 2001a; Providoli et al., 2006) but here in our study we did not find treatment × soil depth interactions neither for bacteria nor fungi.

The observed change of fungal community composition with elevated N deposition was mainly driven by a shift of relative abundance of *Basidiomycota* and *Ascomycota*. Consistent with previous studies that examined the response of soil fungal community composition to N fertilization (Weber et al., 2013), we recovered increased numbers of *Ascomycota* sequences and decreased numbers of *Basidiomycota* sequences (i.e., *Agaricales*) from N-treated soils in all depth intervals. Reduction in *Basidiomycota* abundance may alleviate some of the competitive pressures on *Ascomycota* for resources and thus explain the contrasting changes observed in these phyla (Geisseler and Scow, 2014; Farrer and Suding, 2016; Zhou et al., 2017). This phylum-level composition shift was accompanied by changes on lower taxonomical level that warrant further study. Differential abundant taxa analysis indicated that fungal genera such as the ectomycorrhizal fungi *Hydnum*, *Piloderma*, *Amanita*, and *Tricholoma* showed decreased recovery of sequences in response to N addition. Treseder (2004) and Li et al. (2015) as well observed in their meta-analysis on simulated N deposition a significant decrease of fungal colonization of roots. Because simulated N deposition supplies directly plant-available N, plant investment in ectomycorrhizal fungi may be minimal and result in a reduction of ectomycorrhizal mycelia growth and production (Sims et al., 2007). A decline in the relative abundance of

ectomycorrhizal fungi, in particular members of *Amanitaceae*, *Cortinariaceae*, and *Russulaceae* following long-term N addition has also been reported by others (Burke et al., 2006; Weber et al., 2013; Morrison et al., 2016). However, ectomycorrhizal responses have been shown to be taxon-specific with N enrichment by disfavoring *Cortinarius* species and most *Russula* species, while significantly enhancing the relative abundance of *Russula vinacea* (Morrison et al., 2016). Here, nitrophilic species included ectomycorrhizal as well as saprotrophic fungi. In particular, *Laccaria*, *Hygrophorus*, and *Pachyphlodes*, a truffle-like fungi belonging to the *Pezizaceae*, all known to be ectomycorrhizal associates of trees, were favored by the addition of N.

In contrast to fungi, bacteria were remarkably resistant and did not show changes due to long-term N addition. While the effects of N addition on the diversity of bacterial communities are not always clear, including negative, positive or no effects, changes in the composition across different ecosystems are the rule (Ramirez et al., 2012; Leff et al., 2015; Haas et al., 2018). Studies in mixed hardwood stands, loblolly pine plantations, and boreal forest have all reported either no effect (Burke et al., 2006) or an increase of bacterial richness and diversity after long-term N-addition (Turlapati et al., 2013; Haas et al., 2018). Twenty years of N-addition in a mixed hardwood stand induced a significant increase in diversity as well as a change in composition in both organic and mineral soils (Turlapati et al., 2013). The increase in diversity was attributable to changes in community structure with significantly higher relative abundance of *Acidobacteria*, *Chlamydiae*, and *Proteobacteria* with N addition. In contrast, in our experiment N addition did not change bacterial community structure neither at the phylum level nor at different soil depths after 20 years. Even at lower taxonomic level (e.g., genus) we did not detect significant ($p < 0.05$) responses of specific bacterial taxa to long-term N addition.

Within deeper soil depths we found significant more bacterial sequences from the class *Anaerolineae* of the phylum *Chloroflexi*, independently on the N addition. Members of the phylum *Chloroflexi* are slow growing heterotrophic bacteria, that are ubiquitous in natural ecosystems, whereas *Anaerolineae* become abundant at anaerobic conditions (Yamada and Sekiguchi, 2009; Hartmann et al., 2014). Because of their high clay content, combined with the wet climate of the site, this obviously favors the anoxic classes of *Chloroflexi* like *Anaerolineae* (Vos et al., 2013). Moreover, the increased presence of the methane-producing *Methanocella* and *Methanolinea* in the gleyic soil layers points to prevailing anaerobic conditions that strongly limits the root growth and most probably the response of the soil microbes to long-term moderate N addition.

## CONCLUSIONS

From a functional approach, we conclude that long-term moderate N addition at the Alptal forest site did not strongly affect the soil microbiome and its functioning. Changes due to the treatment were small compared to the heterogeneity of the soil and to differences between soil horizons. The present study including DNA analyses largely confirms the conclusion that the soil microbiome is remarkably resistant to such a chronic low-dose N treatment. We can see some shifts that can be ascribed to the surplus of N that accumulates in the soil, mainly in the composition of the fungal community. Even if the soil microbiome appears to retain its functions and trees are still taking advantage of the additional N to build larger needles and increase their stem growth (Krause et al., 2012), N continues to accumulate in the soil of the treated plots. All the small changes seen so far could intensify in the future and possibly lead to much stronger impacts in a non-linear way. At (slowly decreasing) ambient deposition rates, however, it seems that no negative consequences on the soil microbiome and its function should be feared within the next decades.

## DATA AVAILABILITY STATEMENT

The datasets generated for this study can be found in the NCBI Sequence Read Archive, PRJNA595488.

## AUTHOR CONTRIBUTIONS

PS designed the study and participated in sample collection. IB, MC, BF, and PS contributed to data collection. IB, AD, BF, and PS performed data analysis. IB, BF, and PS wrote the study. All authors commented on previous versions of the manuscript, read and approved the final manuscript.

## FUNDING

This study was partly funded by the Swiss National Science Foundation (SNSF) under the grant C16.0052: Linking forest soil food-web patterns with soil organic matter characteristics across five European biogeographical regions.

## ACKNOWLEDGMENTS

We thank the Central Laboratory, Bernhard Elsner, Simon Baumgartner, and Beat Stierli (Swiss Federal Research Institute WSL) for completing soil analyses and assisting with other laboratory work. We also acknowledge the Genetic Diversity Centre (GDC) of the ETH Zurich and the contribution of scientists at the McGill University and Génome Québec Innovation Center in Montréal, Canada, for performing Illumina MiSeq sequencing.

## SUPPLEMENTARY MATERIAL

The Supplementary Material for this article can be found online at: https://www.frontiersin.org/articles/10.3389/ffgc.2020.00077/full#supplementary-material

## REFERENCES


Abarenkov, K., Henrik Nilsson, R., Larsson, K., Alexander, I. J., Eberhardt, U., Erland, S., et al. (2010). The UNITE database for molecular identification of fungi–recent updates and future perspectives. *New Phytol.* 186, 281–285. doi: 10.1111/j.1469-8137.2009.03160

Aber, J. D. (2002). "Nitrogen saturation in temperate forest ecosystems: current theory, remaining questions and recent advances," in *Progress in Plant Nutrition: Plenary Lectures of the XIV International Plant Nutrition Colloquium. Developments in Plant and Soil Sciences*, eds W. J. Horst, A. Bürkert, N. Claassen, H. Flessa, W. B. Frommer, H. Goldbach, W. Merbach, H.-W. Olfs, V. Römheld, B. Sattelmacher, U. Schmidhalter, M. K. Schenk, and N. von Wirén (Dordrecht: Springer), 179–188.

Allen, S. E. (1989). *Chemical Analysis of Ecological Materials, 2nd Edn*. Oxford, London: Blackwell Scientific Publications.

Allison, S. D., Hanson, C. A., and Treseder, K. K. (2007). Nitrogen fertilization reduces diversity and alters community structure of active fungi in boreal ecosystems. *Soil Biol. Biochem.* 39, 1878–1887. doi: 10.1016/j.soilbio.2007.02.001

Baldrian, P. (2017). Forest microbiome: diversity, complexity and dynamics. *FEMS Microbiol. Rev.* 41, 109–130. doi: 10.1093/femsre/fuw040

Bobbink, R., Hicks, K., Galloway, J., Spranger, R., Alkemade, M., Ashmore, M., et al. (2010). Global assessment of nitrogen deposition effects on terrestrial plant diversity: a synthesis. *Ecol. Appl.* 20, 30–59. doi: 10.1890/08-1140.1

Bowden, R. D., Davidson, E., Savage, K., Arabia, C., and Steudler, P. (2004). Chronic nitrogen additions reduce total soil respiration and microbial respiration in temperate forest soils at the Harvard Forest. *For. Ecol. Manag.* 196, 43–56. doi: 10.1016/j.foreco.2004.03.011

Bowden, R. D., Rullo, G., Stevens, G. R., and Steudler, P. A. (2000). Soil fluxes of carbon dioxide, nitrous oxide, and methane at a productive temperate deciduous forest. *J. Environ. Qual.* 29, 268–276. doi: 10.2134/jeq2000.00472425002900010034x

Boxman, A. W., Blanck, K., Brandrud, T. E., Emmett, B. A., Gundersen, P., Hoger-Vorst, R. F., et al. (1998). Vegetation and soil biota response to experimentally-changed nitrogen inputs in coniferous forest ecosystems of the NITREX project. *For. Ecol. Manag.* 101, 65–79. doi: 10.1016/S0378-1127(97)00126-6

Bredemeier, M., Blanck, K., Xu, Y.-J., Tietema, A., Boxman, A. W., Emmett, B., et al. (1998). Input-output budgets at the NITREX sites. *For. Ecol. Manag.* 101, 57–64. doi: 10.1016/S0378-1127(97)00125-4

Brunner, I., Herzog, C., Galiano, L., and Gessler, A. (2019). Plasticity of fine-root traits under long-term irrigation of a water-limited Scots pine forest. *Front Plant Sci.* 10:701. doi: 10.3389/fpls.2019.00701

Burke, D. J., Kretzer, A. M., Rygiewicz, P. T., and Topa, M. A. (2006). Soil bacterial diversity in a loblolly pine plantation: influence of ectomycorrhizas and fertilization. *FEMS Microbiol. Ecol.* 57, 409–419. doi: 10.1111/j.1574-6941.2006.00125.x

Carnol, M., Cudlin, P., and Ineson, P. (1999). Impacts of $(NH4)_2SO4$ deposition on Norway spruce (Picea abies [L.] Karst) roots. *Water Air Soil Pollut.* 116, 111–120. doi: 10.1023/A:1005250710017

Carnol, M., Ineson, P., Anderson, J. M., Beese, F., Berg, M. P., Bolger, T., et al. (1997). The effects of ammonium sulphate deposition and root sinks on soil solution chemistry in coniferous forest soils. *Biogeochemistry* 38, 255–280. doi: 10.1023/A:1005875505591

Cheng, S. J., Hess, P. G., Wieder, W. R., Thomas, R. Q., Nadelhoffer, K. J., Vira, J., et al. (2019). Decadal fates and impacts of nitrogen additions on temperate forest carbon storage: a data-model comparison. *Biogeosciences* 16, 2771–2793. doi: 10.5194/bg-16-2771-2019

Cotrufo, M. F., Wallenstein, M. D., Boot, C. M., Denef, K., and Paul, E. (2013). The microbial efficiency-matrix stabilization (MEMS) framework integrates plant litter decomposition with soil organic matter stabilization: do labile plant inputs form stable soil organic matter? *Glob. Change Biol.* 19, 988–995. doi: 10.1111/gcb.12113

DeForest, J. L., Zak, D. R., Pregitzer, K. S., and Burton, A. J. (2004). Atmospheric nitrate deposition and the microbial degradation of cellobiose and vanillin in a northern hardwood forest. *Soil Biol. Biochem.* 39, 1878–1887. doi: 10.1016/j.soilbio.2004.02.011

Demoling, F., Nilsson, L. O., and Bååth, E. (2008). Bacterial and fungal response to nitrogen fertilization in three coniferous forest soils. *Soil Biol. Biochem.* 40, 370–379. doi: 10.1016/j.soilbio.2007.08.019

Dise, N. B., and Wright, R. F. (1995). Nitrogen deposition and leaching from European forests. *For. Ecol. Manag.* 71, 153–162. doi: 10.1016/0378-1127(94)06092-W

Edgar, R. C. (2010). Search and clustering orders of magnitude faster than BLAST. *Bioinformatics* 26, 2460–2461. doi: 10.1093/bioinformatics/btq461

Edgar, R. C. (2013). UPARSE: highly accurate OTU sequences from microbial amplicon reads. *Nat. Methods*. 10, 996–998. doi: 10.1038/nmeth.2604

Edgar, R. C., and Flyvbjerg, H. (2015). Error filtering, pair assembly and error correction for next-generation sequencing reads. *Bioinformatics* 31, 3476–3482. doi: 10.1093/bioinformatics/btv401

Edwards, I. P., Zak, D. R., Kellner, H., Eisenlord, S. D., and Pregitzer, K. S. (2011). Simulated atmospheric N deposition alters fungal community composition and suppresses ligninolytic gene expression in a northern hardwood forest. *PLoS ONE* 6:e20421. doi: 10.1371/journal.pone.0020421

Eisenlord, S. D., Freedman, Z., Zak, D. R., Xue, K., He, Z., and Zhou, J. (2013). Microbial mechanisms mediating increased soil C storage under elevated atmospheric N deposition. *Appl. Environ. Microbiol.* 79, 1191–1199. doi: 10.1128/AEM.03156-12

Emmett, B. A., Boxman, D., Bredemeier, M., Gundersen, P., Kjønaas, O. J., Moldan, F., et al. (1998). Predicting the effects of atmospheric nitrogen deposition in conifer stands: evidence from the NITREX ecosystem-scale experiments. *Ecosystems* 1, 352–360. doi: 10.1007/s100219900029

Entwistle, E. M., Zak, D. R., and Edwards, I. P. (2013). Long-term experimental nitrogen deposition alters the composition of the active fungal community in the forest floor. *Soil Sci. Soc. Am. J.* 77, 1648–1658. doi: 10.2136/sssaj2013.05.0179

Erisman, J. W., Galloway, J., Seitzinger, S., Bleeker, A., and Butterbach-Bahl, K. (2011). Reactive nitrogen in the environment and its effect on climate change. *Curr. Opin. Environ. Sustain.* 3, 281–290. doi: 10.1016/j.cosust.2011.08.012

Fan, Y., Miguez-Macho, G., Jobbágy, E. G., Jackson, R. B., and Otero-Casal, C. (2017). Hydrologic regulation of plant rooting depth. *Proc. Natl. Acad. Sci. U. S. A.* 114, 10572–10577. doi: 10.1073/pnas.1712381114

Farrer, E. C., and Suding, K. N. (2016). Teasing apart plant community responses to N enrichment: the roles of resource limitation, competition and soil microbes. *Ecol. Lett.* 19, 1287–1296. doi: 10.1111/ele.12665

Forstner, S. J., Wechselberger, V., Müller, S., Keiblinger, K. M., Díaz-Pinés, E., Wanek, W., et al. (2019a). Vertical redistribution of soil organic carbon pools after twenty years of nitrogen addition in two temperate coniferous forests. *Ecosystems* 22, 379–400. doi: 10.1007/s10021-018-0275-8

Forstner, S. J., Wechselberger, V., Stecher, S., Müller, S., Keiblinger, K. M., Wanek, W., et al. (2019b). Resistant soil microbial communities show signs of increasing phosphorus limitation in two temperate forests after long-term nitrogen addition. *Front. For. Glob. Change* 2:13. doi: 10.3389/ffgc.2019.00073

Freedman, Z. B., Romanowicz, K. J., Upchurch, R. A., and Zak, D. R. (2015). Differential responses of total and active soil microbial communities to long-term experimental N deposition. *Soil Biol. Biochem.* 90, 275–282. doi: 10.1016/j.soilbio.2015.08.014

Frey, B., Niklaus, P. A., Kremer, J., Lüscher, P., and Zimmermann, S. (2011). Heavy-machinery traffic impacts methane emissions as well as methanogen abundance and community structure in oxic forest soils. *Appl. Environ. Microbiol.* 77, 6060–6068. doi: 10.1128/AEM.05206-11

Frey, B., Rime, T., Phillips, M., Stierli, B., Hajdas, I., Widmer, F., et al. (2016). Microbial diversity in European alpine permafrost and active layers. *FEMS Microbiol. Ecol.* 92:fiw018. doi: 10.1093/femsec/fiw018

Frey, S. D., Knorr, M., Parrent, J. L., and Simpson, R. T. (2004). Chronic nitrogen enrichment affects the structure and function of the soil microbial community in temperate hardwood and pine forests. *For. Ecol. Manag.* 196, 159–171. doi: 10.1016/j.foreco.2004.03.018

Frey, S. D., Ollinger, S., Nadelhoffer, K., Bowden, R., Brzostek, E., Burton, A., et al. (2014). Chronic nitrogen additions suppress decomposition and

sequester soil carbon in temperate forests. *Biogeochemistry* 121, 305–316. doi: 10.1007/s10533-014-0004-0

Frossard, A., Donhauser, J., Mestrot, A., Gygax, S., and Frey, B. (2018). Long- and short-term effects of mercury pollution on the soil microbiome. *Soil Biol. Biochem.* 120, 191–199. doi: 10.1016/j.soilbio.2018.01.028

Galloway, J. N., Dentener, F. J., Capone, D. G., Boyer, E. W., Howarth, R. W., Seitzinger, S. P., et al. (2004). Nitrogen cycles: past, present, and future. *Biogeochemistry* 70, 153–226. doi: 10.1007/s10533-004-0370-0

Galloway, J. N., Townsend, A. R., Erisman, J. W., Bekunda, M., Cai, Z., Freney, J. R., et al. (2008). Transformation of the nitrogen cycle: recent trends, questions, and potential solutions. *Science* 320, 889–892. doi: 10.1126/science.1136674

Geisseler, D., and Scow, K. M. (2014). Long-term effects of mineral fertilizers on soil microorganisms—a review. *Soil Biol. Biochem.* 75, 54–63. doi: 10.1016/j.soilbio.2014.03.023

Ghani, A., Dexter, M., and Perrott, K. W. (2003). Hot-water extractable carbon in soils: a sensitive measurement for determining impacts of fertilisation, grazing and cultivation. *Soil Biol. Biochem.* 35, 1231–1243. doi: 10.1016/S0038-0717(03)00186-X

Gregorich, E. G., Beare, M. H., Stoklas, U., and St-Georges, P. (2003). Biodegradability of soluble organic matter in maize-cropped soils. *Geoderma* 113, 237–252. doi: 10.1016/S0016-7061(02)00363-4

Gundale, M. J., From, F., Bach, L. H., and Nordin, A. (2014). Anthropogenic nitrogen deposition in boreal forests has a minor impact on the global carbon cycle. *Glob. Chang. Biol.* 20, 276–286. doi: 10.1111/gcb.12422

Gundersen, P., Callesen, I., and de Vries, W. (1998). Nitrate leaching in forest ecosystems is related to forest floor C/N ratios. *Environ. Pollut.* 102, 403–407. doi: 10.1016/S0269-7491(98)80060-2

Gundersen, P., Christiansen, J. R., Alberti, G., Brüggemann, N., Castaldi, S., Gasche, R., et al. (2012). The response of methane and nitrous oxide fluxes to forest change in Europe. *Biogeosciences* 9, 3999–4012. doi: 10.5194/bg-9-3999-2012

Haas, J. C., Street, N. R., Sjödin, A., Lee, N. M., Högberg, M. N., Näsholm, T., et al. (2018). Microbial community response to growing season and plant nutrient optimisation in a boreal Norway spruce forest. *Soil Biol. Biochem.* 125, 197–209. doi: 10.1016/j.soilbio.2018.07.005

Hagedorn, F., Bucher, J. B., and Schleppi, P. (2001a). Contrasting dynamics of dissolved inorganic and organic nitrogen in soil and surface waters of forested catchments with Gleysols. *Geoderma* 100, 173–192. doi: 10.1016/S0016-7061(00)00085-9

Hagedorn, F., Schleppi, P., Bucher, J. B., and Flühler, H. (2001b). Retention and leaching of elevated N deposition in a forested ecosystem with Gleysols. *Water Air Soil Pollut.* 129, 119–142. doi: 10.1023/A:1010397232239

Hart, S. C., Stark, J. M., Davidson, E. A., and Firestone, M. K. (1994). "Nitrogen mineralization, immobilization, and nitrification," in *Methods of Soil Analysis. Part 2: Microbiological and Biochemical Properties*, eds R. Weaver, S. Angle, P. Bottomley, D. Bezdicek, S. Smith, S., A. Tabatabai, et al. (Madison, WI: Soil Science Society of America), 985–1018. doi: 10.2136/sssabookser5.2.c42

Hartmann, M., Brunner, I., Hagedorn, F., Bardgett, R. D., Stierli, B., Herzog, C., et al. (2017). A decade of irrigation transforms the soil microbiome of a semi-arid pine forest. *Mol. Ecol.* 26, 1190–1206. doi: 10.1111/mec.13995

Hartmann, M., Niklaus, P. A., Zimmermann, S., Schmutz, S., Kremer, J., Abarenkov, K., et al. (2014). Resistance and resilience of the forest soil microbiome to logging-associated compaction. *ISME J.* 8, 226–244. doi: 10.1038/ismej.2013

Hasselquist, N. J., Metcalfe, D. B., and Högberg, P. (2012). Contrasting effects of low and high nitrogen additions on soil $CO_2$ flux components and ectomycorrhizal fungal sporocarp production in a boreal forest. *Glob. Change Biol.* 18, 3596–3605. doi: 10.1111/gcb.12001

Haynes, B. E., and Gower, S. T. (1995). Belowground carbon allocation in unfertilized and fertilized red pine plantations in northern Wisconsin. *Tree Physiol.* 15, 317–325. doi: 10.1093/treephys/15.5.317

Hesse, C. N., Mueller, R. C., Vuyisich, M., Gallegos-Graves, L. V., Gleasner, C. D., Zak, D. R., et al. (2015). Forest floor community metatranscriptomes identify fungal and bacterial responses to N deposition in two maple forests. *Front. Microbiol.* 6:337. doi: 10.3389/fmicb.2015.00337

Högberg, P., Fan, H., Quist, M., Binkley, D., and Tamm, C. O. (2006). Tree growth and soil acidification in response to 30 years of experimental nitrogen loading on boreal forest. *Glob. Change Biol.* 12, 489–499. doi: 10.1111/j.1365-2486.2006.01102.x

Janssens, I. A., Dieleman, W., Luyssaert, S., Subke, J.-A., Reichstein, M., Ceulemans, R., et al. (2010). Reduction of forest soil respiration in response to nitrogen deposition. *Nat. Geosci.* 3, 315–322. doi: 10.1038/ngeo844

Jenkinson, D. S., Brookes, P. C., and Powlson, D. S. (2004). Measuring soil microbial biomass. *Soil Biol. Biochem.* 36, 5–7. doi: 10.1016/j.soilbio.2003.10.002

Joergensen, R. G., and Mueller, T. (1996). The fumigation-extraction method to estimate soil microbial biomass: calibration of the $k_{EN}$ value. *Soil Biol. Biochem.* 28, 33–37. doi: 10.1016/0038-0717(95)00102-6

Krause, K., Cherubini, P., Bugmann, H., and Schleppi, P. (2012). Growth enhancement of *Picea abies* trees under long-term, low-dose N addition is due to morphological more than to physiological changes. *Tree Physiol.* 32, 1471–1481. doi: 10.1093/treephys/tps109

Krause, K., Niklaus, P. A., and Schleppi, P. (2013). Soil-atmosphere fluxes of the greenhouse gases $CO_2$, $CH_4$ and $N_2O$ in a mountain spruce forest subjected to long-term N addition and to tree girdling. *Agric. For. Meteorol.* 181, 61–68. doi: 10.1016/j.agrformet.2013.07.007

Leff, J. W., Jones, S. E., Prober, S. M., Barberán, A., Borer, E. T., Firn, J. L., et al. (2015). Consistent responses of soil microbial communities to elevated nutrient inputs in grasslands across the globe. *Proc. Natl. Acad. Sci. U. S. A.* 112, 10967–10972. doi: 10.1073/pnas.1508382112

Li, W., Jin, C., Guan, D., Wang, Q., Wang, A., Yuan, F., et al. (2015). The effects of simulated nitrogen deposition on plant root traits: a meta-analysis. *Soil Biol. Biochem.* 82, 112–118. doi: 10.1016/j.soilbio.2015.01.001

Liu, X., Yang, Z., Lin, C., Giardina, C. P., Xiong, D., Lin, W., et al. (2017). Will nitrogen deposition mitigate warming-increased soil respiration in a young subtropical plantation? *Agric. For. Meteorol.* 246, 78–85. doi: 10.1016/j.agrformet.2017.06.010

Llado, S., Lopez-Mondejar, R., and Baldrian, P. (2017). Forest soil bacteria: diversity, involvement in ecosystem processes, and response to global change. *Microbiol. Mol. Biol. Rev.* 81, e00063–e00016. doi: 10.1128/MMBR.00063-16

Love, M. I., Huber, W., and Anders, S. (2014). Moderated estimation of fold change and dispersion for RNA-seq data with DESeq2. *Genome Biol.* 15:550. doi: 10.1186/s13059-014-0550-8

Maaroufi, N. I., Nordin, A., Hasselquist, N. J., Bach, L. H., Palmqvist, K., and Gundale, M. J. (2015). Anthropogenic nitrogen deposition enhances carbon sequestration in boreal soils. *Glob. Change Biol.* 21, 3169–3180. doi: 10.1111/gcb.12904

Maaroufi, N. I., Nordin, A., Palmqvist, K., Hasselquist, N. J., Forsmark, B., Rosenstock, N. P., et al. (2019). Anthropogenic nitrogen enrichment enhances soil carbon accumulation by impacting saprotrophs rather than ectomycorrhizal fungal activity. *Glob. Change Biol.* 25, 2900–2914. doi: 10.1111/gcb.14722

McMurdie, P. J., and Holmes, S. (2013). Phyloseq: an R package for reproducible interactive analysis and graphics of microbiome census data. *PLoS ONE* 8:e61217. doi: 10.1371/journal.pone.0061217

Mellert, K. H., and Göttlein, A. (2012). Comparison of new foliar nutrient thresholds derived from van den Burg's literature compilation with established central European references. *Euro. J. For. Res.* 131, 1461–1472. doi: 10.1007/s10342-012-0615-8

Mohn, J., Schürmann, A., Hagedorn, F., Schleppi, P., and Bachofen, R. (2000). Increased rates of denitrification in nitrogen-treated forest soils. *For. Ecol. Manag.* 137, 113–119. doi: 10.1016/S0378-1127(99)00320-5

Moldan, F., and Wright, R. F. (2011). Nitrogen leaching and acidification during 19 years of $NH_4NO_3$ additions to a coniferous-forested catchment at Gårdsjön, Sweden (NITREX). *Environ. Pollut.* 159, 431–440. doi: 10.1016/j.envpol.2010.10.025

Mooshammer, M., Wanek, W., Hämmerle, I., Fuchslueger, L., Hofhansl, F., Knoltsch, A., et al. (2014). Adjustment of microbial nitrogen use efficiency to

carbon:nitrogen imbalances regulates soil N cycling. *Nat. Commun.* 5:3694. doi: 10.1038/ncomms4694

Morier, I., Schleppi, P., Saurer, M., Providoli, I., and Guenat, C. (2010). Retention and hydrolysable fraction of atmospherically deposited nitrogen in two contrasting forest soils in Switzerland. *Eur. J. Soil Sci.* 61, 197–206. doi: 10.1111/j.1365-2389.2010.01226.x

Morrison, E. W., Frey, S. D., Sadowsky, J. J., van Diepen, L. T., Thomas, W. K., and Pringle, A. (2016). Chronic nitrogen additions fundamentally restructure the soil fungal community in a temperate forest. *Fungal Ecol.* 23, 48–57. doi: 10.1016/j.funeco.2016.05.011

Nadelhoffer, K. J., Emmett, B. A., Gundersen, P., Kjønaas, O. J., Koopmans, C. J., Schleppi, P., et al. (1999). Nitrogen deposition makes a minor contribution to carbon sequestration in temperate forests. *Nature* 398, 145–148. doi: 10.1038/18205

Nguyen, N. H., Song, Z. W., Bates, S. T., Branco, S., Tedersoo, L., Menke, J., et al. (2016). FUNGuild: an open annotation tool for parsing fungal community datasets by ecological guild. *Fungal Ecol.* 20, 241–248. doi: 10.1016/j.funeco. 2015.06.006

Oksanen, J., Blanchet, F. G., Friendly, M., Kindt, R., Legendre, P., McGlinn, D., et al. (2017). *Vegan: Community Ecology Package. R Package Version 2.4–4*. Available online at: http://CRAN.Rproject.org/package=vegan

Ostonen, I., Püttsepp, Ü., Biel, C., Alberton, O., Bakker, M. R., Lõhmus, K., et al. (2007). Specific root length as an indicator of environmental change. *Plant Biosyst.* 141, 426–442. doi: 10.1080/11263500701626069

Peng, Y., Chen, G. S., Chen, G. T., Li, S., Peng, T. C., Qiu, X. R., et al. (2017). Soil biochemical responses to nitrogen addition in a secondary evergreen broad-leaved forest ecosystem. *Sci. Rep.* 7:2783. doi: 10.1038/s41598-017-03044-w

Providoli, I., Bugmann, H., Siegwolf, R., Buchmann, N., and Schleppi, P. (2006). Pathways and dynamics of $^{15}NO_3^-$ and $^{15}NH_4^+$ applied in a mountain *Picea abies* forest and in a nearby meadow in central Switzerland. *Soil Biol. Biochem.* 38, 1645–1657. doi: 10.1016/j.soilbio.2005.11.019

Quast, C., Pruesse, E., Yilmaz, P., Gerken, J., Schweer, T., Yarza, P., et al. (2013). The SILVA ribosomal RNA gene database project: improved data processing and web-based tools. *Nucleic Acids Res.* 41, D590–D596. doi: 10.1093/nar/gks1219

R Core Team (2017). *R: A Language and Environment for Statistical Computing*. Vienna: R Foundation for Statistical Computing.

Ramirez, K. S., Craine, J. M., and Fierer, N. (2012). Consistent effects of nitrogen amendments on soil microbial communities and processes across biomes. *Glob. Change Biol.* 18, 1918–1927. doi: 10.1111/j.1365-2486.2012.02639.x

Rime, T., Hartmann, M., and Frey, B. (2016). Potential sources of microbial colonizers in initial soil ecosystem after retreat of an Alpine glacier. *ISME J.* 10, 1625–1641. doi: 10.1038/ismej.2015.238

Robertson, G. P., Wedin, D., Groffmann, P. M., Blair, J. M., Holland, E. A., Nadelhoffer, K. J., et al. (1999). "Soil carbon and nitrogen availability: Nitrogen mineralization, nitrification, and soil respiration potentials," in *Standard Soil Methods for Long-Term Ecological Research*, eds P. Robertson, D. C. Coleman, C. Bledsoe, and P. Sollins (New York, NY: Oxford University Press), 258–271.

Rousk, J., Bååth, E., Brookes, P. C., Lauber, C. L., Lozupone, C., Caporaso, J. G., et al. (2010). Soil bacterial and fungal communities across a pH gradient in an arable soil. *ISME J.* 4, 1340–1351. doi: 10.1038/ismej.2010.58

Saiya-Cork, K. R., Sinsabaugh, R. L., and Zak, D. R. (2002). The effects of long term nitrogen deposition on extracellular enzyme activity in an *Acer saccharum* forest soil. *Soil Biol. Biochem.* 34, 1309–1315. doi: 10.1016/S0038-0717(02)00074-3

Schleppi, P., Curtaz, F., and Krause, K. (2017). Nitrate leaching from a sub-alpine coniferous forest subjected to experimentally increased N deposition for 20 years, and effects of tree girdling and felling. *Biogeochemistry* 134, 319–335. doi: 10.1007/s10533-017-0364-3

Schleppi, P., Hagedorn, F., and Providoli, I. (2004). Nitrate leaching from a mountain forest ecosystem with Gleysols subjected to experimentally increased N deposition. *Water Air Soil Pollut. Focus* 4, 453–467. doi: 10.1023/B:WAFO.0000028371.72044.fb

Schleppi, P., Muller, N., Feyen, H., Papritz, A., Bucher, J., and Flühler, H. (1998). Nitrogen budgets of two small experimental forested catchments at Alptal, Switzerland. *For Ecol. Manag.* 101, 177–185. doi: 10.1016/S0378-1127(97)00134-5

Schmitz, A., Sanders, T., Bolte, A., Bussotti, F., Dirnböck, T., Johnson, J., et al. (2019). Responses of forest ecosystems in Europe to decreasing nitrogen deposition. *Environ. Poll.* 244, 980–994. doi: 10.1016/j.envpol.2018.09.101

Shen, J., Zhang, L. M., Guo, J. F., Ray, J. L., and He, J. Z. (2010). Impact of long-term fertilization practices on the abundance and composition of soil bacterial communities in northeast China. *Appl. Soil Ecol.* 46, 119–124. doi: 10.1016/j.apsoil.2010.06.015

Simpson, D., Andersson, C., Christensen, J. H., Engardt, M., Geels, C., Nyiri, A., et al. (2014). Impacts of climate and emission changes on nitrogen deposition in Europe: a multi-model study. *Atmos. Chem. Phys.* 14, 6995–7017. doi: 10.5194/acp-14-6995-2014

Sims, S. E., Hendricks, J. J., Mitchell, R. J., Kuehn, K. A., and Pecot, S. D. (2007). Nitrogen decreases and precipitation increases ectomycorrhizal extramatrical mycelia production in a longleaf pine forest. *Mycorrhiza* 17, 299–309. doi: 10.1007/s00572-007-0105-x

Sinsabaugh, R. L., Carreiro, M. M., and Repert, D. A. (2002). Allocation of extracellular enzymatic activity in relation to litter composition, N deposition, and mass loss. *Biogeochemistry* 60, 1–24. doi: 10.1023/A:1016541114786

Solberg, S., Dobbertin, M., Reinds, G. J., Lange, H., Andreassen, K., Garcia Fernandez, P., et al. (2009). Analyses of the impact of changes in atmospheric deposition and climate on forest growth in European monitoring plots: a stand growth approach. *For. Ecol. Manag.* 258, 1735–1750. doi: 10.1016/j.foreco.2008.09.057

Thomas, Q. R., Canham, C. D., Weathers, K. C., and Goodale, C. L. (2010). Increased tree carbon storage in response to nitrogen deposition in the US. *Nat. Geosci.* 3, 13–17. doi: 10.1038/ngeo721

Treseder, K. K. (2004). A meta-analysis of mycorrhizal responses to nitrogen, phosphorus, and atmospheric $CO_2$ in field studies. *New Phytol.* 164, 347–355. doi: 10.1111/j.1469-8137.2004.01159.x

Treseder, K. K. (2008). Nitrogen additions and microbial biomass: a meta-analysis of ecosystem studies. *Ecol. Lett.* 11, 1111–1120. doi: 10.1111/j.1461-0248.2008.01230.x

Turlapati, S. A., Minocha, R., Bhiravarasa, P. S., Tisa, L. S., Thomas, W. K., and Minocha, S. C. (2013). Chronic N-amended soils exhibit an altered bacterial community structure in Harvard Forest, MA, USA. *FEMS Microbiol. Ecol.* 83, 478–493. doi: 10.1111/1574-6941.12009

Uroz, S., Buée, M., Deveau, A., Mieszkin, S., and Martin, F. (2016). Ecology of the forest microbiome: highlights of temperate and boreal ecosystems. *Soil Biol. Biochem.* 103, 471–488. doi: 10.1016/j.soilbio.2016.09.006

van der Linde, S., Suz, L. M., Orme, C. D. L., Cox, F., Andreae, H., Asi, E., et al. (2018). Environment and host as large-scale controls of ectomycorrhizal fungi. *Nature* 558, 243–248. doi: 10.1038/s41586-018-0189-9

Vance, E. D., Brookes, P. C., and Jenkinson, D. S. (1987). An extraction method for measuring soil microbial biomass C. *Soil Biol. Biochem.* 19, 703–707. doi: 10.1016/0038-0717(87)90052-6

Vos, M., Wolf, A. B., Jennings, S. J., and Kowalchuk, G. A. (2013). Microscale determinants of bacterial diversity in soil. *FEMS Microbiol. Rev.* 37, 936–954. doi: 10.1111/1574-6976.12023

Wallenstein, M. D., McNulty, S., Fernandez, I. J., Boggs, J., and Schlesinger, W. H. (2006). Nitrogen fertilization decreases forest soil fungal and bacterial biomass in three long-term experiments. *For. Ecol. Manag.* 222, 459–468. doi: 10.1016/j.foreco.2005.11.002

Wang, Q., Garrity, G. M., Tiedje, J. M., and Cole, J. R. (2007). Naïve Bayesian classifier for rapid assignment of rRNA sequences into the new bacterial taxonomy. *Appl. Environ. Microbiol.* 73, 5261–5267. doi: 10.1128/AEM.00062-07

Weber, C. F., Vilgalys, R., and Kuske, C. R. (2013). Changes in fungal community composition in response to elevated atmospheric $CO_2$ and nitrogen fertilization varies with soil horizon. *Front. Microbiol.* 4:78. doi: 10.3389/fmicb.2013.00078

Xu, G.-L., Schleppi, P., Li, M.-H., and Fu, S.-L. (2009). Negative responses of *Collembola* in a forest soil (Alptal, Switzerland) under experimentally increased N deposition. *Environ. Pollut.* 157, 2030–2036. doi: 10.1016/j.envpol.2009.02.026

Yamada, T., and Sekiguchi, Y. (2009). Cultivation of uncultured *Chloroflexi* subphyla: significance and ecophysiology of formerly uncultured *Chloroflexi* "subphylum I" with natural and biotechnological relevance. *Microbes Environ.* 24, 205–216. doi: 10.1264/jsme2.me09151s

Zechmeister-Boltenstern, S., Keiblinger, K. M., Mooshammer, M., Peñuelas, J., Richter, A., Sardans, J., et al. (2015). The application of ecological stoichiometry to plant-microbial-soil organic matter transformations. *Ecol. Monogr.* 85, 133–155. doi: 10.1890/14-0777.1

Zhang, H., Liu, Y., Zhou, Z., and Zhang, Y. (2019). Inorganic nitrogen addition affects soil respiration and belowground organic carbon fraction for a *Pinus tabuliformis* forest. *Forests* 10:369. doi: 10.3390/f10050369

Zhou, Z., Wang, C., Zheng, M., Jiang, L., and Luo, Y. (2017). Patterns and mechanisms of responses by soil microbial communities to nitrogen addition. *Soil Biol. Biochem.* 115, 433–441. doi: 10.1016/j.soilbio.2017.09.015

**Conflict of Interest:** The authors declare that the research was conducted in the absence of any commercial or financial relationships that could be construed as a potential conflict of interest.

frontiers in Forests and Global Change

ORIGINAL RESEARCH
published: 23 July 2020
doi: 10.3389/ffgc.2020.00083

# Soil Phosphorus Dynamics Across a Holocene Chronosequence of Aeolian Sand Dunes in a Hypermaritime Environment on Calvert Island, BC, Canada

*Lee-Ann Nelson*[1,2], *Barbara J. Cade-Menun*[3]*, *Ian J. Walker*[2,4] *and Paul Sanborn*[1,2]

[1] *Ecosystem Science and Management Program, University of Northern British Columbia, Prince George, BC, Canada,* [2] *Hakai Institute, Victoria, BC, Canada,* [3] *Swift Current Research and Development Centre, Agriculture and Agri-Food Canada, Swift Current, SK, Canada,* [4] *School of Geographical Sciences and Urban Planning, School of Earth and Space Exploration, Arizona State University, Tempe, AZ, United States*

Phosphorus (P) is an essential nutrient for plant growth, but soil P concentrations decline with increasing soil age. Phosphorus often limits tree growth within the hypermaritime Coastal Western Hemlock zone in British Columbia, Canada, particularly where parent material with low P concentrations have experienced rapid weathering. To sustainably manage forests in this region, more information is needed about changes in soil P concentrations and dynamics that occur with time. This study characterized the forms and abundance of soil and foliar P compounds using a soil chronosequence developed on aeolian sand dunes on Calvert Island and compared results to chronosequences in other locations. Eight time points were examined, from a modern foredune to a relict, stabilized dune (~10,760 years old). Soil horizons were analyzed for bulk density, pH, and concentrations of total carbon (C), nitrogen (N) and total P (TP), iron (Fe), and aluminum (Al), total organic P ($P_o$), and Mehlich-extractable P and cations. For each site, P forms in L, H and organically-enriched mineral (M) horizons were characterized with solution $^{31}P$ nuclear magnetic resonance spectroscopy (P-NMR), as were foliar samples from tree species spanning all age classes except the youngest dune. This chronosequence followed the Walker and Syers (1976) model, with an exponential decline in TP mass and a humped-shape curve in $P_o$ mass with increasing age. The L horizon had lower TP concentrations than foliage samples, but similar P forms. The H horizons had a greater proportion of DNA, phosphonates and nucleotides than the L horizon and increased proportions of *myo*- and *scyllo*-inositol hexakisphosphate (IHP) with increasing age. The mineral horizons had much lower TP concentrations than other horizons and increased proportions of IHP and DNA with increasing age, which were correlated to increased exchangeable and amorphous Al concentrations. In all sample types, the proportion of orthophosphate declined with increasing age. These results enhance knowledge of P cycling within hypermaritime soils, particularly the P decline that will occur with age. This will aid in the sustainable management of the low-productivity forests typical of these ecosystems.

**Keywords: P-NMR, organic phosphorus, podzolization, forests, western red cedar, western hemlock**

OPEN ACCESS

***Edited by:***
*Friederike Lang,*
*University of Freiburg, Germany*

***Reviewed by:***
*Federica Tamburini,*
*ETH Zürich, Switzerland*
*Wulf Amelung,*
*University of Bonn, Germany*

***Correspondence:**
*Barbara J. Cade-Menun*
*barbara.cade-menun@canada.ca*

***Specialty section:***
*This article was submitted to Forest Soils, a section of the journal Frontiers in Forests and Global Change*

***Received:*** *27 February 2020*
***Accepted:*** *15 June 2020*
***Published:*** *23 July 2020*

***Citation:***
*Nelson L-A, Cade-Menun BJ, Walker IJ and Sanborn P (2020) Soil Phosphorus Dynamics Across a Holocene Chronosequence of Aeolian Sand Dunes in a Hypermaritime Environment on Calvert Island, BC, Canada. Front. For. Glob. Change 3:83. doi: 10.3389/ffgc.2020.00083*

## INTRODUCTION

Phosphorus (P) is one of the most limiting nutrients to plant growth worldwide along with nitrogen (N), and both are integral to the productive functioning of ecosystems. Total P (TP) in soil is divided into various chemical forms (compounds), which vary in their bioavailability and cycling in soil. Molecules of organic P ($P_o$) contain carbon (C), while inorganic P ($P_i$) compounds do not (Condron et al., 2005; Pierzynski et al., 2005). Inorganic $P_i$ compounds include phosphate ($H_2PO_4^-$ or $HPO_4^{2-}$ in the pH range of most soils), and phosphates linked together as pyrophosphate (with two phosphate groups) and polyphosphate (more than two phosphates). Phosphate is the only P form that plants and microbes can directly take from the soil solution, and is the predominant $P_i$ compound in most soils (Schachtman et al., 1998; Stevenson and Cole, 1999). The main $P_o$ compounds can be divided into: orthophosphate monoesters (herein referred to as monoesters), which have one C group per phosphate and include sugar phosphates (e.g., glucose 6-phosphate), mononucleotides such as adenosine monophosphate, and storage compounds such as *myo*-inositol hexakisphosphate (*myo*-IHP, phytate); orthophosphate diesters with two C groups per phosphate (herein referred to as diesters), which include phospholipids and DNA; and phosphonates with a direct C-P bond.

The soil P cycle is controlled by five main pools of P: (1) dissolved within the soil solution; (2) adsorbed to mineral surfaces; (3) precipitated from the soil solution; (4) contained within living microbial biomass; and (5) bound within non-living organic matter (Stevenson and Cole, 1999). Both $P_i$ and $P_o$ compounds are found in all of these pools (Condron et al., 2005; Pierzynski et al., 2005), and P cycling in these pools is controlled by geochemical and biological processes. The soil solution P pool is most critical; P in this pool is directly available for sorption, precipitation, biological uptake and incorporation into organic matter. However, the soil solution P concentration is usually low and soil P moves mainly by diffusion, unlike other nutrients, thereby limiting availability (Schachtman et al., 1998; Stevenson and Cole, 1999). In forests, P cycling is influenced by parent material, plant species and successional stage, and the biological P cycle is generally more dominant in the surface horizons, while geochemical P cycling is more dominant in the mineral horizons (Wood et al., 1984; Cade-Menun et al., 2000a; Lang et al., 2017).

The Walker and Syers (1976) model is the most widely-used model of P change with soil age, and states that Ca-phosphates (Ca-P) will be the first forms of P to be exploited because they are generally the most abundant P forms in the parent material and are more easily solubilized than other P forms. As soil ages and phosphate becomes scarcer, $P_o$ and P sorbed to Fe and Al (hydr)oxides will dominate, including Pi and $P_o$ forms that are tightly sorbed and thus resistant to desorption (occluded P). Therefore, to effectively manage forest soils it is necessary to characterize and measure the concentrations of $P_o$ due to the increasing dominance of $P_o$ with age, especially within P-limited systems (Walker and Syers, 1976).

Declining P with increasing age has been widely documented on soil chronosequences spanning many climates, parent materials, disturbance histories and age ranges (**Table 1**). Depending on the soil forming factors, chronosequences may become depleted of P by different mechanisms. Sandy chronosequences, such as Cooloola (Queensland, Australia), Jurien Bay (Western Australia) and Cox Bay [British Columbia (BC), Canada], generally have parent material with inherently low P concentrations and become P depleted faster than soils with greater initial P concentrations (Vitousek et al., 2010; Turner et al., 2012; Chen et al., 2015; Turner and Laliberté, 2015). The loss of $P_i$ and dissolved $P_o$ via weathering and subsequent leaching is referred to as depletion-driven P limitation, which generally takes millions of years but can occur faster with parent materials with low P concentrations (Vitousek et al., 2010). Other forms of P limitation may be caused by barriers to root exploration or transactional P limitations caused by the slow release of P from minerals compared to other nutrients (Vitousek et al., 2010).

McDowell et al. (2007) proposed that within mineral horizons, pyrophosphate, diesters (including DNA) and *myo*- and *scyllo*-IHP would increase on aging chronosequences as shown on Manawatu (North Island, New Zealand) and Reefton (South Island, New Zealand) chronosequences (**Table 1**; Parfitt, 1979; Shang et al., 1990; Celi and Barberis, 2005). Mineral soil on the Franz Josef chronosequence (South Island, New Zealand) was dominated by DNA that was correlated to OM, and *myo*- and *scyllo*-IHP and other monoesters on the oldest site that were sorbed to amorphous metals (Turner et al., 2007). Unlike the mineral horizon, microbial P compounds dominated the organic horizon on the Haast chronosequence (South Island, New Zealand), illustrating the importance of microbial cycling of P in the forest floor (Turner et al., 2014). The origins of many soil $P_o$ forms are not fully understood; although plants are known to be the source of some compounds such as *myo*-IHP, other compounds such as *scyllo*-IHP have not been identified in plant matter (Makarov et al., 2002; Condron et al., 2005; Turner et al., 2007). Studies characterizing changes in foliar P forms with soil age are limited, although they could be used to link the forms of P found within the L horizon to the surrounding plant species.

In addition to examining P pools with time, nutrient ratios such as NP are frequently utilized in chronosequence studies to indicate potential N or P limitation with age (Parfitt et al., 2005), with Güsewell (2004) suggesting that an NP $<10$ was N-limited and $>20$ was P-limited.

Across a range of chronosequences worldwide, these ratios generally indicate a shift from N limitation on young sites, to co-limitation by N and P on intermediate-aged sites and P limitation on older sites (Vitousek et al., 1995; Richardson et al., 2004; Parfitt et al., 2005; Izquierdo et al., 2013; Hayes et al., 2014). Over time, foliar and organic soil horizon NP ratios may increase to a plateau, like a reverse logistic regression (Richardson et al., 2004; Hayes et al., 2014) or be hump-shaped (Vitousek et al., 1995; Wardle et al., 2004).

Within the Coastal Western Hemlock (CWH) climatic zone of coastal BC, Canada, very wet, hypermaritime variant (CWHvh2; **Figure 1**), low-productivity forests dominated by western redcedar (*Thuja plicata;* Cw*)*, western hemlock

**TABLE 1 |** Chronosequences exhibiting phosphorus (P) decline with age, country, parent material, climate, initial and oldest ages, and the mechanism of P limitation.

| Chronosequence | Country | Parent material | Climate | Initial age | Oldest age | Mechanism of P limitation | References |
|---|---|---|---|---|---|---|---|
| Arjeplog | SWE | Granite boulders, moraine | Temp Bor For | 100 | 6,000 | Sink-driven | (Wardle et al., 1997, 2004; Vitousek et al., 2010) |
| Central Volcanic Plateau | NZL | Rhyolitic tephra overlying graywacke | Temp Rain For | 1,750 | 14,000 | Not verified | (Parfitt et al., 2005; Richardson et al., 2008) |
| Cooloola | AUS | Quartz grains | Sub-trop Rain For | 10 | >600,000 | Low-P PGM, Depletion-driven | (Thompson, 1981; Wardle et al., 2004; Vitousek et al., 2010) |
| Cox Bay | CAN | Sand grains from greywacke, argillite | Temp Rain For | 127 | 550 | Not verified | (Singleton and Lavkulich, 1987a,b) |
| Franz Josef | NZL | Schist, gneiss | Temp Rain For | 22 | 120,000 | Depletion-driven | (Stevens and Walker, 1970; Richardson et al., 2004; Wardle et al., 2004; Parfitt et al., 2005; Turner et al., 2007, 2012) |
| Glacier Bay | USA | Sandstone, limestone with igneous intrusion | Temp Bor For | 12 | 14,000 | Soil barrier | (Noble et al., 1984; Chapin et al., 1994; Wardle et al., 2004; Vitousek et al., 2010) |
| Haast | NZL | Schist, graywacke, argillite | Temp Rain For | 370 | 6,500 | Low-P PGM Depletion-driven | (Eger et al., 2011; Turner et al., 2012, 2014) |
| Hawaiian Substrate Age Gradient | USA | Basalt Tephra | Sub-trop Rain For | 300 | 4,100,000 | Depletion-driven | (Crews et al., 1995; Vitousek and Farrington, 1997; Wardle et al., 2004) |
| Jurien Bay | AUS | Calcareous to aged quartz sand | Med Shrub | 100 | >2,000,000 | Low-P PGM Depletion-driven | (Laliberté et al., 2012, 2013; Turner and Laliberté, 2015) |
| Manawatu | NZL | Sand from feldspars and quartz | Temp For | 1 | 10,000 | Not verified | (Syers and Walker, 1969; Walker and Syers, 1976; McDowell et al., 2007) |
| Mendocino | USA | Graywacke, sandstone | Med For | 100,000 | >500,000 | Depletion-driven Low-P PGM | (Jenny et al., 1969; Merritts et al., 1991; Northup et al., 1998) |
| Reefton | NZL | Granite, graywacke | Temp Rain For | 1,000 | 130,000 | Not verified | (Walker and Syers, 1976; McDowell et al., 2007) |
| San Francisco Volcanic Field | USA | Volcanic scoria | Semi-arid desert | 1,000 | 3,000,000 | Depletion driven Sink-driven | (Selmants and Hart, 2008, 2010) |
| Waitutu | NZL | Mudstone, sandstone | Temp Rain For | 3,000 | 600,000 | Depletion-driven and soil barrier | (Wardle et al., 2004; Parfitt et al., 2005) |

*Adapted from Nelson (2018).*

*Bor For, boreal forest; Med, Mediterranean; PGM, parent geological material; Rain For, rainforest; Shrub, shrubland; Sub-Trop, sub-tropical; Temp, temperate; Trop, tropical.*

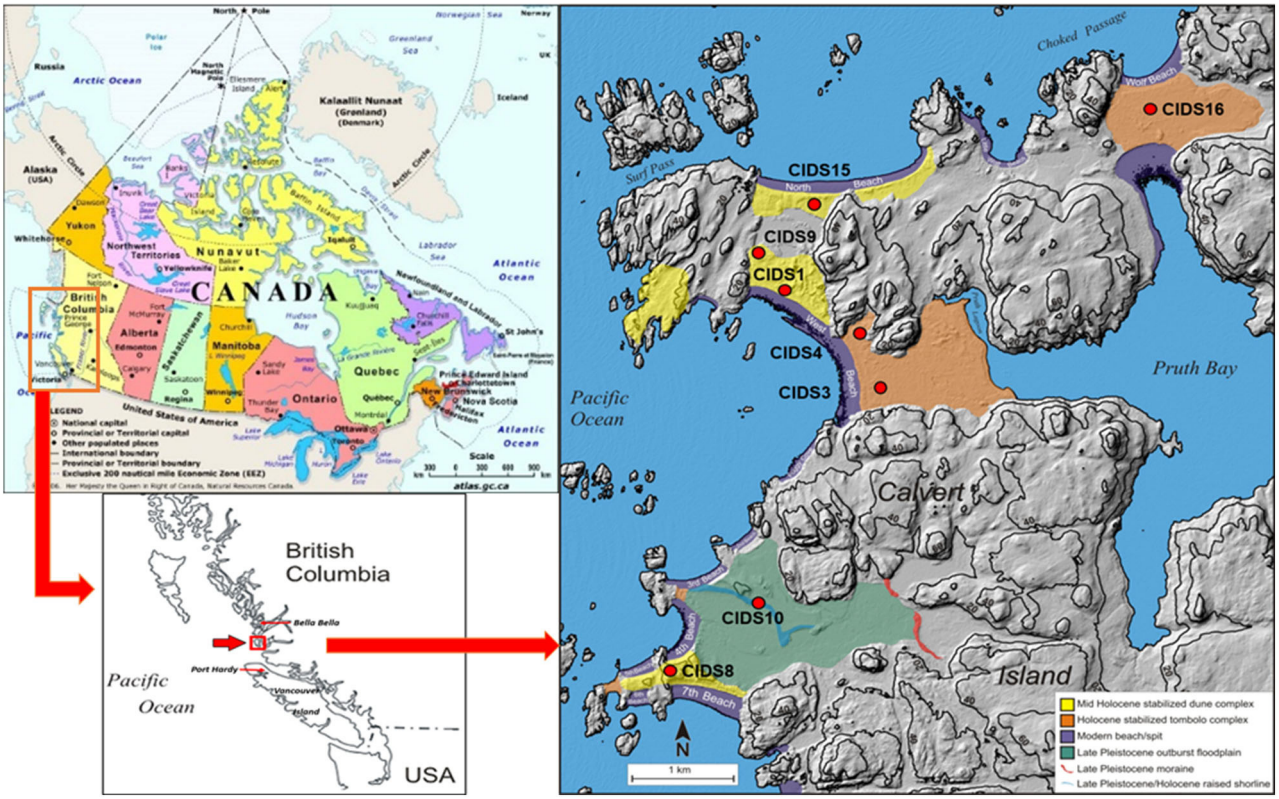


**FIGURE 1 |** Map of study site on Calvert Island, BC, Canada. The map of Canada is from The Atlas of Canada, available at https://www.nrcan.gc.ca/maps-tools-and-publications/maps/atlas-canada/10784. The maps showing more details of the sampling locations are from Nelson (2018), and were adapted from Neudorf et al. (2015). Sampling sites are denoted with red circles.

(*Tsuga heterophylla*; Hw) and shore pine (*Pinus contorta var. contorta*) account for 12% of the North Coast Timber Supply Area or 235,000 ha (Banner et al., 2005). Due to the increasing value of Cw and yellow cedar (*Chamaecyparis nootkatensis*), these lower-productivity areas became of interest economically for timber and fiber production, so a greater ecological understanding was needed and the factors affecting productivity were assessed (Banner et al., 2005). The CWH zone in British Columbia, Canada, is characterized by a temperate, hypermaritime climate. Podzolization is the key process controlling soil development in this region, and soils are characterized by the accumulation of amorphous organic matter and/or the enrichment of Fe and Al in the B horizon (Sanborn et al., 2011). Many soils in the CWH zone have humic-cemented horizons (Bhc) known as ortstein horizons and Fe-enriched cemented horizons (Bfc) known as placic horizons (Banner et al., 1993; Green and Klinka, 1994), designated as Bhm and Bsm horizons, respectively, in the World Reference Base (FAO, 2006). These cemented horizons can impede water flow and can initiate paludification (Ugolini and Mann, 1979; Sanborn et al., 2011; Turner et al., 2012). In the CWH zone, P is often limiting due to rapid weathering of parent material with low P concentrations (Prescott et al., 1993; Kranabetter et al., 2013). Thus, soil P cycling in the CWH zone is typically strongly influenced by soil age.

Within the CWH zone in BC, Canada, researchers have studied a short chronosequence in Cox Bay [> ∼550 y BP (years before present)] and longer chronosequences such as the Naikoon chronosequence on Graham Island (∼550–6,500 y BP; Sanborn and Massicotte, 2010) and the Brooks Peninsula chronosequence on Vancouver Island (> 8,000 y BP; Maxwell, 1997). At Cox Bay, there was a sharp decline in Ca-P within 371 years, associated with rapid podzolization (Singleton and Lavkulich, 1987a,b). The Naikoon and Brooks Peninsula chronosequences also exhibited rapid podzolization and the development of placic horizons, but no in-depth chemical analysis of P within these soils was conducted. The Calvert Island chronosequence is the longest and best-constrained chronosequence on the coast of BC (Neudorf et al., 2015) and is the first study in the region to explore the relationship between soil age and the P cycle, specifically $P_o$.

The overall objective of this study was to examine how the broad pools of P and specific chemical P forms have changed over time in a soil chronosequence developed during the Holocene on aeolian sand dunes within the CWH zone on Calvert Island, on

**TABLE 2 |** The sampling sites used in this study, including chronosequence site name, the most accurate age (in years before present, y BP), location, approximate elevation in meters above mean sea level (m amsl), slope position, aspect, and biogeoclimatic (BEC) site series classification (Green and Klinka, 1994).

| Site name | Fading corrected age (y BP) | Location (Lat/Long coordinates) | Elevation (m amsl) | Slope position | Aspect | BEC site series |
|---|---|---|---|---|---|---|
| CIDS1A | 0 | 51°39.484′ N; 128°08.643′ W | 5.3 | Crest | – | – |
| CIDS1B | | 51°39.479′ N; 128°08.622′ W | | Crest | – | |
| CIDS3A | 105 ± 15 | 51°39.218' N; 128°08.285' W | 3.6 | Level | – | 15-Ss |
| CIDS3B | | 51°39.207′ N; 128°08.273′ W | | Level | – | |
| CIDS4A | 139 ± 17 | 51°39.381' N; 128°08.316' W | 7.8 | Crest | – | 01-CwHw |
| CIDS4B | | 51°39.383' N; 128°08.315' W | | Middle | – | |
| CIDS9A | 605 ± 50 | 51°39.599' N; 128°08.743' W | 8.4 | Crest | – | 03a-CwYc |
| CIDS9B | | 51°39.605' N; 128°08.736' W | | Upper | – | |
| CIDS8A | 3,588 ± 303 | 51°38.480' N; 128°09.109' W | 34.6 | Upper | NW | 14-Ss |
| CIDS8B | | 51°38.484' N; 128°09.106' W | | Crest | SE | |
| CIDS15A | 4,198 ± 332 | 51°39.721' N; 128°08.466' W | 18.0 | Nearly level | – | 01-CwHw |
| CIDS15B | | 51°39.731′ N; 128°08.465' W | | Nearly level | NE | |
| CIDS16A | 7,236 ± 546 | 51°39.967' N; 128°07.067' W | 6.7 | Level | – | 11-CwYc |
| CIDS16B | | 51°39.966' N; 128°07.081' W | | Level | – | |
| CIDS10A | 10,760 ± 864 | 51°38.663' N; 128°08.723' W | 13.0 | Middle | N | 11-CwYc |
| CIDS10B | | 51°38.678' N; 128°08.759' W | | Upper | N | |

*Adapted from Nelson (2018).*

the central coast of BC, Canada. The first research hypothesis was that total C, N and P would change with site age, with TP and $P_o$ following the trends of the Walker and Syers (1976) model.The second objective was to examine how soil $P_o$ compounds varied with increasing age in select organic and mineral soil horizons as well as in dominant foliage species. It was hypothesized that with increasing age, $P_o$ would become an increasingly dominant pool of soil P, with an increase in DNA in the organic horizons and increases in *myo*- and *scyllo*-IHP in the mineral horizons. The third hypothesis was that $P_o$ forms within foliage would be comparable to those within the L horizon, particularly as $P_o$ became a more dominant pool of P with increasing age. The fourth and final hypothesis was that the NP ratios would increase in foliage and organic horizons with increasing age.

# MATERIALS AND METHODS

## Study Area and Sample Collection

The soil chronosequence is located on Calvert Island on the central coast of BC, Canada (**Figure 1**). Soil samples were dated by optically stimulated luminescence (OSL) dating (Neudorf et al., 2015). Eight aeolian sand dunes that developed during a sea-level regression during the Holocene (Eamer et al., 2017) were examined in this study, with ages ranging from a modern foredune to approximately 10,760 y BP (**Table 2**; **Figures S1, S2**). Two sampling locations were examined on each sand dune to capture the variability of soil formation within the dune and age. Sampling locations were chosen to best reflect a stable landscape position (**Table 2**). Additional information regarding the study area can be found in Nelson (2018). Soil sampling was completed in accordance with the Canadian System of Soil Classification (Soil Classification Working Group (SCWG), 1998), which was used to classify the soil horizons. Two soil samples were taken from each genetic horizon. One sample, for basic chemical analysis, was air-dried and sieved to 2 mm. For cemented horizons, a mortar and pestle was used to disaggregate the sample. A coffee grinder was used to grind organic samples. The second sample from each site was oven-dried at 60°C until constant weight to prevent hydrolysis and degradation of P compounds, and was subsequently used for P-NMR analysis.

To examine trends in foliage with increasing age, foliage was collected from two tree species found on the majority of sites, except for the modern dune. These species were Hw, present on 13 of the 16 sites, and Cw, present on 6 of the 16 sites. Samples were also collected from a dominant shrub in most plots, salal (*Gaultheria shallon*). Foliage samples were pruned by hand when possible, or intact green foliage was retrieved off the ground if hand sampling were not feasible, within a 5 m radius plot around each soil pit. All foliage samples were oven-dried at 60°C until constant weight and then ground using a coffee grinder. Foliage samples were composited into groups with equal weights of each dried sample: Group 1, sites CIDS3 and CIDS4; Group 2, of CIDS8, CIDS9 and CIDS15; Group 3, CIDS16, and CIDS10.

## Chemical Analysis

Soil pH was analyzed using a 1:1 soil:water ratio for mineral soils. For samples with high organic matter contents, soil:water ratios ranged from 1:15 to 5:45, depending on viscosity (Kalra and Maynard, 1991). Total C and N were analyzed using a ThermoFischer Scientific Flash 2,000 CHNS. Total C was assumed to be organic C as there were no carbonates in these soils. Total $P_o$ was determined using the ignition method, followed by colorimetric analysis using a Cary-60 UV/vis spectrophotometer (Saunders and Williams, 1955; O'Halloran and Cade-Menun, 2008). The Mehlich method was used to extract P and exchangeable cations [Al, Ca, Fe, and magnesium

(Mg)], and the extracts were analyzed on a Teledyne Leeman Labs Prodigy dual-view ICP-optical emission spectrophotometer (ICP-OES) with a sea spray nebulizer (Mehlich, 1984; Kalra and Maynard, 1991). Sodium pyrophosphate (0.1 N) and acidified ammonium oxalate (0.2 N) were used to extract Fe and Al from mineral samples, followed by ICP-OES analysis (McKeague and Day, 1966; Courchesne and Turmel, 2008). Pyrophosphate-extractable Fe ($Fe_p$) and Al ($Al_p$) represent organically-complexed forms, whereas oxalate-extractable Fe ($Fe_o$) and Al ($Al_o$) represent amorphous and organically-complexed forms. Therefore, the difference between oxalate- and pyrophosphate-extractable Fe and Al provides an indication of how much of these elements occur in amorphous inorganic forms.

Foliage and L horizon samples were analyzed for TP by digestion (Parkinson and Allen, 1975; Cade-Menun and Lavkulich, 1997), followed by colorimetric analysis (Murphy and Riley, 1962) for molybdate-reactive P (MRP). For organic samples total elemental analysis (including TP) was analyzed by closed-vessel microwave acid digestion ICP-OES (Kalra and Maynard, 1991). For mineral samples, total elemental analysis (including TP) was analyzed by high temperature fusion with lithium metaborate/lithium bromide using a Claisse M4 Fluxer followed by ICP-OES.

## Solution Phosphorus NMR Spectroscopy

Analysis of all horizons for one profile revealed that high $P_o$ concentrations could be extracted from organic horizons and organic-matter enriched mineral horizons only, with other mineral horizons containing mainly orthophosphate (**Figure S3**). Thus, L horizons (litter, uppermost organic horizons) and select H (humified lower organic horizons) and humic-enriched mineral (M) horizons were analyzed for each replicate plot, as well as composited foliage samples. The mineral horizons included both A and B horizons, depending on the site, so are designated as M horizons here. The youngest site was not forested, so in the absence of an L horizon, a discontinuous thatch derived from dune grasses was analyzed. Samples [1 g (dry weight) for L horizon and foliage samples, 3 g for organic horizons and 10 g for mineral samples] were extracted with 30-mL of 0.5 M NaOH + 0.1 M $Na_2EDTA$ (NaOH-EDTA), shaken for 4 h in the dark at ∼20°C, and then centrifuged for 15 min at 12,000 × *g* (Cade-Menun and Preston, 1996; Cade-Menun and Liu, 2014). A 1-mL subsample of each supernant was diluted (1:10) with DI water and analyzed using ICP-OES to determine the extract concentrations of P, Al, Ca, Fe, Mg, and Mn. The remaining supernants were filtered through Whatman 42 in a Buchner funnel to remove OM from the sample, frozen, and then lyophilized until dry (∼3 days). The recovery of TP in NaOH-EDTA extracts was calculated (**Table 3**).

The freeze-dried extracts of the select H horizon and M horizon samples were sent to the Stanford Magnetic Resonance Laboratory (SMRL) at Stanford University for NMR analysis. The L horizon and composited foliage samples were analyzed at the Saskatchewan Structural Sciences Center (SSSC) at the University of Saskatoon, due to the closure of the SMRL. At the SMRL, the freeze-dried extracts were prepared for P-NMR analysis by adding 0.5–1.5 ml of $D_2O$, 0.5 ml $H_2O$, 0.5–4.0 ml of NaOH-EDTA extracting solution and 0.5–1.0 mL of 10 M NaOH to increase the sample pH above 12 (Cade-Menun and Liu, 2014). Samples were centrifuged at 3260 × *g* for 5 min. The spectra were obtained on a Varian Inova 600-MHz spectrometer (202.5 MHz for P) with a 10-mm broad band probe. The NMR parameters were: 45° (0.22-μs) pulse, 4.5-s pulse delay, 0.5-s acquisition time, 20°C, and no proton decoupling. Sample LAN30 (CIDS16B, Bhc horizon) was very viscous and had a very low paramagnetic ion (Fe, Mn) content so a 9.5 s pulse delay was used on this sample only. Total NMR analysis for the H and mineral horizon samples ranged from 8 to 16 h, to achieve an acceptable S/N.

At the SSSC, the freeze-dried supernants of the L horizon and foliage samples were prepared by adding 0.6 ml of $D_2O$, $H_2O$ and the NaOH-EDTA extracting solution, as well as 0.4 mL of 10 M NaOH to increase the sample pH above 12. Some samples were very viscous so an additional 0.4 mL each of $D_2O$ and NaOH-EDTA extracting solution were added. All samples were centrifuged at 3260 × *g* for 5 min. Spectra were obtained on a Bruker Avance 500 MHz spectrometer (202.5 MHz for P) with a 10-mm broadband probe. The NMR parameters were: 45° (0.13-μs) pulse, 4.5-s pulse delay, 0.5-s acquisition time, 21°C, and no proton decoupling. Analysis times ranged from 4 to 8 h. During sample analysis at both SMRL and SSSC, selected samples were spiked with different reference compounds after initial NMR analysis, to confirm peak identifications within the monoester region. The chemical shift of compounds were slightly different for each sample type (L vs. H vs. mineral horizons), so a few samples of each sample type were spiked to confirm peak assignments (Cade-Menun, 2015). Spiking compounds included: *myo*-IHP, adenosine monophosphate (AMP), α- and β-glycerophosphate, glucose-1-phosphate, glucose 6-phosphate (g6P), and phosphocholine, all dissolved in NaOH-EDTA, as described in Cade-Menun (2015).

Spectra were processed using NMR Utility Transform Software (NUTS, Acorn NMR, Livermore, CA, 2,000 edition), using 7 Hz line-broadening for the full spectra and 2 Hz line-broadening for finer details, and the orthophosphate peak was adjusted to 6.000 ppm in all samples. Concentrations of P compounds were determined by multiplying the percentage of each P compound by the concentration of P extracted by NaOH-EDTA.

## Statistical Analyses

Due to the small sample set and limited size of the dataset, statistical analysis was performed for the purpose of statistical exploration only. Data were analyzed with STATA 14 IC. Linear and non-linear regression analyses were performed on the masses of TP and $P_o$ to 1 m depth, and on Mehlich P and orthophosphate concentrations with age. The following models were used to examine the data: linear, second order polynomial, Michaelis-Menten, logarithmic, and exponential (decay or increase). Akaike's information criteria and visual examination of the residuals were used to determine the best-fitting model (Gotelli and Ellison, 2004). Parametric pair-wise correlations and non-parametric Spearman correlations were used to test relationships of P forms with other soil parameters. The Shapiro-Wilk normality test and visual examination of box

**TABLE 3 |** Soil pH (in water), total carbon (C), total nitrogen (N), total (TP), and organic P (Po) concentrations within litter (L), humic-enriched organic (H) and mineral (M) horizons, and the recovery of TP in NaOH-EDTA extracts (NE TP).

| Horizon | Age y BP | pH | C (%) | N (%) | CN | TP mg $kg^{-1}$ | CP | NP | $P_o$mg $kg^{-1}$ | $P_o$/TP (%) | $CP_o$ | NE TP (%) |
|---|---|---|---|---|---|---|---|---|---|---|---|---|
| L | 0 | – | – | – | – | 586 (81) | | | – | – | | 73 (1) |
| L | 105 | - | 50 (4.7) | 1.1 (0.3) | 46 (16) | 857 (57) | 584 (94) | 13.3 (2.7) | 531 (112) | 62 (9) | 968 (292) | 88 (5) |
| L | 139 | - | 43 (9.9) | 0.7 (0.0) | 61 (15) | 561 (91) | 768 (52) | 12.9 (2.3) | 448 (23) | 81 (9.1) | 963 (173) | 81 (3) |
| L | 605 | 4.7 (0.1) | 49 (0.9) | 1.0 (0.2) | 50 (9) | 836 (163) | 595 (105) | 12.0 (0.1) | 548 (29) | 67 (16.6) | 894 (64) | 83 (2) |
| L | 3588 | 5.4 (0.4) | 54 (1.1) | 0.6 (0.1) | 86 (11) | 481 (18) | 1116 (19) | 13.1 (1.9) | 432 (65) | 90 (17) | 1258 (216) | 75 (6) |
| L | 4198 | 4.9 (0.1) | 49 (6.5) | 0.7 (0.1) | 74 (1.5) | 449 (30) | 1098 (70) | 14.9 (1.2) | 388 (52) | 86 (5.9) | 1273 (5) | 78 (2) |
| L | 7236 | 4.9 (0.2) | 53 (0.1) | 0.7 (0.1) | 77 (6.5) | 252 (21) | 2125 (176) | 27.5 (0.1) | 426 (45) | 169 (3.8) | 1259 (132) | 76 (8) |
| L | 10760 | 4.2 (0.8) | 38 (5.7) | 0.4 (0.0) | 85 (9.8) | 179 (43) | 2165 (208) | 25.8 (5.4) | 228 (33) | 129 (13.3) | 1676 (11) | 76 (3) |
| H | 0 | – | – | – | – | – | – | – | – | – | – | – |
| H | 105 | 3.5 (0.1) | 54 (1.6) | 1.3 (0.2) | 43 (4.8) | 632 (96) | 858 (106) | 19.9 (0.2) | 440 (42) | 70 (4.0) | 1225 (81) | 29 (6) |
| H | 139 | 3.5 (0.1) | 49 (0.2) | 0.9 (0.0) | 55 (0.8) | 827 (204) | 610 (149) | 11.1 (2.5) | 439 (14) | 55 (12) | 1115 (32) | 49 (8) |
| H | 605 | 3.6 (0.1) | 50 (9.4) | 0.5 (0.1) | 106 (42) | 359 (237) | 1886 (1505) | 16.2 (7.7) | 272 (161) | 78 (6.5) | 2354 (1739) | 66 (37) |
| H | 3588 | 3.9 (0.0) | 55 (0.4) | 0.5 (0.0) | 119 (7) | 263 (19) | 2109 (167) | 17.7 (2.4) | 188 (8.2) | 72 (2.1) | 2940 (149) | 31 (11) |
| H | 4198 | 3.8 (0.0) | 52 (0.1) | 1.3 (0.1) | 41 (4.3) | 777 (56) | 688 (47) | 16.5 (2.9) | 522 (33) | 67 (0.1) | 993 (59) | 42 (0) |
| H | 7236 | 3.3 (0.1) | 58 (0.8) | 0.7 (0.2) | 84 (22) | 331 (126) | 1902 (749) | 22.3 (3.1) | 281 (95) | 86 (3.8) | 2202 (775) | 48 (29) |
| H | 10760 | 3.7 (0.3) | 60 (0.2) | 0.5 (0.2) | 136 (50) | 187 (83) | 3548 (1566) | 25.4 (2.1) | 135 (54) | 73 (3.5) | 4821 (1919) | 42 (1) |
| M | 0 | 7.9 (0.5) | 0.8 (0.4) | 0.03 (0.02) | 34 (9.0) | 234 (5) | 35 (9) | 1.1 (0.8) | 17 (18) | 7.2 (7.8) | 871 (696) | 10 (5) |
| M | 105 | 4.9 (0.4) | 0.3 (0.1) | 0.01 (0.00) | 38 (7.1) | 291 (2) | 9 (4) | 0.2 (0.1) | 25 (0.6) | 8.7 (0.3) | 99 (38) | 12 (4) |
| M | 139 | 4.5 (0.2) | 0.4 (0.2) | 0.01 (0.01) | 34 (5.8) | 148 (8) | 25 (12) | 0.8 (0.5) | 14 (12) | 9.9 (8.8) | 330 (170) | 26 (3) |
| M | 605 | 4.3 (0.4) | 1.4 (1.0) | 0.03 (0.03) | 40 (0.9) | 182 (88) | 100 (102) | 2.5 (2.6) | 20 (7) | 13 (10) | 640 (266) | 32 (28) |
| M | 3588 | 4.6 (0.0) | 2.5 (0.1) | 0.06 (0.0) | 44 (6.4) | 250 (6) | 102 (6) | 2.3 (0.5) | 73 (24) | 29 (10) | 368 (107) | 33 (5) |
| M | 4198 | 4.1 (0.1) | 5.4 (1.1) | 0.12 (0.0) | 47 (5.9) | 165 (12) | 328 (91) | 7.1 (2.8) | 65 (24) | 40 (18) | 855 (149) | 42 (5) |
| M | 7236 | 4.1 (0.1) | 3.7 (0.6) | 0.07 (0.0) | 49 (1.0) | 167 (18) | 218 (11) | 4.4 (1.0) | 35 (5) | 21 (1.0) | 1048 (6) | 34 (1) |
| M | 10760 | 3.8 (0.4) | 7.5 (3.4) | 0.13 (0.0) | 54 (8.4) | 115 (16) | 631 (209) | 11.5 (2.1) | 40 (24) | 33 (16) | 1988 (344) | 53 (31) |

*Values are means (std.dev.); n = 2.*

plots using Stata 14 IC, for each horizon type ($\alpha = 0.05$) were also performed. All NMR data were centered log ratio transformed prior to statistical analyses (Abdi et al., 2015).

# RESULTS

## General Chemical Analyses

Soil pH ranged from 7.5 to 8.6 for the modern foredune and from 2.6 to 5.2 in the forested sites (∼105 y BP and older), with the lowest pH values in samples from the oldest sites (**Table S1**). In the L, H and M horizons, pH was generally similar among samples and was lower in the H horizon than the L horizon (**Table 3**). The greatest pH range with age was observed in the M horizon, from 3.8 in the oldest samples to 7.9 in the modern foredune.

Total C concentrations were greatest in the forest floor and humified horizons (34–60%) and lowest in the mineral horizons (<2%), while total N concentrations were below 1.4% for all samples (**Table 3**, **Table S1**). Carbon and N concentrations were generally similar with age for the L and forest floor horizons, increasing with age in the mineral horizons.

With increasing age, Mehlich-extractable P concentrations declined in all sample types (**Table S2**), and were greatest in the L horizon and least in the mineral horizons (**Figure 2A**). Mehlich-extractable Ca and Mg concentrations were greatest in the surface samples from all sites and decreased with depth, while Mehlich-extractable Al and Fe concentrations generally showed the opposite trend (**Table S2**). The L horizon had the greatest concentration of Mehlich Ca+Mg followed by the H horizon and then the M horizon (**Figure 2B**). Conversely, the mineral horizons had the greatest Mehlich Fe+Al concentrations followed by the H horizon and then the L horizon (**Figure 2C**). In the L horizon, Mehlich Ca+Mg concentrations remained relatively stable with age, exhibiting only a slight decrease with increasing age (**Figure 2**). The H horizon samples maintained stable Ca+Mg concentrations until ∼4,200 years followed by a decline, and there was a sharp decline in the M horizon samples between 0 and 105 years. The L and H horizons had a slight increase in Fe+Al concentrations with age compared to the M horizon, which had a much larger increase with age that peaked around 4,000 years. The H horizon at the ∼7,236 y BP site had an unusually high Fe+Al concentration that was not consistent with other H horizon samples (**Figure 2**).

Concentrations of $Al_p$ and $Al_o$ were similar in samples from profiles up to ∼3,588 y BP, as were $Fe_p$ and $Fe_o$ concentrations, indicating that organically-complexed Fe and Al were predominant in the younger profiles (**Table S1**; Nelson, 2018). In samples from soil profiles from ∼4,198 y BP and older, concentrations of $Al_o$ and $Fe_o$ increased relative to those of $Al_p$ and $Fe_p$, especially at lower depths, indicating an increase in Fe and Al (oxy)hydroxides.

## Soil Phosphorus (Total and Organic P)

Total P concentrations were greatest in the L horizon and decreased with depth (**Table 3**). The CP and NP ratios generally increased from H>L>M horizons, and generally increased with age in all horizons. Concentrations of $P_o$ were greater in the L and H horizons, decreasing substantially in the M horizon. As a proportion of TP, $P_o$ was 52–86% of TP in the L and H horizons. In the M horizon, samples from the sites <605 y BP had a lower proportion of $P_o$ to TP (7.2–13%), which increased to 21–40% of TP in older sites. Within each age category, $CP_o$ was greatest in the H horizon for all but the ∼4,198 y BP site (**Table 3**). For the youngest and oldest sites, the $CP_o$ ratios were comparable in the L and M horizons; for other ages, $CP_o$ was lowest in the M horizon.

## P-NMR Spectroscopy

Extraction with NaOH-EDTA recovered 73–88% of TP from L horizons, 29–66% from H horizons and 10–53% from the M horizons (NE PT, **Table 3**), and 90 ± 9% of TP from the foliar samples (Nelson, 2018). Although TP within the M horizon declined with increasing age, the recovery of P in NaOH-EDTA extracts increased with age and decreasing soil pH.

Example P-NMR spectra are shown in **Figures 3**, **4** and in Nelson (2018). Chemical shifts for foliage and L horizons, H horizons and M horizons are shown in **Tables S3–S5**, respectively. Compounds identified in the monoester region were IHP stereoisomers (*myo, scyllo, neo,* and D-*chiro*), α and β-glycerophosphate, mononucleotides, choline phosphate, g6P and an unidentified peak at ∼5 ppm, labeled as "Unknown" (**Figures 5–8**; **Tables S6**, **S7**) Other unidentified signals in the monoester region were grouped into Mono1 (∼7.0-6.0 ppm chemical shift), Mono2 (∼6.0–3.5 ppm), and Mono3 (3.5–2.5 ppm). The orthophosphate diester region was divided into DNA and other diesters (other diester 1 downfield from DNA; Other Diester 2 upfield from DNA). Because some peaks in the monoester region result from alkaline hydrolysis of RNA and phospholipids during NMR analysis (Makarov et al., 2002; Turner et al., 2003b; Doolette et al., 2009; Cade-Menun, 2015; Schneider et al., 2016), total monoester and diester concentrations were corrected by adding the concentrations of α and β glycerophosphates and mononucleotides to the total diester concentration (cdiesters, cDi), and subtracting them from the total monoester concentration (cmonoesters, cMono). The P-NMR results as percentages for all samples are given in **Tables S6, S7**. Concentrations of P forms are given in **Table S2** and **Figures 5–8**.

Foliage samples from age group 2 for Hw and Cw were compared to the salal samples (**Figure 5**, **Table 4**). Orthophosphate, DNA, α- and β-glycerophosphates, and other diesters were the dominant P compounds in all foliage samples (**Figure 5**, **Table S7**). The Cw and Salal samples were most comparable. Hemlock had the lowest proportion of orthophosphate and greatest proportion of cmonoesters and cdiesters while Cw and Salal had a greater proportion of orthophosphate and lower proportions of cmonoesters and cdiesters. The proportions of total polyphosphates and phosphonate were similar among all foliage species. Both Cw and Salal had all four stereoisomers of IHP and Hw had all but *scyllo*-IHP. With increasing age, the proportion of orthophosphate declined in both Hw and Cw species while cdiesters and cmonoesters increased in proportion (**Figure 5A**). For both Hw and Cw, the concentrations of all forms of P

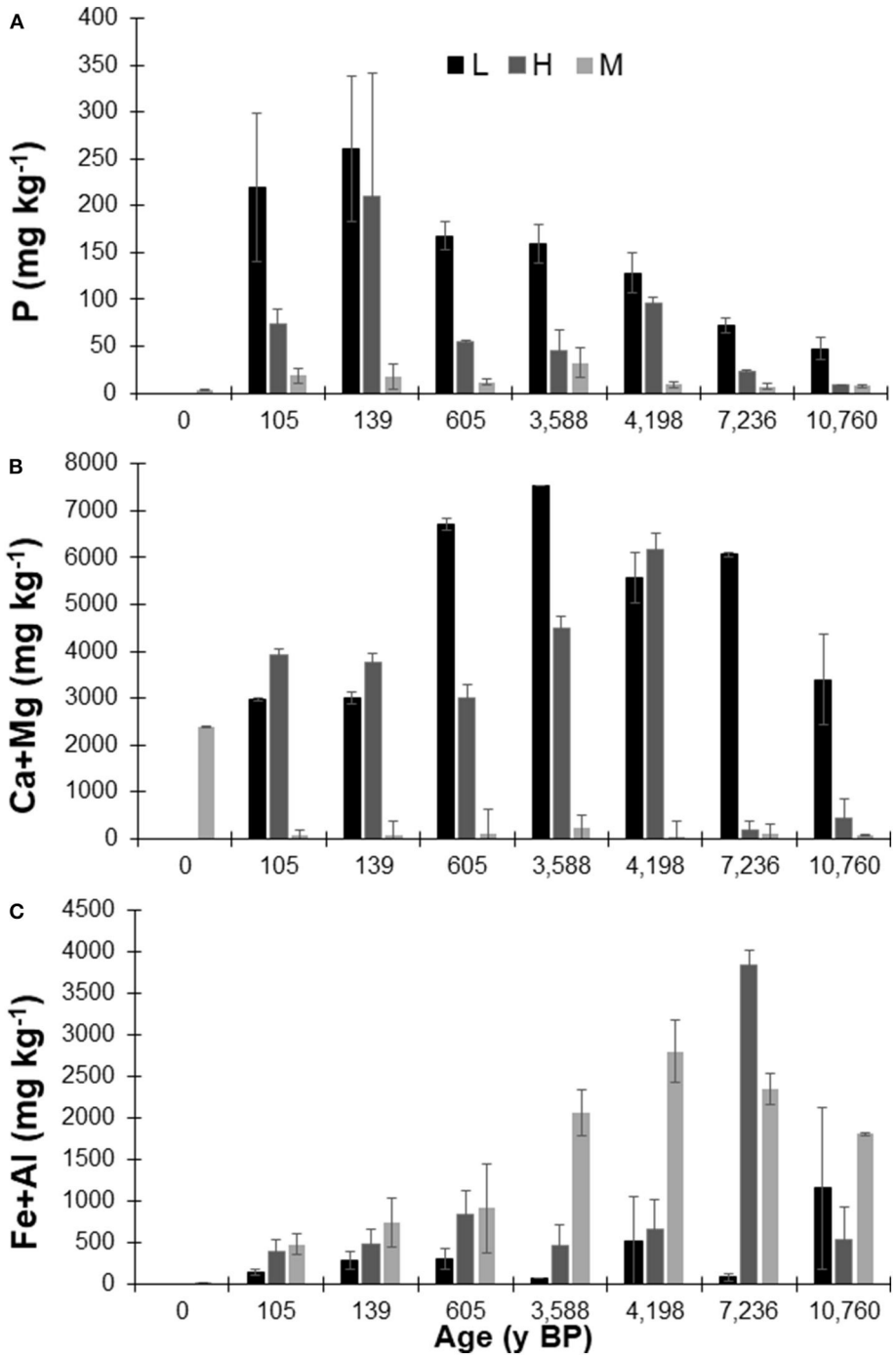


**FIGURE 2 |** Average Mehlich-3 extractable **(A)** phosphorus (P), **(B)** calcium (Ca) + magnesium (Mg) and **(C)** iron (Fe) + aluminum (Al) concentrations within the select litter (L), humic-enriched organic (H) and mineral horizon (M) samples used for P-NMR analysis from the Calvert Island, BC chronosequence. Values are means ± standard deviation; $n = 2$.

declined with increasing age, with the most substantial decline in orthophosphate (**Figure 5B**).

In the L horizon, orthophosphate comprised <40% of extracted P (**Figure 6A**). The next most dominant groups were the cdiesters, followed by pyrophosphate and polyphosphate together (total polyphosphates) and then cmonoesters. The proportion of cmonoesters in the L horizon remained similar throughout the chronosequence, while the proportion of cdiesters generally increased with increasing age. The concentration of all P compound classes of extracted P declined

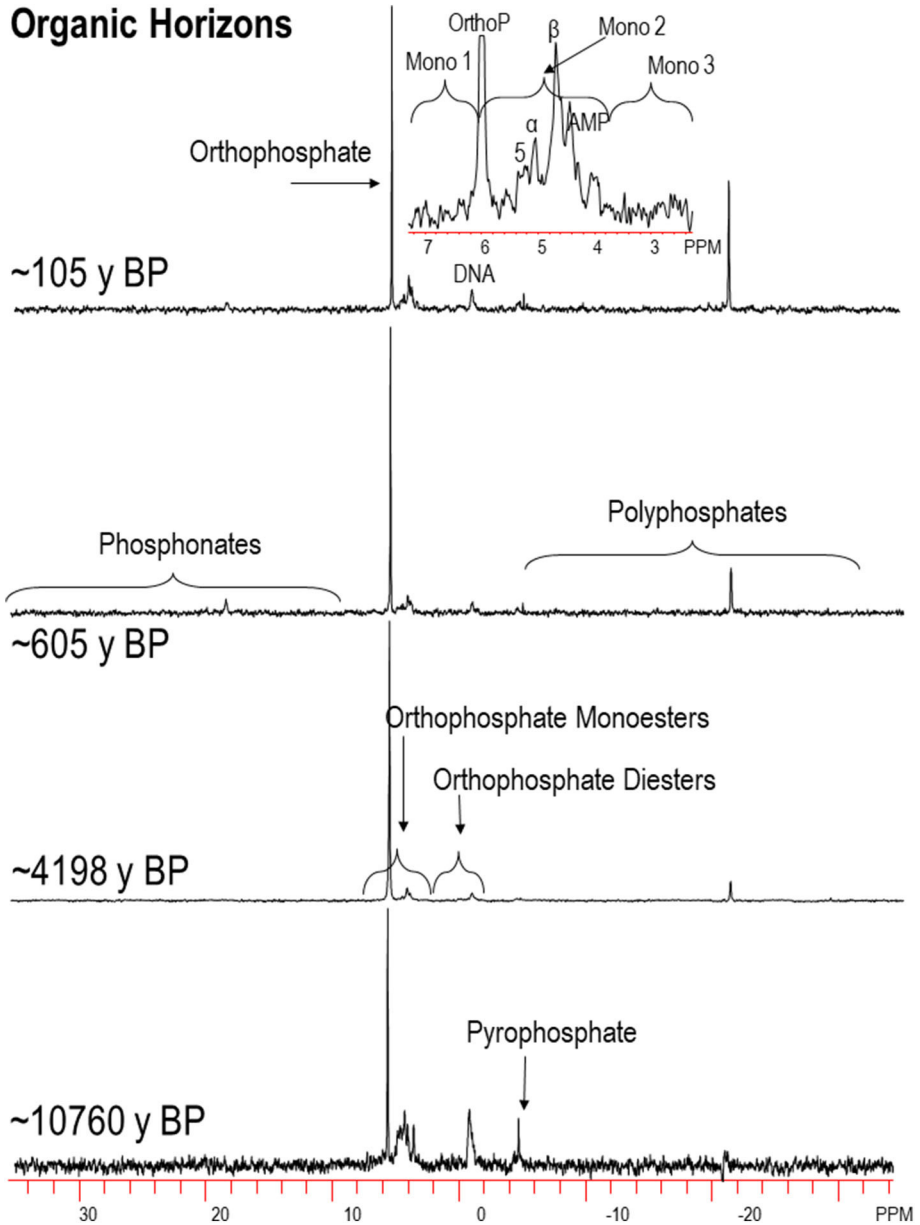


**FIGURE 3 |** Select $^{31}$P-NMR spectra for humic-enriched organic (H) horizon samples along the Calvert Island chronosequence extracted with NaOH-EDTA and processed with 7 Hz line-broadening. OrthoP, orthophosphate, Mono, orthophosphate monoesters; α, α-glycerophosphate; β, β-glycerophosphate; AMP, amino monophosphate; 5, unknown peak, 5 ppm; y BP, years before present. See text for more details.

with increasing age (**Figure 6B**), and there was an apparent shift in the dominance of different P compounds with age. On the youngest site with thatch rather than L horizon, orthophosphate and within the first 100 years, cdiesters became the most dominant forms of P. By ∼10,000 y BP, cdiesters still dominated but the proportion of cmonoesters increased while orthophosphate and total polyphosphates declined.

Within the H horizons, orthophosphate represented a considerable portion of the extracted P on all sites up until ∼7,000 y BP, and then declined (**Figure 7A**). The cmonoesters and cdiesters, in H horizon samples, increased in proportion and concentration (**Figure 7B**) with increasing age. The concentrations of phosphonates and total polyphosphates declined with increasing age.

Within the M horizons, the proportion and concentration of orthophosphate declined with increasing age and was associated with an increase in the proportions of cmonoesters and cdiesters with age (**Figures 8A,B**). The proportions of total

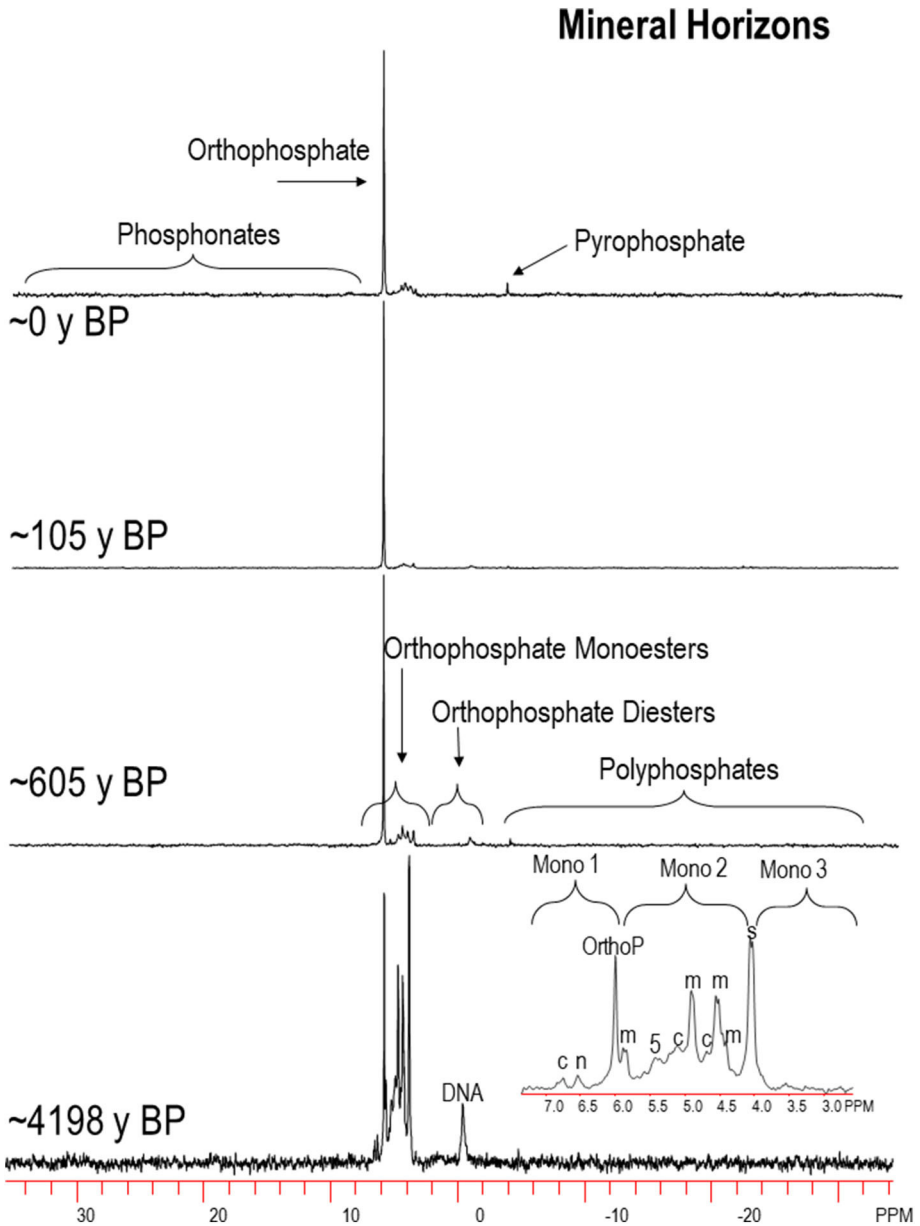


**FIGURE 4 |** Select $^{31}$P-NMR spectra for humic-enriched mineral (M horizon) samples (A or B horizon depending on age) along the Calvert Island chronosequence extracted with NaOH-EDTA and processed with 7 Hz line-broadening. OrthoP, orthophosphate, Mono, orthophosphate monoesters; α, α-glycerophosphate; β, β-glycerophosphate; AMP, amino monophosphate; 5, unknown peak, 5 ppm; y BP, years before present; c, *chiro*-inositol hexaphosphate (IHP); m, *myo*-IHP; n, *neo*-IHP; s, *scyllo*-IHP; See text for more details.

polyphosphates and phosphonates did not fluctuate significantly with age although the concentration of phosphonates increased minimally with increasing age.

Like the foliage and L horizon samples, the concentration of total $P_o$ decreased with age in the H horizon, as did the concentrations of *myo*- and *chiro*- and *neo*-IHP. However, the concentration of *scyllo*-IHP increased (**Table 4**). The concentrations of pyrophosphate and polyphosphates were much lower in the M horizon than other horizons. The M horizon was the only horizon in which total cmonoesters were greater than cdiesters, with *myo*- and *scyllo*-IHP comprising the majority of the cmonoesters (**Table 4**). The ratio of cmonoesters to cdiesters (cM:D) was lowest in the foliage samples and the L horizon (**Table S7**). The cM:D increased in the soil with increasing depth.

The results in **Table S7** clearly demonstrate the need to correct for degradation of diesters to monoesters, especially for organic horizons. Degradation compounds were 22 ± 6 and 22 ± 5% of

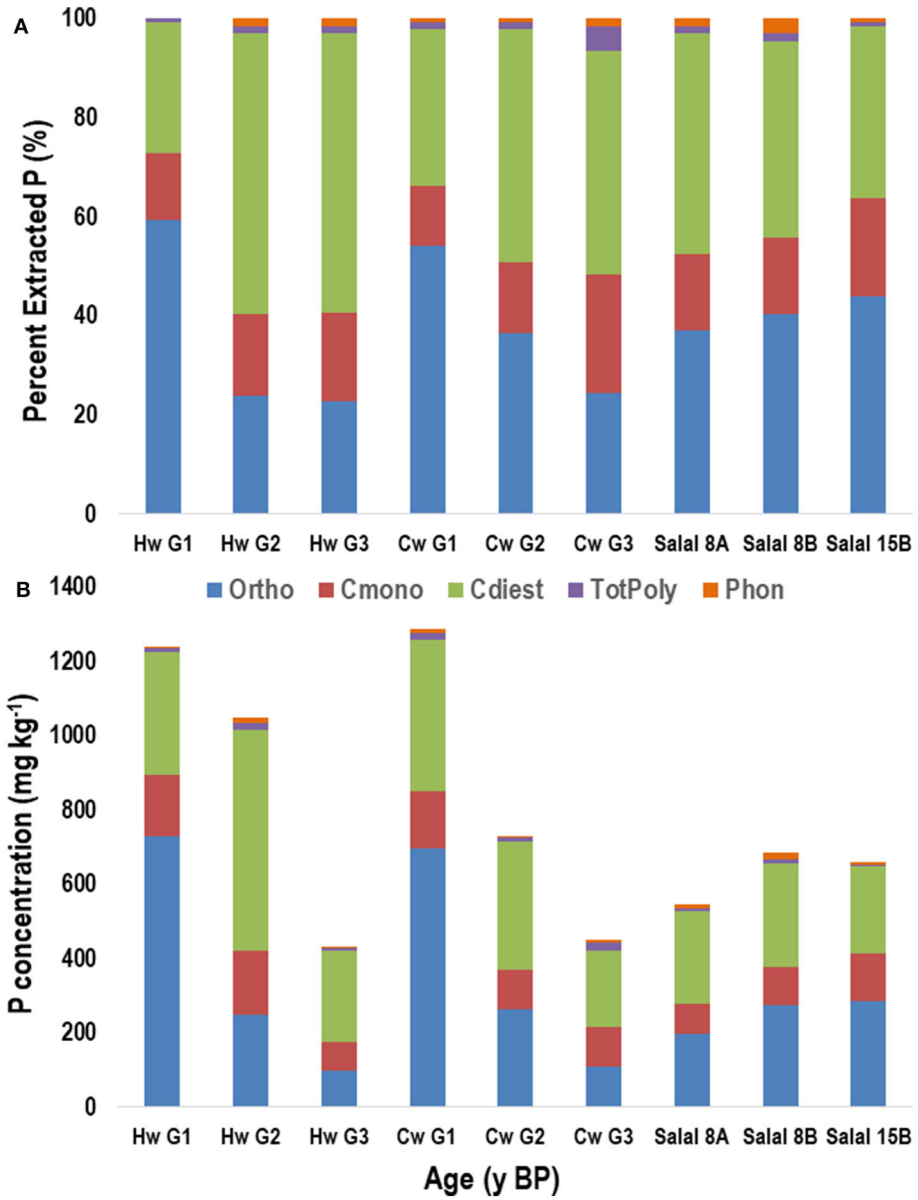


**FIGURE 5 |** Proportion **(A)** and concentration **(B)** of phosphorus (P) in NaOH-EDTA extracts analyzed by P-NMR of three foliage species from the Calvert Island, BC chronosequence: western hemlock (Hw), western redcedar (Cw) and salal by age groupings (G1, G2, G3) or by site (CIDS8A, 8B, 15B). Ortho, orthophosphate; Cmono, Cdi, orthophosphate monoesters and diesters corrected for degradation during analysis; totPoly, total polyphosphates; Phon, phosphonates. Age groupings were made based on soil total P concentrations with G1 representing ages ∼105 to ∼139 years, G2 representing ∼605 to ∼4,198 years and G3 representing ∼7,236 to ∼10,760 years.

the foliage and L horizon samples, respectively, and 10 ± 3 and 9 ± 4% of the O and M horizons. The uncorrected M:D ratio was >1 for all samples, and was >10 in many samples. However, this dropped to <1 for all but the M horizon after correction.

## Exploratory Modeling of P Pools

Linear, second order polynomial and exponential decay models were applied to the masses of TP and $P_o$ to 1 m depth with age (**Figure 9**). The second order polynomial model did not appropriately fit the TP mass data when examined visually. The linear model for TP mass had an appropriate fit but the 4,198 y BP site was identified as an outlier. The exponential decay model had the greatest adjusted $R^2$ (0.982), lowest $P$ (< 0.0001), and best visual fit. For the mass of $P_o$ with time, the linear model did not fit the data and the exponential decay model fit the data statistically but did not corroborate

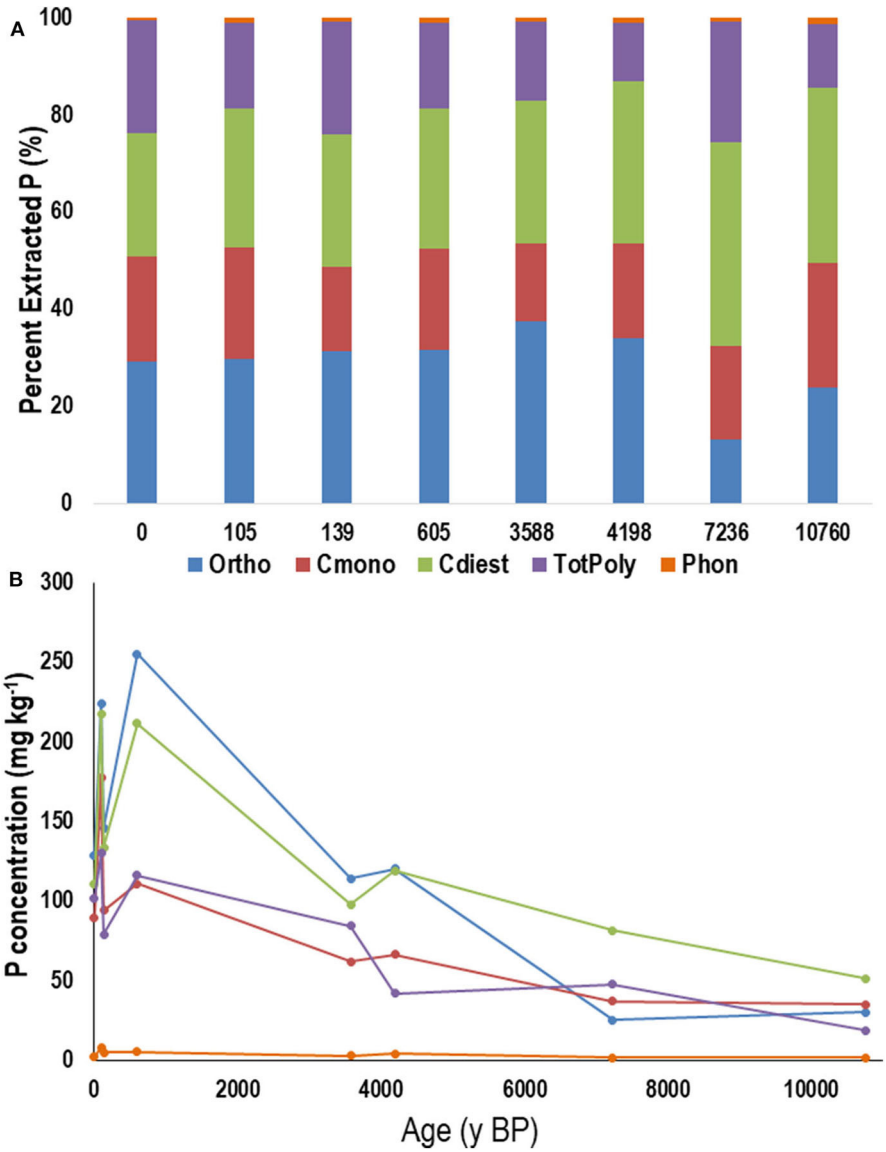


**FIGURE 6 |** Average proportion **(A)** and concentration **(B)** of phosphorus (P) in NaOH-EDTA extracts analyzed by P-NMR for the main groupings of P compounds in the litter (L) horizon from the Calvert Island BC chronosequence. Ortho, orthophosphate; Cmono, Cdi, orthophosphate monoesters and corrected for degradation during analysis; totPoly, total polyphosphates; Phon, phosphonates. Values are means; $n = 2$.

the trends identified in previous studies. The second order polynomial was chosen as the best fit for $P_o$ mass because it appropriately fitted the data and was in accordance with *a priori* knowledge (**Figure 9**, **Table 1**). The concentrations of Mehlich P and orthophosphate in the L, H, and M horizons were modeled with time. The exponential decay model was the best fit for Mehlich P concentration in the L, H, and M horizons and for orthophosphate in the L and M horizons (**Table 5**, **Figures S5**, **S6**). The large variability of orthophosphate concentration with age in the H horizon prevented a significant, explanatory fit of the data.

## Relationships of Select Organic P Compounds With Soil Chemical Parameters

Of the parameters analyzed with correlation analysis, DNA concentration was positively correlated to $Al_o$ concentration ($r^2 = 0.79$, $P < 0.05$), and $Al_o$+$Fe_o$ concentrations ($r^2 = 0.81$, $P < 0.05$). Total IHP concentration in the mineral horizon was significantly correlated to concentrations of total C ($r^2 = 0.91$, $P < 0.001$), $Al_o$ ($r^2 = 0.86$, $P < 0.001$), and $Al_o$+$Fe_o$ ($r^2 = 0.87$, $P < 0.001$), and there was a strong relationship of $Al_o$ and total IHP concentrations for all but the 7,236 y BP sites (**Figure S4**).

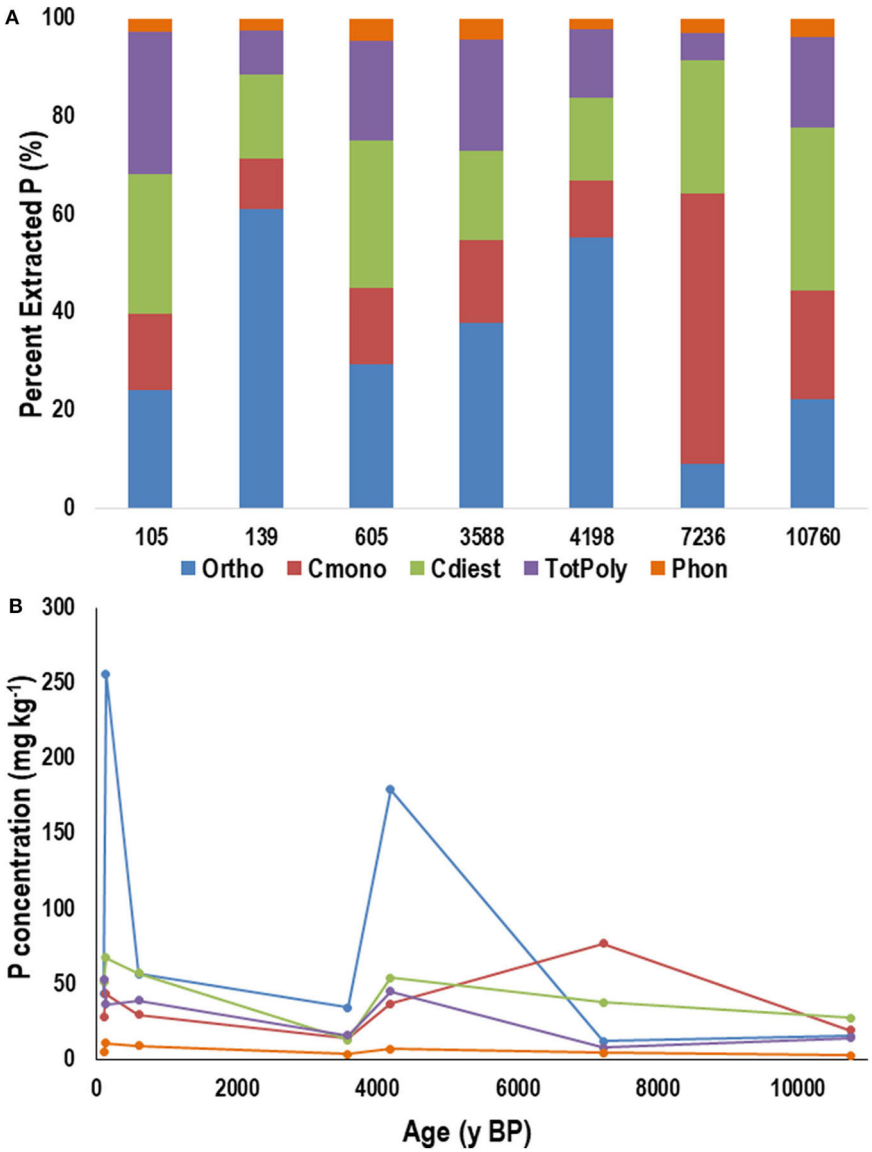


**FIGURE 7 |** Average proportion **(A)** and concentration **(B)** of phosphorus (P) in NaOH-EDTA extracts analyzed by P-NMR for the main groupings of P compounds in the humic-enriched organic (H) horizon from the Calvert Island chronosequence. Ortho, orthophosphate; Cmono, Cdi, orthophosphate monoesters and corrected for degradation during analysis; totPoly, total polyphosphates; Phon, phosphonates. Values are means; $n = 2$.

Mehlich P concentrations within the samples used for P-NMR and orthophosphate concentration determine by P-NMR were also significantly correlated ($r^2 = 0.941$, $P < 0.0001$).

## DISCUSSION

### Comparison of Total, Total Organic, and Mehlich 3 Phosphorus to Other Chronosequences

The Walker and Syers (1976) model suggests that primary mineral P concentrations will rapidly decline within the first ~4,000 years, accompanied by an increase in organic, occluded and non-occluded P forms. In the Calvert Island soils, the mass of TP to 1-m depth followed the typical exponential decline with age (Walker and Syers, 1976). This rapid decline in P concentration with increasing age is similar to the decline in P concentration on the Cox Bay chronosequence, which has a very similar climate (Singleton and Lavkulich, 1987b). Though TP data were not reported for Cox Bay, a linear decline of Ca-P concentrations was apparent in the first 550 years to 1 m depth and an exponential decline of Ca-P concentrations occurred in the first 10 cm of mineral soil (Singleton and Lavkulich, 1987b).

On Calvert Island, total $P_o$ mass displayed a hump-shaped curve that increased until ~4,000 years and then declined. This is characteristic of the Walker and Syers (1976) model: as

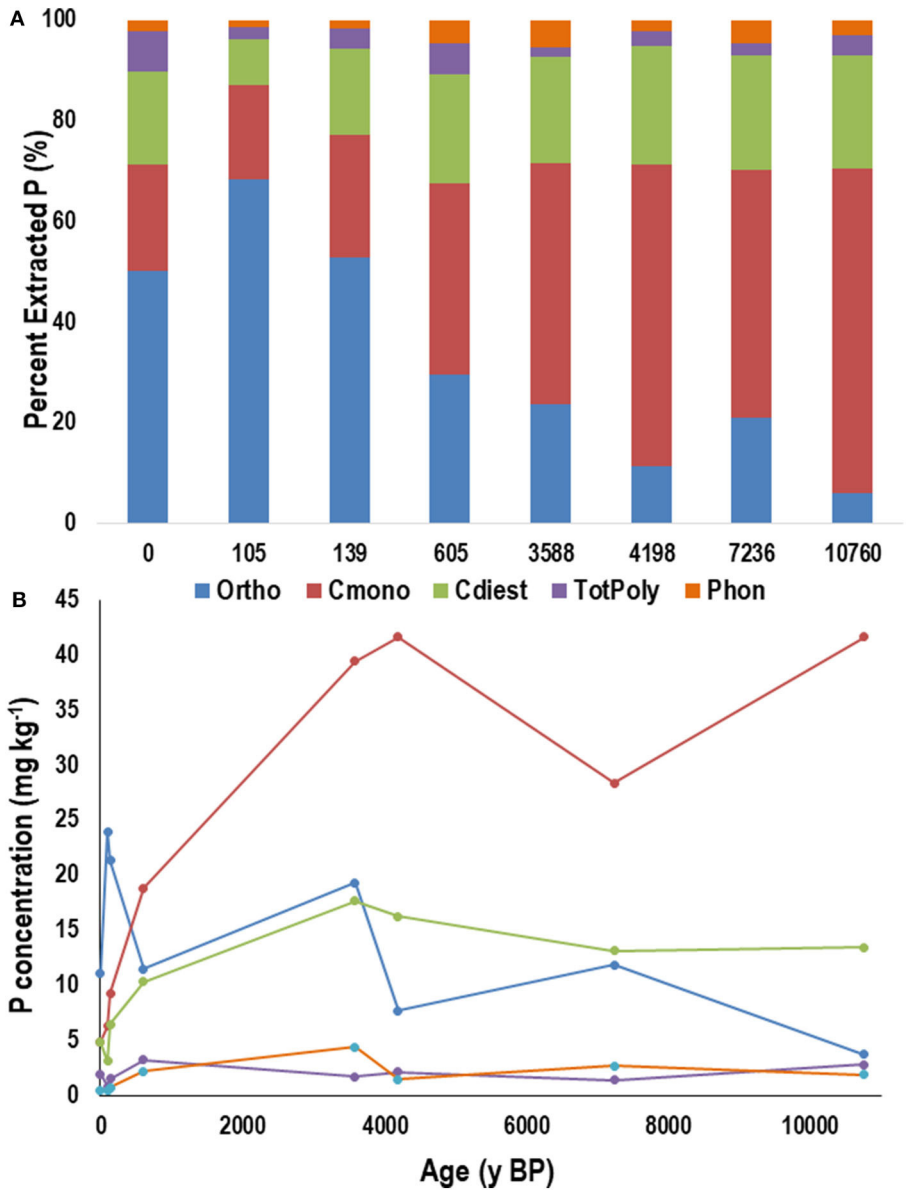


**FIGURE 8 |** Average proportion **(A)** and concentration **(B)** of phosphorus (P) in NaOH-EDTA extracts analyzed by P-NMR for the main groupings of P compounds in the mineral (A or B, depending on age) horizon from the Calvert Island chronosequence. Ortho, orthophosphate; Cmono, Cdi, orthophosphate monoesters and corrected for degradation during analysis; totPoly, total polyphosphates; Phon, phosphonates. Values are means; $n = 2$.

phosphate becomes more scarce with increasing age, less-labile P forms including $P_o$ forms will remain, as well as $P_o$ within soil microorganisms from uptake and immobilization (Quiquampoix and Mousain, 2007). Within organic horizons, the Volcanic plateau (Arizona, USA), Franz Josef, and Waitutu (South Island, New Zealand) chronosequences exhibited a humped decline of $P_o$ concentration with increasing age (Parfitt et al., 2005). The same hump-shaped curve was seen in the mineral horizons on the Reefton, Manawatu, Hawaiian Islands, Jurien Bay, Franz Josef, Cooloola and Mendocino (California, USA) chronosequences (Walker and Syers, 1976; Crews et al., 1995; Richardson et al., 2004; Parfitt et al., 2005; Eger et al., 2011; Izquierdo et al., 2013; Chen et al., 2015; Turner and Laliberté, 2015).

Although the fractionation method used in the Walker and Syers (1976) model was not utilized in this study, fractionation was performed on one profile on the Calvert Island chronosequence (**Figure S3**). Those results suggest that the Mehlich cation data provide a good approximation to fractionation. Thus, TP, $P_o$, exchangeable (Mehlich) P, and the sum of exchangeable (Mehlich) Ca+Mg and Fe+Al concentrations provide an adequate data set to see if the Calvert Island chronosequence follows the general trends of the Walker

**TABLE 4 |** Concentration of P compounds within NaOH-EDTA extracts of soil (Hor) and composited foliage species (Sp.).

| Hor./Sp. | Site age y BP | Tot Pi | Tot Po | Pyro P | Poly P | *myo*-IHP | *chiro*-IHP | *scyllo*-IHP | *neo*-IHP | Oth Mono | DNA | Oth Di |
|---|---|---|---|---|---|---|---|---|---|---|---|---|
| | | mg kg$^{-1}$ | | | | | | | | | | |
| Hw | G1 | 739 | 489 | 2.5 | 7.4 | 25 | 33 | 8.6 | 8.6 | 91 | 123 | 200 |
| Hw | G2 | 266 | 777 | 3.1 | 12.5 | 33 | 17 | 0.0 | 11.5 | 110 | 145 | 446 |
| Hw | G3 | 105 | 327 | 0.4 | 6.0 | 13 | 11 | 0.0 | 4.3 | 50 | 72 | 171 |
| Cw | G1 | 716 | 512 | 3.9 | 15.4 | 41 | 25 | 0.0 | 7.7 | 82 | 94 | 313 |
| Cw | G2 | 276 | 450 | 2.2 | 8.7 | 22 | 17 | 0.0 | 4.4 | 62 | 125 | 215 |
| Cw | G3 | 132 | 316 | 0.9 | 21.1 | 15 | 15 | 3.1 | 5.8 | 68 | 50 | 153 |
| Salal | 8A | 205 | 327 | 0.5 | 7.5 | 21 | 12 | 0.0 | 3.2 | 46 | 27 | 210 |
| Salal | 8B | 283 | 393 | 1.4 | 8.8 | 22 | 11 | 3.4 | 3.4 | 65 | 42 | 226 |
| Salal | 15B | 289 | 356 | 0.0 | 5.2 | 25 | 17 | 4.5 | 4.5 | 77 | 19 | 204 |
| L | 0 | 231 (94) | 199 (43) | 81 (27) | 21 (2.2) | 15.3 (7.2) | 12.2 (1.2) | 2.6 (0.3) | 3.7 (2.0) | 56 (31) | 7.5 (7.8) | 99 (19) |
| L | 105 | 354 (24) | 399 (65) | 80 (20) | 50 (8.0) | 30.1 (9.3) | 22.7 (4.8) | 4.5 (0.5) | 7.4 (4.6) | 113 (54) | 55 (14) | 158 (20) |
| L | 139 | 225 (58) | 229 (0.3) | 56 (6.4) | 23 (8.5) | 18.4 (6.1) | 11.3 (3.3) | 1.2 (1.8) | 4.2 (2.4) | 59 (1.5) | 32 (1.1) | 98 (2.3) |
| L | 605 | 372 (30) | 324 (86) | 72 (30) | 44 (13) | 18.7 (1.2) | 19.0 (10) | 0.0 (00.0) | 6.3 (2.3) | 67 (11) | 35 (23) | 172 (66) |
| L | 3588 | 199 (31) | 160 (14) | 57 (4.0) | 28 (0.1) | 14.0 (4.3) | 7.2 (0.6) | 2.0 (0.4) | 3.1 (2.0) | 36 (16) | 8.1 (7.7) | 87 (8.0) |
| L | 4198 | 163 (43) | 187 (10) | 28 (4.1) | 14 (0.8) | 8.8 (0.4) | 9.8 (1.8) | 2.1 (0.2) | 2.9 (1.0) | 43 (16) | 37 (1.1) | 79 (7.8) |
| L | 7236 | 73 (23) | 118 (18) | 24 (1.7) | 24 (14) | 6.2 (1.9) | 4.4 (0.7) | 0.5 (0.7) | 1.0 (0.0) | 25 (8.8) | 18 (9.8) | 62 (0.1) |
| L | 10760 | 49 (2.4) | 87 (30) | 12 (7.7) | 6.7 (4.8) | 7.0 (2.4) | 3.5 (0.1) | 0.9 (0.0) | 0.9 (0.0) | 23 (8.1) | 4.7 (0.2) | 45 (18) |
| H | 0 | – | – | – | – | – | – | – | – | – | – | – |
| H | 105 | 96 124) | 84 (3.2) | 4.5 (1.6) | 49 (19) | 5.5 (2.2) | 2.8 (0.6) | 1.4 (0.2) | 0.7 (0.2) | 17.5 (1.8) | 15.8 (1.1) | 35 (1.2) |
| H | 139 | 292 (129) | 122 (37) | 7.0 (0.6) | 30 (11) | 4.8 (2.2) | 11.5 (7.0) | 4.8 (2.2) | 2.3 (1.2) | 20.0 (8.5) | 21.2 (6.9) | 46 (2.7) |
| H | 605 | 96 (16) | 96 (6.2) | 7.0 (5.8) | 32 (11) | 4.4 (0.3) | 4.0 (0.2) | 2.1 (1.5) | 1.0 (0.1) | 18.4 (4.9) | 19.3 (0.7) | 38 (7.5) |
| H | 3588 | 51 (27) | 31 (9.1) | 1.6 (0.7) | 15 (3.6) | 1.5 (1.1) | 2.6 (1.6) | 0.9 (0.9) | 0.1 (0.4) | 9.0 (5.4) | 2.5 (2.0) | 10 (0.0) |
| H | 4198 | 224 (31) | 98 (9.0) | 2.8 (0.9) | 42 (2.4) | 4.3 (0.8) | 8.7 (0.6) | 1.6 (0.1) | 1.6 (0.1) | 21.0 (6.8) | 13.9 (6.2) | 40 (5.5) |
| H | 7236 | 20 (0.9) | 119 (36) | 0.8 (0.3) | 7.1 (1.9) | 17.1 (4.7) | 6.5 (0.4) | 13.0 (7.7) | 1.2 (0.3) | 38.9 (9.8) | 5.5 (1.3) | 32 (10.6) |
| H | 10760 | 30 (4.5) | 50 (33) | 2.7 (3.3) | 12 (2.5) | 3.3 (3.3) | 2.0 (1.1) | 2.0 (2.4) | 0.3 (0.1) | 11.9 (9.7) | 10.7 (7.6) | 17 (9.3) |
| M | 0 | 13 (5.5) | 10 (6.6) | 1.3 (1.1) | 0.6 (0.2) | 0.9 (0.4) | 0.9 (0.5) | 0.5 (0.2) | 0.1 (0.1) | 2.4 (1.2) | 0.4 (0.5) | 4.4 (3.7) |
| M | 105 | 25 (8.9) | 9.9 (1.2) | 0.3 (0.1) | 0.6 (0.3) | 1.4 (0.4) | 1.2 (0.3) | 0.8 (0.1) | 0.4 (0.2) | 2.6 (0.3) | 0.8 (0.7) | 2.3 (0.3) |
| M | 139 | 23 (10) | 17 (3.0) | 0.5 (0.1) | 1.0 (0.0) | 2.2 (0.4) | 1.6 (0.6) | 1.4 (1.0) | 0.3 (0.1) | 3.8 (0.2) | 1.8 (1.5) | 4.7 (0.9) |
| M | 605 | 15 (1.3) | 31 (22) | 1.7 (1.9) | 1.5 (1.1) | 7.7 (6.5) | 1.6 (0.7) | 3.2 (2.8) | 0.4 (0.0) | 5.9 (3.8) | 4.1 (3.2) | 6.2 (3.2) |
| M | 3588 | 21 (0.0) | 62 (11) | 0.3 (0.5) | 1.3 (0.1) | 12.2 (2.4) | 3.1 (0.5) | 10.1 (0.5) | 0.9 (0.6) | 13.2 (4.3) | 5.0 (0.9) | 12.7 (6.5) |
| M | 4198 | 9.8 (2.0) | 59 (5.9) | 0.2 (0.1) | 1.9 (0.2) | 15.5 (3.2) | 2.8 (0.2) | 9.7 (2.4) | 0.9 (0.1) | 12.7 (0.0) | 6.1 (1.1) | 10.1 (1.1) |
| M | 7236 | 13 (5.9) | 44 (10) | 0.0 (0.0) | 1.4 (0.2) | 9.4 (4.9) | 2.1 (0.1) | 6.9 (2.3) | 0.7 (0.0) | 9.3 (1.1) | 5.3 (1.5) | 7.9 (0.5) |
| M | 10760 | 6.5 (4.8) | 57 (40) | 0.3 (0.2) | 2.5 (2.0) | 14.0 (8.7) | 2.4 (1.5) | 8.7 (5.8) | 1.0 (1.1) | 15.6 (13.7) | 4.0 (1) | 9.4 (6.7) |

*L, litter horizon; H, humic-enriched organic horizon; M, mineral horizon; Hw, western hemlock; Cw, western redcedar; Pyro P, pyrophosphate; Poly P, polyphosphates; myo-, scyllo-, chiro-, and neo-inositol hexakisphosphates (IHP); Other mono, total orthophosphate monoesters other than IHP, corrected for degradation artifacts; Other Di, total orthophosphate diesters other than DNA, corrected for degradation artifacts. Values are means (std. dev.); n = 2.*

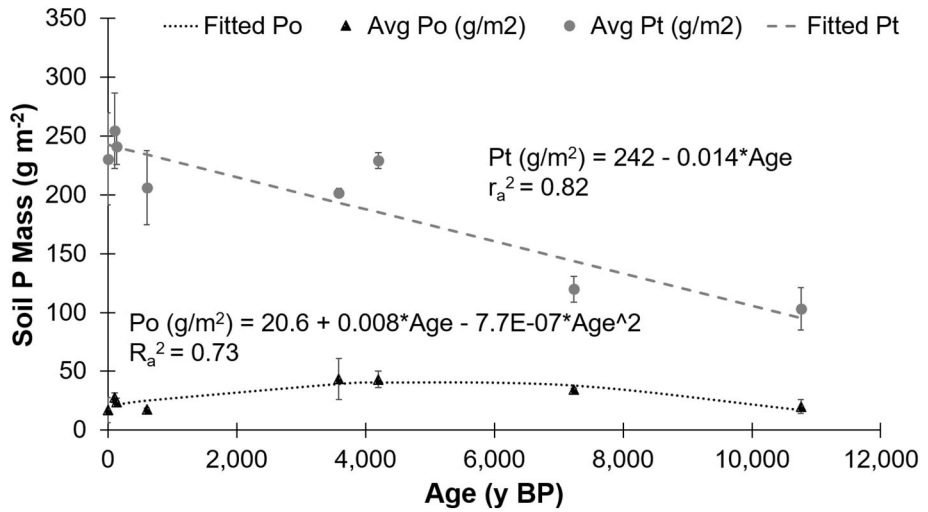


**FIGURE 9 |** Average mass of total phosphorus (Pt) and organic phosphorus (Po) to a 1 m depth with the associated linear and non-linear regression formulas, respectively, and associated *r*-value, for soil sampled from the Calvert Island, BC, chronosequence. Values are means ± standard deviation; $n = 2$.

**TABLE 5 |** Mehlich phosphorus (P) and orthophosphate exponential decay formulas for the litter (L), and select humified organic (H), and mineral (M) horizons with adjusted $R^2$ ($R_a^2$) and *p*-value (p).

| Horizon | Mehlich-P (mg kg$^{-1}$) | | | Orthophosphate (mg kg$^{-1}$) | | |
|---|---|---|---|---|---|---|
| | Formula | $R_a^2$ | *p* | Formula | $R_a^2$ | *p* |
| L | Meh-P = 229.1*0.9999$^{Age}$ | 0.97 | <0.0001 | Ortho-P = 200.3*0.9999$^{Age}$ | 0.90 | 0.0005 |
| H | Meh-P = 123.2*0.9998$^{Age}$ | 0.66 | 0.03 | N/A | N/A | N/A |
| M | Meh-P = 14.9*0.99994$^{Age}$ | 0.62 | 0.02 | Ortho-P = 17.8*0.9999$^{Age}$ | 0.85 | 0.001 |

and Syers (1976) model. For the Calvert Island chronosequence, this can be seen in the exponential decline of Mehlich P concentration with increasing age in all horizons (**Figure S5**), the dramatic decrease in Mehlich Ca and Mg concentrations within ∼105 y BP in the mineral horizon, and the increase in Fe and Al concentrations to ∼4,198 y BP. Effective cation exchange capacity and exchangeable Ca and Mg concentrations also declined with increasing age on the Haast, Mendocino, Cox Bay and Jurien Bay chronosequences (Singleton and Lavkulich, 1987b; Northup et al., 1998; Eger et al., 2011; Turner and Laliberté, 2015). The Calvert Island chronosequence can thus be added to the list of chronosequences worldwide that follow the Walker and Syers (1976) model, regardless of differences in parent material or climate (**Table 1**).

Within organic horizons, TP concentrations declined consistently at the San Francisco Volcanic Field, Franz Josef and Waitutu sites at lower rates than in the mineral horizons (Parfitt et al., 2005), which is comparable to the Calvert Island chronosequence with the exception of the ∼4,198 y BP site. On the Haast chronosequence, TP concentrations in organic horizons declined exponentially, reaching a stable concentration after only 1,000 years that coincided with the development of a mature Podzol (Turner et al., 2012).

Within mineral horizons, TP concentrations declined with age on chronosequences across the world, with significant declines at the Cooloola, Jurien Bay, Franz Josef, Reefton, and Waitutu, Manawatu, and Mendocino sites (Syers and Walker, 1969; Walker and Syers, 1976; Parfitt et al., 2005; Izquierdo et al., 2013; Chen et al., 2015; Turner and Laliberté, 2015). The Haast chronosequence and the Hawaiian substrate age gradient (sub-tropical rain forest) both had rejuvenating dust inputs that buffered TP concentrations within the soil, but a significant decline with age was still apparent (Crews et al., 1995; Kurtz et al., 2001; Eger et al., 2011). Haast also had an increase in TP concentrations following the formation of placic horizons, most likely due to the reduction and subsequent mobilization of Fe (Turner et al., 2012), but this was not seen in the Calvert Island soils, although placic horizons developed.

## Nutrient Ratios

Using the NP ratios suggested by Güsewell (2004), where an NP <10 was N-limited and >20 was P-limited, foliage samples within this study were within the co-limitation or adequate supply region of the ratios. This suggests no limitation of P to plant growth within the foliage, unlike Jurien Bay where the NP ratio within foliage was >20 after 6,700 y (Hayes et al., 2014). The

Mendocino chronosequence also had an increase in NP within foliage with age from 6.0 to 14.4 on Terraces one through five (Izquierdo et al., 2013) and Franz Josef foliage NP was ∼14 after 12,000 years (Richardson et al., 2004). The NP ratio within the L Horizon samples increased with increasing age up to 27.5 for the second oldest site (**Table 3**) which is within the P-limited range (Güsewell, 2004). The NP ratios within the H horizon suggest N and P co-limitation for all but the two oldest sites. In contrast, NP ratios in the M horizon show N limitation in all but the oldest site, which was in the range for co-limitation or adequate supply (Güsewell, 2004). The mineral soils on Calvert Island had a much lower NP ratio compared to other chronosequences spanning similar ages. On the Haast chronosequence the NP ratio did not increase consistently with age, but was 8.6 after 290 years and ∼10 after 6,500 years (Turner et al., 2012). After 6,700 years, the mineral soils from the Jurien Bay chronosequence had NP > 20 suggesting P limitation (Hayes et al., 2014). On the Cooloola chronosequence the NP was 11.5 after 7,500–9,600 years and reached 30.5 after > 460,000 years within the upper 30 cm of mineral soils (Chen et al., 2015). Foliage samples in the current study did not show increasing NP ratios with increasing age as expected; however, the L and H horizons did display the expected trend. Interestingly, the NP ratio in the M horizons suggest N limitation on young sites and possibly co-limitation on the oldest site. Nutrient acquisition strategies and plant communities should be explored on this chronosequence in more detail to further understand foliar nutrients.

## Phosphorus Extraction for P-NMR

Extraction of P, especially $P_o$, with NaOH-EDTA for P-NMR is currently the most quantitative method to recover $P_o$ from soil and other environmental samples (Turner et al., 2005; Cade-Menun and Liu, 2014). The recovery of P in NaOH-EDTA extracts from the foliage and L horizon samples was the greatest of all types of the Calvert Island samples, with a recovery rate >73% of TP. Phosphorus recovery was lower in the H and M horizon samples, and generally increased with age. It was also lower in samples with higher pH. Changes in P recovery with age may be related to humification processes that incorporated $P_o$ within organic matter (Celi and Barberis, 2005), reducing the solubility in NaOH-EDTA. The recovery of TP within this study is comparable to recovery rates from studies of other Podzols on Vancouver Island, BC, such as 71–95% recovery within the LF layer, 32–95% recovery in the H horizon and 4–64% recovery within mineral horizons (Cade-Menun et al., 2000a,b). On the Franz Josef chronosequence, Turner et al. (2007) also observed lower recovery rates on young soils compared to older mineral soils, while Turner et al. (2014) reported lower recovery rates from mineral soil than organic horizons for the Haast chronosequence, especially for soils from younger and older sites. Wang et al. (2019) reported greater P recovery in NaOH-EDTA extracts from L horizons than H horizons for German forests.

Much of the P not extracted by NaOH-EDTA in samples is thought to be occluded $P_i$ (Cade-Menun et al., 2015) With increasing age, $P_o$ dominated and was more easily extractable with NaOH-EDTA than $P_i$ forms that may be precipitated or occluded (Turner et al., 2003a; Turner, 2008). The youngest site (∼0 y BP) was minimally weathered and receives daily influxes of sea spray rich in basic cations, increasing pH relative to the older samples (7.9 vs. 3.8 for M horizon samples). Higher-pH samples generally have lower recoveries with NaOH-EDTA because P bound by Ca and Mg is harder to extract with NaOH-EDTA than P bound to Fe and Al (Turner et al., 2003a; Weyers et al., 2016). With increasing age, both the H and mineral horizons became more enriched in Fe and Al, which corresponds to an increase in the recovery of $P_o$. It is important to note that the mechanisms of P recovery with NaOH-EDTA are not fully understood and more studies should be conducted comparing the extract and the residual P in the remaining sample after extraction with NaOH-EDTA (e.g., Turner, 2008; Cade-Menun and Liu, 2014). It is also important to note that if the majority of unextracted P is $P_i$, then total $P_i$ calculated from NMR spectra will be underestimated in samples with low recovery in NaOH-EDTA, such as for the M horizons of the younger sites.

## Changes in Phosphorus Forms Among Sample Types and With Depth

Different processes control the concentrations and forms of P within the different sample types of this study. In foliage, P forms and concentrations are directly related to the specific plant species and the soil nutrient status (Yan et al., 2019), and in turn control inputs to the L horizon. One $P_o$ compound of particular interest is *myo*-IHP (phytate), which can be a significant component of soil $P_o$. It is a P storage compound commonly found in high concentrations in seeds, and in variable concentrations in other plant materials, and has been widely studied in agriculturally-important crops (Noack et al., 2014). However, there is no published information about *myo*-IHP in plant material of forests such as those found on Calvert Island. In addition to *myo*-IHP, other IHP stereoisomers detected in soils are *chiro*-, *scyllo*-, and *neo*-IHP, which have not been detected in appreciable quantities in plant tissues (Turner, 2007). In soils, the stereoisomers of IHP are either microbially synthesized or are formed from epimerization of *myo*-IHP (Smith and Clark, 1951; Cosgrove, 1980; Martin et al., 2000; Turner and Richardson, 2004; Giles et al., 2011). In the foliage samples from Calvert Island, stereoisomers of IHP were found in plant foliage in varying concentrations depending on the plant species. Redcedar (Cw) and salal foliage had all four IHP stereoisomers, whereas hemlock (Hw) had all stereoisomers except *scyllo*-IHP. It is important to note, however, that these foliage samples were not always collected directly from the plants and were not sterilized prior to extraction. As such, there is a possibility that microbial alteration and epimerization may have occurred and influenced the IHP forms and concentrations. This may also have altered other P compounds such as polyphosphates. However, the high concentrations of diesters in the foliage samples from Calvert Island are consistent with analysis of other plant materials (e.g., Noack et al., 2014; Yan et al., 2019).

The L horizon had lower TP concentrations than the foliage samples, but it appears that there were few alterations to P compounds in the L horizon: the forms of $P_o$ within the L horizon were directly comparable to the foliage samples, which

confirms the third hypothesis of this study. Organic P forms within the foliage and L horizon were dominated by DNA and by the products of diester degradation during P-NMR extraction and analysis, α- and β- glycerophosphates, from phospholipids, and nucleotides, from RNA.

The forms of P within the foliage and L horizon will influence the H horizon, but the direct effect may be diminished by increased biological alteration. The H horizons had P forms similar to those of the L horizon, but there were increases in concentrations of DNA, *scyllo*-IHP, polyphosphates and phosphonates. The differences in P forms between the L and H horizons can be explained by microbial degradation and scavenging. The increased phosphonate concentrations within H horizons are most likely due to differences in the soil microclimate, including wetter condition and different microbial communities due to lower pH. These are ideal conditions for the formation and accumulation of phosphonates, because these conditions limit bacterial activity and subsequently phosphonatase enzyme production (Tate and Newman, 1982; Hawkes et al., 1984; Condron et al., 2005). The specific origins of the phosphonates in these soils are unknown, but phosphonates in general are produced by a number of organisms, including snails (in eggs), protozoa (in cilia), and Actinomyces (Condron et al., 2005). Phosphonates are also found in a number of agricultural chemicals, including herbicides and fungicides, but that is unlikely to be the origin of phosphonates in these soils, given that the study sites are remote and generally undisturbed by human management. The H horizons of the Calvert Island sites were well-humified humic or wood-enriched horizons with an abundance of mycelia, and P can be transported within mycelia as polyphosphate granules (Smith and Read, 1997; Makarov et al., 2002; Oberson and Joner, 2005; Bünemann et al., 2008); thus, an increase in polyphosphate concentrations could be tied to the increased fungal cycling of nutrients. Pyrophosphate may be a storage compound for microbes (Condron et al., 1990), which could explain the increased proportion within the L horizon compared to the foliage and the decline when transitioning to the more active H horizon. It may also originate from degradation of polyphosphates during extraction and NMR analysis (Cade-Menun et al., 2006).

The humic-enriched M horizon had a considerably lower TP concentration compared to the upper horizons. There were few to no roots in the mineral horizons and no identifiable mycelia (Nelson, 2018), which would limit the biological aspects of P cycling in this horizon (Greaves and Webley, 1969). The increase in phosphonates may be attributed to the increasingly wetter conditions with age, because the placic and ortstein horizons that formed between ∼600 and ∼3,500 y BP can impede water flow, making conditions wetter, cooler and more acidic. The dominant $P_o$ forms in the M horizon were *myo*- and *scyllo*-IHP, followed by DNA, nucleotides and *chiro*-IHP and minimal concentrations of glycerophosphates. Mineral horizon samples dominated by orthophosphate had a lower concentration of cmonoesters and the sites dominated by cmonoesters had lower concentrations of orthophosphate. The increased proportion of cmonoesters results from an increase in IHP.

The buildup of IHP and DNA suggests that the controlling process in the mineral horizons of Calvert Island is sorption, because IHP can easily sorb onto humic materials, clays or form insoluble precipitates, making them less likely to be mineralized (Goring and Bartholomew, 1952; Condron et al., 1990; Turner et al., 2002; Giles et al., 2011). This is corroborated by the increase of amorphous and exchangeable Fe and Al in the mineral horizon compared to the other horizons, and there was a clear relationship. Jørgensen et al. (2015) examined IHP stabilization on the Haast chronosequence and suggested that all IHP were sorbed onto amorphous metals. This finding is consistent with the Calvert Island soils. DNA can also be sorbed onto amorphous metals in addition to humic materials (Greaves and Wilson, 1969; Levy-Booth et al., 2007; Turner et al., 2007). Similar to IHP, DNA was correlated to amorphous Fe and Al on the Calvert Island chronosequence.

Cade-Menun et al. (2000a) also used P-NMR to characterize P forms in soils from the CWH zone within Cw-dominated forests. In their study the L and H horizons were dominated by uncorrected monoesters and diesters followed by orthophosphate. The mineral horizons from Cw sites presented in Cade-Menun et al. (2000a) were dominated by orthophosphate and monoesters, similar to Calvert Island. Preston and Trofymow (2000) also used P-NMR to characterize P forms in soils from the CWH zone, however they extracted samples with NaOH and Chelex rather than NaOH-EDTA. They compared the east side of Vancouver Island, BC, in the very dry variant, to the west side in the very wet variant. The west coast soils were characteristic of forests with nutrient restrictions and cool, wet conditions within the CWH zone that are also characteristic of the Calvert Island chronosequence. The young mineral soils on Calvert Island (0–139 y) were comparable to the mineral soils on the west coast of Vancouver Island in Preston and Trofymow (2000), with orthophosphate dominating followed by uncorrected monoesters, and diesters. In other regions of the world, diesters and diester degradation compounds dominated $P_o$ compounds, and pyrophosphate was more abundant, in organic horizons compared to mineral horizons in forest soils of Sweden (Vincent et al., 2012), Russia (Celi et al., 2013), Spain (García-Oliva et al., 2018; Merino et al., 2019), and Taiwan (Lin et al., 2018). In organic forest horizons of Germany, Wang et al. (2019) reported phosphonates in lower organic horizons but not surface litter layers, and generally more pyrophosphate and polyphosphates at the surface than in lower organic horizons.

Another factor that can influence P forms and concentrations in forests is fire. The ∼7,236- and ∼10,760-y BP sites on the Calvert Island chronosequence had evidence of a fire history, with visible fire scars on shore pine (*Pinus contorta* var. *contorta*, and charcoal fragments in soils > 3,500 Y bP (Nelson, 2018). Hoffman et al. (2016a,b) documented fire chronology on northern Calvert Island, with most fires occurring within the last 1,000 years, and found that there was a fire-free period between roughly 7,500 and 5,500 y BP. This suggests that all charcoal found on this chronosequence could be assumed to be <5,500 y BP. The effects of fire on soil P compounds were also investigated within Cw-Hw forests by Cade-Menun et al. (2000b). Post-fire LF and H horizons displayed an increase in $P_i$ following fire since

fire mineralizes $P_o$ forms to phosphate (DeBano and Klopatek, 1988). Similar effects were reported after fire in Spain (García-Oliva et al., 2018; Merino et al., 2019). In Cade-Menun et al. (2000b), after 10 years the effects of fire were diminished and $P_i$ concentrations were comparable to old growth forests. The L and H horizons of the Calvert Island sites with a fire history did not have an apparent increase in phosphate, so the fires that did occur may not have been severe enough to alter soil P forms, or were long enough ago that their effects have diminished.

## Changes in Phosphorus Forms With Site Age

The concentrations of all P forms within the foliage and L and H horizons decreased with increasing age while the concentration of P extracted using NaOH-EDTA increased with age. All samples from Calvert Island (foliage, and L, H, and M horizons) had declining proportions of orthophosphate, with the L horizon exhibiting the least change. The concentration of orthophosphate in the L and M horizon declined exponentially with increasing age (**Figure S6**). This decline in orthophosphate is consistent with the literature because phosphate is a more labile form of P released from primary minerals, plant material and microbes and is subsequently immobilized into microbial and plant tissues, leaving less-labile P forms in soil (Vitousek and Farrington, 1997; McDowell et al., 2007; Bünemann et al., 2008).

Coupled with a decline in orthophosphate concentration and proportion there was an increase in the proportion of $P_o$ in all sample types with age, which is consistent with the second hypothesis for this study. Foliar samples from both Hw and Cw had comparable changes in the P forms with age; however, Hw had a slightly larger increase in the proportion of DNA while Cw had a slightly larger increase in the proportion of monoester 3 category and G6P. The L horizon had a considerable increase in the proportion of cdiesters, the H horizon had an increase in cmonoesters and cdiesters while the M horizon had an increase in the proportion of cMono.

Analysis of the organic horizons on the Haast chronosequence showed an increase in the proportions of phospholipids, DNA and total polyphosphates with age (Turner et al., 2014). Similar to Haast, the H horizons on Calvert Island had an increase in the proportions of cmonoesters and cdiesters with age that can be attributed to an increase in the proportion of DNA, phospholipids, RNA, *myo*- and *scyllo*-IHP and the general monoester 2 category. This is also consistent with the second hypothesis for this study. Interestingly, phosphonates were not detected in the organic horizon on Haast (Turner et al., 2014), whereas phosphonates were detectable on all sites on Calvert Island and slightly increased in proportion with age. This suggests that soil conditions were wetter and more acidic on Calvert Island compared to Haast. It is also consistent with current literature that *myo*- and *scyllo*-IHP increased in proportion with increasing age in the H and mineral horizon samples (McDowell et al., 2007; Turner et al., 2007, 2014) although the concentrations declined between ∼7,236 and ∼10,760 y BP.

On the Franz Josef, Haast, Manawatu and Reefton chronosequences, the proportions of DNA, pyrophosphate, and *myo*-and *scyllo*-IHP increased with increasing age in the mineral horizon (McDowell et al., 2007; Turner et al., 2007, 2014). Similar increases in DNA, *myo*-and *scyllo*-IHP were observed in the mineral horizons on Calvert Island, which fully supports the second hypothesis of the study; however, an increase in pyrophosphate was not apparent. Interestingly, the potential sorption mechanisms for DNA on the Franz Josef and Calvert Island chronosequences differ, with humic material stabilizing DNA on Franz Josef (Turner et al., 2007), and crystalline and amorphous Al on Calvert Island.

Turner et al. (2014) presented a figure of the total IHP concentration and amorphous Al+Fe with increasing age for the Franz Josef chronosequence, and the IHP concentration mirrored the amorphous Al+Fe concentration. The total IHP concentration exhibited a hump shape, with the decline coinciding with the decline in amorphous Fe+Al. The decline in IHP may have been due to biological utilization of these compounds or due to a decline in the stabilization sites for IHP (Turner et al., 2014). As was noted in the previous section, IHP was also correlated to available and amorphous Al and $Al_o$+$Fe_o$ in the Calvert Island chronosequence, although Fe alone was not correlated with IHP. When $Al_o$+$Fe_o$ and total IHP concentration were graphed with age for the Calvert Island chronosequence, the IHP and $Al_o$+$Fe_o$ concentration curves were similar, but the concentration of IHP increases or declines before $Al_o$+$Fe_o$, which differs from the Turner et al. (2014) data (**Figure S4**).

## Ratio of Monoesters to Diesters

For the Calvert Island samples, the cM:D ratio was <1 in the foliage and L horizon, between 0.5 and 2 in the H horizons and greater >1 in the mineral horizons, while the uncorrected M:D ratio was much more variable than the cM:D within all samples types. This suggests that diesters, including degradation products, dominate the foliage, L horizon and sometimes the H horizon, while true monoester compounds (e.g., IHP) are more dominant in the mineral horizon. These data are consistent with our prior conclusion suggesting minimal alteration of the foliage within the L horizon, greater biological cycling and alteration in the H horizon and the dominance of chemisorption processes in the mineral horizons.

The ratio of monoesters to diesters (M:D), or sometimes diester to monoesters (D:M) is widely reported for P NMR literature (e.g., McDowell et al., 2007; Lang et al., 2017), and is thought to reflect $P_o$ lability and mineralization. This is based on the assumption that, in general, monoesters will sorb more readily than diesters, thus restricting their enzymatic hydrolysis. However, there are some flaws with this assumption. First, it makes broad generalizations about sorption by monoesters and diesters that aren't necessarily true for all P species within each category. While IHP sorbs strongly, other monoesters such g6P are not as tightly sorbed (Shang et al., 1996). And while phospholipids do not sorb, DNA will, especially at lower pH. In addition, the degradation of RNA and phospholipids during NMR extraction and analysis requires correction before reporting total monoesters, total diesters or

the M:D (Schneider et al., 2016). Without correction, M:D should be used very cautiously, especially in modeling or to test theories about P-acquisition or P-recycling strategies (Lang et al., 2017).

Studies that have used P-NMR on chronosequences have used uncorrected data with the exception of Vincent et al. (2013) on the Vaserbotten chronosequence in Sweden, although other studies note that due to the degradation of diesters, total diesters are underestimated (McDowell et al., 2007; Turner et al., 2007, 2014). The Vaserbotten chronosequence did not have a significant decline in TP with age so it isn't directly comparable to the Calvert Island chronosequence, but it is interesting to note that Vincent et al. (2013) found that ∼40% of non-IHP monoesters were degradation products of RNA. This supports the current data for Calvert Island about the need to correct for degradation of $P_o$ compounds within NaOH-EDTA extracts. The M:D within mineral soil on the Manawatu and Reefton chronosequence declined with increasing age similarly to Calvert Island (McDowell et al., 2007). However, once the correction for monoesters and diesters was applied, the cM:D actually increased with age on Calvert Island. Due to the increased dominance of IHP with age on Manawatu and Reefton, the cM:D might also be comparable to Calvert Island, reflecting an increased dominance of cmonoesters with age (McDowell et al., 2007).

## CONCLUSIONS

The objective of this study was to examine changes in broad P pools with time using a Holocene soil chronosequence developed on aeolian sand dunes in a hypermaritime climate within the CWH zone on Calvert Island, BC, Canada. The study specifically examines how soil $P_o$ compounds varied with increasing age in organic (L, H) and humic-enriched mineral (M) soil horizons as well as in dominant foliage species. As hypothesized, the Calvert Island chronosequence followed the trends of the Walker and Syers (1976) model with an exponential decline in total P with age and a hump-shaped trend for $P_o$, allowing the Calvert Island chronosequence to be added to the list of chronosequences worldwide that follow the Walker and Syers (1976) P model. As expected, $P_o$ became an increasingly dominant P pool with age, with an increase in DNA in the L and H horizons and increases in *myo*- and *scyllo*-IHP in the M horizons. In all sample types, the proportion of orthophosphate declined with increasing age while the proportion of diesters after correction for degradation (cdiesters) increased with age. There was an increase in the $P_o$ concentration in the M horizons. This was due to increased concentrations of IHP and DNA, which were correlated to total C concentrations and the increased concentration of organically-bound and amorphous Al, and a decline in exchangeable Ca+Mg concentrations that coincided with an increase in concentrations of exchangeable Al+Fe.

The forms of $P_o$ within the foliage and L horizon were comparable as expected, even though the total P concentration of the L horizon was less than the foliage. Several IHP stereoisomers were detected in foliage samples, which is novel given the lack of published data on IHP stereoisomers in plant material from forests in the CWH zone. Ratios of NP increased in L and H horizons but not in foliage samples, with the NP ratios in the M horizons suggesting N limitation on young sites and possible co-limitation by N and P on the oldest site. The information in this study will add to the current understanding of P cycling on the coast of BC and may aid in the management of low-productivity forests that are prevalent in this region.

## DATA AVAILABILITY STATEMENT

The datasets generated for this study are available on request to the corresponding author.

## AUTHOR CONTRIBUTIONS

This work was performed as part of the M.Sc. thesis requirements for L-AN, which was funded by a program led by IW. L-AN was co-supervised by BC-M and PS, with IW on the thesis committee. BC-M conducted some of the NMR analysis and processed and interpreted all NMR spectra. All authors contributed to writing and have read and approved this manuscript.

## FUNDING

Financial support was provided by a research grant from the Tula Foundation and the Hakai Institute to IW and PS and by AAFC A-Base funding (J-00127) to BC-M.

## ACKNOWLEDGMENTS

The authors recognize that this study took place on the traditional territory of the Heiltsuk and Wuikinuxv First Nations and are grateful for the opportunity. The project was supported financially by the Tula Foundation and logistically by the Hakai Institute. The authors are grateful for the support of Eric Peterson and Christina Munck and staff at the Calvert Island field station, especially Lori Johnson for assisting with field work. We thank Dr. Corey Liu for NMR analysis at the Stanford Magnetic Resonance Laboratory and staff at the Saskatchewan Structural Science Center, University of Saskatchewan, for assistance with the NMR work done there. We gratefully acknowledge staff at the BC MECCS Analytical Chemistry Services Laboratory and at the AAFC Swift Current Research and Development Center, especially Katie Hagman, for assistance with sample analysis.

## SUPPLEMENTARY MATERIAL

The Supplementary Material for this article can be found online at: https://www.frontiersin.org/articles/10.3389/ffgc.2020.00083/full#supplementary-material

## REFERENCES


Abdi, D., Cade-Menun, B. J., Ziadi, N., and Parent, L.-E. (2015). Compositional statistical analysis of soil $^{31}$P-NMR forms. *Geoderma* 257–258, 40–47. doi: 10.1016/j.geoderma.2015.03.019

Banner, A., LePage, P., Moran, J., and de Groot, A. (2005). *The Hyp3 Project: Pattern, Process, and Productivity in Hypermaritime Forests of Coastal British Columbia - A Synthesis of 7-Year Results, Spec. Rep. 10.* (Victoria, BC, British Columbia Ministry of Forest, Research Branch), 161.

Banner, A., Mackenzie, W., Haeussler, S., Thomson, S., Pojar, J., and Trowbridge, R. (1993). *A Field Guide to Site Identification and Interpretation for the Prince Rupert Forest Region, LMH No. 26.* (Victoria, BC: Information Services Branch Ministry of Forests), 281.

Bünemann, E., Smernik, R., Marschner, P., and McNeill, A. (2008). Microbial synthesis of organic and condensed forms of phosphorus in acid and calcareous soils. *Soil Biol. Biochem.* 40, 932–946. doi: 10.1016/j.soilbio.2007.11.012

Cade-Menun, B. J. (2015). Improved peak identification in $^{31}$P-NMR spectra of environmental samples with a standardized method and peak library. *Geoderma* 257–258, 102–114. doi: 10.1016/j.geoderma.2014.12.016

Cade-Menun, B. J., Berch, S. M., Preston, C. M., and Lavkulich, L. M. (2000a). Phosphorus forms and related soil chemistry of Podzolic soils on northern Vancouver Island. I. a comparison of two forest types. *Can. J. Forest Res.* 30, 1714–1725. doi: 10.1139/x00-098

Cade-Menun, B. J., Berch, S. M., Preston, C. M., and Lavkulich, L. M. (2000b). Phosphorus forms and related soil chemistry of Podzolic soils on northern Vancouver Island. II. The effects of clear-cutting and burning. *Can. J. For. Res.* 30, 1726–1741. doi: 10.1139/x00-099

Cade-Menun, B. J., He, Z., Zhang,. H., Endale, D. M., Schomberg, H. H., and Liu, C. W. (2015). Stratification of phosphorus forms from long-term conservation tillage and poultry litter application. *Soil Sci. Soc. Am. J.* 79, 504–516. doi: 10.2136/sssaj2014.08.0310

Cade-Menun, B. J., and Lavkulich, L. M. (1997). A comparison of methods to determine total, organic, and available phosphorus in forest soils. *Commun. Soil Sci. Plant Anal.* 28, 651–663. doi: 10.1080/00103629709369818

Cade-Menun, B. J., and Liu, C. W. (2014). Solution phosphorus-31 nuclear magnetic resonance spectroscopy of soils from 2005 to 2013: a review of sample preparation and experimental parameters. *Soil Sci. Soc. Am. J.* 78, 19–37. doi: 10.2136/sssaj2013.05.0187dgs

Cade-Menun, B. J., Navaratnam, J. A., and Walbridge, M. R. (2006). Characterizing dissolved and particulate phosphorus in water with 31P-NMR spectroscopy. *Environ. Sci. Technol.* 40, 7874–7880. doi: 10.1021/es061843e

Cade-Menun, B. J., and Preston, C. (1996). A comparison of soil extraction procedures for $^{31}$P NMR spectroscopy. *Soil Sci.* 161, 770–785. doi: 10.1097/00010694-199611000-00006

Celi, L., and Barberis, E. (2005). "Abiotic stabilization of organic phosphorus in the environment," in *Organic Phosphorus in the Environment*, eds B. L. Turner, E. Frossard, and D. S. Baldwin (Cambridge, MA: CABI Publishing), 113–132. doi: 10.1079/9780851998220.0113

Celi, L., Cerli, C., Turner, B. L., Santoni, S., and Bonifacio, E. (2013). Biogeochemical cycling of soil phosphorus during natural revegetaion of *Pinus sylvestris* on disused sand quarries in Northwestern Russia. *Plant Soil* 367, 121–134. doi: 10.1007/s11104-013-1627-y

Chapin, F. S., Walker, L. R., Fastie, C. L., and Sharman, L. C. (1994). Mechanisms of primary succession following deglaciation at Glacier Bay, Alaska. *Ecol. Monogr.* 64, 149–175. doi: 10.2307/2937039

Chen, C. R., Hou, E. Q., Condron, L. M., Bacon, G., Esfandbod, M., Olley, J., et al. (2015). Soil phosphorus fractionation and nutrient dynamics along the Cooloola coastal dune chronosequence, southern Queensland, Australia. *Geoderma* 257–258, 4–13. doi: 10.1016/j.geoderma.2015.04.027

Condron, L. M., Moir, J., Tiessen, H., and Stewart, J. (1990). Critical evaluation of methods for determining total organic phosphorus in tropical soils. *Soil Sci. Soc. Am. J.* 54, 1261–1266. doi: 10.2136/sssaj1990.03615995005400050010x

Condron, L. M., Turner, B. L., and Cade-Menun, B. J. (2005). "Chemistry and dynamics of soil organic phosphorus," in *Phosphorus: Agriculture and the Environment*, eds J. T. Sims and A. N. Sharpley (Madison, WI: American Society of Agronomy), 87–121. doi: 10.2134/agronmonogr46.c4

Cosgrove, D. J. (1980). *Inositol Phosphates: Their Chemistry, Biochemistry and Physiology*. Amsterdam, NLD: Elsevier. 191.

Courchesne, F., and Turmel, M.-C. (2008). "Extractable Al, Fe, Mn, and Si," *Soil Sampling and Methods of Analysis, 2nd Edn.*, eds M. R. Carter and E. G. Gregorich (Boca Raton, FL: Canadian Society of Soil Science and CRC Press), 307–312.

Crews, T. E., Kitayama, K., Fownes, J. H., Riley, R. H., Herbert, D. A., Mueller-Dombois, D., et al. (1995). Changes in soil phosphorus fractions and ecosystem dynamics across a long chronosequence in Hawaii. *Ecology* 76, 1407–1424. doi: 10.2307/1938144

DeBano, L. F., and Klopatek, J. M. (1988). Phosphorus dynamics of pinyon-juniper soils following simulated burning. *Soil Sci. Soc. Am. J.* 52, 271–277. doi: 10.2136/sssaj1988.03615995005200010048x

Doolette, A., Smernik, R., and Dougherty, W. (2009). Spiking improved solution phosphorus-31 nuclear magnetic resonance identification of soil phosphorus compounds. *Soil Sci. Soc. Am. J.* 73, 919–927. doi: 10.2136/sssaj2008.0192

Eamer, J. B. R., Shugar, D., Walker, I. J., Neudorf, C., Lian, O., Eamer, J. L., et al. (2017). Late Quaternary landscape evolution in a region of stable postglacial relative sea-levels, British Columbia central coast. *Boreas* 47, 738–753. doi: 10.1111/bor.12297

Eger, A., Almond, P. C., and Condron, L. M. (2011). Pedogenesis, soil mass balance, phosphorus dynamics and vegetation communities across a Holocene soil chronosequence in a super-humid climate, south Westland, New Zealand. *Geoderma* 163, 185–196. doi: 10.1016/j.geoderma.2011.04.007

FAO (2006). *Guidelines for Soil Description. 4th Edn.* Rome: Food and Agriculture Organization, 97.

García-Oliva, F., Merino, A., Fonturbel, M. T., Omil, B., Fernández, C., and Vega, J. A. (2018). Severe wildfire hinders renewal of soil P pools by thermal mineralization of organic P in forest soils: Analysis by sequential extraction and $^{31}$P NMR spectroscopy. *Geoderma* 309, 32–40. doi: 10.1016/j.geoderma.2017.09.002

Giles, C., Cade-Menun, B. J., and Hill, J. (2011). The inositol phosphates in soils and manures: abundance, cycling, and measurement. *Can. J. Soil Sci.* 91, 397–416. doi: 10.4141/cjss09090

Goring, C., and Bartholomew, W. (1952). Adsorption of mononucleotides, nucleic acids, and nucleoproteins by clays. *Soil Sci.* 74, 149–164. doi: 10.1097/00010694-195208000-00005

Gotelli, N. J., and Ellison, A. M. (2004). *A Primer of Ecological Statistics*. Sunderland, MA: Sinauer Associates, Inc.

Greaves, M., and Wilson, M. (1969). The adsorption of nucleic acids by montmorillonite. *Soil Biol. Biochem.* 1, 317–323. doi: 10.1016/0038-0717(69)90014-5

Greaves, M. P., and Webley, D. (1969). The hydrolysis of myo-inositol hexaphosphate by soil microorganisms. *Soil Biol. Biochem.* 1, 37–43. doi: 10.1016/0038-0717(69)90032-7

Green, R. N., and Klinka, K. (1994). *A Field Guide for Site Identification and Interpretation for the Vancouver Forest Region, LMH No. 28.* (Victoria, BC: Research Branch, British Columbia Ministry of Forests), 293.

Güsewell, S. (2004). N:P ratios in terrestrial plants: variation and functional significance. *New Phytol.* 164, 243–266. doi: 10.1111/j.1469-8137.2004.01192.x

Hawkes, G. E., Powlson, D. S., Randall, E. W., and Tate, K. R. (1984). A $^{31}$P nuclear magnetic resonance study of the phosphorus species in alkali extracts of soils from long-term field experiments. *Eur. J. Soil Sci.* 35, 35–45. doi: 10.1111/j.1365-2389.1984.tb00257.x

Hayes, P., Turner, B. L., Lambers, H., and Laliberté, E. (2014). Foliar nutrient concentrations and resorption efficiency in plants of contrasting nutrient-acquisition strategies along a 2-million-year dune chronosequence. *J. Ecol.* 102, 396–410. doi: 10.1111/1365-2745.12196

Hoffman, K., Gavin, D., Lertzman, K., Smith, D., and Starzomski, B. (2016b). 13,000 years of fire history derived from soil charcoal in a British Columbia coastal temperate rain forest. *Ecosphere* 7, 1–13. doi: 10.1002/ecs2.1415

Hoffman, K., Gavin, D., and Starzomski, B. (2016a). Seven hundred years of human-driven and climate-influenced fire activity in a British Columbia coastal temperate rainforest. *R Soc. Open Sci.* 3, 1–14. doi: 10.1098/rsos.160608

Izquierdo, J. E., Houlton, B. Z., and van Huysen, T. L. (2013). Evidence for progressive phosphorus limitation over long-term ecosystem development: Examination of a biogeochemical paradigm. *Plant Soil* 367, 135–147. doi: 10.1007/s11104-013-1683-3

Jenny, H., Arkley, R. J., and Schultz, A. (1969). The pygmy forest-Podsol ecosystem and its dune associates of the Mendocino coast. *Madroño* 20, 60–74.

Jørgensen, C., Turner, B. L., and Reitzel, K. (2015). Identification of inositol hexakisphosphate binding sites in soils by selective extraction and solution $^{31}$P NMR spectroscopy. *Geoderma* 257–258, 22–28. doi: 10.1016/j.geoderma.2015.03.021

Kalra, Y. P., and Maynard, D. G. (1991). *Methods Manual for Forest Soil and Plant Analysis*. Edmonton, AB: Forestry Canada Northern Forestry Center, 125.

Kranabetter, J. M., LePage, P., and Banner, A. (2013). Management and productivity of cedar-hemlock-salal scrub forests on the north coast of British Columbia. *For. Ecol. Manage.* 308, 161–168. doi: 10.1016/j.foreco.2013.07.058

Kurtz, A. C., Derry, L. A., and Chadwick, O. A. (2001). Accretion of Asian dust to Hawaiian soils: isotopic, elemental, and mineral mass balances. *Geochim. Cosmochim. Acta* 65, 1971–1983. doi: 10.1016/S0016-7037(01)00575-0

Laliberté, E., Turner, B. L., Costes, T., Pearse, S. J., Wyrwoll, K. H., Zemunik, G., et al. (2012). Experimental assessment of nutrient limitation along a 2-million-year dune chronosequence in the south-western Australia biodiversity hotspot. *J. Ecol.* 100, 631–642. doi: 10.1111/j.1365-2745.2012.01962.x

Laliberté, E., Turner, B. L., Zemunik, G., Wyrwoll, K. H., Pearse, S. J., and Lambers, H. (2013). Nutrient limitation along the Jurien Bay dune chronosequence: response to Uren & Parsons. *J. Ecol.* 101, 1088–1092. doi: 10.1111/1365-2745.12123

Lang, F., Krüger, J., Amelung, W., Willbold, S., Frossard, E., Bünemann, E. K., et al. (2017). Soi phosphorus supply controls P nutrition strategies of beech forest ecosystems in Central Europe. *Biogeochem.* 136, 5–29. doi: 10.1007/s10533-017-0375-0

Levy-Booth, D. J., Campbell, R. G., Gulden, R. H., Hart, M. M., Powell, J. R., Klironomos, J. N., et al. (2007). Cycling of extracellular DNA in the soil environment. *Soil Biol. Biochem.* 39, 2977–2991. doi: 10.1016/j.soilbio.2007.06.020

Lin, C.-W., Tian, G., Pai, C.-W., and Chiu, C.-Y. (2018). Characterization of phosphorus in subtropical coastal sand dune forest soils. *Forests* 9:710. doi: 10.3390/f9110710

Makarov, M., Haumaier, L., and Zech, W. (2002). The nature and origins of diester phosphates in soils: a $^{31}$P-NMR study. *Biol. Fertil. Soils* 35, 136–146. doi: 10.1007/s00374-002-0454-8

Martin, J. B., Laussmann, T., Bakker-Grunwald, T., Vogel, G., and Klein, G. (2000). Neo-inositol polyphosphates in the amoeba *Entamoeba histolytica*. *J. Biol. Chem.* 275, 10134-—10140. doi: 10.1074/jbc.275.14.10134

Maxwell, R. E. (1997). "Soils of Brooks Peninsula" in *Brooks Peninsula: An Ice Age Refugium on Vancouver Island*, (Occasional Paper No. 5.), eds R. J. Hedba and J. C. Haggarty (Victoria, BC: B.C. Min. Environ., Lands and Parks), 4.1–4.49.

McDowell, R. W., Cade-Menun, B. J., and Stewart, I. (2007). Organic phosphorus speciation and pedogenesis: Analysis by solution $^{31}$P nuclear magnetic resonance spectroscopy. *Eur. J. Soil Sci.* 58, 1348–1357. doi: 10.1111/j.1365-2389.2007.00933.x

McKeague, J., and Day, J. (1966). Dithionite-and oxalate-extractable Fe and Al as aids in differentiating various classes of soils. *Can. J. Soil Sci.* 46, 13–22. doi: 10.4141/cjss66-003

Mehlich, A. (1984). Mehlich 3 soil test extractant: a modification of Mehlich 2 extractant. *Commun. Soil Sci. Plant Anal.* 15, 1409–1416. doi: 10.1080/00103628409367568

Merino, A., Jiménez, E., Fernández, C., Fontúrbel, M. T., Campo, J., and Vega, J. A. (2019). Soil organic matter and phosphorus dynamics after low intensity prescribed burning in forests and shrubland. *J. Environ. Manage.* 234, 214–225. doi: 10.1016/j.jenvman.2018.12.055

Merritts, D. J., Chadwick, O. A., and Hendricks, D. M. (1991). Rates and processes of soil evolution on uplifted marine terraces, northern California. *Geoderma* 51, 241–275. doi: 10.1016/0016-7061(91)90073-3

Murphy, J., and Riley, J. P. (1962). A modified single solution method for the determination of phosphate in natural waters. *Anal. Chim. Acta* 27, 31–36. doi: 10.1016/S0003-2670(00)88444-5

Nelson, L.-A. (2018). *Examination of Long-Term Soil Development and Phosphorus Dynamics in a Hypermarine Chronosequence, Calvert Island, British Columbia, Canada*. [MSc. Thesis] (Prince George, BC: University of Northern British Columbia). Available online at: https://unbc.arcabc.ca/

Neudorf, C. M., Lian, O. B., Walker, I. J., Shugar, D. H., Eamer, J. B. R., and Griffin, L. C. M. (2015). Toward a luminescence chronology for coastal dune and beach deposits on Calvert Island, British Columbia central coast, Canada. *Quat. Geochronol.* 30, 275–281. doi: 10.1016/j.quageo.2014.12.004

Noack, S. R., McLaughlin, M. J., Smernik, R. J., McBeath, T. M., and Armstrong, R. D. (2014). Phosphorus speciation in manure wheat and canola plants as affected by phosphorus supply. *Plant Soil* 378, 125–137. doi: 10.1007/s11104-013-2015-3

Noble, M. G., Lawrence, D. B., and Streveler, G. P. (1984). Sphagnum invasion beneath an evergreen forest canopy in southeastern Alaska. *Bryologist* 87, 119–127. doi: 10.2307/3243117

Northup, R. R., Dahlgren, R. A., and McColl, J. G. (1998). Polyphenols as regulators of plant-litter-soil interactions in northern California's pygmy forest: a positive feedback? *Biogeochem.* 42, 189—220. doi: 10.1023/A:1005991908504

Oberson, A., and Joner, E. J. (2005). "Microbial turnover of phosphorus in soil," in *Organic Phosphorus in the Environment*, eds B. L. Turner, E. Frossard, and D. S. Baldwin (Cambridge, MA: CABI Publishing), 133–164. doi: 10.1079/9780851998220.0133

O'Halloran, I. P., and Cade-Menun, B. (2008). "Total and organic phosphorus," in *Soil Sampling and Methods of Analysis, 2nd Edn*., eds M. R. Carter and E. G. Gregorich (Boca Raton, FL: Canadian Society of Soil Science and CRC Press), 265–291. doi: 10.1201/9781420005271.ch24

Parfitt, R. (1979). The availability of P from phosphate-goethite bridging complexes. Desorption and uptake by ryegrass. *Plant Soil* 53, 55–65. doi: 10.1007/BF02181879

Parfitt, R. L., Ross, D. J., Coomes, D. A., Richardson, S. J., Smale, M. C., and Dahlgren, R. A. (2005). N and P in New Zealand soil chronosequences and relationships with foliar N and P. *Biogeochem.* 75, 305—328. doi: 10.1007/s10533-004-7790-8

Parkinson, J., and Allen, S. (1975). A wet oxidation procedure suitable for the determination of nitrogen and mineral nutrients in biological material. *Commun. Soil Sci. Plant Anal.* 6, 1–11. doi: 10.1080/00103627509366539

Pierzynski, G. M., McDowell, R. W., and Sims, J. T. (2005). "Chemistry and dynamics of soil organic phosphorus," in *Phosphorus: Agriculture and the Environment*, eds J. T. Sims and A. N. Sharpley (Madison, WI: American Society of Agronomy), 53–86.

Prescott, C. E., McDonald, M. A., and Weetman, G. F. (1993). Availability of N and P in the forest floors of adjacent stands of western redcedar – western hemlock and western hemlock – amabilis fir on northern Vancouver Island. *Can. J. For. Res.* 23, 605–610. doi: 10.1139/x93-080

Preston, C. M., and Trofymow, J. A. (2000). Characterization of soil P in coastal forest chronosequences of southern Vancouver Island: Effects of climate and harvesting disturbance. *Can. J. Soil Sci.* 80, 633–647. doi: 10.4141/S99-073

Quiquampoix, H., and Mousain, D. (2007). "Enzymatic hydrolysis of organic phosphorus)," in *Organic Phosphorus in the Environment*, eds B. L. Turner R. Frossard, and D. S. Baldwin (Cambridge, MA: CABI Publishing), 89–112. doi: 10.1079/9780851998220.0089

Richardson, S. J., Allen, R. B., and Doherty, J. E. (2008). Shifts in leaf N: P ratio during resorption reflect soil P in temperate rainforest. *Func. Ecol.* 22, 738–745. doi: 10.1111/j.1365-2435.2008.01426.x

Richardson, S. J., Peltzer, D. A., Allen, R. B., McGlone, M. S., and Parfitt, R. L. (2004). Rapid development of phosphorus limitation in temperate rainforest along the Franz Josef soil chronosequence. *Oecologia* 139, 267–276. doi: 10.1007/s00442-004-1501-y

Sanborn, P., Lamontagne, L., and Hendershot, W. (2011). Podzolic soils of Canada: Genesis, distribution, and classification. *Can. J. Soil Sci.* 91, 843–880. doi: 10.4141/cjss10024

Sanborn, P., and Massicotte, H. (2010). *A Holocene Coastal Soil Chronosequence: Naikoon Provincial Park, Graham Island, Haida Gwaii: Progress Report*. Prince George, BC: University of Northern British Columbia. 53.

Saunders, W., and Williams, E. (1955). Observations on the determination of total organic phosphorus in soils. *Eur. J. Soil Sci.* 6, 254–267. doi: 10.1111/j.1365-2389.1955.tb00849.x

Schachtman, D. P., Reid, R. J., and Ayling, S. M. (1998). Phosphorus uptake by plants: from soil to cell. *Plant Physiol.* 116, 447–453. doi: 10.1104/pp.116.2.447

Schneider, K. D., Cade-Menun, B. J., Lynch, D. H., and Voroney, R. P. (2016). Soil phosphorus forms from organic and conventional forage fields. *Soil Sci. Soc. Am. J.* 80, 328–340. doi: 10.2136/sssaj2015.09.0340

Selmants, P. C., and Hart, S. C. (2008). Substrate age and tree islands influence carbon and nitrogen dynamics across a retrogressive semiarid chronosequence. *Global Biogeochem. Cycles* 22, 1–13. doi: 10.1029/2007GB003062

Selmants, P. C., and Hart, S. C. (2010). Phosphorus and soil development: does the Walker and Syers model apply to semiarid ecosystems? *J. Ecol.* 91, 474–484. doi: 10.1890/09-0243.1

Shang, C., Caldwell, D. E., Stewart, J. W. B., Tiessen, H., and Huang, P. M. (1996). Bioavailability of organic and inorganic phosphates adsorbed on short-range ordered aluminum precipitate. *Microb. Ecol.* 31, 29–39. doi: 10.1007/BF00175073

Shang, C., Huang, P., and Stewart, J. (1990). Kinetics of adsorption of organic and inorganic phosphates by short-range ordered precipitate of aluminum. *Can. J. Soil Sci.* 70, 461–470. doi: 10.4141/cjss90-045

Singleton, G. A., and Lavkulich, L. M. (1987a). A soil chronosequence on beach sands, Vancouver Island, British Columbia. *Can. J. Soil Sci.* 67, 795–810. doi: 10.4141/cjss87-077

Singleton, G. A., and Lavkulich, L. M. (1987b). Phosphorus transformations in a soil chronosequence, Vancouver Island, British Columbia. *Can. J. Soil Sci.* 67, 787−793. doi: 10.4141/cjss87-076

Smith, D. H., and Clark, F. E. (1951). Anion-exchange chromatography of inositol phosphates from soil. *Soil Sci.* 72, 353–360. doi: 10.1097/00010694-195111000-00004

Smith, D. H., and Read, D. J. (1997). *Mycorrhizal symbiosis. 2nd Edn*. San Diego, CA: Academic Press. 605.

Soil Classification Working Group (SCWG) (1998). *The Canadian System of Soil Classification. 3rd Edn*. Ottawa, ON: Agriculture and Agri-Food Canada, 202.

Stevens, P. R., and Walker, T. W. (1970). The chronosequence concept and soil formation. *Q. Rev. Biol*. 45, 333–350. doi: 10.1086/406646

Stevenson, F. J., and Cole, M. A. (1999). *Cycles of Soil: Carbon, Nitrogen, Phosphorus, Sulfur and Micronutrients*. New York, NY: Wiley and Sons, Inc., 279–329.

Syers, J. K., and Walker, T. W. (1969). Phosphorus transformations in a chronosequence of soils developed on wind-blown sand in New Zealand. *Eur. J. Soil Sci*. 20, 57–64. doi: 10.1111/j.1365-2389.1969.tb01554.x

Tate, K., and Newman, R. (1982). Phosphorus fractions of a climosequence of soils in New Zealand tussock grassland. *Soil Biol. Biochem*. 14, 191–196. doi: 10.1016/0038-0717(82)90022-0

Thompson, C. H. (1981). Podzol chronosequences on coastal dunes of eastern Australia. *Nature* 91, 59–61. doi: 10.1038/291059a0

Turner, B. L. (2007). "Inositol phosphates in soil: amounts, forms and significance of the phosphorylated inositol stereoisomers," in *Inositol Phosphates: Linking Agriculture and the Environment*, eds B. L. Turner, A. E. Richardson, and E. J. Mullaney (Wallingford: CAB International), 186–207. doi: 10.1079/9781845931520.0186

Turner, B. L. (2008). Soil organic phosphorus in tropical forests: an assessment of the NaOH-EDTA extraction procedure for quantitative analysis by solution $^{31}$P NMR spectroscopy. *Eur. J. Soil Sci*. 59, 453–466. doi: 10.1111/j.1365-2389.2007.00994.x

Turner, B. L., Cade-Menun, B. J., Condron, L. M., and Newman, S. (2005). Extraction of soil organic phosphorus. *Talanta* 66, 294–306. doi: 10.1016/j.talanta.2004.11.012

Turner, B. L., Cade-Menun, B. J., and Westermann, D. T. (2003a). Organic phosphorus composition and potential bioavailability in semi-arid arable soils of the Western United States. *Soil Sci. Soc. Am. J.* 67, 1168–1179. doi: 10.2136/sssaj2003.1168

Turner, B. L., Condron, L. M., Richardson, S. J., Peltzer, D. A., and Allison, V. J. (2007). Soil organic phosphorus transformations during pedogenesis. *Ecosystems* 10, 1166–1181. doi: 10.1007/s10021-007-9086-z

Turner, B. L., Condron, L. M., Wells, A., and Andersen, K. M. (2012). Soil nutrient dynamics during Podzol development under lowland temperate rain forest in New Zealand. *Catena* 97, 50–62. doi: 10.1016/j.catena.2012.05.007

Turner, B. L., and Laliberté, E. (2015). Soil development and nutrient availability along a 2 million-year coastal dune chronosequence under species-rich Mediterranean shrubland in southwestern Australia. *Ecosystems* 18, 287–309. doi: 10.1007/s10021-014-9830-0

Turner, B. L., Mahieu, N., and Condron, L. M. (2003b). Phosphorus-31 nuclear magnetic resonance spectral assignments of phosphorus compounds in soil NaOH–EDTA extracts. *Soil Sci. Soc. Am. J.* 67, 497–510. doi: 10.2136/sssaj2003.4970

Turner, B. L., Papházy, M. J., Haygarth, P. M., and McKelvie, I. D. (2002). Inositol phosphates in the environment. *Phil. Trans. R. Soc. Lond. B* 357, 449–469. doi: 10.1098/rstb.2001.0837

Turner, B. L., and Richardson, A. E. (2004). Identification of *scyllo*-inositol phosphates in soil by solution phosphorus-31 nuclear magnetic resonance spectroscopy. *Soil Sci. Soc. Am. J.* 68, 802–808. doi: 10.2136/sssaj2004.8020

Turner, B. L., Wells, A., and Condron, L. M. (2014). Soil organic phosphorus transformations along a coastal dune chronosequence under New Zealand temperate rain forest. *Biogeochem.* 121, 595–611. doi: 10.1007/s10533-014-0025-8

Ugolini, F. C., and Mann, D. H. (1979). Biopedological origin of peatlands in south east Alaska. *Nature* 281, 366−368. doi: 10.1038/281366a0

Vincent, A. G., Schleucher, J., Gröbner, G., Vestergren, J., Persson, P., Jansson, M., and Giesler, R. (2013). Changes in organic phosphorus composition in boreal forest humus soils: the role of iron and aluminum. *Biogeochem.* 108, 485–499. doi: 10.1007/s10533-011-9612-0

Vincent, A. G., Vestergren, J., Gröbner, G., Persson, P., Schleucher, J., and Giesler, R. (2012). Soil organic phosphorus transformations in a boreal forest chronosequence. *Plant Soil* 367, 149–162. doi: 10.1007/s11104-013-1731-z

Vitousek, P. M., and Farrington, H. (1997). Nutrient limitation and soil development: Experimental test of a biogeochemical theory. *Biogeochem* 37, 63–75. doi: 10.1023/A:1005757218475

Vitousek, P. M., Porder, S., Houlton, B. Z., and Chadwick, O. A. (2010). Terrestrial phosphorus limitation: mechanisms, implications, and nitrogen–phosphorus interactions. *Ecol. Appl.* 20, 5–15. doi: 10.1890/08-0127.1

Vitousek, P. M., Turner, D. R., and Kitayama, K. (1995). Foliar nutrients during long-term soil development in Hawaiian montane rain forest. *J. Ecol.* 76, 712–720. doi: 10.2307/1939338

Walker, T., and Syers, J. K. (1976). The fate of phosphorus during pedogenesis. *Geoderma* 15: 1–19. doi: 10.1016/0016-7061(76)90066-5

Wang, L., Amelung, W., Prietzel, J., and Willbold, S. (2019). Transformation of organic phosphorus compounds during 1500 years of organic soil formation in Bavarian Alpine forests – a $^{31}$P NMR study. *Geoderma* 340, 192–205. doi: 10.1016/j.geoderma.2019.01.029

Wardle, D. A., Walker, L. R., and Bardgett, R. D. (2004). Ecosystem properties and forest decline in contrasting long-term chronosequences. *Science* 305, 509–513. doi: 10.1126/science.1098778

Wardle, D. A., Zackrisson, O., Hörnberg, G., and Gallet, C. (1997). The influence of island area on ecosystem properties. *Science* 277, 1296–1299. doi: 10.1126/science.277.5330.1296

Weyers, E., Strawn, D. G., Peak, D., Moore, A. D., Baker, L. L., and Cade-Menun, B. J. (2016). Phosphorus speciation in calcareous soils following annual dairy manure amendments. *Soil Sci. Soc. Am. J.* 80, 1531–1542. doi: 10.2136/sssaj2016.09.0280

Wood, T. E., Bormann, F. H., and Voigt, G. K. (1984). Phosphorus cycling in a northern hardwood forest: biological and chemical control. *Science* 223, 341–393. doi: 10.1126/science.223.4634.391

Yan, L., Zhang, X., Han, Z., Pang, J., Lambert, H., and Finnegan, P. M. (2019). Responses of foliar phosphorus fractions to soil age are diverse along a 2 Myr dune chronosequence. *New Phytol.* 223, 1621–1633. doi: 10.1111/nph.15910

**Conflict of Interest:** The authors declare that the research was conducted in the absence of any commercial or financial relationships that could be construed as a potential conflict of interest.

frontiers in Forests and Global Change

ORIGINAL RESEARCH
published: 07 August 2020
doi: 10.3389/ffgc.2020.00094

# Goethite-Bound Phosphorus in an Acidic Subsoil Is Not Available to Beech (*Fagus sylvatica* L.)

*Anika Klotzbücher[1]*, Florian Schunck[1,2], Thimo Klotzbücher[1], Klaus Kaiser[1], Bruno Glaser[3], Marie Spohn[4], Meike Widdig[4] and Robert Mikutta[1]*

*[1] Soil Science and Soil Protection, Institute of Agricultural and Nutritional Sciences, Martin Luther University Halle-Wittenberg, Halle (Saale), Germany, [2] Department System Ecotoxicology, Helmholtz Centre for Environmental Research, Leipzig, Germany, [3] Soil Biogeochemistry, Institute of Agricultural and Nutritional Sciences, Martin Luther University Halle-Wittenberg, Halle (Saale), Germany, [4] Department Soil Ecology, Faculty for Biology, Chemistry and Earth Sciences, University of Bayreuth, Bayreuth, Germany*

OPEN ACCESS

**Edited by:**
*Delphine Derrien, INRA Centre Nancy-Lorraine, France*

**Reviewed by:**
*Mark Bakker, Ecole Nationale Supérieure des Sciences Agronomiques de Bordeaux-Aquitaine, France*
*Félix Brédoire, University of Wyoming, United States*
*Jessé Rodrigo Fink, Instituto Federal do Paraná Câmpus Palmas, Brazil*

***Correspondence:**
*Anika Klotzbücher*
*anika.klotzbuecher@landw.uni-halle.de*

**Specialty section:**
*This article was submitted to Forest Soils, a section of the journal Frontiers in Forests and Global Change*

**Received:** *20 May 2020*
**Accepted:** *07 July 2020*
**Published:** *07 August 2020*

**Citation:**
*Klotzbücher A, Schunck F, Klotzbücher T, Kaiser K, Glaser B, Spohn M, Widdig M and Mikutta R (2020) Goethite-Bound Phosphorus in an Acidic Subsoil Is Not Available to Beech (Fagus sylvatica L.). Front. For. Glob. Change 3:94. doi: 10.3389/ffgc.2020.00094*

In forests, where the supply of bioavailable phosphorus (P) from easily weatherable primary minerals is small, plants are thought to recycle P efficiently by uptake of P released from decomposing forest floor material. Yet a share of the P is leached into the subsoil, where it is strongly adsorbed onto the reactive surfaces of pedogenic Fe and Al oxides. This raises the question of whether P leached into subsoil is also recycled. To investigate the mobilization of P bound to hydrous Fe oxides, we conducted a mesocosm experiment in a greenhouse. Beech saplings were grown for 14 months in subsoil material (Bw horizon from the P-poor Lüss beech forest) with added goethite-P adsorption complexes, in either inorganic (orthophosphate) or organic (phytate) form. Four types of control mesocosms were run: soil only and soil mixed with either dissolved orthophosphate or dissolved phytate or goethite. At the end of the experiment, neither total P mass in trees nor P contents in leaves differed between the treatments. According to leaf nutrient contents, plant growth was strongly limited by P in all treatments. Yet total P mass in trees did not increase over the course of the experiment. Thus, despite its P demand, beech was not able to acquire P from goethite surfaces within two vegetation periods. Also P added in dissolved form to the soil before transplanting as well as native soil P were not available. This suggests that, once inorganic and organic P is bound to pedogenic metal oxides in mineral soil, it is not or hardly recycled, which can be an explanation for field data demonstrating quantitatively significant stocks of P in the subsoil of P-deficient forests.

**Keywords: Lüss forest, mesocosm experiment, goethite-P-association, orthophosphate, P recycling system, phosphorus nutrition, plant-available phosphorus, phytate**

## INTRODUCTION

Recent research interest in phosphorus (P) nutrition of European beech (*Fagus sylvatica* L.) forests is triggered by continued decreases in foliar P concentrations over the last decades (Jonard et al., 2015; Talkner et al., 2015). The decrease was attributed to continuing nitrogen (N) deposition and increasing atmospheric carbon (C) dioxide concentrations, which accelerate plant growth and

might thereby induce P limitation (Jonard et al., 2015; Talkner et al., 2015). A conceptual framework for P nutrition of beech forests is provided by Lang et al. (2017), who tested if P acquisition strategies of plants and microbes differ across beech forests with different parent material and soil P stocks using a geosequence approach. In particular, their work suggests that, in forests with young soils, plants and soil organisms mobilize P mainly from primary minerals, and P losses are high ("acquiring strategy." open P cycles), and in forests with mature soils, roots and microorganisms sustain their P demand mainly from the forest floor and soil horizons rich in organic matter, and P losses are low ("recycling strategy," tight P cycles). Their large data set supports the hypothesis of Odum (1969) on the nutrition strategies of vegetation, which presumes that P cycles "tighten" during succession, meaning that P losses due to exports become lower due to an efficient uptake and recycling of P (Odum, 1969). Nevertheless, also in beech forests classified as "P recycling systems" by Lang et al. (2017), a share of the P is leached into subsoil, where it is strongly adsorbed onto reactive surfaces of pedogenic Fe and Al oxides, the most important sorbents for P at low pH (Walker and Syers, 1976; Hinsinger, 2001). This raises the question of whether P in subsoil is also recycled or if it is unavailable for beech.

It is still a matter of debate to what extent oxide-bound P is available to plants. On the one hand, physicochemical research finds that hydrous Fe and Al oxides can bind P forms very strongly via inner sphere complexes (Hinsinger, 2001). The process has been hypothesized as a main cause for the prevalent P limitation of plant growth (Javaid, 2009). On the other hand, it was demonstrated that plants, bacteria, and fungi are able to release P from mineral surfaces for plant uptake (Hinsinger et al., 2018). Beech trees live in symbiosis with ectomycorrhizal fungi, which supply them with P and, in return, receive photosynthates from the plant. One strategy of the plant–microbe system to release P from minerals is dissolution of the mineral by decreasing soil solution pH and thereby coreleasing P. This can be achieved by exudation of protons or low molecular weight organic acids (Hinsinger, 2001). Another strategy is exudation of low molecular weight organic acids, siderophores, or exopolysaccharides, which desorb P from the mineral phases by ligand exchange or complex metal cations involved in P sorption, such as Fe or Al, at low pH (Jones, 1998; Yi et al., 2008; Marschner et al., 2011; Ordoñez et al., 2016; Hinsinger et al., 2018). Thereby, soil exploitation by roots or mycorrhizal hyphae and, more specifically, their surface is crucial for P acquisition as processes are localized in the rhizosphere (Hinsinger, 2001; Lambers et al., 2008).

There is also experimental evidence that oxide-associated P can be available to plants, whereby availability also depends on the P form (Andrino et al., 2019; Klotzbücher et al., 2019; D'Amico et al., 2020). Soil P includes inorganic and organic P; the presumably most persistent P-monoester is phytate (Darch et al., 2014), which might, therefore, predominate in soil. As plants can take up P only as orthophosphate (Vance et al., 2003), organic P must be enzymatically cleaved before it is available to plants (Li et al., 1997). Therefore, plants, bacteria, and fungi exudate phosphatase enzymes, which serve to cleave a phosphate group from its substrates (Margalef et al., 2017). Yet enzymatic hydrolysis of organic P might be hampered by adsorption of organic phosphorylated compounds to mineral phases (George et al., 2016). In addition, the inorganic P that results from the hydrolysis might also adsorb to mineral surfaces, which hampers its uptake by plants.

Recently, D'Amico et al. (2020) exposed mesh bags filled with goethite associated with orthophosphate or phytate for 13 months to P-poor soils of the Italian Alps. Phosphorus was lost from the mesh bags to a larger extent than Fe, suggesting that P was directly released from mineral surfaces. The P release was attributed to ectomycorrhizal activity as fungal growth on the mineral surfaces was detected. The extent of organic P release was smaller than that of inorganic P release. In a mesocosm experiment, Andrino et al. (2019) showed that arbuscular mycorrhiza in symbiosis with tomato were able to acquire orthophosphate and phytate from associations with goethite. Again, more P was plant-available in the treatment with inorganic P. This finding is consistent with the observation that more goethite-associated phosphate than phytate was extractable by an anion exchange resin in $HCO_3^-$ form, which mimics a plant root taking up P (Klotzbücher et al., 2019). In a hydroponic experiment, palisade grass and ruzigrass took up orthophosphate that was associated with goethite or amorphous Al oxide (Merlin et al., 2016). The authors hypothesized that this was due to exudation of organic acids or enzymes by the plants. Also ryegrass was able to take up goethite-associated phosphate in a pot experiment, in which P-loaded goethite was mixed with sand (Parfitt, 1979).

We conducted a mesocosm experiment to test if P from subsoil of the Lüss forest, which was classified as a "P recycling system" by Lang et al. (2017) is available to beech. In more detail, we were interested (i) if P adsorbed to goethite, which is by far the most abundant Fe oxide in soil (Cornell and Schwertmann, 2003), is available to beech, and (ii) if adsorbed organic P is less available than adsorbed inorganic P. Thus, we produced two different goethite-P adsorption complexes using orthophosphate as an inorganic P source and phytate as an organic P source. We mixed the produced adsorption complexes with Lüss subsoil and grew beech saplings for 14 months in experimental pots in a greenhouse. We hypothesized that (i) P from Lüss subsoil and from the goethite-P adsorption complexes is available to beech and that (ii) organic P adsorbed to goethite is less available than adsorbed inorganic P because it not only needs to be desorbed but also mineralized (e.g., by enzymatic cleavage) before it can be taken up by plants.

# MATERIALS AND METHODS

## Preparation of Goethite-P Adsorption Complexes

Goethite was loaded with inorganic P (orthophosphate) or organic P (phytate) to serve as P source for beech saplings in the mesocosm experiment. Solutions containing 1 g P $l^{-1}$ were prepared using $KH_2PO_4$ or K-phytate. The pH was adjusted to 4.0 using HCl or KOH. Goethite (Bayferrox 920 Z, Lanxess,

Köln, Germany) was weighed in portions of 100 g into 1-l bottles and filled with 800 ml of P solutions. Suspensions were shaken overhead for at least 16 h to equilibrate and were afterward centrifuged at 5050 rpm for 45 min at 5°C. Supernatants were withdrawn by suction and discarded. To remove all dissolved P, goethite was resuspended in deionized water by shaking the bottles on a horizontal shaker at 275 rpm for 10 min, and then, they were placed in an ultrasonic bath for 3 min and shaken again in a horizontal shaker at 275 rpm for 10 min. Thereafter, bottles were centrifuged and supernatants were discarded. These steps were repeated until the supernatant had reached an electric conductivity $< 100$ μS. The produced P-loaded goethite was agitated in deionized water and frozen at −20°C. After a few days, samples were freeze-dried, pestled, and sieved $< 250$ μm. All replicates of one treatment were homogenized. To determine the amounts of adsorbed P, aliquots of 50 mg P-loaded goethite were dissolved in 100 ml HCl (32%) for 48 h at 50°C. Concentrations of P and Fe in extracts were determined using inductively coupled plasma-optical emission spectroscopy (ICP-OES, Ultima 2, Horiba Jobin-Yvon, Longjumeau, France). The produced goethite-P adsorption complexes contained 1.17 and 1.84 mg P $g^{-1}$ goethite$^{-1}$ for orthophosphate and phytate loadings, respectively.

## Mesocosm Experiment

### Experimental Setup

Beech saplings of 35–40 cm height were excavated during bud break from the nursery Billen Forst in Bösinghausen, Germany. The nursery was chosen as no mineral fertilizer was applied to saplings; thus, internal P storage of the saplings was assumed not to be too high to render P uptake from soil during the experiment unnecessary. Saplings were stored in darkness at 5°C until transplantation on May 23, 2017. Roots were visibly mycorrhized and additionally inoculated directly before transplanting using a water extract of the organic layer from Lüss forest. The inoculum was prepared by mixing equal masses of material from all organic horizons and extracting it for 48 h in distilled water (soil:solution ratio 1:2) at 4°C. Before inoculation, the extract was diluted 1:1 with deionized water to obtain enough volume; then, all roots were dipped into the extract before each sapling was transplanted into one pot.

Soil was sampled from the Bw horizon of the Hyperdystric Folic Cambisol (Arenic, Loamic, Nechic, Protospodic) of the Lüss Forest (**Table 1**, Lang et al., 2017). After sampling, soil was air dried, sieved to $< 2$ mm, and homogenized. To estimate the total content of Fe in pedogenic Fe oxide phases and associated P, the hot dithionite-citrate-bicarbonate (DCB) extraction was applied as outlined by Mehra and Jackson (1960). To estimate contents of Al and Fe in short range-ordered forms and organic complexes and associated P, extraction with ammonium oxalate at pH 3.0 and 2 h shaking in the dark was carried out according to Schwertmann (1964). Plant-available P was estimated by extraction with sodium bicarbonate (Olsen et al., 1954). The concentrations of extracted Fe, Al, and P were determined by ICP-OES. Results were as follows: $Fe_{DCB}$: 1144 mg $kg^{-1}$, $P_{DCB}$: 28 mg $kg^{-1}$, $Fe_{oxalate}$: 146 mg $kg^{-1}$, $Al_{oxalate}$: 569 mg $kg^{-1}$, $P_{oxalate}$: 11 mg $kg^{-1}$, $P_{Olsen}$: 2 mg $kg^{-1}$.

Each pot contained 7 kg of the subsoil. Six different treatments were installed in 10 replicates each. For the treatments receiving goethite-P adsorption complexes, soil was either mixed with the goethite preloaded with inorganic P (*Goethite* $P_{inorg}$) or with the goethite preloaded with organic P (*Goethite* $P_{org}$). In the corresponding control treatments, either pure goethite (*Goethite*) or only orthophosphate ($P_{inorg}$) or only phytate ($P_{org}$) were added to the soil. Another treatment without any addition to the soil (*Control*) was installed (**Table 2**). For all four treatments receiving P (*Goethite* $P_{inorg}$, *Goethite* $P_{org}$, $P_{inorg}$, $P_{org}$), the additions were normalized to 20 mg P pot$^{-1}$ (2.9 mg P $kg^{-1}$ soil). This amount was chosen as it was more than twice of the P that beech saplings contained at start of the experiment (8.5 ± 1.9 mg P per tree), thus assumed to be enough to cover P demand of beech during the experiment. The added P also represented more than 100% of the bicarbonate-extractable P in the native soil. For the treatment *Goethite* $P_{inorg}$, 17.2 g of the adsorption complex (containing 1.17 mg P $g^{-1}$ goethite$^{-1}$) and for the treatment *Goethite* $P_{org}$, 10.9 g of the adsorption complex (1.84 mg P $g^{-1}$ goethite$^{-1}$) were homogenized with the soil of one pot. For the treatment *Goethite*, the average amount of those two treatments (14.1 g goethite pot$^{-1}$) was homogenized with the soil. For the treatments receiving P without goethite ($P_{inorg}$ and $P_{org}$), corresponding amounts of $KH_2PO_4$ or K-phytate (20 mg P pot$^{-1}$) were added in dissolved form to the soil in pots before saplings were transplanted. To test to what extent both P sources adsorb to the soil, sorption isotherms were produced, suggesting that both P forms were immediately immobilized (**Figure 1**).

Before transplanting, all pots were watered with 1.5 l of a nutrient solution, which contained all essential nutrients except P. Nutrient concentrations in the solution were calculated based on data of soil leachates from the Lüss Forest (unpublished data) by doubling maximum measured concentrations of macronutrients. No data were available for micronutrients; instead concentrations corresponding to those of Hoagland solution were used. The resulting concentrations were 7 mg N $l^{-1}$, 11 mg K $l^{-1}$, 6 mg Ca $l^{-1}$, 2 mg Mg $l^{-1}$, 2 mg S $l^{-1}$, 0.5 mg B $l^{-1}$, 0.01 mg Mo $l^{-1}$, 0.5 mg Mn $l^{-1}$, 0.05 mg Zn $l^{-1}$, and 0.02 mg Cu $l^{-1}$.

### Growing Conditions

The mesocosm experiment (**Figure 2**) was conducted in a greenhouse covering almost two vegetation periods (14 months). During the vegetation periods, temperature was kept between 20 and 25°C, and light intensity was reduced by shading the glass roof. In winter during bud break, temperature in the greenhouse was between 5 and 10°C. Pots were assembled randomly in the greenhouse and were periodically rotated to avoid edge effects in terms of wind from the cooling system and exposition to sunlight. During the first vegetation period, plants were irrigated regularly with the nutrient solution, and thereby volumetric water content was kept between 10 and 20%, which is in range of field capacity of a sandy soil as measured with a time domain reflectometry probe. During bud break and during the second vegetation

**TABLE 1 |** Soil characteristics of the Hyperdystric Folic Cambisol (Arenic, Loamic, Nechic, Protospodic) in the Lüss Forest (the Bw horizon extends from 35 to 106 cm soil depth).

| Horizon | Upper sampling limit (cm) | $P_{total}$ (mg $kg^{-1}$) | $P_{total}$ (g $m^{-2}$) | $P_{citrate}$ (mg $kg^{-1}$) | $P_{citrate}$ (g $m^{-2}$) | $Fe_{DCB}$ (g $kg^{-1}$) | $Fe_{oxalate}$ (g $kg^{-1}$) | $Al_{oxalate}$ (g $kg^{-1}$) | C (mg $g^{-1}$) | pH ($H_2O$) |
|---|---|---|---|---|---|---|---|---|---|---|
| Oi | 13 | 817 | 0.33 | 275 | 0.1 | n.d. | n.d. | n.d. | 502 | 5.7 |
| Oe | 9 | 847 | 2.54 | 259 | 0.8 | n.d. | n.d. | n.d. | 387 | 4.5 |
| Oa | 4 | 671 | 6.71 | 62 | 0.6 | n.d. | n.d. | n.d. | 463 | 3.3 |
| AE | 0- | 196 | 7 | 15 | 0.6 | 1.7 | 0.9 | 0.3 | 97 | 3.5 |
| E | −7 | 119 | 8 | 7 | 0.5 | 2.8 | 1.4 | 0.4 | 18 | 3.8 |
| Bsh | −12 | 118 | 10 | 9 | 0.8 | 4.1 | 3.4 | 0.7 | 14 | 3.8 |
| Bsw | −20 | 129 | 36 | 8 | 2.2 | 4.1 | 3.5 | 1.2 | 10 | 4.2 |
| Bw | −35 | 178 | 201 | 7 | 6.9 | n.d. | n.d. | n.d. | 4 | 4.6 |

*$P_{total}$, total P; $P_{citrate}$, citrate-extractable P; $Fe_{DCB}$, dithionite-citrate-bicarbonate-extractable P; $Fe/Al_{oxalate}$, ammonium oxalate-extractable Fe/Al; n.d., not determined; data from Lang et al. (2017); the subsoil used in this study was sampled from the entire depth of the Bw horizon; further parameters of our subsoil sample were measured and are given in section "Experimental Setup."*

period, plants were regularly watered using deionized water, and nutrient solution was only added in irregular intervals.

Two weeks after transplanting, it turned out that beech saplings were infected with wooly beech scales (*Cryptococcus fagisuga*). To reduce this infection, all trees were regularly sprayed with Imidacloprid, a systemic P-free insecticide (Confidor, Bayer, Leverkusen, Germany). Despite this, the number of replicates was reduced from 10 to 4–8 depending on the treatment. The intensity of damage was not attributed to be a treatment effect as pest outbreak occurred shortly after transplanting. More likely, mortality was controlled by the vitality of individual trees.

### Plant and Soil Sampling and Sample Preparation

To determine biomass and nutrient content of the beech saplings at the start of the experiment, five extra beech saplings were separated into aboveground biomass (stem and branches) and roots, dried at 60°C for 1 week, and stored until the end of the experiment for analyses.

Senesced leaves that fell from trees during both vegetation periods were collected, dried at 60°C for 1 week, and stored until the end of the experiment for analyses.

Trees were harvested after 14 months of growth on July 26, 2018, by cutting stems directly above the soil surface. Soil that stuck to the roots was sampled by carefully removing the root ball from the soil and shaking it within a plastic bag to collect the soil (here referred to as rhizosphere soil). Rhizosphere soil samples were stored at 4°C for a few days until phosphatase activity was analyzed. Trees were separated into leaves, branches, stem, and roots. Plant fractions were dried at 60°C for 1 week.

Dried plant samples were weighed for mass balance calculations. Thereafter, they were first chopped (if necessary) using either a rotor mill or loppers and then ground to fine powder using a vibratory disc mill for nutrient analyses.

**TABLE 2 |** Overview of the treatments of the mesocosm experiment.

| Abbreviation | Explanation |
|---|---|
| *Goethite $P_{org}$* | Lüss Bw horizon mixed with goethite pre-loaded with organic P (phytate) |
| *Goethite $P_{inorg}$* | Lüss Bw horizon mixed with goethite pre-loaded with inorganic P (orthophosphate) |
| *Goethite* | Lüss Bw horizon mixed with pure goethite |
| *$P_{org}$* | Lüss Bw horizon with organic P (phytate) added in dissolved form at start of the experiment |
| *$P_{inorg}$* | Lüss Bw horizon with inorganic P (orthophosphate) added in dissolved form at start of the experiment |
| *Control* | Lüss Bw horizon |

## Plant Analyses

To determine concentrations of P, K, Ca, Mg, Mn, B, Fe, Zn, and Cu, 50 mg of each sample were digested in two replicates using a mixture of 4 ml concentrated $HNO_3$, 1 ml $H_2O_2$ (30%), and 1 ml deionized water for 45 min in a microwave-assisted digestion chamber (MARS 5, CEM, Kamp-Lintfort, Germany). Solutions were filtered through 0.45 µm syringe filters (hydrophobic PTFE, Millex, Merck, Darmstadt, Germany) before measurement by ICP-OES.

Nitrogen content of leaves was analyzed by using a setup of a coupled elemental analyzer (Carlo Erba NC 2500, Thermo Finnigan, Bremen, Germany) and an isotope ratio mass spectrometer (DeltaPlus, Thermo Finnigan, Bremen, Germany), connected by a Conflo III interface (Thermo Finnigan, Bremen, Germany).

## Calculation of Mass Balances

Change of total P (K, Ca, and Mg) mass in trees from the start of the experiment until the end of the experiment, including P (K, Ca, and Mg) lost by leaf fall during both vegetation periods, were calculated as follows:

$$\text{Change [\%]} = \frac{P_{\text{tree end}}\ [\text{mg}] + P_{\text{leaves 2017}}\ [\text{mg}] - P_{\text{tree start}}\ [\text{mg}]}{P_{\text{tree start}}\ [\text{mg}]} \times 100$$

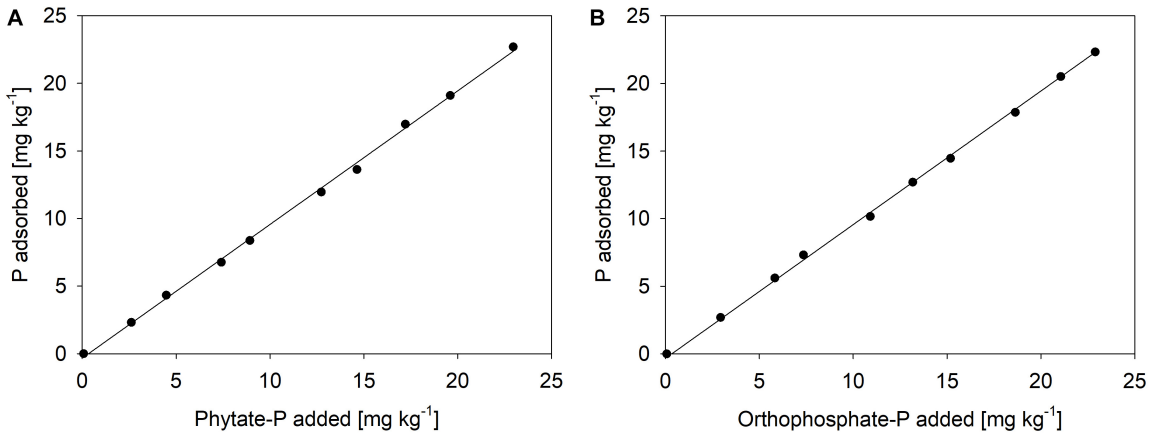


**FIGURE 1 |** Sorption isotherms of **(A)** phytate-P and **(B)** orthophosphate-P to the Lüss Bw horizon, both at pH 4.5 in 1 μM $KClO_4$ solution as a background electrolyte (ca. 100 μS $cm^{-1}$); the amount of P fertilized in the mesocosm experiment equals the second dot (2.8 mg $kg^{-1}$) in both graphics.

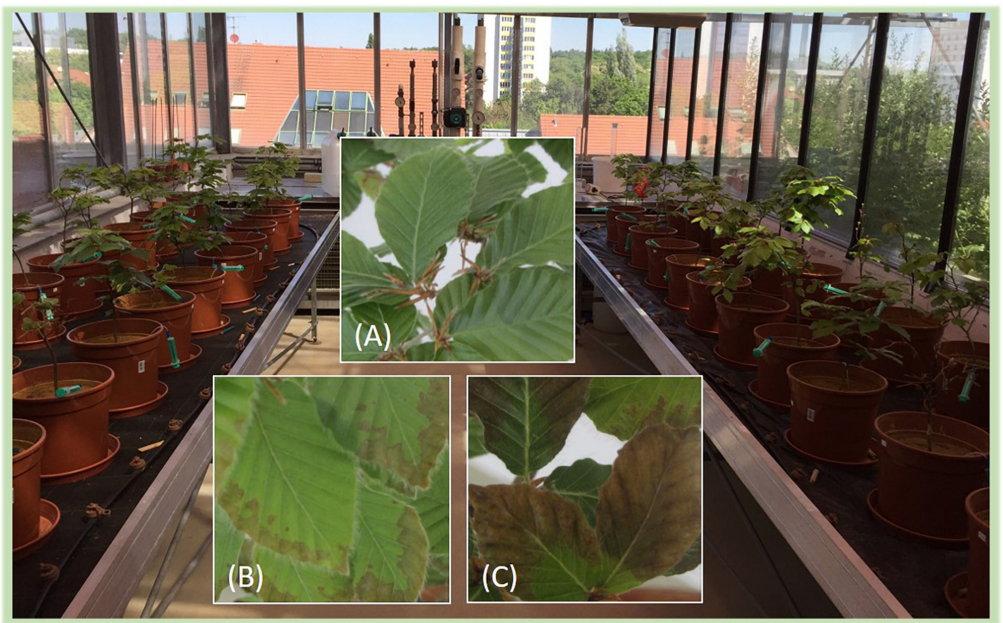


**FIGURE 2 |** Picture of the mesocosm experiment and of leaves **(A)** without symptoms, **(B)** with moderate symptoms, and **(C)** with severe symptoms supposedly caused by P deficiencies.

with

$$\begin{aligned} P_{\text{tree end}}\ [\text{mg}] &= P_{\text{stem end}}\ [\text{mg g}^{-1}]\ \times\ \text{Stem end}\ [\text{g}] \\ &+ P_{\text{branches end}}\ [\text{mg g}^{-1}]\ \times\ \text{Branches end}\ [\text{g}] \\ &+ P_{\text{root end}}\ [\text{mg g}^{-1}]\ \times\ \text{Root end}\ [\text{g}] \\ &+ P_{\text{leaves 2018}}\ [\text{mg g}^{-1}]\ \times\ \text{Leaves 2018}\ [\text{g}] \end{aligned}$$

and

$$P_{\text{leaves 2017}}\ [\text{mg}] = P_{\text{leaves 2017}}\ [\text{mg g}^{-1}]\ \times\ \text{Leaves 2017}\ [\text{g}]$$

and

$$\begin{aligned} P_{\text{tree start}}\ [\text{mg}] &= P_{(\text{stem+branches) start}}\ [\text{mg g}^{-1}] \\ &\times (\text{Stem} + \text{branches})\ \text{start}\ [\text{g}] \\ &+ P_{\text{root start}}\ [\text{mg g}^{-1}]\ \times\ \text{Root start}\ [\text{g}] \end{aligned}$$

Data from the "start" of the experiment refer to the five extra beech saplings that were used to determine biomass and nutrient content of beech saplings at start of the experiment. Data from the "end" of the experiment refer to the individual beech saplings grown in pots. "Leaves 2017" refers to all leaves of the first

**TABLE 3 |** Biomass of beech fractions (g) at start ($n$ = 5) and end of the experiment.

| Fraction | Point of time | Goethite $P_{org}$ $n$ = 8 | Goethite $P_{inorg}$ $n$ = 8 | Goethite $n$ = 7 | $P_{org}$ $n$ = 5 | $P_{inorg}$ $n$ = 4 | Control $n$ = 7 |
|---|---|---|---|---|---|---|---|
| Leaves | 1st season | 1.72 (0.16) | 1.28 (0.13) | 1.24 (0.21) | 1.19 (0.18) | 1.41 (0.37) | 1.58 (0.13) |
| | 2nd season | 2.58 (0.40) | 2.94 (0.40) | 3.25 (0.35) | 2.57 (0.42) | 2.79 (0.25) | 3.18 (0.38) |
| Stem + branches | Start | | | 4.36 (0.96) | | | |
| | End | 6.95 (1.24) | 6.83 (1.01) | 8.06 (0.88) | 5.47 (0.69) | 7.39 (1.10) | 7.38 (0.97) |
| Root | Start | | | 4.68 (1.10) | | | |
| | End | 10.6 (1.55) | 11.9 (1.71) | 11.2 (1.98) | 11.6 (2.96) | 13.4 (1.92) | 11.9 (0.99) |

*Leaves in one vegetation period include the sum of fallen leaves and leaves removed from the tree at the end of the experiment. Values in parentheses show the standard error of the arithmetic mean. No significant differences between the treatments were detected.*

vegetation period, and "leaves 2018" refers to all leaves of the second vegetation period.

## Analysis of Phosphatase Activity in Rhizosphere Soil

Phosphatase activity was determined using the fluorogenic substrate 4-methylumbelliferyl-phosphate according to Marx et al. (2001); German et al. (2011), and Herold et al. (2014). One g of moist rhizosphere soil was homogenized in 50 ml of sterile water by shaking for 20 min. The soil was then pipetted into black 96-well microplates (Brand GmbH und Co., KG, Wertheim, Germany), diluted with 50 µl sterile deionized water, and 100 µl substrate solution was added. Samples were preincubated in the dark at 15°C for 30 min and subsequently measured fluorometrically after 0, 60, 120, and 180 min using a microplate reader (Infinite 200 PRO, Tecan, Männedorf, Switzerland). Fluorescence was corrected for quenching of the soil as well as for the fluorescence of substrate and soil (German et al., 2011). Enzyme activity was calculated from the slope of net fluorescence over incubation time.

## Statistical Analyses

Statistical analyses were performed using the package *ggpubr* of R version 3.4.4. Data were tested for normal distribution by quantile–quantile plots and the Shapiro-Wilk test. In case of parametric data sets, analysis of variance followed by multiple student's *t*-tests were performed; number of comparisons were corrected after Holm (1979). In the case of non-parametric data sets, a Kruskal-Wallis test was performed, and *post hoc* analysis was conducted with a Wilcoxon-rank-sum test; number of comparisons were corrected after Holm (1979). A significance level of $\alpha = 0.05$ was applied.

# RESULTS

## Biomass Production

During the experimental period of 14 months, biomass of the trees increased on average by 154% from 9.0 ± 2.1 g (standard error, SE) to 23.0 ± 1.2 g, including fallen leaves during both vegetation periods. At the end of the experiment, biomass of all plant fractions (leaves, stem, and roots) did not significantly differ between the treatments (**Table 3**).

## Phosphorus Uptake

At the end of the experiment, P contents of leaves did not significantly differ between the treatments; on average, it was 0.52 ± 0.01 (SE) mg $g^{-1}$ and, thus, far below the threshold value of 0.95 mg $g^{-1}$ for deficiency symptoms of beech (**Figure 3**) as reported by Göttlein (2015). During the second vegetation period, P content of leaves was significantly lower than during the first vegetation period, decreasing on average by 19% (**Table 4**). The P content of stems also decreased during the experiment on average by 77% and that of roots by 68%.

Phosphorus contents did not differ between the treatments for leaves of the first vegetation period, leaves of the second vegetation period (sum of fallen leaves and leaves removed from trees at the end of the experiment), and stems at the end of the experiment (**Table 4**). Only for roots at the end of the experiment, P content was significantly higher in the treatment $P_{org}$ than in all other treatments (**Table 4**).

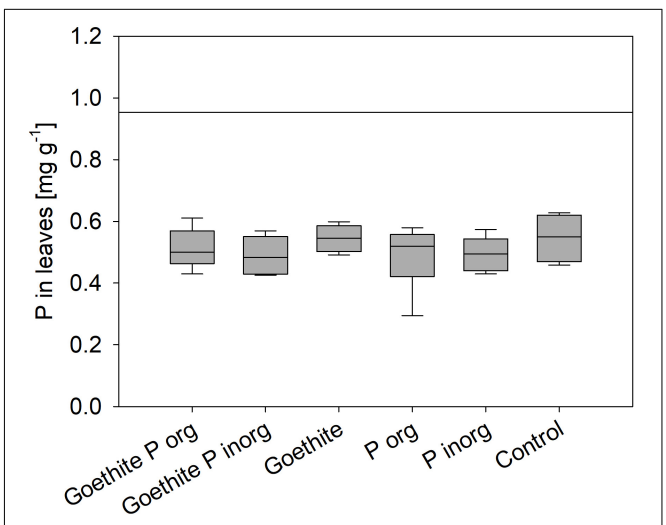


**FIGURE 3 |** Phosphorus content of leaves at the end of the experiment; error bars represent standard errors; no statistical differences between treatments were detected. Black line represents threshold value for P deficiency symptoms (Göttlein, 2015).

**TABLE 4 |** Phosphorus contents of beech fractions (mg $g^{-1}$) at the start ($n$ = 4 because one sample was lost during nutrient analysis) and end of the experiment.

| Fraction | Point of time | Goethite $P_{org}$ $n$ = 8 | Goethite $P_{inorg}$ $n$ = 8 | Goethite $n$ = 7 | $P_{org}$ $n$ = 5 | $P_{inorg}$ $n$ = 4 | Control $n$ = 7 |
|---|---|---|---|---|---|---|---|
| Leaves | 1st season | 0.63 (0.04) | 0.66 (0.04) | 0.65 (0.04) | 0.62 (0.01) | 0.63 (0.06) | 0.65 (0.02) |
| | 2nd season | 0.54 (0.03) | 0.52 (0.02) | 0.49 (0.02) | 0.48 (0.01) | 0.59 (0.01) | 0.47 (0.04) |
| Stem + branches | Start | | | 0.97 (0.09) | | | |
| | End | 0.22 (0.01) | 0.22 (0.01) | 0.20 (0.01) | 0.20 (0.01) | 0.22 (0.01) | 0.24 (0.01) |
| Root | Start | | | 0.84 (0.11) | | | |
| | End | 0.28 (0.01)[a] | 0.30 (0.01)[a] | 0.27 (0.01)[a] | 0.24 (0.01)[b] | 0.28 (0.01)[a] | 0.27 (0.01)[a] |

*Phosphorus in leaves in one vegetation period includes P in fallen leaves and leaves removed from the tree at the end of the vegetation period/harvest. Values in parentheses show the standard error of the arithmetic mean. Treatments with the same letter are not significantly different at α = 0.05. No letters were added when treatments did not differ significantly.*

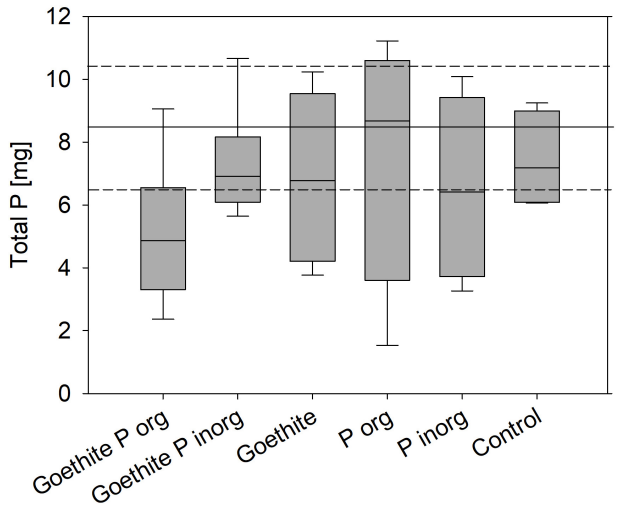


**FIGURE 4 |** Boxplots represent the sum of total P in trees at the end of the experiment and P lost with leaves during the first and second vegetation period; error bars represent standard errors; no statistical differences between treatments were detected. Black line marks total P in saplings at the start of the experiment; dashed lines represent standard error.

The results suggest that, during the experiment, no P was taken up from soil in any of the treatments because the sum of total P stored in plants at the end of the experiment plus the P lost with fallen leaves during both vegetation periods did not significantly differ from total P in the trees at the start of the experiment. The sum of total P stored in plants at the end of the experiment plus the P lost with fallen leaves during both vegetation periods did also not significantly differ between the treatments (**Figure 4**).

## Uptake of Further Essential Nutrients

At the end of the experiment, contents of K, Ca, Mg, Mn, B, Fe, Zn, and Cu in leaves were also compared to threshold values for deficiency symptoms (**Table 5**) reported by Göttlein (2015). For Ca, measured contents were slightly below the threshold (i.e., on average, 3.7 ± 0.1 mg $g^{-1}$ compared to 4.0 mg $g^{-1}$); for all other nutrients, measured contents were above the threshold.

In contrast to P, total amounts of K, Ca, and Mg in trees increased strongly during the experiment (**Figure 5**); total K mass in trees increased by 255%, Ca mass by 829%, and Mg mass by 36%. Thus, uptake of Ca and K was faster than biomass production (**Figure 5**).

## Phosphatase Activity

Mean phosphatase activity in the rhizosphere at the end of the experiment was 96 nmol $g^{-1}$ $soil^{-1}$ $h^{-1}$ across all treatments. Mean values of the treatments ranged from 48 to 191 nmol $g^{-1}$ $soil^{-1}$ $h^{-1}$ in the *Goethite* $P_{org}$ and $P_{org}$ treatments, respectively. Overall, phosphatase activity in rhizosphere at the end of the experiment did not differ significantly between treatments (**Figure 6**).

**TABLE 5 |** Contents of essential nutrient elements in leaves at the end of the experiment in comparison to threshold values for deficiency level (Göttlein, 2015).

| Nutrient element | Goethite $P_{org}$ $n$ = 8 | Goethite $P_{inorg}$ $n$ = 8 | Goethite $n$ = 7 | $P_{org}$ $n$ = 5 | $P_{inorg}$ $n$ = 4 | Control $n$ = 7 | Threshold value |
|---|---|---|---|---|---|---|---|
| N (mg $g^{-1}$) | 18.03 (0.79) | 18.66 (0.61) | 18.59 (0.43) | 19.34 (0.75) | 20.65 (0.60) | 19.09 (0.39) | 16.65 |
| K (mg $g^{-1}$) | 13.26 (0.58) | 9.79 (0.61) | 11.05 (0.38) | 11.47 (0.83) | 11.16 (0.51) | 11.13 (0.48) | 4.75 |
| Ca (mg $g^{-1}$) | 3.88 (0.22) | 3.61 (0.21) | 3.89 (0.16) | 3.32 (0.26) | 3.72 (0.35) | 3.85 (0.15) | 4.00 |
| Mg (mg $g^{-1}$) | 1.31 (0.11) | 1.23 (0.10) | 1.41 (0.09) | 1.48 (0.17) | 0.93 (0.14) | 1.10 (0.12) | 0.70 |
| Mn (mg $g^{-1}$) | 1.53 (0.15) | 1.32 (0.09) | 1.56 (0.05) | 1.42 (0.15) | 1.52 (0.17) | 1.55 (0.12) | 0.50 |
| B (μg $g^{-1}$) | 234 (21) | 255 (23) | 221 (12) | 204 (13) | 288 (18) | 228 (18) | 100 |
| Fe (μg $g^{-1}$) | 288 (82) | 197 (32) | 208 (28) | 277 (57) | 137 (3) | 181 (36) | 35 |
| Zn (μg $g^{-1}$) | 39 (3) | 40 (2) | 42 (4) | 43 (3) | 40 (3) | 37 (4) | 20 |
| Cu (μg $g^{-1}$) | 22 (3) | 27 (3) | 26 (2) | 30 (4) | 27 (4) | 25 (2) | 5 |

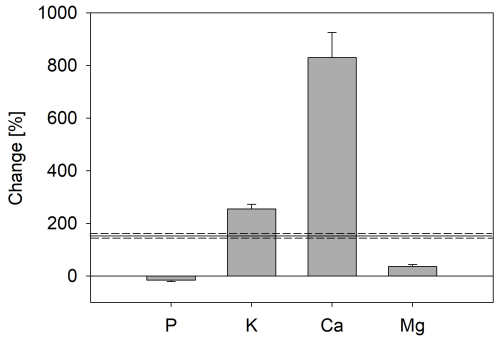


**FIGURE 5 |** Change of total nutrient mass in trees from the start (four saplings) until end of the experiment, including nutrients lost by leaf fall during both vegetation periods (trees of all treatments were pooled); error bars represent standard errors. Black line marks increase of total biomass during the experiment; dashed lines represent standard error.

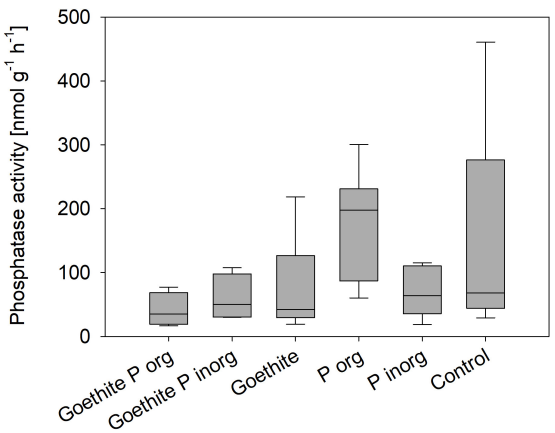


**FIGURE 6 |** Phosphatase activity in the rhizosphere at the end of the experiment; no statistical differences between treatments were detected.

# DISCUSSION

## Phosphorus From Lüss Subsoil and From the Added Adsorption Complexes Is Not Available to Beech

Our first hypothesis that P from Lüss subsoil and from the goethite-P adsorption complexes is available to beech was not confirmed in our experiment. The three main findings supporting rejection of the hypothesis are (i) addition of goethite-P adsorption complexes did not affect P uptake by plants although leaf P contents were far below a deficiency level, (ii) addition of dissolved P did not enhance P uptake by beech as it was rapidly immobilized in soil by adsorption to minerals, and (iii) native P from the subsoil was not available to beech as, despite P limitation, beech leaves were only supplied with P by P redistribution within the plant tissue. In the following, these reasons are explained in detail.

(i) The addition of goethite-P adsorption complexes did not affect P uptake by plants although P content of leaves was far below a deficiency level for beech of 0.95 mg $g^{-1}$ reported by Göttlein (2015). In our experiment, for the given leaf biomass, only 1.1 ± 0.1 mg P would have been required by a tree of each treatment to reach the threshold value for leaf P content. Even though this amount accounts for only 5.5% of the added P (20 mg P $pot^{-1}$), plants were not able to use the supplied P. For comparison, leaf P contents of adult trees in the Lüss Forest were 1.2 ± 0.1 mg $g^{-1}$ (Lang et al., 2016), and mature leaves of young trees from the Lüss Forest had similar P contents (Zavišic and Polle, 2018). In a mesocosm experiment in which saplings from Lüss were grown in Lüss soil from the A horizon and the forest floor, leaf P contents of only 0.7 ± 0.3 mg $g^{-1}$, thus below the deficiency level, were observed, but saplings did take up P from the soil (Hofmann et al., 2016). Meller et al. (2019) conducted a cross-growth experiment, in which soil and beech saplings from sites with the lowest and highest P contents along the geosequence (Lang et al., 2017), Lüss and Bad Brückenau, were used. Lowest leaf P contents of 0.94 ± 0.06 mg $g^{-1}$ were reported for beech saplings from the Lüss Forest grown in pots with soil from Bad Brückenau. The authors found that internal P allocation within the tree is a better indicator for P availability in soil than leaf P contents. Nevertheless, in none of the cited experiments were leaf P contents as low as in our experiment with a mean of all treatments of 0.52 ± 0.1 mg $g^{-1}$. Another hint for P limitation of trees was that all saplings showed signs of stress in both vegetation periods (**Figure 2**). Leaf tips browned and/or brown spots appeared on the leaf area; then signs expanded to the whole leaf and some leaves crinkled and fell off. Even if no descriptions of P limitation symptoms were found in literature for deciduous trees, similar symptoms were described for P deficiency of plants in general (Zorn et al., 2016).

(ii) The reason for the lack of uptake of dissolved P is likely the strong sorption by the used subsoil material. In accordance with the considerable contents of Fe and Al oxides in the used subsoil, the sorption isotherms for orthophosphate and phytate of the Lüss subsoil (**Figure 1**) suggest nearly complete adsorption of the supplied P by mineral surfaces. The sorption isotherms indicate that sorption even at the eightfold P input was 92–99%. Thus, in the mesocosm experiment, only a small portion of the free sorption sites was necessary to retain virtually all added P. In comparison with experiments in which beech saplings from Lüss were grown in mesocosms with either forest floor and topsoil horizon (Spohn et al., 2018) or with a mixture of soil from the A and B horizons (Hofmann et al., 2016), beech was able to take up added orthophosphate in dissolved form. This can be explained by a lower number of sorption sites for P in soils of those experiments than in soil from the Bw horizon used in our mesocosm experiment. Rapid adsorption of added orthophosphate in Lüss soil might also have taken place in a mesocosm experiment by Hauenstein et al. (2018). In this experiment, radioactive $^{33}$P-labeled orthophosphate was applied to beech saplings in pots filled with Lüss soil from the top three mineral horizons with or without the organic layer. In the treatment with the organic layer, radioactivity in the xylem sap of

beech was higher than in the treatment without an organic layer, probably because P immediately adsorbed to oxide surfaces in the mineral soil horizons but remained available in the organic layer. Hence, sorption onto oxide surfaces is a process that competes with plants for the supplied P; i.e., in soils rich in sorption sites, P availability remains low even after large inputs of potentially available P forms.

(iii) Data on P allocation across plant parts suggest that native P from the subsoil horizon (*Control*) was likewise not bioavailable. We noticed that beech leaves of all treatments were only supplied with P by redistribution within plant tissue during the experiment as indicated by decreasing P contents in stems, branches, and roots from the start to the end of the experiment. Improvement of the internal P recycling was shown to be a strategy of trees to cope with low P in the environment (Côté et al., 2002; Hofmann et al., 2016; Netzer et al., 2017; Hauenstein et al., 2018; Meller et al., 2019). In our experiment, initial internal P storage of beech was so low that beech was not able to compensate for low P availability by P redistribution only, but additional P from soil would have been required to cover the P demand. Surprisingly, leaf biomass increased from the first to the second vegetation period even if it was shown that growth reduction is another strategy of beech trees to cope with low P supply (Yang et al., 2016; Zavišic and Polle, 2018; Meller et al., 2019). Increasing P deficiency from the first to the second vegetation period might also be attributed to a dilution effect of P in plant tissue by biomass increase. Biomass increase was larger for roots than for stems and branches; the rapid root growth might have been one attempt (without effect) of beech to access more P by increasing the root/shoot ratio and the root/soil interface. The total root surface area of plants is one major factor limiting P uptake besides P concentration at the absorbing root surface and the distribution of roots in the soil (Lambers et al., 2008).

The factors limiting P uptake depicted by Lambers et al. (2008) might also explain why our results differ from results of Merlin et al. (2016) and Klotzbücher et al. (2019). In the study of Klotzbücher et al. (2019) it was shown that 43% of goethite-associated phosphate and 6% of goethite-associated phytate were extracted by an anion exchange resin in $HCO_3^-$ form, which mimics a plant root taking up P. The resin was placed together with P-loaded goethite in ultrapure water. Phosphorus release was driven by the chemical gradient of P between goethite and solution, and an equilibrium state was permanently changed by P removal by the resin. Compared to this experiment, in our mesocosm experiment, the P concentration in the solid phase and, therefore, also in the soil solution was much lower. Also P diffusion was probably much slower in the pot experiments than in the solution with the resin as P diffusion is known to be slow in soil (Barber, 1995). Further, rooting of the pots and thus the absorbing root surface was very limited (when removing the roots from the pots, we realized that root balls did not fill the whole pot volume). In the study of Merlin et al. (2016), goethite-associated P (and Al oxide-associated P) was available for palisade grass and ruzigrass. As their experiments were conducted in nutrient solutions (without soil), results fit those of P extraction from solution by the resin.

Our results also differ from those of Parfitt (1979); Andrino et al. (2019), and D'Amico et al. (2020), who showed that P associated with goethite was at least partly bioavailable in studies using soil or solid substrates instead of nutrient solutions. In the study of Andrino et al. (2019), arbuscular mycorrhiza associated with tomato plants were able to acquire goethite-associated P. On the one hand, this finding might differ from our results because different types of plants and mycorrhiza were studied. On the other hand, also spatial P distribution in the substrates differed between the experimental setups. In the experiment of Andrino et al. (2019), either pure orthophosphate-loaded goethite was applied or phytate-loaded goethite mixed with pure goethite (same substrate volumes, normalized to P) was offered in a chamber accessible for fungal hyphae only. In our experiment, the P-loaded goethite accounted for only 0.2% of the substrate although P-loadings of goethite were similar. Thus, P concentrations at the absorbing hyphae surfaces (and, in our experiment, also root surfaces) were much higher in the experiment of Andrino et al. (2019). D'Amico et al. (2020) conducted (to our knowledge) the only published experiment in which goethite-P associations were exposed to P-poor surroundings in the field. The study sites are located in the Italian Alps, where European Larch is grown. Goethite-P associations were exposed in mesh bags mixed with quartz sand. High P losses of the mesh bags in combination with ectomycorrhizal colonization were attributed to P release by mycorrhizal fungi. However, due to the experimental setup, it was not possible to test if mobilized P was taken up by trees or if it was readsorbed to mineral surfaces in soil. In the study of Parfitt (1979), ryegrass was able to take up goethite-associated phosphate in a pot experiment in which adsorption complexes were mixed with sand. Probably, P uptake was possible because the lack of other adsorption sites for P in the sand. Taken together, the results of the discussed studies and our mesocosm experiment suggest that P adsorbed to goethite can (at least partly) be released by a plant-microbe system. In substrates without abundant free adsorption sites for P, the released P is plant-available after release from oxides; however, when many free adsorption sites are abundant, such as in our experiment, these are more competitive than plants regarding the desorbed P.

Results of our mesocosm experiment fit to those of Pastore et al. (2020), who showed that goethite-associated phosphate is hardly available to microorganisms especially at low concentrations of easily degradable organic C, which is an important driver for P release by microorganisms (Brucker et al., 2020). In our mesocosm experiment, C-limitation by microbes might, thus, be a further reason why microbes did not release sufficient P from goethite in our C-poor subsoil.

In general, our results suggest that, once P is bound to pedogenic metal oxides in mineral soil, it is no longer recycled, which can be an explanation for field data demonstrating quantitatively significant stocks of P in subsoil of P deficient forests (Lang et al., 2017), such as in Lüss (**Table 1**). Supposedly, in P recycling systems, P leaching from the forest floor to subsoil is not recycled; i.e., trees entirely rely on P from the organic layer or organic-rich topsoil as suggested by Lang et al. (2017) and confirmed by Leuschner et al. (2006) and

Hauenstein et al. (2018). Further, our results are in line with low P availability in highly weathered (thus, Fe and Al oxide-rich) soils under tropical forests (Reed et al., 2010). Generally, in acidic and deeply weathered tropical soils, P-availability is low as a large portion of soil P occurs as bound to and/or occluded in Fe and Al oxides (Jones and Oburger, 2011).

### Both Inorganic and Organic P Adsorbed to Goethite Were Not Available to Beech

Our second hypothesis of organic P adsorbed to goethite being less available than adsorbed inorganic P because it requires not only desorption, but also mineralization (e.g., by enzymatic cleavage) before being taken up by plants is not confirmed as none of the two P sources was available. Even though phosphatase activity varied slightly between the treatments, there were no significant differences. A global meta-analysis showed that average acid phosphatase activities in deciduous forests amount up to 14,500 nmol $g^{-1}$ $h^{-1}$ (Margalef et al., 2017) – much higher than the phosphatase activities measured in our study. However, studies show that phosphatase activities decrease rapidly with soil depth (Taylor et al., 2002; Zhang et al., 2005; Herold et al., 2014). In subsoil horizons (45-105 cm depth) phosphomonoesterase activity of around 1000 nmol $g^{-1}$ $h^{-1}$ in rhizosphere and around 75 nmol $g^{-1}$ $h^{-1}$ in bulk soil were measured in an agricultural field (Uksa et al., 2015). Similar to our study, Herold et al. (2014) found phosphatase activities of around 122 nmol $g^{-1}$ $h^{-1}$ in the Bw horizon of a nutrient-poor sandy forest soil. An explanation for the low phosphatase activities could be low microbial biomass C concentrations in combination with C-limitation of microbes in this C- and P-poor subsoil (Herold et al., 2014) as well as the plants' nutrient limitation.

As described in section "Phosphorus From Lüss Subsoil and From the Added Adsorption Complexes Is Not Available to Beech," organic P adsorbed to goethite was shown to be less available than adsorbed inorganic P in other studies (Andrino et al., 2019; Klotzbücher et al., 2019; D'Amico et al., 2020). This was probably caused by slower desorption of organic P than of inorganic P in the study of D'Amico et al. (2020), in which mycorrhizal colonization of the goethite-P-complexes was measured, and in the study of Klotzbücher et al. (2019), in which desorption induced by a chemical gradient was determined. Desorption rates for organic P from goethite might have been lower than those for inorganic P because of stronger bindings of organic P than of inorganic P to goethite. In the study of Andrino et al. (2019), P uptake by plants was lower for organic than for inorganic P; thus, either slower desorption from goethite and/or the necessity of mineralization of organic P might have caused the difference in availability. However, in our mesocosm experiment, in which even inorganic P was unavailable to beech, both inorganic and organic P were either not released from oxides or rapidly readsorbed to oxides after release.

## CONCLUSION

In the conducted mesocosm experiment, we have shown that beech was not able to take up organic or inorganic P from a subsoil in which P was bound to pedogenic Fe and Al oxides, which additionally provided free adsorption sites. Neither native soil P nor P added in dissolved form nor P from added goethite-P adsorption complexes was taken up by beech saplings. This was attributed to rapid adsorption of dissolved P to hydrous Fe and Al oxides and rapid readsorption of P possibly released by oxides. Thus, oxides were more competitive in taking up and retaining P than plants. Obviously, P from goethite-P adsorption complexes might only be acquired by plant-microbe systems in environments with little other adsorption sites for P. Our results support the view that in P-poor forest ecosystems classified as P recycling systems, trees rely on P from the organic matter and on tree internal P recycling. We conclude for P recycling systems that P leached from decomposing forest floor to subsoil is not or hardly recycled. Further, our results point at a critical view of extractions estimating plant-available P in soil, such as the method using an anion exchange resin in $HCO_3^-$ form in a water extract because it does not consider additional free adsorption sites for P in soil, which might prevent P uptake by plants due to rapid P adsorption.

## DATA AVAILABILITY STATEMENT

The original contributions presented in the study are included in the article, further inquiries can be directed to the corresponding author.

## AUTHOR CONTRIBUTIONS

AK, TK, KK, RM, and BG designed the experiment. AK and FS conducted the experiment. MS and MW analyzed phosphatase activity. FS and AK analyzed all other data. AK wrote the manuscript with contributions from all authors.

## FUNDING

The study was carried out in the framework of the priority program 1685 "Ecosystem Nutrition: Forest Strategies for limited Phosphorus Resources" funded by the German Federal Ministry of Education and Research (DFG, MI 1377/7-2). We further acknowledge the financial support within the funding program "Open Access Publishing" by the DFG.

## ACKNOWLEDGMENTS

We acknowledge Simon Clausing for ordering beech saplings from the nursery and sharing his expertise on mycorrhiza. We thank Sonia Meller for practical advice during planning of the experiment. We thank Prof. Dr. Edgar Peiter for the allowance to use the greenhouse chamber and Dr. Margret Köck for her technical assistance. We are thankful for the scientific and technical support during the greenhouse experiment by Dr. Bastian Meier. We thank Alexandra Boritzki, Christine Krenkewitz, Miriam Kempe, and Christian Treptow for their work in the greenhouse and laboratory.

## REFERENCES


Andrino, A., Boy, J., Mikutta, R., Sauheitl, L., and Guggenberger, G. (2019). Carbon investment required for the mobilization of inorganic and organic phosphorus bound to goethite by an arbuscular mycorrhiza (*Solanum lycopersicum* x *Rhizophagus irregularis*). *Front. Environ. Sci.* 7:26. doi: 10.3389/fenvs.2019.00026

Barber, S. A. (1995). *Soil nutrient Bioavailability: A Mechanistic Approach*. New York, NY: John Wiley & Sons.

Brucker, E., Kernchen, S., and Spohn, M. (2020). Release of phosphorus and silicon from minerals by soil microorganisms depends on the availability of organic carbon. *Soil Biol. Biochem.* 143:107737. doi: 10.1016/j.soilbio.2020.107737

Cornell, R. M., and Schwertmann, U. (2003). *The Iron Oxides: Structure, Properties, Reactions, Occurrences and Uses*. Hoboken, NJ: John Wiley & Sons.

Côté, B., Fyles, J. W., and Djalilvand, H. (2002). Increasing N and P resorption efficiency and proficiency in northern deciduous hardwoods with decreasing foliar N and P concentrations. *Ann. For. Sci.* 59, 275–281. doi: 10.1051/forest:2002023

D'Amico, M., Almeida, J. P., Barbieri, S., Castelli, F., Sgura, E., Sineo, G., et al. (2020). Ectomycorrhizal utilization of different phosphorus sources in a glacier forefront in the Italian Alps. *Plant Soil* 446, 81–95. doi: 10.1007/s11104-019-04342-0

Darch, T., Blackwell, M. S., Hawkins, J., Haygarth, P. M., and Chadwick, D. (2014). A meta-analysis of organic and inorganic phosphorus in organic fertilizers, soils, and water: implications for water quality. *Crit. Rev. Environ. Sci. Technol.* 44, 2172–2202. doi: 10.1080/10643389.2013.790752

George, T. S., Hinsinger, P., and Turner, B. L. (2016). *Phosphorus in Soils and Plants–Facing Phosphorus Scarcity*. Berlin: Springer.

German, D. P., Weintraub, M. N., Grandy, A. S., Lauber, C. L., Rinkes, Z. L., and Allison, S. D. (2011). Optimization of hydrolytic and oxidative enzyme methods for ecosystem studies. *Soil Biol. Biochem.* 43, 1387–1397. doi: 10.1016/j.soilbio.2011.03.017

Göttlein, A. (2015). Grenzwertbereiche für die ernährungsdiagnostische Einwertung der Hauptbaumarten Fichte, Kiefer, Eiche, Buche. *Allg For. Jagdztg* 186, 110–116.

Hauenstein, S., Neidhardt, H., Lang, F., Krüger, J., Hofmann, D., Pütz, T., et al. (2018). Organic layers favor phosphorus storage and uptake by young beech trees (*Fagus sylvatica* L.) at nutrient poor ecosystems. *Plant Soil* 432, 289–301. doi: 10.1007/s11104-018-3804-5

Herold, N., Schöning, I., Berner, D., Haslwimmer, H., Kandeler, E., Michalzik, B., et al. (2014). Vertical gradients of potential enzyme activities in soil profiles of European beech, Norway spruce and Scots pine dominated forest sites. *Pedobiologia* 57, 181–189. doi: 10.1016/j.pedobi.2014.03.003

Hinsinger, P. (2001). Bioavailability of soil inorganic P in the rhizosphere as affected by root-induced chemical changes: a review. *Plant Soil* 237, 173–195. doi: 10.1023/A:1013351617532

Hinsinger, P., Herrmann, L., Lesueur, D., Robin, A., Trap, J., Waithaisong, K., et al. (2018). Impact of roots, microorganisms and microfauna on the fate of soil phosphorus in the rhizosphere. *Annu. Plant Rev. Online* 48, 377–407. doi: 10.1002/9781119312994.apr0528

Hofmann, K., Heuck, C., and Spohn, M. (2016). Phosphorus resorption by young beech trees and soil phosphatase activity as dependent on phosphorus availability. *Oecologia* 181, 369–379. doi: 10.1007/s00442-016-3581-x

Holm, S. (1979). A simple sequentially rejective multiple test procedure. *Scand. J. Stat.* 6, 65–70.

Javaid, A. (2009). Arbuscular mycorrhizal mediated nutrition in plants. *J. Plant Nutr.* 32, 1595–1618. doi: 10.1080/01904160903150875

Jonard, M., Fürst, A., Verstraeten, A., Thimonier, A., Timmermann, V., Potočić, N., et al. (2015). Tree mineral nutrition is deteriorating in Europe. *Global Change Biol.* 21, 418–430. doi: 10.1111/gcb.12657

Jones, D. L. (1998). Organic acids in the rhizosphere – a critical review. *Plant and Soil* 205, 25–44. doi: 10.1023/A:1004356007312

Jones, D. L., and Oburger, E. (2011). "Solubilization of phosphorus by soil microorganisms," in *Phosphorus in Action. Biological Processes in Soil Phosphorus Cycling*, eds E. K. Bünemann, A. Oberson, and E. Frossard, (Berlin: Springer-Verlag), 169–198. doi: 10.1007/978-3-642-15271-9_7

Klotzbücher, A., Kaiser, K., Klotzbücher, T., Wolff, M., and Mikutta, R. (2019). Testing mechanisms underlying the Hedley sequential phosphorus extraction of soils. *J. Plant Nutr. Soil Sci.* 182, 570–577. doi: 10.1002/jpln.201800652

Lambers, H., Raven, J. A., Shaver, G. R., and Smith, S. E. (2008). Plant nutrient-acquisition strategies change with soil age. *Trends Ecol. Evol.* 23, 95–103. doi: 10.1016/j.tree.2007.10.008

Lang, F., Bauhus, J., Frossard, E., George, E., Kaiser, K., Kaupenjohann, M., et al. (2016). Phosphorus in forest ecosystems: new insights from an ecosystem nutrition perspective. *J. Plant Nutr Soil Sci.* 179, 129–135. doi: 10.1002/jpln.201500541

Lang, F., Krüger, J., Amelung, W., Willbold, S., Frossard, E., Bünemann, E., et al. (2017). Soil phosphorus supply controls P nutrition strategies of beech forest ecosystems in Central Europe. *Biogeochemistry* 136, 5–29. doi: 10.1007/s10533-017-0375-0

Leuschner, C., Meier, I. C., and Hertel, D. (2006). On the niche breadth of Fagus sylvatica: soil nutrient status in 50 Central European beech stands on a broad range of bedrock types. *Ann. For. Sci.* 63, 355–368. doi: 10.1051/forest:2006016

Li, M., Osaki, M., Honma, M., and Tadano, T. (1997). Purification and characterization of phytase induced in tomato roots under phosphorus-deficient conditions. *Soil Sci. Plant Nutr.* 43, 179–190. doi: 10.1080/00380768.1997.10414726

Margalef, O., Sardans, J., Fernández-Martínez, M., Molowny-Horas, R., Janssens, I. A., Ciais, P., et al. (2017). Global patterns of phosphatase activity in natural soils. *Sci. Rep.* 7, 1–13. doi: 10.1038/s41598-017-01418-8

Marschner, P., Crowley, D., and Rengel, Z. (2011). Rhizosphere interactions between microorganisms and plants govern iron and phosphorus acquisition along the root axis – model and research methods. *Soil Biol. Biochem.* 43, 883–894. doi: 10.1016/j.soilbio.2011.01.005

Marx, M.-C., Wood, M., and Jarvis, S. C. (2001). A microplate fluorimetric assay for the study of enzyme diversity in soils. *Soil Biol. Biochem.* 33, 1633–1640. doi: 10.1016/S0038-0717(01)00079-7

Mehra, O. P., and Jackson, M. L. (1960). Iron oxide removal from soils and clay by a dithionite-citrate system buffered with sodium bicarbonate. *Clays Clay Minererals* 7, 317–327. doi: 10.1016/B978-0-08-009235-5.50026-7

Meller, S., Frossard, E., and Luster, J. (2019). Phosphorus allocation to leaves of beech saplings reacts to soil phosphorus availability. *Front. Plant Sci.* 10:744. doi: 10.3389/fpls.2019.00744

Merlin, A., Rosolem, C. A., and He, Z. (2016). Non-labile phosphorus acquisition by *Brachiaria*. *J. Plant Nutri.* 39, 1319–1327. doi: 10.1080/01904167.2015.1109117

Netzer, F., Schmid, C., Herschbach, C., and Rennenberg, H. (2017). Phosphorus-nutrition of European beech (*Fagus sylvatica* L.) during annual growth depends on tree age and P-availability in the soil. *Environ. Exp. Bot.* 137, 194–207. doi: 10.1016/j.envexpbot.2017.02.009

Odum, E. P. (1969). The strategy of ecosystem development. *Science* 164, 267–270. doi: 10.5822/978-1-61091-491-8_20

Olsen, S. R., Cole, C. V., Watanabe, F. S., and Dean, L. A. (1954). *Estimation of Available Phosphorus in Soils by Extraction with Sodium Bicarbonate*. Washington, DC: USDA.

Ordoñez, Y. M., Fernandez, B. R., Lara, L. S., Rodriguez, A., Uribe-Vélez, D., and Sanders, I. R. (2016). Bacteria with phosphate solubilizing capacity alter mycorrhizal fungal growth both inside and outside the root and in the presence of native microbial communities. *PLoS One* 11:e0154438. doi: 10.1371/journal.pone.0154438

Parfitt, R. L. (1979). The availability of P from Phosphate-goethite bridging complexes. Desorption and uptake by ryegrass. *Plant Soil* 53, 55–65. doi: 10.1007/BF02181879

Pastore, G., Kaiser, K., Kernchen, S., and Spohn, M. (2020). Microbial release of apatite- and goethite-bound phosphate in acidic forest soils. *Geoderma* 370:114360. doi: 10.1016/j.geoderma.2020.114360

Reed, S. C., Townsend, A. R., Taylor, P. G., and Cleveland, C. C. (2010). "Phosphorus cycling in tropical forests growing on highly weathered soils," in *Phosphorus in Action*, eds E. Bünemann, A. Oberson, and E. Frossard, (Berlin: Springer), 339–369. doi: 10.1007/978-3-642-15271-9_14

Schwertmann, U. (1964). Differenzierung der Eisenoxide des Bodens durch Extraktion mit Ammoniumoxalat-Lösung. *Zeitschrift für Pflanzenernährung Düngung Bodenkunde* 105, 194–202. doi: 10.1002/jpln.3591050303

Spohn, M., Zavišić, A., Nassal, P., Bergkemper, F., Schulz, S., Marhan, S., et al. (2018). Temporal variations of phosphorus uptake by soil microbial biomass and young beech trees in two forest soils with contrasting phosphorus stocks. *Soil Biol. Biochem.* 117, 191–202. doi: 10.1016/j.soilbio.2017.10.019

Talkner, U., Meiwes, K. J., Potočić, N., Seletković, I., Cools, N., De Vos, B., et al. (2015). Phosphorus nutrition of beech (*Fagus sylvatica* L.) is decreasing in Europe. *Ann. For. Sci.* 72, 919–928. doi: 10.1007/s13595-015-0459-8

Taylor, J. P., Wilson, B., Mills, M. S., and Burns, R. G. (2002). Comparison of microbial numbers and enzymatic activities in surface soils and subsoils using various techniques. *Soil Biol. Biochem.* 34, 387–401. doi: 10.1016/S0038-0717(01)00199-7

Uksa, M., Schloter, M., Kautz, T., Athmann, M., Köpke, U., and Fischer, D. (2015). Spatial variability of hydrolytic and oxidative potential enzyme activities in different subsoil compartments. *Biol. Fertil. Soils* 51, 517–521. doi: 10.1007/s00374-015-0992-5

Vance, C. P., Uhde-Stone, C., and Allan, D. L. (2003). Phosphorus acquisition and use: critical adaptations by plants for securing a nonrenewable resource. *New Phytol.* 157, 423–447. doi: 10.1046/j.1469-8137.2003.00695.x

Walker, T. W., and Syers, J. K. (1976). The fate of phosphorus during pedogenesis. *Geoderma* 15, 1–19. doi: 10.1016/0016-7061(76)90066-5

Yang, N., Zavišić, A., Pena, R., and Polle, A. (2016). Phenology, photosynthesis, and phosphorus in European beech (*Fagus sylvatica* L.) in two forest soils with contrasting P contents. *J. Plant Nutr. Soil Sci.* 179, 151–158. doi: 10.1002/jpln.201500539

Yi, Y., Huang, W., and Ge, Y. (2008). Exopolysaccharide: a novel important factor in the microbial dissolution of tricalcium phosphate. *World J. Microbiol. Biotechnol.* 24, 1059–1065. doi: 10.1007/s11274-007-9575-4

Zavišic, A., and Polle, A. (2018). Dynamics of phosphorus nutrition, allocation and growth of young beech (*Fagus sylvatica* L.) trees in P-rich and P-poor forest soil. *Tree Physiol.* 38, 37–51. doi: 10.1093/treephys/tpx146

Zhang, Y.-M., Wu, N., Zhou, G.-Y., and Bao, W.-K. (2005). Changes in enzyme activities of spruce (*Picea balfouriana*) forest soil as related to burning in the eastern Qinghai-Tibetan Plateau. *Appl. Soil Ecol.* 30, 215–225. doi: 10.1016/j.apsoil.2005.01.005

Zorn, W., Marks, G., Heß, H., and Bergmann, W. (2016). *Handbuch zur Visuellen Diagnose von Ernährungsstörungen bei Kulturpflanzen*. Berlin: Springer-Verlag.

**Conflict of Interest:** The authors declare that the research was conducted in the absence of any commercial or financial relationships that could be construed as a potential conflict of interest.

frontiers in Forests and Global Change

ORIGINAL RESEARCH
published: 19 August 2020
doi: 10.3389/ffgc.2020.00095

# Fine Root Size and Morphology of Associated Hyphae Reflect the Phosphorus Nutrition Strategies of European Beech Forests

*Caroline A. E. Loew*[1]*, *Helmer Schack-Kirchner*[1], *Siegfried Fink*[2] and *Friederike Lang*[1]

[1] Laboratory Soil Ecology, Department of Environment and Natural Resources, Institute of Soil Ecology, Organization Albert-Ludwigs-University Freiburg, Freiburg, Germany, [2] Laboratory Forest Botany, Department of Environment and Natural Resources, Institute of Forest Botany, Organization Albert-Ludwigs-University Freiburg, Freiburg, Germany

OPEN ACCESS

**Edited by:**
Andreas Schindlbacher, Austrian Research Centre for Forests (BFW), Austria

**Reviewed by:**
Xiao-Tao Lu, Institute of Applied Ecology (CAS), China
Junwei Luan, International Center for Bamboo and Rattan, China

***Correspondence:**
Caroline A. E. Loew
caroline.loew@bodenkunde.uni-freiburg.de

**Specialty section:**
This article was submitted to Forest Soils, a section of the journal Frontiers in Forests and Global Change

**Received:** 11 April 2020
**Accepted:** 10 July 2020
**Published:** 19 August 2020

**Citation:**
Loew CAE, Schack-Kirchner H, Fink S and Lang F (2020) Fine Root Size and Morphology of Associated Hyphae Reflect the Phosphorus Nutrition Strategies of European Beech Forests. Front. For. Glob. Change 3:95. doi: 10.3389/ffgc.2020.00095

Roots are among the major controls of nutrient and C cycles and together with mycorrhizal fungi they are assumed to play a key role especially in the P nutrition of forest ecosystems. Current publications emphasized that the size distribution of fine roots reflects the crucial impact of roots on biogeochemical cycles. However, we know hardly anything about the spatial distribution of fine root size classes and their specific surface as well as the distribution of mycorrhizal fungi among different size classes in undisturbed soils. We used a novel method based on epifluorescence microscopy to analyze fine roots in undisturbed soil samples. We expected that based on these analyses proposed differences between P-rich and P-poor soils get clearer than based on routine methods for fine root analysis. This was examined at two European beech forests in Germany at silicate rock that differ in P supply by the parent material. We analyzed the fine root frequency, size distribution and surface based on resin impregnated cross sections taken from undisturbed soil samples. Fine roots were classified according to their size and morphology of associated ectomycorrhiza (ECM). After staining with acridine orange these root traits were analyzed and quantified with epifluorescence microscopy. We found that more than 82 % of the absorbing surface was associated with roots having a diameter smaller than 100 $\mu$m. The fine root surface area present per square meter of soil was 388 $m^2$ at the P-poor site and 220 $m^2$ at the P-rich site. In addition, the percentage of mycorrhization of the fine root surface was 47 % at the P-poor site and only 38 % at the P-rich site. The biggest root length density and the highest absorbing fine root surface with mycorrhization and abundance of extramatrical mycelia (EM) was observed in the forest floor (+4 to 0 cm) at the P-poor site and in the subsoil (−79 to −100 cm) at the P-rich site. Our results confirm that beech trees adapt their root traits according to P availability showing higher absorbing surface at the P-poor site compared to the

P-rich site. In contrast, at the soil-profile scale, rooting density (RLD) and mycorrhization increased with P availability thereby showing an efficient way of root and mycorrhizal fungi placement. Overall, distinct differences in fine root traits, between the P-rich and P-poor site were most evident for fine roots smaller than 100 $\mu$m.

**Keywords: phosphorus-nutrition, fine root length, ectomycorrhiza, beech forests, root size class, epifluorescence microscopy, polished soil sections**

## 1. INTRODUCTION

Roots are less accessible for researchers than above-ground plant compartments and are widely assumed to bear still a lot of unidentified possibilities of adaptation (Finér et al., 2011). Current papers indicate the prominent role of roots in C sequestration (Ruess et al., 2003; Clemmensen et al., 2013) and nutrient cycling (Johnson and Turner, 2019). The high relevance of roots for phosphorus nutrition of higher plants originates from the low mobility of P in soils (Raghothama and Karthikeyan, 2005). At many sites, P is among the limiting factors of forest growth (Lang et al., 2017). It has been shown that beech forests evolved many mechanisms to adapt to P scarcity. Since declining P leaf contents observed for European beech forests (Jonard et al., 2015; Talkner et al., 2015) might indicate disturbance of those mechanisms they are currently in the center of scientific debate. Lang et al. (2017) found a shift in P nutrition strategies of beech forest ecosystems, depending on the P supply provided by the soils. At sites with low stocks in soil P, beech forests maintain their P supply by recycling of P from organic sources, while the acquisition of P from mineral resources controls P nutrition at high soil P stocks (Raghothama and Karthikeyan, 2005). Till now, it is unknown, if fine root spatial and size distribution as well as mycorrhization reflect nutrition strategies (Lopez-Bucio et al., 2000; Plassard and Dell, 2010; Hauenstein et al., 2018). In general, size distribution and surface area of very small roots (<100 $\mu$m) and the morphology of the associated mycorrhizal fungi have hardly been analyzed. This is especially true for samples with undisturbed soil structure. About 95% of all trees in forest ecosystems, especially in boreal and temperate biomes, have ectomycorrhiza symbiosis (Smith and Read, 2009). In terms of P uptake, the extramatrical mycelium (EM) produced by ectomycorrhizal fungi (ECM) is a key factor (Read, 1984; Plassard and Dell, 2010). It improves P uptake by increasing the size of the explored soil volume (Lynch, 1995) whereby the depletion zone may extend far beyond the rhizosphere (Bolan, 1991; Marschner and Dell, 1994; Tibbett and Sanders, 2002) and thus overcomes the limits of the slow diffusion of P in the soil, which is assumed to be not more than a few millimeters (Williamson and Alexander, 1975; Schachtman et al., 1998; Plassard and Dell, 2010; Demand et al., 2017). Furthermore, Nylund and Wallander (1992) determined that the production of the EM for *Pinus sylvestris* L. is induced by P starvation. Thus, we assume that European beech trees of the above-mentioned recycling and acquiring systems show different rooting density, depth distribution, and mycorrhization depending on P availability.

Most published root data is based on mass or length of washed-out roots (Böhm, 1979; Colpaert et al., 1992; Van Noordwijk et al., 2000). However, this procedure has problems regarding the size distribution of roots in soils. It has been found that especially fine roots (<1 mm) are underestimated (Bengough et al., 1992; Rousseau et al., 1994). The quantification of hyphae spreading out from the Hartig net to build extramatrical mycelium is even more challenging (Colpaert et al., 1992; Rousseau et al., 1994). A variety of methods have been developed to quantify the biomass of extramatrical mycelium in soils, including mini-rhizotrons and in-growth mesh bags. Yet, due to disturbance of soil samples or artificial growing conditions, these methods are inadequate to quantitatively describe roots and their mycorrhizal traits in soils. Consequently, to provide information on the effective absorbing root surface area, multiple studies have requested that roots should be characterized and quantified in undisturbed soil samples (Jones et al., 1990; Rousseau et al., 1994; Hinsinger et al., 2011; Peñuelas et al., 2013). We suggest a micro morphological approach to quantify and characterize fine roots which has also been used by Tippkötter et al. (1986), Altemüller (1989), and Schack-Kirchner et al. (2000). This means, shortly, that roots are left in their soil environment but are analyzed on two-dimensional areas such as thin sections or faces prepared otherwise. Our study aim was to analyze those characteristics of fine roots (<2 mm) with major relevance for P uptake: size distribution, surface area, specific root length, and the mycorrhization as well as the morphology of mycorrhizal fungi within undisturbed soil environment. We compared soils from two European beech forests, one developed from P-rich substrate, the other from P-poor substrate. We expected that based on micro morphological root analyzes proposed differences between P-rich and P-poor soils get more clear than based on routine methods for fine root analysis. Our approach was based on epifluorescence microscopy of resin impregnated polished soil sections taken from undisturbed soil cores. To our knowledge, this study is the first approach of *in situ* quantification of the absorbing root surfaces in their undisturbed environment.

## 2. MATERIALS AND METHODS

### Site Characteristics

Soil and stand characteristics including P stocks of the study sites Bad Brueckenau (BBR, P-rich site) and Unterluess (LUE, P-poor site) are reported in **Table 1**. As a proxy for P availability, citric acid extractable $P_{inorganic}$ according to Manghabati et al. (2018) is listed per soil horizon in **Table 2**. The experiment is focused

**TABLE 1 |** Site and stand characteristics of the study sites Bad Brueckenau (BBR) and Unterluess (LUE) (Lang et al., 2017).

| Properties | BBR | LUE |
|---|---|---|
| Geographical coordinates | 50°35′N, 9°92′E | 52°83′N, 10°36′E |
| Soil type (WRB, 2015) | Dystric skeletic cambisol (Hyperhumic. Loamic) | Hyperdystric folic cambisol (Arenic. Loamic. Nechic. Protospodic) |
| Parent material | Basaltic rock | Sandy till |
| Humus form (Ad-hoc-AG Boden, 2005) | Mull-like Moder | Mor-like Moder |
| Texture—topsoil (WRB, 2015) | Silty clay loam | Loamy sand |
| Texture—subsoil (WRB, 2015) | Loam | Sand |
| Elevation [m] | 809 | 115 |
| Precipitation [mm] | 1,031 | 779 |
| Total basal area $m^2$ $ha^{-1}$ | 35.6 *Fagus sylvatica* (99%), *Acer pseudoplatanus* (1%) | 36.7 *Fagus sylvatica* (91%), *Quercus petraea* (9%) |
| Stand age [a] | 137 | 132 |
| Stem density [n $ha^{-1}$] | 595 | 520 |
| P Stocks to 1 m [kg $ha^{-1}$] | 9,040 | 164 |

exclusively on four soil horizons per site (Oa, Ah/AhE, Bw/Bsw, and Cw). BBR, is located in the Rhoen mountains in North Bavaria, and LUE, is in the North German lowlands. Both study sites belong to the Level II intensive monitoring plots of the Pan-European International Cooperative Program on assessment and monitoring of air pollution effects for the forests (ICP Forests) under the supervision of UNECE (Lorenz, 1995). Though the stocks and availability of P substantially differ between the two sites, leaf concentrations of P are similar (Lang et al., 2017).

## 2.1. Root-Mycorrhiza Investigations

### 2.1.1. Root System Sampling and Soil Preparation

For the quantitative investigation of fine roots (<2 mm), we used a three-level hierarchical sampling design (**Figure 1**). On the first level, we sampled undisturbed soil cores at three sampling points (three beech trees) considered to be representative of the sites BBR and LUE and with low coverage of herbs or shrubs to avoid non-beech roots and at a distance from the next stem of about 1 m. Soil cores with a diameter of 8 cm and a length of 20 cm were taken with a root auger up to 1 m in depth. In BBR, we had to take clods below 40 cm instead of soil cores due to the high stone content. Immediately after sampling, we identified and counted the visible fine roots (1–2 mm) (Kreutzer, 1961) by the core break method (Böhm, 1979). On the second level, we subsampled the surrounding of four randomly chosen visible fine roots (1–2 mm) per analyzed soil horizon with "mini cores" for microscopic analysis.

These mini cores (**Figure 1**) are tubes formed out of perforated aluminum plate with a diameter of 1.5 cm and a length of 2 cm. These were pushed into the soil around a fine root (1–2 mm). The mini cores and the Cw clods were next placed in rectangle casting molds (EPDM rectangle mold, 55 × 30 × 22 mm, Buehler, Esslingen am Neckar, Germany).

For the third level, immediately after cutting out and placing the mini cores were fixed in 2.5% glutardialdehyde aqueous solution (Tippkötter et al., 1986) to stop microbial activity and to conserve roots and other biological tissues. Dehydration was then performed using a five-step ascending acetone concentration of 50%, 80%, and three times 100% for 3 days to prevent shrinking or deformation (Tippkötter and Ritz, 1996). The dehydrated soil samples were then embedded in a low viscosity epoxy resin (Serva Electrophoresis GmbH; Heidelberg; Germany, Application note "Modified Spurr," "Modification E") (Serva Electrophoresis GmbH, 2007). After complete filling of the pore space, acetone was replaced by resin. The resin content was sequentially increased from 20 to 100% in five steps based on preliminary tests. To ensure that all pores were filled with epoxy resin, the actual impregnation was carried out with 100% epoxy resin under a vacuum for 24 h.

The final polymerization took place for 16 h at 70°C. The cured soil cores were mounted onto aluminum plates with hot melting adhesive and were cut horizontally into three to five 1–2 mm slices using a diamond saw. These slices were ground with sand paper in declining grid size from P320 to P800 and P1200, and finally polished with $Al_2O_3$ powder with declining grain size from 5, 1, and 0.3 $\mu$m. Low viscosity erosion oil (EDM180 from Ilocut, Diermeier Energie GmbH, Munich, Germany) was used as cutting and grinding fluid to avoid swelling (Schack-Kirchner et al., 2000). The individual soil samples were finally glued onto the microscope slides with a two compound epoxy adhesive glue and cleaned with paraldehyde. Since the soil slices did not perfectly correspond to the mini core surface area, we quantified the soil filled surface area of each soil slice with image analysis (ImageJ, Version1.51f).

The surface of the polished soil slices was stained with acridine orange. According to Schack-Kirchner et al. (2000) for the coloring of hyphae embedded in polyester resin was modified as follows: In preliminary tests we found an optimum staining contrast in epoxy resin specimen by using a mixture of seven parts 0.1% acridine orange in 100% ethanol to three parts 0.1% acridine orange in 10% hydrochloric acid. It was applied for 10 min and the staining was done in closed boxes to prevent the evaporation of ethanol. After the dye was removed with a cloth, the soil slabs were left to stand for a further 20 min before being examined by Zeiss Axio Zoom V16 fluorescence zoom microscope (Carl Zeiss AG; Jena, Germany). For the fluorescence illumination, a HXP 200C illuminator with a mercury short-arc reflector lamp was used. The microscope was equipped with a PlanNeoFluar Z2.3x/0.57 FWD 10.6 mm objective and a filter combination of BP450-490/FT510/LP515.

The digital microscope camera AxioCam HRC (Carl Zeiss AG; Jena, Germany) has a CCD sensor type with a pixel resolution of 1.4 megapixel with 1,388 × 1,040 with a pixel size of 6.45 $\mu$m. The pictures were further analyzed with the imaging software ZEN 2012 (Version 1.1.2.0, Carl Zeiss AG; Jena, Germany).

**TABLE 2 |** The citric acid extractable P for the respective sampled soil horizon (Oh, Ah, Bw, and Cw) of the two study sites Bad Brückenau (BBR) and Unterluess (LUE) (Lang et al., 2017).

| Site | Horizon | Soil depth cm | $pH_{H_2O}$ | $P_{citr}$ mg $kg^{-1}$ | C % | N % | CEC meq $kg^{-1}$ | BS % |
|---|---|---|---|---|---|---|---|---|
| BBR | Oa | +2 to 0 | 5.3 | 326 | 48.2 | 2.07 | 543 | 79 |
| BBR | Ah | 0 to −7 | 4.2 | 39 | 9.7 | 0.65 | 261 | 10 |
| BBR | Bw | −33 to −51 | 4.9 | 64 | 3.4 | 0.25 | 149 | 26 |
| BBR | Cw | −79 to −100 | 5.7 | 141 | 1.1 | 0.09 | 148 | 45 |
| LUE | Oa | +4 to 0 | 3.3 | 54 | 46.3 | 1.75 | 557 | 13 |
| LUE | AhE | 0 to −7 | 3.5 | 10 | 9.7 | 0.38 | 109 | 8 |
| LUE | Bsw | −65 to −79 | 4.6 | 3 | 0.4 | 0.03 | 38 | 7 |
| LUE | Cw | −88 to −100 | 4.6 | 3 | 0.2 | 0.02 | 23 | 9 |

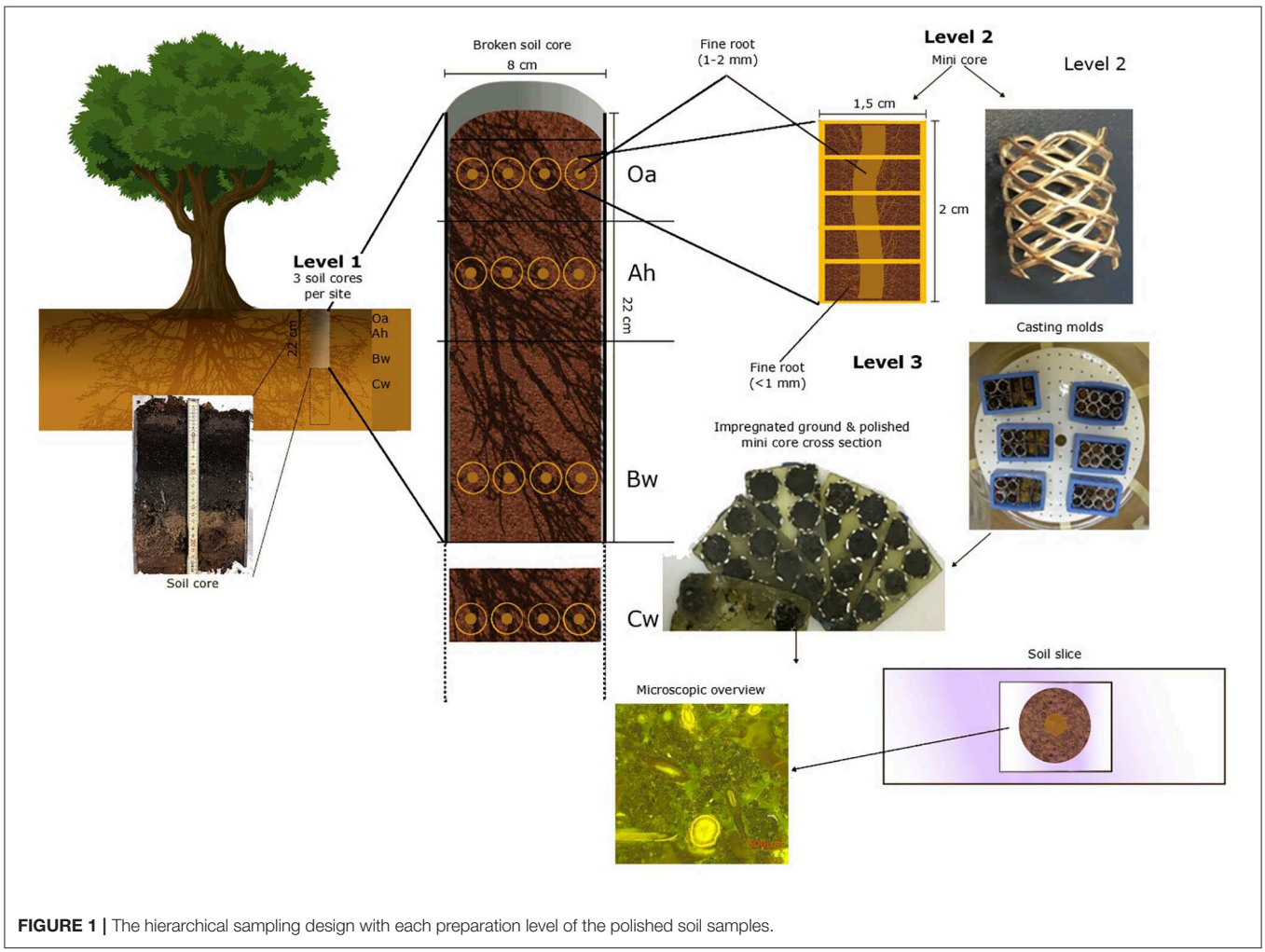


**FIGURE 1 |** The hierarchical sampling design with each preparation level of the polished soil samples.

By illumination with blue light, fresh plant material, hyphae, and bacteria fluoresced in a spectrum from yellow to yellow-green. However, a color difference between hyphae and other plant material was not visible. Therefore, roots and fungi were classified and determined by differences in morphology that could be easily distinguished such as diameter, form, or the appearance of hyphae mantle. The respective cell structures of roots and fungi could be clearly distinguished.

A total of 384 microscopic samples distributed evenly over both sites were evaluated. We included only intact roots in our data set. First, we differentiated between fine roots having a diameter of 1–2 mm, and those having a diameter <1 mm in

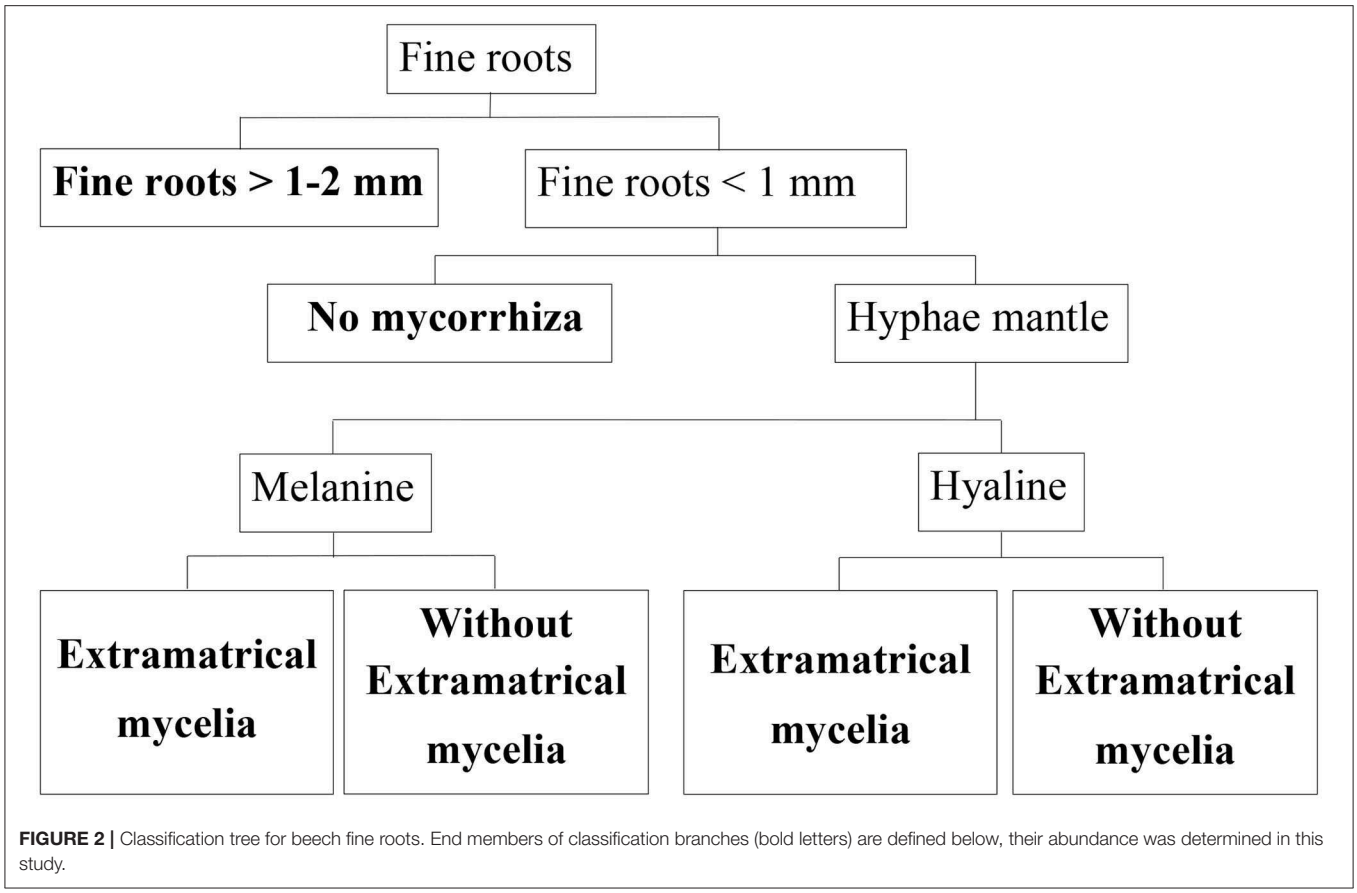


**FIGURE 2 |** Classification tree for beech fine roots. End members of classification branches (bold letters) are defined below, their abundance was determined in this study.

ZEN 2012 (**Figure 2**). We used a spherical graphic primitive interactively placed into the boundaries of the root cross section to measure the minimum ferret diameter representing the diameter even when roots are cut non-perpendicular to their axis. Second, for each root, the existence of mycorrhization was analyzed based on presence/absence of hyphae mantle. Since melanine hyphae are not stained by acridine orange, whereas hyaline hyphae are, we were able to differentiate between melanine and hyaline hyphae as described in Schack-Kirchner et al. (2000) (**Figure 2**).

### 2.1.2. Classification of Fine Roots

Roots were assigned to different morphological classes according to diameter, existence of a hyphae mantle, type of hyphae, and emanating hyphae as an indication of EM (**Figure 2**). For this classification, each root cross section on the specimen was assessed. With our microscopic method it is possible to differentiate low order absorptive roots with no secondary development and roots with mainly transport functions based on absence/presence of fully developed cortexes and xylem as suggested by McCormack et al. (2015). Nearly none of our cross sections showed fully developed cortex.

Microscopic images of different fine root classes are shown exemplary in **Figure 3**.

### 2.1.3. Calculations

For the first level (**Figure 1**) the fine root (1–2 mm) frequency per surface area was calculated as:

$$\frac{N_{1-2\ mm}}{A_{Ac}} \tag{1}$$

with $A_{Ac}$ as the area of the vertical root-auger core surface and $N_{1-2\ mm}$ as the number of visible fine roots tips (1–2 mm). For the second level (**Figure 1**) the fine root (<1 mm) of the mini core cross section were counted to calculate the frequency:

$$\frac{N_{<1\ mm}}{A_{Mc}} \tag{2}$$

With $A_{MC}$ as the area of mini core surface and $N_{<1\ mm}$ as the number of fine roots (<1 mm). Finally, the number of fine roots (<1 mm) was averaged across the vertical repetitions of up to five slices. By assuming that the detected cross sections of roots were part of an isotropic multitude of vectors in 3 D space, fine root length densities (RLD/cm $cm^{-3}$; $\frac{L_R}{V_S}$ in Weibel, 1980) were derived from the number of cross sections per area (Weibel, 1980; Schack-Kirchner et al., 2000; Van Noordwijk et al., 2000):

$$RLD = \frac{L_R}{V_S} = \alpha * \frac{N_R}{A_S} \tag{3}$$

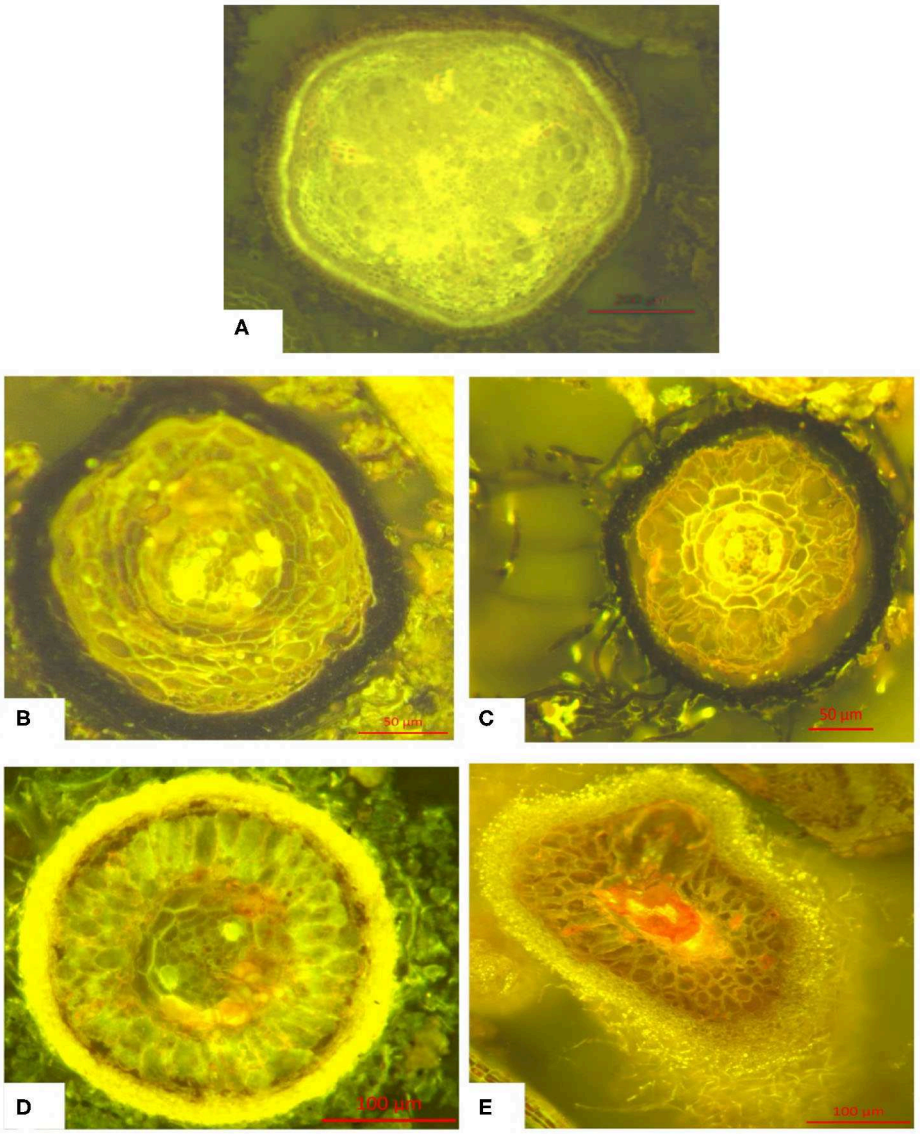


**FIGURE 3 |** Typical morphology of the classes of fine roots (<1 mm) defined above: **(A)** Fine root without hyphae mantle (without mycorrhization), **(B)** Fine root with melanine hyphae mantle, **(C)** Fine root with hyaline hyphae mantle, **(D)** Fine root with melanine hyphae mantle and melanine extramatrical mycelium, **(E)** Fine root with hyaline hyphae mantle and hyaline extramatrical mycelium. Further information can be found in **Figure S1**.

where $L_R$ is the root length [cm], $V_S$ is the soil volume [$cm^3$], $\alpha$ is the dimensionless factor of isotropy (we assumed complete isotropy with $\alpha = 2$; Weibel, 1980), $N_R$ is the number of the counted fine roots, and $A_S$ is the soil area. Based on the specific RLD ($L_R/V_S$), thickness of each horizon H and average diameter $\bar{d}$ for each fine root trait per horizon, we calculated the fine root surface area index (RAI/$m^2$ $m^{-3}$) per soil volume:

$$RAI = \pi * \bar{d} * RLD * H \quad (4)$$

The RAI was related to the stand area, separately for each genetic soil horizon, as a proxy for the absorbing fine root surface considering the thickness of each horizon. The calculations were carried out for the different fine root classes.

### 2.1.4. Statistics

From each mini core we assessed four to five cross sections. The root-observations have been averaged because these samples are not statistically independent. From each soil horizon we obtained 12 averaged mine core data sets of root counts originating from three soil cores. Because variability of root counts within soil cores was much lower than between soil horizons and average results of the respective soil cores individually reflected already the overall horizon pattern, we regarded the averaged mine core results as statistically independent, so we have

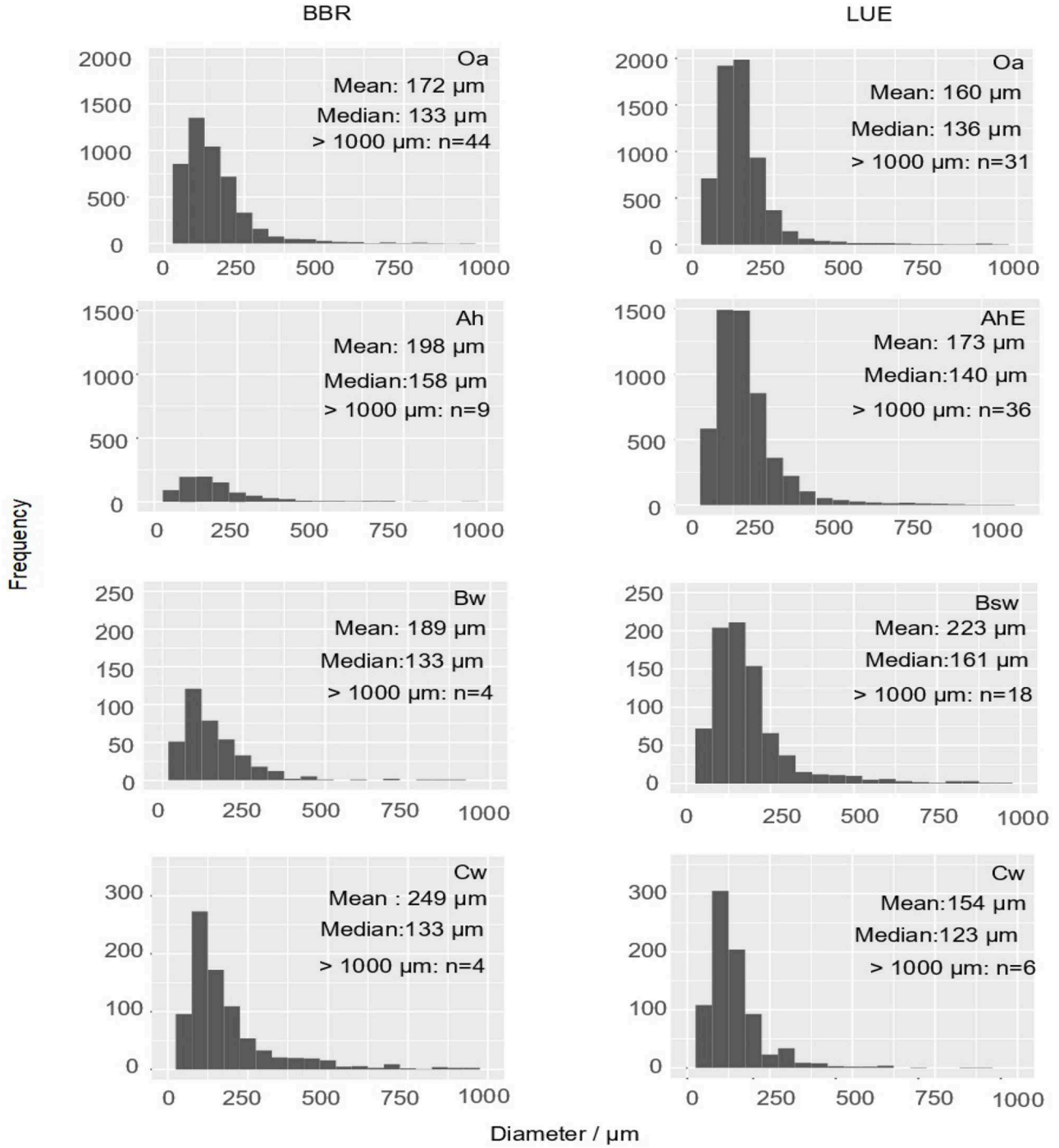


**FIGURE 4 |** Histograms display the absolute frequency of fine root cross sections (<1,000 $\mu$m) as diameter distributions of the mini cores (about 2 $cm^2$) of both sites and each horizon. The arithmetic mean and the median of diameters of the fine roots <1,000 $\mu$m as well as the number of roots >1,000 $\mu$m are inserted as numbers.

$N = 12$. To test the observed differences in medians for statistical significance we used the multiple non-parametric multiple Dunn's test with Bonferroni correction (Kruskal–Wallis-test, $p < 0.05$) (https://cran.r-project.org/web/packages/dunn.test/dunn.test.pdf).

## 3. RESULTS

In total, we measured and classified 6,969 fine roots (<1 mm) in BBR and 13,587 fine roots (<1 mm) in LUE. Diameters >500 $\mu$m were observed rarely, the frequency maximum was

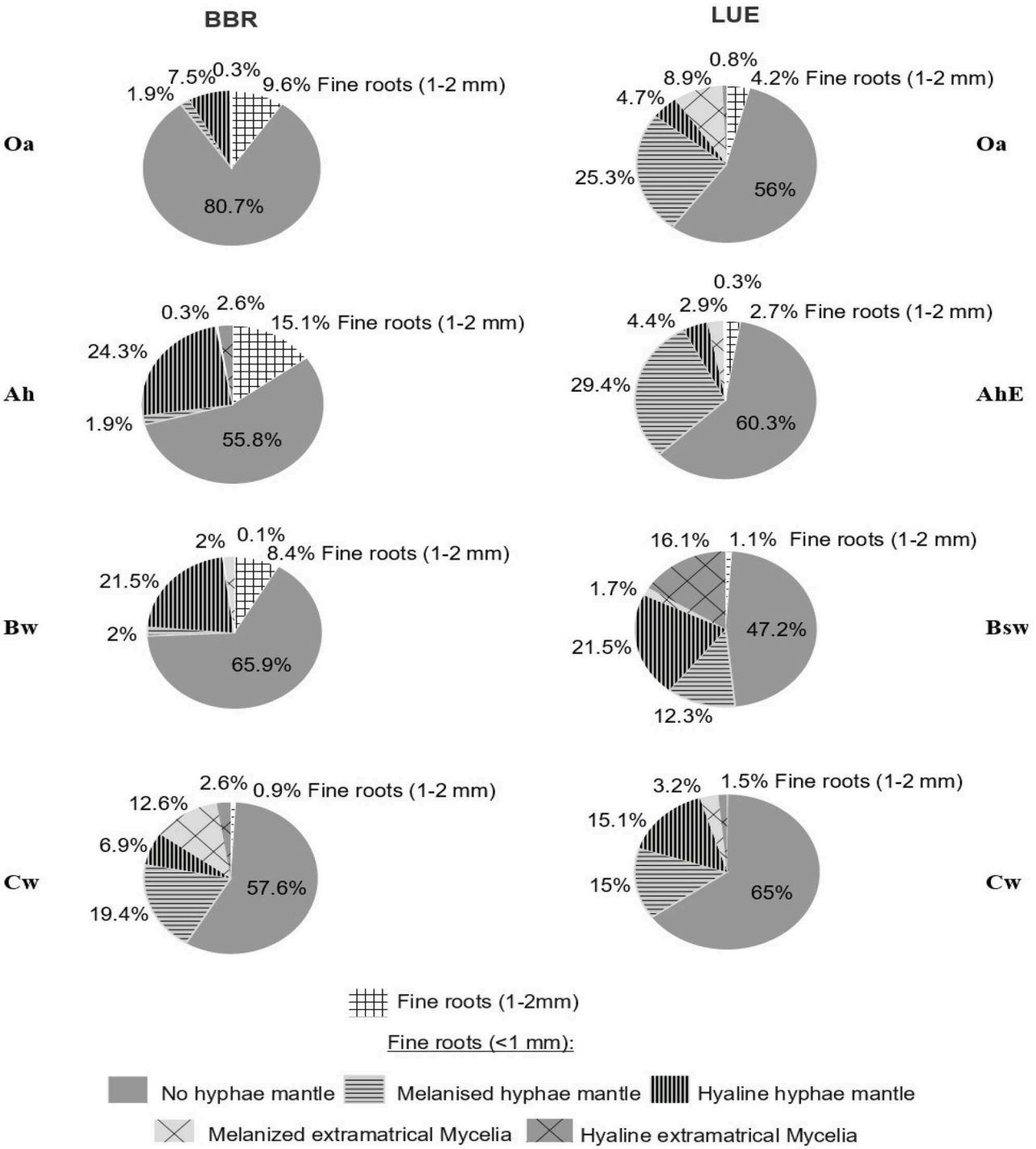


**FIGURE 5 |** Relative frequency of the different fine root classes per horizons and sites.

usually below 100 $\mu$m. (**Figure 4**). Roots (d > 1 mm) were found only sporadically. By far the highest number of fine roots were found in the topsoil of LUE.

In general, the degree of mycorrhization was lower at BBR than at LUE. The least share of mycorrhizal roots at BBR was observed in the Oa horizon (<9.7%) and at LUE in the Cw horizon (33.1%, **Figure 5**). In comparison, horizons with the highest portion of mycorrhizal roots were the Cw horizon in BBR (41.5%) and in the Bsw horizon in LUE(>51%).

**TABLE 3 |** The calculated root length density (RLD) and the ratio of root length density (RLD) <1 mm to root length density (RLD) (1–2 mm) are compared to the $RLD_{sieving-scanningmethod}$ of sieving-scanning method of Lang et al. (2017) at the same sites.

| Site | Horizon | $RLD_{1-2\ mm}$ cm cm$^{-3}$ | $RLD_{<1\ mm}$ cm cm$^{-3}$ | $\frac{R_{<1\ mm}}{R_{1-2\ mm}}$ | $RLD_{sieving\text{-}method}$ cm cm$^{-3}$ |
|---|---|---|---|---|---|
| BBR | Oa | 11.5 | 120 | 10 | 0.29 |
| BBR | Ah | 4.75 | 31 | 7 | 2.01 |
| BBR | Bw | 1.7 | 20 | 12 | 0.46 |
| BBR | Cw | 0.5 | 54 | 106 | 0.12 |
| LUE | Oa | 8.08 | 191 | 24 | 5.37 |
| LUE | AhE | 4.2 | 164 | 37 | 1.38 |
| LUE | Bsw | 0.46 | 41 | 89 | 0.27 |
| LUE | Cw | 0.05 | 33 | 60 | 0 |

*The mean root length density and standard deviation for all mini core samples per soil core horizon and site are listed in* ***Figure S4****. The mean root length density. Furthermore, the box plots of the RLD over all mini core mean values together with the result of the Dunn-test for each median are represented in* ***Figure S5****.*

The highest portion of fine roots (<1 mm) with extramatrical mycelium was found in the Cw horizon of BBR (13%) and in the Bsw horizon of LUE (16%). In addition, at BBR the portion of hyaline mycelia was higher than at LUE.

The highest relative portion of fine roots (<1 mm) with EM were found in the Cw horizon of BBR (12.6%) and in the Bsw horizon of LUE (16.1%), the lowest portion were in the Oa horizon of BBR (0.3%)and in the AhE and the Bsw horizon of LUE (3.2%). Melanine mycorrhization dominated in the topsoil of LUE and in the Cw horizon of BBR, hyaline mycorrhization dominated in the Ah horizon of BBR and in the Bsw horizon of LUE. In the Oa, AhE, and Cw horizons of LUE and in the Bw and Cw of BBR, the EM was dominated by melanine hyphae, whereas the other horizons of BBR and LUE were dominated by hyaline EM.

In BBR, the $RLD_{1-2\ mm}$ [cm cm$^{-3}$] consistently decreased with depth while the $RLD_{<1\ mm}$ [cm cm$^{-3}$] decreased from the Oa to the Bw horizon but rose again in the Cw horizon (**Table 3**). In LUE, both fine root length densities revealed a steady decrease with depth (**Table 3**). At both sites, the ratio of $RLD_{<1\ mm}$ to $RLD_{1-2\ mm}$ increased with depth except the Ah horizon in BBR. However, in LUE this ratio was consistently two to six times higher than in BBR.

From each soil horizon we obtained 12 averaged mine core data sets of root counts originating from 3 soil cores. All soil cores are similar (**Figure S4**) which is why all mini core samples can be considered as an independent sample (**Figure S4**). For these we calculated root length density (RLD) and the ratio of root length density (RLD) <1 mm to root length density (RLD) (1–2 mm) are represented. Furthermore, we compared the RLD of our method with the $RLD_{sieving-scanningmethod}$ of a routine sieving-scanning method of Lang et al. (2017) also performed at both sites (**Table 3**).

In the following it is analyzed whether the horizons within the profiles or whether the same horizons of the different profiles differ (**Figure 6**). It can be clearly seen that the variability is between the soil cores, which means that the heterogeneity within the horizons is not so significant.

Based on the RLD and mean diameter (**Figure 5**), we calculated a root surface area index (RAI) [m$^2$ m$^{-3}$], (**Figure 7**). If RAI is related to the genetic horizon depths up to 1 m soil depth, the weighted RAI is obtained (right bar). We regard this weighted cumulative RAI as a measure of as the potentially absorbing area per stand area. In LUE the total this RAI is almost twice as high and the mycorrhizal RAI almost three times as high as in BBR. The horizon-specific RAIs reveal the disproportionately high contribution of the only 11 cm thick organic topsoils (Oa and AhE) in LUE and the only 2 cm thick Oa horizon and 21 cm Cw horizon in BBR.

In **Figure 8**, we have related the RLD to the soil concentration of available P, which reaches 300 $mg\ kg^{-1}$ in the Oa of BBR and only 50 $mg\ kg^{-1}$ in the Oa in LUE. The general pattern at both sites was an increase in total RLD of fine roots <1 mm with P availability regardless of soil depth. However, the total mycorrhizal root length and its share in the total root length do not show a clear pattern. To test the influence of P on the RLD distribution, we tested correlations between the different RLDs and P, soil texture, pH, base cations, etc. for each site separately (**Figures S2**, **S3**). However, we could not find any influence on the root length density in our correlations, except the soil P content (**Figures S2**, **S3**).

# 4. DISCUSSION

## 4.1. The Method Applied

We observed that 82% of the absorbing root surface was bound to fine roots having a diameter smaller than 100 $\mu$m. These results were in contrast to results reported by Weemstra et al. (2017) that most of the fine roots of European beech were part of the diameter classes 200–750 $\mu$m. In agreement, also other studies indicated low abundance of root diameter classes smaller than 500 $\mu$m (e.g., Leuschner et al., 2001). A direct comparison of visual and microscopic scanning approaches provided in **Table 3** supports that visual methods in particular fail to quantify the roots smaller than 1 mm (**Table 3**). In agreement, also the roots surface seems to be strongly underestimated by conventional methods (Jackson et al., 1996; Kirfel et al., 2019) sieving-scanning or washing-scanning cause losses especially of small fine roots. Furthermore, picking out roots manually, also results in an underestimation of fine roots since only roots seen by eyes without the support of a microscope, are selected.

Functional traits of roots are in the center of current research (McCormack et al., 2015). An advantage of our method is the possibility to differentiate between absorptive roots and roots with mainly transport functions based on anatomic features (section 2.1.2, **Figure 3**). Thus, we could verify directly that all cross sections of fine roots corresponded to the morphology of absorptive roots according to McCormack et al. (2015). Furthermore, the distinction between intact roots and those with developed or initial symptoms of decay is easily performed on the cross sections. Using undisturbed soil samples and epifluorescence microscopy, we were able to quantify the

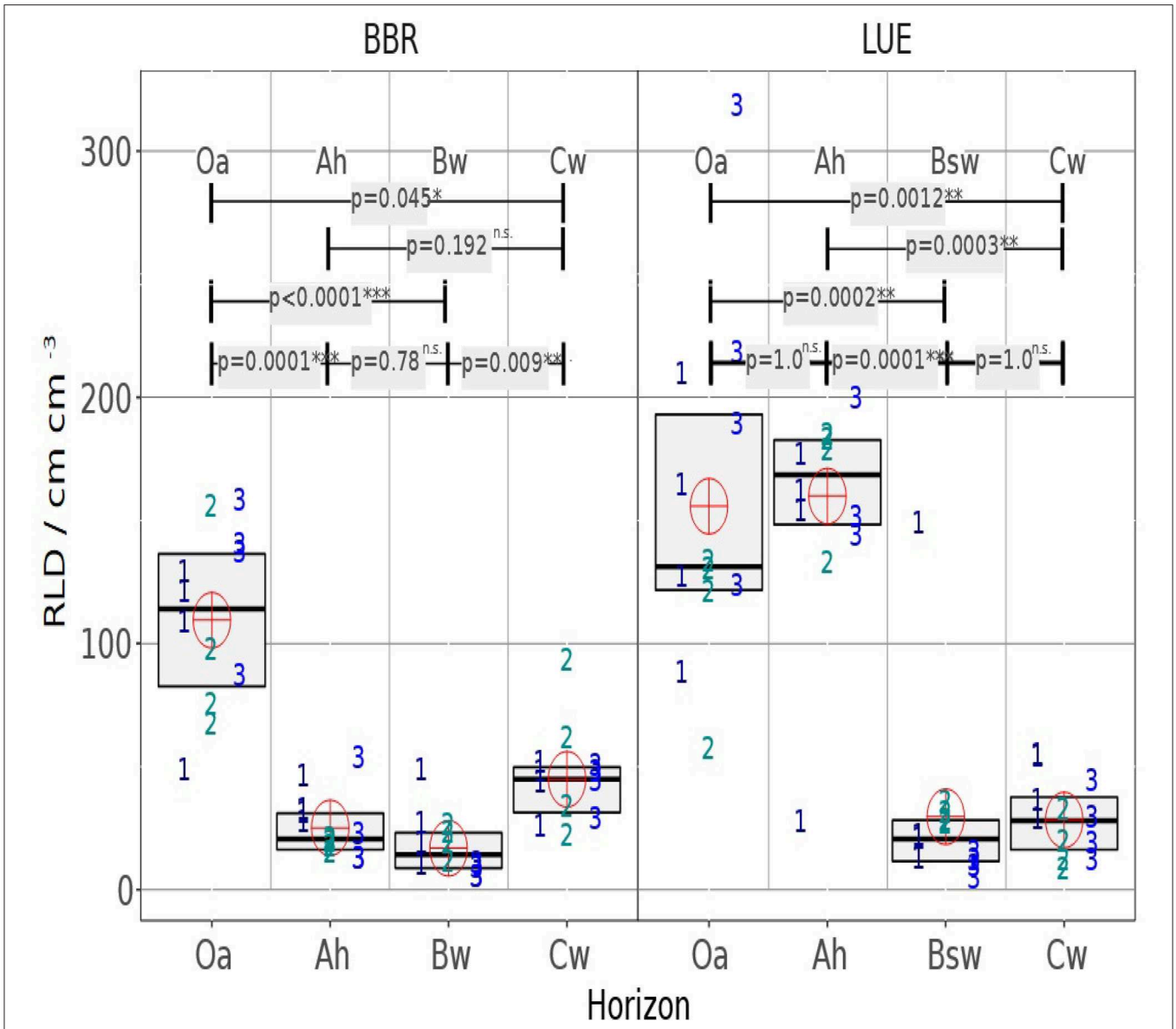


**FIGURE 6 |** The RLD boxplot chart shows the median and interquartile range (IQR) for four mini cores of three drill cores, each and for the studied horizons. Symbol numbers indicate the drill core number of the analyzed minicore the cross indicates the mean value of all 4 × 3 mini cores per horizon. The upper part of the graph shows the *p*-value of the Dunn test for the different medians.

absorbing root surface and associated fungi. The method reliably differentiates between hyphae forming a mantel or EM. Based on our results it was possible to calculate the total absorbing root area root-fungi associations, which is a crucial component of plant-uptake models (Schnepf and Roose, 2006).

## 4.2. Controls of Rooting Density and Abundance of Root Classes

Our results confirm that beech trees adapt their root traits according to P availability, as shown by the efficient way of mycorrhization. This leads to a generally higher absorbing area at the P-poor site compared to the P-rich site, which compensates for the low P fluxes from soil to root surface. Soil texture, pH-value, and other soil chemical parameters can have an influence on fine roots, so many studies address this aspect. In order to test these influences, a correlation of the fine root length density and the absorbing fine root surface per site with the soil chemical parameters (Ca, Fe, K, Mg, Mn, Na) as well as with the soil texture and pH-value was performed. We could only observe a positive correlation between root length density and soil P-content (**Figures S2**, **S3**). This indicates that P could have a significant influence on the root length density. However, we cannot claim that only P has an influence on the root length density. The significant negative correlation between the soil pH value and the fine root length density could be linked to an

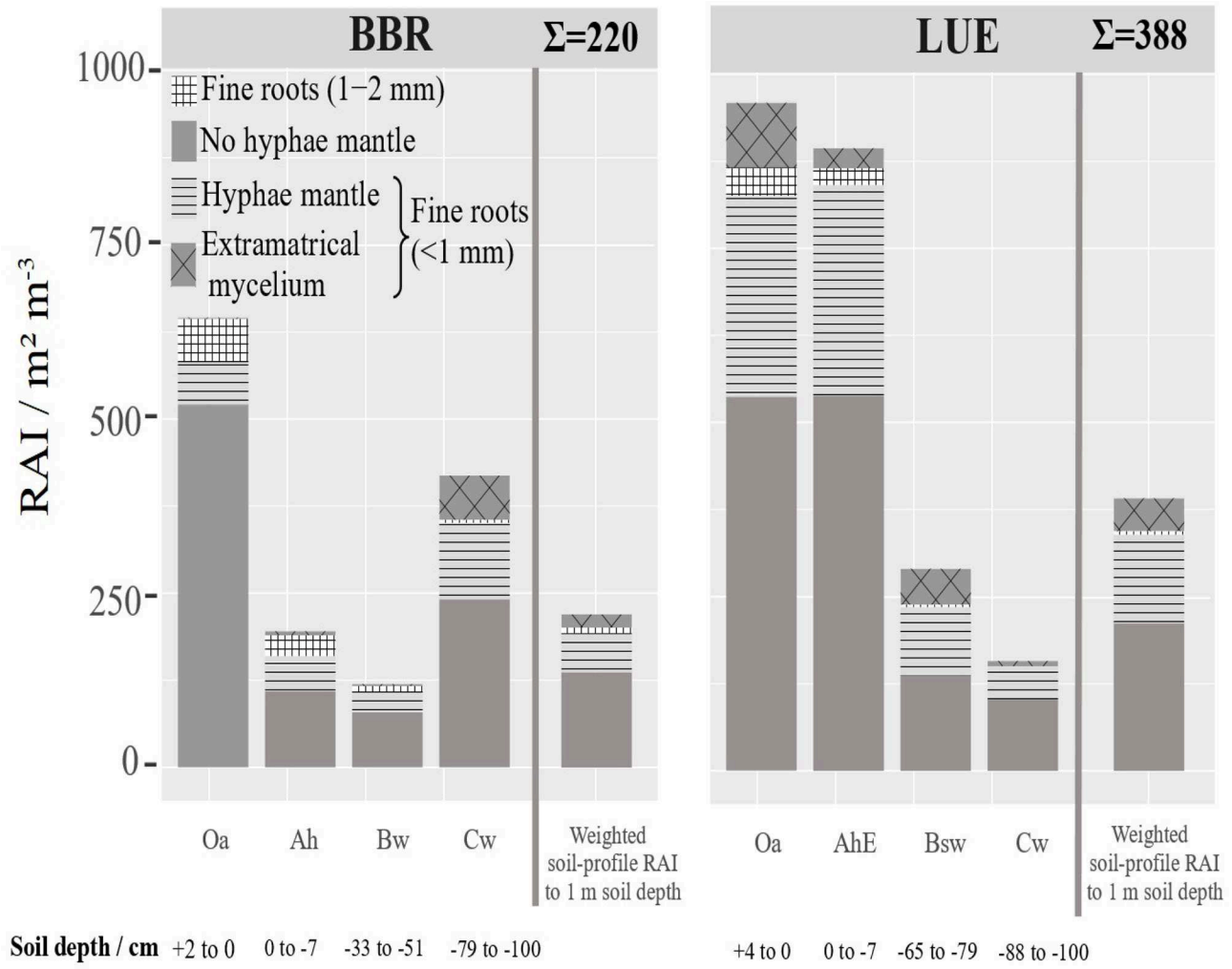


**FIGURE 7 |** Depth distribution of the root surface area index (RAI) (<2 mm) [$m^2$ $m^{-3}$] at BBR and LUE separately for the analyzed horizons. The fine root surface area down to 1 m soil depth related to ground area [$m^2$ $m^{-3}$] was estimated based on the thickness of horizons and is presented as cumulative bar. For LUE the Of horizon was added in fine root surface area index. For error bars see **Figure S4**. The mean root length density and standard deviation.

indirect correlation, an inter-correlation with the $PO_4$ content. Thus, it can be excluded that the pH value causes the site specific differences between these two sites. This is in line with Richter et al. (2007, 2013) who show that there is an influence of base saturation and pH values on the fine roots of beech, but that this influence is smaller than expected. Now both LUE and BBR can be assigned to the base saturation group >5%, since for example the AhE horizon of LUE has a base saturation of 7% and the Ah horizon of BBR of 20%.

In our study $RLD_{<1\ mm}$ was significantly higher at the P-poor site LUE than at the P-rich site BBR, whereas $RLD_{1-2\ mm}$ showed no significant difference. The maximum ratio between $RLD_{<1\ mm}$ and $RLD_{1-2\ mm}$ was two to six times higher at the P-poor site than at the P-rich site.

Thus, the soil profile scale shows that the surface area and mycorrhization of fine roots (<1 mm) increase with P availability. The significant correlation between the ratio of mycorrhizal RLD to citrate-extractable $PO_4$ at both sites (**Figures S2**, **S3**) indicated that root growth and mycorrhization is concentrated on horizons with high P availability. In contrast, comparing different sites, Fitter (1985) observed increasing specific root length with decreasing P availability. This is in agreement with our results regarding the comparison of the two different sites. At the P-poor site, LUE, the root length density is much higher than at the P-rich site BBR. Yet, the highest $RLD_{<1\ mm}$ was found at both sites in the two Oa horizons with the highest concentration of available P (**Table 1**, **Figure 8**). This statement is consistent with the observations of with Meier and Leuschner (2008), Meinen et al. (2009a,b) who showed that beech has a flat root system with the majority (approx. 75%) of fine roots in the Oa and in the topsoil (Meier and Leuschner, 2008; Meinen et al., 2009a,b) this is especially true for P-poor sites (Jonard et al., 2015). In agreement, in our study, the depth distribution of fine roots clearly differed at both sites: LUE had most of the fine roots in the forest floor and topsoil horizon, with 88% of the total fine roots occurring in the upper 11 cm of the soil (**Figure 4**), whereas

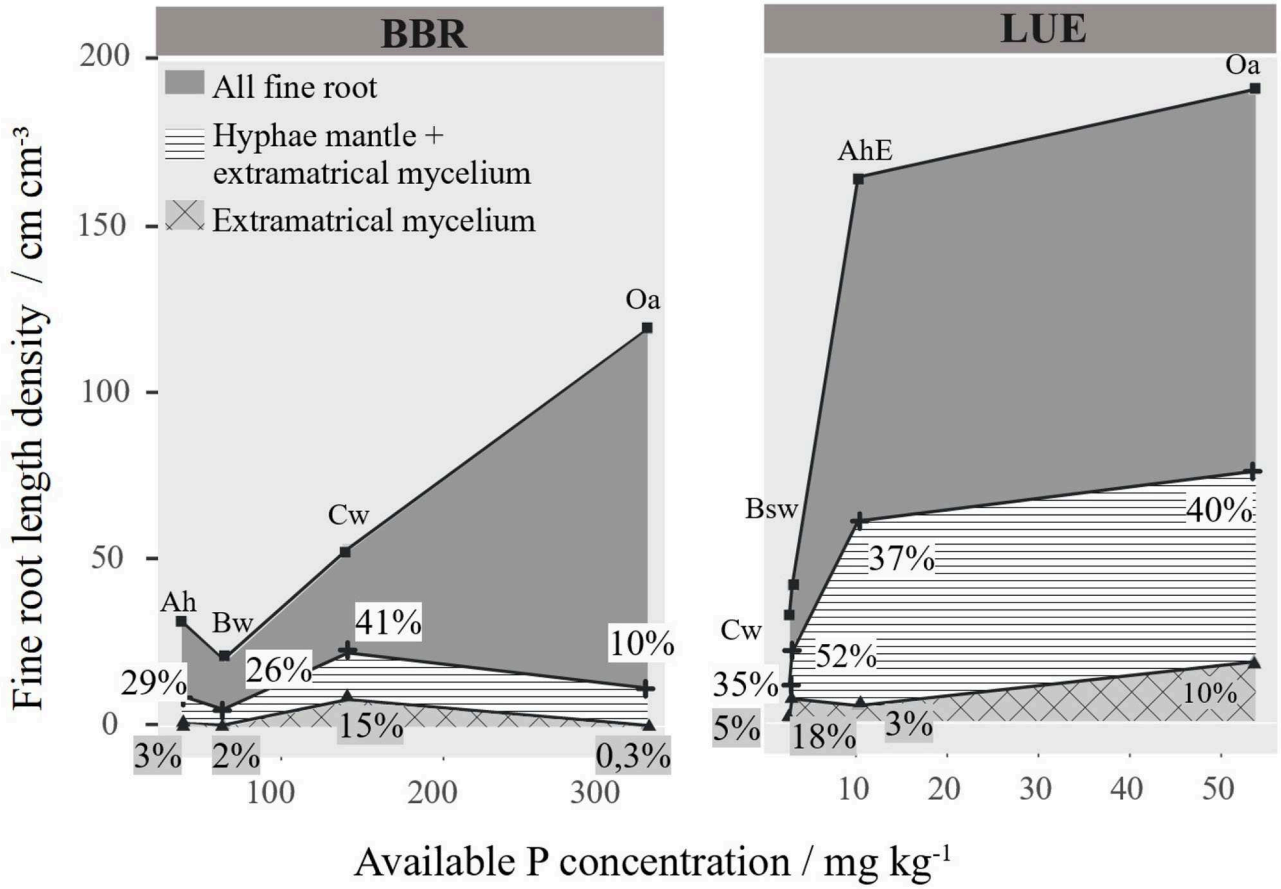


**FIGURE 8 |** Mycorrhizal and non-mycorrhizal fine root length density (RLD) [cm cm$^{-3}$] per horizon arranged to site specific available phosphorus. Percentage of the different mycorrhizal root lengths are given as numbers.

the root length density of the Cw horizon was much higher at BBR than at LUE (**Table 3**).

Further, the total mycorrhizal root length density is much higher in BBR the P-rich site than at the P-poor site LUE. According to Tatry et al. (2009) uptake rates in plant parts with ECM are two to three times higher than in root parts without mycorrhizal fungi, which supports the hypothesis that the greater proportion of mycorrhizal root length is found at the P-poor site. Also, Jones et al. (1990) showed that P inflow rates of ECM roots are about two times higher than those of non-mycorrhizal roots. Furthermore, mycorrhizal fungi can store P (Harley, 1989; MacFall and Slack, 1991) and thus possibly buffering phases of P starvation, which may also reflect an adaptation to low P availability. The low degree of mycorrhization in the Oa horizon of BBR and Cw of LUE seems to contradict the 100% mycorrhization for these sites reported by Zavišić et al. (2016). However, their results exclusively referred to the root tips, while our topological cross-sectional method examined the degree of mycorrhization over the entire root length and thus did not contradict his data. Mycorrhizal fungi can extend their RAI and their spatial coverage by forming EM. According to Nylund and Wallander (1992), this is promoted by low P contents. Therefore, the high frequency of mycorrhizal fungi and the high share of extramatrical mycelium, might help sustain sufficient P uptake at the site LUE in spite of low P availability.

The share of melanine and hyaline mycelia is different for different sites and horizons. Nosanchuk and Casadevall (2003) showed that melanin plays a protective role in unfavorable environments. One function of melanin could be the tolerance to water stress (Fernandez and Koide, 2013) and the protection against dehydration through storage of melanin in cell walls that in turn reduces water loss (Kogej et al., 2006). In contrast to hyaline cells, melanine cells have a high biosorptive capacity for numerous ions, which improves plant growth for plants in toxic environments (Fogarty and Tobin, 1996). Also, metal ions bound to melanin protect against toxicity and inhibition of extracellular hydrolytic enzymes (Fogarty and Tobin, 1996). This enables melanin to prevent enzymatic degradation (Nosanchuk and Casadevall, 2003) and makes hyphae more resistant to decay (Fernandez and Koide, 2013). Consequently, these properties increase the lifespan of melanine roots, thereby maintaining the P supply from litter or mineral soil as needed. The differences between both sites can be explained by the rough harsh soil chemical and physical soil properties at LUE with its higher acidity and sandy texture that could trigger water and mechanical stress. In BBR with its higher pH and water holding capacity, the

environment for hyphae is probably more favorable. The higher robustness of melanine hyphae could also explain the strong dominance of the melanine hyphae in the EM. Extramatrical mycelium is more vulnerable to extreme conditions than hyphae in the mantle around the root, which is where we observed more hyaline hyphae. Finally, we cannot provide any information on mycorrhizal species composition, since our fine root classes are based on simple morphological characteristics. Such data have been provided for the study sites by Zavišić et al. (2018). Their molecular genetic determination of mycorrhizal fungi identified 14 different fungal morphotypes with 25 taxa by ITS sequencing. He showed that both sites had different taxa, with the greater biodiversity being found at the P-rich site indicating that different morphotypes might be linked to different species composition.

### 4.3. Root-Mycorrhizal Fungi Associations and P Nutrition Strategies of Beech Forest Ecosystems

As hypothesized we found clear differences between the traits of root/mycorrhizal associations at both sites, which would not have been identified by routine methods for fine root quantification: We found higher RLD on the P-poor than on the P-rich site and a higher portion of mycorrhizal root surface. Within the soil profiles, the plants clearly concentrate non-mycorrhizal roots in the P-rich horizons. In general, the different root morphology would support the different P nutrition strategies assumed for P-poor and P-rich beech forests (Lang et al., 2017). At the P-rich site BBR where the forest ecosystem is assumed to acquire P from mineral resources we observed a high percentage of overall root surface in the Cw subsoil horizon besides the Oa horizon. This intense rooting in the subsoil seems to be mirrored by the concentration of soil organic matter at 1 m soil depth. The $C_{org}$ content at BBR is still 11 mg C $g^{-1}$ at this depth, while at the site LUE we only measured 1 mg C $g^{-1}$. This might indicate, that small fine roots neglected by conventional approaches represent a major source for deep-soil organic matter. In contrast, root length density was extremely high in the Oa and the AhE horizon in the P-poor ecosystem LUE, which is assumed to sustain its P supply by taking up P mobilized from organic matter. The prominent role of the Oa horizon for P uptake at the site LUE is further supported by its extension. Forest floor mass at LUE was five times higher than at site BBR.

## 5. CONCLUSION

The results of our quantitative micro morphological cross sections analyzes of undisturbed soil samples, are in agreement with the idea that we could show that beech forest nutrition strategies are reflected in the distribution of fine roots and the associated mycorrhization of European beech forests. The method gives new insights into the distribution and morphological traits of absorptive roots in forest stands including the size of the RAI and the degree and type of mycorrhization. Overall our study indicates, that the major part of fine roots had been overseen by conventional approaches for fine root quantification. Based on the detailed root information provided to confine idea of adaptation to forest ecosystem on P scarcity, which has to be validated by future studies: The depth distribution of the fine roots was controlled by P availability. Intense root growth in regions with high P availability, is compensated by reduced root growth in areas with low P availability. This mechanism would enhance the realization of either recycling or acquiring by European beech. As a consequence, the contrasting overall high rooting density at P-poor sites and the overall low rooting density at high-P sites is unlikely to be directly triggered by soil solution concentrations but seem to be rather the result of long-term adaptation to P scarcity.

## DATA AVAILABILITY STATEMENT

The raw data supporting the conclusions of this article will be made available by the authors, without undue reservation.

## AUTHOR CONTRIBUTIONS

CL carried out the experiment, analyses, and wrote the first draft of the manuscript. CL and HS-K performed the statistical analysis. All authors contributed to manuscript revision, read, and approved the submitted version.

## FUNDING

The project was funded by the German Research Foundation (DFG, GZ: LA 1398/12-2 AOBJ: 632054).

## ACKNOWLEDGMENTS

The authors gratefully acknowledge to be part of the priority program 1685 Ecosystem Nutrition: Forest Strategies for limited Phosphorus Resources.

## SUPPLEMENTARY MATERIAL

The Supplementary Material for this article can be found online at: https://www.frontiersin.org/articles/10.3389/ffgc.2020.00095/full#supplementary-material

## REFERENCES

Ad-hoc-AG Boden (2005). *Bodenkundliche Kartieranleitung: Ed.: Bundesanstalt für Geowissenschaften und Rohstoffe in Zusammenarbeit mit den Staatlichen Geologischen Diensten. E. Schweizerbart'sche Verlagsbuchhandlung (Nägele und Obermiller), 5th Edn*. Hanover.

Altemüller, H.-J. (1989). *Zur Fluoreszenzmikroskopischen Darstellung Biologischer Objekte in Boden-dünnschliffen*. Mitteilungen der Deutschen Bodenkundlichen Gesellschaft, 517–522.

Bengough, A. G., Mackenzie, C. J., and Diggle, A. J. (1992). Relations between root length densities and root intersections with horizontal and vertical planes using root growth modelling

in 3-dimensions. *Plant Soil* 145, 245–252. doi: 10.1007/BF00010353

Böhm, W. (1979). *Methods of Studying Root Systems, Vol. 33 of Ecological Studies*. Berlin: Springer. doi: 10.1007/978-3-642-67282-8

Bolan, N. S. (1991). A critical review on the role of mycorrhizal fungi in the uptake of phosphorus by plants. *Plant Soil* 134, 189–207. doi: 10.1007/BF00012037

Clemmensen, K. E., Bahr, A., Ovaskainen, O., Dahlberg, A., Ekblad, A., Wallander, H., et al. (2013). Roots and associated fungi drive long-term carbon sequestration in boreal forest. *Science* 339, 1615–1618. doi: 10.1126/science.1231923

Colpaert, J. V., Van Assche, J. A., and Luijtens, K. (1992). The growth of the extramatrical mycelium of ectomycorrhizal fungi and the growth response of *Pinus sylvestris* L. *New Phytol*. 120, 127–135. doi: 10.1111/j.1469-8137.1992.tb01065.x

Demand, D., Schack-Kirchner, H., and Lang, F. (2017). Assessment of diffusive phosphate supply in soils by microdialysis. *J. Plant Nutr. Soil Sci*. 180, 220–230. doi: 10.1002/jpln.201600412

Fernandez, C. W., and Koide, R. T. (2013). The function of melanin in the ectomycorrhizal fungus cenococcum geophilum under water stress. *Fungal Ecol*. 6, 479–486. doi: 10.1016/j.funeco.2013.08.004

Finér, L., Ohashi, M., Noguchi, K., and Hirano, Y. (2011). Fine root production and turnover in forest ecosystems in relation to stand and environmental characteristics. *For. Ecol. Manage*. 262, 2008–2023. doi: 10.1016/j.foreco.2011.08.042

Fitter, A. H. (1985). "Functional significance of root morphology and root system architecture," in *Ecologicai Interactions in Soil*, eds A. H. Fitter, D, Atkinson, D. J. Read, and M. B. Usher (Oxford, UK: Blackwell Scientific Publications), 87–106.

Fogarty, R. V., and Tobin, J. M. (1996). Fungal melanins and their interactions with metals. *Enzyme Microb. Technol*. 19, 311–317. doi: 10.1016/0141-0229(96)00002-6

Harley, J. L. (1989). The significance of mycorrhiza. *Mycol. Res*. 92, 129–139. doi: 10.1016/S0953-7562(89)80001-2

Hauenstein, S., Neidhardt, H., Lang, F., Krüger, J., Hofmann, D., Pütz, T., et al. (2018). Organic layers favor phosphorus storage and uptake by young beech trees (*Fagus sylvatica* l.) at nutrient poor ecosystems. *Plant Soil* 432, 289–301. doi: 10.1007/s11104-018-3804-5

Hinsinger, P., Brauman, A., Devau, N., Gérard, F., Jourdan, C., Laclau, J.-P., et al. (2011). Acquisition of phosphorus and other poorly mobile nutrients by roots. Where do plant nutrition models fail? *Plant Soil* 348:29. doi: 10.1007/s11104-011-0903-y

Jackson, R. B., Canadell, J., Ehleringer, J. R., Mooney, H. A., Sala, O. E., and Schulze, E. D. (1996). A global analysis of root distributions for terrestrial biomes. *Oecologia* 108, 389–411. doi: 10.1007/BF00333714

Johnson, D. W., and Turner, J. (2019). Nutrient cycling in forests: a historical look and newer developments. *For. Ecol. Manage*. 444, 344–373. doi: 10.1016/j.foreco.2019.04.052

Jonard, M., Fürst, A., Verstraeten, A., Thimonier, A., Timmermann, V., Potočič, N., et al. (2015). Tree mineral nutrition is deteriorating in Europe. *Glob. Change Biol*. 21, 418–430. doi: 10.1111/gcb.12657

Jones, M. D., Durall, D. M., and Tinker, P. B. (1990). Phosphorus relationships and production of extrametrical hyphae by two types of willow ectomycorrhizas at different soil phosphorus levels. *New Phytol*. 115, 259–267. doi: 10.1111/j.1469-8137.1990.tb00451.x

Kirfel, K., Heinze, S., Hertel, D., and Leuschner, C. (2019). Effects of bedrock type and soil chemistry on the fine roots of European beech-a study on the belowground plasticity of trees. *For. Ecol. Manage*. 444, 256–268. doi: 10.1016/j.foreco.2019.04.022

Kogej, T., Gorbushina, A. A., and Gunde-Cimerman, N. (2006). Hypersaline conditions induce changes in cell-wall melanization and colony structure in a halophilic and a xerophilic black yeast species of the genus trimmatostroma. *Mycol. Res*. 110, 713–724. doi: 10.1016/j.mycres.2006.01.014

Kreutzer, K. (1961). Wurzelbildung junger waldbäume auf pseudogleyböden. *Forstwiss. Centralbl*. 80, 356–392. doi: 10.1007/BF01821447

Lang, F., Krüger, J., Amelung, W., Willbold, S., Frossard, E., Bünemann, E. K., et al. (2017). Soil phosphorus supply controls p nutrition strategies of beech forest ecosystems in central Europe. *Biogeochemistry* 136, 5–29. doi: 10.1007/s10533-017-0375-0

Leuschner, C., Hertel, D., Coners, H., and Büttner, V. (2001). Root competition between beech and oak: a hypothesis. *Oecologia* 126, 276–284. doi: 10.1007/s004420000507

Lopez-Bucio, J., de La Vega, O M, Guevara-Garcia, A., and Herrera-Estrella, L. (2000). Enhanced phosphorus uptake in transgenic tobacco plants that overproduce citrate. *Nat. Biotechnol*. 18, 450–453. doi: 10.1038/74531

Lorenz, M. (1995). International co-operative programme on assessment and monitoring of air pollution effects on forests-icp forests-. *Water Air Soil Pollut*. 85, 1221–1226. doi: 10.1007/BF00477148

Lynch, J. (1995). Root architecture and plant productivity. *Plant Physiol*. 109, 7–13. doi: 10.1104/pp.109.1.7

MacFall, J. S., and Slack, S. A. (1991). Effects of hebeloma arenosa on growth and survival of container-grown red pine seedlings (*Pinus resinosa*). *Can. J. For. Res*. 21, 1459–1465. doi: 10.1139/x91-205

Manghabati, H., Kohlpaintner, M., Ettl, R., Mellert, K., Blum, U., and Göttlein, A. (2018). Correlating phosphorus extracted by simple soil extraction methods with foliar phosphorus concentrations of *Picea abies* (l.) h. karst. and *Fagus sylvatica* (l.). *J. Plant Nutr. Soil Sci*. 181, 547–556. doi: 10.1002/jpln.201700536

Marschner, H., and Dell, B. (1994). Nutrient uptake in mycorrhizal symbiosis. *Plant Soil* 159, 89–102. doi: 10.1007/BF00000098

McCormack, M. L., Dickie, I. A., Eissenstat, D. M., Fahey, T. J., Fernandez, C. W., Guo, D., et al. (2015). Redefining fine roots improves understanding of below-ground contributions to terrestrial biosphere processes. *New Phytol*. 207, 505–518. doi: 10.1111/nph.13363

Meier, I. C., and Leuschner, C. (2008). Belowground drought response of European beech: fine root biomass and carbon partitioning in 14 mature stands across a precipitation gradient. *Glob. Change Biol*. 14, 2081–2095. doi: 10.1111/j.1365-2486.2008.01634.x

Meinen, C., Hertel, D., and Leuschner, C. (2009a). Biomass and morphology of fine roots in temperate broad-leaved forests differing in tree species diversity: is there evidence of below-ground overyielding? *Oecologia* 161, 99–111. doi: 10.1007/s00442-009-1352-7

Meinen, C., Leuschner, C., Ryan, N. T., and Hertel, D. (2009b). No evidence of spatial root system segregation and elevated fine root biomass in multi-species temperate broad-leaved forests. *Trees* 23, 941–950. doi: 10.1007/s00468-009-0336-x

Nosanchuk, J. D., and Casadevall, A. (2003). The contribution of melanin to microbial pathogenesis. *Cell. Microbiol*. 5, 203–223. doi: 10.1046/j.1462-5814.2003.00268.x

Nylund, J.-E., and Wallander, H. (1992). "Chapter 5: Ergosterol analysis as a means of quantifying mycorrhizal biomass," in *Methods in Microbiology, Vol. 24*, eds J. Norris, D. Read, and A. Varma (Sweden: Academic Press), 77–88. doi: 10.1016/S0580-9517(08)70088-6

Pe nuelas, J., Poulter, B., Sardans, J., Ciais, P., van der Velde, M., Bopp, L., et al. (2013). Human-induced nitrogen-phosphorus imbalances alter natural and managed ecosystems across the globe. *Nat. Commun*. 4:2934. doi: 10.1038/ncomms3934

Plassard, C., and Dell, B. (2010). [duplikat] phosphorus nutrition of mycorrhizal trees. *Tree Physiol*. 30, 1129–1139. doi: 10.1093/treephys/tpq063

Raghothama, K. G., and Karthikeyan, A. S. (2005). Phosphate acquisition. *Plant Soil* 274:37. doi: 10.1007/s11104-004-2005-6

Read, D. (ed.). (1984). *The Ecology and Physiology of the Fungal Mycelium British Mycological Society Symposium: The Structure and Function of the Vegetative Mycelium of Mycorrhizal Roots, Vol. 8*. Cambridge: Cambridge University Press.

Richter, A. K., Hajdas, I., Frossard, E., and Brunner, I. (2013). Soil acidity affects fine root turnover of European beech. *Plant Biosyst*. 147, 50-59. doi: 10.1080/11263504.2012.742471

Richter, A. K., Walthert, L., Frossard, E., and Brunner, I. (2007). Does low soil base saturation affect fine root properties of European beech (*Fagus sylvatica* l.)? *Plant Soil* 298, 69–79. doi: 10.1007/s11104-007-9338-x

Rousseau, J. V., Sylvia, D. M., and Fox, A. J. (1994). Contribution of ectomycorrhiza to the potential nutrient-absorbing surface of pine. *New Phytol*. 128, 639–644. doi: 10.1111/j.1469-8137.1994.tb04028.x

Ruess, R. W., Hendrick, R. L., Burton, A. J., Pregitzer, K. S., Sveinbjornssön, B., Allen, M. F., et al. (2003). Coupling fine root dynamics with ecosystem carbon cycling in black spruce forests of interior alaska. *Ecol. Monogr*. 73, 643–662. doi: 10.1890/02-4032

Schachtman, D. P., Reid, R. J., and Ayling, S. M. (1998). Phosphorus uptake by plants: from soil to cell. *Plant Physiol*. 116, 447–453. doi: 10.1104/pp.116.2.447

Schack-Kirchner, H., Wilpert, K. V., and Hildebrand, E. E. (2000). The spatial distribution of soil hyphae in structured spruce-forest soils. *Plant Soil* 224, 195–205. doi: 10.1023/A:1004806122105

Schnepf, A., and Roose, T. (2006). Modelling the contribution of arbuscular mycorrhizal fungi to plant phosphate uptake. *New Phytol*. 171, 669–682. doi: 10.1111/j.1469-8137.2006.01771.x

Serva Electrophoresis GmbH (2007). *Embedding in Electron Microscopy*.

Smith, S. E., and Read, D. J. (2009). *Mycorrhizal Symbiosis, 3rd Edn*. Amsterdam: Elsevier; Academic Press.

Talkner, U., Meiwes, K. J., Potočič, N., Seletković, I., Cools, N., de Vos, B., et al. (2015). Phosphorus nutrition of beech (*Fagus sylvatica* l.) is decreasing in Europe. *Ann. For. Sci*. 72, 919–928. doi: 10.1007/s13595-015-0459-8

Tatry, M.-V., Kassis, E. E., Lambilliotte, R., Corratgé, C., van Aarle, I., Amenc, L. K., et al. (2009). Two differentially regulated phosphate transporters from the symbiotic fungus *Hebeloma cylindrosporum* and phosphorus acquisition by ectomycorrhizal *Pinus pinaster*. *Plant J*. 57, 1092–1102. doi: 10.1111/j.1365-313X.2008.03749.x

Tibbett, M., and Sanders, F. E. (2002). Ectomycorrhizal symbiosis can enhance plant nutrition through improved access to discrete organic nutrient patches of high resource quality. *Ann. Bot*. 89, 783–789. doi: 10.1093/aob/mcf129

Tippkötter, R., and Ritz, K. (1996). Evaluation of polyester, epoxy and acrylic resins for suitability in preparation of soil thin sections for *in situ* biological studies. *Geoderma* 69, 31–57. doi: 10.1016/0016-7061(95)00041-0

Tippkötter, R., Ritz, K., and Darbyshire, J. F. (1986). The preparation of soil thin sections for biological studies. *J. Soil Sci*. 37, 681–690. doi: 10.1111/j.1365-2389.1986.tb00396.x

Van Noordwijk, M., Brouwer, G., Meijboom, F., do Rosário G. Oliveira, M., and Bengough, A. G. (2000). "Trench profile techniques and core break methods," in *Root Methods*, eds A. L. Smit, A. G. Bengough, C. Engels, M. Noordwijk, S. Pellerin, and S. C. Geijn (Berlin; Heidelberg: Springer Berlin Heidelberg), 211–233. doi: 10.1007/978-3-662-04188-8_7

Weemstra, M., Sterck, F. J., Visser, E. J. W., Kuyper, T. W., Goudzwaard, L., and Mommer, L. (2017). Fine-root trait plasticity of beech (*Fagus sylvatica*) and spruce (*Picea abies*) forests on two contrasting soils. *Plant Soil* 415, 175–188. doi: 10.1007/s11104-016-3148-y

Weibel, E. R. (1980). *Theoretical Foundations, Vol. 2 of Stereological Methods*. London: Academic Press.

Williamson, B., and Alexander, I. J. (1975). Acid phosphatase localised in the sheath of beech mycorrhiza. *Soil Biol. Biochem*. 7, 195–198. doi: 10.1016/0038-0717(75)90037-1

WRB (ed.). (2015). *World Reference Base for Soil Resources 2014, Update 2015: International Soil Classification System for Naming Soils and Creating Legends for Soil Maps*. World Soil Resources Reports. FAO, Rome.

Zavišić, A., Nassal, P., Yang, N., Heuck, C., Spohn, M., Marhan, S., et al. (2016). Phosphorus availabilities in beech (*Fagus sylvatica* l.) forests impose habitat filtering on ectomycorrhizal communities and impact tree nutrition. *Soil Biol. Biochem*. 98, 127–137. doi: 10.1016/j.soilbio.2016.04.006

Zavišić, A., Yang, N., Marhan, S., Kandeler, E., and Polle, A. (2018). Forest soil phosphorus resources and fertilization affect ectomycorrhizal community composition, beech p uptake efficiency, and photosynthesis. *Front. Plant Sci*. 9:463. doi: 10.3389/fpls.2018.00463

**Conflict of Interest:** The authors declare that the research was conducted in the absence of any commercial or financial relationships that could be construed as a potential conflict of interest.

frontiers in Forests and Global Change

ORIGINAL RESEARCH
published: 15 September 2020
doi: 10.3389/ffgc.2020.542738

# Impacts of Fertilization on Biologically Cycled P in Xylem Sap of *Fagus sylvatica* L. Revealed by Means of the Oxygen Isotope Ratio in Phosphate

*Simon Hauenstein, Micha Nebel and Yvonne Oelmann**

*Geoecology, Department of Geosciences, University of Tübingen, Tübingen, Germany*

OPEN ACCESS

**Edited by:**
*Jaane Krüger, University of Education Freiburg, Germany*

**Reviewed by:**
*Nicole Wellbrock, Thuenen Instutitute of Forest Ecology, Germany*
*Katelyn Elise Gray, University of Delaware, United States*

***Correspondence:**
*Yvonne Oelmann*
*yvonne.oelmann@uni-tuebingen.de*

**Specialty section:**
*This article was submitted to Forest Soils, a section of the journal Frontiers in Forests and Global Change*

**Received:** *13 March 2020*
**Accepted:** *24 August 2020*
**Published:** *15 September 2020*

**Citation:**
*Hauenstein S, Nebel M and Oelmann Y (2020) Impacts of Fertilization on Biologically Cycled P in Xylem Sap of Fagus sylvatica L. Revealed by Means of the Oxygen Isotope Ratio in Phosphate. Front. For. Glob. Change 3:542738. doi: 10.3389/ffgc.2020.542738*

Studies on the effect of high atmospheric N deposition report inconsistent results on forest productivity and N cycling which might be related to P availability in soil and subsequently affect tree P nutrition. We wanted to test the effects of (i) site i.e., a P-poor versus a P-rich site and of (ii) fertilization (N, P, N+P) on inorganic P (Pi) and organic P (Po) concentrations as well as on biologically cycled phosphate (inferred from the O isotope signature after adding an $^{18}O$-enriched label) in xylem sap. We measured Pi and Po concentrations and the O isotope signature in phosphate ($\delta^{18}O_{Pi}$) in xylem sap of beech (*Fagus sylvatica* L.) trees two and 14 days after addition of $^{18}O$-enriched water to the organic layer in a full factorial fertilization experiment (control, +N, +P, +NP) at two sites differing in P availability. Higher P concentrations in xylem sap at the P-rich than at the P-poor site originated from accelerated biological P cycling indicated by incorporation of $^{18}O$ from the isotope label into phosphate in xylem sap shortly after labeling. At this site, $\delta^{18}O_W$ values of xylem sap after label application remained close to background $\delta^{18}O_W$ values of soil solution. We speculate that in contrast to P uptake, trees took up water from deeper (non-$^{18}O$-labeled) soil layers. At the P-poor site, the $^{18}O$ label was recovered both in xylem sap water and phosphate in xylem sap, the latter only after 14 days. These results imply that trees relied on the organic layer for P acquisition and water uptake. However, biological processes associated with an incorporation of $^{18}O$ from the label were slower at the P-poor than at the P-rich site. P addition (P, NP) increased Pi concentrations in xylem sap at the P-rich site. Based on $\delta^{18}O_{Pi}$ values in xylem sap, the additional P originated both from the fertilizer and from accelerated biological P cycling in soil. We conclude that P-poor sites likely suffer more from climate change in case of an increased frequency of droughts because as opposed to P-rich sites both water and nutrient uptake will be affected.

**Keywords: $^{18}O$ labeling, organic P mobilization, phosphorus nutrition, forest floor, soil, beech, phosphorus uptake**

## INTRODUCTION

Phosphorus (P) is an essential agent in a variety of vital processes like the build-up of DNA, RNA, and cell membranes, energy transfer via free nucleotides and carbon metabolism. Therefore, P is of paramount importance for plant growth and ecosystem performance (Marschner, 2002; Scheerer et al., 2018). Based on the decrease of foliar P concentrations during the last decades, P is suspected to limit the growth of trees (*Fagus sylvatica* L.; *Pinus sylvestris* L.) in forests and thus, forest productivity (Prietzel and Stetter, 2010; Jonard et al., 2015).

The drivers for P limitation in European forest ecosystems are mainly associated with anthropogenic activities. In particular, continuously high deposition of atmospheric N and increased $CO_2$ concentrations due to climate change accelerate forest growth, consequently resulting in enhanced P demands by trees (Jonard et al., 2015; Talkner et al., 2015). However, the effect of increased N supply on forest growth reported so far are not consistent. Magill et al. (2004) found that forest growth was increased by N fertilization whereas N fertilization had no effect in several other studies (Nadelhoffer et al., 2004; Finzi, 2009; Lovett et al., 2013). Given an unbalanced N and P deposition together with the crucial role of phosphorus (P) in plant development, ecosystems are gradually moving from N to P limitation (Peñuelas and Sardans, 2012; Peñuelas et al., 2013). Gaudio et al. (2015) describe N limitation in forests to become crucial under climate scenarios where the turnover rate of organic matter is slow and N deposition continues to decrease. Consequently, other nutrients such as P could also become limiting in the future or are already limiting in nutrient−poor ecosystems (Jonard et al., 2012). For soils, Mo et al. (2015) found that N addition resulted in an overall decline in nutrient availability (except N), which seemed to result from a decline in litter decomposition and increased soil acidification. Waldrop and Firestone (2004) reported that excess N reduced the production of enzymes involved in decomposition, particularly in lignin degradation. Thus, soil respiration and decomposition were reduced, while soil-organic matter accumulation in fertilized soils was increased (Pregitzer et al., 2007; Nave et al., 2009; Janssens et al., 2010). Therefore, positive growth responses of trees to N fertilization might be constrained by negative fertilization effects on decomposition rates. In addition, missing effects of N fertilization might be due to the fact that elements other than N limit forest growth.

Jonard et al. (2015) as well as Talkner et al. (2015) consider P as the upcoming limiting factor in nutrient poor forest ecosystems which yet has to be approved by P fertilization trials (Polglase et al., 1992; Clarholm, 1993). The effect of P fertilization likely depends on the type of nutrient acquisition in ecosystems. In "acquiring ecosystems," e.g., on young, nutrient-rich or just P-rich soils, P is mobilized from P-containing minerals in the soil and subsequently taken up by trees (Odum, 2014; Lang et al., 2016). In forests on old, highly weathered and/or P-poor soils, trees mainly rely on the mobilization from organically bound P in soil organic matter ("recycling ecosystems;" Hauenstein et al., 2018). Augusto et al. (2017) consider the parent material as the principal component controlling P availability in soils, beside the progression of pedogenesis, or climatic controls. This view is supported by Porder and Ramachandran (2012), who showed that parent material serves as a control of bioavailable P in soil. Findings of forest ecosystem adaptions toward a "recycling" system along decreasing nutrient supply from different parent materials are described by several authors (Lang et al., 2016, 2017; Hansson et al., 2020; Legout et al., 2020). In case of such P-poor soils, P fertilization increased forest growth/productivity (Blevins et al., 2006; Trichet et al., 2009; Turner and Lambert, 2015). This effect was likely driven by soil processes exemplary described by Mo et al. (2015) who found that the addition of P to soils containing very little available P resulted in a significant "priming" effect, which stimulated microbial activity and nutrient turnover of litter, whereas no effect of P addition was observed in soils containing sufficiently available P. This is in line with Bergkemper et al. (2016) who described a shift in bacterial communities which led to increased organic P acquisition on P-poor soils, whereas in P-rich soils inorganic P acquisition dominated. By contrast, several authors reported the downregulation of enzyme activity slowing down P mobilization from organic P after the addition of water soluble mineral P to soil irrespective of initial P availability in soil (DeForest et al., 2012; Marklein and Houlton, 2012; Shaw and DeForest, 2013). Whether these P fertilization effects on P availability in soil translate into tree P uptake via xylem sap has hardly been studied (Prietzel and Stetter, 2010). We expect that N and P fertilization effects on forest growth and nutrient availability in soil are reflected in P uptake by trees i.e., P concentrations in xylem sap. In xylem sap, the addition of water-soluble mineral P to soil likely increases Pi concentrations by direct uptake of fertilizer P and by increased uptake from biologically cycled P originating from a stimulation of biological activity in soil.

To distinguish biological P mobilization processes from other processes, recent studies used the ratio of stable oxygen (O) isotopes in phosphate ($\delta^{18}O_{Pi}$) (Pistocchi et al., 2018; Hacker et al., 2019). This is possible because only biological processes involve an exchange between O atoms in phosphate and O atoms in ambient water (Blake et al., 2005), while no such exchange takes place during the dissolution of P-containing minerals and the desorption of $H_2PO_4^-/HPO_4^{2-}$ from charged surfaces (Liang and Blake, 2007). Particularly if the O isotope signature of ambient water is modified via isotope labeling by $^{18}$O-enriched- or $^{18}$O-depleted water, mobilization processes or distinct P sources can be identified (Hacker et al., 2019). Accordingly, an incorporation of O atoms from $^{18}$O-enriched ambient water into phosphate by biological activity in soil should be visible in $\delta^{18}O_{Pi}$ values of xylem sap once phosphate has been taken up by trees. Given the assumption that an acquiring ecosystem relies much less on nutrient release from organic matter via biological activity than a recycling ecosystem does, different contributions of biologically cycled phosphate i.e., different extents of $^{18}$O-enrichment, in xylem sap can be expected. Similarly, a stimulation of biological activity in the soil by P fertilization should be reflected in a greater contribution of biologically cycled phosphate particularly so in the recycling ecosystem.

Our objectives were to test the effects of (i) site i.e., an acquiring versus a recycling ecosystem, and of (ii) fertilization (N, P, N+P) on Pi and Po concentrations as well as on biologically cycled phosphate (inferred from the O isotope signature after adding an $^{18}O$ label) in xylem sap.

# MATERIALS AND METHODS

## Study Sites

In the frame of the priority program SPP 1685 "Ecosystem Nutrition, Forest Strategies for limited Phosphorus Resources" (Lang et al., 2016), two temperate beech forest sites were selected for the purpose of this study. The site "Bad Brückenau" (BBR) is located in Bavaria, southeastern Germany in a midrange mountain area of the Rhön (50°35′N, 9°92′E). The potential natural vegetation at the site BBR is Hordelymo-Fagetum (Lang et al., 2017). The forest stand comprises 99% *Fagus sylvatica* L. and 1% *Acer pseudoplatanus* L. Mean stand age of beech is 137 years with an average height of 26.8 m, a mean (breast height) diameter of 36.8 cm and a tree density of 335 individuals per hectare. At this site, mull-like Moder forest floors on dystric skeletic Cambisols developed on alkaline igneous rocks/metamorphites (Haußmann and Lux, 1997). The order of organic soil horizons (IUSS WG WRB, 2015) was as follows, for LUE: Oi (3 cm) – Oe (4 cm) – Oa (1 cm) and for BBR: Oi (3 cm) – Oe (3 cm). Mean annual air temperature and the mean sum of annual precipitation are 5.8°C and 1031 mm, respectively (Level II ICP-forest monitoring; Lorenz, 1995). At the site BBR yearly atmospheric N deposition was 13.8 kg N $ha^{-1}$ (measured between 2009 and 2012; personal communication Dietrich, H.-P., LWF-Bayern, Germany). For more detailed site characteristics see Lang et al. (2017). During the experimental course, soil temperature at a depth of 0.05 m was, on average, of 13.0 ± standard deviation (SD) 0.4°C. During this period of time, 26.6 mm throughfall were reported (personal communication Dr. Meesenburg, NW-FVA, Germany). The site "Lüss" (LUE) is located in Lower Saxony, northwestern Germany in the Lüneburg Heath (52°83′N, 10°36′E). The potential natural vegetation at the site LUE is Luzulo-Fagetum (Lang et al., 2017). The forest stand comprises 91% *F. sylvatica* and 9% *Quercus petrea* (MATTUSCHKA) LIEBL. Mean stand age of beech is 132 years with an average height of 27.3 m, a mean (breast height) diameter of 27.5 cm and a tree density of 480 individuals per hectare. Organic layers and soil types are classified as a mor-like Moder forest floor on hyperdystric folic Cambisols developed from Pleistocene sands. The mean annual air temperature is 8°C and the annual sum of precipitation amounts to 779 mm (Level II ICP-forest monitoring; Lorenz, 1995). During the experimental course, the mean soil temperature mean at a depth of 0.06 m was 9.3 ± SD 0.1°C and 23.8 mm throughfall were observed (personal communication Mr. Dietrich, LWF-Bayern, Germany). At the site LUE, yearly atmospheric N deposition was 10 kg N $ha^{-1}$ (measured between 2009 and 2012; personal communication Dietrich, H.-P., LWF-Bayern, Germany). Sites were selected according to their bioavailability of P, thus showing the ecosystem adaptions to different parent materials. We assume the influence of the climate conditions to be important but not fundamental for the development and adaptions of the forest ecosystems on these sites.

## Fertilization Experiment

At both sites, a full-factorial fertilization experiment was established in April-May 2016. The experiment comprised a control and three fertilization treatments: N addition (150 kg N $ha^{-1}$ $year^{-1}$ as $NH_4NO_3$), P addition (50 kg N $ha^{-1}$ $year^{-1}$ as $KH_2PO_4$), N+P addition (combination of N and P addition). Control and treatment plots (20 m × 20 m) were established in triplicates which were randomly distributed in the stands while keeping a minimum distance of 20 m between plots (**Figure 1**). Each plot contained at least two individuals of adult beech trees (*F. sylvatica* L.) with a diameter at breast height of 46.8 ± SD 3.65 cm at the site BBR and 48.8 ± SD 5.81 cm at the site LUE and an approximate age of 120 years.

The control and the N addition treatments received KCl to account for the addition of K in P-containing treatments. The addition of N was split into five parts (30 kg N $ha^{-1}$ each) in spring, summer, and autumn to account for the seasonal demand of trees and to reduce leaching losses. The addition of P took place once a year along with the N addition in spring. The fertilizer addition was carried out in dissolved form by means of garden sprayers. The experiment was conducted in July/August 2017. We acknowledge that by restricting the fertilization to N and P, we did exclude the potential limitation of forest growth by elements other than N and P which was speculated by Jonard et al. (2012). We tried to simulate a conservative estimate of maximum N input for the next decade of atmospheric N deposition. Nevertheless, similar to many other forest fertilization experiments, our fertilization approach did not take into account direct interactions between the fertilizer and the canopy which would have occurred had we manipulated atmospheric deposition directly.

## Labeling by $^{18}O$-Enriched Water

The isotope labeling took place June 19–21, 2017 at the site BBR and June 12–14, 2017 at the site LUE. We used an area of 10.8 $m^2$ around each tree individual for the application of $^{18}O$-enriched water. This area was formed by two circles with an identical center in the middle of each tree with radii of 0.4 and 1.9 m. We prepared $^{18}O$-enriched water by diluting tap water with $^{18}O$-enriched water (>98 atom% $^{18}O$, Hyox $^{18}O$, rotem, Arava, Israel) aiming at $\delta^{18}O$ values of soil solution of around +40‰. Assuming thermodynamic equilibrium fractionation (Chang and Blake, 2015), $\delta^{18}O_{Pi}$ values of +61.7‰ would result (see calculations for realized $\delta^{18}O_W$ values of soil solution in **Supplementary Figure S1**). We applied the $^{18}O$-enriched water using a syringe (100 ml, Vektenxi, amazon.de) that was composed of a 12 cm long needle with a closed tip and five outlet holes (1 mm diameter). We injected the $^{18}O$-enriched water into the Oe horizon and the injection depth was adapted to the site-specific forest floor structure in order to be centered in the Oe horizon. To assure homogeneous application of the label, the area was divided into eight subareas. 60 injections of 2.5 ml water were allocated randomly to each subarea. In total, 1.2 l of $^{18}O$-enriched water

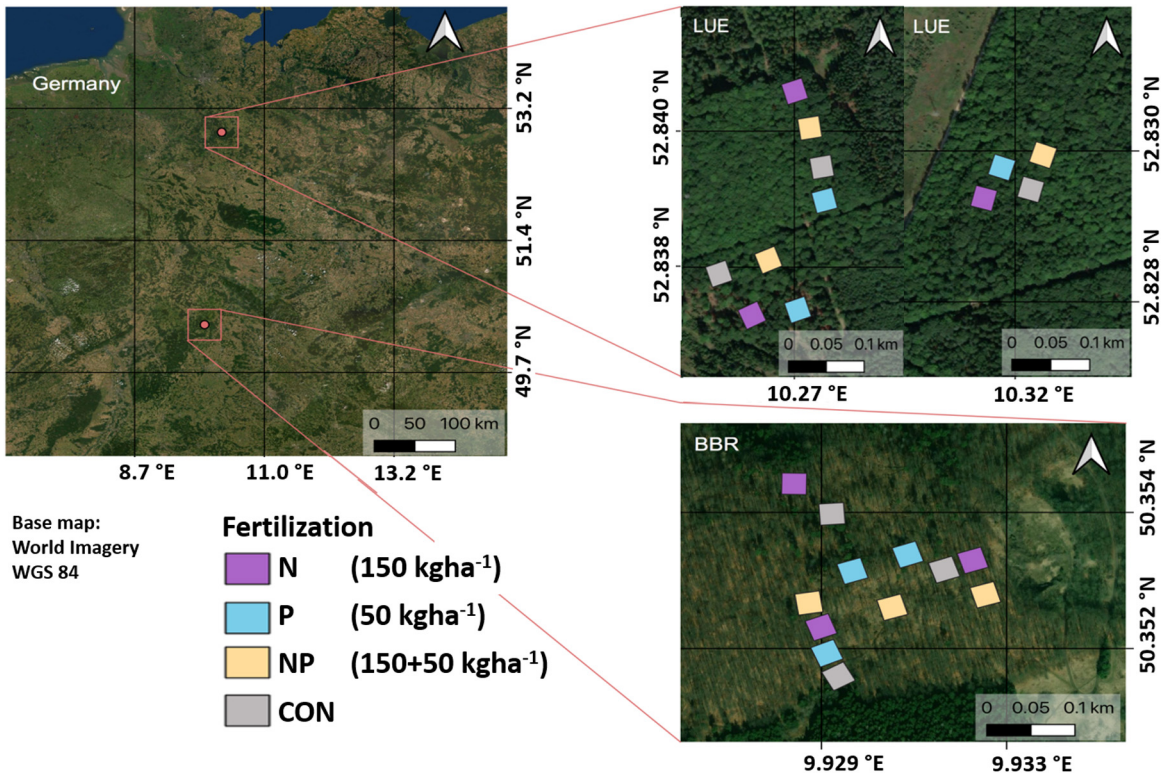


**FIGURE 1 |** Sitemap: experimental design of the fertilizer treatments (done in triplicate). The amount of fertilizer applied is given in brackets in kg $ha^{-1}$ $year^{-1}$. Nitrogen (N) and phosphorus (P) were applied as $NH_4NO_3$ and $KH_2PO_4$, respectively. Note that the control and N treatment received KCl to ease comparison with the P treatment which included the addition of K as well. Courtesy by Jaane Krüger; Source: Esri, Maxar, GeoEye, Earthstar Geographics, CNES/Airbus DS, USDA, USGS, Aerogrid, IGN, and the GIS User Community. To minimize visual distance of one triplicate of fertilized plots in LUE the coordinate system is adapted adequately, BBR = Bad Brückenau; LUE = Lüss.

was applied in the prescribed area around each tree individual and this equals 2.1% (BBR) and 1.7% (LUE) of the average soil water content in the organic layers. To check for resulting labeling of soil water, organic layer samples were taken and stored in gas-tight vials until isotope analysis.

## Xylem Sap Extraction and Sample Purification

In total, we sampled 48 trees (2 sites × 4 treatments × 2 time steps × 6 replicates). Two time steps were necessary to cover the potential duration until $^{18}O$-enriched phosphate originating from incorporation of $^{18}O$ from the water label in soil were taken up by the trees. To follow the uptake of $^{18}O$-enriched phosphate, we extracted xylem sap. To this end, branches (diameter of 0.8–2 cm) were harvested by tree climbers from the middle canopy. Directly after harvesting, we removed 2 cm of bark and cambium to prevent contamination with phloem constituents and tightly pulled a PE hose over the twigs. The twigs were placed in the Scholander pressure bomb (Soilmoisture 3000 Series Plant Water Status Console). The pressure was applied as $N_2$ gas (Grade 3). This procedure was repeated until a minimum amount of 30 ml xylem sap was extracted. Directly after sampling the xylem sap was filtered through 1.2 μm PET syringe filters (CHROMAFIL Xtra PET-120/25, MACHEREY-NAGEL GmbH & Co. KG, Düren, Germany). The samples were stored in a portable fridge at 4°C. Aliquots were split for $\delta^{18}O_W$ (1 ml) and $\delta^{18}O_{Pi}$ analyses.

Because some organic P compounds might be rapidly transformed into Pi in xylem sap, we processed xylem sap samples each day directly after returning from the field. We purified Pi following the protocol of Weiner et al. (2011) and added anion exchange resin membranes (VWR International GmbH, Bruchsal, Germany) to the xylem sap samples. After 16 h of shaking, the membranes were removed, rinsed with $H_2O$ and eluated by $HNO_3$. Eluates were again stored in a portable fridge at 4°C until preparation for isotope analysis in the laboratory. In the laboratory, the eluate was used for precipitation of silver phosphate as described by Weiner et al. (2011). In brief, the mineral precipitation and dissolution of ammonium phospho-molybdate was followed by mineral precipitation and dissolution of magnesium ammonium phosphate. After removal of cations and proof of the absence of chloride, silver phosphate was precipitated.

## Chemical Analyses

Concentration of inorganic P (Pi) in xylem was determined spectrophotometrically with a continuous flow analyzer (CFA,

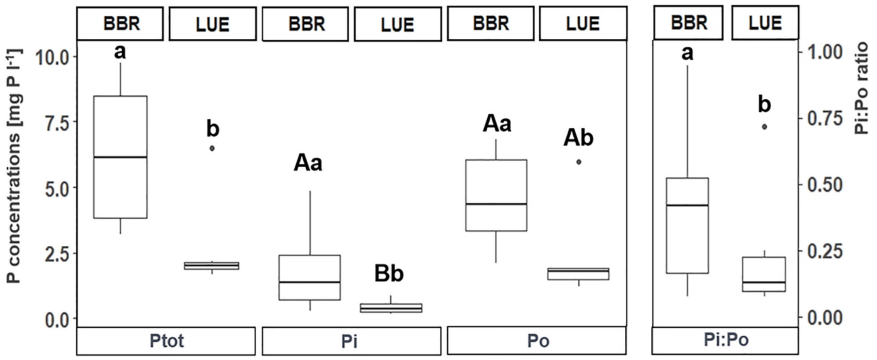


**FIGURE 2 |** Total (Ptot), inorganic (Pi) and organic (Po) phosphorus concentrations (mg P $l^{-1}$), and Pi:Po ratios in xylem sap of trees in the control plots. Note that Pi:Po ratios refer to the second *y*-axis. For ease of reading, samples were pooled from both sampling periods but treated separately for statistical analyses. Lowercase letters indicate differences between sites whereas uppercase letters indicate significant differences between Pi and Po concentrations of a given site. BBR = Bad Brückenau; LUE = Lüss.

AA3, XY2, Seal-Analytic, Norderstedt, Germany) at λ = 660 nm, using the method of Murphy and Riley (1962). Concentration of total P in xylem as well as total dissolved P concentrations in soil extraction solutions were measured by means of Inductively Coupled Plasma/Optical Emission Spectrometry (ICP-OES, PerkinElmer Optima 5300 DVGermany) at λ P 213.617. Organic P concentrations (Po) were calculated as the difference between total P and Pi concentrations (Toor et al., 2006). Limits of detection were 0.02 mg P $l^{-1}$ for CFA and 0.05 mg P $l^{-1}$ for ICP-OES.

Soil water for O isotope analysis was gathered by cryoextraction (Orlowski et al., 2013). $\delta^{18}O$ values of soil water extracts as well as of xylem sap were measured by cavitiy ring down spectroscopy (PICARRO Santa Clara, California, USA). The analysis of O isotope ratios of silver phosphate was carried out by means of a TC/EA (PYRO cube) coupled in continuous flow to an IRMS (IsoPrime100, both Elementar Analysensysteme; Hanau, Germany). Three triplicate subsamples (if enough silver phosphate was available) of each sample were weighed in silver capsules together with a small amount of glassy carbon powder to promote CO formation during combustion (Thermofisher scientific, Type 1, Kandel, Germany). The purity of the precipitated silver phosphate was ensured by the close match of standards and samples regarding the regression of O yield on analyte weight (**Supplementary Figure S2**). Calibration and drift-corrections were accomplished by repeated measurements of two international benzoic acid standards, IAEA 601 and IAEA 602 ($\delta^{18}O$ = +23.3 and +71.4‰, respectively; distributed by the International Atomic Energy Agency, Vienna, Austria), and one internal $Ag_3PO_4$ standard ($\delta^{18}O$ = +10.2‰). The standard deviation of triplicate measurements was ±0.6‰.

## Calculations and Statistical Analyses

General site effects were derived from a comparison of control plots between sites. In these cases, differences between sites were tested using a student's *t*-test. For single time steps and the complete design (i.e., including all treatments), we used a repeated measures ANOVA with site as between-subject factor and treatment (fertilization) as within-subject factor. Furthermore, we tested whether calculated differences between treatments (Δ) significantly deviated from zero based on a *t*-test against zero. For time series, a repeated measures ANOVA was conducted with site as between-subject factor and time step as within-subject factor. If the prerequisite for statistical analyses was violated (non-normal distribution), Wilcoxon tests were performed instead. Statistical analysis was carried out by IBM SPSS Statistics 22.

# RESULTS

## Site Effects on P Concentrations in Xylem Sap

Across control plots of both sites, Pi and Po concentrations ranged from 0.1 to 4.8 and 1.2 to 6.7 mg P $l^{-1}$, respectively. On average, we found Pi concentrations of 1.1 ± standard error (SE) 0.4 mg P $l^{-1}$ and Po concentrations of 3.4 ± SE 0.6 mg P $l^{-1}$. In general, the variability of P concentrations in xylem was high at both sites (coefficient of variation [CV] 41% in BBR and 63% in LUE). The mean Pi:Po ratio was 0.33 ± SE 0.08. We found significantly higher Ptot, Pi, and Po concentrations and Pi:Po ratios in BBR than in LUE (**Figure 2**). In LUE, Po concentrations were 4.3 times higher than Pi concentrations (**Figure 2**).

## Site Effects on the O Isotope Signature of Soil Water, Xylem Sap, and Phosphate of Xylem Sap After Application of $^{18}O$-Enriched Water

The application of $^{18}O$-enriched water in the Oe horizon increased $\delta^{18}O_W$ values of soil solution to +41 ± SE 5‰ across sites and sampling dates and this represented a substantial increase as compared to $\delta^{18}O_W$ values before label application (BBR: −8.2‰ ± SD 0.9‰, LUE: −9.1‰ ± SD 0.5‰, **Figure 3A**). This increase was similarly observed in BBR and LUE (compare boxplots and dashed red line in **Figure 3A**). Despite the successful

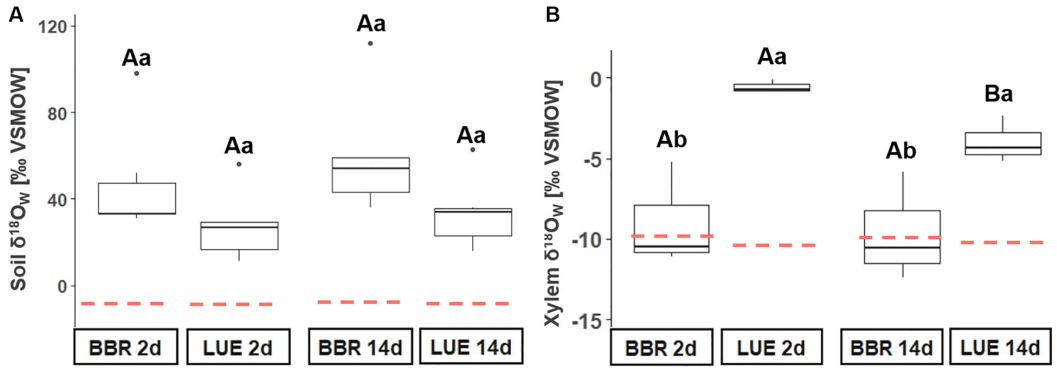


**FIGURE 3 |** Oxygen isotope signatures ($\delta^{18}O$) of xylem sap water (xylem $\delta^{18}O_W$, a), and soil water (soil $\delta^{18}O_W$, b) of control plots on the two sampling dates (2 d and 14 d = 2 days and 14 days, respectively) after addition of $^{18}O$-enriched water. Lowercase letters indicate significant differences between sites, whereas uppercase letters refer to significant differences between sampling dates. Red dashed lines show the background oxygen isotope signatures ($\delta^{18}O$) before $^{18}O$ addition **(A)** background: BBR: –8.2‰ ± SD 0.9‰, LUE: –9.1‰ ± SD 0.5‰, **(B)** background: BBR: –9.8‰, LUE: –10.6‰; BBR = Bad Brückenau; LUE = Lüss.

and consistent $^{18}O$ labeling of soil water at both sites, $\delta^{18}O_W$ values in xylem sap after labeling did not differ from those observed before label application in BBR (**Figure 3B**). By contrast, $\delta^{18}O_W$ values of xylem sap in LUE were higher after than before labeling and significantly higher than in BBR at both sampling dates (**Figure 3B**). In LUE, $\delta^{18}O_W$ values of xylem sap significantly decreased with time (**Figure 3B**).

At both sampling dates after the application of $^{18}O$-enriched water (2 and 14 days), $\delta^{18}O_{Pi}$ values of xylem sap were significantly different to the background $\delta^{18}O_{Pi}$ values in xylem sap (mean $\delta^{18}O_{Pi}$ background = −9.15‰ in BBR and −2.26‰ in LUE). In BBR, the difference significantly decreased from 26.1 ± SE 1.7‰ to 7.8 ± SE 2.4‰ during the period from 2 to 14 days after label application (**Figure 4**). In LUE, the difference was 9.8 ± SE 3.1‰ and 13.9 ± SE 2.2‰ 2 and 14 days after label application, respectively (**Figure 4**). Notably, the variation in $\delta^{18}O_{Pi}$ values of xylem sap was smallest 2 days after label application in BBR (coefficient of variation [CV] 16% as opposed to 75% after 14 days), whereas in LUE $\delta^{18}O_{Pi}$ values of xylem sap varied the least 14 days after label application (CV 78 and 39% after 2 and 14 days, respectively).

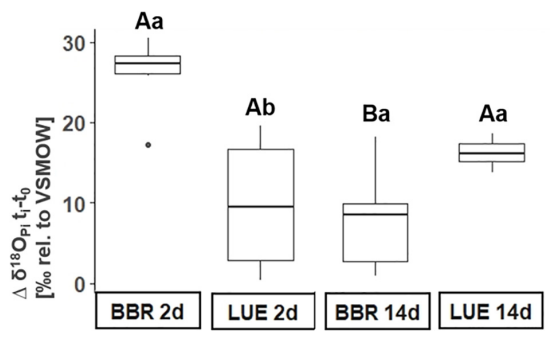


**FIGURE 4 |** Difference between oxygen isotope signatures of inorganic phosphate ($\delta^{18}O_{Pi}$) in xylem sap before (background, t0) and after addition of $^{18}O$-enriched water (ti) in the control plots. ti refers to the two time points after label application (2 d and 14 d = 2 days and 14 days, respectively). Lowercase letters indicate significant differences between sites, whereas uppercase letters refer to significant differences between sampling dates. BBR = Bad Brückenau; LUE = Lüss.

## Fertilizer Effects on P Concentrations and O Isotope Signatures of Phosphate in Xylem Sap

We found only few effects of fertilization on P concentrations in xylem sap. In BBR, N+P addition significantly increased Ptot and Pi concentrations while P addition resulted only in increased Pi concentrations in xylem sap of fertilized as compared to non-fertilized trees (**Figures 5A,B** and **Supplementary Figure S3**). As a consequence, the Pi:Po ratio of xylem sap was significantly higher in the P-fertilized than the non-fertilized trees in BBR (**Figure 5D**). Total P concentrations in xylem sap of fertilized trees were increased as compared to non-fertilized trees by P addition in LUE (**Figure 5**, but see **Supplementary Figure S3**). $\delta^{18}O_{Pi}$ values of xylem sap were enriched in $^{18}O$ irrespective of fertilizer treatments in BBR two days and in LUE 14 days after labeling (**Supplementary Figure S4**). Strikingly, only P fertilization (P and NP) resulted in an $^{18}O$-enrichment of phosphate in xylem sap on the other sampling dates at each site (14 days in BBR and 2 days in LUE, **Supplementary Figure S4**). However, $\delta^{18}O_{Pi}$ values of xylem sap were not affected by fertilization treatments (**Supplementary Figure S5**).

# DISCUSSION

## Site Effects on P Concentrations and O Isotope Signatures of Phosphate in Xylem Sap

The ranges of 0.1 to 4.8 mg P $l^{-1}$ (Pi) and 1.2 to 6.7 mg P $l^{-1}$ (Po) in our study were in the lower range of Pi and Po concentrations of xylem sap reported in the literature (Pi: 0.5 to 70 mg P $l^{-1}$; Po: 0.5 to 80 mg P $l^{-1}$) (Bollard, 1960; Saur

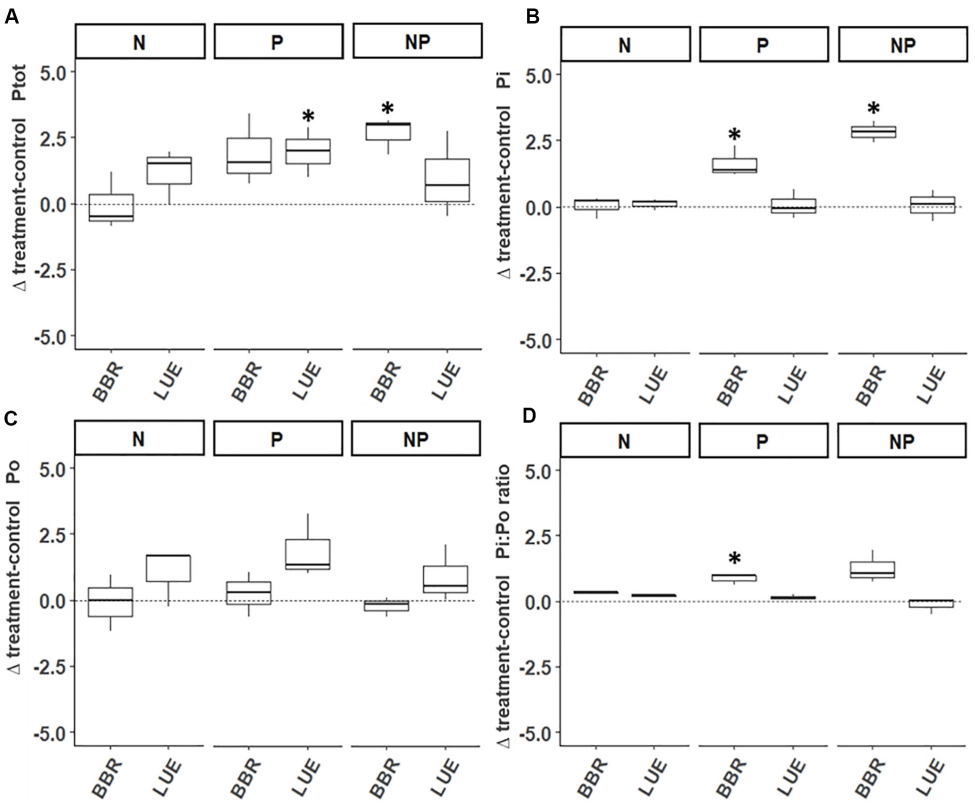


**FIGURE 5 |** Difference in phosphorus concentrations (mg P l-1) in xylem sap between fertilized trees (N, P, N+P) and non-fertilized trees (control) 14 days after application of 18O-enriched water. Differences are displayed separately for total phosphorus (Ptot, **A**), inorganic phosphorus (Pi, **B**), organic phosphorus (Po, **C**) and the ratio of Pi to Po **(D)**. Asterisks above boxplots indicate differences significantly deviating from zero (i.e., the control). BBR = Bad Brückenau; LUE = Lüss.

et al., 1995; Prima-Putra and Botton, 1998; Netzer et al., 2017). In line with our hypotheses, xylem sap total P concentrations were 2.3-fold higher in BBR than in LUE (**Figure 2**) and this was corroborated by 10-fold higher $NaHCO_3$-P-extractable P concentrations in soil in BBR as compared to LUE (Hauenstein et al., 2018). Therefore, site-specific P availability in soil was reflected in P concentrations of xylem sap. The significantly higher Pi:Po ratios in xylem sap at the P-rich site BBR compared to the P-poor site LUE indicates an intensified uptake of inorganic P from soil solution. By contrast, the low Pi:Po ratios at the P-poor site LUE could be indicative of the uptake of Po. In line, Scheerer et al. (2019) showed that small P-containing organic molecules can be taken up directly (i.e., intact) by trees. Alternatively, low Pi:Po ratios might be indicative of tree-internal P cycling. For example, Netzer et al. (2017) described higher Po concentrations in xylem at P-poor sites postulating intensified tree internal P remobilization and enhanced internal P cycling efficiency. This is further corroborated by a larger difference in P concentrations between leaf litter and fresh leaves and thus, higher P resorption, in LUE as compared to BBR (Lang et al., 2017). In summary, not only transformations of Po to Pi in organic layers (Hauenstein et al., 2018) but also Po uptake and tree-internal cycling are decisive for P nutrition of trees at the P-poor site.

Because neither site nor date influenced $\delta^{18}O$ values of soil solution (**Figure 3A**) and because of constant temperatures as well as negligible rainfall events during the experimental course, we can exclude both the $^{18}O$-enrichment of soil water via evaporation (Kendall and McDonnell, 1998) and the dilution of the $^{18}O$ tracer in soil solution via rainfall. Despite the continuous $^{18}O$-enrichment of soil solution water at both sites, we observed an $^{18}O$-enrichment of xylem sap in LUE only (**Figure 3B**). Therefore, trees in LUE took up water from the organic layer to which we added the isotope label. In line, >40% of the total fine roots (down to 1 m) are located in the organic layers in LUE (Hauenstein et al., 2018) and trees rely on the organic layer for water uptake. By contrast, 9% of the total fine roots can be found in the organic layer in BBR (Hauenstein et al., 2018) and thus, water uptake to a main proportion likely originates from deeper soil layer that we did not label. We observed differences in $\delta^{18}O$ values of xylem water between sampling dates in LUE (**Figure 3**). These might indicate water uptake from deeper non-labeled soil layers in LUE as well. However, the absolute difference of 3.3‰ is too small to pinpoint shifting patterns during the experimental course.

We found significantly increased $\delta^{18}O_{Pi}$ values of xylem sap at both sites (**Figure 4**). Notably, at both sites differences in $\delta^{18}O_{Pi}$ values after and before labeling were sufficiently

large (+15‰) to exceed potential "small" isotope fractionation of ca. 3‰ associated with active transporter-driven P uptake (Blake et al., 2005; Gross and Angert, 2015). Furthermore, the incorporation of $^{18}O$ into phosphate in xylem sap might originate from tree-internal biological processes. According to textbook knowledge, neither do microorganisms colonize the protoplast-free tracheids enabling xylem sap flow nor do extracellular enzymes exist in xylem sap. Therefore, xylem-internal biological processes resulting in an incorporation of $^{18}O$-enriched xylem water into phosphate in xylem sap are highly unlikely. The only plausible explanation of a tree-internal $^{18}O$ incorporation into phosphate would be an exchange between phloem – containing P-containing metabolites produced in metabolically active plant organs such as leaves – and xylem. During metabolic reactions in leaves, O atoms from cell water are incorporated into phosphate (Pfahler et al., 2013). Because in our study, xylem sap water was enriched in $^{18}O$, this biological incorporation would be visible in xylem if there was a connection between phloem and xylem. We did not measure $\delta^{18}O$ values of cell water or $\delta^{18}O_{Pi}$ values in leaves. However, we can roughly estimate $\delta^{18}O_{Pi}$ values in metabolically active P fractions in leaves. Leaf cell water is enriched in $^{18}O$ caused by preferential evaporative losses of $H_2{}^{16}O$ (Dongmann et al., 1974). Gan et al. (2002) found a difference between xylem and leaf mesophyll water ranging from +22.1 to +24.4‰ in cotton leaves. Based on $\delta^{18}O$ values of xylem sap water in our study (**Figure 3**), $\delta^{18}O$ values of leaf water of +14‰ (BBR) and +21‰ (LUE) would result. During metabolic reactions in leaves, all four O atoms in phosphate molecules are exchanged with those of cell-water-O and this reaction is accompanied by a temperature-dependent equilibrium fractionation (Pfahler et al., 2013) similar to observations of microbial metabolism (Blake et al., 2005). Applying the equation provided by Chang and Blake (2015) for a temperature of 13 and 8.5°C (mean soil temperature in 5 cm depth during the experiment in BBR and LUE, respectively), $\delta^{18}O_{Pi}$ values in leaves of 39‰ in BBR and 47‰ in LUE would result. Because estimated $\delta^{18}O_{Pi}$ values in leaves are far from those we observed and because we are not aware of studies on an exchange between xylem and phloem, we postulate that $^{18}O$-enriched phosphate in xylem sap originates from the uptake of phosphate previously biologically cycled in soil rather than from tree-internal biological cycling of P. This assumption is in line with our finding that the biological incorporation of $^{18}O$ from $^{18}O$-enriched ambient water into phosphate was visible at both sites and was in line with the $^{18}O$ enrichment of soil water but not of xylem sap water.

Interestingly, for the P-rich site BBR, Pi and water uptake seemed to be decoupled since phosphate contained the $^{18}O$ label while xylem sap did not (**Figures 3**, **4**). A decoupling of P and water uptake from different soil layers is plausible due to the energy-dependent active Pi uptake (Schachtman et al., 1998). Trees can adapt the active Pi uptake to changing conditions, for example to the seasonal variation in P supply (Netzer et al., 2017). Therefore, an active uptake of Pi is not necessarily linked to water uptake. Conversely, the location of water and P uptake seem to be identical, namely the organic layer, at the P-poor site LUE since the $^{18}O$ enrichment of soil water, xylem sap and phosphate in xylem sap match (**Figures 3**, **4**). This is corroborated by the site-specific fine root distribution (Hauenstein et al., 2018) and in line with our hypotheses identifying distinct ecosystem adaptions to P-poor sites. Beside water acquisition, this might also be an adaption of trees to P limitation, by expanding their fine roots to locations of P acquisition. Nevertheless, we cannot pinpoint the exact location of water uptake due to a lack of data on $\delta^{18}O_W$ values of deeper soil layers.

Since the $\delta^{18}O_{Pi}$ values of xylem sap in BBR exhibit little variability and are highly enriched in $^{18}O$ already 2 days after label application (**Figure 4**), $^{18}O$ from ambient water seem to be rapidly incorporated into phosphate which was subsequently taken up by trees in BBR. This short time scale is in line with the time scale of minutes to a few weeks until all four O atoms of a phosphate molecule are exchanged by O from isotopically labeled ambient water (Gross et al., 2015; von Sperber et al., 2017; Helfenstein et al., 2018). The incorporation of $^{18}O$ from ambient water into phosphate is mediated by enzymes such as pyrophosphatases in microorganisms (Blake et al., 2005), or mono-/diesterases (Liang and Blake, 2006; Sperber et al., 2014). The fast occurrence of the $^{18}O$ label in xylem sap of BBR is corroborated by higher microbial activity (Heuck and Spohn, 2016; Pistocchi et al., 2018) as well as higher phosphatase activity (Lang et al., 2017) reported for BBR as compared to LUE. At the P-poor site LUE, a distinct occurrence of the $^{18}O$ label occurred after 14 days (**Figure 4**). The slower appearance of the $^{18}O$ label corresponds to a slower forest floor turnover rate of 39 years in LUE compared to 5 years in BBR (Lang et al., 2017) illustrating a hampered biological activity in LUE. The slow turnover rates are linked to a greater contribution of fungi as compared to bacteria in organic matter decomposition. This is corroborated by Zavišić and Polle (2018) who highlights the importance of ectomycorrhrizal fungi (EMF) for P uptake by beech trees on P-poor sites. Similarly, Zavišić et al. (2016) pinpoint the intense colonization of root tips by EMF in the organic layers. In summary, high availability of P in soil is reflected in tree P nutrition in acquiring ecosystems such as BBR. In these ecosystems, because of high biological activity, P supply of trees originates from biological processes and is not necessarily linked to water supply. The source of P supply is similar in acquiring and recycling ecosystems, however, the retarded biological processes result in less favorable P nutrition of trees in recycling as compared to acquiring ecosystems.

## Fertilizer Effects on P Concentrations and O Isotope Signatures of Phosphate in Xylem Sap

We found that P addition alone and in combination with N increased Pi concentrations in xylem sap of BBR (**Figure 5**). Because data on tree growth or biomass are not available, it remains unclear whether the increased P uptake we observed for xylem sap was driven by fertilizer-induced increased biomass production or by growth-independent "luxury" P uptake. Other studies indicate that increased P uptake is mostly associated to growth-related increased P demand of trees (Goswami et al., 2018). At first sight, one might guess that the increased P uptake

derives from the fertilizer source itself. If this was the case, the O isotope signature of the fertilizer would predominate without shifts caused by biological cycling. However, $^{18}O$ enrichment of phosphate in xylem sap took place (**Figure 4**) and cannot be explained by fertilizer uptake because the fertilizer was not enriched in $^{18}O$ ($\delta^{18}O_{Pi}$ values = +19‰). Furthermore, $\delta^{18}O_{Pi}$ values were $^{18}O$-enriched irrespective of treatment at the dates where the label was most intensely recovered in xylem sap at each site (BBR: 2 days, LUE: 14 days; **Figure 4** and **Supplementary Figure S5**). At the dates where label recovery was not as pronounced (BBR: 14 days; LUE 2 days), P fertilization (P, NP) still significantly increased $\delta^{18}O_{Pi}$ values in xylem sap which was not the case for the control and N treatment (**Supplementary Figure S5**). Because of our interpretation of the $^{18}O$-enrichment as a result of biological $^{18}O$ incorporation into phosphate prior to P uptake (see previous chapter on site effects), we infer that (i) fertilizer-P was cycled biologically i.e., taken up and released by soil microorganisms, and/or (ii) P fertilization stimulated biological activity in soil (Mo et al., 2015) and thereby increased biological incorporation of $^{18}O$ into phosphate prior to uptake by trees.

## CONCLUSION

Our $^{18}O$ labeling approach highlights decoupled water and P uptake at the P-rich site BBR representing an acquiring ecosystem. By contrast, trees relied on the organic layer for both water and P uptake at the P-poor site LUE (recycling ecosystem). Foresters should consider that ecosystem resilience particularly at P-poor ecosystems might be strongly influenced by processes that deteriorate the organic matter and subsequently changes the forest floor structure and thereby its function as a place of water retention and nutrient retention from leaching to mineral soil layers. In this regard, ongoing N deposition and increasing soil temperatures especially in the forest floor due to climate change have the potential to considerably change forest floor turnover dynamics. Our results further suggest that N deposition fosters the biological release of P in soil, and the subsequent uptake by trees could serve to meet the N-induced increased P demand. Therefore, in the short run N deposition does not necessarily induce P limitation.

## DATA AVAILABILITY STATEMENT

The datasets generated for this study are available on request to the corresponding author.

## AUTHOR CONTRIBUTIONS

YO conceived the idea of the study. SH and MN conducted the study. SH and YO was jointly wrote the manuscript. All authors contributed to the article and approved the submitted version.

## FUNDING

The authors gratefully acknowledge funding by the German Research Foundation (DFG) (Oe516/6-2 in the priority program 1685).

## ACKNOWLEDGMENTS

This project was carried out in the framework of the priority programme 1685 "Ecosystem Nutrition: Forest Strategies for limited Phosphorus Resources". We are grateful for support by the forest tree climbers from Michael Furche Baumservice and Baumfällung de Vries. We want to thank the SPP coordinators (Prof. Dr. Friederike Lang and Dr. Jaane KrÃijger, University of Freiburg, Germany) for their support. Furthermore, we thank all people involved in establishing and maintaing the monitoring sites as well as the fertilization experiment.

## SUPPLEMENTARY MATERIAL

The Supplementary Material for this article can be found online at: https://www.frontiersin.org/articles/10.3389/ffgc.2020.542738/full#supplementary-material

## REFERENCES

Augusto, L., Achat, D. L., Jonard, M., Vidal, D., and Ringeval, B. (2017). Soil parent material-A major driver of plant nutrient limitations in terrestrial ecosystems. *Glob. Change Biol.* 23, 3808–3824. doi: 10.1111/gcb.13691

Bergkemper, F., Schöler, A., Engel, M., Lang, F., Krüger, J., Schloter, M., et al. (2016). Microbial phosphorus turnover in soil. *Environ. Microbiol.* 18, 1988–2000. doi: 10.1111/1462-2920.13188

Blake, R. E., O'Neil, J. R., and Surkov, A. V. (2005). Biogeochemical cycling of phosphorus Insights from oxygen isotope effects of phosphoenzymes. *Am. J. Sci.* 305, 596–620. doi: 10.2475/ajs.305.6-8.596

Blevins, L. L., Prescott, C. E., and van Niejenhuis, A. (2006). The roles of nitrogen and phosphorus in increasing productivity of western hemlock and western redcedar plantations on northern Vancouver Island. *For. Ecol. Manag.* 234, 116–122. doi: 10.1016/j.foreco.2006.06.029

Bollard, E. G. (1960). Transport in the Xylem. *Plant Physiol.* 11, 141–166.

Chang, S. J., and Blake, R. E. (2015). Precise calibration of equilibrium oxygen isotope fractionations between dissolved phosphate and water from 3 to 37°C. *Geochimica Cosmochimica Acta* 150, 314–329. doi: 10.1016/j.gca.2014.10.030

Clarholm, M. (1993). Microbial biomass P, labile P, and acid phosphatase activity in the humus layer of a spruce forest, after repeated additions of fertilizers. *Biol. Fert. Soils* 16, 287–292. doi: 10.1007/bf00369306

DeForest, J. L., Smemo, K. A., Burke, D. J., Elliott, H. L., and Becker, J. C. (2012). Soil microbial responses to elevated phosphorus and pH in acidic temperate deciduous forests. *Biogeochemistry* 109, 189–202. doi: 10.1007/s10533-011-9619-6

Dongmann, G., Nrnberg, H. W., Frstel, H., and Wagener, K. (1974). On the enrichment of H2 18O in the leaves of transpiring plants. *Radiat. Environ. Biophys.* 11, 41–52. doi: 10.1007/BF01323099

Finzi, A. C. (2009). Decades of atmospheric deposition have not resulted in widespread phosphorus limitation or saturation of tree demand for nitrogen

in southern New England. *Biogeochemistry* 92, 217–229. doi: 10.1007/s10533-009-9286-z

Gan, K. S., Wong, S. C., Yong, J. W. H., and Farquhar, G. D. (2002). 18 O spatial patterns of vein xylem water, leaf water, and dry matter in cotton leaves. *Plant Physiol.* 130, 1008–1021. doi: 10.1104/pp.007419

Gaudio, N., Belyazid, S., Gendre, X., Mansat, A., Nicolas, M., Rizzetto, S., et al. (2015). Combined effect of atmospheric nitrogen deposition and climate change on temperate forest soil biogeochemistry: a modeling approach. *Ecol. Model.* 306, 24–34. doi: 10.1016/j.ecolmodel.2014.10.002

Goswami, S., Fisk, M. C., Vadeboncoeur, M. A., Garrison-Johnston, M., Yanai, R. D., and Fahey, T. J. (2018). Phosphorus limitation of aboveground production in northern hardwood forests. *Ecology* 99, 438–449. doi: 10.1002/ecy.2100

Gross, A., and Angert, A. (2015). What processes control the oxygen isotopes of soil bio-available phosphate? *Geochim. Cosmochim. Acta* 159, 100–111. doi: 10.1016/j.gca.2015.03.023

Gross, A., Turner, B. L., Wright, S. J., Tanner, E. F. J., Reichstein, M., Weiner, T., et al. (2015). Oxygen isotope ratios of plant available phosphate in lowland tropical forest soils. *Soil Biol. Biochem.* 88, 354–361. doi: 10.1016/j.soilbio.2015.06.015

Hacker, N., Wilcke, W., and Oelmann, Y. (2019). The oxygen isotope composition of bioavailable phosphate in soil reflects the oxygen isotope composition in soil water driven by plant diversity effects on evaporation. *Geochim. Cosmochim. Acta* 248, 387–399. doi: 10.1016/j.gca.2018.11.023

Hansson, K., Laclau, J.-P., Saint-André, L., Mareschal, L., van der Heijden, G., Nys, C., et al. (2020). Chemical fertility of forest ecosystems. Part 1: common soil chemical analyses were poor predictors of stand productivity across a wide range of acidic forest soils. *For. Ecol. Manag.* 461:117843. doi: 10.1016/j.foreco.2019.117843

Hauenstein, S., Neidhardt, H., Lang, F., Krüger, J., Hofmann, D., Pütz, T., et al. (2018). Organic layers favor phosphorus storage and uptake by young beech trees (*Fagus sylvatica* L.) at nutrient poor ecosystems. *Plant Soil* 432, 289–301. doi: 10.1007/s11104-018-3804-5

Haußmann, T., and Lux, W. (1997). *Dauerbeobachtungsflächen zur Umweltkontrolle im Wald: Level II ; Erste Ergebnisse*. BMELF (Bundesministerium für Ernährung, Landwirtschaft und Forsten). Bonn, Germany.

Helfenstein, J., Tamburini, F., Sperber, C. V., Massey, M. S., Pistocchi, C., Chadwick, O. A., et al. (2018). Combining spectroscopic and isotopic techniques gives a dynamic view of phosphorus cycling in soil. *Nat. Commun.* 9:3226. doi: 10.1038/s41467-018-05731-2

Heuck, C., and Spohn, M. (2016). Carbon, nitrogen and phosphorus net mineralization in organic horizons of temperate forests: stoichiometry and relations to organic matter quality. *Biogeochemistry* 131, 229–242. doi: 10.1007/s10533-016-0276-7

IUSS WG WRB. (2015). "World reference base for soil resources 2014, update 2015," in *International Soil Classification System for Naming Soils and Creating Legends for Soil Maps*. World Soil Resources Reports No. 106. (Rome: FAO), 153–154.

Janssens, I. A., Dieleman, W., Luyssaert, S., Subke, J.-A., Reichstein, M., Ceulemans, R., et al. (2010). Reduction of forest soil respiration in response to nitrogen deposition. *Nat. Geosci.* 3, 315–322. doi: 10.1038/ngeo844

Jonard, M., Furst, A., Verstraeten, A., Thimonier, A., Timmermann, V., Potocic, N., et al. (2015). Tree mineral nutrition is deteriorating in Europe. *Glob. Change Biol.* 21, 418–430. doi: 10.1111/gcb.12657

Jonard, M., Legout, A., Nicolas, M., Dambrine, E., Nys, C., Ulrich, E., et al. (2012). Deterioration of Norway spruce vitality despite a sharp decline in acid deposition: a long-term integrated perspective. *Glob. Change Biol.* 18, 711–725. doi: 10.1111/j.1365-2486.2011.02550.x

Kendall, C., and McDonnell, J. J. (1998). *Isotope Tracers in Catchment Hydrology*. Amsterdam: Elsevier.

Lang, F., Bauhus, J., Frossard, E., George, E., Kaiser, K., Kaupenjohann, M., et al. (2016). Phosphorus in forest ecosystems: new insights from an ecosystem nutrition perspective. *J. Plant Nutr. Soil Sci.* 179, 129–135. doi: 10.1002/jpln.201500541

Lang, F., Krüger, J., Amelung, W., Willbold, S., Frossard, E., Bünemann, E. K., et al. (2017). Soil phosphorus supply controls P nutrition strategies of beech forest ecosystems in Central Europe. *Biogeochemistry* 127:255. doi: 10.1007/s10533-017-0375-0

Legout, A., Hansson, K., van der Heijden, G., Laclau, J.-P., Mareschal, L., Nys, C., et al. (2020). Chemical fertility of forest ecosystems. Part 2: towards redefining the concept by untangling the role of the different components of biogeochemical cycling. *For. Ecol. Manag.* 461:117844. doi: 10.1016/j.foreco.2019.117844

Liang, Y., and Blake, R. E. (2006). Oxygen isotope signature of Pi regeneration from organic compounds by phosphomonoesterases and photooxidation. *Geochim. Cosmochim. Acta* 70, 3957–3969. doi: 10.1016/j.gca.2006.04.036

Liang, Y., and Blake, R. E. (2007). Oxygen isotope fractionation between apatite and aqueous-phase phosphate: 20–45 °C. *Chem. Geol.* 238, 121–133. doi: 10.1016/j.chemgeo.2006.11.004

Lorenz, M. (1995). International Co-operative programme on assessment and monitoring of air pollution effects on forests-ICP forests-. *Water Air Soil Pollut.* 85, 1221–1226. doi: 10.1007/BF00477148

Lovett, G. M., Arthur, M. A., Weathers, K. C., Fitzhugh, R. D., and Templer, P. H. (2013). Nitrogen addition increases carbon storage in soils, but not in trees, in an Eastern U.S. deciduous forest. *Ecosystems* 16, 980–1001. doi: 10.1007/s10021-013-9662-3

Magill, A. H., Aber, J. D., Currie, W. S., Nadelhoffer, K. J., Martin, M. E., McDowell, W. H., et al. (2004). Ecosystem response to 15 years of chronic nitrogen additions at the Harvard Forest LTER, Massachusetts, USA. *For. Ecol. Manag.* 196, 7–28. doi: 10.1016/j.foreco.2004.03.033

Marklein, A. R., and Houlton, B. Z. (2012). Nitrogen inputs accelerate phosphorus cycling rates across a wide variety of terrestrial ecosystems. *New Phytol.* 193, 696–704. doi: 10.1111/j.1469-8137.2011.03967.x

Marschner, H. (ed.). (2002). "Introduction, definition, and classification of mineral nutrients," in *Marschner's Mineral Nutrition of Higher Plants, 2 Edn.* (Academic Press), 3–5. doi: 10.1016/B978-0-08-057187-4.50007-2

Mo, Q., Zou, B., Li, Y., Chen, Y., Zhang, W., Mao, R., et al. (2015). Response of plant nutrient stoichiometry to fertilization varied with plant tissues in a tropical forest. *Sci. Rep.* 5:14605. doi: 10.1038/srep14605

Murphy, J., and Riley, J. P. (1962). A modified single solution method for the determination of phosphate in natural waters. *Anal. Chim. Acta* 27, 31–36. doi: 10.1016/S0003-2670(00)88444-5

Nadelhoffer, K. J., Colman, B. P., Currie, W. S., Magill, A., and Aber, J. D. (2004). Decadal-scale fates of tracers added to oak and pine stands under ambient and elevated N inputs at the Harvard Forest (USA). *For. Ecol. Manag.* 196, 89–107. doi: 10.1016/j.foreco.2004.03.014

Nave, L. E., Vance, E. D., Swanston, C. W., and Curtis, P. S. (2009). Impacts of elevated N inputs on north temperate forest soil C storage, C/N, and net N-mineralization. *Geoderma* 153, 231–240. doi: 10.1016/j.geoderma.2009.08.012

Netzer, F., Schmid, C., Herschbach, C., and Rennenberg, H. (2017). Phosphorus-nutrition of European beech (*Fagus sylvatica* L.) during annual growth depends on tree age and P-availability in the soil. *Environ. Exp. Bot.* 137, 194–207. doi: 10.1016/j.envexpbot.2017.02.009

Odum, E. P. (2014). "The strategy of ecosystem development," in *The Ecological Design and Planning Reader*, ed. F. O. Ndubisi (Washington, DC: Island Press/Center for Resource Economics), 203–216. doi: 10.5822/978-1-61091-491-8_20

Orlowski, N., Frede, H.-G., Brüggemann, N., and Breuer, L. (2013). Validation and application of a cryogenic vacuum extraction system for soil and plant water extraction for isotope analysis. *J. Sens. Sens. Syst.* 2, 179–193. doi: 10.5194/jsss-2-179-2013

Peñuelas, J., Poulter, B., Sardans, J., Ciais, P., van der Velde, M., Bopp, L., et al. (2013). Human-induced nitrogen-phosphorus imbalances alter natural and managed ecosystems across the globe. *Nat. Commun.* 4:2934. doi: 10.1038/ncomms3934

Peñuelas, J., and Sardans, J. (2012). The role of plants in the effects of global change on nutrient availability and stoichiometry in the plant-soil system. *Plant Physiol.* 160, 1741–1761. doi: 10.1104/pp.112.208785

Pfahler, V., Dürr-Auster, T., Tamburini, F., Bernasconi, M. S., and Frossard, E. (2013). 18 O enrichment in phosphorus pools extracted from soybean leaves. *New Phytol.* 197, 186–193. doi: 10.1111/j.1469-8137.2012.04379.x

Pistocchi, C., Mészáros, É, Tamburini, F., Frossard, E., and Bünemann, E. K. (2018). Biological processes dominate phosphorus dynamics under low phosphorus availability in organic horizons of temperate forest soils. *Soil Biol. Biochem.* 126, 64–75. doi: 10.1016/j.soilbio.2018.08.013

Polglase, P. J., Jokela, E. J., and Comerford, N. B. (1992). Phosphorus, nitrogen, and carbon fractions in litter and soil of Southern pine plantations. *Soil Sci. Soc. Am. J.* 56, 566–573. doi: 10.2136/sssaj1992.03615995005600020036x

Porder, S., and Ramachandran, S. (2012). The phosphorus concentration of common rocks—a potential driver of ecosystem P status. *Plant Soil* 367, 41–55. doi: 10.1007/s11104-012-1490-2

Pregitzer, K. S., Burton, A. J., Zak, D. R., and Talhelm, A. F. (2007). Simulated chronic nitrogen deposition increases carbon storage in Northern Temperate forests. *Glob. Change Biol.* 14, 142–153. doi: 10.1111/j.1365-2486.2007.01465.x

Prietzel, J., and Stetter, U. (2010). Long-term trends of phosphorus nutrition and topsoil phosphorus stocks in unfertilized and fertilized Scots pine (*Pinus sylvestris*) stands at two sites in Southern Germany. *For. Ecol. Manag.* 259, 1141–1150. doi: 10.1016/j.foreco.2009.12.030

Prima-Putra, D., and Botton, B. (1998). Organic and inorganic compounds of xylem exudates from five woody plants at the stage of bud breaking. *J. Plant Physiol.* 153, 670–676. doi: 10.1016/S0176-1617(98)80219-8

Saur, E., Brechet, C., Lambrot, C., and Masson, P. (1995). Micronutrient composition of xylem sap and needles as a result of P-fertilization in maritime pine. *Trees* 10, 52–54. doi: 10.1007/BF00197780

Schachtman, D. P., Reid, R. J., and Ayling, S. M. (1998). Phosphorus uptake by plants: from soil to cell. *Plant Physiol.* 116, 447–453. doi: 10.1104/pp.116.2.447

Scheerer, U., Netzer, F., Bauer, A. F., and Herschbach, C. (2018). Measurements of 18 O-Pi uptake indicate fast metabolism of phosphate in tree roots. *Plant Biol.* 21, 565–570. doi: 10.1111/plb.12922

Scheerer, U., Trube, N., Netzer, F., Rennenberg, H., and Herschbach, C. (2019). ATP as phosphorus and nitrogen source for nutrient uptake by *Fagus sylvatica* and Populus x Canescens roots. *Front. Plant Sci.* 10:378. doi: 10.3389/fpls.2019.00378

Shaw, A. N., and DeForest, J. L. (2013). The cycling of readily available phosphorus in response to elevated phosphate in acidic temperate deciduous forests. *Appl. Soil Ecol.* 63, 88–93. doi: 10.1016/j.apsoil.2012.09.008

Sperber, C. V., Kries, H., Tamburini, F., Bernasconi, S. M., and Frossard, E. (2014). The effect of phosphomonoesterases on the oxygen isotope composition of phosphate. *Geochim. Cosmochim. Acta* 125, 519–527. doi: 10.1016/j.gca.2013.10.010

Talkner, U., Meiwes, K. J., Potoèiæ, N., Seletkoviæ, I., Cools, N., Vos, B. D., et al. (2015). Phosphorus nutrition of beech (*Fagus sylvatica* L.) is decreasing in Europe. *Ann. For. Sci.* 72, 919–928. doi: 10.1007/s13595-015-0459-8

Toor, G. S., Hunger, S., Derek Peak, J., Thomas Sims, J., and Sparks, D. L. (2006). Advances in the characterization of phosphorus in organic wastes: environmental and agronomic applications. *Acta Sci. Agron.* 89, 1–72. doi: 10.1016/S0065-2113(05)89001-7

Trichet, P., Bakker, M. R., Augusto, L., Alazard, P., Merzeau, D., and Saur, E. (2009). Fifty Years of fertilization experiments on pinus pinaster in Southwest france: the importance of phosphorus as a fertilizer. *For. Sci.* 55, 390–402.

Turner, J., and Lambert, M. J. (2015). Long-term growth responses to phosphatic fertilisers in a Pinus radiata plantation. *Austral. For.* 78, 207–218. doi: 10.1080/00049158.2015.1071679

von Sperber, C., Lewandowski, H., Tamburini, F., Bernasconi, S. M., Amelung, W., and Frossard, E. (2017). Kinetics of enzyme-Řcatalysed oxygen isotope exchange between phosphate and water revealed by Raman spectroscopy. *J. Raman Spectrosc.* 48, 368–373. doi: 10.1002/jrs.5053

Waldrop, M. P., and Firestone, M. K. (2004). Altered utilization patterns of young and old soil C by microorganisms caused by temperature shifts and N additions. *Biogeochemistry* 67, 235–248. doi: 10.1023/B:BIOG.0000015321.51462.41

Weiner, T., Mazeh, S., Tamburini, F., Frossard, E., Bernasconi, S. M., Chiti, T., et al. (2011). A method for analyzing the δ18O of resin-extractable soil inorganic phosphate. *Rapid Commun. Mass Spectrom.* 25, 624–628. doi: 10.1002/rcm.4899

Zavišić, A., and Polle, A. (2018). Dynamics of phosphorus nutrition, allocation and growth of young beech (*Fagus sylvatica* L.) trees in P-rich and P-poor forest soil. *Tree Physiol.* 38, 37–51. doi: 10.1093/treephys/tpx146

Zavišić, A., Nassal, P., Yang, N., Heuck, C., Spohn, M., Marhan, S., et al. (2016). Phosphorus availabilities in beech (*Fagus sylvatica* L.) forests impose habitat filtering on ectomycorrhizal communities and impact tree nutrition. *Soil Biol. Biochem.* 98, 127–137. doi: 10.1016/j.soilbio.2016.04.006

**Conflict of Interest:** The authors declare that the research was conducted in the absence of any commercial or financial relationships that could be construed as a potential conflict of interest.

frontiers in Forests and Global Change

ORIGINAL RESEARCH
published: 15 September 2020
doi: 10.3389/ffgc.2020.00100

# Organic Nutrients Induced Coupled C- and P-Cycling Enzyme Activities During Microbial Growth in Forest Soils

*Sebastian Loeppmann*[1,2]*, *Andreas Breidenbach*[1], *Sandra Spielvogel*[2], *Michaela A. Dippold*[1] and *Evgenia Blagodatskaya*[3,4]

[1] Biogeochemistry of Agroecosystems, Georg-August-University, Göttingen, Germany, [2] Institute of Plant Nutrition and Soil Science, Christian-Albrechts-University, Kiel, Germany, [3] Department of Soil Ecology, Helmholtz Centre for Environmental Research - UFZ, Halle (Saale), Germany, [4] Agro-Technology Institute, RUDN University, Moscow, Russia

Besides environmental and soil physical drivers, the functional properties of microbial populations, i. e., growth rate, enzyme production, and maintenance requirements are dependent on the microbes' environment. The soil nutrition status and the quantity and quality of the substrate input, both infer different growth strategies of microorganisms. It is uncertain, how enzyme systems respond during the different phases of microbial growth and retardation in soil. The objective of this study was to uncover the changes of microbial functioning and their related enzyme systems in nutrient-poor and nutrient-rich beech forest soil during the phases of microbial growth. We determined microbial growth via kinetic approach by substrate-induced respiratory response of microorganisms, enabling the estimation of total, and growing biomass of the microbial community. To induce microbial growth we used glucose, while yeast extract simulated additional input of nutrients and factors indicating microbial residues (i.e., necromass compounds). Microbial growth on glucose showed a 12–18 h delay in associated enzyme activity increase or the absence of distinct activity responses ($V_{max}$). β-glucosidase and chitinase (NAG) demonstrated clear differences of $V_{max}$ in time and between P-rich and P-poor soils. However, during microbial growth on glucose + yeast extract, the exponential increase in enzymatic activity was clearly stimulated accompanied by a delay of 8–12 h, smoothing the differences in nutrient-acquisition dynamics between the two soils. Furthermore, cross-correlation of β-glucosidase and acid phosphatase between the two sites demonstrated harmonized time constraints, which reflected the establishment of comparable and balanced enzymatic systems within the decomposition network. The network accelerated nutrient acquisition to maintain microbial growth, irrespective of the contrasting soil properties and initial nutrient stocks, indicating similar tradeoffs of C- and P- cycling enzymes in both soils. This reflects comparable temporal dynamics of activities in nutrient-poor and nutrient-rich soil when the glucose + yeast extract was added. During lag phase and phase of exponential microbial growth, substrate turnover time of all enzymes was shortened in nutrient-poor forest soil exclusively, reflecting that the quality of the added substrate strongly matters during all stages of microbial growth in soil.

**Keywords: substrate utilization, soil nutrition, microbial activity, enzyme kinetics, microbial necromass, time series analysis, european beech forests, microbial growth kinetics**

OPEN ACCESS

***Edited by:***
*Edith Bai,*
*Institute of Applied Ecology (CAS), China*

***Reviewed by:***
*Jörg Schnecker,*
*University of Vienna, Austria*
*Frank Hagedorn,*
*Snow and Landscape Research (WSL), Switzerland*

***Correspondence:**
*Sebastian Loeppmann*
*s.loeppmann@soils.uni-kiel.de*

***Specialty section:***
*This article was submitted to Forest Soils, a section of the journal Frontiers in Forests and Global Change*

***Received:*** *13 February 2020*
***Accepted:*** *29 July 2020*
***Published:*** *15 September 2020*

***Citation:***
*Loeppmann S, Breidenbach A, Spielvogel S, Dippold MA and Blagodatskaya E (2020) Organic Nutrients Induced Coupled C- and P-Cycling Enzyme Activities During Microbial Growth in Forest Soils. Front. For. Glob. Change 3:100. doi: 10.3389/ffgc.2020.00100*

## INTRODUCTION

Temperate forest soils store significant quantities of the terrestrial organic carbon (SOC) (Jobbágy and Jackson, 2000) which are continuously microbially processed. Soil microorganisms decompose and transform organic substrates, varying in quality, and quantity under impact of biotic and abiotic factors (Kowalchuk and Stephen, 2001; Jansson and Prosser, 2013). Due to specific abiotic conditions of temperate forest ecosystems (e.g., pH), fungi often dominate over bacteria in soil microbial community, and such a dominance is usually distinctly associated with a particular soil horizon (Baldrian et al., 2012). Additionally, the diversity of yeast species is much broader in forest biomes than in other natural ecosystems (Maksimova and Chernov, 2004). The abundance of fungal taxa is mainly driven by the C/N ratio and by the content of phosphorus in the soil as compared to other edaphic factors (Lauber et al., 2008). Enormous microbial diversity ensures sustainability of the community due to high functional redundancy of various species, however, it does not necessarily mean high microbial activity and functioning. An ability to maintain ecologically relevant biogeochemical processes such as SOC and nutrient cycling (Roszak and Colwell, 1987) is ensured by the capacity of soil microorganisms to switch from dormancy to growth adjusting their functional traits accordingly to changing environmental and climatic conditions (Lennon and Jones, 2011; Wallenstein and Burns, 2011; Blagodatskaya and Kuzyakov, 2013). During growth and turnover, microorganisms process primarily plant-derived organic substrates transforming them to secondary C sources in form of microbial residues (i.e., necromass). If microbial residues are not stabilized, they are further decomposed and thus, are fueling the active microbial community. As a result of microbial turnover, up to 50% of soil organic matter (SOM) originates from microbial residues (Liang et al., 2011; Miltner et al., 2012). Up to now, our knowledge on its nutrition potential for plants and the active microbial community is still limited.

Along with strong functional redundancy, microbial functional diversity ensures sustainable mechanisms in the community, and the ecosystem (Petchey et al., 2006; Wagg et al., 2019), which still remains a missing link between biodiversity patterns and ecosystem functions (Bardgett and Putten, 2014). Microbial functional diversity is increasingly recognized in science, as these patterns provide a more powerful test of theory than taxonomic richness (Lamanna et al., 2014; Louca et al., 2018). However, we are still lacking knowledge on soil microbial functional diversity and related enzyme systems, especially in forest ecosystems (Lang et al., 2016).

Besides traditional methods such as viable counts or the measurements of optical density of microorganisms (**Figure 1**), microbial growth can be determined by kinetic approach, via the substrate-induced respiratory response of microorganisms. This enables the estimation of total and growing biomass of the glucose-consuming, i.e., the major part of the entire microbial community (Panikov, 1995; Panikov and Sizova, 1996). By combining substrate-induced respiration (SIR) (Anderson and Domsch, 1986) and substrate-induced growth respiration (SIGR) of microbial cells (Panikov, 1995) we are able to estimate soil microbial biomass as well as its growing proportion. Despite that the SIGR approach is based on the unlimited exponential microbial growth induced by an excess of substrate, the steepness of the growth curve (determined by $CO_2$ evolution rate) is different in soils varying in abiotic or biotic properties (Panikov, 1991; Blagodatsky et al., 2000). All the mentioned techniques can determine the typical microbial growth curves of

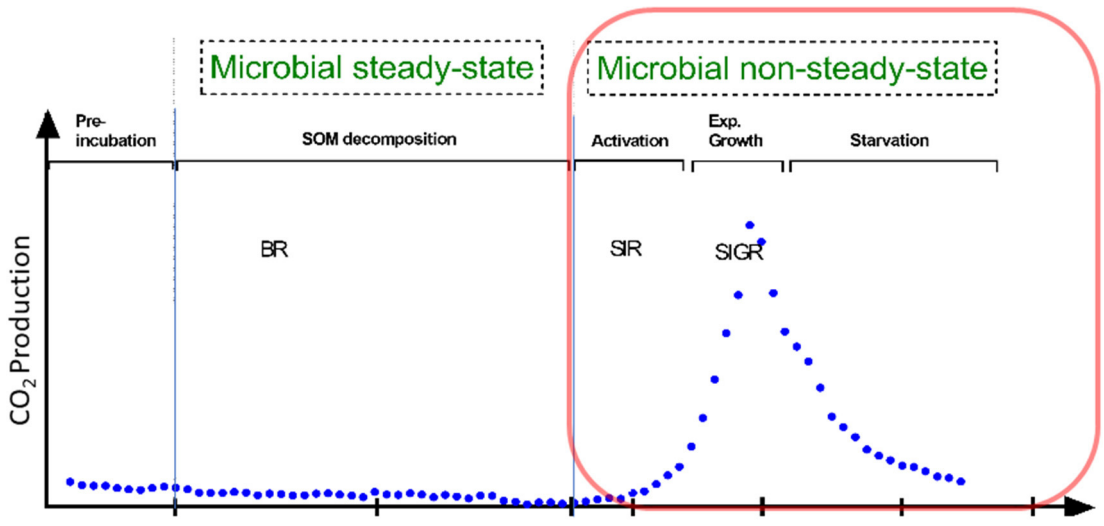


**FIGURE 1 |** Conceptional soil microbial respiration: We focused on microbial non-steady state condition, reflecting the phases of microbial growth (lag, exponential growth). This is in contrast to the basal respiration (BR) without any additional substrate addition. Soil activation leads to increased protein synthesis in the early exponential phase; protein for motility occurs mainly at mid-exponential phase; in the late expontential phase typically accounts for stress resistance, since substratre gets scarce; stationary phase reflects stable to slight decreasing microbial biomass. Substrate-induced respiration (SIR) and substrate-induced growth respiration (SIGR) are commonly used to determine microbial growth parameter and microbial biomass.

microorganisms during microbial non-steady state (increase in microbial respiration/abundance, **Figure 1**). These growth curves show different phases of microbial growth, namely (1) lag, (2) exponential, (3) stationary and 4) death phase (**Figure 1**). In general, the lag phase metabolism may include the activation of signaling pathways and specific transcriptional changes which might lead to the upregulation of protein assembly, nucleotide metabolism, lipopolysaccharide biosynthesis, respiration, and other processes which are needed for differentiation and multiplication (Hamill et al., 2020). These processes occur during lag phase, initiate exponential growth and cell divisions (Panikov, 1991). The stationary phase of microbial growth is characterized by stable (not increasing) microbial net biomass, which is more relevant for hemostat cultures, whereas it cannot be often detected in soils.

Substrates of contrasting quality may favor microbial guilds with different intrinsic properties (e.g., maximum specific growth rates), while substrate amount and availability may affect duration of lag-time and exponential growth phases. Since nutrient acquisition is linked stoichiometrically to microbial growth dynamics, the production of extracellular enzymes is a basic strategy for microorganisms to prevent nutrient scarcity. There is still uncertainty, how soil enzyme systems support microbial growth during lag-, exponential-, and death phase. To survive under unfavorable environmental conditions and to be ready to metabolize the occasional substrate input, soil microorganisms can maintain a dynamic state, ready to adapt immediately to environmental changes by means of a wide range of genotypic and phenotypic accommodations. For example, cell mechanisms such as (i) modification of enzyme synthesis to take up growth-limiting nutrients, (ii) modulation of uptake rates for available nutrients, and (iii) coordination of anabolic processes to maintain balanced growth (van den Berg, 2001). The functional traits of the dominating population, i.e., specific growth rate, enzyme production and maintenance requirements are dependent on both the soil nutrition status, and the availability of the fresh substrate input. Especially, bacteria have developed sophisticated mechanisms to adapt to soil C availability. For example, the presence of glucose often prevents the use of other, secondary, carbon sources. This preference for glucose over other carbon sources has been termed glucose repression or, more generally, carbon catabolite repression (CCR) (Deutscher, 2008). Nowadays, CCR is defined as a regulatory phenomenon by which the expression of functions for the use of secondary carbon sources and the activities of the corresponding enzymes are reduced in the presence of a preferred carbon source (Görke and Stülke, 2008). Since CCR has been revealed in most free-living heterotrophic bacteria, including facultatively autotrophic bacteria, 5–10% of all bacterial genes are subjected to CCR (Liu et al., 2005). The selection of the preferred carbon source reflects an important factor in relation to the bacterial growth rate, and therefore competitive success with other microorganisms (Görke and Stülke, 2008).

Among numerous enzyme-mediated processes, several are usually specifically addressed due to their relevance for decomposition of SOM and therefore, for acquisition of elements (i.e., C, N, and P), which are critical for plant-microbial interactions and finally, for biochemical cycles. These processes are related to (1) decomposition of cellulose-like compounds—the most abundant components in plant tissues by cellulolytic enzymes (Blifernez-Klassen et al., 2012); (2) the proteolysis, which is of major importance in heterogeneous soil ecosystems, as it is considered as rate- limiting step during N mineralization (Weintraub and Schimel, 2005). For example, proteases such as exopeptidases (e.g., leucine-aminopeptidase) catalyze the hydrolysis of the terminal amino acids of polypeptide chains (Landi et al., 2011). (3) Decomposition of organic compounds is an important source of phosphorus acquisition due to relatively high abundance of organic P forms in soil. Therefore, specific enzymes, e.g., phytase and acid phosphor-mono- and di-esterase are released in large quantities by e.g., microbes and plants to access P forms in organic sources (Nannipieri et al., 2012; Jarosch et al., 2019).

The objective of this study was to unravel the changes of microbial functioning and their related enzyme systems in nutrient-poor (site Luess, LUE) and nutrient-rich (site Mitterfels, MIT) forest soil during phases of microbial growth. Therefore, we either used glucose, as simple substrate or a combination of glucose and yeast extract, reflecting a different substrate quality for microbial utilization. Glucose was used because the fraction of glucose-consuming microorganisms is generally large and relatively constant across different soil types and glucose is one of the most abundant sugars exuded by roots (Ottow, 2011). As an additional source of substrate, we used yeast extract because it consists of organic nutritional compounds similar to microbial (in large extent fungal) residues present in forest ecosystems. Yeast extract contains a broad range of sugars, phosphates, proteins and lipids, purines and pyrimidines (RNA type), $Mg^{2+}$ and $Ca^{2+}$, chitosan, and chitin (Bartnicki-Garcia and Nickerson, 1962; Pronk, 2002).

We hypothesized that during lag phase (i) an acceleration of enzyme activity in soil with lower nutrient status would occur, (ii) enzyme activity would be altered by the addition of yeast extract in nutrient-poor compared to nutrient-rich soil, as the enzymes' affinity is assumed to change. We further hypothesized that during exponential growth: (iii) microorganisms would increase enzyme activity, mining for additional nutrients in order to maintain growth. This effect may be more pronounced in the nutrient-poor soil, because of lower initial soil resources. We also hypothesized that (iv) the glucose + yeast extract amendment would reduce enzyme activity, which can either affect the synthesis of catabolic enzymes via global or specific regulators or inhibit the uptake of a carbon source (Park et al., 2006; Deutscher, 2008). For growth retardation, we hypothesized that (v) enzymatic activity would be maintained at a high level and it would not decrease with respiration.

# MATERIALS AND METHODS

## Experimental Sites and Soil Sampling

The nutrient-poor field site is located at lower Saxon plain, a landscape that is predominantly shaped by Pleistocene glaciation. The nutrient-rich soil was sampled from the forest monitoring station Mitterfels (MIT), situated on the eastern front ridge of the Bavarian Forest. We sampled the Ah horizon of the

nutrient-poor and the A(e)h of nutrient-rich soil in June 2017 and immediately started the incubation experiment. Both studied forest sites showed acidic pH values (Bergkemper et al., 2016; Lang et al., 2017).

## Experimental Setup

We incubated 1.5 g of moist soil in a small flask inserted into the larger tube with the sodium hydroxide to trap the $CO_2$ at 22°C and measured $CO_2$ production via changes in electric conductivity by rapid automated bacterial Impedance technique (RABIT) (Don Whitley Scientific Limited, UK) (Fehlhaber and Krüger, 1998). The indirect technique of RABIT provides a flexible and calibrated impedance method which monitors the amount of carbon dioxide produced by growing organisms. Soil samples were kept in closed systems (microcosm) under quasi-stationary conditions and the evolved $CO_2$ was measured every 20 min. After 24 h the $CO_2$ efflux showed stable values and we started the experiment. A first sampling determined the background values of enzymes activity in the soils without the addition of any substrate. Thereafter, two treatments for substrate addition were established (1) glucose (2) glucose + yeast extract. Substrate concentrations, enough for unlimited exponential growth of microorganisms, were estimated based on preliminary experiments and were adjusted in a rate equivalent to ∼100% of the microbial biomass C, measured in the field. Glucose with nutrients (1.9 mg $g^{-1}$ $(NH_4)SO_4$, 2.25 mg $g^{-1}$ $K_2HPO_4$ and 3.8 mg $g^{-1}$ $MgSO_4$-$7H_2O$) was added to the soil as solutions via micro-pipetting onto the surface of the soil. Yeast extract amounted 0.3 mg per g soil (C ∼258 and N ∼30 μg $g^{-1}$), so that it could not serve as essential C-source to induce exponential microbial growth. Substrates were dissolved and added to the soil as a solution, to reach a resulting moisture to the 60% of WHC. A destructive sampling design was chosen to determine enzyme kinetics during the phases of exponential microbial growth and retardation. Details on experimental duration and time spans of measurements are shown in **Figure 4**. Microbial biomass was determined by substrate-induced respiration (SIR) based on $CO_2$ efflux measured the first 4 h after substrate addition (Anderson and Domsch, 1986; Anderson and Joergensen, 1997) and the conversion factor of 30 suggested by Kaiser et al. (1992) was used. Overall, SIR is a sensitive method and well-reproducible (Heinemeyer et al., 1989).

## Soil Extracellular Enzyme Activities

We determined the enzyme activities of β-glucosidase, acid phosphatase, β-N-Acetylglucosaminidase (NAG), and leucine-aminopeptidase. An aliquot of 0.5 g soil of the sample was sonicated in 50 ml autoclaved millipore water in sterile jars for 2 min at low energy level. Aliquots of 50 μl of aliquot were pipetted in 96-well-microplates (Brand pureGrade, black) while stirring the soil suspension. Additionally, we buffered the solution either with 80 ml 0.1 M MES buffer, at pH 6.1 for β-glucosidase, NAG, and phosphatase, or with 0.05 M TRIZMA buffer, at pH 6.8 for leucine-aminopeptidase. Lastly, 100 μl substrate solutions with the following concentrations were filled into the wells: 20, 40, 60, 80, 100, 200, 400 μmol substrate g $soil^{-1}$. Microplates were set to a temperature of 21°C and agitated before determination of fluorescence (excitation 360 nm; emission 450 nm) via an automated fluorometric plate-reader (Wallac 1420, Perkin Elmer, Turku, Finland) after 30, 60, 90, and 120 min.

We used Michaelis Menten kinetics a non-linear regression to estimate the maximal enzyme (potential) activity ($V_{max}$), (Stemmer, 2004; Sinsabaugh et al., 2010; Nannipieri et al., 2012). Each soil sample was measured as an analytical triplicate.

$$v = (V_{max} x\ [S]) / (K_m + [S]) \quad (1)$$

The reaction rate (v) is mediated by enzymes. $V_{max}$ reflects maximal decomposition rates at saturating substrate concentrations; $K_m$ is the concentration of substrate at half-maximum activity and thus is a value which has a negative correlation with the enzyme affinity to the substrate. The substrate turnover time was determined by $(K_m+S)/V_{max}$ (Panikov, 1991; Larionova et al., 2007).

## Growth Rate Model

The use of substrate-induced growth respiration (SIGR) to disentangle the soil microbial biomass, its active part and maximum specific growth rate has become a common tool in soil science (Blagodatsky et al., 2000). SIGR differs from SIR method in terms of the phase of $CO_2$ evolution and time interval (Loeppmann et al., 2016a). The change in $CO_2$ production (p) with time (t) in soil amended with glucose and nutrients was calculated by Equation (2), where A (uncoupled respiration) = $(1–r_0)\ Q'x_0$, B (coupled respiration) = $r_0\ Q\ x_0$, and $\mu = Y_{CO2}\ (Q–Q')$. Therefore, the steepness of the growth curve represents the intrinsic functional trait of the growing microbial population and it can be estimated by the maximum specific growth rate after the fitting of experimental data to Equation (2) (Wutzler et al., 2012).

$$CO_2\ (t) = A + B\ \exp\ (\mu t) \quad (2)$$

According to Panikov (1995), the specific respiration activity measured under excess substrate is denoted as Q, and the cyanide-resistant fraction Q'; the productive fraction of the total respiration is then equal to Q–Q'. $Y_{CO2}$ is yield of biomass C per unit of respired C-$CO_2$, assumed to be constant during the experiment and equal to 1. The parameters of Equation (5) were fitted by minimizing the least- square sum using MODEL MAKER-3 software (SB Technology Ltd). Fitting was restricted to the part of the curve that corresponded to unlimited exponential growth, as indicated by maximum values of r, F, and Q statistic criteria. $r_0$ was calculated from the ratio of A:B (Panikov and Sizova, 1996).

$$r_0 = \frac{B\,(1-\lambda)}{A + B\,(1-\lambda)} \quad (3)$$

where $\lambda = (Q–Q')/Q$ and may be accepted as a basic stoichiometric constant = 0.9 (Panikov and Sizova, 1996). The total glucose-metabolizing microbial biomass (sustaining+growing; $x_0$) was calculated as following:

$$x_0 = \frac{B\lambda Y_{CO_2}}{r_0 \mu} \quad (4)$$

The growing microbial biomass (GMB, $x_0$') was calculated using the equation: $x_0$

$$x'_0 = x_0 r_0 \quad (5)$$

The lag period ($t_{lag}$) was determined as the time interval from substrate amendment to the moment when the increasing rate of growth-related respiration [B exp(mt)] became as high as the rate of respiration uncoupled from the growth of microorganisms [A] [Equation (1)]. $t_{lag}$ was calculated using the parameters of the approximated respiration curve by the following equation:

$$t_{lag} = \frac{\ln(A/B)}{\mu} \quad (6)$$

## Determination of dsDNA Content

For quantitative soil DNA extraction, we used the MP Bio kits (MP Biomedicals, Germany). DNA extraction was performed during lag phase according to the manufacturer's protocol with 0.5 g of fresh moist soil treated by the FastDNA® SPIN kit for Soil (MP Biomedicals, Germany). Detailed information on extraction and quantification of dsDNA can be found in Loeppmann et al. (2018). A conversion factor of 5.0 was used to convert mg DNA $g^{-1}$ soil to mg microbial biomass C $g^{-1}$ soil (Anderson and Martens, 2013; Loeppmann et al., 2018).

## Statistics

Significant effects of process parameter (e.g., $\mu_{max}$) between treatments (substrate and soil) were assessed by ANOVA at $p < 0.05$. The parameters of the equation were fitted by minimizing the least-square sum using GraphPad Version 8 software (Prism, USA). The normality distribution of the data was checked using the Shapiro-Wilks test and if necessary, transformed to log distribution. Equality of variances were analyzed by Levene's test. The degree of linear association between pairs of values separated by a given distance was obtained from the self- or autocorrelation using PAST4.01 (Hammer and Harper, 2006) which allowed an observation of temporal processes at and between local maxima and minima within the sampled domain. In general, physical, chemical, and biological reactions occurring rapidly manifest smaller temporal correlation lengths than those occurring more slowly. The 95% confidence band is technically appropriate only at each individual lag, not for the complete autocorrelation function. Cross correlation was used to compare the two different time series, covering the same time span (Miller, 1979). Prior to cross correlation analysis the data was de-trended to prevent non-stationarity (Podobnik and Stanley, 2008) and pre-whitened to remove spurious correlations, based on temporal dependencies between adjacent values of the input time-series. This technique removes the influences from the output time-series (Shumway and Stoffer, 2017). Parameter optimization was restricted to the applied model Equation 2, as indicated by maximum values of statistic criteria: $r^2$, the fraction of total variation explained by the model defined as ratio of model weighted sum of squares to total weighted sum of squares.

# RESULTS

## Activation and Growth of Soil Microorganisms

The $CO_2$ response of microbial respiration to glucose addition was 83% higher in nutrient-rich (Mitterfels) than in nutrient-poor soil (Luess) reflecting a stronger microbial activation and higher total biomass C (**Figure 2**, **Table 2**). A similar pattern was depicted for nutrient-rich soil after combined substrate addition, showing an increase of 48% compared to nutrient-poor soil.

The maximum specific growth rate of microorganisms was significantly higher (34% for glucose; 17% glucose + yeast extract) in nutrient-poor soil than in nutrient-rich soil (**Figure 3**), indicating a faster microbial turnover and shorter generation times. Although, the growth rate was similar in nutrient-poor soil irrespective of the type of substrate addition, the proportion of growing microbial biomass increased by three times, and the lag time shortened by 6 h in yeast extract vs. sole glucose treatment (**Table 1**). This indicates a positive feedback of the additional growth factors derived from the yeast

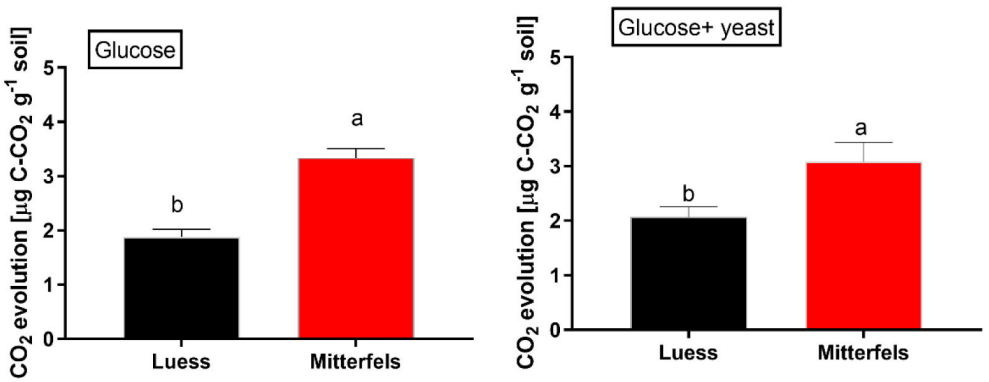


**FIGURE 2 |** Soil substrate-induced respiration (SIR) including standard error of mean (SEM) measured by $CO_2$ production in two forest soils planted with beech. Significant differences between the sites are denoted by lower case letters at a significance level of $p < 0.05$. Note, SIR-derived $CO_2$ is measured before exponential growth phase sets in.

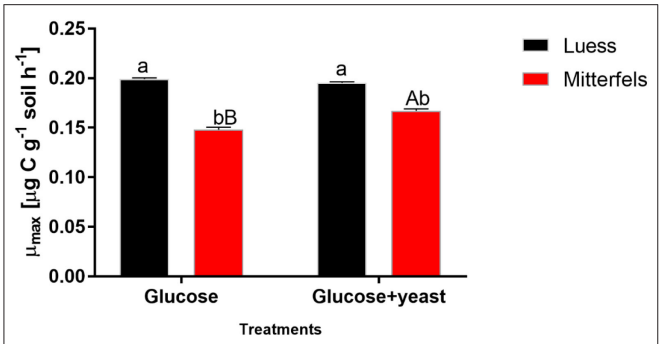


**FIGURE 3 |** Maximum specific growth rates including SEM of soil microorganisms after the addition of either glucose or the combination of glucose and yeast extract. Significant differences ($P < 0.05$) between sites were denoted by lower-case letters. Capital letters denote significant differences between the substrate addition at identical level.

**TABLE 1 |** Position and site characteristics were adapted from Lang et al. (2017).

| **Position and site characteristics** | | | |
|---|---|---|---|
| | | **Mitterfels** | **Luess** |
| Gauss-krueger | Easting | 4564502 | 3585473 |
| Coordinates | Northing | 5426906 | 5857057 |
| | m.a.s.l (m) | 1299 | 115 |
| Annual mean temperature | (°C) | 4.5 | 8 |
| Annual precipitation | (mm) | 1299 | 779 |
| **Forest stand** | | | |
| Main tree | | European beech | European beech |
| Species | | Fagus sylvatica | Fagus sylvatica |
| **Soil** | | | |
| Soil type | | Hyperdystric chromic | Hyperdystric folic |
| WRB 2014 | | Folic cambisol | Cambisol |
| Humus layer | | Moder | More-like moder |
| Parent material | | Paragneis | Sandy till |
| Microbial biomass C | ($\mu g\ g^{-1}$) | 795 | 192 |
| Soil organic C | ($mg\ g^{-1}$) | 175 | 92 |
| Total soil N | ($mg\ g^{-1}$) | 10 | 4 |
| Total soil P | ($mg\ kg^{-1}$) | 1281 | 178 |

*Soil microbial biomass content was adapted from Bergkemper et al. (2016), and determined by chloroform fumigation extraction. All other soil parameter, such as soil organic C and total N and P content were measured in the Ah horizon before incubation was started. Aboveground and belowground P pools of ecosystems reflect the current state of interactions between P availability of soils and P uptake and usage by plants and microorganisms occurring at these sites (Lang et al., 2017).*

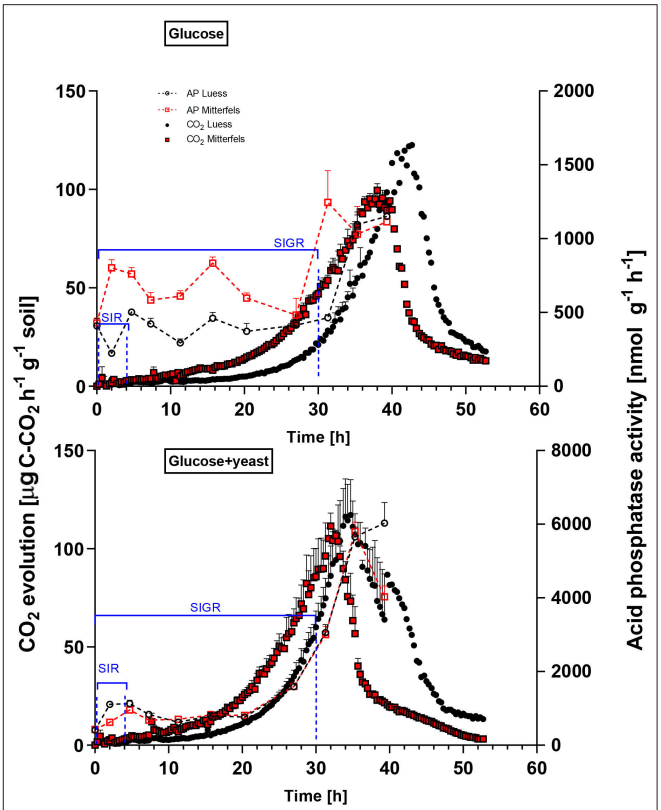


**FIGURE 4 |** Microbial growth curves and potential enzyme activities (dotted lines) are shown including SEM for soils treated with glucose vs. glucose + yeast extract. The nutrient-poor soil is denoted by black circles, whereas nutrient-rich soil is highlighted in red squares. The values given at time point zero, reflected the control, namely without the addition of any substrate. The time interval chosen for calculation of SIR are denoted in blue brackets. For kinetic parameters of SIGR, the whole curve including lag phase is required for modeling, which is also shown in blue.

extract. The active microbial biomass proportion increased by 5% and the lag time shortened by 4 h in nutrient-rich soil (**Table 1**). The dsDNA-derived microbial biomass C content during the first 10 h after substrate addition (taken as an average) was slightly higher when the glucose + yeast extract was added irrespective of the soil. This was in line with the faster specific growth rate of microorganisms in nutrient-poor soil (**Figure 4**).

β-glucosidases and NAG demonstrated higher activity in nutrient-rich than in nutrient-poor soil prior substrate addition ($t = 0$) (**Figure 5**). After glucose addition, activity of β-glucosidases did not increase during exponential microbial growth in nutrient-rich soil (MIT) (**Figure 5**), indicating stable enzymatic functioning on C utilization throughout experimental duration. However, β-glucosidase demonstrated strong response to glucose addition in nutrient-poor soil (LUE), by increasing activity during exponential growth of microorganisms. Correspondingly, the $CO_2$ efflux increased in nutrient-poor soil (**Figure 4**).

Activity of β-glucosidase and acid phosphatase increased with microbial growth curves when the glucose + yeast extract was added and reached the maximum in the phase of microbial retardation. Acid phosphatase activity showed more steady time constraint after the glucose + yeast extract addition compared

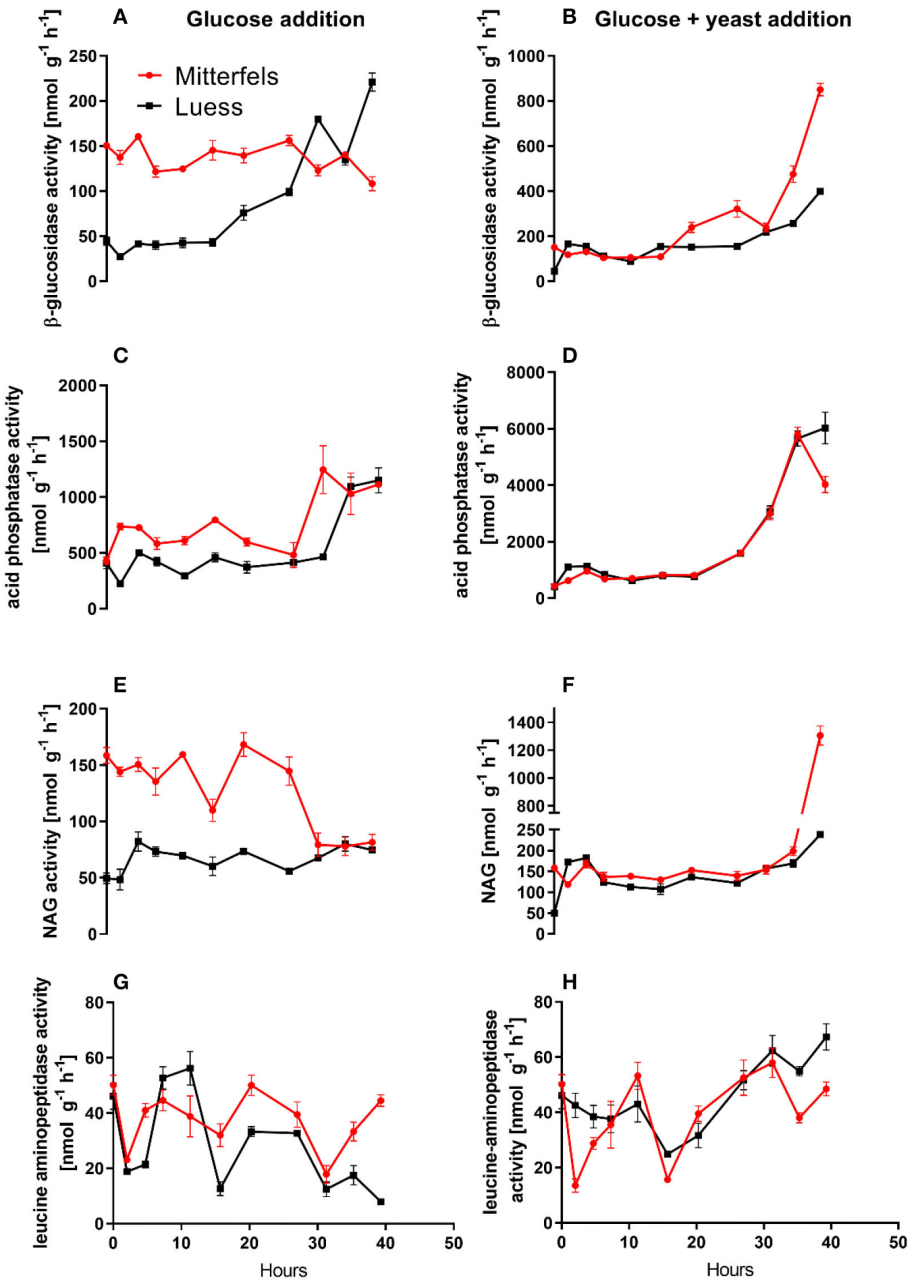


**FIGURE 5 |** Potential activities ($V_{max}$) including standard error of mean of C- N- and P-cycling enzymes during microbial growth and retardation. **(A,B)** beta-glucosidase, **(C,D)** acid phosphatase, **(E,F)** NAG, **(G,H)** leucine-aminopeptidase.

to the amendment of sole glucose. Moreover, we found stronger responses of enzymes and their substrate turnover times in nutrient-poor than in nutrient-rich soil. The additional substrate input of yeast extract induced a greater shortage of substrate turnover time in nutrient-poor soil (**Figure 8**), which was in line with a faster microbial growth rate (**Figure 3**). Overall, the turnover time was enzyme-specific, being the shortest for acid phosphatase and the longest for leucine aminopeptidases during both, lag time and exponential growth (**Table 2**).

## Self- and Cross- Correlation

Single substrate addition increased the self-correlation of acid phosphatase (till a lag of 3 h) more in nutrient-poor than in nutrient-rich soil (**Figure 6**), reflecting increased predictability of enzyme activities during microbial growth because of the stability of kinetic reaction parameters such as the Michaelis-Menten constant. The glucose + yeast extract addition increased autocorrelation length of acid phosphatase in both soils (**Figure 6**). In comparison, β-glucosidase exhibited contrasting

**TABLE 2 |** Microbial growth respiration parameters, such as lag phase ($T_{lag}$), actively growing microbial biomass (MB) according to Panikov (1995) and substrate-induced respiration derived microbial biomass content after Anderson and Domsch (1986) including the conversion factor used by Kaiser et al. (1992).

| | $T_{lag}$ (h) | Growing MB (μg C/g) | Growing MB (%) | SIR-derived MB (μg C/g) |
|---|---|---|---|---|
| **Glucose** | | | | |
| Nutrient-poor soil (LUE) | 18a | 4b | 0.3 | 1263a |
| Nutrient-rich soil (Mit) | 12a | 49a | 3.9 | 2258a |
| **Glucose+yeast** | | | | |
| Nutrient-poor soil (LUE) | 12a | 13a | 1.0 | 1411a |
| Nutrient-rich soil (MIT) | 8a | 63a | 5.0 | 2083a |

*Significant differences between glucose and glucose + yeast extract were denoted by lower-capital letters ($P < 0.05$).*

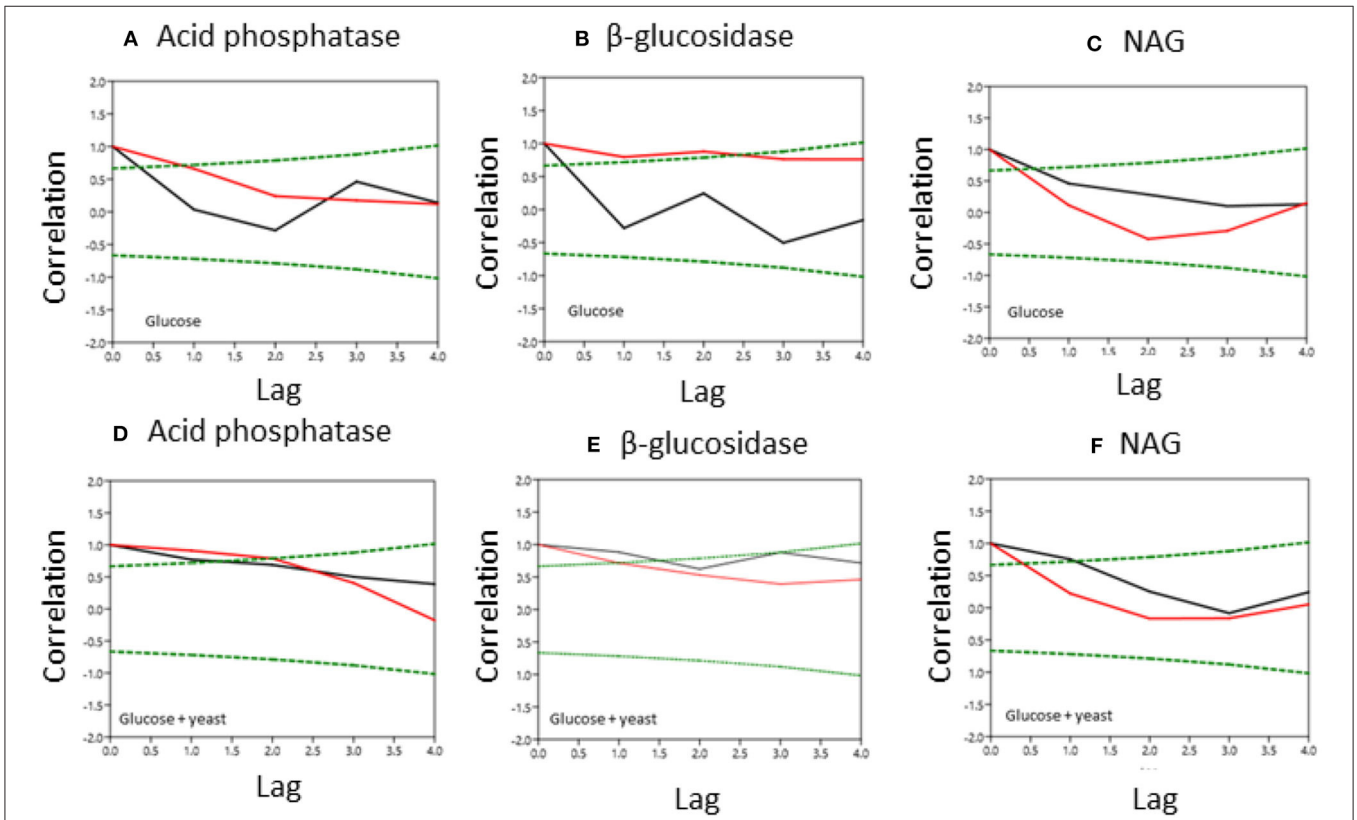


**FIGURE 6 |** Normalized covariance function of enzyme activities during microbial growth in nutrient-poor (black line) and nutrient-rich (red line) soils. Upper graphs show glucose amendment and below graphs depict glucose + yeast extract. The x-axis shows the lag in hours and y-axis the correlation coefficient. The green dashed line denotes the confidence bands ($P < 0.05$), reflecting the significant confidence interval of autocorrelation. **(A, D)** acid phosphatase, **(B,E)** beta-glucosidase; **(C,F)** NAG.

time constraints by glucose addition, where only nutrient-poor soil was stable ($r \sim 0.6$ at lag 3 h). Adding both substrates the autocorrelation of β-glucosidase revealed $r > 0.4$, accounting a lag of 2 h at each of the sites.

To test for similarities between the sites cross-correlation of enzyme activities was performed. Cross-correlation of acid phosphatase activity between nutrient-rich and nutrient-poor soil revealed a significant ($P < 0.05$) relation till a lag of −1.5 h for both sites by adding glucose (**Figure 7**). However, for the glucose + yeast extract, the cross-correlation of acid phosphatase between nutrient-poor and nutrient-rich soil was highly significant till a lag of −1.5 h and also to a lag of 1.5 h between the two site, indicating harmonized time constraints of acid phosphatase during the phase of microbial growth. Strongest cross-correlation between nutrient-poor and nutrient-rich soil was exhibited for the C-cycling enzyme β-glucosidase reflecting a high degree of similarity of the two time series between the sites during exponential growth of

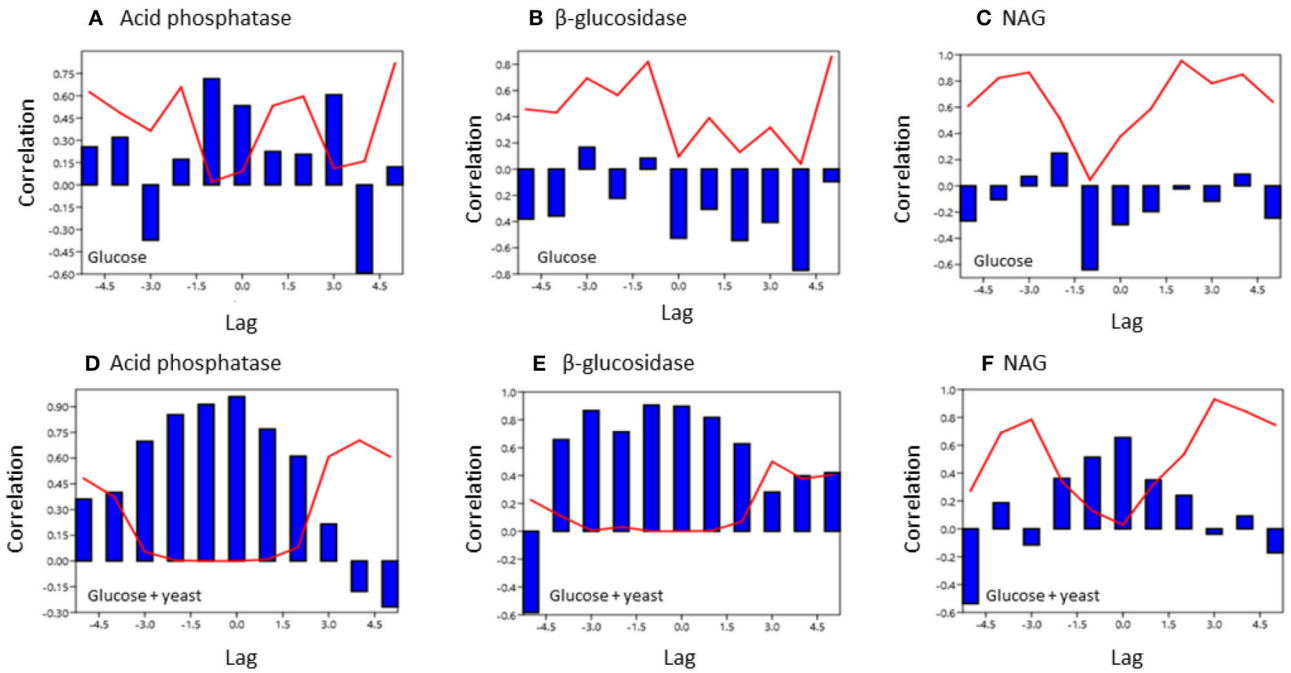


**FIGURE 7 |** Cross covariance function of enzyme activities during microbial growth was computed between the two soils of contrasting nutrient content. The x-axis shows the lag in hours and y-axis the correlation coefficient. The red line denotes the level of significance ($P < 0.05$) at a specific lag. **(A,D)** acid phosphatase, **(B,E)** beta-glucosidase; **(C,F)** NAG.

microorganisms ($r > 0.6$ up to a lag of −3 h; $P < 0.05$) (**Figure 7**).

# DISCUSSION

## Microbial Growth After Substrate Addition in Contrasting Forest Soils

During non-steady state of microbial growth, we detected higher microbial biomass and higher proportion of growing microbial biomass along with a shorter lag time in nutrient-rich than in nutrient-poor soil, which reflected a well-adapted microbial response to the added substrate as well as the higher initial nutrient stock (Loeppmann et al., 2016a,b; Lang et al., 2017). However, the maximum specific growth rate of microorganisms was higher in nutrient-poor soil, indicating faster growing microorganisms than in nutrient-rich soil. The fact that most microbial groups existed at both sites (43% of identified microbial groups) (Bergkemper et al., 2016) does not necessarily imply that the communities were similar. Nevertheless, we assume a high sustainability potential due to broad microbial diversity independent from the soil nutrient status. However, significant differences of microbial specific growth rates between sites indicated wide disparity in microbial community structure (Fuhrman, 2009). This reflects the high abundance of unique bacterial groups in nutrient-poor soil, which points to a specific adaption of the community to P limitation at this site (Bergkemper et al., 2016). Despite the fact that specific growth rate reflects the respiratory response of microbial community as a whole (Panikov, 1995; Panikov and Sizova, 1996), it mainly characterizes a few or even single microbial assemblies dominating competition for a single input of glucose (Mau et al., 2015). As single glucose addition is insufficient to activate large number of glucose-metabolizing taxa (Mau et al., 2015), the SIGR approach does not alter functional structure of the community and it simulates an occasional input of available substrate under conditions of substrate excess (Ehlers et al., 2010).

The glucose + yeast extract addition increased the specific growth rate of microbes by 15% solely in the nutrient-rich soil (**Figure 3**). We did not reveal any repression of respiration by CCR (Deutscher, 2008) compared with sole glucose addition, presumably due to relatively low input of yeast extract insufficient to initiate microbial growth. In contrast, glucose was quickly metabolized during exponential growth causing microbial starvation and growth retardation instead of catabolite repression. Another explanation could be that CCR occurred in a very short-term immediately after substrate addition to soil. We revealed that glucose repressed an activity of enzymes related to cleavage of carbohydrates and proteins but only in short-term (10 h). This infers that those bacteria affected by CCR may be easily outcompeted by other microorganisms during phase of exponential growth. In addition, the enzyme activity was more stable (smooth) and more synchronous with $CO_2$ evolution with the amendment of glucose + yeast extract indicating an absence of catabolic repression.

The addition of yeast extract along with glucose to nutrient-poor soil increased maximum specific growth rate, shortened

the lag phase and enhanced the portion of growing microbial biomass compared to the amendment of glucose. This clearly indicated that the substrate diversity and quality are of great importance during lag and exponential microbial growth. We determined 2–3-times higher potential $\beta$-glucosidase, acid phosphatase and NAG activity in nutrient-rich than in nutrient-poor soil with the addition of glucose. As a result of NAG activity, amino sugars derived from peptidoglycan (bacterial cell walls, e.g., microbial necromass) and chitin (fungal cell walls) decomposition could have contributed substantially to the

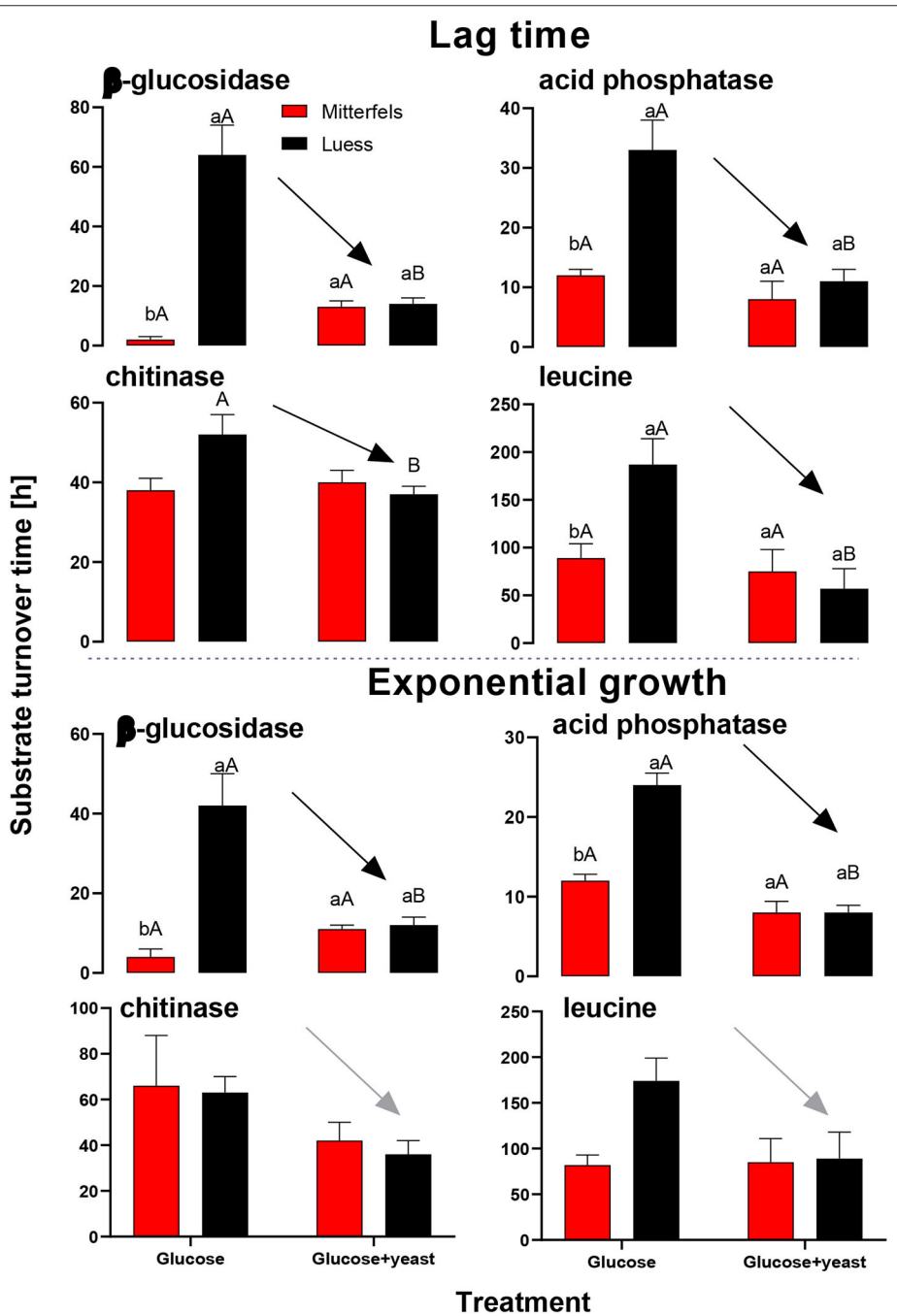


**FIGURE 8 |** Substrate turnover time of C-, N-, and P-cycling extracellular enzymes during lag phase and exponential growth of microorganisms according to Tischer et al. (2015). The nutrient-poor site is shown by black and the nutrient-rich by red bars. As substrates either glucose or the combination of glucose and yeast extract was added to two soils of nutrient stocks (**Table 1**). Significant differences between substrate addition were denoted by capital letters at a level of significance of $P < 0.05$. Lower letters indicate the significant differences between the sites at identical level.

dissolved organic N pool (Hu et al., 2018) and subsequently fueling microbial demands (Geisseler et al., 2009).

Limitations in gene expression may play a role in generating phenotypic diversity, which is advantageous in fluctuating environments, at the expenses of decreasing growth rates (Kim et al., 2020). Since acid phosphatases have been shown to correlate with the soil microbial C content and with abundance of bacterial phoN genes in the field (Spohn et al., 2018), we assume optimized trade-offs between resource allocation and growth of microorganisms.

By the addition of glucose + yeast extract, the lag phase of growing microorganisms shortened irrespective of the initial nutrient content (**Table 2**), reflecting an advanced adaptation to the newly available resources, fueling a balanced, and less stressed metabolic network (Hamill et al., 2020). However, the substrate turnover time of C-, N-, and P-cycling extracellular enzymes during lag phase and exponential growth of microorganisms was stable in nutrient-rich soil, whereas the substrate turnover time of enzymes was strongly shortened in nutrient-poor soil (**Figure 8**). This indicates that organic nutrients derived from the yeast extract were the preferential source to overcome microbial resource scarcity only in nutrient-poor soil.

The dsDNA-derived microbial biomass in nutrient-poor soil was close to the one of nutrient-rich soil (**Figure 9**), reflecting stronger activation potential of microorganisms in soil of lower initial MBC content. This was in line with the faster specific growth rate of microorganisms in nutrient-poor soil.

Microbial growth is often preceded by adapting the physiological state of the microbial cells, during the lag phase (Madar et al., 2013). A recent study on single cells has revealed that individual bacteria vary in the time required to reach first cell division (Bertrand, 2019) and that with increasing number of stressed or nutrient limited cells, the lag phase becomes longer and the time-points at which individual cells begin dividing show increased scattering (Smelt et al., 2002; Guillier et al., 2006).

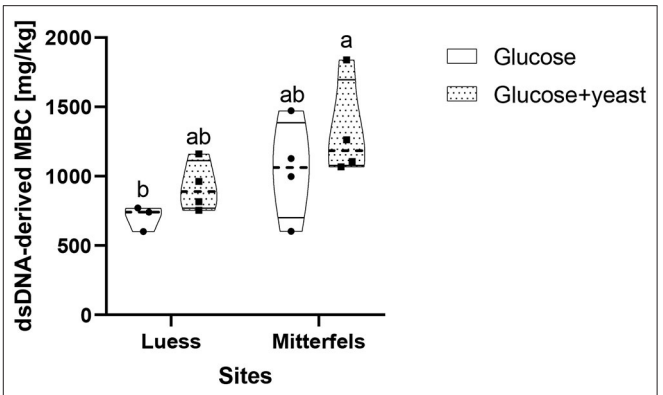


**FIGURE 9 |** Violin plot of dsDNA-derived microbial biomass C (MBC) content during the first 10 h after substrate addition for nutrient-poor soil (Luess) and nutrient-rich soil (Mitterfels). The dashed line shows the median of MBC, the dots denote the replicates and the thin black line the quartiles. The lower-capital letter depicts the significant differences between sites at a level of 0.1.

## Enzyme Activities During the Phase of Microbial Growth

Acid phosphatase activity increased during microbial growth in both, nutrient-rich and nutrient-poor soil. The maximum of potential acid phosphatase activities was reached in the phase of microbial growth retardation. This may be explained by the active excretion of phosphatases or their release by cell lysis after death, which reflect a crucial portion in the build-up of indigenous soil phosphatase activity (Jarosch et al., 2019). When microbes start to mine for nutrients, they invest in enzyme production related to their specific needs. Many different pathways of organics' degradation, including amino acid, glycolytic, and fatty acid pathways, utilize enzyme cascades processing a broad range of substrates, which increases the chance of microbial recycling of dead cell residues. Therefore, in order to avoid the detection of $CO_2$ derived from microbial recycling experimental our duration was kept short.

The substrate turnover time was enzyme-specific and ranged from hours to days. During microbial growth substrate turnover of enzymes was shorter than reported from the field (natural forest) under steady state, ranging from 0.6 days for acid phosphatase to 646 days for α-glucosidase (Tischer et al., 2015). The addition of glucose + yeast extract increased β-glucosidase and NAG activity during lag phase exclusively in nutrient-poor soil. Strongest effects on activities and estimated substrate turnover time of enzymes were detected in nutrient-poor soil when both substrates were added in combination, implying a strong affinity to these substrates and therefore, an adequate strategy on the recycling of organic compounds.

By adding the substrate combination cross-correlation of β-glucosidase and acid phosphatase between the two sites demonstrated harmonized time constraints, which reflected the establishment of comparable and balanced enzymatic systems for substrate utilization during lag time. Consequently, accelerating nutrient acquisition to maintain microbial growth, irrespective of contrasting soil properties, and initial nutrient stocks, was demonstrated by the temporal interpolation between their measured values. This clearly indicates similar tradeoffs of C- and P- cycling enzymes in both soils reflecting comparable temporal dynamics of enzyme activities in nutrient-poor and nutrient-rich soil during the phase of microbial growth when the glucose + yeast extract was added. Due to the individual composition of compound-classes of different decomposability, necromass of different microbial groups, such as yeast residues, reflect a wide range of decomposition rates (Six et al., 2006). Despite the different decomposability of microbial cell wall components during microbial steady state, no difference in the mean residence time of necromass C in soil among bacteria, actinobacteria, and fungi was found (Throckmorton et al., 2012). Here, during microbial non-steady state conditions a faster microbial turnover was present in nutrient-poor soil suggesting faster recycling of microbial necromass-derived nutrients and reduced necromass C stabilization in nutrient-poor than in nutrient-rich forest soils.

## SUMMARY

Up to 34% faster specific growth rates of microorganisms, albeit of a small proportion of actively growing microbial biomass, were revealed in nutrient-poor than in nutrient-rich soil. This clearly showed the fast adaptation and activation of microorganisms, able to quickly uptake and grow fast on the sudden (single) substrate input. Therefore, a faster microbial turnover occurred in nutrient-poor soil, which shifted microbial substrate utilization and resulted in a shortened lag phase of microbial growth, irrespective of the initial soil nutrient status, because faster microbial activation and nutrient acquisition dynamics in the presence of additional microbial residues i.e., yeast extract took place. This was in line with a strong reduction of substrate turnover time of all enzymes in nutrient-poor soil. Cross-correlation analysis of enzyme activities between the two sites demonstrated harmonized time constraints of enzyme systems which reflected the establishment of comparable and balanced enzymatic systems within the decomposition network. This became evident as similar tradeoffs of C- and P- cycling enzymes occurred in both soils. However, significant differences in microbial community structure, due to high abundance of unique bacterial groups in nutrient-poor soil, indicated a specific adaption of the community to P limitation at this site. Glucose repressed an activity of enzymes related to cleavage of carbohydrates and proteins only in short-term (10 h), inferring that those bacteria affected by catabolic repression may be easily outcompeted by other soil microorganisms during exponential growth. Especially, β-glucosidase and acid phosphatase underlined an activity synchronous with $CO_2$ evolution when glucose + yeast extract was added, which indicates an absence of bacterial catabolic repression during microbial growth in soil.

## DATA AVAILABILITY STATEMENT

All datasets generated for this study are included in the article/supplementary material.

## AUTHOR CONTRIBUTIONS

EB and SL developed an idea. EB, SL, and MD developed the project and contributed to the interpretation of the results. SL, AB, and SS wrote the manuscript, which was read and revised by all co-authors. SL performed statistics and data evaluation with support by SS. All authors listed have made a substantial, direct and intellectual contributions to the work, and approved it for publication.

## FUNDING

Financial support was provided by the Deutsche Forschungsgemeinschaft (DFG) and acknowledge the experimental design of the Priority (Ecosystem nutrition: forest strategies for limited phosphorus resources, SPP1685) by grants to SS 200021E- 171173 and M.D. (DFG, DI 2136/6). The publication was prepared with the support of the RUDN University program 5-100. We acknowledge financial support by DFG within the funding programme Open Access Publizieren.

## REFERENCES

Anderson, T.-H., and Domsch, K. H. (1986). Carbon assimilation and microbial activity in soil. *Zeitschrift Für Pflanzenernährung Und Bodenkunde*, 149, 457–468. doi: 10.1002/jpln.19861490409

Anderson, T.-H., and Joergensen, R. G. (1997). Relationship between SIR and FE estimates of microbial biomass C in deciduous forest soils at different pH. *Soil Biol. Biochem.* 29, 1033–1042. doi: 10.1016/S0038-0717(97)00011-4

Anderson, T. H., and Martens, R. (2013). DNA determinations during growth of soil microbial biomasses. *Soil Biol. Biochem.* 57, 487–495. doi: 10.1016/j.soilbio.2012.09.031

Baldrian, P., Kolarík, M., Štursová, M., Kopecký, J., Valášková, V., Větrovský, T., et al. (2012). Active and total microbial communities in forest soil are largely different and highly stratified during decomposition. *ISME J.*6, 248–258. doi: 10.1038/ismej.2011.95

Bardgett, R. D., and Putten, W. H. (2014). Belowground biodiversity and ecosystem functioning. *Nature* 515, 505–511. doi: 10.1038/nature13855

Bartnicki-Garcia, S., and Nickerson, W. J. (1962). Isolation, composition, and structure of cell walls of filamentous and yeast-like forms of Mucor rouxii. *Biochim. et Biophys. Acta* 58, 102–119. doi: 10.1016/0006-3002(62)90822-3

Bergkemper, F., Welzl, G., Lang, F., Krüger, J., Schloter, M., and Schulz, S. (2016). The importance of C, N and P as driver for bacterial community structure in German beech dominated forest soils. *J. Plant Nutrit. Soil Sci.* 179, 472–480. doi: 10.1002/jpln.201600077

Bertrand, R. L. (2019). Lag phase - a dynamic, organized, adaptive, and evolvable period that prepares bacteria for cell division. *J. Bacteriol.* 201:e00697-18. doi: 10.1128/JB.00697-18

Blagodatskaya, E., and Kuzyakov, Y. (2013). Active microorganisms in soil: critical review of estimation criteria and approaches. *Soil Biol. Biochem.* 67, 192–211. doi: 10.1016/j.soilbio.2013.08.024

Blagodatsky, S. A., Heinemeyer, O., and Richter, J. (2000). Estimating the active and total soil microbial biomass by kinetic respiration analysis. *Biol. Fertil. Soils* 32, 73–81. doi: 10.1007/s003740000219

Blifernez-Klassen, O., Klassen, V., Doebbe, A., Kersting, K., Grimm, P., Wobbe, L., et al. (2012). Cellulose degradation and assimilation by the unicellular phototrophic eukaryote Chlamydomonas reinhardtii. *Nat. Commun.* 3:1214. doi: 10.1038/ncomms2210

Deutscher, J. (2008). The mechanisms of carbon catabolite repression in bacteria. *Curr. Opin. Microbiol.* 11, 87–93. doi: 10.1016/j.mib.2008.02.007

Ehlers, K., Bakken, L. R., Frostegård, Å., Frossard, E., and Bünemann, E. K. (2010). Phosphorus limitation in a Ferralsol: impact on microbial activity and cell internal P pools. *Soil Biol. Biochem.* 42, 558–566. doi: 10.1016/j.soilbio.2009.11.025

Fehlhaber, K., and Krüger, G. (1998). The study of Salmonella enteritidis growth kinetics using rapid automated bacterial impedance technique. *J. Appl. Microbiol.* 84, 945–949. doi: 10.1046/j.1365-2672.1998.00410.x

Fuhrman, J. A. (2009). Microbial community structure and its functional implications. *Nature* 459, 193–199. doi: 10.1038/nature08058

Geisseler, D., Horwath, W. R., and Doane, T. A. (2009). Significance of organic nitrogen uptake from plant residues by soil microorganisms as affected by carbon and nitrogen availability. *Soil Biol. Biochem.* 41, 1281–1288. doi: 10.1016/j.soilbio.2009.03.014

Görke, B., and Stülke, J. (2008). Carbon catabolite repression in bacteria: many ways to make the most out of nutrients. *Nat. Rev. Microbiol.* 6, 613–624. doi: 10.1038/nrmicro1932

Guillier, L., Pardon,. P., and Augustin, J. C. (2006). Automated image analysis of bacterial colony growth as a tool to study individual lag time distributions of immobilized cells. *J. Microbiol. Meth.* 65, 324–334. doi: 10.1016/j.mimet.2005.08.007

Hamill, P. G., Stevenson, A., McMullan, P. E., Lewis, A. D. R., Sudharsan, S., Stevenson, K. E., et al. (2020). Microbial lag phase can be indicative of, or independent from, cellular stress. *Sci Rep*. 10:5948. doi: 10.1038/s41598-020-62552-4

Hammer, Ø., and Harper, D. A. T. (2006). PAST. Paleontological statistics. version 2.07. *Reference manual. Blackwell Publ.* 351. doi: 10.1016/j.bcp.2008.05.025

Heinemeyer, O., Insam, H., Kaiser, E. A., and Walenzik, G. (1989). Soil microbial biomass and respiration measurements: an automated technique based on infra-red gas analysis. *Plant Soil* 116, 191–195. doi: 10.1007/BF02214547

Hu, Y., Zheng, Q., Zhang, S., Noll, L., and Wanek, W. (2018). Significant release and microbial utilization of amino sugars and D-amino acid enantiomers from microbial cell wall decomposition in soils. *Soil Biol. Biochem.* 123, 115–125. doi: 10.1016/j.soilbio.2018.04.024

Jansson, J. K., and Prosser, J. I. (2013). Microbiology: the life beneath our feet. *Nature* 494, 40–41. doi: 10.1038/494040a

Jarosch, K. A., Kandeler, E., Frossard, E., and Bünemann, E. K. (2019). Is the enzymatic hydrolysis of soil organic phosphorus compounds limited by enzyme or substrate availability? *Soil Biol. Biochem.* 139:107628. doi: 10.1016/j.soilbio.2019.107628

Jobbágy, E. G., and Jackson, R. B. (2000). The vertical distribution of soil organic carbon and its relation to climate and vegetation. *Ecol. Appl.* 10, 423–436. doi: 10.1890/1051-0761(2000)0100423:TVDOSO2.0.CO;2

Kaiser, E. A., Mueller, T., Joergensen, R. G., Insam, H., and Heinemeye, O. (1992). Evaluation of methods to estimate the soil microbial biomass and the relationship with soil texture and organic matter. *Soil Biol. Biochem*. 24, 675–683. doi: 10.1016/0038-0717(92)90046-Z

Kim, J., Darlington, A., Salvador, M., Utrilla, J., and Jiménez, J. I. (2020). Trade-offs between gene expression, growth and phenotypic diversity in microbial populations. *Curr. Opin. Biotechnol.* 62, 29–37. doi: 10.1016/j.copbio.2019.08.004

Kowalchuk, G. A., and Stephen, J. R. (2001). Ammonia-oxidizing bacteria: a model for molecular microbial ecology. *Ann. Rev. Microbiol.* 55, 485–529. doi: 10.1146/annurev.micro.55.1.485

Lamanna, C., Blonder, B., Violle, C., Kraft, N. J., Sandel, B., Šímová, I., et al. (2014). Functional trait space and the latitudinal diversity gradient. *Proc. Natl. Acad. Sci.U.S.A.* 111, 13745–13750. doi: 10.1073/pnas.1317722111

Landi, L., Renella, G., Giagnoni, L., and Nannipieri, P. (2011). Activities of proteolytic enzymes. *Methods soil enzymology*, 9, 247–260.

Lang, F., Bauhus, J., Frossard, E., George, E., Kaiser, K., Kaupenjohann, M., et al. (2016). Phosphorus in forest ecosystems: new insights from an ecosystem nutrition perspective. *J. Plant Nut. Soil Sci.* 179, 129–135. doi: 10.1002/jpln.201500541

Lang, F., Krüger, J., Amelung, W., Willbold, S., Frossard, E., Bünemann, E. K., et al. (2017). Soil phosphorus supply controls, P., nutrition strategies of beech forest ecosystems in Central Europe. *Biogeochemistry* 136, 5–29. doi: 10.1007/s10533-017-0375-0

Larionova, A. A., Yevdokimov, I. V., and Bykhovets, S. S. (2007). Temperature response of soil respiration is dependent on concentration of readily decomposable C. *Biogeosciences* 4, 1073–1081. doi: 10.5194/bg-4-1073-2007

Lauber, C. L., Strickland, M. S., Bradford, M. A., and Fierer, N. (2008). The influence of soil properties on the structure of bacterial and fungal communities across land-use types. *Soil Biol. Biochem.* 40, 2407–2415. doi: 10.1016/j.soilbio.2008.05.021

Lennon, J. T., and Jones, S. E. (2011). Microbial seed banks: the ecological and evolutionary implications of dormancy. *Nat. Rev. Microbiol.* 9, 119–130. doi: 10.1038/nrmicro2504

Liang, C., Cheng, G., Wixon, D. L., and Balser, T. C. (2011). An Absorbing Markov Chain approach to understanding the microbial role in soil carbon stabilization. *Biogeochemistry* 106, 303–309. doi: 10.1007/s10533-010-9525-3

Liu, M., Durfee T., Cabrera, J., Zhao, K., Jin, D. J., and Blattner, G. R. (2005). Global transcriptional programs reveal a carbon source foraging strategy by *Escherichia coli*. *J. Biol. Chem*. 280, 15921–15927. doi: 10.1074/jbc.M414050200

Loeppmann, S., Blagodatskaya, E., Pausch, J., and Kuzyakov, K. (2016b). Substrate quality affects kinetics and catalytic efficiency of exo-enzymes in rhizosphere and detritusphere. *Soil Biol. Biochem.* 92, 111–118. doi: 10.1016/j.soilbio.2015.09.020

Loeppmann, S., Semenov, M., Blagodatskaya, E., and Kuzyakov, Y. (2016a). Substrate quality affects microbial- and enzyme activities in rooted soil. *J. Plant Nut. Soil Sci.* 179, 39–47. doi: 10.1002/jpln.201400518

Loeppmann, S., Semenov, M., Kuzyakov, Y., and Blagodatskaya, E. (2018). Shift from dormancy to microbial growth revealed by RNA: DNA ratio. *Ecol. Indicat.* 85, 603–612. doi: 10.1016/j.ecolind.2017.11.020

Louca, S., Polz, M. F., Mazel, F., Albright, M. B., Huber, J. A., O'Connor, M. I., et al. (2018). Function and functional redundancy in microbial systems. *Nat. Ecol. Evol.* 2, 936–943. doi: 10.1038/s41559-018-0519-1

Madar, D., Dekel, E., Bren, A., Zimmer, A., Porat, Z., and Alon, U. (2013). Promoter activity dynamics in the lag phase of *Escherichia coli*. *BMC Syst. Biol.* 7:136. doi: 10.1186/1752-0509-7-136

Maksimova, I. A., and Chernov, I. Y. (2004). Community structure of yeast fungi in forest biogeocenoses. *Microbiology* 73, 474–481. doi: 10.1023/B:MICI.0000036994.21650.3a

Mau, R. L., Liu, C. M., Aziz, M., Schwartz, E., Dijkstra, P., Marks, J. C., et al. (2015). Linking soil bacterial biodiversity and soil carbon stability. *ISME J.* 9, 1477–1480. doi: 10.1038/ismej.2014.205

Miller, S. E. (1979). Univariate residual cross-correlation analysis: an application to beef prices. *North Central J. Agri. Econ.* 141–146. doi: 10.2307/1349421

Miltner, A., Bombach, P., Schmidt-Brücken, B., and Kästner, M. (2012). SOM genesis: microbial biomass as a significant source. *Biogeochemistry* 111, 41–55. doi: 10.1007/s10533-011-9658-z

Nannipieri, P., Giagnoni, L., Renella, G., Puglisi, E., Ceccanti, B., Masciandaro, G., et al. (2012). Soil enzymology: classical and molecular approaches. *Biol. Fert. Soils* 48, 743–762. doi: 10.1007/s00374-012-0723-0

Ottow, J. C. (2011). Ottow, J. C. (2011). *Mikrobiologie von Böden: Biodiversität, Ökophysiologie und Metagenomik*. Springer-Verlag.

Panikov, N. S. (1991). *Kinetika rosta mikroorganizmov*. Nauka Moscow, 117–118.

Panikov, N. S. (1995). *Microbial Growth Kinetics*. Chapman Hall: London.

Panikov, N. S., and Sizova, M. V. (1996). A kinetic method for estimating the biomass of microbial functional groups in soil. *J. Microbiol. Methods* 24, 219–230. doi: 10.1016/0167-7012(95)00074-7

Park, Y. H., Lee, B. R., Seok, Y. J., and Peterkofsky, A. (2006). *In vitro* reconstitution of catabolite repression in *Escherichia coli*. *J. Biol. Chem.* 281, 6448–6454. doi: 10.1074/jbc.M512672200

Petchey, O., and Kevin, L., Gaston, J. (2006). Functional diversity: back to basics and looking forward. *Ecol. Lett.* 9, 741–758. doi: 10.1111/j.1461-0248.2006.00924.x

Podobnik, B., and Stanley, H. E. (2008). Detrended cross-correlation analysis: a new method for analyzing two nonstationary time series. *Phys. Rev. Lett.* 100:084102. doi: 10.1103/PhysRevLett.100.084102

Pronk, J. T. (2002). MINIREVIEWS auxotrophic yeast strains in fundamental and applied research. *Appl. Environ. Microbiol.* 68, 2095–2100. doi: 10.1128/AEM.68.5.2095-2100.2002

Roszak, D. B., and Colwell, R. R. (1987). Survival strategies of bacteria in the natural environment. *Microbiol. Rev.* 51:365. doi: 10.1128/MMBR.51.3.365-379.1987

Shumway, R. H., and Stoffer, D. S. (2017). *Time Series Analysis and its Applications: with R Examples*. Springer. doi: 10.1007/978-3-319-52452-8

Sinsabaugh, R. L., Hill, B. H., Shah, J. J. F., and Follstad Shah, J. J. (2010). Ecoenzymatic stoichiometry of microbial organic nutrient acquisition in soil and sediment. *Nature* 468:122. doi: 10.1038/nature09548

Six, J., Frey, S. D., Thiet, R. K., and Batten, K. M. (2006). Bacterial and fungal contributions to carbon sequestration in agroecosystems. *Soil Sci. Soc. Am. J.* 70, 555–569. doi: 10.2136/sssaj2004.0347

Smelt, J. P., Otten, G. D., and Bos, A. P. (2002). Modelling the effect of sublethal injury on the distribution of the lag times of individual cells of Lactobacillus plantarum. *Int. J. Food Microbiol.* 73, 207–212. doi: 10.1016/S0168-1605(01)00651-1

Spohn, M., Zavišić, A., Nassal, P., Bergkemper, F., Schulz, S., Marhan, S., et al. (2018). Temporal variations of phosphorus uptake by soil microbial biomass and young beech trees in two forest soils with contrasting phosphorus stocks. *Soil Biol. Biochem.* 117, 191–202. doi: 10.1016/j.soilbio.2017.10.019

Stemmer, M. (2004). Multiple-substrate enzyme assays: a useful approach for profiling enzyme activity in soils? *Soil Biol. Biochem.* 36, 519–527. doi: 10.1016/j.soilbio.2003.11.004

Throckmorton, H. M., Bird, J. A., Dane, L., Firestone, M. K., and Horwath, W. R. (2012). The source of microbial C has little impact on soil organic matter stabilisation in forest ecosystems. *Ecol. Lett.* 15, 1257–1265. doi: 10.1111/j.1461-0248.2012.01848.x

Tischer, A., Blagodatskaya, E., and Hamer, U. (2015). Microbial community structure and resource availability drive the catalytic efficiency of soil enzymes under land-use change conditions. *Soil Biol. Biochem.* 89, 226–237. doi: 10.1016/j.soilbio.2015.07.011

van den Berg, H. A. (2001). How microbes can achieve balanced growth in a fluctuating environment. *Acta Biotheor.* 49, 1–21. doi: 10.1023/A:1010267821884

Wagg, C., Schlaeppi, K., Banerjee, S., Kuramae, E. E., and van der Heijden, M. G. (2019). Fungal-bacterial diversity and microbiome complexity predict ecosystem functioning. *Nat. Commun.* 10:4841. doi: 10.1038/s41467-019-12798-y

Wallenstein, M. D., and Burns, R. G. (2011). Ecology of extracellular enzyme activities and organic matter degradation in soil: a complex community-driven process. *Methods Soil Enzymol.* 9, 35–55. doi: 10.2136/sssabookser9.c2

Weintraub, M. N., and Schimel, J. P. (2005). Seasonal protein dynamics in Alaskan arctic tundra soils. *Soil Biol. Biochem.* 37, 1469–1475. doi: 10.1016/j.soilbio.2005.01.005

Wutzler, T., Blagodatsky, S. A., Blagodatskaya, E., and Kuzyakov, Y. (2012). Soil microbial biomass and its activity estimated by kinetic respiration analysis - statistical guidelines. *Soil Biol. Biochem.* 45, 102–112. doi: 10.1016/j.soilbio.2011.10.004

**Conflict of Interest:** The authors declare that the research was conducted in the absence of any commercial or financial relationships that could be construed as a potential conflict of interest.

frontiers in Forests and Global Change

ORIGINAL RESEARCH
published: 23 September 2020
doi: 10.3389/ffgc.2020.535397

# Impact of Climate Change on Soil Hydro-Climatic Conditions and Base Cations Weathering Rates in Forested Watersheds in Eastern Canada

*Daniel Houle[1,2]*, Charles Marty[3], Fougère Augustin[4,5], Gérald Dermont[6] and Christian Gagnon[1]*

*[1] Science and Technology Branch, Environment Canada and Climate Change, Montreal, QC, Canada, [2] Ouranos, Montréal, QC, Canada, [3] Carbone Boréal, Département des Sciences Fondamentales, Université du Québec à Chicoutimi, Saguenay, QC, Canada, [4] Centre d'Étude de la Forêt, Université du Québec à Montréal, Montréal, QC, Canada, [5] Service Canadien des Forêts, Centre de Foresterie des Laurentides, Sainte-Foy, QC, Canada, [6] Independent Researcher, Lévis, QC, Canada*

OPEN ACCESS

**Edited by:**
*Klaus Kaiser, Martin Luther University Halle-Wittenberg, Germany*

**Reviewed by:**
*Salim Belyazid, Stockholm University, Sweden*
*Hui Wang, Chinese Academy of Forestry, China*
*Pavel Kram, Czech Geological Survey, Czechia*

***Correspondence:**
*Daniel Houle*
*daniel.houle2@canada.ca*

**Specialty section:**
*This article was submitted to Forest Soils, a section of the journal Frontiers in Forests and Global Change*

**Received:** *15 February 2020*
**Accepted:** *03 September 2020*
**Published:** *23 September 2020*

**Citation:**
*Houle D, Marty C, Augustin F, Dermont G and Gagnon C (2020) Impact of Climate Change on Soil Hydro-Climatic Conditions and Base Cations Weathering Rates in Forested Watersheds in Eastern Canada. Front. For. Glob. Change 3:535397. doi: 10.3389/ffgc.2020.535397*

Increases in mean annual air temperature (MAAT) and mean annual precipitation (MAP) are projected for north eastern North America, which will alter soil hydro-climatic conditions and hence the rate of many soil processes. Among them, chemical weathering of soil minerals is an essential source of base cations (BC) which controls the acid-base status of surface waters and is crucial for forest nutrition. In this modeling study, MAAT and MAP projections from a regional and a global climate models were first used to project changes in soil temperature (MAST) and soil water content (SWC) with the ForStem and ForHym models for 21 eastern Canadian forested catchments. The models predicted an increase in MAST by 2.03–2.05°C and 2.87–3.42°C for the 2041–2070 and 2071–2100 periods, respectively, and a small decrease (<5%) in SWC. In a second step, these projected changes in MAST and SWC were used to estimate changes in BC weathering rates (WR) and soil pH with the geochemical model PROFILE. The simulations indicated that BC WR would increase by 13–15% and 20–22% for the 2041–2070 and 2071–2100 periods, respectively. The increase in BC WR was accompanied by an increase not only in base cation concentrations, but also in soil pH at most sites, suggesting that future temperature increase has the potential to ameliorate the acid-base status and the fertility of soils in eastern Canada through its impact on WR.

**Keywords: soil weathering, climate change, forest ecosystems and biogeochemical processes, tree nutrition, surface water acidity**

## INTRODUCTION

Recent climatic simulations have shown that mean annual air temperature (MAAT) may rise by up to 4–7°C by the end of the century relative to the 1971–2000 period under a scenario of high greenhouse gas (GHG) emissions (RCP 8.5) in southern Québec, Canada (Ouranos, 2015). This increase will impact soil temperature and moisture, two variables that play a key role in several

processes in forest ecosystems, including soil organic matter (SOM) mineralization (Melillo et al., 2002; Davidson and Janssens, 2006), nitrification (Gessler et al., 2004; Groffman et al., 2009; Durán et al., 2014), tree growth and forest productivity (Gessler et al., 2004; Hernandez-Santana et al., 2009) and forest fire intensity and frequency (Rennenberg et al., 2006). Over long periods of time, such changes could also affect the distribution and composition of forests. In addition, soil temperature and moisture have a strong impact on the rate of chemical weathering of soil minerals (White and Blum, 1995), which is the main source of essential nutrients for tree nutrition such as base cations (BC) and other essential elements (e.g., P, Fe, Mn). A 44-year study in Iceland has shown a positive effect of MAAT on chemical and mechanical weathering rates (WRs) in glacial catchments (Gislason et al., 2009). Higher weathering rates driven by increasing temperatures was also suggested to explain increased alkalinity and pH of lake waters for 47 temperate and boreal catchments in the province of Quebec, Canada (Houle et al., 2010). More recently, it was shown that MAAT and precipitation had a positive effect on BC budget and concentrations in lake water across 72 forested catchments of eastern Canada (Augustin et al., 2015b). Results reported by Li et al. (2016) also showed a strong positive correlation between mean annual temperature and the rate of $CO_2$ consumption associated with the weathering of basaltic rocks. Although these studies suggest an increase in chemical weathering rates in response to climate warming, potential reduction of soil moisture resulting from increased evapotranspiration (Milly, 1992) associated with higher temperature may nevertheless counteract the increase in soil processes due to warmer temperatures. Such a mechanism has been reported for microbial SOM mineralization and nitrification rates (Venterea et al., 2003; Groffman et al., 2009; Durán et al., 2014).

A wide range of methodological approaches have been developed to quantify BC WRs (Augustin et al., 2016). These include soil profile mass balance calculations (Brimhall et al., 1991; Egli and Fitze, 2000), watershed input-output budgets (Clayton, 1979; Velbel, 1985), laboratory dissolution experiments (Chou and Wollast, 1984; Oelkers et al., 1994), test-mineral techniques (Ranger et al., 1990), strontium isotope ratio methods

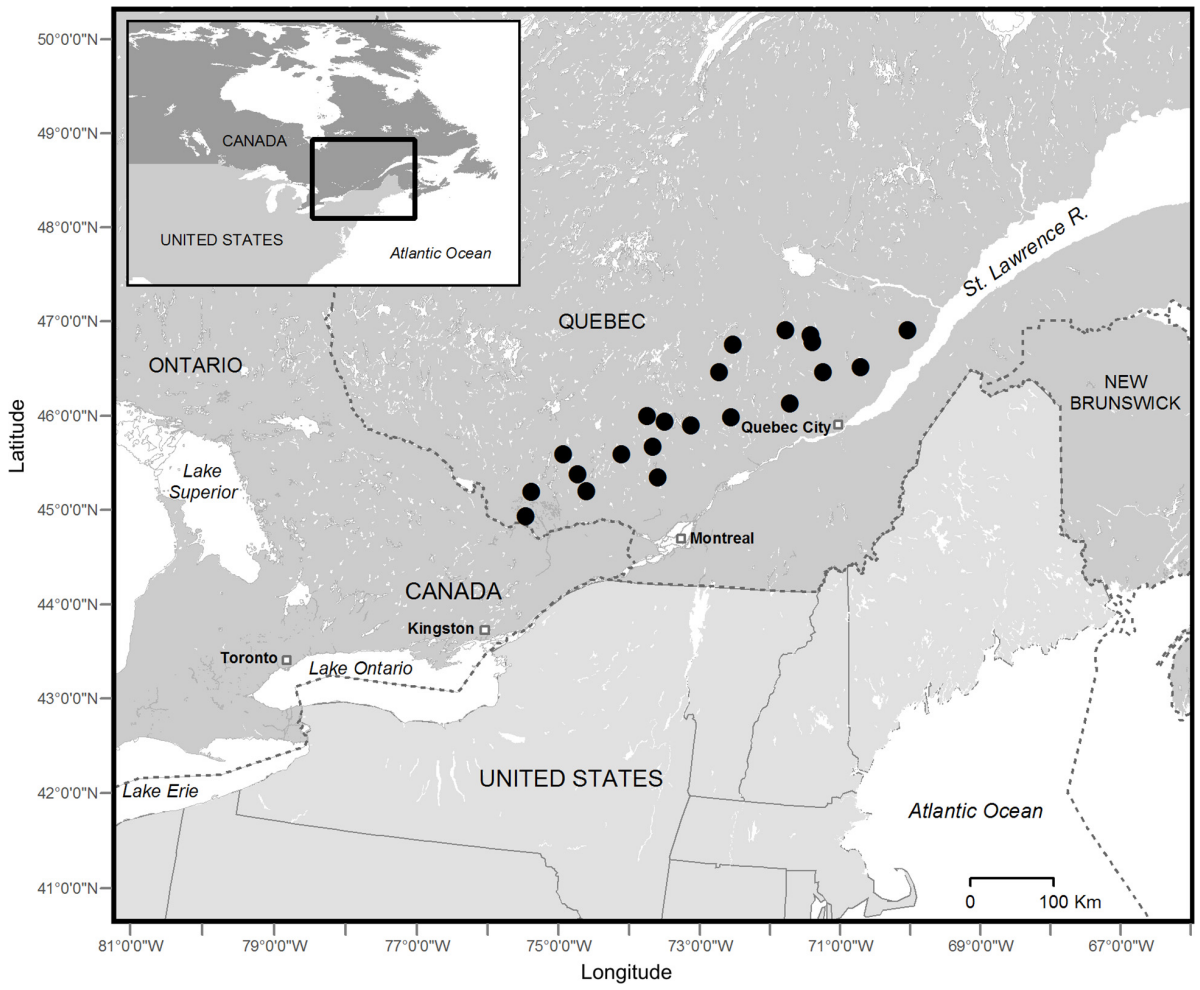


**FIGURE 1 |** Location of the study sites.

(Åberg et al., 1989), as well as geochemical modeling using the MAGIC (Cosby et al., 2001) or PROFILE models (Warfvinge and Sverdrup, 1992). The geochemical model PROFILE is widely used to evaluate chemical and geochemical processes involved in forest soils and watersheds (Koptsik et al., 1999; Duan et al., 2002; Duchesne and Houle, 2006; Sverdrup, 2009; Erlandson Lampa et al., 2020). Previous works have shown that PROFILE is enough powerful to reproduce spatial geographical gradients in WRs for relatively large areas with contrasted mineralogy (Houle et al., 2012b; Augustin et al., 2016), while yielding reliable BC WRs (Jönsson et al., 1995). Since soil temperature and moisture both greatly affect the chemical, physical, and biological processes that are occurring in soils, it is essential to better understand how climate change will affect resulting future soil conditions. However, changes in soil moisture and temperature cannot be directly deduced from projected changes in air temperature or precipitation. For example, an increase in winter air temperature would have a slight impact on soil temperature because of the insulation properties of the snowpack. Although global and regional climate models have a land surface scheme that can diagnose soil temperature and moisture, their use is limited for site-specific studies because their spatial resolution is too coarse to allow taking the characteristics of soils specific to each site into account (presence of organic soils, organic soil depth, mineral soil depth, root zone depth, clay content, soil porosity, vegetation type, etc.). The objectives of this study were thus: (1) to predict climate change impact on soil moisture and temperature at 21 forested catchments of the Quebec portion of the Long-Range Transport of Airborne Pollutants (LRTAP) program; and (2) to simulate future BC WRs, soil pH, and BC availability associated with changes in soil temperature and moisture by using the geochemical model PROFILE.

# MATERIALS AND METHODS

## Study Sites and Sampling

The study took place in 21 forested watersheds of the LRTAP-Quebec network. All watersheds are located in the temperate and boreal forests of the province of Quebec, Canada, within a ∼90 000 km$^2$ area defined as a 150 km wide strip, parallel to the St. Lawrence River (**Figure 1**) and it has been extensively

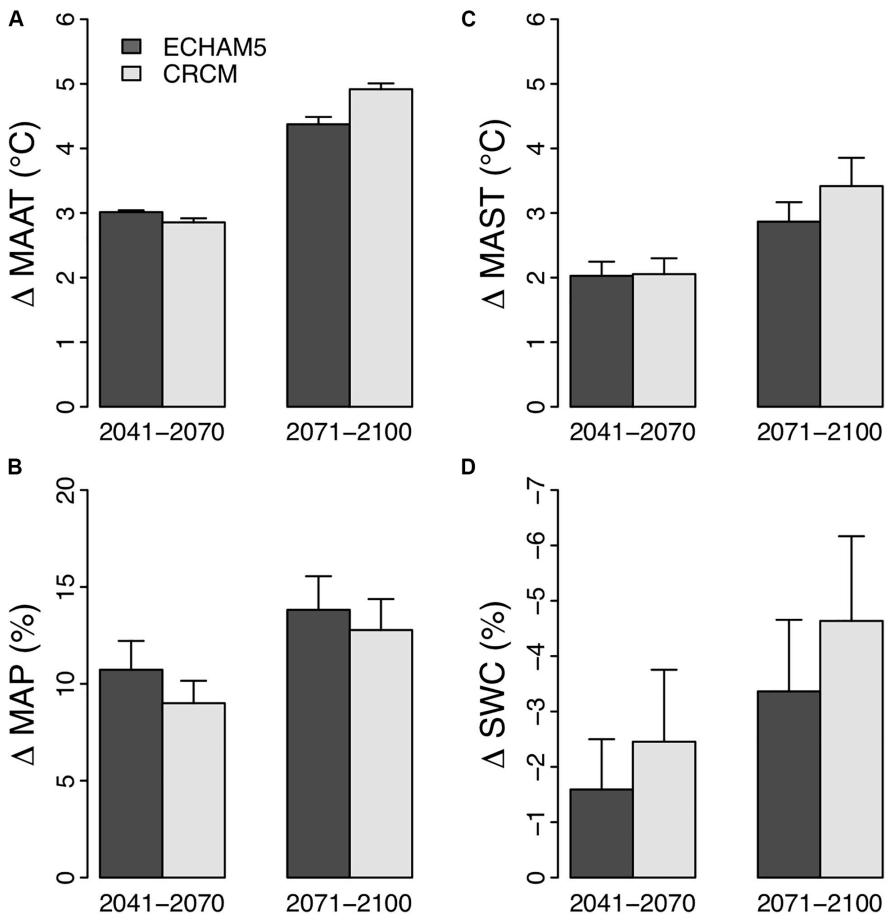


**FIGURE 2 |** Changes in mean annual air temperature (MAAT) **(A)**, mean annual precipitation (MAP) **(B)**, mean annual soil temperature (MAST) **(C)** and soil water content (SWC) **(D)** between the reference period (1971–2000) and the 2041–2070 and 2071–2100 periods. MAAT and MAP values were projected by the ECHAM 5 (global) and CRCM (regional) climate models and were used as inputs in the FORHYM-FORSTEM model for MAST and SWC projections.

described in previous studies (Houle et al., 2012b; Augustin et al., 2015a, 2016). In this region, the Canadian Shield is composed of bedrocks formed during the Precambrian, which consists mainly of igneous (granite, syenite, anorthosite) and metamorphic (gneiss, granitic gneiss, paragneiss) rocks.

Site boundaries were delimited from topographical maps analysis (1:20,000). Catchments surface areas are indicated in Houle et al. (2012b). The 21 catchments comprised no peat bogs and are protected by a provincial law against forest harvesting and major human activity. Most of them are only accessible by helicopter. The vegetation ranges from forests dominated by sugar maple (*Acer saccharum* Marsh.) in the southwest, to balsam fir (*Abies balsamea* L.) or black spruce (*Picea mariana* Mill.) in the northeast of the study area (Houle et al., 2006; Marty et al., 2015). The soils in the watersheds are mainly orthic humo-ferric or ferro-humic podzols. These types of soils are typically shallow, covered with a humus layer of 7–10 cm underlained by a thin (sometime discontinuous) eluviated Ae horizon and with a thick B-horizon (Houle et al., 2012b). The thickness of the till deposit is not exactly known for each catchment but it typically reaches 2–4 m (including the developed soil profile) at mid-slope. The C-horizon, which gets rapidly heavily compacted with depth, lies on the impermeable rock of the Canadian Shield.

Soil sampling was conducted during the summer and fall of 2001 and 2002. Details about sampling procedure can be found elsewhere (Augustin et al., 2015a; Marty et al., 2015, 2017). Briefly, three soil pits were dug to a depth of about 1 m within each site. The soil profiles locations were evenly distributed on flat surfaces around the lake perimeter, approximately 50 m from the lake shore. Percent volume of large stone was visually estimated in the field. The Munsell Soil Color Chart (Munsell Soil Color Charts, 1994) were used to characterize the soil colors. The organic soil layers (L, F, and H) were sampled with a 177 $cm^2$ sampling frame up to the top of the mineral horizons. The thickness of both organic and mineral horizons was measured and soils were sampled by genetic horizons. Main mineral horizons were also core sampled (diameter, 53 mm; length, 60 mm) to determine bulk density and their thickness measured in the field.

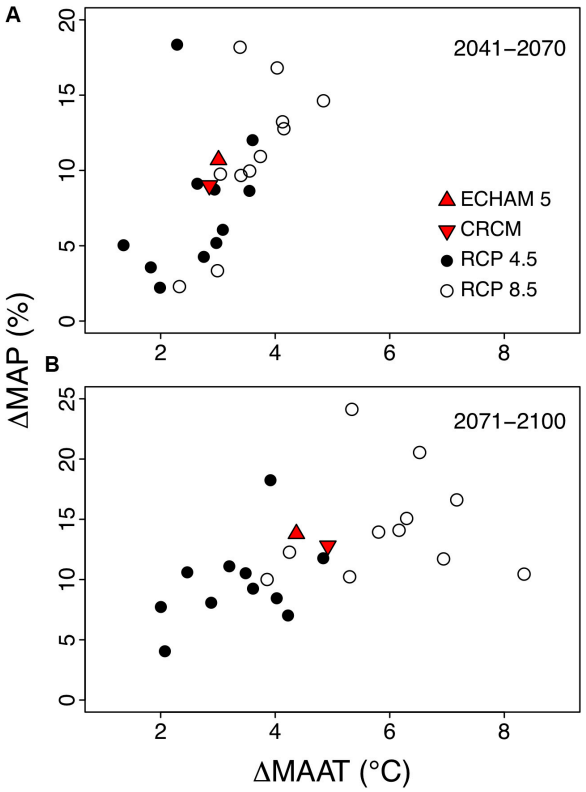


**FIGURE 3 |** Relative changes in mean annual precipitation (MAP) and mean annual air temperature (MAAT) for the study region as projected by 11 models under two GHG emission scenarios (RCP 4.5 and RCP 8.5) for the periods 2041–2070 **(A)** and 2071–2100 **(B)**. Projected changes by the climate models used in this study for coupled simulations (ECHAM 5 and CRCM) are also shown on the graphs. The 11 reference models are: ACCESS1.3, BNU-ESM, CMCC-CMS, CanESM2, GFDL-ESM2M, HadGEM2, INM-CM4, IPSL-CM5A-LR, IPSL-CM5B-LR, MPIESM-LR, and NorESM.

## Climate Models and Projections of Soil Moisture and Temperature

Average monthly air temperatures, rainfall and the fraction of precipitation falling as snow were generated for each catchment over the reference period (1971–2000) with the BioSIM model (Régnière and Bolstad, 1994; Régnière and St-Amant, 2007), based on historical observations as described in Houle et al. (2012a). For each catchment, simulations of the same variables were also performed for the reference as well as two other distinct periods (2041–2070, and 2071–2100), using two climate models: (i) the global model ECHAM 5 (member 1 SRES A1B) (300 × 300 km grid) that has a median behavior among a large set of global climate models (**Figure 3**); and (ii) the Canadian Regional Climate Model (CRCM 4.2.3 AET CGCM3.1v2 member 4 SRES A2) that was developed within the framework of the existing global climate modeling (Scinocca et al., 2016). MAAT and MAP were then computed for the reference and the two other distinct periods. Changes in MAAT and MAP were expressed as the difference between values simulated for the 2041–2070 and 2071–2100 periods on the one hand, and the reference period (1971–2000) on the other hand.

Climate data derived from BioSIM as well as both the regional and global models described above were used as inputs in the forest hydrology model ForHyM and the forest soil temperature model ForSTeM to simulate mean annual soil temperature (MAST) and soil water content (SWC), respectively, for the reference (1971–2000) as well as the 2041–2070 and the 2071–2100 periods (Arp and Yin, 1992; Yin and Arp, 1993; Houle et al., 2002, 2012a). The ForHyM sub-model simulates variations in soil water content and the main hydrological flows among the different compartments of a forest ecosystem. Regarding the ForSTeM sub-model, it simulates soil temperatures at the desired depths (here within the rooting zone, at ∼28 cm depth), while accounting for the latent heat transfers due to freeze-thaw events as well as changes in the thermal properties of the soil. The two models were calibrated for three distinct forest ecosystems

(maple, fir and spruce) based on site characteristics (canopy density, soil texture, horizon depths, extent of root zone, etc.) and on long-term and high temporal resolution measurements of soil temperature and humidity at different depths (Houle et al., 2012b). The model performance was very good with low calibration effort, and it has been observed that calibration had a very low impact on future soil temperature and SWC projections (Houle et al., 2012b). Changes in SWC and MAST were computed as the difference between values simulated for the 2041–2070 and 2071–2100 periods on the one hand, and the reference period on the other hand.

## Soil Solution Chemistry and Mineral Weathering Rate Estimates

Soil solution pH and BC concentration, as well as BC weathering rate (WR) were simulated for the 62 pedons distributed within the 21 catchments (2–3 pedons per site), using the geochemical model PROFILE (Warfvinge and Sverdrup, 1992; Sverdrup and Warfvinge, 1995, 1999). This model requires several input data, such as climate conditions, soil properties (e.g., mineralogical composition, specific surface area, soil moisture, soil temperature) and vegetation cover characteristics. Data acquisition methods regarding soil properties and site characteristics for the 21 watersheds were described elsewhere (Houle et al., 2012b; Augustin et al., 2015a). Only a brief description is provided here for some parameters. Determination of soil texture distribution (clay, sand and silt) was conducted on air-dried soil samples sieved through a 2 mm-sieve as described in Augustin et al. (2015a). Specific soil surface area was calculated from measured grain size distribution, dry bulk density, and coarse fragments according to Jönsson et al. (1995). Total elemental concentrations in soil was obtained by X-ray fluorescence (XRF) spectrometry, a non-consumptive technique for multi-element determination. These data were then used to quantitatively estimate the mineralogical composition of the soil samples with the stoichiometric model UPPSALA (Sverdrup, 1990; Sandén and Warfvinge, 1992; Houle et al., 2012b; Augustin et al., 2015a). Soil water content and temperature used in PROFILE were simulated with ForHyM and ForSTeM as described above.

# RESULTS

## Baseline and Projected Climate and Soil Hydro-Climatic Conditions

The 21 sites exhibited substantial ranges in MAAT (−1.1 to 5.1°C) and MAP (960–1,600 mm) (**Table 1**). MAST and SWC, respectively, ranged from 1.98 to 6.24°C and from 0.159 to 0.269 $m^3$ $m^{-3}$. For the 21 watersheds, average increases in MAAT of 3.01 ± 0.03°C and 4.38 ± 0.11°C were projected with the global model (ECHAM5) for the 2041–2070 and 2071–2100 periods, respectively, whereas the regional model (CRCM) projected increases by 2.85 ± 0.06°C

**TABLE 1 |** Sites characteristics for the reference period (1971–2000).

| | | | | | | Concentrations ($\mu mol_c$ $l^{-1}$) | | | |
|---|---|---|---|---|---|---|---|---|---|
| | MAAT (°C) | MAST (°C) | MAP (m $yr^{-1}$) | SWC ($m^3$ $m^{-3}$) | Soil pH | $Ca^{2+}$ | $Mg^{2+}$ | $K^+$ | $Na^+$ |
| Adanys | 1.33 | 2.68 | 0.96 | 0.269 | 5.3 | 88 | 48 | 25 | 79 |
| Blais | 4.27 | 5.62 | 1.07 | 0.194 | 6.2 | 352 | 100 | 21 | 25 |
| Boisvert | 2.12 | 2.68 | 0.96 | 0.159 | 4.7 | 63 | 40 | 12 | 34 |
| Chomeur | 1.55 | 3.65 | 1.13 | 0.251 | 5.2 | 80 | 40 | 21 | 66 |
| Clair | 5.01 | 4.82 | 0.99 | 0.191 | 6.4 | 715 | 151 | 32 | 34 |
| Daniel | 0.66 | 3.31 | 1.20 | 0.212 | 4.7 | 54 | 29 | 11 | 36 |
| David | 3.84 | 5.60 | 0.99 | 0.199 | 6.4 | 539 | 128 | 26 | 32 |
| Des joncs | 2.28 | 4.71 | 1.12 | 0.208 | 5.7 | 129 | 55 | 21 | 73 |
| Des papillons | 2.64 | 4.51 | 1.07 | 0.207 | 6.0 | 271 | 81 | 19 | 23 |
| Duck | 4.08 | 6.24 | 1.22 | 0.208 | 6.2 | 383 | 136 | 31 | 31 |
| Eclair | 2.50 | 1.98 | 1.07 | 0.244 | 5.7 | 118 | 65 | 28 | 100 |
| Fauvette | 1.64 | 4.26 | 1.06 | 0.246 | 5.9 | 156 | 108 | 31 | 106 |
| General White | 3.16 | 4.66 | 1.06 | 0.208 | 5.6 | 152 | 71 | 25 | 66 |
| Josselin | 0.19 | 4.19 | 1.60 | 0.231 | 5.0 | 41 | 25 | 11 | 30 |
| Laurent | 2.50 | 3.80 | 1.12 | 0.210 | 5.0 | 71 | 42 | 17 | 47 |
| Lemaine | 0.61 | 4.59 | 1.36 | 0.261 | 5.3 | 64 | 36 | 17 | 51 |
| McLeod | −1.09 | 2.65 | 1.43 | 0.216 | 4.8 | 61 | 31 | 13 | 34 |
| Najoua | 1.99 | 5.03 | 1.33 | 0.250 | 5.3 | 60 | 33 | 18 | 52 |
| Pothier | 2.24 | 3.47 | 1.19 | 0.212 | 5.5 | 95 | 55 | 19 | 70 |
| Thomas | 0.87 | 2.58 | 1.17 | 0.251 | 4.7 | 46 | 24 | 8 | 26 |
| Truite rouge | 2.27 | 5.58 | 1.30 | 0.213 | 5.2 | 95 | 48 | 13 | 15 |

*MAAT and MAP values were simulated with BioSim, MAST and soil water content (SWC) values with ForStem and ForHym, respectively. Soil pH and base cation concentrations were simulated by PROFILE for mineral soil's B-horizon (see "Materials and Methods" section for details).*

and 4.92 ± 0.09°C, respectively (**Figure 2A**). ECHAM 5 also predicted average increases in MAP by 10.7 and 13.8% (125 ± 29 mm and 160 ± 28 mm) for the 2041–2070 and 2071–2100 periods respectively, whereas CRCM predicted increases by 9.0 and 12.8% (104 ± 20 mm and 147 ± 21 mm), respectively (**Figure 2B**). The projected MAAT and MAP values by the two models are close to the median values of 11 other simulations under high and low GHG emissions scenarios (RCP4.5 and RCP8.5, respectively) (**Figure 3**). When fed with the results of the climate models, the ForSTeM-ForHyM models projected an increase in MAST by 2.05 ± 0.25°C and 2.03 ± 0.22°C for the 2041–2070 and by 3.42 ± 0.44°C and 2.87 ± 0.30°C for the 2071–2100 periods relative to the reference period (**Figure 2C**), while only small changes in SWC (<5%) were projected for both models and periods (**Figure 2D**).

**TABLE 2 |** Ranges and mean (SD) values for base cations weathering rates (WR; $kmol_c\ ha^{-1}\ yr^{-1}$) during the reference period (1971–2000) as simulated by PROFILE.

| | Weathering rates (WR; $kmol_c\ ha^{-1}\ yr^{-1}$) | | | | |
|---|---|---|---|---|---|
| | **Ca** | **Mg** | **K** | **Na** | **Σ BC** |
| Range | 0.21–3.39 | 0.15–0.83 | 0.05–0.19 | 0.07–0.53 | 0.54–4.36 |
| Mean (SD) | 0.96 (0.97) | 0.38 (0.20) | 0.12 (0.03) | 0.25 (0.14) | 1.70 (1.11) |

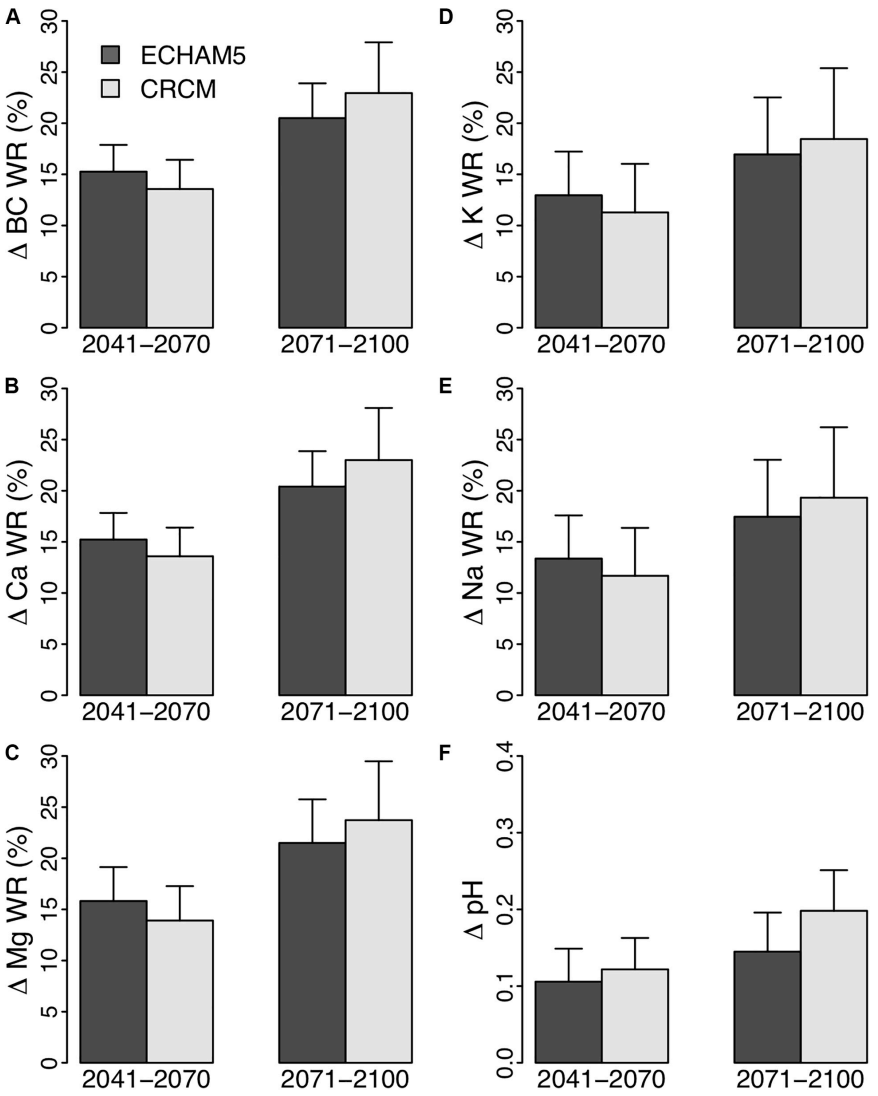


**FIGURE 4 |** Mean (±SD) relative changes in base cation weathering rates (ΔWR; %) **(A–E)** and pH **(F)** for the periods 2041–2070 and 2071–2100 relative to the reference period (1971–2000) with climate projections generated by the ECHAM 5 (global) and CRCM (regional) climate models.

## Base Cation Weathering Rate Projections

Weathering rates estimates reported here for the reference period (1971–2000) are presented in **Table 2**. The obtained results are close to those reported by Houle et al. (2012a) but differed slightly because the climate inputs were slightly different for the time period considered, i.e., 1971–2000 here as compared to 1997–2002 for Houle et al. (2012a). Across the study sites, total BC WRs simulated using PROFILE ranged from 0.54 to 4.36 $kmol_c$ $ha^{-1}$ $yr^{-1}$ and averaged 1.70 ± 1.11 $kmol_c$ $ha^{-1}$ $yr^{-1}$ for the reference period (**Table 2**). The simulations showed large ranges in individual base cation weathering rates across the 21 sites, especially for Ca (0.21–3.39 $kmol_c$ $ha^{-1}$ $yr^{-1}$).

Projected increases in the sum of BC WRs averaged 13–15% and 20–22% for the 2041–2070 and 2071–2100 periods, respectively (**Figure 4A**). Ca and Mg increases ranged from 13 to 16% (2041–2070) and from 20 to 24% (2071–2100) (**Figures 4B,C**), but were slightly lower for K and Na with values of 11–13% and 17–19% for the 2041–2070 and 2071–2100 periods, respectively (**Figures 4D,E**).

## Simulated pH and Base Cation Concentrations in the Soil Solution

There was a large variation in BC concentrations in soils among sites (**Table 1**). Among BC, $Ca^{2+}$ had the largest contribution to total BC concentration (range of 41–715 $\mu mol_c$ $l^{-1}$; average of 190 ± 194 $\mu mol_c$ $l^{-1}$), followed by $Mg^{2+}$ (range of 24–151 $\mu mol_c$ $l^{-1}$; average of 67 ± 41 $\mu mol_c$ $l^{-1}$), $Na^+$ (range of 15–106 $\mu mol_c$ $l^{-1}$; average of 48 ± 25 $\mu mol_c$ $l^{-1}$) and $K^+$ (range of 8–32 $\mu mol_c$ $l^{-1}$; average of 20 ± 7 $\mu mol_c$ $l^{-1}$). The sum of BC concentration simulated for each site is strongly correlated to total lake BC concentration (**Figure 5**) showing that the model is able to reproduce the spatial variability pattern within the study area although simulated values were slightly higher. Model simulations indicate that soil BC concentrations would increase in the future (**Figure 6**). However, the magnitude of the projected increases varied markedly among sites, cations and climate projections. The increase was more pronounced with CRCM than ECHAM 5 climate projections, and for $Ca^{2+}$, $Mg^{2+}$ and $K^+$ than for $Na^+$. On average, $Ca^{2+}$, $Mg^{2+}$ and $K^+$ concentrations in the soil would increase by 8–21% and 15–35% respectively in 2041–2070 and 2071–2100 relative to the reference period, and by slightly less for $Na^+$ (6–17% and 13–27%). The increased BC concentration resulted in a slight average increase in soil pH from 5.5 ± 0.6 (reference period) to 5.6 ± 0.6 (2041–2070) and 5.7 ± 0.6 (2071–2100) (**Figure 4F**).

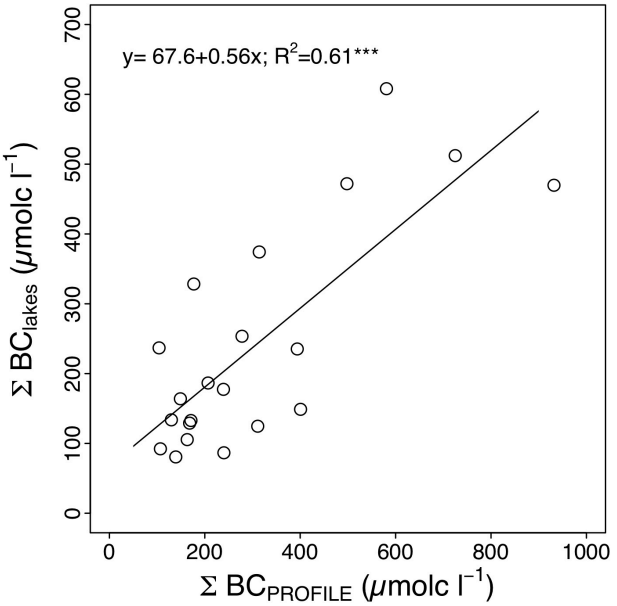


**FIGURE 5 |** Relationship between projected (Σ $BC_{PROFILE}$; $\mu mol_c$ $l^{-1}$) base cation concentrations in the soil solution and measured base cation concentrations in lake water (Σ $BC_{lakes}$; $\mu mol_c$ $l^{-1}$) at the study for the reference period (1971–2000).

# DISCUSSION

The average increases in mean annual temperature (MAAT) and mean annual precipitation (MAP) projected by the CRCM and ECHAM 5 climate models (+2.9 and 4.8°C, and +9 and 13% for the 2041–2070 and 2071–2100 periods, respectively) are very close to the median values of a large ensemble of climate simulations for both periods (**Figure 3**). We assessed the impact of these projected changes in MAAT and MAP on soil hydroclimatic variables, namely mean annual soil temperature (MAST) and soil water content (SWC), using forests hydrological models. Based on changes in MAST and SWC, future base cations (BC) weathering rates (WR) as well as soil pH and BC concentrations in soil solutions were simulated with the geochemical model PROFILE. We therefore estimated the potential changes in chemical WR and BC availability that would result from changes in soil hydroclimatic conditions only. We deliberately made not attempts to model the influence of other factors caused by global change that could potentially affect these variables such as changes in atmospheric nitrogen and sulfur depositions, changes in forest growth rates or changes in land use. The latter are too uncertain, especially forest dynamics which could be affected not only by increasing temperatures but also by changes in the rate of natural perturbations such as fires, insect outbreaks and droughts. We discuss the results of the study in relation to previous works and with respect to their general implications and also, limitations.

## Projected Changes in Soil Hydro-Climatic Conditions

Our results indicate that climate change will result in an average MAST increase by 2°C in 2041–2070 and 3.5°C by the end of the century. These increases represent on average 69% of the increases in air temperature, mostly due to the insulating impact of the snow cover during winter (Zhang et al., 2005; Sushama et al., 2006; Jungqvist et al., 2014), which corroborates other projections for temperate and boreal soils in Canada and Scandinavian countries (Houle et al.,

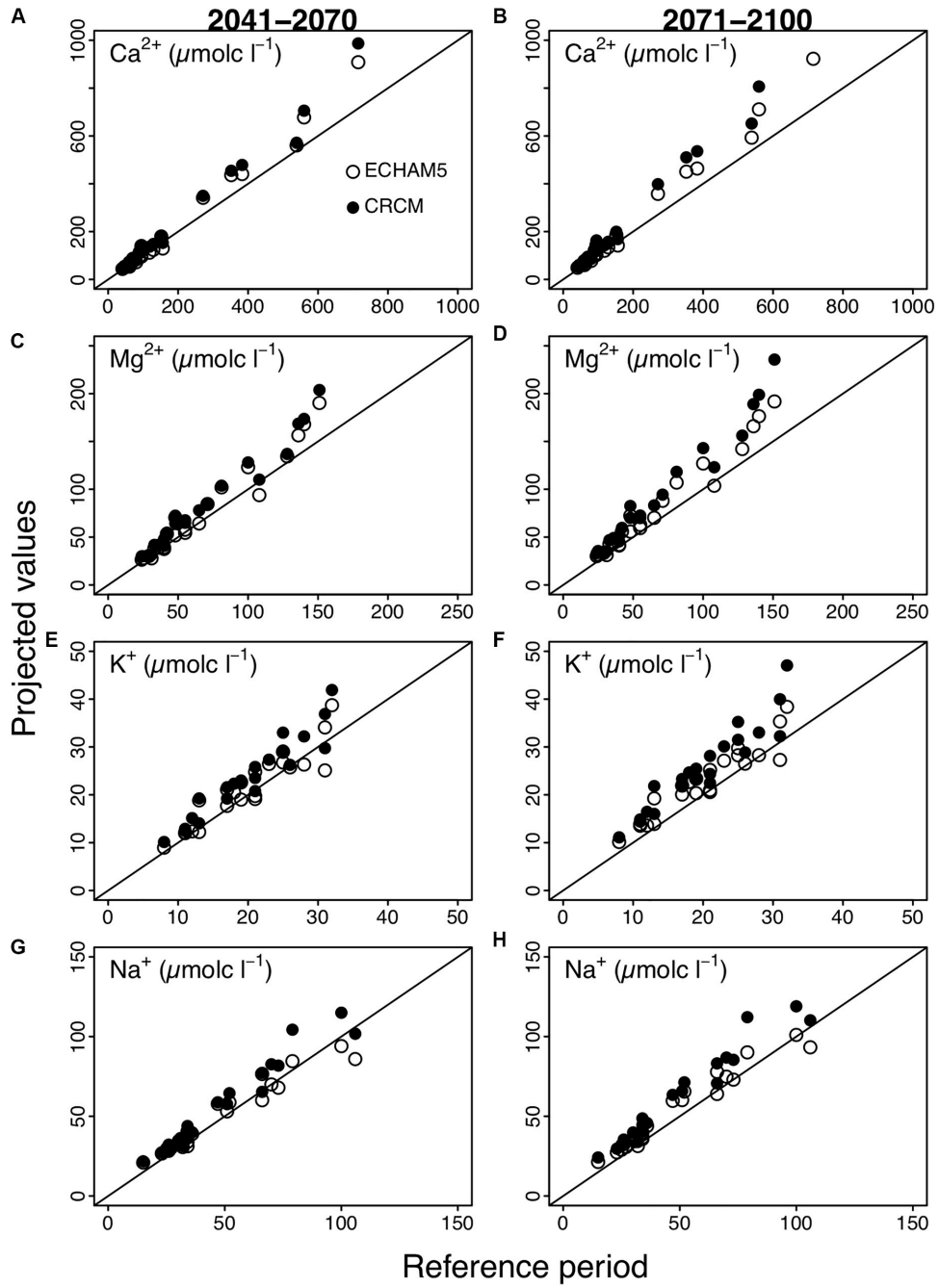


**FIGURE 6 |** Soil base cation concentrations ($\mu mol_c\ l^{-1}$) for the reference period (*x*-axis, 1971–2000) vs. the 2041–2070 **(A,C,E,G)** and 2071–2100 **(B,D,F,H)** periods as projected by the ECHAM 5 (global) and CRCM (regional) climate models. The full line is the 1:1 line.

2012b; Jungqvist et al., 2014). Jungqvist et al. (2014) simulated the effects of climate change on soil temperature in four forested catchments along a climatic gradient in Sweden and found that future changes in winter soil temperature were rather strongly dependent on projected snow cover (Jungqvist et al., 2014), highlighting the complexity of projecting soil winter temperature in snow-dominated area (Mott et al., 2018). Our data also showed higher variability in simulated MAST data compared to MAAT. This is the result of site-specific characteristics such as topography, vegetation, soil characteristics, snow pack depth and duration. Despite a 9–15% projected increase in MAP, a small decrease in average annual soil water content (<5%) was projected for both future periods (**Figure 2D**) relative to the reference period because of the impact of increased MAAT on evapotranspiration (Houle et al., 2012b).

## Future Changes in BC Weathering Rates

The estimates of BC WR simulated with the PROFILE model for the reference period are within the range reported for southern Quebec or similar soil types using other methods (Courchesne et al., 2002; Schaller et al., 2009; Augustin et al., 2016, 2018). The data show substantial BC WR increases (+ 11–25%) for the two future periods relative to the reference period. Our projected range of future BC WR is consistent with other studies including data published by Gislason et al. (2009) who showed positive relationships between MAAT and chemical weathering in 8 catchments in Iceland. Akselsson et al. (2016) projected weathering rate increases of 20–30% in Swedish soils in response to a soil warming of 2–3°C, which is slightly higher than our projected values. Within the conditions of our simulations (i.e., significant soil temperature increases with small decreases in soil water content), 79% of changes in BC WR was explained by changes in MAST (**Figure 7**) while no significant relationship was obtained between WR and SWC changes (data not shown). According to the slope of the regression line, BC WR is projected to increase by around 7% for each 1°C rise in MAST. A slightly higher value of 9% was obtained by Belyazid and Giuliana (2019) for coniferous forest soils in Sweden using the ForSAFE model.

However, our results may be conservative as the simulation did not take the length of the growing season into account. In cold regions, warmer air temperature lead to longer growing season (Euskirchen et al., 2006; Öquist and Laudon, 2008), reduced number of frost days and smaller duration of the snowpack (Jungqvist et al., 2014). As a result, the seasonality of biological activity in the soils would be affected (Kaiser et al., 2010, 2011), with more intense activity commencing earlier and continuing later as growing season extends. Such conditions would lengthen the period during which weathering reactions are taking place in addition to the soils being warmer, thereby potentially increasing the annual weathering rate. For forested catchments of eastern Canada, the length of the growing season was positively correlated with BC WR (Augustin et al., 2015b, 2018).

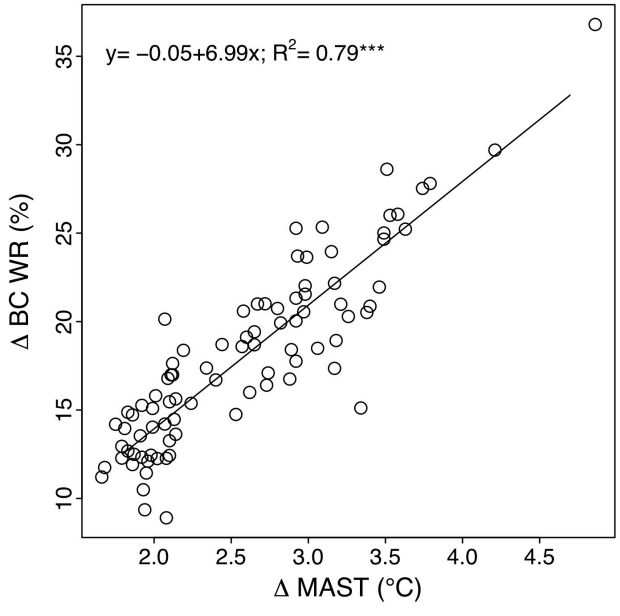


**FIGURE 7 |** Relationship between changes in base cations weathering rate (ΔBC WR; %) and changes in mean annual soil temperature (Δ MAST; °C). Values are derived from PROFILE projections from the 2041–2070 and 2071–2100 periods. The line is the linear regression ($P < 0.005$).

## Projected Soil pH and BC Concentrations in the Soil Solution

Because soil solution and surface waters are strongly influenced by the biogeochemical processes that occur in the surrounding soils, including mineral weathering (Hairston and Fussmann, 2002), it is likely that the factors affecting BC mineral weathering in soils influence chemical properties of the soil solution (Ryan and Kahler, 1987). The projected WR increases were accompanied by increases in BC concentration in the soil solution (+6–35%). The capability of the PROFILE model to yield realistic BC concentrations (**Figure 5**) and to reproduce its spatial variability in the studied region (Houle et al., 2012b; Augustin et al., 2016) supports the validity of our projections. The projected increases by up to 31% in $Ca^{2+}$ concentrations may have a significant beneficial impact on acid-base status of soils and potentially forest productivity. The region under study has actually been affected by acid rain in the last decades, which has led to reduced Ca availability in soils (Houle et al., 1997) and tree growth (Duchesne et al., 2002). In addition, the projected soil warming will likely increase forest floor respiration rate as well as soil organic matter decomposition (Marty et al., 2019), which will release nutrients (among which base cations) in the soil solution which may stimulate tree growth, at least in the short term (Melillo et al., 2011). Our simulations agree with previous observations that the temporal variation in pH and alkalinity in surface water drained from forested catchments were mainly controlled by temperature and not only by decreasing precipitation acidity (Houle et al., 2010), suggesting that increased BC WR, driven by warming temperature, are already involved in the actual recovery of surface water chemistry (acid-base status). Overall our results suggest that climate warming has the potential to improve the acid-base status of surface waters as well as to maintain forest growth by increasing BC availability for trees (Schaberg and Hawley, 2010; Moore et al., 2012).

## CONCLUSION

This study shows that the projected climate warming in the region (increase in MAAT by 2.85–3.01°C and 4.38–4.92°C for the 2041–2070 and 2071–2100 periods, respectively) would result in a MAST increase of 2.03–2.05°C and 2.87–3.42°C during the same periods. Meanwhile, soil moisture would only decrease slightly (<−5%) due to the increase in MAP by 9–14%. According to model simulations, these future soil conditions would increase BC WR and thereby soil pH and BC concentration in the soil solution, contributing to increase the

acid-base status of surface waters and fertility of the soils. In our simulations, acidic ions depositions were kept constant (i.e., at actual levels). It is, however, likely that the observed decreasing trends in S and N depositions in the study area (Houle et al., 2010, 2014, 2015; Marty et al., 2012) will be prolonged in the future, which would further increase the beneficial effect of higher weathering rates on soil conditions. It is, however, important to underline that such an increase in BC WR was likely made possible because SWC was only slightly decreased ($<-5\%$) by the increase in evapo-transpirative demand associated with increased MAST, due to substantial projected increase in MAP for the region under study (**Figure 3**). It is likely that for any regions where precipitation will stay constant or decrease in the future, decreased SWC may limit the stimulation of higher MAST on BC WR. Our study has nevertheless limitation since the PROFILE model is driven by annual climate inputs. As a result, other climate change impacts on WR driven by seasonality such as changes in growing season length or increasing probability of summer drought (resulting in lower SWC) have not been quantified. Also, other impacts of climate change such as a potential increase of nutrients demands by trees due to a speculated positive impact of higher temperature on growth may eventually result in lower BC availability. The present study represents a first step in trying to project future WR in response to climate change in eastern North-America. More research is needed to model these complex biogeochemical processes and refine these projections.

## DATA AVAILABILITY STATEMENT

The datasets generated for this study are available on request to the corresponding author.

## AUTHOR CONTRIBUTIONS

DH designed the study. GD made the simulations. CM made the first data analysis. All authors contributed to data interpretation and writing of the manuscript.

## REFERENCES


Åberg, G., Jacks, G., and Hamilton, P. J. (1989). Weathering rates and 87Sr/86Sr ratios: an isotopic approach. *J. Hydrol.* 109, 65–78. doi: 10.1016/0022-1694(89)90007-3

Akselsson, C., Olsson, J., Belyazid, S., and Capell, R. (2016). Can increased weathering rates due to future warming compensate for base cation losses following whole-tree harvesting in spruce forests? *Biogeochemistry* 128, 89–105. doi: 10.1007/s10533-016-0196-6

Arp, P. A., and Yin, X. W. (1992). Predicting water fluxes through forests from monthly precipitation and mean monthly air temperature records. *Can. J. For. Res.* 22, 864–877. doi: 10.1139/x92-116

Augustin, F., Houle, D., and Courchesne, F. (2018). An approach at estimating present day base cation weathering rates: a case study for the Hermine watershed, Canada. *Biogeochemistry* 140, 127–144. doi: 10.1007/s10533-018-0479-1

Augustin, F., Houle, D., Gagnon, C., and Courchesne, F. (2015a). Long-term mineral weathering in forested catchments of the Canadian shield, Québec. *Geoderma* 247–248, 12–23. doi: 10.1016/j.geoderma.2015.01.016

Augustin, F., Houle, D., Gagnon, C., and Courchesne, F. (2016). Evaluation of three methods for estimating the weathering rates of base cations in forested catchments. *Catena* 144, 1–10. doi: 10.1016/j.catena.2016.04.022

Augustin, F., Houle, D., Gagnon, C., Couture, S., and Courchesne, F. (2015b). Partitioning the impact of environmental factors on lake concentrations and catchment budgets for base cations in forested ecosystems. *Appl. Geochem.* 53, 1–12. doi: 10.1016/j.apgeochem.2014.11.013

Belyazid, S., and Giuliana, Z. (2019). Water limitation can negate the effect of higher temperatures on forest carbon sequestration. *Eur. J. For. Res.* 138, 287–297. doi: 10.1007/s10342-019-01168-4

Brimhall, G. H., Lewis, C. J., Ford, C., Bratt, J., Taylor, G., and Warin, O. (1991). Quantitative geochemical approach to pedogenesis importance of parent material reduction, volumetric expansion, and eolian influx in laterization. *Geoderma* 51, 51–91. doi: 10.1016/0016-7061(91)90066-3

Chou, L., and Wollast, R. (1984). Study of the weathering of albite at room temperature and pressure with a fluidized bed reactor. *Geochim. Cosmochim. Acta* 48, 2205–2218. doi: 10.1016/0016-7037(84)90217-5

Clayton, J. L. (1979). "Nutrient supply to soil by rock weathering," in *Impact of Intensive Harvesting on Forest Nutrient Cycling*, ed. A. Leaf (Syracuse, NY: State University of New York), 75–96.

Cosby, B. J., Ferrier, R. C., Jenkins, A., and Wright, R. F. (2001). Modelling the effects of acid deposition: refinements, adjustments and inclusion of nitrogen dynamics in the MAGIC model. *Hydrol. Earth Syst. Sci.* 5, 499–517. doi: 10.5194/hess-5-499-2001

Courchesne, F., Hallé, J. P., and Turmel, M. C. (2002). Bilans élémentaires holocèneset altération des minéraux dans trois sols forestiers du Québec méridional. *Géog. Phys. Quatern.* 56, 3–124.

Davidson, E. A., and Janssens, I. A. (2006). Temperature sensitivity of soil carbon decomposition and feedbacks to climate change. *Nature* 440, 165–173. doi: 10.1038/nature04514

Duan, L., Hao, J., Xie, S., Zhou, Z., and Ye, X. (2002). Determining weathering rates of soils in China. *Geoderma* 110, 205–225. doi: 10.1016/s0016-7061(02)00231-8

Duchesne, L., and Houle, D. (2006). Base cation cycling in a pristine watershed of the Canadian boreal forest. *Biogeochemistry* 78, 195–216. doi: 10.1007/s10533-005-4174-7

Duchesne, L., Ouimet, R., and Houle, D. (2002). Basal area growth of sugar maple in relation to acid deposition, stand health, and soil nutrients. *J. Environ. Qual.* 31, 1676–1683. doi: 10.2134/jeq2002.1676

Durán, J., Morse, J. L., Groffman, P. M., Campbell, J. L., Christenson, L. M., Driscoll, C. T., et al. (2014). Winter climate change affects growing-season soil microbial biomass and activity in northern hardwood forests. *Glob. Chang. Biol.* 20, 3568–3577. doi: 10.1111/gcb.12624

Egli, M., and Fitze, P. (2000). Formulation of pedologic mass balance based on immobile elements: a revision. *Soil Sci.* 165, 437–443. doi: 10.1097/00010694-200005000-00008

Erlandson Lampa, M., Sverdrup, H. U., Bishop, K. H., Belyazid, S., Ameli, A., and Köhler, S. J. (2020). Catchment export of base cations: improved mineral dissolution kinetics influence the role of water transit time. *Soil* 6, 231–244. doi: 10.5194/soil-6-231-2020

Euskirchen, E., McGuire, A. D., Kicklighter, D. W., Zhuang, Q., Clein, J. S., Dargaville, R. J., et al. (2006). Importance of recent shifts in soil thermal dynamics on growing season length, productivity, and carbon sequestration in terrestrial high latitude ecosystems. *Glob. Chang. Biol.* 12, 731–750. doi: 10.1111/j.1365-2486.2006.01113.x

Gessler, A., Keitel, C., Nahm, M., and Rennenberg, H. (2004). Water shortage affects the water and nitrogen balance in Central European beech forests. *Plant Biol.* 6, 289–298. doi: 10.1055/s-2004-820878

Gislason, S. R., Oelkers, E. H., Eiriksdottir, E. S., Kardjilov, M. I., Gisladottir, G., Sigfusson, B., et al. (2009). Direct evidence of the feedback between climate and weathering. *Earth Planet. Sci. Lett.* 277, 213–222. doi: 10.1016/j.epsl.2008.10.018

Groffman, P. M., Hardy, J. P., Fisk, M. C., Fahey, T. J., and Driscoll, C. T. (2009). Climate variation and soil carbon and nitrogen cycling processes in a Northern Hardwood Forest. *Ecosystems* 12, 927–943. doi: 10.1007/s10021-009-9268-y

Hairston, N. G. Jr., and Fussmann, G. F. (2002). "Lake ecosystems," in *Encyclopedia Life Science*, ed. eLS (London: Macmillian Reference Ltd), 1–3. doi: 10.1038/npg.els.0003191

Hernandez-Santana, V., Martinez-Vilalta, J., Martinez-Fernandez, J., and Williams, M. (2009). Evaluating the effect of drier and warmer conditions on water use by Quercus pyrenaica. *For. Ecol. Manage.* 258, 1719–1730. doi: 10.1016/j.foreco.2009.07.038

Houle, D., Bouffard, A., Duchesne, L., Logan, T., and Harvey, R. (2012a). Projections of future soil temperature and water content for three Southern Quebec forested sites. *J. Clim.* 25, 7690–7701. doi: 10.1175/jcli-d-11-00440.1

Houle, D., Couture, S., and Gagnon, C. (2010). Relative role of decreasing precipitation sulfate and climate on recent lake recovery. *Global Biogeochem. Cycles* 24:GB4029. doi: 10.1029/2009GB003757

Houle, D., Duchesne, L., Ouimet, R., Paquin, R., Meng, F. R., and Arp, P. A. (2002). Evaluation of the FORHYM2 model for prediction of hydrologic fluxes and soil temperature at the Lake Clair Watershed (Duchesnay, Quebec). *For. Ecol. Manage.* 159, 249–260. doi: 10.1016/s0378-1127(01)00438-8

Houle, D., Lamoureux, P., Bélanger, N., Bouchard, M., Gagnon, C., Couture, S., et al. (2012b). Soil weathering rates in 21 catchments of the Canadian Shield. *Hydrol. Earth Syst. Sci.* 16, 685–697. doi: 10.5194/hess-16-685-2012

Houle, D., Marty, C., and Duchesne, L. (2015). Response of canopy nitrogen uptake to a rapid decrease in bulk nitrate deposition in two eastern Canadian boreal forests. *Oecologia* 177, 29–37. doi: 10.1007/s00442-014-3118-0

Houle, D., Marty, C., Duchesne, L., and Gagnon, C. (2014). Humus layer is the main locus of secondary SO4 production in boreal forests. *Geochim. Cosmochim. Acta* 126, 18–29. doi: 10.1016/j.gca.2013.10.038

Houle, D., Ouimet, R., Couture, S., and Gagnon, C. (2006). Base cation reservoirs in soil control the buffering capacity of lakes in forested catchments. *Can. J. Fish. Aquat. Sci.* 63, 471–474. doi: 10.1139/f06-007

Houle, D., Paquin, R., Camiré, C., Ouimet, R., and Duchesne, L. (1997). Response of the Lake Clair Watershed (Duchesnay, Québec) to changes in precipitation chemistry (1988-1994). *Can. J. For. Res.* 27, 1813–1821. doi: 10.1139/x97-143

Jönsson, C., Warfvinge, P., and Sverdrup, H. (1995). Uncertainty in predicting weathering rate and environmental stress factors with the PROFILE model. *Water Air Soil Pollut.* 81, 1–23. doi: 10.1007/bf00477253

Jungqvist, G., Oni, S. K., Teutschbein, C., and Futter, M. N. (2014). Effect of climate change on soil temperature in swedish boreal forests. *PLoS One* 9:e93957. doi: 10.1371/journal.pone.0093957

Kaiser, C., Fuchslueger, L., Koranda, M., Gorfer, M., Stange, C. F., Kitzler, B., et al. (2011). Plants control the seasonal dynamic of microbial N cycling in a beech forest soil by belowground C allocation. *Ecology* 92, 1036–1051. doi: 10.1890/10-1011.1

Kaiser, C., Koranda, M., Kitzler, B., Fuchslueger, L., Schnecker, J., Schweiger, P., et al. (2010). Belowground carbon allocation by trees drive seasonal pattern of extracellular enzyme activities by altering microbial community composition in a beech forest soil. *New Phytol.* 187, 843–858. doi: 10.1111/j.1469-8137.2010.03321.x

Koptsik, G., Teveldal, S., Aamlid, D., and Venn, K. (1999). Calculations of weathering rate and soil solution chemistry for forest soils in the Norwegian–Russian border area with the PROFILE model. *Appl. Geochem.* 14, 173–185. doi: 10.1016/s0883-2927(98)00048-1

Li, G., Hartmann, J., Derry, L. A., West, A. J., You, C. F., Long, X., et al. (2016). Temperature dependence of basalt weathering. *Earth Planet. Sci. Lett.* 443, 59–69. doi: 10.1016/j.epsl.2016.03.015

Marty, C., Houle, D., Duchesne, L., and Gagnon, C. (2012). Canopy interaction with precipitation and sulphur deposition in two boreal forests of Quebec, Canada. *Environ. Pollut.* 162, 354–360. doi: 10.1016/j.envpol.2011.12.007

Marty, C., Houle, D., and Gagnon, C. (2015). Effect of the relative abundance of conifers versus hardwoods on soil δ13C enrichment with soil depth in eastern Canadian forests. *Ecosystems* 18, 629–642. doi: 10.1007/s10021-015-9852-2

Marty, C., Houle, D., Gagnon, C., and Courchesne, F. (2017). The relationships of soil total nitrogen concentrations, pools and C:N ratios with climate, vegetation types and nitrate deposition in temperate and boreal forests of eastern Canada. *Catena* 152, 163–172. doi: 10.1016/j.catena.2017.01.014

Marty, C., Piquette, J., Morin, H., Bussières, D., Thiffault, N., Houle, D., et al. (2019). Nine years of in situ soil warming and topography impact the temperature sensitivity and basal respiration rate of the forest floor in a Canadian boreal forest. *PLoS One* 14:e0226909. doi: 10.1371/journal.pone.0226909

Melillo, J. M., Butler, S., Johnson, J., Mohan, J., Steudler, P., Lux, H., et al. (2011). Soil warming, carbon-nitrogen interactions, and forest carbon budgets. *Proc. Natl. Acad. Sci. U.S.A.* 108, 9508–9512. doi: 10.1073/pnas.1018189108

Melillo, J. M., Steudler, P. A., Aber, J. D., Newkirk, K., Lux, H., Bowles, F. P., et al. (2002). Soil warming and carbon-cycle feedbacks to the climate system. *Science* 298, 2173–2176. doi: 10.1126/science.1074153

Milly, P. C. D. (1992). Potential evapotranspiration and soil moisture in general circulation models. *J. Clim.* 5, 209–226. doi: 10.1175/1520-0442(1992)005<0209:peasmi>2.0.co;2

Moore, J. D., Ouimet, R., and Duchesne, L. (2012). Soil and sugar maple response 15 years after dolomitic lime application. *For. Ecol. Manage.* 281, 130–139. doi: 10.1016/j.foreco.2012.06.026

Mott, R., Vionnet, V., and Grünewald, T. (2018). The seasonal snow cover dynamics: review on wind-driven coupling processes. *Front. Earth Sci.* 6:197. doi: 10.3389/feart.2018.00197

Munsell Soil Color Charts (1994). *Munsell Color, Macbeth Division of Kollmorgen Instruments Corporation*.

Oelkers, E. H., Schott, J., and Devidal, J. L. (1994). The effect of aluminum, pH, and chemical affinity on the rates of aluminosilicate dissolution reactions. *Geochim. Cosmochim. Acta* 58, 2011–2024. doi: 10.1016/0016-7037(94)90281-x

Öquist, M., and Laudon, H. (2008). Winter soil frost conditions in boreal forests control growing season soil CO2 concentration and its atmospheric exchange. *Glob. Chang. Biol.* 14, 2839–2847. doi: 10.1111/j.1365-2486.2008.01669.x

Ouranos (2015). *Vers L'adaptation. Synthèse des Connaissances sur les Changements Climatiques au Québec. Édition* 2015. Montréal: Ouranos, 415.

Ranger, J., Robert, M., Bonnaud, P., and Nys, C. (1990). Les minéraux-test, une approche expérimentale in situ de l'altération biologique et du fonctionnement des écosystèmes forestiers. Effets des types de sols et des essences feuillues et résineuses. *Ann. Sci. For.* 47, 529–550. doi: 10.1051/forest:19900601

Régnière, J., and Bolstad, P. (1994). Statistical simulation of daily air temperature patterns eastern North America to forecast seasonal events in insect pest management. *Environ. Entomol.* 23, 1368–1380. doi: 10.1093/ee/23.6.1368

Régnière, J., and St-Amant, R. (2007). Stochastic simulation of daily air temperature and precipitation from monthly normals in North America north of Mexico. *Int. J. Biometeorol.* 51, 415–430. doi: 10.1007/s00484-006-0078-z

Rennenberg, H., Loreto, F., Polle, A., Brilli, F., Fares, S., Beniwal, R. S., et al. (2006). Physiological responses of forest trees to heat and drought. *Plant Biol.* 8, 556–571. doi: 10.1055/s-2006-924084

Ryan, D. F., and Kahler, D. M. (1987). Geochemical and mineralogical indications of pH in lakes and soils in central New Hampshire in the early Holocene. *Limnol. Oceanogr.* 32, 751–757. doi: 10.4319/lo.1987.32.3.0751

Sandén, P., and Warfvinge, P. (1992). *Modelling Groundwater Response to Acidification: Report from the Swedish Integrated Groundwater Acidification Project. Coll. Reports Hydrology, no* 5. Lund: Lund University, 186.

Schaberg, P. G., and Hawley, G. J. (2010). "Disruption of calcium nutrition at Hubbard Brook Experimental Forest (New Hampshire) alters the health and productivity of red spruce and sugar maple trees and provides lessons pertinent to other sites and regions," in *Proceedings of the Conference on the Ecology and Management of High-Elevation Forests in the Central and Southern Appalachian Mountains. 2009 May 14-15; Slatyfork, WV. Gen. Tech. Rep. NRS-P-64*, eds Rentch, S. James, Schuler, and M. Thomas (Newtown Square, PA: U.S. Department of Agriculture), 190–200.

Schaller, M., Blum, J. D., Hamburg, S. P., and Vadeboncoeur, M. A. (2009). Spatial variability of long-term chemical weathering rates in the White Mountains, New Hampshire, USA. *Geoderma* 154, 294–301. doi: 10.1016/j.geoderma.2009.10.017

Scinocca, J. F., Kharin, V. V., Jiao, Y., Qian, M. W., Lazare, M., Solheim, L., et al. (2016). Coordinated global and regional climate modeling. *J. Clim.* 29, 17–35. doi: 10.1175/JCLI-D-15-0161.1

Sushama, L., Laprise, R., and Allard, M. (2006). Modeled current and future soil thermal regime for northeast Canada. *J. Geophys. Res.* 111:D18111. doi: 10.1029/2005JD007027

Sverdrup, H. (1990). *The Kinetics of Base Cation Release Due to Chemical Weathering*. Lund: Lund University Press, 246.

Sverdrup, H. (2009). Chemical weathering of soil minerals and the role of biological processes. *Fungal Biol. Rev.* 23, 94–100. doi: 10.1016/j.fbr.2009.12.001

Sverdrup, H., and Warfvinge, P. (1995). Critical loads of acidity for Swedish forest ecosystems. *Ecol. Bull.* 44, 75–89.

Sverdrup, H., and Warfvinge, P. (1999). Calculating field weathering rates using a mechanistic geochemical model PROFILE. *Appl. Geochem.* 8, 273–283. doi: 10.1016/0883-2927(93)90042-f

Velbel, M. A. (1985). Geochemical mass balances and weathering rates in forested watersheds of the Southern Blue Ridge. *Am. J. Sci.* 285, 904–930. doi: 10.2475/ajs.285.10.904

Venterea, R. T., Lovett, G. M., Groffman, P. M., and Schwarz, P. A. (2003). Landscape patterns of net nitrification in a northern hardwood-conifer forest. *Soil Sci. Soc. Am. J.* 67, 527–539. doi: 10.2136/sssaj2003.0527

Warfvinge, P., and Sverdrup, H. (1992). Calculating critical loads of acid deposition with PROFILE—a steady-state soil chemistry model. *Water Air Soil Pollut.* 63, 119–143. doi: 10.1007/bf00475626

White, A. F., and Blum, A. E. (1995). Effects of climate on chemical weathering in watersheds. *Geochim. Cosmochim. Acta* 59, 1729–1747. doi: 10.1016/0016-7037(95)00078-e

Yin, X. W., and Arp, P. A. (1993). Predicting forest soil temperatures from monthly air temperature and precipitation records. *Can. J. For. Res.* 23, 2521–2536. doi: 10.1139/x93-313

Zhang, Y., Chen, W., Smith, S. L., Riseborough, D. W., and Cihlar, J. (2005). Soil temperature in Canada during the twentieth century: complex responses to atmospheric climate change. *J. Geophys. Res.* 110:D03112.

**Conflict of Interest:** The authors declare that the research was conducted in the absence of any commercial or financial relationships that could be construed as a potential conflict of interest.

frontiers in Forests and Global Change

ORIGINAL RESEARCH
published: 25 September 2020
doi: 10.3389/ffgc.2020.535117

# Plant Nutritional Status Explains the Modifying Effect of Provenance on the Response of Beech Sapling Root Traits to Differences in Soil Nutrient Supply

*Sonia Meller[1,2], Emmanuel Frossard[2], Marie Spohn[3] and Jörg Luster[1]**

[1] Forest Soils and Biogeochemistry, Swiss Federal Institute for Forest, Snow and Landscape Research WSL, Birmensdorf, Switzerland, [2] Institute of Agricultural Sciences, Swiss Federal Institute of Technology ETH, Zurich, Switzerland, [3] Soil Ecology, University of Bayreuth, Bayreuth, Germany

Forests dominated by beech (*Fagus sylvatica* L.) cover large parts of Europe where they occupy a broad ecological niche in terms of soil fertility. This indicates a large potential to adapt to different soil conditions over long time periods. Recent changes in tree mineral nutrition across Europe raise the question to what degree beech can acclimate to changing soil conditions in the short term. In this study, we aimed at assessing the plasticity of root traits and rhizosphere properties of young beech trees from populations that are adapted to either high or low nutrient supply, when growing in soils differing in their fertility. We sampled beech saplings from two forest sites of contrasting nutrient supply, most distinctly in terms of phosphorus. We grew them for 2 years in rhizoboxes in mineral soil either from their own site or from the other site. We assessed the influence of the factors "plant origin" and "current soil" on root traits and rhizosphere properties. Fine root traits related to growth (biomass, length), architecture (branching), and morphology (diameter) responded strongly to the factor "current soil." Provenance (factor "plant origin") modified the response. The modifying effect was consistent with an influence of the plant status in those nutrients, which were not in sufficient supply in the soil. An additional genotypic difference in the sensitivity of the beech saplings to different soil nutrient supply could not be excluded. Fine root parameters normalized for length, mass, or volume (root tip density and frequency, specific root length and area, and root tissue density) did not differ among the treatments. Differences in percentage of mycorrhizal root tips and rhizosphere parameters related to phosphorus mobilization potential (pH, abundance of organic acid anions, and phosphatase activity) were small and mainly determined by the "current soil." Provenance had only a minor modifying effect, possibly due to differences in the ability of the plants to transfer carbon compounds from the shoot to the root and the fungal partner. Our results indicate a high plasticity of young beech trees to adapt their root system to different soil nutrient supply, thereby also taking into account internal nutrient reserves.

**Keywords: root growth, root architecture, root morphology, mycorrhizal colonization, rhizosphere, potential phosphatase activity, organic acid anions, acid forest soil**

OPEN ACCESS

***Edited by:***
*Sebastian Loeppmann, Christian-Albrechts-Universität zu Kiel, Germany*

***Reviewed by:***
*Stefano Mazzoleni, University of Naples Federico II, Italy*
*Maria Teresa Ceccherini, University of Florence, Italy*

***Correspondence:**
*Jörg Luster*
*joerg.luster@wsl.ch*

***Specialty section:***
*This article was submitted to Forest Soils, a section of the journal Frontiers in Forests and Global Change*

***Received:*** *14 February 2020*
***Accepted:*** *31 August 2020*
***Published:*** *25 September 2020*

***Citation:***
*Meller S, Frossard E, Spohn M and Luster J (2020) Plant Nutritional Status Explains the Modifying Effect of Provenance on the Response of Beech Sapling Root Traits to Differences in Soil Nutrient Supply. Front. For. Glob. Change 3:535117. doi: 10.3389/ffgc.2020.535117*

## INTRODUCTION

Forests dominated by European beech (*Fagus sylvatica* L.) cover large parts of Europe where climatic conditions are suitable (Durrant et al., 2016). Considering the distribution of important tree species in temperate forests, beech belongs to a group that is relatively insensitive to differences in soil nutrient supply (Walthert and Meier, 2017) and thus occurs at a wide range of soil chemical properties including strongly acid to alkaline pH, as well as low to high N and P availability (Leuschner et al., 2006). This indicates a large potential of beech to adapt to different soil nutrient supply over long periods of time. Considering the recent changes in tree mineral nutrition across Europe (Jonard et al., 2015), the question arises to what degree beech can acclimate to changing soil conditions in the short term. Of particular concern is phosphorus (P), since plant-available P occurs at only low concentrations in the soil solution, while most P is present in unavailable forms adsorbed to reactive surfaces of the soil solid phase or is bound in minerals or soil organic matter (Hinsinger, 2001).

Root–soil interactions have been shown to play a major role in adaptation to given soil conditions in relation to nutrient acquisition. Such interactions can include alterations of root growth, architecture and morphology, formation of mycorrhizae, and root exudation affecting nutrient availability in the rhizosphere (Richardson et al., 2009).

Root growth, architecture and morphology can be highly plastic in response to soil nutrient availability (Hodge et al., 2009). In particular, alterations in reaction to low soil availability of P and major nutrient cations (Mg, K, and Ca) that have been found across a large range of plant species include inhibition of primary root growth and promotion of lateral root growth (Gruber et al., 2013; Niu et al., 2013). Relations are not so clear in the case of N, which is demonstrated by maximum root length and branching of the model plant *Arabidopsis* at intermediate N limitation (Kiba and Krapp, 2016), and effects on branching depend in addition on the chemical form of N (nitrate or ammonium). While these mechanisms have been well established for crops, evidence for trees is scarce, and assessing effects of nutrient availability in the field is often made difficult by interaction with other soil properties such as texture (Weemstra et al., 2017), environmental factors such as the availability of water (Hertel et al., 2013) or light (Minotta and Pinzauti, 1996), or stand age (Finér et al., 2007). Preferential root proliferation in nutrient-enriched patches and layers has been observed frequently (Hodge, 2006; Chen et al., 2016). Particularly important for trees growing in nutrient-poor soils in temperate forests is preferential exploration of the topsoil, including the organic surface layer (Borken et al., 2007; Hauenstein et al., 2018).

Uptake via the mycorrhizal pathway is of major importance for N and P nutrition of trees in temperate zones (Plassard and Dell, 2010; Chalot and Plassard, 2011). While fertilization with P often decreases mycorrhization in inoculation experiments (Garbaye and Wilhelm, 1985; Kazantseva et al., 2009), under field conditions, relationships between soil P availability and measures of mycorrhization or mycorrhizal P uptake are less clear and might differ seasonally (Yang et al., 2016; Spohn et al., 2018). In most studies on the effect of N availability, mycorrhizal colonization increased with decreasing N availability (e.g., Brunner and Brodbeck, 2001; Sun et al., 2010); however, under natural concentration gradients, higher colonization was also found at lower C:N ratios (Hawkins et al., 2015). Under field conditions, the effects of both N and P supply on mycorrhization have to be considered as well (e.g., Bahr et al., 2013). Studies assessing host effects on ectomycorrhizal fungi provide a variable picture on the degree to which trees can actively shape the rhizosphere fungal community (Ishida et al., 2007; Lang et al., 2017; Spohn et al., 2018). There can also be competition between fungal partner and host plant, leading to limited nutrient transfer to the host (e.g., Simon et al., 2017).

On a small scale in the rhizosphere, root exudation can lead to an increase in the abundance of compounds that potentially increase the bioavailability of P, including protons, low-molecular-weight organic acid anions, and phosphatases (Hinsinger et al., 2011). However, under field conditions, it is often difficult to differentiate between the different sources of these compounds. Organic acid anions and phosphatases can be produced and released to the soil by roots, mycorrhizal hyphae, and free-living microorganisms (Gianfreda and Ruggiero, 2006; Oburger et al., 2011; Plassard et al., 2011). Therefore, also little is known to which degree plants are able to influence the P mobilization potential in their rhizosphere directly via root exudation and/or indirectly via stimulating microbial activity and growth or shaping the soil microbial community. For example, root exudates can stimulate P mineralization by heterotrophic bacteria in the rhizosphere (Spohn et al., 2013). Phosphatase activity (PA) in soil is often linked to soil P availability (Marklein and Houlton, 2012; Hofmann et al., 2016), but this relation can be masked, e.g., by the generally strong correlation with soil organic matter content (Nannipieri et al., 2011). The root exudation of organic acid anions may be induced by a low P nutritional status of the plant, as has been shown for crops (Hinsinger, 2001). However, it can also be a reaction to other conditions such as high Al concentrations in acid soils (Richardson et al., 2009) or be part of constitutive release of excess carbon (Heim et al., 2001; Eldhuset et al., 2007). Although proton exudation by roots can be induced by P deficiency (e.g., Shahbaz et al., 2006), alteration of rhizosphere pH often depends on the form of mineral nitrogen taken up by the plant (Riley and Barber, 1971; Hinsinger, 2001).

Signaling of the plant nutritional status has been shown to be involved in controlling root development, initiating mycorrhizal symbiosis, and producing and exuding mobilizing substances (Chalot and Plassard, 2011; George et al., 2011; Niu et al., 2013; Xuan et al., 2017). Thus, differences in this status could affect the root response of beech populations that are adapted to sites differing in resource availability, when growing in soils with different nutrient supply. However, genotypic differences related to adaptation to specific site conditions could also be involved. Beech populations across central Europe have been shown to be genetically closely related in terms of neutral markers, such as microsatellite loci, but to differ in genes related to adaptive traits (e.g., Buiteveld et al., 2007). Nevertheless, genotypic diversity has often been found to be larger within than among populations, also including also adaptive traits (e.g., Cuervo-Alarcon et al.,

2018). In contrast to the lack of studies on acclimation to changes in nutrient supply, the ability of beech populations from sites with different climatic conditions to acclimate, in the short term, to increased drought frequency has recently received much attention (Meier and Leuschner, 2008; Cuervo-Alarcon et al., 2018). Specifically, Meier and Leuschner (2008) found that while root traits, such as relative fine root growth and turnover, of beech populations from sites differing in precipitation responded generally strongly to drought treatment, the effect of provenance was small. Aboveground adaptive traits related to resource acquisition such as photosynthetic activity have been considered in the so-called "resource economics" framework (Craine, 2009). This differentiates between "acquisitive" and "conservative resource strategies" exhibited by plants growing at resource-rich and resource-poor sites, respectively. However, Weemstra et al. (2016) concluded from their review that there is little evidence for root physiological and morphological traits being indicative of specific nutrient acquisition strategies. Specifically, fine root diameter had often been found to correlate with root longevity and therefore been considered a respective potential belowground indicator. Taking together the information on genotypic relations among beech populations, their acclimation to drought, and relation between belowground plant traits and nutrient acquisition strategies, we do not expect strong genotypic provenance effects on root traits during acclimation to a different soil nutrient supply.

In this study, we aimed at assessing the plasticity of root traits and rhizosphere properties of young beech trees from populations, which are adapted to either high or low nutrient supply, when growing in soils differing in their fertility. To this end, we sampled beech saplings from two forest sites differing most distinctly in the supply P. We grew the saplings in mineral soil either from their own site or from the other site. In all four experimental treatments, we assessed the influence of the factors "plant origin" and "current soil" on root growth, architecture and morphology, mycorrhization, and the occurrence of P mobilizing compounds in the rhizosphere. In this "cross-exchange" approach, the factor "current soil" was considered to reflect differences not only in physicochemical soil properties but also in microbial communities adapted to these properties. Potential confounding effects by differences in so-called "plant-soil feedback" (reviewed, e.g., by Bever et al., 2012), are expected to be small when comparing different populations of the same plant species (Wagner et al., 2011; Gundale et al., 2014).

We hypothesized, first, that the assessed root traits and rhizosphere parameters are determined mainly by the factor "current soil." We hypothesized, second, that the factor "plant origin" modifies the effects of the soils and that the modifying effect can be attributed mainly to differences in the plant nutritional status.

# MATERIALS AND METHODS

## Plant and Soil Materials

Plant and soil materials were collected at the core research sites of the priority programme 1685 "Ecosystem nutrition" of the German Science Foundation (DFG)[1] in Unterlüss (Lower Saxony, Germany, LUE) and Bad Brückenau (northern Bavaria, Germany, BBR). The sites both sustain mature mono-specific beech stands, but differ in environmental conditions and soil properties (Lang et al., 2017), as summarized in **Supplementary Table S1**. The site LUE has a drier climate than the site BBR. The soil at BBR contains more N and P than the one at LUE in terms of total element stocks, as well as concentrations in organic surface layer and mineral soil. In particular, the P concentration in the mineral soil is much higher at BBR, whereas the organic surface layer is an important source of N and P at LUE. Both organic surface layer and mineral soil at LUE are more acidic and exhibit a lower base saturation than their BBR counterparts. Furthermore, the mineral soil at BBR has a loamy texture with a higher cation exchange capacity than the sandy mineral soil at LUE. Mature beeches are of similar age and height at both sites, however, their average diameter is much smaller at LUE.

Saplings of beech (*F. sylvatica* L.) of similar size were collected during their dormancy period in December 2014 and stored at 4°C with their roots embedded in soil until planting. Based on tree-ring counting, they were between 12 and 15 years old at the end of our experiment (Meller et al., 2019). Total N contents in various plant compartments were determined by combustion using an elemental analyzer (NC 2500, Carlo Erba Instruments), and total P, Mg, K, and Ca contents were determined by inductively coupled plasma optical emission spectrometry of digests (for details, see Meller et al., 2019).

Soil materials were taken from the Bh horizon in LUE and the uppermost part of the Bv horizon in BBR. This choice represented a compromise between root density within the soil profile—and thus potential importance for nutrient uptake—and organic matter content of the material being sufficiently low to not interfere with the assessment of rhizosphere properties. Soils were air-dried at 15°C, sieved to 4 mm, and homogenized. Plant residues were removed. Selected physical and chemical properties of the soils are summarized in **Table 1** and were mostly determined as described by Meller et al. (2019). Sequential P extraction was performed according to Hedley et al. (1982) as modified by Tiessen and Moir (2006). In **Table 1**, resin exchangeable inorganic P ($P_{resin}$), inorganic P ($P_i$) in various extracts (0.5 M $NaHCO_3$, 0.1 M NaOH before and after sonication, 1 M HCl, concentrated HCl), and organic P ($P_{org}$) in the $NaHCO_3$ and NaOH extracts are shown. The soil material from BBR exhibited a finer texture; a higher pH; a higher content in exchangeable nutrient cations; a higher organic carbon content; lower $C_{org}/N_{tot}$, $C_{org}/P_{org}$, and $N_{tot}/P_{org}$ ratios; and much higher concentrations of all inorganic and organic P fractions than the material from LUE. On the other hand, the LUE soil exhibited a higher proportion of $P_{org}$ than the BBR soil, and the base cation-to-Al ratio was similar in both soils.

## Experimental Setup

In April 2015, rhizoboxes were set up with beech saplings planted either in the soil from their site of origin or in the contrasting soil from the other site. In a completely randomized design,

[1] http://www.ecosystem-nutrition.uni-freiburg.de/

**TABLE 1 |** Properties of the soil materials from the forest sites Bad Brückenau (BBR, Bv horizon) and Unterlüss (LUE, Bh horizon); BC/Al refers to the ratio between the sum of exchangeable base cations (Mg, K, Ca) and exchangeable Al; inorganic P ($P_i$) and organic P ($P_{org}$) used in element ratios refer to the respective total extractable fractions; data are from Meller et al., 2019 except for the concentration of P fractions.

| | | BBR Bv | LUE Bh |
|---|---|---|---|
| **General soil properties** | | | |
| Sand | ($g\ kg^{-1}$) | 287 | 811 |
| Clay | ($g\ kg^{-1}$) | 253 | 43 |
| pH in $H_2O$ | | 4.8 | 4.0 |
| Sum of exchangeable Mg, K, Ca | ($mmol_c\ kg^{-1}$) | 3.3 | 1.4 |
| BC/Al | ($mol_c\ mol_c^{-1}$) | 0.08 | 0.07 |
| $C_{org}$ | ($g\ kg^{-1}$) | 41.2 | 18.5 |
| $N_{tot}$ | ($g\ kg^{-1}$) | 3.2 | 0.7 |
| **Inorganic P ($P_i$)** | | | |
| resin $P_i$ | ($mg\ kg^{-1}$) | 5.3 | 0.4 |
| $NaHCO_3$ extractable $P_i$ | ($mg\ kg^{-1}$) | 88.2 | 1.9 |
| NaOH extractable $P_i$ | ($mg\ kg^{-1}$) | 334.9 | 5.9 |
| NaOH extractable sonic $P_i$ | ($mg\ kg^{-1}$) | 52 | 1.2 |
| 1 M HCl extractable $P_i$ | ($mg\ kg^{-1}$) | 240 | 1.6 |
| $HCl_{conc}$ extractable $P_i$ | ($mg\ kg^{-1}$) | 195.9 | 18.1 |
| Total extractable $P_i$ (without residual P) | ($mg\ kg^{-1}$) | 916.3 | 29.1 |
| **Organically bound P ($P_{org}$)** | | | |
| $NaHCO_3$ extractable $P_{org}$ | ($mg\ kg^{-1}$) | 78.9 | 12.3 |
| NaOH extractable $P_{org}$ | ($mg\ kg^{-1}$) | 1036.2 | 42.5 |
| NaOH extractable sonic $P_{org}$ | ($mg\ kg^{-1}$) | 140.9 | 34.3 |
| Total extractable $P_{org}$ (without residual P) | ($mg\ kg^{-1}$) | 1256 | 89.1 |
| $P_{org}/P_i$ | ($g\ g^{-1}$) | 1.37 | 3.07 |
| **Stoichiometric ratios** | | | |
| $C_{org}/N_{tot}$ | ($g\ g^{-1}$) | 12.8 | 24.7 |
| $C_{org}/P_{org}$ | ($g\ g^{-1}$) | 33 | 208 |
| $N_{tot}/P_{org}$ | ($g\ g^{-1}$) | 2.6 | 8.4 |

each treatment was replicated six times. The rhizoboxes had inner dimensions of 60 cm × 25 cm × 1.5 cm. They consisted of PVC walls and a removable transparent front plate made of polymethyl methacrylate. The soil was filled into the boxes at a bulk density of 1.2 kg/dm$^3$. After 1 week of soil conditioning under irrigation as described below, the saplings were planted. At this time point, saplings possessed up to 10-cm-long tap roots of 0.5–1.5 cm diameter but almost no fine roots, which presumably had died off during storage. The roots were washed with tap water to remove sticking soil, and approximately 2 cm of tap root was cut to stimulate new root formation. For each tree, the front plate of one rhizobox was opened, the roots pressed into the soil, and the front plate closed again. Rhizoboxes were placed in a greenhouse with temperature control (day, 22 ± 2°C; night, 18 ± 2°C), natural light, and shading from the direct sun. Since shading with movable blinds was the only means for active cooling, at some days in summer, temperatures higher than 22°C occurred for short periods. The soil was kept dark by covering the rhizoboxes with black plastic foil, and to stimulate the formation of a quasi-planar root system along the front plate, the rhizoboxes were inclined at an angle of about 30°. Soil water potential in the rhizoboxes was kept at approximately -8 kPa by using irrigation tubes ("Rhizon irrigators," Rhizosphere research products, Wageningen, The Netherlands), providing P-free artificial rain solution based on the composition of natural precipitation [2.1 μM $K_2SO_4$, 3.7 μM $Na_2SO_4$, 3.0 μM $CaCl_2$, 4.4 μM $CaSO_4$, 1.9 μM $MgCl_2$, 26.4 μM $NH_4NO_3$, and 2.0 μM $Ca(NO_3)_2$; Holzmann et al., 2016]. During summer, additional periodic irrigation from the top was needed to compensate for high evapotranspiration. At the end of the first growing season (end of September 2015), the rhizoboxes were placed outside of the greenhouse, but protected by a roof, to induce dormancy. In November 2015, they were moved to a dark cold room at 4°C and periodically irrigated with artificial rain from the top. End of March 2016, after the last frost, the rhizoboxes were moved first to the protected area outside of the greenhouse, and in May, after appearance of the first leaves, back into the greenhouse with temperature control set to the same conditions as in the year before.

## Measurement of Rhizosphere Parameters

In August 2015 and 2016, non-destructive and minimally invasive membrane-based methods were applied to the surface-exposed roots after carefully removing the front plate. For each rhizobox, all measurements, as described in detail in the following paragraphs, were performed on the same day in the following order: pH (8–9 a.m.), exchangeable anions (10 a.m. to 1 p.m.), and potential PA (2–4 p.m.). For this, the rhizoboxes were laying horizontally on their back side. Two or three rhizoboxes were assessed per day within 2 weeks, and the order of replicates among the four treatments was selected randomly. Five replicates per plant/soil combination were selected. Since some of the LUE saplings growing in LUE soil died during the first months after planting, replication was only 3 in this case.

## pH Distribution

The pH in the rhizosphere was mapped using prototypes of planar optodes with an optimal measurement range between pH 3.5 and 5.0 and signal detection by a VisiSens camera (PreSens GmbH, Regensburg, Germany). The optodes consisted of a 10-μm-thick foil composed of a proton-permeable polymer matrix, with a pH-sensitive and a pH-insensitive dye fixed in this matrix. Upon contact with soil or buffer solution, pH is measured as the ratio between the fluorescence of the pH-sensitive indicator dye and the fluorescence of the pH-insensitive reference dye (for more details of the principle, refer to Blossfeld and Gansert, 2007). For this, photos taken with the VisiSens camera were separated into a red and green channel corresponding to the fluorescence of the sensitive and non-sensitive fluorophores, respectively. For calibration, small pieces of optodes were equilibrated in a buffer of pH 4 overnight and then placed for 30 min in buffered standard solutions with pH values ranging from 3 to 5. Five to ten measurements of each membrane were averaged. The calibration curve was sigmoidal with a quasi-linear range and thus optimum sensitivity, between pH 3.5 and 4.5. For soil measurements, optodes of about 1 × 2 to

$2 \times 2$ cm$^2$ were equilibrated in pH 4 buffer overnight, applied to the terminal part of at least three newly grown roots per rhizobox including the surrounding soil, and left to equilibrate for 15 min, protected with a small piece of clear acrylic glass. In initial tests, an equilibration time of 15 min was found to be optimum to reach stable conditions and to avoid artifacts caused by drying of the membrane at longer application times. Then, photos were taken with the VisiSens camera using a cylindric aluminum spacer of 6 cm length between camera and acrylic glass. In order to cover its whole area, several overlapping partial areas of each optode were measured, and photos were subsequently merged into one image using Adobe Photoshop (**Supplementary Figure S1**). After use, optodes were rinsed with deionized water and stored in a buffer of pH 4 in a dark plastic bag at 4°C, because they are damaged by drying and re-wetting and exposure to light. After overlaying the pH maps with a mask for the location of the roots, using Adobe Photoshop, two zones were defined: root surface (values in the middle of the root) and bulk soil (>2 mm from root edge). Averaged values of bulk soil and root surface per rhizobox were used in the statistical analysis.

## Nutrient and Organic Acid Anions

Nutrient and organic acid anions (nitrate, phosphate, sulfate, oxalate, and citrate) were collected from the rhizosphere using anion exchange membranes (AEMs; Shi et al., 2011). Strips of AEMs (2 cm × 0.5 cm; No. 55164 2S, BDH Laboratory Supplies, United Kingdom) were soaked in deionized water for 24 h and then converted into $HCO_3^-$ form by equilibration with 2.2 ml of various agents per cm$^2$ as follows: (i) for 10 min with 0.5 M HCl, (ii) twice for 1 h with 0.5 M NaCl, and (iii) three times for 30 min with 0.5 M $NaHCO_3$. In between and at the end, the AEMs were rinsed with deionized water and stored in deionized water at 4°C until use. The membranes were applied to at least three newly grown roots including tip, elongation zone, side roots, and the respective rhizosphere per rhizobox for 3 h, covered with a plastic sheet to keep them moist during this time. After collection, the AEMs were rinsed with deionized water to remove sticking soil and extracted for 3 h with 0.3 ml of 1.75 M HCl in 2 ml Eppendorf tubes (opened periodically to release an excess of $CO_2$ produced) using an end-over-end shaker at room temperature. The extracts were measured with ion chromatography (Thermo Scientific DIONEX ICS-3000 with InGuard Ag and Na Column 9*24 mm, an Ultratrace Anion Concentrator Column and a conductivity detector). Data from all membranes per rhizobox were averaged.

## Potential PA

Spatial distribution of potential PA in the rhizosphere and bulk soil was mapped using zymography as developed by Spohn and Kuzyakov (2013) with slight modifications. Polyamide membranes (pore size 0.45 μm, Sartorius Stedim Biotech GmbH, Goettingen, Germany) were coated with 4-methylumbelliferyl phosphate (MUF-P, Sigma-Aldrich) by soaking in a 12 mM solution of this substrate in $10^{-4}$ M HCl (unbuffered solution with pH similar to soil pH) directly before application. Membranes of approximately 150 cm$^2$ and varying shapes—to match the roots—were applied to newly grown long roots including the surrounding soil with a 1 mm protective layer of agarose gel (in $10^{-4}$ M HCl) between membrane and soil for 20 min. After incubation, the membrane was exposed to UV light (366 nm) in a dark chamber (UV cabinet camag, Muttenz, Switzerland) to visualize the fluorescence of the reaction product (4-Methylumbelliferone, MUF). Images (RGB) of the membrane were taken from a fixed distance of 28 cm using a Nikon D3200 Camera with an AF-S Nikkor 18–55 mm lens. Of all zymograms, several images were taken with different exposures. For quantification, an image without overexposure was selected and compared with the image of a series of MUF standards taken with the same exposure. Standards were prepared by soaking small pieces of the membrane in solutions of MUF in $10^{-4}$ M HCl with concentrations of 0, 35, 70, 130, and 200 μM MUF, yielding a linear calibration curve. The amount of MUF per unit area was calculated based on the amount of solution taken up and the surface of the membrane. The images of the standard curve and zymograms required further processing for which the intensities of the green channel of the RGB images were used without conversion (Image J version 1.18; Schneider et al., 2012). First, a correction was made for variations in light reaching the camera sensor. In our setting, this variation had a circular shape with a maximum near the center of the image and decreasing linearly toward the peripheries. Maximum and gradient of the corresponding function were defined based on spatial variations in light reflection from the homogeneous table background, which was part of each image. For this, we wrote a custom R [version 3.1.2 (2014-10-31)] code. Then, the intensities of individual pixels of zymograms, membranes with unreacted substrate, and standards were scaled based on this function. Second, the zymograms were corrected for background fluorescence of unreacted substrate on a piece of membrane that was not placed in contact with the soil but photographed in the same image. Third, we overlaid the corrected zymograms with masks representing the root distribution. For this, visible roots in a photograph of the open rhizobox were traced manually using Adobe Photoshop. This drawing, together with markings for the edges of the rhizobox was laid over a photograph of the rhizobox with substrate-soaked membranes applied. From this, masks were created showing root distribution and markings for the edges of the membranes. Finally, the mirrored masks were laid over the zymograms and the membrane markings in the masks aligned with the membranes in the zymogram. Intensities assigned to pixels on the root surface and in the bulk soil (areas > 2 mm from the edge of a root mask) were ranked and calibrated using a standard curve obtained as described above. For each rhizobox value, median values of PA for root and bulk soil of all individual membranes applied to this box were averaged.

## Root Morphology

The whole root systems of the saplings were excavated at the end of the experiment (August 2016), rinsed with tap water, and then scanned and analyzed for morphological characteristics using the WinRHIZO software employing 0.1 mm steps for root diameter. Specific root length (m g$^{-1}$) was calculated as length of fine roots (diameter ≤ 2 mm) divided by their dry mass (M), specific

root area ($m^2$ $kg^{-1}$) as surface of fine roots divided by M, and root tissue density (RTD) (kg $m^{-3}$) as M divided by volume of fine roots. Root tip density and frequency are expressed as number of root tips per unit length and per unit dry mass of fine roots, respectively. Branching was calculated as the number of forks divided by the total length of fine roots. In order to determine the mycorrhization of root tips for a given sapling, the whole fine root system was cut into small pieces, which were mixed in a bowl filled with water. Three replicate subsamples of 30 ml of root suspension were transferred to a petri dish each. The number of mycorrhized and non-mycorrhized root tips was counted for each replicate using a binocular, and the percentages of mycorrhized root tips were averaged.

## Carbon, Nitrogen, and Phosphorus in Soil Microbial Biomass

At the end of the experiment, bulk soil and rhizosphere soil—defined as soil sticking to the roots after gentle shaking—were collected from the rhizoboxes. Microbial biomass C and N ($C_{mic}$, $N_{mic}$) were determined using chloroform fumigation–extraction (Brookes et al., 1985), following the detailed instructions by Voroney et al. (2006). Specifically, soils were fumigated for 24 h and extracted with 0.5 M $K_2SO_4$ at a soil-to-extractant ratio of 1:5. Organic C and total N in the extracts were measured using a TOC/TN analyzer (Shimadzu TOC-V). The measured values for $C_{mic}$ and $N_{mic}$ were used without factors accounting for soil-specific recovery. Microbial biomass P ($P_{mic}$) was determined using the hexanol fumigation method introduced by Kouno et al. (1995) as described by Bünemann et al. (2004). Briefly, slurries of 0.5 g soil in 30 ml of deionized water with and without addition of 1 ml of hexanol were incubated together with an AEM in bicarbonate form (for preparation see above) for 16 h. Then, the AEMs were removed and extracted with 0.5 M HCl. Phosphate in the extracts was analyzed colorimetrically using malachite green (Ohno and Zibilske, 1991) and a phosphate standard curve in 0.5 M HCl. The re-sorption of P released by hexanol fumigation was accounted for by employing a third replicate incubation with addition of a suitable P spike as described by Bünemann et al. (2004).

## Statistical Analysis

All analyses were performed in R [R version 3.1.2 (2014-10-31)]. Differences among individual treatments were assessed by using analysis of variance (ANOVA) followed by a Tukey *post hoc* test. In addition, results were tested for an influence of the factors "plant origin" and "current soil" as well as their interactions using two-way ANOVA. The following variables were log transformed to meet the requirements of the ANOVA: concentrations of resin-extractable phosphate in the first and second season, exchangeable nitrate in the first season, foliar N/Ca ratios in the first and second season, foliar K concentrations and N/P ratios in the second season. Because of unequal group sizes, we used the ANOVA model from the R package "car" that employs a "type II" test of the factors (for details of the definition of "type II" testing in "car," refer to the respective reference manual)[2].

# RESULTS

## Nutritional Status of the Beech Saplings

During the experiment, the nutritional status of the beech saplings underwent a drastic change from mainly reflecting their site of origin in the first growing season to a major influence of the experimental soil in the second growing season. Important exceptions were K with a strong additional influence of the factor "current soil" already in the first season and P with a still strong additional effect of the factor "plant origin" in the second season. The respective data are provided in **Table 2** and described in more detail in the following.

Foliar concentrations and concentration ratios in the first growing season revealed, irrespective of the soil, a higher supply of beech saplings from LUE with N and a lower supply with P and Mg than saplings from BBR. Compared to leaves of BBR plants, leaves of LUE plants exhibited about 10% higher N, 30% lower P, and 50% lower Mg concentrations, as well as about 50% higher N/P and twice as high N/Mg ratios. These differences were not all significant, but the corresponding effect of the factor "plant origin" was. The additional influence of the factor "current soil" on foliar K in the first growing season was stronger for saplings from LUE than from BBR. As a consequence, foliar K concentrations were about 40% higher for LUE plants growing in LUE soil than in all other treatments. These differences were significant, as were the effects of both experimental factors and their interaction. Similar differences were observed for the N/K ratios (35 and 15% lower for LUE and BBR saplings, respectively, when comparing growth in LUE with growth in BBR soil), but only the factor "current soil" was significant.

In the second growing season and irrespective of their site of origin, the leaves of saplings growing in the BBR soil exhibited a lower supply with N and K but a higher supply with Mg and Ca than leaves of saplings growing in the LUE soil. The corresponding effects of the factor "current soil" on foliar concentrations and concentration ratios were all significant except for N/K. The same applied to the respective differences between plants from the same origin growing in the different soils. The smallest difference was about 25% for N concentrations of BBR saplings, and the largest difference was about 100% for Mg concentrations of saplings from both sites of origin. Additional small but significant effects of the factor "plant origin" indicated that LUE plants were better supplied with N, and less supplied with Mg and Ca than BBR plants when comparing growth in the same soil. The respective differences in Ca concentrations were small and not significant. By contrast, differences in N concentrations and N/Mg ratios were large (30 and 250%, respectively) and significant, but only for growth in the LUE soil. The strong combined effects of both factors, "current soil" and "plant origin," on foliar P were expressed by 50% lower P concentrations and five times higher N/P ratios for LUE than

[2]https://cran.r-project.org/web/packages/car/car.pdf

**TABLE 2 |** Nutrient concentrations and ratios in full season leaves, as well as average nutrient concentrations in the whole plant for beech (*Fagus sylvatica* L.) saplings originating from the sites Bad Brückenau (BBR) and Unterlüss (LUE), respectively.

| | | | | | | Source of variation | | |
|---|---|---|---|---|---|---|---|---|
| | | BBR in BBR | BBR in LUE | LUE in BBR | LUE in LUE | Current soil | Plant origin | Current soil × plant origin |
| **Leaves season 1** | | | | | | | | |
| N | (mg g$^{-1}$) | 21.5 ± 0.9*a* | 21.0 ± 0.9*a* | 23.3 ± 0.4*a* | 24.2 ± 1.5*a* | 1.2 ns | 7.2* | 0.6 ns |
| P | (mg g$^{-1}$) | 1.2 ± 0.1*ab* | 1.4 ± 0.1*a* | 0.9 ± 0.1*b* | 1.0 ± 0.1*ab* | 2.0 ns | 9.9** | 0.2 ns |
| Mg | (mg g$^{-1}$) | 2.5 ± 0.2*a* | 2.0 ± 0.2*ab* | 1.3 ± 0.2*b* | 1.2 ± 0.1*b* | 3.9 ns | 28*** | 1.1 ns |
| K | (mg g$^{-1}$) | 4.4 ± 0.3*b* | 4.9 ± 0.3*b* | 4.7 ± 0.3*b* | 7.1 ± 0.6*a* | 16.2** | 9.4** | 8.3* |
| Ca | (mg g$^{-1}$) | 7.0 ± 0.3*a* | 5.7 ± 0.7*a* | 7.8 ± 0.5*a* | 6.4 ± 1.6*a* | 3.5 ns | 1.2 ns | 0.01 ns |
| N/P | (g g$^{-1}$) | 18 ± 1*bc* | 15 ± 2*c* | 25 ± 2*a* | 24 ± 3*ab* | 1.1 ns | 19** | 0.1 ns |
| N/Mg | (g g$^{-1}$) | 9 ± 1*b* | 11 ± 1*b* | 19 ± 2*a* | 21 ± 2*a* | 1.7 ns | 33*** | 0.0 ns |
| N/K | (g g$^{-1}$) | 4.9 ± 0.2*a* | 4.3 ± 0.1*ab* | 5.1 ± 0.3*a* | 3.4 ± 0.1*b* | 18*** | 0.9 ns | 4.1 ns |
| N/Ca | (g g$^{-1}$) | 3.1 ± 0.2*a* | 3.9 ± 0.5*a* | 3.1 ± 0.2*a* | 4.3 ± 1.0*a* | 4.4 ns | 0.04 ns | 0.2 ns |
| **Leaves season 2** | | | | | | | | |
| N | (mg g$^{-1}$) | 16.1 ± 1.3*c* | 22.0 ± 1.5*b* | 17.6 ± 0.9*bc* | 28.4 ± 1.0*a* | 38*** | 7.3* | 3.5 ns |
| P | (mg g$^{-1}$) | 1.6 ± 0.1*a* | 0.9 ± 0.1*b* | 0.9 ± 0.1*b* | 0.7 ± 0.3*b* | 14** | 13** | 3.1 ns |
| Mg | (mg g$^{-1}$) | 2.8 ± 0.3*a* | 1.5 ± 0.2*b* | 2.4 ± 0.2*a* | 1.1 ± 0.5*b* | 28*** | 2.6 ns | 0.04 ns |
| K | (mg g$^{-1}$) | 5.9 ± 0.6*b* | 9.4 ± 1.0*a* | 5.5 ± 0.2*b* | 11.3 ± 0.4*a* | 36*** | 0.3 ns | 1.9 ns |
| Ca | (mg g$^{-1}$) | 6.9 ± 0.4*ab* | 4.1 ± 0.2*c* | 8.3 ± 0.5*a* | 5.0 ± 1.1*bc* | 32*** | 5.3* | 0.3 ns |
| N/P | (g g$^{-1}$) | 11 ± 1*c* | 25 ± 2*ab* | 20 ± 2*b* | 51 ± 15*a* | 41*** | 20*** | 0.0 ns |
| N/Mg | (g g$^{-1}$) | 6 ± 0.3*b* | 16 ± 2*b* | 7 ± 1*b* | 39 ± 12*a* | 29*** | 7.8* | 9.2** |
| N/K | (g g$^{-1}$) | 2.9 ± 0.4*a* | 2.4 ± 0.2*a* | 3.2 ± 0.1*a* | 2.5 ± 0.02*a* | 4.2 ns | 0.8 ns | 0.2 ns |
| N/Ca | (g g$^{-1}$) | 2.4 ± 0.2*b* | 5.4 ± 0.4*a* | 2.2 ± 0.1*b* | 6.3 ± 1.4*a* | 81*** | 0.0 ns | 1.2 ns |
| **Whole plant** | | | | | | | | |
| N | (mg g$^{-1}$) | 5.8 ± 0.3*b* | 8.2 ± 0.6*a* | 5.8 ± 0.3*b* | 9.5 ± 0.5*a* | 47*** | 1.6 ns | 2.3 ns |
| P | (mg g$^{-1}$) | 0.9 ± 0.1*a* | 0.7 ± 0.1*b* | 0.4 ± 0.03*c* | 0.3 ± 0.1*c* | 12** | 72*** | 0.1 ns |
| Mg | (mg g$^{-1}$) | 1.5 ± 0.1*a* | 1.1 ± 0.1*b* | 1.3 ± 0.1*ab* | 0.7 ± 0.1*c* | 43*** | 14** | 2.7 ns |
| K | (mg g$^{-1}$) | 2.5 ± 0.1*b* | 3.2 ± 0.1*a* | 2.1 ± 0.1*b* | 3.3 ± 0.3*a* | 54*** | 1.8 ns | 2.8 ns |
| Ca | (mg g$^{-1}$) | 3.5 ± 0.2*ab* | 3.1 ± 0.1*b* | 4.1 ± 0.2*a* | 4.1 ± 0.3*a* | 1.5 ns | 15** | 1.8 ns |

*The saplings were grown in material from the Bv horizon at BBR or from the Bh horizon at LUE. The first four data columns show mean values ± standard error of replicate plants; different letters indicate significant differences between means according to the Tukey post hoc test. The last three columns show results of the two-way analysis of variance on the factors "current soil" and "plant origin"; shown are $F_{(1,\ 14)}$ values for the factors and their interactions; statistical significance is indicated as ***P < 0.001, **P < 0.01, *P < 0.05; ns, not significant. P data are taken from Meller et al. (2019).*

BBR plants growing in the soil from their own site, and values in between for the other two treatments.

The average concentrations of N, Mg, and K in the whole plant at the end of the experiment in the second growing season reflected the situation in the leaves and were also determined mainly by the factor "current soil." By contrast, average P concentrations in the whole plant were still mainly determined by the factor "plant origin" and were about 50% lower in saplings from LUE than from BBR, when comparing growth in the same soil. In addition, average Ca concentrations were determined significantly by "plant origin" only with about 25% higher values in saplings from LUE than BBR.

## Growth, Architectural, and Morphological Traits of Fine Roots

Fine root traits of the beech saplings at the end of the experiment related to size, branching, and diameter were mainly determined by the "current soil," but with an additional effect of "plant origin," which was more pronounced for growth in the LUE soil. The respective data are presented in **Table 3** and **Figure 1**, and the results of the ANOVA are shown in **Table 4**.

Irrespective of their origin, beech saplings exhibited a larger root system—in terms of mass, length, and number of root tips—in the BBR than the LUE soil. However, the respective trait differences were larger for saplings from LUE (three to five times higher values in BBR than LUE soil) than for saplings from BBR (about 50–75% higher values in BBR than LUE soil). The differences were not all significant, but the effects of both experimental factors were in all cases. Furthermore, beech saplings from LUE growing in soil from LUE had developed a fine root system with half the branching of plants in all other treatments. This led to a significant interaction between the two experimental factors.

Fine root diameters were identical for saplings from both sites of origin when growing in soil from BBR, with 40% of all fine roots being thinner or equal to 0.1 mm. By contrast, the distribution of root diameter categories differed between the plants from the two sites of origin for growth in the LUE soil. When compared to the growth in the

**TABLE 3 |** Morphological traits of fine roots (<2 mm diameter), as measured during the second growing season in a rhizobox experiment with beech (*Fagus sylvatica* L.) saplings originating from the sites Bad Brückenau (BBR) and Unterlüss (LUE), respectively.

| | | BBR in BBR | BBR in LUE | LUE in BBR | LUE in LUE |
|---|---|---|---|---|---|
| Total mass | (g) | 2.6 ± 0.4*a* | 1.5 ± 0.4*ab* | 1.9 ± 0.2*ab* | 0.6 ± 0.2*b* |
| Total length | (m) | 9.1 ± 0.6*a* | 5.6 ± 1.0*b* | 7.6 ± 0.8*ab* | 1.7 ± 0.4*c* |
| Branching | ($cm^{-1}$) | 14.8 ± 0.7*a* | 12.6 ± 0.6*a* | 15.1 ± 0.9*a* | 7.4 ± 0.2*b* |
| Number of root tips | (no.) | 29′213 ± 2′674*a* | 19′449 ± 2′525*a* | 25′2497 ± 3′868*a* | 4′804 ± 869*b* |
| Root tip density | ($cm^{-1}$) | 3.9 ± 0.3*a* | 4.1 ± 0.1*a* | 3.9 ± 0.4*a* | 3.7 ± 0.4*a* |
| Specific root length | ($m\ g^{-1}$) | 37 ± 4*a* | 41 ± 4*a* | 44 ± 6*a* | 28 ± 4*a* |
| Specific root area | ($m^2\ kg^{-1}$) | 35 ± 3*a* | 39 ± 4*a* | 40 ± 5*a* | 30 ± 4*a* |
| Root tissue density | ($kg\ m^{-3}$) | 201 ± 15*a* | 198 ± 21*a* | 190 ± 20*a* | 265 ± 36*a* |
| Root tip frequency | ($mg^{-1}$) | 12.1 ± 1.8*a* | 14.7 ± 1.9*a* | 14.3 ± 2.3*a* | 8.4 ± 1.3*a* |
| Mycorrhization | (%) | 49 ± 3*ab* | 66 ± 7*a* | 42 ± 2*b* | 51 ± 8*ab* |

*The saplings were grown in material from the Bv horizon at BBR or from the Bh horizon at LUE. Mass-based parameters are as or related to dry weight. Data represent mean values ± standard error of replicate plants; different letters indicate significant differences between means according to the Tukey post hoc test.*

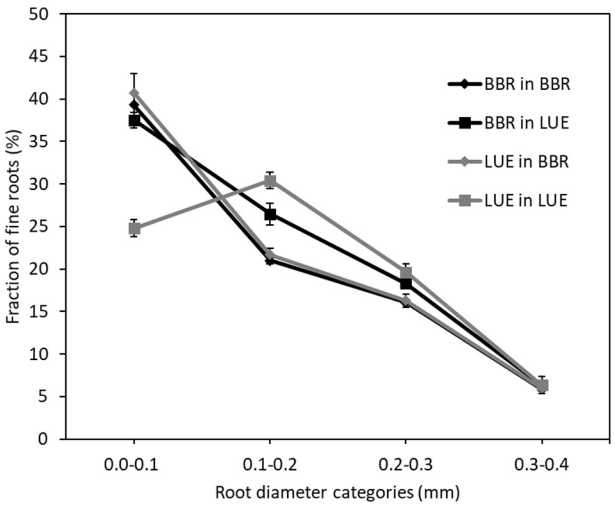


**FIGURE 1 |** Fractions of fine roots in different diameter categories in (%) of total length of fine roots with diameter ≤ 2 mm, as measured in August of the second growing season in a rhizobox experiment with beech (*Fagus sylvatica* L.) saplings originating from the sites Bad Brückenau (BBR) and Unterlüss (LUE). The saplings were grown in material from the Bv horizon at BBR or from the Bh horizon at LUE. Data represent mean values ± SE for replicate saplings ($n$ = 5, except $n$ = 3 for LUE in LUE); lines serve as visual aid only.

**TABLE 4 |** Two-way analysis of variance for different fine root traits of beech (*Fagus sylvatica* L.) saplings, as measured in the second growing season of a rhizobox experiment; saplings originated from the sites Bad Brückenau (BBR) and Unterlüss (LUE) (factor "plant origin") and were grown in material from the Bv horizon at BBR or from the Bh horizon at LUE (factor "current soil"); shown are $F_{(1,\ 14)}$ values for the factors and their interactions; statistical significance is indicated as ***$P < 0.001$, **$P < 0.01$, *$P < 0.05$; ns, not significant.

| | Source of variation | | |
|---|---|---|---|
| | Current soil | Plant origin | Current soil × plant origin |
| Total mass | 13.4** | 6.4* | 0.0*ns* |
| Total length | 35.4*** | 10.3** | 2.3*ns* |
| Branching | 37.8*** | 6.5* | 13.3** |
| Number of root tips | 23.2*** | 7.7* | 3.2*ns* |
| Root tip density | 1.9*ns* | 0.9*ns* | 3.3*ns* |
| Specific root length | 0.8*ns* | 0.0*ns* | 3.7*ns* |
| Specific root area | 0.1*ns* | 0.0*ns* | 2.8*ns* |
| Root tissue density | 1.9*ns* | 0.9*ns* | 3.3*ns* |
| Root tip frequency | 0.2*ns* | 0.3*ns* | 4.6* |
| *Fractions of root diameter categories:* | | | |
| 0.0–0.1 mm | 17.4*** | 5.0* | 14.4** |
| 0.1–0.2 mm | 59.9*** | 5.0* | 3.4*ns* |
| 0.2–0.3 mm | 17.9*** | 1.0*ns* | 0.7*ns* |
| 0.3–0.4 mm | 2.5*ns* | 0.1*ns* | 0.0*ns* |
| Mycorrhization | 7.7* | 3.9*ns* | 0.7*ns* |

BBR soil, LUE plants growing in LUE soil exhibited a lower proportion of the thinnest roots but higher proportions of roots with diameters between 0.1 and 0.3 mm. On the other hand, BBR plants growing in LUE soil exhibited the same proportion of thinnest roots, a higher proportion of roots between 0.1 and 0.3 mm, and a lower proportion of fine roots larger than 0.4 mm, when compared to growth in BBR soil.

In contrast to the aforementioned root traits, fine root parameters normalized for length, mass, or volume (root tip density and frequency, specific root length and area, and RTD) were equal for all four plant-soil combinations (**Table 3**) and the experimental factors did not exert any significant effect (**Table 4**).

## Mycorrhizal Colonization of Fine Roots and Soil Microbial Biomass

After two growing seasons, mycorrhizal colonization of root tips did not differ strongly among the four treatments. Fine roots of saplings from the same site of origin tended to be more highly colonized when growing in the LUE than the BBR soil (**Table 3**). The corresponding effect of the factor "current soil" was significant (**Table 4**). On the other hand, in the same soil, BBR plants tended to have more highly colonized roots than LUE plants. The corresponding effect of the factor "plant origin" was weak [$F_{(1,\ 14)} = 3.9$; $P = 0.06$].

**TABLE 5 |** Soil microbial biomass C, N, and P concentrations (per dry weight) in the bulk soil (bulk) and the rhizosphere (RS), as well as ratios in the rhizosphere, as measured during the second growing season in a rhizobox experiment with beech (*Fagus sylvatica* L.) saplings originating from the sites Bad Brückenau (BBR) and Unterlüss (LUE).

| | | BBR in BBR | BBR in LUE | LUE in BBR | LUE in LUE |
|---|---|---|---|---|---|
| $C_{mic}$ bulk | (mg $kg^{-1}$) | 224 ± 13*a* | 51 ± 8*b* | 219 ± 17*a* | 43 ± 16*b* |
| $C_{mic}$ RS | (mg $kg^{-1}$) | 259 ± 13*a* | 65 ± 7*b* | 251 ± 15*a* | 48 ± 11*b* |
| $N_{mic}$ bulk | (mg $kg^{-1}$) | 31.6 ± 0.9*a* | 5.0 ± 0.6*b* | 31.6 ± 1.7*a* | 4.7 ± 0.9*b* |
| $N_{mic}$ RS | (mg $kg^{-1}$) | 35.7 ± 0.8*a* | 8.0 ± 0.7*b* | 32.8 ± 0.8*a* | 4.4 ± 1.4*b* |
| $P_{mic}$ bulk | (mg $kg^{-1}$) | 6.2 ± 1.5*a* | 1.9 ± 0.2*ab* | 4.4 ± 1.2*ab* | 1.2 ± 0.4*b* |
| $P_{mic}$ RS | (mg $kg^{-1}$) | 5.9 ± 1.1*a* | 2.4 ± 0.4*a* | 5.2 ± 1.2*a* | 2.3 ± 0.3*a* |
| $C_{mic}/N_{mic}$ bulk | (g $g^{-1}$) | 7.1 ± 0.6*a* | 10.5 ± 1.6*a* | 7.0 ± 0.7*a* | 10.3 ± 4.6*a* |
| $C_{mic}/N_{mic}$ RS | (g $g^{-1}$) | 7.3 ± 0.4*b* | 8.0 ± 0.5*ab* | 7.6 ± 0.4*b* | 11.6 ± 2.4*a* |
| $C_{mic}/P_{mic}$ bulk | (g $g^{-1}$) | 49.6 ± 19*a* | 25.8 ± 4.6*a* | 84.8 ± 31*a* | 67.7 ± 49*a* |
| $C_{mic}/P_{mic}$ RS | (g $g^{-1}$) | 58 ± 19*a* | 29 ± 6*a* | 86 ± 39*a* | 26 ± 2*a* |
| $N_{mic}/P_{mic}$ bulk | (g $g^{-1}$) | 6.5 ± 2.1*ab* | 2.4 ± 0.1*b* | 11.2 ± 3.3*a* | 5.1 ± 1.8*ab* |
| $N_{mic}/P_{mic}$ RS | (g $g^{-1}$) | 5.2 ± 0.4*ab* | 3.5 ± 0.9*ab* | 6.3 ± 1.3*a* | 2.3 ± 0.6*b* |

*The saplings were grown in material from the Bv horizon at BBR or from the Bh horizon at LUE. Data represent mean values ± standard error of replicate rhizoboxes; different letters indicate significant differences between means according to the Tukey post hoc test.*

Microbial biomass in bulk soil and rhizosphere at the end of the experiment was much higher in the BBR than the LUE soil with almost no effect of the origin of the beech saplings growing in the soil. Microbial biomass C ($C_{mic}$) in BBR soil was about 4.5 times, that in $N_{mic}$ was about 6 times, and that in $P_{mic}$ was about 3 times higher than in LUE soil (**Table 5**). The differences in $C_{mic}$ and $N_{mic}$ were significant, while those in $P_{mic}$ were not. The corresponding effects of the factor "current soil" were highly significant for $C_{mic}$ and $N_{mic}$, but only weakly significant for $P_{mic}$ (**Table 6**). The $C_{mic}$:$N_{mic}$ ratios in LUE soil tended to be a bit higher, the $C_{mic}$:$P_{mic}$ ratios were up to three times lower, and the $N_{mic}$:$P_{mic}$ ratios were two to three times lower than in the BBR soil. Considering both bulk soil and rhizosphere data for all plant-soil combinations, there was a weakly significant rhizosphere effect for $C_{mic}$ ($P = 0.02$) and $N_{mic}$ ($P = 0.008$) with slightly higher concentrations in the rhizosphere.

**TABLE 6 |** Analysis of variance for microbial biomass C, N, and P ($C_{mic}$, $N_{mic}$, $P_{mic}$) in bulk soil (bulk) and rhizosphere (RS), the difference between pH on the root and in the bulk soil (ΔpH), resin extractable anions (nitrate, phosphate, oxalate, and citrate) in the rhizosphere, and phosphatase activity (PA) on the root and in the bulk soil, as measured in the first and/or second growing season of a rhizobox experiment with beech (*Fagus sylvatica* L.) saplings; saplings originated from the sites Bad Brückenau (BBR) and Unterlüss (LUE) (factor "plant origin"), and were grown in material from the Bv horizon at BBR or from the Bh horizon at LUE (factor "current soil"); shown are $F_{(1,\ 14)}$ values for the factors and their interactions; statistical significance is indicated as $^{***}P < 0.001$, $^{**}P < 0.01$, $^{*}P < 0.05$; ns, not significant.

| | Source of variation | | |
|---|---|---|---|
| | Current soil | Plant origin | Current soil × plant origin |
| $C_{mic}$ bulk (season 2) | 138.73*** | 0.16*ns* | 0.017*ns* |
| $C_{mic}$ RS (season 2) | 221.70*** | 0.78*ns* | 0.10*ns* |
| $N_{mic}$ bulk (season 2) | 525.93*** | 0.04*ns* | 0.03*ns* |
| $N_{mic}$ RS (season 2) | 922.03*** | 12.17** | 0.13*ns* |
| $P_{mic}$ bulk (season 2) | 11.60** | 1.86*ns* | 0.03*ns* |
| $P_{mic}$ RS (season 2) | 5.06* | 0.24*ns* | 0.05*ns* |
| ΔpH (season 2) | 0.22*ns* | 1.27*ns* | 0.00*ns* |
| Nitrate (season 1) | 19.54*** | 4.13*ns* | 0.49*ns* |
| Nitrate (season 2) | 3.62*ns* | 0.05*ns* | 1.01*ns* |
| Phosphate (season 1) | 14.57** | 0.04*ns* | 1.20*ns* |
| Phosphate (season 2) | 1.29*ns* | 0.08*ns* | 0.43*ns* |
| Oxalate (season 1) | 1.51*ns* | 10.96** | 1.21*ns* |
| Oxalate (season 2) | 4.55* | 0.15*ns* | 0.58*ns* |
| Citrate (season 1) | 0.15*ns* | 3.50*ns* | 0.49*ns* |
| Citrate (season 2) | 0.14*ns* | 1.71*ns* | 0.14*ns* |
| PA root (season 1) | 9.15** | 0.18*ns* | 0.01*ns* |
| PA root (season 2) | 6.20* | 3.24*ns* | 0.97*ns* |
| PA bulk soil (season 1) | 2.69*ns* | 0.92*ns* | 0.93*ns* |
| PA bulk soil (season 2) | 11.89** | 8.05* | 3.43*ns* |
| PA/$P_{mic}$ root (season 2) | 1.53*ns* | 1.28*ns* | 0.33*ns* |
| PA/$P_{mic}$ bulk (season 2) | 3.94*ns* | 2.30*ns* | 1.12*ns* |

## Rhizosphere Properties

Although the variability of all measured rhizosphere properties was large and differences among treatments were mostly not significant, ANOVA revealed significant effects of the experimental factors. Most of the parameters differed between the first and the second growing season in terms of magnitude, effects of the two experimental factors, or both. The influence of the factor "current soil" was higher in most cases in both years except for a larger effect of "plant origin" on the abundance of low-molecular-weight organic acids in the first growing season. The respective data are shown in **Figures 2–4**, and the results of the ANOVA are shown in **Table 6**.

In the second growing season, we observed small pH increases from bulk soil to the roots for all plant-soil combinations (**Figure 2**). However, effects of neither "plant origin" nor "current soil" were significant. Unfortunately, measurements performed in the first growing season provided no reliable data.

Resin-extractable nitrate in the rhizosphere exhibited different patterns in the two growing seasons (**Figure 3A**). Comparing growth in the BBR with growth in the LUE soil in the first year, nitrate in the rhizosphere of roots of BBR and LUE plants was about three and five times higher, respectively. The respective influence of the factor "current soil" was significant. In the second

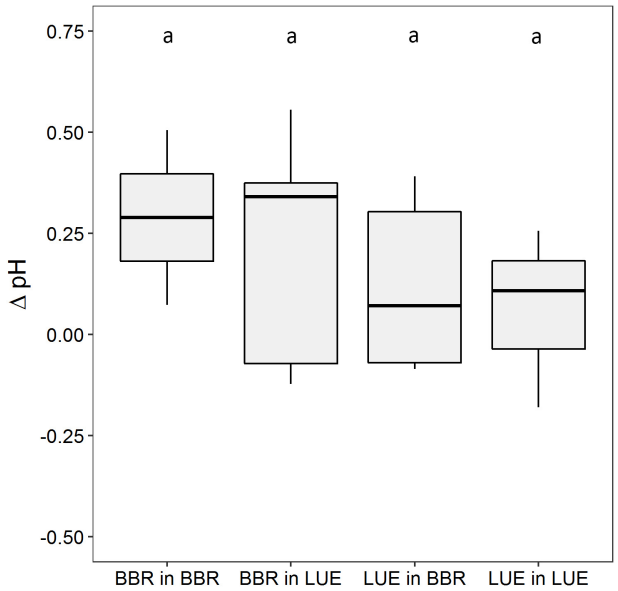


**FIGURE 2 |** Difference between pH measured with optodes on the surface of roots and in the bulk soil (ΔpH) in August of the second growing season in a rhizobox experiment with beech (*Fagus sylvatica* L.) saplings originating from the sites Bad Brückenau (BBR) and Unterlüss (LUE). The saplings were grown in material from the Bv horizon at BBR or from the Bh horizon at LUE. Shown are box plots based on values for replicate rhizoboxes in the second growing season ($n$ = 5, except $n$ = 3 for LUE in LUE and $n$ = 2 for BBR in BBR); different letters indicate significant differences between means according to the Tukey *post hoc* test.

growing season, nitrate concentrations remained similar to the first year in the BBR soil but increased strongly in the LUE soil and were larger than in the BBR soil. The differences were not significant, though, and the effect of the factor "current soil" was weak [$F_{(1,\ 14)}$ = 3.6; $P$ = 0.08].

During the first growing season, resin-extractable phosphate was also significantly determined by the factor "current soil" with about two times higher concentrations in the BBR than the LUE soil (**Figure 3B**). In the second growing season, the pattern remained the same as a trend and concentrations were generally higher but also more variable than in the first growing season.

Oxalate and citrate were the only detectable resin-extractable low-molecular-weight organic acid anions, with oxalate occurring in about 10 times higher amounts than citrate (**Figures 3C,D**). In the first growing season, amounts of oxalate in the rhizosphere of the BBR plants were around 5 nmol $cm^{-2}$, while amounts in the rhizosphere of LUE plants were about two times lower (BBR soil) or below the detection limit of 0.05 nmol $cm^{-2}$ (LUE soil). This pattern led to a significant effect of "plant origin." Citrate showed the same trends, but the effect of "plant origin" was not significant. In the second growing season, amounts of oxalate were generally lower than in the first year at around 0.15 nmol $cm^{-2}$. There was no plant effect anymore, but a weak effect of "current soil" with a tendency to slightly higher amounts in the LUE soil. The few cases of detectable amounts of citrate suggest a similar, but not significant, effect of "plant origin" as in the first year.

In general, potential PA was highest on the main roots, intermediate on the side roots, and lowest in the bulk soil (see example in **Supplementary Figure S2**). During the first growing season, PA tended to be higher in the BBR than in the LUE soil, irrespective of the origin of the beech saplings (median values differed by about 15% in the bulk soil and by about 25% on the root; **Figure 4A**). This effect of "current soil" was significant for PA on roots but not for the bulk soil. In the second growing season, up to 30% lower PA were measured than in the first year, but the patterns among the treatments remained similar. The respective effect of "current soil" was significant for PA on roots and in the bulk soil. In contrast to the first year, the soil effect was overlaid by a weak effect of "plant origin"—albeit significant in the case of bulk soil—with a tendency to slightly higher values for saplings from BBR. In contrast to PA, PA per unit microbial P ($PA/P_{mic}$) exhibited a tendency toward higher values in the LUE soil, both on the root and in the bulk soil (**Figure 4B**).

# DISCUSSION

## Availability of Nutrients in the Soil and Plant Nutritional Status

Our results showed that after two growing seasons, the nutrient concentrations in different compartments of the beech saplings, irrespective of their provenance, had become largely determined by the experimental soil, with the notable exception of P (**Table 2**). In this section, we discuss these results by first reflecting on the soil conditions and plant characteristics at the sampling sites and then evaluating the plant nutritional status in our experiment as basis for the discussion of root and rhizosphere data in the following sections.

The comparison of the climatic conditions and soil properties at the two sites indicates more favorable conditions for plant growth at BBR than LUE in terms of both water and nutrients. An overall adaptation of the ecosystem at LUE to the low fertility of the mineral soil is the recycling of nutrients via a thick organic surface layer (Bünemann et al., 2016; Lang et al., 2017).

While the beech population at BBR is putatively autochthonous, this is not certain for the one at LUE (Dietrich and Meesenburg, personal communications). Nevertheless, considering (i) the generally close relationship between beech populations from different sites (see section "Introduction"), (ii) the age of the stands, and (iii) the generally strong selection of trees at the juvenile stage, which allows for fast adaptation (e.g., Kremer et al., 2012), trait differences between beeches at the two sites are likely to a large degree due to adaptation to the specific site conditions. These adaptations are expressed in a slower growth of the mature beeches at LUE than at BBR, as is indicated by a smaller stem diameter. When grown under identical climatic conditions in undisturbed soil cores from their own site, saplings from natural rejuvenation at LUE produced smaller leaves with a lower photosynthetic activity and stomatal conductance than saplings from natural rejuvenation at BBR (Yang et al., 2016; Zavišić et al., 2018). In particular,

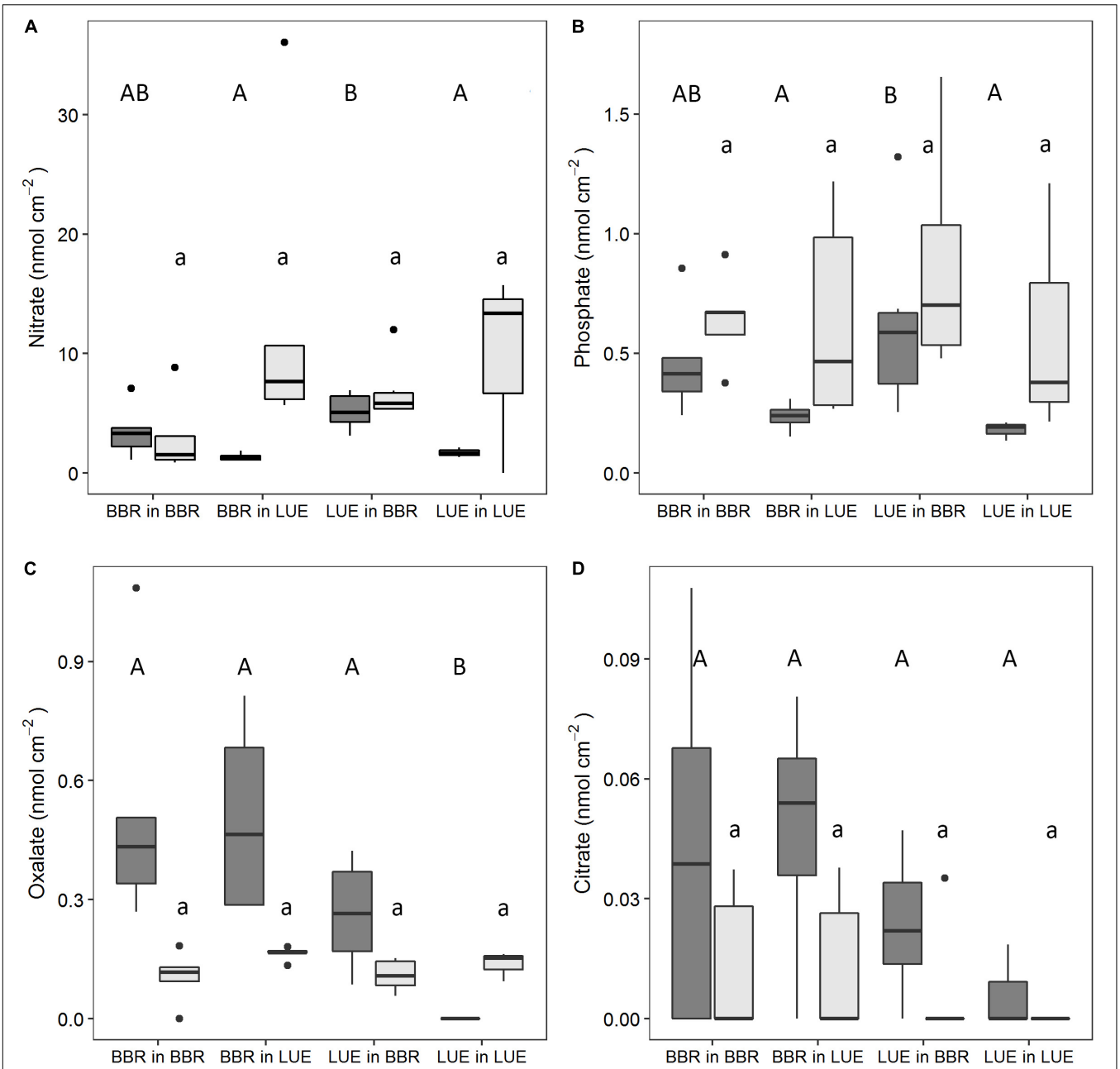


**FIGURE 3 |** Nitrate **(A)**, phosphate **(B)**, oxalate **(C)**, and citrate **(D)** collected with anion exchange membranes in the rhizosphere in a rhizobox experiment with beech (*Fagus sylvatica* L.) saplings originating from the sites Bad Brückenau (BBR) and Unterlüss (LUE). The saplings were grown in material from the Bv horizon at BBR or from the Bh horizon at LUE. Shown are box plots based on values for replicate rhizoboxes in August of the first (dark gray) and second (light gray) season ($n$ = 5, except $n$ = 3 for LUE in LUE); different letters indicate significant differences between means according to the Tukey *post hoc* test (uppercase letters, first growing season; lowercase letters, second growing season).

the difference in photosynthetic activity can be considered an indication of a more conservative resource strategy of the beech saplings at LUE (Craine, 2009; Weemstra et al., 2016). Comparing foliar nutrient concentrations and nutrient ratios with threshold values by Mellert and Göttlein (2012); ratios) and Göttlein (2015); concentrations in mature trees), the mature beeches at BBR exhibited a balanced nutrition except for a latent deficiency in K and N/K ratios above the normal range, while the trees at LUE showed a latent deficiency in P and N/P, N/Mg, and N/Ca ratios above the normal range. A lower P nutritional status of juvenile beech trees from LUE than from BBR was documented by Zavišić et al. (2018). They found a respective difference in P concentration for all plant compartments.

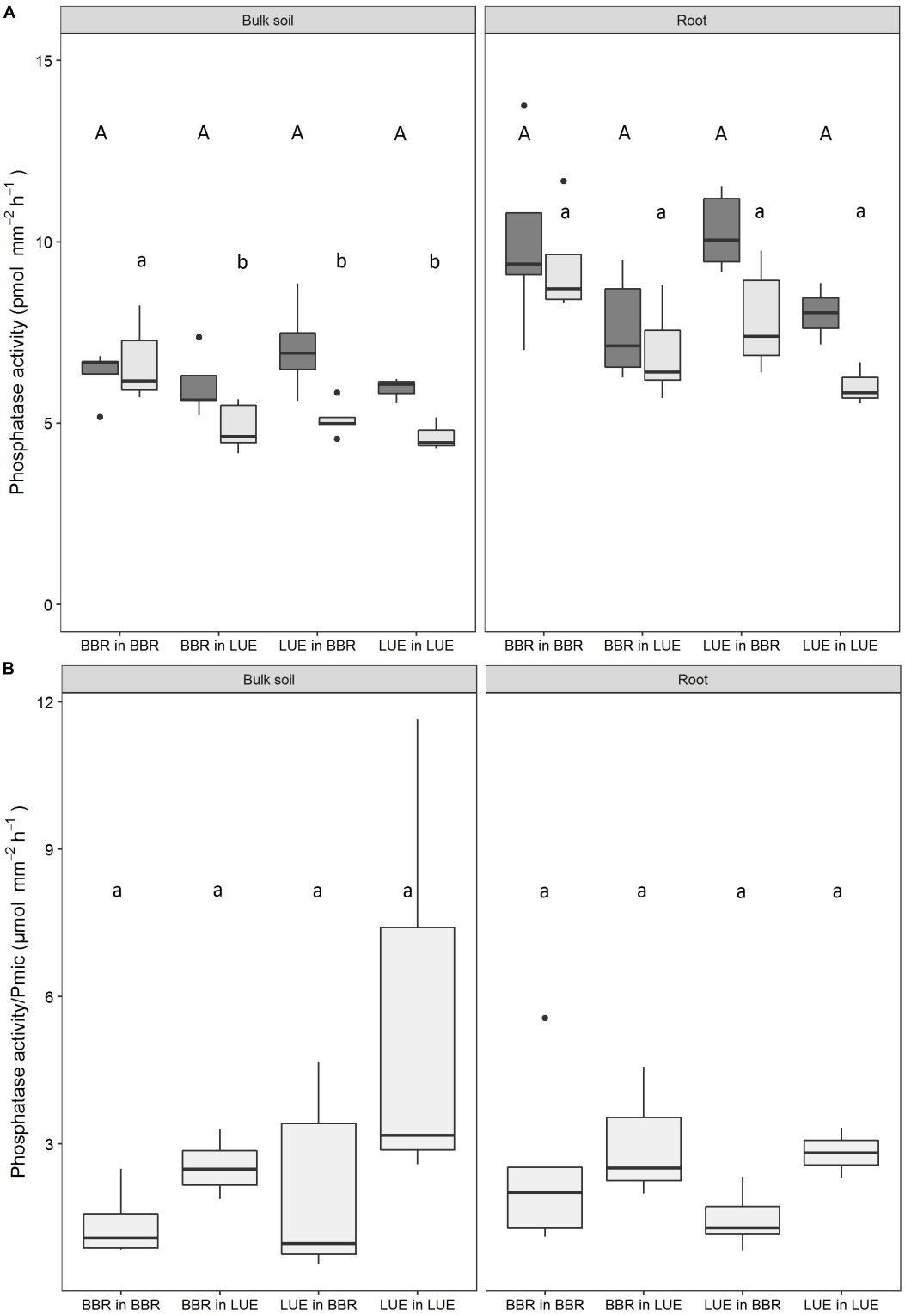


**FIGURE 4 |** Potential phosphatase activity (PA) measured in the bulk soil and on the surface of the roots using zymography **(A)** and the ratio between potential PA and microbial P ($P_{mic}$) in bulk soil and in the rhizosphere (PA on the root divided by $P_{mic}$ in the rhizosphere) **(B)** in a rhizobox experiment with beech (*Fagus sylvatica* L.) saplings originating from the sites Bad Brückenau (BBR) and Unterlüss (LUE). The saplings were grown in material from the Bv horizon at BBR or from the Bh horizon at LUE. Shown are box plots based on values for replicate rhizoboxes in August of the first (dark gray) and second (light gray) season ($n$ = 5, except $n$ = 3 for LUE in LUE); different letters indicate significant differences between means according to the Tukey *post hoc* test (uppercase letters, first growing season; lowercase letters, second growing season).

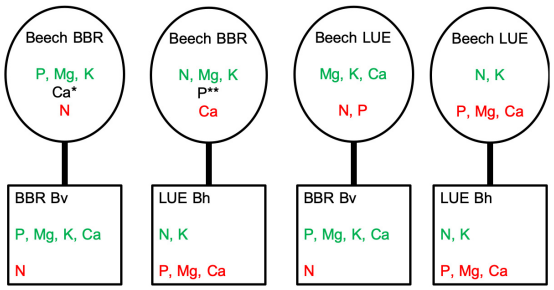


**FIGURE 5 |** Evaluation of plant nutritional status and effective nutrient availability in the soil in a rhizobox experiment with beech (*Fagus sylvatica* L.) saplings originating from the sites Bad Brückenau (BBR) and Unterlüss (LUE). The saplings were grown in material from the Bv horizon at BBR or from the Bh horizon at LUE. For the plant nutritional status (i) the comparison of foliar nutrient concentrations and ratios (**Table 2**) with published threshold values (Mellert and Göttlein, 2012; Göttlein, 2015; green normal or surplus; red deficient or above/below normal) and (ii) the average nutrient concentrations in the whole plant (green low, red high) are considered; the assessments agree except for *: foliar Ca in deficient range, N/Ca in normal range; **: foliar P in deficient range, N/P above normal range, whole plant P high; effective nutrient availability in the soil (green sufficient, red not sufficient) is estimated from the influence of the factor "current soil" on the plant nutritional status in the second year of the experiment.

The beech saplings from natural rejuvenation used in our experiment were of similar age to those investigated by Yang et al. (2016) and Zavišić et al. (2018). In contrast to the strong influence of "current soil" on the N, Mg, and K concentrations in the second year, P concentrations in different plant compartments were still similar to P concentrations of saplings from the two sites when grown in their natural soil (Zavišić et al., 2018). In the following, we assess the relative nutritional status of the saplings and its change during the experiment (i) by evaluating the foliar nutrient concentrations based on threshold values for juvenile beech trees by Göttlein (2015) and foliar N-to-nutrient ratios based on threshold values by Mellert and Göttlein (2012) and (ii) by comparing the average concentrations in the whole plant among the treatments. **Figure 5** summarizes the results of this assessment for the second year. The figure also shows the results of an assessment of the effective nutrient availability in the soil. This assessment is based on the influence of the factor "current soil" on the nutrient concentrations in the plant as it should reflect what the plant effectively took up from the soil. According to this assessment, saplings from LUE growing in the soil from LUE exhibited in both years a low P, Mg, and Ca status and thus reflected well the nutritional status at the provenance site throughout the experiment. When saplings from LUE were growing in the soil from BBR, they also maintained a low P status throughout the experiment, but were low in K instead of Mg and Ca in the first year, and became low in N in the second year (although N/P was still above normal). In the first year, and irrespective of the "current soil" the saplings from BBR were low in K, as were the mature trees at this site. In the second year, the K status had improved, but N was low when growing in the soil from BBR, and Ca was low when growing in the soil from LUE. In the latter case, the P status was low in terms of foliar concentrations but still high when considering the concentrations in the whole plant. The reason for the low N status in the second year of saplings growing in the BBR soil becomes apparent neither from the chemical properties of our experimental soils, nor when inspecting the microbial C, N, and P concentrations and related nutrient ratios in the second year. A possible explanation is competition between beech saplings and mycorrhizal partner expressed as limited transfer of N to the plant (Simon et al., 2017). While ammonium has been shown to be the preferred N form taken up by mycorrhizal roots of beech (Gessler et al., 2005), nitrate appears to be much better transferred to the plant (Leberecht et al., 2016). This explanation is thus consistent with the tendency to lower resin-extractable nitrate in the BBR than the LUE soil in the second year. In summary, based on the assessment of the plant nutritional status at the end of the experiment, two of the experimental treatments represent the growth of beech saplings differing in P and Mg status in a soil that does not provide sufficient P, Mg, and Ca. In the other two treatments, beech saplings differing in P status grew in soil that did not provide sufficient N (**Figure 5**).

## Root Growth and Morphology

The dominant effect of the experimental factor "current soil" on root growth, as well as on architectural and morphological root traits, demonstrates a high plasticity of the root system of juvenile beech trees when growing in soils differing in nutrient supply (**Tables 3**, **4** and **Figure 1**). The stronger reaction of the beech saplings from LUE than BBR to the differences in soil nutrient supply points to a modifying effect of the factor "plant origin" and thus of provenance. We cannot rule out that this may be due to a genotypic difference in sensitivity. However, taking into account the assessment of plant nutritional status and effective soil nutrient availability at the end of our experiment from the previous section, the provenance effect is also consistent with an influence of the plant nutritional status. In this respect, and for growth in a given soil, those nutrients are critical, which are not in sufficient supply in this soil. Specifically, when grown in the LUE soil, which did not provide sufficient P, Mg, and Ca, the beech saplings from the two sites differed in their P and Mg status and their fine roots strongly differed in growth, branching, and diameter. By contrast, when grown in the BBR soil, the saplings from the two sites exhibited a very similar root system, particularly in terms of branching and fine root diameter. In this case, the saplings differed mainly in their nutritional status in P, which was supplied sufficiently by the soil, but not in their status in N, which was not supplied sufficiently by the soil. Furthermore, when accepting the modifying role of the plant nutritional status, the results suggest that the observed differences in root traits can be mainly attributed to differences in the supply of P and/or Mg rather than N. To further examine this, we compare in the following our findings on specific root traits with the results from earlier studies on the effects of P, Mg, or N supply.

Our results on biomass and length of fine roots (**Table 3**) are consistent with either inhibition of root growth by low P and/or Mg supply or its stimulation by low N supply. They are thus in agreement with the general finding that P and Mg starvation inhibit primary root growth (Gruber et al., 2013; Niu et al., 2013).

Effects of differences in N supply on root growth are less clear. This is emphasized, e.g., by results for the model plant *Arabidopsis* showing that mild N deficiency increases and strong N deficiency decreases root growth (Gruber et al., 2013). Independent on the considered nutrient, findings are more variable under natural than under controlled laboratory conditions. For beech under natural conditions, only small effects of soil fertility on root growth have been found (Leuschner et al., 2004). This can be attributed partly to interaction with other factors that can affect root growth, such as soil texture (Hertel et al., 2013; Weemstra et al., 2017), water availability (Leuschner et al., 2004; Hertel et al., 2013), stand age (Finér et al., 2007), or light (Minotta and Pinzauti, 1996; Yang et al., 2016). Soil texture cannot be excluded as a factor explaining differences in root growth between our two experimental soils. However, such an effect would be opposite to results of earlier studies that found higher fine root growth of beech in sandy than loamy or clayey soils (Hertel et al., 2013; Weemstra et al., 2017).

The lower root branching of the saplings from LUE growing in LUE soil than of the ones in all other treatments (**Table 3**) is mainly consistent with inhibition by a low combined P and/or Mg supply from soil and plant reserves. This is in contrast to the findings of many studies across different plant species, including trees, that P starvation promotes lateral root growth (Niu et al., 2013; Zhou et al., 2018). However, a lower branching at low P availability was observed earlier for pine (Theodorou and Bowen, 1993).

Our results on root diameter (**Figure 1**) are consistent with thicker fine roots at low P and/or Mg supply or with finer fine roots at low N supply. There are conflicting reports on how fine root diameter depends on soil P availability. Considering only trees, Yan et al. (2019) found thicker fine roots at low P supply for various tree species, but Razaq et al. (2017) found the opposite for maple. Reports on the effect of different N supply on root diameter are more coherent. Mostly thinner roots at low N supply have been reported for trees (e.g., Razaq et al., 2017; Yan et al., 2017). There are little indications that the differences in fine root diameter in our experiment are affected by genotypic differences in plant "resource strategy" (Weemstra et al., 2016; see also the section "Introduction"). On one hand, the relatively thick fine roots of saplings from LUE when growing in the soil from LUE could reflect a "conservative resource strategy" as expressed by these saplings at their site of origin. On the other hand, when the same saplings were grown in the BBR soil, they exhibited thin roots of the same diameter as those of saplings from BBR, which are rather indicative of an "acquisitive resource strategy." Vice versa, the BBR saplings formed significantly thicker roots when growing in the soil from LUE.

In contrast to growth, branching, and diameter, fine root traits normalized for length, mass, or volume were insensitive to differences in nutrient supply (**Tables 3**, **4**). Generally, these traits appear not to be affected strongly or uniformly by soil P availability. Again, considering only trees, specific root length (SRL) was found to be smaller at lower P supply, e.g., for spruce (Clemensson-Lindell and Asp, 1995), while the opposite was found, e.g., for pine (Zhang et al., 2013). The few reports on RTD show rather higher values at lower P supply (e.g., Zhang et al., 2013). There are more studies that investigated these root traits in dependence on N supply, but also for this nutrient, the results are variable. A higher SRL at higher N supply was observed, e.g., for larch (Liu et al., 2009) and the opposite was observed, e.g., for maple (Razaq et al., 2017). A higher specific root area at low N supply was reported, e.g., for spruce (Gong and Zhao, 2019). RTD was higher at low N availability, e.g., for spruce (Gong and Zhao, 2019), while the opposite was observed, e.g., for poplar (Yan et al., 2019).

In summary, the comparison with the literature shows that attributing the differences in root traits mainly to differences in the combined supply from soil and plant reserves in P and/or Mg, is consistent with earlier findings on root growth. On the other hand, N supply may have played an additional role determining fine root diameter.

In our "cross-exchange" setup, it cannot be completely ruled out that differences in "plant-soil feedback" may have affected the results on root growth and morphology. In particular, better growth of beech saplings from LUE in BBR than LUE soil would be consistent with negative plant-soil feedback. This kind of feedback is a commonly observed mechanism that has developed between plant species and soil microbial communities over longer time periods and helps to maintain the diversity of plant communities (Bever et al., 2012). It is based on specific root exudates stimulating host-specific pathogens, which in turn restrict root development. This can be enhanced by "auto-toxicity" effects of extracellular DNA leached from decomposed litter and accumulated in the soil (Mazzoleni et al., 2015; Nagler et al., 2018). The absence of such inhibitory effects can lead to better growth when plants are transferred to a "foreign" soil. However, in contrast to different plant species, different populations of the same plant species appear to exhibit similar feedback when grown in the same soil, as was shown for grasses (Wagner et al., 2011) and trees (Gundale et al., 2014). Considering the latter studies and the similar root growth of the beech saplings from BBR in both soils, we conclude that negative plant-soil feedback likely had a negligible effect on root growth and morphology in our experiment.

## Mycorrhizal Colonization

Compared to root traits, mycorrhizal inoculation appeared to be relatively insensitive to the treatments. Nevertheless, as for root traits, the results indicate soil properties as the main and plant provenance as a modifying factor (**Tables 3**, **4**). Taking into account our assessment of plant nutritional status and effective nutrient availability (section "Availability of Nutrients in the Soil and Plant Nutritional Status"), there are two potential explanations for higher mycorrhization of beech saplings from the same site when growing in the LUE than the BBR soil. This behavior could be related either to the lower P availability in the LUE soil or to a reaction of the plants to the limited transfer of N from the fungal partners in the BBR soil, as postulated above.

Although a weak effect, the somewhat higher mycorrhization of beech saplings from BBR than LUE, when considering growth in the same soil (**Table 3**), may point to a higher ability of the saplings with an overall higher nutritional status to provide the fungal partner with carbon compounds. A similar enhancing

effect of high plant nutritional status was observed for stimulation of root growth of *Helianthus* in reaction to reduced N supply (Bowsher et al., 2016).

## Phosphorus Mobilization Potential in the Rhizosphere

As for mycorrhizal inoculation, the results from the second year of our experiment indicate a less sensitive reaction of rhizosphere properties related to P mobilization to the treatments than root traits (**Figures 2–4** and **Table 6**). Among these properties, the potential to mineralize organic P appeared to be most strongly affected with a main influence of the factor "current soil."

Higher rhizosphere concentrations of phosphate in the BBR than LUE soil, irrespective of plant origin, as observed in the first year (**Figure 3B**), reflect the better P availability in the former soil. The general increase in exchangeable phosphate concentrations between the first and the second year points to a respective difference in the balance between P mobilization and uptake by organisms. A similar reasoning may apply for the increase in nitrate from the first to the second year in the LUE soil (**Figure 3A**). The importance of nitrate for the N nutrition of our beech saplings was also indicated by the general increase of pH in the rhizosphere. Root exudation of $OH^-$ in exchange for $NO_3^-$ is well known (e.g., Marschner et al., 1996). As a side effect, in acid soils, a pH increase in the rhizosphere, as observed in our experiment (**Figure 2**), could contribute to a better P solubility due to a decrease of the positive soil surface charge density and thus weaker sorption of phosphate (Hinsinger, 2001).

As reviewed in section "Introduction," the source of organic acid anions in the rhizosphere can be root exudation, exudation by mycorrhizal hyphae, or release by free-living microorganisms, but it is difficult to distinguish between the different sources. Following a similar argument as for exchangeable phosphate and nitrate, the much larger oxalate and citrate concentrations in the first than the second year (**Figures 3C,D**), in particular in the BBR soil, point to a difference in the balance between exudation/release to and microbial degradation in the rhizosphere. The significance of microbial degradation for the effectiveness of low-molecular-weight organic acid anions in mobilization of sorbed or mineral bound inorganic P was emphasized earlier (e.g., Hinsinger, 2001). The higher concentration of organic acid anions in the rhizosphere of the BBR than the LUE saplings in the first year is likely related to a higher constitutive root exudation by the saplings from BBR, which increased the organic acid anion concentrations either directly or via stimulation of the production and release by free living microorganisms. Studies on trees have so far provided no evidence for organic acid anion exudation by roots being induced by specific soil conditions (Heim et al., 2001; Eldhuset et al., 2007). The weak effect of "current soil" in the second growing season with slightly higher abundance of oxalate in the rhizosphere of saplings growing in LUE than BBR soil was thus more likely due to lower microbial degradation than a reaction to lower soil P availability.

The higher PA in the BBR than the LUE soil in both years (**Figure 4A**) is in good agreement with results for mineral bulk soil from the same sites (Bünemann et al., 2016; Spohn et al., 2018), and with the often observed good correlation between PA and soil organic matter content (Feller et al., 1994; Nannipieri et al., 2011). However, PA per unit microbial P, representing the relative investment of the microorganisms in phosphatases, tended to be higher in the LUE than the BBR soil and suggests a reaction to the differences in P supply (**Figure 4B**). The lower PA in the second than the first growing season in all treatments, both on the roots and in the soil, may be explained as feedback to an increased P availability in the rhizosphere as indicated by the resin-extractable phosphate concentrations. Soil PA has been shown to react sensitively to increased P availability (Marklein and Houlton, 2012; Hofmann et al., 2016). The stronger reaction in the treatments with saplings from LUE is in good agreement with the results by Hofmann et al. (2016) who found a significant fertilization effect only in the rhizosphere of LUE saplings and not in the one of BBR saplings when growing in soil from their own site.

As organic acid anions, phosphatases can be produced and released by roots, mycorrhizal hyphae, and free-living microorganisms (see the section "Introduction"). The higher PA on the roots than in the bulk soil in our experiment can then be attributed either to production and release by the roots or to stimulation of microbial enzyme production in the rhizosphere by root exudation of easily degradable carbon compounds. Hofmann et al. (2016) argued that root exudation of such compounds could, in addition, alleviate the main C limitation of the microorganisms, as found for mineral soils from BBR and LUE by Heuck et al. (2015), and as a consequence induce P deficiency and further stimulate production of phosphatases. Similarly, the significant plant effect in the second growing season with slightly higher PA in the treatments with saplings from BBR could be explained by the higher constitutive root exudation by these saplings, as discussed above.

# CONCLUSION

From our cross-exchange experiment with beech saplings and mineral soil material from two acid forest sites differing in nutrient supply, we draw the following conclusions.

Beech saplings exhibited a high plasticity in adapting their root system to soils, differing in their nutrient supply, in terms of root traits related to growth, architecture, and morphology. The results confirm our first hypothesis that the plastic reactions were determined mainly by the soil properties. Confirming our second hypothesis, plant provenance had a modifying effect that was consistent with an influence of the plant status in those nutrients, which were not in sufficient supply in the soil. However, we cannot completely rule out an additional genotypic difference between the beech saplings from LUE and BBR in their sensitivity to differences in soil nutrient supply.

Compared to root traits, differences among treatments in mycorrhizal inoculation and rhizosphere parameters related to P mobilization were small and mainly determined by the soil properties. Plant origin had only a minor modifying effect,

possibly due to differences in the ability to transfer carbon compounds from the shoot to the root and the fungal partner.

## DATA AVAILABILITY STATEMENT

The datasets generated for this study are available on request to the corresponding author.

## AUTHOR CONTRIBUTIONS

JL, EF, and SM designed the experiment. SM and JL collected the plant and soil materials used in the study. SM set up and carried out the experiment, performed most of the chemical analyses, analyzed the data, and wrote the first version of the manuscript. MS provided the expertise in measuring phosphatase activity. All authors contributed significantly to the final version of the manuscript.

## FUNDING

The project was carried out in the framework of the Priority Program SPP 1685 "Ecosystem Nutrition" of the German and Swiss National Science Foundations (DFG and SNF, respectively). This particular project was funded by the SNF project no. 149138 and by internal funds of the Swiss Federal Research Institute WSL.

## ACKNOWLEDGMENTS

The forest research stations "Bayerische Landesanstalt für Wald und Forstwirtschaft" (LWF) and "Nordwestdeutsche Forstliche Versuchsanstalt" (NW-FVA) provided access to the field sites. The following groups at the Swiss Federal Research Institute WSL provided technical assistance: the technical support at Birmensdorf and the workshop at Davos helped with construction of the rhizoboxes, the experimental garden operated and maintained the greenhouse, the central analytical laboratories carried out part of the chemical analyses, and the soil physical and chemical laboratories provided various technical support. We thank Jaane Krüger (Soil Ecology, University of Freiburg i.B.), Klaus Kaiser (Soil Science and Soil Protection, Martin-Luther University Halle-Wittenberg), and Jörg Prietzel (Soil Science, TU Munich) for providing data on soil properties at the sampling sites; Henning Meesenburg (NW-FVA) and Hans-Peter Dietrich (LWF) for providing data on foliar concentrations at the sampling sites and information on site history; and Christoph Sperisen (WSL) for advice on genetic relationships among beech forests.

## SUPPLEMENTARY MATERIAL

The Supplementary Material for this article can be found online at: https://www.frontiersin.org/articles/10.3389/ffgc.2020.535117/full#supplementary-material

## REFERENCES

Bahr, A., Ellström, M., Akselsson, C., Ekblad, A., Mikusinska, A., and Wallander, H. (2013). Growth of ectomycorrhizal fungal mycelium along a Norway spruce forest nitrogen deposition gradient and its effect on nitrogen leakage. *Soil Biol. Biochem.* 59, 38–48. doi: 10.1016/j.soilbio.2013.01.004

Bever, J. D., Platt, T. G., and Morton, E. R. (2012). Microbial population and community dynamics on plant roots and their feedbacks on plant communities. *Annu. Rev. Microbiol.* 66, 265–283. doi: 10.1146/annurev-micro-092611-150107

Blossfeld, S., and Gansert, D. (2007). A novel non-invasive optical method for quantitative visualization of pH dynamics in the rhizosphere of plants. *Plant Cell Environ.* 30, 176–186. doi: 10.1111/j.1365-3040.2006.01616.x

Borken, W., Kossmann, G., and Matzner, E. (2007). Biomass, morphology and nutrient contents of fine roots in four Norway spruce stands. *Plant Soil* 292, 7–93. doi: 10.1007/s11104-007-9204-x

Bowsher, A. W., Miller, B. J., and Donovan, L. A. (2016). Evolutionary divergences in root system morphology, allocation, and nitrogen uptake in species from high- versus low-fertility soils. *Funct. Plant Biol.* 43, 129–140. doi: 10.1071/FP15162

Brookes, P. C., Landman, A., Pruden, G., and Jenkinson, D. S. (1985). Chloroform fumigation and the release of soil nitrogen: a rapid direct extraction method to measure microbial biomass nitrogen in soil. *Soil Biol. Biochem.* 17, 837–842.

Brunner, I., and Brodbeck, S. (2001). Response of mycorrhizal Norway spruce seedlings to various nitrogen loads and sources. *Environ. Poll.* 114, 223–233.

Buiteveld, J., Vendramin, G. G., Leonardi, S., Kamer, K., and Geburek, T. (2007). Genetic diversity and differentiation in European beech (*Fagus sylvatica* L.) stands varying in management history. *For. Ecol. Manag.* 247, 98–106. doi: 10.1016/j.foreco.2007.04.018

Bünemann, E. K., Augstburger, S., and Frossard, E. (2016). Dominance of either physicochemical or biological phosphorus cycling processes in temperate forest soils of contrasting phosphate availability. *Soil Biol. Biochem.* 101, 85–95. doi: 10.1016/j.soilbio.2016.07.005

Bünemann, E. K., Bossio, D. A., Smithson, P. C., Frossard, E., and Oberson, A. (2004). Microbial community composition and substrte use in a highly weathered soil as affected by crop rotation and P fertilization. *Soil Biol. Biochem.* 36, 889–901. doi: 10.1016/j.soilbio.2004.02.002

Chalot, M., and Plassard, C. (2011). "Ectomycorrhiza and nitrogen provision to the host tree," in *Ecological Aspects of Nitrogen Metabolism in Plants, First Edition*, eds J. C. Polacco and C. D. Todd (Hoboken, NJ: John Wiley & Sons Inc), 69–94.

Chen, W., Koide, R. T., Adams, T. S., DeForest, J. L., Cheng, L., and Eissenstat, D. M. (2016). Root morphology and mycorrhizal symbioses together shape nutrient foraging strategies of temperate trees. *Proc. National Acad. Sci. U.S.A.* 113, 8741–8746. doi: 10.1073/pnas.1601006113

Clemensson-Lindell, A., and Asp, H. (1995). Fine-root morphology and uptake of 32P and 35S in a Norway spruce (*Picea abies* (L.) Karst.) stand subjected to various nutrient and water supplies. *Plant Soil* 173, 147–155.

Craine, J. (2009). *Resource Strategies of Wild Plants*. Princeton, NJ: Princeton University Press.

Cuervo-Alarcon, L., Arend, M., Muller, M., Sperisen, C., Finkeldey, R., and Krutovsky, K. V. (2018). Genetic variation and signatures of natural selection in populations of European beech (*Fagus sylvatica* L.) along precipitation gradients. *Tree Genet. Genom.* 14:84. doi: 10.1007/s11295-018-1297-2

Durrant, T. H., de Rigo, D., and Caudullo, G. (2016). *Fagus sylvatica* and other beeches in Europe: distrubution, habitat, usage and threats. *Eur. Atlas For. Tree Spec.* 2016, 130–131. doi: 10.2788/038466

Eldhuset, T. D., Swensen, B., Wickstrøm, T., and Wollebæk, G. (2007). Organic acids in root exudates from *Picea abies* seedlings influenced by mycorrhiza and aluminum. *J. Plant Nutr. Soil Sci.* 170, 645–648. doi: 10.1002/jpln.200700005

Feller, C., Frossard, E., and Brossard, M. (1994). Activité phosphatasique de quelques sols tropicaux à argile 1:1. Répartition dans les fractions granulométriques. *Can. J. Soil Sci.* 74, 121–129.

Finér, L., Helmisaari, H.-S., Lõhmus, K., Majdi, H., Brunner, I., Børja, I., et al. (2007). Variation in fine root biomass of three European tree species: beech (*Fagus sylvatica* L.), Norway spruce (*Picea abies* L. Karst.), and Scots pine (*Pinus sylvestris* L.). *Plant Biosyst.* 141, 394–405.

Garbaye, J., and Wilhelm, M. E. (1985). Facteurs limitants et aspects dynamiques de la mycorhization contrôlée de *Fagus silvatica* Lin. par *Hebeloma crustuliniforme* (Bull. ex Saint-Amans) Quél, sur tourbe fertilisée. *Annal. Sci. For.* 42, 53–68. doi: 10.1051/forest:19850104

George, T. S., Fransson, A.-M., Hammond, J. P., and White, P. J. (2011). "Phosphorus nutrition: rhizosphere processes, plant response and adaptations," in *Phosphorus in Action, Soil Biology*, Vol. 26, eds E. K. Bünemann, A. Oberson, and E. Frossard (Berlin: Springer), 245–271.

Gessler, A., Jung, K., Gasche, R., Papen, H., Heidenfelder, A., Börner, E., et al. (2005). Climate and forest management influence nitrogen balance of European beech forests: microbial N transformations and inorganic N net uptake capacity of mycorrhizal roots. *Eur. J. For. Res.* 124, 95–111. doi: 10.1007/s10342-005-0055-9

Gianfreda, L., and Ruggiero, P. (2006). "Enzyme activities in soil," in *Nucleic Acids and Proteins in Soil*, eds P. Nannipieri and K. Smalla (Berlin: Springer-Verlag), 257–311.

Gong, L., and Zhao, J. (2019). The response of fine root morphological and physiological traits to added nitrogen in Schrenk's spruce (*Picea schrenkiana*) of the Tianshan mountains, China. *PeerJ* 7:e8194. doi: 10.7717/peerj.8194

Göttlein, A. (2015). Ranges of threshold values for the nutritional assessment of the main tree species spruce, pine, oak and beech. *Allg. Forst Jagd-Ztg.* 186, 110–116.

Gruber, B. D., Giehl, R. F. H., Friedel, S., and von Wirén, N. (2013). Plasticity of the Arabidopsis root system under nutrient deficiencies. *Plant Phys.* 163, 161–179. doi: 10.1104/pp.113.218453

Gundale, M. J., Kardol, P., Nilsson, M.-C., Nilsson, U., Lucas, R. W., and Wardle, D. A. (2014). Interactions with soil biota shift from negative to positive when a tree species is moved outside its native range. *New Phytol.* 202, 415–421. doi: 10.1111/nph.12699

Hauenstein, S., Neidhardt, H., Lang, F., Krüger, J., Hofmann, D., Pütz, T., et al. (2018). Organic layers favor phosphorus storage and uptake by young beech trees (*Fagus sylvatica* L.) at nutrient poor ecosystems. *Plant Soil* 432, 289–301. doi: 10.1007/s11104-018-3804-5

Hawkins, B. J., Jones, M. D., and Kranabetter, J. M. (2015). Ectomycorrhizae and tree seedling nitrogen nutrition in forest restoration. *New For.* 46, 747–771. doi: 10.1007/s11056-015-9488-2

Hedley, M. J., White, R. E., and Nye, P. H. (1982). Plant-induced changes in the rhizosphere of Rape (*Brassica napus* ver. Emerald) seedlings. III. Changes in L Value, Soil Phosphate Fractions and Phosphatase Activity. *New Phytol.* 91, 45–56.

Heim, A., Brunner, I., Frey, B., Frossard, E., and Luster, J. (2001). Root exudation, organic acids, and element distribution in roots of Norway spruce seedlings treated with aluminum in hydroponics. *J. Plant Nutr. Soil Sci.* 164, 519–526. doi: 10.1002/1522-2624(200110)164:5<519::AID-JPLN519<3.0.CO;2-Y

Hertel, D., Strecker, T., Müller-Haubold, H., and Leuschner, C. (2013). Fine root biomass and dynamics in beech forests across a precipitation gradient - Is optimal resource partitioning theory applicable to water-limited mature trees? *J. Ecol.* 101, 1183–1200. doi: 10.1111/1365-2745.12124

Heuck, C., Weig, A., and Spohn, M. (2015). Soil microbial biomass C:N:P stoichiometry and microbial use of organic phosphorus. *Soil Biol. Biochem.* 85, 119–129. doi: 10.1016/j.soilbio.2015.02.029

Hinsinger, P. (2001). Bioavailability of soil inorganic P in the rhizosphere as affected by root-induced chemical changes?: a review. *Plant Soil* 237, 173–195.

Hinsinger, P., Brauman, A., Devau, N., Gérard, F., Jourdan, C., Laclau, J.-P., et al. (2011). Acquisition of phosphorus and other poorly mobile nutrients by roots. Where do plant nutrition models fail? *Plant Soil* 348, 29–61. doi: 10.1007/s11104-011-0903-y

Hodge, A. (2006). Plastic plants and patchy soils. *J. Exp. Bot.* 57, 401–411. doi: 10.1093/jxb/eri280

Hodge, A., Berta, G., Doussan, C., Merchan, F., and Crespi, M. (2009). Plant root growth, architecture and function. *Plant Soil* 321, 153–187. doi: 10.1007/s11104-009-9929-9

Hofmann, K., Heuck, C., and Spohn, M. (2016). Phosphorus resorption by young beech trees and soil phosphatase activity as dependent on phosphorus availability. *Oecologia* 181, 369–379. doi: 10.1007/s00442-016-3581-x

Holzmann, S., Missong, A., Puhlmann, H., Siemens, J., Bol, R., Klumpp, E., et al. (2016). Impact of anthropogenic induced nitrogen input and liming on phosphorus leaching in forest soils. *J. Plant Nutr. Soil Sci.* 179, 443–453. doi: 10.1002/jpln.201500552

Ishida, T. A., Nara, K., and Hogetsu, T. (2007). Host effects on ectomycorrhizal fungal communities insight from eight host species in mixed conifer–broadleaf forests. *New Phytol.* 174, 430–440.

Jonard, M., Fürst, A., Verstraeten, A., Thimonier, A., Timmermann, V., Potoèiæ, N., et al. (2015). Tree mineral nutrition is deteriorating in Europe. *Glob. Chang. Biol.* 21, 418–430. doi: 10.1111/gcb.12657

Kazantseva, O., Bingham, M., Simard, S. W., and Berch, S. M. (2009). Effects of growth medium, nutrients, water, and aeration on mycorrhization and biomass allocation of greenhouse-grown interior Douglas-fir seedlings. *Mycorrhiza* 20, 51–66. doi: 10.1007/s00572-009-0263-0

Kiba, T., and Krapp, A. (2016). Plant nitrogen acquisition under low availability: regulation of uptake and root architecture. *Plant Cell Phys.* 54, 707–714. doi: 10.1093/pcp/pcw052

Kouno, K., Tuchiya, Y., and Ando, T. (1995). Measurement of soil microbial phosphorus by anion exchange membrane method. *Soil Biol. Biochem.* 27, 1353–1357.

Kremer, A., Ronce, O., Robledo-Arnuncio, J. J., Guillaume, F., Bohrer, G., Nathan, R., et al. (2012). Long-distance gene flow and adaptation of forest trees to rapid climate change. *Ecol. Lett.* 15, 378–392.

Lang, F., Krüger, J., Amelung, W., Willbold, S., Frossard, E., Bünemann, E. K., et al. (2017). Soil phosphorus supply controls P nutrition strategies of beech forest ecosystems in Central Europe. *Biogeochemistry* 136, 5–29. doi: 10.1007/s10533-017-0375-0

Leberecht, M., Dannenmann, M., Tejedor, J., Simon, J., Rennenberg, H., and Polle, A. (2016). Segregation of nitrogen use between ammonium and nitrate of ectomycorrhizas and beech trees. *Plant Cell Environ.* 39, 2691–2700. doi: 10.1111/pce.12820

Leuschner, C., Hertel, D., Schmid, I., Koch, O., Muhs, A., and Hölscher, D. (2004). Stand fine root biomass and fine root morphology in old-growth beech forests as a function of precipitation and soil fertility. *Plant Soil* 258, 43–56.

Leuschner, C., Meier, I. C., and Hertel, D. (2006). On the niche breadth of *Fagus sylvatica*: soil nutrient status in 50 Central European beech stands on a broad range of bedrock types. *Ann. For. Sci.* 63, 355–368. doi: 10.1051/forest:2006016

Liu, J., Mei, L., Gu, J., Quan, X., and Wang, Z. (2009). Effects of nitrogen fertilization on fine root biomass and morphology of *Fraxinus mandshurica* and *Larix gmelinii*: a study with in-growth core approach. *Shengtaixue Zazhi* 28, 1–6.

Marklein, A. R., and Houlton, B. Z. (2012). Nitrogen inputs accelerate phosphorus cycling rates across a wide variety of terrestrial ecosystems. *New Phytol.* 193, 696–704. doi: 10.1111/j.1469-8137.2011.03967.x

Marschner, H., Kirkby, E. A., and Cakmak, I. (1996). Effect of mineral nutritional status on shoot-root partitioning of photoassimilates and cycling of mineral nutrients. *J. Exp. Bot.* 47, 1255–1263. doi: 10.1093/jxb/47.Special_Issue.1255

Mazzoleni, S., Bonanomi, G., Incerti, G., Chiusano, M. L., and Termolino, P. (2015). Inhibitory and toxic effects of extracellular self-DNA in litter: a mechanism for negative plant-soil feedbacks? *New Phytol.* 205, 1195–1210. doi: 10.1111/nph.13121

Meier, I. C., and Leuschner, C. (2008). Genotypic variation and phenotypic plasticity in the drought response of fine roots of European beech. *Tree Phys.* 28, 297–309.

Meller, S., Frossard, E., and Luster, J. (2019). Phosphorus allocation to leaves of beech saplings reacts to soil phosphorus availability. *Front. Plant Sci.* 10:744. doi: 10.3389/fpls.2019.00744

Mellert, K. H., and Göttlein, A. (2012). Comparison of new foliar nutrient thresholds derived from van den Burg's literature compilation with established central European references. *Eur. J. For. Res.* 131, 1461–1472. doi: 10.1007/s10342-012-0615-8

Minotta, G., and Pinzauti, S. (1996). Effects of light and soil fertility on growth, leaf chlorophyll content and nutrient use efficiency of beech (*Fagus sylvatica* L.) seedlings. *For. Ecol. Manag.* 86, 61–71.

Nagler, M., Insam, H., Pietramellara, G., and Ascher-Jenull, J. (2018). Extracellular DNA in natural environments: features, relevance and applications. *Appl. Microbiol. Biotechnol.* 102, 6343–6356. doi: 10.1007/s00253-018-9120-4

Nannipieri, P., Giagnoni, L., Landi, L., and Renella, G. (2011). "Role of phosphatase enzymes in soil," in *Phosphorus in Action, Soil Biology*, Vol. 26, eds E. K. Bünemann, A. Oberson, and E. Frossard (Berlin: Springer), 215–243.

Niu, Y. F., Chai, R. S., Jin, G. L., Wang, H., Tang, C. X., and Zhang, Y. S. (2013). Responses of root architecture development to low phosphorus availability: a review. *Ann. Bot.* 112, 391–408. doi: 10.1093/aob/mcs285

Oburger, E., Jones, D. L., and Wenzel, W. W. (2011). Phosphorus saturation and pH differentially regulate the efficiency of organic acid anion-mediated P solubilization mechanisms in soil. *Plant Soil* 341, 363–382. doi: 10.1007/s11104-010-0650-5

Ohno, T., and Zibilske, L. M. (1991). Determination of low concentrations of phosphorus in soil extracts using malachite green. *Soil Sci. Soc. Am. J.* 55, 892–895.

Plassard, C., and Dell, B. (2010). Phosphorus nutrition of mycorrhizal trees. *Tree Phys.* 30, 1129–1139. doi: 10.1093/treephys/tpq063

Plassard, C., Louche, J., Ali, M. A., Duchemin, M., Legname, E., and Cloutier-Hurteau, B. (2011). Diversity in phosphorus mobilisation and uptake in *Ectomycorrhizal* fungi. *Annals For. Sci.* 68, 33–43. doi: 10.1007/s13595-010-0005-7

Razaq, M., Zhang, P., Shen, H., and Salahuddin, J. (2017). Influence of nitrogen and phosphorous on the growth and root morphology of *Acer mono*. *PLoS One* 12:e0171321. doi: 10.1371/journal.pone.0171321

Richardson, A. E., Hocking, P. J., Simpson, R. J., and George, T. S. (2009). Plant mechanisms to optimise access to soil phosphorus. *Crop Pasture Sci.* 60, 124–143. doi: 10.1071/CP07125

Riley, D., and Barber, S. A. (1971). Effect of ammonium and nitrate fertilization on phosphorus uptake as related to root-induced pH changes at the root-soil interface. *Soil Sci. Soc. Am. J.* 35, 300–306. doi: 10.2136/sssaj1971.03615995003500020035x

Schneider, C. A., Rasband, W. S., and Eliceiri, K. W. (2012). NIH Image to ImageJ: 25 years of image analysis. *Nat. Methods* 9, 671–675.

Shahbaz, A. M., Oki, Y., Adachi, T., Murata, Y., and Khan, M. H. R. (2006). Phosphorus starvation induced root-mediated pH changes in solubilization and acquisition of sparingly soluble P sources and organic acids exudation by Brassica cultivars. *Soil Sci. Plant Nutr.* 52, 623–633. doi: 10.1111/j.1747-0765.2006.00082.x

Shi, S., Condron, L., Larsen, S., Richardson, A. E., Jones, E., Jiao, J., et al. (2011). *In situ* sampling of low molecular weight organic anions from rhizosphere of radiata pine (*Pinus radiata*) grown in a rhizotron system. *Env. Exp. Bot.* 70, 131–142. doi: 10.1016/j.envexpbot.2010.08.010

Simon, J., Dannenmann, M., Pena, R., Gessler, A., and Rennenberg, H. (2017). Nitrogen nutrition of beech forests in a changing climate: importance of plant-soil-microbe water, carbon, and nitrogen interactions. *Plant Soil* 418, 89–114.

Spohn, M., Ermak, A., and Kuzyakov, Y. (2013). Microbial gross organic phosphorus mineralization can be stimulated by root exudates–a $^{33}$P isotopic dilution study. *Soil Biol. Biochem.* 65, 254–263.

Spohn, M., and Kuzyakov, Y. (2013). Distribution of microbial-and root-derived phosphatase activities in the rhizosphere depending on P availability and C allocation–Coupling soil zymography with 14C imaging. *Soil Biol. Biochem.* 67, 106–113.

Spohn, M., Zavišić, A., Nassal, P., Bergkemper, F., Schulz, S., and Marhan, S. (2018). Temporal variations of phosphorus uptake by soil microbial biomass and young beech trees in two forest soils with contrasting phosphorus stocks. *Soil Biol. Biochem.* 117, 191–202. doi: 10.1016/j.soilbio.2017.10.019

Sun, Y., Gu, J.-C., Zhuang, H.-F., and Wang, Z.-Q. (2010). Effects of ectomycorrhizal colonization and nitrogen fertilization on morphology of root tips in a *Larix gmelinii* plantation in northeastern China. *Ecol. Res.* 25, 295–302. doi: 10.1007/s11284-009-0654-x

Theodorou, C., and Bowen, G. D. (1993). Root morphology, growth and uptake of phosphorus and nitrogen of *Pinus radiata* families in different soils. *For. Ecol. Manag.* 56, 43–56.

Tiessen, H., and Moir, J. O. (2006). "Chapter 25: Characterization of available P by sequential extraction," in *Soil Sampling and Methods of Analysis Canadian Society of Soil Science*, 2nd Edn, eds M. Carter and E. Gregorich (Milton Park: Taylor and Francis).

Voroney, R. P., Brookes, P. C., and Beyaert, R. P. (2006). "Chapter 49: Soil microbial biomass C, N, P, and S," in *Soil Sampling and Methods of Analysis, Canadian Society of Soil Science*, 2nd Edn, eds M. Carter and E. Gregorich ( Milton Park: Taylor and Francis).

Wagner, V., Antunes, P. M., Ristow, M., Lechner, U., and Hensen, I. (2011). Prevailing negative soil biota effect and no evidence for local adaptation in a widespread Eurasian grass. *PLoS One* 6:e17580. doi: 10.1371/journal.pone.0017580

Walthert, L., and Meier, E. S. (2017). Tree species distribution in temperate forests is more influenced by soil than climate. *Ecol. Evol.* 7, 9473–9484. doi: 10.1002/ece3.3436

Weemstra, M., Mommer, L., Visser, E. J. W., van Ruijven, J., Kuyper, T. W., Mohren, G. M. J., et al. (2016). Towards a multidimensional root trait framework: a tree root review. *New Phytol.* 211, 1159–1169. doi: 10.1111/nph.14003

Weemstra, M., Sterck, F. J., Visser, E. J. W., Kuyper, T. W., Goudzwaard, L., and Mommer, L. (2017). Fine-root trait plasticity of beech (*Fagus sylvatica*) and spruce (*Picea abies*) forests on two contrasting soils. *Plant Soil* 415, 175–188. doi: 10.1007/s11104-016-3148-y

Xuan, W., Beeckman, T., and Xu, G. (2017). Plant nitrogen nutrition: sensing and signaling. *Curr. Opin. Plant Biol.* 39, 57–65. doi: 10.1016/j.pbi.2017.05.010

Yan, G., Chen, F., Zhang, X., Wang, J., Han, S., Xing, Y., et al. (2017). Spatial and temporal effects of nitrogen addition on root morphology and growth in a boreal forest. *Geoderma* 303, 178–187.

Yan, X.-L., Wang, C., Ma, X., and Wu, P. (2019). Root morphology and seedling growth of three tree species in southern China in response to homogeneous and heterogeneous phosphorus supplies. *Trees* 33, 1283–1297. doi: 10.1007/s00468-019-01858-x

Yang, N., Zavišić, A., Pena, R., and Polle, A. (2016). Phenology, photosynthesis, and phosphorus in European beech (*Fagus sylvatica* L.) in two forest soils with contrasting P contents. *J. Plant Nutr. Soil Sci.* 179, 151–158. doi: 10.1002/jpln.201500539

Zavišić, A., Yang, N., Marhan, S., Kandeler, E., and Polle, A. (2018). Forest soil phosphorus resources and fertilization affect ectomycorrhizal community composition, beech P uptake, and photosynthesis. *Front. Plant Sci.* 9:463. doi: 10.3389/fpls.2018.00463

Zhang, Y., Zhou, Z., and Yang, Q. (2013). Genetic variations in root morphology and phosphorus efficiency of *Pinus massoniana* under heterogeneous and homogeneous low phosphorus conditions. *Plant Soil* 364, 93–104. doi: 10.1007/s11104-012-1352-y

Zhou, X.-B., Jia, Z.-M., and Wang, D.-B. (2018). Effects of limited phosphorus supply on growth, root morphology and phosphorus uptake in citrus rootstocks seedlings. *Int. J. Agric. Biol.* 20, 431–436. doi: 10.17957/IJAB/15.0553

**Conflict of Interest:** The authors declare that the research was conducted in the absence of any commercial or financial relationships that could be construed as a potential conflict of interest.

frontiers in Environmental Science

ORIGINAL RESEARCH
published: 29 September 2020
doi: 10.3389/fenvs.2020.564778

# In or Out of Equilibrium? How Microbial Activity Controls the Oxygen Isotopic Composition of Phosphate in Forest Organic Horizons With Low and High Phosphorus Availability

*Chiara Pistocchi[1,2], Éva Mészáros[1,3], Emmanuel Frossard[1], E. K. Bünemann[1,4] and Federica Tamburini[1]**

[1] Institute of Agricultural Science, ETH Zürich, Zurich, Switzerland, [2] Eco&Sols, Montpellier SupAgro, Univ Montpellier, CIRAD, INRAE, IRD, Montpellier, France, [3] Department of Biosystems Science and Engineering, ETH Zürich, Basel, Switzerland, [4] Department of Soil Sciences, Research Institute of Organic Agriculture FiBL, Frick, Switzerland

OPEN ACCESS

**Edited by:**
Roland Bol,
Helmholtz Association of German Research Centres (HZ), Germany

**Reviewed by:**
Alon Angert,
Hebrew University of Jerusalem, Israel
Steve Granger,
Rothamsted Research,
United Kingdom

***Correspondence:**
Federica Tamburini
federica.tamburini@usys.ethz.ch

**Specialty section:**
This article was submitted to Biogeochemical Dynamics, a section of the journal Frontiers in Environmental Science

**Received:** 22 May 2020
**Accepted:** 24 August 2020
**Published:** 29 September 2020

**Citation:**
Pistocchi C, Mészáros É, Frossard E, Bünemann EK and Tamburini F (2020) In or Out of Equilibrium? How Microbial Activity Controls the Oxygen Isotopic Composition of Phosphate in Forest Organic Horizons With Low and High Phosphorus Availability. Front. Environ. Sci. 8:564778. doi: 10.3389/fenvs.2020.564778

While there are estimates of the abiotic processes contribution to soil phosphorus (P) availability, less is known about the contribution of biological processes. Two main enzymatic processes involved in soil P cycling are known to alter the oxygen isotopic composition of phosphate ($\delta^{18}$O-P), each in a different way, through the cleavage of the P–O bond: the intracellular P turnover and the organic P hydrolysis. The former induces isotopic equilibration between phosphate and water and is considered the major process affecting soil available P via microbial P release. The latter induces depleted $\delta^{18}$O-P in the phosphate released from the mineralization of organic P. We studied P dynamics in organic horizons of two contrasting soils (low- and high-P availability) from temperate beech forests. We labeled the soil with $^{18}$O-enriched water and followed changes in the $\delta^{18}$O-P of different soil P pools in the presence or absence of added leaf litter during 3 months of incubation. $\delta^{18}$O-P values of almost all P pools progressively increased indicating oxygen incorporation from the enriched soil water into phosphate via the above-mentioned enzymatic processes. $\delta^{18}$O-P of available P increased more in the P-rich soil than in the P-poor soil and approached the isotopic equilibrium between phosphate and water, revealing the impact of microbial P release into the available P pool. However, in the P-poor soil, the available P brought the isotopic signature induced by phosphatase enzymes, indicating that it was mostly originated from the hydrolysis of organic P. Therefore, under P-limiting conditions, the isotopic effect of organic P hydrolysis can outweigh the isotopic equilibrium effect. Finally, two independent isotopic approaches with $^{33}$P and $\delta^{18}$O-P provided very similar estimates of P exchanged between the available P and other inorganic soil pools. This suggests that $\delta^{18}$O-P can be successfully used to trace P fluxes, provided that the underlying processes do not break the P–O bonds of the phosphate molecule.

**Keywords: soil, isotopic labeling, phosphatase, microbial phosphorus, mineralization**

## INTRODUCTION

In forest ecosystems, plants and their mycorrhizae take up most of their phosphorus (P) as dissolved orthophosphate ($PO_4^{3-}$, hereafter phosphate) from the soil solution, which represents often a small proportion of the total P in soil. The soil solution is continuously replenished by abiotic processes, such as the release of P from sorbed phases, by the dissolution of P containing minerals, and by biological processes, namely mineralization of organic P (Po). Microbes mineralize Po from plant litter and soil organic matter via enzymatic hydrolysis. The newly released P is taken up by microbes (immobilization), sorbed to the soil solid phases or replenishes the soil solution. Upon cell death, microbial P ultimately enters the non-living Po and inorganic P pools, thus constituting a potentially available P pool.

While there are estimates of the contribution of abiotic inorganic P pools to P availability (Helfenstein et al., 2020), less is known about the contribution of biological processes. This contribution varies widely, depending on factors such as land-use and inorganic P availability (Becquer et al., 2014; Bünemann, 2015; Pistocchi et al., 2018). Integrating this knowledge into soil P cycling models is crucial to predict the effects of changing environmental conditions, such as the ones induced by climate change, or of global P resources scarcity on net primary production.

Assessing soil P dynamics is challenging, because exchanges between P pools often occur without net changes in pool size. The use of radioactive tracers $^{33}$P and $^{32}$P is to date the sole option to quantify gross P fluxes, such as gross P immobilization and mineralization (Bünemann, 2015 and references therein), the transfer from the soil to the plant (Frossard et al., 2011 and references therein) and the fate of P added with plant residues or fertilizers (Fardeau et al., 1995; Daroub et al., 2000; Pistocchi et al., 2018). Studies on various forest soils have highlighted the impact of Po mineralization on P fluxes notably when inorganic P availability is low (Achat et al., 2009; Mooshammer et al., 2012; Spohn et al., 2013; Bünemann et al., 2016; Pistocchi et al., 2018).

Although radioisotopes have several advantages (e.g., negligible P mass addition, direct P tracing, simple to analyze), they also have several drawbacks related to safety issues, short half-lives, and low sensitivity to biological P fluxes when the baseline of isotopic dilution, i.e., the flux due to abiotic processes, is high (Pistocchi et al., 2018; Siegenthaler et al., 2020).

In the last two decades, many studies have shown that biological processes involved in soil P cycling alter the isotopic composition of oxygen in phosphate ($\delta^{18}$O-P) through the cleavage of the P–O bond and the incorporation of O atoms from water (Tamburini et al., 2012 and references therein). Whereas in the absence of biological activity, the P–O bond is stable and exchanges of oxygen (O) between phosphate and water are negligible. Two main enzyme-mediated processes have an impact on $\delta^{18}$O-P. Firstly, intracellular P turnover controlled by the enzyme inorganic pyrophosphatase leads to the complete exchange of the four O atoms in phosphate with O from water. This reaction produces a temperature-dependent isotopic equilibrium between phosphate and water (Longinelli and Nuti, 1973; Chang and Blake, 2015).

Secondly, the intra- and extracellular phosphatase enzymes incorporate one or two O atoms from water into phosphate released by the breakdown of Po compounds (P mono- and diesters). One O atom is incorporated during the hydrolysis of a phosphomonoester and two O atoms are incorporated during the hydrolysis of a phosphodiester. These transfers are associated with an enzyme-dependent fractionation. Most phosphatase enzymes (e.g., alkaline and acid phosphatase and phytase) have a negative fractionation factor, meaning they release phosphate with a depleted $\delta^{18}$O-P (Liang and Blake, 2006b; von Sperber et al., 2014, 2015).

The $\delta^{18}$O-P of available P in the soil can be affected by these processes through various mechanisms. Phosphate ions released by microorganisms to the soil solution potentially contribute a $\delta^{18}$O-P close to isotopic equilibrium, as influenced by the intracellular inorganic pyrophosphatase (Zohar et al., 2010; Poll et al., 2006). Negative offsets from isotopic equilibrium may be caused by the hydrolysis of Po compounds by extracellular or intracellular phosphatase enzymes (Helfenstein et al., 2018). Positive offsets might result from the uptake of phosphate by organisms, as they preferentially take up lighter phosphate isotopologues, thus increasing the $\delta^{18}$O-P of the extracellular phosphate pool (Blake et al., 2005; Lis et al., 2019).

An approach used to detect the main biological processes affecting soil P cycling consists of labeling the soil solution with $^{18}$O-enriched water (Bauke et al., 2017; Siebers et al., 2018; Siegenthaler et al., 2020). Enzyme-mediated processes inducing the P–O bond cleavage are therefore detected by tracing the incorporation of O from water into specific phosphate pools.

Tracing P fluxes with this approach is possible provided that the process generating the P flux does not induce a cleavage of the P–O bond, i.e., phosphate is transferred as intact molecule. Abiotic processes, such as sorption/desorption and precipitation/dissolution meet this condition. Additionally, phosphate ions are sorbed or precipitate with negligible isotopologues discrimination (Liang and Blake, 2006b; Jaisi et al., 2010). Through these abiotic processes, the $\delta^{18}$O-P of phosphate acquired via biological processes can be transferred to other inorganic P pools present in the solid phase. This was observed in a study on Andosols along a rainfall gradient, where P bound to calcium was found to carry an equilibrium isotopic signature after losing the $\delta^{18}$O-P of the original parent material (Helfenstein et al., 2018).

Within the German Priority Program SPP1685 "Ecosystem Nutrition: Forest Strategies for Limited Phosphorus Resources" we studied P dynamics and the biological contribution to P availability in organic horizons (Oe) of two contrasting (low- and high-P availability) and well-characterized soils from temperate forests. We chose organic horizons, as they are essential for the recycling of nutrients in forests, supplying up to 99% of plant P demand where inorganic P availability is low (Brandtberg et al., 2004; Jonard et al., 2009; Hauenstein et al., 2018).

We labeled the soil with $^{18}$O-enriched water and measured the $\delta^{18}$O-P from different soil P pools in the presence or absence of added leaf litter at several time points during 3 months of incubation. In parallel, we conducted an identical incubation with $^{33}$P to quantify P fluxes, as reported in Pistocchi et al. (2018). The results of the present study will be discussed also in relation to this parallel study and the analysis of microbial community composition of Mészáros et al. (2020).

Our hypothesis was that under low P availability, the prevalence of Po mineralization on P fluxes would cause a negative offset in the $\delta^{18}$O-P of the available P due to the negative fractionation of phosphatase enzymes. Under high P availability conditions, we expected the $\delta^{18}$O-P of available P pool to be affected by either (i) abiotic exchanges with mineral phases: in this case, we would observe no incorporation of oxygen from water into phosphate; or (ii) microbial P turnover: in this case, the $\delta^{18}$O-P of the available P would approach isotopic equilibrium. Additionally, we measured the $\delta^{18}$O-P in alkaline and acid-extractable P to trace abiotic exchanges of these pools with the available P. Finally, we made the hypothesis that O incorporation from labeled water into P pools is proportional to microbial activity as suggested by Melby et al. (2013).

# MATERIALS AND METHODS

## Sites, Soil Sampling and Preparation

The soil organic horizons come from two European Beech forest sites in Germany (*Fagus sylvatica* L., 100–120 years old). The site Bad Brückenau (BBR) is located at about 800 m above sea level (asl) in Northern Bavaria (50°21′7.26″N, 9°55′44.53″E). The site Lüss (LUE) is located at 100 m asl in Lower Saxony (52°50′21.77″N, 10°16′2.37″E). The soils are classified as Dystric Skeletic Cambisol (Hyperhumic, Loamic; IUSS Working Group WRB, 2006) and developed on basalt bedrock, and as a Hyperdystric Folic Cambisol (Arenic, Loamic, Nechic, Protospodic), developed on Pleistocene sand, respectively. The texture of the mineral topsoil in BBR is silty clay loam, while in LUE is loamy sand. A detailed description of the two sites is reported in Lang et al. (2017).

At each site, we collected samples from the leaf litter deposited during the previous autumn and from the organic horizons, in April, 2015 at LUE and May, 2015 at BBR. Litter was collected from the soil surface, and then five to six subsamples were taken from the Oe horizon at each site and bulked into a composite sample (hereafter referred to as BBR and LUE *soil*, respectively).

The soil was sieved while moist to < 5 mm. The litter was dried at 35°C, manually crushed and sieved twice to collect the fraction between 20 and 5 mm. Soil and litter samples were stored at 4°C for a period of 2 weeks (BBR) to 1 month (LUE) before the experiment.

The gravimetric water content of field moist soil was determined by drying for 20 h at 105°C. The water holding capacity (WHC) of the field moist soils was determined by saturating the soils with water and then allowing gravitational water to drain by putting them in a sand bath for 4 h.

## Experimental Design and Incubation Experiment

The soils were split in two and two incubations were undertaken. The first was the labeling experiment with $^{18}$O enriched water. The second was a soil respiration experiment to measure $CO_2$ produced as an indicator of microbial activity under the same condition of the labeling experiment. The two incubations lasted 93 and 97 days, respectively.

In both cases, the experiment design had two factors: the soil (BBR and LUE) and the litter treatment, which included the absence [non-amended treatment (NL)] or presence [leaf-litter amended treatment (L)] of leaf litter amendment. All treatments were replicated three times for the labeling experiment and four times for the respiration experiment.

Before splitting the soil, a 3-week pre-incubation at approximately 40% of the maximum WHC was undertaken, during which we monitored the respiration to obtain constant soil respiration rates (Oehl et al., 2001).

For the labeling experiment, soils were weighed in polyethylene zip lock bags (equivalent of 108 g dry soil each) and randomly assigned to the treatments. The labeling solution was prepared with 98% $^{18}$O-enriched water (Sercon Limited, Crewe, United Kingdom, the final $\delta^{18}$O in the labeling water was = 34.30‰). Three ml of the labeling solution was added to each of the three replicate bags, spread on the top of the soil by pipetting and then mixed for 1 min by hand through agitating the bag. This process was then repeated to add a total of nine and 12 ml of labeling solution per bag, for BBR and LUE soils, respectively. The added volumes increased the BBR and LUE soils water content to approximately 50% of their WHC. Finally, litter was added to half of the bags, in the ratio of 10 mg per g of dry soil, equivalent to 4.6 mg C $g^{-1}$ soil, which corresponds approximately to natural leaf litter inputs at the two sites (Lang et al., 2017). The bags were left slightly open and arranged in a completely randomized design, in plastic trays which were covered and incubated in the dark at 19°C. To reduce evaporation, which affects the $\delta^{18}$O of soil water, the air moisture was kept approximately constant by placing a beaker with water in each tray.

The labeling experiment was combined with sequential extractions. Concentrations of P were measured in resin-extractable P (inorganic available P, hereafter referred to as $P_{res}$) and hexanol-labile P pools ($P_{hex}$) at days 0, 4, 11, 29, and 93 after labeling. Additionally, at days 0, 4, and 93 we performed a modified Hedley sequential extraction (Tiessen and Moir, 1993; Tamburini et al., 2018) to follow the fate of $^{18}$O into other P pools (see section "Soil Phosphorus Pools Concentrations").

For the soil respiration experiment, a set of subsamples (10 g dry weight equivalent) including all soil × litter treatment combinations was prepared on day 0 adding ultrapure $H_2O$ instead of the labeling solution. Each sample was placed in an air-tight jar (1 L volume) with an alkaline trap made of 20 ml 0.2 M NaOH solution, including four blanks without soil. The

jars were then incubated together with the labeled samples. The $CO_2$ emitted by the soil was measured at weekly intervals by back titration of the trapping solution (Alef, 1995).

## Analytical Methods

### Soil General Characteristics and Phosphatase Activity

For a detailed description of soil general characteristics and of the corresponding analytical methods refer to Pistocchi et al. (2018).

Potential acid and alkaline phosphatase activities were determined on soil/water suspensions by microplate fluorescence assay (Marx et al., 2001; Poll et al., 2006). A 4-methylumbelliferon (MUF) substrate was added to six replicates of soil/water suspensions under either acidic (pH 6.1) or alkaline (pH 11) conditions. Fluorescence was read on a fluorescence plate reader (Biotek FLx800, Fisher Scientific GmbH, Schwerte, Germany). The analysis was done on 1 g dry weight equivalent samples taken at days 0, 4, 11, 29, and 93 and subsequently frozen until analyzed.

### Soil Phosphorus Pools Concentrations

The Hedley sequential extraction scheme was upscaled and adapted for $\delta^{18}$O-P analysis (Tamburini et al., 2018). The initial step of the sequential extraction follows the method proposed by Kouno et al. (1995) and modified by Bünemann et al. (2004). First, two moist soil subsamples were treated in parallel: one subsample was extracted with anion exchange resins (BDH #55164, 12 cm × 4 cm, $P_{res}$), the other was fumigated with liquid hexanol and extracted with anion exchange resins ($P_{hex}$). In the upscaled version, the amount of soil, resins and hexanol were adapted to obtain sufficient amount of P for isotope analyses, e.g., up to 100 g equivalent dry soil for LUE, keeping the solid to liquid ratio 1:15 (Tamburini et al., 2018). We did not include a P spiked subsample for quantifying the P recovery according to the method, as this was done in the parallel experiment with $^{33}$P tracing (Pistocchi et al., 2018). The $P_{res}$ is a proxy of the available P, while the difference between $P_{hex}$ and $P_{res}$ provides an estimate of the microbial P ($P_{mic}$).

The soil residue of the subsample extracted with hexanol was used for the subsequent steps of the sequential extraction. First, it was extracted with NaOH/EDTA, targeting the inorganic and organic P bound to Fe and Al oxides (hereafter $Pi_{NaOH}$ and $Po_{NaOH}$). After removing the resins, NaOH and EDTA disodium salt were added to the soil suspensions in solid form to reach the required concentration (0.25 M NaOH and 0.05 M EDTA). After 16 h shaking, the samples were centrifuged (5300 *g* for 15 min), filtered through Millipore nylon filters (0.8 μm), and the filtrates were collected for $Pi_{NaOH}$ and $Po_{NaOH}$ determination and purification for isotopes analyses.

Subsequently, the soil residue was extracted with 1 M HCl, targeting sparingly soluble P bound to Ca ($Pi_{HCl}$), but in acidic soil likely including P bound to Fe and Al oxyhydroxides not entirely extracted during the previous step (Werner et al., 2017). A volume of 1 M HCl was added to the soil residue in the proportion of 10–1 and the extracts collected after shaking overnight and filtering using glass fiber filters (0.8 μm, Millipore).

The concentrations of $P_{res}$, $P_{hex}$, $Pi_{NaOH}$, and $Pi_{HCl}$ were determined colorimetrically (UV-1800, Shimadzu, Canby, United States) with the malachite green method (Ohno and Zibilske, 1991). The organic fraction, $Po_{NaOH}$, was determined by difference with the total P concentration in the NaOH–EDTA extract, measured after liquid digestion with concentrated nitric acid and potassium persulfate.

### Oxygen Isotopic Values

#### *Oxygen isotopic values in soil water and phosphate*

Soil water was quantitatively extracted by cryogenic vacuum extraction (Orlowski et al., 2013) for each combination of soil per treatment at days 0, 4, 11, 29, and 93 after labeling. Oxygen isotopic composition of the soil water ($\delta^{18}$Ow) was measured by equilibration with $CO_2$ using a gas bench (Thermo Scientific GasBench II) connected to an isotope ratio mass spectrometer (Thermo Scientific Delta V plus) at the facilities of the Department of Earth Science of the ETH Zürich (Seth et al., 2006). Calibration was made with international standards SMOW (Standard Mean Ocean Water), SLAP (Standard Light Antarctic Precipitation), and GISP (Greenland Ice Sheet Precipitation), distributed by the International Atomic Energy Agency (IAEA, Vienna, Austria). Results are reported in the standard delta notation ($\delta^{18}$O) as per mill deviation to the Vienna Standard Mean Ocean Water (VSMOW). Reproducibility of the measurements based on repeated measurements of internal standards was better than 0.03‰.

The $P_{res}$, $P_{hex}$, and $Pi_{HCl}$ extracts were purified following the protocol of Tamburini et al. (2010) and modified by Pistocchi et al. (2014). In NaOH–EDTA extracts, both $Po_{NaOH}$ and $Pi_{NaOH}$ are present and a separation prior the purification is needed. According to Tamburini et al. (2018), the NaOH–EDTA pool was divided into high-molecular weight (mostly organic) and low-molecular weight (mostly inorganic) compounds using size exclusion gel chromatography with a Sephadex G25 Medium, presenting a 5 KDa cut-off (ÄKTAprime plus, GE Healthcare Bio-Sciences AB, Uppsala, Sweden). The inorganic pool was purified following the standard protocol, after a precipitation of magnesium ammonium phosphate, which targets inorganic P. The organic pool was hydrolysed by UV radiation, with one split containing $^{18}$O-enriched water to check for possible incorporation of O into the newly formed inorganic phosphate.

The P concentration in NaOH–EDTA extracts from LUE was not high enough for the separation–purification procedure and therefore only the $\delta^{18}$O-P values of the initial $Po_{NaOH}$ ($\delta^{18}$O-$Po_{NaOH}$) are presented.

Purified phosphate in the form of $Ag_3PO_4$ was weighted in silver capsules in two or three analytical replicates each consisting in 300–600 μg of $Ag_3PO_4$ and a small amount of glassy carbon powder. Samples were analyzed on a thermal conversion elemental analyzer (vario PYRO cube, Elementar Analysensysteme GmbH, Langenselbold, Germany), coupled to an IsoPrime 100 isotopic ratio mass spectrometer (IRMS) at the Laboratory of the Plant Nutrition Group (ETH Zürich). In each run, repeated measurements of internal $Ag_3PO_4$ standard (Acros Organics, Geel, Belgium, $\delta^{18}$O = 14.2‰), two benzoic acid international standards (IAEA 601: $\delta^{18}$O = 23.1‰, IAEA 602 $\delta^{18}$O = 71.3‰), and in-house made standards were included for instrumental drift correction

and calibration. The $\delta^{18}O$ composition is expressed in the delta notation with respect to VSMOW (Vienna Standard Mean Ocean Water). The $\delta^{18}O$-P of a specific P pool is referred to as: $\delta^{18}O\text{-}P_{\text{pool identification}}$. Analytical uncertainties, as determined from the replicate analysis of the standards, were of 0.4‰.

***Oxygen isotopic values in leaf litter***

Samples of the LUE and BBR leaf litter used in the incubation were extracted and purified according to the protocol of Tamburini et al. (2018). The protocol targets two pools extracted sequentially: the metabolic Pi with trichloroacetic acid (TCA) and the organic P with NaOH–EDTA. In detail, plant material weighed in duplicate (6 g each) was first crushed with the help of liquid $N_2$ and then extracted with either $^{18}O$-labeled or unlabeled 0.3 M TCA. The supernatants were separated after homogenization with a Polytron (Kinematica AG, Lucerne, Switzerland) and shaking (0.5 h) via filtration with glass fiber filters (APFF04700 Merck Millipore). The residue was further extracted with 0.25 M NaOH – 0.05 M $Na_2(EDTA)_2{\cdot}H_2O$, following the protocol described in Noack et al. (2014).

The TCA and NaOH–EDTA supernatants were measured for Pi ($Pi_{TCA}$, $Pi_{NaOH\_litter}$) and Po ($Po_{TCA}$, $Po_{NaOH\_litter}$) and purified for $\delta^{18}O$-P analysis, following the procedure described by Pfahler et al. (2013) and Tamburini et al. (2018), respectively.

## Data Analyses

### Expected $\delta^{18}O$-P at Isotopic Equilibrium and From Organic P Hydrolysis

The expected $\delta^{18}O$-P of phosphate in equilibrium with soil water ($\delta^{18}O\text{-}P_{eq}$) was calculated for each time point rearranging the equation from Chang and Blake (2015) as follows:

$$\delta^{18}O\text{-}P_{eq} = e\hat{}(14.43/T + 26.54/1000) * (\delta^{18}Ow + 1000) - 1000 \quad (1)$$

where $T$ is the temperature in K during the incubation and $\delta^{18}Ow$ (‰) is the measured oxygen isotopic composition of soil water.

The expected $\delta^{18}O$-P of phosphate released from hydrolysis of phosphoesters ($\delta^{18}O\text{-}P_{Pase}$) via phosphatase enzymes was calculated according to this equation:

$$\delta^{18}O\text{-}P_{Pase} = x \times (\delta^{18}O\text{-}Po) + (1 - x) \times (\delta^{18}Ow + \varepsilon) \quad (2)$$

where $x$ is the proportion of O atoms inherited from the phosphate group in the Po compound (0.75 for phosphomonoester and 0.5 for phosphodiester), $\delta^{18}O$-Po (‰) is the O isotopic composition of the phosphate group in the Po compound, $\delta^{18}Ow$ (‰) is the measured O isotopic composition of soil water, and $\varepsilon$ (‰) is the enzyme-specific fractionation factor. Here we estimated $\delta^{18}O$-Po as the measured isotopic composition of Po extracted by NaOH–EDTA ($\delta^{18}O\text{-}Po_{NaOH}$) either from soil or leaf litter (see **Table 1** and sections "Oxygen isotopic values in soil water and phosphate" and "Oxygen isotopic values in leaf litter").

### Calculation of $\delta^{18}O$-P

The oxygen isotopic composition of phosphate in the $P_{mic}$ pool ($\delta^{18}O\text{-}P_{mic}$), was calculated with a mass balance equation (Tamburini et al., 2012):

$$\delta^{18}O\text{-}P_{mic} = (\delta^{18}O\text{-}P_{hex} \times P_{hex} - \delta^{18}O\text{-}P_{res} \times P_{res})/(P_{hex} - P_{res}) \quad (3)$$

where $\delta^{18}O\text{-}P_{hex}$ (‰) and $\delta^{18}O\text{-}P_{res}$ (‰) are the oxygen isotopic composition of phosphate in the hexanol and resin extracts, respectively, and $P_{hex}$ (mg P $kg^{-1}$) and $P_{res}$ (mg P $kg^{-1}$) are the P concentrations in the corresponding extracts. When $\delta_{18}O\text{-}P_{hex}$ and $\delta_{18}O\text{-}P_{res}$ were close, i.e., a difference of less than twice the standard deviation of analytical replicates (< 0.8‰), the $\delta^{18}O\text{-}P_{hex}$ was taken directly as $\delta^{18}O\text{-}P_{mic}$. We did not apply any conversion factor (Kp) to correct for incomplete recovery of $P_{mic}$ due to possible ineffectiveness of the fumigant. Indeed, we cannot assume that all $P_{mic}$ compartments, including the ones non-extractable with hexanol, have the same isotopic composition.

Some extractions were done in duplicate with $^{18}O$ labeled and unlabeled reagents, i.e., TCA, UV digestion of the organic pool of NaOH–EDTA and HCl, to track the incorporation of labeled oxygen into the $\delta^{18}O$-P via inorganic hydrolysis (Tamburini et al., 2010). If incorporation was detected, the actual $\delta^{18}O$-P was calculated according to Pistocchi et al. (2017):

$$\delta^{18}O\text{-}P = (\delta^{18}O\text{-}P_l \times \delta^{18}Ow_{nl} - \delta^{18}O\text{-}P_{nl} \times \delta^{18}Ow_l)/(\delta^{18}O\text{-}P_l - \delta^{18}O\text{-}P_{nl} - \delta^{18}Ow_l + \delta^{18}Ow_{nl}) \quad (4)$$

where $\delta^{18}O\text{-}P_l$ (‰) and $\delta^{18}O\text{-}P_{nl}$ (‰) are the oxygen isotopic composition of phosphate for the labeled and unlabeled samples, respectively, and accordingly $\delta^{18}Ow_l$ (‰) and $\delta^{18}Ow_{nl}$ (‰) the oxygen isotopic composition of labeled and unlabeled extraction solution. When hydrolysis was negligible, as in most cases, the subsamples were considered as duplicates.

### Incorporation of O From Water Into Phosphate

Through the process of labeling with $^{18}O$-enriched water, it is possible to calculate how much O from soil water was incorporated into phosphate molecules of a specific P pool over time. Oxygen incorporation (%) was calculated as the slope of the straight line between two points in the $\delta^{18}Ow$-$\delta^{18}O$-P plot (Liang and Blake, 2006a):

$$\text{O incorporation} = (\delta^{18}O\text{-}P_t - \delta^{18}O\text{-}P_{t0})/(\delta^{18}Ow_t - \delta^{18}Ow_{t0}) \times 100 \quad (5)$$

Where $\delta^{18}Ow_t$ and $\delta^{18}Ow_{t0}$ are the oxygen isotopic compositions of soil water and $\delta^{18}O\text{-}P_t$ and $\delta^{18}O\text{-}P_{t0}$ are the oxygen isotopic compositions of phosphate in a given pool at time point t and at day 0, respectively.

Incorporations of 25 or 50% indicate that overall one out of four or two out of four O atoms, respectively, are incorporated from water into phosphate. 100% O incorporation indicates all four O of phosphate derived from water.

For $\delta^{18}O$-P values obtained with the Equations 3, 4, and 5 the mean and standard deviation per sample were obtained with a Monte Carlo error propagation simulation (Anderson, 1976).

**TABLE 1 |** General characteristics of the two studied Oe horizons at site Lüss (LUE) and Bad Brückenau (BBR).

| Soil Property or Variable | Unit | LUE | BBR |
|---|---|---|---|
| Humus form and humus layer thickness | – | Mor-like Moder (13 cm) | Mull-like Moder (5 cm) |
| Water holding capacity | g $g^{-1}$ | 2.92 | 3.26 |
| $pH_{H2O}$ | – | 3.55 | 3.70 |
| Organic Carbon | g C $kg^{-1}$ | 364 | 237 |
| Organic Nitrogen | g N $kg^{-1}$ | 16.7 | 14.8 |
| Microbial Carbon ($C_{mic}$) | mg C $kg^{-1}$ | 1,047 | 844 |
| Microbial Nitrogen | mg N $kg^{-1}$ | 238 | 152 |
| Microbial P ($P_{mic}$) | mg P $kg^{-1}$ | 55.6 | 98.8 |
| Total P | mg P $kg^{-1}$ | 485 | 2,564 |
| Organic P | mg P $kg^{-1}$ | 371 | 1,523 |
| Available P ($P_{res}$) | mg P $kg^{-1}$ | 3.0 | 34.7 |
| Corg: Norg | mol/mol | 25.4 | 18.7 |
| $C_{mic}$: $N_{mic}$ | mol/mol | 5.1 | 6.5 |
| Corg: Porg | mol/mol | 2,949 | 426.4 |
| $C_{mic}$: $P_{mic}$ | mol/mol | 48.6 | 21.1 |
| Acid phosphatase potential activity (day 1) | nmol $g^{-1}$ $h^{-1}$ | 19,207 | 16,098 |
| Alkaline phosphatase potential activity (day 1) | nmol $g^{-1}$ $h^{-1}$ | 146 | 74 |
| Metabolic quotient ($cCO_2$; 1) | $\mu$g C–$CO_2$ $\mu g^{-1}$ Cmic $h^{-1}$ | 4.5 | 2.6 |
| $\delta^{18}$O-P of organic P (2) | ‰ | 22.47 | 17.22 |
| $\delta^{18}$O-P of leaf litter, TCA (3) | ‰ | 13.48 | 17.06 |
| $\delta^{18}$O-P of leaf litter, NaOH (3) | ‰ | 20.42 | 18.58 |

*(1) Unit $CO_2$ respired per unit microbial carbon. Calculated using steady respiration rate measured in the present study. (2) Oxygen isotopes composition of organic P from 25 M sodium hydroxide – 0.05 M sodium EDTA soil extract. (3) Oxygen isotopes composition of P in leaf litter, TCA, 0.3 M Trichloroacetic acid extract; NaOH, 0.25 M sodium hydroxide – 0.05 M sodium EDTA extract.*

Calculations were repeated 10 million times by varying the $\delta^{18}$O signatures according to their mean and standard deviations. For the $\delta^{18}Ow_s$, we assumed a standard deviation of 0.03‰ corresponding to the analytical error.

### Statistical Analyses

A two-way ANOVA (1st factor = litter application, 2nd factor = date) was applied to analyze the variables measured during the incubation for each soil separately except the respiration rates. These latter were analyzed with a mixed model, where the litter amendment was the fixed factor and the time of the measurement (weekly) a random factor with the replicate nested in it. Model simplification (one-way ANOVA) was done when possible or when data were missing, e.g., $\delta^{18}O\text{-}Po_{NaOH}$ in LUE soil. In some cases, there were not enough replicates for statistical tests. These results are discussed qualitatively. The Tukey test was used for *post hoc* comparison. The Student's paired *t*-test was used when comparing single dates and cumulative values, after checking for homogeneity of variances. The Shapiro–Wilk test was used to assess normality of the data. All analyses were performed in R 3.1.1 (R version 3.1.1, R Core Team).

## RESULTS

### Soil Respiration

The soil respiration declined during the first 3–4 weeks by approximately 10 and 25% for LUE and BBR soils, respectively. After the first month, the respiration remained approximately constant (**Figure 1**). The soil respiration of LUE soil was almost double that of the one measured for BBR soil. Similarly, the metabolic quotient $cCO_2$, calculated with the average respiration rates over the last 8 weeks, was almost double in LUE soil (**Table 1**).

During the first 4 weeks, differences between treatments were detectable, with leaf litter-amended soils showing higher respiration rates (**Figure 1**). This resulted in a cumulative additional carbon (C) release for the litter-amended soils of 3.4 and 11.1% for LUE and BBR soils, respectively, significant only for the latter (**Supplementary Table 1 SI**).

### Soil General Characteristics and Potential Phosphatases Activity

The two soils were acidic (3.77 and 3.65 for BBR and LUE soil, respectively) but differed in almost all considered variables (**Table 1**). In particular, concentration of total, organic and available P was much higher in BBR than in LUE soil.

Potential acid phosphatase activity was similar for LUE and BBR soils, while potential alkaline phosphatase activity was double in LUE soil, although much lower than the acid phosphatase activity (**Table 1** and **Supplementary Figure 1SI**). Therefore, for the calculation of the expected value from Po hydrolysis by phosphatases with Equation 2 we used the fractionation factor (ε) of – 10‰ attributed to acid phosphatases (von Sperber et al., 2014). No differences were found between litter treatments.

### The Concentration and $\delta^{18}$O-P of Resin-Extractable and Microbial P Pools

In both LUE and BBR soils the concentration of $P_{res}$ increased, while $P_{mic}$ remained largely stable over the study time with small

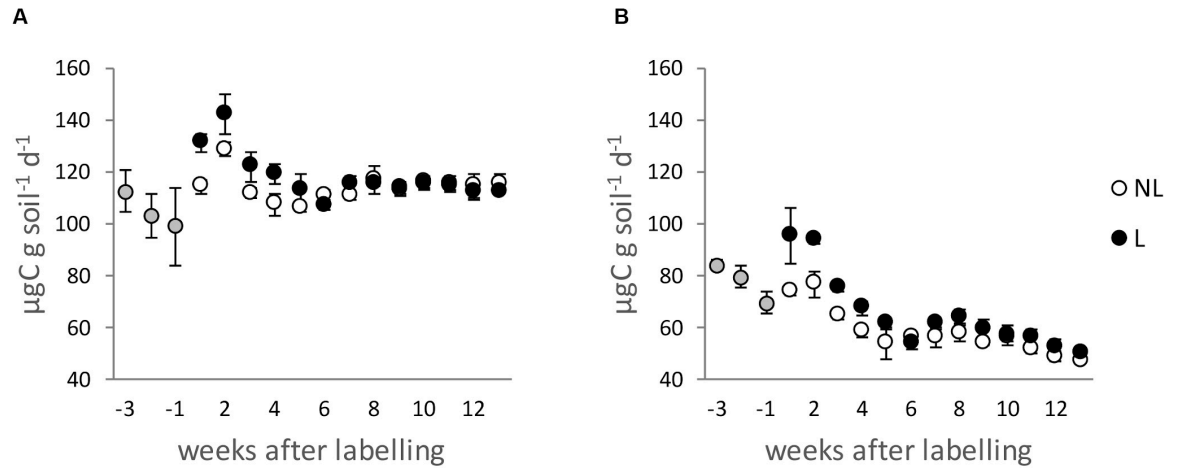


**FIGURE 1 |** $CO_2$ emitted from Lüss (LUE; **A**) and Bad Brückenau (BBR; **B**) soils during the incubation. Gray circles indicate respiration rates during the pre-incubation period, white circles the respiration rates in the non-amended treatment (NL) and black circles in the leaf-litter amended treatment (L). Error bars indicate replicates standard deviation.

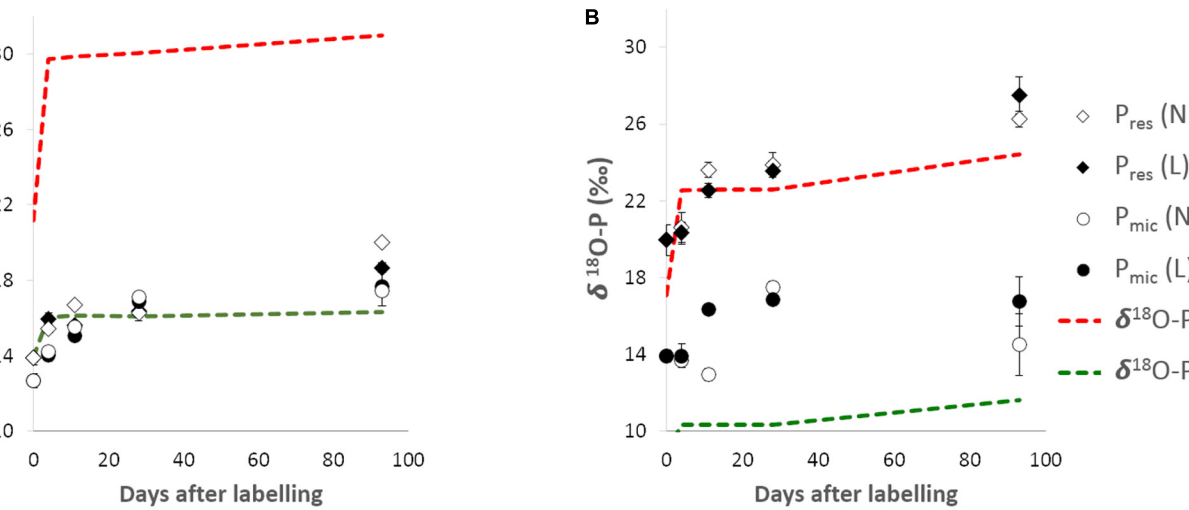


**FIGURE 2 |** The $\delta^{18}$O-P of available P ($P_{res}$) and microbial P ($P_{mic}$) pools in Lüss (LUE; **A**) and Bad Brückenau (BBR; **B**) soils over the course of the incubation. The expected isotopic equilibrium between phosphate and water (Equation 1) is indicated by the red dotted line and the expected isotopic signature of phosphate from organic P (Po) hydrolysis of soil organic matter via acid phosphatase (Equation 2) is indicated by the green dotted line. Error bars indicate replicates standard deviation. NL, non-amended; L, leaf litter-amended.

fluctuation in the low P LUE soil and decreased significantly in the high P BBR soil (**Supplementary Table 2 SI**). In the litter-amended BBR soil the $P_{res}$ was slightly higher, with a mean effect size of + 2.1 mg kg$^{-1}$. The litter addition increased the $P_{mic}$ slightly in both soils, with a mean effect size of + 4.9 and + 4.4 mg kg$^{-1}$ for LUE and BBR, respectively (**Supplementary Table 2 SI**).

The $\delta^{18}O\text{-}P_{res}$ and $\delta^{18}O\text{-}P_{mic}$ increased by several units during the incubation in both LUE and BBR soils (**Figure 2**). Therefore, incorporation of O from labeled soil water into phosphate occurred.

For the low P LUE soil, both $\delta^{18}O\text{-}P_{res}$ and $\delta^{18}O\text{-}P_{mic}$ had a similar initial value (13.9 and 12.7‰, respectively) and both followed a slight increasing trend over the duration irrespective of the application of leaf litter. This change in value was similar to that predicted by the $\delta^{18}O\text{-}P_{Pase}$, i.e., expected from the hydrolysis of Po via acid phosphatases (Equation 2; **Figure 2A**).

For the high P BBR soil, however, the initial values of $\delta^{18}O\text{-}P_{res}$ and $\delta^{18}O\text{-}P_{mic}$ were different: 19.9‰ *vs.* 14.0‰, respectively. The $\delta^{18}O\text{-}P_{mic}$ increased slightly over time and remained below the expected equilibrium between phosphate and water ($\delta^{18}O\text{-}P_{eq}$ in Equation 1), whereas the $\delta^{18}O\text{-}P_{res}$ approached and exceeded the $\delta^{18}O\text{-}P_{eq}$ by day 93 (**Figure 2B**). The $\delta^{18}O\text{-}P_{mic}$ values were in average lower for the non-amended treatment ($p < 0.05$).

For both soils, the picture does not change if we consider the $\delta^{18}O\text{-}P_{Pase}$ values calculated using the Po in the litter, as they are similar to the ones from soil Po (see $\delta^{18}O\text{-}P_{Pase}$ litter, **Supplementary Table 2 SI**).

## The Concentration and $\delta^{18}$O-P of NaOH- and HCl-Extractable Pools

In the LUE soil incubation, concentrations of the inorganic pools $Pi_{NaOH}$ and $Pi_{HCl}$ remained approximately stable during the incubation. The organic pool, $Po_{NaOH}$, increased slightly ($+$ 36.8 mg kg$^{-1}$ at day 93). No differences were detected between the litter amended and non-amended treatments (**Table 3**).

In BBR, a slight increase (mean effect size of $+$ 49.0 mg kg$^{-1}$ at day 93) of the $Pi_{NaOH}$ was registered over the incubation time. The $Pi_{HCl}$ and $Po_{NaOH}$ remained stable over the incubation time. No differences due to the leaf litter addition were observed (**Table 3**).

The $\delta^{18}O\text{-}Pi_{HCl}$ in the LUE soil incubation had a slight increase ($+$ 1‰). We could not analyze the $\delta^{18}O\text{-}Pi_{NaOH}$ or $\delta^{18}O\text{-}Po_{NaOH}$ in LUE soil because of the insufficient amount of P extracted. In the BBR soil, we detected a significant increase of the $\delta^{18}$O-P of both inorganic and organic pools. The $\delta^{18}O\text{-}Pi_{NaOH}$ increased by 4.4‰, as an average of the L and NL treatments. A similar increase was measured for the $\delta^{18}O\text{-}Pi_{HCl}$ (**Table 3**). Despite those increases neither $\delta^{18}O\text{-}Pi_{NaOH}$ nor $\delta^{18}O\text{-}Pi_{HCl}$ reached the corresponding value of the available P ($P_{res}$) at day 93, meaning that they did not completely equilibrate with the $P_{res}$ at the end of the incubation. Similarly, the $\delta^{18}O\text{-}Po_{NaOH}$ also increased slightly, but by only approximately 1‰ at the end of the incubation.

Differences due to the litter addition were found in the BBR soil for the $\delta^{18}O\text{-}Po_{NaOH}$ ($+$ 1‰ for the L treatment at day 4) and for the $\delta^{18}O\text{-}Pi_{HCl}$ ($-$2.3‰ for the L treatment at day 93).

## $^{18}$O Incorporation Into P Pools

The addition of $^{18}$O-enriched water successfully increased O isotopic ratio of soil water (**Supplementary Table 3 SI**) and resulted in incorporation of $^{18}$O from water into major soil P pools. The trend, however, differed in the two soils. In LUE, both the $P_{res}$ and $P_{mic}$ incorporated O at similar rate: around one out of four O atoms per phosphate (25%) were exchanged in the first 20–30 days of incubation and up to two out of four (50%) were exchanged after 93 days (**Figure 3A**). In BBR instead, the $^{18}$O from water was incorporated faster, but it did not exceed 50% in the $P_{mic}$ by day 93, while it had reached 90% in the $P_{res}$, suggesting an almost complete exchange of the four O of phosphate with water (**Figure 3B**). A decline of the O incorporation in $P_{mic}$ in the BBR soil was observed between the second-last and the last sampling. This decline was more pronounced in the treatment without litter. A stronger relationship was found between O incorporation in Pres and cumulated respiration in BBR soil as compared to LUE (**Figure 4A**).

# DISCUSSION

The increase in $\delta^{18}$O-P value of almost all P pools indicates that biological processes were involved in P cycling in both soils, as the exchange of oxygen between soil phosphate and water involves enzymatic reactions (Tudge, 1960).

## Biological Processes Affecting Available P in the Low P Availability LUE Soil

Under low P availability, $\delta^{18}O\text{-}P_{mic}$ and $\delta^{18}O\text{-}P_{res}$ were very similar and followed the same temporal trend (**Figure 2A**). There are three potential explanations for this pattern: (i) There was phosphate efflux from $P_{mic}$ to $P_{res}$, so the $P_{res}$ pool was strongly influenced by the $P_{mic}$ pool as observed in other P-poor soils (Tamburini et al., 2012; Weiner et al., 2018); (ii) There was no phosphate efflux from $P_{mic}$ to $P_{res}$, but the dominant enzymatic processes were the same in both pools, thus imprinting the same isotopic signature; finally (iii) There was no phosphate efflux from $P_{mic}$ to $P_{res}$, and the two pools were impacted by different enzymatic processes which resulted in similar $\delta^{18}O$-P just by chance.

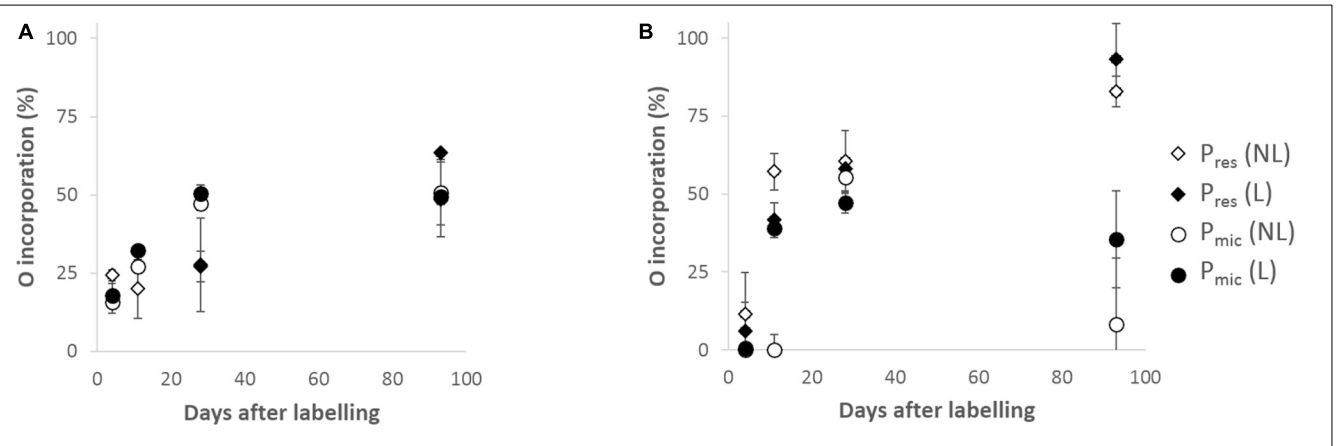


**FIGURE 3 |** Oxygen incorporation from water into available P ($P_{res}$) and microbial P ($P_{mic}$) pools according to Equation 5 in Lüss (LUE; **A**) and Bad Brückenau (BBR; **B**) soils during the incubation. Error bars indicate standard deviation from Monte Carlo error propagation. NL, non-amended; L, leaf litter-amended.

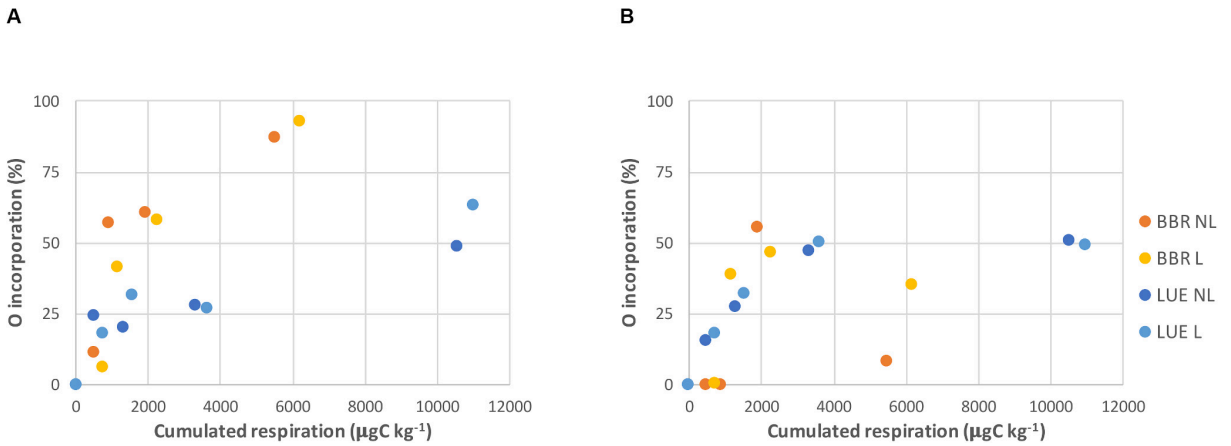


**FIGURE 4 |** Oxygen incorporation from labeled water into the available ($P_{res}$; **A**) and microbial P ($P_{mic}$; **B**) in Bad Brückenau (BBR) and Lüss (LUE) soils against cumulated respiration. NL, non-amended; L, leaf litter-amended.

The parallel $^{33}$P dilution experiment showed that gross mineralization strongly contributed to the $P_{res}$ pool. It also highlighted a fast and important P immobilization into the microbial biomass (around 95% of gross mineralization, see Pistocchi et al., 2018). The $^{33}$P experiment, however, gave no direct evidence of an efflux from $P_{mic}$ to $P_{res}$. This may point either to the first or to the second explanation. Lis et al. (2019) observed in an *in vitro* experiment that cyanobacteria growing under P-depleted conditions took up P through phosphate specific transporters (Pst) without leaking it. Therefore, the second explanation, i.e., no or little phosphate efflux from $P_{mic}$ to $P_{res}$ and same dominant enzymatic processes, is more likely (see **Figure 5A** modified after Lis et al., 2019). However, compared to their study we did not observe isotopic equilibrium in the intracellular and extracellular P.

Of further consideration is that both $\delta^{18}$O-$P_{mic}$ and $\delta^{18}$O-$P_{res}$ were similar to the value expected for phosphomonoester hydrolysis over the first 30 days of incubation (one out of four O was exchanged with water, see **Figure 2A**). According to a two end-members mass balance including the isotopic equilibrium ($\delta^{18}$O-$P_{eq}$, Equation 1) and the $\delta^{18}$O-$P_{Pase}$ (Equation 2), this contribution represented almost 100% of the $P_{res}$ over this period.

By the end of the incubation, the O incorporation into $P_{res}$ had attained 50% (two out of four O atoms exchanged with water; **Figure 3A**), suggesting the contribution of other processes. There are two possible explanations: (i) that a single enzymatic process which incorporates two O atoms from water into phosphate was prevailing; or (ii) two or more processes contributed, resulting in 50% average O incorporation. The first explanation would be that the extracellular hydrolysis of phosphodiesters was occurring. However, Lang et al. (2017) found that the potential activity of phosphodiesterases over phosphomonoesterases was very low at this site. The contribution of multiple processes is, therefore, more likely. A two end-members balance including $\delta^{18}$O-$P_{eq}$ and $\delta^{18}$O-$P_{Pase}$ as previously hypothesized, suggests that phosphate derived from monoester hydrolysis constitutes about 80% of the $P_{res}$ at the end of the incubation. Interestingly, this value agrees with the results of parallel $^{33}$P incubation, where 94% of P exchanged with the soil solution came from gross mineralization (Pistocchi et al., 2018).

We conclude that under low P availability, both the $P_{res}$ and the $P_{mic}$ pools were dominated by phosphomonoesterase catalyzed reactions.

The attainment of the isotopic equilibrium was until now considered the main biological effect influencing the available P, corresponding to $P_{res}$ as defined in this study, via the release of intracellular phosphate ions (Zohar et al., 2010; Tamburini et al., 2012; Stout et al., 2014; Weiner et al., 2018; Lis et al., 2019). Our results support the hypothesis that under P-limiting conditions, the isotopic effect of Po hydrolysis can outweigh the isotopic equilibrium effect driven by inorganic pyrophosphatase in both $P_{mic}$ and $P_{res}$ pools (**Figure 5A**).

## Biological Processes Affecting Available P in the High P Availability BBR Soil

Under high P availability, the $P_{res}$ pool carried a very distinct isotopic signature from the $P_{mic}$ pool (**Figure 2B**). The $\delta^{18}$O-$P_{res}$ was close to or higher than the $\delta^{18}$O-$P_{eq}$ (isotopic equilibrium between phosphate and water, Equation 1), while $\delta^{18}$O-$P_{mic}$ was in between $\delta^{18}$O-$P_{eq}$ and the $\delta^{18}$O-$P_{Pase}$ (Equation 2).

The contribution of P from leaf litter does not explain the $\delta^{18}$O-$P_{res}$ values, as we did not find significant differences between litter treatments. The exchange with other soil P pools via sorption/desorption or precipitation/dissolution does not explain them either, as the $Pi_{NaOH}$ and $Pi_{HCl}$ all had lower $\delta^{18}$O-P than $\delta^{18}$O-$P_{res}$ (see **Table 2**), although these P pools likely exchanged phosphate ions with the $P_{res}$ pool (see section "Exchanges Between Available P and Other Inorganic and Organic P Pools").

The incorporation of O atoms from labeled water was around 90% in the $P_{res}$ pool by day 93, suggesting the prevalence of a process that leads to an exchange of all four O atoms. The

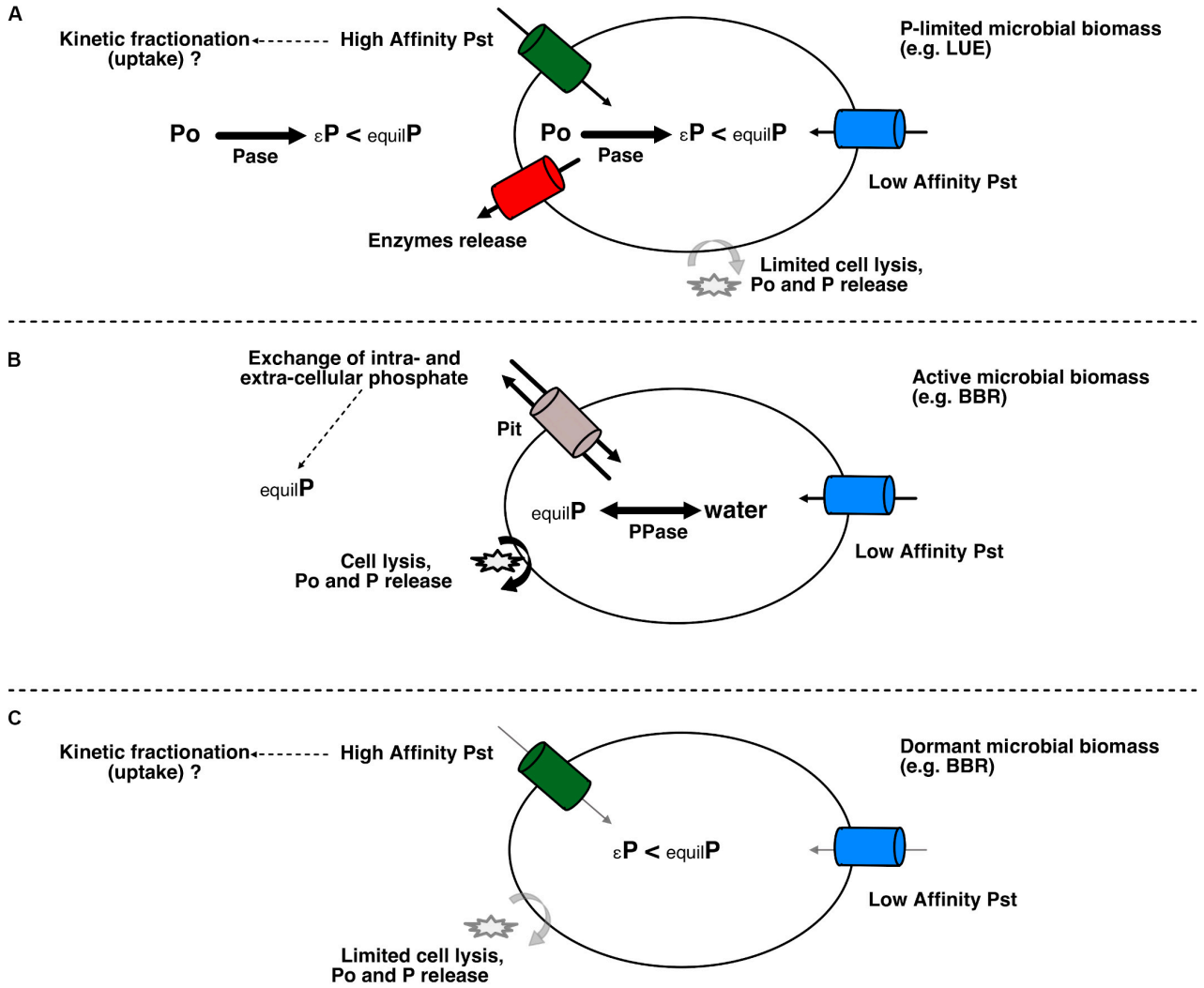


**FIGURE 5 |** Schematic representation of microbial processes under active stressed or dormant status and their effect on $\delta^{18}$O-$P_{res}$ and $\delta^{18}$O-$P_{mic}$ adapted with permission from Lis et al. (2019). Copyright (2019) American Chemical Society. **(A)** Case of microbes under low P conditions [e.g., Lüss (LUE) soil]. Intracellular P is not at isotopic equilibrium, since inorganic pyrophosphatase (PPase) is not dominant and other enzymes, e.g., phosphomonoesterase, are controlling the $\delta^{18}$O-$P_{mic}$. Only influx of phosphate ions is observed through phosphate specific transporters (high and low affinity Pst) and cell lysis might be limited. Phosphatase enzymes are actively excreted by the cells to hydrolyse Po compounds. These enzymatic reactions imprint an isotopic kinetic effect on the $\delta^{18}$O-$P_{res}$. **(B)** Case of microbes not limited by any environmental factor [e.g., active microbes in Bad Brückenau (BBR) soils]. Oxygen in intracellular phosphate is equilibrated with oxygen in water via the action of PPase. Intracellular phosphate is leaked out to the soil environment by either the low affinity Pit transporter or cell lysis (see Lis et al., 2019). $\delta^{18}$O-$P_{res}$ is controlled by the intracellular P and exhibits an equilibrium signature. **(C)** Case of microbes in a dormant state (limited by factors other than P availability, such as in BBR soils): uptake from the soil solution is limited and intracellular processes (e.g., phosphatases catalyzed reactions or other processes guaranteeing the minimal functioning of the cell; see Blagodatskaya and Kuzyakov (2013)] are imprinting an isotopic kinetic effect on $\delta^{18}$O-$P_{mic}$. This portion of the microbial biomass have little impact on the $P_{res}$. EquilP, phosphate with oxygen at equilibrium with oxygen in water; εP, phosphate released from hydrolysis of Po with a kinetic isotope imprint.

only known enzyme which could cause a complete exchange of O atoms with water is the inorganic pyrophosphatase (Cohn, 1958), which is mostly intracellular (Poll et al., 2006). However, the $P_{mic}$ pool in the BBR soil, showed consistently lower O incorporation when compared to the $P_{res}$. The presence of different microorganisms in either active or dormant states, all extracted with hexanol but carrying different isotopic signatures, could possibly explain the difference in $\delta^{18}$O-P between $P_{res}$ and $P_{mic}$ pools. However, only the active microbial community would carry a signature close to $\delta^{18}$O-$P_{eq}$ and contribute to the $P_{res}$ via P uptake, intracellular turnover and release (Siegenthaler et al., 2020). Indeed, inorganic pyrophosphatase is involved in DNA synthesis, amongst other processes, and therefore is more active when cells are growing (Kottur and Nair, 2018). The microorganisms in a dormant state would interact poorly with the $P_{res}$ pool and incorporate less O from water (see section "$\delta^{18}$O-P and Microbial Activity" for more discussion).

The O incorporation of close to 90% (**Figure 2B**) implies that almost all the phosphate in the final $P_{res}$ pool (i.e., 45.8 and 49.8 mg $kg^{-1}$, for the NL and L treatment, respectively)

**TABLE 2 |** Concentration and $\delta^{18}$O-P values of inorganic and organic P pools over the incubation period.

| Treatment | Days | $\delta^{18}$O-$Pi_{NaOH}$ | | | $\delta^{18}$O-$Po_{NaOH}$ | | | $\delta^{18}$O-$Pi_{HCl}$ | | | $Pi_{NaOH}$ | | | $Po_{NaOH}$ | | | $Pi_{HCl}$ | | |
|---|---|---|---|---|---|---|---|---|---|---|---|---|---|---|---|---|---|---|---|
| | | Mean | SD | *n* | Mean | SD | *n* | Mean | SD | *n* | Mean | SD | *n* | Mean | SD | *n* | Mean | SD | *n* |
| | | **LUE** | | | | | | | | | | | | **LUE** | | | | | |
| | 0 | nm | nm | – | 22.47 | nm | 1 | 21.82 | 0.12 | 2 | 95 | 3 | 3 | 168 | 37 | 3 | 7.2 | 0.1 | 3 |
| NL | 4 | nm | nm | – | nm | nm | – | 19.30 | 0.29 | 2 | 105 | 3 | 3 | 176 | 17 | 3 | 5.7 | 0.3 | 3 |
| L | 4 | nm | nm | – | nm | nm | – | nm | nm | - | 106 | 2 | 3 | 150 | 32 | 3 | 5.5 | 0.3 | 3 |
| NL | 93 | nm | nm | – | nm | nm | – | 22.68 | 0.51 | 2 | 102 | 5 | 3 | 203 | 7 | 3 | 7.5 | 1.7 | 3 |
| L | 93 | nm | nm | – | nm | nm | – | 22.55 | 0.24 | 2 | 105 | 4 | 3 | 206 | 45 | 3 | 5.2 | 0.3 | 3 |
| | | **Time effect** | | | | | | | | | | | | **Time effect** | | | | | |
| | | – | | | – | | | *** | (1) | | ns | | | * | | | ns | | |
| | | **Litter effect** | | | | | | | | | | | | **Litter effect** | | | | | |
| | | – | | | – | | | ns | (1) | | ns | | | ns | | | ns | | |
| | | **BBR** | | | | | | | | | | | | **BBR** | | | | | |
| | 0 | 16.52 | 0.85 | 2 | 17.22 | 0.81 | 3 | 17.47 | 0.36 | 2 | 658 | 9 | 3 | 1,320 | 68 | 3 | 98.6 | 10.2 | 3 |
| NL | 4 | 18.65 | 0.80 | 2 | 16.90 | 0.29 | 3 | 19.17 | nm | 1 | 621 | 39 | 3 | 1,426 | 118 | 3 | 83.4 | 9.4 | 3 |
| L | 4 | 18.92 | nm | 1 | 17.93 | 0.91 | 2 | 19.23 | nm | 1 | 660 | 10 | 2 | 1,386 | 186 | 3 | 81.1 | 23.7 | 3 |
| NL | 93 | 21.12 | nm | 1 | 18.34 | 0.38 | 2 | 21.94 | 0.21 | 3 | 720 | 50 | 3 | 1,569 | 342 | 3 | 91.1 | 19.9 | 3 |
| L | 93 | 22.38 | nm | 1 | 18.55 | 0.37 | 2 | 19.67 | 0.30 | 3 | 699 | 13 | 3 | 1,552 | 248 | 3 | 114.7 | 9.8 | 3 |
| | | **Time effect** | | | | | | | | | | | | **Time effect** | | | | | |
| | | *** | (1) | | ** | | | *** | | | *** | | | ns | | | ns | | |
| | | **Litter effect** | | | | | | | | | | | | **Litter effect** | | | | | |
| | | – | | | * | | | *** | | | ns | | | ns | | | ns | | |

*$Pi_{NaOH}$, NaOH–EDTA-extractable inorganic P; $Po_{NaOH}$, NaOH–EDTA-extractable organic P; $Pi_{HCl}$, HCl-extractable inorganic P; L, leaf litter-amended; NL, non-amended. Significance levels according to two-way ANOVA, where not differently specified: *** $p < 0.001$; ** $p < 0.01$; * $p < 0.05$; ns, non-significant; nm, not measurable. (1) Significance value from a 1-way ANOVA.*

underwent intracellular P turnover catalyzed by inorganic pyrophosphatases over the investigated period. Part of this efflux from $P_{mic}$ corresponded to a net loss, more pronounced in the NL treatment, which in turn translated in a net increase of $P_{res}$ (**Supplementary Table 2 SI**) and a transfer to other Pi or Po pools (see section "Exchanges Between Available P and Other Inorganic and Organic P Pools").

At the end of the incubation, the $\delta^{18}$O-$P_{res}$ was higher than the expected equilibrium by + 3.0‰. Recent studies on temperate forest soils reported enriched isotopic ratios compared to expected equilibrium after a period of incubation (Gross and Angert, 2017; Weiner et al., 2018). They attributed this positive offset to the steady-state between the efflux of intracellular P at isotopic equilibrium and the P uptake by microbes inducing isotopic enrichment of the extracellular phosphate ions (Blake et al., 2005; Lis et al., 2019). Although this effect could explain our finding, this explanation appears unlikely. Firstly, in our system $P_{res}$ increased during the incubation period, which does not fit into a Rayleigh fractionation model, which describes the kinetic fractionation induced by P uptake (Blake et al., 2005). Secondly, the mentioned studies observed the effect of P uptake by cells mostly under low environmental P conditions, which is not the case in the BBR soil.

It can also not be ruled out that a possible contribution from an unknown extracellular process occurred, leading to the exchange of four O atoms between phosphate and water, and/or the partial contribution of mineralization of Po compounds with heavy $\delta^{18}$O-P.

## $\delta^{18}$O-P and Microbial Activity

Saaby Johansen et al. (1991) and Melby et al. (2013) showed a positive relationship between $\delta^{18}$O-P de-labeling and respiration in incubation experiments with addition of $^{18}$O-labeled phosphate. Siegenthaler et al. (2020) suggested that a high incorporation of O from labeled water into the $P_{mic}$ pool reflects a high microbial activity.

In this study, we observed a higher respiration rate, therefore a higher microbial activity, in the low P LUE soil when compared to the high P BBR soil. Similarly, the microbial respiration per unit microbial biomass (metabolic quotient, $cCO_2$) of the LUE soil was twice the value recorded for the BBR soil (**Table 1**). In contrast, the O incorporation into the $P_{res}$ per unit $CO_2$ respired was lower in LUE soil (**Figure 4A**).

The dominance of phosphomonoesterase catalyzed reactions in the $P_{res}$ pool of the LUE soil (see section "Biological Processes Affecting Available P in the Low P Availability LUE Soil")

explains the lower O incorporation. This together with the higher $cCO_2$ might indicate differences in the microbial communities composition and/or a stronger investment of the LUE microbial community into Po mining via the production of extracellular phosphatase enzymes (Manzoni et al., 2010; Spohn and Chodak, 2015). The community composition analyses of Mészáros et al. (2020) and the $\delta^{18}$O-P data of the present study suggest that both factors possibly contribute simultaneously.

The O incorporation into the $P_{mic}$ pool was similar in the two soils during the first month of incubation, then lower in the BBR soil, which showed a strong decrease in the non-amended treatment (**Figures 3B**, **4B**).

We assumed earlier (section "Biological Processes Affecting Available P in the High P Availability BBR Soil") that in the BBR soil only part of the microbial community was actively turning over P and imprinting an isotopic equilibrium signature on it. The below-equilibrium $\delta^{18}$O-$P_{mic}$ and corresponding O incorporation resulted, therefore, from the relative contribution of $\delta^{18}$O-$P_{mic}$ at the isotopic equilibrium and $\delta^{18}$O-$P_{mic}$ below isotopic equilibrium. Lower $\delta^{18}$O-$P_{mic}$ would either occur because of the dominance of intracellular phosphomonoesterase reactions or because of little exchange of O between intracellular phosphate and labeled water (Chen et al., 2019). Since the $\delta^{18}$O-$P_{mic}$ was lower than isotopic equilibrium already before the labeling, the first explanation seems more likely. The two typologies outlined in **Figures 5B,C** would, therefore, contribute to the $\delta^{18}$O-$P_{mic}$ in the BBR soil.

The decrease in the O incorporation in the $\delta^{18}$O-$P_{mic}$ of the non-amended BBR soil by the end of the incubation was concomitant with a strong decrease in $P_{mic}$ concentration (**Supplementary Table 2 SI**). These effects could be determined by a decrease in the activity of microbial cells or a shift in the microbial community composition in response to less favorable environmental conditions (Fanin et al., 2013; Mooshammer et al., 2014). The respiration rates were very similar between treatments over the last 2 months of incubation (**Figure 1**). However, the analysis of microbial community composition showed a shift in both the fungal and bacterial communities. Additionally, the bacterial community changed differently in the amended and non-amended treatments over the last incubation period (Mészáros et al., 2020). The second explanation seems, therefore, more likely.

In LUE the incorporation of O from labeled water into $P_{mic}$ was driven by phosphomonoesterase catalyzed reactions as for $P_{res}$ (see section "Biological Processes Affecting Available P in the Low P Availability LUE Soil"). Pfahler et al. (2013) reported $\delta^{18}$O-P of soybean leaves decreased under P-limiting conditions and suggested this was the result of increased recycling of Po within plant tissue. Therefore, P-limiting conditions might induce a tighter intracellular Po recycling and translate in below-equilibrium $\delta^{18}$O-$P_{mic}$ values (**Figure 5A**). Interestingly, we found below-equilibrium $\delta^{18}$O-$P_{mic}$ also in non-incubated samples taken at the site LUE at two different dates (unpublished results), which suggests this effect is not an artifact of the incubation.

In summary, despite similar below-equilibrium $\delta^{18}$O-$P_{mic}$ in LUE and BBR soils, data such as $\delta^{18}$O-$P_{res}$, respiration rates and microbial communities composition, suggest a tighter P cycling in LUE. Interestingly, such differences were not reflected in different potential acid phosphatases activities (**Table 1** and **Supplementary Figure 1** in SI). Our data also suggest that the relationship between microbial activity and O incorporation into phosphate is not simply proportional as we initially hypothesized but likely modulated by P availability.

## Exchanges Between Available P and Other Inorganic and Organic P Pools

Due to the low extractable P concentration in LUE, we can only discuss results from the BBR soil.

In the parallel $^{33}$P experiment the $P_{res}$ and the $Pi_{NaOH}$ were shown to exchange rapidly in the BBR soil, with the tracer found in the $Pi_{NaOH}$ pool after 4 days. This suggests a fast exchange process, such as sorption/desorption. However, 3-months of incubation were not sufficient to attain a complete exchange between these two pools (Pistocchi et al., 2018).

As these exchanges are abiotic, i.e., without P–O bond cleavage, it is possible to trace P fluxes also with the $\delta^{18}$O-P, provided that the two exchanging pools have different initial isotopic signatures.

**TABLE 3 |** Estimation of P exchange fluxes in the Bad Brückenau (BBR) soil between the available and other inorganic P pools over 93 days according to a mass balance ($\delta^{18}$O-P data from this study) or to an isotopic dilution approach ($^{33}$P data from Pistocchi et al., 2018).

| | | $\delta^{18}$O-P Mass Balance | | $^{33}$P Isotopic Dilution | |
|---|---|---|---|---|---|
| ***P* pool** | **Treatment** | **Proportion of the P pool exchanged (1)** | **mg kg$^{-1}$ day$^{-1}$ P exchanged** | **Proportion of the P pool exchanged (2)** | **mg kg$^{-1}$ day$^{-1}$ P exchanged** |
| $Pi_{NaOH}$ | NL | 0.47 | 3.5 | 0.47 | 3.5 |
| | L | 0.53 | 3.9 | 0.54 | 4.0 |
| $Pi_{HCl}$ | NL | 0.51 | 0.5 | 0.29 | 0.8 |
| | L | 0.22 | 0.3 | 0.31 | 0.9 |

*L, leaf litter-amended; NL, non-amended. (1) proportion of the P pool exchanged* $= (\delta^{18}O\text{-}P\,(target\ pool)_{(t)} - \delta^{18}O\text{-}P\,(target\ pool)_{(0)})/(\delta^{18}O\text{-}P_{res(t)} - \delta^{18}O\text{-}P\,(target\ pool)_{(0)})$*, where 0 and t represent the day 0 and a time t (93 days), respectively, and* $\delta^{18}O\text{-}P_{res\,(t)}$ *is the oxygen isotopes ratio of the available P at time t. (2) According to the equation of Fardeau et al. (1995)* $q_{(t)} = Q\,(r_{(t)}/R)$*, where* $q_{(t)}$ *is the proportion of P exchanged in the target pool at time t, r is the radioactivity in the target pool, R is the total radioactivity introduced, and Q is the mass of the labeled pool (in this case the available P).*

The increase of the $\delta^{18}$O-$Pi_{NaOH}$ suggests that phosphate ions were transferred from an enriched P pool, presumably $P_{res}$. As was found with the $^{33}$P, the $Pi_{NaOH}$ and the $P_{res}$ did not attain similar isotopic compositions by the end of the incubation. On the contrary, their isotopic signature diverged, due to a large increase of the $\delta^{18}$O-$P_{res}$ (see **Table 3** and **Supplementary Table 2 SI**). It would appear that over the time scale of this incubation study, the biological processes that led to the isotopic enrichment of the $P_{res}$ had a stronger effect than the ions exchange with the $Pi_{NaOH}$ pool.

A mass balance, assuming constant P concentrations over the incubation, yields an exchange flux between $P_{res}$ and $Pi_{NaOH}$ of approximately 3.5–3.9 mg $kg^{-1}$ $day^{-1}$, which is similar to estimates provided by the $^{33}$P tracing experiment (**Table 3**).

The $\delta^{18}$O-$Pi_{HCl}$ also increased over time, suggesting an exchange with an isotopically enriched P pool. Similarly, we assume that the $Pi_{HCl}$ exchanged phosphate ions with the $P_{res}$ pool via abiotic reactions, allowing us to trace P fluxes via the $\delta^{18}$O-P. Through a mass balance calculation, we estimated 0.3–0.5 mg $kg^{-1}$ $day^{-1}$ of P was exchanged on average between these two P pools (**Table 3**).

The addition of leaf litter resulted in a slightly lower $\delta^{18}$O-$Pi_{HCl}$ at the end of the incubation (**Table 2**). To explain this, we have to assume that an abiotic transfer of depleted phosphate from the litter to the $Pi_{HCl}$ has occurred. Although the inorganic P in the litter had a slightly depleted $\delta^{18}$O-P (17.06‰ for the TCA extract, see **Table 1**), the amount of inorganic P contained within the litter was small compared to the $Pi_{HCl}$ pool. Furthermore, no other differences in other inorganic P pools of the leaf litter-amended soils were observed. Therefore, we cannot exclude the lower $\delta^{18}$O-$P_{HCl}$ was not simply a processing error.

In summary, the $P_{res}$ exchanged mostly with the $Pi_{NaOH}$ pool, which is in agreement with previous studies on BBR (Lang et al., 2017; Pistocchi et al., 2018) or on low-pH and Fe/Al oxides-rich soils (Buehler et al., 2002; Helfenstein et al., 2020).

The $\delta^{18}$O-$Po_{NaOH}$ increased slightly in the BBR soil (+ 1.1–1.3‰ in the NL and L treatment, respectively). The effect of leaf litter on the $\delta^{18}$O-$Po_{NaOH}$ was minor, as a difference between the treatments was only observed at day 4, and this subsequently leveled out. The increase in microbial activity observed in the first few weeks after the addition of the litter could have determined a faster turnover of Po derived from microbes. If the microbial Po was isotopically enriched as a consequence of the incorporation of O from labeled water, it would enrich the $\delta^{18}$O-$Po_{NaOH}$ once released from cells. Unfortunately, the $\delta^{18}$O-P of microbial Po is unknown, which prevents the calculation of its contribution to the $Po_{NaOH}$ pool. Measuring the isotopic signature of microbial Po or single microbial metabolites constitutes a major research gap that needs to be investigated in order to better clarify Po dynamics (Tamburini et al., 2018).

## CONCLUSION

Until now the isotopic equilibrium between phosphate and water was believed to be the main biological effect on microbial and available P. Here, we show that a below-equilibrium signature can be still an indicator of control of microbial P on the available P via Po hydrolysis reactions. This effect is possibly induced by P limiting conditions for microbes.

Labeling with $^{18}$O-water allowed the identification of the major biological process contributing to available P where radioisotope tracers fail because of low sensitivity, i.e., high baseline of isotopic dilution, as in the case of P-rich soils. Two independent isotopic approaches ($^{33}$P and $\delta^{18}$O-P) provided very similar estimates of P exchanged between the $P_{res}$ and $Pi_{NaOH}$ pools. This suggests that $\delta^{18}$O-P can be successfully used to trace P fluxes, provided that the underlying processes do not break the P – O bonds of the phosphate molecule.

## DATA AVAILABILITY STATEMENT

The dataset on fungal and bacterial community composition discussed in this study can be found in the Portail Data INRAE V1 repository (https://doi.org/10.15454/XOFCHY).

## AUTHOR CONTRIBUTIONS

CP wrote the manuscript with the inputs from all the co-authors. CP and ÉM conducted the experiments and performed the analyses. EF, FT, EB, and CP contributed to the experiment design. All authors contributed to the article and approved the submitted version.

## FUNDING

This work was funded by the Swiss National Science Foundation (SNF project 200021E-149130). The ETH Library funded the publication fee.

## ACKNOWLEDGMENTS

We want to acknowledge Friedericke Lang and Jaane Krueger for the project coordination, their support in sampling organization, and the many information they provided. We are also very grateful to the two reviewers for providing valuable and detailed comments to the manuscript. We also want to thank Laurie Schönholzer for her support in the laboratory analysis.

## SUPPLEMENTARY MATERIAL

The Supplementary Material for this article can be found online at: https://www.frontiersin.org/articles/10.3389/fenvs.2020.564778/full#supplementary-material

## REFERENCES


Achat, D. L., Bakker, M. R., Augusto, L., Saur, E., Dousseron, L., Morel, C., et al. (2009). Evaluation of the phosphorus status of P-deficient podzols in temperate pine stands: combining isotopic dilution and extraction methods. *Biogeochemistry* 92, 183–200. doi: 10.1007/s10533-008-9283-7

Alef, K. (1995). "Soil respiration," in *Methods in Soil Microbiology and Biochemistry*, eds K. Alef, and P. Nannipieri (San Diego, CA: Alef K. and Nannipieri P).

Anderson, G. M. (1976). Error propagation by the Monte Carlo method in geochemical calculations. *Geochim. Cosmochim. Acta* 40, 1533–1538. doi: 10.1016/0016-7037(76)90092-2

Bauke, S. L., Sperber, C., von Siebers, N., Tamburini, F., and Amelung, W. (2017). Biopore effects on phosphorus biogeochemistry in subsoils. *Soil Biol. Biochem.* 111, 157–165. doi: 10.1016/j.soilbio.2017.04.012

Becquer, A., Trap, J., Irshad, U., Ali, M. A., and Claude, P. (2014). From soil to plant, the journey of P through trophic relationships and ectomycorrhizal association. *Front. Plant Sci.* 5:548. doi: 10.3389/fpls.2014.00548

Blagodatskaya, E., and Kuzyakov, Y. (2013). Active microorganisms in soil: critical review of estimation criteria and approaches. *Soil Biol. Biochem.* 67, 192–211. doi: 10.1016/j.soilbio.2013.08.024

Blake, R. E., O'Neil, J. R., and Surkov, A. V. (2005). Biogeochemical cycling of phosphorus: insights from oxygen isotope effects of phosphoenzymes. *Am. J. Sci.* 305, 596–620. doi: 10.2475/ajs.305.6-8.596

Brandtberg, P.-O., Bengtsson, J., and Lundkvist, H. (2004). Distributions of the capacity to take up nutrients by *Betula* spp. and Picea abies in mixed stands. *For. Ecol. Manag.* 198, 193–208. doi: 10.1016/j.foreco.2004.04.012

Buehler, S., Oberson, A., Rao, I. M., Friesen, D. K., and Frossard, E. (2002). Sequential phosphorus Extraction oof a 33P-labeled Oxisol under contrasting agricultural systems. *Soil Sci. Soc. Am. J.* 66, 868–877. doi: 10.2136/sssaj2002.0868

Bünemann, E. K. (2015). Assessment of gross and net mineralization rates of soil organic phosphorus – A review. *Soil Biol. Biochem.* 89, 82–98. doi: 10.1016/j.soilbio.2015.06.026

Bünemann, E. K., Augstburger, S., and Frossard, E. (2016). Dominance of either physicochemical or biological phosphorus cycling processes in temperate forest soils of contrasting phosphate availability. *Soil Biol. Biochem.* 101, 85–95. doi: 10.1016/j.soilbio.2016.07.005

Bünemann, E. K., Steinebrunner, F., Smithson, P. C., Frossard, E., and Oberson, A. (2004). Phosphorus dynamics in a highly weathered soil as revealed by isotopic labeling techniques. *Soil Sci. Soc. Am. J.* 68, 1645–1655. doi: 10.2136/sssaj2004.1645

Chang, S. J., and Blake, R. E. (2015). Precise calibration of equilibrium oxygen isotope fractionations between dissolved phosphate and water from 3 to 37°C. *Geochim. Cosmochim. Acta* 150, 314–329. doi: 10.1016/j.gca.2014.10.030

Chen, J., Seven, J., Zilla, T., Dippold, M. A., Blagodatskaya, E., Kuzyakov, Y., et al. (2019). Microbial C:N:P stoichiometry and turnover depend on nutrients availability in soil: a 14C, 15N and 33P triple labelling study. *Soil Biol. Biochem.* 131, 206–216. doi: 10.1016/j.soilbio.2019.01.017

Cohn, M. (1958). Phosphate-water exchange reaction catalyzed by inorganic pyrophosphatase of yeast. *J. Biol. Chem.* 230, 369–380.

Daroub, S. H., Pierce, F. J., and Ellis, B. G. (2000). Phosphorus fractions and fate of phosphorus-33 in soils under plowing and no-tillage. *Soil Sci. Soc. Am. J.* 64, 170–176. doi: 10.2136/sssaj2000.641170x

Fanin, N., Fromin, N., Buatois, B., and Hättenschwiler, S. (2013). An experimental test of the hypothesis of non-homeostatic consumer stoichiometry in a plant litter–microbe system. *Ecol. Lett.* 16, 764–772. doi: 10.1111/ele.12108

Fardeau, J. C., Guiraud, G., and Marol, C. (1995). The role of isotopic techniques on the evaluation of the agronomic effectiveness of P fertilizers. *Nutr. Cycling Agroecosyst.* 45, 101–109. doi: 10.1007/bf00790659

Frossard, E., Achat, D. L., Bernasconi, S. M., Bünemann, E. K., Fardeau, J.-C., Jansa, J., et al. (2011*). "The use of tracers to investigate phosphate cycling in soil–plant systems," in *Phosphorus in Action*. (Berlin: Bunemann E. K).

Gross, A., and Angert, A. (2015). What processes control the oxygen isotopes of soil bio-available phosphate? *Geochim. Cosmochim. Acta* 159, 100–111.

Gross, A., and Angert, A. (2017). Use of 13 C- and phosphate 18 O-labeled substrate for studying phosphorus and carbon cycling in soils: a proof of concept: 13 C- and P- 18 O dual-labeled substrate to trace soil C and P cycling. *Rapid Commun. Mass Spectrom.* 31, 969–977. doi: 10.1002/rcm.7863

Hauenstein, S., Neidhardt, H., Lang, F., Krüger, J., Hofmann, D., Pütz, T., et al. (2018). Organic layers favor phosphorus storage and uptake by young beech trees (*Fagus sylvatica* L.) at nutrient poor ecosystems. *Plant Soil* 432, 289–301. doi: 10.1007/s11104-018-3804-5

Helfenstein, J., Pistocchi, C., Oberson, A., Tamburini, F., Goll, D. S., Frossard, E., et al. (2020). Estimates of mean residence times of phosphorus in commonly considered inorganic soil phosphorus pools. *Biogeosciences* 17, 441–454. doi: 10.5194/bg-17-441-2020

Helfenstein, J., Tamburini, F., von Sperber, C., Massey, M. S., Pistocchi, C., Chadwick, O. A., et al. (2018). Combining spectroscopic and isotopic techniques gives a dynamic view of phosphorus cycling in soil. *Nat. Commun.* 9:3226.

IUSS Working Group WRB (2006). *World Reference Base for Soil Resources 2006 – A Framework for International Classification, Correlation and Communication*. Rome: Food and Agriculture Organization of the United Nations.

Jaisi, D. P., Blake, R. E., and Kukkadapu, R. K. (2010). Fractionation of oxygen isotopes in phosphate during its interactions with iron oxides. *Geochim. Cosmochim. Acta* 74, 1309–1319. doi: 10.1016/j.gca.2009.11.010

Jonard, M., Augusto, L., Morel, C., Achat, D. L., and Saur, E. (2009). Forest floor contribution to phosphorus nutrition: experimental data. *Ann. For. Sci.* 66:510. doi: 10.1051/forest/2009039

Kottur, J., and Nair, D. T. (2018). Pyrophosphate hydrolysis is an intrinsic and critical step of the DNA synthesis reaction. *Nucleic Acids Res.* 46, 5875–5885. doi: 10.1093/nar/gky402

Kouno, K., Tuchiya, Y., and Ando, T. (1995). Measurement of soil microbial biomass phosphorus by an anion exchange membrane method. *Soil Biol. Biochem.* 27, 1353–1357. doi: 10.1016/0038-0717(95)00057-l

Lang, F., Krüger, J., Amelung, W., Willbold, S., Frossard, E., Bünemann, E. K., et al. (2017). Soil phosphorus supply controls P nutrition strategies of beech forest ecosystems in Central Europe. *Biogeochemistry* 136, 5–29. doi: 10.1007/s10533-017-0375-0

Liang, Y., and Blake, R. E. (2006a). Oxygen isotope composition of phosphate in organic compounds: isotope effects of extraction methods. *Organic Geochem.* 37, 1263–1277. doi: 10.1016/j.orggeochem.2006.03.009

Liang, Y., and Blake, R. E. (2006b). Oxygen isotope signature of Pi regeneration from organic compounds by phosphomonoesterases and photooxidation. *Geochim Cosmochim. Acta* 70, 3957–3969. doi: 10.1016/j.gca.2006.04.036

Lis, H., Weiner, T., Pitt, F. D., Keren, N., and Angert, A. (2019). Phosphate Uptake by Cyanobacteria Is Associated with Kinetic Fractionation of Phosphate Oxygen Isotopes. *ACS Earth Space Chem.* 3, 233–239. doi: 10.1021/acsearthspacechem.8b00099

Longinelli, A., and Nuti, S. (1973). Revised phosphate-water isotopic temperature scale. *Earth Planet. Sci. Lett.* 19, 373–376. doi: 10.1016/0012-821x(73)90088-5

Manzoni, S., Trofymow, J. A., Jackson, R. B., and Porporato, A. (2010). Stoichiometric controls on carbon, nitrogen, and phosphorus dynamics in decomposing litter. *Ecol. Monogr.* 80, 89–106. doi: 10.1890/09-0179.1

Marx, M.-C., Wood, M., and Jarvis, S. C. (2001). A microplate fluorimetric assay for the study of enzyme diversity in soils. *Soil Biol. Biochem.* 33, 1633–1640. doi: 10.1016/s0038-0717(01)00079-7

Melby, E. S., Soldat, D. J., and Barak, P. (2013). Biological decay of 18O-labeled phosphate in soils. *Soil Biol. Biochem.* 63, 124–128. doi: 10.1016/j.soilbio.2013.03.020

Mészáros, É, Pistocchi, C., Frossard, E., Buenemann, E. K., and Tamburini, F. (2020*). Changes of fungal and bacterial community composition of forest organic horizons with low and high phosphorus availability, Portail Data INRAE, V1. doi: 10.15454/XOFCHY

Mooshammer, M., Wanek, W., Schnecker, J., Wild, B., Leitner, S., Hofhansl, F., et al. (2012). Stoichiometric controls of nitrogen and phosphorus cycling in decomposing beech leaf litter. *Ecology* 93, 770–782.

Mooshammer, M., Wanek, W., Zechmeister-Boltenstern, S., and Richter, A. (2014). Stoichiometric imbalances between terrestrial decomposer communities and their resources: mechanisms and implications of microbial adaptations to their resources. *Front. Microbiol.* 5:22. doi: 10.3389/fmicb.2014.00022

Noack, S. R., Smernik, R. J., McBeath, T. M., Armstrong, R. D., and McLaughlin, M. J. (2014). Assessing crop residue phosphorus speciation using chemical fractionation and solution 31P nuclear magnetic resonance spectroscopy. *Talanta* 126, 122–129. doi: 10.1016/j.talanta.2014.03.049

Oehl, F., Oberson, A., Sinaj, S., and Frossard, E. (2001). Organic phosphorus mineralization studies using isotopic dilution techniques. *Soil Sci. Soc. Am. J.* 65, 780–787. doi: 10.2136/sssaj2001.653780x

Ohno, T., and Zibilske, L. (1991). Determination of low concentrations of phosphorus in soil extracts using malachite green. *Soil Sci. Soc. Am. J.* 55, 892–895. doi: 10.2136/sssaj1991.03615995005500030046x

Orlowski, N., Frede, H. G., Brüggemann, N., and Breuer, L. (2013). Validation and application of a cryogenic vacuum extraction system for soil and plant water extraction for isotope analysis. *J Sensors Sensor Syst.* 2, 179–193. doi: 10.5194/jsss-2-179-2013

Pfahler, V., Dürr-Auster, T., Tamburini, F., Bernasconi, S. M., and Frossard, E. (2013). 18 O enrichment in phosphorus pools extracted from soybean leaves. *New Phytol.* 197, 186–193. doi: 10.1111/j.1469-8137.2012.04379.x

Pistocchi, C., Mészáros, É, Tamburini, F., Frossard, E., and Bünemann, E. K. (2018). Biological processes dominate phosphorus dynamics under low phosphorus availability in organic horizons of temperate forest soils. *Soil Biol. Biochem.* 126, 64–75.

Pistocchi, C., Tamburini, F., Gruau, G., Ferhi, A., Trevisan, D., Dorioz, J. M., et al. (2017). Tracing the sources and cycling of phosphorus in river sediments using oxygen isotopes: methodological adaptations and first results from a case study in France. *Water Res.* 111, 346–356.

Pistocchi, C., Tamburini, F., Savoye, L., Sebilo, M., Baneschi, L., Lacroix, D., et al. (2014*). Développement d'une méthode d'extraction et purification des phosphates à partir de matrices sédimentaires pour l'analyse isotopique de leur oxygène. *Le cahier des techniques de l'INRA* 81, 1–23.

Poll, C., Ingwersen, J., Stemmer, M., Gerzabek, H., and Kandeler, E. (2006). Mechanisms of solute transport affect small-scale abundance and function of soil microorganisms in the detritusphere. *Eur. J. Soil Sci.* 57, 583–595. doi: 10.1111/j.1365-2389.2006.00835.x

Saaby Johansen, H., Middelboe, V., and Larsen, S. (1991). *Delabelling of 18O Enriched Phosphate Added to Soil as a Function of Biological Activity in the Soil*. Vienna: IAEA.

Seth, B., Schneider, C., and Storck, F. (2006). Improved reliability of oxygen isotopic analysis of water using the Finnigan GasBench II periphery of a continuous flow isotope ratio mass spectrometer by backflushing of the sampling line. *Rapid Commun. Mass Spectrom.* 20, 1049–1051. doi: 10.1111/j.1365-2389.2006.00835.x

Siebers, N., Bauke, S. L., Tamburini, F., and Amelung, W. (2018). Short-term impacts of forest clear-cut on P accessibility in soil microaggregates: an oxygen isotope study. *Geoderma* 315, 59–64. doi: 10.1016/j.geoderma.2017.11.024

Siegenthaler, M. B., Tamburini, F., Frossard, E., Chadwick, O. A., Vitousek, P., Chiara, P., et al. (2020). A dual isotopic (32P and 18O) incubation study to disentangle mechanisms controlling phosphorus cycling in soils from a climatic gradient (Kohala, Hawaii). *Soil Biol. Biochem.* 149:107920. doi: 10.1016/j.soilbio.2020.107920

Spohn, M., and Chodak, M. (2015). Microbial respiration per unit biomass increases with carbon-to-nutrient ratios in forest soils. *Soil Biol. Biochem.* 81, 128–133. doi: 10.1016/j.soilbio.2014.11.008

Spohn, M., Ermak, A., and Kuzyakov, Y. (2013). Microbial gross organic phosphorus mineralization can be stimulated by root exudates – A 33P isotopic dilution study. *Soil Biol. Biochem.* 65, 254–263. doi: 10.1016/j.soilbio.2013.05.028

Stout, L. M., Joshi, S. R., Kana, T. M., and Jaisi, D. P. (2014). Microbial activities and phosphorus cycling: an application of oxygen isotope ratios in phosphate. *Geochim. Cosmochim. Acta* 138, 101–116. doi: 10.1016/j.gca.2014.04.020

Tamburini, F., Bernasconi, S. M., Angert, A., and Frossard, E. (2010). A method for the analysis of the δ18O of inorganic phosphate extracted from soils with HCl. *Eur. J. Soil Sci.* 61, 1025–1032. doi: 10.1111/j.1365-2389.2010.01290.x

Tamburini, F., Pfahler, V., Bünemann, E. K., Guelland, K., Bernascon, S. M., Frossard, E., et al. (2012). Oxygen isotopes unravel the role of microorganisms in phosphate cycling in soils. *Environ. Sci. Technol.* 46, 5956–5962. doi: 10.1021/es300311h

Tamburini, F., Pistocchi, C., Helfenstein, J., and Frossard, E. (2018). A method to analyse the isotopic composition of oxygen associated with organic phosphorus in soil and plant material. *Eur. J. Soil Sci.* 69, 816–826. doi: 10.1111/ejss.12693

Tiessen, H., and Moir, J. O. (1993). "Characterization of Available P by Sequential Extraction," in *Soil Sampling and Methods of Analysis*, eds M. R. Carter, and E. G. Gregorich (Ann Arbor, MI: Carter M.R).

Tudge, A. P. (1960). A method of analysis of oxygen isotopes in orthophosphate—its use in the measurement of paleotemperatures. *Geochim. Cosmochim. Acta* 18, 81–93. doi: 10.1016/0016-7037(60)90019-3

von Sperber, C., Kries, H., Tamburini, F., Bernasconi, S. M., and Frossard, E. (2014). The effect of phosphomonoesterases on the oxygen isotope composition of phosphate. *Geochim. Cosmochim. Acta* 125, 519–527. doi: 10.1016/j.gca.2013.10.010

von Sperber, C., Tamburini, F., Brunner, B., Bernasconi, S. M., and Frossard, E. (2015). The oxygen isotope composition of phosphate released from phytic acid by the activity of wheat and Aspergillus niger phytase. *Biogeosciences* 12, 4175–4184. doi: 10.5194/bg-12-4175-2015

Weiner, T., Gross, A., Moreno, G., Migliavacca, M., Schrumpf, M., Reichstein, M., et al. (2018). Following the turnover of soil bioavailable phosphate in mediterranean savanna by oxygen stable isotopes. *J. Geophys. Res.* 123, 1850–1862. doi: 10.1029/2017JG004086

Werner, F., Mueller, C. W., Thieme, J., Gianoncelli, A., Rivard, C., Höschen, C., et al. (2017). Micro-scale heterogeneity of soil phosphorus depends on soil substrate and depth. *Sci. Rep.* 7:3203. doi: 10.1038/s41598-017-03537-8

Zohar, I., Shaviv, A., Young, M., Kendall, C., Silva, S., Paytan, A., et al. (2010). Phosphorus dynamics in soils irrigated with reclaimed waste water or fresh water — A study using oxygen isotopic composition of phosphate. *Geoderma* 159, 109–121. doi: 10.1016/j.geoderma.2010.07.002

**Conflict of Interest:** The authors declare that the research was conducted in the absence of any commercial or financial relationships that could be construed as a potential conflict of interest.

frontiers in Forests and Global Change

ORIGINAL RESEARCH
published: 15 October 2020
doi: 10.3389/ffgc.2020.543112

# Modeling Soil Responses to Nitrogen and Phosphorus Fertilization Along a Soil Phosphorus Stock Gradient

*Lin Yu*†, Bernhard Ahrens, Thomas Wutzler, Sönke Zaehle and Marion Schrumpf*

*Max Planck Institute for Biogeochemistry, Jena, Germany*

In this study, we investigate the responses of soil organic carbon (C) to nitrogen (N) and phosphorus (P) additions along a soil P stock gradient of five beech forest stands in Germany, using a modeling approach. Two different soil models with coupled C, N, and P cycles are used to simulate fertilization experiments conducted at the study sites. The first model, the stand-alone soil module of QUINCY (QUINCY-soil, Thum et al., 2019), is a conventional soil model that uses first-order kinetics to describe soil organic matter (SOM) turnover and represents microbial biomass only implicitly. The second model, the Jena Soil Model (JSM) (Yu et al., 2020), is a novel microbial soil model, which explicitly simulates microbial dynamics and describes the turnover of SOM as the consequence of several interactive processes, such as microbially mediated depolymerization of litter and SOM, organo-mineral association, and vertical transport. We applied both site-level models to five study sites and compared the modeled soil profile with observations. In addition, model scenarios were conducted to simulate the fertilization of N and P, and we further evaluate the effect of soil P stock, plant litter quality, and SOM CNP stoichiometry, on the responses of soil (heterotrophic) respiration ($R_s$) to nutrient addition. We found that the fitness between simulated and observed SOM profiles (defined as normalized root mean square ratios, $K_{nrmsr}$) were generally better in JSM than in QUINCY-soil ($K_{nrmsr}$ larger by 0.03 ± 0.10 to 0.16 ± 0.06 for various soil measurements at all sites); The general pattern of observed $R_s$ responses to nutrient fertilization, that N addition decreases $R_s$ whereas P addition increases it, can be reproduced by JSM but not by QUINCY-soil. Our results indicated that a detailed explicit description of microbial processes and organo-mineral association is required to model plant-soil-microbial interactions, thus to better reproduce SOM profiles and their responses to nutrient additions. It highlights the need to better represent these processes in future model developments.

**Keywords: phosphorus, nitrogen, microbe, stoichiometry, soil models**

OPEN ACCESS

***Edited by:***
*Sebastian Loeppmann, Christian-Albrechts-Universität zu Kiel, Germany*

***Reviewed by:***
*Lucia Fuchslueger, University of Vienna, Austria*
*Zachary E. Kayler, University of Idaho, United States*

****Correspondence:***
*Lin Yu*
*lyu@bgc-jena.mpg.de*

***†Present address:***
*Lin Yu, Centre for Environmental and Climate Research, Lund University, Lund, Sweden*

***Specialty section:***
*This article was submitted to Forest Soils, a section of the journal Frontiers in Forests and Global Change*

***Received:*** *15 March 2020*
***Accepted:*** *23 September 2020*
***Published:*** *15 October 2020*

***Citation:***
*Yu L, Ahrens B, Wutzler T, Zaehle S and Schrumpf M (2020) Modeling Soil Responses to Nitrogen and Phosphorus Fertilization Along a Soil Phosphorus Stock Gradient. Front. For. Glob. Change 3:543112. doi: 10.3389/ffgc.2020.543112*

## INTRODUCTION

Macronutrients such as nitrogen (N) and phosphorus (P) are capable of regulating major functions (e.g., photosynthesis and respiration) of higher plants (Engels et al., 2011; Hawkesford et al., 2012), and can thus affect the future forest carbon (C) balance (Fernández-Martínez et al., 2014; Wieder et al., 2015). Although changes of terrestrial C cycling are more easily observed aboveground

than belowground (Pan et al., 2011; Jonard et al., 2015, Zhu et al., 2016), many studies have shown that belowground biogeochemical processes, such as C allocation, decomposition, nutrient uptake, and mineralization, strongly control the C-nutrient interactions of forest ecosystems. For example, increased atmospheric $CO_2$ concentration has been shown to increase belowground C allocation (Norby et al., 2004; Ellsworth et al., 2017), and to facilitate plant N uptake (Finzi et al., 2007) and soil P mining (Jiang et al., 2020) in free-air $CO_2$ enrichment studies. A similarly large number of studies have shown that changes of nutrient inputs (fertilization, deposition changes, nutrient stock gradients, etc.) can affect forest ecosystem C cycling by changing plant nutrient uptake, litter and soil organic matter (SOM) decomposition, and nutrient mineralization (see reviews of Johnson and Turner, 2019, Janssens et al., 2010 and references therein). These processes mostly occur belowground and are driven by interactions between plants, soil, and microorganisms (Čapek et al., 2018; Mori et al., 2018). Plant production and microbial activity rely on nutrient availability so that the response of soil C storage to global changes is expected to be modulated by soil nutrient contents (Fernández-Martínez et al., 2014; Wieder et al., 2015). However, while a range of soil models coupling carbon and nutrient cycles are already available (e.g., Schimel and Weintraub, 2003; Moorhead and Sinsabaugh, 2006), only the latest ones have an explicit representation of microbial activity or consider the full vertical profile (e.g., Abramoff et al., 2017; Sulman et al., 2019, Yu et al., 2020). It remains to be tested if the microbial-explicit models can better reproduce interactions between C and nutrient cycling in soils, both along gradients in soil nutrient contents, or under fertilization or increased nutrient deposition.

Soil respiration ($R_s$), which consists of autotrophic respiration and heterotrophic respiration, is commonly used as a key indicator to study the response of SOM dynamic to perturbation (Bond-Lamberty et al., 2018; Carey et al., 2016). The negative response of $R_s$ to N addition is well-known and generally consistent across studies. For instance, Janssens et al. (2010) have shown a reduction of forest soil respiration in response to increasing N deposition, particularly in temperate forest soils. The meta-analysis of Zhou et al. (2014) confirmed the finding in the forest ecosystem and pointed out that the magnitude of $R_s$ responses was positively correlated with changes in root and microbial biomass as well as soil organic C (SOC) content. In contrast, in other biomes, such as croplands, grasslands, and deserts, $R_s$ was enhanced in response to N addition (Zhong et al., 2016; Zhou et al., 2014).

However, the response of $R_s$ to P addition is less investigated compared to that of N addition. The very first global meta-analysis of $R_s$ to P addition (Feng and Zhu, 2019) has shown that $R_s$ is significantly increased by 17.4% in tropical forests but decreased by 13.7% in wetlands in response to P addition. Although many studies tend to agree that P addition generally causes increases in $R_s$ and soil microbial biomass (Fanin et al., 2012; Liu et al., 2013, Jing et al., 2017; Meyer et al., 2018, Spohn and Schleuss, 2019), there are also some studies reporting no effects (Groffman and Fisk, 2011; Wang et al., 2019) or a reduction in $R_s$ (Wang et al., 2017) in response to P addition. The soil P stock has been found to be one of the key factors regulating the P cycling strategy in beech forests (Lang et al., 2017). For instance, soil P has also been proposed as one potential reason for different responses to P addition in P fertilization studies at several beech forest sites (Kohler et al., 2019; Spohn and Widdig, 2017, Netzer et al., 2019). These studies have found that soil P stock can impact plant and soil processes, such as retranslocation (Kohler et al., 2019) or microbial turnover (Spohn and Widdig, 2017). These impacts are less notable for aboveground plant traits, such as foliar N and P contents, compared to belowground traits, such as the root biomass and forest floor turnover time (Lang et al., 2017).

Most studies conducting both N and P additions have pointed to contrasting effects of N and P addition imposed on heterotrophic respiration (Fisk et al., 2015; Poeplau et al., 2016, Ren et al., 2016; Stiles et al., 2018, Liu et al., 2019), that is N addition decreases heterotrophic respiration whereas P addition increases it. The proposed mechanisms of these studies are different effects of N and P on microbial and SOM turnover, i.e., microbial nutrient mining. The microbial N mining hypothesis (Moorhead and Sinsabaugh, 2006) predicts an increase in SOM decomposition when N availability decreases. The N mining always involves C mineralization but P mining does not, leading to different respiration responses after nutrient addition (Craine et al., 2007). An alternative hypothesis is that the competition of inorganic P with SOC for adsorption sites in the soil could help release organic C to microbes after P but not N addition (Mori et al., 2018; Spohn and Schleuss, 2019). Moreover, how these processes are affected by soil nutrient availabilities is largely unknown.

Process-based models are powerful tools to identify and quantify important processes as well as to test hypotheses within complex terrestrial ecosystems (e.g., Medlyn et al., 2016; Zaehle et al., 2014). The importance to account for N cycle or novel microbial processes has been shown by earlier soil model studies. For example, soil priming effect, i.e., the change in SOM decomposition caused by plant root activity (Kuzyakov et al., 2000), was found to be affected by the litter C:N ratio (Abramoff et al., 2017; Wutzler et al., 2017), the SOM stability (Huang et al., 2018), and mycorrhizal association types (Sulman et al., 2017, 2019), thus further influence the soil respiration and C storage. Recent developments in these models have focused on representations of the P cycle (Goll et al., 2017; Thum et al., 2019, Zhu et al., 2019) and microbial processes (Sulman et al., 2019; Yu et al., 2020), which provide a new opportunity to investigate soil responses to nutrient additions. One important assumption in these models of the P cycle is the so-called bio-mineralization process, which accounts for an additional soil P mining pathway that does not involve C release (McGill and Cole, 1981; Wang et al., 2010). The bio-mineralization has been quantified as one of the main sources for plant P supply in many modeling studies (Goll et al., 2012; Thum et al., 2019, Wang et al., 2010; Yu et al., 2018) and also identified as an important process regulating the SOM C:P ratio (Yu et al., 2020).

In this study, we investigate the effects of soil P stock on soil responses to N and P additions by applying two soil models to

five study sites with a soil P stock gradient. The two models, QUINCY-soil model and Jena Soil Model (JSM), share many common features and the same code base but differ in the way SOM formation and turnover are represented. We firstly identify if and how SOM and its CNP stoichiometry are affected by a natural gradient in soil P stock. This was done by comparing simulations of the two models with different SOM formation representation with observations from beech forests growing on soils with different P stocks. Secondly, we verify if the two models can reproduce the observed soil respiration ($R_s$) response to N or P fertilization often observed from experiments, with a decline in $R_s$ with N-, but an increase with P-addition and test if the results vary with initial soil P stock along the tested gradient. An ongoing fertilization experiment was simulated at the five study sites for this purpose to evaluate short- and long-term responses of SOM to nutrient additions. We hypothesize that the more mechanistic Jena Soil Model should better reproduce the observed SOM stoichiometry and $R_s$ responses to nutrient addition compared to the more conventional QUINCY-soil model. Lastly, we aim to identify which features, i.e., process representation or model structure, of the two models are affecting the simulated $R_s$ responses to nutrient addition, and discuss recommendations for improving soil C, N, and P interaction representations in terrestrial biosphere models (TBMs) in the future. This is done by conducting further model scenarios and sensitivity analyses.

# MATERIALS AND METHODS

## Descriptions of Study Sites

Five mature beech forest stands in Germany [Bad Brückenau (BBR), Mitterfels (MTF), Vessertal (VES), Conventwald (COM), and Lüss (LUE)] were selected as study sites. Because all five sites are the Level II intensive monitoring plots in the Pan-European International Co-operative Program for the assessment and monitoring of air pollution effects on forests (ICP Forests) and have been continuously monitored with soil and tree properties for 15–25 years. They are also the main study sites of the research project SPP1685 "Ecosystem Nutrition" (Lang et al., 2017), which aims for investigating the P cycling strategies of forests with varying soil P stocks.

The total soil P stock (g P/m$^2$, down to 1 m depth) decreases strongly along the gradient: BBR > MTF > VES > COM > LUE. This decrease is concurrent with increasing soil N:P ratios in the topsoil (0–30 cm) along the gradient, and decreasing P concentration in the litterfall, including leaf litter and fine roots in forest floor and mineral soil (**Table 1**). Such a decreasing trend along the gradient is less remarkable in soil P content (mg P/kg soil) and available P content [mg P/kg soil, resin P and $NaHCO_3$ extracted P in Hedley fractionation (Klotzbücher et al., 2019)], due to a noticeably lower stone content at MTF than VES (**Table 1**). Other soil properties, including soil organic and microbial C contents as well as soil and microbial C:N:P ratios, do not show clear trends along the total soil P gradient. Other vegetation traits such as tree height, diameter, and foliar N and P contents are similar among the sites (Lang et al., 2017). With respect to the soil texture, the subsoil is generally more sandy than the topsoil at all study sites; the most P-rich site, BBR, is meanwhile the siltiest site and the most P-poor site, LUE, is the sandiest site (**Table 1**, Lang et al., 2017).

## Models

In this study, we employ two contrasting stand-alone soil models implemented into the QUantifying Interactions between terrestrial Nutrient CYcles and the climate system (QUINCY)

**TABLE 1 |** Site characteristics of the study sites Bad Brückenau (BBR), Mitterfels (MTF), Vessertal (VES), Conventwald (COM), and Lüss (LUE), reproduced from data in Lang et al. (2017).

| Study sites | BBR | MTF | VES | COM | LUE |
|---|---|---|---|---|---|
| **Chemical and microbial characteristics of topsoil (0–30 cm)/subsoil (30–100 cm)** | | | | | |
| Ptot (mg kg$^{-1}$) | 3057/2012 | 986/872 | 990/984 | 681/436 | 131/178 |
| Pavail (mg kg$^{-1}$) | 99.1/60.3 | 34.9/23.3 | 56.0/74.6 | 17.1/7.0 | 4.1/2.6 |
| SOC (mg g$^{-1}$) | 77.1/20.9 | 60.9/23.4 | 58.2/17.7 | 82.7/16.3 | 18.8/5.1 |
| Soil C:N | 14.1/13.2 | 18.2/18.3 | 16.3/16.2 | 22.7/18.2 | 23.6/16.7 |
| Soil N:P | 3.6/2.4 | 5.1/3.3 | 6.2/4.4 | 8.5/5.7 | 16.5/3.7 |
| Mic C ((g g$^{-1}$) | 1223 | 795 | 810 | 1392 | 192 |
| Mic C:N | 14 | 10 | 13 | 11 | 16 |
| Mic N:P | 0.9 | 0.7 | 0.8 | 1.3 | 1.2 |
| **Texture of the topsoil (0–30 cm)/subsoil (30–100 cm) and total stone content** | | | | | |
| Clay (%) | 35/20 | 17/8 | 18/8 | 21/11 | 6/6 |
| Silt (%) | 54/49 | 31/35 | 46/35 | 39/40 | 18/14 |
| Sand (%) | 11/31 | 51/57 | 36/57 | 40/49 | 76/80 |
| Stone content (%) | 78 | 25 | 63 | 69 | 43 |
| **P concentrations in leaf litter and fine roots** | | | | | |
| P in leaf litter (g m$^{-2}$ a$^{-1}$) | 0.229 | 0.213 | n.d. | n.d. | 0.156 |
| P fine roots forest floor (mg g$^{-1}$) | 0.96 | 0.96 | 0.93 | 0.8 | 0.76 |
| P fine roots mineral soil (s.d.) (mg g$^{-1}$) | 0.88 (0.27) | 0.82 (0.14) | 0.77 (0.13) | 0.49 (0.17) | 0.54 (0.27) |

**TABLE 2 |** Comparison of model features between the soil module in QUINCY (QUINCY-soil) and Jena Soil model (JSM).

| Model/features | | QUINCY-soil | JSM |
|---|---|---|---|
| Model structure | CNP-enabled | Yes | Yes |
| | vertical soil profile | Yes | Yes |
| | SOC (litter included) pools | 2 (5) | 5 (8) |
| | DOM | No | Yes |
| | Mineral-associated C | No | Yes |
| | SOM stoichiometry | Prescribed | Flexible |
| | enzyme pool | No | Implicit |
| | Microbial biomass | Implicit | Explicit |
| Model process | SOM Decomposition | First-order kinetics | Reversed Michaelis–Menten (M–M) kinetics |
| | Litter turnover† | First-order kinetics | First-order kinetics and M–M kinetics |
| | Mineralization | SOM-dependent | Microbe-dependent |
| | Respiration | SOM-dependent | Microbe-dependent |
| | OC sorption | No | Langmuir isotherm |
| | N dynamics | Yes | No |
| | Temperature and moisture response | Yes | Yes |
| | carbon-use-efficiency‡ | Prescribed, pool-specific | Flexible, microbes only |

†*The turnover of polymeric litter in JSM is described with M–M kinetics.* ‡*For QUINCY-soil, carbon transfer efficiency is used as an approximation of carbon-use-efficiency. DOM, dissolved organic matter; OC, organic carbon.*

TBM with fully coupled C, N, and P cycles and water and energy balances (Thum et al., 2019). The two models, QUINCY-soil and Jena Soil Model, share some common structures and processes of the QUINCY framework, such as soil layering, calculations of soil temperature, moisture, and water transport, litter pooling, woody litter turnover, and most inorganic P cycling processes (**Table 2** and **Figure 1**).

The QUINCY-soil model as applied in the standard version of the QUINCY model applies first-order kinetics for SOM decomposition for 15 vertical soil levels, broadly following the CENTURY approach (Parton et al., 1988). In addition, it accounts for vertical transport through bioturbation fluxes, such as movements caused by soil fauna and animals, as well as the advection of soluble mineral nutrients.

The Jena Soil Model (JSM) is a microbe-based, vertically explicit soil carbon model with integrated N and P cycles (Yu et al., 2020). It represents the turnover and formation of SOM based on mechanistic descriptions of soil processes such as microbially mediated depolymerization, organo-mineral association, and transport of dissolved organic matter (DOM) as well as bioturbation following the COMISSION model (Ahrens et al., 2015). JSM applies different kinetics to different processes, such as Michaelis–Menten kinetics for depolymerization and microbial uptake, Langmuir isotherm for the organo-mineral association and phosphate adsorption, and first-order kinetics for woody litter turnover (**Table 2**).

The main differences between the two models originate from the representation of SOM formation and turnover processes (**Table 2** and **Figure 1**). In QUINCY-soil, decomposed litter enters a SOM pool with fast turnover, which implicitly contains microbial biomass. The fast SOM pool stabilizes into the slowly overturning SOM pool and the slow SOM pool can also be destabilized back to the fast SOM pool. All these processes, i.e., litter decomposition, and SOM stabilization/destabilization, are described with first-order kinetics and happen at the same time with heterotrophic respiration (**Figure 1**, upper panel). In QUINCY-soil, the stoichiometry of the fast SOM pool adjusts linearly to the soluble N concentration with a heuristic function, in which the stoichiometry adjustment occurs instantaneously as the soluble N concentration changes, whereas the slow SOM pool is assumed to have fixed C:N:P ratio. All the C transfer processes have a prescribed C transfer efficiency, which determines the rate of respiration flux (**Table 2** and **Figure 1**).

Contrary, in JSM, polymeric litter needs to be first depolymerized to DOM and then enters an explicit microbial pool, which represents microbial biomass with a fixed ratio of C, N, and P. The microbial residue (necromass) pool could also be depolymerized to DOM, and both pools can be adsorbed to mineral surfaces up to a maximum sorption capacity, forming more recalcitrant SOM. The depolymerization rate is calculated using reverse Michaelis–Menten kinetics, limited by the microbial biomass C; the microbial DOM uptake and growth rate is described using Michaelis–Menten kinetics, limited by the substrate (DOM); the organo-mineral association is calculated with Langmuir isotherm, constrained by a C sorption capacity, which is related with soil clay and silt contents (Ahrens et al., 2015). In JSM, only the microbial stoichiometry is fixed, and the stoichiometry of all the other SOM pools depends on the C:N:P ratios of the influx and efflux of substrates. These fluxes retain the stoichiometry of their source SOM pools unless the microbial community's element use efficiencies change during the process (**Figure 1**, Yu et al., 2020). The respiration rate in JSM mainly depends on the microbial growth and its carbon use efficiency (CUE), which adjusts with nutrient availability (**Table 2** and **Figure 1**).

In this study, we refer to $R_s$ only as heterotrophic respiration, since root respiration is not described in our models. Therefore we only qualitatively compare the $R_s$ responses of model simulations with the general pattern that is often observed from experiments partly because a qualitative analysis is sufficient for our aim, and partly due to an absence of $R_s$ observations from the simulated study sites to directly compare to model results.

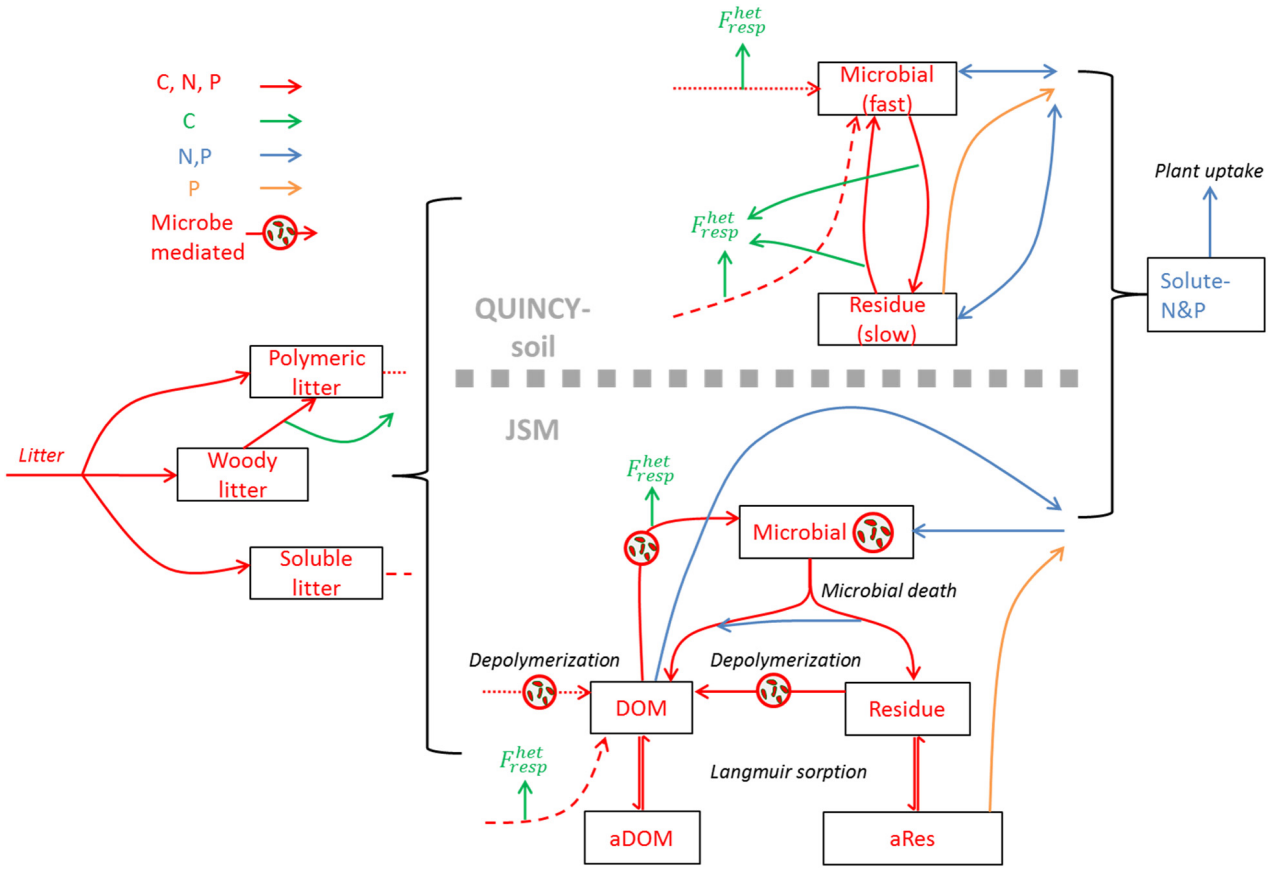


**FIGURE 1 |** Model structure comparison between QUINCY-soil and Jena Soil Model (JSM). The fast SOM pools in JSM include the Microbial, DOM, and Residue pools, and the slow SOM pools refer to the mineral-adsorbed DOM (aDOM) and residue (aRes) pools. The soil litter pool in both models refer to the woody, polymeric, and soluble litter; both models share the same litter distribution process, and the effluxes from polymeric and soluble litter are distinguished with dash line types.

## Model Protocols, Scenarios, and Sensitivity Analysis

### Model Protocols

Both models require soil temperature, moisture, and litterfall as forcing data, which were generated by running the full QUINCY model (including the respective soil submodel and vegetation processes), for 500 years at each site. To account for the natural litter P gradient in **Table 1**, we modified the QUINCY model outputs at VES, COM, and LUE sites to replicate the observed trend in litter P concentrations. The soil texture profiles for all the sites were obtained from observations and were used by both models as inputs. The time series of N deposition for each site was extrapolated from Lamarque et al. (2010) and Lamarque et al. (2011). For the P deposition, model estimates of nutrient and dust fluxes from Brahney et al. (2015) and Chien et al. (2016) were used. Site-specific climate data were taken from the nearest grid-cell of the daily CRU-NCEP (Viovy, 2018), as described in Thum et al. (2019). The initialization of litter and soil inorganic P pools in both models followed the protocol in Yu et al. (2020), in which each study site is initialized with its observed Hedley P pool sizes. The initialization of SOM pools assumed the same total CNP contents of litter and SOM for each site, however, specific pool sizes differ between the two models given their different pool structure and vertical distribution of SOM. The microbial C:N:P ratios in JSM were parameterized using the field observations (Lang et al., 2017).

### Model Scenarios

We first ran both models at all the study sites to evaluate their performances against observed SOM profiles and to set up the baseline for the N and P fertilization scenarios, referring to this scenario as the control treatment (CK). We spun up both models for 900 years before 1920 to guarantee that a stable SOM profile has been reached (see also Yu et al., 2020), and ran the model for 150 years (1920–2070). Both spin-up and model simulation used the same 1-year soil and litter forcing generated as described in the previous section. We used the JSM parameterization from our previous study (Yu et al., 2020) which was calibrated at the VES site, as for the QUINCY-soil model, we used the parameterization from Thum et al. (2019)'s study and tuned the SOM stoichiometry parametrization (**Table 3**) in the allowable range to match the observed SOM stoichiometry at VES. To explore the modeled soil responses to N and P additions, we conducted a model scenario to reproduce ongoing field N x P fertilization experiments, which

**TABLE 3 |** Parameter for sensitivity analysis.

| Symbol | Description | Value | Unit | Model |
|---|---|---|---|---|
| $x_{SOM^{N:P}_{fast,max}}$ | N:P ratio of fast SOM pool | 30.98 | mol/mol | QUINCY-soil |
| $f_x$ | Slope of fast SOM C:N to mineral soil N | 102000 | kg/mol | QUINCY-soil |
| $x_{SOM^{C:N}_{slow}}$ | C:N ratio of slow SOM pool | 14 | mol/mol | QUINCY-soil |
| $x_{SOM^{C:N}_{slow}}$ | N:P ratio of slow SOM pool | 11.07 | mol/mol | QUINCY-soil |
| $x^{C:N}_{mic}$ | Microbial C:N ratio | 15.17 | mol/mol | JSM |
| $x^{N:P}_{mic}$ | Microbial N:P ratio | 1.77 | mol/mol | JSM |

consists of an N addition treatment (N-add), and a P addition treatment (P-add). In the N-add treatment, 150 kg N/ha was added as ammonium nitrate ($NH_4NO_3$) to each study site at five dates (30 kg per dosage): September 16, 2016; April 17, 2017; June 17, 2017; September 17, 2017; May 18, 2018. In the P-add treatment, 50 kg/ha P was added once as potassium dihydrogen phosphate ($KH_2PO_4$) on September 16, 2016 (Jaane Krüger, personal communication). The added N accounts for 0.5, 0.9, 1.0, 1.3, and 2.0% of the total soil N at the sites along the soil P gradient (BBR > MTF > VES > COM > LUE), respectively; the added P accounts for 0.1, 0.6, 0.6, 1.3, and 2% of the total soil P at the sites along the soil P gradient, respectively. The simulation ends in 2070, allowing for a long-term (>50 years) perspective of the fertilization scenarios. To test the effect of litter quality on soil responses to nutrient addition, we implemented a model scenario, in which all the five sites have equal litter C:P ratio, for the control, N addition, and P addition treatments (Lit-CK, Lit-N-add, and Lit-P-add). According to the field observations (**Table 1**), the litter C:P ratios of all the five sites in equal-litter scenarios were set as that of BBR and MTF in the CK scenario, meaning that VES, COM, and LUE sites were 10, 20, and 30% lower than their values in the CK scenario, respectively.

### Sensitivity Analysis

To explore the effects of SOM stoichiometry on soil responses to nutrient addition, we tested the sensitivity of both models to changes of parameters that control SOM stoichiometry, using a hierarchical Latin hypercube design, which is a robust, scalable Monte Carlo-type stratified sampling approach that is used in many areas of science and engineering (LHS, Zaehle et al., 2005). For JSM, the SOM stoichiometry is an emerging property of flexible SOM stoichiometry, which is regulated by fixed microbial stoichiometry, therefore we varied the microbial C:N and N:P ratios between 75 and 125% of the default values to form a set of 50 LHS samples (**Table 3**), i.e., parameter sets. For QUINCY-soil, the SOM stoichiometry is determined by the prescribed stoichiometry of individual SOM pools. Therefore we selected four SOM stoichiometry parameters and varied each parameter between 75 and 125% of the default values to form another set of 80 LHS samples (**Table 3**). For each LHS sample in each model, we ran the three treatments (CK, N-add, P-add) for the VES site in parallel, and firstly evaluated the model output from all the CK LHS model runs in terms of soil C, N, and P stocks, soil respiration, and mineralization rates of N and P; secondly, we calculated the fertilization responses, i.e., output differences between N-add and CK as well as between P-add and CK for each LHS sample, and evaluated the output in term of respiration only.

All statistical tests were carried out with the RStudio software (R Core Team, 2013). Trend analyses were carried out with the Mann–Kendall test (M–K test) of the Kendall R package (McLeod, 2011). In the Mann–Kendall test, the tau ($\tau$) value varies between −1 and 1, where −1 represents a decreasing trend and 1 represents an increasing trend. The match between the modeled soil profile and observed soil profile was evaluated with a normalized root mean square ratio term, $K_{\mathrm{nrmsr}}$, which is modified to represent the average proportions between modeled and measured values.

$$K_{\mathrm{nrmsr}} = \sqrt{\frac{\sum_1^n K_{\mathrm{i}}^2}{n}}, \quad \text{where } K_{\mathrm{i}} = \min\left(\frac{Mod_i}{Meas_{\mathrm{i}}}, \frac{Meas_{\mathrm{i}}}{Mod_i}\right)$$

$K_{\mathrm{i}}$ is the variable representing the ratio between simulated and observed values at the observed $i_{\mathrm{th}}$ layer. Since the observation depths differed from the model soil layer depths, $K_{\mathrm{i}}$ values can only be compared using volumetric units. Although each depth shares the same weight in the calculation, $K_{\mathrm{nrmsr}}$ is weighted toward topsoil due to the increasing sampling intervals. To balance the influences of overestimation and underestimation, $K_{\mathrm{i}}$ is always normalized between 0 and 1 where 1 represents a perfect match of simulated and observed values.

## RESULTS

### Comparison of Observed and Simulated Soil Profiles

The simulated soil profiles of original (CK) and equal-litter (Lit-CK) control treatments for both JSM and QUINCY-soil model (referred to as QS in annotations of figures and tables) were compared with observed data (**Figure 2**). Although both models were tuned to the VES site, JSM better represented the SOC, soil inorganic P (SIP), soil organic P (SOP), and SOM profile C:N ratio, as the $K_{\mathrm{nrmsr}}$ values of JSM were greater than QUINCY-soil by 0.12, 0.16, 0.19, and 0.09, respectively (**Supplementary Table S1**). In contrast, QUINCY-soil underestimated SIP contents and failed to capture the decreases of C:N and C:P ratios with increasing soil depth (**Figure 2** and **Supplementary Table S2**). For the simulations of the other four sites, which used the calibration to VES, we observed similar differences between the two models. The goodness of fits between simulations and observations were similar as at VES (**Supplementary Table S1**), especially for soil C:N and C:P ratios (**Figure 2**). However, JSM performed better than QUINCY-soil in simulating SIP ($K_{\mathrm{nrmsr}}$ greater by $0.13 \pm 0.16$, **Supplementary Table S1**) and SOP ($K_{\mathrm{nrmsr}}$ greater by $0.16 \pm 0.06$, **Supplementary Table S1**) contents as well as SOM C:N ($K_{\mathrm{nrmsr}}$ greater by $0.06 \pm 0.05$, **Supplementary Table S1**) and C:P ($K_{\mathrm{nrmsr}}$ greater by $0.03 \pm 0.10$, **Supplementary Table S1**) ratios (**Figures 2C,D**). The simulation results from CK treatment better reproduced topsoil C:P ratio and SIP content compared

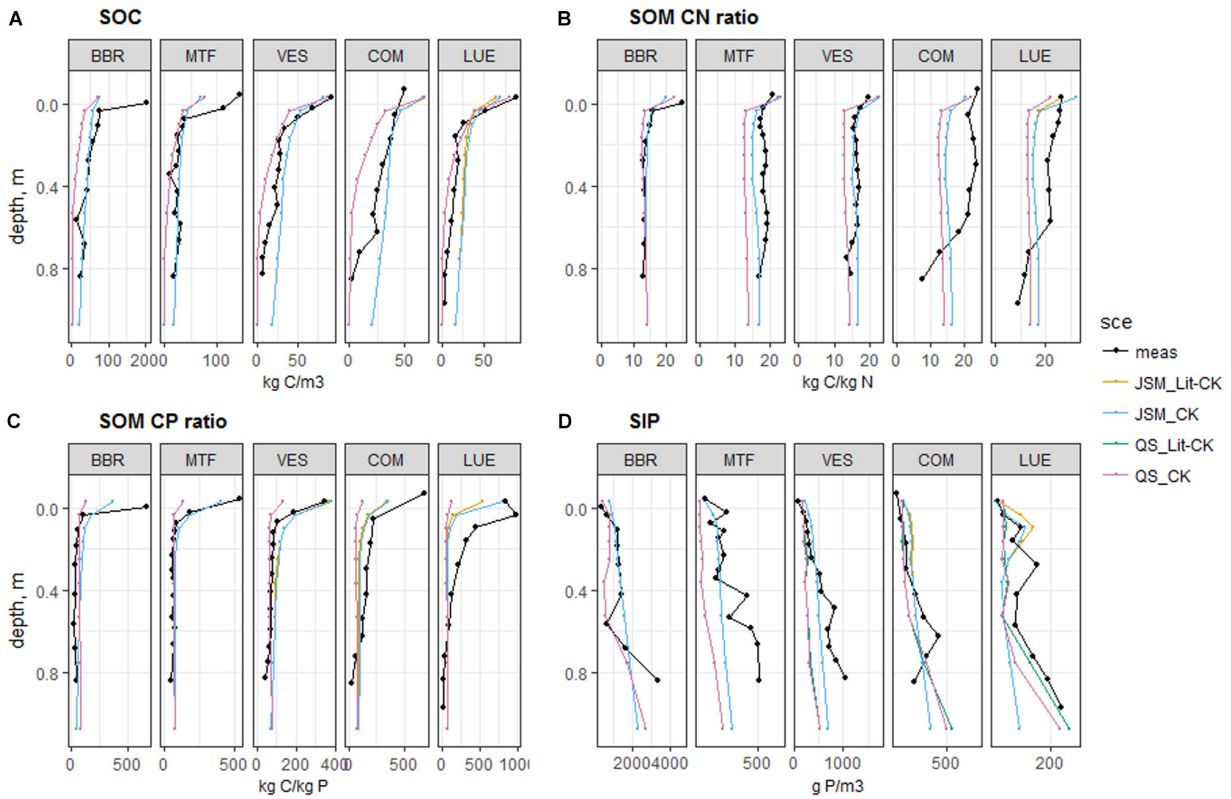


**FIGURE 2 |** Simulated and observed **(A)** SOC content, **(B)** C:N ratio in SOM, **(C)** C:P ratio in SOM, **(D)** SIP content at the study sites up to 1 m soil depth. Black lines and dots: observations; colored lines and dots: simulated mean values by control (CK) and equal-litter control (Lit-CK) treatments. Simulated means were calculated using data from the last 10 years of model experiments.

to the Lit-CK treatment, particularly at the most P-poor site LUE, demonstrating the need to correctly account for litter P concentration in these simulations, and thus an adequate representation of this process across sites.

Based on field measurements, we detected a slightly decreasing trend in SOC content, strong decreasing trends in soil organic N (SON), SOP, and SIP contents, and slight increasing trends in soil C:N, C:P, and N:P ratios along the decreasing soil P gradient (BBR > MTF > VES > COM > LUE) (**Table 4**). With respect to our models, JSM was generally much better in reproducing the observed trends along the P gradient by capturing the trends in SOC (M–K test τ of observation vs. JSM: −0.6 vs. −0.6), SOP (M−K τ: −1 vs. −0.6), and SIP (M−K τ: −0.8 vs. −0.8) contents and SOM C:N ratio (M−K τ: 0.6 vs. 0.6), whereas QUINCY-soil model only captured the SIP (M−K τ of observation vs. QS: −0.8 vs. −0.6) trend. JSM could capture the SOP trend with realistic stoichiometry in litter forcing (CK, **Table 4**), indicating the important role of litter stoichiometry on SOM formation. Both models did not reproduce observed trends of soil C:P and N:P ratios along the soil P gradient, but JSM performed much better in reproducing the observed decreasing trends of C:P (M−K τ of observation vs. JSM: −0.96 to −0.67 vs. −0.83 to −0.68) and N:P (M−K τ: −0.89 to −0.67 vs. −0.89 to −0.71) ratios with increasing soil depth (**Supplementary Table S2**).

## Modeled Soil C Cycling Responses to Nutrient Additions

The addition of nutrients affected C cycling and storage in the model scenarios at most study sites (**Table 5** and **Figure 3**).

**TABLE 4 |** The tau (τ) values of the Mann–Kendall trend test for main soil variables along the soil P gradient (BBR > MTF > VES > COM > LUE) of field measurements and control (CK) and equal-litter (Lit-CK) scenarios for JSM and QUINCY-soil (QS) models.

| Var/ Sce | Measurement | JSM_CK | JSM_Lit-CK | QS-CK | QS_Lit-CK |
|---|---|---|---|---|---|
| SOC | −0.6 | −0.6 | −0.6 | 0.2 | 0.2 |
| SON | −1 | −0.4 | −0.4 | 0.2 | 0.2 |
| SOP | −1 | −0.6 | 0 | 0.2 | 0.2 |
| SIP | −0.8 | −0.8 | −0.8 | −0.6 | −0.6 |
| RhoCor | 0 | 0.4 | 0.4 | 0.6 | 0.6 |
| CNr | 0.6 | 0.6 | 0.6 | 0.2 | 0.2 |
| CPr | 0.8 | 0.2 | 0.2 | 0 | 0 |
| NPr | 0.8 | 0.2 | 0 | 0 | 0 |

*RhoCor: bulk density corrected with organic matter content; CNr, CPr, and NPr: SOM C:N, C:P, and N:P ratios, respectively. All the τ values are calculated based on the sum or the normalized mean soil property values down to 1 m soil. Negative τ value indicates a decreasing trend along the P gradient and vice versa.*

**TABLE 5 |** Simulated soil respiration responses (g C/m$^2$) of model scenarios at all study sites.

| Treatment | Study sites/Model variants | BBR | MTF | VES | COM | LUE | τ (M–K test) |
|---|---|---|---|---|---|---|---|
| N-add | JSM_CK | −0.029 | −0.11 | −1e-9 | −0.0003 | −0.052 | 0 |
| | JSM_Lit-CK | −0.029 | −0.11 | −1e-5 | −0.001 | −0.387 | −0.2 |
| | QS_CK | 0.002 | −0.025 | 0.058 | 0.021 | 0.0004 | 0.2 |
| | QS_Lit-CK | 0.002 | −0.025 | 0.058 | 0.021 | 0.0004 | 0.2 |
| P-add | JSM_CK | −5.02 | −11 | −14.4 | −16.8 | 12.33 | −0.2 |
| | JSM_Lit-CK | −5.02 | −11 | −4.06 | −7.45 | −29.6 | −0.4 |
| | QS_CK | 0 | 0 | 0 | 0 | 0 | NA |
| | QS_Lit-CK | 0 | 0 | 0 | 0 | 0 | NA |

*The values are calculated as the long-term (55 years) differences of total soil respiration between the control (CK, Lit-CK) and their respective fertilization treatments. The tau (τ) values of the Mann–Kendall trend test (M–K test) are calculated along the soil P gradient (BBR > MTF > VES > COM > LUE) for each model scenario.*

According to the mass balance, an increase in $R_s$, i.e., a positive response, led to a decrease in C storage and *vice versa*. The addition of N (N-add) led to decreased $R_s$ in JSM at all sites, and increased $R_s$ in QUINCY-soil at all sites except MTF. The addition of P (P-add) led to strong $R_s$ decreases in JSM but caused no $R_s$ responses in QUINCY-soil (**Table 5**). Our simulations indicated that N-add in both models led to increases of microbial biomass and residue C (C_fast in **Figure 3**) and decreases of soil litter C pool. Litter C decrease was offset by an increase in fast C, therefore, resulting in negative $R_s$ responses in JSM; While in QUINCY-soil, there was no offset of litter loss by the fast C pool and the model simulated $R_s$ increases (**Figures 3A,B**). P-add in JSM also generally increased the microbial biomass C, which led to stronger depolymerization and $R_s$ increases at the P-poor LUE site, but not at other sites (**Figures 3C,D**).

### Effects of Soil P Stock, Litter Quality, and Temporal Responses

The effect of the soil P gradient on $R_s$ responses to nutrient addition was not found, since no clear trends were confirmed along the soil P gradient (BBR > MTF > VES > COM > LUE) in any of the model scenarios (**Table 5**). In QUINCY-soil, there were no $R_s$ responses to P addition at all study sites (**Figures 3C,D**), while in JSM, we did see a different pattern of $R_s$ responses to P addition at the P-poor LUE site compared to the other four sites. Meanwhile, the negligibly small $R_s$ responses to N addition at two middle sites (VES and COM) also showed that soil P was not controlling the responses to N addition in JSM (**Figure 3**). In QUINCY-soil, $R_s$ responses were not sensitive to litter C:P ratios, indicated by the same $R_s$ responses in CK and Lit-CK scenarios (**Table 5**). However, in JSM, $R_s$ responses to P and N additions were changed by decreasing litter C:P ratios, particularly at LUE. A 30% decrease of litter C:P ratio changed $R_s$ response to P-add from positive to negative mainly due to a decrease in litter-C, which was not seen at VES or COM (where a decrease of 10 and 20% of litter C:P ratio was applied, respectively).

## Modeled Soil Nutrient Responses to Nutrient Additions

We noticed divergent temporal patterns of the two models' N responses to N-add (**Figure 4** and **Supplementary Figure S1**). In QUINCY-soil, a substantial amount of N was quickly incorporated to fast SOM via microbial uptake after N addition (between 0.6 and 1.5 g N for all study sites) and then slowly released and taken up by plants, whilst in JSM, most of N was quickly taken up by plants after fertilization and only a minor amount (<0.01 g N/m$^2$) was incorporated into SOM (**Supplementary Figure S1**). This difference primarily reflects the difference in the representation of SOM stoichiometry, where the QUINCY-soil model applies a heuristic function to decrease SOM C:N with increasing N availability, whereas stoichiometric changes in JSM occur only by changing the magnitude of organic pools, resulting in the much slower responses of simulated SOM after nutrient additions.

The responses of soil P pools to P-add were largely different from the responses of N pools to N-add due to the presence of SIP pools and inorganic P cycling processes. The two models' responses to P addition also largely differed (**Figures 4**, **5**, **6** and **Supplementary Table S3**) due to their distinct representations of SOM processes. In JSM, of all the added P (P-add: 1.14 g P/m$^2$ for each site) in various treatments at all study sites, 40–60% was stored in SOM, 25–50% taken up by plants, and 10–20% was stored as SIP (**Supplementary Table S3** and **Figure 4**). However, in QUINCY-soil, no P was stored in SOM and the storage of the added P in SIP varied greatly among sites and treatments, from 15% to almost 50%. We also noticed that the response of P cycling processes after P addition was different in JSM and QUINCY-soil (**Figures 4**, **5**, **6**). P-add in QUINCY-soil led to an immediate spike of phosphate adsorption followed by a continuous increase of plant P uptake and a decrease in bio-mineralization (**Figures 5B**, **6B**). However, in JSM, P-add led to an increase in adsorption as well as to an instantaneous decrease in bio-mineralization (except LUE), followed by continuous desorption and alternating changes of net P mineralization, microbial P uptake (**Figures 5**, **6**).

## Effect of SOM Stoichiometry (Sensitivity Analysis)

In general, outputs and nutrient addition responses of JSM and QUINCY-soil showed similar overall sensitivities to changes in SOM stoichiometry parameterization (**Figure 7A**). In both models, SOM stocks and P mineralization were most sensitive to parameter uncertainty. However, in QUINCY-soil, respiration, net N mineralization, as well as SOC and SIP contents

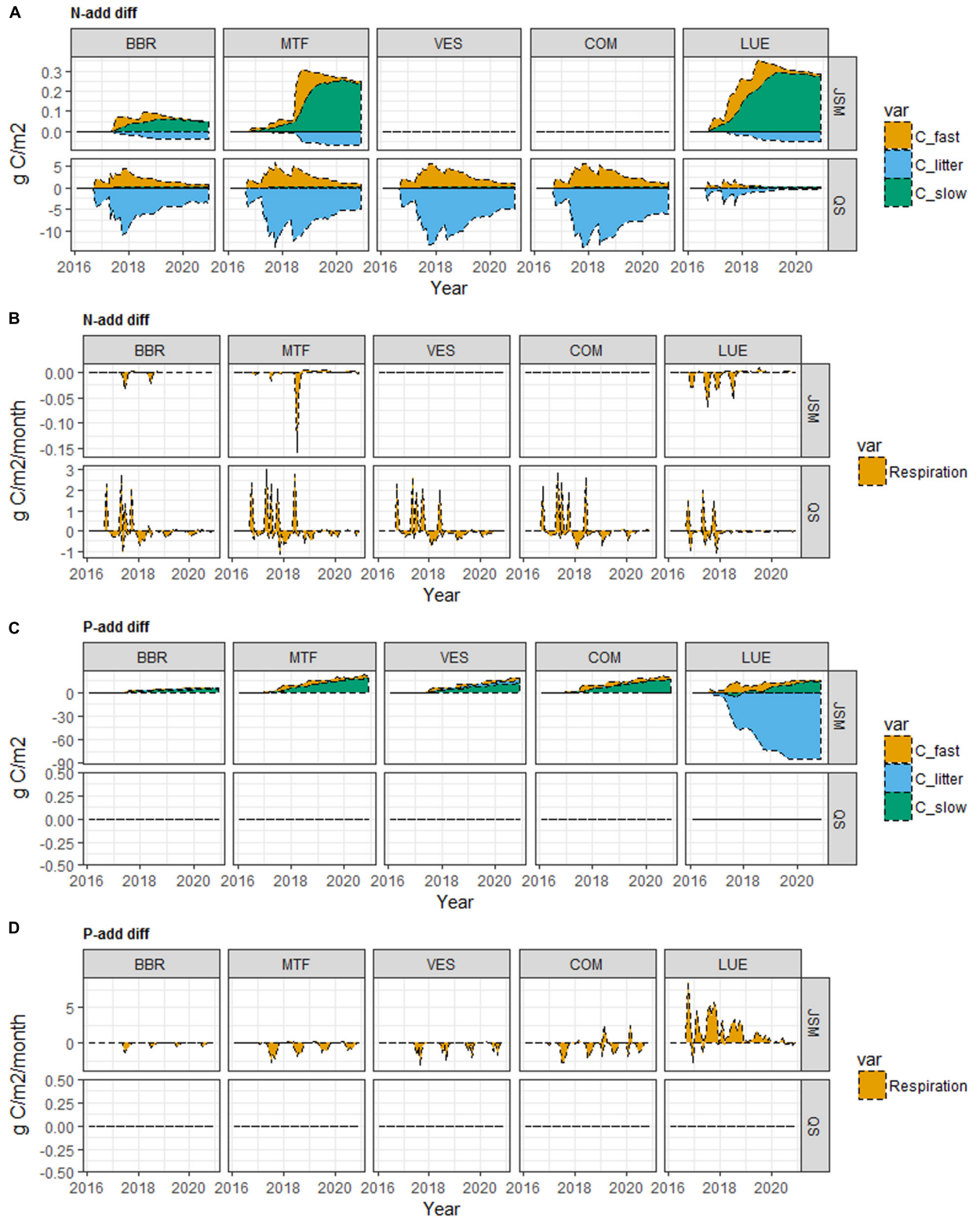


**FIGURE 3 |** Simulated SOC and soil respiration responses to N addition (**A,B**, N-add diff), and P addition (**C,D**, P-add diff) of JSM and QUINCY-soil (QS) at the study sites along the soil P gradient (BBR > MTF > VES > COM > LUE). Fast C refers to C in microbe, microbial residue and dissolved organic matter (DOM) pools in JSM, and C in fast SOM pool in QUINCY-soil; slow C refers to C in mineral-associated DOM and mineral-associated residue pools in JSM, and C in slow SOM pool in QUINCY-soil; litter C refers to C in litter in both models. Time for N addition: September 2016; April 2017; June 2017; September 2017; May 2018. Time for P addition: September 2016.

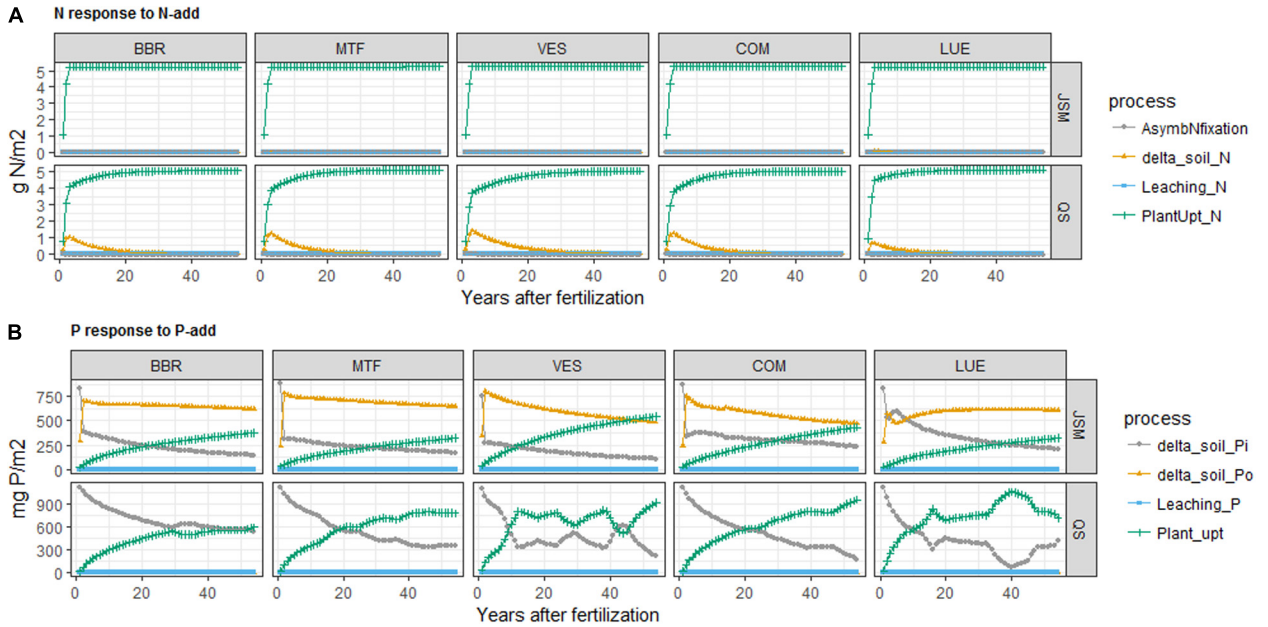


**FIGURE 4 |** Simulated changes of **(A)** N budget after N addition (N-add) and **(B)** P budget after P addition (P-add) in JSM and QUINCY-soil (QS) at the study sites along the soil P gradient (BBR > MTF > VES > COM > LUE). The proposed processes for the N budget are: N fixation, SON change, N leaching, and plant N uptake; the proposed processes for P budget are: SIP change, SOP change, P leaching, and plant P uptake.

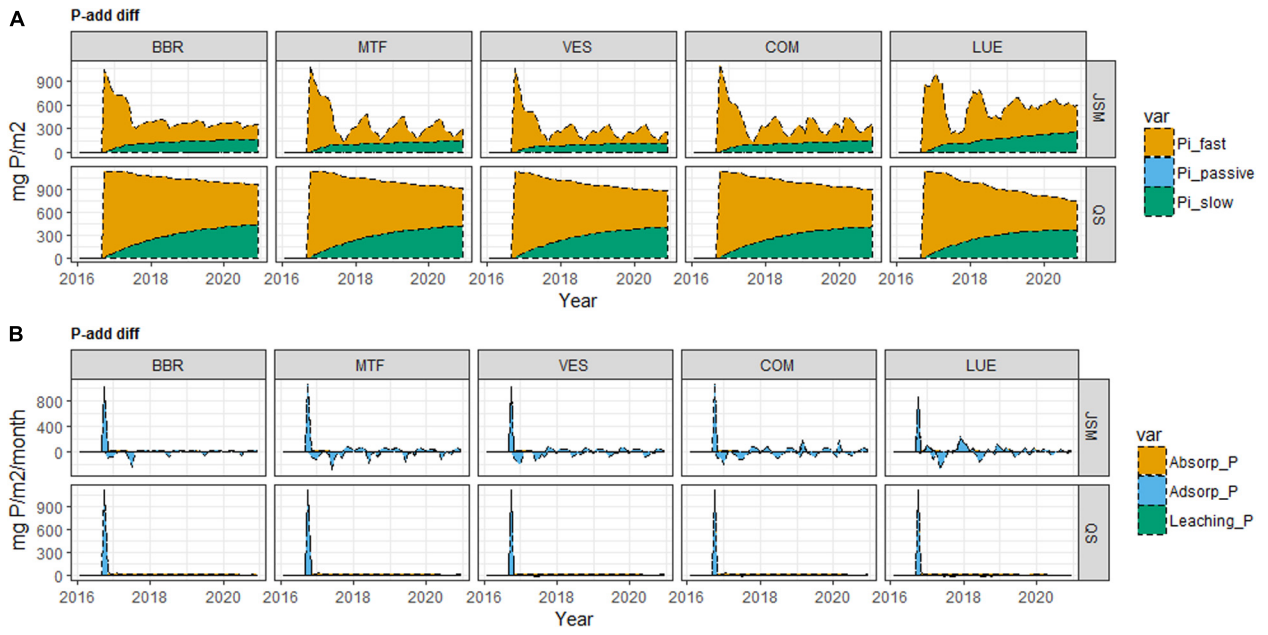


**FIGURE 5 |** Simulated **(A)** soil inorganic P (SIP) pool responses and **(B)** inorganic P cycling processes responses to P addition (P-add diff) of JSM and QUINCY-soil (QS) at the study sites along the soil P gradient (BBR > MTF > VES > COM > LUE). In both models, fast Pi refers to soluble and labile inorganic P pools, slow Pi refers to strongly sorbed P pool, and passive Pi refers to occluded and primary P pools; adsorption (adsorp_P) and absorption (absorp_P) refer to transfer of P from soluble pool to labile pool and from labile pool to sorbed pool, respectively. Time for P addition: September 2016.

showed no sensitivity to uncertainty in parameters of the SOM stoichiometry. Contrary, with JSM, soil stoichiometry also influenced those model outputs. One key difference between the two models, as shown in **Figure 7B**, is their different responses to N and P additions. The $R_s$ responses to N addition in QUINCY-soil were constrained around the median value, but they highly deviated from the median value in JSM. Regarding P addition, QUINCY-soil had no $R_s$ responses in

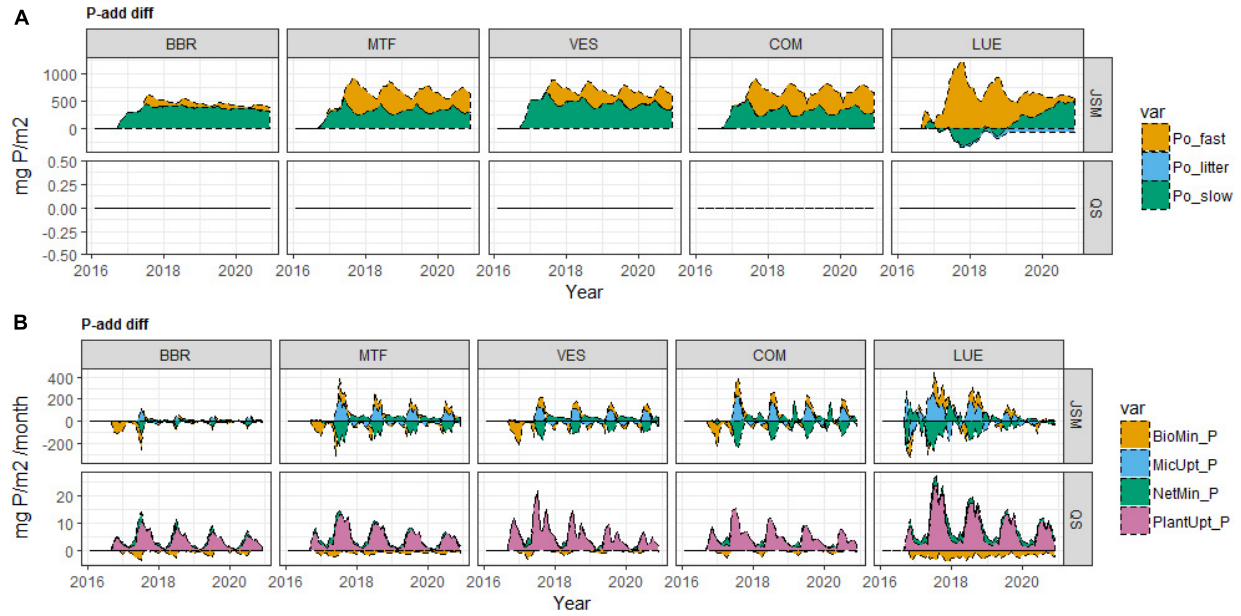


**FIGURE 6 |** Simulated **(A)** soil organic P (SOP) pool responses and **(B)** organic P cycling processes responses to P addition (P-add diff) of JSM and QUINCY-soil (QS) at the study sites along the soil P gradient (BBR > MTF > VES > COM > LUE). Fast P refers to P in microbe, microbial residue and dissolved organic matter (DOM) pools in JSM, and P in fast SOM pool in QUINCY-soil; slow P refers to P in mineral-associated DOM and mineral-associated residue pools in JSM, and P in slow SOM pool in QUINCY-soil; litter P refers to P in litter in both models. Organic P cycling processes include bio-mineralization, microbial uptake, net mineralization, and plant uptake of P. Time for P addition: September 2016.

each LHS sample; while JSM had strong negative $R_s$ responses that were much constrained to the median value compared to N addition (**Figure 7B**). With respect to the magnitude and direction of $R_s$ responses to nutrient additions, P-add in JSM had strongest negative responses (−189.32 mg C/year) and N-add in JSM had weakest positive responses (0.07 mg C/year), but we noticed that of all the three treatments, $R_s$ responses could be either positive or negative depending on SOM stoichiometry parameterization.

# DISCUSSION

## Effects of Soil Phosphorus Gradient on SOM Profiles

By comparing the model simulations of both models with observations of SOM profiles from the soil P stock gradient (BBR > MTF > VES > COM > LUE), we have found that the JSM is generally better than QUINCY-soil in reproducing the observed SOM profiles (such as SOC, SOP, SIP, and soil C:N ratio, **Supplementary Table S1**) as well as capturing the observed effect of the soil P gradient on other soil properties (such as SOC, SOP, and soil C:N ratio, **Table 4**) along the P gradient. Lang et al. (2017) have found that some ecosystem traits, i.e., the proportion of diester P in soil, the residence time of forest floor, fine root biomass, and P content in leaf litter and fine-roots (**Table 1**), define the P nutrition and distinguish P cycling strategy of these sites along the soil P stock gradient (BBR > MTF > VES > COM > LUE). These ecosystem traits are better correlated with soil P stock, rather than foliage P. Our further analysis of field observation data has indicated, that this soil P stock gradient is also correlated with decreasing SOC and SON contents, and slightly increasing soil C:N, C:P, and N:P ratios (**Table 4**). These observational trends are better reproduced by JSM. Since the major difference between the two models are the microbially mediated C, N, and P interactions of SOM formation and turnover, this suggests that connections between soil P and C, N cycling are to a large extend regulated by these microbial interactions (**Table 2** and **Figure 1**). Moreover, the fact that the soil P gradient is highly correlated with other ecosystem properties such as fine root biomass and forest floor residence time, with important implications for SOM storage, turnover and depth profiles, highlights the need that TBM should also be able to reproduce plant-soil-microbe interactions in a way to capture these patterns along nutrient gradients.

## Simulated Soil Responses to Nutrient Addition

The general pattern of observed $R_s$ responses to nutrient addition, that N addition decreases soil respiration whereas P addition increases it (Feng and Zhu, 2019; Zhou et al., 2014), is not fully reproduced by either model. However, many reported $R_s$ responses from literature are not consistent with the general pattern due to specific site conditions (Wang et al., 2017, Zeng and Wang, 2015, Groffman and Fisk, 2011); therefore, modeling can help understand the driving mechanisms.

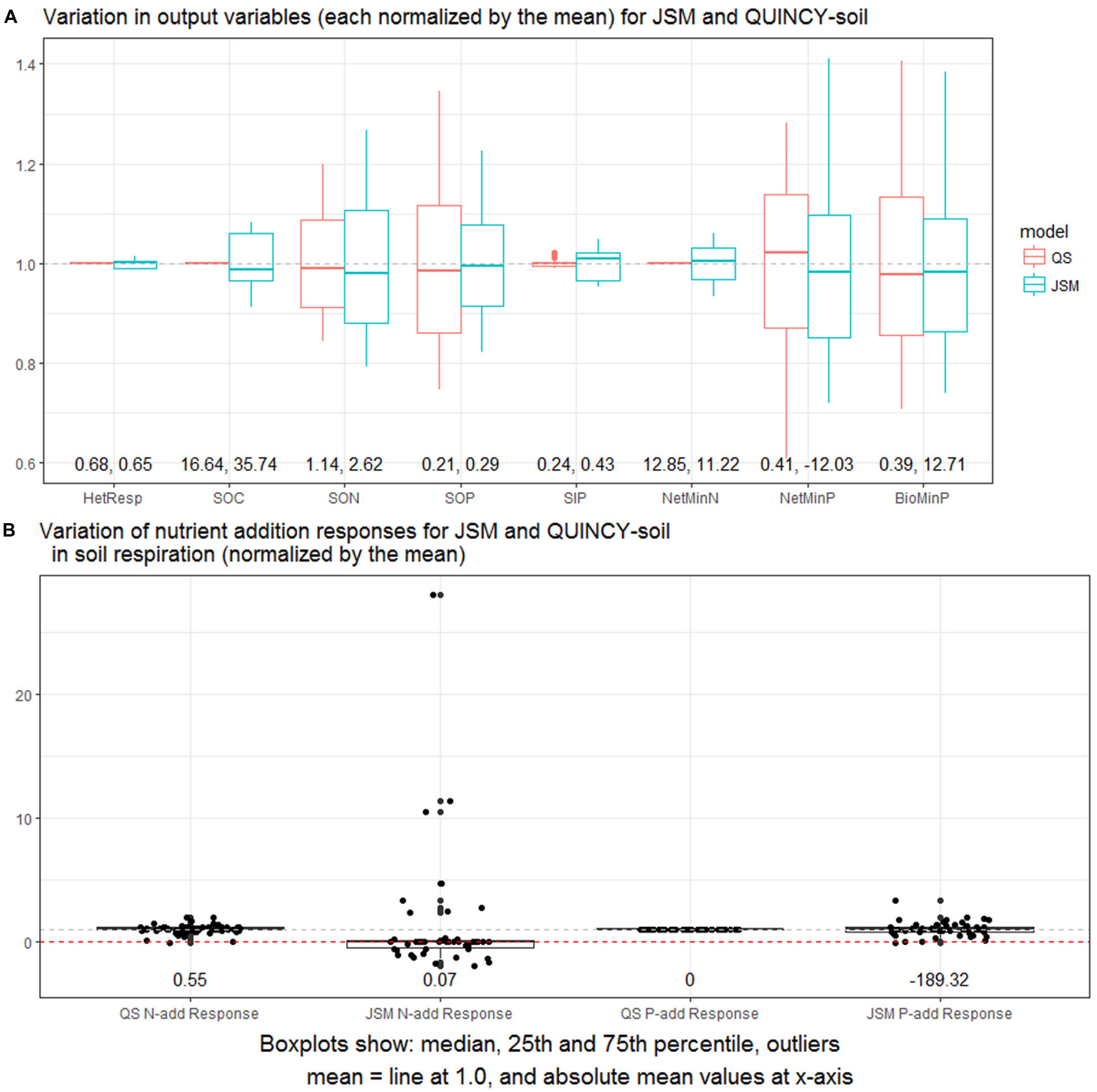


**FIGURE 7 | (A)** Normalized output variations in the LHS sensitivity analysis for JSM and QUINCY-soil (QS). The selected output variables include respiration, total soil organic C, N, and P, total soil inorganic P, net mineralization of N and P, and P bio-mineralization. **(B)** Normalized variations of soil respiration responses (mg C/year) to nutrient additions in the LHS sensitivity analysis for JSM and QUINCY-soil. The plots are based on data from the last 10 years of simulations.

QUINCY-soil simulated $R_s$ increases to N addition at all study sites and simulated no $R_s$ changes to P addition in all the model scenarios and sensitivity tests (**Table 5** and **Figure 7**). The key assumption in QUINCY-soil is that the $R_s$ responses to nutrient addition are solely regulated by a heuristic function between soluble N concentration and soil C:N ratio, which aims at mimicking a long-term pattern between N availability and SOM stoichiometry of a fully coupled plant-soil system, rather than describing the process response such as nutrient mining (Meyer et al., 2018) or priming effects (Dijkstra et al., 2013). With respect to N addition in QUINCY-soil, the soluble N concentration increased after N addition, which generally decreased the C:N ratio in the fast SOM pool (**Figure 1**, Parton et al., 1988). A decreased C:N ratio of fast SOM pool spontaneously increased microbial N demand in QUINCY-soil, which was compensated through increasing litter decomposition, thus leading to an increase in $R_s$. In some cases, if the site is rich in N, such an increase in $R_s$ could be interrupted due to our prescribed minimum C:N ratio of fast SOM pool, which might be the reason for negative $R_s$ responses to N additions in few occasions (**Table 5** and **Figure 7**). Such a mechanism is not described between soluble phosphate concentration and SOM C:P ratio, leading to no $R_s$ responses to P addition under different soil P, litter quality, fertilization type or SOM stoichiometry in QUINCY-soil.

Jena Soil Model was able to reproduce the $R_s$ decreases to N addition, but only simulated an $R_s$ increase to P addition in the most P-poor site LUE and $R_s$ decreases at other sites (**Table 5** and **Figure 3**). The fact that in JSM, $R_s$ increased after P addition only at the very P-poor site agrees with the finding that P-poor tropical soils usually have positive $R_s$ responses to P addition while other soils not (Hui et al., 2019; Feng and Zhu, 2019, Fanin et al., 2012). Although $R_s$ decreases can be simulated after N and P addition in JSM, the reasons are different for N and P. N addition leads to a decreased N mining and thus decreased respiration, while P addition leads to increased SOC sequestration thus decreased respiration. In JSM, N- and P-add increased the microbial biomass at all study sites but the increases of microbial biomass were much higher when P was added (**Figure 3**), because the microbial biomass was extremely P demanding in our model parameterization, indicated by the very low microbial N:P ratios (ca. 1, **Table 1**) compared to the global average value (ca. 6, Xu et al., 2013). N and P additions reduced the microbial mining of N (N mineralization, **Supplementary Figure S1**) and P (P bio-mineralization, **Figure 6**) in JSM, respectively. Since the N mining was always associated with C decomposition, a decrease in N mineralization led to a corresponding decrease of respiration in most cases. However, for P, the decrease of P mining did not directly lead to a change of stable SOC pool but only to an increase of microbial biomass C, which further resulted in an increased of C in microbial residue and mineral-associated residue pool, thus reducing respiration.

The magnitude of respiration responses in JSM depended on several interacting processes, such as microbial growth, organo-mineral association, enzyme allocation and depolymerization (**Figure 1**), and was sensitive to changes of soil P stock, litter quality, and microbial stoichiometry (**Table 5**, **Figure 3**, and **Supplementary Figure S1**). Moreover, P addition did not reduce the mining of P (**Figure 6B**) and led to a strong increase of microbial biomass at LUE, indicating a P limitation in microbial biomass. The litter decomposition was thus enhanced due to much larger decomposer biomass, leading to an increase in respiration. Alternatively, an increase in respiration after N addition in JSM could also be caused by a decrease of microbial CUE after N addition (cases in sensitivity tests, data not shown), but such a mechanism seems not supported by lab analysis at a grassland site (Spohn et al., 2016), in which the authors observed an increase of microbial CUE after N fertilization. One caveat of JSM simulations was the much stronger $R_s$ response to P-add than N-add, which still held under varying microbial stoichiometry in the sensitivity test (**Table 5** and **Figure 7**). But such a pattern is not supported by any observational evidence. This might be because JSM ignored the N demand of enzyme allocation, which simply underestimated the N demand of soil microbial processes.

## IMPLICATIONS FOR SOIL MODELING AND FIELD OBSERVATION

Both models used in this study are stand-alone soil models, meaning that no feedback from vegetation was considered, including the responses of root growth or respiration. Therefore it is not possible to directly compare our simulations to many field studies due to the lack of a complete plant-soil-microbe framework (Čapek et al., 2018). Nevertheless, based on our simulations we can identify fields for the further developments of soil models or soil modules in TBMs, and also discuss the implications of our model simulations for collecting and interpreting future field observations.

Jena Soil Model and QUINCY-soil generally performed differently in reproducing the observed soil profiles, as well as simulating soil responses to N and P additions under different litter qualities, fertilization types, and SOM stoichiometry at all study sites. This shows that alternative assumptions about SOM formation and turnover can lead to substantial differences in model simulations and their sensitivity to perturbations. The better performance of JSM to reproduce SOC and soil C:N ratio may be mainly due to the representation of the organo-mineral association (as discussed in section "Effects of Soil Phosphorus Gradient on SOM Profiles"), which is not represented in QUINCY-soil. The relative better performances of JSM to reproduce SON and SOP trends under realistic litter P inputs indicates that correct litter qualities are essential to model different SOM conditions. Unlike stand-alone soil models, in which litter stoichiometry is part of model inputs, TBMs usually model the litter stoichiometry as an important prognostic variable. Therefore this importance of litter quality highlights the challenges in TBMs to correctly simulate vegetation and soil responses to P gradients. Furthermore, the much better performances of JSM in capturing vertical trends of soil C:P and N:P ratios (**Supplementary Table S2**) implied that the spatial pattern of SOM is strongly regulated by the vertical explicitness of soil microbial and organo-mineral association processes (Yu et al., 2020; Ahrens et al., 2015), which should also be represented in TBMs.

The added N in both models was both taken up by plants in the long term (>50 years), but their short-term (<1 year) responses differed. In JSM, almost all the added N was quickly taken up by plants but in QUINCY-soil, nearly 20% of added N was also instantaneously incorporated into SOM (**Supplementary Figure S1**). The fast microbial assimilation of N did occur in JSM but was less visible in N pools because their sizes changed much slower compared to QUINCY-soil (**Figure 4** and **Supplementary Figure S1**). This imposed an obstacle to directly compare our results with field $^{15}N$ tracer studies (e.g., Goodale, 2017) because the recovery of $^{15}N$ signals is the evidence of N exchange between N pools and does not necessarily imply pool size changes. The slow response of N pool to N addition in JSM may be due to the fixed microbial C:N ratio, which does not allow microbes to take up excess N. However, $R_s$ increased shortly after N addition but leveled out in the long term to a negative response in QUINCY-soil (**Figure 3** and **Table 5**). This contradicted the reported short- and long-term observations that N addition led to decreased $R_s$ (Stiles et al., 2018; Poeplau et al., 2016, Janssens et al., 2010, Camenzind et al., 2018). However, we note that the model currently misses the decline of root growth to nitrogen addition, and associated

with this the decline in fresh C input as an energy source for SOM decomposition. The divergence between short- and long-term responses has brought up a noteworthy question for the modeling community. Should we directly apply an empirical relationship derived from long-term observations (the heuristic function discussed in section "Simulated Soil Responses to Nutrient Addition") in models, or should we describe the processes mechanistically to achieve such a relationship in a progressive manner? For the purpose of describing short-term responses, the heuristic function is not suitable, and our findings also suggest the mechanistic description is better than the heuristic function in simulating the long-term C responses to N addition (**Table 5**).

With respect to P addition, the two models disagreed on the fates of added P and $R_s$ responses. QUINCY-soil predicted no long-term effects of SOM cycling to P addition and all the added P ended up either being taken by plants or stored as SIP (**Supplementary Table S3** and **Figure 4**). This was obviously against the results from isotopic experiments conducted at soils from BBR and LUE in which a large proportion of isotopic signals were recovered in SOM (Spohn et al., 2018). JSM predicted strong microbial biomass increases and $R_s$ responses, which seems to agree with the observed pattern (Feng and Zhu, 2019), and a large proportion of P stored as SOP (**Supplementary Table S3** and **Figure 4**). We found no effect of initial soil P stock on $R_s$ responses to nutrient addition by our simulations, but we did see effects on responses of bio-mineralization ($\tau = 0.8$, M–K test) and microbial P uptake ($\tau = 0.8$, M–K test) to the P addition along the soil P gradient (BBR > MTF > VES > COM > LUE). These were caused by a stronger reduction of bio-mineralization and a weaker increase of microbial P uptake in P rich site than P poor site.

The JSM simulation suggested that the key process to regulate this response is the P mining process, i.e., bio-mineralization, as we noticed that the simulated $R_s$ increase after P addition concurred with the exceptional responses of bio-mineralization (**Figure 6**). As discussed in section "Simulated Soil Responses to Nutrient Addition" and Yu et al. (2020), the C and N costs of bio-mineralization seem essential to describe the C, N, and P interactions of plant-soil-microbe systems and need to be included in models but were not yet implemented in the current JSM version. Moreover, the bio-mineralization rate in JSM was significantly higher than in QUINCY-soil (**Figure 7A**), indicating that the P cycling is very different between explicit and implicit microbial dynamics. Therefore, we do see a reasonable need to improve the soil C, N, and P interactions in TBMs, particularly in the sense of improving SOM P cycling, and our simulations have shown that the inclusion of microbial dynamics and processes might be a plausible solution.

Our findings suggest that the more detailed explicit description of microbial processes and organo-mineral association is required to reproduce observed SOM profiles, to capture SOM trends in the depth profile and along the soil P stock gradient, and to model soil responses to N and P additions. Therefore, these processes should be included in the TBMs in the future.

Moreover, some intriguing patterns in the model simulations, particularly those in JSM, could be potentially enlightening to field studies. For example, we have found a systematic belowground P stress at our study sites, because the JSM simulations show that microbial biomass increments and soil respiration responses are both much higher in P addition than in N addition. It seems a very interesting pattern but needs to be validated with field data. Additionally, diverging temporal effects between short-term and long-term fates of added nutrients in our simulations (**Figure 4**) suggest the necessity of better experiment designs to tackle the long-term effects of nutrient fertilization. In the other hand, to understand the short-term soil responses to nutrient fertilization, our model simulations indicate that microbial processes or properties, such as microbial biomass, stoichiometry, and CUE as well as nutrient mineralization, are important and should be better tracked in future field or lab studies.

## DATA AVAILABILITY STATEMENT

The datasets generated for this study are available on request to the corresponding author.

## AUTHOR CONTRIBUTIONS

SZ, MS, and LY conceived the manuscript idea. LY ran the model simulations. All authors contributed to the interpretation of the results and wrote the manuscript.

## FUNDING

This work was supported by the framework of Priority Program SPP 1685 "Ecosystem Nutrition: Forest Strategies for Limited Phosphorus Resources" of the German Research Foundation (DFG), grant no. ZA 763/2-1 and SCHR 1181/3-1. SZ was supported by the European Research Council (ERC) under the European Union's Horizon 2020 research and innovation programme (grant agreement No 647204, QUINCY).

## ACKNOWLEDGMENTS

We are grateful to Friederike Lang, Jaane Krüger, and other co-workers for measuring and sharing the data, to Jan Engel and Tea Thum for technical assistance in model simulation, and to Kendalynn Morris for assistance in literature search.

## SUPPLEMENTARY MATERIAL

The Supplementary Material for this article can be found online at: https://www.frontiersin.org/articles/10.3389/ffgc.2020.543112/full#supplementary-material

## REFERENCES


Abramoff, R. Z., Davidson, E. A., and Finzi, A. C. (2017). A parsimonious modular approach to building a mechanistic belowground carbon and nitrogen model. *J. Geophys. Res. Biogeosci.* 122, 2418–2434. doi: 10.1002/2017jg003796

Ahrens, B., Braakhekke, M. C., Guggenberger, G., Schrumpf, M., and Reichstein, M. (2015). Contribution of sorption, DOC transport and microbial interactions to the 14C age of a soil organic carbon profile: Insights from a calibrated process model. *Soil Biol. Biochem.* 88, 390–402. doi: 10.1016/j.soilbio.2015.06.008

Bond-Lamberty, B., Bailey, V. L., Chen, M., Gough, C. M., and Vargas, R. (2018). Globally rising soil heterotrophic respiration over recent decades. *Nature* 560, 80–83. doi: 10.1038/s41586-018-0358-x

Brahney, J., Mahowald, N., Ward, D. S., Ballantyne, A. P., and Neff, J. C. (2015). Is atmospheric phosphorus pollution altering global alpine lake stoichiometry? *Glob. Biogeochem. Cycles* 29, 1369–1383. doi: 10.1002/2015gb005137

Camenzind, T., Hättenschwiler, S., Treseder, K. K., Lehmann, A., and Rillig, M. C. (2018). Nutrient limitation of soil microbial processes in tropical forests. *Ecol. Monogr.* 88, 4–21. doi: 10.1002/ecm.1279

Čapek, P., Manzoni, S., Kaštovská, E., Wild, B., Diáková, K., Bárta, J., et al. (2018). A plant–microbe interaction framework explaining nutrient effects on primary production. *Nat. Ecol. Evol.* 2, 1588–1596. doi: 10.1038/s41559-018-0662-8

Carey, J. C., Tang, J., Templer, P. H., Kroeger, K. D., Crowther, T. W., Burton, A. J., et al. (2016). Temperature response of soil respiration largely unaltered with experimental warming. *Proc. Natl. Acad. Sci. U.S.A.* 113, 13797–13802.

Chien, C.-T., Mackey, K. R. M., Dutkiewicz, S., Mahowald, N. M., Prospero, J. M., and Paytan, A. (2016). Effects of African dust deposition on phytoplankton in the western tropical Atlantic Ocean off Barbados. *Glob. Biogeochem. Cycles* 30, 716–734. doi: 10.1002/2015gb005334

Craine, J. M., Morrow, C., and Fierer, N. (2007). Microbial nitrogen limitation increases decomposition. *Ecology* 88, 2105–2113. doi: 10.1890/06-1847.1

Dijkstra, F. A., Carrillo, Y., Pendall, E., and Morgan, J. A. (2013). Rhizosphere priming: a nutrient perspective. *Front. Microbiol.* 4:216. doi: 10.3389/fmicb.2013.00216

Ellsworth, D. S., Anderson, I. C., Crous, K. Y., Cooke, J., Drake, J. E., Gherlenda, A. N., et al. (2017). Elevated CO2 does not increase eucalypt forest productivity on a low-phosphorus soil. *Nat. Clim. Change* 7, 279–282. doi: 10.1038/nclimate3235

Engels, C., Kirkby, E., and White, P. (2011). "Mineral nutrition, yield and source–sink relationships," in *Marschner's Mineral Nutrition of Higher Plants*, ed. P. Marschner (Waltham: Academic Press), 85–134. doi: 10.1016/b978-0-12-384905-2.00005-4

Fanin, N., Barantal, S., Fromin, N., Schimann, H., Schevin, P., and Hättenschwiler, S. (2012). Distinct microbial limitations in litter and underlying soil revealed by carbon and nutrient fertilization in a tropical rainforest. *PLoS One* 7:e49990. doi: 10.1371/journal.pone.0049990

Feng, J., and Zhu, B. (2019). A global meta-analysis of soil respiration and its components in response to phosphorus addition. *Soil Biol. Biochem.* 135, 38–47. doi: 10.1016/j.soilbio.2019.04.008

Fernández-Martínez, M., Vicca, S., Janssens, I. A., Sardans, J., Luyssaert, S., Campioli, M., et al. (2014). Nutrient availability as the key regulator of global forest carbon balance. *Nat. Clim. Change* 4, 471–476. doi: 10.1038/nclimate2177

Finzi, A. C., Norby, R. J., Calfapietra, C., Gallet-Budynek, A., Gielen, B., Holmes, W. E., et al. (2007). Increases in nitrogen uptake rather than nitrogen-use efficiency support higher rates of temperate forest productivity under elevated CO<sub>2</sub&gt. *Proc. Natl. Acad. Sci. U.S.A.* 104, 14014–14019. doi: 10.1073/pnas.0706518104

Fisk, M., Santangelo, S., and Minick, K. (2015). Carbon mineralization is promoted by phosphorus and reduced by nitrogen addition in the organic horizon of northern hardwood forests. *Soil Biol. Biochem.* 81, 212–218. doi: 10.1016/j.soilbio.2014.11.022

Goll, D. S., Brovkin, V., Parida, B. R., Reick, C. H., Kattge, J., Reich, P. B., et al. (2012). Nutrient limitation reduces land carbon uptake in simulations with a model of combined carbon, nitrogen and phosphorus cycling. *Biogeosciences* 9, 3547–3569. doi: 10.5194/bg-9-3547-2012

Goll, D. S., Vuichard, N., Maignan, F., Jornet-Puig, A., Sardans, J., Violette, A., et al. (2017). A representation of the phosphorus cycle for ORCHIDEE (revision 4520). *Geosci. Model Dev.* 10, 3745–3770. doi: 10.5194/gmd-10-3745-2017

Goodale, C. L. (2017). Multiyear fate of a 15N tracer in a mixed deciduous forest: retention, redistribution, and differences by mycorrhizal association. *Glob. Change Biol.* 23, 867–880. doi: 10.1111/gcb.13483

Groffman, P. M., and Fisk, M. C. (2011). Phosphate additions have no effect on microbial biomass and activity in a northern hardwood forest. *Soil Biol. Biochem.* 43, 2441–2449. doi: 10.1016/j.soilbio.2011.08.011

Hawkesford, M., Horst, W., Kichey, T., Lambers, H., Schjoerring, J., Møller, I. S., et al. (2012). "Functions of macronutrients," in *Marschner's Mineral Nutrition of Higher Plants*, ed. P. Marschner (Waltham: Academic Press), 135–189. doi: 10.1016/b978-0-12-384905-2.00006-6

Huang, Y., Guenet, B., Ciais, P., Janssens, I. A., Soong, J. L., Wang, Y., et al. (2018). ORCHIMIC (v1.0), a microbe-mediated model for soil organic matter decomposition. *Geosci. Model Dev.* 11, 2111–2138. doi: 10.5194/gmd-11-2111-2018

Hui, D., Porter, W., Phillips, J. R., Aidar, M. P. M., Lebreux, S. J., Schadt, C. W., et al. (2019). Phosphorus rather than nitrogen enhances CO2 emissions in tropical forest soils: evidence from a laboratory incubation study. *Eur. J. Soil Sci.* 71, 495–510. doi: 10.1111/ejss.12885

Janssens, I. A., Dieleman, W., Luyssaert, S., Subke, J. A., Reichstein, M., (2010). Reduction of forest soil respiration in response to nitrogen deposition. *Nat. Geosci.* 3, 315–322. doi: 10.1038/ngeo844

Jiang, M., Medlyn, B. E., Drake, J. E., Duursma, R. A., Anderson, I. C., Barton, C. V. M., et al. (2020). The fate of carbon in a mature forest under carbon dioxide enrichment. *Nature* 580, 227–231.

Jing, Z., Chen, R., Wei, S., Feng, Y., Zhang, J., and Lin, X. (2017). Response and feedback of C mineralization to P availability driven by soil microorganisms. *Soil Biol. Biochem.* 105, 111–120. doi: 10.1016/j.soilbio.2016.11.014

Johnson, D. W., and Turner, J. (2019). Tamm review: nutrient cycling in forests: a historical look and newer developments. *For. Ecol. Manag.* 444, 344–373. doi: 10.1016/j.foreco.2019.04.052

Jonard, M., Fürst, A., Verstraeten, A., Thimonier, A., Timmermann, V., Potočić, N., et al. (2015). Tree mineral nutrition is deteriorating in Europe. *Glob. Change Biol.* 21, 418–430. doi: 10.1111/gcb.12657

Klotzbücher, A., Kaiser, K., Klotzbücher, T., Wolff, M., and Mikutta, R. (2019). Testing mechanisms underlying the Hedley sequential phosphorus extraction of soils. *J. Plant Nutr. Soil Sci.* 182, 570–577. doi: 10.1002/jpln.201800652

Kohler, M., Niederberger, J., Wichser, A., Bierbaß, P., Rötzer, T., Spiecker, H., et al. (2019). Using tree rings to reconstruct changes in soil P availability – Results from forest fertilization trials. *Dendrochronologia* 54, 11–19. doi: 10.1016/j.dendro.2019.01.001

Kuzyakov, Y., Friedel, J. K., and Stahr, K. (2000). Review of mechanisms and quantification of priming effects. *Soil Biol. Biochem.* 32, 1485–1498. doi: 10.1016/s0038-0717(00)00084-5

Lamarque, J. F., Bond, T. C., Eyring, V., Granier, C., Heil, A., Klimont, Z., et al. (2010). Historical (1850–2000) gridded anthropogenic and biomass burning emissions of reactive gases and aerosols: methodology and application. *Atmos. Chem. Phys.* 10, 7017–7039. doi: 10.5194/acp-10-7017-2010

Lamarque, J.-F., Kyle, G. P., Meinshausen, M., Riahi, K., Smith, S. J., van Vuuren, D. P., et al. (2011). Global and regional evolution of short-lived radiatively-active gases and aerosols in the representative concentration pathways. *Clim. Change* 109:191. doi: 10.1007/s10584-011-0155-0

Lang, F., Krüger, J., Amelung, W., Willbold, S., Frossard, E., Bünemann, E. K., et al. (2017). Soil phosphorus supply controls P nutrition strategies of beech forest ecosystems in central Europe. *Biogeochemistry*. 136, 5–29. doi: 10.1007/s10533-017-0375-0

Liu, H., Zhou, G., Bai, S. H., Song, J., Shang, Y., He, M., et al. (2019). Differential response of soil respiration to nitrogen and phosphorus addition in a highly phosphorus-limited subtropical forest. *China. For. Ecol. Manag.* 448, 499–508. doi: 10.1016/j.foreco.2019.06.020

Liu, L., Zhang, T., Gilliam, F. S., Gundersen, P., Zhang, W., Chen, H., et al. (2013). Interactive effects of nitrogen and phosphorus on soil microbial communities in a tropical forest. *PLoS One* 8:e61188. doi: 10.1371/journal.pone.0061188

McGill, W. B., and Cole, C. V. (1981). Comparative aspects of cycling of organic C, N, S and P through soil organic matter. *Geoderma* 26, 267–286. doi: 10.1016/0016-7061(81)90024-0

McLeod, A. I. (2011). *Kendall Rank Correlation and Mann–Kendall Trend Test. R Package Version 2.2.*

Medlyn, B. E., De Kauwe, M. G., Zaehle, S., Walker, A. P., Duursma, R. A., Luus, K., et al. (2016). Using models to guide field experiments: a priori predictions for

the CO2 response of a nutrient- and water-limited native Eucalypt woodland. *Glob. Change Biol.* 22, 2834–2851. doi: 10.1111/gcb.13268

Meyer, N., Welp, G., Rodionov, A., Borchard, N., Martius, C., and Amelung, W. (2018). Nitrogen and phosphorus supply controls soil organic carbon mineralization in tropical topsoil and subsoil. *Soil Biol. Biochem.* 119, 152–161. doi: 10.1016/j.soilbio.2018.01.024

Moorhead, D. L., and Sinsabaugh, R. L. (2006). A theoretical model of litter decay and microbial interaction. *Ecol. Monogr.* 76, 151–174. doi: 10.1890/0012-9615(2006)076[0151:atmold]2.0.co;2

Mori, T., Lu, X., Aoyagi, R., and Mo, J. (2018). Reconsidering the phosphorus limitation of soil microbial activity in tropical forests. *Funct. Ecol.* 32, 1145–1154. doi: 10.1111/1365-2435.13043

Netzer, F., Pozzi, L., Dubbert, D., and Herschbach, C. (2019). Improved photosynthesis and growth of poplar during nitrogen fertilization is accompanied by phosphorus depletion that indicates phosphorus remobilization from older stem tissues. *Environ. Exp. Bot.* 162, 421–432. doi: 10.1016/j.envexpbot.2019.03.017

Norby, R. J., Ledford, J., Reilly, C. D., Miller, N. E., and Neill, E. G. (2004). Fine-root production dominates response of a deciduous forest to atmospheric CO<sub>2</sub> enrichment. *Proc. Natl. Acad. Sci. U.S.A.* 101, 9689–9693. doi: 10.1073/pnas.0403491101

Pan, Y., Birdsey, R. A., Fang, J., Houghton, R., Kauppi, P. E., Kurz, W. A., et al. (2011). A large and persistent carbon sink in the world's forests. *Science* 333, 988–993.

Parton, W. J., Stewart, J. W. B., and Cole, C. V. (1988). Dynamics of C, N, P and S in grassland soils: a model. *Biogeochemistry* 5, 109–131. doi: 10.1007/bf02180320

Poeplau, C., Herrmann, A. M., and Kätterer, T. (2016). Opposing effects of nitrogen and phosphorus on soil microbial metabolism and the implications for soil carbon storage. *Soil Biol. Biochem.* 100, 83–91. doi: 10.1016/j.soilbio.2016.05.021

R Core Team (2013). *R: A Language and Environment for Statistical Computing*. Vienna: R Core Team.

Ren, F., Yang, X., Zhou, H., Zhu, W., Zhang, Z., Chen, L., et al. (2016). Contrasting effects of nitrogen and phosphorus addition on soil respiration in an alpine grassland on the Qinghai-Tibetan Plateau. *Sci. Rep.* 6:34786.

Schimel, J. P., and Weintraub, M. N. (2003). The implications of exoenzyme activity on microbial carbon and nitrogen limitation in soil: a theoretical model. *Soil Biol. Biochem.* 35, 549–563. doi: 10.1016/s0038-0717(03)00015-4

Spohn, M., Pötsch, E. M., Eichorst, S. A., Woebken, D., Wanek, W., and Richter, A. (2016). Soil microbial carbon use efficiency and biomass turnover in a long-term fertilization experiment in a temperate grassland. *Soil Biol. Biochem.* 97, 168–175. doi: 10.1016/j.soilbio.2016.03.008

Spohn, M., and Schleuss, P.-M. (2019). Addition of inorganic phosphorus to soil leads to desorption of organic compounds and thus to increased soil respiration. *Soil Biol. Biochem.* 130, 220–226. doi: 10.1016/j.soilbio.2018.12.018

Spohn, M., and Widdig, M. (2017). Turnover of carbon and phosphorus in the microbial biomass depending on phosphorus availability. *Soil Biol. Biochem.* 113, 53–59. doi: 10.1016/j.soilbio.2017.05.017

Spohn, M., Zavišić, A., Nassal, P., Bergkemper, F., Schulz, S., Marhan, S., et al. (2018). Temporal variations of phosphorus uptake by soil microbial biomass and young beech trees in two forest soils with contrasting phosphorus stocks. *Soil Biol. Biochem.* 117, 191–202. doi: 10.1016/j.soilbio.2017.10.019

Stiles, W. A. V., Rowe, E. C., and Dennis, P. (2018). Nitrogen and phosphorus enrichment effects on CO2 and methane fluxes from an upland ecosystem. *Sci. Total Environ.* 618, 1199–1209. doi: 10.1016/j.scitotenv.2017.09.202

Sulman, B. N., Brzostek, E. R., Medici, C., Shevliakova, E., Menge, D. N. L., and Phillips, R. P. (2017). Feedbacks between plant N demand and rhizosphere priming depend on type of mycorrhizal association. *Ecol. Lett.* 20, 1043–1053. doi: 10.1111/ele.12802

Sulman, B. N., Shevliakova, E., Brzostek, E. R., Kivlin, S. N., Malyshev, S., Menge, D. N. L., et al. (2019). Diverse mycorrhizal associations enhance terrestrial c storage in a global model. *Glob. Biogeochem. Cycles* 33, 501–523. doi: 10.1029/2018gb005973

Thum, T., Caldararu, S., Engel, J., Melanie, K., Marleen, P., Reiner, S., et al. (2019). A new model of the coupled carbon, nitrogen, and phosphorus cycles in the terrestrial biosphere (QUINCY v1.0; revision 1996). *Geosci. Model Dev.* 12, 4781–4802. doi: 10.5194/gmd-12-4781-2019

Viovy, N. (2018). *CRUNCEP Version 7 - Atmospheric Forcing Data for the Community Land Model. Research Data Archive at the National Center for Atmospheric Research, Computational and Information Systems Laboratory*. Available online at: https://doi.org/10.5065/PZ8F-F017. (accessed December 15, 2019).

Wang, J., Li, Q., Fu, X., Dai, X., Kou, L., Xu, M. S., et al. (2019). Mechanisms driving ecosystem carbon sequestration in a Chinese fir plantation: nitrogen versus phosphorus fertilization. *Eur. J. Forest Res.* 138, 863–873. doi: 10.1007/s10342-019-01208-z

Wang, Q., Zhang, W., Sun, T., Chen, L. C., Pang, X. Y., Wang, Y. P., et al. (2017). N and P fertilization reduced soil autotrophic and heterotrophic respiration in a young Cunninghamia lanceolata forest. *Agric. For Meteorol.* 232, 66–73. doi: 10.1016/j.agrformet.2016.08.007

Wang, Y. P., Law, R. M., and Pak, B. (2010). A global model of carbon, nitrogen and phosphorus cycles for the terrestrial biosphere. *Biogeosciences* 7, 2261–2282. doi: 10.5194/bg-7-2261-2010

Wieder, W. R., Cleveland, C. C., Smith, W. K., and Todd-Brown, K. (2015). Future productivity and carbon storage limited by terrestrial nutrient availability. *Nat. Geosci.* 8, 441–444. doi: 10.1038/ngeo2413

Wutzler, T., Zaehle, S., Schrumpf, M., Ahrens, B., and Reichstein, M. (2017). Adaptation of microbial resource allocation affects modelled long term soil organic matter and nutrient cycling. *Soil Biol. Biochem.* 115, 322–336. doi: 10.1016/j.soilbio.2017.08.031

Xu, X., Thornton, P. E., and Post, W. M. (2013). A global analysis of soil microbial biomass carbon, nitrogen and phosphorus in terrestrial ecosystems. *Glob. Ecol. Biogeogr.* 22, 737–749. doi: 10.1111/geb.12029

Yu, L., Ahrens, B., Wutzler, T., Schrumpf, M., and Zaehle, S. (2020). Jena soil model (JSM v1.0; revision 1934): a microbial soil organic carbon model integrated with nitrogen and phosphorus processes. *Geosci. Model Dev.* 13, 783–803. doi: 10.5194/gmd-13-783-2020

Yu, L., Zanchi, G., Akselsson, C., Wallander, H., and Belyazid, S. (2018). Modeling the forest phosphorus nutrition in a southwestern swedish forest site. *Ecol. Modell.* 369, 88–100. doi: 10.1016/j.ecolmodel.2017.12.018

Zaehle, S., Medlyn, B. E., De Kauwe, M. G., Walker, A. P., Dietze, M. C., Hickler, T., et al. (2014). Evaluation of 11 terrestrial carbon–nitrogen cycle models against observations from two temperate Free-Air CO2 Enrichment studies. *New Phytol.* 202, 803–822. doi: 10.1111/nph.12697

Zaehle, S., Sitch, S., Smith, B., and Hatterman, F. (2005). Effects of parameter uncertainties on the modeling of terrestrial biosphere dynamics. *Glob. Biogeochem. Cycles* 19:GB3020.

Zeng, W., and Wang, W. (2015). Combination of nitrogen and phosphorus fertilization enhance ecosystem carbon sequestration in a nitrogen-limited temperate plantation of Northern China. *For. Ecol. Manag.* 341, 59–66. doi: 10.1016/j.foreco.2015.01.004

Zhong, Y., Yan, W., and Shangguan, Z. (2016). The effects of nitrogen enrichment on soil CO2 fluxes depending on temperature and soil properties. *Glob. Ecol. Biogeogr.* 25, 475–488. doi: 10.1111/geb.12430

Zhou, L., Zhou, X., Zhang, B., Lu, M., Luo, Y., Liu, L., et al. (2014). Different responses of soil respiration and its components to nitrogen addition among biomes: a meta-analysis. *Glob. Change Biol.* 20, 2332–2343. doi: 10.1111/gcb.12490

Zhu, Q., Riley, W. J., Tang, J., Collier, N., Hoffman, F. M., Yang, X., et al. (2019). Representing nitrogen, phosphorus, and carbon interactions in the E3SM land model: development and global benchmarking. *J. Adv. Model. Earth Syst.* 11, 2238–2258. doi: 10.1029/2018ms001571

Zhu, Z., Piao, S., Myneni, R. B., Huang, M., Zeng, Z., Canadell, J. G., et al. (2016). Greening of the earth and its drivers. *Nat. Clim. Change* 6, 791–795.

**Conflict of Interest:** The authors declare that the research was conducted in the absence of any commercial or financial relationships that could be construed as a potential conflict of interest.

The reviewer LF declared a past co-authorship with one of the authors SZ to the handling editor.

frontiers in Forests and Global Change

ORIGINAL RESEARCH
published: 21 December 2020
doi: 10.3389/ffgc.2020.550884

# The Cumulative Amount of Exuded Citrate Controls Its Efficiency to Mobilize Soil Phosphorus

*Helmer Schack-Kirchner*, Caroline A. Loew and Friederike Lang*

*Department of Soil Ecology, Institute of Forest Sciences, Albert-Ludwigs- Universität, Freiburg, Germany*

Root exudation of citrate is discussed as mechanism to mobilize P from the soils' solid phase. Microbial processes can mitigate the mobilization efficiency of citrate. Due to higher microbial activity in topsoils compared to subsoils, we hypothesized a lower mobilization efficiency of exuded citrate in topsoils than in the subsoils. As a model system we used microdialysis (MD) probes and we followed diffusive fluxes of citrate from the perfusate into the soil and of phosphate from the soil into the dialysate in three soil horizons (Oa, Ah, Bw) of a Fagus sylvatica L. stand Cambisol. Three different MD perfusates with a KCl background concentration have been used: control, 1, and 3 mmol $L^{-1}$ citric acid. Fluxes have been measured after 24, 48, and 144 h. The high-citrate perfusate increased the cumulative 144 h P-influx by a factor of 8, 13, and 113 in the Oa, Ah, and Bw horizon, respectively. With the high-citrate treatment, P mobilization efficiency decreased over time, whereas for the low citrate, P mobilization efficiency had a maximum at day 2. Minimum P mobilization efficiency of citrate was 1:25,000 mol phosphate per mol citrate in the Oa horizon between days 2 and 6, and maximum was 1:286 in the Bw-horizon during day 2. An increasing citrate efflux over time indicated an increasing sink term for citrate in the soil due to microbial decay or immobilization processes. Cumulative phosphate influx could be fitted to cumulative citrate efflux and soil horizon in a logarithmic model explaining 87% of the variability. For the first time, we could follow the localized P-uptake with citrate exudation over several days. Cumulative citrate efflux as the main control of P-mobilization has been barely discussed yet, however, it could explain some gaps in the role of carboxylates in the rhizosphere. Batch experiments are not capable to elucidate microscale dynamic competition for phosphate and carboxylates. MD is a promising tool for spatially explicit investigation of phosphate–citrate exchange, since such detailed insights in are not possible with batch experiments. In combination with the analysis of microbial properties, this technique has a huge potential to identify mobilization processes in soils as induced by citrate.

**Keywords: forest soil, microdialysis, rhizosphere, carboxylates, microbial citrate attenuation**

OPEN ACCESS

***Edited by:***
*Andreas Schindlbacher, Austrian Research Centre for Forests (BFW), Austria*

***Reviewed by:***
*Lukas Kohl, University of Helsinki, Finland*
*Lucia Fuchslueger, University of Vienna, Austria*

****Correspondence:***
*Helmer Schack-Kirchner helmer.schack-kirchner@soil.uni-freiburg.de*

***Specialty section:***
*This article was submitted to Forest Soils, a section of the journal Frontiers in Forests and Global Change*

***Received:*** *10 April 2020*
***Accepted:*** *26 October 2020*
***Published:*** *21 December 2020*

***Citation:***
*Schack-Kirchner H, Loew CA and Lang F (2020) The Cumulative Amount of Exuded Citrate Controls Its Efficiency to Mobilize Soil Phosphorus. Front. For. Glob. Change 3:550884. doi: 10.3389/ffgc.2020.550884*

## 1. INTRODUCTION

Of all nutrients, phosphorus has the highest discrepancy between the concentrations in leaf dry mass and soil solution. The relation of both, Degryse et al. (2009) calls it "concentration factor," easily exceeds $10^5$ in which case the uptake of phosphorus in 1 kg of dry leaf mass based on soil-water mass flow would require a water volume of 10 $m^3$ that is difficult to imagine. Reasons are

not only small P stocks in many forest soils (Lang et al., 2017) but also the high affinity of P to the soil solid phase (Schachtman et al., 1998; Hinsinger et al., 2011). Therefore, root systems had to develop efficient strategies to sustain the required leaf-P concentrations. First, they possess high-affinity carriers that virtually deplete the soil solution against huge concentration gradients between soil solution and root cells (Schachtman et al., 1998; Scheerer et al., 2019). Second, they associate with mycorrhizal fungi (Bucher, 2007; Zavišić et al., 2018) or form specialist root systems, such as cluster roots (Lambers et al., 2015). Third, they change the chemical environment of the rhizosphere by emitting mobilizing substances either themselves or in association with microorganisms (Hinsinger, 2001; Richardson et al., 2011).

One group of such substances intensely discussed in this context are carboxylates, i.e., anions of organic acids, such as oxalate, malate, and citrate (Jones, 1998; Richardson et al., 2011; Gerke, 2015). Carboxylates can increase P-mobility by ligand exchange on oxidic surfaces, and by dissolution of metal-P complexes and subsequent chelating of the cationic species of Ca, Fe, or Al. This helps keeping orthophosphates in solution. By decreasing the pH the solubility of metal-P complexes is increased (Barrow et al., 2018). Also, P bound in oxide-organic surfaces is well-mobilized by carboxylates. Renella et al. (2007) reported a strong increase of phosphatase activity by stimulation of microbial activity due to carboxylate exudation. It is well-documented that these effects can increase plant uptake. However, the mechanisms of P mobilization in the root–soil interface by carboxylates are still not fully clear (Richardson et al., 2011; Gerke, 2015). In this context, it has to be considered that microbial decay of carboxylates reduces their half life to a few hours (van Hees et al., 2002; Oburger et al., 2009). By this way microorganisms possibly hamper mobilization of P by carboxylate exudation (Barrow et al., 2018).

Most experimental data of carboxylate-based P mobilization was provided by batch experiments (e.g., Fox and Comerford, 1992; Gerke et al., 2000; Oburger et al., 2009), in some cases including suppression of biotic activity (Henintsoa et al., 2017; Barrow et al., 2018). The assessment of P mobilization in these experiments is mainly based on equilibrium conditions and does not consider depletion of soil solution by roots and dynamic replenishment by the solid phase. To improve the shortcoming of routine methods, Menezes-Blackburn et al. (2016) used diffusive gradient in thin film extraction (DGT). However, citric and oxalic acid had to be added in one single dose that was equilibrated with the soil–water mixture. This method is still far from typical rhizosphere processes. An experimental alternative to DGT that allows the constant release of carboxylates from a spatially discrete source like a root surface is microdialysis (MD). MD is based on highly miniaturized flow-through membranes that enrich soil solutes in the dialysate and release perfusate-solutes by diffusion. Various MD applications in soil science are listed in the comprehensive review of Buckley et al. (2020). The applicability of this dynamic extraction technique for soil phosphate including the effect of citric acid has been shown first by Demand et al. (2017). McKay Fletcher et al. (2019) measured the short-time dynamic of citrate release on P absorption to parameterize a rhizosphere model. As mentioned above, a comprehensive process description of the interaction between carboxylate exudation and P absorption is challenging. However, MD experiments simulate P mobilization by exudating fine root better than other infinite-sink extraction methods (Brackin et al., 2017; Demand et al., 2017; McKay Fletcher et al., 2019).

The aim of our study was to track for the first time absorption of the phosphate by MD probes with and without exudation of citric acid over several days. Citric acid turned out to be one of the most efficient rhizosphere carboxylates to mobilize phosphorus (Wang et al., 2008; Gerke, 2015). Furthermore, P-concentration in citric acid batch extracts of soil samples is regarded as a reasonable proxy for the foliar nutrition status of central European forest trees (Fäth et al., 2019) and it is the base of several P-mobilizing studies (e.g., Gerke, 2015; Barrow et al., 2018).

In the soil environment, citric acid is subject to fast microbial degradation and when it is supplied continuously it can stimulate the microbial community (Renella et al., 2007). Therefore, we hypothesized a decreasing P-mobilizing efficiency during continuous citrate exudation. van Hees et al. (2002) reported a strong decline in citrate mineralization with soil depth and decreasing SOM. Based on their observations, we expected the strongest decrease in citrate P-mobilizing efficiency over time in the SOM-rich topsoil and the lowest decrease in the deeper mineral soil.

Another aim of this study was to calculate an exudation efficiency as the molar ratio between citrate efflux and net gain of P from the MD flux data. This relation would be an important aspect to assess the plant's costs of P acquisition (Raven et al., 2018).

## 2. MATERIALS AND METHODS

### 2.1. Study Site and Sample Treatment

Soil samples have been collected in a beech-forest (Fagus sylvatica L.) in the Rhön mountains close to the town of Bad Brückenau, northern Bavaria/Germany. The soil developed on periglacial layers of basalt rock, and is classified as dystric sceletic Cambisol (hyperhumic, loamic) (FAO, 2015). We sampled the Oa, Ah, and Bw horizons. The site belongs to the core sites of the priority research program "Ecosystem nutrition" on forest-P nutrition and is the site with the highest phosphorus stocks (Lang et al., 2017). Altitude is 809 m a.s.l., mean annual temperature is 5.8°C, and precipitiation 1,031 mm/year. Properties of the sampled soil horizons are listed in **Table 1**.

Soil samples have been prevented from drying and have been stored at 4°C. Within 1 week after sampling field-fresh soil material has been homogenized by passing through a 2 mm sieve. Homogenization leveled the expected small-scale heterogeneity of the samples without inducing strong effects on P-mineralization processes (Bünemann et al., 2016). Round plastic containers (200 $cm^3$, diameter 9 cm, height 4 cm) for the MD experiments have been used. The containers have been filled to a predefined height with a soil mass involving field moisture and organic matter to achieve a bulk density of 0.52, 0.9, and 1.0 g $cm^{-3}$ for Oa, Ah, and Bw, respectively. The final water

**TABLE 1 |** Characteristics of the sampled soil horizons (Lang et al., 2017).

| Parameter | Oa | Ah | Bw |
|---|---|---|---|
| Soil depth/cm | +2 to 0 | 0 to –7 | –33 to –51 |
| Bulk density/g cm$^{-3}$ | 0.01 | 0.73 | 1.2 |
| Texture/mg g$^{-1}$ sand/silt/clay | –/–/– | 90/540/370 | 370/480/150 |
| $C_{org}$/mg g$^{-1}$ | 482 | 125 | 11 |
| N/mg g$^{-1}$ | 20 | 9 | 0.9 |
| $P_{total}$[a]/mg kg$^{-1}$ | 1,571 | 3,266 | 1,844 |
| $P_{citrate}$ (ICP)[b]/mg kg$^{-1}$ | 390 | 121 | 174 |
| $P_{citrate}$ (Molyb.)[c]/mg kg$^{-1}$ | 326 | 39 | 141 |
| C/N/g·g$^{-1}$ | 22.3 | 15.3 | 12.7 |
| C/P/g·g$^{-1}$ | 307 | 44.2 | 6.1 |
| $pH_{H2O}$ | 5.3 | 4.0 | 5.2 |
| CEC/mmol$_C$ kg$^{-1}$ | 543 | 260 | 150 |
| Base sat. Σ(Ca,Mg,K)/CEC | 78 | 15 | 45 |
| exchangbl. Ca/mmol$_C$ kg$^{-1}$ | 304 | 32 | 29 |
| $Fe_{oxalate}$/g kg$^{-1}$ | – | 32 | 13 |
| $Fe_{dithionite}$/g kg$^{-1}$ | – | 33 | 23 |

[a] *HF-digestion.*
[b] *Extraction with 50 mmol L$^{-1}$ citric acid, total P by atomic emission spectroscopy.*
[c] *Same extraction, but "inorganic P" by molybdene-blue photometric.*

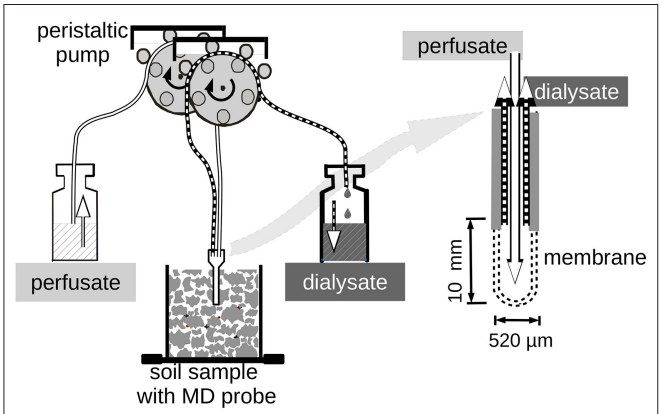


**FIGURE 1 |** Overview of the microdialysis (MD) setup.

content has been adjusted to 85% water-filled pore space. This is a compromise between ensuring a capillary continuum at the membrane surface and leaving a sufficient air-filled porosity to avoid P-mobilization caused by reduction of Fe and Mn-oxides. Furthermore, the experimental setup limited the maximum diffusion distance to the fully oxygenated air to 2 cm, which makes reductive Fe-mobilizing unlikely.

## 2.2. Microdialysis Experiments

The microdialysis extractions of the soil samples followed the proceeding described in Demand et al. (2017). We used CMA 20 Elite concentric MD probes (CMA Microdialysis AB, Kista, Sweden) equipped with a polyarylethersulfone (PAES) membrane with 20 kDa molecular cutoff. The membrane cylinder had 0.52 mm diameter and 10 mm vertical length. Fluid transport through the probes was achieved by a 24 channel peristaltic pump (Ismatec IPC-N 24, Cole Partner GmbH, Wertheim, Germany) with a minimum rotor speed of 0.11 min$^{-1}$. The recommended pump tubes for minimum flow rates turned out to be not stable enough to produce a constant flow over more than 12 h. The longlife tubing (PharMed Ismaprense SC0323, Cole Partner GmbH, Wertheim, Germany) was not available with a minimum diameter smaller than 0.64 mm. Because this was not adequate to achieve the targeted low flow rate of 3 µL min$^{-1}$ by constant rotation, we used the pumps in intermittent mode with 2.6 s pumping and 17.4 s pause corresponding to a nominal flow rate of 3.22 µL min$^{-1}$. The actual flow rates through the MD-probes with these settings were around 3 µL min$^{-1}$ but varied slightly between pumps and probes. Furthermore, pump rate increased when not all 24 rotors of a pump were used. Therefore, we monitored the flux rates during the experiments for calculation of efflux and influx data. To minimize losses of perfusate when MD probes were in contact with the non-saturated soil, a push-pull technique (Li et al., 2008) has been used. This technique is based on forcing fluid flow of both, perfusate and dialysate by mounting transport tubes on the coupled rotors of the multi-channel peristaltic pump. Perfusate loss has been monitored by comparing the soil mass before and after the MD extractions. The setup is outlined in **Figure 1**.

Tubing and probes have been conditioned by pumping deionized water through the system for 16 h. Setup and probes have then been tested for P recovery with a perfusate of 15 mmol$^{-1}$ KCl at the flow rate setting of 3.22 µ L min$^{-1}$ in a stirred 0.84 µ mol L$^{-1}$ phosphate solution over 20 h. In this experiment, P recovery varied between 5 and 15% with a median of 10.8%. This was only half the recovery observed by Demand et al. (2017) with a similar setup, but with a 10 times higher phosphate concentration in the outer medium.

Three different perfusates have been applied. Demand et al. (2017) demonstrated the strong effect of the ionic strength of the perfusate on P recovery. Therefore, we used a 15 mmol$^{-1}$ KCl solution as the control perfusate and as the base electrolyte for the two citric acid treatments with 1 and 3 mmol L$^{-1}$ addition of citrate anions as citric acid monohydrate ($C_6H_8O_7{\cdot}H_2O$).

For the soil experiments 6 MD probes have been inserted into the soil within one plastic container. This left a 10 cm$^2$ free space around each probe to avoid interference during the extraction time. Before sampling of dialysates, the probes have been flushed for 3 min with 23 µ L min$^{-1}$ to remove air bubbles. Dialysates have been sampled over 6 d separately for three subsequent periods: 0–24, 24–48, and 48–144 h. Temperature was kept constant at 15°C. With the three horizons and three perfusates, in total nine treatments have been tested. For each treatment, six individual dialysates of MD probes have been sampled (plus six extra replications for the control in Bw), yielding in total 180 dialysates. Actual flow rates were determined based on the weight of the sampled dialysate divided by perfusion time. Concentrations of phosphate, citrate, and chloride have been analyzed to calculate rates of absorption from and release into the soil. Average exchange between MD membrane and soil has been calculated from the change of concentration between dialysates and perfusates multiplied by the respective flow rate. The loss of

**TABLE 2 |** Cumulative phosphate influx (medians ±95% confidence limits) into MD probes during 6 days (144 h).

| | P/nmol cm$^{-2}$ | | |
|---|---|---|---|
| | Soil horizon | | |
| Citrate in perfusate | Oa | Ah | Bw |
| No | 6.1 ±1.33 | 2.4 ±0.56 | 0.8 ±0.22 |
| 1 mmol L$^{-1}$ | 23.8 ±1.86 | 13.2 ±0.93 | 48.0 ±6.28 |
| 3 mmol L$^{-1}$ | 50.0 ±11.84 | 32.2 ±31.55 | 87.1 ±16.75 |

*Effect of p-values of the robust anova was 0.003 for horizon, 0.001 for perfusate, and 0.001 for interaction (perfusate × horizon).*

perfusate into the soil samples was around 5%, but reached up to 20% in the Bw horizon. Because the soil samples could only be weighted at the end of the experiment and not together with each dialysate vial, a quantitative consideration of this term is not yet possible. For future experiments, we will foresee separate perfusate vials allowing to track the perfusate loss.

## 2.3. Analytics

Phosphate in the dialysate has been analyzed with the molybdenum-blue method by using a continuous flow analyzer (SAN Plus, Skalar Analytical B.V., The Netherlands) equipped with a 50 cm extended light-path cell (Zhang and Chi, 2002). Limit of detection was around 7 nmol L$^{-1}$, limit of quantification around 20 nmol L$^{-1}$ based on the 95% confidence limit of a 5-point calibration. Citrate and chloride concentrations have been analyzed with capillary-zone electrophoresis (Agilent Technologies, Waldbronn, Germany) according to the procedure of Göttlein and Blasek (1996).

## 2.4. Calculations and Statistics

From the molar relation of the citrate-increased P-influx and the related citrate efflux, we calculated an efficiency term (Equation 1):

$$E_{cit} = \frac{Q_{P,(+cit)} - Q_{P,(-cit)}}{Q_{cit}} \quad (1)$$

with $E_{cit}$ the efficiency of citrate to mobilize P, $Q_P$ the molar influx of P with citrate in the perfusate (+cit) and without (−cit), and $Q_{cit}$ the molar efflux of citrate. $Q_{cit}$ is the product of the dialysate-flow rate and the difference between perfusate and dialysate concentration of citrate. Statistics have been calculated with R-statistics version 3.5.0 (R Core Team, 2018). The observed fluxes (**Table 2**, **Figure 2**) and citrate P-mobilization efficiencies (**Figure 3**) have been tested with robust 2-way analyses of variance (anova) from the R-statistics package *WRS* (Mair and Wilcox, 2020). We used the function *t2way* to reveal significant effects of soil horizon and citrate treatment on the cumulative fluxes (**Table 2**). For the fluxes over time (**Figure 2**) and for the mobilization efficiency (**Figure 3**), we used the mixed-anova function *bwsplit* to reveal significant effects of sampling time and citrate treatment. In this anova, the differences between sampling times have been regarded as within-subject effects (repeated measurements on individual probes) and the citrate treatment as between-subject (group) effect. Additionally, we reported in the graphics the approximated 95% confidence limits of the median (McGill et al., 1978) to facilitate the localization of significant differences. We based the regression of P-influx over citrate efflux on a log-log model of the medians as a robust approach. With these transformations, we achieved a normal distribution of the P-influx data (Shapiro-test). In the error estimation, this aggregation is considered by the strong reduction of the number of degrees of freedom. The model formula was:

$$log_{10}\left(\sum Q_P\right) = (I_0 + I_{hor}) + (S_0 + S_{hor}) \cdot log_{10}\left(\sum -Q_{cit}\right) \quad (2)$$

with $\Sigma Q_P$ and $\Sigma - Q_{Cit}$ the cumulated molar fluxes of phosphate and the opposite flux of citrate, $I_0$, $I_{Hor}$, $S_0$, and $S_{Hor}$ the intercept and the slope. Both are composed of a basic term (subscript "0") that covers the Oa horizon and a further additive term of slope and intercept (subscript "hor") that covers the modifications for Ah and Bw horizon.

# 3. RESULTS

P-influx of MD depended on the citrate concentration of the perfusate. Maximum cumulative 144 h influx (**Table 2**) without citrate was in the Oa horizon and minimum in the Bw-subsoil. With the high-citrate perfusate, the ranking changed and maximum influx was in the Bw horizon. There was an interaction between the effects of citrate concentration of perfusate and time (**Figures 2A,B**, **Table 3**). With the control and the high-citrate treatment P influx decreased continuously over time, while for the low-citrate treatment P influx reached a maximum after 48 h. By trend, both citrate treatments produced highest P influx for the samples of the Bw subsoil, whereas with the control P-influx decreased with soil depth from Oa to the Bw. The highest relative P-mobilization effect of citrate was observed for samples of the Bw horizon between 48 and 144 h where the median of P influx raised from 6.9E-7 (control) to 1.05E-4 nmol cm$^{-2}$ s$^{-1}$ (high citrate), i.e., by a factor of 157. The continuous decrease of P influx over time with the control is in agreement with a depletion of the probe environment by diffusion with or without first-order desorptive replenishment.

Cumulative P-influx (**Table 2**) of both citrate treatments did not reflect the gradation of the batch-citrate extractable P in **Table 1** neither for the molybdenum active part, nor the total P in the citrate extract. Maximum concentration of batch-citrate extractable P was found in the Oa horizon and minimum in the Ah: On a volume base it was for total citrate-extractable P [$P_{cit}$ (ICP)] 195, 108, and 174 µg cm$^{-3}$, and for inorganic [$P_{cit}$ (Molyb.)] 163, 35, and 141 µg cm$^{-3}$ in Oa, Ah, and Bw, respectively. This does not correlate to the clear maximum of MD-P influx in the Bw horizon. The minimum of batch-extractable P in the Ah horizon coincides only with the MD influx of low citrate but not with the high citrate perfusate where MD-P influx of the Ah horizon was close to that of the Oh horizon.

In all horizons and all perfusates efflux of chloride (**Figure 2D**) decreased strongly from day 1 to 2 followed by a constant efflux

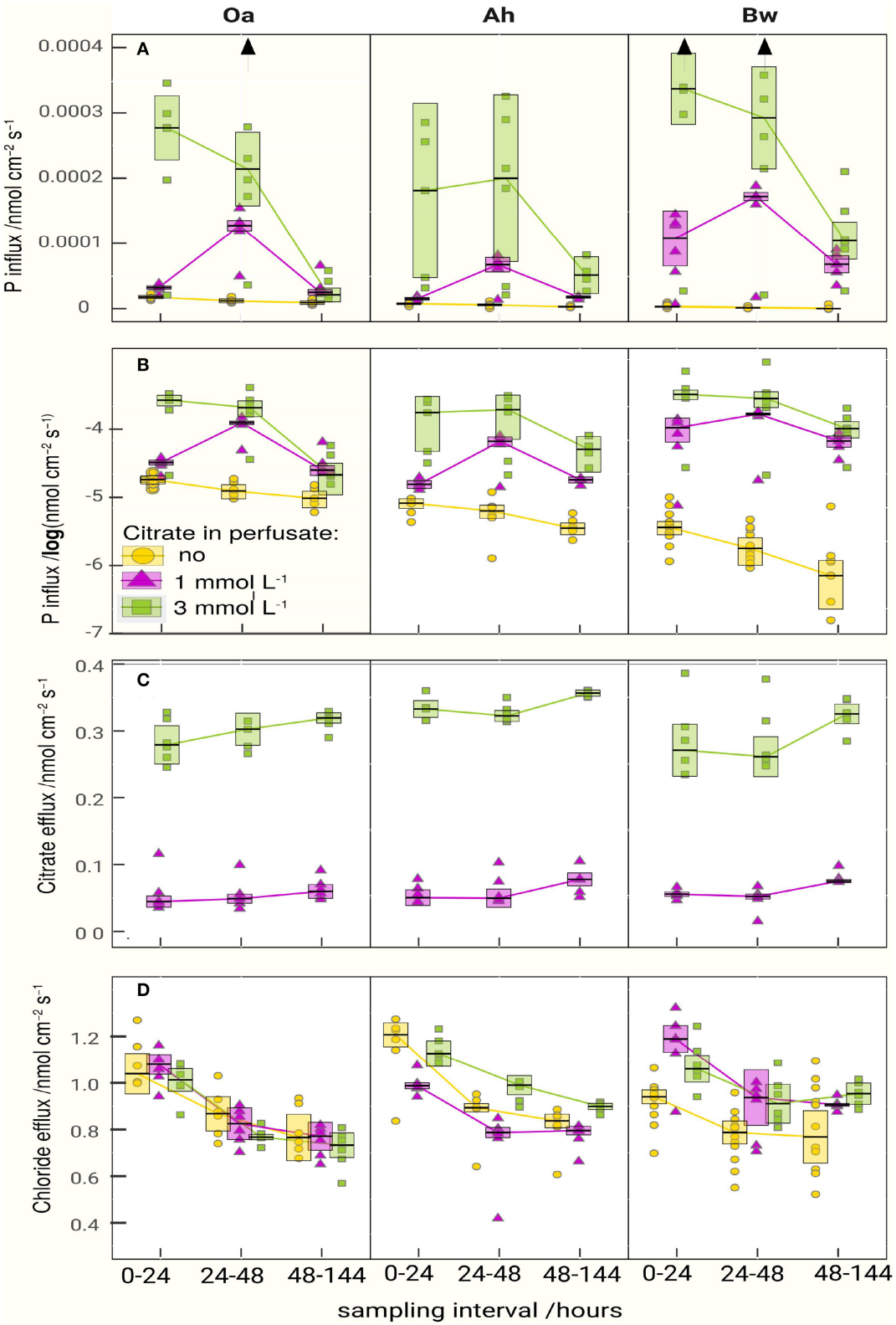


**FIGURE 2 |** Fluxes of phosphate **(A,B)**, citrate **(C)**, and chloride **(D)** between soil and microdialysis probes. The boxes represent the approximated 95% confidence limit of the median (anova statistics is presented in **Table 3**). The lines are connecting medians indicating the temporal pattern. For the phosphate influx, the plot is repeated with logarithmic scaling in **(B)** to highlight the gradation of the P-absorption between control and citrate treatments. Vertical arrows in the upper graph symbolize outliers beyond the maximum axis value.

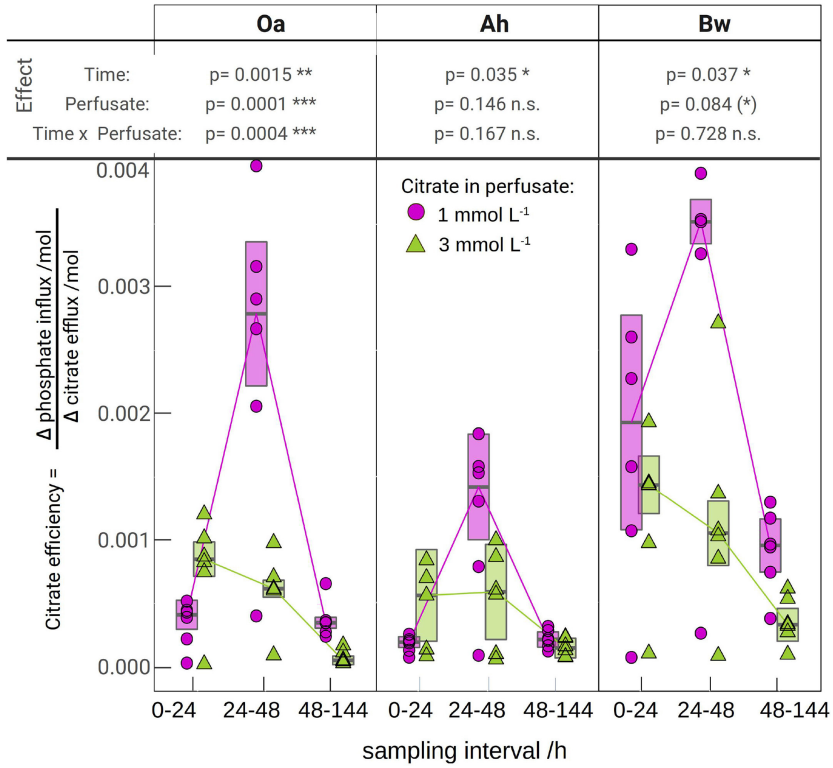


**FIGURE 3 |** The molar efficiency of citrate to release phosphate, calculated as the ratio of flux changes between the respective citrate perfusate and the control (Equation 1). The lines are connecting medians indicating the temporal pattern. The error bars limit the approximated 95% confidence limits of the medians, the tabled *p*-values come from a robust mixed 2-way anova (c.f. that was applied separately for each soil horizon. Significance of *p*-values is symbolized by: (*)< 0.1, * < 0.05, ** <0.01, *** < 0.001).

**TABLE 3 |** Comparison of fluxes reported in **Figure 2**: *p*-values of the robust 2-way mixed anova considering within-subject effects (repeated measurement of probes over time) and between-subject effects (perfusates).

| Horizon | Oa | | | Ah | | | Bw | | |
|---|---|---|---|---|---|---|---|---|---|
| **Flux** | ***P*** | **Citrate** | **Chloride** | ***P*** | **Citrate** | **Chloride** | ***P*** | **Citrate** | **Chloride** |
| **EFFECT** | | | | | | | | | |
| Perfusate | 0.0003 *** | <0.0001 *** | 0.41 n.s. | 0.0001 *** | <0.0001 *** | 0.0006 *** | <0.0001 *** | 0.0006 *** | 0.0011 ** |
| Time | <0.0001 *** | 0.072 (*) | <0.0001 *** | 0.0021 ** | 0.034 * | <0.0001 *** | 0.0006 *** | 0.018 * | 0.0002 *** |
| Time × perf. | <0.0001 *** | 0.45 n.s. | 0.53 n.s. | 0.0001 ** | 0.51 n.s. | 0.041 * | 0.065 (*) | 0.19 n.s. | 0.03 * |

*The anova was applied separately for each soil horizon, significance of p-values is symbolized with: (*)<0.1, *<0.05, **<0.01, ***<0.001.*

or a further decrease to day 3–6. Final $Cl^-$ efflux was only 70–90% of that of day 1. This pattern can easily be attributed to a transient diffusion process of an ion that does not interact with the solid phase and approaches a steady-state efflux. Citrate efflux (**Figure 2C**), in contrast, increased over time with all treatments and horizons (for the Oa horizon, the *p*-value is 0.072, **Table 3**; in this case, we have to classify the increase as tendency). Horizon-specific effects could not be revealed.

**Figure 3** shows the calculated efficiencies of citrate efflux to mobilize P according to Equation (1). Individual MD-probe observations have been used for P-influx [$Q_{P,(+cit)}$] of the citrate treatments and the respective citrate efflux ($Q_{cit}$). The median of the control P-influx of the respective horizon, perfusate, and time has been used for the term $Q_{P,(-cit)}$. The highest P yield for a given citrate efflux was observed in the Bw horizon with low citrate at day 2 with 0.0035 mol·mol$^{-1}$, i.e., 286 citrate

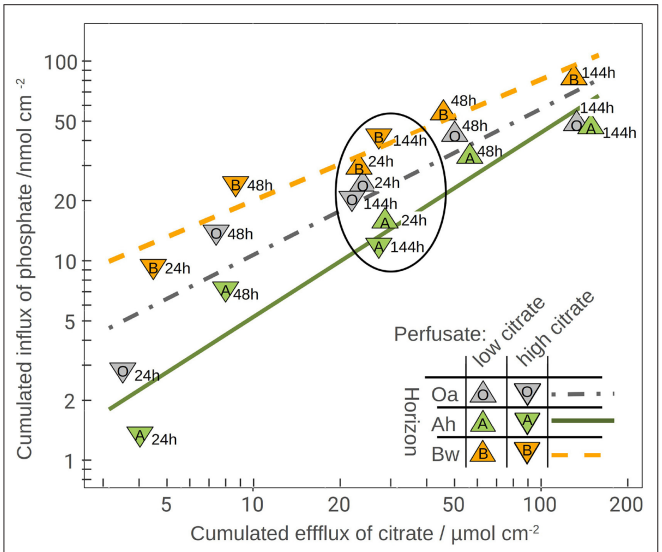


**FIGURE 4 |** Phosphate influx over citrate efflux together with the logarithmic model fitting (model parameters in **Table 4**). The numbers right of the symbols are the time in hours. The ellipse highlights the overlapping results of both perfusate-citrate concentrations where the values of the low citrate treatment cover 144 h efflux and those of the high-citrate treatment only 24 h.

**TABLE 4 |** Coefficients of the regression model of cumulated *P*-influx over cumulated citrate efflux (Equation 2 displayed in **Figure 4**), with *p*-values of coefficients: **<0.01, ***<0.001.

| Horizon | Oa | Ah | Bw |
|---|---|---|---|
| $I_0$ | — | 1.895 | — |
| | — | $p = 0.005$** | — |
| $I_{Hor}$ | 0 | −1.077 | 0.768 |
| | | $p = 0.206$ | $p = 0.379$ |
| $S_0$ | — | 0.731 | — |
| | — | $p = 0.0001$*** | — |
| $S_{Hor}$ | 0 | 0.192 | −0.125 |
| | | $p = 0.32$ | $p = 0.53$ |

*Adj.* $r^2 = 0.87$.

molecules were needed to harvest one additional phosphate. Lowest efficiency was observed in the Oa horizon with high-citrate treatment between 48 and 144 h with 0.00004 mol·mol$^{-1}$ or 25.000 citrate molecules needed for one additional phosphate. Efficiency of the high-citrate treatment decreased progressively from day 1 to 3–6, whereas low-citrate treatment showed a maximum efficiency during day 2.

The plot of the cumulated phosphate absorption over cumulated citrate efflux (**Figure 4**) exhibits a logarithmic trend and could be fitted by a regression model (Equation 2). The coefficients of the model are listed in **Table 4**. In the plot three sections along the x-axis can be distinguished: Points left of the drawn ellipse stem only from the low citrate treatment, points right of ellipse only from the high citrate treatment. Points within the ellipse come from both treatments equally and form a smooth transition between the citrate treatments. P-influx after 144 h of low-citrate efflux was virtually the same as P-influx of 24 h of high-citrate efflux. This can also be expressed in terms of citrate efficiency (Equation 1). The 24 h efficiency of high-citrate treatment has been taken directly from **Figure 3**, and the 144 h efficiency of the low-citrate treatment has been calculated from the cumulative fluxes of phosphate and citrate. In the Oa horizon, the 144 h low and the 24 h high efficiency were 0.001 and 0.00084, respectively, in the Ah 0.00055 and 0.00051, and in the Bw 0.0021 and 0.0014 mol mol$^{-1}$. In neither of the three horizons, the 144 h low and the 24 h high P-efficiencies revealed significant differences (Wilcoxon rank test). The close similarity of the efficiencies in the soil horizons are notable insofar that the major control of P mobilization by citrate was the cumulated efflux of citrate and that this was independent of time or citrate concentration.

# 4. DISCUSSION

## 4.1. Citrate Efflux

Citrate efflux from the MD probes into the soil increased P influx into the MD probes. Beyond that, the specific time patterns of P-influx and citrate efflux during the 6-days experiment merit specific analysis. The volume of soil that is influenced by the activity of a living root is defined as rhizosphere with a radius in the µm-range up to cm (Hinsinger et al., 2009). The radius of an "MD-rhizosphere" is limited by the modification of solute concentrations that can also trigger modifications of biotic activity. The efflux from the perfusate increased concentrations of $K^+$, $Cl^-$, and citrate in the solution surrounding the MD-probe. For an ion that does not interact with the solid phase, such as $Cl^-$, a transient growth of the dispersal volume together with flattened concentration gradients near the MD membrane can be expected. In our results, this was reflected by the decreasing diffusional loss of $Cl^-$ with time (**Figure 2**). The efflux characteristics of Cl are crucial for our interpretations since it is an ion that hardly interacts with microbes or the solid phase. Chloride reveals the typical efflux pattern dominated by diffusion. Though we can assume the same transport physics for citrate and Cl anions, the development of citrate efflux over time is completely different. We observed a decreasing Cl efflux over time, but an increasing citrate efflux. Diffusion of solutes revealing a stronger interaction to the solid phase than Cl would slow down in a similar way. A solute depletion by first-order kinetics (adsorption, precipitation) or Michaelis–Menten kinetics would delay a saturation, but never lead to an increase of diffusional loss over time. Precipitation of citrate by polyvalent cations can neither explain increasing diffusional loss since this process would follow zero-order kinetics, resulting in constant citrate efflux, nor it can be explained by citrate adsorption, since this would cause decreasing citrate efflux over time. The most obvious explanation for increasing efflux is microbial decay or metabolization of citrate with increasing rates after begin of efflux. In the following, we summarize evidence from literature supporting this assumption. In soils, citrate is easily metabolized or degraded by microorganisms and reveals short half life of only up to some hours (Jones, 1998; van Hees

et al., 2002). This would not cause increasing efflux rates into the MD environment as long as the microbial citrate sink is controlled by constant concentration-dependent kinetics. Several models of citrate concentration around exuding roots are based on decay constants (Geelhoed et al., 1999; Schnepf et al., 2012; McKay Fletcher et al., 2019). When parametrized with literature-based decay constants these models yield a radius of 0.1 and 0.4 cm around the exuding surface where citrate concentrations approach zero. In these models, citrate efflux decreases over time. This type of citrate efflux characteristics was observed by McKay Fletcher et al. (2019) in a 20 h MD experiment. However, the assumption of constant rates of concentration-dependent citrate decay in the rhizosphere is questionable. Fujii et al. (2012) observed an increase of Michaelis–Menten parameters of carboxylate decay in the rhizosphere vs. bulk soil.

Here it has to be emphasized that carboxylate exudation by actual roots is a dynamic process insofar, that the efflux is concentrated at the rather short-living root tip (Canarini et al., 2019). This means a root grows toward a soil spot devoid of an active root and often with higher availability of water or nutrients. There, it begins to exude, e.g., citrate, an easily available additional energy source for microorganisms that will stimulate the microbial community. Root exuded low-molecular organic acids exert a particularly strong rhizosphere priming effect (Renella et al., 2007; Keiluweit et al., 2015; Shahzad et al., 2015), which describes a microbial carbon mineralization in the rhizosphere that releases more $CO_2$ than could be expected from the amount of exudates (Kuzyakov, 2002). Modification of the microbial community is an important trait of the rhizosphere (Hinsinger et al., 2011; Kaiser et al., 2011). Therefore, it is unlikely that biotic activity in the rhizosphere as well as in the vicinity of a MD probe in a living soil remains unchanged during hours and days following the emergence of a local citrate source. In contrast to first-order processes, a microbial stimulation counteracts a saturation and can cause an increasing diffusional efflux of citrate. In our experiments, diffusional efflux of citrate increased by a factor up to 1.57 within 6 days. This factor is also the minimum estimate of increased decay in the direct vicinity of the MD membrane. This is evident from the physics of diffusion: An increase of efflux needs a proportional lowering of the citrate concentration directly at the membrane surface. The actual increase of the rate of microbial decay was nevertheless higher by an unknown factor, because a part of the initial diffusion efflux was not used solely by microbes, but contributed to a transient adsorption by the solid phase near the membrane (Gerke et al., 2000).

We hypothesized a stronger effect of microbial citrate consumption on P-mobilization in the topsoil horizons rich in SOM. This would have been supported by a stronger increase of citrate efflux with time in the Oa and Ah horizon than in the Bw horizon, but for this effect there is no direct evidence in the results. Overall, the data do not allow a detailed analysis of the rising citrate efflux over time. Furthermore, without additional data on soil respiration conclusions on time patterns of microbial stimulation remain speculative. As shown by Stenström et al. (1998), the delay and the further trend of soil respiration after stimulation by added substrate depend on the composition of the microbial community with members whose population grow and others that only increase their metabolism in response to an addition of easily available substrate. The authors found that increase in soil respiration by growing microbial populations is stronger, but begins later than increased substrate mineralization by a non-growing population.

## 4.2. Phosphate Mobilization

Generally, it is assumed that microbial decay of citrate lowers its efficiency to mobilize phosphate (Geelhoed et al., 1999; Barrow et al., 2018) because microbial loss reduces citrate concentrations responsible for P-mobilization processes, such as ligand exchange, surface reactions, or chelating of Fe. We hypothesized therefore an increasing efficiency of citrate to mobilize phosphate with decreasing SOM as a proxy for microbial activity and thereby citrate decay according to van Hees et al. (2002). In accordance with our hypothesis, we observed uniformly higher mobilizing efficiencies of citrate in the Bw horizon than in the topsoil (Oa and Ah horizon). Independently of a priming by citrate in the MD vicinity a higher density of potentially citrate consuming microorganisms would lower the citrate concentration in the soil solution and additionally could compete with the MD membranes for mobilized phosphate.

We parametrized a regression model that explains 87% of the total variation of phosphate influx into the MD probes solely based on the cumulative citrate efflux and the soil horizon (**Table 4**). The model is thus independent of time and citrate concentration in the perfusate. The logarithmic trend implies a decreasing marginal benefit of citrate exudation for phosphate mobilization. Until now, cumulative efflux has barely been discussed as the main control of P-mobilization by citrate. Results supporting the relevance of cumulative efflux of carboxylates were obtained by Fox et al. (1990). The authors applied one single dose of oxalate to a soil sample and extracted soil solution after 12 h and compared the results to sequential extractions after applying smaller doses over several days. They obtained congruent curves of P yield plotted over the cumulative amount of added oxalate. Though the authors did not discuss the mechanisms that cause this phenomenon, they emphasized the important ecological role of small, but continuous release of carboxylates mobilizing strongly adsorbed solutes like Al or P.

Most existing studies of P mobilization by carboxylates focus on equilibrium concentration as controlling factor (Hinsinger, 2001), probably because batch extraction is a common approach and equilibrium coefficients allow a straightforward implementation of numeric models. In contrast, McKay Fletcher et al. (2019) related the P mobilization potential of citrate efflux in an MD experiment to the efflux rate of citrate. However, their results do not contradict our findings because the experiments were limited to 20 h. Low efflux rates need to be observed with extended exposure times. Citrate efficiencies plotted in **Figure 3** indicate that there exists, however, a threshold of cumulated citrate efflux to mobilize P. With the high-citrate treatment we observed a strong decrease of mobilization efficiency over time. The extremely low phosphate extra yield in the Oa horizon after 48 h of citrate efflux implies

high costs of phosphate mobilization. With low citrate efflux initial mobilizing efficiency, however, was low and not until the second day it reached a marked peak to decrease again during the period between day 3 and 6. This is not in compliance with the logarithmic model in **Figure 4**, which implies a continuous decrease of the specific efficiency: The more citrate was released, the lower its ability to mobilize additional P. In the logarithmic fit, the reduced initial low-citrate efficiency is reflected by the systematically negative residuals of the 24 h low-citrate observations in **Figure 4**.

Gerke et al. (2000) described a threshold of citrate concentration on the solid phase implying also a minimum dissolved citrate concentration where the dissolved phosphate concentration begins to increase. In the dynamic MD extraction, such a sharp threshold cannot be expected, but with low citrate concentrations in solution, a stronger competition between phosphate mobilization and other processes of citrate immobilization is probable (Jones and Brassington, 1998). Filling up the most selective citrate adsorption positions in the direct vicinity of the membrane can therefore explain the delayed maximum efficiency in case of low citrate. A similar effect could be hypothesized for selective microbial uptake of phosphate around the membranes. In the high-citrate treatment, this possible threshold is masked by the high amount of exuded citrate in the first 24 h, which is close to the 144 citrate efflux of the low-citrate treatment. With the experimental data of our study, a quantitative limitation of the scope of the logarithmic model is not yet possible. For the lower threshold, a high-citrate efflux has to be tested with reduced time steps.

Adsorption/desorption characteristics of citrate and phosphate are mostly non-linear (Gerke et al., 2000), i.e., at low concentrations a higher fraction is bound to the solid phase. When only desorption from the solid phase is considered, phosphate mobilization independently of the applied citrate concentration is therefore remarkable. Possibly, processes of P mobilization are much more diverse than those included in the established quantitative models. Kinetics of obviously relevant rhizosphere processes, such as stepwise P release from supramolecular SOM structures by citrate (Clarholm et al., 2015) or the absorption of "leftover" P of SOM-mineralization triggered by the priming effect of citrate (Renella et al., 2007; Dijkstra et al., 2013) is difficult to quantify. A further validation of cumulative carboxylate efflux as major control of P-mobilization needs application of a wider variation of efflux rates and an overlapping of resulting efflux over several points in time. This should be amended by quantification of citrate-triggered change of soil respiration. If cumulative efflux proved to be a generalizable control of P mobilization, a discussion of the underlying mechanisms would be needed.

Because MD-influx originates from an unknown volume, it cannot be converted directly to batch extracted P. A distance-weighted distribution of the P-influx can only be obtained by parametrizing models with diffusion, adsorption, and decay data (Schnepf et al., 2012; McKay Fletcher et al., 2019). Nevertheless, MD P-influx data of our three soil horizons did not reflect the differences and ranking of phosphate mobilized with citrate-batch extraction (**Table 1**). Because our experiments yielded the first quantitative data on P-absorption of a citric acid exuding membrane in soil environment over several days, a direct reference to existing studies is not available. One important difference to batch experiments is the MD membrane acting as an additional sink for dissolved P that competes with chelating species, adsorbing surfaces (Barrow, 2017), and microbial uptake (Schneider et al., 2017). In such a far-from equilibrium dynamic, each single interacting citrate molecule can mobilize a phosphate whose fate is determined by the spatial arrangement of sinks and the diffusion speed (McKay Fletcher et al., 2020). The probability of a dissolved P to reach the MD surface decreases by both diffusion time and the number of opportunities to be re-immobilized. Therefore, the competetiveness of the MD surfaces strongly increases with decreasing distance between the place of mobilization and the absorbing membrane. As Raynaud et al. (2008) illustrated by modeling spatial interaction of rhizosphere processes, it could be beneficial for a root when the concentration of a mobilizing solute around a root drops in a narrow radius because this decreases the share of the mobilized nutrients that are lost for the exuding root.

MD assesses far-from equilibrium dynamics that cannot be modeled with equilibrium constants involving instantaneous exchange. By leveling desorption/adsorption kinetics and the microscale-spatial distribution of both exchanging surfaces and microorganisms, an equilibrium experiment can barely reflect the specific low-distance competetiveness of an absorbing membrane. Furthermore, the standard citrate extraction procedure applied for the values in **Table 1** is based on a concentration of 50 mmol $L^{-1}$ of citrate, which is much higher than we induced directly at the membrane surface.

A critical point of our study are the absolute concentrations we applied. Carboxylate concentrations in the rhizosphere are generally higher than in the bulk soil (Jones, 1998; Fujii et al., 2012). There is an evidence of increased carboxylate exudation when roots grow in soils with limited P availability (Hoffland et al., 1989) including European beech (De Feudis et al., 2016). However, citrate concentrations of 1 mmol $L^{-1}$ or more are barely observed in soil solution (Except in the vicinity of specialist root structures, such as cluster roots; Lambers et al., 2015). In topsoil solutions of beech stands, Shen et al. (1996) measured citrate concentrations below 1 µmol $L^{-1}$. In bulk soil solutions citrate concentrations solution rarely exceed 50 µmol $L^{-1}$ (Jones, 1998), in forest floor of coniferous stands they may approach 500 µmol $L^{-1}$ (van Hees et al., 2005a).

Though soil-solution sampling in the rhizosphere is challenging (Luster et al., 2009), it is assumed that natural concentrations of citrate are lower than those applied in most experiments (Hinsinger, 2001). From the existing data of low rhizosphere concentrations and low exudation rates, Richardson et al. (2011) recognize only a "modest" evidence that organic anion release of non-cluster root plants can improve P nutrition. Maximum concentrations in our experiment were directly at the membrane–soil contact zone. They can be easily estimated due to the low membrane thickness and its high porosity (Demand et al., 2017), where the diffusional flux causes a marginal gradient. Therefore, concentrations at the outer membrane surface were close to the perfusate of 1, respectively 3 mmol $L^{-1}$.

The point-like membrane-surface concentration is not equal to a rhizosphere concentration that is always defined on a volume base. Until now rhizosphere concentration measurements are limited in the spatial resolution to 1–2 mm (Fujii et al., 2012) or in case of micro-suction cups to 1 cm (Dessureault-Rompré et al., 2006). As mentioned above, the localized exudation of this easily degradable organic carbon causes very steep concentration gradients around the sources approaching zero within an mm range. Reliable data of exudation rates of individual tree roots are scarce (Preece and Peñuelas, 2016; Oburger and Jones, 2018). By relating mineralization kinetics and the concentrations in bulk-soil solution, van Hees et al. (2005b) calculated soil-mass related production rates of citrate for podzolic forest soils between 0.4 and 600 nmol $g^{-1}$ $day^{-1}$. Considering the fast mineralization, van Hees et al. (2005a) assumed turnover rates up to 80 $day^{-1}$ for the dissolved part and 10 $day^{-1}$ for total carboxylates including the adsorbed part. These high turnover rates require a permanent replenishment of the soil solution. Roots play an important role in this replenishment (Nguyen, 2003). However, both time and spot of exudation of carboxylates in root systems can be highly localized (Hinsinger et al., 2011; Canarini et al., 2019). This means until now we do not know the maximum citrate concentrations directly at exuding root tips. There are furthermore scaling challenges because potentially an important part of phosphate is mobilized in pores with diameters below 10 µm, which are barely accessible to microscopic concentration measurements. Though it would be desirable to extend the range of citrate concentrations in the MD-experiments toward lower values, existing information on efflux rates of root citrate does not exclude the local occurrence of high concentrations directly at the root surface or in individual pores in direct contact to the membrane surface.

### 4.3. Conclusions

Following phosphate influx into MD probes and synchronous efflux of citrate over several days yielded novel insights into soil P-mobilization. A surprising result was the rather complex patterns of P-influx modified by time, soil-horizon, and perfusate concentration that could be aggregated in a logarithmic model. This model predicts cumulated phosphate influx by the cumulated citrate efflux independently of time and efflux rate. We conclude therefore that processes other than sorption/desorption or precipitation/solution control the mobilization efficiency of exuded citrate in soil. Our data are consistent with the assumption that in this context microbial decomposition or immobilization processes are central. Our data also show that in soils with high concentrations of adsorbed phosphate, the exudation of citrate in the subsoil is more beneficial for the plant roots' P uptake than in the SOM-rich topsoil. The logarithmic character of the model implies a decreasing marginal benefit of citrate exudation, which can probably be related to stimulation of microbial activity by citrate and an increasing distance between mobilization of phosphate and membrane uptake. Both effects lower the competitiveness of the uptaking membrane to other processes. In order to deepen our knowledge of P-mobilization by carboxylates, the presented MD approach should be amended with (a) lower citrate efflux rates but longer observation time, (b) analyses of soil microbial activity with high time resolution, and (c) on-site use of spatial MD grids. Our results confirm that the developed advancement of MD application is promising for the identification of P mobilization processes in soils mediated by plant roots but also indicate still open questions regarding this issue. Nevertheless, we agree with Brackin et al. (2017) who called the MD method "Roots-eye view."

## DATA AVAILABILITY STATEMENT

The raw data supporting the conclusions of this article will be made available by the authors, without undue reservation.

## AUTHOR CONTRIBUTIONS

HS-K contributed to the experimental design and data analysis and wrote the major part of the manuscript. CL contributed to the experimental design, carried out respectively supervised the experiment, and did the data analysis. FL conceptualized the project, wrote the funding application, and contributed to the manuscript. All authors contributed to the article and approved the submitted version.

## FUNDING

The project was funded by the German Research Foundation (DFG, GZ: LA 1398/12-2 AOBJ: 632054).

## ACKNOWLEDGMENTS

The authors gratefully acknowledge A. Thiemann, C. Gabriel, and M. P. Haas who carefully conducted experiments and analyses.

## REFERENCES

Barrow, N. (2017). The effects of pH on phosphate uptake from the soil. *Plant Soil* 410, 401–410. doi: 10.1007/s11104-016-3008-9

Barrow, N., Debnath, A., and Sen, A. (2018). Mechanisms by which citric acid increases phosphate availability. *Plant Soil* 423, 193–204. doi: 10.1007/s11104-017-3490-8

Brackin, R., Atkinson, B. S., Sturrock, C. J., and Rasmussen, A. (2017). Roots-eye view: using microdialysis and microCT to non-destructively map root nutrient depletion and accumulation zones. *Plant Cell Environ.* 40, 3135–3142. doi: 10.1111/pce.13072

Bucher, M. (2007). Functional biology of plant phosphate uptake at root and mycorrhiza interfaces. *New Phytol.* 173, 11–26. doi: 10.1111/j.1469-8137.2006.01935.x

Buckley, S., Brackin, R., Jämtgård, S., Näsholm, T., and Schmidt, S. (2020). Microdialysis in soil environments: current practice and future perspectives. *Soil Biol. Biochem.* 143:107743. doi: 10.1016/j.soilbio.2020.107743

Bünemann, E. K., Augstburger, S., and Frossard, E. (2016). Dominance of either physicochemical or biological phosphorus cycling processes in temperate forest soils of contrasting phosphate availability. *Soil Biol. Biochem.* 101, 85–95. doi: 10.1016/j.soilbio.2016.07.005

Canarini, A., Kaiser, C., Merchant, A., Richter, A., and Wanek, W. (2019). Root exudation of primary metabolites: mechanisms and their roles in plant responses to environmental stimuli. *Front. Plant Sci.* 10:157. doi: 10.3389/fpls.2019.00420

Clarholm, M., Skyllberg, U., and Rosling, A. (2015). Organic acid induced release of nutrients from metal-stabilized soil organic matter-the unbutton model. *Soil Biol. Biochem.* 84, 168–176. doi: 10.1016/j.soilbio.2015.02.019

De Feudis, M., Cardelli, V., Massaccesi, L., Bol, R., Willbold, S., Cocco, S., et al. (2016). Effect of beech (*Fagus sylvatica* L.) rhizosphere on phosphorous availability in soils at different altitudes (central Italy). *Geoderma* 276, 53–63. doi: 10.1016/j.geoderma.2016.04.028

Degryse, F., Smolders, E., Zhang, H., and Davison, W. (2009). Predicting availability of mineral elements to plants with the DGT technique: a review of experimental data and interpretation by modelling. *Environ. Chem.* 6, 198–218. doi: 10.1071/EN09010

Demand, D., Schack-Kirchner, H., and Lang, F. (2017). Assessment of diffusive phosphate supply in soils by microdialysis. *J. Plant Nutr. Soil Sci.* 180, 220–230. doi: 10.1002/jpln.201600412

Dessureault-Rompré, J., Nowack, B., Schulin, R., and Luster, J. (2006). Modified micro suction cup/rhizobox approach for the *in-situ* detection of organic acids in rhizosphere soil solution. *Plant Soil* 286, 99–107. doi: 10.1007/s11104-006-9029-z

Dijkstra, F. A., Carrillo, Y., Pendall, E., and Morgan, J. A. (2013). Rhizosphere priming: a nutrient perspective. *Front. Microbiol.* 4:216. doi: 10.3389/fmicb.2013.00216

FAO (Ed.). (2015). *World Reference Base for Soil Resources 2014, Update 2015: International Soil Classification System for Naming Soils and Creating Legends for Soil Maps*. World Soil Resources Reports. Rome: FAO.

Fäth, J., Kohlpaintner, M., Blum, U., Göttlein, A., and Mellert, K. H. (2019). Assessing phosphorus nutrition of the main european tree species by simple soil extraction methods. *For. Ecol. Manag.* 432, 895–901. doi: 10.1016/j.foreco.2018.10.007

Fox, T., and Comerford, N. (1992). Influence of oxalate loading on phosphorus and aluminum solubility in spodosols. *Soil Sci. Soc. Am. J.* 56, 290–294. doi: 10.2136/sssaj1992.03615995005600010046x

Fox, T., Comerford, N., and McFee, W. (1990). Kinetics of phosphorus release from spodosols: effects of oxalate and formate. *Soil Sci. Soc. Am. J.* 54, 1441–1447. doi: 10.2136/sssaj1990.03615995005400050038x

Fujii, K., Aoki, M., and Kitayama, K. (2012). Biodegradation of low molecular weight organic acids in rhizosphere soils from a tropical montane rain forest. *Soil Biol. Biochem.* 47, 142–148. doi: 10.1016/j.soilbio.2011.12.018

Geelhoed, J., Van Riemsdijk, W., and Findenegg, G. (1999). Simulation of the effect of citrate exudation from roots on the plant availability of phosphate adsorbed on goethite. *Eur. J. Soil Sci.* 50, 379–390. doi: 10.1046/j.1365-2389.1999.00251.x

Gerke, J. (2015). The acquisition of phosphate by higher plants: effect of carboxylate release by the roots. A critical review. *J. Plant Nutr. Soil Sci.* 178, 351–364. doi: 10.1002/jpln.201400590

Gerke, J., Beißner, L., and Römer, W. (2000). The quantitative effect of chemical phosphate mobilization by carboxylate anions on P uptake by a single root. I. The basic concept and determination of soil parameters. *J. Plant Nutr. Soil Sci.* 163, 207–212. doi: 10.1002/(SICI)1522-2624(200004)163:2<207::AID-JPLN207>3.0.CO;2-P

Göttlein, A., and Blasek, R. (1996). Analysis of small volumes of soil solution by capillary electrophoresis. *Soil Sci.* 161, 705–715. doi: 10.1097/00010694-199610000-00007

Henintsoa, M., Becquer, T., Rabeharisoa, L., and Gerard, F. (2017). Geochemical and microbial controls of the effect of citrate on phosphorus availability in a ferralsol. *Geoderma* 291, 33–39. doi: 10.1016/j.geoderma.2016.12.020

Hinsinger, P. (2001). Bioavailability of soil inorganic P in the rhizosphere as affected by root-induced chemical changes: a review. *Plant Soil* 237, 173–195. doi: 10.1023/A:1013351617532

Hinsinger, P., Bengough, A. G., Vetterlein, D., and Young, I. M. (2009). Rhizosphere: biophysics, biogeochemistry and ecological relevance. *Plant Soil* 321, 117–152. doi: 10.1007/s11104-008-9885-9

Hinsinger, P., Brauman, A., Devau, N., Gérard, F., Jourdan, C., Laclau, J.-P., et al. (2011). Acquisition of phosphorus and other poorly mobile nutrients by roots. Where do plant nutrition models fail? *Plant Soil* 348:29. doi: 10.1007/s11104-011-0903-y

Hoffland, E., Findenegg, G. R., and Nelemans, J. (1989). Solubilization of rock phosphate by rape: II. Local root exudation of organic acids as response to P-starvation. *Plant Soil* 113, 161–165. doi: 10.1007/BF02280176

Jones, D., and Brassington, D. (1998). Sorption of organic acids in acid soils and its implications in the rhizosphere. *Eur. J. Soil Sci.* 49, 447–455. doi: 10.1046/j.1365-2389.1998.4930447.x

Jones, D. L. (1998). Organic acids in the rhizosphere–a critical review. *Plant Soil* 205, 25–44. doi: 10.1023/A:1004356007312

Kaiser, C., Fuchslueger, L., Koranda, M., Gorfer, M., Stange, C. F., Kitzler, B., et al. (2011). Plants control the seasonal dynamics of microbial N cycling in a beech forest soil by belowground C allocation. *Ecology* 92, 1036–1051. doi: 10.1890/10-1011.1

Keiluweit, M., Bougoure, J. J., Nico, P. S., Pett-Ridge, J., Weber, P. K., and Kleber, M. (2015). Mineral protection of soil carbon counteracted by root exudates. *Nat. Clim. Change* 5, 588–595. doi: 10.1038/nclimate2580

Kuzyakov, Y. (2002). Factors affecting rhizosphere priming effects. *J. Plant Nutr. Soil Sci.* 165, 382–396. doi: 10.1002/1522-2624(200208)165:4<382::AID-JPLN382>3.0.CO;2-#

Lambers, H., Martinoia, E., and Renton, M. (2015). Plant adaptations to severely phosphorus-impoverished soils. *Curr. Opin. Plant Biol.* 25, 23–31. doi: 10.1016/j.pbi.2015.04.002

Lang, F., Krüger, J., Amelung, W., Willbold, S., Frossard, E., Bünemann, E. K., et al. (2017). Soil phosphorus supply controls P nutrition strategies of beech forest ecosystems in central europe. *Biogeochemistry* 136, 5–29. doi: 10.1007/s10533-017-0375-0

Li, Z., Hughes, D., Urban, J. P., and Cui, Z. (2008). Effect of pumping methods on transmembrane pressure, fluid balance and relative recovery in microdialysis. *J. Membr. Sci.* 310, 237–245. doi: 10.1016/j.memsci.2007.10.051

Luster, J., Göttlein, A., Nowack, B., and Sarret, G. (2009). Sampling, defining, characterising and modeling the rhizosphere—the soil science tool box. *Plant Soil* 321, 457–482. doi: 10.1007/s11104-008-9781-3

Mair, P., and Wilcox, R. (2020). Robust statistical methods in R using the WRS2 package. *Behav. Res. Methods* 52, 464–488. doi: 10.3758/s13428-019-01246-w

McGill, R., Tukey, J. W., and Larsen, W. A. (1978). Variations of box plots. *Am. Stat.* 32, 12–16. doi: 10.1080/00031305.1978.10479236

McKay Fletcher, D., Shaw, R., Sánchez-Rodríguez, A., Daly, K., Van Veelen, A., Jones, D., et al. (2019). Quantifying citrate-enhanced phosphate root uptake using microdialysis. *Plant Soil*. doi: 10.1007/s11104-019-04376-4. [Epub ahead of print].

McKay Fletcher, D. M., Ruiz, S., Dias, T., Petroselli, C., and Roose, T. (2020). Linking root structure to functionality: the impact of root system architecture on citrate-enhanced phosphate uptake. *New Phytol.* 227, 376–391. doi: 10.1111/nph.16554

Menezes-Blackburn, D., Paredes, C., Zhang, H., Giles, C. D., Darch, T., Stutter, M., et al. (2016). Organic acids regulation of chemical-microbial phosphorus transformations in soils. *Environ. Sci. Technol.* 50, 11521–11531. doi: 10.1021/acs.est.6b03017

Nguyen, C. (2003). Rhizodeposition of organic C by plants: mechanisms and controls. *Agronomie* 23, 375–396. doi: 10.1051/agro:2003011

Oburger, E., and Jones, D. L. (2018). Sampling root exudates-mission impossible? *Rhizosphere* 6, 116–133. doi: 10.1016/j.rhisph.2018.06.004

Oburger, E., Kirk, G. J., Wenzel, W. W., Puschenreiter, M., and Jones, D. L. (2009). Interactive effects of organic acids in the rhizosphere. *Soil Biol. Biochem.* 41, 449–457. doi: 10.1016/j.soilbio.2008.10.034

Preece, C., and Peñuelas, J. (2016). Rhizodeposition under drought and consequences for soil communities and ecosystem resilience. *Plant Soil* 409, 1–17. doi: 10.1007/s11104-016-3090-z

R Core Team (2018). *R: A Language and Environment for Statistical Computing*. Vienna: R Foundation for Statistical Computing.

Raven, J. A., Lambers, H., Smith, S. E., and Westoby, M. (2018). Costs of acquiring phosphorus by vascular land plants: patterns and implications for plant coexistence. *New Phytol.* 217, 1420–1427. doi: 10.1111/nph.14967

Raynaud, X., Jaillard, B., and Leadley, P. W. (2008). Plants may alter competition by modifying nutrient bioavailability in rhizosphere: a modeling approach. *Am. Nat.* 171, 44–58. doi: 10.1086/523951

Renella, G., Landi, L., Valori, F., and Nannipieri, P. (2007). Microbial and hydrolase activity after release of low molecular weight organic compounds by a model root surface in a clayey and a sandy soil. *Appl. Soil Ecol.* 36, 124–129. doi: 10.1016/j.apsoil.2007.01.001

Richardson, A. E., Lynch, J. P., Ryan, P. R., Delhaize, E., Smith, F. A., Smith, S. E., et al. (2011). Plant and microbial strategies to improve the phosphorus efficiency of agriculture. *Plant Soil* 349, 121–156. doi: 10.1007/s11104-011-0950-4

Schachtman, D. P., Reid, R. J., and Ayling, S. M. (1998). Phosphorus uptake by plants: from soil to cell. *Plant Physiol.* 116, 447–453. doi: 10.1104/pp.116.2.447

Scheerer, U., Netzer, F., Bauer, A., and Herschbach, C. (2019). Measurements of 18O-Pi uptake indicate fast metabolism of phosphate in tree roots. *Plant Biol.* 21, 565–570. doi: 10.1111/plb.12922

Schneider, K. D., Voroney, R. P., Lynch, D. H., Oberson, A., Frossard, E., and Bünemann, E. K. (2017). Microbially-mediated P fluxes in calcareous soils as a function of water-extractable phosphate. *Soil Biol. Biochem.* 106, 51–60. doi: 10.1016/j.soilbio.2016.12.016

Schnepf, A., Leitner, D., and Klepsch, S. (2012). Modeling phosphorus uptake by a growing and exuding root system. *Vadose Zone J.* 11:vzj2012.0001. doi: 10.2136/vzj2012.0001

Shahzad, T., Chenu, C., Genet, P., Barot, S., Perveen, N., Mougin, C., et al. (2015). Contribution of exudates, arbuscular mycorrhizal fungi and litter depositions to the rhizosphere priming effect induced by grassland species. *Soil Biol. Biochem.* 80, 146–155. doi: 10.1016/j.soilbio.2014.09.023

Shen, Y., Ström, L., Jönsson, J. Ä., and Tyler, G. (1996). Low-molecular organic acids in the rhizosphere soil solution of beech forest (*Fagus sylvatica* L.) cambisols determined by ion chromatography using supported liquid membrane enrichment technique. *Soil Biol. Biochem.* 28, 1163–1169. doi: 10.1016/0038-0717(96)00119-8

Stenström, J., Stenberg, B., and Johansson, M. (1998). Kinetics of substrate-induced respiration (SIR): theory. *Ambio* 27, 35–39. doi: 10.1080/010503998420630

van Hees, P. A., Jones, D. L., Finlay, R., Godbold, D. L., and Lundström, U. S. (2005a). The carbon we do not see—the impact of low molecular weight compounds on carbon dynamics and respiration in forest soils: a review. *Soil Biol. Biochem.* 37, 1–13. doi: 10.1016/j.soilbio.2004.06.010

van Hees, P. A., Jones, D. L., and Godbold, D. L. (2002). Biodegradation of low molecular weight organic acids in coniferous forest podzolic soils. *Soil Biol. Biochem.* 34, 1261–1272. doi: 10.1016/S0038-0717(02)00068-8

van Hees, P. A., Jones, D. L., Nyberg, L., Holmström, S. J., Godbold, D. L., and Lundström, U. S. (2005b). Modelling low molecular weight organic acid dynamics in forest soils. *Soil Biol. Biochem.* 37, 517–531. doi: 10.1016/j.soilbio.2004.08.014

Wang, Y., He, Y., Zhang, H., Schroder, J., Li, C., and Zhou, D. (2008). Phosphate mobilization by citric, tartaric, and oxalic acids in a clay loam ultisol. *Soil Sci. Soc. Am. J.* 72, 1263–1268. doi: 10.2136/sssaj2007.0146

Zavišić, A., Yang, N., Marhan, S., Kandeler, E., and Polle, A. (2018). Forest soil phosphorus resources and fertilization affect ectomycorrhizal community composition, beech P uptake efficiency, and photosynthesis. *Front. Plant Sci.* 9:463. doi: 10.3389/fpls.2018.00463

Zhang, J.-Z., and Chi, J. (2002). Automated analysis of nanomolar concentrations of phosphate in natural waters with liquid waveguide. *Environ. Sci. Technol.* 36, 1048–1053. doi: 10.1021/es011094v

**Conflict of Interest:** The authors declare that the research was conducted in the absence of any commercial or financial relationships that could be construed as a potential conflict of interest.

frontiers in Forests and Global Change

ORIGINAL RESEARCH
published: 20 January 2021
doi: 10.3389/ffgc.2020.577364

# Forest Soil Colloids Enhance Delivery of Phosphorus Into a Diffusive Gradient in Thin Films (DGT) Sink

*Alexander Konrad*[1]*, *Benjamin Billiy*[1], *Philipp Regenbogen*[1], *Roland Bol*[2], *Friederike Lang*[3], *Erwin Klumpp*[2] *and Jan Siemens*[1]

[1] *Institute of Soil Science and Soil Conservation, Justus-Liebig University Giessen, Giessen, Germany,* [2] *Research Centre Jülich, Institute of Bio- and Geosciences, Agrosphere (IBG-3), Jülich, Germany,* [3] *Faculty of Environment and Natural Resources, Chair of Soil Ecology, University of Freiburg, Freiburg im Breisgau, Germany*

Phosphorus (P) is preferentially bound to colloids in soil. On the one hand, colloids may facilitate soil P leaching leading to a decrease of plant available P, but on the other hand they can carry P to plant roots, thus supporting the P uptake of plants. We tested the magnitude and the kinetics of P delivery by colloids into a P sink mimicking plant roots using the Diffusive Gradients in Thin-Films (DGT) technique. Colloids were extracted with water from three forest soils differing in parent material using a method based on dispersion and sedimentation. Freeze-dried colloids, the respective bulk soil, and the colloid-free extraction residue were sterilized and mixed with quartz sand and silt to an equal P basis. The mixtures were wetted and the diffusive fluxes of P into the DGTs were measured under sterile, water unsaturated conditions. The colloids extracted from a P-poor sandy podzolic soil were highly enriched in iron and organic matter compared to the bulk soil and delivered more P at a higher rate into the sink compared to bulk soil and the colloid-free soil extraction residue. However, colloidal P delivery into the sink was smaller than P release and transport from the bulk soil developed on dolomite rock, and with no difference for a soil with intermediate phosphorus-stocks developed from gneiss. Our results provide evidence that both the mobility of colloids and their P binding strength control their contribution to the plant available P-pool of soils. Overall, our findings highlight the relevance of colloids for P delivery to plant roots.

**Keywords: plant nutrition, ecosystem nutrition, colloid-facilitated transport, cambisol, beech, DGT technique, phosphorus, soil**

OPEN ACCESS

***Edited by:***
*Jennifer L. Soong, Colorado State University, United States*

***Reviewed by:***
*Erik Smolders, KU Leuven, Belgium*
*Hao Zhang, Lancaster University, United Kingdom*

***Correspondence:**
*Alexander Konrad*
*alexander.konrad@umwelt.uni-giessen.de*

***Specialty section:***
*This article was submitted to Forest Soils, a section of the journal Frontiers in Forests and Global Change*

***Received:*** *29 June 2020*
***Accepted:*** *22 December 2020*
***Published:*** *20 January 2021*

***Citation:***
*Konrad A, Billiy B, Regenbogen P, Bol R, Lang F, Klumpp E and Siemens J (2021) Forest Soil Colloids Enhance Delivery of Phosphorus Into a Diffusive Gradient in Thin Films (DGT) Sink. Front. For. Glob. Change 3:577364. doi: 10.3389/ffgc.2020.577364*

## INTRODUCTION

Intact forest ecosystems are of extraordinary relevance for biodiversity, the functioning of biogeochemical cycles, landscape water balance and human health (Watson et al., 2018). Phosphorus (P) is an essential element for all living organisms (Elser et al., 2007) and a major limiting factor for the productivity of forest ecosystems, as well as an important driver for soil and ecosystem development (Vitousek et al., 2010; Lang et al., 2017). Recent studies indicate that forests may lose their ability to recycle P due to climate change and enhanced global nitrogen (N) input (Jonard et al., 2015). Understanding the functioning of forest ecosystems and their nutrient cycles is therefore of utmost importance for their protection and sustainable use.

Natural soil colloids (diameter <1,000 nm) embody the smallest particulate phase in soils. Colloids bind larger amounts of P through their high specific surface area compared to other soil

components (de Jonge et al., 2004). These particles are formed through weathering, the formation of secondary minerals and the incomplete degradation of organic material (e.g., Missong et al., 2016). Due to their small size, colloids are subject to Brownian motion so that they diffuse through the soil solution, whereby smaller particles are more strongly influenced by the Brownian motion and diffuse faster than large colloids (e.g., Molnar et al., 2019).

The importance of colloids for P-binding and -transport in agricultural soils, which receive P-containing fertilizers, has been recognized for quite some time (e.g., Haygarth et al., 1997; Jacobsen et al., 1997; de Jonge et al., 2004; Heathwaite et al., 2005; Ilg et al., 2005; Jiang et al., 2015; Li et al., 2020). More recently, the importance of colloids for P-binding and –transport was also shown for unfertilized forest soils (Bol et al., 2016; Gottselig et al., 2017a,b, 2020; Missong et al., 2018a,b; Wang et al., 2020). These studies revealed that the P-content of colloids of acidic forest soils was up to 16 times larger than the P-contents of the corresponding bulk soils (Missong et al., 2018b). They also showed that up to 91% of the P leached from forest topsoils was not truly dissolved, but bound to colloids (Missong et al., 2018a). Determined by field flow fractionation, these colloids could be subdivided into three size classes of particles smaller than 25 nm rich in organic carbon (C), particles between 25 and 240 nm composed mainly of organic C, iron (Fe), silicon (Si), and aluminum (Al), and finally particles between 240 and 500 nm with an important contribution of phyllosilicates (Missong et al., 2018a). In calcareous forest soils, calcium (Ca) was the primary metallic element in water-dispersible colloids (WDC) (Wang et al., 2020).

The availability of P bound to colloids for plant uptake is crucial for evaluating the relevance of particle-facilitated P-leaching and redistribution for P-cycling in ecosystems. If the P bound to colloids would be well-accessible for plants, then transport of P from intensely rooted topsoils into deep subsoils or out of the ecosystem together with colloids would have severe consequences for the P supply to the vegetation and the stability of ecosystems. Montalvo et al. (2015a) demonstrated that colloids from a volcanic soil (Andosol) could also act as P-carriers supporting the diffusional transport of P to plant roots and the subsequent P-uptake of plants in hydroponic systems, while no such effect was observed for particles derived from a strongly weathered tropical soil (Oxisol). Based on their finding that ortho-P and hexamethaphosphate bound to Fe-oxide colloids were well-accessible for spinach grown in nutrient solution, Bollyn et al. (2017) emphasized the potential role of pedogenic Fe-oxides for the P-availability in soils and the possibility of using synthetic Fe-oxides as nanofertilizer facilitating P transport to roots. Therefore, an important question is whether colloids from more widely distributed soils of temperate climate zones, like Cambisols, could also support the diffusional P transport to roots and whether this process does also occur in porous media under water-unsaturated moisture conditions. Unsaturated porous media provide many opportunities for attachment of colloids to water-solid interfaces and water-air interfaces or their entrapment in thin water films (Kretzschmar et al., 1999; Flury and Aramrak, 2017). Hence, the enhancement of diffusional colloidal P transport to roots or similar P sinks might be less relevant in water-unsaturated porous media, like most terrestrial soils, than in hydroponic systems. Indeed, Bollyn et al. (2019) observed no additional fertilizer effect of P bound to Fe-oxide nanoparticles compared to soluble $KH_2PO_4$ when added to strongly weathered tropical soils. They argued that the much smaller diffusion coefficient of colloids compared to ortho-phosphate in combination with its lower bioavailability were responsible for this lacking additional fertilizer effect in relation to ortho-phosphate. Nevertheless, the experiments of Bollyn et al. (2019) demonstrated that P bound to Fe-oxides increased plant growth and P uptake relative to a zero P control, indicating that it can be used by plants at least partly.

We examined the delivery of P bound to natural soil colloids from forest soils to artificial P sinks in comparison to P-delivery from colloid-free soil and bulk soil. To this end, we extracted colloids from three forest soils differing in parent material and soil P stock with water. For each of the three soils, the colloids, the colloid-free extraction residue and the respective bulk soil were mixed with quartz silt and sand and P-delivery into artificial P-sinks was quantified at a moisture content equal to 90% water-holding capacity using the Diffusive Gradients in Thin-Films technique (DGT) (Zhang et al., 1998). DGT is based on the continuous depletion of P in the soil solution around the sampler. Reduced P concentrations are then compensated by desorption of P from the soil solid phase. DGT therefore measures the P fraction that can be released into soil water and transported to a sink after soil solution depletion, thus simulating the diffusive uptake of P by plant roots (Kruse et al., 2015). For soils in which P uptake by plants is limited by diffusion, DGT is a good predictor of plant-available P (Degryse et al., 2009), since DGT mainly extracts plant-available P as shown by $^{33}P$ isotope dilution studies (Six et al., 2012; Mason et al., 2013). Considering that the mobility of WDC by diffusion and the lability of colloid-bound P are important drivers for their role in ecosystems, the DGT technique provides valuable insights into the behavior of WDC at the root-soil interface. We hypothesized that: (1) colloids deliver more P at a faster rate into the P-sink than bulk soil and colloid-free residual soil, and that (2) soil properties control the magnitude and the kinetics of colloid-facilitated P-delivery into a nutrient sink according to their impact on colloid mobility, the partitioning of P between WDC and non-dispersible soil material and the P binding strength of colloids. Thus, soil properties control the potential relevance of colloids for plant nutrition.

**Abbreviations:** Al, aluminum; C, carbon; Ca, calcium; Co, cobalt; DGT, Diffusive Gradients in Thin-Films; DOM, dissolved organic matter; FDR, false discovery rate; Fe, iron; ICP-OES, inductively coupled plasma optical emission spectrometry; LUE, Lüss; MAN, Mangfall; MIT, Mitterfels; NTA, nanoparticle tracking analysis; OM, organic matter; P, phosphorus; Si, silicon; WDC, water-dispersible colloids.

## MATERIALS AND METHODS

### Forest Sites

Disturbed soil samples from A-horizons and the O/A-transition horizon were collected from three mature beech forest sites in Germany in a sampling campaign in summer 2017. All sites

**TABLE 1 |** Characteristics of the study sites Mangfall (MAN), Mitterfels (MIT) and Lüss (LUE) (Prietzel et al., 2016; Lang et al., 2017).

| Study site | MAN | MIT | LUE |
|---|---|---|---|
| Location (WGS84) | N: 47.608364° | N: 48.976008° | N: 52.838967° |
| | E: 11.817519° | E: 12.879879° | E: 10.267250° |
| Soil type (WRB, 2015) | Rendzic Leptosol (Rendzina) | Hyperdystric chromic folic cambisol (Humic, Loamic, Nechic) | Hyperdystric folic cambisol (Arenic, Loamic, Nechic, Protospodic) |
| Parent material | Dolostone (Triassic) | Paragneiss | Sandy till |
| Humus form (*ad-hoc*-AG Boden 2005) | Mull | Moder | Mor-like moder |
| Altitude (m a.s.l.) | 1,130 | 1,023 | 115 |
| Mean annual precipitation (mm) | 2,110 | 1,299 | 779 |
| pH (measured in $H_2O$) | 7 | 3.8 | 3.5 |
| $P_{resin}$ A horizon (mg $kg^{-1}$) | 56 | 70 | 11 |

**TABLE 2 |** Elemental composition of P-sources of the study sites Mangfall (MAN), Mitterfels (MIT), and Lüss (LUE) after microwave-assisted extraction and ICP-OES and TOC/TN measurements in [g $kg^{-1}$], including C:N and C:P ratios.

| Site | Fraction | Elemental composition [g $kg^{-1}$] | | | | | | C:N ratio | C:P ratio |
|---|---|---|---|---|---|---|---|---|---|
| | | Al | Ca | Fe | *P* | C | *N* | | |
| MAN | Bulk soil | 38.59 | 71.61 | 20.84 | 0.97 | 199.40 | 9.30 | 21:1 | 151:1 |
| | Residual soil | 36.79 | 73.92 | 19.93 | 0.97 | 172.80 | 7.40 | 23:1 | 191:1 |
| | WDC | 76.08 | 26.02 | 36.84 | 1.57 | 111.80 | 10.20 | 11:1 | 39:1 |
| MIT | Bulk soil | 34.00 | 0.87 | 29.22 | 1.17 | 178.50 | 8.60 | 21:1 | 115:1 |
| | Residual soil | 32.48 | 0.89 | 28.14 | 1.04 | 253.20 | 13.50 | 19:1 | 215:1 |
| | WDC | 49.72 | 0.85 | 60.65 | 3.26 | 305.60 | 39.30 | 8:1 | 48:1 |
| LUE | Bulk soil | 5.84 | 0.41 | 3.92 | 0.14 | 58.60 | 2.30 | 52:1 | 119:1 |
| | Residual soil | 5.17 | 0.41 | 3.44 | 0.13 | 164.40 | 6.50 | 52:1 | 1,107:1 |
| | WDC | 43.96 | 0.98 | 49.14 | 1.91 | 244.80 | 16.30 | 15:1 | 77:1 |

were similar with regard to their forest stand characteristics (tree species composition and stand age), while they differed in the source material of soil formation (**Table 1**) and therefore in their soil P-stock and -availability (Lang et al., 2016, 2017; Prietzel et al., 2016). The soil sampled at the Mitterfels site (MIT) developed on paragneiss and had the highest P content (**Tables 1**, **2**), followed by the sample from the calcareous site Mangfall (MAN) located in the dolomite alps the with a slightly smaller P content, while the sample from the sandy podzolic soil of the site Lüss (LUE) had a much smaller P content (**Tables 1**, **2**). For further information regarding the sites visit https://www.ecosystem-nutrition.uni-freiburg.de/.

## Extraction and Preparation of Water-Dispersible Colloids

Water-dispersible colloids (WDC) were extracted from topsoil samples from the MAN, MIT and LUE sites following an extraction routine based on suspension in water with subsequent sedimentation and centrifugation steps developed by Séquaris and Lewandowski (2003) and Missong et al. (2016). The centrifugation times for the separation of colloids were determined according to Hathaway (1956) to separate the WDC fraction <700 nm. First 0.2 L demineralized water was added to 100 g sample material and shaken on an overhead shaker for 6 h. Subsequently 0.6 L demineralized water was added, the suspension was left to settle for 20 min and the supernatant was pipetted off. The supernatant was centrifuged at 4,000 g for 4 min and the supernatant was removed by pipette. The supernatant after centrifugation was centrifuged again at 14,000 g for 90 min and the supernatant discarded, thus we potentially lost the smallest WDC. The amount of P bound to WDC lost with the supernatants was quantified through separation from dissolved P using dialysis tubes (Spectrum™ Labs Spectra/Por™ 7, Repligen Corporation, Rancho Dominguez, USA) with subsequent colorimetric measurements (Van Veldhoven and Mannaerts, 1987). The sedimented portion after this process step formed the WDC P-source, while the sedimented soil components after shaking and sedimentation, as well as the sedimented soil components after centrifugation at 4,000 g formed the colloid-free residual soil fraction. The WDC suspensions obtained by extraction were shock-frozen in 45 mL PE bottles using liquid nitrogen. The caps of the PE bottles were then removed and replaced with fine-pored filters (GE Whatman™ SG81, GE Healthcare Bio-Sciences, Marlborough, USA) for freeze-drying (Christ Beta 1–8 LSCplus, Martin Christ Gefriertrocknungsanlagen GmbH, Osterode am Harz, Germany). The dried WDC powders were subsequently transferred into 1 L PE bottles and homogenized for 6 h using an overhead shaker.

Bulk soil and residual soil (residue of the WDC-extraction) were dried in a drying cabinet at 40°C. After drying, bulk soil, residual soil and WDC were sterilized with a $^{60}Co$ source as described by Dalkmann et al. (2014) to prevent microbial cycling of P. Total C and -N contents of the P-sources were measured using an vario MAX cube (Elementar Analysensysteme GmbH, Langenselbold, Germany). Aliquots (0.5 g) of the three different P-source materials were digested using 5 mL 69% $HNO_3$, 3 mL 30% $H_2O_2$ (both ROTIPURAN® Supra, Carl Roth GmbH + Co. KG, Karlsruhe, Germany) and 5 mL $H_2O$ by microwave-assisted extraction (Öztan and Düring, 2012) and the P-contents were determined by inductively coupled plasma optical emission spectrometry (ICP-OES) (Agilent 720 ICP-OES ES, Agilent Technologies Inc., Santa Clara, USA) as specified in DIN ISO 22036:2009-06 at the element-specific wavelength of 213.618 nm. Particle size distributions of WDC were obtained by Nanoparticle Tracking Analysis (NTA). Three replicates of WDC suspension from every site were analyzed using the laser unit NanoSight LM 14 (Malvern Panalytical Ltd., Malvern, United Kingdom) combined with the microscope NanoSight LM 10 (Malvern Panalytical Ltd., Malvern, United Kingdom). Images were evaluated by the NTA 3.0 software (Malvern Panalytical Ltd., Malvern, United Kingdom) (**Supplementary Material 1**).

## Test System

A mixture of 60 mass-% quartz sand and 40 mass-% quartz silt (20.5 g in total, Gebrüder Dorfner GmbH & Co., Hirschau, Germany) were filled into 60 mL screw-cap beakers made of polycarbonate (Thermo Fisher Scientific, Waltham, Massachusetts, USA). The particle size composition of the quartz mixture determined according to DIN 19683/2 was 1.0% medium sand, 60.4% fine sand, 20.0% coarse silt, 12.3% medium silt, 4.1% fine silt, and 2.2% clay. After autoclaving, the beakers were opened in a sterile environment and the equivalent of 1 mg P of a P-source [bulk soil, residual soil or WDC of the sites MAN, MIT, and LUE, as well as an ortho-phosphate solution (Certipur®, Merck KGaA, Darmstadt, Germany) as a positive control] was filled into a screw-cap beaker. The screw-cap beakers were closed again and mixed for 6 h on an overhead shaker (Heidolph REAX 2, Heidolph Instruments GmbH & CO. KG, Schwabach, Germany). The screw-cap beakers were then opened again in a sterile environment and autoclaved water was added with an air cushion pipette until 90% of the water holding capacity was reached. The water holding capacity of the porous media including the individual soil fractions was determined in preliminary tests according to Alef (1998, p. 106). The screw cap beakers were then closed for 24 h. During this time, an equilibrium of P between the added water and the soil solid phase was established. The screw-cap beakers were opened again in the sterile environment and one DGT [LSLP-NP Loaded DGT device for P and metals (B) in soil, DGT Research, Quernmore, Great Britain] was inserted in each beaker and gently pressed into the substrate. The screw cap beakers were closed and the DGTs were removed after 24, 48, 72, 120, and 168 h, with three DGTs per treatment removed after 48 h. The ambient temperature during the experiment was kept constant at 22 ± 0.3°C. The semi-permeable filter membranes were rinsed with demineralized water afterwards to stop the mass transport into the device. The DGTs were opened at the groove of the housing and the diffusion layers together with the semipermeable membrane, as well as the ferrihydrite gels were transferred to 2 mL Safelock tubes (Eppendorf AG, Hamburg, Germany) and stored at 4°C until further analysis. The ferrihydrite gels were than eluted with 0.25 M $H_2SO_4$ as described by Zhang et al. (1998). The P-concentrations of the eluates were determined using the method of Van Veldhoven and Mannaerts (1987) after formation of phosphomolybdate complexes with malachite green and measured at 630 nm by a UV/Vis photometer (T80 Spectrophotometer, PG Instruments Ltd., Lutterworth, Great Britain) (**Supplementary Material 2**). Additionally the diffusion layers of the disassembled DGTs after 168 h exposure time to the P-sources were rinsed with water and Al, Ca, Fe, and P concentrations in the gels were determined using ICP-OES after microwave-assisted digestion similar to the P-sources, using 5 mL 69% $HNO_3$, 3 mL 30% $H_2O_2$, and 5 mL $H_2O$ for each gel. Due to the harsh extractant used and the high temperatures, the resulting concentrations can be interpreted as total elemental concentrations.

## Statistical Analysis

The statistical evaluation of the measurements after 48 h was performed with R (version 3.5.1, The R Foundation for Statistical Computing, Vienna, Austria) and RStudio (version 1.1.456, RStudio Inc., Boston, USA). The software packages used included lme4 (v. 1.1.21), lsmeans (v. 2.30.0) multcomp (v. 1.4.10), and multcompView (v. 0.1.7). The script can be found in the **Supplementary Material 3**. The cumulated amount of P in the sinks delivered from the bulk soil, residual soil, or WDC of the sites after 48 h were investigated by pairwise comparisons using the *t*-test statistics after testing of homogeneity of variances (Bartlett, 1937). The mean values of the pairwise comparisons were adjusted using the false discovery rate (FDR) (Benjamini and Hochberg, 1994). The kinetics of P accumulation in the DGTs after 24, 48, 72, 120, and 168 h were calculated and evaluated with SigmaPlot Version 12.0 (Systat Software GmbH, Erkrath, Germany). The transport of P from the P-source into the sink of the DGT device is controlled by two kinetic processes, the desorption of P from the solid phase (WDC, bulk soil or residual soil) into the aqueous phase and the diffusion of dissolved P (and colloidal P) through the aqueous phase into the DGT. Both kinetic processes result in a decreasing amount of P delivered to the DGTs per unit time with increasing duration of the experiment. We therefore decided to describe the delivery of P into the DGTs by means of an empirical first order law of velocity model that lumps the desorption rate constant and the diffusion rate constant into one effective parameter (Atkins and de Paula, 2013, p. 840):

$$A_t = A_0 \times (1 - e^{-pt})$$

With $A_0$ as the total amount of P delivered into the P-sinks up to $t = \infty$ [μg], $p$ as the release and transport rate of P [$h^{-1}$] and $t$ as the time of measurement [h]. We assume that the number of five points of time of our experiments would not have allowed

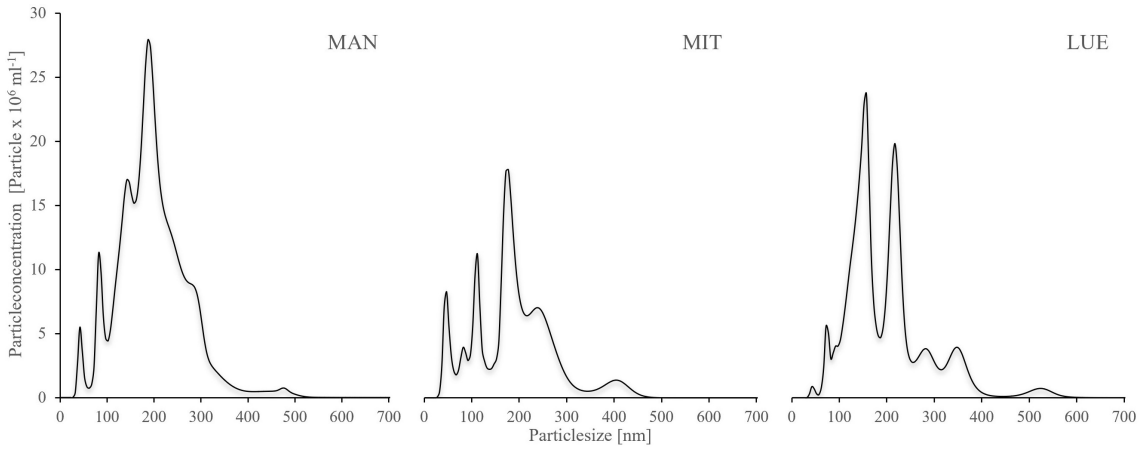


**FIGURE 1 |** Size distribution of the WDC extracted from the topsoils of the sites Mangfall (MAN), Mitterfels (MIT), and Lüss (LUE), determined using Nanoparticle Tracking Analysis (NTA). NTA is capable of measuring natural colloids >50 nm, thus smaller particles were not detected. Size distribution showed three main peaks across all three sites, one around 50 nm, one between 100–150 nm and one around 200–250 nm. Most larger particles were found at MAN, followed by MIT and LUE. A tabular list of particle sizes and particle concentrations is given in the **Supplementary Material 1**.

the estimation of desorption rate constants and diffusion rate constants independently.

# RESULTS

## Elemental Composition of Soils and Their Fractions

The largest Al- and Ca-concentrations were found for MAN soil (**Table 2**), while MIT soil showed the largest Fe-concentrations. The WDC of all three sites were enriched in the elements Al, Fe, and P compared to the bulk soil and the residual soil (WDC > bulk soil > residual soil). Most striking is the much stronger enrichment of Fe (WDC/bulk soil ratio of 13:1) and P (WDC/bulk soil ratio of 14:1) in the WDC of the sandy site LUE compared to the MAN soil (Fe ratio of 1.8:1, P ratio of 1.6:1) and MIT soil (Fe ratio of 2.1:1, P ratio of 2.8:1). Moreover, WDC had smaller C:N and C:P ratios than bulk soil and residual soil. While C was enriched in the WDC fraction of MIT and LUE in comparison to the bulk soil, a depletion of C was found for MAN. Analysis of the supernatants after centrifugation at 14,000 g revealed that 3.3% (LUE), 2.9% (MIT), and 0.6% (MAN) of WDC bound P got discarded during WDC extraction.

## WDC Size Distribution

The mean size of the WDC particles was similar for the three sites with an average of 195 nm for MAN (median 188 nm), 188 nm for MIT (median 180 nm), and 195 nm for LUE (median 173 nm). However, the size distribution of particles differed between sites (**Figure 1**). The WDC size distribution was characterized by three main peaks, one around 50 nm particle size, one around 100–150 nm particle size and one around 200–250 nm particle size. The share of the largest size fraction of the particles decreased in the order MAN > MIT > LUE. The WDC of LUE contained the largest concentration of the medium-sized collodial particles. Data from NTA can be found in the **Supplementary Material 1**.

## Delivery of P Into the DGTs

The largest amounts of P were found in the DGTs in contact with the ortho-phosphate—solution of the positive control (24 h: 37.3 μg; 48 h: 51.2 μg, 47.7 μg, 44.6 μg; 72 h: 40.18 μg; 120 h: 60.1 μg; and 168 h: 63.0 μg). The regression models of the P-supply into the DGTs and the statistical evaluation of the DGT measurements after 48 h revealed differences in the supply of P from the bulk soils, WDC and residual soils of the different sites into the DGTs (MAN < MIT < LUE) (**Figure 2** and **Table 3**). Furthermore, the order of the rates of P–release and –transport from the three P-sources into the DGTs varied between sites. While P-release and –transport increased in the order WDC < residual soil < bulk soil for MAN, the order was residual soil < bulk soil = WDC for MIT, and residual soil < bulk soil < WDC for LUE. Multiple pairwise comparisons of the cumulated P quantities in the DGTs after 48 h between the P-sources showed no significant differences ($p < 0.05$) at the MAN site. However, significant differences between residual soil on the one hand and bulk soil and WDC on the other hand at the MIT site, and significantly different rates of P-release and -transport between all fractions at the LUE site (**Table 3**) were observed. The WDC of the P-rich, calcareous MAN site supplied the smallest P quantities in the experiment both over 48 h and the entire (168 h) measurement period. In contrast, the largest P quantities from P-sources derived from soil were delivered by the WDC of the LUE site, which after 48 h supplied on average 74 times the quantity of P as the WDC of the MAN site (**Table 3**). In addition to the highest cumulated P quantities, the regression model for the P-release and –transport from the WDC of the LUE site into the DGTs indicated no decrease in the P-replenishment rate over the experimental time span of 168 h (**Figure 2**). Furthermore, when disassembling the DGTs in contact with the WDC of the LUE

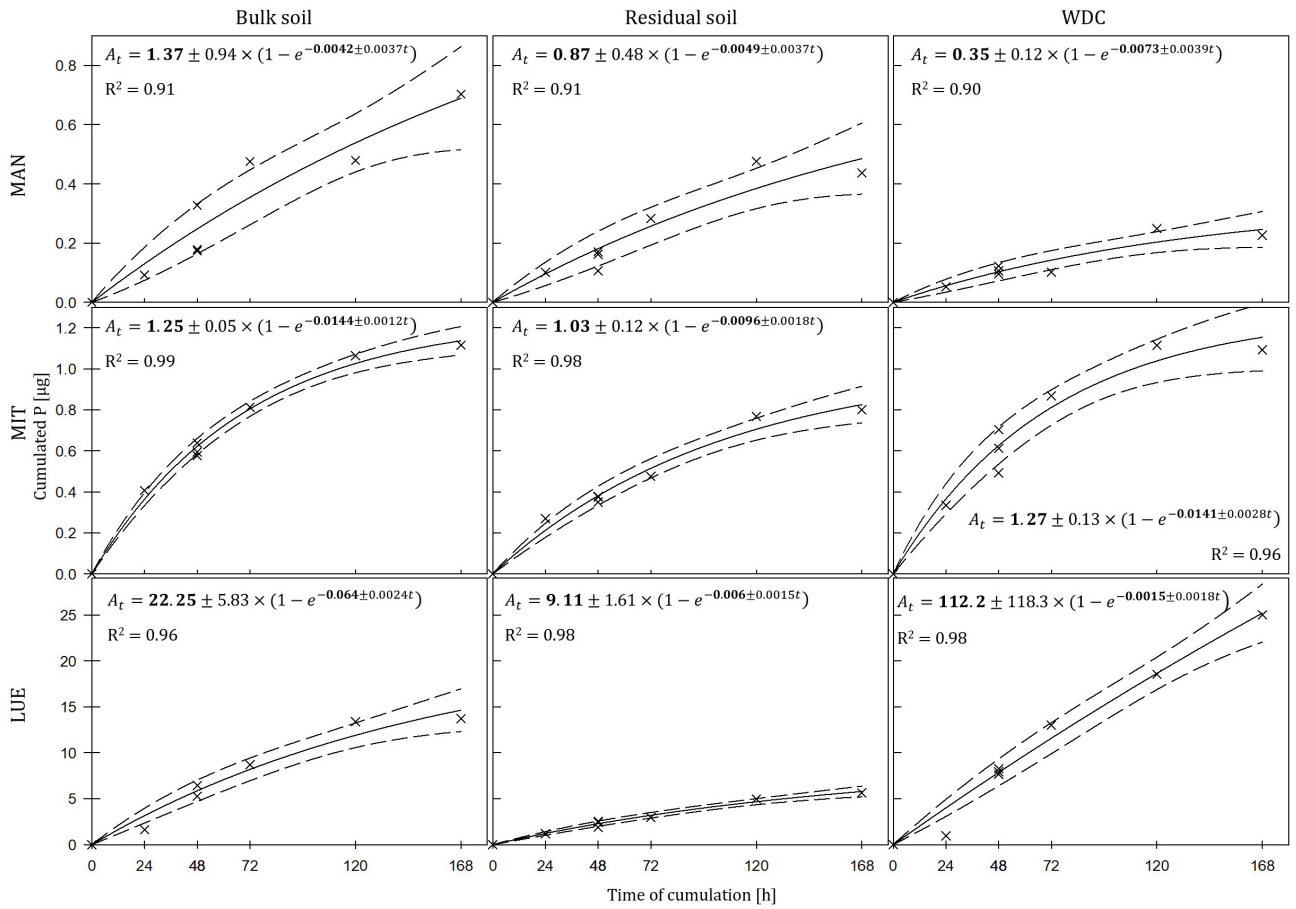


**FIGURE 2 |** Kinetics of P-delivery by bulk soil, residual soil, and WDC of the sites Mangfall (MAN), Mitterfels (MIT), and Lüss (LUE). P quantities cumulated in DGTs after 24, 48, 72, 120, and 168 h are displayed with crosshairs, the regression models with lines and the corresponding 95% confidence intervals with dashed lines. Note the different scaling of y-axes for the three sites. The estimated parameters are shown in bold ± their standard error.

site a dark brown suspension between diffusion gel and filter membrane and a coloration of the diffusion gel (**Figure 3**), as well as a dark brown coloration of the nutrient sinks themselves (**Figure 4**) were recognized. These colorations also occurred to a small extent in the gel layers and nutrient sinks that were in contact with the WDC fraction of the MIT site, while they were absent in gel layers and nutrient sinks that were in contact with the WDC fraction of the MAN site. The elemental analyzes of the diffusion layers after 168 h exposure time to the P-sources by ICP-OES after microwave-assisted extraction revealed that gels used for bulk soil and the colloid-free soil residuals from the calcareous site MAN contained the largest amount of Ca in the experimental setup, while no Ca was traceable in the gels in contact with WDC from this site (**Table 4**). Furthermore, Al and Fe were absent in the diffusion layer in contact with WDCs extracted from MAN. In contrast, the highest amounts of Al and Fe were detected in the colored gel of the WDC from the LUE site, while the WDCs from the Fe-rich MIT site contained in comparison only marginal amounts of Fe in the gel.

# DISCUSSION

## P-Release From the Solid Phase of the Different Soils and Soil Fractions

The delivery of P to the DGTs by different P-sources reflected the speciation, binding, and solubility of P in the soils. Prietzel et al. (2016) demonstrated with X-ray absorption near-edge structure spectroscopy (XANES) that in the Ah horizon of the calcareous MAN site, P is present mainly in organic form (either bound to Ca, most likely as precipitate of Ca and inositol hexakisphosphate or as unsorbed organic P), as well as in inorganic form bound to Al-(hydr)oxides. These P-forms show low solubility (precipitates) or desorbability [Al-(hydr)oxides] at the given pH-value of 7.0, resulting in marginal amounts of P transported into the sinks compared to MIT and LUE. The sandy soil of the LUE site features a low sorption capacity for inorganic P (Lang et al., 2017). In line with this limited P sorption capacity, a large fraction of water-soluble P of most likely microbial origin was detected for the Ae horizon at LUE (Lang et al., 2017). Both, the limited P sorption capacity of the soil material and the large

**TABLE 3 |** Mean values and standard deviations of P delivered into the DGTs within 48 h by different P-sources ($n = 3$).

| Site | Soil fraction | Mean [μg] | *SD* | Group |
|---|---|---|---|---|
| MAN | Bulk soil | 0.227 | 0.071 | a |
| | Residual soil | 0.147 | 0.029 | a |
| | WDC | 0.108 | 0.012 | a |
| MIT | Bulk soil | 0.603 | 0.026 | a |
| | Residual soil | 0.368 | 0.013 | b |
| | WDC | 0.603 | 0.086 | a |
| LUE | Bulk soil | 5.661 | 0.561 | a |
| | Residual soil | 2.291 | 0.287 | b |
| | WDC | 7.961 | 0.246 | c |

*Significant differences in the accumulated amount of P in the DGTs delivered by the P-sources from each site were determined by multiple pairwise comparisons after testing for variance homogeneity (Bartlett, 1937). Mean values of the pairwise comparisons were adjusted using the "False discovery rate" (Benjamini and Hochberg, 1994). Different letters in the rightmost column indicate significantly different P delivery by P-sources of the same sampling site Mangfall (MAN), Mitterfels (MIT), or Lüss (LUE) ($p < 0.05$).*

fraction of water-soluble P likely promoted the delivery of P by the LUE bulk soil in the DGTs.

## Delivery of P Bound to WDC Into the DGTs

Water-dispersible colloids from the P-poor LUE site delivered significantly more P into the DGTs than the bulk soil or the colloid-free residual P-source. The almost linear increase in cumulated P over time from the LUE WDC indicated the immediate compensation of the depleted P concentration in the pore water surrounding the DGTs. This phenomenon was not observed for any other soil fraction at the other sites. Noteworthy, the amount of P cumulated over the measurement period of 168 h in the DGTs in contact with the LUE WDC exceeded the P-capacity of the DGTs of 6.7 μg (Zhang et al., 1998). Although P can be sorbed to the ferrihydrite P-sink above this P-capacity, the ferrihydrite binding sites were already loaded to such extent that P-species were likely not immediately removed from the gel surrounding the ferrihydrite so that the rate of P-accumulation in the DGTs should have decreased over time (Davison and Zhang, 2012). Considering the distinctly increased Fe and P content in the WDC fraction compared to the bulk soil at the site LUE, the measured P flux into the DGT, as well as the coloration of diffusion gel and nutrient sink inside the DGTs (**Figures 3**, **4**), the intensive P delivery by LUE WDC could have been caused by mobile OM-Al(Fe)-P complexes (Gerke, 2010) dissolved organically-bound P (e.g., phosphate esters) and mobile OM-Al- and Fe-containing WDC (Jiang et al., 2017). This assumption is supported by the analysis of the diffusion gels using ICP-OES, showing the diffusion of Al, Ca, and Fe into the samplers. Because the gels were rinsed thoroughly before digestion, we assume that most measured complexes, molecules, and WDC have diffused into the gels and were not just attached to its surface. Since the diffusion layer and the nutrient sink use the same type of gel, P-containing compounds that diffused into the diffusion layer may have also diffused into the nutrient sink over time. It must be stated that the use of the colorimetric method might exclude a part of organic P transported into the DGT. The digestion of the gels with 0.25 M $H_2SO_4$ and the malachite green method however likely released most P bound to DOM (Baldwin, 1998), OM-Al/Fe complexes (Gerke, 2010), and colloids (Stainton, 1980) through hydrolysis and quantified it in addition to ortho-phosphate. Nevertheless, we likely underestimated the total amount of P translocated into the sinks.

The potential of the DGT technique to measure the transport of colloids into a nutrient sink depends on whether these compounds can diffuse through the filter membrane and the diffusive gel layer during the time of the experiment (Davison and Zhang, 2012). The polyethersulfone filter membrane used in the DGTs has a pore width of 450 nm and should be permeable for most WDC in our experiment. While (Zhang and Davison, 1999) stated the average pore size of polyacrylamide gels cross-linked with agarose derivative used for diffusive gel layers with radii >5 nm, van der Veeken et al. (2008) demonstrated the diffusion of latex particles with radii up to 129 nm into these gels. However, diffusion coefficients ($D_c$) strongly decrease with increasing spherical diameter of the particle according to the Stokes-Einstein equation. As a result, WDC particles or large molecules diffuse much slower than ions like ortho-phosphate. For example, $D_c$ in water is 9.5 $10^{-11}$ $m^2$ $s^{-1}$ for a spherical particle of 5 nm, 5.95 $10^{-12}$ $m^2$ $s^{-1}$ for 80 nm, and 2.4 $10^{-12}$ $m^2$ $s^{-1}$ for 200 nm diameter ($T = 295.15$ K, **Supplementary Material 4**). We used particle $D_c$ to estimate the distance they could travel due to Brownian motion based on their "mean squared displacement." The square root of this estimate indicated that very small particles of 5 nm diameter could have moved 10 mm on average during the 168 h of the experiment, much more than the thickness of the diffusion layer of 0.8 mm. Further calculations, now assuming an equal mix of 5, 80, and 200 nm sized colloids and a density of 2 g $cm^{-3}$ for all particles estimate colloid concentrations to be in the order of 1.7–5.1 $10^{-8}$ mol $l^{-1}$. These concentrations could have been large enough to cause a potential diffusion of all added 5 nm colloids and even 21% of the added 80 nm diameter colloids across the diffusion layer into the DGT sink during the 168 h of our experiment (**Supplementary Material 4**). Hence, it appeared possible that the diffusion of mobile colloids was an important reason for the fast and constant delivery of P into the DGTs in contact with the LUE WDC.

Unfortunately the used particle tracking analysis is not able to quantify natural colloids <50 nm properly due to technical restrains (Gallego-Urrea et al., 2011). Therefore, a larger portion of particles smaller than 50 nm might have been present in the WDC of LUE than indicated by the NTA data of **Figure 1**. Overall, the results for the LUE site supported our hypothesis that colloids supply P more efficiently into a P sink than bulk soil or colloid-free residual soil.

Montalvo et al. (2015a,b) demonstrated that colloids and nanoparticles carry P to root surfaces, thereby contributing to the P supply and uptake of plants in hydroponic systems and under water-saturated soil conditions. However, especially in most agricultural soils except Hydragic Anthrosols (WRB, 2015, "paddy rice soils"), water-saturated conditions occur rarely and if, then only for very limited periods of time. Under more common

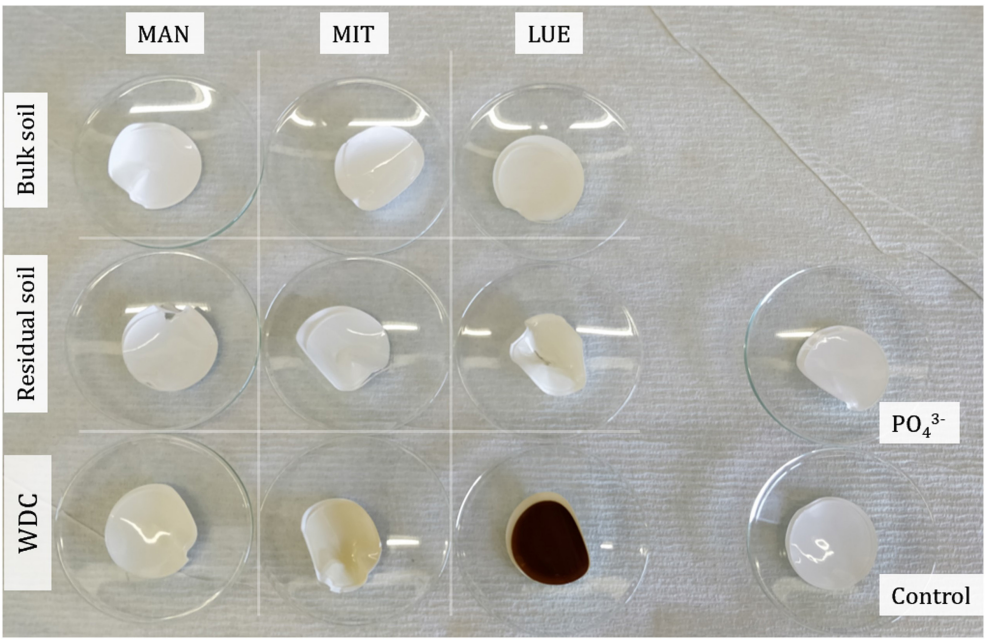


**FIGURE 3 |** Diffusion gels and filter membranes of the disassembled DGTs after 168 h accumulation time of all *P*-sources and sites. The diffusion gel of the WDC from the site Lüss (LUE) showed a strong coloration due to the diffusion of WDC into the gel.

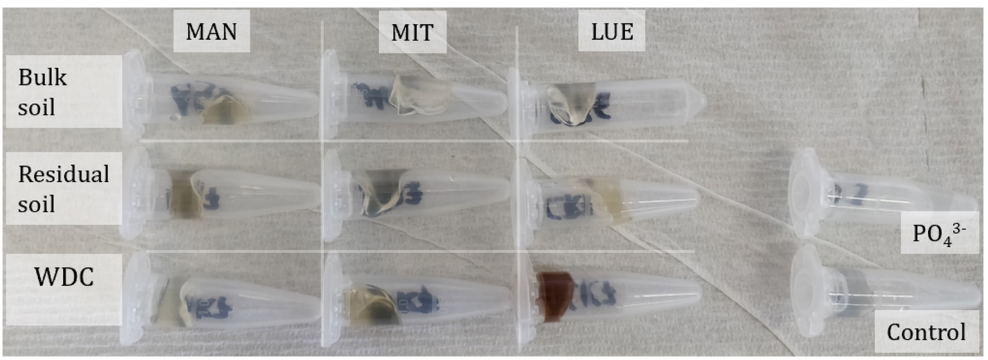


**FIGURE 4 |** Ferrihydrite gel nutrient sinks of the disassembled DGTs after 168 h accumulation time of all soil fractions and sites following their extraction with sulfuric acid. The nutrient sink of WDC of the site Lüss (LUE) showed a strong coloration due to the diffusion of WDC into the sink.

unsaturated conditions the mobility of colloids and nanoparticles in porous media like soils is strongly reduced by interception of particles at water-air interfaces or in thin water films (e.g., Kretzschmar et al., 1999; Flury and Aramrak, 2017). The results of our experiment for the LUE site indicated that colloids can likely carry P to a sink also under water-unsaturated conditions.

## Soil pH, WDC Composition, and P-Speciation as Drivers for WDC Mobility and P-Delivery

While the WDC from LUE delivered P at a quick rate, the results for MAN and MIT did not show increased P supply into the DGTs compared to the bulk soil. This suggested that soil properties, as well as the WDC properties controlled their mobility and the binding strength of WDC-P. Since the lowest P quantities were delivered by WDC from the calcareous site MAN and neither coloration of the DGT diffusive gels were visible nor Al, Ca, or Fe were detectable after digestion by ICP-OES, we assumed that the extracted MAN WDC lack OM-Fe-/Al-P complexes and small P-bearing colloids that contributed to the P-flux into the sinks at LUE. Wang et al. (2020) showed that in the Oh and Ah horizons of the MAN site, P was mainly bound to WDC >240 nm rich in Al and Si, which were likely formed from phyllosilicates (Missong et al., 2018a). These larger WDC were not able to diffuse into the sinks of the DGTs due to their size. Two reasons, high $Ca^{2+}$ concentrations and a circumneutral pH value of the soil might limited the mobility of the small

**TABLE 4 |** Elemental composition of diffusion layer gels after 168 h in contact with the P-sources of the sites Mangfall (MAN), Mitterfels (MIT), and Lüss (LUE) in mg $gel^{-1}$.

| Site | Fraction | Elemental composition [mg $gel^{-1}$] | | | |
|---|---|---|---|---|---|
| | | Al | Ca | Fe | *P* |
| MAN | Bulk soil | <LOD | 0.031 | 0.003 | 0.006 |
| | Residual soil | <LOD | 0.029 | <LOD | 0.004 |
| | WDC | <LOD | <LOD | <LOD | <LOD |
| MIT | Bulk soil | 0.002 | <LOD | 0.006 | 0.004 |
| | Residual soil | 0.004 | 0.010 | 0.009 | 0.004 |
| | WDC | <LOD | 0.006 | 0.004 | 0.004 |
| LUE | Bulk soil | <LOD | <LOD | <LOD | <LOD |
| | Residual soil | 0.002 | 0.007 | 0.009 | 0.006 |
| | WDC | 0.018 | 0.016 | 0.058 | 0.007 |
| Matrix blank | 1 | 0.001 | 0.012 | 0.002 | 0.004 |
| | 2 | <LOD | 0.011 | 0.001 | 0.004 |
| | 3 | <LOD | 0.007 | 0.001 | 0.004 |

*Water-dispersible colloids (WDC) from MAN and MIT showed no increased concentrations for aluminum (Al), calcium (Ca), iron (Fe), and phosphorus (P) compared to blank gels, while WDC from LUE were enriched in these elements, indicating the diffusion of compounds derived from WDC into the DGTs at this site. <LOD indicates elemental concentrations below detection limit.*

WDC from MAN and the P-release into the dissolved phase from these particles. Large concentrations of $Ca^{2+}$ released from the MAN soil derived from dolomite rock might have promoted the flocculation of these clay mineral particles in the porous media. Flocculated WDC would not diffuse in the soil solution or with a much lower rate than single particles because of their larger hydrodynamic radius and mass (Banchio et al., 1999). Furthermore, flocculated WDC may have been retained in the pore space, which in turn may have changed the permeability of the porous medium (Molnar et al., 2019). Moreover, the pH value of 7.0 of the MAN bulk soil was closer to the point of zero charge of many soil components compared to the pH values of the acidic forest soils in MIT and LUE, which may have led to aggregation of the MAN WDC. Aggregation has been demonstrated for example for titanium nanoparticles in porous media at pH values close to the point of zero charge of the nanoparticles (Dunphy Guzman et al., 2006). Contrary to MAN, the WDC from the acidic forest soils of MIT and LUE were likely better dispersed at pH values much lower than the particles point of zero charge. The strong binding of (dissolved) organic matter to Fe- and Al-(hydr)oxides at low pH values (Kaiser et al., 1997) can promote the mobilization of particles (Kretzschmar et al., 1995; Philippe and Schaumann, 2014; Cheng and Saiers, 2015), thus enhancing also the mobility of P bound to these particles. The (weak) podzolic features of the LUE soil would support the theory of diffusion of OM-Fe/Al-P complexes into the DGTs. Missong et al. (2018b) found indications of a translocation of WDC-bound P from the topsoil to the Bsv horizon of the LUE soil. Similarly, Wood et al. (1984), Turner et al. (2012), Celi et al. (2013), and Wu et al. (2014) reported translocation of P during podzolization. However, according to Lang et al. (2017) podzolization was not promoting P transport to greater soil depths at the LUE site.

Although comparable amounts of Al and Fe were added with the WDC from the MIT soil as with WDC from the LUE soil to the quartz sand and silt mixture, 10 times less Fe was found in the diffusion layer of the DGT in contact with MIT colloids, and no Al was detectable. The larger Fe contents of the MIT WDC potentially reflected a stronger cementation of individual colloids, which might have reduced their mobility.

## CONCLUSIONS

Our study demonstrates the enhanced delivery of P by colloids compared to bulk soil and colloid-free soil extraction residue into DGTs in a porous medium under unsaturated conditions. This underpins the relevance of natural colloids for the supply of soil P to plants. Therefore, leaching of these colloids from intensely rooted topsoils to deep subsoils with few roots, or the export of these particles with surface runoff or interflow can decrease the plant availability of P in terrestrial ecosystems. The magnitude and kinetics of colloid-facilitated P delivery likely depend on the mobility of colloids and the strength of the binding of P to the colloids. Building up on previous work on this issue we could confirm that the mobilization of P by and from mobile colloids plays a crucial role for DGT extraction of P.

## DATA AVAILABILITY STATEMENT

The original contributions presented in the study are included in the article/**Supplementary Material**, further inquiries can be directed to the corresponding author/s.

## AUTHOR CONTRIBUTIONS

RB, EK, and JS formulated the hypotheses. AK and JS conceived the experiment. RB, EK, and FL gave feedback regarding the concept and theory in all phases of the study. AK, BB, PR, and JS sampled the soils. AK, BB, and PR carried out the experiments. AK performed statistical analyses and wrote a first draft of the manuscript. All authors discussed the results and contributed to the final manuscript.

## FUNDING

This study was funded in the framework of the Priority Program SPP 1685 Ecosystem Nutrition-Forest Strategies for Limited Phosphorus Resource of the Deutsche Forschungsgemeinschaft (DFG SI 1106/8-1, 2).

## ACKNOWLEDGMENTS

Thanks to Astrid Jäger, Diedrich Steffens, and Caroline Löw for their comments that helped to improve the experimental design. We also thank Elke Müller, Elke Schneidenwind, and Ann-Kathrin Nimführ for their technical assistance in the laboratory, as well as Jan Wolff for the provision of resin-P data for the topsoil at the Mangfall (MAN) site. We gratefully acknowledge the help of Daniel F. Kaiser, Sebastian Loeppmann,

Marius Schmitt, and Jaane Krüger during the sampling of soils. Without the help of Daniel F. Kaiser and Linda Vogt we never would have been able to extract many kilograms of soil for the isolation of colloids. Big thanks to Jaane Krüger also for organizing and administrating our collaboration.

## SUPPLEMENTARY MATERIAL

The Supplementary Material for this article can be found online at: https://www.frontiersin.org/articles/10.3389/ffgc.2020.577364/full#supplementary-material

## REFERENCES


Alef, K. (ed.). (1998). *Methods in Applied Soil Microbiology and Biochemistry*. London: Academic Press.

Atkins, P. W., and de Paula, J. (2013). *Physikalische Chemie (5. Auflage)*. Weinheim: WileyVCH Verlag GmbH and Co. KGaA.

Baldwin, D. S. (1998). Reactive "organic" phosphorus revisited. *Water Res.* 32, 2265–2270. doi: 10.1016/S0043-1354(97)00474-0

Banchio, A. J., Nägele, G., and Bergenholtz, J. (1999). Viscoelasticity and generalized Stokes–Einstein relations of colloidal dispersions. *J. Chem. Phys.* 111, 8721–8740. doi: 10.1063/1.480212

Bartlett, M. S. (1937). Properties of sufficiency and statistical tests. *Proc. R. Soc.* 160, 268–282. doi: 10.1098/rspa.1937.0109

Benjamini, Y., and Hochberg, Y. (1994). Controlling the false discovery rate: a practical and powerful approach to multiple testing. *J. R. Stat. Soc. Ser. B* 57, 289–300.

Bol, R., Julich, D., Brödlin, D., Siemens, J., Kaiser, K., Dippold, M. A., et al. (2016). Dissolved and colloidal phosphorus fluxes in forest ecosystems-an almost blind spot in ecosystem research. *J. Plant Nutr. Soil Sci.* 179, 425–438. doi: 10.1002/jpln.201600079

Bollyn, J., Castelein, L., and Smolders, E. (2019). Fate and bioavailability of phosphorus loaded to iron oxyhydroxide nanoparticles added to weathered soils. *Plant Soil* 438, 297–311. doi: 10.1007/s11104-019-04008-x

Bollyn, J., Faes, J., Fritzsche, A., and Smolders, E. (2017). Colloidal-bound polyphosphates and organic phosphates are bioavailable: a nutrient solution study. *J. Agric. Food Chem.* 65, 6762–6770. doi: 10.1021/acs.jafc.7b01483

Celi, L., Cerli, C., Turner, B. L., Santoni, S., and Bonifacio, E. (2013). Biogeochemical cycling of soil phosphorus during natural revegetation of Pinus sylvestris on disused sand quarries in Northwestern Russia. *Plant Soil* 367, 121–134. doi: 10.1007/s11104-013-1627-y

Cheng, T., and Saiers, J. E. (2015). Effects of dissolved organic matter on the co-transport of mineral colloids and sorptive contaminants. *J. Contam. Hydrol.* 177–178, 148–157. doi: 10.1016/j.jconhyd.2015.04.005

Dalkmann, P., Siebe, C., Amelung, W., Schloter, M., and Siemens, J. (2014). Does long-term irrigation with untreated wastewater accelerate the dissipation of pharmaceuticals in soil? *Environ. Sci. Technol.* 48, 4963–4970. doi: 10.1021/es501180x

Davison, W., and Zhang, H. (2012). Progress in understanding the use of diffusive gradients in thin films (DGT) – back to basics. *Environ. Chem.* 9, 1–13. doi: 10.1071/EN11084

de Jonge, L. W., Moldrup, P., Rubaek, G. H., Schelde, K., and Djurhuus, J. (2004). Particle leaching and particle-facilitated transport of phosphorus at field scale. *Vadose Zone J.* 3, 462–470. doi: 10.2113/3.2.462

Degryse, F., Smolders, E., Zhang, H., and Davison, W. (2009). Predicting availability of mineral elements to plants with the DGT technique: a review of experimental data and interpretation by modelling. *Environ. Chem.* 6, 198–218. doi: 10.1071/EN09010

Dunphy Guzman, K. A., Finnegan, M. P., and Banfield, J. F. (2006). Influence of surface potential on aggregation and transport of titania nanoparticles. *Environ. Sci. Technol.* 40, 7688–7693. doi: 10.1021/es060847g

Elser, J. J., Bracken, M. E. S., Cleland, E. E., Gruner, D. S., Harpole, W. S., Hillebrand, H., et al. (2007). Global analysis of nitrogen and phosphorus limitation of primary producers in freshwater, marine and terrestrial ecosystems. *Ecol. Lett.* 10, 1135–1142. doi: 10.1111/j.1461-0248.2007.01113.x

Flury, M., and Aramrak, S. (2017). Role of air-water interfaces in colloid transport in porous media: a review: air-water interfaces and colloid transport. *Water Resour. Res.* 53, 5247–5275. doi: 10.1002/2017WR020597

Gallego-Urrea, J. A., Tuoriniemi, J., and Hassellöv, M. (2011). Applications of particle-tracking analysis to the determination of size distributions and concentrations of nanoparticles in environmental, biological and food samples. *TrAC Trends Analyt. Chem.* 30, 473–483. doi: 10.1016/j.trac.2011.01.005

Gerke, J. (2010). Humic (organic matter)-Al(Fe)-phosphate complexes: an underestimated phosphate form in soils and source of plant-available phosphate. *Soil Sci.* 175, 417–425. doi: 10.1097/SS.0b013e3181f1b4dd

Gottselig, N., Amelung, W., Kirchner, J. W., Bol, R., Eugster, W., Granger, S. J., et al. (2017a). Elemental composition of natural nanoparticles and fine colloids in european forest stream waters and their role as phosphorus carriers: colloids in european forest streams. *Glob. Biogeochem. Cycles* 31, 1592–1607. doi: 10.1002/2017GB005657

Gottselig, N., Nischwitz, V., Meyn, T., Amelung, W., Bol, R., Halle, C., et al. (2017b). Phosphorus binding to nanoparticles and colloids in forest stream waters. *Vadose Zone J.* 16, 1–12. doi: 10.2136/vzj2016.07.0064

Gottselig, N., Sohrt, J., Uhlig, D., Nischwitz, V., Weiler, M., and Amelung, W. (2020). Groundwater controls on colloidal transport in forest stream waters. *Sci. Total Environ.* 717:134638. doi: 10.1016/j.scitotenv.2019.134638

Hathaway, J. C. (1956). Procedure for clay mineral analyses used in the sedimentary petrology laboratory of the U.S. geological survey. *Clay Min.* 3, 8–13. doi: 10.1180/claymin.1956.003.15.05

Haygarth, P. M., Warwick, M. S., and House, W. A. (1997). Size distribution of colloidal molybdate reactive phosphorus in river waters and soil solution. *Water Res.* 31, 439–448. doi: 10.1016/S0043-1354(96)00270-9

Heathwaite, L., Haygarth, P., Matthews, R., Preedy, N., and Butler, P. (2005). Evaluating colloidal phosphorus delivery to surface waters from diffuse agricultural sources. *J. Environ. Qual.* 34, 287–298. doi: 10.2134/jeq2005.0287a

Ilg, K., Siemens, J., and Kaupenjohann, M. (2005). Colloidal and dissolved phosphorus in sandy soils as affected by phosphorus saturation. *J. Environ. Qual.* 34, 926–935. doi: 10.2134/jeq2004.0101

Jacobsen, O. H., Moldrup, P., Larsen, C., Konnerup, L., and Petersen, L. W. (1997). Particle transport in macropores of undisturbed soil columns. *J. Hydrol.* 196, 185–203. doi: 10.1016/S0022-1694(96)03291-X

Jiang, X., Bol, R., Cade-Menun, B. J., Nischwitz, V., Willbold, S., Bauke, S. L., et al. (2017). Colloid-bound and dissolved phosphorus species in topsoil water extracts along a grassland transect from Cambisol to Stagnosol. *Biogeosciences* 14, 1153–1164. doi: 10.5194/bg-14-1153-2017

Jiang, X., Bol, R., Nischwitz, V., Siebers, N., Willbold, S., Vereecken, H., et al. (2015). Phosphorus containing water dispersible nanoparticles in arable soil. *J. Environ. Qual.* 44, 1772–1781. doi: 10.2134/jeq2015.02.0085

Jonard, M., Fürst, A., Verstraeten, A., Thimonier, A., Timmermann, V., Potočić, N., et al. (2015). Tree mineral nutrition is deteriorating in Europe. *Glob. Change Biol.* 21, 418–430. doi: 10.1111/gcb.12657

Kaiser, K., Guggenberger, G., Haumaier, L., and Zech, W. (1997). Dissolved organic matter sorption on sub soils and minerals studied by 13C-NMR and DRIFT spectroscopy. *Eur. J. Soil Sci.* 48, 301–310. doi: 10.1111/j.1365-2389.1997.tb00550.x

Kretzschmar, R., Borkovec, M., Grolimund, D., and Elimelech, M. (1999). Mobile subsurface colloids and their role in contaminant transport. *Adv. Agron.* 66, 121-193. doi: 10.1016/s0065-2113(08)60427-7

Kretzschmar, R., Robarge, W. P., and Amoozegar, A. (1995). Influence of natural organic matter on colloid transport through saprolite. *Water Resour. Res.* 31, 435–445. doi: 10.1029/94WR02676

Kruse, J., Abraham, M., Amelung, W., Baum, C., Bol, R., Kühn, O., et al. (2015). Innovative methods in soil phosphorus research: a review. *J. Plant Nutr. Soil Sci.* 178, 43–88. doi: 10.1002/jpln.201400327

Lang, F., Bauhus, J., Frossard, E., George, E., Kaiser, K., Kaupenjohann, M., et al. (2016). Phosphorus in forest ecosystems: new insights from an ecosystem nutrition perspective. *J. Plant Nutr. Soil Sci.* 179, 129–135. doi: 10.1002/jpln.201500541

Lang, F., Krüger, J., Amelung, W., Willbold, S., Frossard, E., Bünemann, E. K., et al. (2017). Soil phosphorus supply controls P nutrition strategies of beech forest ecosystems in central Europe. *Biogeochemistry* 136, 5–29. doi: 10.1007/s10533-017-0375-0

Li, F., Liang, X., Li, H., Jin, Y., Jin, J., He, M., et al. (2020). Enhanced soil aggregate stability limits colloidal phosphorus loss potentials in agricultural systems. *Environ. Sci. Eur.* 32:17. doi: 10.1186/s12302-020-0299-5

Mason, S. D., McLaughlin, M. J., Johnston, C., and McNeill, A. (2013). Soil test measures of available P (Colwell, resin and DGT) compared with plant P uptake using isotope dilution. *Plant Soil* 373, 711–722. doi: 10.1007/s11104-013-1833-7

Missong, A., Bol, R., Nischwitz, V., Krüger, J., Lang, F., Siemens, J., et al. (2018a). Phosphorus in water dispersible-colloids of forest soil profiles. *Plant Soil* 427, 71–86. doi: 10.1007/s11104-017-3430-7

Missong, A., Bol, R., Willbold, S., Siemens, J., and Klumpp, E. (2016). Phosphorus forms in forest soil colloids as revealed by liquid-state 31 P-NMR. *J. Plant Nutr. Soil Sci.* 179, 159–167. doi: 10.1002/jpln.201500119

Missong, A., Holzmann, S., Bol, R., Nischwitz, V., Puhlmann, H., v. Wilpert, K., et al. (2018b). Leaching of natural colloids from forest topsoils and their relevance for phosphorus mobility. *Sci. Total Environ.* 634, 305–315. doi: 10.1016/j.scitotenv.2018.03.265

Molnar, I. L., Pensini, E., Asad, M. A., Mitchell, C. A., Nitsche, L. C., Pyrak-Nolte, L. J., et al. (2019). Colloid transport in porous media: a review of classical mechanisms and emerging topics. *Transp. Porous Med.* 130, 129–156. doi: 10.1007/s11242-019-01270-6

Montalvo, D., Degryse, F., and McLaughlin, M. J. (2015a). Natural colloidal P and its contribution to plant P uptake. *Environ. Sci. Technol.* 49, 3427–3434. doi: 10.1021/es504643f

Montalvo, D., McLaughlin, M. J., and Degryse, F. (2015b). Efficacy of hydroxyapatite nanoparticles as phosphorus fertilizer in andisols and oxisols. *Soil Sci. Soc. Am J.* 79, 551–558. doi: 10.2136/sssaj2014.09.0373

Öztan, S., and Düring, R.-A. (2012). Microwave assisted EDTA extraction—determination of pseudo total contents of distinct trace elements in solid environmental matrices. *Talanta* 99, 594–602. doi: 10.1016/j.talanta.2012.06.042

Philippe, A., and Schaumann, G. E. (2014). Interactions of dissolved organic matter with natural and engineered inorganic colloids: a review. *Environ. Sci. Technol.* 48, 8946–8962. doi: 10.1021/es502342r

Prietzel, J., Klysubun, W., and Werner, F. (2016). Speciation of phosphorus in temperate zone forest soils as assessed by combined wet-chemical fractionation and XANES spectroscopy. *J. Plant Nutr. Soil Sci.* 179, 168–185. doi: 10.1002/jpln.201500472

Séquaris, J.-M., and Lewandowski, H. (2003). Physicochemical characterization of potential colloids from agricultural topsoils. *Colloids Surfaces A* 217, 93–99. doi: 10.1016/S0927-7757(02)00563-0

Six, L., Pypers, P., Degryse, F., Smolders, E., and Merckx, R. (2012). The performance of DGT versus conventional soil phosphorus tests in tropical soils - an isotope dilution study. *Plant Soil* 359, 267–279. doi: 10.1007/s11104-012-1192-9

Stainton, M. P. (1980). Errors in molybdenum blue methods for determining orthophosphate in freshwater. *Can. J. Fish. Aquat. Sci.* 37, 472–478. doi: 10.1139/f80-061

Turner, B. L., Condron, L. M., Wells, A., and Andersen, K. M. (2012). Soil nutrient dynamics during podzol development under lowland temperate rain forest in New Zealand. *Catena* 97, 50–62. doi: 10.1016/j.catena.2012.05.007

van der Veeken, P. L. R., Pinheiro, J. P., and van Leeuwen, H. P. (2008). Metal speciation by DGT/DET in colloidal complex systems. *Environ. Sci. Technol.* 42, 8835–8840. doi: 10.1021/es801654s

Van Veldhoven, P. P., and Mannaerts, G. P. (1987). Inorganic and organic phosphate measurements in the nanomolar range. *Analyt. Biochem.* 161, 45–48. doi: 10.1016/0003-2697(87)90649-X

Vitousek, P. M., Porder, S., Houlton, B. Z., and Chadwick, O. A. (2010). Terrestrial phosphorus limitation: mechanisms, implications, and nitrogen–phosphorus interactions. *Ecol. Appl.* 20, 5–15. doi: 10.1890/08-0127.1

Wang, L., Missong, A., Amelung, W., Willbold, S., Prietzel, J., and Klumpp, E. (2020). Dissolved and colloidal phosphorus affect P cycling in calcareous forest soils. *Geoderma* 375:114507. doi: 10.1016/j.geoderma.2020.114507

Watson, J. E. M., Evans, T., Venter, O., Williams, B., Tulloch, A., Stewart, C., et al. (2018). The exceptional value of intact forest ecosystems. *Nat. Ecol. Evol.* 2, 599–610. doi: 10.1038/s41559-018-0490-x

Wood, T., Bormann, F. H., and Voigt, G. K. (1984). Phosphorus cycling in a northern hardwood forest: biological and chemical control. *Science* 223, 391–393. doi: 10.1126/science.223.4634.391

WRB (2015). *World Reference Base for Soil Resources 2014, Update 2015*. International soil classification system for naming soils and creating legends for soil maps. World soil resources reports. FAO, Rome.

Wu, Y., Prietzel, J., Zhou, J., Bing, H., Luo, J., Yu, D., et al. (2014). Soil phosphorus bioavailability assessed by XANES and Hedley sequential fractionation technique in a glacier foreland chronosequence in Gongga Mountain, Southwestern China. *Sci. China Earth Sci.* 57, 1860–1868. doi: 10.1007/s11430-013-4741-z

Zhang, H., and Davison, W. (1999). Diffusional characteristics of hydrogels used in DGT and DET techniques. *Analyt. Chim. Acta* 398, 329–340. doi: 10.1016/S0003-2670(99)00458-4

Zhang, H., Davison, W., Gadi, R., and Kobayashi, T. (1998). *In situ* measurement of dissolved phosphorus in natural waters using DGT. *Analyt. Chim. Acta* 370, 29–38. doi: 10.1016/S0003-2670(98)00250-5

**Conflict of Interest:** The authors declare that the research was conducted in the absence of any commercial or financial relationships that could be construed as a potential conflict of interest.

The reviewer ES declared a past co-authorship with one of the author RB to the handling Editor.

frontiers in Forests and Global Change

ORIGINAL RESEARCH
published: 23 February 2021
doi: 10.3389/ffgc.2020.604200

# Soil Phosphorus Speciation and Availability in Meadows and Forests in Alpine Lake Watersheds With Different Parent Materials

*Thomas Heron[1], Daniel G. Strawn[1]*, Mariana Dobre[1], Barbara J. Cade-Menun[2], Chinmay Deval[1], Erin S. Brooks[1], Julia Piaskowski[1], Caley Gasch[3] and Alex Crump[1]*

[1] College of Agricultural and Life Sciences, University of Idaho, Moscow, ID, United States, [2] Agriculture and Agri-Food Canada, Swift Current Research and Development Centre, Swift Current, SK, Canada, [3] Department of Soil Science, North Dakota State University, Fargo, ND, United States

OPEN ACCESS

**Edited by:**
*Friederike Lang,*
*University of Freiburg, Germany*

**Reviewed by:**
*Joerg Schaller,*
*Leibniz Center for Agricultural Landscape Research (ZALF), Germany*
*Hui Wang,*
*Chinese Academy of Forestry, China*
*Sara L. Bauke,*
*University of Bonn, Germany*

***Correspondence:**
*Daniel G. Strawn*
*dgstrawn@uidaho.edu*

**Specialty section:**
*This article was submitted to Forest Soils, a section of the journal Frontiers in Forests and Global Change*

**Received:** *08 September 2020*
**Accepted:** *23 December 2020*
**Published:** *23 February 2021*

**Citation:**
*Heron T, Strawn DG, Dobre M, Cade-Menun BJ, Deval C, Brooks ES, Piaskowski J, Gasch C and Crump A (2021) Soil Phosphorus Speciation and Availability in Meadows and Forests in Alpine Lake Watersheds With Different Parent Materials. Front. For. Glob. Change 3:604200. doi: 10.3389/ffgc.2020.604200*

In the Lake Tahoe Basin in California and Nevada (USA), managing nutrient export from watersheds into streams and the lake is a significant challenge that needs to be addressed to improve water quality. Leaching and runoff of phosphorus (P) from soils is a major nutrient source to the lake, and P loading potential from different watersheds varies as a function of landscape and ecosystem properties, and how the watershed is managed. In this research, P availability and speciation in forest and meadow soils in the Lake Tahoe Basin were measured at two watersheds with different parent material types. Soils developed on andesitic parent materials had approximately twice as much total P compared to those developed on granitic parent materials. Regardless of parent material, organic P was 79–92% of the total P in the meadow soils, and only 13–47% in the forest soils. Most of the soil organic P consisted of monoester P compounds, but a significant amount, especially in meadow soils, was diester P compounds (up to 30% of total extracted P). Water extractable P (WEP) concentrations were ∼10 times greater in the granitic forest soils compared to the andesitic forest soils, which had more poorly crystalline aluminosilicates and iron oxides that retain P and thus restrict WEP export. In the meadow soils, microbial biomass P was approximately seven times greater than the forest soils, which may be an important sink for P leached from upland forests. Results show that ecosystem and parent material are important attributes that control P speciation and availability in the Lake Tahoe Basin, and that organic P compounds are a major component of the soil P and are available for leaching from the soils. These factors can be used to develop accurate predictions of P availability and more precise forest management practices to reduce P export into Lake Tahoe.

**Keywords: forest phosphorus, soil phosphorus, phosphorus NMR, phosphorus availability, phosphorus leaching, phosphorus speciation**

## INTRODUCTION

Lake Tahoe, located in the Sierra Nevada Mountain range in California and Nevada, is the sixth largest lake by volume in the United States. It is classified as an ultra-oligotrophic lake, meaning that it has naturally low nutrient concentrations and low primary production, and it is renowned for the clarity of its water (Hatch et al., 2001; Goldberg et al., 2015). In recent years, however, water clarity in Lake Tahoe has declined, with Secchi depth readings decreasing from ∼31 m in 1968 to 21.6 m in 2018 (Schladow, 2019). As a result of non-point-source nutrient loading, primary production in Lake Tahoe has increased by ∼6% per year (Jassby et al., 1999; Roberts and Reuter, 2010).

Historically, algae growth in Lake Tahoe has been co-limited by nitrogen (N) and phosphorus (P) (Hatch et al., 1999). However, as has been observed for lakes worldwide (Elser et al., 2009), increased atmospheric N loading and N deposition have altered plankton species and N:P stoichiometry, shifting nutrient limitation in Lake Tahoe to P (Hatch et al., 1999; Goldberg et al., 2015). A recent lake-clarity model demonstrated that a return to the historical Secchi depth reading in Lake Tahoe would be possible within 20 years if P loading were reduced by at least 2.75% per year (Sahoo et al., 2010). However, to control P sources and subsequent loading into surface waters, a full understanding of P cycling and species in soils in the Lake Tahoe Basin is required.

The physical forms of P that can enter and cycle in lakes are defined as particulate P that is >0.45 μm, and solution P that can pass through a 0.45-μm filter that consists of dissolved and colloidal P (Bol et al., 2016). Colloidal P particles are 1 to 1,000 nm in diameter and the colloids less than 450 nm can pass through a 0.45 μm filter (Jiang et al., 2017), and can thus be mobilized through soils and remain suspended in surface waters. Dissolved, colloidal, or particulate P species can be organic [bound to a carbon (C) group] or inorganic (singular or multiple phosphate groups). Short-term changes in Lake Tahoe primary productivity are well-explained by dissolved inorganic and organic P loads from Lake Tahoe Basin streams, which contribute up to 1,000 kg of dissolved P annually (Hatch et al., 1999). Different forms of P, both physically and chemically, differ in their mobility, environmental reactivity, and bioavailability. Dissolved molybdate-reactive phosphate (MRP), also known as soluble reactive phosphate (SRP), is the most readily bioavailable form (Hatch et al., 1999; Sahoo et al., 2010). Thus, to manage Lake Tahoe Basin landscapes for P-load reduction requires knowledge of soil P species and pools, and their potential for release and transport into surface waters.

About 6% of the Lake Tahoe Basin is considered urban and has been developed for residential and commercial use. Phosphorus inputs within the urban portion of the Basin account for 18% of total P inputs into the lake (Sahoo et al., 2013). In the non-urban regions of the Basin, 50% are covered by forests with yellow pine associations (TRPA, 2015) containing Jeffrey pine (*Pinus jeffreyi* Balf.), white fir [*Abies concolor* (Gord. and Glend.) Lindl. Ex Hildebr.], incense cedar [*Calocedrus decurrens* (Torr.) Florin], and sugar pine (*Pinus labertiana* Douglas); and another 17% of the Tahoe Basin landscape are red fir associations containing red fir (*Abies magnifica* A. Murray bis), Jeffrey pine and Lodgepole pine (*Pinus contorta* Douglas ex Loudon). Wet and dry meadows comprise 2 and 1% of non-urban land, respectively, and contain grasses, sedges, and rushes (TRPA, 2015). Soils in the Lake Tahoe Basin are developed on andesitic, granitic, or mixed parent materials (Coats et al., 2016). Studies in the Eastern Sierra Nevada have shown that forest soils on granitic parent materials can have substantially higher extractable-P concentrations than those developed on andesitic parent materials (Johnson et al., 1997; Coats et al., 2016). However, it is unclear the mechanistic processes that are responsible for these differences.

In soils, inorganic and organic P molecular species have distinct potential for uptake by vegetation or mobilization out of the soil profile. Uselman et al. (2012) suggested that the amount of dissolved organic P in soil solution is largely dependent on the type and amount of above- and below-ground organic matter. Some forest-soil P is exported as particulate P (Prairie and Kalff, 1988). The amount of eroded particulate P that is exported from a site depends on three factors: (1) site geography (slope, climate, and geology); (2) site management (harvest, thinning, and development); and (3) wildfire history (Miller et al., 2006). Particulate P that enters streams and lakes is not directly available for uptake by aquatic organisms, although it can be released as dissolved P from the particles and then is bioavailable to support aquatic algae growth (Young et al., 1985; Reid et al., 2018).

A significant fraction of forest P exists in the plant litter and O horizons that can be illuviated into lower depths in the soil profile or be lost in runoff (Miller et al., 2010; Bol et al., 2016). Miller et al. (2005, 2006) observed that organic horizons on forest floors in Lake Tahoe Basin have high levels of water-soluble P that may be a source of P loading to streams via overland or subsurface flow, the latter of which moves through and reacts with soils. Phosphorus leached from O horizons can be transported into the soils through several mechanisms, depending on the soil physical properties that facilitate preferential vs. matrix flow (Julich et al., 2017; Luo et al., 2019). In alpine environments, spring snowmelt runoff is an important mechanism of P loading because it transports dissolved, colloidal, and particulate P from decomposed forest litter and soils, which can then emerge as subsurface P loading to streams and lakes (Backnäs et al., 2012).

Estimates suggest that groundwater sources make up 15% by mass of total P loading to Lake Tahoe (Roberts and Reuter, 2010). Furthermore, 61% (3,700 kg) of the annual total dissolved P that is found in Lake Tahoe Basin groundwater is believed to be derived from natural sources from unimpacted non-urban areas, predominantly from overlying forest litter P pools and P released from the adsorbed and mineral-bound soil P pool (U.S. Army Corp of Engineers, 2003). Sohrt et al. (2019) used an end-member mixing model that included soil water input to predict that up to 92% of the stream P in a mixed deciduous/evergreen forest in Europe was leached from the mineral soil horizons. Considering the hydrologic interfaces in the soil, it follows that in the Lake Tahoe Basin forests, soil P biogeochemistry is an important factor that controls P discharge into surface waters, and to reduce P loads released from forests it is imperative to understand how site and management factors impact P solubility and mobility.

Although meadows comprise a small area of the Lake Tahoe Basin watershed, they are important controllers of P entering streams because they are transitional zones connecting terrestrial and aquatic ecosystems and are commonly located adjacent to forests (Roby et al., 2015). Some meadows in the Lake Tahoe Basin are categorized as stream environment zones (SEZ), which is a designation used by the Lake Tahoe Basin Management Unit for an area of high value and management priority based on ecosystem services, including the filtering and storage of nutrients in runoff (Roby et al., 2015). Forest-derived P is commonly hydrologically transported through meadow ecosystems, which can act as either sinks that intercept P or sources that release P to streams and lakes. Several groups have studied the capacity of riparian systems to perform these functions. For example, Casey and Klaine (2001) studied P adsorption behavior in meadow soils, including Cumulic Humaquepts (similar taxa are found in some Lake Tahoe Basin meadows), and demonstrated the importance of sorption capacity as a mechanism of nutrient attenuation. They determined that soil P concentration was 100 times below concentrations that would cause soil solution P levels to exceed U.S. Environmental Protection Agency recommendations for lentic waters. In contrast, Hoffmann et al. (2006) found a net loss of P via leaching from soils in riparian meadows during two of three sampling years. In a later study, Hoffmann et al. (2009) concluded that, although sedimentation in riparian buffers is an important mechanism of P retention, these buffers may eventually become significant sources of dissolved reactive P release to surface or groundwater. Gergans et al. (2011) studied nutrient flow through a Lake Tahoe watershed that included a riparian meadow ecosystem and observed that the meadow soils were sources of phosphate into a nearby stream and that the release varied with season. The contrasting reports of nutrient retention and release from meadows highlight the complex nature of meadow biogeochemical processes that can make them either sources or sinks of P into surface waters.

Organic P species in forest soils have been shown to be a dominant loading factor to surface waters (Condron et al., 2005; Sohrt et al., 2017). Backnäs et al. (2012) observed higher soluble organic P (labile monoester and diester P species) in surface horizons of Podzol soils in a mixed-coniferous forest in Finland compared to deeper soils. Anderson and Magdoff (2005) observed higher levels of labile organic P than inorganic P in leachate from packed soil columns leached with DNA (diester P) and orthophosphate solutions. Missong et al. (2016) separated bulk soil extractions from forest soils into colloidal and electrolytic fractions and found most of the extractable P was organic bound P (diesters) on colloids. Brödlin et al. (2019b) studied P forms in soils from three different parent materials in deciduous forests and observed a tendency for organic P to dominate mobilized dissolved P. Bol et al. (2016) reviewed organic P in forested soils and concluded that, although it is a significant component of P cycling, the lack of knowledge of organic P species creates a "blind spot in ecosystem research." Therefore, the dynamics and vulnerability of P leached from both forest and adjacent meadow soils needs to be investigated to understand the potential impact on water quality. This is especially true in watersheds like in the Lake Tahoe Basin, where nutrients leached through forest soils are major inputs into the lake.

In this paper, we investigated the influence of parent material and ecosystem type on soil P species and solubility in the Lake Tahoe Basin. We hypothesized that there would be distinct P biogeochemistry in forest and meadow ecosystems, and that granitic and andesitic parent materials would influence total and available soil P, as well as the amount and type of organic P. Speciation of P in the soils was determined by extraction and $^{31}$P nuclear magnetic resonance spectroscopy (P-NMR) to elucidate organic and inorganic P species. Water-extractable, exchangeable, and microbial-biomass bound soil P were measured to determine soil P fractions that are potentially soluble and labile. These extractions are good predictors of P immobilization and potential runoff from soils (Pote et al., 1996; Campo et al., 1998; Vadas et al., 2005; Wang et al., 2010; Pistocchi et al., 2018).

# METHODS

## Study Sites and Sample Collection

Soils were sampled from two subalpine meadow systems (Paige Meadow and Meeks Meadow) and their adjacent forests. The research sites are located on the west shore of the Lake Tahoe Basin (**Figure 1**). Paige Meadow is an alluvial floodplain surrounded by forested hillslopes of terminal moraines at elevation ∼2,115 m. Meeks Meadow is situated in an elongated glacial valley trough floodplain (elevation ∼1,905 m), confined on both sides by steep forested hillslopes of lateral moraines. Separate lobes of the Sierran Ice Cap extended over the present-day locations of both meadows, carving out their current floodplain topographic environments (Ehlers and Gibbard, 2003). At Paige Meadow and its surrounding forest, soils developed on glacial deposits of eroded basaltic and andesitic rocks from Miocene- through Pleistocene-age volcanic activity (Kortemeier et al., 2018). The geologic substrate of the Meeks Meadow watershed is primarily granodiorite eroded from a glacial drift of till and outwash (Saucedo, 2005). Both meadows contain perennial grasses mixed with sedges, rushes, and forbs (Soil Survey Staff, 2007). The forest surrounding Paige Meadow is a red fir forest association, while the forest next to Meeks Meadow consists of a yellow pine association (Soil Survey Staff, 2007; TRPA, 2015). Climatic data from Tahoe City and Rubicon SNOTEL stations show approximate cumulative precipitation of 900 mm and a mean annual temperature of 7.5°C (USDA-NRCS, 2019). Soils at nearby SNOTEL stations fall under a xeric soil moisture and frigid soil temperature regimes. At each location, 3–5 soil profiles were viewed to 20–40 cm depth and characterized using either a shovel or corer. The descriptions of the soils were done following USDA NRCS soil description methods (Schoeneberger et al., 2012).

Eight locations from each ecosystem-parent material type were sampled in June, August, and October of 2018 (**Figure 1**). Samples were taken from the top 15 cm of the soil below the O horizon using a 10-cm diameter soil auger. At each of the

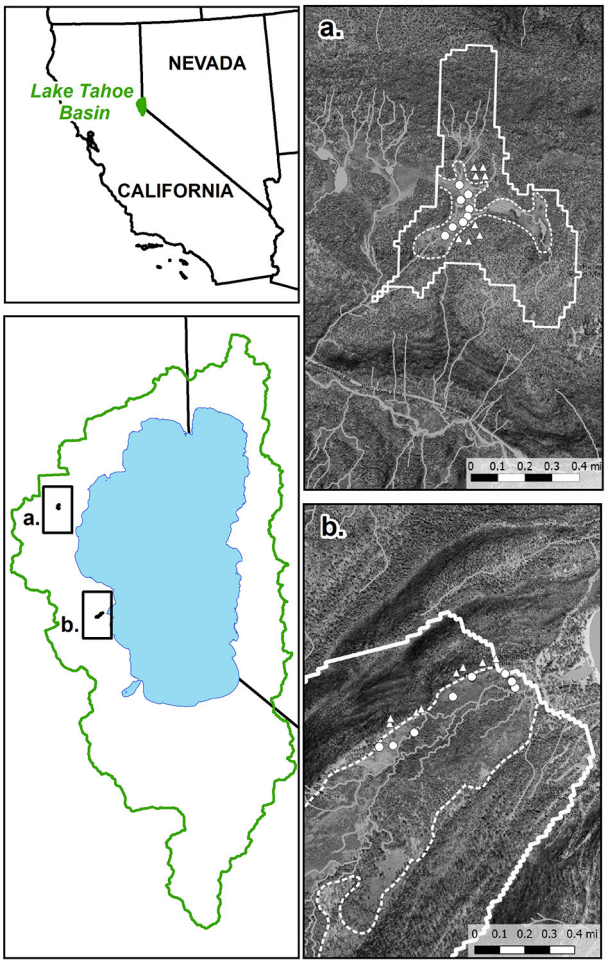


**FIGURE 1 |** Andesitic watershed at Paige Meadow **(a)** and granitic watershed at Meeks Meadow **(b)**. Solid lines are watershed boundaries. Dashed lines separate forest soils from meadow soils, based on map units from the SSURGO database. Circles are meadow sampling sites and triangles are forest sampling sites.

eight replicate locations, a composite sample was collected by mixing three sub-samples from 1 m radius. After sampling, the soils were stored on ice while in transport to the lab. A portion of each sample was sieved (<2 mm) and oven-dried at 50°C, and the remainder was stored undried in re-sealable plastic bags at 4°C and sieved (<2 mm) immediately prior to analysis. At each site seven to fourteen 7-cm diameter by 15-cm depth intact cores were sampled for bulk density measurement. O-horizon samples were taken by compositing material from several locations at each forest site into a bag that was thoroughly mixed. For P-NMR analysis and P availability extractions, field-moist samples were used, and P concentrations were adjusted using the percent moisture content determined by the difference in mass of water between the field-moist and oven-dried samples. Other analyses used 50°C oven-dried soils.

# Laboratory Analyses

## Soil Characterization

Replicate samples from the June 2018 sampling were analyzed for pH, percent sand, and concentrations of total organic C (TOC), total N (TN), and oxalate-extractable iron (Fe), aluminum (Al), silicon (Si), and P. Soils pH was measured on soils at 1:1 soil to 18-megaohm deionized water mass ratio. Percent sand by mass was measured by sieving the < 2 mm soil fraction through a 63 μm sieve. Bulk density was measured in cores dried at ∼50°C and corrected for rocks using granite and andesite density of 2.65 and 2.60 g $cm^{-3}$, respectively (Soil Survey Staff, 2014). Concentrations of TOC and TN were measured using a CNS dry combustion analyzer (Shimadzu Corporation, Oregon). Soils were extracted for poorly crystalline iron and aluminum oxides in a 1:50 solid-solution ratio of 0.2 M ammonium oxalate solution in darkness (Soil Survey Staff, 2014), shaken for 4 h, allowed to settle overnight, centrifuged (1,500 × *g* for 30 min), filtered (0.22 μm diameter PES membrane filter), and analyzed by inductively coupled plasma-atomic emission spectrometry (ICP-AES, Thermo Scientific, Waltham, Massachusetts) that was calibrated using ISO traceable standards.

## Soil Total P

A subset of samples from granitic meadow ($n = 6$), granitic forest ($n = 6$), andesitic meadow ($n = 5$), and andesitic forest ($n = 5$) soils were analyzed for total P (TP) concentration by an analytical laboratory (Bureau Veritas, Inc.; Vancouver, BC; ISO/IEC 17025 and ISO 9001) using a two-step multi-acid ($HNO_3$-$HClO_4$-HF, and HCl) heated-digestion and analysis by ICP-mass spectrometry.

## Total Organic Soil P by Ignition

Total soil organic P concentrations of the same subset of samples used for P-NMR analysis were measured using the ignition method (Saunders and Williams, 1955; Cade-Menun and Lavkulich, 1997). Duplicate 0.5 g subsamples of oven-dried soil were weighed. One replicate was incinerated at 550°C over a 2 h ramp-up period and maintained at this temperature for an additional 1 h followed by a 2-hr cool down. Both samples were then extracted in 1:60 solid-solution ratio of 1 N $H_2SO_4$, shaken for ∼16 h, centrifuged at 1,500 × *g* for 15 min, and the supernatant was decanted and analyzed colorimetrically (Murphy and Riley, 1962). Total organic P was calculated as the difference between incinerated and non-incinerated samples. The P concentration in the incinerated sample is an estimate of soil total P ($TP_{inc}$).

## Soil P Speciation by P-NMR Analysis

A subset of samples that included at least two replicates from each soil/ecosystem type were selected for P NMR analysis to identify concentrations and speciation of organic P in the soils. Following standard extraction procedures for P NMR (Cade-Menun and Preston, 1996; Cade-Menun and Liu, 2014), 2 g dry-mass equivalent undried soil subsamples were suspended in 25 ml of 0.5 M NaOH and 0.1 M $Na_2$-EDTA solution, shaken for 4 h, centrifuged at 1,500 × *g* for 20 min, and the supernatant was decanted and freeze-dried. A 1 ml aliquot of extract was

taken from each sample, diluted 1:10 with deionized water, and analyzed by ICP-AES for total P, Fe, and manganese (Mn) concentrations. The P-NMR spectroscopy was conducted at the University of Idaho's Department of Chemistry. Approximately 0.24 g of freeze-dried extract powder from each sample was dissolved in 0.9 ml of NaOH-EDTA solution and 0.1 ml and $D_2O$ and 0.5 ml of this solution was placed in a 5-mm NMR tube. The NMR spectra were obtained at 202.48 MHz on a 500 MHz Bruker Avance III spectrometer equipped with a 5-mm broadband probe. The 1D $^{31}P$ spectra were acquired with 67.5° pulses, at 30°C, with proton decoupling, and a total recycle delay (pre-scan delay plus acquisition time) of 4 s, for 3,000–8,000 scans, determined by signal-to-noise ratios. This delay time will be sufficient for relaxation based on the ratio of P/Fe+Mn in these samples (McDowell et al., 2006; Cade-Menun and Liu, 2014). Spectra were plotted with 7 Hz line-broadening for the main spectra and 2 Hz line-broadening to assess finer details. Peak areas were computed by integration and visual inspection using NUTS software (Acorn NMR, Livermore CA, 2000 edition), with correction for the degradation of orthophosphate diesters (Cade-Menun and Liu, 2014; Schneider et al., 2016). Peak assignments were made from the literature and confirmed using phytate and β-glycerophosphate spikes (Cade-Menun, 2015).

### Extractable Soil P

Concentrations of labile soil P were measured using water-extractable P (WEP), Bray-1 P (B1P), and microbial biomass P (MBP) methods. Field-moist soil samples were extracted for WEP in a 1:10 solid-solution ratio of 18 megaohm deionized water, shaken for 1 h, centrifuged (1,500 x *g*) for 10 min, and filtered through 0.45-μm diameter PES membrane filters (Kuo, 1996; Self-Davis et al., 2009). An aliquot was subsampled from the filtered extract for molybdate colorimetry (Murphy and Riley, 1962). Colorimetry measures phosphate that reacts with molybdate (MRP), which is used as an estimation of inorganic P in solution. However, some organic P compounds may hydrolyze during the colorimetric reaction and are included in the MRP measurement, while complex inorganic P compounds such as polyphosphates will not react with molybdate (Haygarth and Sharpley, 2000; Worsfold et al., 2016). Therefore, we hereafter refer to WEP MRP as $WEP_{MR}$. The total P in the WEP was analyzed by ICP-AES. The difference between the total WEP and $WEP_{MR}$ concentrations is operationally defined as molybdate-unreactive ($WEP_{MU}$), which primarily consists of P associated with organic, non-hydrolysable, and colloidal forms (Haygarth et al., 1997; Haygarth and Sharpley, 2000). In addition to soil extraction, five subsamples from composite O-horizon samples from each forest were ground, passed through a 2-mm sieve, and extracted at 1:50 solid solution ratio for WEP and $WEP_{MR}$.

Field-moist soils were extracted for Bray-1 P (B1P) as described in Sims (2009). An aliquot of the Bray-1 extract was filtered through a 0.45-μm PES membrane filter and measured colorimetrically ($B1P_{MR}$) and by ICP-AES (B1P). The difference between B1P and $B1P_{MR}$ is the B1P molybdate unreactive ($B1P_{MU}$).

Microbial biomass P (MBP) was measured by treating a 1 g dry-mass equivalent sample of undried soil using 1 ml of chloroform, placing it under a vacuum with a beaker of ∼30 ml of chloroform, allowing it to evaporate for 24 h, and then extracting with the Bray-1 P extractant (Voroney et al., 2008; Reddy et al., 2013). In acidic soils, Bray-1 is a better extract for microbial biomass P than Na-bicarbonate extract (Oberson et al., 1997; Wu et al., 2000). Microbial biomass P was calculated as the difference between chloroform-fumigated and unfumigated samples, without an efficiency correction factor.

## Statistical Analyses

The three seasonal samples of WEP, B1P, and MBP were pooled in the statistical analysis using a mixed model to estimate the random and fixed effects. Extract concentrations that were below the method detection limit (MDL) of the ICP (0.05 mg $kg^{-1}$ for WEP and B1P and 0.1 mg $kg^{-1}$ for MBP) were assigned values ½ MDL. The extract data were analyzed with a generalized linear mixed model using a log-normal distribution. Landscape type, parent material, and their interaction were evaluated as fixed effects, and sample point was evaluated as a random effect. Repeated measurements on the concentrations from the sample points were modeled using a compound symmetry covariance structure. For all variables except total WEP and $WEP_{MU}$, sample identification effects were estimated at each time point. Model fit was assessed by examining the log-likelihoods and inspecting residual plots. All analyses were performed in R version 3.6 (R Core Team, 2019) using the packages "nlme" (Pinheiro, 2019) for model building and ANOVA and "emmeans" (Lenth, 2019) for finding the estimated marginal means and conducting comparisons. Tukey honest significance difference (HSD) test ($p < 0.05$) was used to test significance for the following paired comparisons: andesitic-meadow vs. andesitic forest, granitic-meadow vs. granitic forest, andesitic forest vs. granitic forest, and andesitic meadow vs. granitic meadow.

All other soil data were tested for significance by fitting the data to the analysis of variance (ANOVA) linear models, and Tukey HSD test was used for assessing statistical differences ($p < 0.05$) between treatment means. Pearson's correlation coefficients were used to evaluate the strength of relationships between soil properties (Origin Lab, Northampton, MA).

# RESULTS

## Soil Characterization

Upper soil profile descriptions for each watershed are listed in **Supplementary Table 1**. Both meadow soils are mapped as Inceptisols, and typically have aquic conditions in spring and early summer (Soil Survey Staff, 2007). Meadow soils had a darker chroma of 1 compared to chroma between 2 and 3 in the forest soils. The taxonomic descriptions of the meadow soils include subgroups Cumulic Humaquept at Paige Meadow and Cumulic Humaquept and Aquic/Oxyaquic Dystroxerept at Meeks Meadow. The difference between these subgroups is a higher seasonal water table and an epipedon thick enough to qualify as either mollic or umbric in Cumulic Humaquepts. The Aquic and Oxyaquic Dystroxerepts at Meeks Meadow have slightly deeper water tables and dark ochric epipedons (∼ 15 cm) that verge on meeting the thickness requirement of a mollic or

umbric epipedon. The forest soils surrounding Paige Meadow are mapped as Humic Vitrixerands. The forest soils at Meeks are mapped as Humic Dystroxerepts.

Organic horizons were ∼6 cm thick at the granitic forest sites (**Supplementary Table 1**), and 1.5–2 cm thick at the andesitic sites. At the granitic forest sites, the decomposed litter could be separated into Oi and Oe horizons. In contrast, at sampling time (October 2018), only an Oe horizon was present in the litter at the andesitic forest site, suggesting a greater litter decomposition rate. Forest canopy coverage at the sites are similar: 49% at the andesitic site and 41% at the granitic site (Landfire, 2020). In the meadows, O horizons were 0.5–3 cm thick.

The pH of the meadow and forest soils ranged from pH 5.3 to 6.0, with meadows slightly lower than forests (**Table 1**). Average sand content was similar in the granitic meadow, granitic forest, and andesitic meadow (84, 87, and 88%, respectively), but it was significantly lower (75%) in the andesitic forest soils (**Table 1**). Bulk density of the forest and meadow soils ranged from 0.78 to 1.46 g $cm^{-3}$. The andesitic soils had significantly lower bulk densities than the granitic soils (**Table 1**). The andesitic forest soils contain the most poorly crystalline iron and aluminum oxides (measured by oxalate extraction), which is consistent with Andisol classification by the USDA NRCS (Soil Survey Staff, 1999). Oxalate-extractable Fe and Al were not significantly different among the other three ecosystem-parent material types (**Table 1**). Oxalate-extractable Si concentrations followed the same patterns as Fe and Al concentrations. Oxalate-extractable P concentrations were significantly higher in andesitic forest soil than the other soils, and significantly lower in granitic meadow soils compared to granitic forest soils. Soil TOC concentrations were significantly different between the two forests (**Table 1**), but not the two meadows, and were not significantly different between meadows and forests within each watershed. Granitic forest soils contained the lowest average TOC concentration of all four ecosystem-parent material types, while andesitic forest soil had the highest average TOC concentration. The average TN concentration was approximately three times higher in the andesitic meadow soils compared to the andesitic forest soils (**Table 1**) and was higher in the andesitic forest soils than the granitic forest. Total N concentrations in the granitic forest and granitic meadow soils were not significantly different.

**TABLE 1 |** Soil physicochemical properties of replicates sampled in June 2018.

| | Granitic meadow | | Granitic forest | | Andesitic meadow | | Andesitic forest | |
|---|---|---|---|---|---|---|---|---|
| pH | 5.38 (0.07) | B | 5.84 (0.12) | A | 5.35 (0.08) | B | 5.49 (0.11) | AB |
| Sand (%) | 84 (1.1) | A | 88 (0.6) | A | 87 (1.0) | A | 75 (1.3) | B |
| Oxalate-Al (%) | 0.139 (0.030) | B | 0.242 (0.028) | B | 0.239 (0.012) | B | 1.65 (0.142) | A |
| Oxalate-Fe (%) | 0.195 (0.028) | B | 0.244 (0.022) | B | 0.236 (0.049) | B | 0.725 (0.027) | A |
| Oxalate-Si (%) | 0.027 (0.006) | B | 0.034 (0.005) | B | 0.043 (0.002) | B | 0.431 (0.053) | A |
| Oxalate-P (%) | 0.010 (0.008) | C | 0.036 (0.007) | B | 0.023 (0.004) | BC | 0.069 (0.007) | A |
| TOC (%) | 4.57 (0.91) | AB | 2.77 (0.35) | B | 5.19 (0.56) | AB | 5.36 (0.47) | A |
| TN (%) | 0.200 (0.043) | B | 0.061 (0.015) | B | 0.485 (0.051) | A | 0.153 (0.012) | B |
| PSI[a] | 0.029 (0.003) | B | 0.072 (0.010) | A | 0.047 (0.003) | B | 0.029 (0.002) | B |
| Bulk density[b] (g $cm^{-3}$) | 1.26 (0.05) | B | 1.68 (0.08) | A | 0.91 (0.10) | C | 1.20 (0.06) | BC |

*[a]PSI = P-saturation index = oxalate-P/(oxalate-Al + oxalate-Fe). [b]< 2 mm. Values are means (n = 8) and values in parentheses are standard errors of mean. Values with the same letters are not significantly different between sites (α =0.05).*

## Soil Total P

The mean total soil P concentrations (TP) in the soils developed on andesitic parent materials were significantly higher than those for the soils developed on the granitic parent materials (**Figure 2**). Differences between forest and meadow soils within either watershed were not significant. The estimated total P concentrations via incineration and $H_2SO_4$ extraction for the soil samples analyzed by P-NMR were similar to the total P measured from three acid digestion (slope = 0.95, $r^2$ = 0.95; **Supplementary Table 2**). The total P stocks for the 0–15 cm mineral soils calculated using the mean bulk densities were 0.69, 1.10, 1.22, and 1.81 Mg $Ha^{-1}$ for the granitic meadow, granitic forest, andesitic meadow, and andesitic forest, respectively.

## Speciation of Soil P

In the meadow soils, total organic P concentrations determined from incineration and $H_2SO_4$ extraction were 79–92% of the $TP_{inc}$ (**Figure 3**, **Supplementary Table 2**). Organic P concentrations in the forest soils were much lower (13–47% of the $TP_{inc}$) than in the meadow soils.

The NaOH-EDTA extraction efficiency ranged from 33 to 75% of total soil P (**Supplementary Table 2**). The P not extracted by NaOH-EDTA is considered to be predominantly mineral-bound

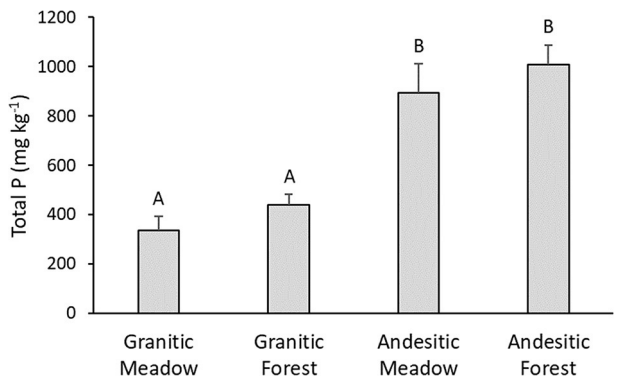


**FIGURE 2 |** Mean total soil phosphorus. Error bars are standard errors. Values with the same letter are not significantly different (α =0.05), *n* = 6 for granitic parent material sites and *n* = 5 for andesitic parent material sites.

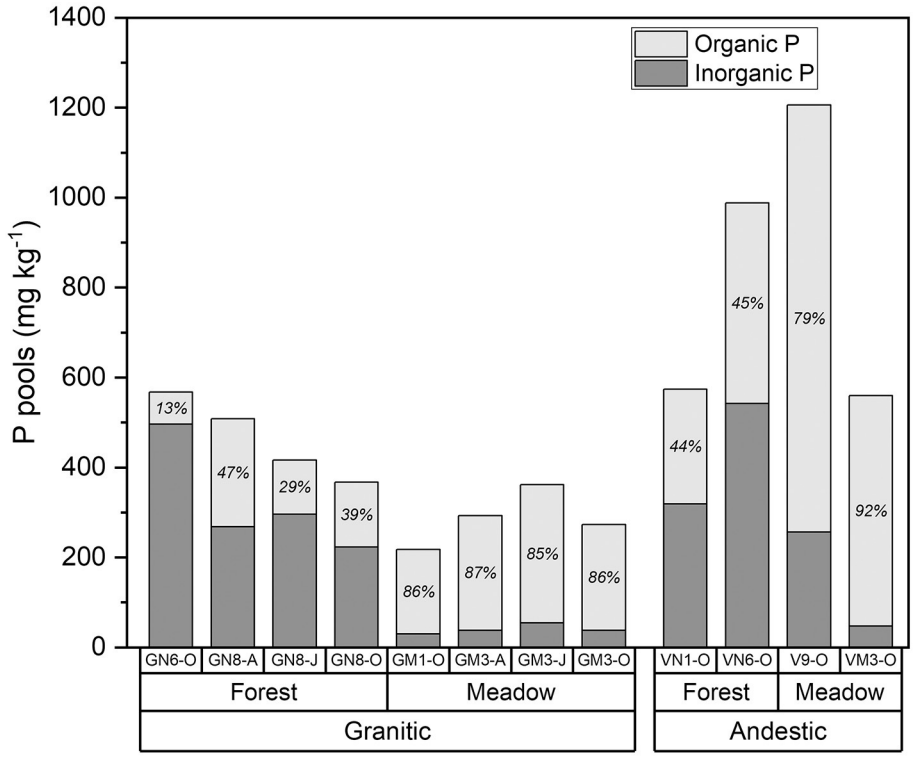


**FIGURE 3 |** Organic and inorganic P in forest and meadow soils from andesitic and granitic parent materials determined by difference of $H_2SO_4$ extraction of non-incinerated and incinerated soils. Numbers within bars are percent organic P.

inorganic P and not readily available to the soil solution or for biological cycling (Cade-Menun et al., 2015).

Example P-NMR spectra are shown in **Figure 4**, the concentrations (and percentage of extracted P) are shown in **Supplementary Table 3**, the grouping of these P species into pools (total organic and inorganic P) and compound classes (total polyphosphates, etc.) are shown in **Supplementary Table 4**, and the chemical shifts of the identified P compounds are shown in **Supplementary Table 5**. The concentrations of the main P compound classes within each ecosystem and parent material type are shown in **Figure 5**.

Inorganic P compounds identified in the NaOH-EDTA extracts by NMR include orthophosphate, pyrophosphate, and polyphosphates. Pyrophosphate and polyphosphates were grouped together as total polyphosphates (**Supplementary Table 4**), and all three were summed together as inorganic P (**Supplementary Table 4**, **Figure 5**). For all soils, orthophosphate was the dominant inorganic P form, and for forest soils developed on both parent materials it comprised the majority of P in the NaOH-EDTA extracts (71.2–84.7% for granitic forests; 51.7–69.3% for andesitic forests). In contrast, the percentages and concentrations of all inorganic P compounds were much lower in meadow soils developed on both parent materials, averaging 21% of extracted P (**Figure 5**). There were no clear trends among the ecosystem and parent material soil types for pyrophosphate or polyphosphates, which were present in all samples, ranging from at 2.1–4.9% of NaOH-EDTA extracted P.

The percentage organic P determined by P-NMR on the soil extracts was directly correlated with the percentage determined using incineration and $H_2SO_4$ extraction ($r^2$ = 0.95, **Supplementary Figure 1**). For all soil types, all the major organic P compound classes were identified: phosphonates, orthophosphate monoesters (hereafter called monoesters), and orthophosphate diesters (hereafter called diesters). The phosphonates included several different peaks (**Supplementary Table 5**), indicating that a number of different compounds were present, but these were not specifically identified. Concentrations of phosphonates ranged from 1.4 to 10.3 mg $kg^{-1}$ (0.7–4.9% of extracted P) and were generally higher in meadows than forests.

Monoesters identified in the P-NMR spectra included four stereoisomers of inositol hexakisphosphate (IHP): *myo*-IHP (phytate), *scyllo*-IHP, *neo*-IHP, and D-*chiro*-IHP. Of these, *myo*-IHP was the predominant P form and was generally more abundant in meadows than forests. For most of the soil samples, *myo*-IHP exceeded the sum of the other three stereoisomers. Other specifically identified monoesters were glucose 6-phosphate (0.6–2.1% of extracted P), choline phosphate (0.3–1.3%), α-glycerophosphate (0.3–2.8%), β-glycerophosphate (0.7–5.7%), nucleotides (1.3–12.8%), and an unidentified peak at ∼5 ppm, which was present in all

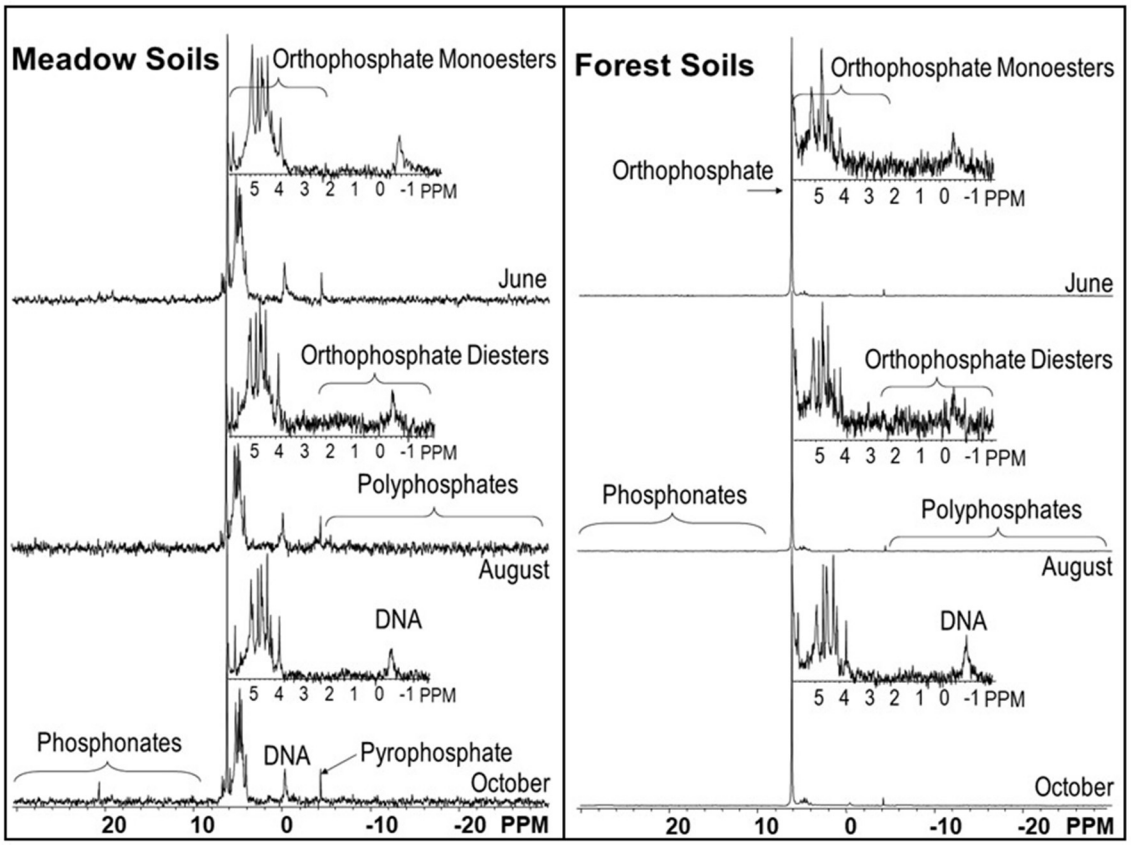


**FIGURE 4 |** NMR spectra from NaOH-EDTA extracts of forest and meadow soils from the granitic site.

samples at 0.7–9.2% of the extracted P. Although peaks for α-glycerophosphate, β-glycerophosphate, and nucleotides are present in the monoester region of spectra, they originate during NaOH-EDTA extraction and P-NMR analysis as a result of degradation of diesters in the original soil samples (Cade-Menun, 2015; Schneider et al., 2016). Thus, the peak areas from these compounds were subtracted from the monoester peak areas and included with the diesters.

Peaks representing diester compounds were separated into DNA (0.5–5.9%), Diester 1 (2.33 to −0.27 ppm, 0.6–8.7%), and Diester 2 (−0.9 to −3.72 ppm, 0.2–3.4%). The Diester 1 region included phospholipids and lipoteichoic acids, while the compounds in the Diester 2 region have not been specifically identified. The proportions and concentrations of P in these three diester regions were generally greater in meadows than forests for both parent materials. Total diesters (cDiesters), calculated by including the degradation compounds from the monoesters, confirmed that the percentages of cDiesters were greater in meadows than forests, and concentrations were greater in andesitic forests and meadows than the granitic forests and meadows, respectively (**Supplementary Table 4**, **Figure 5**).

The average of the replicate NMR results (**Figure 5**) shows that in the meadow soils the three major organic P compound classes were greater in concentration than in the forest soils. In meadow soils, cMonester was 50.3% (107 mg $kg^{-1}$), cDiester was 25.8% (52.1 mg $kg^{-1}$), and phosphonates were 3.0% (5.6 mg $kg^{-1}$). In forest soils, cMonester was 15.7% (42.5 mg $kg^{-1}$), cDiester was 8.5% (22.2 mg $kg^{-1}$), and phosphonates were 1.3% (3.4 mg $kg^{-1}$). The ratio of cMonesters to cDiesters was over 1 for all soils, indicating that monoesters were the dominant P compound class in both ecosystems. In meadow soils, total IHP concentrations comprised about one third of the cMonoesters 17.3% (33.5 mg $kg^{-1}$) but were half of the cMonoesters in forest soils 7.7% (20.9 mg $kg^{-1}$).

## Effects of Parent Material and Ecosystem on Extractable P

In evaluating the extractable P concentrations, main effects were calculated as well as interactions (**Supplementary Table 6**). For all the WEP and B1P extractions, there were crossover interactions between parent material and ecosystem type (**Supplementary Figure 3**). Thus, the effect of ecosystem should be interpreted in context of parent material, and vice versa.

The mean total WEP ($WEP_{Total}$) concentrations from all the paired interactions (parent material within ecosystem type and ecosystem type within parent material type) were significantly different from each other (**Supplementary Table 6**). The granitic forest soils had the greatest mean $WEP_{Total}$

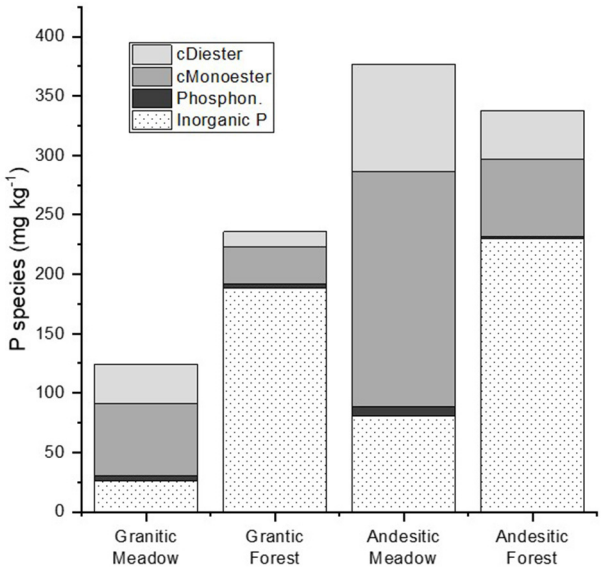


**FIGURE 5 |** Mean P species in soils measured using 31-NMR analysis of NaOH-EDTA extracts of soils. The monoester and diester values were corrected for degradation (denoted with "c" prefix). Inorganic P is the sum of the inorganic orthophosphate and polyphosphate compounds.

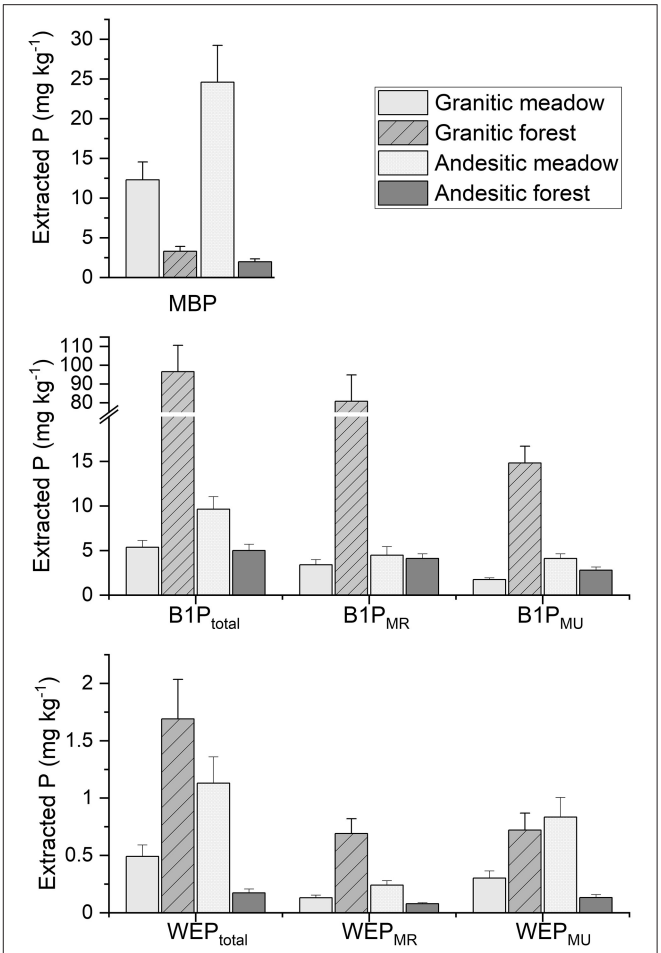


**FIGURE 6 |** Estimated marginal means for water extractable P (WEP) (bottom), Bray 1 extractable P (B1P) (middle), and microbial biomass P (MBP) (top) from soil samples from the different ecosystem and parent material sites. WEP and B1P extract subscripts indicate total solution P, molybdate reactive P (MR), and molybdate unreactive P (MU). Error bars are the standard errors.

concentration of the four ecosystem-parent material types (**Figure 6**). The andesitic forest soils had the lowest mean $WEP_{Total}$ concentration. $WEP_{MU}$ comprised the largest fraction of WEP (**Supplementary Table 6**) in all ecosystem-parent material types. This suggests that most of the WEP exists as soluble organic P compounds or as inorganic P complexed to colloids instead of as dissolved phosphate.

The mean total B1P concentration from the granitic forest soils was more than 10 times greater than the mean B1P concentration from the other soils (**Figure 6**). The B1P concentrations at the two forest soils were significantly different, as were the meadow to forest comparisons (**Supplementary Table 6**). However, the B1P from the andesitic meadow and granitic meadow soils were not significantly different. Most of the B1P was molybdate reactive P (**Supplementary Table 6**), suggesting B1P was predominantly inorganic P extracted from the soil.

The mean MBP concentrations for the meadow soils were approximately seven times more than the mean MBP concentrations from the forest soils (17.4 mg $kg^{-1}$ compared to 2.55 mg $kg^{-1}$, **Supplementary Table 6**). All paired comparisons for the interactions were significantly different. The andesitic meadow soils had the greatest MBP concentrations, followed by the granitic meadow soils (**Figure 6**).

## Water Soluble P of Soil O Horizons

The WEP and $WEP_{MR}$ concentrations from composite O-horizon samples are shown in **Table 2**. The less decomposed Oi composite sample from the granitic site had greater WEP concentrations than the Oe sample.

**TABLE 2 |** Mean[a] WEP and $WEP_{MR}$ extract concentrations from composite samples of the O horizons from the forested sites.

| | Granitic forest | | Andesitic forest | |
|---|---|---|---|---|
| | $WEP_{MR}$ mg $kg^{-1}$ | WEP mg $kg^{-1}$ | $WEP_{MR}$ mg $kg^{-1}$ | WEP mg $kg^{-1}$ |
| Oi | 184 | 254 | - | - |
| Oe | 73.8 | 111 | 107 | 159 |

[a] *Mean of five subsamples from field composite samples. Relative standard deviations of the replicate analyses were between 1 and 6%.*

# DISCUSSION

## Parent Material Effects on Soil P

Total P concentrations in unfertilized soils are typically linked to P content of the parent material, which is the source of P and is also an important control of soil mineralogy that

affects P retention (Gardner, 1990; Porder and Ramachandran, 2013; Hahm et al., 2014). The granitic Meeks Meadow soils developed on granodiorite eroded from glacial till and outwash, while the andesitic soils at Paige Meadow developed on glacial deposits of eroded basaltic and andesitic volcanic rock. In a database of P concentrations of common rock types, mean total P concentrations of granodiorite and granite are 810 and 568 mg $kg^{-1}$, respectively, while mean total P concentrations of basalt, andesite, and basaltic-andesite are 1,304, 1,150, and 1,551 mg $kg^{-1}$ (Porder and Ramachandran, 2013). Total P concentrations in Tahoe soils developed in andesitic parent materials were over two times greater than in soils developed in the granitic parent materials (**Figure 2**), which is consistent with expected differences based on parent material.

In addition to P inputs from parent materials, other P inputs and losses from the soil also affect soil TP concentrations. Phosphorus released from parent material by weathering is taken up by plants and microbes and converted to other P forms and can also be leached out of the soil profile. It has been noted that total P concentrations in forest soils decrease over time (Yang and Post, 2011; Deiss et al., 2018; Nelson et al., 2020). There are no clear trends for WEP, B1P, or MBP concentrations between the granitic or andesitic watersheds (**Figure 6**, **Supplementary Table 6**). However, there were significant differences for WEP, B1P, and MBP when the interaction of parent material type and ecosystem were considered (**Supplementary Figure 3**). The granitic forest soils had much greater WEP and B1P concentrations than the andesitic forest soils, despite having lower TP concentrations. This suggests greater P availability, or more labile P, in the granitic forest soils than in the andesitic forest soils. The labile P is available to either efflux out of the soil or be taken up by plants, thus causing a decrease in TP concentration in the soil. Johnson et al. (1997) reported significantly higher concentrations for a B1P-type extraction from andesitic forest soils than granitic forest soils at other locations in the Lake Tahoe Basin, but did not report concentrations for other P pools such as TP. Brödlin et al. (2019a) observed that in sandy soils derived from glacial-till parent materials in a European deciduous forest, greater P leaching occurred than in soils derived from volcanic rock. Thus, for the granitic forest soils in Lake Tahoe, the decreased TP concentration is both due to the decreased parent material rock-P inputs and export of available P out of the soil. Since the meadow soils are depositional environments, the TP concentrations in these soils reflect the parent material trends as well: andesitic meadows have more TP than granitic meadows. But differences in labile P are not as great as the differences between the forest soils. Thus in the meadows, other ecosystem processes are more important in controlling the availability of the soil P.

In the soils of the current study, soil properties were not clearly delineated by parent material alone. Soil pH was more closely related to ecosystem type than parent materials (**Table 1**), and concentrations of oxalate-extractable Al, Fe, Si and P, and sand content of the andesitic forest were significantly different from the andesitic meadow and the granitic forest and meadow (**Table 1**). The andesitic forest soil properties are due to the andesitic-parent material contributions, while the andesitic meadow is in a depositional environment collecting eroded soils transported from surrounding landscapes. In addition, the hydraulic conditions and vegetative community dynamics of the meadow create pedogenic processes that can overshadow the andic soil properties. Thus, the meadow soil has less andesitic parent material influences, even though it is within a predominantly andesitic parent material landscape. The A horizon in the andesitic forest soils is only 6 cm thick, and thus some of the soil properties in the 15 cm cores sampled from this site were impacted by Bw horizon material (**Supplementary Table 1**). At nearly all of the other sites, except one andesitic meadow profile, A horizons are more than 15 cm thick, and thus the cores represent the pedogenic horizons. The inclusion of Bw material in the andesitic forest soil sample may have contributed to its distinct properties as compared to the other soil cores; however, the mineral properties of this sample as measured by the oxalate extractable Fe, Al, and Si (**Table 1**) are indicative of andic soils, which have high concentrations of poorly crystalline aluminum and iron oxides in both the surface and subsurface horizons. Thus, the andesitic soil samples, while composed of A and B horizon soils, have mineral properties that are indicative of the andesitic parent materials from which the soils developed and the soil P properties from this sample are indicative of the top 15 cm of the soil.

Soil P sorption capacity is related to clay minerals and iron and aluminum oxides (Gerard, 2016). The andesitic forest soils had the lowest sand content and the highest concentrations of amorphous iron hydroxides and aluminosilicates (**Table 1**), suggesting that P adsorption on mineral surfaces will be strong in these soils (Khare et al., 2005; Redel et al., 2008). Phosphorus complexed as Al or Fe-organic matter ternary complexes are also common in andesitic soils (Gerke and Hermann, 1992; Gerke, 2010). Oxalate-extractable P was positively correlated to oxalate extractable Fe, Al, and Si ($r = 0.82$, 0.85, 0.82, respectively; **Supplementary Figure 2**) and the highest concentrations of oxalate-extractable P were in the andesitic forest soils (**Table 1**), confirming the relation of the soil P to the andesitic soil minerals.

Sorption capacity will influence both inorganic and organic P forms. Total organic P in the Lake Tahoe soils does not appear to be related to the parent material, beyond the differences in TP already discussed, and is clearly more influenced by ecosystem (**Figure 3**; **Supplementary Table 2**). For specific organic P forms, correlations of concentrations of *myo*-IHP and other IHP stereoisomers with concentrations of oxalate-extractable Fe and Al have been widely reported for soils and are thought to demonstrate the sorption of these compounds to amorphous iron hydroxides and aluminosilicates (Jorgensen et al., 2015; Nelson et al., 2020). The average of the percentage of total extracted IHP (**Supplementary Table 4**) for the eight granitic soils was similar to that for the four andesitic soils (13.1 and 11.3% respectively), while the average concentrations of total IHP in andesitic soils were double those of the granitic soils (41.2 vs. 20.2 mg $kg^{-1}$). The same trend was also observed for DNA and the general Diester 1 category (**Supplementary Table 3**). In acidic soils, adsorption of DNA occurs, and its NaOH-EDTA-extracted concentrations have been correlated with those of oxalate-extracted Fe and Al (Condron et al., 2005; Nelson et al.,

2020). However, the Diester 1 category includes phospholipids and lipoteichoic acids, which do not sorb to soil minerals (Condron et al., 2005). The differences in concentrations of these compounds and compound classes are consistent with differences in total concentrations of P in the NaOH-EDTA extracts (**Supplementary Table 2**), which are consistent with total concentrations of soil P (**Figure 2**), so may simply reflect trends in total P rather than selective binding of P compounds.

## Ecosystem Type and Soil P

Although TP concentration did not differ between ecosystem types at the two different parent material watersheds, total organic P measured by the incineration method was substantially greater in meadow soils than forest soils (85.5 vs. 36.2%, averaging data from **Figure 3**). The same trend was observed for total organic P determined by P-NMR, even though the recovery of total P was lower in NaOH-EDTA extracts from meadow soils (40.8%) than forest (61.9%, averaging data in **Supplementary Table 2**), which could underestimate inorganic P. Chiu et al. (2005) measured P-NMR spectra in NaOH-EDTA extracts from subalpine grassland and forest soils and observed a similar fractionation of inorganic and organic P forms between the two ecosystems. In addition to differences in total organic P, P-NMR revealed differences in P forms and compound classes between the two ecosystem types (**Figure 3**, **Supplementary Table 4**).

The forest and meadow ecosystems differ in vegetation, elevation, and slope position, all of which influence P cycling. The plant species in the meadows have above and below-ground vegetation that can readily decompose compared to forests (Margalef et al., 2017). In forests, litter is deposited onto the forest floor and gets incorporated into an Oi horizon that decomposes to an Oe horizon. An Oi horizon with identifiable pine needles was observed in the granitic soil, but not the andesitic forest. This may be due to andesitic soil properties that increase soil moisture retention, which facilitates greater microbial decomposition rates and thus quicker breakdown of forest litter (Sun et al., 2017). Different species of plants and even the same species of plants growing under different soil fertility conditions will contribute different P species (Noack et al., 2014) that can change with depth in the soil profile (Nelson et al., 2020).

The vegetation from these ecosystems was not analyzed by P-NMR, so we cannot say with certainty the P forms input from plants. However, *myo*-IHP is widely recognized as a plant P compound (Condron et al., 2005). Other compounds may originate from plants or microbes or can be produced by alteration of plant-P compounds (Condron et al., 2005). In the soils of this study, microbial P (MBP) concentrations were greater in meadow soils than they were in forest soils. However, in coniferous forests, the majority of microbial activity and P cycling occurs in the O horizon, associated with the hyphal mat of ectomycorrhizal fungi at the soil-organic matter interface (Plassard et al., 2011; Nelson et al., 2020). This may account for difference in P forms and MBP concentrations between these ecosystems and would be consistent with the substantially higher WEP concentrations in O horizons (**Table 2**) than mineral soils in the forest.

Availability of soil P controls P immobilization into microbial biomass (Olander and Vitousek, 2004; Yang and Post, 2011; Spohn and Widdig, 2017; Pistocchi et al., 2018). For example, Pistocchi et al. (2018) observed that during incubation of a deciduous forest soil with low available P, P cycling between soil and microbial biomass was conservative, while in soil with higher available P there was more exchange between microbial-bound P and inorganic soil P pools (i.e., mineral-bound P). Thus, in forest soils, when P availability exceeds biological demands, geochemical processes (adsorption and precipitation) predominate over immobilization by microbes (Olander and Vitousek, 2004); this implies that geochemical processes control P availability for leaching or root uptake in the mineral soil horizons. In the andesitic soils, the decreased labile P concentrations (**Figure 6**) inhibit microbial P fixation, causing low MBP. Aluminum toxicity is another cause of decreased MBP in the andic forest soils because high soluble Al concentrations inhibit microbial enzyme production, including phosphatase, thereby limiting P immobilization (Kunito et al., 2016).

Another possible cause of the MBP increase in the meadow soils compared to the forest soils is the increase in N availability in the meadow soils (**Table 2**). Microbes mineralize organic P for microbial uptake using phosphatase enzymes, which require N for production (Vitousek et al., 2010; Marklein and Houlton, 2012). Total N and MBP were significantly correlated ($r = 0.81$) (**Supplementary Figure 3**). Thus, the occurrence of sufficient N availability for phosphatase generation in the meadows facilitates degradation of organic P compounds, and subsequently, the biologically available P can be immobilized by microbes. Soil moisture may also play a factor, with greater moisture in the meadows increasing microbial activity.

Mycorrhizal association may also greatly influence P cycling. The ectomycorrhizal fungi found in forests will produce more phosphatases than endomycorrhizae associated with meadow plants (Plassard et al., 2011; Margalef et al., 2017). They will also produce organic acids such as oxalate (Plassard et al., 2011). These will desorb both inorganic and organic P, and both organic acids and phosphatases may need to be present simultaneously to mineralize organic P (Giles et al., 2018). This could also account for the reduced organic P concentrations in these forests compared to meadows.

In meadows, high seasonal water tables can have a significant impact on soil properties that influences P cycling. This, combined with high organic C concentrations, can mask the influence of mineralogy on labile P (Sah et al., 1989; Johnston et al., 1995). Sah et al. (1989) observed that C availability controlled P availability in wetland soils: when total organic C concentration exceeded 0.8%, it promoted the reduction of ferric ($Fe^{3+}$) oxides, which decreased sorption capacity of the soil for P. Alternatively, during periods of flooding, the precipitation of ferrous iron-phosphate minerals such as vivianite may occur (Zhang et al., 2003; Heiberg et al., 2010; Rothe et al., 2016), which is less soluble upon drainage because the P remains occluded by oxidized iron-hydroxide minerals that form when the vivianite oxidizes (Sah and Mikkelsen, 1986b). The seasonal redox cycles that occur in wetland soils may decrease P leaching compared to unflooded soils, even after soils remained drained

over 4 months (Sah and Mikkelsen, 1986a). In contrast, Gergans et al. (2011) proposed that excess sulfate in Tahoe Basin wetland soils facilitates production of iron sulfides during reducing conditions that make Fe unavailable when the soils re-oxidize to adsorb phosphate and organic P compounds, thus making soil P more available for continued leaching in these wetland soils. Based on the varying results of the studies discussed above, there are several factors that influence P speciation in Lake Tahoe Basin meadows, including seasonal flooding, high organic matter, and Fe biogeochemical transformations. These factors may be more important than parent materials for controlling P mobility. The presence of higher concentrations of phosphonates in meadow soils compared to forest soils is also consistent with higher moisture levels (Condron et al., 2005), and higher diester concentrations have also been reported for poorly drained soils compared to well-drained soils (Young et al., 2013).

## Labile Soil P and Potential Loss to Lake Tahoe

Soil P buffering capacity is the degree to which soil can adsorb or release P from exchange sites to maintain dissolved P concentrations in the soil solution (Holford, 1997). Soils with larger total P reserves are considered to have greater buffering capacity to replenish P taken up by plants or leached out of the soil (Daly et al., 2015). An estimate of soil P buffering capacity is the P saturation index (PSI), which is calculated as concentrations of oxalated-extracted P divided by the sum of the oxalate-extracted Fe and Al (Schoumans, 2009). For the Lake Tahoe watershed soils, PSI was 0.029 and 0.072 for the granitic meadow and forest soils, and 0.047 and 0.029 for the andesitic meadow and forest soil (**Table 1**).

Of the extractants used in this study, WEP measures the most labile P, B1P extracts less labile P that is sorbed to the soil, and oxalate or NaOH-EDTA extract both labile P and P that is more tightly held by soil through either adsorption complexes, mineral-bound P, or larger organic P compounds. In all of the Lake Tahoe Basin soils, B1P concentrations were approximately an order of magnitude greater than WEP concentrations (**Figure 6**), suggesting a large amount of adsorbed P is released by the B1P extractant that is not released by water extraction. Although a stronger P buffering capacity is expected in the andesitic forest soils, where the highest TP was observed, the lower PSI in these soils suggests there is excess P sorption capacity on high-adsorption affinity iron and aluminum oxides, thus causing the lower concentrations of labile P (WEP and B1P) as compared to the granitic forest soils. The B1P extractant apparently did not access the P in the andesitic soils that was either strongly adsorbed, had formed Al or Fe-P mineral phases with low solubility (Negrín et al., 1996), or was complexed as Al or Fe-organic matter ternary complexes, which are common in andesitic soils (Gerke and Hermann, 1992; Gerke, 2010). The NaOH-EDTA extracts removed a much greater amount of the total P than the B1P extracts (**Supplementary Table 6**) but were similar in concentration to those of oxalate-extractable P (**Table 1**). Thus, there appears to be a large reserve of P associated with iron oxide and allophane minerals in the andesitic forest soils that is not readily available for release to the soil solution.

Analysis of the NaOH-EDTA soil extracts from the andesitic forests by P-NMR showed that 26–46% of the extracted P was organic P species (**Supplementary Table 4**). This organic P fraction in the andesitic soils may be slowly available to plants and microbes that release organic acids, which enhance P release through competitive exchange (Harrold and Tabatabai, 2006), and which may be synergistic with hydrolysis of organic P compounds by phosphatases (Giles et al., 2018).

Most of the WEP in forests and meadow soils from Lake Tahoe was not reactive with molybdate blue chemistry ($WEP_{MU}$) (**Figure 6**, **Supplementary Table 6**). The source of water-extractable organic P compounds are inputs from plants and soil microbes. The predominance of $WEP_{MU}$ from both forest and meadow soils in the Lake Tahoe Basin is a potential source of mobile P that most likely consists of organic P compounds (Worsfold et al., 2016). The labile organic P compounds can be transported to Lake Tahoe by vertical and lateral transport processes, especially during high intensity events that cause preferential flow through macropores, which are common in coniferous forest soils (Luo et al., 2019). Organic P species have been reported in soil leachate, snowmelt runoff, and samples of river inlet and floodplain waters during flooding events (Toor et al., 2003; Cade-Menun et al., 2006; Wiens et al., 2019), and in water-extractable colloids from grasslands and forests (Missong et al., 2016; Jiang et al., 2017).

Water-soluble P from leaf litter is an important source of labile P return to the soil (Uselman et al., 2012; Sohrt et al., 2019). In a separate study of soluble P from O horizons from Lake Tahoe Basin (unpublished data), nine samples were collected from forest and meadow sites near the Paige Meadow and Meeks Bay watersheds. WEP concentrations in these samples ranged from 54 to 209 mg $kg^{-1}$ (mean = 122 mg $kg^{-1}$, standard deviation = 45 mg $kg^{-1}$), indicating that WEP concentrations in the O-horizon samples are highly variable throughout the two watersheds. Based on the two Oe composite samples (**Table 2**), molybdate-reactive P (inorganic P) was the predominant phase of WEP (67% in both the granitic and andesitic forests). The concentration of P from the composite Oi horizon sample from the granitic site was more than twice that of the Oe horizon sample, suggesting P is lost from the litter as it decomposes (**Table 2**).

The Oe WEP concentration was ∼58 times greater than soil A horizon WEP concentration in the granitic forest soils, and 690 times greater than in andesitic forest soils. Miller et al. (2005) measured soluble P from O horizons of Lake Tahoe Basin forest soils using laboratory simulated precipitation and snowmelt leaching experiments and observed 46 mg $kg^{-1}$ of soluble P leached from the less decomposed Oi horizon and 28 mg $kg^{-1}$ from the more decomposed Oe horizon. The O horizons in the Miller et al. (2005) study came from Jeffrey and Sugar Pine forests in a granitic watershed. Although the Miller et al. (2005) water extraction methods were different than those used in this study, both the Miller et al. (2005) leaching experiment and this study's granitic forest O-horizon samples (**Table 2**) have more water-soluble P in the minimally decomposed Oi horizons compared to the more decomposed Oe horizons.

Approximately one-third of the WEP from the O horizon samples was $WEP_{MU}$, which could be a considerable source of

organic P mobilized into the soil and possibly to the surface water, depending on the organic P species and reactivity. Both the granitic and andesitic sites have a similar vegetative density (41 vs. 49%) (Landfire, 2020), thus, vegetative P inputs to the soils should be similar in the two watersheds. However, based on the greater WEP and B1P concentrations in the granitic forest soils, P outputs to streams and groundwater are expected to be much greater from these systems; this is due to the lower sorption capacity of the soils that allows for a significant amount of P release in the extractions. Uhlig and von Blanckenburg (2019) estimated that P inventory of the forest litter in montane, temperate forest ecosystems can only sustain vegetative demand for a few decades, and that continuous release of P from parent rocks must occur to sustain forest growth. The different adsorption capacities of the andesitic and granitic soils in the Lake Tahoe forests can have a major influence on the timescales of P availability and its cycling between the forests, litter, and parent material.

There are several sinks for WEP from forest litter: it can be taken up by plants and microorganisms for internal cycling; leached into the soil where it may adsorb, be immobilized, or further leached into ground water; or be transported off site via surface runoff of dissolved P or eroded P-containing particles. Although concentrations of WEP in the O horizons are much greater than the soils, it is a much smaller total P pool in the ecosystem than soil P, which is large and stores much of the WEP leached into it from O horizons (Yang and Post, 2011). The high concentrations of soluble P in the Lake Tahoe Basin O horizon samples indicate that a large flux of available P can enter the soil. Much of this flux occurs during spring snowmelt. The fate of this O horizon-sourced P is a function of the characteristics of soil biological and physical properties and site hydrology.

Ohara et al. (2011) recorded that more than 90% of field-observed hillslope drainage in a Lake Tahoe watershed occurred as subsurface lateral flow through the soil. Thus, soil reactions are important processes controlling P transport to surface waters, which would be especially high during periods of continuous snowmelt. These processes are impacted by the species of soluble P in the soils, which both the soil extractions and soil P-NMR analyses suggest are both inorganic and organic P species.

When streams near our research sites experience peak discharge, molybdate-unreactive fractions make up 61–67% of filterable (<0.45 μm) P [**Supplementary Figure 4** (USGS, 2016)]. Therefore, molybdate-reactive and unreactive fractions in these nearby streams during snowmelt more closely reflect the WEP fractionation of soils (50–74% $WEP_{MU}$; **Supplementary Table 6**) than $WEP_{MU}$ from O horizons (28–36%; **Table 2**). A possible explanation of this is that during high-flow periods, the inorganic (molybdate-reactive) P species are attenuated by forest and meadow soils leading to net exports of organic forms. Thus, the flowing solution reflects the $WEP_{MU}$ fraction leaching from the soil. Bol et al. (2016) conducted an extensive review of P fluxes in forested ecosystems and concluded that P loss as colloidal-organic P that is exported from soil profiles through macropores during high-intensity rainfall events is likely a critical factor in P export. Colloidal organic P would be included in the $WEP_{MU}$ fraction in this study. Considering that organic P increases in the stream in the Lake Tahoe Basin during high-intensity events (**Supplementary Figure 4**), preferential-flow path loading is a likely scenario occurring in forest and meadow watersheds in the Lake Tahoe Basin. However, to explain the molybdate unreactive ratio of the stream water, there must be attenuation of the inorganic P as it moves through the preferential flow paths; otherwise the ratio of inorganic to organic P forms in the stream water would be more similar to the ratios in the O-horizon extracts. Alternatively, forest soils may be transporting P-laden water through preferential flow paths where P attenuation is minimal, but as the flow continues toward the streams, it is intercepted by riparian meadows that have fewer preferential flow paths, enhanced groundwater storage, and greater microbial activity that immobilizes orthophosphate, causing the soil water that exfiltrates into the streams to have a greater proportion of $WEP_{MU}$ than what is leached from the forest O horizons. A third mechanism of inorganic P attenuation that may enrich Lake Tahoe Basin stream waters with molybdate unreactive P is preferential adsorption of inorganic P within the stream on suspended particles eroded from soils. Since the highest total suspended solids occurs during high runoff events, adsorption may be significant enough to alter the dissolved inorganic and organic solution composition during these periods.

Because molybdate unreactive P (organic P) accounted for the majority of WEP from the Lake Tahoe Basin soils (**Figure 6**), it is likely the most vulnerable for transport as lateral flow during spring snowmelt or exfiltration from meadows, thereby increasing the P load in surface waters. The high concentrations of P released from litter suggests that forest management practices that remove timber and deposit deep layers of chopped fresh organic matter (mastication) to prevent erosion may be creating a potential source of P that can be leached into surface waters—at least in the short-term time it takes for the material to degrade. In watersheds with soils developed on granitic parent materials, this would be especially problematic. A beneficial focus of future research would be an examination of the speciation of P in the forest O horizons and comparison to P forms in both forest and meadow soils, as well as measurement of soil and stream water samples for P-species composition. Additionally, evaluation of the subsoil deeper than 15 cm should be done to account for how P reactions influence leaching through the deeper soil profile.

## CONCLUSION

In soils in the Lake Tahoe Basin, P storage shifts from sorption on minerals in forests, to immobilization in microbial biomass in meadows. In forested hillslopes, adsorbed P may be gradually depleted if it is leached from the soil into ground and surface water. The degree of P depletion depends on the parent materials from which the soils developed (granitic vs. andesitic). In soils developed on andesitic parent materials, forest cycling of P is mediated by the high adsorption capacity of P on andic minerals, while in soils derived from granitic parent materials the increased resistance to weathering creates coarser-textured soils and fewer

soil clays, causing a decreased P adsorption capacity. As a result, granitic soils have greater potential P mobilization into groundwater and lateral runoff into surface waters.

Organic P was a predominant water-extractable fraction from all soils. Total organic P concentration was greater in meadow soils than forest soils, and in all soils of this study, orthophosphate monoesters were the main organic P compound class, even after correcting for diester degradation during analysis. The organic P compounds in the soils can be leached into the surface waters. Once in the surface water, mineralization of the organic P compounds can make phosphate available to aquatic organisms, causing surface water quality degradation.

Results from this study provide insights into speciation of P in forest and meadow soils and show the importance of parent materials on P availability. This information can be used to better understand which ecosystems present the most risks for P loading into Lake Tahoe, which will allow for better forest management practices to prevent P export into feeder streams and groundwater that discharge into the lake. Current management strategies use controlled burns and erosion prevention strategies to prevent P loss from Lake Tahoe Basin soils into the lake. Resource managers need to consider the highly variable sources of P in the Basin to decide which watersheds are most vulnerable to P loss, such as the granitic forest watersheds, and match management strategy to site properties to optimize the site management for decreased P loss.

## DATA AVAILABILITY STATEMENT

The original contributions presented in the study are included in the article/**Supplementary Material**, further inquiries can be directed to the corresponding author/s.

## AUTHOR CONTRIBUTIONS

TH conducted the research and reported it as part of a MS thesis at the University of Idaho. DS is the corresponding author and led all aspects of the research and writing of this manuscript. MD, CD, EB, and CG designed the research and assisted with experiments and data interpretation. BC-M conducted NMR data analyses and interpretation as well as helped interpret all of the experimental data. JP did the mixed-model statistical analyses of the data and consulted in data interpretation. AC assisted with conducting experiments and collecting and analyzing data. All authors contributed to writing and editing of the article and approved the submitted version.

## FUNDING

This work was supported by AFRI program (Grant No. 2016-67020-25320/project accession no. 1009827) from the USDA National Institute of Food and Agriculture.

## ACKNOWLEDGMENTS

We appreciate assistance with NMR experiments by Alex Blumenfeld in the University of Idaho Chemistry Department, and assistance with O horizon water extractable P measurements by Tiffany Perez.

## SUPPLEMENTARY MATERIAL

The Supplementary Material for this article can be found online at: https://www.frontiersin.org/articles/10.3389/ffgc.2020.604200/full#supplementary-material

## REFERENCES

Anderson, B. H., and Magdoff, F. R. (2005). Relative movement and soil fixation of soluble organic and inorganic phosphorus. *J. Env. Qual.* 34, 2228–2233. doi: 10.2134/jeq2005.0025

Backnäs, S., Laine-Kaulio, H., and Klove, B. (2012). Phosphorus forms and related soil chemistry in preferential flowpaths and the soil matrix of a forested podzolic till soil profile. *Geoderma* 189, 50–64. doi: 10.1016/j.geoderma.2012.04.016

Bol, R., Julich, D., Brödlin, D., Siemens, J., Kaiser, K., Dippold, M. A., et al. (2016). Dissolved and colloidal phosphorus fluxes in forest ecosystems: an almost blind spot in ecosystem research. *J. Plant Nutr. Soil Sci.* 179, 425–438. doi: 10.1002/jpln.201600079

Brödlin, D., Kaiser, K., and Hagedorn, F. (2019a). Divergent patterns of carbon, nitrogen, and phosphorus mobilization in forest soils. *Front. Glob. Chang.* 2:66. doi: 10.3389/ffgc.2019.00066

Brödlin, D., Kaiser, K., Kessler, A., and Hagedom, F. (2019b). Drying and rewetting foster phosphorus depletion of forest soils. *Soil Biol. Biochem.* 128, 22–34. doi: 10.1016/j.soilbio.2018.10.001

Cade-Menun, B., and Liu, C. W. (2014). Solution phosphorus-31 nuclear magnetic resonance spectroscopy of soils from 2005 to 2013: a review of sample preparation and experimental parameters. *Soil Sci. Soc. Am. J.* 78, 19–37. doi: 10.2136/sssaj2013.05.0187dgs

Cade-Menun, B. J. (2015). Improved peak identification in P-31-NMR spectra of environmental samples with a standardized method and peak library. *Geoderma* 257, 102–114. doi: 10.1016/j.geoderma.2014.12.016

Cade-Menun, B. J., He, Z. Q., Zhang, H. L., Endale, D. M., Schomberg, H. H., and Liu, C. W. (2015). Stratification of phosphorus forms from long-term conservation tillage and poultry litter application. *Soil Sci. Soc. Am. J.* 79, 504–516. doi: 10.2136/sssaj2014.08.0310

Cade-Menun, B. J., and Lavkulich, L. M. (1997). A comparison of methods to determine total, organic, and available phosphorus in forest soils. *Comm. Soil Sci. Plant Anal.* 28, 651–663. doi: 10.1080/00103629709369818

Cade-Menun, B. J., Navaratnam, J. A., and Walbridge, M. R. (2006). Characterizing dissolved and particulate phosphorus in water with P-31 nuclear magnetic resonance spectroscopy. *Env. Sci. Tech.* 40, 7874–7880. doi: 10.1021/es061843e

Cade-Menun, B. J., and Preston, C. M. (1996). A comparison of soil extraction procedures for P-31 NMR spectroscopy. *Soil Sci.* 161, 770–785. doi: 10.1097/00010694-199611000-00006

Campo, J., Jaramillo, V. J., and Maass, J. M. (1998). Pulses of soil phosphorus availability in a Mexican tropical dry forest: effects of seasonality and level of wetting. *Oecologia* 115, 167–172. doi: 10.1007/s004420050504

Casey, R. E., and Klaine, S. J. (2001). Nutrient attenuation by a riparian wetland during natural and artificial runoff events. *J. Env. Qual.* 30, 1720–1731. doi: 10.2134/jeq2001.3051720x

Chiu, C. Y., Pai, C. W., and Yang, K. L. (2005). Characterization of phosphorus in sub-alpine forest and adjacent grassland soils by chemical extraction and phosphorus-31 nuclear magnetic resonance spectroscopy. *Pedobiologia* 49, 655–663. doi: 10.1016/j.pedobi.2005.06.007

Coats, R., Lewis, J., Alvarez, N. L., and Arneson, P. (2016). Temporal and spatial trends in nutrient and sediment loading to Lake Tahoe, California-Nevada, USA. *J. Am. Water Resour. Assoc.* 52, 1347–1365. doi: 10.1111/1752-1688.12461

Condron, L. M., Turner, B. L., and Cade-Menun, B. J. (2005). "Chemistry and Dynamics of Soil Organic Phosphorus," in *Phosphorus: Agriculture and the Environment*, eds J. T. Sims and A. N. Sharpley (Madison, WI: American Society of Agronomy), 87–121. doi: 10.2134/agronmonogr46.c4

Daly, K., Styles, D., Lalor, S., and Wall, D. P. (2015). Phosphorus sorption, supply potential and availability in soils with contrasting parent material and soil chemical properties. *Eur. J. Soil Sci.* 66, 792–801. doi: 10.1111/ejss.12260

Deiss, L., de Moraes, A., and Maire, V. (2018). Environmental drivers of soil phosphorus composition in natural ecosystems. *Biogeoscience* 15, 4575–4592. doi: 10.5194/bg-15-4575-2018

Ehlers, J., and Gibbard, P. L. (2003). Extent and chronology of glaciations. *Quaternary Sci. Rev.* 22, 1561–1568. doi: 10.1016/S0277-3791(03)00130-6

Elser, J. J., Andersen, T., Baron, J. S., Bergstrom, A. K., Jansson, M., Kyle, M., et al. (2009). Shifts in Lake N:P stoichiometry and nutrient limitation driven by atmospheric nitrogen deposition. *Science* 326, 835–837. doi: 10.1126/science.1176199

Gardner, L. R. (1990). The role of rock weathering in the phosphorus budget of terrestrial watersheds. *Biogeochemistry* 11, 97–110. doi: 10.1007/BF00002061

Gerard, F. (2016). Clay minerals, iron/aluminum oxides, and their contribution to phosphate sorption in soils - a myth revisited. *Geoderma* 262, 213–226. doi: 10.1016/j.geoderma.2015.08.036

Gergans, N., Miller, W. W., Johnson, D. W., Sedinger, J. S., Walker, R. F., and Blank, R. R. (2011). Runoff water quality from a Sierran upland forest, transition ecotone, and riparian wet meadow. *Soil Sci. Soc. Am. J.* 75, 1946–1957. doi: 10.2136/sssaj2011.0001

Gerke, J. (2010). Humic (organic matter)-Al(Fe)-phosphate complexes: an underestimated phosphate form in soils and source of plant-available phosphate. *Soil Sci.* 175, 417–425. doi: 10.1097/SS.0b013e3181f1b4dd

Gerke, J., and Hermann, R. (1992). Adsorption of orthophosphate to humic-Fe-Complexes and to amorphous Fe-oxide. *Z. Pflanzen. Bodenk.* 155, 233–236. doi: 10.1002/jpln.19921550313

Giles, C. D., Richardson, A. E., Cade-Menun, B. J., Mezeli, M. M., Brown, L. K., Menezes-Blackburn, D., et al. (2018). Phosphorus acquisition by citrate- and phytase-exuding Nicotiana tabacum plant mixtures depends on soil phosphorus availability and root intermingling. *Physiol. Plantarum* 163, 356–371. doi: 10.1111/ppl.12718

Goldberg, S. J., Ball, G. I., Allen, B. C., Schladow, S. G., Simpson, A. J., Masoom, H., et al. (2015). Refractory dissolved organic nitrogen accumulation in high-elevation lakes. *Nat. Commun.* 6:6347. doi: 10.1038/ncomms7347

Hahm, W. J., Riebe, C. S., Lukens, C. E., and Araki, S. (2014). Bedrock composition regulates mountain ecosystems and landscape evolution. *Proc. Natl. Acad. Sci. U.S.A.* 111, 3338–3343. doi: 10.1073/pnas.1315667111

Harrold, S. A., and Tabatabai, M. A. (2006). Release of inorganic phosphorus from soils by low-molecular-weight organic acids. *Comm. Soil Sci. Plant Anal.* 37, 1233–1245. doi: 10.1080/00103620600623558

Hatch, L. K., Reuter, J. E., and Goldman, C. R. (1999). Relative importance of stream-borne particulate and dissolved phosphorus fractions to Lake Tahoe phytoplankton. *Can. J. Fish Aquatic Sci.* 56, 2331–2339. doi: 10.1139/f99-166

Hatch, L. K., Reuter, J. E., and Goldman, C. R. (2001). Stream phosphorus transport in the Lake Tahoe basin, 1989-1996. *Environ. Monit. Assess* 69, 63–83. doi: 10.1023/A:1010752628576

Haygarth, P. M., and Sharpley, A. N. (2000). Terminology for phosphorus transfer. *J. Env. Qual.* 29, 10–15. doi: 10.2134/jeq2000.00472425002900010002x

Haygarth, P. M., Warwick, M. S., and House, W. A. (1997). Size distribution of colloidal molybdate reactive phosphorus in river waters and soil solution. *Water Res.* 31, 439–448. doi: 10.1016/S0043-1354(96)00270-9

Heiberg, L., Pedersen, T. V., Jensen, H. S., Kjaergaard, C., and Hansen, H. C. B. (2010). A comparative study of phosphate sorption in lowland soils under oxic and anoxic conditions. *J. Env. Qual.* 39, 734–743. doi: 10.2134/jeq2009.0222

Hoffmann, C. C., Berg, P., Dahl, M., Larsen, S. E., Andersen, H. E., and Andersen, B. (2006). Groundwater flow and transport of nutrients through a riparian meadow - field data and modelling. *J. Hydrol.* 331, 315–335. doi: 10.1016/j.jhydrol.2006.05.019

Hoffmann, C. C., Kjaergaard, C., Uusi-Kamppa, J., Hansen, H. C. B., and Kronvang, B. (2009). Phosphorus retention in riparian buffers: review of their efficiency. *J. Env. Qual.* 38, 1942–1955. doi: 10.2134/jeq2008.0087

Holford, I. C. R. (1997). Soil phosphorus: its measurement, and its uptake by plants. *Aust. J. Soil Res.* 35, 227–239. doi: 10.1071/S96047

Jassby, A. D., Goldman, C. R., Reuter, J. E., and Richards, R. C. (1999). Origins and scale dependence of temporal variability in the transparency of Lake Tahoe, California-Nevada. *Limnol. Oceanogr.* 44, 282–294. doi: 10.4319/lo.1999.44.2.0282

Jiang, X. Q., Bol, R., Cade-Menun, B. J., Nischwitz, V., Willbold, S., Bauke, S. L., et al. (2017). Colloid-bound and dissolved phosphorus species in topsoil water extracts along a grassland transect from Cambisol to Stagnosol. *Biogeoscience* 14, 1153–1164. doi: 10.5194/bg-14-1153-2017

Johnson, D. W., Susfalk, R. B., and Dahlgren, R. A. (1997). Nutrient fluxes in forests of the eastern Sierra Nevada mountains, United States of America. *Global Biogeochem. Cy* 11, 673–681. doi: 10.1029/97GB01750

Johnston, C. A., Pinay, G., Arens, C., and Naiman, R. J. (1995). Influence of soil properties on the biogeochemistry of a beaver meadow hydrosequence. *Soil Sci. Soc. Am. J.* 59, 1789–1799. doi: 10.2136/sssaj1995.03615995005900060041x

Jorgensen, C., Turner, B. L., and Reitzel, K. (2015). Identification of inositol hexakisphosphate binding sites in soils by selective extraction and solution P-31 NMR spectroscopy. *Geoderma* 257, 22–28. doi: 10.1016/j.geoderma.2015.03.021

Julich, D., Julich, S., and Feger, K.-H. (2017). Phosphorus in preferential flow pathways of forest soils in Germany. *Forests* 8:19. doi: 10.3390/f8010019

Khare, N., Hesterberg, D., and Martin, J. D. (2005). XANES investigation of phosphate sorption in single and binary systems of iron and aluminum oxide minerals. *Env. Sci. Tech.* 39, 2152–2160. doi: 10.1021/es049237b

Kortemeier, W., Calvert, A., Moore, J. G., and Schweickert, R. (2018). Pleistocene volcanism and shifting shorelines at Lake Tahoe, California. *Geosphere* 14, 812–834. doi: 10.1130/GES01551.1

Kunito, T., Isomura, I., Sumi, H., Park, H. D., Toda, H., Otsuka, S., et al. (2016). Aluminum and acidity suppress microbial activity and biomass in acidic forest soils. *Soil Biol. Biochem.* 97, 23–30. doi: 10.1016/j.soilbio.2016.02.019

Kuo, S. (1996). "Phosphorus," in *Methods of Soil Analysis*, ed. D.L. Sparks. (Madison, WI: Soil Science Society of America), 869.

Landfire (2020). Forest Canopy Cover Layer, LANDFIRE 2.0.0. U.S. Department of the Interior, Geological Survey. Available online at: http://landfire.cr.usgs.gov/viewer/ [accessed March, 2020].

Lenth, R. (2019). "Emmeans: Estimated Marginal Means, aka Least-Squares Means," in: *Package for R.* 1.4.2 ed.).

Luo, Z., Niu, J., Zhang, L., Chen, X., Zhang, W., Xie, B., et al. (2019). Roots-enhanced preferential flows in deciduous and coniferous forest soils revealed by dual-tracer experiments. *J. Env. Qual.* 48, 136–146. doi: 10.2134/jeq2018.03.0091

Margalef, O., Sardans, J., Fernandez-Martinez, M., Molowny-Horas, R., Janssens, I. A., Ciais, P., et al. (2017). Global patterns of phosphatase activity in natural soils. *Sci. Rep.* 7:1337. doi: 10.1038/s41598-017-01418-8

Marklein, A. R., and Houlton, B. Z. (2012). Nitrogen inputs accelerate phosphorus cycling rates across a wide variety of terrestrial ecosystems. *New Phytol.* 193, 696–704. doi: 10.1111/j.1469-8137.2011.03967.x

McDowell, R. W., Stewart, I., and Cade-Menun, B. J. (2006). An examination of spin-lattice relaxation times for analysis of soil and manure extracts by liquid state phosphorus-31 nuclear magnetic resonance spectroscopy. *J. Env. Qual.* 35, 293–302. doi: 10.2134/jeq2005.0285

Miller, W. W., Johnson, D. E., Loupe, T. M., Sedinger, J. S., Carroll, E. M., Murphy, J. H., et al. (2006). Nutrients flow from runoff at burned forest site in Lake Tahoe Basin. *California Agriculture* 60, 65–71. doi: 10.3733/ca.v060n02p65

Miller, W. W., Johnson, D. W., Denton, C., Verburg, P. S. J., Dana, G. L., and Walker, R. F. (2005). Inconspicuous nutrient laden surface runoff from mature forest Sierran watersheds. *Water Air Soil Poll.* 163, 3–17. doi: 10.1007/s11270-005-7473-7

Miller, W. W., Johnson, D. W., Karam, S. L., Walker, R. F., and Weisberg, P. J. (2010). A synthesis of Sierran forest biomass management studies and potential effects on water quality. *Forests* 1, 131–153. doi: 10.3390/f1030131

Missong, A., Bol, R., Willbold, S., Siemens, J., and Klumpp, E. (2016). Phosphorus forms in forest soil colloids as revealed by liquid-state 31P-NMR. *J. Plant Nutr. Soil Sci.* 179, 159–167. doi: 10.1002/jpln.201500119

Murphy, J., and Riley, J. P. (1962). A modified single solution method for determination of phosphate in natural waters. *Anal. Chim. Acta* 26, 31–36. doi: 10.1016/S0003-2670(00)88444-5

Negrín, M. A., Espino-Mesa, M., and Hernández-Moreno, J. M. (1996). Effect of water: soil ratio on phosphate release: P, aluminium and fulvic acid associations

in water extracts from Andisols and Andic soils. *Eur. J. Soil Sci*. 47, 385–393. doi: 10.1111/j.1365-2389.1996.tb01412.x

Nelson, L., Cade-Menun, B., Walker, I., and Sanborn, P. (2020). Soil phosphorus dynamics across a Holocene chronosequence of aeolian sand dunes on Calvert Island, BC, Canada. *Front. For. Glob. Chang*. 3:83. doi: 10.3389/ffgc.2020.00083

Noack, S. R., McLaughlin, M. J., Smernik, R. J., McBeath, T. M., and Armstrong, R. D. (2014). Phosphorus speciation in mature wheat and canola plants as affected by phosphorus supply. *Plant Soil* 378, 125–137. doi: 10.1007/s11104-013-2015-3

Oberson, A., Friesen, D. K., Morel, C., and Tiessen, H. (1997). Determination of phosphorus released by chloroform fumigation from microbial biomass in high P sorbing tropical soils. *Soil Biol. Biochem*. 29, 1579–1583. doi: 10.1016/S0038-0717(97)00049-7

Ohara, N., Kavvas, M. L., Easton, D., Dogrul, E. C., Yoon, J. Y., and Chen, Z. Q. (2011). Role of snow in runoff processes in a subalpine hillslope: field study in the Ward Creek Watershed, Lake Tahoe, California, during 2000 and 2001 water years. *J. Hydrol. Eng*. 16, 521–533. doi: 10.1061/(ASCE)HE.1943-5584.0000348

Olander, L. P., and Vitousek, P. M. (2004). Biological and geochemical sinks for phosphorus in soil from a wet tropical forest. *Ecosystems* 7, 404–419. doi: 10.1007/s10021-004-0264-y

Pinheiro, J. (2019). "Linear and nonlinear mixed effects models," in *Package* for R.).

Pistocchi, C., Meszaros, E., Tamburini, F., Frossard, E., and Bunemann, E. K. (2018). Biological processes dominate phosphorus dynamics under low phosphorus availability in organic horizons of temperate forest soils. *Soil Biol. Biochem*. 126, 64–75. doi: 10.1016/j.soilbio.2018.08.013

Plassard, C., Louche, J., Ali, M. A., Duchemin, M., Legname, E., and Cloutier-Hurteau, B. (2011). Diversity in phosphorus mobilisation and uptake in ectomycorrhizal fungi. *Ann. Forest Sci*. 68, 33–43. doi: 10.1007/s13595-010-0005-7

Porder, S., and Ramachandran, S. (2013). The phosphorus concentration of common rocks-a potential driver of ecosystem P status. *Plant Soil* 367, 41–55. doi: 10.1007/s11104-012-1490-2

Pote, D. H., Daniel, T. C., Sharpley, A. N., Moore, P. A., Edwards, D. R., and Nichols, D. J. (1996). Relating extractable soil phosphorus to phosphorus losses in runoff. *Soil Sci. Soc. Am. J*. 60, 855–859. doi: 10.2136/sssaj1996.03615995006000030025x

Prairie, Y. T., and Kalff, J. (1988). Particulate phosphorus dynamics in headwater streams. *Can. J. Fish Aquatic Sci*. 45, 210–215. doi: 10.1139/f88-024

R Core Team (2019). *R: A Language and Environment for Statistical Computing*. Vienna: R Foundation for Statistical Computing.

Reddy, K. R., Chua, T., and Richardson, C. J. (2013). "Organic phosphorus mineralization in wetland soils," in *Methods in Biogeochemistry of Wetlands,* eds. K.R. Reddy and P.B. DeLaune. (Madison, WI: Soil Science Society of America), 683–700. doi: 10.2136/sssabookser10.c35

Redel, Y., Rubio, R., Godoy, R., and Borie, F. (2008). Phosphorus fractions and phosphatase activity in an Andisol under different forest ecosystems. *Geoderma* 145, 216–221. doi: 10.1016/j.geoderma.2008.03.007

Reid, K., Schneider, K., and McConkey, B. (2018). Components of phosphorus loss from agricultural landscapes, and how to incorporate them into risk assessment tools. *Front. Earth Sci*. 6:135. doi: 10.3389/feart.2018.00135

Roberts, D. M., and Reuter, J. E. (2010). *Lake Tahoe Total Maximum Daily Load Technical Report-California and Nevada*. Lahontan Water Board and Nevada Division of Environmental Protection.

Roby, K., O'Neil-Dunne, J., Romsos, S., Loftis, W., MacFaden, S., Saah, D., et al. (2015). "A review of stream environment zone definitions, field delineation criteria and indicators, classification systems, and mapping – collaborative recommendations for stream environment zone program updates", *(eds.) Spatial Informatics Group (SIG) University of Vermont and Spatial Analysis Laboratory (UVM-SAL) and the United States Department of Agriculture Natural Resource Conservation Service* (NRCS).).

Rothe, M., Kleeberg, A., and Hupfer, M. (2016). The occurrence, identification and environmental relevance of vivianite in waterlogged soils and aquatic sediments. *Earth-Sci. Rev.* 158, 51–64. doi: 10.1016/j.earscirev.2016.04.008

Sah, R. N., and Mikkelsen, D. S. (1986a). Sorption and bioavailability of phosphorus during the drainage period of flooded-drained soils. *Plant Soil* 92, 265–278. doi: 10.1007/BF02372640

Sah, R. N., and Mikkelsen, D. S. (1986b). Transformations of inorganic phosphorus during the flooding and draining cycles of soil. *Soil Sci. Soc. Am. J*. 50, 62–67. doi: 10.2136/sssaj1986.03615995005000010012x

Sah, R. N., Mikkelsen, D. S., and Hafez, A. A. (1989). Phosphorus behavior in flooded-drained soils. 3. Phosphorus desorption and availability. *Soil Sci. Soc. Am. J*. 53, 1729–1732. doi: 10.2136/sssaj1989.03615995005300060020x

Sahoo, G. B., Nover, D. M., Reuter, J. E., Heyvaert, A. C., Riverson, J., and Schladow, S. G. (2013). Nutrient and particle load estimates to Lake Tahoe (CA-NV, USA) for total maximum daily load establishment. *Sci. Total Environ*. 444, 579–590. doi: 10.1016/j.scitotenv.2012.12.019

Sahoo, G. B., Schladow, S. G., and Reuter, J. E. (2010). Effect of sediment and nutrient loading on Lake Tahoe optical conditions and restoration opportunities using a newly developed lake clarity model. *Water Resour. Res*. 46:W10505. doi: 10.1029/2009WR008447

Saucedo, G. J. (2005). *Geologic Map of the Lake Tahoe Basin, California and Nevada, 1:100,000 Scale*. Sacramento, CA: California Geological Survey.

Saunders, W. M. H., and Williams, E. G. (1955). Observations on the determination of total organic phosphorus in soils. *J. Soil Sci*. 6, 254–267. doi: 10.1111/j.1365-2389.1955.tb00849.x

Schladow, G. (2019). *Tahoe State of the Lake Report 2019*. UC Davis News and Media Relations.

Schneider, K. D., Cade-Menun, B. J., Lynch, D. H., and Voroney, R. P. (2016). Soil phosphorus forms from organic and conventional forage fields. *Soil Sci. Soc. Am. J*. 80, 328–340. doi: 10.2136/sssaj2015.09.0340

Schoeneberger, P. J., Wysocki, D. A., Benham, E. C., and Soil Survey Staff (2012). *Field Book for Describing and Sampling Soils.* Lincoln, NE: Natural Resources Conservation Service, National Soil Survey Center.

Schoumans, O. (2009). "Determination of the Degree of Phosphate Saturation in Noncalcareous Soils," in *Methods of Phosphorus Analysis for Soils, Sediments, Residuals, and Waters*, eds. J. Kovar and G. Pierzynski (Raleigh, NC: North Carolina State University; Southern Cooperative Series Bulletin).

Self-Davis, M., Moore, P., and Joern, B. (2009). "Water or Dilute Salt-Extractable Phosphorus in Soil," in *Methods of Phosphorus Analysis for Soils, Sediments, Residuals, and Waters,* eds. J. Kovar and G. Pierzynski. (Raleigh, NC: North Carolina State University: Southern Cooperative Series Bulletin), 22–24.

Sims, J. (2009). "Soil Test Phosphorus: Principles and Methods," in *Methods of Phosphorus Analysis for Soils, Sediments, Residuals, and Waters*, eds. J. Kovar and G. Pierzynski. (Raleigh, NC: North Carolina State University: Southern Cooperative Series Bulletin), 9–19.

Sohrt, J., Lang, F., and Weiler, M. (2017). Quantifying components of the phosphorus cycle in temperate forests. *Wires Water* 4, 1–36. doi: 10.1002/wat2.1243

Sohrt, J., Uhlig, D., Kaiser, K., von Blanckenburg, F., Siemens, J., Seeger, S., et al. (2019). Phosphorus fluxes in a temperate forested watershed: canopy leaching, runoff sources, and in-stream transformation. *Front. Glob. Chang* 2:85. doi: 10.3389/ffgc.2019.00085

Soil Survey Staff (1999). *Soil Taxonomy: A Basic System of Soil Classification for Making and Interpreting Soil Surveys. U.S. Department of Agriculture Handbook 436: Natural Resources Conservation Service*.

Soil Survey Staff (2014). "Kellogg Soil Survey Laboratory Methods Manual", in: *Soil Survey Investigations Report No. 42 Version 5.* (Lincoln, NE: Kellogg Soil Survey Laboratory).

Soil Survey Staff, N. R. C. S. (2007). *Soil Survey of the Tahoe Basin Area, California and Nevada*. Washington, DC: United States Department of Agriculture. Available online at: http://soils.usda.gov/survey/printed_surveys/ (accessed January 26, 2021).

Spohn, M., and Widdig, M. (2017). Turnover of carbon and phosphorus in the microbial biomass depending on phosphorus availability. *Soil Biol. Biochem*. 113, 53–59. doi: 10.1016/j.soilbio.2017.05.017

Sun, L., Teramoto, M., Naishin, L., Yazaki, T., and Hirano, T. (2017). Comparison of litter-bag and chamber methods for measuring $CO_2$ emissions from leaf litter decomposition in a temperate forest. *J. Ag Meteorol*. 73, 59–67. doi: 10.2480/agrmet.D-16-00012

Toor, G. S., Condron, L. M., Di, H. J., Cameron, K. C., and Cade-Menun, B. J. (2003). Characterization of organic phosphorus in leachate from a grassland soil. *Soil Biol. Biochem*. 35, 1317–1323. doi: 10.1016/S0038-0717(03)00202-5

TRPA (2015). *"2015 Threshold Evaluation Report", (ed.) Tahoe Regional Planning Agency*. Available online at: http://www.trpa.org/regional-plan/threshold-evaluation/ (accessed January 26, 2021).

U.S. Army Corp of Engineers (2003). *Lake Tahoe Basin framework study ground water evaluation, Lake Tahoe Basin, California and Nevada (ed.)*. California: U.S. Army Corp of Engineers Sacramento District.

Uhlig, D., and von Blanckenburg, F. (2019). How slow rock weathering balances nutrient loss during fast forest floor turnover in montane, temperate forest ecosystems. *Front. Earth Sci.* 7:159. doi: 10.3389/feart.2019.00159

USDA-NRCS (2019). Snow Telemetry (SNOTEL) and Snow Course Data and Products. Available online at: https://www.wcc.nrcs.usda.gov/snow/: Natural Resource Conservation Service and National Water and Climate Center.

Uselman, S. M., Qualls, R. G., and Lilienfein, J. (2012). Quality of soluble organic C, N, and P produced by different types and species of litter: root litter versus leaf litter. *Soil Biol. Biochem.* 54, 57–67. doi: 10.1016/j.soilbio.2012.03.021

USGS (2016). USGS Water Data for the Nation. Available online at: https://waterdata.usgs.gov/nwis:USGS.

Vadas, P. A., Kleinman, P. J. A., Sharpley, A. N., and Turner, B. L. (2005). Relating soil phosphorus to dissolved phosphorus in runoff: a single extraction coefficient for water quality modeling. *J. Env. Qual.* 34, 572–580. doi: 10.2134/jeq2005.0572

Vitousek, P. M., Porder, S., Houlton, B. Z., and Chadwick, O. A. (2010). Terrestrial phosphorus limitation: mechanisms, implications, and nitrogen-phosphorus interactions. *Ecol. Appl.* 20, 5–15. doi: 10.1890/08-0127.1

Voroney, R. P., Brookes, P. C., and Beyaert, R. (2008). "Soil Microbial Biomass C, N, P and S," in *Soil Sampling and Methods of Analysis,* eds. M.R. Carter and E.G. Gregorich. (Boca Raton, FL: CRC Press), 637–651.

Wang, Y. T., Zhang, T. Q., Hu, Q. C., Tan, C. S., O'Halloran, I. P., Drury, C. F., et al. (2010). Estimating dissolved reactive phosphorus concentration in surface runoff water from major Ontario soils. *J. Env. Qual.* 39, 1771–1781. doi: 10.2134/jeq2009.0504

Wiens, J. T., Cade-Menun, B. J., Weiseth, B., and Schoenau, J. J. (2019). Potential phosphorus export in snowmelt as influenced by fertilizer placement method in the Canadian prairies. *J. Env. Qual.* 48, 586–593. doi: 10.2134/jeq2018.07.0276

Worsfold, P., McKelvie, I., and Monbet, P. (2016). Determination of phosphorus in natural waters: a historical review. *Anal. Chim. Acta* 918, 8–20. doi: 10.1016/j.aca.2016.02.047

Wu, J., Li, J. B., Zhao, J., and Miller, R. (2000). Dynamic characterization of phospholipid/protein competitive adsorption at the aqueous solution/chloroform interface. *Colloid Surface A* 175, 113–120. doi: 10.1016/S0927-7757(00)00543-4

Yang, X., and Post, W. M. (2011). Phosphorus transformations as a function of pedogenesis: a synthesis of soil phosphorus data using Hedley fractionation method. *Biogeoscience* 8, 2907–2916. doi: 10.5194/bg-8-2907-2011

Young, E. O., Ross, D. S., Cade-Menun, B. J., and Liu, C. W. (2013). Phosphorus speciation in riparian soils: a phosphorus-31 nuclear magnetic resonance spectroscopy and enzyme hydrolysis study. *Soil Sci. Soc. Am. J.* 77, 1636–1647. doi: 10.2136/sssaj2012.0313

Young, T. C., DePinto, J. V., Martin, S. C., and Bonner, J. S. (1985). Algal-available particulate phosphorus in the Great Lakes Basin. *J. Great Lakes Res.* 11, 434–446. doi: 10.1016/S0380-1330(85)71788-1

Zhang, Y. S., Lin, X. Y., and Werner, W. (2003). The effect of soil flooding on the transformation of Fe oxides and the adsorption/desorption behavior of phosphate. *J. Plant Nutr. Soil Sci.* 166, 68–75. doi: 10.1002/jpln.200390014

**Conflict of Interest:** The authors declare that the research was conducted in the absence of any commercial or financial relationships that could be construed as a potential conflict of interest.

frontiers in Forests and Global Change

ORIGINAL RESEARCH
published: 13 May 2021
doi: 10.3389/ffgc.2021.543037

# Phosphorus Leaching From Naturally Structured Forest Soils Is More Affected by Soil Properties Than by Drying and Rewetting

*Lukas Gerhard[1]*, Heike Puhlmann[1], Margret Vogt[2] and Jörg Luster[2]*

*[1] Department of Soil and Environment, Forest Research Institute Baden Württemberg, Freiburg, Germany, [2] Forest Soils and Biogeochemistry, Swiss Federal Institute for Forest, Snow and Landscape Research (WSL), Birmensdorf, Switzerland*

Foliar phosphorus (P) concentrations in beech trees are decreasing in Europe, potentially leading to reductions in the trees' growth and vitality. In the course of climate change, drying and rewetting (DRW) cycles in forest soils are expected to intensify. As a consequence, P leakage from the root zone may increase due to temporarily enhanced organic matter mineralization. We addressed the questions whether sites with different soil properties, including P pools, differ in their susceptibility to DRW-induced P leaching, and whether this is affected by the DRW intensity. A greenhouse experiment was conducted on naturally structured soil columns with beech saplings from three sites representing a gradient of soil P availability. Four DRW cycles were conducted by air-drying and irrigating the soils over 4 hours (fast rewetting) or 48 hours (slow rewetting). Leachates below the soil columns were analyzed for total P, and molybdate reactive P (considered as inorganic P). The difference was considered to represent organically bound P. Boosted regression trees were used to examine the effects of DRW and soil characteristics on P leaching. Contrary to a first hypothesis, that P leaching increases upon rewetting with the intensity of the preceding desiccation phase, intense soil drying (to pF 3.5 to 4.5) did not generally increase P leakage compared to moderate drying (to pF 2 to 3). However, we observed increased inorganic P concentrations and decreased organic P concentrations in leachates after drying to matric potentials above pF 4. Also against our expectations, fast rewetting did not lead to higher leakage of P than slow rewetting. However, the results confirmed our third hypothesis that the site poorest in P, where P recycling is mainly limited to the humus layer and the uppermost mineral soil, lost considerably more P during DRW than the other two sites. The results of our experiment with naturally structured soils imply that intensified drying and rewetting cycles, as predicted by climate-change scenarios, may not *per se* lead to increased P leaching from forest soils. Soil properties such as soil organic carbon content and texture appear to be more important predictors of P losses.

**Keywords: phosphorus leaching, drying-rewetting, temperate beech forest, undisturbed soil columns, mesocosm, dissolved organic carbon, boosted regression trees**

OPEN ACCESS

***Edited by:***
*Sebastian Loeppmann, Christian-Albrechts-Universität zu Kiel, Germany*

***Reviewed by:***
*Antra Boca, Latvia University of Agriculture, Latvia*
*Per Marten Schleuss, University of Bayreuth, Germany*

****Correspondence:***
*Lukas Gerhard*
*l.gerhard@posteo.de*

***Specialty section:***
*This article was submitted to Forest Soils, a section of the journal Frontiers in Forests and Global Change*

***Received:*** *15 March 2020*
***Accepted:*** *19 April 2021*
***Published:*** *13 May 2021*

***Citation:***
*Gerhard L, Puhlmann H, Vogt M and Luster J (2021) Phosphorus Leaching From Naturally Structured Forest Soils Is More Affected by Soil Properties Than by Drying and Rewetting. Front. For. Glob. Change 4:543037. doi: 10.3389/ffgc.2021.543037*

## INTRODUCTION

As an essential plant nutrient, phosphorus (P) is of paramount importance for the nutrition of beech trees (Fagus sylvatica L.). Temporal decoupling of P acquisition and growth, and internal P trade-off between storage tissues and leaves are physiological strategies enabling this species to flexibly adapt to different soil P availabilities (Zavišić and Polle, 2017; Meller et al., 2019). In this context, cycling and re-utilization of P within the ecosystem are crucial for P nutrition of beech. As Odum (1969) hypothesized, the cycling of P as part of plant nutritional strategies becomes tighter as an ecosystem matures, shifting from open to closed P cycles, with increasing importance of detritus for nutrient recycling. Total P uptake from forest trees has been found to be an order of magnitude higher than P supplied from chemical weathering, which indicates that P is efficiently re-utilized from the forest floor. However, despite nutrient recycling, the finite organic P pool in the forest floor is short-lived and susceptible to continuous losses through plant litter erosion or its dissolution and export (Uhlig and von Blanckenburg, 2019).

Lang et al. (2016) argue that the soilss' P status (in terms of their carbon/phosphorous (C/P) ratios or total P pools) may be the most influential factor for forest P nutrition, and that different ecosystems of similar maturity may display differing tightness in their P cycling, depending on the soil's P status. They propose that at sites rich in P, the nutrient is predominantly acquired from weathered primary soil minerals ("P acquiring strategy"). In contrast, P recycled from organic material becomes an important nutrient source at P-poor sites, leading to a tightening of the P cycle and a minimization of ecosystem P losses ("P recycling strategy").

The soil solution, containing both dissolved organic and inorganic P forms, is the central compartment of the P cycle in forests (Weihrauch and Opp, 2018). Mobilized P that is neither taken up by plants nor immobilized by microbes or sorbed, can be leached from the topsoil into the subsoil. Leaching of P from the subsoil is considered small, due to the high P binding capacity there (Heathwaite and Dils, 2000; Sinaj et al., 2002). However, leaching may be triggered when under certain conditions, interactions of soil pore water and soil matrix are hampered (Julich et al., 2017; Makowski et al., 2020).

Soil moisture is an abiotic key factor controlling nutrient fluxes (Meier and Leuschner, 2014). Prolonged dry spells alternating with heavy rains can create new preferential pathways for P, initiate leaching processes and thereby open up gaps in an ecosystem's P cycle (Sohrt et al., 2017).

In a changing climate, prolonged periods of drought alternating with more intense rain events ("drying and rewetting events," DRW) are predicted to occur more often (Trenberth, 2011; Coumou and Rahmstorf, 2012). As a result, fluctuations in soil moisture are likely to become more extreme in many environmental settings (Zwiers et al., 2013). As compared to constantly moist soil, the rewetting of dry soil is known to induce pulses of $CO_2$ efflux and nutrient leaching associated with the mineralization of organic matter, called the Birch effect (after Birch, 1958). Barnard et al. (2020) list six main causes for this mineralization pulse: cell lysis from microbial necromass; organic matter becoming more accessible to microbial decomposition after disruption of soil aggregates; exposure of mineralizable C after desorption of soluble organic compounds associated with minerals; restoration of water film connectivity that enables microorganisms to access substrates by diffusion; a net increase in resource availability for microorganisms upon rewetting due to sustained exoenzyme activity despite reduced microbial activity during soil drying; microbial release and catabolization of osmolytes accumulated in response to drying. All these processes also affect P mobilization in soil (Barnard et al., 2020). The DRW-induced release of P is primarily derived from biotic processes such as microbial cell lysis (e.g., Blackwell et al., 2010; Achat et al., 2012; Dinh et al., 2017; Pezzolla et al., 2019; Makowski et al., 2020) and soil organic matter mineralization (Wu and Brookes, 2005; Butterly et al., 2009; Chen et al., 2021). Microbial cell lysis has been found to enhance leaching mainly of organic P (Turner and Haygarth, 2001; Turner et al., 2003; Blackwell et al., 2009). However, also the leaching of inorganic P has been associated with cell lysis (Brödlin et al., 2019; Khan et al., 2019), possibly due to the rapid mineralization of released organic compounds rich in P (Annaheim et al., 2013; Dinh et al., 2016). Apart from biotic processes, abiotic processes may release both organic and inorganic P upon DRW. The disruption of soil aggregates (Bünemann et al., 2013) as well as desorption and increased organic matter solubility (Frossard et al., 2000; Turner and Haygarth, 2003; Butterly et al., 2009) were found to increase leakage of inorganic P. Turner and Haygarth (2003) discuss that physical disruption of organic matter coatings is the primary mechanism contributing to the increase in extractable inorganic P upon soil drying, but that dry conditions also reduce the specific surface area and thus the P sorption capacity of increasingly crystalline Fe and Al oxides.

Drying and rewetting has been found to increase the mobility of P in experiments performed with sieved soil, for example by Dinh et al. (2017) and Brödlin et al. (2019) from O and A horizons of forest soils, by Forber et al. (2017) from agricultural soils and by Blackwell et al. (2013) and Bünemann et al. (2013) from grassland soils. Blackwell et al. (2009) found that the rate of rewetting significantly changed the concentrations of dissolved and particulate P in the leachate, with highest concentrations being observed under fastest rewetting. Similarly, Messing et al. (2015) found in a field study on clay soil under agriculture that increased rain intensities enhanced losses of total P and inorganic P. Preferential flow, e.g., through macropores, has been found to be an important pathway for the translocation of particulate (Julich et al., 2017; Makowski et al., 2020) or colloidal (Missong et al., 2018) P within soils after irrigation events. Other than the rate of rewetting, the duration (Forber et al., 2017) and degree (Dinh et al., 2017; Brödlin et al., 2019; Gao et al., 2020) of drying, as well as the frequency of DRW cycles (Chen et al., 2016, 2021; Dinh et al., 2016) have been studied. Forber et al. (2017) identified 7–15 drying days as critical breakpoints after which substantially more P was found in mineral soil solution. Also, Brödlin et al. (2019) found that longer and warmer dry spells enhanced P release after drought,

most likely due to increasing osmotic stress levels exerted on microorganisms. Dinh et al. (2017) identified a pF of 4 as a critical degree of desiccation of artificial soils, above which microbial P release increased substantially upon rewetting and continued to increase up to pF 6. Regarding repeated DRW cycles, Dinh et al. (2016) found no increase in P release after repeated DRW, whereas Chen et al. (2016) report decreases in microbial P, yet increases in inorganic P upon frequent DRW. Further, in a study by Chen et al. (2021), three repeated DRW cycles affected biotic and abiotic processes differently, with most biotic indicators, including microbial P, quickly adjusting to the treatment.

All above-mentioned studies on DRW-induced P release were performed on sieved, homogenized soil. DRW studies on undisturbed soil samples are rare. Batch experiments on disturbed soils, however, appear to be of limited use in predicting P release rates from naturally structured soils. For example, Forsmann and Kjaergaard (2014) found that P release rates from sieved soils were hardly correlated with actual P release rates, which illustrates the overall influence of the soil structure on P transport processes. To our knowledge, so far only one DRW study on P release used undisturbed soil columns, however only from forest floors (Hömberg and Matzner, 2017). The authors found that DRW caused a significant short-term increase in concentrations and leachate fluxes of dissolved P, with a stronger effect on organic than on inorganic P.

In experimental soil science, percolation experiments with undisturbed soil columns are a viable alternative to in-field experiments and allow the study of nutrient transport in naturally structured soils (e.g., Hildebrand, 1994; Thaysen et al., 2014; Holzmann et al., 2016). These studies showed that soil aggregate surfaces and adjacent macropores are selectively and systematically depleted of nutrients. Hildebrand (1994) found the soil structure to heavily delay nutrient release from aggregate surfaces into the pore space compared to homogenized soil. Those findings have been confirmed by several studies (e.g., Horn and Taubner, 1989; Hantschel et al., 1994; Vogt and Matschonat, 1997; Schlotter et al., 2012).

Despite ongoing research, overall understanding of leaching of P from forest soils is still fragmentary, which implies a lack of detailed studies quantifying such P losses (Bol et al., 2016). In particular, it remains less understood (a) how rain events and fast soil infiltration affect P translocation, (b) how strongly P fractions differ in their susceptibility to leaching and (c) how various ecosystem properties are involved in P leaching processes. To approach these questions we conducted a multivariate soil mesocosm experiment. Specifically we wanted to test the following hypotheses: (H1) intense soil drying compared to moderate drying increases P leakage upon rewetting, possibly due to P release from lysed microbial cells, (H2) fast rewetting leaches more P than slow rewetting, due to induced macropore flow and reduced uptake of P by plants and microorganisms, and (H3) more P is released upon rewetting from soils with low sorption capacity, in particular organically bound P.

# MATERIALS AND METHODS

## Study Sites and Collection of Soil Columns

We took samples from three different sites in Germany with mature European beech (Fagus sylvatica L.) stands: Bad Brückenau (BBR), Vessertal (VES) and Lüss (LUE). The soils represent a gradient in available and total P stocks (total P: BBR 904 g $m^{-2}$, VES 464 g $m^{-2}$, LUE 164 g $m^{-2}$, to 1 m soil depth). **Table 1** summarizes other important site characteristics. The sites differ with respect to humus form (BBR: mull-like moder, VES: moder, LUE: mor-like moder), texture (BBR: silty clay loam, VES: loam, LUE: loamy sand) and sesquioxide contents. The soil in LUE shows signs of podzolization. Soil microbial activity is higher in VES than in BBR and LUE (Lang et al., 2017). According to the concept proposed by Lang et al. (2016), the site BBR is categorized as an "acquiring" forest ecosystem, whereas LUE corresponds to a "recycling" forest ecosystem. VES is considered an intermediate site (Lang et al., 2017).

In March 2017, we sampled naturally structured soil columns including young beech trees from natural regeneration. We retrieved the soil samples by driving acrylic glass cylinders (inner diameter: 7.4 cm, height: 30 cm) into the soil, using a metal cartridge with a lid to protect the trees. Sampled soil columns comprised 15 to 24 cm of the top mineral soil as well as the organic layers (Oi, Oe, Oa). The sampled forest floor varied in thickness between 4 and 8 cm, the P-poor

**TABLE 1 |** Basic site and soil characteristics of the three sampling sites Bad Brückenau (BBR), Vessertal (VES) and Lüss (LUE) for the upper 20 cm soil. Feo and Alo, are proxies for sesquioxide content. Fe/Al suffix "o": oxalate extracted. Data retrieved from Lang et al. (2017).

| Study site | BBR | VES | LUE |
|---|---|---|---|
| Soil type (WRB, 2015) | Dystric skeletic cambisol | Hyperdystric skeletic chromic cambisol | Hyperdystric folic cambisol |
| Parent material | Basalt | Trachyandesite | Sandy till |
| Humus form | Mull-like Moder | Moder | Mor-like Moder |
| Altitude (m a.s.l.) | 809 | 810 | 115 |
| Precipitation (mm $a^{-1}$) | 1,031 | 1,200 | 779 |
| Texture (WRB, 2015) | Silty clay loam | Loam | Loamy sand |
| Sand% | 9 | 30 | 76 |
| Silt% | 55 | 47 | 19 |
| Clay% | 37 | 24 | 5.5 |
| pH mineral soil ($H_2O$) | 4.2 | 3.9 | 3.7 |
| Feo (g $kg^{-1}$) | 33 | 8 | 2 |
| Alo (g $kg^{-1}$) | 11 | 6 | 1 |
| Resin extractable P of A horizon (mg $kg^{-1}$) | 116 | 40 | 11 |
| Total P stocks up to 1 m soil depth and forest floor (g $m^{-2}$) | 904 | 464 | 164 |

site LUE exhibiting the thickest and the P-rich site BBR the thinnest humus layer. Due to the abundance of fresh litter in spring, Oi layers were thick irrespective of the humus form. To prevent translocation of organic layer material into the mineral soil during the sampling process, we carefully removed the humus layer within and around the sampling spot before soil extraction and added it to the soil column later. Beech saplings were about 30 to 60 cm high. After storage at 5°C in a cooling chamber until May 2017, we moved the mesocosms to the greenhouse.

## Conditioning

The DRW experiments were preceded by a 14-month conditioning phase starting in May 2017, in order to reduce possible effects of the soil sampling (e.g., disruption of roots and soil aggregates) on the DRW results. We equipped all mesocosms with vertically installed MPS 6 sensors (Decagon) which continuously monitored matric potential and soil temperature in the center of the mineral soil. Air humidity and temperature in the greenhouse were also monitored throughout the experiment. During conditioning, we irrigated the mesocosms with 20 to 40 ml of irrigation solution every second to third day to maintain a matric potential of around -10 kPa. Especially in the warm summer period, however, matric potentials in the mesocosms occasionally decreased between the irrigations to values below this target value. For irrigation, a solution was used which resembled the average precipitation water from around Freiburg i.B., Germany (detailed information provided in Holzmann et al., 2016). From mid-December 2017 to mid-March 2018, we set up a cooling case around the mesocosms to simulate winter conditions. Soil temperatures varied between 7 and 10°C during this period.

## Drying and Rewetting

We conducted four DRW cycles between 17th of July and 20th of September 2018. Between the DRW cycles, there were 20-day intervals, in which all mesocosms were treated as during the conditioning phase. During the drying phase of a DRW cycle, irrigation was suspended for 3 to 5 days to achieve a moderate drying to pF values between 2 and 3 (LUE soils) or 2 and 3.5 (BBR and VES soils), or for 5 to 8 days to achieve an intense drying to pF values between 3 and 4 (LUE soils) or 3.5 and 5 (BBR and VES soils). We rewetted by continuously watering each mesocosm with 250 ml over 4 hours (fast rewetting) or over 48 hours (slow rewetting), simulating 58 l $m^{-2}$ of rainfall. The irrigated water volume and the duration of the rewetting phase were chosen based on records of regional precipitation data (Malitz and Ertel, 2015) and available water capacities of the soils. Estimated return periods of the simulated rain events are 40, 30 and 50 years for the 4 hour rain, and 1.5, 1.5, and 4 years for the 48 hour rain for BBR, VES and LUE, respectively. We realized three combinations of drying intensity and rewetting duration: (1) moderate drying and slow rewetting (MOD-S), (2) intense drying and slow rewetting (DRY-S), and (3) intense drying and fast rewetting (DRY-F). We used five replicate mesocosms per variant from each of the three sites. All mesocosms of one variant were irrigated simultaneously. Irrigation of the different variants started with a slight time offset within a few hours. Each mesocosm was exposed to the same DRW variant (either MOD-S, DRY-S or DRY-F) throughout the four DRW cycles.

Irrigation water was supplied to each mesocosm from a 250 ml glass bottle by use of a peristaltic pump (Ismatec). The pump constantly delivered the irrigation solution to about 5 cm above the soil surface via silicone tubing, from where it dripped down at the preset rate. We manually changed the position of the dripping tube every 15 min to facilitate even water distribution over the mesocosm surface.

## Experimental Boundary Conditions

Regardless of the DRW variant, rewetting aimed at saturating the mesocosms to matric potentials at or above −10 kPa. With very few exceptions, this was achieved for all DRW cycles and mesocosms. However, the location in a greenhouse entailed a certain susceptibility to environmental influences and therefore, conditions varied to some extent among the four DRW cycles. The second DRW cycle, for instance, took place in a considerably warmer period than the other three, which resulted in approximately 4°C higher soil temperatures. Apart from varying atmospheric conditions, differences between the sites with respect to the water retention characteristics complicated the aim to achieve similar matric potentials during the desiccation phase, and LUE samples generally remained wetter than samples from BBR and VES. Reasons for this could be a lower water uptake by the trees, a decreased evaporation due to hampered capillary rise through sand and the presence of an Oh horizon with a particularly high water retention capacity in the LUE soils compared to the other two sites. The mere effect of the drying and rewetting intensities on the leaching of P is therefore not easily comparable among the different sites.

## Matric Potential During DRW

Average matric potentials before rewetting were for DRY-S and DRY-F: BBR: −2,004 ± 1,093 kPa, VES: −1,607 ± 824 kPa, LUE: −457 ± 645 kPa, and for MOD-S: BBR: −335 ± 465 kPa, VES: −176 ± 282 kPa, LUE: −16 ± 16 kPa. In the fast rewetting variant, the measured matric potential reached values around -10 kPa (upper measurement limit of the MPS 6 sensors) within 3.7 ± 3.0 hours on average after start of the irrigation, while in the slow rewetting variants it took on average 9.7 ± 9.9 hours (MOD-S) and 25.9 ± 13.1 hours (DRY-S) (**Figure 1**). After the experiment, we retrieved soil cores of 100 $cm^3$ from the lower part of the mesocosms, and determined the volumetric water content at -6.3 kPa (field capacity).

## Sampling and Chemical Analysis

Soil solution was collected at the bottom of the mesocosms with filter plates (ROBU GmbH) which consisted of borosilicate glass 3.3 and had a pore size of 10–16 μm. The leachate was collected in separate 500 ml borosilicate glass bottles, which were constantly cooled in a water bath to 12–15°C. During rewetting and for several hours thereafter, we reduced the air pressure inside the collection bottles by 6–8 kPa through a connected vacuum pump (KNF Neuberger GmbH). Thus,

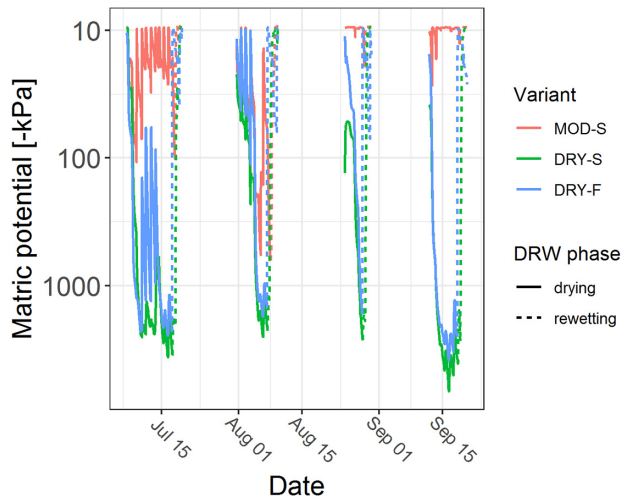


**FIGURE 1 |** Matric potential of mesocosms from Bad Brückenau over the course of the four DRW cycles. MOD-S, moderate drying, slow rewetting; DRY-S, intense drying, slow rewetting; DRY-F, intense drying, fast rewetting.

water-logging, anaerobic soil conditions and, as a consequence, reductive P mobilization were avoided. We sampled the leachates during each DRW cycle. For this, we emptied the glass bottles at the beginning of a cycle and transferred the leached solution from the bottles into storage containers at the end of a cycle.

Until analysis, the leachates were stored for 4 to 8 weeks at 5°C. Despite cooling, some enzymatic transformation of organic P likely occurred during the storage, so inorganic P leaching is probably somewhat overestimated in our data. We analyzed total phosphorus (TP) of the leachates after digestion of unfiltrated soil solution with $K_2S_2O_8$ and $H_2SO_4$ and addition of ascorbic acid solution. Molybdate reactive phosphorus (MRP) as well as all other chemical parameters were determined in soil solution that was filtered through 0.45 µm cellulose acetate filters. Total minus molybdate reactive P was considered to represent organically bound P including colloidal organic P (molybdate unreactive P, MUP). TP, MRP, dissolved organic carbon (DOC), total nitrogen (TN) and $NH_4$ were measured with a San++ Continuous Flow Analyzer (Skalar Analytical B.V.). Al, Fe, $NO_3$, $SO_4$, Cl, Si, Mn, Zn, Mg, K, Ca and Na were analyzed with an 881 Compact IC pro (Deutsche METROHM GmbH & Co. KG). Soil solution pH was measured with an A 220 pH meter (Denver Instrument). For a detailed explanation of chemical analyses see Holzmann et al. (2016).

Leachate obtained from individual mesocosms was not always sufficient for a complete laboratory analysis. In those cases, we combined leachates from replicate samples (same site, same DRW variant) to obtain an analyzable leachate volume. If leachate was still not sufficient, TP analysis was prioritized over other parameters, hence more observations are available for TP ($n$ = 154) than for MRP and MUP ($n$ = 137). The total P loss (P load) within a DRW cycle was determined by multiplying the leachate volumes by the P concentrations.

## Statistical Analysis and Model Building

To compare P leaching between the different DRW variants and the different sites, we firstly applied a Wilcoxon signed-rank test at 5% error probability.

We then used Boosted Regression Trees (BRTs) to analyze the effect of experimental variants, environmental conditions as well as soil and soil solution properties on P leakage. BRT modelling seemed appropriate due to its ability to handle different types of predictor variables, outliers and missing data (Elith et al., 2008). BRTs fit multiple regression trees and combine them, using a combination of the ordinary regression tree approach and boosting, thereby potentially improving the predictive performance compared to standard regression methods which produce a single model (Buston and Elith, 2011). All predictor variables are ranked according to their relative influence (RI) on the response variable (De'Ath, 2007). Partial dependence plots (Friedman and Meulman, 2003) were used to visualize the effect of a given predictor on the response, while all other predictors are held at their mean value (Greenwell, 2017).

We built BRTs for the leachate concentrations of MRP, MUP and TP, the ratio of MUP/TP as well as the total loss of MRP, MUP and TP during each DRW cycle. We increased the number of predictor variables included in the BRTs in three hierarchical steps. Firstly, we fitted basic models ("Level I BRTs") with the predictors SITE (BBR, VES or LUE), INT (MOD or DRY for the drying intensity), IRR_RATE (SLOW or FAST for the applied rewetting rate) and CYCLE (1, 2, 3 or 4 for the consecutive DRW cycles).

Secondly ("Level II BRTs"), we added predictor variables that are specific to the DRW cycle of each individual mesocosm: PSI_START (log-transformed matric potential just before rewetting [log10(hPa)]), RW_TIME (duration of rewetting [min], derived from matric potential sensor readings), WRET (water retention during irrigation = irrigated volume - leached volume [ml]), MESO_FC (field capacity of the individual mesocosm [mm]), and SOIL_TEMP (soil temperature [°C]). Air temperature [°C] and air humidity [%] were tested as predictor variables to clarify that the number of the DRW cycle was not a mere proxy for the prevailing climatic conditions.

Thirdly ("Level III BRTs"), we included soil solution chemical parameters in the final models: pH, DOC ([mg $l^{-1}$]) and NH4_N (ammonium-N [mg $l^{-1}$]). $NO_3$_N (nitrate-N [mg $l^{-1}$]), DIN = $NH_4$_N + $NO_3$_N (dissolved inorganic nitrogen [mg $l^{-1}$]) and TN (total nitrogen [mg $l^{-1}$]) were dropped in the process of model development due to their high correlation with the stronger predictor NH4_N (Pearson correlation coefficients $> | \pm 0.7|$). Likewise, Al (total aluminum [mg $l^{-1}$]), Fe (total iron [mg $l^{-1}$]), and DON (dissolved organic nitrogen [mg $l^{-1}$], TN – DIN) were dropped in favor of DOC. To make these selections, we calculated separate BRT models with only one of the intercorrelated predictor variables (DIN, $NO_3$_N, $NH_4$_N, TN, and Al, Fe, DOC, DON) at a time. We then chose the predictor that contributed to the model with the highest score of explained variance.

We tested all other parameters available from soil solution analysis (Si, Mn, Zn, Mg, K, Ca, Na, Cl, and $SO_4$) for their influence on P response variables, but rejected them due to their negligible impact. Because of their skewed distribution, the values of the predictors Al, Fe, DOC, NH4_N, and DON were log-transformed.

All analyses were conducted in R (R Core Team, 2019). We used the dismo (Hijmans et al., 2017) and gbm (Greenwell et al., 2019) packages based on scripts provided by Elith et al. (2008) and Elith and Leathwick (2017) to model BRTs and examine the models for predictor interactions. The applied gbm.step function uses cross validation of simulated vs. measured P concentrations and loads to estimate the optimum number of trees. As some randomness usually improves model accuracy and reduces overfitting (Friedman, 2002), models were built using randomly selected 50% of the data at each iteration (bag fraction = 0.5). To obtain models with at least 1,000 trees, we used a learning rate of 0.002, which was increased to 0.003 when the number of fitted trees exceeded 10,000. To allow for the fitting of interactions between predictor effects, tree complexity was set to 5. As measures for predictive performance, we calculated the variance explained by the BRT models according to Derville et al. (2016), as well as the cross-validation variance according to Sutcliffe et al. (2013).

# RESULTS

## Effects of DRW Variants and Site on Phosphorus Leaching as Revealed by Rank Testing

Phosphorus in the leachates was composed to a larger degree of molybdate unreactive phosphorus (MUP) than of molybdate reactive phosphorus (MRP; **Figure 2**; for details see below). While the experimental drying-rewetting (DRW) variants (MOD-S, DRY-S, DRY-F) had no effect on either P fraction, when considering soil columns from all three sites (**Figure 2A**), there were differences when comparing data from given sites (see **Supplementary Table 1**). DRY-S resulted in the lowest total phosphorus (TP) concentrations in BBR and VES leachates (22.9 ± 9.3 and 27.9 ± 13.2 µg $l^{-1}$, respectively), as well as the lowest MUP concentrations in BBR (12.8 ± 8.5 µg $l^{-1}$) and the second lowest MUP concentrations in VES (15.6 ± 9.1 compared to 15.3 ± 6.7 µg $l^{-1}$ in DRY-F). Contrarily, LUE leachates showed the highest concentrations of TP and MUP in DRY-S (63.2 ± 25.7 and 54.8 ± 24.6 µg $l^{-1}$, respectively). As for MRP concentrations, MOD-S, DRY-S and DRY-F only had a noticeable effect in VES leachates (12.2 ± 16.2, 10.8 ± 13.2 and 16.8 ± 12.8 µg $l^{-1}$, respectively). We found significant differences when comparing data from the three sites, but irrespective of DRW variant (**Figure 2B**). MRP concentrations in leachates from VES soil (14 ± 10.3 µg $l^{-1}$) were significantly and about 1.5 times higher than in leachates from BBR (8.6 ± 4.6 µg $l^{-1}$) and LUE (9.2 ± 5.0 µg $l^{-1}$). By contrast, both TP and MUP concentrations in leachates from LUE soil (TP: 50.9 ± 26.4 µg $l^{-1}$; MUP: 41.7 ± 24.3 µg $l^{-1}$) were significantly and about two times higher than in leachates from VES soil (TP: 32.7 ± 14.3 µg $l^{-1}$; MUP: 18.7 ± 10.8 µg $l^{-1}$) and BBR soil (TP: 26.6 ± 10.1 µg $l^{-1}$; MUP: 17.0 ± 10.1 µg $l^{-1}$). As a consequence, also the relative proportion of MUP (MUP/TP) was significantly higher in LUE soil leachates (0.79 ± 0.14) than in leachates from VES (0.57 ± 0.21) and BBR (0.61 ± 0.24) soils. As higher P concentrations generally coincided with higher leachate volumes, the inter-site differences described above for P concentrations also applied to P loads (not shown).

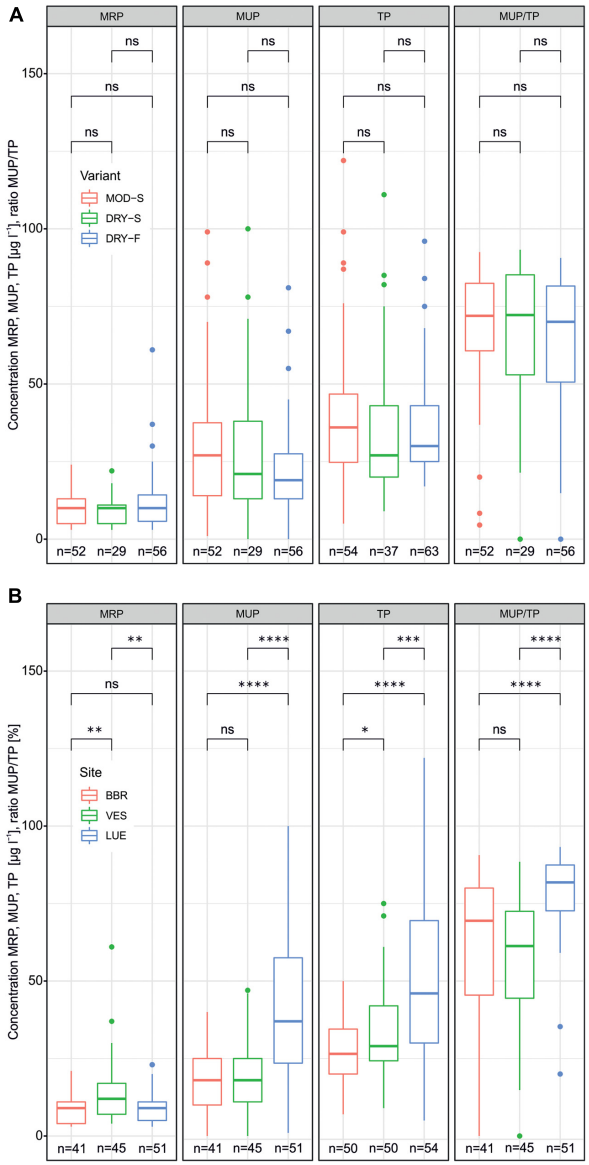


**FIGURE 2 |** Leachate concentrations of molybdate reactive phosphorus (MRP), molybdate unreactive phosphorus (MUP), total phosphorus (TP) and MUP/TP ratios for the three different DRW variants (MOD-S, DRY-S, DRY-F on x-axis) **(A)** and the three sampling sites (BBR, VES, LUE on x-axis) **(B)**. Asteriks indicate significance at $^{*}P < 0.05$, $^{**}P < 0.01$, $^{***}P < 0.005$, $^{***}P < 0.001$ (Wilcoxon test), ns indicates no significance.

In addition to the site related differences, concentrations and loads of both P fractions differed among the individual DRW cycles (see **Supplementary Table 1**). While, irrespective of site, MRP concentrations gradually declined continuously from the first to the fourth cycle, MUP and TP concentrations were minimum either in the second cycle (BBR, VES) or in the fourth cycle (LUE). The effects of the DRW cycle on our results was revealed in more detail by the boosted regression tree analysis, as described in the following.

## Level I Boosted Regression Trees (BRTs) for P Concentrations in Soil Leachates

Basic BRT analysis, testing for the relative effects of the predictors site, drying intensity before rewetting, irrigation rate during rewetting, and DRW cycle, and visualized in partial dependence plots (**Figure 3**), revealed distinct differences between the behavior of MRP and MUP in leachates during rewetting. The DRW cycle had a dominant effect on MRP with a RI of 59.9% (**Table 2**), leading to a continuous decrease from the 1st to the last cycle (**Figure 3**, **Supplementary Table 1**). The RI of site was only 25.8% with higher MRP concentrations in VES leachates than BBR and LUE leachates (**Figures 2**, **3**). By contrast, site had a somewhat higher RI on MUP, TP and MUP/TP (48.6, 44.3, and 49.5%, respectively; **Table 2**) than DRW cycle (37, 42.4, and 38.5%, respectively; **Table 2**). As also shown by rank testing (see above), leachates from LUE exhibited higher values of MUP, TP and MUP/TP than BBR and VES leachates (**Figure 3**). As shown for MRP, also the MUP and TP concentrations were maximum in the first DRW cycle. However, there was no continuous decrease during the following cycles, and the relative contribution of MUP was maximum in the last cycle (**Figure 3**).

Neither drying intensity before rewetting (MOD, DRY; RI between 3.3 and 6.6%) nor irrigation rate during rewetting (SLOW, FAST; RI between 5.3 and 11%) had a strong effect on P leaching from the soil columns. The only noticeable effect were somewhat higher MRP concentrations (only in VES) and lower MUP concentrations (only in LUE) after fast than slow rewetting (see **Supplementary Table 1**, **Figure 3**).

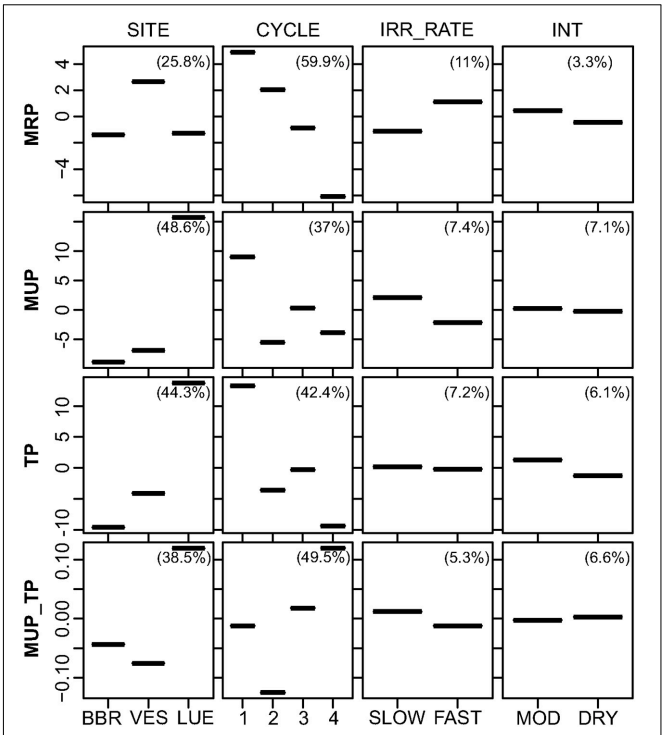


**FIGURE 3 |** Partial dependence plots for Level I BRTs, showing fitted effects of predictor variables (IRR_RATE: irrigation rate, INT: drying intensity) on MRP, MUP, TP concentrations and MUP/TP ratios with all other predictor variables held at their mean. Percentages in plots list the relative influence of each predictor on the respective response variable. The response variables on the y-axis have been centered by subtracting their mean.

## Including DRW Parameters: Level II BRTs for Leachate P Concentrations

The partial dependence plots for level II BRTs are shown in **Figure 4**. These BRTs were performed with the predictors from level I BRTs (site, DRW cycle, etc.) and predictor variables specific to individual mesocosms (field capacity MESO_FC, water retention during rewetting WRET, soil temperature, desiccation intensity before rewetting PSI_START, duration of rewetting RW_TIME, etc.). PSI_START and RW_TIME replaced the "two-level" predictors intensity before rewetting and irrigation rate during rewetting from the level I BRTs. Site (RI between 14.7 and 28.9%) and DRW cycle number (RI between 18.4 and 31.3%; **Table 2**) remained strong predictors for all response variables also for Level II BRTs (**Figure 4**). However, also the newly included predictors exhibited strong effects. Concentrations of all P fractions were affected strongly by water retention during irrigation (RI between 14.5 and 22.4%) and field capacity (RI between 14.5 and 16.9%; **Table 2**), with concentrations decreasing with increasing water retention or field capacity (**Figure 4**). On the other hand, the relative proportion of MUP increased with increasing water retention to about 130 ml and decreased with further increasing water retention (RI 13.2%). Desiccation intensity prior to rewetting (PSI_START, RI between 16 and 20.6%; **Table 2**) was another influential predictor for all P fractions. MRP concentrations increased with increasing PSI_START in the moist range to about pF 2.5, decreased slightly with increasing dryness and increased again in the very dry range above pF 4 (**Figure 4**). By contrast, MUP and TP concentrations increased up to pF 2.2, and then decreased with increasing dryness. The relative proportion of MUP decreased steadily with increasing dryness. The MUP/TP ratio was the only parameter which in addition was strongly affected by soil temperature (RI 25.9%), showing a marked decrease with increasing soil temperature.

In strong contrast to the two-level predictor irrigation rate (see level I BRTs), the individual duration of rewetting (RW_TIME) was among the important predictors for TP and MUP (RI 12.7 and 16.5%, respectively; **Table 2**). However, an examination of the interactions between RW_TIME and SITE (data not shown) revealed that only for LUE samples TP and MUP concentrations increased with longer rewetting times.

**TABLE 2 |** Output from Boosted Regression Trees (BRTs); The explained (cross-validated, CV) variance of the models, and the relative influences of predictor variables (INT: Drying intensity, IRR_RATE: Irrigation rate, MESO_FC: Field capacity of mesocosm, SOIL_TEMP: Soil temperature, PSI_START: Matric potential before rewetting, WRET: Water retained during rewetting, RW_TIME: Duration of rewetting, DOC: Concentration of dissolved organic carbon, NH4_N: Concentration of ammonium-N) on concentrations of molybdate reactive phosphorus (MRP), molybdate unreactive phosphorus (MUP), total phosphorus (TP) and MUP/TP ratios (BRTs Level I, II, III), and the respective P loads (BRTs Level III). Blank fields indicate that the predictor was dropped during simplifying of the BRT model.

| | | P concentrations | | | | | | | | | | | | P loads | | |
|---|---|---|---|---|---|---|---|---|---|---|---|---|---|---|---|---|
| | | BRTs Level I | | | | BRTs Level II | | | | BRTs Level III | | | | BRTs Level III | | |
| **Response variable** | | **MRP** | **MUP** | **TP** | **MUP/TP** | **MRP** | **MUP** | **TP** | **MUP/TP** | **MRP** | **MUP** | **TP** | **MUP/TP** | **MRP** | **MUP** | **TP** |
| Explained variance [%] | | 49.7 | 55.5 | 51.4 | 49.0 | 75.9 | 67.8 | 71.4 | 58.6 | 89.4 | 82.8 | 72.2 | 63.3 | 65.8 | 83.7 | 85.7 |
| Explained CV variance [%] | | 38.9 | 43.1 | 43.4 | 34.3 | 47.5 | 43.5 | 44.8 | 35.0 | 47.7 | 53.7 | 50.0 | 35.2 | 40.6 | 52.9 | 61.8 |
| Relative influence [%] | SITE | 25.8 | 48.6 | 44.3 | 38.5 | 14.7 | 28.9 | 20.5 | 21.8 | 14.3 | | 4.2 | 7.8 | 9.4 | | |
| | CYCLE | 59.9 | 37.0 | 42.4 | 49.5 | 31.3 | 20.1 | 20.7 | 18.4 | 25.4 | 14.0 | 14.6 | | 20.2 | | 6.8 |
| | INT | 3.3 | 7.1 | 6.1 | 6.6 | | | | | | | | | | | |
| | IRR_RATE | 11.0 | 7.4 | 7.2 | 5.3 | | | | | | | | | | | |
| | MESO_FC | | | | | 15.5 | 16.9 | 14.2 | | 15.9 | | 8.4 | | | | |
| | SOIL_TEMP | | | | | | | | 25.9 | | | | 23.8 | 10.2 | | |
| | PSI_START | | | | | 16.0 | 17.6 | 17.0 | 20.6 | | | | 10.6 | 9.8 | 11.9 | 8.1 |
| | WRET | | | | | 22.4 | | 14.5 | 13.2 | 19.7 | | 8.4 | 10.1 | 40.7 | 30.0 | 38.5 |
| | RW_TIME | | | | | | 16.5 | 12.7 | | | | | | | | |
| | pH | | | | | | | | | | 27.3 | 10.4 | 16.1 | | 21.8 | 15.3 |
| | DOC | | | | | | | | | | 33.9 | 35.4 | 12.0 | | 18.7 | 16.9 |
| | NH4_N | | | | | | | | | 24.8 | 24.9 | 28.9 | 19.5 | 9.6 | 17.6 | 14.4 |

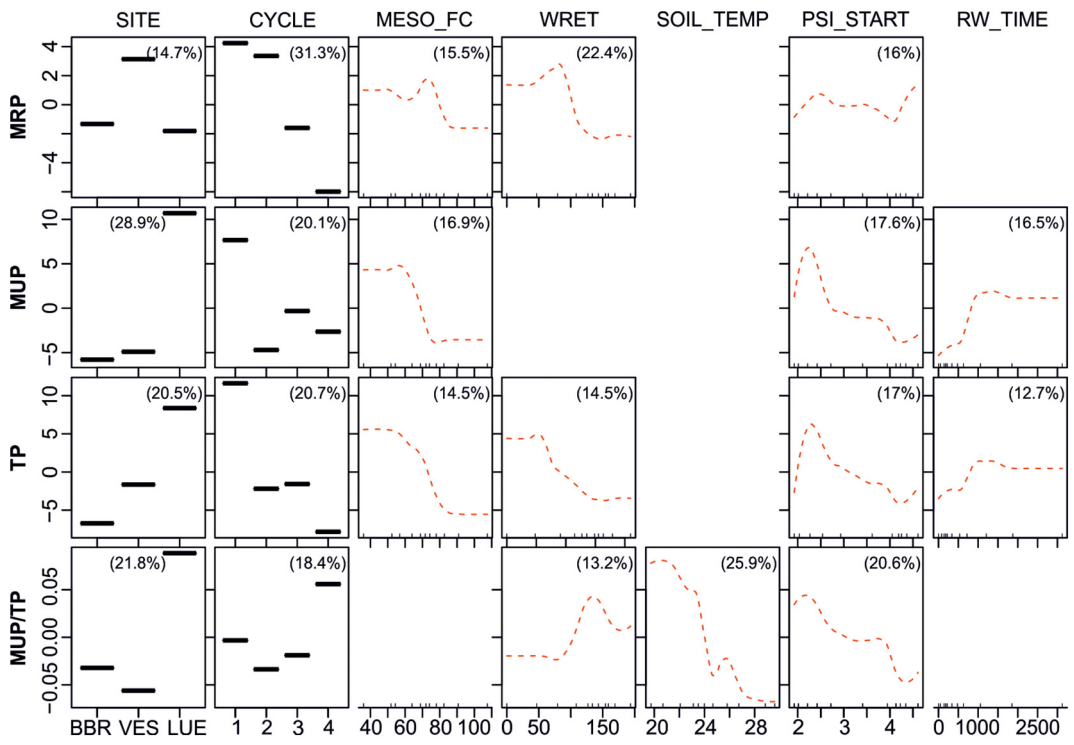


**FIGURE 4 |** Partial dependence plots for Level II BRTs, showing fitted effects of predictor variables (MESO_FC: Field capacity of mesocosm [mm], WRET: Water retained during rewetting [ml], SOIL_TEMP: soil temperature [°C], PSI_START: Matric potential before rewetting [log10(hPa)], RW_TIME: duration of rewetting [min] on MRP, MUP, TP concentrations and MUP/TP ratios with all other predictor variables held at their mean. Red dotted lines are loess smoothed curves. Percentages in plots list the relative influence of each predictor on the respective response variable. The response variables on the y-axis have been centered by subtracting their mean. Blank fields indicate that the predictor was dropped during simplifying of the BRT model. Ticks at the base of the plots indicate the distribution, in deciles, of the predictor variable on the x-axis.

### Including Leachate Chemical Composition: Level III BRTs for Leachate P Concentrations and Loads

Including soil solution parameters (DOC and NH4_N concentrations, pH) as additional predictors in the BRTs reduced mainly the RI of the three-level predictor SITE, while one or more of the soil solution parameters became highly influential (see partial dependence plots in **Figure 5**). The concentrations of all P fractions as well as the relative proportion of MUP were strongly influenced by NH4_N concentrations (RI ranging from 19.5 to 28.9%), with P concentrations and ratios increasing with NH4_N up to a threshold of 0.5 $\mu g\ l^{-1}$. Furthermore, MUP, TP and MUP/TP increased with increasing DOC concentrations (RI between 12 and 35.4%). Soil solution acidity (pH) showed a strong (RI 27.3%) but varying effect on MUP between pH 4.5 and 5.0, whereas the relative proportion of MUP decreased sharply between pH 4.0 and 4.5 (**Figure 5**).

Interactive relations (not shown) between the predictor site and the predictors DOC, NH4_N and pH suggest that the predicted effects of DOC, NH4_N and soil acidity on the concentrations of P fractions are a reflection of inherent differences between LUE and the other two sites. The leachates from LUE (see **Supplementary Table 1**) exhibited varying concentrations of DOC ($35.2 \pm 29.8\ mg\ l^{-1}$), that were, however, distinctly higher than DOC concentrations in leachates from BBR ($8.5 \pm 3.5\ mg\ l^{-1}$) and VES ($12.6 \pm 6.6\ mg\ l^{-1}$). The concentrations of NH4_N ($3.5 \pm 5.3\ mg\ l^{-1}$) in LUE leachates were also higher than those in leachates from BBR and VES (both $1.1 \pm 0.1\ mg\ l^{-1}$). LUE leachates were also more acidic (mean pH 4.3) than leachates from VES (mean pH 5.0) and BBR (mean pH 5.7).

Since loads of leached P fractions were calculated by multiplying the leached volume of each rewetting phase with the respective concentrations of MRP, MUP and TP, all loads were reduced by an increasing water retention during rewetting (WRET) as the strongest predictor in the BRTs (RI between 30 and 40.7%; see partial dependence plots in **Figure 6**). Responses to most other predictor variables were similar to the respective P concentrations.

## DISCUSSION

### P Leakage Decreases Over Time

The total P concentrations in leachates were in a similar range as in previous leachate studies examining the same sites (Holzmann et al., 2016; Makowski et al., 2020). Organic P dominated the leakage from all three sites (mean MUP/TP ratios ranging from 57 to 80%), which has also been observed by a number of other authors (e.g., Turner and Haygarth, 2001; Blackwell et al., 2010) and is explained by the greater affinity of MRP to the soil solid phase (Kaiser et al., 2003; George et al., 2018). However, our findings are in contrast with observations of Holzmann et al. (2016); Brödlin et al. (2019), and Makowski et al. (2020), where MRP dominated leachates from mineral soil. We found mean ratios of MUP/TP to be about a third higher in leachates from LUE than from BBR and VES, which is due to the thicker humus layer containing a higher share of organic P in LUE.

While leachate volumes remained approximately constant throughout the four DRW cycles, P concentrations in the leachates decreased steadily. The consecutive number of the DRW cycle was included in all BRT models for MUP, MRP and TP concentrations, as well as for MRP and TP loads. The steady decrease of MRP concentrations from the first to the fourth cycle points to a progressive depletion of the exchangeable inorganic P pool and its declining replenishment from organic matter mineralization. The strikingly higher MUP (and thus TP) concentrations in the first DRW cycle compared to subsequent cycles indicate a flushing of soil organic matter during the first rewetting ("Birch effect"). This is in line with observations of a distinct P flushing during the first hours of irrigation of desiccated soil in a field experiment by Makowski et al. (2020). The particularly low MUP concentrations in the second DRW cycle are possibly due to the higher soil temperatures (compared to the third and fourth cycle) that enhanced enzymatic depolymerization and mineralization of organic matter (e.g., Conant et al., 2011; Bailey et al., 2019). Since we did not observe a concomitant increase in MRP concentrations during the second cycle, the mineralized P was likely taken up by trees or microorganisms.

### Drier Soil Does Not Leach More P Upon Rewetting

Our observations only partly confirm our hypothesis (1) that increasing intensity of desiccation would lead to higher P leakage upon rewetting. Contrary to our expectations, MUP and TP concentrations as well as MUP/TP ratios decreased in the leachates with increasing degree of drying, predominantly in the VES samples. MRP showed a tendency to increase after more intense desiccation, especially above pF 4. This is in agreement with the results of Khan et al. (2019), who observed increased leaching of dissolved inorganic P when soils were more desiccated prior to rewetting. Our results partially agree with findings of Brödlin et al. (2019), who observed (in organic and topsoil material from LUE and BBR) a considerably greater mobilization of inorganic, but also organic P after an initiate harsh dry spell (drying at 40°C for 72 h) compared to a subsequent moderate one (drying at 20°C for one month). While the potential effect of a first flush is not discussed by Brödlin et al. (2019), the authors argue that a harsher drying exerts higher osmotic stress on microorganisms and thereby affects drought-induced P release of primarily microbial origin. Our results suggest that a drying to a matric potential up to pF 4 does not affect P leaching, but losses of P increase above pF 4. This is also in line with Dinh et al. (2017), who found microbial P release under DRW to critically increase upon desiccation to above pF 4. Apart from the magnitude of desiccation (i.e., the achieved matric potential), the established drying phase in our experiment was possibly too short to induce a substantial release of P from microbial cell lysis. For example, Khan et al. (2019) found that after an intensive drying period of 14 days, rewetting released significantly more microbially derived P from soils than after

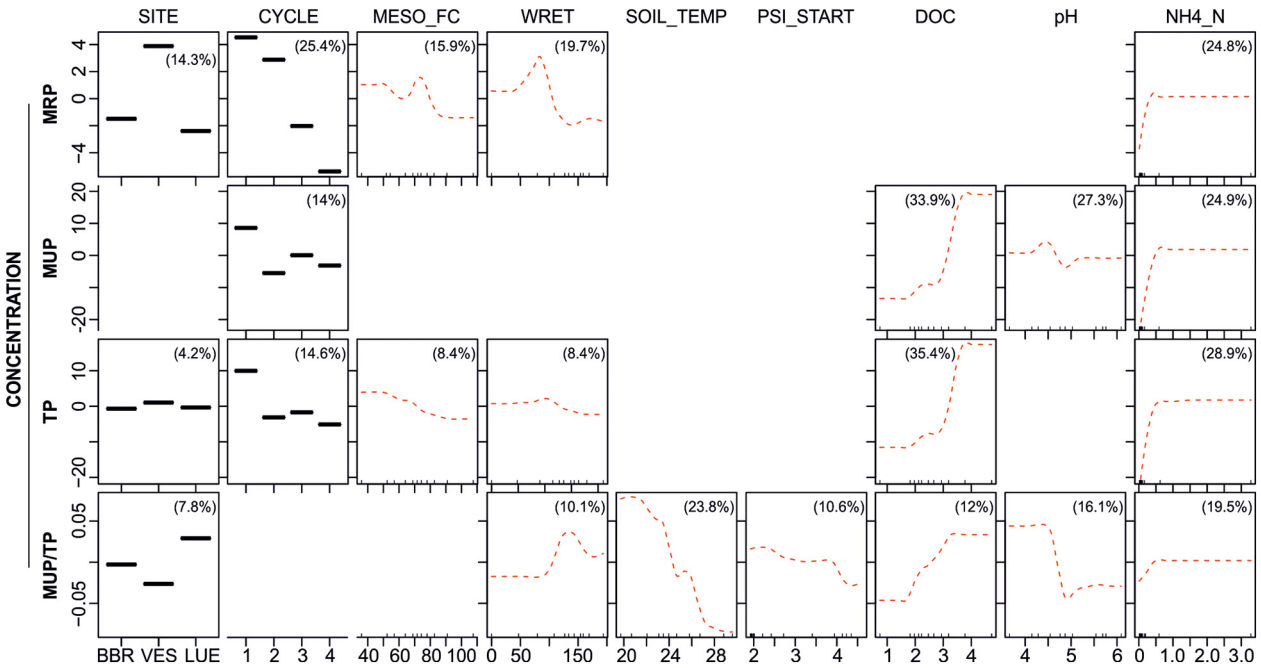


**FIGURE 5 |** Partial dependence plots for Level III BRTs, showing fitted effects of predictor variables (MESO_FC: Field capacity of mesocosm [mm], WRET: Water retained during rewetting [ml], SOIL_TEMP: soil temperature [°C], PSI_START: Matric potential before rewetting [log10(hPa)], DOC: concentration of dissolved organic carbon (log-transformed), NH4_N: concentration of ammonium-nitrate (log-transformed)) on MRP, MUP, TP concentrations and MUP/TP ratios with all other predictor variables held at their mean. Red dotted lines are loess smoothed curves. Percentages in plots list the relative influence of each predictor on the respective response variable. The response variables on the y-axis have been centered by subtracting their mean. Blank fields indicate that the predictor was dropped during simplifying of the BRT model. Ticks at the base of the plots indicate the distribution, in deciles, of the predictor variable on the x-axis.

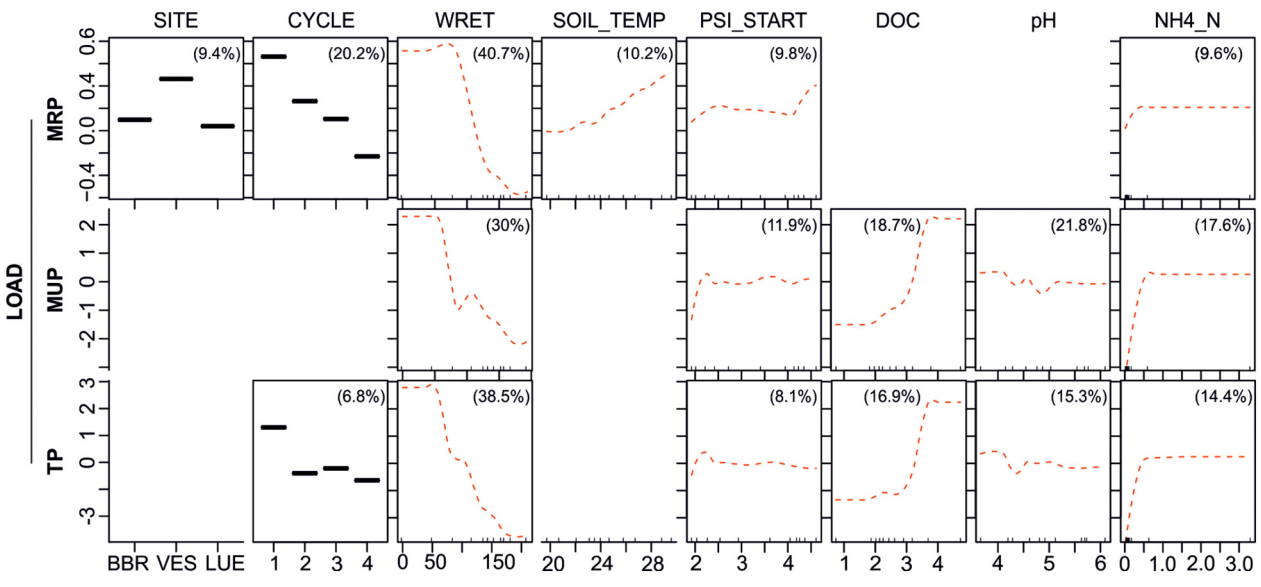


**FIGURE 6 |** Partial dependence plots for Level III BRTs, showing fitted effects of predictor variables (WRET: Water retained during rewetting [ml], SOIL_TEMP: soil temperature [°C], PSI_START: Matric potential before rewetting [log10(hPa)], DOC (concentration of dissolved organic carbon (log-transformed), NH4_N: concentration of ammonium-nitrate (log-transformed)) on MRP, MUP and TP loads with all other predictor variables held at their mean. Red dotted lines are loess smoothed curves. Percentages in plots list the relative influence of each predictor on the respective response variable. The response variables on the y-axis have been centered by subtracting their mean. Blank fields indicate that the predictor was dropped during simplifying of the BRT model. Ticks at the base of the plots indicate the distribution, in deciles, of the predictor variable on the x-axis.

two days of intensive drying. Lower survival of bacteria with increasing desiccation time was also observed by Meisner et al. (2015, 2017), while fungi probably survived desiccation better (Schimel, 2018). Overall, it appears that the microbial community in our experiment was able to largely outlast and recover from the desiccation phases (3 to 5 days for moderate and 5 to 8 days for intensive drying) (cf. Gao et al., 2020; Schimel, 2018). Parts of the bacterial community likely adapted to drought stress by developing epigenetical traits, e.g., by the production of extracellular polymeric substances during soil drying (Schimel, 2018). This may have altered soil repellency, decreased organic matter mobility (Barnard et al., 2020) and thereby hampered the leaching of soil organic P (George et al., 2018). Possibly, this process explains why desiccation to values below pF 4 did not further intensify P leaching in our experiment.

In addition to biotic processes, abiotic factors such as aggregate disruption (Bünemann et al., 2013) and desorption (Butterly et al., 2009) modify the response of soils to DRW cycles. However, the breakdown of soil aggregates by drying and rewetting is unlikely to have played a role in our experiment because it usually occurs only at very large rewetting magnitudes (Barnard et al., 2020). Accordingly, we found that in BBR and VES, which have loamy soils with a distinct soil structure, MRP (but not MUP) leaching was only slightly increased when subjected to harsher drying. The elevated leaching of MRP is possibly an effect of both, the release of adsorbed inorganic P in the mineral soil (Butterly et al., 2009) and microbial P release (Dinh et al., 2017).

Taken together, our results suggest that the upshock, i.e., the change in soil water potential between desiccation and rewetting achieved in our experiment, was not the main driver behind the stimulated P leaching and that site properties had a stronger influence. Future DRW experiments should investigate the individual effects of drying intensity and rewetting rate by more intense upshocks.

## Fast Rewetting Does Not Affect P Leaching More Than Slow Rewetting

Based on our results, we must reject our hypothesis (2) that P concentrations in leachate are elevated after fast rewetting compared to slower rewetting. Overall, rewetting time had very little effect on the P leakage in BBR. In VES, faster rewetting was associated with slightly increased MRP leaching, but had no effect on MUP and TP. LUE samples had lower MUP and TP concentrations and slightly higher MRP concentrations under fast rewetting than under slow rewetting. The fact that organic P leaching reacted to the rewetting rate mainly in the LUE samples, where the organic layer and its potentially mobilizable organic P pool are larger than in BBR (Hauenstein et al., 2018) and VES (Lang et al., 2017), underlines the role of dissolved organic matter for the translocation of organic P. This was also reflected in the higher DOC concentrations in LUE leachates than in BBR and VES. The comparatively low response of the BBR samples to the rewetting intensity can be explained by the lower mineralization rate and the higher storage capacity for nutrients at this site.

During fast rewetting of dried soil, water is more likely to pass the soil via macropores and leach particulate P (Makowski et al., 2020). In the loamy soils from BBR and VES, matrix retention of the irrigation water was higher under slow rewetting, which indicates a rapid passage of the irrigation water through macropores under fast rewetting. However, contrary to our expectations, this was not associated with higher leachate P concentrations (except for slightly increased MRP leaching in VES). Despite the occurrence of macropore flow, the BBR and VES soils apparently retained phosphorus effectively in the soil matrix. The high clay and sesquioxide contents seemingly allow effective physical adsorption and ligand exchange at exchange sites (Kalbitz et al., 2000) despite the rapid water movement. In the sandy LUE samples, with no visible signs of soil aggregation, MRP was, in agreement with our hypothesis, higher under fast than under slow rewetting. Resaturation of the mesocosms was achieved on average after 83 ml of irrigation after slow rewetting, but only after 166 ml under fast rewetting, which hints at the occurrence of preferential flow also in the highly water-conductive LUE soil.

## More P Is Released Upon Rewetting From Soils With Low Sorption Capacity

In agreement with hypothesis (3), soil solution MRP, MUP and TP concentrations differed significantly between the sites. LUE, the site with the smallest P stock and the lowest sorption capacity, had leachate MUP und TP concentrations that were about a factor of two higher than in VES and BBR. However, TP and MUP leaching did not differ between the other two sites, BBR and VES, despite higher soil P stocks and sorption capacities in BBR. MRP concentrations were comparably low in LUE and BBR, and highest in leachates from VES. The generally very low P leaching from BBR has been linked to low release of P from organic matter (Hauenstein et al., 2018; Brödlin et al., 2019). In addition, the higher sorption capacity as well as a reduced apatite solubility in the less acidic BBR soil (Holzmann et al., 2016) may explain the lower P leaching from BBR than from VES.

This contrasts the findings of Holzmann et al. (2016); Brödlin et al. (2019), and Makowski et al. (2020), where MRP dominates leachates of mineral soil solution. The concentrations of leached MRP were low at all three sites, and generally lower than MUP.

The higher MRP concentrations in the VES soil leachates agree with findings of Julich et al. (2017), who observed higher shares of inorganic labile P in TP in O and A horizons from VES compared to BBR and LUE. The soil matrix in VES contains less sesquioxides than in BBR (see **Table 1**), which, together with the lower pH, explains the less strong binding of inorganic P to the soil matrix. Another possible cause for the comparatively high MRP concentrations in VES is the higher biological activity and thus potentially higher mobilization of inorganic P at this site. This is reflected in higher P leaf concentrations, lower $C_{mic}/P_{mic}$ ratios, larger $P_{org}$/TP ratios and higher C stocks in the mineral soil compared to BBR and LUE (Lang et al., 2017). In addition, the bacterial community in VES is more diverse and less dominated by specialized taxa than in BBR and LUE

(Bergkemper et al., 2016), which may favor the mineralization of organically bound P.

According to the Level II BRTs, an increasing field capacity (MESO_FC) decreased the leachate concentrations of MUP and TP, especially in LUE. This confirms the expectation that sites with low water storage capacity have a higher risk of P loss because of the concomitant reduced ability to retain soluble organic nutrients there. DOC concentrations, which are three to four times higher in LUE than in BBR and VES, explained large parts of the observed variance in the leachate P concentrations. LUE leachates had higher C/P ratios, which likely results from higher C/P ratios of the mineral soil, the soil organic matter and the microbiome at this site (Lang et al., 2017). In our data, Al, Fe and DON were highly correlated with DOC (R2: 0.82, 0.80, and 0.73, respectively) and thus also positively related to MUP and TP concentrations in leachate, but not with MRP. This is in line with the generally acknowledged simultaneous dynamics of MUP/TP and DOC as reflections of dissolved organic matter release, which increases upon physico-chemical solubilization and microbial breakdown, and decreases with mineral sorption (e.g., Kalbitz et al., 2000; Kaiser et al., 2003; Zederer and Talkner, 2018; Brödlin et al., 2019; Wanek et al., 2019).

## CONCLUSION

We subjected mesocosms with young beech trees growing in approximately 20 cm undisturbed mineral soil plus organic layer to four consecutive DRW cycles. P concentrations in leachates decreased with each cycle. Neither the intensity of drying nor the rewetting rate affected the P leaching as hypothesized: Intensive drying or fast rewetting did not generally enhance P release. We found that an increasing water retention capacity of the soils led to decreasing P concentrations in the leachates. At all sites, MUP contributed predominantly to TP and more MUP and TP leached from the sandy site LUE than from the loamy soils from BBR and VES. The release of MUP and TP was best explained by released DOC. This indicates that the solubilization of organic matter, to some extent enhanced by DRW events, entails the release and translocation of organic P. This mobilized organic P may be mineralized and taken up by plants, or leached from the soil. These losses may be especially high in soils with a coarse texture that are in addition often inherently nutrient poor and where biological processes are critical to maintain P supply. Our results confirm previous findings that leaching of organic P can be a relevant source of potential P losses from ecosystems.

## DATA AVAILABILITY STATEMENT

The datasets generated for this study are available on request to the corresponding author.

## AUTHOR CONTRIBUTIONS

HP, JL, and LG designed the study and wrote the manuscript, with input from MV. LG, HP, MV, and JL collected samples. LG set up the DRW experiment and conducted the experiment with support from HP. LG and HP performed data analysis. All authors contributed to the article and approved the submitted version.

## FUNDING

This work was funded by the German Research Foundation (DFG) as a part of the Priority Program 1685 "Ecosystem Nutrition: Forest Strategies for limited Phosphorus Resources" (grant no. PU 405/1-1), as well as by the Swiss National Science Foundation (SNF, grant no. 200021E-171172).

## ACKNOWLEDGMENTS

We thank Joshua Braun-Wimmer and Roland Hoch for indispensable support during field work and throughout the whole process of experimental and data handling work. We also thank the laboratory workers at the FVA Freiburg for their dedicated analytical work and support. We also thank the two reviewers whose comments and suggestions helped improving and clarify this manuscript.

## SUPPLEMENTARY MATERIAL

The Supplementary Material for this article can be found online at: https://www.frontiersin.org/articles/10.3389/ffgc.2021.543037/full#supplementary-material

## REFERENCES

Achat, D. L., Augusto, L., Gallet-Budynek, A., and Bakker, M. R. (2012). Drying-induced changes in phosphorus status of soils with contrasting soil organic matter contents–Implications for laboratory approaches. *Geoderma* 187, 41–48. doi: 10.1016/j.geoderma.2012.04.014

Annaheim, K. E., Rufener, C. B., Frossard, E., and Bünemann, E. K. (2013). Hydrolysis of organic phosphorus in soil water suspensions after addition of phosphatase enzymes. *Biol. Fertil. Soils* 49, 1203–1213. doi: 10.1007/s00374-013-0819-1

Bailey, V. L., Pries, C. H., and Lajtha, K. (2019). What do we know about soil carbon destabilization? *Environ. Res. Lett.* 14:083004. doi: 10.1088/1748-9326/ab2c11

Barnard, R. L., Blazewicz, S. J., and Firestone, M. K. (2020). Rewetting of soil: revisiting the origin of soil CO2 emissions. *Soil Biol. Biochem.* 147:107819. doi: 10.1016/j.soilbio.2020.107819

Bergkemper, F., Welzl, G., Lang, F., Krüger, J., Schloter, M., and Schulz, S. (2016). The importance of C, N and P as driver for bacterial community structure in German beech dominated forest soils. *J. Plant Nutr. Soil Sci.* 179, 472–480. doi: 10.1002/jpln.201600077

Birch, H. F. (1958). The effect of soil drying on humus decomposition and nitrogen availability. *Plant Soil* 10, 9–31. doi: 10.1007/bf01343734

Blackwell, M., Brookes, P., de la Fuente-Martinez, N., Murray, P., Snars, K., Williams, J., et al. (2009). Effects of soil drying and rate of re-wetting on concentrations and forms of phosphorus in leachate. *Biol. Fertil. Soils* 45, 635–643. doi: 10.1007/s00374-009-0375-x

Blackwell, M., Carswell, A., and Bol, R. (2013). Variations in concentrations of N and P forms in leachates from dried soils rewetted at different rates. *Biol. Fertil. Soils* 49, 79–87. doi: 10.1007/s00374-012-0700-7

Blackwell, M. S. A., Brookes, P. C., de la Fuente-Martinez, N., Gordon, H., Murray, P. J., Snars, K. E., et al. (2010). "Phosphorus solubilization and potential transfer to surface waters from the soil microbial biomass following drying–rewetting and freezing–thawing," in *Advances in Agronomy*, Vol. 106, ed. D. L. Sparks (Cambridge, MA: Academic Press), 1–35. doi: 10.1016/s0065-2113(10)06001-3

Bol, R., Julich, D., Brödlin, D., Siemens, J., Kaiser, K., Dippold, M. A., et al. (2016). Dissolved and colloidal phosphorus fluxes in forest ecosystems—an almost blind spot in ecosystem research. *J. Plant Nutr. Soil Sci.* 179, 425–438. doi: 10.1002/jpln.201600079

Brödlin, D., Kaiser, K., Kessler, A., and Hagedorn, F. (2019). Drying and rewetting foster phosphorus depletion of forest soils. *Soil Biol. Biochem.* 128, 22–34. doi: 10.1016/j.soilbio.2018.10.001

Bünemann, E. K., Keller, B., Hoop, D., Jud, K., Boivin, P., and Frossard, E. (2013). Increased availability of phosphorus after drying and rewetting of a grassland soil: processes and plant use. *Plant Soil* 370, 511–526. doi: 10.1007/s11104-013-1651-y

Buston, P. M., and Elith, J. (2011). Determinants of reproductive success in dominant pairs of clownfish: a boosted regression tree analysis. *J. Anim. Ecol.* 80, 528–538. doi: 10.1111/j.1365-2656.2011.01803.x

Butterly, C. R., Bünemann, E. K., McNeill, A. M., Baldock, J. A., and Marschner, P. (2009). Carbon pulses but not phosphorus pulses are related to decreases in microbial biomass during repeated drying and rewetting of soils. *Soil Biol. Biochem.* 41, 1406–1416. doi: 10.1016/j.soilbio.2009.03.018

Chen, H., Jarosch, K. A., Mészáros, É, Frossard, E., Zhao, X., and Oberson, A. (2021). Repeated drying and rewetting differently affect abiotic and biotic soil phosphorus (P) dynamics in a sandy soil: a 33P soil incubation study. *Soil Biol. Biochem.* 153:108079. doi: 10.1016/j.soilbio.2020.108079

Chen, H., Lai, L., Zhao, X., Li, G., and Lin, Q. (2016). Soil microbial biomass carbon and phosphorus as affected by frequent drying–rewetting. *Soil Res.* 54, 321–327. doi: 10.1071/sr14299

Conant, R. T., Ryan, M. G., Ågren, G. I., Birge, H. E., Davidson, E. A., Eliasson, P. E., et al. (2011). Temperature and soil organic matter decomposition rates–synthesis of current knowledge and a way forward. *Global Change Biol.* 17, 3392–3404. doi: 10.1111/j.1365-2486.2011.02496.x

R Core Team (2019). *R: A Language and Environment for Statistical Computing*. Vienna: R Foundation for Statistical Computing.

Coumou, D., and Rahmstorf, S. (2012). A decade of weather extremes. *Nat. Clim. Change* 2, 491–496. doi: 10.1038/nclimate1452

De'Ath, G. (2007). Boosted trees for ecological modeling and prediction. *Ecology* 88, 243–251. doi: 10.1890/0012-9658(2007)88[243:btfema]2.0.co;2

Derville, S., Constantine, R., Baker, C., Oremus, M., and Torres, L. (2016). Environmental correlates of nearshore habitat distribution by the critically endangered maui dolphin. *Mar. Ecol. Prog. Ser.* 551, 261–275. doi: 10.3354/meps11736

Dinh, M.-V., Guhr, A., Spohn, M., and Matzner, E. (2017). Release of phosphorus from soil bacterial and fungal biomass following drying/rewetting. *Soil Biol. Biochem.* 110, 1–7. doi: 10.1016/j.soilbio.2017.02.014

Dinh, M.-V., Schramm, T., Spohn, M., and Matzner, E. (2016). Drying–rewetting cycles release phosphorus from forest soils. *J. Plant Nutr. Soil Sci.* 179, 670–678. doi: 10.1002/jpln.201500577

Elith, J., and Leathwick, J. (2017). *Boosted Regression Trees for Ecological Modeling. R Documentation*. Available online: http://citeseerx.ist.psu.edu/viewdoc/download?doi=10.1.1.1068.3627&rep=rep1&type=pdf (accessed January 31, 2019).

Elith, J., Leathwick, J. R., and Hastie, T. (2008). A working guide to boosted regression trees. *J. Anim. Ecol.* 77, 802–813. doi: 10.1111/j.1365-2656.2008.01390.x

Forber, K. J., Ockenden, M. C., Wearing, C., Hollaway, M. J., Falloon, P. D., Kahana, R., et al. (2017). Determining the effect of drying time on phosphorus solubilization from three agricultural soils under climate change scenarios. *J. Environ. Qual.* 46, 1131–1136. doi: 10.2134/jeq2017.04.0144

Forsmann, D. M., and Kjaergaard, C. (2014). Phosphorus release from anaerobic peat soils during convective discharge—effect of soil Fe: P molar ratio and preferential flow. *Geoderma* 223, 21–32. doi: 10.1016/j.geoderma.2014.01.025

Friedman, J. H. (2002). Stochastic gradient boosting. *Comput. Stat. Data Anal.* 38, 367–378.

Friedman, J. H., and Meulman, J. J. (2003). Multiple additive regression trees with application in epidemiology. *Stat. Med.* 22, 1365–1381. doi: 10.1002/sim.1501

Frossard, E., Condron, L. M., Oberson, A., Sinaj, S., and Fardeau, J. (2000). Processes governing phosphorus availability in temperate soils. *J. Environ. Qual.* 29, 15–23. doi: 10.2134/jeq2000.00472425002900010003x

Gao, D., Bai, E., Li, M., Zhao, C., Yu, K., and Hagedorn, F. (2020). Responses of soil nitrogen and phosphorus cycling to drying and rewetting cycles: a meta-analysis. *Soil Biol. Biochem.* 148:107896. doi: 10.1016/j.soilbio.2020.107896

George, T. S., Giles, C. D., Menezes-Blackburn, D., Condron, L. M., Gama-Rodrigues, A. C., Jaisi, D., et al. (2018). Organic phosphorus in the terrestrial environment: a perspective on the state of the art and future priorities. *Plant Soil* 427, 191–208. doi: 10.1007/s11104-017-3391-x

Greenwell, B., Boehmke, B., Cunningham, J., and Developers, G. (2019). *gbm: Generalized Boosted Regression Models*. Available online at: https://CRAN.R-project.org/package=gbm (accessed October 22, 2019).

Greenwell, B. M. (2017). pdp: an R Package for constructing partial dependence plots. *R J.* 9, 421–436. doi: 10.32614/rj-2017-016

Hantschel, R. E., Flessa, H., and Beese, F. (1994). An automated microcosm system for studying soil ecological processes. *Soil Sci. Soc. Am. J.* 58, 401–404. doi: 10.2136/sssaj1994.03615995005800020023x

Hauenstein, S., Neidhardt, H., Lang, F., Krüger, J., Hofmann, D., Pütz, T., et al. (2018). Organic layers favor phosphorus storage and uptake by young beech trees (Fagus sylvatica L.) at nutrient poor ecosystems. *Plant Soil* 432, 289–301. doi: 10.1007/s11104-018-3804-5

Heathwaite, A., and Dils, R. (2000). Characterising phosphorus loss in surface and subsurface hydrological pathways. *Sci. Total Environ.* 251, 523–538. doi: 10.1016/s0048-9697(00)00393-4

Hijmans, R. J., Phillips, S., Leathwick, J., and Elith, J. (2017). *dismo: Species Distribution Modeling*. Available online at:https://cran.r-project.org/web/packages/dismo/index.html (accessed May 15, 2019).

Hildebrand, E. E. (1994). The heterogeneous distribution of mobile ions in the rhizosphere of acid forest soils: facts, causes and consequences. *J. Environ. Sci. Health Part A* 29, 1973–1992. doi: 10.1080/10934529409376159

Holzmann, S., Missong, A., Puhlmann, H., Siemens, J., Bol, R., Klumpp, E., et al. (2016). Impact of anthropogenic induced nitrogen input and liming on phosphorus leaching in forest soils. *J. Plant Nutr. Soil Sci.* 179, 443.–453. doi: 10.1002/jpln.201500552

Hömberg, A., and Matzner, E. (2017). Effects of drying and rewetting on soluble phosphorus and nitrogen in forest floors: an experiment with undisturbed columns. *J. Plant Nutr. Soil Sci.* 181, 177–184. doi: 10.1002/jpln.201700380

Horn, R., and Taubner, H. (1989). Effect of aggregation on potassium flux in a structured soil. *Z. Pflanz. Bodenkunde* 152, 99–104. doi: 10.1002/jpln.19891520118

Julich, D., Julich, S., and Feger, K.-H. (2017). Phosphorus in preferential flow pathways of forest soils in Germany. *Forests* 8:19. doi: 10.3390/f8010019

Kaiser, K., Guggenberger, G., and Haumaier, L. (2003). Organic phosphorus in soil water under a European beech (Fagus sylvatica L.) stand in northeastern Bavaria, Germany: seasonal variability and changes with soil depth. *Biogeochemistry* 66, 287–310. doi: 10.1023/B:BIOG.0000005325.86131.5f

Kalbitz, K., Solinger, S., Park, J.-H., Michalzik, B., and Matzner, E. (2000). Controls on the dynamics of dissolved organic matter in soils: a review. *Soil Sci.* 165, 277–304. doi: 10.1097/00010694-200004000-00001

Khan, S. U., Hooda, P. S., Blackwell, M. S. A., and Busquets, R. (2019). Microbial biomass responses to soil drying-rewetting and phosphorus leaching. *Front. Environ. Sci.* 7:00133. doi: 10.3389/fenvs.2019.00133

Lang, F., Bauhus, J., Frossard, E., George, E., Kaiser, K., Kaupenjohann, M., et al. (2016). Phosphorus in forest ecosystems: new insights from an ecosystem nutrition perspective. *J. Plant Nutr. Soil Sci.* 179, 129–135. doi: 10.1002/jpln.201500541

Lang, F., Krüger, J., Amelung, W., Willbold, S., Frossard, E., Bünemann, E. K., et al. (2017). Soil phosphorus supply controls P nutrition strategies of beech forest ecosystems in Central Europe. *Biogeochemistry* 136, 5–29. doi: 10.1007/s10533-017-0375-0

Makowski, V., Julich, S., Feger, K.-H., and Julich, D. (2020). Soil phosphorus translocation via preferential flow pathways: a comparison of two sites with different phosphorus stocks. *Front. For. Glob. Change* 3:00048. doi: 10.3389/ffgc.2020.00048

Malitz, G., and Ertel, H. (2015). *KOSTRA-DWD-2010, Starkniederschlagshöhen für Deutschland (Bezugszeitraum 1951 bis 2010). Abschlussbericht, Deutscher Wetterdienst (DWD)*. Offenbach: Abteilung Hydrometeorologie.

Meier, I., and Leuschner, C. (2014). Nutrient dynamics along a precipitation gradient in European beech forests. *Biogeochemistry* 120, 51–69. doi: 10.1007/s10533-014-9981-2

Meisner, A., Leizeaga, A., Rousk, J., and Bååth, E. (2017). Partial drying accelerates bacterial growth recovery to rewetting. *Soil Biol. Biochem.* 112, 269–276. doi: 10.1016/j.soilbio.2017.05.016

Meisner, A., Rousk, J., and Bååth, E. (2015). Prolonged drought changes the bacterial growth response to rewetting. *Soil Biol. Biochem.* 88, 314–322. doi: 10.1016/j.soilbio.2015.06.002

Meller, S., Frossard, E., and Luster, J. (2019). Phosphorus allocation to leaves of beech saplings reacts to soil phosphorus availability. *Front. Plant Sci.* 10:744. doi: 10.3389/fpls.2019.00744

Messing, I., Joel, A., Wesström, I., and Strock, J. (2015). Influence of higher rain intensities on phosphorus movements in the upper half meter of macroporous clay soil. *Acta Agri. Scand. B Soil Plant Sci.* 65, 93–99. doi: 10.1080/09064710.2014.996588

Missong, A., Holzmann, S., Bol, R., Nischwitz, V., Puhlmann, H., von Wilpert, K., et al. (2018). Leaching of natural colloids from forest topsoils and their relevance for phosphorus mobility. *Sci. Total Environ.* 634, 305–315. doi: 10.1016/j.scitotenv.2018.03.265

Odum, E. P. (1969). The strategy of ecosystem development. *Science* 164, 262–270. doi: 10.1126/science.164.3877.262

Pezzolla, D., Cardenas, L. M., Mian, I. A., Carswell, A., Donovan, N., Dhanoa, M. S., et al. (2019). Responses of carbon, nitrogen and phosphorus to two consecutive drying–rewetting cycles in soils. *J. Plant Nutr. Soil Sci.* 182, 217–228. doi: 10.1002/jpln.201800082

Schimel, J. P. (2018). Life in dry soils: effects of drought on soil microbial communities and processes. *Ann. Rev. Ecol. Evol. Syst.* 49, 409–432. doi: 10.1146/annurev-ecolsys-110617-062614

Schlotter, D., Schack-Kirchner, H., Hildebrand, E. E., and von Wilpert, K. (2012). Equivalence or complementarity of soil-solution extraction methods. *J. Plant Nutr. Soil Sci.* 175, 236–244. doi: 10.1002/jpln.201000399

Sinaj, S., Stamm, C., Toor, G. S., Condron, L. M., Hendry, T., Di, H. J., et al. (2002). Phosphorus exchangeability and leaching losses from two grassland soils. *J. Environ. Qual.* 31, 319–330. doi: 10.2134/jeq2002.3190

Sohrt, J., Lang, F., and Weiler, M. (2017). Quantifying components of the phosphorus cycle in temperate forests. *Wiley Interdiscip. Rev. Water* 4:e1243. doi: 10.1002/wat2.1243

Sutcliffe, P. R., Mellin, C., Pitcher, C. R., Possingham, H. P., and Caley, M. J. (2013). Regional-scale patterns and predictors of species richness and abundance across twelve major tropical inter-reef taxa. *Ecography* 37, 162–171. doi: 10.1111/j.1600-0587.2013.00102.x

Thaysen, E. M., Jessen, S., Ambus, P., Beier, C., Postma, D., and Jakobsen, I. (2014). Technical note: mesocosm approach to quantify dissolved inorganic carbon percolation fluxes. *Biogeosciences* 11, 1077–1084. doi: 10.5194/bg-11-1077-2014

Trenberth, K. E. (2011). Changes in precipitation with climate change. *Clim. Res.* 47, 123–138. doi: 10.3354/cr00953

Turner, B. L., Driessen, J. P., Haygarth, P. M., and Mckelvie, I. D. (2003). Potential contribution of lysed bacterial cells to phosphorus solubilisation in two rewetted Australian pasture soils. *Soil Biol. Biochem.* 35, 187–189. doi: 10.1016/s0038-0717(02)00244-4

Turner, B. L., and Haygarth, P. M. (2001). Biogeochemistry: phosphorus solubilization in rewetted soils. *Nature* 411:258. doi: 10.1038/35077146

Turner, B. L., and Haygarth, P. M. (2003). Changes in bicarbonate-extractable inorganic and organic phosphorus by drying pasture soils. *Soil Sci. Soc. Am. J.* 67, 344–350. doi: 10.2136/sssaj2003.3440

Uhlig, D., and von Blanckenburg, F. (2019). How slow rock weathering balances nutrient loss during fast forest floor turnover in montane, temperate forest ecosystems. *Front. Earth Sci.* 7:159. doi: 10.3389/feart.2019.00159

Vogt, R., and Matschonat, G. (1997). Patterns of soil solution composition in acid forest soils: differences between undisturbes and bulk samples. *Z. Pflanz. Bodenkunde* 160, 549–554. doi: 10.1002/jpln.19971600505

Wanek, W., Zezula, D., Wasner, D., Mooshammer, M., and Prommer, J. (2019). A novel isotope pool dilution approach to quantify gross rates of key abiotic and biological processes in the soil phosphorus cycle. *Biogeosciences* 16, 3047–3068. doi: 10.5194/bg-16-3047-2019

Weihrauch, C., and Opp, C. (2018). Ecologically relevant phosphorus pools in soils and their dynamics: the story so far. *Geoderma* 325, 183–194. doi: 10.1016/j.geoderma.2018.02.047

WRB (2015). *World Reference Base for Soil Resources 2014, Update 2015: International Soil Classification System for Naming Soils and Creating Legends for Soil Maps*. Rome: FAO, 192.

Wu, J., and Brookes, P. C. (2005). The proportional mineralisation of microbial biomass and organic matter caused by air-drying and rewetting of a grassland soil. *Soil Biol. Biochem.* 37, 507–515. doi: 10.1016/j.soilbio.2004.07.043

Zavišić, A., and Polle, A. (2017). Dynamics of phosphorus nutrition, allocation and growth of young beech (Fagus sylvatica L.) trees in P-rich and P-poor forest soil. *Tree Physiol.* 38, 37–51. doi: 10.1093/treephys/tpx146

Zederer, D. P., and Talkner, U. (2018). Organic P in temperate forest mineral soils as affected by humus form and mineralogical characteristics and its relationship to the foliar P content of European beech. *Geoderma* 325, 162–171. doi: 10.1016/j.geoderma.2018.03.033

Zwiers, F. W., Alexander, L. V., Hegerl, G. C., Knutson, T. R., Kossin, J. P., Naveau, P., et al. (2013). "Climate extremes: challenges in estimating and understanding recent changes in the frequency and intensity of extreme climate and weather events," in *Climate Science for Serving Society: Research, Modeling and Prediction Priorities*, eds G. R. Asrar and J. W. Hurrell (Dordrecht: Springer Netherlands), 339–389. doi: 10.1007/978-94-007-6692-1_13

**Conflict of Interest:** The authors declare that the research was conducted in the absence of any commercial or financial relationships that could be construed as a potential conflict of interest.

frontiers in Forests and Global Change

ORIGINAL RESEARCH
published: 31 May 2021
doi: 10.3389/ffgc.2021.684069

# Leaching of Phosphomonoesterase Activities in Beech Forest Soils: Consequences for Phosphorus Forms and Mobility

*Jasmin Fetzer[1,2]*, Sebastian Loeppmann[3,4], Emmanuel Frossard[1], Aamir Manzoor[4], Dominik Brödlin[2], Klaus Kaiser[5] and Frank Hagedorn[2]*

*[1] Department of Environmental Systems Science, ETH Zurich, Zurich, Switzerland, [2] Forest Soils and Biogeochemistry, Swiss Federal Institute for Forest, Snow and Landscape Research WSL, Birmensdorf, Switzerland, [3] Department of Plant Nutrition and Soil Science, Christian-Albrechts University, Kiel, Germany, [4] Department of Biogeochemistry of Agroecosystems, Georg-August University, Göttingen, Germany, [5] Soil Science and Soil Protection, Martin Luther University Halle-Wittenberg, Halle, Germany*

OPEN ACCESS

**Edited by:**
*Andreas Schindlbacher, Austrian Research Centre for Forests (BFW), Austria*

**Reviewed by:**
*Alan Feest, University of Bristol, United Kingdom*
*Lukas Kohl, University of Helsinki, Finland*

***Correspondence:**
*Jasmin Fetzer*
*jasmin.fetzer@wsl.ch*

**Specialty section:**
*This article was submitted to Forest Soils, a section of the journal Frontiers in Forests and Global Change*

**Received:** *22 March 2021*
**Accepted:** *04 May 2021*
**Published:** *31 May 2021*

**Citation:**
*Fetzer J, Loeppmann S, Frossard E, Manzoor A, Brödlin D, Kaiser K and Hagedorn F (2021) Leaching of Phosphomonoesterase Activities in Beech Forest Soils: Consequences for Phosphorus Forms and Mobility. Front. For. Glob. Change 4:684069. doi: 10.3389/ffgc.2021.684069*

Phosphomonoesterases play an important role in the soil phosphorus (P) cycle since they hydrolyze P monoester to phosphate. Their activity is generally measured in soil extracts, and thus, it remains uncertain how mobile these enzymes are and to which extent they can be translocated within the soil profile. The presence of phosphomonoesterases in soil solutions potentially affects the share of labile dissolved organic P (DOP), which in turn would affect P leaching. Our study aimed at assessing the production and leaching of phosphomonoesterases from organic layers and topsoil horizons in forest soils and its potential effect on dissolved P forms in leachates obtained from zero-tension lysimeters. We measured phosphomonoesterase activities in leached soil solutions and compared it with those in water extracts from litter, Oe/Oa, and A horizons of two beech forests with a contrasting nitrogen (N) and P availability, subjected to experimental N × P fertilization. In addition, we determined phosphate and DOP. In soil solutions leached from litter, Oe/Oa, and A horizons, phosphomonoesterase activities ranged from 2 to 8 $\mu$mol $L^{-1}$ $h^{-1}$ during summer, but remained below detection limits in winter. The summer values represent 0.1–1% of the phosphomonoesterase activity in soil extracts, indicating that enzymes can be translocated from organic layers and topsoils to greater soil depths. Activities of phosphomonoesterases obtained by water extracts were greater in the organic layer of the P-poor site, while activities of those in soil solutions were similar at the two sites. Nitrogen addition increased phosphomonoesterase activities in leached soil solutions of the organic layer of the N- and P-poor soil. Using a modeling approach, we estimated that approx. 76% of the initial labile DOP was hydrolyzed to dissolved inorganic P within the first 24 h. Back calculations from measured labile DOP revealed an underestimation of approx. 15% of total dissolved P, or 0.03 mg $L^{-1}$. The observed leaching of

phosphomonoesterases implies that labile organic P could be hydrolyzed in deeper soil horizons and that extended sample storage leads to an underestimation of the contribution of DOP to total dissolved P leaching. This has been neglected in the few field studies measuring DOP leaching.

**Keywords: dissolved organic phosphorus, N x P fertilization experiment, hydrolysis, leaching, phosphate, sample storage, organic layers**

## INTRODUCTION

Phosphorus (P) is an essential and, in some regions, a limiting nutrient in forest ecosystems (Wardle et al., 2004; Vitousek et al., 2010). There are also indications for a deteriorated P nutrition in European temperate forests ecosystems (Talkner et al., 2015). Potential reasons are uncertain but may include a long-term depletion of ecosystems in P, an imbalance between nitrogen (N) and P inputs due to global change (Peñuelas et al., 2013) or a co-limitation by N (Harpole et al., 2011). Phosphomonoesterases play an important role in the P cycle by hydrolyzing organic P compounds – P monoesters – to phosphate. Therefore, the activity of extracellular phosphomonoesterases controls the P form in soil which in turn determines its mobility and bioavailability in the plant and soil system. Phosphomonoesterases can be released into extra-cellular environments either actively by bacteria, roots, mycorrhizae, fungi, protists, earthworms, and other fauna or passively from the leakage of cytoplasm due to cell lysis (Spiers and McGill, 1979; Dick, 2011). Process rates catalyzed by enzymes depend on their activity (frequently expressed as the maximal potential rate $V_{max}$) and affinity for substrates (expressed by the Michaelis-Menten constant $K_M$, defined as the substrate concentration at half of $V_{max}$). Since phosphomonoesterases form a diverse group of enzymes, these kinetic parameters represent a weighted mean of the individual characteristics of present phosphomonoesterases (Nannipieri et al., 2011). As N is essential for the production of phosphomonoesterases, soil N availability may represent an important co-limiting factor for P acquisition by plants and microbes mediated by phosphomonoesterases (Olander and Vitousek, 2000; Margalef et al., 2017; Widdig et al., 2019).

The activities of phosphomonoesterases are generally measured in extracts of homogenized soils. Although it was shown that soil extracts yield higher concentrations and different compositions of dissolved organic matter than soil solutions obtained by zero-tension lysimeters (Christ and David, 1994; Fröberg et al., 2003; Hagedorn et al., 2004), few attempts have been made to determine the activities of phosphomonoesterases directly in soil solutions from field experiments. In drainage systems of agricultural land, Wirth et al. (2008) observed the translocation of hydrolases by percolating leachates, indicating that enzymes can be indeed mobile. Toor et al. (2003) detected phosphatase activity in lysimeter solutions in fertilized grassland soils, concluding that organic P could be mineralized during leaching. Some laboratory experiments (e.g., Denison et al., 1998; Turner et al., 2002) indicated that the activities of phosphomonoesterases could be a potential source of error for dissolved inorganic P (DIP) determination. In agreement, Turner et al. (2002) related low concentrations of "labile dissolved organic P (DOP)" in water-extracts from grassland soils (quantified by hydrolysis with phosphomonoesterases) as compared to "non-labile DOP" to the presence of phosphomonoesterases in these extracts, which rapidly transform labile DOP compounds before they can be measured. The hydrolysis of P mono-esters in soil solutions does not only affect the contribution of labile DOP, but also the mobility of P in soils since some organic forms of P are less prone to sorptive retention compared to phosphate (Frossard et al., 1989; Qualls and Haines, 1991a; Kaiser et al., 2003; Brödlin et al., 2019a). Also, phosphate is more available to plants and microorganisms and could be retained more strongly in the system by biological uptake. So far, the few field experiments in forest soils quantifying leaching of various organic and inorganic P forms (e.g., Qualls and Haines, 1991b; Kaiser et al., 2001) have not been considering the possible consequences of enzymatic alterations of P forms. If phosphomonoesterases would be present in soil solutions as suggested by grassland studies and water extractions of soils, they could be translocated to deeper soils, where they could transform P monoesters to the hydrologically more immobile phosphate. In soil solution, phosphomonoesterases could also change the distribution of P forms after sampling with extended storage, which may lead to misinterpretations of P leaching and cycling.

Our study aimed at assessing phosphomonoesterase activities in leachates and soil solutions obtained by free draining lysimeters from organic layers and mineral topsoil horizons of two beech forests and its effects on P forms (DIP, labile and non-labile DOP fractions). We studied soils of two beech forests developed from either P-poor sandy till or P-rich basalt with a different N and P status. To have a larger span in N and P availabilities and to account for possible N and P co-limitation, we took advantage of a full factorial N × P fertilization experiment at the two sites. Our objectives were (i) to investigate the phosphomonoesterase activities and its drivers in leachates and soil solutions percolating from organic layers and mineral topsoils, (ii) to relate these activities in soil solutions to the activity in conventional soil extracts, and finally (iii) to estimate the possible impact of enzymatic hydrolysis of labile DOP in leached soil solutions for P mobility in the soils. We hypothesized that there are substantial phosphomonoesterase activities in soil solutions, which causes a rapid hydrolysis of labile DOP, and changes the contribution of DOP and DIP to total dissolved P. The consequences of the rapid P hydrolysis would be an altered mobility and bioavailability of P in soil and an underestimation of the contribution of DOP to the P leaching in soil.

# MATERIALS AND METHODS

## Study Sites

The study sites Lüss (LUE) and Bad Brückenau (BBR) are mature beech forest stands with strongly differing soil P stocks (**Tables 1**, **2**). The soil at LUE with low P stocks is a sandy Cambisol that developed from glacial till, has a thick organic layer, and shows indications of initial podzolization. The soil at BBR is a loamy Cambisol that formed from a P-rich basaltic rock which is characterized by a thin organic layer. The availability and potential net mineralization of P are substantially higher at BBR than at LUE (**Table 2**).

## Experimental Set-Up and *in situ* Measurements

### N x P Fertilization Experiment

A full factorial N and P fertilization experiment was set up and replicated three times at each site. Plots of 20 m × 20 m were established with 20 m distance between each of them. The plots were fertilized with either N, P, or N × P; an unfertilized plot served as control. From 2016 to 2018, five doses of $NH_4NO_3$ were applied amounting to a total of 150 kg N $ha^{-1}$. In 2016, 50 kg P $ha^{-1}$ were applied as $KH_2PO_4$. To compensate for the salt input in the P fertilized plots, 63 kg K $ha^{-1}$ were applied as KCl on the control and N fertilized plots.

### Zero-Tension Lysimeters

In November 2017, we installed zero-tension lysimeters at both sites at three depths: (i) below the litter horizon (Oi), (ii) below the fermented/humified horizon (Oe/Oa), and (iii) in the mineral topsoil horizon [A(e)h]. The lysimeters at the three depths were spatially separated, not beneath each other. Two types of lysimeters were used. For the litter and Oe/Oa horizon, we used 20 cm × 20 cm plates made from acrylic glass, with a mesh on top and three holes to ensure contact with the soil underneath and allowing access by soil fauna (**Supplementary Figure 1A**). O-rings, 0.3 cm high, were mounted around the holes to prevent water loss. The two lower sides of the plate are framed with a 2 cm high rim. The outlet was placed at the joint of the rims and the plate. A net of 0.5 mm mesh size was fitted into the outlet, to prevent clogging of the tube by coarse particles. The lysimeter in the mineral topsoil was a 19.5 cm × 25.5 cm pod with a 3.3 cm high rim and a bottom outlet equipped with the same mesh as the plate lysimeters. The pod was filled with three layers acid-washed quartz sand of different grain sizes (**Supplementary Figures 1B,C**).

For the installation of the lysimeters, a 1 $m^2$ square was selected and a pit was dug along the lower side. For the A horizon lysimeter, a soil block of at least double the area of the lysimeter was removed. Then, soil was removed from the envisaged place of the lysimeter and sieved to <2 mm. The lysimeters were placed into soil slightly sloping toward the pit. The top of the lysimeters was covered with the sieved soil to ensure a pore continuum with the soil above and finally the soil block was placed back on top of the lysimeter. The plate lysimeters beneath the litter and the Oe/Oa horizons were installed by removing the litter or the entire organic layer and placing them onto the top of the lysimeters. Again, the lysimeters were placed inclined toward the pit. The outlets of all lysimeters were connected to polyethylene bottles placed in the pits, connected by a silicone tube. After installation of the lysimeters, the plots were left to recover from disturbance for 5 months.

**TABLE 1 |** Characteristics of the two study sites, the P-rich site Bad Brückenau (BBR) and the P-poor site Lüss (LUE), for more detailed information please see Lang et al. (2017).

| | BBR (P-rich) | LUE (P-poor) |
|---|---|---|
| Location | N: 50.351800° E: 09.927478° | N: 52.838967° E: 10.267250° |
| Elevation (m a.s.l.) | 809 | 115 |
| Slope / aspect | 10 ± 3° / distributed at a shallow hilltop | No slope /– |
| Mean annual temperature (°C) | 5.8 | 8.0 |
| Mean annual precipitation (mm) | 1,031 | 779 |
| Forest stand | Beech | Beech |
| Parent material | Basalt | Sandy till |
| Soil type | Dystric skeletic Cambisol (hyperhumic, loamic) | Hyperdystric folic Cambisol (arenic, loamic, nechic, protospodic) |
| pH ($CaCl_2$) at 0-5 cm | 3.2 | 3.0 |
| Humus layer | Mull-type moder | Mor-type moder |

### Irrigation and Sampling

Leachates and soil solutions were collected under standardized conditions by irrigating the plots with 20 L $h^{-1}$ $m^{-2}$ of artificial rain water in February/March 2019 and in July 2019 to cover seasonal extremes. Artificial rainwater was prepared using P- and N-free solutes to match local throughfall with pH of 5.5 and electrical conductivity of 25 μS $cm^{-1}$. The artificial rainwater was applied using an Accu-Power sprayer from Birchmeier (Birchmeier Sprühtechnik AG, Switzerland), set to a constant spray rate of 0.3 L $min^{-1}$, which allowed a homogeneous application of the 20 L over the plot area (1 $m^2$) within 1 h. Soil solutions collected in the PE-bottles were stored in powered cooling boxes and transported within 24–48 h to the laboratory. Phosphomonoesterase activities were analyzed with unfiltered samples stored at 4°C. All other analyses were performed with samples passed through 0.45 μm nitrocellulose filters (GVS Life Sciences, Zola Predosa, Italy), and stored at 4°C until analysis.

## Leachate Analysis

Dissolved total P concentrations in soil solutions were measured with ICP-OES (Ultima 2, Horiba Jobin-Yvon, Longjumeau, France), DIP was estimated spectrophotometrically as molybdate-reactive P (MRP), using the molybdate-ascorbic acid method (Murphy and Riley, 1962), using a flow injection analyzer (Scan+, Skalar, Breda, The Netherlands). Dissolved organic P, defined as molybdate-unreactive P (MUP), was calculated as the difference between total P and DIP. Concentrations of dissolved organic carbon (DOC) and total nitrogen (TN) were measured with a FormacsHT/TN analyzer (Skalar). Dissolved nitrate concentrations were measured by ion chromatography

**TABLE 2 |** Phosphorus (P), carbon (C), and nitrogen (N) forms from the non-fertilized litter layer, Oe/Oa horizon, and A horizon of the two study sites Bad Brückenau (BBR, P-rich) and Lüss (LUE, P-poor).

| Site | Horizon | Horizon thickness | Total soil C | Total soil N | Total soil P | C stock | N stock |
|---|---|---|---|---|---|---|---|
| | | cm | mg $g^{-1}$ | mg $g^{-1}$ | mg $g^{-1}$ | g C $m^{-2}$ | g N $m^{-2}$ |
| BBR | Litter | 2.0 | 451 | 17.0 | 0.96 | 135.0 | 5.10 |
| BBR | Oe/Oa | 2.5 | 352 | 19.4 | 2.30 | 703.0 | 38.9 |
| BBR | A | 5.0 | 178 | 12.0 | 3.02 | 3,553 | 240 |
| LUE | Litter | 4.5 | 391 | 14.9 | 0.79 | 313.0 | 12.0 |
| LUE | Oe/Oa | 6.0 | 316 | 11.8 | 0.53 | 3,787 | 141 |
| LUE | A | 5.0 | 69.7 | 3.40 | 0.17 | 2,613 | 128 |

| Site | Horizon | P stock | $P_{citr}$ ($PO_4$-P) [a] | $P_{org}$ of $P_{tot}$ [a] | Soil C: $P_{tot}$ | Soil $N_{tot}$: $P_{tot}$ | Net-DIP rel. [b] | Net-DOP rel. [b] |
|---|---|---|---|---|---|---|---|---|
| | | g P $m^{-2}$ | mg $kg^{-1}$ | % | – | – | μg DIP g $soil^{-1}$* | μg DOP g $soil^{-1}$* |
| BBR | Litter | 0.29 | 315 | 56 | 470 | 17.7 | 310 | 40.0 |
| BBR | Oe/Oa | 4.60 | 326 | 48 | 153 | 8.43 | 84.6 | 18.0 |
| BBR | A | 60.5 | 58.0 | 54 | 58.9 | 3.97 | 2.07 | 1.34 |
| LUE | Litter | 0.63 | 226 | 78 | 495 | 18.9 | 32.0 | 21.7 |
| LUE | Oe/Oa | 6.35 | 140 | 78 | 596 | 22.3 | 60.2 | 7.46 |
| LUE | A | 6.34 | 10.0 | 50 | 410 | 20.0 | 1.25 | 1.06 |

*$P_{citr}$, citric acid extractable P as proxy for plant available P; $P_{org}$ of $P_{tot}$, share of organic P to total P; Net-P rel., potential net dissolved inorganic P (DIP) release at 20°C; Net-DOP rel., potential net dissolved organic P (DOP) release at 20°C.*
*[a]Data from Lang et al. (2017).*
*[b]Data from Brödlin et al. (2019a).*
**During incubation over 33 weeks.*

(ICS 3000, Dionex, Sunnyvale, CA, United States) and dissolved ammonium concentrations with a FIAS-300 (Perkin-Elmer, Waltham, MA, United States). Electrical conductivity was measured with a LF 325 probe (WTW, Weilheim, Germany) and pH with a LL electrode (Metrohm, Herisau, Switzerland). In the unfiltered leachates and soil solutions, colloidal P was determined in different size classes according to the procedure by Missong et al. (2018) to estimate non-dissolved P fractions, allowing for comparisons between filtered and unfiltered samples.

## Kinetics of Phosphomonoesterase Activities

Potential extracellular phosphomonoesterase activities were measured in samples from litter, Oe/Oa, and A horizons, as well as in soil solutions. For organic and A horizons, 0.5 g moist material was weighed in sterilized 100 mL glass bottles with polypropylene lids, then 50 mL of sterilized water was added, and the suspensions were shaken at 20 rpm for 30 min at 22°C on a horizontal shaker. Thereafter, soil suspensions were sonicated (UW2200, Bandelin) at 40 J $s^{-1}$ pulsed energy output for 2 min, transferred to sterilized petri dishes, continuously stirred, and then 50 μL aliquots were pipetted into 96-well microplates. The wells received 100 μL of fluorogenic P monoester substrate (4-methylumbelliferyl-phosphate; $C_{10}H_7O_6PNa_2$) at six concentrations (5, 20, 50, 100, 200, and 300 μM) plus 50 μL 2-(N-morpholino)ethanesulfonic acid ($C_6H_{13}NO_4SNa_{0.5}$) buffer. The reaction pH was 6.1 and the temperature 22°C. Fluorescence was measured after 0, 1, 2, and 3 h reaction time at 355 nm excitation and 460 nm emission wavelength with a slit width of 25 nm, using a Victor 1,420–050 Multi label Counter (Perkin Elmer). For soil solutions, we used 1 mL of sample, processed similarly but without sonication. To compensate for measuring close to the detection limit of enzyme activity in the soil solutions, three analytical replicates were processed. Note, the term phosphomonoesterases as used here, covers all enzymes capable of cleaving the mono-ester bond of added fluorogenic substrate.

## Quantification of Labile DOP by Enzyme Addition Assays

Labile DOP was estimated as the fraction potentially hydrolyzable by added phosphomonoesterases (Turner et al., 2002). The soil solutions for the enzyme additions assays were sampled monthly with zero-tension lysimeters at the P-rich site in 2013 and 2014. We could not analyze soil solutions from the P-poor site because of possible in-solution hydrolysis during long transportation times. Therefore, samples from another beech forest site were used were used to cross-validate the results from BBR. The site Mitterfels (MIT) is as well characterized by a Cambisol, but developed from paragneiss (**Supplementary Material 2**). Soil solutions were collected from beneath the organic forest floor and at 20 cm soil depth in the mineral topsoil. At both sites, eight solution samples were collected and pooled per depth. The samples were transported to the laboratory within 22 h after collection, filtered through 0.45 μm nitrocellulose filters (GVS Life Sciences) and stored at 4°C in polyethylene bottles.

Samples were analyzed for P forms as described above. To obtain measurable concentrations of various DOP fractions, samples were freeze-dried on a lyophilizator (BETA 1–8, Christ, Osterrode, Germany), pooled over a 3-months period for winter (December 2013–March 2014) and for summer (June-August 2014), then re-dissolved in 20–50 mL of autoclaved

ultrapure water, and well mixed on a vortex (Select Vortex, Select BioProducts, United States). Despite these measures, several values in the mineral soil were close to or below the detection limit.

The enzyme addition assays on the concentrated soil solutions were carried out according to Annaheim et al. (2013), using five analytical replicates. 20 μL of phosphomonoesterase solution, made from phosphomonoesterase lyophilisate and ultra-pure water, was added to 200 μL of sample solution. Additionally, 40 μL of MES buffer (pH = 5.4) and 40 μL ultrapure water were added. During preparation of the assays, well-plates and phosphomonoesterases were constantly kept on ice to prevent unspecific hydrolysis. The well plates were sealed with self-adhesive film (no. 781390, Brand, Wertheim, Germany) to prevent evaporation and incubated for 24 h on a laboratory shaker (Tecan, Männedorf, Switzerland) at 37°C and 40 rpm. After incubation, DIP was determined colorimetrically, using the malachite green method (Ohno and Zibilske, 1991) and total P via acid persulfate digestion in an autoclave (Tiessen and Moir, 1993), followed by colorimetric DIP determination with the malachite green method.

## Data Analysis, Calculations, and Statistics

### Michaelis-Menten Kinetics

The hydrolysis rate $v$ can be described by the Michaelis-Menten equation [1]

$$v = V_{max} * \frac{[S]}{K_M + [S]} \quad (1)$$

where $v$ is the reaction rate in μmol $L^{-1}$ $h^{-1}$ and [S] is the substrate concentration in μmol $L^{-1}$, here the amount of labile DOP. $V_{max}$ (μmol $L^{-1}$ $h^{-1}$ for leached soil solutions or μmol $g^{-1}$ $h^{-1}$ for soil) is the maximal potential reaction rate and $K_M$ (μmol $L^{-1}$) is defined as the substrate concentration at half $V_{max}$. $V_{max}$ and $K_M$ were estimated with the "drm" function of the R package "drc" with the two parameter MM model (MM.2).

### Calculations of Net Fluxes and Leachable Fractions

Phosphomonoesterase activities in soil solutions indicate transport to deeper soil horizons, and thus, represent the "leachable fraction" as compared to the soil's total phosphomonoesterase activities. To estimate the leachable fraction, we first upscaled the enzyme activities in leachates to the 20 L of artificial rainfall applied per $m^2$ (**Supplementary Material 3**). "Total" potential phosphomonoesterase activities in the soil (as defined by the activity in soil extracts) were calculated by multiplying the $V_{max}$ per gram dry soil with the total soil mass per $m^2$ (**Supplementary Material 2**). The ratio of phosphomonoesterase activities per 20 L per $m^2$ to the activity in 1 $m^2$ soil was defined as "leachable fraction."

### Modeling of Labile DOP Hydrolysis in Soil Solutions

We modeled the labile DOP hydrolysis in soil solutions based on estimated Michaelis-Menten kinetic parameters $V_{max}$ and $K_M$, total P concentrations (measured in 2019), and fractions of labile DOP in soil solutions (measured 2013/2014). Equation [2] is based on the Michaelis-Menten equation [1].

$$DIP_t = \int_{t'=0}^{t'=t} V_{max} * \frac{labileDOP_0 - DIP_{t'}}{K_M + labileDOP_0 - DIP_{t'}} d_{t'} \quad (2)$$

with $DIP_t$ being the product released over time t and $labileDOP_0$ the initial substrate concentration at time point t = 0. The equation was solved with the "deSolve" package in R (Soetaert et al., 2010). Equations can be found in **Supplementary Material 4**.

Literature data (**Table 3**) and results from our own enzyme addition assay were used to approximate the fractions of labile and non-labile DOP. The following assumptions were made: (i) All inorganic P in the soil solutions originates from organic P, however, mineralization of labile organic P starts instantly upon release in the soil solution. In organic and mineral topsoil horizons, P input from weathering of P-containing primary and secondary minerals is negligible, since older topsoils are depleted in P-containing minerals (Prietzel et al., 2013). We are aware that microbial cells can contain up to 30% of their P in inorganic P forms (Bünemann et al., 2011), but the contribution of inorganic P from microbial cells to total P in soil solutions is small enough to be neglected. (ii) DOP in the sample consists of 20% labile DOP (**Table 3**). (iii) Enzyme activity $V_{max}$ remains constant. In filtered samples, as commonly used for P analysis, microorganisms should be largely removed by filtration at 0.45 μm, however, there might still be some active microorganisms in the leachates that could produce new enzymes. In balance, enzymes can become mineralized during the storage period. (iv) Enzyme activity follows a temperature dependency of on average $Q_{10}$ = 1.7 (Kroehler and Linkins, 1988; Trasar-Cepeda and Gil-Sotres, 1988; Hui et al., 2013; Menichetti et al., 2015; Min et al., 2019), which was considered to be constant for the entire time period of sample storage, transport, and laboratory processing. (v) There is no enzyme activation and deactivation over the storage period and the solutions are perfectly mixed. Since the mass of micro-particles in samples is constant, net sorption of enzymes, and therefore, net activity will not change.

### Statistical Analysis With Linear Mixed Effects Models

We assessed treatment effects using linear mixed-effects models. According to the experimental design, we included blocks (three blocks per site containing the full fertilization treatment) as random effects, and site, N and P inputs, and horizon as fixed effects. We used the *lmer* function from the *lme4* package (Bates et al., 2015). Due to divergence from normal distributed residuals, total P, $V_{max}$, and $K_M$ values were log-transformed for statistical analysis. *P*-values were obtained with the *lmerTest* package (Kuznetsova et al., 2017). For all statistical analyses, effects were considered significant at $p < 0.05$. Due to relatively low number of replicates and therefore, limited statistical power, we designated *p*-values $\geq 0.05$ but $< 0.1$ as marginally significant. Error estimates given in the text and error bars in figures are standard errors of the means. All analyses were performed using R version 3.6.3 (R Core Team, 2020).

**TABLE 3 |** Results of enzyme addition assays conducted with phosphomonoesterase addition in 2013/2014 on soil solutions from the P-rich site Bad Brückenau (BBR), and results from enzyme addition assays from literature with leached soil solutions and soil extracts.

| Study | Phosphomonoesterase-labile DOP (% of DOP)* | | | Non-labile DOP (% of DOP)** | | | Medium | Ecosystem |
|---|---|---|---|---|---|---|---|---|
| | Min*** | Max*** | Mean | Min*** | Max*** | Mean | | |
| This study BBR- Litter layer | 20 | 39 | 29 | 61 | 93 | 71 | Leachate | Forest soil |
| This study BBR- A horizon | 0 | 49 | 25 | 51 | 100 | 75 | Leachate | Forest soil |
| Toor et al. (2003) | 7 | 36 | 23 | 79# | 9# | – | Leachate | Grassland soil |
| Turner et al. (2002) | 0 | 20 | 6 | 40 | 90 | – | Soil-water extract | Pasture soil |
| Keller et al. (2012) | 10 | 15 | – | 61 | 67 | – | NaOH-EDTA soil extract | Agricultural soil |
| Jarosch et al. (2015) | 9 | 57 | 21 | 14 | 67 | 44 | NaOH-EDTA soil extract | Agricultural soil |
| Annaheim et al. (2013) | 6 | 39 | – | 6 | 39 | – | Soil-water suspension | Grassland soil |
| Annaheim et al. (2015) | 5 | 16 | 11 | 51 | 68 | 56 | NaOH-EDTA soil extract | Agricultural soil |

*Hydrolyzable by phosphomonoesterase, or classified as simple or labile monoesters/monoester-like.*
***Enzyme-stable, depends on how many different enzymes were added/were naturally in theolution.*
****Different soils and soil depths and ecosystems.*
*#Hydrolysis without any addition of commercial phosphatases.*
*DOP, Dissolved organic phosphorus.*

# RESULTS

## Phosphorus Forms in the Leachate and Soil Solutions

Total dissolved P concentrations in soil solutions differed significantly among horizons ($p_{\text{Horizon}} < 0.01$), but not between sites ($p_{\text{Site}} = 0.31$). In summer, total P concentrations of non-fertilized litter, Oe/Oa, and A horizons averaged 0.15, 0.09, and 0.06 mg P $L^{-1}$ in the P-poor soil. In the P-rich soil, total P from unfertilized litter, Oe/Oa, and A horizons averaged 0.36, 0.26, and 0.26 mg P $L^{-1}$ ($p_{\text{Horizon}} < 0.01$, **Figure 1**). In winter, total P concentrations were significantly smaller, averaging 0.05 mg P $L^{-1}$ at the P-rich site and 0.03 mg P $L^{-1}$ at the P-poor site ($p_{\text{Season}} < 0.01$). Higher total P concentrations in summer than in winter were mainly due to higher DIP concentrations in summer. Organic P accounted for 17–24% of total P in summer; the share of organic P was higher in winter ($p_{\text{Season}} < 0.01$), ranging from 36 to 80%. Phosphorus fertilization increased total P leaching, especially in the litter ($p_{+P} = 0.05$, $p_{\text{Site:N:P}} < 0.01$) and in the Oe/Oa horizon ($p_{+N:P} = 0.03$). In contrast, N fertilization showed no significant influence on P leaching, at any site and for any season.

Analysis of P-bearing colloids in unfiltered samples showed that all colloids were smaller than 0.45 μm (A. Missong, personal communication, August 25, 2019), indicating that total P analyzed in filtered leachates (**Figure 1**) were representative for unfiltered leachates. In the organic horizons (litter and Oe/Oa), less than 10% of P was associated with colloids, while in the A horizon colloid-associated P accounted for approx. 15% of total P at the P-rich site and approx. 25% at the P-poor site.

Enzyme addition assays with leachates from the P-rich soil showed that, averaged over the winter and summer, 30% of DOP in the litter layer and 25% of the DOP in the A horizon could be potentially enzymatically hydrolyzed (**Figure 2**), being 0.015 and 0.0004 mg P $L^{-1}$, respectively. These contents of labile DOP corresponded to 7% of total P for the litter layer and 3% of total P for the mineral horizon. There was no consistent significant difference in labile DOP between seasons. Analyses of P forms at the additional site MIT gave similar ranges of DOP fractions (**Supplementary Material 4**).

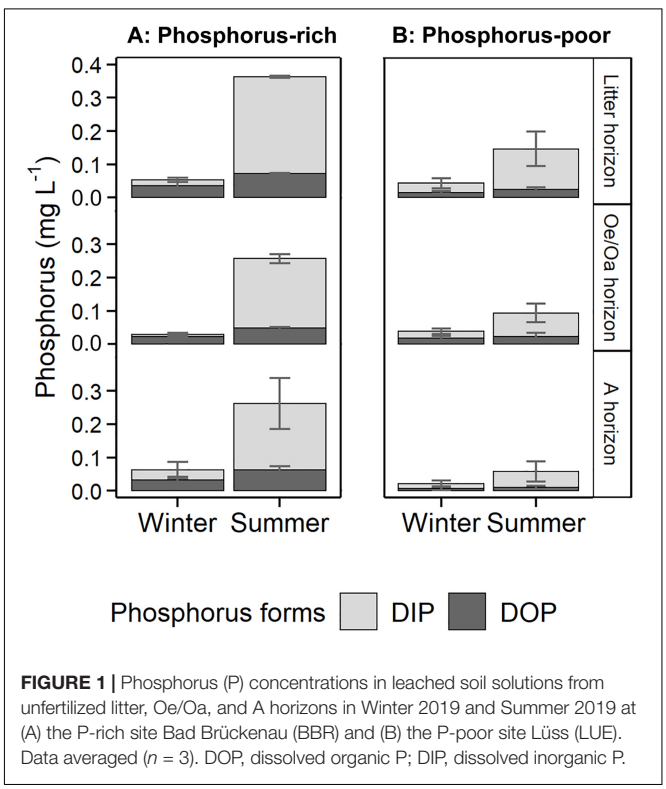


**FIGURE 1 |** Phosphorus (P) concentrations in leached soil solutions from unfertilized litter, Oe/Oa, and A horizons in Winter 2019 and Summer 2019 at (A) the P-rich site Bad Brückenau (BBR) and (B) the P-poor site Lüss (LUE). Data averaged ($n = 3$). DOP, dissolved organic P; DIP, dissolved inorganic P.

## Phosphomonoesterase Activities in Leachate and Soil Solutions

In soil solutions leached in summer, potential phosphomonoesterase activities ($V_{max}$) ranged between 1.89 and 8.09 μmol $L^{-1}$ $h^{-1}$ (**Supplementary Material 5**). At the P-rich site, activity was highest in the solutions leached from the litter, but similar for the Oe/Oa and A horizons (**Figure 3**). At

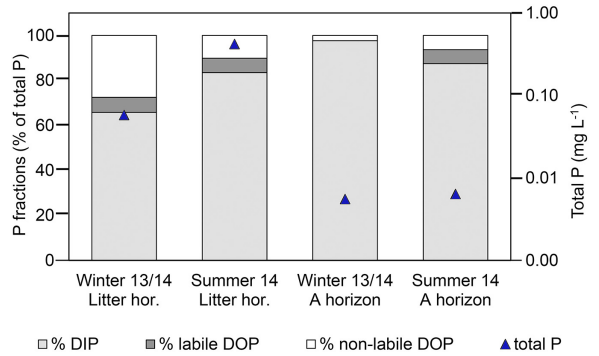


**FIGURE 2 |** Phosphorus (P) forms in leached soil solutions from the litter and the A horizon at the P-rich site Bad Brückenau (BBR) in Winter 2013/2014 and Summer 2014, as revealed by enzyme addition assays with phosphomonoesterase addition; DIP, dissolved inorganic P; DOP, dissolved organic P.

the P-poor site, solutions leached from the A horizon revealed the same $V_{max}$ as those from the litter horizon, while it was lower for solutions from the Oe/Oa horizon ($p_{Horizon} < 0.01$). There were no significant site effects ($p_{Site}$ = n.s.). In winter, phosphomonoesterase activities were mostly below detection limit (data not shown).

The $K_M$ of phosphomonoesterases, reflecting the enzyme affinity for the substrate, ranged between 3 and 205 μmol $L^{-1}$ in soil solutions, with large differences between sites ($p_{Site} < 0.01$) and with soil depth ($p_{Horizon}$ = 0.03) (**Supplementary Material 5**). The P-poor sandy soil exhibited on average 8.5-fold higher $K_M$ values than the P-rich soil. The two sites showed also a different depth patterns, with slight changes in $K_M$ values with depth in the P-poor site, but a distinct decline in $K_M$ in the P-rich soil, from 17.4 ± 2 μmol $L^{-1}$ in the litter layer to 3.80 ± 0.4 μmol $L^{-1}$ in the A horizon (**Figure 4**, bottom left).

At the P-rich site BBR, fertilization with N and P did not significantly alter phosphomonoesterase activities in leached soil solutions (**Supplementary Material 5**). In the litter horizon of the P-poor site, N addition caused increased $V_{max}$ of phosphomonoesterases ($p_{Site:N} < 0.05$, $p_{N:P} = 0.06$). In the Oe/Oa horizon, the addition of P resulted in slightly lower $V_{max}$ than for the control ($p_{+P} = 0.08$, $p_{Site:N:P} < 0.05$). In contrast, $K_M$ was only significantly affected by the fertilization treatments in the Oe/Oa horizon at the P-rich site ($p_{Site:P} < 0.05$; $p_{Site:N:P} < 0.05$) (**Supplementary Material 5**).

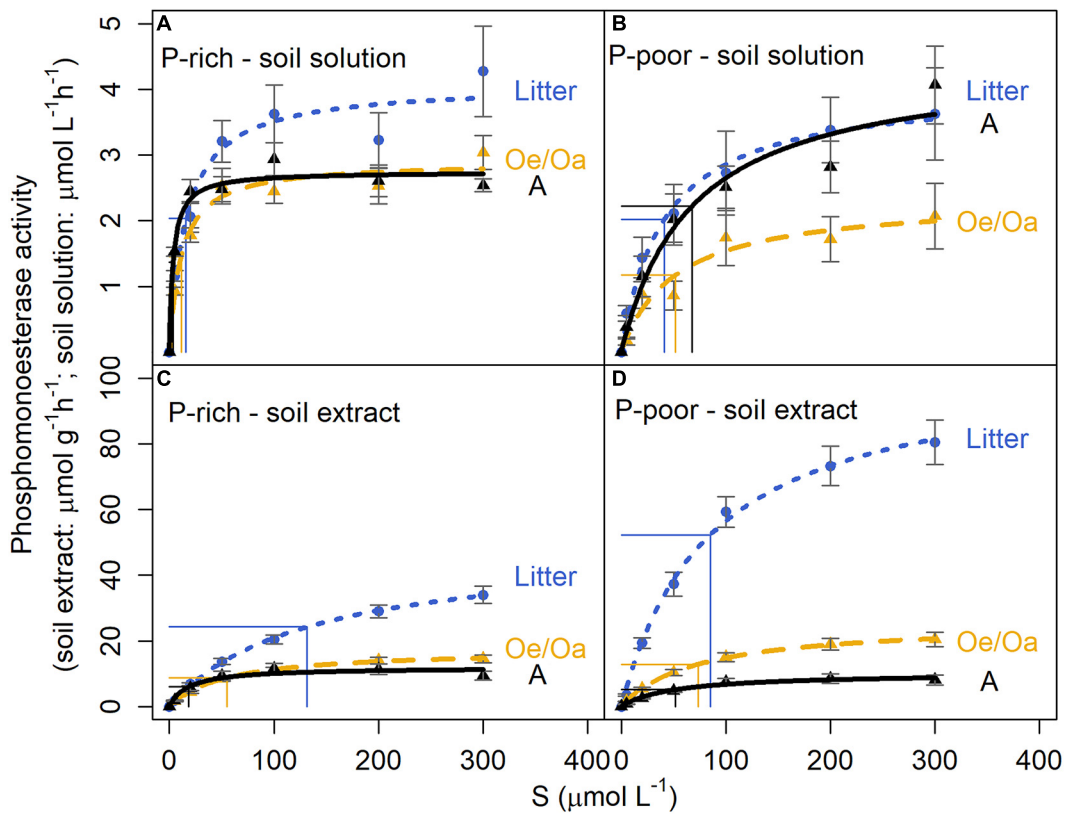


**FIGURE 3 |** Reaction rates of phosphomonoesterase in leached soil solutions and soil extracts from litter, Oe/Oa, and Ah horizons at the P-rich site Bad Brückenau (BBR) and the P-poor site Lüss (LUE) as dependent on substrate concentration (S). **(A)** Phosphomonoesterase activity in leached soil solutions from BBR; **(B)** Phosphomonoesterase activity in leached soil solutions from LUE; **(C)** Phosphomonoesterase activity in soil extracts from BBR; **(D)** Phosphomonoesterase activity in soil extracts from LUE. Horizontal lines are half potential activity ($V_{max}$) and vertical lines the Michalis-Menten constant $K_M$. Symbols = experimental data, lines = approximation by Michaelis-Menten kinetics. Data from July 2019. Error bars as standard error ($n$ = 12, averaged over all fertilization treatments).

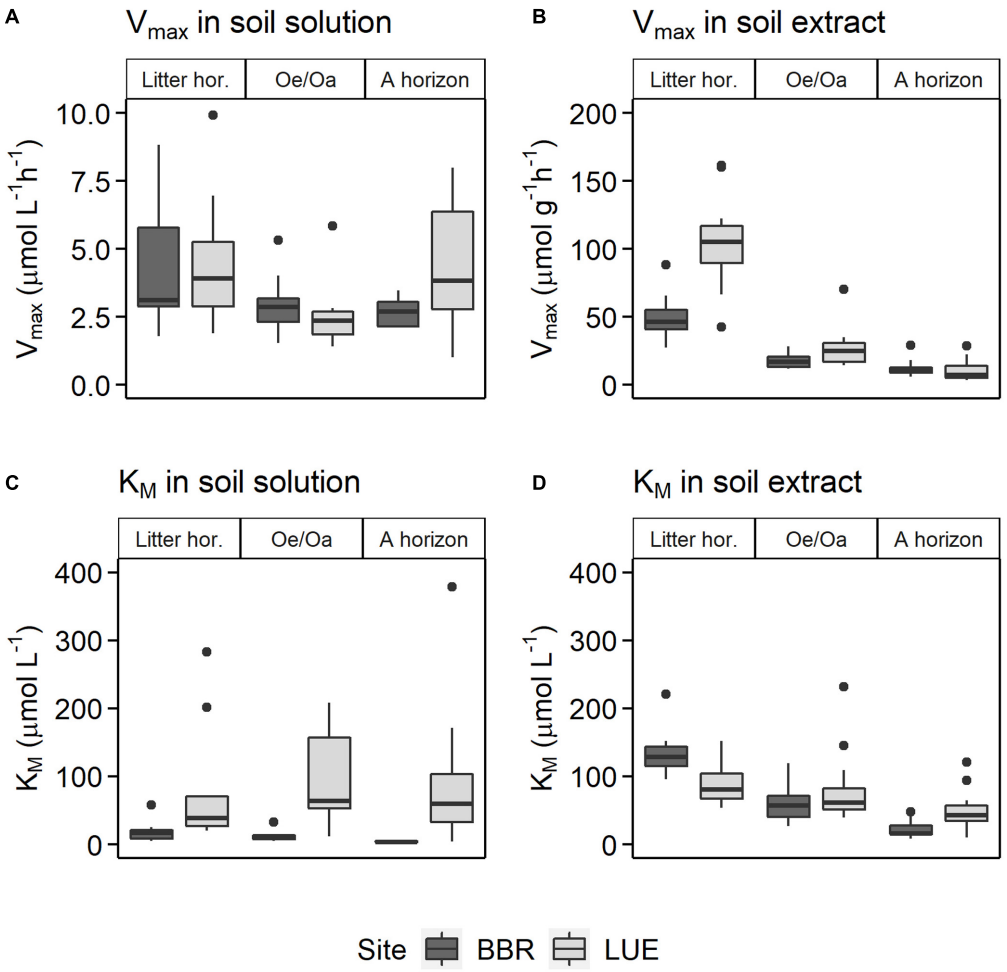


**FIGURE 4 |** Patterns of the Michaelis-Menten kinetic parameters **(A,B)** $V_{max}$ and **(C,D)** $K_M$ in **(A,C)** leached soil solutions and **(B,D)** soil extracts of litter, Oe/Oa, and A horizons at the P-rich site Bad Brückenau (BBR) and the P-poor site Lüss (LUE) averaged over fertilization treatments ($n$ = 12). Data from July 2019.

## Phosphomonoesterase Activities in Soil Extracts

In the soil extracts, potential phosphomonoesterase activities ($V_{max}$) ranged between 6 and 128 µmol $g^{-1}$ $h^{-1}$ (**Supplementary Material 5**). Activity was highest in the litter horizon and decreased strongly with soil depth at both sites ($p_{Horizon} < 0.01$) (**Figures 3**, **4**). $V_{max}$ was higher at the P-poor than at the P-rich site, especially in the litter ($p_{Site} = 0.01$), but statistically not significant in the Oe/Oa and A horizon. The decrease in $V_{max}$ with soil depth was more pronounced in the P-rich soil than in the P-poor soil. $K_M$ in soil extracts ranged between 16 and 142 µmol $L^{-1}$, being highest in the litter layer and decreasing with soil depth ($p_{Horizon} < 0.01$; **Figure 4** and **Supplementary Material 5**).

The depth pattern of $V_{max}$ and $K_M$ differed between sites (**Figure 4**). For the P-rich soil, $V_{max}$ and $K_M$ consistently decreased from litter horizon to Ah horizon in soil solutions as well as in soil extracts. At the P-poor site, they decreased with depth only in the soil extracts, but not in soil solutions.

Total potential phosphomonoesterase activities ($V_{max}$) in soil extracts per horizon and square meter amounted to 4–155 mmol $h^{-1}$ $m^{-2}$. In soil solutions, $V_{max}$ of phosphomonoesterases ranged from 38 to 164 µmol $h^{-1}$ $m^{-2}$ after irrigation with 20 L of artificial rain water. Accordingly, phosphomonoesterase activities in leached soil solutions ranged from 0.1 to 1% of the phosphomonoesterase activities measured in soil extracts. The highest proportion of leached enzyme activity (ratio of enzyme activity in leaching vs. soil extract) was observed for the litter horizon of the P-rich site, the lowest for the mineral A horizons (**Table 4**).

There was no correlation between $V_{max}$ and $K_M$ of phosphomonoesterases with pH, electrical conductivity, total organic C, and total N of soil solutions. Kinetic parameters of phosphomonoesterases in leached soil solutions and extracts were not significantly related to DIP but to DOP in the soil solutions (**Supplementary Material 6**).

## Modeling of DOP Hydrolysis in Leached Soil Solutions

Modeling DOP hydrolysis in soil solutions using measured $V_{max}$ and $K_M$ values shows that 50% of labile DOP is mineralized within 5 and 91 h due to the presence of enzymes (**Figure 5**). The

**TABLE 4 |** Potential phosphomonoesterase activity ($V_{max}$) in leached soil solutions and soil extracts from unfertilized plots per horizon and square meter.

| Site | Horizon | $V_{max}$ leachate | | SE $V_{max}$ leachate | $V_{max}$ soil | | SE $V_{max}$ soil | Leached % of activity in soil | | SE |
|---|---|---|---|---|---|---|---|---|---|---|
| | | $\mu mol\ h^{-1}\ m^{-2}$ | | | $mmol\ h^{-1}\ m^{-2}$ | | | % | | |
| BBR | Litter | 83.0 | ± | 11.4 | 24.7 | ± | 4.5 | 0.35 | ± | 0.05 |
| BBR | Oe/Oa | 56.7 | ± | 3.7 | 30.7 | ± | 2.9 | 0.19 | ± | 0.03 |
| BBR | A | 58.2 | ± | 2.5 | 327 | ± | 105 | 0.03 | ± | 0.00 |
| LUE | Litter | 75.6 | ± | 5.8 | 102 | ± | 11 | 0.08 | ± | 0.01 |
| LUE | Oe/Oa | 118 | ± | NA | 285 | ± | 50 | 0.07 | ± | 0.00 |
| LUE | A | 51.9 | ± | 13.7 | 507 | ± | 230 | 0.03 | ± | 0.01 |

*Data from litter, Oe/Oa, and A horizons at Bad Brückenau (BBR) and Lüss (LUE). Leached percentage of activity in soil extracts defined as ratio of $V_{max}$ in soil solutions to $V_{max}$ in soil extracts. SE: Standard error, n = 3. Data from July 2019.*

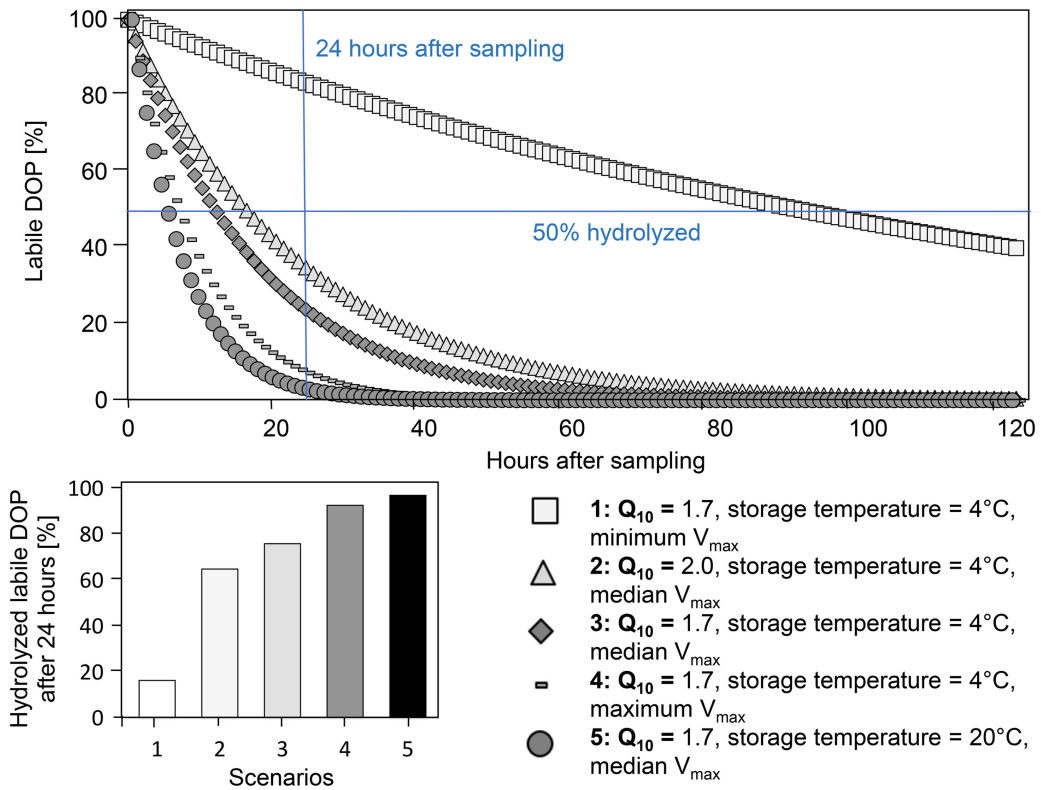


**FIGURE 5 |** Hydrolysis of labile dissolved organic phosphorus (DOP) in leached soil solutions estimated within a range of $V_{max}$ values: lowest, median, and highest $V_{max}$ derived from this study, including two storage temperatures, and two $Q_{10}$ values. $V_{max}$ and $K_M$ from 2019.

model is based on measured P concentrations in leachates and a labile DOP fraction based on literature values of 20% (**Table 3**).

We tested the rate of labile DOP hydrolysis in soil solutions, with five scenarios covering a range of measured $V_{max}$ values of the soils studied (minima, maxima, and median), two $Q_{10}$ values, and two temperatures during storage (**Figure 5**): The $Q_{10}$ values reflecting the range in literature did not influence hydrolysis rates strongly (scenario 2 vs. 3: $Q_{10}$: 1.7 vs. 2.0; Kroehler and Linkins, 1988; Trasar-Cepeda and Gil-Sotres, 1988; Hui et al., 2013; Menichetti et al., 2015; Min et al., 2019). In comparison, $V_{max}$ values had stronger influence on the hydrolysis rate (scenario 1,3,4), with the lowest hydrolysis rate at minimal $V_{max}$. As expected, storage at 4°C showed lower hydrolysis rates than storage at 20°C (scenario 3 vs. 5, **Figure 5**). At median $V_{max}$ (scenario 3), 76% of the labile DOP was hydrolyzed within the first 24 h (**Figure 5**).

Applying the model with the median $V_{max}$ value to the measured labile DOP fractions in leached soil solutions from 2013/2014 and a transport and storage time of 22 h before analysis, suggested that at the time of sampling, the fraction of labile DOP was between 21 and 24% of total P. However, the measured proportions were only 0–7% (**Table 5**) of total P. Consequently, even when labile DOP is rapidly measured after sampling, labile DOP is strongly underestimated by approx. 15% (**Table 5** and **Supplementary Material 7**), which corresponds to an absolute difference of 0.03 mg P $L^{-1}$.

**TABLE 5 |** Back-estimation of fractions of phosphorus (P) forms to the time point of sampling in leached soil solutions from the litter and the A horizon (20 cm depth) in winter 2013/2014 and summer 2014 at the P-rich site Bad Brückenau (BBR).

| Site | Soil depth | Season | Hours | Total P | DIP | Labile DOP | Labile DOP | Non-labile DOP at 22 h* |
|---|---|---|---|---|---|---|---|---|
| | cm | | After sampling | μmol $L^{-1}$ | % of total P | % of total P | % of DOP | % of total P |
| BBR | 0 | Winter 13/14 | 0 (estimated) | 1.87 | 48 | 24 | 47 | 27 |
| BBR | 0 | Winter 13/14 | 22 (measured) | 1.87 | 66 | 6.7 | 20 | 27 |
| BBR | 0 | Summer 14 | 0 (estimated) | 13.57 | 69 | 21 | 68 | 10 |
| BBR | 0 | Summer 14 | 22 (measured) | 13.57 | 83 | 6.4 | 39 | 10 |
| BBR | 20 | Winter 13/14 | 0 (estimated) | 0.18 | 98 | *0.0* | *0.0* | *2.3*** |
| BBR | 20 | Winter 13/14 | 22 (measured) | 0.18 | 98 | 0.0 | 0.0 | 2.3 |
| BBR | 20 | Summer 14 | 0 (estimated) | 0.21 | 71 | 22 | 78 | 6.3 |
| BBR | 20 | Summer 14 | 22 (measured) | 0.21 | 87 | 6.2 | 49 | 6.3 |

*Estimates are based on P fractions measured 22 h after sampling. The back-estimation is based on the DOP hydrolysis model using following parameters: $V_{max}$ = 1.69 μmol $L^{-1}$ $h^{-1}$, $Q_{10}$ = 1.7, temperature = 4°C. DIP, dissolved inorganic P; DOP, dissolved organic P.*
**Not hydrolyzable by phosphomonoesterases – assumed to stay constant over time.*
***No back-estimation possible because of lack of presence of labile DOP at time of measurement.*

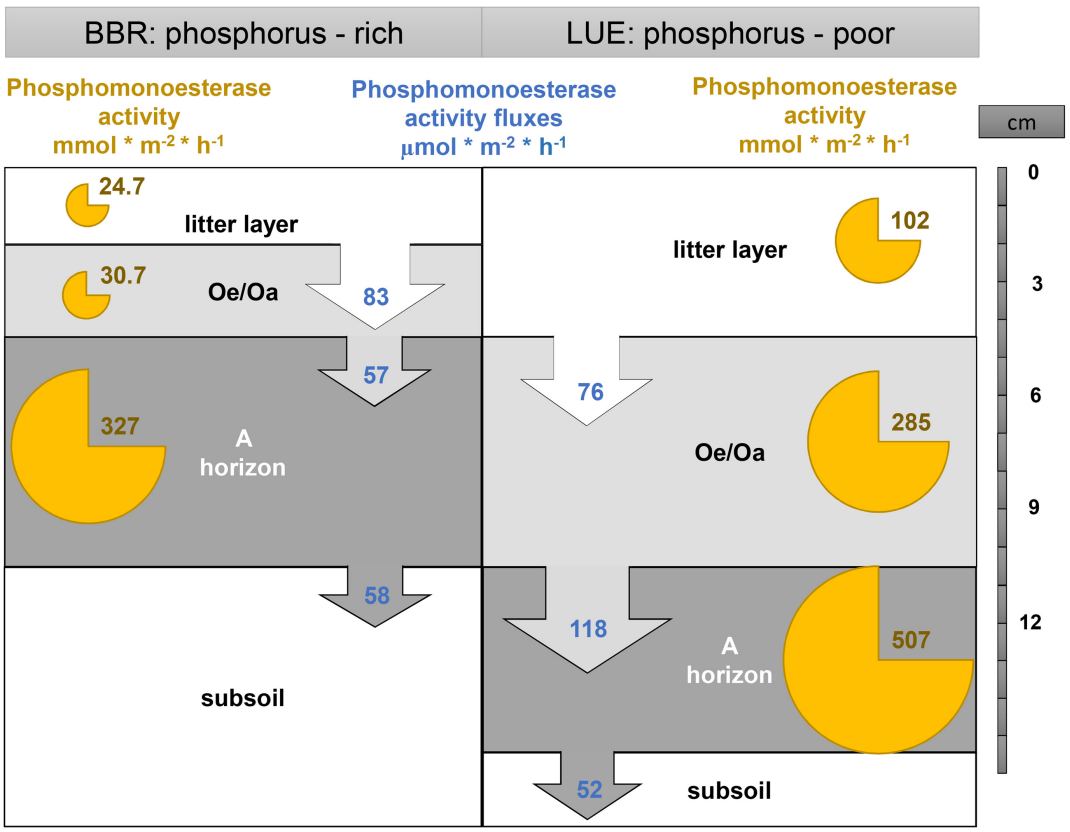


**FIGURE 6 |** Conceptual model of down-transport of phosphomonoesterase activities in the unfertilized plots with percolating water as compared to total phosphomonoesterase activity per horizon and $m^2$ (as defined by activity in soil extracts). Phosphomonoesterase activity ($V_{max}$) in soil horizon: in mmol $m^{-2}$ $h^{-1}$, net phosphomonoesterase activity fluxes in μmol $m^{-2}$ $h^{-1}$. Data from July 2019.

## DISCUSSION

The finding of active phosphomonoesterases being present in soil solutions implies that labile forms of DOP can be rapidly hydrolyzed either *in situ* or *ex situ* after sampling. This result suggests (i) that subsoils are continuously supplied with active enzymes from the surface horizons, for instance with water passing through macro-pores, and (ii) that hydrolysis of labile DOP in samples alters the composition of P forms during leachate collection and processing. Both may lead to an underestimation of DOP leaching in soils.

## Production and Mobility of Phosphomonoesterases

### Production

The greater production of phosphomonoesterases (approximated by the activity in soil extracts, **Figure 6**) in the organic horizons of the P-poor soil than in the P-rich soil probably results from the stronger demand for P from the hydrolysis of organic P by microorganisms, roots, and their associate mycorrhizal fungi (Spiers and McGill, 1979; Olander and Vitousek, 2000; Hofmann et al., 2016). This explanation is supported by a $^{33}P$ labeling study showing that the processing and recycling of organically bound P is more pronounced at the P-poor site with a thick forest floor, whereas at the P-rich site with more narrow C:P and N:P ratios, P release from mineral sources is more dominant (Bünemann et al., 2016). In the leachate of the P-poor site, $V_{max}$ increased after N fertilization (+N and +N × P) in the litter layer and the mineral soil, whereas P fertilization had no significant effect on $V_{max}$, These findings could be either explained by a removal of a N limitation of phosphomonoesterase production at the nutrient-poor site LUE, or by a stimulation of microbial activity that in turn requires more P, since this soil is probably co-limited in both nutrients. In the Oe/Oa horizon of the P-poor soil, N and P seem to be both limiting, as their addition (+P and +N × P) decreased $V_{max}$ in leached soil solution, pointing to a lowered demand after fertilization and hence, lower enzyme production. In contrast to the low-nutrient site, fertilization had no effect on $V_{max}$ at the nutrient-rich site. These results suggest that the susceptibility to changes in phosphomonoesterase production due to N and P fertilization depends on site-specific N:P ratios, as noted in various meta-analyses (Marklein and Houlton, 2012; Margalef et al., 2017).

The strong differences in $K_M$ between both sites point at contrasting soil characteristics. In the P-rich soil, the higher substrate affinity (lower $K_M$) shows that the enzymes can hydrolyze phosphomonoester at low concentrations. One reason could be higher contents of sorptive minerals to which monoesters can bind in the P-rich soil. In the P-rich soil, the Oe/Oa horizon had lower C contents and hence a greater contribution of the mineral phase than in the P-poor soil (**Table 2**). This is likely related to a greater bioturbation in the biological more active and P-rich soil, promoting the transfer of Al and Fe oxides from the mineral soil into organic layers (Clarholm and Skyllberg, 2013). The effect might be supported by larger contents of Al and Fe oxides in the topsoil horizon at the P-rich than the P-poor site (Lang et al., 2017).

### Transport

In contrast to the results from soil extracts where contact between enzymes and substrates is facilitated, the mobility of substrate and active enzymes for enabling hydrolysis is much more important under field conditions, where e.g., adsorption to solid particles prevents contact (Burns et al., 2013; Schimel et al., 2017). Despite the differences in the production of phosphomonoesterases (approximated by soil extracts), their activity in leached soil solutions ($V_{max}$) from the organic horizons was similar at both sites (**Figure 6**). The higher leaching rate at the P-rich site (corresponding to 0.2% of phosphomonoesterase activity in the Oe/Oa horizon) than at the P-poor site (0.1% of phosphomonoesterase activity in the Oe/Oa horizon) can be attributed to the much thicker organic horizons at the P-poor site leading to a longer contact time between enzymes, monoester, and potential sorption sites. Moreover, enzymes might largely be leached from the direct vicinity of the sampling devices, which leads to smaller relative leaching of enzymes produced. In the solutions leached from the A horizons, the patterns were different. Here, the higher $V_{max}$ at the P-poor site than at the P-rich site could either result from the higher production of phosphomonoesterases at lower P availability at the P-poor site or from less sorption of phosphomonoesterases. The mineral soil at the P-poor site is sandy and has low contents of sorptive minerals while the soil at the P-rich site is a clayey loam (Lang et al., 2017), with larger capacity to retain charged compounds such as enzymes. Moreover, water percolation rates are higher in the sandy P-poor soil (unpublished data; A. Manzoor), which promotes vertical mobilization and transport of enzymes, similar as observed for microorganisms (Banfield et al., 2018). As phosphomonoesterases can be transported either dissolved in percolating water, adsorbed to suspended or dispersed particles, or within microbes (Nannipieri et al., 2011; Hoang et al., 2016), unfiltered samples are needed to assess phosphomonoesterase mobility and activity within soils. In the soils studied, colloidal transport was of minor importance for P translocation (A. Missong, pers. communication).

The comparison of phosphomonoesterase activities in leached soil solutions in the field and in soil extracts provides novel insights to the dynamic nature and mobility of phosphomonoesterases in soils. Since phosphomonoesterase activities in soil extracts show that enzymes are released from each horizon, and hence, are prone to leaching, one might expect that rates of enzyme leaching cumulatively increase from one to the next organic horizons, where typically almost no sorption takes place. However, there is no such cumulative effect; enzyme activities in leached soil solutions show even a slight decline of phosphomonoesterase activities with soil depth. As at the same time, enzymes can be produced in each soil horizon, released to the deeper soil horizons, or degraded, the 'gross' removal of phosphomonoesterase activities from percolating soil solution is much greater than anticipated from the changes in phosphomonoesterase activities in soil solutions with depth (**Figure 6**). Seemingly, the continuous deactivation or mineralization of enzymes in percolating soil solution is (almost) compensated by the release of new enzymes in the organic horizons. This points at rapid turnover of these enzymes in soils, however, determining the rates is difficult (Burns et al., 2013; Schimel et al., 2017) and estimates range up to several weeks (Schimel et al., 2017).

In the mineral soil, decreasing phosphomonoesterase activities in leached soil solution are likely due to either a smaller production, or a sorption of enzymes as well as substrates. Sorption reduces substrate accessibility or causes deactivation of the enzyme due to changes in its tertiary structure (Allison and Jastrow, 2006; Nannipieri et al., 2011). Despite sorption

and deactivation processes, there is a net flux of active phosphomonoesterases to deeper soil depths. The hydrolyzing activity of phosphomonoesterases in percolating soil water may promote retention of P in the mineral soil by hydrolyzing the hydrologically more mobile phosphomonoesters into less mobile phosphate (Bol et al., 2016). This is in accordance with findings of Brödlin et al. (2019b), who measured less net P release in the A horizon than in the organic horizons at the study sites, likely due to strong sorption of released phosphate.

### Seasonal Patterns

In addition to the observed patterns among and within soils, phosphomonoesterase activities in leached soil solutions showed a clear seasonality with substantially smaller enzyme activities in winter than in summer, despite standardized irrigation. As microbial biomass was shown to be rather constant throughout the year (Holmes and Zak, 1994), seasonal differences can be more likely ascribed to changes in microbial activity or in the composition of the microbial communities (Yan et al., 2017). Apart of the general increase in phosphatase activities with rising temperature (Shaw and Cleveland, 2020), additional physical and biological factors may explain the seasonal differences. Low enzymatic activities in winter could be due to lower phosphomonoesterases production with overall lower biological activity or to a lower P demand or lower N availability in winter (Chen et al., 2003; Margalef et al., 2017). Dilution or depletion by high leaching fluxes during snow melt may additionally contribute to low enzymatic activities (Wirth et al., 2008). However, we observed substantially smaller phosphomonoesterase activities during winter at both sites, but only the P-rich site received considerable amounts of snow. At the P-poor site, soil moisture contents were similar during the winter and summer sampling, with values of approx. 0.17 $m^3$ $m^{-3}$ at 5 cm depth (**Supplementary Material 8**). Therefore, the observed seasonal patterns of phosphomonoesterase activities mirror most likely the temperature-related biological processes. This conclusion is supported by the smaller share of DIP to total P leaching in winter, suggesting that hydrolysis of organic P is reduced at low temperatures (**Figure 2**). A lower biological P demand during winter would be associated with higher DIP concentrations.

## Implications

The presence of active phosphomonoesterases in leachates obtained from free-draining lysimeters even after filtration at 0.45 μm has consequences for the quantification of P forms in soil solutions. It may result in overestimation of DIP in soil solutions due to hydrolysis of DOP, especially when samples are collected over longer periods as well as during prolonged sample storage. However, it is important to note that measurements of total P are not affected by enzymatic hydrolysis, and thus, total P leaching fluxes represent a solid measure.

Sensitivity analysis of the labile DOP hydrolysis model used revealed little influence of the variations in P concentrations and fractions of P forms on model outcome (**Supplementary Material 9**). We therefore presume that our modeling of rather rapid DOP hydrolyzation rates is (i) rather robust and (ii) applicable to soils covering a great span of P availabilities. Testing for the range of $Q_{10}$ values observed for phosphomonoesterase activities indicated that both, the range of $Q_{10}$ values found in literature (Kroehler and Linkins, 1988; Trasar-Cepeda and Gil-Sotres, 1988; Hui et al., 2013; Menichetti et al., 2015; Min et al., 2019; **Supplementary Material 9**) and the observed model variations due to changes in $Q_{10}$ were small. The largest influence on the hydrolysis rate is exerted by the $V_{max}$ and $K_M$ values that were inherent properties of the soils studied. Despite the distinct differences between the two soils and their horizons, and the large ranges of N and P availabilities covered, the model estimation resulted in comparable hydrolysis times of labile DOP. Our estimate of 76% hydrolyzed labile DOP within 24 h is slightly higher than in the study by Shand and Smith (1997) showing that in a soil solution from a peaty Podzol (0–15 cm soil depth) the share of MRP to total P in increased from 15 to 50% within 24 h after sampling.

Our results also suggest that labile DOP fractions in soil solutions have to be interpreted with care. For instance, the contributions of labile DOP in solutions of forest soils observed here, averaging 20 ± 7% of DOP, as well as those at 70 cm soil depth under a fertilized grassland (23% labile DOP of DOP; Toor et al., 2003) are likely underestimates. Back calculations indicated that at the time of sampling, the fraction of labile DOP of DOP must have been about 30% higher in our study (corresponding to a difference of approx. 15% of total P). This assumption is in agreement with Turner et al. (2002) explaining low contents of labile DOP (approx. 5% of total P) in soil water extracts. They argued that that there must be considerably higher inputs of labile orthophosphate monoesters from plants and microorganisms to the soil, which, however, must have been hydrolyzed within short time after their release. Despite the likely presence of many different P-hydrolyzing enzymes in soil solution, DOP was still detectable even after prolonged storage time, implying that a substantial fraction of DOP is non-hydrolyzable.

The overestimation of DIP in soil water may also lead to an overestimation of phosphate mobility in soils. For instance, despite high sorption capacity, phosphate has been measured in solutions of forested mineral subsoil (Bol et al., 2016). One reason could be preferential flow that transported phosphate rapidly to the subsoils. However, another explanation would be that mobile DOP has been transported into the subsoil and became hydrolyzed to DIP by dissolved enzymes either in situ or after sampling. This would not affect assumptions on the potential bioavailability of leached P, but would cause underestimation the mobility of ester-bound P (Frossard et al., 1989; Kaiser et al., 2003; Bol et al., 2016). Also, these findings suggest that non-labile DOP is most prone to be leached, and therefore might the dominant P form in soils with prevalent leaching of DOP (Kaiser et al., 2000; Qualls, 2000). At the long-term perspective, P depletion of soils might thus be driven by mobile non-labile DOP forms. Leaching of DOP was not affected by fertilization, suggesting independent availability of N and P within ecosystems, which is agreement with studies in soils of contrasting nutrient availability (Hedin et al., 2003).

### Outlook

Measuring phosphomonoesterase activities in leached soil solution provides a potentially complementary approach to the soil extract method. Considering the presence of active DOP hydrolyzing phosphomonoesterases in soil solution advances the understanding the P cycling in soil. The current associated uncertainty of the actual chemical composition of P at the time of sampling exacerbates inferences about P mobility and leaching. Consequently, a standardized measurement procedure is needed to compare the leaching of P forms across sites and horizons. Total P is not affected by the enzyme-driven DOP hydrolysis, and thus, the most reliable variable to track P leaching. Our results are likely applicable to other enzyme groups, for example to other P enzymes, but also enzymes in the C, N, and sulfur cycle.

## DATA AVAILABILITY STATEMENT

The datasets presented in this study can be found in online repositories. The names of the repository/repositories and accession number(s) can be found below: https://www.envidat.ch/#/metadata/jfetzer-phosphatase-leaching.

## AUTHOR CONTRIBUTIONS

FH, KK, EF, JF, and SL contributed to conception and design of the study. JF, SL, and AM conducted the field experiments. JF, DB, SL, and AM conducted laboratory experiments and analyses. JF did the data analyses, the data visualization, and wrote the first draft of the manuscript. All authors contributed to the interpretation of the findings and to the manuscript revision, they read and approved the submitted version.

## FUNDING

We gratefully acknowledge the financial support by the Swiss National Science Foundation (SNF) (project no. 171171) that supports JF, DB, and FH, as well as the German Research Foundation (DFG) that funded the priority program SPP 1685 "Ecosystem nutrition: Forest strategies for limited phosphorus resources" (grants KA1673/9-1 and 2, supporting JF, FH, KK, and DB). SL and AM acknowledge grant 200021E- 171173, given to Prof. S. Spielvogel.

## ACKNOWLEDGMENTS

We thank all people involved in establishing and maintaining the monitoring sites as well as the fertilization experiment. Many thanks to R. Köchli, I. Vögtli, L. Jansing, and D. Kaiser for great help during the field work. We also thank the WSL central laboratory (A. Schlumpf, K. v. Känel, J. Bollenbach, U. Graf, and D. Pezzotta) and the WSL forest soil laboratory (A. Zürcher and D. Christen) for chemical analyses and support as well as A. Boritzki at the Halle soil laboratory for the phosphorus measurements.

## SUPPLEMENTARY MATERIAL

The Supplementary Material for this article can be found online at: https://www.frontiersin.org/articles/10.3389/ffgc.2021.684069/full#supplementary-material

## REFERENCES

Allison, S. D., and Jastrow, J. D. (2006). Activities of extracellular enzymes in physically isolated fractions of restored grassland soils. *Soil Biol. Biochem.* 38, 3245–3256. doi: 10.1016/j.soilbio.2006.04.011

Annaheim, K. E., Doolette, A. L., Smernik, R. J., Mayer, J., Oberson, A., Frossard, E., et al. (2015). Long-term addition of organic fertilizers has little effect on soil organic phosphorus as characterized by 31P NMR spectroscopy and enzyme additions. *Geoderma* 257–258, 67–77. doi: 10.1016/j.geoderma.2015.01.014

Annaheim, K. E., Rufener, C. B., Frossard, E., and Bünemann, E. K. (2013). Hydrolysis of organic phosphorus in soil water suspensions after addition of phosphatase enzymes. *Biol. Fertil. Soils* 49, 1203–1213. doi: 10.1007/s00374-013-0819-1

Banfield, C. C., Pausch, J., Kuzyakov, Y., and Dippold, M. A. (2018). Microbial processing of plant residues in the subsoil – The role of biopores. *Soil Biol. Biochem.* 125, 309–318. doi: 10.1016/j.soilbio.2018.08.004

Bates, D., Mächler, M., Bolker, B., and Walker, S. (2015). Fitting linear mixed-effects models using lme4. *J. Stat. Softw.* 67:120116. doi: 10.18637/jss.v067.i01

Bol, R., Julich, D., Brödlin, D., Siemens, J., Kaiser, K., Dippold, M. A., et al. (2016). Dissolved and colloidal phosphorus fluxes in forest ecosystems–an almost blind spot in ecosystem research. *J. Plant Nutr. Soil Sci.* 179, 425–438. doi: 10.1002/jpln.201600079

Brödlin, D., Kaiser, K., and Hagedorn, F. (2019a). Divergent patterns of carbon, nitrogen, and phosphorus mobilization in forest soils. *Front. For. Glob. Chang.* 2:66. doi: 10.3389/ffgc.2019.00066

Brödlin, D., Kaiser, K., Kessler, A., and Hagedorn, F. (2019b). Drying and rewetting foster phosphorus depletion of forest soils. *Soil Biol. Biochem.* 128, 22–34. doi: 10.1016/j.soilbio.2018.10.001

Bünemann, E. K., Augstburger, S., and Frossard, E. (2016). Dominance of either physicochemical or biological phosphorus cycling processes in temperate forest soils of contrasting phosphate availability. *Soil Biol. Biochem.* 101, 85–95. doi: 10.1016/j.soilbio.2016.07.005

Bünemann, E. K., Oberson, A., and Frossard, E. (2011). *Phosphorus in Action – Biological Processes and Soil Phosphorus Cycling*. Berlin: Springer-Verlag, doi: 10.1016/j.soilbio.2003.10.001

Burns, R. G., DeForest, J. L., Marxsen, J., Sinsabaugh, R. L., Stromberger, M. E., Wallenstein, M. D., et al. (2013). Soil enzymes in a changing environment: current knowledge and future directions. *Soil Biol. Biochem.* 58, 216–234. doi: 10.1016/j.soilbio.2012.11.009

Chen, C. R., Condron, L. M., Davis, M. R., and Sherlock, R. R. (2003). Seasonal changes in soil phosphorus and associated microbial properties under adjacent grassland and forest in New Zealand. *For. Ecol. Manage* 177, 539–557. doi: 10.1016/S0378-1127(02)00450-4

Christ, M., and David, M. B. (1994). Fractionation of dissolved organic carbon in soil water: effects of extraction and storage methods. *Commun. Soil Sci. Plant Anal.* 25, 3305–3319. doi: 10.1080/00103629409369266

Clarholm, M., and Skyllberg, U. (2013). Translocation of metals by trees and fungi regulates pH, soil organic matter turnover and nitrogen availability in acidic forest soils. *Soil Biol. Biochem.* 63, 142–153. doi: 10.1016/j.soilbio.2013.03.019

Denison, F. H., Haygarth, P. M., House, W. A., and Bristow, A. W. (1998). The measurement of dissolved phosphorus compounds: evidence for hydrolysis during storage and implications for analytical definitions in environmental analysis. *Int. J. Environ. Anal. Chem.* 69, 111–123. doi: 10.1080/03067319808032579

Dick, R. P. (2011). *Methods of Soil Enzymology*, ed. R. P. Dick Madison Available online at: https://dl.sciencesocieties.org/publications/books/abstracts/sssabookseries/methodsofsoilen/161

Fröberg, M., Berggren, D., Bergkvist, B., Bryant, C., and Knicker, H. (2003). Contributions of Oi, Oe and Oa horizons to dissolved organic matter in forest floor leachates. *Geoderma* 113, 311–322. doi: 10.1016/S0016-7061(02)00367-1

Frossard, E., Stewart, J. W. B., and St Arnaud, R. J. (1989). Distribution and mobility of phosphorus in grassland and forest soils of Saskatchewan. *Can. J. Soil Sci.* 69, 401–416. doi: 10.4141/cjss89-040

Hagedorn, F., Saurer, M., and Blaser, P. (2004). A $^{13}$C tracer study to identify the origin of dissolved organic carbon in forested mineral soils. *Eur. J. Soil Sci.* 55, 91–100. doi: 10.1046/j.1365-2389.2003.00578.x

Harpole, W. S., Ngai, J. T., Cleland, E. E., Seabloom, E. W., Borer, E. T., Bracken, M. E. S., et al. (2011). Nutrient co-limitation of primary producer communities. *Ecol. Lett.* 14, 852–862. doi: 10.1111/j.1461-0248.2011.01651.x

Hedin, L. O., Vitousek, P. M., and Matson, P. A. (2003). Nutrient losses over four million years of tropical forest development. *Ecol. Res.* 84, 2231–2255. doi: 10.1890/02-4066

Hoang, D. T. T., Pausch, J., Razavi, B. S., Kuzyakova, I., Banfield, C. C., and Kuzyakov, Y. (2016). Hotspots of microbial activity induced by earthworm burrows, old root channels, and their combination in subsoil. *Biol. Fertil. Soils* 52, 1105–1119. doi: 10.1007/s00374-016-1148-y

Hofmann, K., Heuck, C., and Spohn, M. (2016). Phosphorus resorption by young beech trees and soil phosphatase activity as dependent on phosphorus availability. *Oecologia* 181, 369–379. doi: 10.1007/s00442-016-3581-x

Holmes, W. E., and Zak, D. R. (1994). Soil microbial biomass dynamics and net nitrogen mineralization in northern hardwood ecosystems. *Soil Sci. Soc. Am. J.* 58, 238–243. doi: 10.2136/sssaj1994.03615995005800010036x

Hui, D., Mayes, M. A., and Wang, G. (2013). Kinetic parameters of phosphatase: a quantitative synthesis. *Soil Biol. Biochem.* 65, 105–113. doi: 10.1016/j.soilbio.2013.05.017

Jarosch, K. A., Doolette, A. L., Smernik, R. J., Tamburini, F., Frossard, E., and Bünemann, E. K. (2015). Characterisation of soil organic phosphorus in NaOH-EDTA extracts: a comparison of 31P NMR spectroscopy and enzyme addition assays. *Soil Biol. Biochem.* 91, 298–309. doi: 10.1016/j.soilbio.2015.09.010

Kaiser, K., Guggenberger, G., and Haumaier, L. (2003). Organic phosphorus in soil water under a European beech (*Fagus sylvatica* L.) stand in northeastern Bavaria, Germany: seasonal variability and changes with soil depth. *Biogeochemistry* 66, 287–310.

Kaiser, K., Guggenberger, G., Haumaier, L., and Zech, W. (2001). Seasonal variations in the chemical composition of dissolved organic matter in organic forest floor layer leachates of old-growth Scots pine (*Pinus sylvestris* L.) and European beech (*Fagus sylvatica* L.) stands in northeastern Bavaria, Germany. *Biogeochemistry* 55, 103–143. doi: 10.1023/A:1010694032121

Kaiser, K., Guggenberger, G., and Zech, W. (2000). Organically bound nutrients in dissolved organic matter fractions in seepage and pore water of weakly developed forest soils. *Acta Hydrochim. Hydrobiol.* 28, 411–419.

Keller, M., Oberson, A., Annaheim, K. E., Tamburini, F., Mäder, P., Mayer, J., et al. (2012). Phosphorus forms and enzymatic hydrolyzability of organic phosphorus in soils after 30 years of organic and conventional farming. *J. Plant Nutr. Soil. Sci.* 175, 385–393. doi: 10.1002/jpln.201100177

Kroehler, C. J., and Linkins, A. E. (1988). The root surface phosphatases of *Eriophorum vaginatum*: effects of temperature, pH, substrate concentration and inorganic phosphorus. *Plant Soil* 105, 3–10. doi: 10.1007/BF02371136

Kuznetsova, A., Brockhoff, P. B., and Christensen, R. H. B. (2017). lmerTest Package: tests in linear mixed effects models. *J. Stat. Softw.* 82:34107. doi: 10.18637/jss.v082.i13

Lang, F., Krüger, J., Amelung, W., Willbold, S., Frossard, E., Bünemann, E. K., et al. (2017). Soil phosphorus supply controls P nutrition strategies of beech forest ecosystems in Central Europe. *Biogeochemistry* 136, 5–29. doi: 10.1007/s10533-017-0375-0

Margalef, O., Sardans, J., Fernández-Martínez, M., Molowny-Horas, R., Janssens, I. A., Ciais, P., et al. (2017). Global patterns of phosphatase activity in natural soils. *Sci. Rep.* 7:1337. doi: 10.1038/s41598-017-01418-8

Marklein, A. R., and Houlton, B. Z. (2012). Nitrogen inputs accelerate phosphorus cycling rates across a wide variety of terrestrial ecosystems. *New Phytol.* 193, 696–704. doi: 10.1111/j.1469-8137.2011.03967.x

Menichetti, L., Reyes Ortigoza, A. L., García, N., Giagnoni, L., Nannipieri, P., and Renella, G. (2015). Thermal sensitivity of enzyme activity in tropical soils assessed by the Q10 and equilibrium model. *Biol. Fertil. Soils* 51, 299–310. doi: 10.1007/s00374-014-0976-x

Min, K., Buckeridge, K., Ziegler, S. E., Edwards, K. A., Bagchi, S., and Billings, S. A. (2019). Temperature sensitivity of biomass-specific microbial exo-enzyme activities and $CO_2$ efflux is resistant to change across short- and long-term timescales. *Glob. Chang. Biol.* 25, 1793–1807. doi: 10.1111/gcb.14605

Missong, A., Bol, R., Nischwitz, V., Krüger, J., Lang, F., Siemens, J., et al. (2018). Phosphorus in water dispersible-colloids of forest soil profiles. *Plant Soil* 427, 71–86. doi: 10.1007/s11104-017-3430-7

Murphy, J., and Riley, J. P. (1962). A modified single solution method for the determination of phosphate in natural waters. *Anal. Chim. Acta* 27, 31–36. doi: 10.1016/S0003-2670(00)88444-5

Nannipieri, P., Giagnoni, L., Landi, L., and Renella, G. (2011). "Role of phosphatase enzymes in soil," in *Phosphorus in Action*, eds E. Bünemann, A. Oberson, and E. Frossard (Berlin: Springer Berlin Heidelberg), 215–243. doi: 10.1007/978-3-642-15271-9_9

Ohno, T., and Zibilske, L. M. (1991). Determination of low concentrations of phosphorus in soil extracts using malachite green. *Soil Sci. Soc. Am. J.* 55, 892–895.

Olander, L. P., and Vitousek, P. M. (2000). Regulation of soil phosphatase and chitinase activity by N and P availability. *Biogeochemistry* 49, 175–190. doi: 10.1023/A:1006316117817

Peñuelas, J., Poulter, B., Sardans, J., Ciais, P., van der Velde, M., Bopp, L., et al. (2013). Human-induced nitrogen–phosphorus imbalances alter natural and managed ecosystems across the globe. *Nat. Commun.* 4,:2934. doi: 10.1038/ncomms3934

Prietzel, J., Dümig, A., Wu, Y., Zhou, J., and Klysubun, W. (2013). Synchrotron-based P K-edge XANES spectroscopy reveals rapid changes of phosphorus speciation in the topsoil of two glacier foreland chronosequences. *Geochim. Cosmochim. Acta* 108, 154–171. doi: 10.1016/j.gca.2013.01.029

Qualls, R. G. (2000). Comparison of the behavior of soluble organic and inorganic nutrients in forest soils. *For. Ecol. Manage* 138, 29–50.

Qualls, R. G., and Haines, B. L. (1991a). Fluxes of dissolved organic nutrients and humic substances in a deciduous forest. *Ecology* 72, 254–266.

Qualls, R. G., and Haines, B. L. (1991b). Geochemistry of dissolved organic nutrients in water percolating through a forest ecosystem. *Soil Sci. Soc. Am. J.* 55, 1112–1123. doi: 10.2136/sssaj1991.03615995005500040036x

R Core Team (2020). *R: A Language and Environment for Statistical Computing*. Vienna: R Foundation for Statistical Computing.

Schimel, J., Becerra, C. A., and Blankinship, J. (2017). Estimating decay dynamics for enzyme activities in soils from different ecosystems. *Soil Biol. Biochem.* 114, 5–11. doi: 10.1016/j.soilbio.2017.06.023

Shand, C. A., and Smith, S. (1997). Enzymatic release of phosphate from model substrates and P compounds in soil solution from a peaty podzol. *Biol. Fertil. Soils* 24, 183–187. doi: 10.1007/s003740050229

Shaw, A. N., and Cleveland, C. C. (2020). The effects of temperature on soil phosphorus availability and phosphatase enzyme activities: a cross-ecosystem study from the tropics to the Arctic. *Biogeochemistry* 151, 113–125. doi: 10.1007/s10533-020-00710-6

Soetaert, K., Petzoldt, T., and Setzer, R. W. (2010). Solving differential equations in R: package deSolve. *J. Stat. Softw.* 33:37742. doi: 10.18637/jss.v033.i09

Spiers, G. A., and McGill, W. B. (1979). Effects of phosphorus addition and energy supply on acid phosphatase production and activity in soils. *Soil Biol. Biochem.* 11, 3–8. doi: 10.1016/0038-0717(79)90110-X

Talkner, U., Meiwes, K. J., Potočić, N., Seletković, I., Cools, N., De Vos, B., et al. (2015). Phosphorus nutrition of beech (Fagus sylvatica L.) is decreasing in Europe. *Ann. For. Sci.* 72, 919–928. doi: 10.1007/s13595-015-0459-8

Tiessen, H., and Moir, J. O. (1993). "Characterization of available P by sequential extraction," in *Soil Sampling and Methods of Analysis*, eds M. R. Carter and E. G. Gregorich (Pinawa, MB: Canadian Society of Soil Science), 293–306.

Toor, G. S., Condron, L. M., Di, H. J., Cameron, K. C., and Cade-Menun, B. J. (2003). Characterization of organic phosphorus in leachate from a grassland soil. *Soil Biol. Biochem.* 35, 1317–1323. doi: 10.1016/S0038-0717(03)00202-5

Trasar-Cepeda, M. C., and Gil-Sotres, F. (1988). Kinetics of acid phosphatase activity in various soils of galicia (NW Spain). *Soil Biol. Biochem.* 20, 275–280. doi: 10.1016/0038-0717(88)90003-X

Turner, B. L., McKelvie, I. D., and Haygarth, P. M. (2002). Characterisation of water-extractable soil organic phosphorus by phosphatase hydrolysis. *Soil Biol. Biochem.* 34, 27–35. doi: 10.1016/S0038-0717(01)00144-4

Vitousek, P. M., Porder, S., Houlton, B. Z., and Chadwick, O. A. (2010). Terrestrial phosphorus limitation: mechanisms, implications, and nitrogen – phosphorus interactions. *Ecol. Appl.* 20, 5–15. doi: 10.1890/08-0127.1

Wardle, D. A., Walker, L. R., and Bardgett, R. D. (2004). Ecosystem properties and forest decline in contrasting long-term chronosequences. *Science* 305, 509–513. doi: 10.1126/science.1098778

Widdig, M., Schleuss, P. M., Weig, A. R., Guhr, A., Biederman, L. A., Borer, E. T., et al. (2019). Nitrogen and phosphorus additions alter the abundance of phosphorus-solubilizing bacteria and phosphatase activity in grassland soils. *Front. Environ. Sci.* 7:185. doi: 10.3389/fenvs.2019.00185

Wirth, S., Höhn, A., and Müller, L. (2008). Translocation of soil enzyme activity by leachates from different agricultural drainage systems. *Int. J. Soil Sci.* 3, 52–61. doi: 10.3923/ijss.2008.52.61

Yan, G., Xing, Y., Xu, L., Wang, J., Dong, X., Shan, W., et al. (2017). Effects of different nitrogen additions on soil microbial communities in different seasons in a boreal forest. *Ecosphere* 8, 1–19. doi: 10.1002/ecs2.1879

**Conflict of Interest:** The authors declare that the research was conducted in the absence of any commercial or financial relationships that could be construed as a potential conflict of interest.

frontiers in Forests and Global Change

ORIGINAL RESEARCH
published: 29 June 2021
doi: 10.3389/ffgc.2021.696983

# Phosphorus Availability Alters the Effect of Tree Girdling on the Diversity of Phosphorus Solubilizing Soil Bacterial Communities in Temperate Beech Forests

*Antonios Michas[1], Giovanni Pastore[2], Akane Chiba[1,3], Martin Grafe[1], Simon Clausing[4], Andrea Polle[4], Michael Schloter[1,5], Marie Spohn[2,6] and Stefanie Schulz[1]**

*[1] Research Unit Comparative Microbiome Analysis, Helmholtz Zentrum München, Neuherberg, Germany, [2] Department of Soil Biogeochemistry, Bayreuth Center of Ecology and Environmental Research (BayCEER), University of Bayreuth, Bayreuth, Germany, [3] Crop Physiology, TUM School of Life Sciences, Technical University of Munich, Freising, Germany, [4] Forest Botany and Tree Physiology, University of Göttingen, Göttingen, Germany, [5] Chair of Soil Science, TUM School of Life Sciences, Technical University of Munich, Freising, Germany, [6] Biogeochemistry of Forest Soils, Swedish University of Agricultural Sciences, Uppsala, Sweden*

OPEN ACCESS

**Edited by:**
*Sebastian Loeppmann, Christian-Albrechts-Universität zu Kiel, Germany*

**Reviewed by:**
*Bang-Xiao Zheng, University of Helsinki, Finland*
*Aamir Manzoor, University of Göttingen, Germany*

***Correspondence:**
*Stefanie Schulz*
*stefanie.schulz@helmholtz-muenchen.de*

**Specialty section:**
*This article was submitted to Forest Soils, a section of the journal Frontiers in Forests and Global Change*

**Received:** *18 April 2021*
**Accepted:** *07 June 2021*
**Published:** *29 June 2021*

**Citation:**
*Michas A, Pastore G, Chiba A, Grafe M, Clausing S, Polle A, Schloter M, Spohn M and Schulz S (2021) Phosphorus Availability Alters the Effect of Tree Girdling on the Diversity of Phosphorus Solubilizing Soil Bacterial Communities in Temperate Beech Forests. Front. For. Glob. Change 4:696983. doi: 10.3389/ffgc.2021.696983*

Phosphorus (P) solubilization is an important process for P acquisition by plants and soil microbes in most temperate forests. The abundance of inorganic P solubilizing bacteria (PSB) is affected by the P concentration in the soil and the carbon input by plants. We used a girdling approach to investigate the interplay of root-derived C and initial P content on the community composition of *gcd*-harboring bacteria as an example of PSB, which produce gluconic acid. We hypothesized that *gcd*-harboring PSB communities from P-poor sites are more vulnerable to girdling, because of their lower diversity, and that a shift in *gcd*-harboring PSB communities by girdling is caused by a response of few, mostly oligotrophic, taxa. We used a high-throughput metabarcoding approach targeting the *gcd* gene, which codes for the quinoprotein glucose dehydrogenase, an enzyme involved in the solubilization of inorganic P. We compared the diversity of *gcd*-harboring PSB in the mineral topsoil from two temperate beech forests with contrasting P stocks, where girdling was applied and compared our data to the respective control plots with untreated young beech trees. At both sites, *gcd*-harboring PSB were dominated by Proteobacteria and *Acidobacteria*, however, with differences in relative abundance pattern on the higher phylogenetic levels. The P-poor site was characterized by a high relative abundance of *Kaistia*, whereas at the P-rich site, *Dongia* dominated the *gcd*-harboring bacterial communities. Girdling induced an increase in the relative abundance of *Kaistia* at the P-poor site, whereas other bacterial groups of the family *Rhizobiaceae* were reduced. At the P-rich site, major microbial responders differed between treatments and mostly *Bradyrhizobium* and *Burkholderia* were positively affected by girdling in contrast to uncultured *Acidobacteria*,

where reduced relative abundance was found. Overall, these effects were consistent at different time points analyzed after the introduction of girdling. Our data demonstrate that plant-derived carbon influences community structure of *gcd*-harboring bacteria in temperate beech forest soils.

**Keywords: beech, *gcd* gene, girdling, P solubilizing bacteria, quinoprotein glucose dehydrogenase**

## INTRODUCTION

The availability of phosphorus (P) in soil is essential for the growth of plants and the functioning of soil biomes. Soil microbes can exploit different inorganic and organic P sources via several solubilization and mineralization pathways (Sharma et al., 2013). Microbial solubilization of inorganic P in soil promotes plant nutrition (Satyaprakash et al., 2017), the mitigation of drought stress (Shintu and Jayaram, 2015) and the recovery of soil P, e.g., after ecosystem restoration processes (Liang et al., 2020), and it is accomplished by several processes, like the release of protons or secretion of organic acids and siderophores (Sashidhar and Podile, 2010). The secreted organic acids include a diverse range of acids, such as citric acid, oxalic acid, formic acid, and malic acid, among which gluconic acid is considered to be the most important (Goldstein, 1995; Rodríguez and Fraga, 1999; Alori et al., 2017). The formation of gluconic acid from glucose is the result of the expression of the bacterial *gcd* gene, which encodes for the quinoprotein glucose dehydrogenase and the pyrroloquinoline quinon cofactor. As Gcd is a membrane bound enzyme, the oxidation of glucose directly leads to external acidification and subsequent solubilization of mineral bound inorganic P (Goldstein et al., 1993; Goldstein, 1995; Yang et al., 2017; Rasul et al., 2019), and can be considered as an important mechanisms for the solubilization of inorganic P Gram negative bacteria.

P availability in soil affects the structure and abundance of *gcd*-harboring bacterial communities. Previous studies have shown that the diversity and abundance of phosphate solubilizing bacteria (PSB) increase (Pastore et al., 2020; Spohn et al., 2020) or decrease (Bergkemper et al., 2016b; Kurth et al., 2020) at forest sites with low P availability. Further *gcd e*xpression is directly controlled by phosphate concentration (Zeng et al., 2016). However, the role of the availability of other nutrients, e.g., carbon (C) or nitrogen (N), as well as the stoichiometry of those nutrients for the abundance and diversity of PSB are still poorly understood.

The input of organic material into soil, e.g., by root exudation, changes the soil nutrient content and can shift the carbon to phosphorus ratio (C:P) with pronounced effects on the structure of the plant associated microbiome and the phenotype of single microorganisms (Kuzyakov et al., 2007; Koranda et al., 2011; Meier et al., 2017; Vives-Peris et al., 2020). In addition, the release of plant exudates stimulates microbial mobilization of P in the rhizosphere (Spohn et al., 2013). A $^{13}$C-labeling experiment demonstrated that different PSB were attracted by root-derived C in P-poor (e.g., *Bacillales*) and P-rich (e.g., *Rhizobiales*) soils (Long et al., 2018). In addition, single compounds of root exudates may act as a modulator for P turnover, for example citramalic acid and salicylic acid for inorganic P solubilization (Tawaraya et al., 2006; Khorassani et al., 2011). In a recent study, Clausing et al. (2021) demonstrated that tree girdling, which reduces the release of plant photosynthates into soil (Högberg et al., 2001; Kleinsteuber et al., 2008; Zeller et al., 2008; Kaiser et al., 2010, 2015; Pena et al., 2010), significantly reduced the P uptake of plants and increased the abundance of *gcd*-harboring bacteria in the mineral topsoil of beech forests. Girdling significantly increased the potential for microbial inorganic P solubilization in the mineral topsoil only at the P-poor site, while other microbial driven P turnover processes like the mineralization of organic P were not significantly affected.

The results from Clausing et al. (2021) and the previously demonstrated importance of gluconic acid for inorganic P solubilization (Goldstein, 1995; Rodríguez and Fraga, 1999; Alori et al., 2017) gave us the motivation to investigate feedback loops of plant-derived C and shifts in the stoichiometry of soil C:P on the diversity of *gcd*-harboring PSB. For this purpose, we used a molecular barcoding approach based on the *gcd* gene to assess changes in diversity and community composition in response to P and C availability. We analyzed soil samples from a tree girdling experiment, which was performed at two sites with contrasting soil P stocks in temperate beech forests. Samples were taken at two time points after girdling and compared to the respective controls, where no girdling was applied. We hypothesized that (1) the *gcd* community from P-poor sites is more vulnerable to girdling, because of their lower diversity. (2) The increase in abundance of *gcd*-harboring bacteria observed by Clausing et al. (2021) is associated with an increase in the relative abundance of few taxa, rather than a uniform growth of the whole *gcd* community.

## MATERIALS AND METHODS

### Experimental Design

The experimental design has been previously described in detail by Clausing et al. (2021). Briefly, the experiment was conducted at two beech (*F. sylvatica L.*) forests in Germany, Bad Brückenau (BBR: 5579975 N, 3566195 E) and Luess (LUE: 5857057 N, 3585473 E), with different soil properties. Among others, soils differed in total P content; BBR topsoil contained approximately 0.9 mg $P_{tot}$ $g^{-1}$ of dry mass (P-rich), compared to 0.02 mg $P_{tot}$ $g^{-1}$ dry mass at the LUE site (P-poor). The average soil $C:P_{org}$ ratios were 59 and 493 g $g^{-1}$ for BBR and LUE, respectively, (Lang et al., 2017). Experimental plots (4 $m^2$) with young beech trees (10 years) were established at both forest sites in May 2017. In June 2017, all trees in half of each plot were girdled by removal of a strip of bark around the stem. This treatment interrupts the C

flux into the soil. Trees in the other half of the plot were separated by a lawn edge and left untreated. Composite samples consisting of eight soil cores per subplot were collected one (T1) and eight (T2) weeks after girdling from each replicate plot. Bulk topsoil samples from three plots per site were sieved (mesh width: 4 mm) and divided into two aliquots in the field. One aliquot was frozen in liquid nitrogen and stored at −80°C for molecular barcoding. The second aliquot was dried (40°C, 14 days) for calculating soil dry weight.

## Nucleic Acid Extraction and Amplicon Sequencing of the *gcd* Gene

Total nucleic acids were isolated from 0.5 g of frozen soil per sample by mechanical cell disruption using a Precellys 24 homogenisator (5 m $s^{-1}$; 30 s; Bertin Technologies, France), followed by organic solvent extraction according to Lueders et al. (2004). The modified protocol is described by Clausing et al. (2021). A sample without soil served as extraction blank for subsequent sequencing analysis. The amount of DNA was quantified using a NanoDrop 1000 spectrophotometer (Thermo Fisher Scientific, Germany) and the purity was assessed based on the ratio of absorbance of 280/260 nm. Extracted samples were stored at −20°C until further processing.

The amplicon library preparation of *gcd* genes from the soil samples was performed in triplicates according to Bergkemper et al. (2016a) using the same primer pair as for the qPCR analysis in the study of Clausing et al. (2021), *gcd*-FW and *gcd*-RW, with the following modifications. PCR master mix contained 1× High Fidelity PCR Buffer, 1 U Platinum® Taq DNA Polymerase High Fidelity (Invitrogen, Germany), 5 pmol of each primer, 0.06% bovine serum albumin, 2 mM $MgSO_4$, 0.2 mM dNTP, and 50 ng of DNA template in 25 μl total volume. Equal volumes of extraction blank and nuclease-free water were used as non-template controls. The amplification profile was as follows: initial denaturation 94°C for 2 min, 35 amplification cycles of 94°C (30 s), 57°C (60 s) and 72°C (45 s), and final extension at 72°C for 7 min. The presence of DNA fragments of the correct size was confirmed by agarose gel (1%) electrophoresis. A second PCR (10 cycles) was performed with 2 μl of the first PCR product and 2 μl of each of the same primers containing the overhangs for Illumina sequencing. Triplicates were combined and the products were purified using Agencourt AMPure XP beads (0.8 × sample volume; Beckman Coulter Inc., United States). The length and quantity of the fragments were assessed using a Fragment Analyzer Automated CE System (Advanced Analytical Technologies Inc., United States). Barcoded sequences and indices were incorporated by the following PCR reaction: 1 × NEBNext High Fidelity Master Mix (New England BioLabs Ltd., United Kingdom), 2.5 μl of each indexing primer (Nextera® XT Index Kit v2) and 5 ng of the purified template in a 25 μl final volume. Indexed amplicons were purified using Agencourt AMPure XP beads and analyzed by the Fragment Analyzer System as described above. Libraries were diluted to 4 nM, equimolar pooled and sequenced on a MiSeq instrument (Illumina, United States) using the MiSeq Reagent Kit v3 for 600 cycles.

## Bioinformatic and Statistical Analysis

The raw amplicon sequencing data was processed with a modified version of the protocol by Bergkemper et al. (2016a). Briefly, adapter sequences and low quality bases (minimum Phred score: 15) were trimmed and short reads (minimum length: 50 bp) were discarded using AdapterRemoval v2.1.7 (Schubert et al., 2016). Paired reads were merged and chimeras were removed using the *qiime dada2 denoise-paired* command (N-terminal trimming: 10 bp; C-terminal trimming: 235 and 170 bp for forward and reverse reads, respectively; maximum expected errors: 3) of the DADA2 R package v1.3.4 (Callahan et al., 2016) in Qiime2 v2018.8.0[1] (Caporaso et al., 2010). The merged reads were used to infer amplicon sequence variants (ASVs) at the same step. Open reading frames (ORFs) were predicted from the merged reads using FragGeneScan v1.19 (Rho et al., 2010) and were subsequently annotated to functions using hmmsearch (HMMER v3.1b2; [2]) against selected Hidden Markov Models (HMMs) obtained from the TIGRFAM v15.0 database[3]. Overlapping motifs were removed, results were quality filtered (maximum *e*-value: 1e-5) and the sequences assigned to the target gene were extracted from the original datasets. The "positive" sequences were taxonomically aligned to the non-redundant NCBI database (January 2018) using Kaiju v1.4.4 (mismatches allowed in greedy mode: 5; Menzel et al., 2016). The datasets can be found in the Sequence Read Archive[4].

Diversity calculations and statistical analysis of *gcd* amplicon sequencing data, as well as data visualization, were performed using R v3.5.2 (R Core Team,, 2015) and RStudio v1.2.5033. Rarefaction curves were produced with the *rarecurve* command of the "vegan" package (Oksanen et al., 2019); the negative control contained no ASVs. The abundances of ASVs were normalized by calculating relative (%) abundances. Alpha (α−) diversity indices were calculated with the *richness* and *diversity* commands of the "microbiome" package (Lahti and Shetty, 2012-2017) and beta (β−) diversity was explored by non-metric multidimensional scaling (NMDS) analysis based on Bray-Curtis dissimilarity calculations with the *metaMDS* command of package "vegan." ASVs assigned to the same genus were merged using the "phyloseq" package (McMurdie and Holmes, 2013) and the results were visualized using "phyloseq" and "ggplot2" (Wickham, 2016). Common *gcd*-harboring ASVs were defined as the ASVs detected in all replicate plots of each treatment and detected using the online tool of Bioinformatics and Evolutionary Genomics group, Gent, Belgium[5]. The impact of site and girdling treatment on Shannon diversity, was tested per sampling time point by robust 2-way ANOVAs on trimmed means using the *t2way* command of the "WRS2" package (Mair and Wilcox, 2019). The impact of girdling was further tested by pairwise comparisons between the girdled and the respective control plots individually per sampling point at each site by robust 1-way ANOVAs on trimmed means using the *t1way* command

[1] https://qiime2.org/
[2] http://hmmer.org/
[3] ftp://ftp.jcvi.org/pub/data/TIGRFAMs/
[4] https://www.ncbi.nlm.nih.gov/sra/PRJNA694833
[5] http://bioinformatics.psb.ugent.be/webtools/Venn/

of the "WRS2" package. Additionally, the impact of site, girdling treatment and sampling time point on the taxonomic profiles of *gcd* gene datasets was tested by PERMANOVA with 999 permutations using the *adonis* command of the "vegan" package. The results are summarized in **Supplementary Table 1**. Differences in the relative abundances of the detected *gcd*-harboring genera due to site and girdling treatment, were detected by multiple comparisons (robust 1-way ANOVAs on trimmed means, as described above) followed by Benjamini-Hochberg *p*-value adjustment. In all tests, effects were considered significant when the *p*-value was $<0.05$.

## RESULTS

For the analysis of the diversity of *gcd*-harboring PSB, we used a molecular barcoding approach based on sequencing of the *gcd* gene. Overall, we generated a total of 3.5 Mbp reads which could be assigned to 2,517 different ASVs. Among those, 2,515 ASVs contained ORFs and 2,496 of them had a significant hit against the *gcd*-specific HMM, confirming the validity of the applied method. Rarefaction analysis revealed sufficient coverage of major ASVs in all datasets (**Supplementary Figure 2**).

Shannon diversity analysis revealed a significantly higher diversity of *gcd*-harboring bacteria at the BBR site, compared to LUE, at both time points (*p*-values = 0.02; **Figure 1A**, **Supplementary Table 1**) and a decrease from T1 to T2. At BBR, diversity was slightly lower in the girdled plots compared to the control plots for both time points, while the opposite effect was observed at LUE. However, these effects did not reach statistical significance.

The comparison of β-diversity revealed that the structure of *gcd*-harboring bacteria differed between the two sites (*p*-value $< 0.01$). Whereas at LUE all samples clustered closely together (with one exception at T1) and neither girdling nor time point had a significant effect on the β-diversity, individual response pattern toward girdling and time point were observed at BBR for each plot. As the responses differed for each plot, an overall assessment of the shifts did not reach significance (**Figure 1B** and **Supplementary Table 1**).

At both sites, almost 90% of the obtained ASVs were annotated as putative Proteobacteria belonging to the genera *Bradyrhizobium*, *Dongia*, *Kaistia,* as well as other bacteria of the family *Rhizobiaceae*, which could not be further assigned to a genus. Moreover, a high proportion of reads linked to putative uncultured *Acidobacteria* was detected at both sites. However, the relative abundance of the dominant genera differed at both sites (**Figure 2A**). Whereas at BBR almost 50% of the reads could be assigned to uncultured *Acidobacteria* and *Dongia*, ASVs linked to *Kaistia* were dominating the *gcd*-harboring bacterial community at LUE. With the exception of *Kaistia*, differences in the relative abundances of the detected genera between the two sites were not statistically significant, as a result of the huge variability of β-diversity between replicates mostly at BBR (**Figure 2B**). Girdling influenced the relative abundance of ASVs linked to the dominant genera (**Figure 2**). At LUE, at both time points, an increase in relative abundance of ASVs linked to *Kaistia* was observed, which was complemented by a reduced relative abundance of other ASVs linked to putative members of the family *Rhizobiaceae,* which so far have not been further classified. Differences between the two sampling time points were only detected for ASVs, which were not part of the dominant groups listed above. For example, at the control subplots slight increases in the relative abundance of ASV grouped as *Agrobacterium* and *Pseudomonas* was visible, whereas in the subplots subjected to girdling ASVs linked to *Paraburkholderia* were slightly increased in relative abundance. This shift was also confirmed

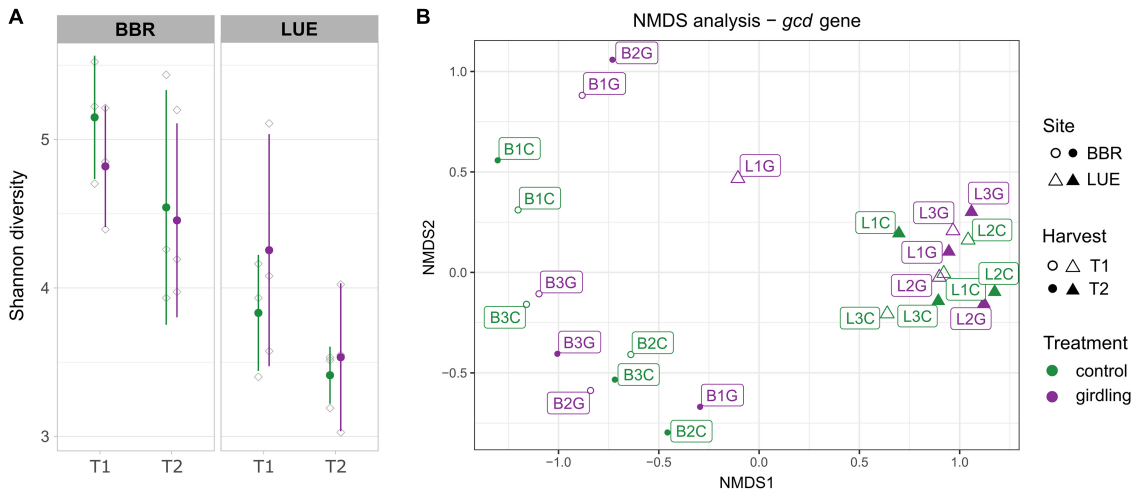


**FIGURE 1 |** Diversity analysis of the amplified *gcd* gene based on the detected ASVs. **(A)** Shannon diversity. Green and purple lines include the samples obtained from the control and girdled plots, respectively. Gray shapes present the individual replicates and error bars the standard deviation between replicates. **(B)** Non-metric multidimensional scaling analysis (NMDS). The sampled sites, sampling time point and treatments are shown by different shape, filling and color, respectively. Labels indicate the number of the replicate sampled plot.

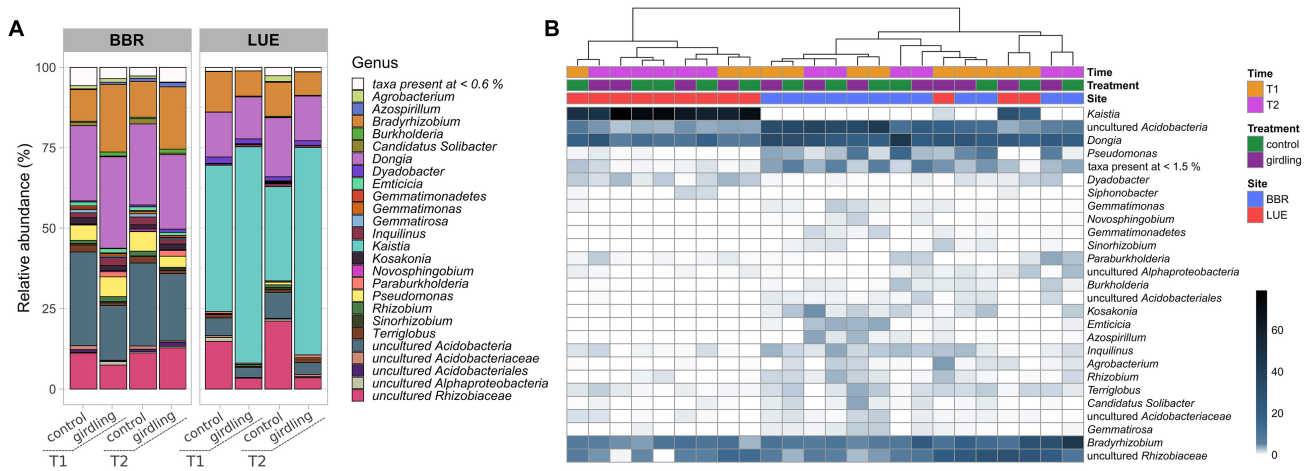


**FIGURE 2 |** Taxonomic assignment at the genus level of ASVs obtained by *gcd* gene amplicon sequencing. **(A)** Stacked barplots of mean relative abundance (%) values. Only genera with >0.6% relative abundance are shown. **(B)** Heatmap of relative abundances (%) in individual replicate samples clustered based on their profile similarity. Only genera with >1.5% relative abundance are shown.

by a cultivation based approach (**Supplementary Figure 3**, **Supplementary Methods**).

At BBR mostly ASVs linked to *Bradyrhizobium* and *Burkholderia* were affected by girdling, as numbers increased at both time points of sampling as a result of girdling. At the same time, there was a trend to reduced numbers of ASVs belonging to uncultured *Acidobacteria*. At T1 also ASVs linked to uncultured bacteria of the family *Rhizobiaceae* were negatively affected. In addition, differences accounting for the sampling time point were observed, which affected mostly the relative abundance of ASVs assigned to *Azospirillum* independent from the treatment. A time point depending response was observed for ASVs linked to *Agrobacterium*, which were increased in relative abundance at T2 in the control treatments compared to all other variants.

As the NMDS analysis revealed strong differences between replicate plots, we identified consistent ASVs among the replicate plots (common *gcd*-harboring ASVs) and compared them between the control and girdling treatments at T1 and T2 (**Figure 3**). The responses to girdling were more pronounced at BBR compared to LUE, as the number of unaffected ASVs was lower at BBR compared to LUE. Interestingly at both sites the overall number of common *gcd*-harboring ASVs for the girdled and control subplots, respectively, was lower at T2 compared to T1, indicating an increased fluctuation over time (**Figure 3A**). Most common *gcd*-harboring ASVs could be assigned to *Dongia* at BBR and *Dongia* and *Kaistia* at LUE, again confirming the importance of these proteobacterial groups for inorganic P solubilization at both sites. The analysis at the level of individual ASVs revealed differences also for the major bacterial genera which are shared between both sites, differences on the level of ASVs indicating differing species composition e.g., for *Dongia* for both sites (**Figure 3B**). In addition, also girdling specific effects mostly at BBR were observed for *Dongia*, with clear differences in the ASV composition as a result of girdling.

## DISCUSSION

Clausing et al. (2021) previously investigated the effect of girdling on the plant and soil microbial P mobilization processes at BBR (P-rich) and LUE (P-poor). Following the reduced efflux of dissolved organic C from the roots caused by girdling, plant root biomass and plant P uptake decreased especially at the P-poor site, indicating that the stimulation of *gcd*-harboring PSB by plant-derived C is an important factor with a strong feedback on plant performance. In this study, we investigated the diversity of *gcd*-harboring PSB communities as affected by girdling at two sites with contrasting P stocks.

The most abundant genera detected at both sites potentially belonged to the orders *Rhizobiales*, *Rhodospirillales*, and the phylum *Acidobacteria*, which have also been previously detected by both amplicon and shotgun metagenomic sequencing (Bergkemper et al., 2016a,b). Considering that these dominant genera harbor also genes encoding for phosphatases (Weon et al., 2008; Ragot et al., 2015; Kim et al., 2016; Grönemeyer et al., 2017), they can potentially exploit both inorganic and organic P sources depending on the changes in soil C:P stoichiometry. Thus, it is possible that girdling causes significant changes in the P acquisition strategy of *gcd*-harboring PSB, which may explain partly that the observed changes in the diversity pattern of *gcd*-harboring PSB were less pronounced than expected, and strong shifts might occur on the level of transcriptomes and associated phenotypes rather than the level of genomes.

However, we observed that the decrease in plant-derived C affected the diversity of *gcd*-harboring PSB at both sites, but response pattern of *gcd*-harboring PSB toward girdling were not consistent at both sites. At the P-rich site (BBR), we observed that the overall high diversity of potential *gcd*-harboring PSB which is present at this site, slightly decreased after the girdling of plants, while the diversity of *gcd*-harboring PSB at the P-poor site was favored by girdling and the subsequent low plant P uptake,

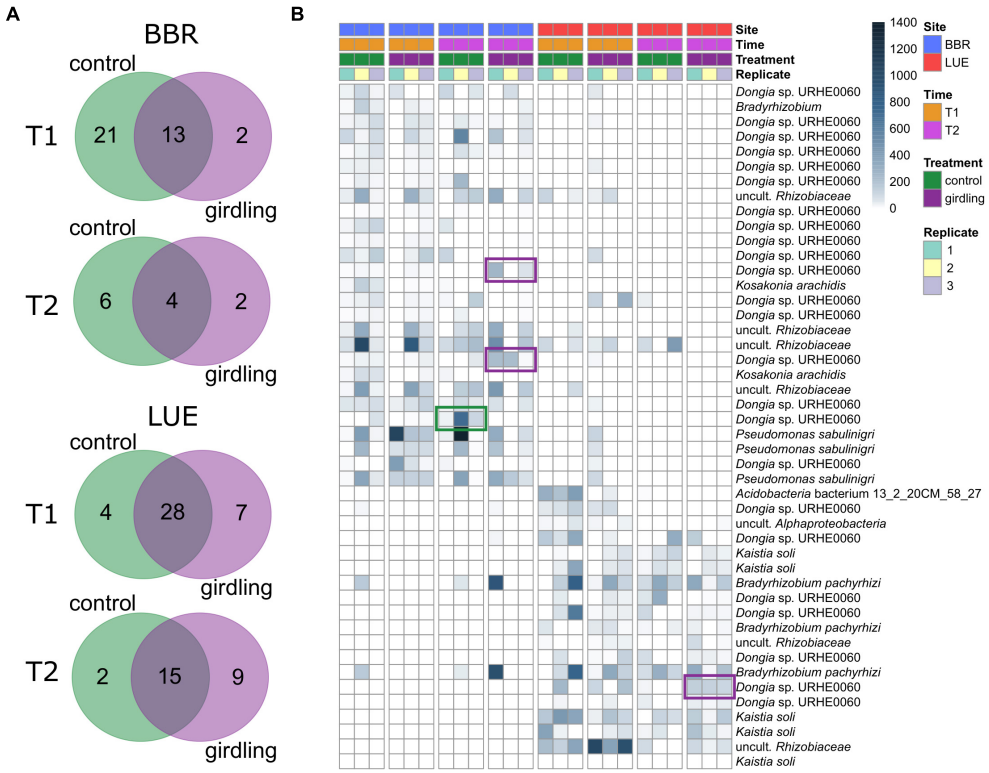


**FIGURE 3 | (A)** Unique and shared common *gcd*-harboring ASVs between treatments. Common *gcd*-harboring ASVs were defined as the ASVs detected in all replicate plots of each treatment. **(B)** Relative abundance of unique ASVs and their taxonomic affiliation on the species level. The color bar indicates the number of reads assigned to each ASV, after normalization of the datasets. The ASVs that responded 8 weeks after girdling are marked in a green or purple frame.

which is in line with the observation of Clausing et al. (2021) who observed an increasing abundance of *gcd*-harboring PSB (**Supplementary Figure 1**).

The opposite response pattern at the two sites might be linked to differences in the stoichiometry of available C and P. In this regard, strong competition of beech roots and soil microbes in P-poor compared to P-rich conditions has been shown for LUE (Clausing and Polle, 2020). Here, the diversity and abundance of *gcd*-harboring PSB at LUE increased as a result of the girdling. The reduced competition of bacteria and plants for P resulted in an increase in diversity despite the reduced available C pools. Changes mostly occurred in the family of *Rhizobiaceae,* which opposed the seasonal fluctuation observed in the control plots. While some genera of the *Rhizobiaceae* were negatively impacted, *Kaistia* benefited from girdling. Whereas many *Rhizobiaceae* form tight interactions with plants (Alves et al., 2014) and may share with them the low amounts of available P, *Kaistia* as a mostly free living genus, might directly fight for P with plants, when plants are active in P acquisition as on the control subplots. In fact *Kaistia* spp. have been detected in various environments, including wastewater soils, river sediments and an anaerobic reactor (Im et al., 2004; Lee et al., 2007; Jin et al., 2012) indicating a large flexibility toward different C sources. Thus, the reduced performance by the plants as a result of girdling may have a negative impact on the plant associated bacteria of the *Rhizobiaceae*, but free living bacteria of the same family may benefit.

At BBR, where control subplots are characterized by a generally low soil C:P ratio, it might be argued that girdling induces a situation where C becomes the limiting factor and not all *gcd*-harboring PSB present in the control subplots are capable to tolerate these conditions. However, the reduced relative abundance of *Acidobacteria*, which can be considered as bacteria with an oligotrophic lifestyle (Kielak et al., 2016) and thus an indicator for reduced stocks of available C, is in contradiction to this postulation. In contrast, we observed an increase of ASVs assigned to *Bradyrhizobium*, *Burkholderia, and Paraburkholderia*. The latter was also confirmed by a cultivation based approach (**Supplementary Figure 3**). Most of these bacteria can form strong interactions with plant roots and have been often considered as part of the plant holobiont (Hassani et al., 2018). However, several *Burkholderia* species are known to change their lifestyle depending on plant fitness and change their mode of interaction from plant beneficial to plant pathogens (Rojas-Rojas et al., 2019). These shifts might be triggered by the availability and quality of root exudates. As plant growth promoting bacteria, *Burkholderia* may benefit from root exudates, whereas as plant pathogens they are capable to degrade cell wall compounds like cellulose or lignin to invade the root interior. The ability to degrade lignin has been described for a

number of *Burkholderia* strains (Morya et al., 2019). Thus, at BBR a girdling induced shift in C quality might be more important than total C availability. Because of the high concentrations of available P, microbes, which are capable to degrade more complex organic materials like plant-derived cellulose or lignin, might become dominant members after girdling. As this flexibility in C use is restricted to some bacterial families only, the reduced diversity pattern observed may be a consequence of shifts in C quality. When T1 and T2 are compared, we expect that this is not the endpoint of community changes after girdling as, for example, the common ASVs detected in the control and girdling treatment still decreased (**Figure 3**). Rasche et al. (2011) observed significant girdling effects even in the second year after girdling. However, long-term girdling effects might be also a consequence of lower fine root biomass or earlier tree senescence, which interferes with the girdling effects (Kaiser et al., 2010). Differences, e.g., in relation to the increase in relative abundance of *Agrobacterium* at T2, were found. *Agrobacterium spp*. are known as degraders for bacterial cellulose (Sieger et al., 1995). Thus, their increase in relative abundance might indicate a secondary succession after girdling, where a number of bacteria which benefit from the changed C quality at T1 die off and their cell wall materials are consumed by others, again benefiting from the overall sufficiently available P.

Beyond shifts in the relative abundance of genera also shifts in ASVs belonging to one species were observed. This was mainly true for the dominant genera, including *Dongia*. This might indicate functional redundancy within the dominant genera, as some ASVs consistently increased in the girdled plots while being absent in the respective control and the other way around. Different preferences of genus ecotypes were also reported previously (Chase et al., 2018), but to prove this mechanism, additional isolation approaches are needed to compare the traits of responding species on whole genome level. Moreover, some bacteria might have obtained the ability to solubilize inorganic P by horizontal gene transfer, as it was demonstrated recently for some proteobacteria like *Bradyrhizobium* (Liang et al., 2020). The question if the identified groups received their capability for the solubilization of inorganic P by horizontal gene transfer of *gcd* genes or by coevolution cannot be disentangled by an amplicon sequencing approach, but needs additional isolation experiments, which allow the comparison of the phylogeny based on 16S rRNA genes and for the *gcd* gene for the same isolate. However, this approach is beyond the scope of this study and also comes along with all limitations related to cultivation experiments like selecting for bacteria preferring copiotrophic conditions, which especially introduced a strong bias for communities isolated from LUE, which is underlined by the low number of different PSB isolates obtained from LUE (**Supplementary Figure 3**)."

## CONCLUSION

Short-term responses of young-beech trees toward girdling were observed at both sites with different responding taxa. As interactions of girdling and season were not significant, the different response pattern observed could be most likely linked to the different soil C:P ratios at the two sites and the factors limiting microbial performance.

The majority of observed shifts in *gcd*-harboring PSB community structure were consistent for the two time points. However, this does not imply that no additional long-term changes in *gcd*-harboring PSB community composition could be observed as a result of girdling after T2. In addition, it needs to be taken into account that the study was performed with relatively young beech trees, which may differ in their exudation pattern as well as strategies to exploit nutrients from trees of older age classes. Furthermore, tree specific effects need to be taken into account despite the fact that bulk soil was sampled, where the direct influence of the trees is limited. But phytoalexins and other compounds are highly persistent in soil and thus might strongly influence all soil microbiome members, including *gcd*-harboring PSB. Thus, future studies might include different tree ages or species as well as the presence and activity of other PSB that do not harbor the *gcd* gene, and were consequently excluded from our current analysis.

## DATA AVAILABILITY STATEMENT

The datasets presented in this study can be found in online repositories. The names of the repository/repositories and accession number(s) can be found below: https://www.ncbi.nlm.nih.gov/, PRJNA694833 https://www.ncbi.nlm.nih.gov/genbank/, MW806976-MW807204.

## AUTHOR CONTRIBUTIONS

AP, MSc, MSp, and SS designed the experiment. SC performed the experiment and collected samples. GP performed cultivation and sequenced isolates. MG extracted soil DNA, generated and analyzed qPCR data, prepared amplicon libraries. AC analyzed amplicon sequencing data. AM performed statistical analysis, visualized results, and wrote the manuscript. AM, MSc, MSp, and SS conceptualized the manuscript. All authors contributed to revisions and approved the final manuscript.

## FUNDING

The work has been funded by the Deutsche Forschungsgemeinschaft in frame of the Priority Program SPP1685 "Ecosystem Nutrition" (SCHL 446/20-2, SCHU 2907/3-2, PO362/22-2, and SP1389/5-2).

## ACKNOWLEDGMENTS

The authors are grateful to Susanne Kublik for sequencing the amplicon libraries.

## SUPPLEMENTARY MATERIAL

The Supplementary Material for this article can be found online at: https://www.frontiersin.org/articles/10.3389/ffgc.2021.696983/full#supplementary-material

**Supplementary Figure 1 |** Absolute counts of *gcd* copies $g^{-1}$ of dry soil as also shown previously in Clausing et al. (2021). Green and purple bars include the samples obtained from the control and girdled plots, respectively. Errors bars present the standard deviation between replicates. Statistically significant differences between plots with girdled trees and the respective controls are presented by *.

**Supplementary Figure 2 |** Constructed rarefaction curves of the sequenced *gcd* gene libraries, showing the number of ASVs detected by means of sequencing depth.

**Supplementary Figure 3 | (A)** Relative number (%) of PSB cultures to total number of cultures obtained by cultivation on Pikovskaya's agar. Green and purple bars include the samples obtained from the control and plots with girdled trees, respectively. Error bars present the standard deviation between replicates. Statistically significant differences between girdled and the respective controls are presented by *. **(B)** Taxonomic assignment of the isolated PSB cultures at the genus level.

**Supplementary Table 1 |** Statistical analysis of the copy numbers, Shannon diversity and taxonomic profiles of amplified *gcd* genes, as well as the relative number of PSB cultures. When applicable, the test statistics (Q and F. model), degrees of freedom (df) and the respective *p*-values are presented. Significant differences ($p$-value $< 0.05$) are marked with orange color.

**Supplementary Methods |** Description of the isolation and characterization of PSB based on cultivation on Pikovskaya agar.

## REFERENCES


Alori, E. T., Glick, B. R., and Babalola, O. O. (2017). Microbial phosphorus solubilization and its potential for use in sustainable agriculture. *Front. Microbiol.* 8:971. doi: 10.3389/fmicb.2017.00971

Alves, L. M. C., de Souza, J. A. M., de Mello Varani, A., and de Macedo Lemos, E. G. (2014). "The Family Rhizobiaceae," in *The Prokaryotes*, eds E. Rosenberg, E. F. DeLong, S. Lory, E. Stackebrandt, and F. Thompson, (Berlin: Springer), 419–437.

Bergkemper, F., Kublik, S., Lang, F., Krüger, J., Vestergaard, G., Schloter, M., et al. (2016a). Novel oligonucleotide primers reveal a high diversity of microbes which drive phosphorus turnover in soil. *J. Microbiol. Methods* 125, 91–97. doi: 10.1016/j.mimet.2016.04.011

Bergkemper, F., Schöler, A., Engel, M., Lang, F., Krüger, J., Schloter, M., et al. (2016b). Phosphorus depletion in forest soils shapes bacterial communities towards phosphorus recycling systems. *Environ. Microbiol.* 18, 1988–2000. doi: 10.1111/1462-2920.13188

Callahan, B. J., Mcmurdie, P. J., Rosen, M. J., Han, A. W., Johnson, A. J. A., and Holmes, S. P. (2016). DADA2: high-resolution sample inference from Illumina amplicon data. *Nat. Methods* 13, 581–583. doi: 10.1038/nmeth.3869

Caporaso, J., Kuczynski, J., Stombaugh, J., Bittinger, K., Bushman, F. D., Costello, E. K., et al. (2010). QIIME allows analysis of high-throughput community sequencing data. *Nat. Methods* 7, 335–336.

Chase, A. B., Gomez-Lunar, Z., Lopez, A. E., Li, J., Allison, S. D., Martiny, A. C., et al. (2018). Emergence of soil bacterial ecotypes along a climate gradient. *Environ. Microbiol.* 20, 4112–4126. doi: 10.1111/1462-2920.14405

Clausing, S., Pena, R., Song, B., Müller, K., Mayer-Gruner, P., Marhan, S., et al. (2021). Carbohydrate depletion in roots impedes phosphorus nutrition in young forest trees. *New Phytol.* 229, 2611–2624. doi: 10.1111/nph.17058

Clausing, S., and Polle, A. (2020). Mycorrhizal Phosphorus Efficiencies and Microbial Competition Drive Root P Uptake. *Front. For. Glob. Change* 3:54. doi: 10.3389/ffgc.2020.00054

Grönemeyer, J. L., Bünger, W., and Urek, B. (2017). Bradyrhizobium namibiense sp. nov., a symbiotic nitrogen-fixing bacterium from root nodules of lablab purpureus, hyacinth bean, in Namibia. *Int. J. Syst. Evol. Microbiol.* 67, 4884–4891.

Goldstein, A. H. (1995). Recent progress in understanding the molecular genetics and biochemistry of calcium phosphate solubilization by gram negative bacteria. *Biol. Agric. Hortic.* 12, 185–193. doi: 10.1080/01448765.1995.9754736

Goldstein, A. H., Rogers, R. D., and Mead, G. (1993). Mining by Microbe: separating phosphate from ores via bioprocessing. *Nat. Biotechnol.* 11, 1250–1254. doi: 10.1038/nbt1193-1250

Hassani, M. A., Durán, P., and Hacquard, S. (2018). Microbial interactions within the plant holobiont. *Microbiome* 6:58. doi: 10.1186/s40168-018-0445-0

Högberg, P., Nordgren, A., Buchmann, N., Taylor, A. F. S., Ekblad, A., Högberg, M. N., et al. (2001). Large-scale forest girdling shows that current photosynthesis drives soil respiration. *Nature* 411, 789–792. doi: 10.1038/35081058

Im, W.-T., Yokota, A., Kim, M.-K., and Lee, S.-T. (2004). Kaistia adipata gen. nov., sp. nov., a novel .ALPHA.-proteobacterium. *J. Gen. Appl. Microbiol.* 50, 249–254. doi: 10.2323/jgam.50.249

Jin, L., Kim, K. K., Lee, H. G., Ahn, C. Y., and Oh, H. M. (2012). Kaistia defluvii sp. nov., isolated from river sediment. *Int. J. Syst. Evol. Microbiol.* 62, 2878–2882. doi: 10.1099/ijs.0.038687-0

Kaiser, C., Kilburn, M. R., Clode, P. L., Fuchslueger, L., Koranda, M., Cliff, J. B., et al. (2015). Exploring the transfer of recent plant photosynthates to soil microbes: mycorrhizal pathway vs direct root exudation. *New Phytol.* 205, 1537–1551. doi: 10.1111/nph.13138

Kaiser, C., Koranda, M., Kitzler, B., Fuchslueger, L., Schnecker, J., Schweiger, P., et al. (2010). Belowground carbon allocation by trees drives seasonal patterns of extracellular enzyme activities by altering microbial community composition in a beech forest soil. *New Phytol.* 187, 843–858. doi: 10.1111/j.1469-8137.2010.03321.x

Khorassani, R., Hettwer, U., Ratzinger, A., Steingrobe, B., Karlovsky, P., and Claassen, N. (2011). Citramalic acid and salicylic acid in sugar beet root exudates solubilize soil phosphorus. *BMC Plant Biol.* 11:121. doi: 10.1186/1471-2229-11-121

Kielak, A. M., Barreto, C. C., Kowalchuk, G. A., van Veen, J. A., and Kuramae, E. E. (2016). The ecology of Acidobacteria: moving beyond genes and genomes. *Front. Microbiol.* 7:744. doi: 10.3389/fmicb.2016.00744

Kim, D. U., Lee, H., Kim, H., Kim, S. G., and Ka, J. O. (2016). Dongia soli sp. nov., isolated from soil from Dokdo. Korea. *Antonie Van Leeuwenhoek* 109, 1397–1402.

Kleinsteuber, S., Schleinitz, K. M., Breitfeld, J., Harms, H., Richnow, H. H., Vogt, C., et al. (2008). Molecular characterization of bacterial communities mineralizing benzene under sulfate-reducing conditions. *FEMS Microbiol. Ecol.* 66, 143–157. doi: 10.1111/j.1574-6941.2008.00536.x

Koranda, M., Schnecker, J., Kaiser, C., Fuchslueger, L., Kitzler, B., Stange, C. F., et al. (2011). Microbial processes and community composition in the rhizosphere of european beech - the influence of plant C exudates. *Soil Biol. Biochem.* 43, 551–558. doi: 10.1016/j.soilbio.2010.11.022

Kurth, J. K., Albrecht, M., Karsten, U., Glaser, K., Schloter, M., and Schulz, S. (2020). Correlation of the abundance of bacteria catalyzing phosphorus and nitrogen turnover in biological soil crusts of temperate forests of Germany. *Biol. Fertil. Soils* 57, 1–14.

Kuzyakov, Y., Hill, P. W., and Jones, D. L. (2007). Root exudate components change litter decomposition in a simulated rhizosphere depending on temperature. *Plant Soil* 290, 293–305. doi: 10.1007/s11104-006-9162-8

Lahti, L., and Shetty, S. (2012-2017). *microbiome R package*. Available online at: http://microbiome.github.io (accessed October 30, 2019).

Lang, F., Krüger, J., Amelung, W., Willbold, S., Frossard, E., Bünemann, E. K., et al. (2017). Soil phosphorus supply controls P nutrition strategies of beech forest ecosystems in Central Europe. *Biogeochemistry* 136, 5–29. doi: 10.1007/s10533-017-0375-0

Lee, H. W., Yu, H. S., Liu, Q. M., Jung, H. M., An, D. S., Im, W. T., et al. (2007). Kaistia granuli sp. nov., isolated from anaerobic granules in an upflow

anaerobic sludge blanket reactor. *Int. J. Syst. Evol. Microbiol.* 57, 2280–2283. doi: 10.1099/ijs.0.65023-0

Liang, J. L., Liu, J., Jia, P., Yang, T. T., Zeng, Q. W., Zhang, S. C., et al. (2020). Novel phosphate-solubilizing bacteria enhance soil phosphorus cycling following ecological restoration of land degraded by mining. *ISME J.* 14, 1600–1613. doi: 10.1038/s41396-020-0632-4

Long, X. E., Yao, H., Huang, Y., Wei, W., and Zhu, Y. G. (2018). Phosphate levels influence the utilisation of rice rhizodeposition carbon and the phosphate-solubilising microbial community in a paddy soil. *Soil Biol. Biochem.* 118, 103–114. doi: 10.1016/j.soilbio.2017.12.014

Lueders, T., Manefield, M., and Friedrich, M. W. (2004). Enhanced sensitivity of DNA- and rRNA-based stable isotope probing by fractionation and quantitative analysis of isopycnic centrifugation gradients. *Environ. Microbiol.* 6, 73–78. doi: 10.1046/j.1462-2920.2003.00536.x

Mair, P., and Wilcox, R. (2019). Robust statistical methods in R using the WRS2 package. *Behav. Res. Methods* 52, 464–488. doi: 10.3758/s13428-019-01246-w

McMurdie, P. J., and Holmes, S. (2013). phyloseq: an R package for reproducible interactive analysis and graphics of microbiome census data. *PLoS One* 8:e61217. doi: 10.1371/journal.pone.0061217

Meier, I. C., Finzi, A. C., and Phillips, R. P. (2017). Root exudates increase N availability by stimulating microbial turnover of fast-cycling N pools. *Soil Biol. Biochem.* 106, 119–128. doi: 10.1016/j.soilbio.2016.12.004

Menzel, P., Ng, K. L., and Krogh, A. (2016). Fast and sensitive taxonomic classification for metagenomics with Kaiju. *Nat. Commun.* 7:11257.

Morya, R., Kumar, M., Singh, S. S., and Thakur, I. S. (2019). Genomic analysis of Burkholderia sp. ISTR5 for biofunneling of lignin-derived compounds. *Biotechnol. Biofuels* 12:277. doi: 10.1186/s13068-019-1606-5

Oksanen, J., Blanchet, F. G., Friendly, M., Kindt, R., Legendre, P., McGlinn, D., et al. (2019). *Vegan: Community Ecology Package*. Available online at: https://cran.r-project.org/package=vegan (accessed April 09, 2020).

Pastore, G., Kernchen, S., and Spohn, M. (2020). Microbial solubilization of silicon and phosphorus from bedrock in relation to abundance of phosphorus-solubilizing bacteria in temperate forest soils. *Soil Biol. Biochem.* 151:108050. doi: 10.1016/j.soilbio.2020.108050

Pena, R., Offermann, C., Simon, J., Naumann, P. S., Geßler, A., Holst, J., et al. (2010). Girdling affects ectomycorrhizal fungal (EMF) diversity and reveals functional differences in EMF community composition in a beech forest. *Appl. Environ. Microbiol.* 76, 1831–1841. doi: 10.1128/aem.01703-09

R Core Team, (2015). *R: A Language And Environment For Statistical Computing*. Vienna: R foundation for statistical computing.

Ragot, S. A., Kertesz, M. A., and Bünemann, E. K. (2015). phoD alkaline phosphatase gene diversity in soil. *Appl. Environ. Microbiol.* 81, 7281–7289.

Rasche, F., Knapp, D., Kaiser, C., Koranda, M., Kitzler, B., Zechmeister-Boltenstern, S., et al. (2011). Seasonality and resource availability control bacterial and archaeal communities in soils of a temperate beech forest. *ISME J.* 5, 389–402. doi: 10.1038/ismej.2010.138

Rasul, M., Yasmin, S., Suleman, M., Zaheer, A., Reitz, T., Tarkka, M. T., et al. (2019). Glucose dehydrogenase gene containing phosphobacteria for biofortification of Phosphorus with growth promotion of rice. *Microbiol. Res.* 223–225, 1–12. doi: 10.1016/j.micres.2019.03.004

Rho, M., Tang, H., and Ye, Y. (2010). FragGeneScan: predicting genes in short and error-prone reads. *Nucleic Acids Res.* 38:e191. doi: 10.1093/nar/gkq747

Rodríguez, H., and Fraga, R. (1999). Phosphate solubilizing bacteria and their role in plant growth promotion. *Biotechnol. Adv.* 17, 319–339. doi: 10.1016/s0734-9750(99)00014-2

Rojas-Rojas, F. U., López-Sánchez, D., Meza-Radilla, G., Méndez-Canarios, A., Ibarra, J. A., and Estrada-de los Santos, P. (2019). The controversial Burkholderia cepacia complex, a group of plant growth promoting species and plant, animals and human pathogens. *Rev. Argent. Microbiol.* 51, 84–92.

Sashidhar, B., and Podile, A. R. (2010). Mineral phosphate solubilization by rhizosphere bacteria and scope for manipulation of the direct oxidation pathway involving glucose dehydrogenase. *J. Appl. Microbiol.* 109, 1–12. doi: 10.1111/j.1365-2672.2009.04654.x

Satyaprakash, M., Nikitha, T., Reddi, E. U. B., Sadhana, B., and Satya Vani, S. (2017). Phosphorous and Phosphate Solubilising Bacteria and their Role in Plant Nutrition. *Int. J. Curr. Microbiol. Appl. Sci.* 6, 2133–2144. doi: 10.20546/ijcmas.2017.604.251

Schubert, M., Lindgreen, S., and Orlando, L. (2016). AdapterRemoval v2: rapid adapter trimming, identification, and read merging. *BMC Res. Notes* 9:88. doi: 10.1186/s13104-016-1900-2

Sharma, S. B., Sayyed, R. Z., Trivedi, M. H., and Gobi, T. A. (2013). Phosphate solubilizing microbes: sustainable approach for managing phosphorus deficiency in agricultural soils. *Springerplus* 2:587.

Shintu, P. V., and Jayaram, K. M. (2015). Phosphate solubilising bacteria (Bacillus polymyxa)-An effective approach to mitigate drought in tomato (Lycopersicon esculentum Mill.). *Trop. Plant Res.* 2, 17–22.

Sieger, C. H. N., Kroon, A. G. M., Batelaan, J. G., and van Ginkel, C. G. (1995). Biodegradation of carboxymethyl celluloses by Agrobacterium CM-1. *Carbohydr. Polym.* 27, 137–143. doi: 10.1016/0144-8617(95)00039-A

Spohn, M., Ermak, A., and Kuzyakov, Y. (2013). Microbial gross organic phosphorus mineralization can be stimulated by root exudates - A 33P isotopic dilution study. *Soil Biol. Biochem.* 65, 254–263. doi: 10.1016/j.soilbio.2013.05.028

Spohn, M., Zeißig, I., Brucker, E., Widdig, M., Lacher, U., and Aburto, F. (2020). Phosphorus solubilization in the rhizosphere in two saprolites with contrasting phosphorus fractions. *Geoderma* 366:114245. doi: 10.1016/j.geoderma.2020.114245

Tawaraya, K., Naito, M., and Wagatsuma, T. (2006). Solubilization of insoluble inorganic phosphate by hyphal exudates of arbuscular mycorrhizal fungi. *J. Plant Nutr.* 29, 657–665. doi: 10.1080/01904160600564428

Vives-Peris, V., de Ollas, C., Gómez-Cadenas, A., and Pérez-Clemente, R. M. (2020). Root exudates: from plant to rhizosphere and beyond. *Plant Cell Rep.* 39, 3–17. doi: 10.1007/s00299-019-02447-5

Weon, H. Y., Lee, C. M., Hong, S. B., Kim, B. Y., Yoo, S. H., Kwon, S. W., et al. (2008). *Kaistia soli* sp. nov., isolated from a wetland in Korea. *Int. J. Syst. Evol. Microbiol.* 58, 1522–1524.

Wickham, H. (2016). *ggplot2: Elegant Graphics for Data Analysis*. New York: Springer-Verlag.

Yang, Y., Wang, N., Guo, X., Zhang, Y., and Ye, B. (2017). Comparative analysis of bacterial community structure in the rhizosphere of maize by high-throughput pyrosequencing. *PLoS One* 12:e0178425. doi: 10.1371/journal.pone.0178425

Zeller, B., Liu, J., Buchmann, N., and Richter, A. (2008). Tree girdling increases soil N mineralisation in two spruce stands. *Soil Biol. Biochem.* 40, 1155–1166. doi: 10.1016/j.soilbio.2007.12.009

Zeng, Q., Wu, X., and Wen, X. (2016). Effects of Soluble Phosphate on Phosphate-Solubilizing Characteristics and Expression of *gcd* Gene in *Pseudomonas* frederiksbergensis JW-SD2. *Curr. Microbiol* 72, 198–206. doi: 10.1007/s00284-015-0938-z

**Conflict of Interest:** The authors declare that the research was conducted in the absence of any commercial or financial relationships that could be construed as a potential conflict of interest.

The reviewer, AM, declared a shared affiliation, though no other collaboration, with the authors, SC and AP, to the handling editor.

# Advantages of publishing in Frontiers

**OPEN ACCESS**
Articles are free to read for greatest visibility and readership

**FAST PUBLICATION**
Around 90 days from submission to decision

**HIGH QUALITY PEER-REVIEW**
Rigorous, collaborative, and constructive peer-review

**TRANSPARENT PEER-REVIEW**
Editors and reviewers acknowledged by name on published articles

**Frontiers**
Avenue du Tribunal-Fédéral 34
1005 Lausanne | Switzerland

**Visit us:** www.frontiersin.org
**Contact us:** frontiersin.org/about/contact

**REPRODUCIBILITY OF RESEARCH**
Support open data and methods to enhance research reproducibility

**DIGITAL PUBLISHING**
Articles designed for optimal readership across devices

**FOLLOW US**
@frontiersin

**IMPACT METRICS**
Advanced article metrics track visibility across digital media

**EXTENSIVE PROMOTION**
Marketing and promotion of impactful research

**LOOP RESEARCH NETWORK**
Our network increases your article's readership